

Proceedings of the  
**XXI INTERNATIONAL  
MINERAL PROCESSING  
CONGRESS**

Rome, Italy  
July 23 - 27, 2000



P. Massacci (Editor)

VOLUME **C**  
ORAL SESSIONS

ELSEVIER

Proceedings of the

XXI INTERNATIONAL  
MINERAL PROCESSING  
CONGRESS

## IMPC INTERNATIONAL STEERING COMMITTEE

Mr. Jacques Astier	Prof. Eric Forsberg (chairman)	Prof. Cyril T. O'Connor
Dr Robin Batterham	Prof. Douglas W. Fuerstenau	Dr. Ponisseril Somasundaran
Prof. Jean M.Cases	Dr. Stephen T. Hall	Prof Kazimierz Sztaba
Prof. Valentin A. Chanturiya	Dr. Vladimir Hencel	Prof. Roberto C. Villas-Bôas
Mr. Rod D. Elvish	Prof Heinz Hoberg	
Prof James A. Finch	Prof. Paolo Massacci	

## IMPC INTERNATIONAL SCIENTIFIC COMMITTEE

Prof. Sayed Abid Hussain	Prof. Wijnand L. Dalmijn	Mr. Hugo Nielson
Dr. Jantore N. Abishev	Dr. Jacques de Cuyper	Prof. Cyril T. O'Connor
Dr. Georgios Anastassakis	Prof. Zeki Dogan	Dr. Peter Pilov
Mr. Jacques Astier	Mr. Rodney D. Elvish	Prof. Knut Sandvik
Dr. George Ayat	Prof. James A. Finch	Dr. Ponisseril Somasundaran
Mr. M.K Batra	Mr. Baba-Ahmed Fodil	Prof. Hans-Jörg Steiner
Dr. Robin Batterham	Prof Eric Forsberg (chairman)	Prof. R. Sturua
Prof. Refaat T. Boulos	Dr. Stephen T. Hall	Prof. Kazimierz Sztaba
Mr. Aurelien Brâncusi	Prof. Kari Heiskanen	Prof. Roberto C. Villas-Bôas
Prof. Jean M. Cases	Dr. Vladimir Hencel	Prof. Takahide Wakamatsu
Prof. Sergio Castro	Prof. Heinz Hoberg	Prof. Dianzou Wang
Prof. Valentin A. Chanturiya	Prof. Errol G. Kelly	Dr. Lordwell K. Witika
Prof. Barbabas Csöke	Prof. Paolo Massacci	

## XXI IMPC AWARD COMMITTEE

Dr. Robin Batterham	Prof. Paolo Massacci (chairman)
Dr. John A. Herbst	Prof. Cyril T. O'Connor
Prof. Heinz Hoberg	

## XXI IMPC ORGANIZING, SCIENTIFIC AND EDITORIAL COMMITTEES

Dr. Carlo Abbruzzese	Prof. Marcello Ghiani
Dr. Michele Agus	Prof. Silvestro Giuliani
Prof. Giovanni Badino	Prof. Massimo Guarascio
Prof. Alberto Bonfiglioli	Dr. Floriana La Marca
Prof. Giuseppe Bonifazi	Prof. Anna Marabini
Prof. Fulvio Ciancabilla	Prof. Paolo Massacci (chairman)
Dr. Laura Cutaia	Dr. Giuseppe Sappa
Dr. Vincenzo Gente	Dr. Silvia Serranti

## XXI IMPC PRODUCTION COMMITTEE

Dr. Clarissa Bagnini	Dr. Carla Nobili
Mrs. Giovanna Cassisa (scientific secretary)	Mr. Alessandro Serrani
Mrs. Gabriella Comandini	Mrs. Gabriella Silvaggi
Mrs. Domenica Liburdi	Mrs. Ludovica Valori
Dr. Flora Nania	Mrs. Maria Pilar Zuniga
Mrs. Ariella Neustadt	

Developments in Mineral Processing, 13

Proceedings of the  
**XXI INTERNATIONAL  
MINERAL PROCESSING  
CONGRESS**

VOLUME **C**  
ORAL SESSIONS



Edited by

**Paolo Massacci**

University of Rome "La Sapienza"  
Department of Chemical, Raw Material and Metallurgical Engineering,  
Rome, Italy



2000

ELSEVIER

AMSTERDAM - LAUSANNE - NEW YORK - OXFORD - SHANNON - SINGAPORE - TOKYO

ELSEVIER SCIENCE B.V.  
Sara Burgerhartstraat 25  
P.O. Box 211, 1000 AE Amsterdam, The Netherlands

© 2000 Elsevier Science B.V. All rights reserved.

This work is protected under copyright by Elsevier Science, and the following terms and conditions apply to its use:

**Photocopying**

Single photocopies of single chapters may be made for personal use as allowed by national copyright laws. Permission of the Publisher and payment of a fee is required for all other photocopying, including multiple or systematic copying, copying for advertising or promotional purposes, resale, and all forms of document delivery. Special rates are available for educational institutions that wish to make photocopies for non-profit educational classroom use.

Permissions may be sought directly from Elsevier Science Global Rights Department, PO Box 800, Oxford OX5 1DX, UK; phone: (+44) 1865 843830, fax: (+44) 1865 853333, e-mail: [permissions@elsevier.co.uk](mailto:permissions@elsevier.co.uk). You may also contact Global Rights directly through Elsevier's home page (<http://www.elsevier.nl>), by selecting 'Obtaining Permissions'.

In the USA, users may clear permissions and make payments through the Copyright Clearance Center, Inc., 222 Rosewood Drive, Danvers, MA 01923, USA; phone: (978) 7508400, fax: (978) 7504744, and in the UK through the Copyright Licensing Agency Rapid Clearance Service (CLARCS), 90 Tottenham Court Road, London W1P 0LP, UK; phone: (+44) 171 631 5555; fax: (+44) 171 631 5500. Other countries may have a local reprographic rights agency for payments.

**Derivative Works**

Tables of contents may be reproduced for internal circulation, but permission of Elsevier Science is required for external resale or distribution of such material. Permission of the Publisher is required for all other derivative works, including compilations and translations.

**Electronic Storage or Usage**

Permission of the Publisher is required to store or use electronically any material contained in this work, including any chapter or part of a chapter.

Except as outlined above, no part of this work may be reproduced, stored in a retrieval system or transmitted in any form or by any means, electronic, mechanical, photocopying, recording or otherwise, without prior written permission of the Publisher.

Address permissions requests to: Elsevier Science Rights & Permissions Department, at the mail, fax and e-mail addresses noted above.

**Notice**

No responsibility is assumed by the Publisher for any injury and/or damage to persons or property as a matter of products liability, negligence or otherwise, or from any use or operation of any methods, products, instructions or ideas contained in the material herein. Because of rapid advances in the medical sciences, in particular, independent verification of diagnoses and drug dosages should be made.

First edition 2000

Library of Congress Cataloging in Publication Data

A catalog record from the Library of Congress has been applied for.

ISBN: 0 444 50283 1

© The paper used in this publication meets the requirements of ANSI/NISO Z39.48-1992 (Permanence of Paper).  
Printed in The Netherlands.

## GOLDEN NUGGETS

Mystery and sacredness surround the origins of those activities that are grouped under the name of Mineral Processing.

In all cultures, mineral products, just as vegetable products, are considered living parts of the earth. The original act of picking a piece fruit, putting out fire or exploiting mineral from the earth, which was considered sacrilegious, was punished by exile, slavery and segregation, as happened to *Adam*, *Prometheus* and *Hephaistos* according to Mediterranean mythology.

The defying gesture of man confronting the sacredness of nature, while condemning him to suffer in order to obtain its fruit, at the same time emancipates him and makes him protagonist of his destiny; it makes him an artificer of a new world, built according to the limits of man himself.

*Homo faber* thus becomes capable of taking the place of the generative force of the earth, favoring the processes of growth and accelerating the generative action to the point of transformation of matter and energy into materials. The alchemist crowns this acceleration by researching the final transformation of all raw materials into the incorruptible gold.

A set of rules and codes of professional behavior emerge from this experience, which culminate in the *De La Pirotechnia* by *Biringuccio* and in the *De Re Metallica* by *Agricola*, whose purpose is not simply that of passing on the production processes and the transformation of raw materials, but that rather more ambitious task of revealing the means of recognizing the harmony in the rules inherent in the management of the natural resources.

By exceeding empirical rules handed down by the masters of Art, Science and Technology are developed at the University, the headquarters in which the alchemic experiment matures, and adopt physical and mathematical models of processes that are the very foundation of modern Mineral Processing.

*Tradition, Science, and Technology* outline a long course through the history of man, with myths and mysteries, secrets, know-how's, scientific discoveries and technical applications.

The history of Mineral Processing describes a course back to an origin rich in symbolism, followed by strong consolidated experiments, and, finally, suitable of refined rational analysis and efficient synthesis of models.

The XXI IMPC, following the tradition initiated in 1952, traces a trip through the development of scientific knowledge and the most recent industrial applications, in order to compare know how's of scientists and technicians with the perspectives for the research and for the industrial activity in the sector of Mineral Processing, which now also definitely include topics of waste treatment, recycling and soil remediation.

This series of *Golden Nuggets* volumes, after an accurate process of cleaning, re-cleaning, and polishing, includes 270 texts selected after a preliminary call for papers (with a response of 650 abstracts), which were then refined after review.

All manuscripts were first reviewed in a draft form by a 40 reviewers. In spite of the fact that rules of compilation were pre-established, the reworked, final versions have

been formatted in such a way as to guarantee a uniform look for the proceedings. The editor took the liberty of introducing essential layout changes, as well as correcting grammar, spelling and style when this was most needed and requested by reviewers.

The works collected in the first two volumes (A and B), which focus mainly on the presentation of scientific and technological innovations, are designed to be presented in the oral sessions of the XXI International Mineral Processing Congress.

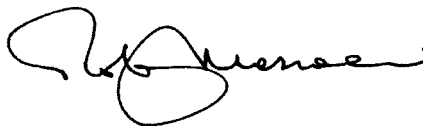
The works collected in the last volume (C), which are focused mainly on the presentation of new advanced applications, are designed for presentation in the posters sessions of the same Congress.

All of the people involved in the editing process need to be thanked: the authors, the reviewers, the members of the scientific and editorial committee, and the members of the production staff, with special thanks to the scientific secretary, who assured continuous contact between authors and editor.

To all people, incoming in Rome attending the XXI IMPC: *felici faustoque ingressui*.

Rome, March 20th 2000

Paolo Massacci  
Chairman of the XXI IMPC Organizing  
Scientific and Editorial committee



#### **PATRONAGE**

The XXI International Mineral Processing Congress takes place under the high patronage of the President of the Italian Republic and under the patronage of the Minister for University, Technical and Scientific Research.

#### **SPONSORSHIP**

The XXI International Mineral Processing Congress is held on invitation of: Università di Roma "La Sapienza", Consiglio Nazionale delle Ricerche (National Research Center), Ordine degli Ingegneri di Roma (Italian Engineering Association), Provincia di Roma, Comune di Catanzaro and Consorzio Interuniversitario Nazionale per l'Ingegneria delle Georisorse (Italian Interuniversity Society for Georesources Engineering among the Universities of Bologna, Cagliari, Roma "La Sapienza" and Trieste).

#### **MEMORIAL**

While the activities for preparation of the XXI IMPC were in progress, Prof. Gianfranco Ferrara, an authoritative exponent of the International Steering Committee and the National Organizing Committee of the Congress, passed away. His suggestions remain with us as a precious guide for completion of this edition.

# **XXI INTERNATIONAL MINERAL PROCESSING CONGRESS**

## **STRUCTURE OF THE PROCEEDINGS**

### **Volume A - Oral Sessions**

1. Mineral and Material Characterization
2. Mineral Liberation
3. Process Simulation and Control
4. Comminution, Classification and Agglomeration
5. Fine Particle Processing
6. Hydro and Biohydrometallurgy
7. Physical Separation Processing

### **Volume B - Oral Sessions**

- 8a. Flotation - Kinetics and Modelling
- 8b. Flotation - Surface Chemistry and Reagents
9. Plant and Process Design
10. Process of Complex Ores
11. Processing of Raw Materials for Glass and Ceramics
- 12a. Waste Treatment and Recycling
- 12b. Waste Treatment and Recycling (Effluent treatment)
13. Soil Remediation

### **Volume C - Poster Sessions**

1. Mineral and Material Characterization
2. Mineral Liberation
3. Process Simulation and Control
4. Comminution, Classification and Agglomeration
5. Fine Particle Processing
6. Hydro and Biohydrometallurgy
7. Physical Separation Processing
- 8a. Flotation - Kinetics and Modelling
- 8b. Flotation - Surface Chemistry and Reagents
9. Plant and Process Design
10. Process of Complex Ores
11. Processing of Raw Materials for Glass and Ceramics
- 12a. Waste Treatment and Recycling
- 12b. Waste Treatment and Recycling (Effluent Treatment)
13. Soil Remediation



**TABLE OF CONTENTS****A1 - Mineral and Material Characterization**

<b>The Mathematical Characterization of Raw Materials - A Basis to Design Machines</b> G. Unland	A1-1
<b>Lithological Composition and Ore Grindability Sensors, based on Image Analysis</b> A. Casali, G. Vallebuona, C. Pérez, G. D. González, R. Vargas	A1-9
<b>Automated Characterisation of Non-Stoichiometric Minerals</b> D. Sutherland, P. Gottlieb, A. Butcher, E. Ho Tun	A1-17
<b>Color Classification of Kaolin Typologies by Neural Networks</b> A.B. Valim, C.O. Petter, R. Gliese, S. Sabedot	A1-24
<b>On-Line Xrd Analysers for Slurry Samples. Problems and Solutions</b> J. Nikolov, I. Madsen	A1-30
<b>Martian Soil and Human Exploration</b> T.P. Meloy, M.C. Williams	A1-37
<b>Beneficiation and Mechanical-Chemical Alterations of Natural Zeolites</b> T.S. Yusupov, H. Heegn, L.G. Shumskaya	A1-44
<b>Selective Data Mining for Material Selection</b> D. Pace, G. Bonifazi, F. La Marca, P. Massacci	A1-52
<b>Substantiation of Classification of Coals by Use of their Structural-Chemical Parameters</b> A.M. Gyulmaliev, I.V. Eremin	A1-64

**A2 - Mineral Liberation**

<b>Stereological Correction of Mineral Liberation Grade Distributions</b> S. J. Spencer, D. N. Sutherland	A2-1
<b>Liberation Model Considering Preferential Breakage at Mineral Boundaries</b> S. Owada, T. Naraki, K. Takeda	A2-9
<b>Mineral Liberation Analysis - A Review of Some Recent Developments</b> R.P. King, C.L. Schneider	A2-16
<b>Liberation of a Particle-Composite Material</b> J. Tomas, M. Schreier	A2-24
<b>Liberation of Valuable Inclusions in Ores and Slags by Electrical Pulses</b> U. Andres, I. Timoshkin, J. Jirestig, H. Stallknecht	A2-36

**A3 – Process Simulation and Control**

<b>Scale-up of Tower Mill Performance Using Modeling and Simulation</b> A. Jankovic, S. Morrell	A3-1
--	------

<b>Column Flotation of Low Cassiterite Contained Slimes: Modeling and Scale-up Using Pilot Plant Data</b>	
L.O. Filippov	A3-8
<b>Micro-Scale Physical Model to Account for Energy Spectrum Distribution in the Ball Mill for Sophisticated Performance Prediction</b>	
T. Inoue, K. Okaya	A3-16
<b>Flotation Process Control on a Pgm Flotation Circuit</b>	
A. Singh, J. Schubert	A3-24
<b>Gain Scheduling Control of a Cement Grinding Circuit Based on its Fuzzy Model</b>	
S. Matsuo, Y. Okano	A3-32
<b>“Data Mining” for Mining Data</b>	
H. Hyötyniemi, V. Hasu, J. Hätönen, R. Ylinen	A3-39
<b>Identification of the Distributed Efficiency of a Particle Separation System</b>	
G.D. Schena, R.J. Gochin	A3-46
<b>Experimental Research of Industrial Flotation Machines Process Dynamics</b>	
K. Kalinowski, R. Kaula	A3-54
<b>An Algorithm for Fault Detection and Isolation Using Mass Balance Constraints</b>	
D. Hodouin, A. Berton	A3-59
<b>Dynamic Flowsheet Simulation: a New Tool for Mine Through Mill Optimization</b>	
J.A. Herbst, W.T. Pate	A3-66
<b>The Locus of Flotation Performance</b>	
M.A. Vera, J-P. Franzidis, E.V. Manlapig	A3-74
<b>Mineral Processing Process Optimization and Collaboration at the Industrial Desktop</b>	
O.A. Bascur, J.P. Kennedy	A3-83
<b>Establishing the Neural Network Models for Grinding Systems</b>	
Y. Mao, B. Chen, J. Gao, Y. Liu	A3-92
<b>Fine Grinding by High Pressure Roll Mill</b>	
A. Bertagnolli, D. Romano, R. Levi	A3-100
<b>Simulation of Biotreatments in Complex Mineral Processes</b>	
S. Brochot, P. Cézac, M.V. Durance, G. Fourniguet, J.C. Guillaneau, D. Morin, J. Villeneuve	A3-108
<b>Identification and Multivariable Nonlinear Predictive Control of a Pilot Flotation Column</b>	
M. Milot, A. Desbiens, R. del Villar, D. Hodouin	A3-120
 <b>A4 – Comminution, Classification and Agglomeration</b>	
<b>Dry Vibration Milling of Blast-Furnace Slag Cement – Parameter Study</b>	
Y.M. Wang, K.S.E. Forsberg	A4-1
<b>Monitoring of Sag Mill Performance Using Acoustic Emissions</b>	
S.J. Spencer, J.J. Campbell, K.R. Weller, Y. Liu	A4-13

<b>Influences of Operating Parameters and Shape Factor of Particles on Performances of a Dynamic Air Classifier</b> G. Baudet, M. Bizi, A. Chahdi, H. Gaboriau, A. Seron	<b>A4-21</b>
<b>Improving the Air Classification Process by Optimal Operating Parameters</b> J. Kolacz	<b>A4-31</b>
<b>Investigations on Abrasive Particle Stress in Spouted Beds and Agitation Cells</b> H.Z. Kuyumcu, L. Rolf	<b>A4-38</b>
<b>Vibration Grinding of Copper and Aluminum Metal by-Products</b> L. Kuzev, S. Seksenov	<b>A4-44</b>
<b>Mechanical Induced Changes in Structure and Properties of Solids</b> H. Heegn	<b>A4-52</b>
<b>Mixture Grinding in the High-Pressure Roll Mill</b> A.-Z.M. Abouzeid, D.W. Fuerstenau	<b>A4-60</b>
<b>Advances in the Theory and Practice of Hydrocyclone Technique</b> T. Neesse, F. Donhauser	<b>A4-69</b>
<b>Vortex Flow in Flat-Bottomed Hydrocyclones: Leading Order Steady Solution</b> J. Collantes, F. Concha	<b>A4-77</b>
<b>Agglomeration Methods in Particle Engineering</b> W. Pietsch	<b>A4-87</b>
<b>Pressure and Shear on the Roller Surfaces of High Pressure Roller Mills</b> U. Sander, K. Schönert	<b>A4-97</b>
<b>Effect of Grinding Methods on Flotation of Sulphide Ores</b> R. Kalapudas, J. Leppinen, K. Heiskanen, P. Koivistoinen	<b>A4-104</b>
<b>Advances in the Theory and Practice of Novel Comminution Technology</b> Y. C. Lo	<b>A4-112</b>
<b>Iron Ore Pellet Binding Mechanisms Pozzolanic vs. Physical Binders</b> S.J. Ripke, S.K. Kawatra	<b>A4-120</b>
<b>Mathematical Models of the Behavior of Malleable Metals in Tumbling Mills</b> M. Noaparast, A.R. Laplante	<b>A4-128</b>
<b>Experimental Investigation of Compacting in Roll Presses with Gravity and Screw Feed</b> B. Csöke, I. Tarján, J. Faitli	<b>A4-132</b>
 <b>A5 – Fine Particle Processing</b>	
<b>A New Concept for the Process Design of Flocculation Processes</b> M. Nagel, P. Ay	<b>A5-1</b>
<b>Characterization and Investigation on the Sorption Behavior of Steelmaking Flue Dust</b> L.-M. Wu, Z.-X. Sun, W. Forsling	<b>A5-8</b>
<b>Enhancing Top-Size Control in Ultra Fine Grinding</b> M. Agus, G. Alfano, P. Saba, M. Surracco	<b>A5-16</b>

<b>Development of a New Method of Waste Water Treatment by Hetero-Flocculation with Fluorite</b> S. Mori, T. Furuyama	A5-23
<b>The Role of Coagulants and Flocculants in the Control of Compressional Dewatering of Mineral Slurries</b> K.E. Bremmell, R.G. de Kretser, P.J. Scales, D.V. Boger, T.W. Healy	A5-30
<b>Dispersion of Oil in Electrolyte Solutions</b> H. Polat, M. Polat, S. Chander	A5-37
<b>Preparation of Inorganically Modified Bentonites Suitable for Thickener and Thixotropic Agents</b> H.J. Koroğlu, S. Kocakuşak, K. Akçay, H. Yüzer, Ö.T. Savaşçı, Y. Bilge, R. Tolun	A5-45
<b>Drag Force on Spheres Settling in Gas-Fluidized Beds</b> L.B. Wei, J. Chen	A5-50
<b>Flocculation of Fine Calcite Particles with <i>Corynebacterium Xerosis</i></b> S.R. Haas, F.R. Nascimento, I.A.H. Schneider	A5-56
<b>Polymer Induced Flocculation /Dispersion of Colloidal Iron Oxide and Alumina Suspensions</b> P. Somasundaran, K. Das Kalyan, Pradip	A5-62
<b>Role of Hydrogen Bonding in Reagent Adsorption for Enhanced Separation Efficiency</b> M. Bjelopavlic, H. El-Shall, B.M. Moudgil	A5-69

## **A6 – Hydro and Biohydrometallurgy**

<b>Cyanide Recycling Using Ion Exchange Resins. Application to the Treatment of Gold-Copper Ores</b> V.A. Leão, R.S. Costa, V.S.T. Ciminelli	A6-1
<b>Recovery of Silver and Barite from Silver Plant Tailings and their Economical Evaluation</b> H. Dinçer, G. Önal	A6-9
<b>Manganese and Zinc Removal from Cobalt Sulfate Solutions by Means of Solvent Extraction</b> K. Kongolo, D.M. Mwema, P.M. Kyony, K. Mfumu	A6-14
<b>Cobalt-Magnesium Separation by Solvent Extraction with Bis(2,4,4-Trimethylpentyl) Monothiophosphinic Acid</b> S.L. Agatzini, P.E. Tsakiridis	A6-22
<b>Leaching of Precious Metals from Secondary Sources Using Halogen Salts</b> K.N. Han	A6-33
<b>Zinc Powder Cementation of Gold from Ammoniacal Thiosulphate Solutions</b> R. Ravaglia, O. Barbosa-Filho	A6-41
<b>The Use of Jet Reactor Technology in the Extraction of Valuable Minerals</b> L. Lorenzen	A6-48
<b>Thiocyanate Technology for Processing Silver-Bearing Ores and Concentrates</b> S.B. Leonov, V.V. Elshin, Y.E. Golodkov	A6-56

<b>A Novel Process for Radioactive Impurity Removal from Zircon Sands</b> H. Aral	A6-60
<b>Direct Acid Leaching of Pyrolusite Ore</b> I.A. Ibrahim, E.A. Abdel-Aal, A.A. Ismail, A.K. Ismail	A6-67
<b>Thiosulfate Leaching of Gold from a Mechanochemically Pretreated Complex Sulfide Concentrate</b> P. Baláz, J. Ficeriová, E. Boldižárová, M. Háber, S. Jeleň, R. Kammel	A6-74
<b>Polygermanates and Their Role in the Obtaining GeO<sub>2</sub> from Zinc Concentrates</b> A. de la Cuadra, A. Hernández, F.J. Alguacil	A6-82
<b>Electrowinning of Gold from Cyanide Solutions</b> G. Cifuentes, C. Vargas, J. Simpson, R. Esteban	A6-87
<b>Supported Liquid Membranes in Metals Recovery and Concentration</b> R. Molinari, M.G. Buonomenna, E. Drioli	A6-95
<b>The Use of Silver-Bearing Concentrates in Bacterial Leaching of Chalcopyrite-Containing Ore Material</b> J. Wang, Y. Hu, D. Wang, G. Qiu, K. Zhong	A6-103
<b>A Comparison of Pyrite Oxidation Capability of Three Major Groups of Acidophilic Iron Oxidizing Bacteria</b> S.A. Bagheri, M. Oliazadeh, M. Tabatabae, A.R. Shahverdi	A6-110

## **A7 – Physical Separation Processing**

<b>Evaluation of the Effectiveness of Separation Processes According to the Obtained Feed-Segregation Rate</b> K.S. Sztaba	A7-1
<b>Packed Column Jig Sets New Standards in Iron Ore Concentration</b> D.C. Yang, P. Bozzato, G. Ferrara	A7-8
<b>Correlation between the Electrical Properties of Quartz, Feldspar and Wollastonite Minerals and their Tribo-Electric Separation Potential</b> H.R. Manouchehri, K. Hanumantha Rao, K.S.E. Forssberg	A7-17
<b>Advances in Cryomagnetic Separation Process: Industrial Minerals and Waste Effluent</b> G. Gillet, F. Diot, M. Lenoir	A7-27
<b>Prediction of the Performance of Low-Intensity Wet-Magnetic Separators in the Processing of Partly Altered Magnetite Ores</b> H.J. Steiner, A. Boehm	A7-35
<b>A New Electrostatic Separator for Fine Particles</b> R. Ciccu, M. Ghiani, R. Peretti, A. Serci, A. Zucca	A7-42
<b>Possibility of Howlite and Colemanite Concentration by Multi-stage D.M.S. Processes</b> M. Ignjatovic, R. Maric, N. Magdalinovic, M. Trumic, R. Ignjatovic	A7-52
<b>Layer Model of Stratification during Screening</b> M. Soldinger	A7-59
<b>In-Plant Testing of the Hydrofloat Separator</b> M. Mankosa, R. Merwin, J. Kohmuench, G. Luttrell	A7-69

<b>Hi Filters to Superconducting HGMS: The New Generation</b>	
A. Stadtmuller, S. Fawell	A7-78
<b>Novel Tubular Electrostatic Separators</b>	
A.I. Mesenyashin	A7-89
<b>Influence of Particle Shape on Dynamic DMS Processes</b>	
G. Ferrara, P. Bevilacqua, L. De Lorenzi, M. Zanin	A7-95
<b>High Temperature Superconductors for Magnetic Separation</b>	
J.H.P. Watson, L. Bolt	A7-105
<b>Theoretical Aspects of Fine Particles Separation</b>	
A.V. Bogdanovich, A.M. Bazilevsky, V.V. Yermakov, V.S. Pugachev, A.P. Samosy, V.V. Moshninov	A7-115
<b>Study on Producing Low Ash Coal with Triboelectrostatic Separator</b>	
X.X. Zhang, C.H. Duan, J.C. Qian	A7-121
<b>B8a – Flotation – Kinetics and Modelling</b>	
<b>The Role of Surface Forces in Flotation Kinetics</b>	
R.-H. Yoon	B8a-1
<b>Effect of the Suspension State on the Entrainment in Flotation Machines</b>	
E.A. Guerra, H. Schubert	B8a-8
<b>The Use of an Ejector-Aerated Baffled Column for Finely Disseminated Sulfide Ore Flotation</b>	
V.S. Babineti, P. Ilie, G.M. Filip, S. Krausz	B8a-16
<b>Factors Affecting the Flotation of Free Gold in the Presence of Refractory Gold</b>	
J.S.J. Van Deventer A.J. Teague, C. Swaminathan	B8a-24
<b>Modeling the Influence of the Froth Phase on Recovery in Batch and Continuous Flotation Cells</b>	
Z.T. Mathe, M.C. Harris, C.T. O'Connor	B8a-33
<b>Contact Angle and Thin Film Studies on the Cationic Collector/Silica Flotation System</b>	
R.J. Pugh, L. Alexandrova, F. Tiberg, L. Grigorov	B8a-40
<b>Selective Flotation of Enargite and Chalcopyrite</b>	
W.T. Yen, J. Tajadod	B8a-49
<b>New Investigations on the Rupture Process of Thin Liquid Films at the Particle-Bubble Adhesion</b>	
H.J. Schulze, K.W. Stöckelhuber, J. Mahnke	B8a-56
<b>Hydrodynamics of Conventional Flotation Cells with External Air Blow and its Effect on Metallurgical Results</b>	
G.N. Anastassakis	B8a-64
<b>Optimization of Collector, Slime Modifier and Frother Usage in Potash Ore Flotation</b>	
J.S. Laskowski, X.-M. Yuan, E.A. Alonso	B8a-71
<b>Particle-Bubble-Water Contact Angle Based on Flotation in a Hallimond Tube</b>	
J. Drzymala, V. Vigdergauz	B8a-79

<b>Boltzman's Model of Flotation Kinetics</b> P. Lazić, N. Čalić	<b>B8a-87</b>
<b>Bioflotation of Sulfide Minerals in the Presence of Heterotrophic and Chemolithotrophic Bacteria</b> P.K. Sharma, K. Hanumantha Rao, K.A. Natarajan, K.S.E. Forsberg	<b>B8a-94</b>
<b>Non-Equilibrium Thermodynamics in the Oxidation and Flotation of Sulfides</b> V. Avdokhin, V. Morozov	<b>B8a-104</b>
<b>Removal of Deleterious Elements from Copper Sulfide Concentrate</b> J.A. Mielczarski, J. Cases, E. Mielczarski, P. Marion, P. de Donato, M. Kongolo, O. Barres, E. Bouquet, M. Fordham, C. Valente	<b>B8a-111</b>
<b>Regularities of Hydrophobisation and Flotation of Salt-Like Minerals</b> A.A. Abramov	<b>B8a-120</b>
<b>Deep Mechanical Flotation Machines with Axial Impellers and Flotation Columns with Jet Aerators</b> N.F. Mescheriakov, R.H. Sabirov, N.I. Rets	<b>B8a-131</b>
<b>Reduction of Graphite in Lead Concentrate During Flotation of a Complex Lead-Zinc Ore from Rajpura - Dariba, India</b> K. Das Kalyan, T.K. Rao, Pradip, V. Rangarajan, N.K. Sharma, R.K. Gaur, V.P. Kohad	<b>B8a-138</b>
<b>Flotation in a Pulsating Medium</b> G. Krasnov, A. Lavrinenko, D. Krapivny, O. Frolov	<b>B8a-146</b>
<b>Effect of High-Intensity (Pre)Conditioning of Pulp on the Flotation of Sulphide Ores</b> C. Aldrich, D. Feng	<b>B8a-152</b>
<b>The Use of an Image Processing Based Sensor for On-Line Analysis of Flotation Performance</b> B.A. Wright, C.G. Sweet, J.J. Francis, G. de Jager, D.J. Bradshaw, J.J. Cilliers	<b>B8a-158</b>
<b>Processing of Iron Ore by Reverse Column Flotation</b> E.C. Dowling, J. Hebbard, T.C. Eisele, S.K. Kawatra	<b>B8a-163</b>
<b>Comparative Studies of the Surface Acid-Base Properties of Pyrites from Coal and Ore Sources</b> A.M. Raichur, X.H. Wang, B.K. Parekh	<b>B8a-171</b>
<b>3d Froth Modeling by Image Analysis</b> G. Bonifazi, P. Massacci, A. Meloni	<b>B8a-178</b>
<b>Column Flotation Improves Metallurgical Results in Non-Ferrous Ore Concentration and Matte Separation</b> I.I. Maksimov, M.F. Yemelyanov, T.Y. Koltunova, I.S. Satayev	<b>B8a-190</b>

## **B8b – Flotation – Surface Chemistry and Reagents**

<b>The Synergistic Interactions of Mixtures of Thiol Collectors in the Flotation of Sulphide Minerals</b> C. Helbig, D.J. Bradshaw, P.J. Harris, C.T. O'Connor, H. Baldauf	<b>B8b-1</b>
<b>Surface Properties of Diamonds in Kimberlites Processing</b> V. Chanturiya, V. Zuev, E. Trofimova, Y. Dikov, V. Bogachev, G. Dvoichenkova	<b>B8b-9</b>

<b>Copper Selective Collectors in the Separation of Sulfide Minerals</b> D. Fornasiero, W.Z. Shen, J. Ralston	<b>B8b-17</b>
<b>The Effect of Polymeric Depressants and Inorganic Dispersants on the Surface Characteristics of Talc</b> M.A. Dalvie, P.J Harris, D.J. Bradshaw	<b>B8b-25</b>
<b>Landfill Leachate as a Frother and Collector in Froth Flotation</b> S.T. Hall	<b>B8b-33</b>
<b>Effect of Ca<sup>2+</sup> and S<sub>2</sub>O<sub>3</sub><sup>2-</sup> on the Flotation of Pentlandite in Real Ore System</b> N. Schreithofer, V. Kirjavainen, K. Heiskanen, R. Ahveninen	<b>B8b-40</b>
<b>Surface Properties and Floatability of Enargite</b> S.H. Castro, S. Honores	<b>B8b-47</b>
<b>Spin-Marked Reagents in Flotation</b> P. Solozhenkin, V. Nebera, V. Larin	<b>B8b-54</b>
<b>Mineral/Solution Equilibria and the Flotation Chemistry of Magnesite with Oleate Collector</b> D.W. Fuerstenau, A. Lopez-Valdivieso, S. Kmet	<b>B8b-62</b>
<b>Liquid-Liquid Extraction of Fine Oxide Particles Using Chelating Reagent as Collector</b> E. Kusaka, K. Maegawa, Y. Fukunaka, R. Ishii	<b>B8b-70</b>
<b>Semiconductor Energy-Band Theory of Sodium Humate Interacting with Sulphide Minerals and its Application in Flotation Separation</b> Q. Feng, J. Chen, Y. Lu	<b>B8b-78</b>
<b>Effect of Calcium on Sphalerite Activation with Copper</b> C. Sui, D. Lascelles, J.A. Finch	<b>B8b-87</b>
<b>The Effect of Pulp Potential Control on the Metallurgical Performance of a Lead/Copper Bulk Flotation Stage</b> A. Uribe-Salas, F. Nava-Alonso, E. Martínez-Cavazos, R. Pérez-Garibay	<b>B8b-96</b>
<b>Technology for Copper-Zinc Flotation by Electro Chemical Treatment</b> V. Panayatov, K. Kovachev, G. Önal, Z. Doğan, H. Dinçer, G. Bulut, M. Panayotova, V. Ninova	<b>B8b-103</b>
<b>Floatability of Zircon with Sodium Oleate</b> R.A. Muratoğlu, Ç. Hoşten, Y. Topkaya, M. Akser	<b>B8b-109</b>
<b>Mineral Separation in the Processing of Complex Nickel-Copper Ores Using Chelating Agents</b> S. Kelebek, C. Tukul	<b>B8b-116</b>
<b>Enhancing Flotation Recovery of Phosphate Ore by Nonionic Surfactant</b> H. Sis, S. Chander	<b>B8b-124</b>
<b>Adsorption of the Thiol Compound on Gold and Pyrite and its Influence on Their Selective Flotation</b> M.B.M. Monte, F.F. Lins, J.F. Oliveira	<b>B8b-131</b>
<b>On the Fundamentals of the Surface Chemistry of Cadmium Ion Flotation</b> I.B. Scorzelli, A.L. Fragomeni, M.L. Torem	<b>B8b-138</b>
<b>Investigations Into the Surface Chemistry of Some Sulfide Minerals Using a Natural Polysaccharide</b> R.K. Rath, S. Subramanian	<b>B8b-144</b>



<b>Selective Flotation of Chalcopyrite and Pyrite and the Effect of Ore Type</b> Q. Broadbent, D. Yan, R. Dunne	<b>B8b-152</b>
<b>Polyoxyethylene Nonionic Surfactants as Collectors in the Flotation of Quartz and Feldspar: Effects Induced by the Addition of Cationic Surfactant</b> M.S. EL Salmawy, E. Kusaka, T. Wakamatsu	<b>B8b-160</b>
<b>Electrochemical and Electrokinetic Properties of Carrollite and Chalcopyrite and their Flotation Behaviour</b> L.K. Witika	<b>B8b-168</b>
<b>Study on the Effect of Collector Type and Collector Mixing in Coal Flotation</b> A.M. Saleh, A.M. Ramadan, M.R. Moharam	<b>B8b-177</b>

## **B9 – Plant and Process Design**

<b>Flowsheet Optimization Using Simulation: A Gravity Concentrator Using Reichert Cones</b> R.P. King	<b>B9-1</b>
<b>Application of Multifeed Circuits for Coal and Molybdenite Flotation</b> D.W. Fuerstenau, M.C. Williams, W. Hu	<b>B9-10</b>
<b>Industrial Practice of Phosphate Ore Flotation at Serrana-Araxá, Brazil</b> R.C. Guimaraes, A.E. C. Peres	<b>B9-17</b>
<b>Re-Engineering of the Uranium Ore Flowsheet</b> F. Aurelian, D.P. Georgescu, L. Andrei, N. Udrea	<b>B9-24</b>
<b>Treatment of Gold Tailings with the 3PC-Column Flotation</b> L. Valderrama, J. J. Da Rosa, M. Santander, J. Rubio	<b>B9-30</b>

## **B10 – Process of Complex Ores**

<b>Removal of Magnesium from Phosphates and Phosphoric Acid</b> P. Blazy, E.A. Jdid	<b>B10-1</b>
<b>An Equation of State for Trona Solutions</b> H. Haynes Jr., P. De Filippis	<b>B10-9</b>
<b>The Role of O<sub>2</sub>, N<sub>2</sub> and Their Mixture at Different Proportions of N<sub>2</sub> on the Formation of Sodium Chromate</b> M.E.H. Shalabi, N.A. El-Hussiny, F.Z Shebel, S. El-Affifi	<b>B10-16</b>
<b>Comprehensive Processing of Copper-Sulfide Ores Resulting in the Production of Rare Metal Concentrates</b> Z. Abisheva, A. Zagorodnyaya, T. Bukurov, B. Beisembaev, E. Bochevskaya, M. Abaidildinov	<b>B10-22</b>
<b>Processing of Oxidized Zinc-Lead Bearing Raw Materials</b> V. Lukanov, M. Bitimbaev	<b>B10-30</b>

## **B11 – Processing of Raw Materials for Glass and Ceramics**

<b>Development of Iron Removal Process Design for High Purity Silica Sands Production by Oxalic Acid Leaching</b> F. Veglio, C. Abbruzzese, B. Passariello, F. Ullu, L. Toro	<b>B11-1</b>
---	--------------

**The Benefits of Blast Furnace Slag for Glass Production**

M.F. Eskibalci, B. Ipekoğlu

**B11-9**

**B12a – Waste Treatment and Recycling**

**Various Kinds of Plastics and Paper Separation Using Electrostatic Separation and the Combination of Sink-Float Separation and Flotation for Recycling**

T. Fujita, N. Haruki, G. Dodbiba, P. Jing, T. Miyazaki, E. Kuzuno

**B12a-1**

**Mechanical Processing of Low Grade Printed Circuit Boards**

J.A. van Houwelingen, C. Le Guern

**B12a-9**

**Environmental Protection from Mineral Wastes**

S. Hoffman

**B12a-18**

**Transfer of Mineral Process Models to Waste Treatment**

K.L. Sandvik, J. Villeneuve, M.V. Durance, H. Védrine

**B12a-26**

**Instruments for Improving the Material Flow of Aluminum Alloy Recycling**

H. Hoberg, J. Meier-Kortwig, S. Wolf

**B12a-35**

**Utilization of Fly Ash in Mineral Wool Production**

I. Simovic, Z. Micevic, S. Djekic

**B12a-43**

**Flotation of Plastics Using Combined Treatments**

N. Fraunholz, S.J.M. Kooijman, W.L. Dalmijn

**B12a-49**

**Plastic Waste Grinding**

F. Ciancabilla, A. Bonoli

**B12a-56**

**Recycling of Rare Earth Luminophores Originating from Discharge Lamps**

E. Gock, B. Schimroszyk, J. Kähler, U. Waldek

**B12a-63**

**B12b – Waste Treatment and Recycling (Effluent Treatment)**

**Decontamination of Cadmium from Industrial Liquid Waste by Coconut Fiber**

A. Espinola, R. Adamian, L.M.B. Gomes

**B12b-1**

**Production of H<sub>2</sub>S By Sulfate-Reducing Bacteria in a Two-Column Gas/Liquid Reactor for the Purification of Metal-Containing Effluents**

F. Battaglia-Brunet, S. Foucher, I. Ignatiadis, D. Morin

**B12b-9**

**Water Treatment of Manganese-Rich Mine Drainage by Manganese-Oxidizing Bacteria at Neutral Ph**

K. Sasaki, K. Kurosawa, H. Konno

**B12b-18**

**Bioprocessing of Actinoids by Using Microorganisms**

T. Sakaguchi

**B12b-25**

**The Treatment of Acid Mine Drainage through the Precipitation of Ettringite**

F.W. Petersen

**B12b-33**

**B13 – Soil Remediation**

**Complexing Agent Using both Chemical and Electrochemical Processes for the Removal of Heavy Metals from a Contaminated Soil**

A. Djordem, D.E. Akretche, H. Kerdjoudj

**B13-1**

<b>Novel and Efficient Technology for Contaminated Soil Cleanup</b> K. Szymocha, W. Pawlak, J. Kramer	<b>B13-9</b>
<b>Distributions of Contaminants in Electrokinetic Processing of Fine-Grained Soils</b> M. Niinae, T. Aoe, W. Kishi, T. Sugano, K. Aoki	<b>B13-17</b>
<b>Remediation of Contaminated Sandy Soil Fractions Using High-Performance Attrition</b> B. Schricker, H. Tiefel, T. Neesse	<b>B13-24</b>
<b>Removal of Oil Contaminants from Soil by Flotation</b> M. Niewiadomski, J. Nalaskowski, J. Hupka, J.D. Miller	<b>B13-31</b>
<b>Chemical Processes for Radioactive Waste Treatment</b> T. Dovbysheva	<b>B13-38</b>

### **C1 – Mineral and Material Characterization**

<b>Characterization of Particles by Means of Laser Light Diffraction and dynamic Light Scattering</b> U. Foerter-Barth, U. Teipel	<b>C1-1</b>
<b>Industrial Treatment of Raw Agate: Spectrocolorimetry and Scanning Electron Microscopy (Sem) Analyses</b> L.C.B. Tubino, C.H. Sampaio	<b>C1-8</b>
<b>Back-Scattered Electron Imaging of a Lateritic Iron Ore and its Applications in Process Mineralogy</b> A. Alcover Neto, R. Neumann, C.L.Schneider	<b>C1-17</b>
<b>Chemical Reactivity of Different Phosphate Minerals for Direct Application as Fertilizers</b> S.I. Mostafa, T.A. Bibawi, A. A. Yehia, I.A. Ibrahim	<b>C1-25</b>

### **C2 - Mineral Liberation**

<b>Poor Manganese Ore Dressing on the Basis of Mineralogical-Technological Studies</b> E.L. Chanturiya, T.V. Bashlykova, N.I. Potkonen, A.R. Makavetskas	<b>C2-1</b>
<b>Prospective of Electric Impulse Processes for the Study of the Structure and Processing of Mineral Raw Materials</b> A. Usov, V.Tsukerman	<b>C2-8</b>

### **C3 – Process simulation and Control**

<b>Pulp-Froth Interface Control in the Flotation Column</b> A.C. Maffei, I.L. de Oliveira Luz	<b>C3-1</b>
<b>Acoustic Emissions from the Impact of Particles and their Application to On-Line Monitoring for Zirconia Micro-Agglomerate Production in Liquids</b> T. Hirajima, M. Tsunekawa	<b>C3-8</b>
<b>Strategies for Fuzzy Control of a Water/Air Column</b> M.T. Carvalho, F. Durão	<b>C3-17</b>

<b>Improving Controllability on Flotation Columns</b> L.G. Bergh, J.B. Yianatos	C3-24
<b>Cost Cutting in Optimizing a Flotation Unit by Use of Statistical Methods</b> H.-C. Haarmann, R. Janitschek, E. Beeker	C3-32
<b>Validation of the Discrete Element Method (DEM) by Comparing Predicted Load Behaviour of a Grinding Mill with Measured Data</b> M.H. Moys, M.A. van Nierop, J.C. van Tonder, G. Glover	C3-39
<b>Design and Implementation of an On-Line Optimizing Control System for Processing the Sadiola Hill Oxidised Gold Ore</b> T. Mulpeter, O. Guyot	C3-45
<b>On-Line Prediction of Transient Phenomena in the Slag Phase during Ilmenite Smelting</b> J.J. Eksteen, M.A. Reuter	C3-55
<b>The Uniform Description of Mineral Processes by Methods of Compound Distributions of Material Features</b> T. Tumidajski	C3-65
<b>Arma Type Model for Copper Ore Flotation</b> K. Trybalski, J. Cieply	C3-72
 <b>C4 – Comminution, Classification and Agglomeration</b>	
<b>Operational Work Index for Grinding Plants</b> G.D. González, C. Pérez, A. Casali, G. Vallebuona, R. Vargas	C4-1
<b>Magotteaux Automatic Ball Charger (Abc)</b> W. Conger, P. Amelynck	C4-8
<b>Breakage Parameters of Chromite and Simulation of the Product-Size Distributions</b> M.Yekeler, U. Ulusoy, I. Akbaba	C4-16
<b>Run-of-Mine Milling Pilot Plant Test Work</b> B. Clermont	C4-22
<b>The Effect of Viscosity on Small-Diameter Hydrocyclones' Performance in Desliming Process</b> M.V. Possa, J.R.B. Lima	C4-29
<b>Drum Granulation of Mineral Raw Materials with Different Particle Size Distributions</b> T. Gluba, A. Obraniak	C4-36
<b>Studies on Comminution Mechanism of the Dry Tower Mill Kd-3</b> A. Shibayama, S. Mori, A. Bissombolo	C4-44
<b>Improvement in Classification Performance of Turbo Classifiers by Reducing the Inertia Counter-Rotating Vortices</b> J. Liu, B. Chen, D. Xu	C4-53
<b>Optimized Production Scale Classifier for Finest Cuts at High Capacities</b> M. Adam, S. Zampini	C4-58
<b>The Influence of Comminution Method to Particle Shape</b> M. Oja, R. Tuunila	C4-64

<b>Maxmill - a Field Report about the Application of a Stirred Ball Mill with Increased Economic Efficiency for Grinding of Minerals</b> J. Sachweh	C4-72
<b>The Kelsey Fine Autogenous Grinding (Fag) Mill</b> B. Kelly, D. Geraghty	C4-80
<b>The Effect of Using Concave Surfaces as Grinding Media</b> F.L. von Krüger, J.D. Donda, M.A.R. Drummond, A.E.C. Peres	C4-86
<b>Studies in Fine Grinding in an Attritor Mill</b> P. Raghuraman, R. Rajiv Raman, B. Pitchumani	C4-94
<b>Role of Particle Microstructure in Comminution</b> L.M. Tavares	C4-99

### **C5 – Fine Particle Processing**

<b>Formation of Fine Particles with Compressed Gases</b> U. Teipel, U. Foerter-Barth	C5-1
<b>Dewatering of Fine Granular Materials by Vibrating Screens with Superposed Capillary Suction</b> A. Ettmayr, W. Stahl, K. Keller, G. Sauer	C5-8
<b>Production of Rheological Additives for Solvent Based Paint from Turkish Bentonite</b> K. Cinku, B. Ipekoglu, Y. Bilge	C5-16
<b>Flocculation and Adsorption-Desorption Mechanism of Polymers on Albite</b> I. Kurşun, B. Ipekoğlu, M.S. Çelik, Y. Kaytaç	C5-24
<b>TheoRy and Applications of Hydrophobic Flocculation Technology</b> S. Song, S. Lu	C5-31

### **C6 – Hydro and Biohydrometallurgy**

<b>The Dissolution and Interactions of Gibbsite Particles in Alkaline Media</b> J. Addai-Mensah, J. Dawe, J. Ralston	C6-1
<b>Evaluation of an Hcl Process for Leaching of Low-Grade Highly Siliceous Bauxite Ore from Khushab, Pakistan</b> S.A. Hussain, R. Jamal	C6-8
<b>Application of Solvent Impregnated Resin to the Treatment of Heavier Rare Earth Residue</b> J. Shibata, S. Matsumoto, H. Yamamoto	C6-15
<b>Gold Extraction from Kaymaz Gold Ore by Thiourea Leaching</b> S. Örgül, Ü. Atalay	C6-22
<b>Synthesis of Aragonite by the Carbonation Process Using Stainless Refining Dust in Iron &amp; Steel Plants</b> J.H. Ahn, K.S. Choi, H. Kim, S.H. Yoon, J.S. Kim, G.W. Sung, K.H. Lee	C6-29
<b>Development of an Iron Removal Process from Kaolin by Thiourea Leaching: Kinetic and Related Statistical Analysis</b> F. Vegliò, F. Beolchini	C6-36

<b>Application of Thiobacillus Ferrooxidans by Bacterial Desulfurization of Coal</b> P. Fečko, V. Sedláčková	C6-43
<b>The Adsorption of Precious and Base Metals on Xad7 Ion Exchange Resin</b> E.R. Els, L. Lorenzen, C. Aldrich	C6-50
<b>The Influence of Precipitation Variables on the Aggregation and Crystalline Structure of Stabilized Zirconia Powders</b> A.P.A. Oliveira, M.L. Torem	C6-57
<b>Solvent Extraction of Cu (Ii) and Fe (Iii) using Lix 1104sm</b> P. Navarro, J. Simpson, F.J. Alguacil	C6-64
<b>A Comparison of Lix984® and Non-Conventional Reagents as Copper Extractants</b> J.B.A. Paulo, J.Y.P. Leite	C6-70
<b>Development and Application of Filblast Mass Transfer Technology in Hydrometallurgical Processing</b> B.J. Sceresini, G. Nguyen	C6-77
<b>Selective Separation of Yttrium from Chemical Concentrate of Rare Earth</b> E. Panturu, D.P. Georgescu, F. Aurelian, N. Udrea	C6-84

## **C7 – Physical Separation Processing**

<b>The Separation of Coarse Particles by a Moving Froth Bed</b> J.S.J. van Deventer, W.A. van Dyk, L. Lorenzen	C7-1
<b>A New Magnetic Separator and Classifier: Case Study</b> P.A. Augusto, J.P. Martins	C7-9
<b>Removal of Sulfur and Mineral Matter from Coal Slurry by a Pilot Scale Wet Magnetic Separator</b> H. Dinçer, G. Ateşok, M.Z. Doğan, Ş. Girgin, F. Boylu, Ö. Yüksel	C7-15
<b>Study of Separation of Refractory Sulfide Minerals by Hgms</b> Y. Zhang, S. Liu, W. Fu	C7-22
<b>Electrostatic Feldspar/Quartz Separation without Hydrofluoric Acid Reduces Pollution</b> S. Dorfner, H. Tröndle, U. Jakobs	C7-30
<b>Assessment of Multistage Turbulent Cross-Flow Aeroseparation of Building Rubble</b> J. Tomas, T. Gröger	C7-34
<b>Separation Technology Based on Segregation Effects in Fast Gravity Flows</b> V. Dolgunin, A. Ukolov, A. Romanov, A. Kudy, A. Klimov	C7-44
<b>Trapped Vortex Magnetic Separation (Tvms)</b> Z. Li, J.H.P. Watson	C7-50
<b>General Trends of Gravity Separation</b> M. Barsky, E. Barsky	C7-57

**C8a – Flotation – Kinetics and Modelling**

- An Investigation into the Enrichment of Phosphate Slime by Column Flotation**  
H. Ipek, H. Ozdag C8a-1
- An Investigation on the Effects of Ore Grade and Particle-Liberation Size in Gold Recovery by Coal-Oil-Gold Agglomerate Flotation**  
Y. Cilingir, S. Sen C8a-6
- Characterization of Rigid Spargers and Selection for Flotation Columns**  
C.O. Gomez, R. Escudero, J.A.Finch C8a-14
- An Interactive Dynamic Flotation Model Framework**  
O.A. Bascur C8a-21
- A Computational Fluid Dynamics (CFD) Model for a Bubble Separation Tank**  
P.R. Desam, A. Datta, J. D. Miller C8a-32
- Characterization of the Flotation Froth Structure and Color by Machine Vision (Chaco)**  
G. Bonifazi, V. Giancontieri, A. Meloni, S. Serranti, F. Volpe, R. Zuco, H. Koivo, J. Hätönen, H. Hyötyniemi, A. Niemi, P. Sipari, H. Kuopanporrti, R. Ylinen, I. Heikkila, S. Lahteenmaki, J. Miettunen, O. Stephasson, W. Wang, L.E. Carlsson C8a-39

**C8b – Flotation – Surfact Chemistry and Reagents**

- New Synthetic Polymeric Depressants for Sulfide and Non-Sulfide Minerals**  
D.R. Nagaraj C8b-1
- Valorisation of Molybdenite from Majdanpek Copper Concentrate**  
D. Salatic, V. Salatic C8b-9
- Characterisation of the Surfaces of Galena and Sphalerite in the Presence of Dithionite**  
C. Sui, J.A. Finch, J.E. Nasset, J. Kim, S. Lajoie C8b-15
- Collector Properties of New Flotation Reagent Z-96**  
Z.S. Markovic, R. Stanojlovic, G. Milenkovic, Z. Petkovic C8b-23
- Beneficiation of Fine Bituminous Coal by Column Flotation**  
B. Gürsu, C. Hiçyılmaz, S. Bilgen C8b-29
- Studies of Surface and Sorption Behaviour of Saline and Clay Carbonate Minerals in Electrolytes**  
S. Titkov, N. Panteleeva, A. Chistyakov, L. Pimkina, I. Mikhaylova C8b-36
- Activation of Xanthate Flotation of Pyrite by Ammonium Salts Following it's Depression by Lime**  
X. Xiaojun, Ş. Kelebek C8b-43
- Modified Hydroxamate Collectors for Kaolin Flotation**  
C. Basilio, R.A. Lowe, A. Gorken, L. Magliocco, R. Hagy C8b-51
- Monitoring the Distribution of Flotation Chemicals at an Industrial Mineral Processing Plant**  
M.S. Miettinen, P.M. Stén, J.O. Leppinen, H.J. Lehto C8b-56
- Azine Compounds Application in Separation of Polymetallic Sulfide Concentrates**  
T.I. Yushina, A.A. Abramov C8b-63

- On Certain Aspects Controlling Selectivity of Non-Sulfide Mineral Flotation**  
A.V. Kurkov, V.V. Shatalov, I.V. Pastukhova C8b-71
- Purification of Brazilian Kaolin Clay by Flotation**  
A.B. Luz, I. Yildirim, R-H. Yoon C8b-79
- Ways to Increase the Efficiency of Flotation Process for Complex Ores**  
V. Beloborodov, K. Fedotov C8b-84

### **C9 – Plant and Process Design**

- Technology for Separation of Non-Ferrous Metal Minerals with Similar Physical and Chemical Properties**  
A.V. Tarasov, V.A. Bocharov C9-1
- Physical Separation Processing of a Bulk Tin-Tungsten Pre-Concentrate Into its Individual Constituents for Commercial Applications**  
A.T. Sutaone, S.K. Ghosh, K.S. Raju C9-7
- Old Tailings Dumps of Concentrating Plants as a Source of Raw Minerals**  
V.M. Izoitko, Y.N. Shumskaya C9-13

### **C10 – Process of Complex Ores**

- Pre-Concentration of a Low-Grade Sulfidic Copper Ore from Murgul-Çakmakkaya Region of Turkey**  
A. Gül, G. Önal C10-1
- Processing of Valuable Vein-Minerals, as Molybdenite, Monazite, Magnetite, Pyrite and Ilmenite**  
M. Zlagnean, N. Tomus, C. Vasile, I. Vasile C10-5

### **C11 – Processing of Raw Materials for Glass and Ceramics**

- Carrier Flotation of Alunite from Kaolin Clay**  
S. Koca, H. Koca C11-1
- Multicolor Optical Sorting: a Large Scale Application in a Feldspar Treatment Plant in Sardinia - Italy**  
B. Anselmi, H. Harbeck C11-9
- Beneficiation of Low Grade Feldspar Ores for the Ceramics Industry**  
M. Agus, R. Angius, M. Ghiani, R. Peretti, A. Serci, A. Zucca C11-17
- Beneficiation of Sand from the Sava-River Bed**  
B. Salopek, G. Bedeković C11-26
- Controlled Processing of Raw Materials for Ceramic Paste Components**  
F. Durão, L. Cortez, T. Carvalho, C. Pires, A. Felicio, I. Rodrigues, R. Lourenço, C. Tareco, G. Brito C11-32
- Beneficiation Studies on A Spodumene Ore from Portugal**  
A. Botelho de Sousa, M.M. Amarante, M. Machado Leite C11-40



**C12a – Waste Treatment and Recycling****Comminution of Scrap and Metals in Shredders with Horizontally and Vertically Mounted Rotor**G. Timmel, S. Sander, G. Schubert C12a-1**Employment of Foundry Wastes**M.C. Zanetti, C. Clerici, D. Sandrin, M. Operto C12a-9**Production of Magnetite Powder and Recovery of Non-Ferrous Metals from Steel Making Residues**A. Delalio, Z. Bajger, P. Baláz, F. Castro C12a-15**Interactions Between the Toner Composites and Cellulose and Their Implication to Flotation Deinking**Y. Hu, D. Wang, J.D. Miller C12a-20**Beneficiation of Brass Ashes**S. Timur, S. Gürmen, G. Orhan, C. Arslan, I. Duman C12a-27**The Liberation of Impregnated Gold from Wood Chips**W. Martin, F.W. Petersen, A.B. Nesbitt C12a-34**Recycling of Industrial Waste Materials: Recovery of Aluminum from Leftover Bottle Cap-Liner Materials**S. Sano, M. Nikaidoh, K. Yanagawa, Y. Kanda C12a-40**Characterization and Recycling of Amalgam from Dental Clinics**J.Y. Pereira Leite, C. Pereira de Souza C12a-46**C12b – Waste Treatment and Recycling (Effluent Treatment)****New Technique for the Separation of Finely Dispersed Mercury from Philippine Small-Scale Gold Amalgamation Effluent**L.J.G. Lanticse, E.P. Clemente, H.D. Mendoza C12b-1**Treatment of Dye Bearing Effluents from Brazilian Agate Industry**E. Carissimi, T.M. Pizzolato, A. Zoch, C. Mistura, E.L. Machado, I.A.H. Schneider C12b-9**C13 – Soil Remediation****Microbial in Situ Treatment of Soils Contaminated with Radionuclides**S.N. Groudev, P.S. Georgiev, I.I. Spasova C13-1**Humic Acids from Coal as a Reagent to Soil Remediation**E.G. Gorlov., V.V. Rodae, O.G. Ryzhkov, D.M. Koledin C13-7

# **MINERAL AND MATERIAL CHARACTERIZATION**

This Page Intentionally Left Blank

<b>Characterization of Particles by Means of Laser Light Diffraction and dynamic Light Scattering</b> U. Foerter-Barth, U. Teipel	<b>C1-1</b>
<b>Industrial Treatment of Raw Agate: Spectrocolorimetry and Scanning Electron Microscopy (Sem) Analyses</b> L.C.B. Tubino, C.H. Sampaio	<b>C1-8</b>
<b>Back-Scattered Electron Imaging of a Lateritic Iron Ore and its Applications in Process Mineralogy</b> A. Alcover Neto, R. Neumann, C.L.Schneider	<b>C1-17</b>
<b>Chemical Reactivity of Different Phosphate Minerals for Direct Application as Fertilizers</b> S.I. Mostafa, T.A. Bibawi, A. A. Yehia, I.A. Ibrahim	<b>C1-25</b>

This Page Intentionally Left Blank

## CHARACTERIZATION OF PARTICLES BY MEANS OF LASER LIGHT DIFFRACTION AND DYNAMIC LIGHT SCATTERING

U. Foerter-Barth, U. Teipel

Fraunhofer Institut fuer Chemische Technologie (ICT)  
Pfinztal, Germany

### Abstract

The laser light diffraction uses the scattering of light, arising from the disturbance of the propagation of light waves due to their interaction with particles, to determine the particle size and the particle size distribution. Laser light diffraction analysis equipment is able to characterize particulate systems in the range from 0.5  $\mu\text{m}$  up to 3,500  $\mu\text{m}$ .

The principle of dynamic light scattering takes advantage of the fluctuation of scattered light intensities due to the Brownian motion of particles in the submicron range. The measuring range, covered by dynamic light scattering, reaches from 5 nm to 3  $\mu\text{m}$  < 5  $\mu\text{m}$ , the upper limit depending on the specific weight of the particles.

The laser light diffraction and the dynamic light scattering belong to the optical procedures. Their features are the short times, needed for analysis, and the good reproducibility of the obtained results.

*Keywords: particle size, particle size distribution, laser light diffraction, dynamic light scattering*

### Introduction

When a light wave (wavelength  $\lambda$ ) encounters a particle (diameter  $x$ , index of refraction  $n$ ) the propagation direction of the light wave is altered. This scattering can be caused by diffraction, refraction and reflection.

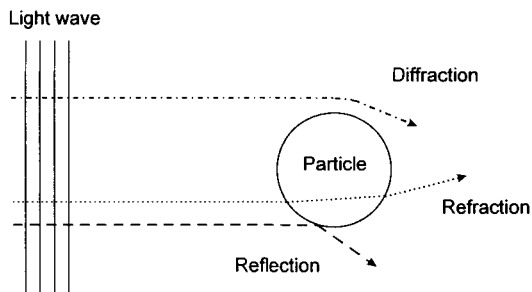


Figure 1: Scattering of light on a single particle.

The ratio of  $I$ , the intensity of the scattered light, to the illumination intensity  $I_0$ , depends on the angle of observation  $\theta$ , the index of refraction  $n$ , the wavelength of light  $\lambda$  and the particle diameter  $x$ :

$$\frac{I}{I_0} = f(\theta, n, \lambda, x) \quad (1)$$

The Mie parameter  $\alpha$  can be used to describe the combined effect of  $\lambda$  and the particle size, the latter expressed in terms of the spherical circumference  $\pi \cdot x$ :

$$\alpha = \frac{\pi \cdot x}{\lambda} \quad (2)$$

Three ranges can be distinguished:

$\alpha \ll 1$	Rayleigh scattering range
$0.5 < \alpha < 10$	Mie scattering range
$\alpha \gg 1$ ( $\alpha \approx 10$ or greater)	Fraunhofer range (geometric optics apply).

Rayleigh scattering is characterized by a total forward-backward symmetry of the scattered light, i.e. as much light is scattered back toward the source as forward, away from the source. For Rayleigh scattering, the intensity of the scattered light is proportional to the 6<sup>th</sup> power of the particle diameter and inversely proportional to the 4<sup>th</sup> power of the wavelength  $\lambda$ .

Mie scattering makes possible particle size analysis based on scattered light for particles larger than about 0.1  $\mu\text{m}$ .

As the parameter  $\alpha$  increases through the Mie range, i.e. as the particle diameter size increases, the proportion of light scattered in the forward direction becomes very much larger than that scattered back toward the source. Mie scattering intensities are proportional to the 4<sup>th</sup> power of the particle diameter.

In the range where the laws of geometric optics apply, the narrow cone of forward-scattered light is primarily determined by diffraction. The refraction and reflection scattering components can be disregarded (von Fraunhofer, 1817). The intensity of the scattered light is proportional to the 2<sup>nd</sup> power of the particle diameter.

### Laser light diffraction

Laser light diffraction analysis is based on the diffraction of parallel, collimated rays of laser light as they pass through a measuring chamber. Each particle causes a characteristic diffraction pattern in the detector based on the particle's size and shape. The diffraction pattern, which consists light maxima and dark minima, is projected onto a detector.

The use of a Fourier lens ensures that, for particles of the same size and shape, the location of the projected image is independent of the location of the particle in the measuring cell. The distance  $s$  of the maxima and minima to the optical axis depends on particle size, and their intensity depends on the proportion of particles in the sample having that size.

Because the detector elements are arranged in rings, the light and dark diffraction pattern of a sample is recorded with radial symmetry. This means that only spherical particles will be analyzed exactly, as only they produce a diffraction pattern consisting of light and dark concentric rings (diffraction rings).

The particle size distribution in the sample can be calculated by applying the Fraunhofer Approximation (which assumes non-reflecting, spherical particles) to the intensity distribution measured on the diffraction rings. This approximation is very accurate for particles larger than about 3  $\mu\text{m}$ , because their low-angle, forward-scattering (small  $\theta$ ) intensity is primarily determined by diffraction of the source beam at the particle surfaces (Mie parameter  $\alpha > \sim 10$ ).

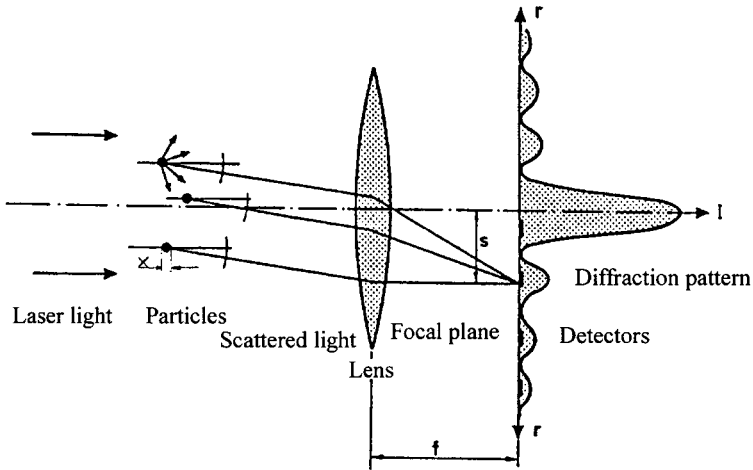


Figure 2: Laser light diffraction principle.

The Fraunhofer Approximation gives the relationship between the intensity of the scattered light  $I$  to the particle diameter  $x$  and the distance  $r$  from the image to the optical axis on the focal plane, in the following equation (Airy, 1837):

$$I(r, x) = I_0 \cdot \left( \frac{\pi \cdot x^2}{4 \cdot f \cdot \lambda} \right)^2 \cdot \left[ \frac{2 \cdot J_1 \left( \frac{\pi \cdot r \cdot x}{\lambda \cdot f} \right)}{\frac{\pi \cdot r \cdot x}{\lambda \cdot f}} \right]^2 \quad (3)$$

where  $J_1$  is the first order Bessel function of the first kind, and  $f$  is the focal length of the lens.

The light scattered by the various particles superimposes additively, so that the size distribution of the sample can be calculated from the light intensity distribution of the scattered light.

The Fraunhofer Approximation is insufficient for smaller particles ( $0.5 < \alpha < 10$ ), because the light scattered is spread over large angles  $\theta$  and results from several different scattering phenomena superimposed.

In such cases, the Mie theory must be used to calculate the exact relationship between particle size and scattering distribution (Mie, 1908).

The Mie theory requires knowledge of the optical characteristics of the (homogeneous) particle material, i.e. the complex index of refraction  $m$ :

$$m = n - i \cdot \kappa \quad (4)$$

where :

$n$  = index of refraction

$\kappa$  = absorption index  $\sim k$  = absorption coefficient

This makes possible laser analysis of homogeneous, transparent, reflective, and refractive or light-absorbing particles (Teipel et al., 1995 and 1996).



### Dynamic light scattering

Dynamic light scattering relies on Brownian motion for determining the size of suspended particles. Brownian motion is the random, disordered motion of particles caused by random collisions with solvent or gas molecules. Smaller particles recoil more strongly and thus generally show higher velocities. In general, the larger the particle, the lower the velocity. The velocity observed can be related to particle size with the help of the diffusion coefficient  $D$ . The particles must not be subject to any other superimposed motion, i.e. they must be neither sinking nor rising in the medium. In addition to particle size, the density or rather the density difference between particles and medium is important in determining the upper measuring range limit. If the particles are dispersed in a high-viscosity medium to prevent sedimentation, the Brownian motion effects will also be dampened. The temperature must be uniform throughout the sample volume in order to prevent currents in the dispersing medium.

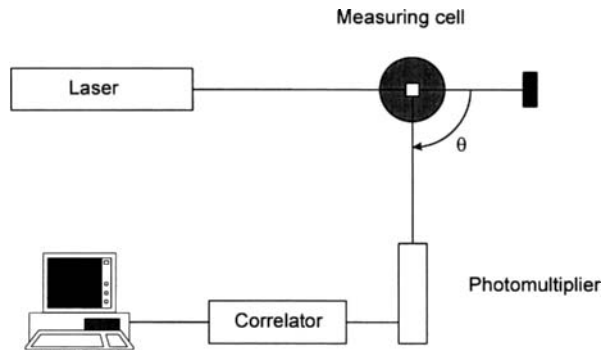


Figure 3: Dynamic light scattering measuring device.

Figure 3 shows the functional blocks of a dynamic light scattering measuring device. The laser light scattered in the sample is usually measured at an angle of  $90^\circ$ , but there are instruments that permit measuring at various angles. The signal is amplified in a photomultiplier. The Brownian motion interactions with the particles cause fluctuations in the scattered light intensity, which are analyzed in a correlator. In the correlator, the current level of a signal level is compared with the level from an earlier point in time. If the signal is compared with itself ( $\Delta t = 0$ ), then the correlation is perfect. If the delay time  $\Delta t$  is in the nanosecond to millisecond range, the correlation between the signal at time  $t$  and  $t+\Delta t$  is still very good. The correlation at  $t+2\Delta t$  can still be considered to be good. The correlation falls as the time interval increases, until there is no correlation remaining whatsoever. By multiplying the intensities at  $t\dots t+n\Delta t$  and summing over the measured time interval, the correlator computes the autocorrelation function. For monodisperse particles the following correlation equation applies:

$$g(\tau) = e^{-D K^2 \tau}; \tau = \text{delay interval} \quad (5)$$

$K$  can be calculated as follows:

$$K = \frac{4 \cdot \pi \cdot n}{\lambda} \cdot \sin \frac{\theta}{2} \quad (6)$$

These values depend on the device and/or measurement conditions:  $n$  is the index of refraction of the dispersing medium for wavelength  $\lambda$ , the wavelength of laser light used,  $\theta$  is the observation angle of the scattered light, and  $D$  is the diffusion coefficient of the particles. With the help of the Stokes-Einstein relation,  $D$  can be used to calculate the particle diameter:

$$x = \frac{k \cdot T}{3 \cdot \pi \cdot \eta \cdot D} \quad (7)$$

This equation, derived by Einstein from Stokes' law for frictional force on spheres in an ideal fluid, uses the Boltzmann constant  $k$  to relate the absolute temperature  $T$ , the diffusion coefficient  $D$  and the viscosity  $\eta$  to the particle diameter  $x$ .

The exponential function given earlier can be curve-fit to a line on a semi-logarithmic plot. The slope of the line gives the average particle diameter, weighted by intensity. This procedure can only be used with monodisperse samples.

If the semi-logarithmic plot diverges from a line, then the measured autocorrelation function can be approximated by a polynomial (cumulative analysis). A second-degree polynomial is usually employed. The linear coefficient provides the average diameter, and the quadratic coefficient a measure of the deviation, the polydispersion index  $PI$  (Teipel et al., 1995 and 1996). This analysis technique is not suitable, however, when the deviation is very large or multimodal.

Approaches to describing complex dispersion distributions have been developed, for example multi-exponential analysis, CONTIN analysis and the NNLS (non-negative least square) procedure (Koppel, 1972, Provencher, 1982, Provencher and Stepanek, 1996).

## Results

The results of the laser light diffraction, presented in this contribution, were obtained by using the Mastersizer S of Malvern Instruments Ltd.. This spectrometer works with a He-Ne laser at a wavelength  $\lambda$  of 632.8 nm. Particle size analysis can be done in a range from 0.5  $\mu\text{m}$  to 3,500  $\mu\text{m}$ . The measuring range is fixed by varying the focal length  $f$ . Different fractions of glass beads ( $n = 1.53$ ), dispersed in demineralized water ( $n = 1.33$ ) were examined. The calculation of the size distribution was carried out by applying the Fraunhofer Approximation and the Mie theory.

Figure 4 shows the volume frequency distribution  $q_v(x)$  of a monomodal sample of glass beads with a median  $x_{50,3}$  of 115.2  $\mu\text{m}$  and a Sauter diameter  $x_s$  of 113.4  $\mu\text{m}$ . At this size range, the evaluation by Fraunhofer and by Mie, using the refractive index  $n=1.53$  and an absorption coefficient  $k = 0.001$ , provide identical values of the distribution.

Figure 5 shows the results for glass beads with a median  $x_{50,3}$  of approximately 13  $\mu\text{m}$ . Fraunhofer delivers a median  $x_{50,3}$  of 13.7  $\mu\text{m}$  and a Sauter diameter  $x_s$  of 6.9  $\mu\text{m}$ . A fraction of fine particles, which is not really existing, is indicated. Consequently,

quently, the Sauter diameter of the whole fraction is strongly reduced. Using the correct complex refractive index of glass beads ( $n = 1.53$ ,  $k = 0.001$ ), the evaluation by Mie provides the real particle size distribution.

Only for large particles (Mie parameter  $\alpha$ ), the Fraunhofer Approximation, which is valid for spherical and non-reflecting particles, correctly determines the size distribution of glass beads. For transparent particles, and when the differences of the refractive indices of particles and continuous phase are small, the Mie theory has to be applied, but using the correct values for  $n$  and  $k$  because false values tend to false size distributions.

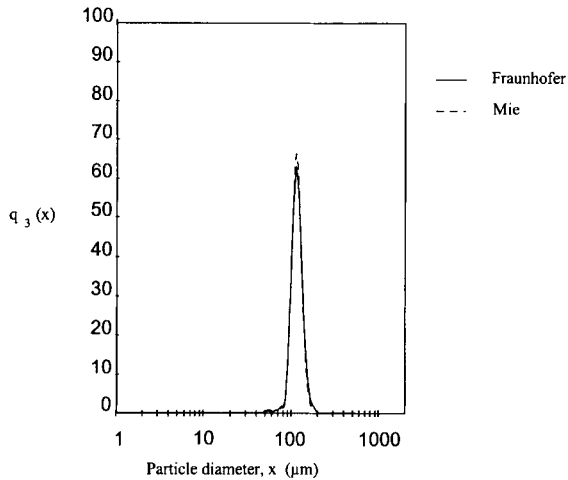


Figure 4: Volume frequency distribution  $q_3(x)$  of glass beads with a median  $x_{50,3} = 115.2 \mu\text{m}$ ; analysed by Fraunhofer and by Mie.

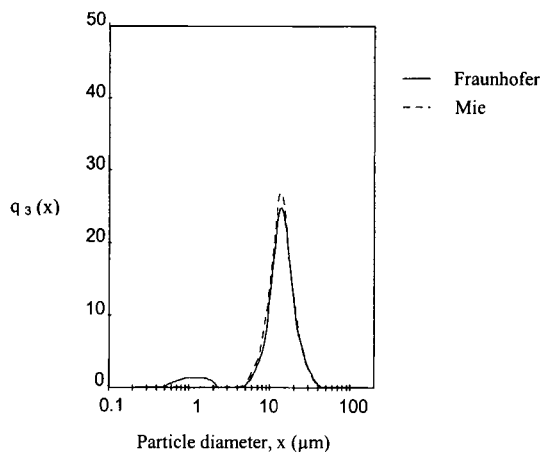


Figure 5: Volume frequency distribution  $q_3(x)$  of glass beads with a median  $x_{50,3} 13 \mu\text{m}$ ; analysed by Fraunhofer and by Mie.

The Zetasizer 3000 of Malvern Instruments Ltd. was used for the investigation of the dynamic light scattering. The instrument is equipped with a He-Ne laser. The measuring range reaches from 5 nm to 5  $\mu\text{m}$ , the upper limit depending on the specific weight of the particles to be examined.

Several latex standards in aqueous solution were investigated, both phases having similar densities to avoid sedimentation (disturbance of Brownian motion).

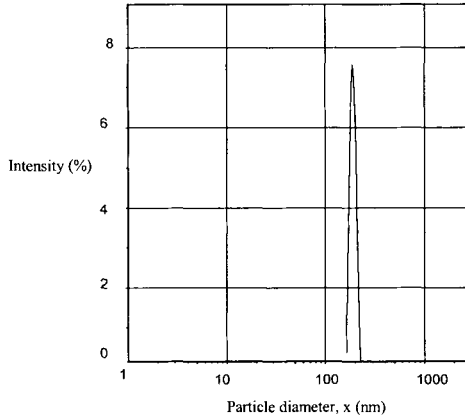


Figure 6: Intensity-weighted plot of a 200 nm standard; cumulative analysis.  
Mean diameter: 194 nm.

Figure 6 shows the plot of a standard with a mean diameter of 200 nm. The mean intensity-weighted particle diameter, detected by dynamic light scattering and analyzed by the cumulative method, was 194 nm.

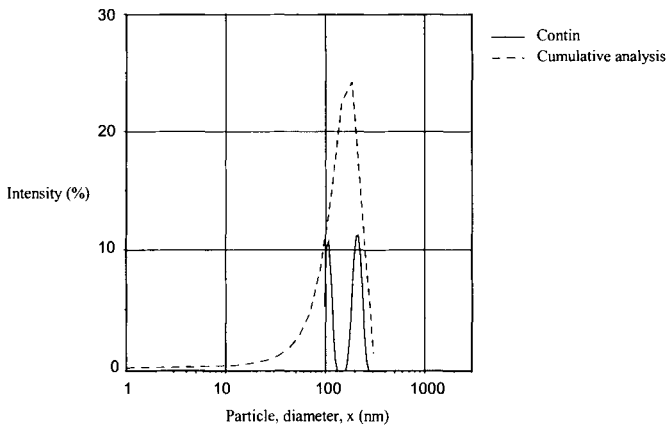


Figure 7: Intensity-weighted plot of a latex mixture; *Contin* analysis and cumulative analysis.

Figure 7 shows the plot of the mixture of a 100 nm and a 200 nm latex standard (volume ratio 1:1). Applying the CONTIN analysis, correct determination of the size as well as of the quantity of the mixture is given. The cumulative analysis is not sufficient for the evaluation of bimodal distributions because only a mean particle diameter and a value for the width of the distribution (PI) can be provided.

If the diameter ratio of bimodal distributions becomes less than 1:2, no valid evaluation will be possible by any analysis. For particulate systems, consisting of very small and very large particles, it can happen within the region of Rayleigh scattering that the intensity signal of the small particles is put out by the signal of the large ones ( $I \sim x^6$ ). In general, multimodal distributions are very difficult to evaluate.

### References

- Airy, G.B., 1837. On the diffraction of an object with circular aperture. *Trans. Camb. Phil. Soc.*, 5, pp. 283-290.
- Koppel, D.E., 1972. Analysis of macromolecular polydispersity in intensity correlation spectroscopy: The method of cumulants. *J. Chem. Phys.* 57, pp. 4814-4820.
- Mie, G., 1908. Beiträge zur Optik trüber Medien. *Annalen der Physik*, 25, pp. 377-445.
- Provencher, S.W. and Stepanek, P., 1996. Global analysis of dynamic light scattering autocorrelation functions. *Part. Part. Syst. Charact.* 13, pp. 291-294.
- Provencher, S.W., 1982. CONTIN- A general program for the regularized solution of linear integral equations. *Comput. Phys. Comm.* 27, pp. 213 - 229.
- Teipel, U., Siegl, T. and Aksel, N., 1995 and 1996. Größenanalyse transparenter Partikel mit Hilfe der Laserbeugungsspektrometrie Teil 1 u. 2. *VFI Der Versuchs- und Forschungsingenieur* (28), 2, pp. 39-41 and (29), 2, pp. 38-40.
- von Fraunhofer, J., 1817. Bestimmung des Brechungs- und Farberstreuungsvermögens verschiedener Glasarten. *Gilberts Annalen der Physik*, 56, pp. 193-

## **INDUSTRIAL TREATMENT OF RAW AGATE: SPECTROCOLORIMETRY AND SCANNING ELECTRON MICROSCOPY (SEM) ANALYSES**

L.C.B. Tubino, C.H. Sampaio

Laboratory Mineral Processing, Tecnology Center, Engineering College,  
Federal University of Rio Grande do Sul, Porto Alegre, Brazil

### **Abstract**

This work's main objective is to present the techniques used for optimization of the process of industrial staining of raw agate geodes extracted from small operations in the Rio Grande do Sul State, southern Brazil. This optimization is accomplished through the comparative control of hot and cold staining techniques, the analysis of the colors obtained in the staining process, and the recognition of the structures that compose the bands of the agate and their capacity to absorb the coloring solutions. The duration needed for the impregnation of the agate with the coloring agent used in the chemical treatment is directly related to the type of chemical solution and its temperature. The Spectrocolorimeter's results, according to the CIELab system, and the emphasis on the tonality and chromaticity of the samples are employed to analyze the colors obtained in the staining process. The analysis of the agate by means of scanning electron microscopy (SEM) points out the different types of microstructures that form the banding of this material, as well as the relationship of this banding with other minerals, mainly quartz in crystal and milky forms. This recognition of the banding characteristics is important, since it determines the capacity of the agate to absorb the coloring agent during the staining process.

*Keywords: agate, process, spectrophotometry and SEM*

### **Introduction**

The Rio Grande do Sul State has been recognized as the greatest world producer of raw agate and, as a consequence, has assumed a major responsibility in the supply of this raw material to foreign consumer markets, especially to countries such as Germany, Japan, the United States and others (Souza and Sampaio, 1994).

The utilization of agate is largely diversified, though the most widespread use is as personal or home-embellishment material. Agates are also manufactured as precision parts for the laboratory, in crucibles, milling bodies, etc. (Mattos, 1974).

With the employment of cutting machines, geodes are pre-formed, washed and subject to chemical-thermal treatment, whereas agates are stained - mainly in green, blue, red and black - to improve the product's final quality.

### **Methods**

#### *Chemical-thermal treatment*

The coloring solutions used to dye the agate can be prepared at room temperature (cold staining) or in a hot bath (hot staining). The agate pieces are placed in perforated baskets, disposed side by side inside the stainless steel vats, in contact with the

standardized coloring solutions. After staying the necessary time in solution, pieces are removed from the recipients and dried in an oven at a temperature of 60 °C, for a period of 12 h. Soon after, they're submitted to thermal treatment, where fixation of the green, red and black colors will take place. This treatment is not necessary in order to obtain a blue color.

In this stage of the process, the agate pieces are assembled in stainless steel or metal vats and covered by a layer of fine sand, whose main function is to homogeneously dissipate the heat conduction along the pieces inside the muffle furnace. Here the black pieces are submitted to temperatures that vary from 180 °C to 200 °C, the green pieces from 200 °C to 220 °C, and the red pieces from 240 °C to 260 °C, for over a period of 24 h. After completion of the procedure, the pieces will be sanded, polished and later placed for sale. As a final result of the industrial staining process of the agate pieces, a certain color is obtained from impregnation of the coloring solutions, resulting from the arrangement of parameters such as solution type, duration in the solution, choice of the cold or the hot method and respective calcination temperature.

#### *Colorimetric analysis*

The use of a method to qualify and to quantify the resulting color will contribute to definition of the optimum parameters to be used in the process. The equipment used for data collection was the Ultra Scan model of the HunterLab Spectrocolorimeter associated with the Universal software. This equipment was standardized with a D65 luminous source that excludes speculating and is without an ultra-red filter, and measurements were collected in the CIELab system. The equipment was always calibrated at the beginning of the data collection session. To accomplish measurements with the Spectrocolorimeter, the following parameters were used for analysis of the proposed methods: L\* (regarding the body brightness, which varies from 0 (black) to 100 (white)); a\* (regarding values in the axis of red (+ a\*) and green (- a\*) colors that vary from 0 to 60); b\* (regarding values in the axis of yellow (+ b\*) and blue (- b\*) colors that vary from 0 to 60); C\* (which represents the sample's chromaticity); and h° (which represents the angle whose tangent is b\*/a\*, which indicates the quadrant and the direction in which the material's tonality develops). Several measurements were accomplished for each plate of treated agate, and the final values of L\*, a\*, b\*, C\* and h° used in the calculations are the mean values corresponding to the number of observations accomplished for each sample. This procedure was necessary to minimize the effect caused by the different types of bands that form the agates (the material's heterogeneity).

For the comparison of the cold and hot staining methods, colorimetric measurements were accomplished with agate plates colored in green and blue. Moreover, the experiment was set up to analyze the efficiency of the process, comparing the duration (in days) in the respective coloring solutions, by means of the chromatic parameters of the pieces.

The solution for the green color was prepared as an aqueous solution containing chromic acid, ammonium chloride and distilled water. For the experiment, the samples denominated Umbu-02 and Umbu-08 were used. For the blue color, two different aqueous solutions were prepared. The first was composed of potassium ferrocyanide and distilled water, and the second was made of ferrous sulfate, sulfuric

acid and distilled water. The agate plates were submitted to different durations in solution, according to the following approach: with a fixed time for the material in the first solution and varied in the second solution, and also in the inverse way. For this experiment, the samples used were denominated Umbu-03 and Umbu-07.

### *Scanning Electron Microscope*

The geodes, constituted by the agate and its associated minerals, such as quartz, calcite, zeolite and apofillites, present several filling patterns, identified by the different banding types. The filling pattern found in the agates from Rio Grande do Sul State is described in the Table I by Brum et al. (1994).

Table I: Filling pattern and agate variety.

Filling pattern	Agate variety
Without banding (massive)	Muscous or dendritic agate - Mosquito agate
Concentric banding	Banded or striped agate - Orbicular agate Onyx - Iris agate
Parallel banding	Uruguay agate - Onyx
Concentric and parallel banding	Scenical or landscape agate
Complex filling	Tubular agate - Scenical or landscape agate

The individual bands that form the banding of the agate geode present different colors, sizes, forms, transparency and porosity as a function of the structural arrangement, which can be observed with the aid of the scanning electron microscope. To analyze and later to correlate the micro-crystalline structures that individualize a certain band of the agate with a greater or smaller capacity to absorb the coloring chemical solutions, several standardized specimens were prepared according to the following description. The specimens were cut in a cylindrical form 1 cm in diameter, then treated with a set of sandpaper. Soon after, they were polished by using a 4-micrometer diamond powder and finally were submitted to an attack by HF (hydrofluoric acid) for 30 s. After being coated with gold, samples were then analyzed by the scanning electron microscope (Flörke et al., 1982). The bandwidth varies randomly by millimetric rates. When the agate is polished at its cross-section, then prepared and examined in the SEM, the banded aspect is determined on the scale of a micron to a sub-micron, for zones in concentric succession. (Frondele, 1978 and 1985).

## **Results**

### *Green Staining*

To test the efficiency of the hot and cold staining processes for obtaining the green coloration in agate plates, the samples Umbu-02 and Umbu-08 were submitted to the same values for the duration in solution (3, 5, 7 and 11 days) and calcination temperature (220 °C), presenting the results shown in Tables II-V.

In the hot staining process, the plates of agate Umbu-02 presented chromaticity in 3 and in 5 days, on the order of 17.92 and 16.72, with tonality angles of 9°52' and 6°13'. These results are very close to those for samples of 7 and 11 days, with values of 16.50 and 16.03, and tonality angles respectively equal to 2°01' and 6°52', as shown in Table II. In terms of the revenue of the process, it can be affirmed from the obtained



results, that the plates dyed for 3 days in hot solution would already be ready for commercialization.

Table II: Parameters of the sample Umbu-02, green-dyed, hot process.

UMBU-02 – Green (calcination temperature = 220 °C)				
Hot Process = 60 °C				
T (day)	3	5	7	11
L*	39.51	36.66	35.50	34.82
a*	- 17.65	- 16.61	- 16.45	- 15.91
b*	- 3.07	- 1.81	- 0.58	- 1.92
C* hot	17.92	16.72	16.50	16.03
h° - quadrant	9°52' - 3q	6°13' - 3q	2°01' - 3q	6°52' - 3q

In the cold staining process, the plates of agate Umbu-02 presented chromaticity in 11 days on the order of 13.83, with an angle of tonality of 0°37', followed by the 5-days and 7-day samples, with chromaticity values of 12.47 and 12.32, and tonality angles respectively equal to 0°19' and 4°09', as shown in Table III. In terms of the revenue of the process, it can be affirmed from the obtained results, that the plates dyed for 5 days in cold solution would already be completed for commercialization. Usually, the analysis of the C\* value obtained is not alone capable of expressing the best performance of the hot and cold staining methods or of discerning them. It is still needed to observe the angular tendency of the tonality and its respective quadrant, which many times can indicate the evolution of the tonality acquired by the agate plate.

Table III: Parameters of the sample Umbu-02, green-dyed, cold process.

UMBU-02 – Green (calcination temperature = 220 °C)				
Cold Process				
T (day)	3	5	7	11
L*	38.35	42.45	41.76	36.21
a*	- 11.09	- 12.47	- 12.27	- 13.81
b*	2.07	0.07	0.89	- 0.15
C* cold	11.43	12.47	12.33	13.83
h° - quadrant	10°34' - 2q	0°19' - 2q	4°09' - 2q	0°37' - 3q

In the hot staining process of the Umbu-08 agate plates, specimens were analyzed after 3, 5, 7 and 11 days in solution. The plates stained during 3 days were distinguished from the others by a chromaticity value on the order of 17.42 and an angle of tonality of 6°06', as can be seen in Table IV. In terms of revenue of the process, it can be affirmed, based on the obtained results, that the plates stained during 3 days or more in hot solution would be ready for commercialization.

In the cold staining process, the Umbu-08 agate plates with 11 and 7 days presented chromaticity values on the order of 18.08 and 17.86, with tonality angles equal to 1°31' and 5°47' - values higher than those obtained for the samples of 3 days and 5 days, with chromaticity values of 15.80 and 14.71 and tonality angles respectively equal to 2°17' e 4°24', as seen in Table V.

Table IV: Parameters of the sample Umbu-08, green-dyed, hot process.

UMB-08 – Green (Calcination Temperature = 220 °C)				
Hot process = 60 °C				
T (days)	3	5	7	11
L*	28.78	28.79	30.08	26.75
a*	- 15.77	- 17.31	- 15.70	- 15.54
b*	- 2.69	- 1.85	- 2.68	- 2.67
C* hot	16.00	17.42	15.93	15.76
h° - quadrant	9°40' - 3q	6°06' - 3q	9°41' - 3q	9°45' - 3q

In terms of revenue of the process, it can be affirmed, based on the obtained results, that the plates that remain for 5 days in cold solution would already be completed for commercialization.

Table V: Parameters of the sample Umbu-08, green-dyed, cold process.

UMB-08 – Green (Calcination Temperature = 220 °C)				
Cold process				
T (days)	3	5	7	11
L*	35.72	30.88	28.10	24.50
a*	- 14.65	- 15.43	- 17.76	- 18.06
b*	- 1.13	3.36	- 1.80	0.48
C* cold	14.71	15.80	17.86	18.08
h° - quadrant	4°24' - 3q	12°17' - 2q	5°47' - 3q	1°31' - 2q

### Blue staining

In staining to blue, samples were initially immersed in the ferrocyanide solution for a given period, and afterwards in the iron sulfate solution. The periods here are written as X-Y, where X = time in the first solution and Y=time in the second solution. To test the efficiency of the hot and cold staining processes for obtaining the blue color in agate plates, two samples denominated Umbu-03 and Umbu-07 were used. Results for these samples are shown in Tables VI-IX.

In the hot staining process, the plates of the Umbu-03 agate were analyzed after 3-1, 3-2, 3-4 and 4-2 days in solution, and the plates with 4-2 and 3-2 days presented resulting chromacity values on the order of 15.36 and 14.15, and tonality angles of respectively 86°33' and 86°04'. Even the sample for 3-1 days presented a chromacity value of 15.75 and a tonality angle of 62°52', as seen in Table VI. The differing values for the sample of 3-1 days is due to the excessive impregnation of potassium ferrocyanide contained in the first solution, compared with the iron sulfate contained in the second, which gave a green-blue tonality to the sample that is checked by its position in the third quadrant.

In terms of the revenue of the process, it can be affirmed, based on the obtained results, that the plates dyed for 3-2 days or more in hot solution would already be completed for commercialization.

In the cold staining process, the plates with 3-2 and 3-4 days presented chromaticity values on the order of 13.73 and 13.70, with tonality angles of 79°49' and 82°19' respectively, as in Table VII. The sample 3-1 presents the same effect as in the previous treatment, with green-blue tonality.

Table VI: Parameters of the sample Umbu-03, blue-dyed, hot process.

UMB-03 - Blue				
Hot process = 60 °C				
T (days)	3-1	3-2	3-4	4-2
L*	8.19	4.17	3.42	4.58
a*	- 7.18	0.97	0.99	- 0.92
b*	- 14.01	- 14.12	- 10.05	-15.31
C* hot	15.75	14.15	10.09	15.36
h° - quadrant	62°52' - 3q	86°04' - 4q	84°22' - 4q	86°33' - 3q

In terms of revenue of the process, based on the obtained results, it can be affirmed that the plates dyed for 3-2 days or more in cold solution would already be completed for commercialization.

Table VII: Parameters of the sample Umbu-03, blue-dyed, cold process.

UMB-03 - Blue				
Cold process				
T (days)	3-1	3-2	3-4	4-2
L*	7.78	5.28	4.75	-
a*	- 5.28	- 2.38	- 1.83	-
b*	- 12.75	- 13.27	- 13.58	-
C* cold	13.81	13.73	13.70	-
h° - quadrant	67°30' - 3q	79°49' - 3q	82°19' - 3q	-

In the hot staining process, the plates of Umbu-07 agate were analyzed after 3-1, 3-2, 3-4, 4-2 and 4-5 days in solution, and the plates for 3-2, 3-4 and 4-2 days presented quite close chromaticity values and tonality angles, followed by the plate for 4-5 days, all in the fourth quadrant. Only the plate for 3-1 days differs from the others, with a chromaticity value on the order of 21.02, and a tonality angle of 51°46', as seen in Table VIII. This sample's differing values are due to the excessive impregnation of potassium ferrocyanide contained in the first solution, in relation to the iron sulfate contained in the second, giving a green-blue tonality to the sample, which is confirmed by its position in the third quadrant. In terms of revenue of the process, based on the obtained results, it can be affirmed that the plates dyed 3-2 days or more in hot solution would be ready for commercialization.

Table VIII: Parameters of the sample Umbu-07, blue-dyed, hot process.

UMB-07 - Blue					
Hot Process = 60 °C					
T (days)	3-1	3-2	3-4	4-2	4-5
L*	12.54	5.82	6.36	7.00	5.65
a*	- 13.00	3.36	3.71	3.80	3.04
b*	- 16.50	- 23.50	- 23.42	- 23.69	- 20.74
C* hot	21.02	23.74	23.71	24.00	20.96
h° - quadrant	51°46' - 3q	81°51' - 4q	81°00' - 4q	80°53' - 4q	81°36' - 4q

In the cold staining process, the plates with 3-2 and 3-4 days presented chromaticity values on the order of 17.56 and 18.78, with tonality angles of respectively 79°30' and

82°31', as can be seen in Table IX. In terms of the revenue of the process, based on the obtained results, it can be affirmed that the plates dyed for 3-2 days or more in cold solution would be ready for commercialization.

Table IX: Parameters of the sample Umbu-07, blue-dyed, cold process.

UMBU-07 – Blue					
Cold process					
T (days)	3-1	3-2	3-4	4-2	4-5
L*	10.35	7.35	7.41	-	-
a*	-12.14	-3.20	-2.45	-	-
b*	-12.78	-17.27	-18.62	-	-
C* frio	17.63	17.56	18.78	-	-
h°-quadrant	46°28' – 3q	79°30' - 3q	82°31' - 3q	-	-

### Microstructures

For observations accomplished with the aid of the scanning electron microscope, it was possible to relate the 3 microstructures that compose the bands of the agates that directly influence the final result of the staining process: translucent microcrystalline, compact microcrystalline and fibrous microcrystalline (see Figure 1).

The translucent microcrystalline band is formed by microcrystalline translucent quartz, crystallized in the trigonal system, and commonly appears in the geodes as concentric or parallel bands, with thicknesses varying from millimeters to centimeters. It presents a very low degree of porosity, absorbing very little of the coloring solutions.

The compact microcrystalline band is formed of microcrystalline milky quartz crystallized in the trigonal system, and appears as often in concentric as in parallel forms in the geodes. It doesn't absorb the coloring solutions. However, when the piece that possesses it is submitted to thermal treatment, it will acquire a whitish tonality, giving the piece a quite interesting and appreciable contrast. The fibrous microcrystalline band is formed of translucent and porous quartz fibers disposed perpendicularly to the elongation of the banding. It is crystallized in the trigonal system and occurs in all of the agate geodes, forming successive concentric or parallel bands. This is the main agate's structure for staining, absorbing all types of coloring solutions.

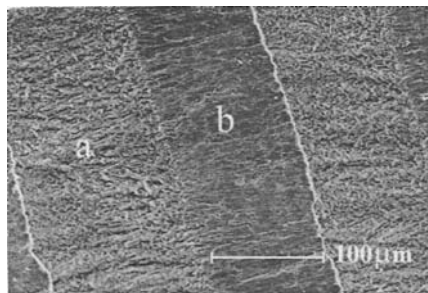


Figure 1: Microstructures: fibrous in (a) and compact in (b).

## **Conclusions**

With the colorimetric data obtained with a CIELab system Spectrocolorimeter, it was possible to compare the performance of the two methods of industrial staining used in the Rio Grande do Sul. The hot staining process presented a better performance in relation to the cold method, as much for the green color, which needs thermal treatment, as for the blue color, which doesn't use this step of the treatment for color fixation. This better chromatic performance observed with the hot-colored agate plates was identified with the aid of the parameters  $L^*$ ,  $a^*$ ,  $b^*$ ,  $C^*$  and the tonality angle  $h^\circ$ . The operational optimization of the industrial staining process can be reached with a residence period in solution that varies from 3 to 5 days for the green color and from 3-2 for the blue.

Recognition of the banded structures described in the text and their relationship to the capacity to absorb the coloring solutions used in the staining process, with the aid of the scanning electron microscope, became important parameters for characterizing the agates' deposits in the Rio Grande do Sul State, in order to seek industrial processes.

## **References**

- Brum, T.M.M., Juchem, P.L. and Fischer, A.C., 1994. Padrões de preenchimento da ágata do Rio Grande de Sul. XXXVIII Congresso Brasileiro de Geologia, Balneário Camboriú-SC, 201-202.
- Flörke, O.W. et al., 1982. Water in microcrystalline quartz of volcanic origin: agates. *Contributions to Mineralogy and Petrology*, August, 324-333.
- Frondel, C., 1978. Characters of quartz fibers. *American Mineralogist*, 63, 17-27.
- Frondel, C., 1985. Systematic compositional zoning in the quartz fibers of agates. *American Mineralogist*, 70, 975-979.
- Mattos, L.E., 1974. Perfil analítico da ágata. DNPM, Bol. 29, Rio de Janeiro, 18.
- Souza, J.C. and Sampaio, C.H., 1994. Industrialização de pedras preciosas no Rio Grande do Sul – estado da arte. IIIº Congresso Ítalo-Brasileiro de Engenharia de Minas, setembro, Verona, Itália.

## BACK-SCATTERED ELECTRON IMAGING OF A LATERITIC IRON ORE AND ITS APPLICATIONS IN PROCESS MINERALOGY

A. Alcover Neto\*, R. Neumann\*, C. L. Schneider<sup>o</sup>

\*Centro de Tecnologia Mineral, CETEM  
Rua 4, Quadra D, Rio de Janeiro, RJ 21941-590, Brazil  
<sup>o</sup>University of Utah, 1460 East 135 South Room 412  
Salt Lake City, UT 84112-0114, USA

### Abstract

A hydrocyclone treating an itabirite iron ore was sampled, characterized in detail using modern image analysis techniques and modeled. Some of the most interesting results from this investigation were: the itabirite studied is highly porous; this property may be advantageous in direct reduction applications; two types of porosity are present; one is macroscopic and the other microscopic; the micro-pores in this itabirite are interconnected. Porosity liberation in the size range studied is associated to the macro pores; the process of liberation in this itabirite is quick, probably aided by liberation by detachment; the regimen inside the hydrocyclone is closer to turbulent than it is to laminar regimen; the density of the slurry in the separation zone must be used instead of the density of the liquid.

It is anticipated that lateritic iron ores in general may present significant porosity, and this must be taken into consideration when evaluating image analysis results from this type of ores.

*Keywords: liberation, hydrocyclone, image analysis, modeling*

### Introduction

The work reported here originated from a need to implement quantitative image analysis for mineralogical characterization at CETEM's process mineralogy laboratory. CETEM is a fully equipped center for mineral technologies with services ranging from small scale lab tests to full pilot scale testing of most unit operations in mineral processing. Services and testing are supported by a complete chemical analysis laboratory, and a process mineralogy laboratory that includes modern X-Ray diffraction and an excellent Leica S-440 SEM equipped with X-Ray micro-analysis and a solid-state back-scattered electron detector. A research project in tandem with the University of Utah Center for Minerals Technology and SAMARCO, a major iron ore producing company in Brazil was carried out at CETEM. The aim was to execute a project that would cover most areas related to liberation characterization and process mineralogy, including the implementation of the techniques developed at the University of Utah at CETEM's mineralogy laboratory. The work consisted of a sampling campaign around a hydrocyclone operating in closed circuit with a ball mill at SAMARCO's Germano plant. Samples were collected in the feed, overflow and underflow of the cyclone cluster, and all pertinent operation data recorded. The dry samples were screened using standard sieving, and delivered to CETEM for analysis. The work that ensued was that of sampling, mounting, grinding and polishing, carbon coating and image acquisition, all using standard techniques. The LEICA S-440

SEM is capable of unattended image acquisition and this is a crucial advantage since for proper statistics, about 50 images must be acquired from each narrow size sample, and for the 30 samples, 10 from each stream, this translates to 1,500 images to be acquired. Although unattended operation capability is largely due to stage configuration, capability of running 3 samples at a time in the chamber and a good stage control interface, it is also very important to maintain beam stability during the hours while the system is operating automatically. Combined with an even coating of carbon on the surface of the mounts, beam stability is perhaps the strongest feature of this SEM. Once the contrast and brightness are set according to the requirements for proper phase discrimination and the automated image processing procedures that followed, the peaks corresponding to the epoxy mounting media, quartz, goethite and hematite and magnetite, the main mineral components of this ore, are found at or near the preset gray levels in all images, without need for detector gain adjustments or any other kind of intervention during the acquisition process.

The LEICA system has a number of features designed for qualitative analysis. One of them is the visual display of the images at high contrast, even when actual contrast is poor. This feature must to be turned off for quantitative analysis, so that the images generated are true high-contrast images. This also helps in adjusting the solid state detector to the proper level of gain. Also, the image histogram can be displayed with the image, facilitating the adjustment of contrast and brightness.

Once a good image acquisition procedure was in place, implementation of the MMIA™ software package developed at the University of Utah was required. MMIA™ is developed under Solaris™, which is not available at CETEM. The low cost solution was to port MMIA™ to Linux. The workstations controlling the LEICA system, running a DOS based OS, and the Linux workstation were networked to CETEM's LAN, and communication could be established using standard TCP/IP over Ethernet. This is the basis for interfacing the image acquisition system with the MMIA™ image analysis system. With the implementation of a GUI for file exchange and management, implementation of MMIA™ at CETEM was completed. Following the required implementation, the proposed work included training in image processing techniques, measurement of linear and areal liberation, stereological correction, process mineralogy calculations, and modeling and simulation of the cyclone with the liberation information obtained at CETEM. This was expected to be a straight forward repetition of work routinely done at the University of Utah. However, due to the lateritic characteristics of the itabirite iron ore, the high porosity associated to the iron bearing minerals must be characterized before any useful result can be obtained. This is usually not necessary for the non-lateritic ores such as taconite, lending novelty to the itabirite characterization. Furthermore, liberation had never been fully characterized for any of the Brazilian itabirites, even though liberation plays an important role in obtaining the high grade concentrates that are required for pelletization. Finally, modeling the hydrocyclone with measured liberation spectra had never been reported in the literature, and this exercise uncovered some long debated aspects of hydrocyclone operation in the light of the traditional Plitt (1976) model.

### **Itabirite image analysis**

The itabirite studied is mainly composed of quartz, goethite, hematite and magnetite. The average atomic numbers of hematite and magnetite are too close to allow for

discriminating these two phases at the contrast levels used in this work. Goethite, quartz and the epoxy mounting media can be discriminated from hematite and magnetite so that whenever all phases are present in significant amounts, 4 peaks could be clearly identified in the gray level histogram of the solid-state backscatter electron image. The epoxy peak was located at about gray level 30 by adjusting the brightness level and then contrast was adjusted so that the peak corresponding to hematite/magnetite was located at gray level 220. At first inspection, the images show particle cross-sections with significant amounts of porosity. Direct measurement in porous sections is not feasible, and the best course of action is to fill the features prior to measurement, using apparent densities to reconcile grades and volumetric grades after measurement. The quartz in the itabirite has very little observable internal porosity, and it was assumed that all porosity is associated to the iron bearing minerals, with advantage, since pores located at the interface between quartz and an iron phase cannot be correctly identified as belonging to one phase or another. On the other hand, pores located completely inside quartz features were filled with quartz phase. Linear grade and areal grade distributions were measured on ternary images with a phase corresponding to the epoxy mounting media, one corresponding to gangue, mostly quartz and another that included goethite, hematite and magnetite, thus giving liberation of iron bearing minerals against the gangue minerals. Because grades must be reconciled, the amount of porosity associated to the iron bearing minerals was recorded and saved for each image in each specimen. Furthermore, the volume fractions of goethite were measured in each image. This is important because goethite's density is considerably less than that of hematite, and because goethite and hematite are abundant phases in the itabirite, mass fractions calculated from volume fractions may be strongly influenced by the relative amounts of goethite and hematite. The mass fraction of any particular phase in a mineral system can be calculated when the volume fractions and densities of all phases present are known. When the volume fractions measured include the volume of the pores associated, then apparent densities must be used instead of phase densities. In any case, porosity must be known before mass fractions can be calculated. Other measurements carried out included feature and phase perimeters, chord length distributions and feature area distribution.

### **Qualitative and quantitative assessment of porosity by image analysis**

The problem of quantitative analysis of the itabirite is better understood when one surveys every back-scattered electron image generated on all samples originating from each stream and size range. As an attempt to illustrate the essence of this process, two images from samples of hydrocyclone overflow are shown side by side in Figure 1, one from large particles at low magnification and one from small particles at high magnification. Significant amounts of porosity can be readily seen in the large particles and comparatively less porosity is seen in the small particles.

Also, the general shape of the particles in both images is significantly different, with the large particles showing concavities in the perimeter of the cross-sections indicating that the fracture surface intercepts the unbroken ore pores frequently, while in the small particles the shape is significantly more convex, indicating that the process of pore liberation is not as significant at this size. This process has impact in the hydrocyclone operation, as particles with higher porosity tend to concentrate in the overflow stream



while the less porous particles tend to concentrate in the underflow stream. The evolution of measured porosity with stream and size shown in Figure 2 confirms this tendency.

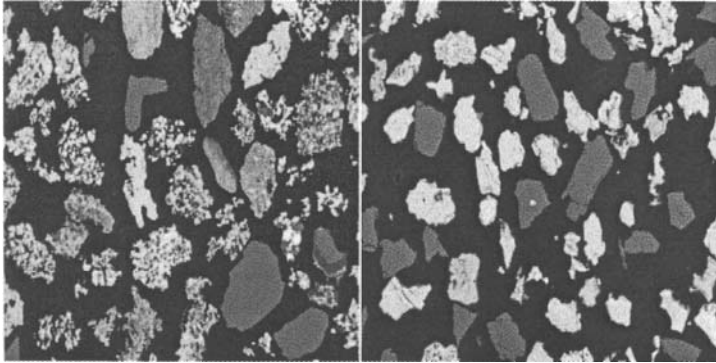


Figure 1: Cyclone overflow particles. Left image from  $841 \times 589 \mu\text{m}^2$  particles at 20x magnification. Right image from  $44 \times 37 \mu\text{m}^2$  particle at 600x magnification.

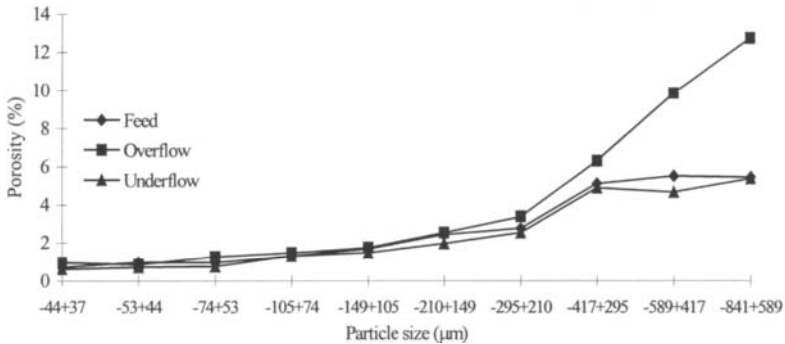


Figure 2: Macro-porosity evolution in iron bearing minerals.

### Reconciliation of chemical and image analysis grades

Chemical assay of iron ore is performed routinely in a number of laboratories in Brazil. Nine samples, three from each stream, were selected and sent to two certified laboratories for detailed chemical analysis, and the mass fractions of quartz, goethite, hematite and magnetite determined. The assays from both labs were in agreement. The estimated mass fractions of quartz from image analysis, using the measured porosity in each sample, are shown in Figure 3, and this is compared with the results of the chemical assays.

Clearly the mass fractions of quartz were consistently underestimated in all samples, and this ultimately lead to the conclusion that the measured porosity by image analysis was consistently underestimated in all samples. The nature of the porosity of this itabirite began to be understood when particle density measurement was undertaken using a helium pycnometer. The measured densities were equal to the theoretical densities of the

phases, given the contributions of each phase as calculated using chemical assay results. In clear terms, all the pores that are present in the particles and that can be clearly seen under the microscope, were filled with helium during the picnometer measurement. The inexorable conclusion is that all pores must be connected to each other and to the particle surface, since the helium flows freely through the pores.

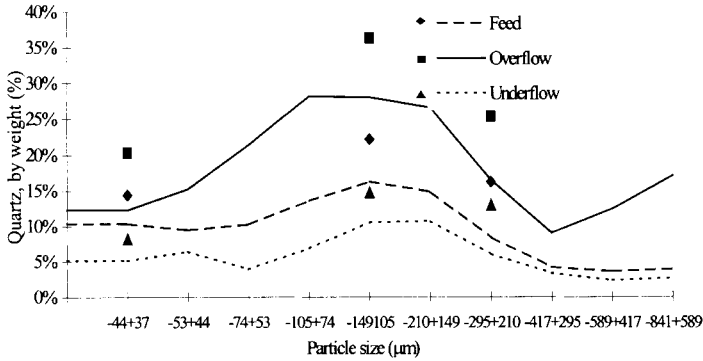


Figure 3: Quartz assays from chemical (symbols) and I.A. (lines) calculated using the measured macro-porosity.

Interestingly enough, the same problem in reconciling I.A. results with chemical assays have been reported by Fandrich (1998) who measured liberation in a lateritic iron oxide sample probably originated in South Africa, and reported a significant degree of porosity not visible to QEM\*SEM used in that work, and in the work reported by Srivastava et al. (1999) who studied the Kiriburu lateritic iron ore of India. Also corroborating the presence of micro-porosity, is the amenability of some itabirites to direct reduction processes. Sampaio et al. (1997) showed that the kinetics of direct reduction of a Brazilian itabirite was considerably faster when using H<sub>2</sub> when compared to CO as reduction gas in a fluidized bed reactor, and attributed this to the presence of inter-crystalline micro-pores.

Because magnetite cannot be distinguished from hematite in back-scattered electron images, it was assumed that magnetite and hematite constituted a single phase. This assumption can be considered mild in this case since only small amounts of magnetite is present, less than 5% by weight. Also, it was assumed that the same amount of porosity is present in the goethite phase and the hematite/magnetite phase, which may be unrealistic, but does not prevent porosity to be evaluated in a general basis. With these assumptions, porosity can be calculated using

$$P = 1 - \frac{\rho_{Qz} V_{Qz}}{\rho_G \bar{V}_G + \rho_{HM} \bar{V}_{HM}} \left[ \frac{1}{M_{Qz}} - 1 \right] \quad (1)$$

where  $\rho_{Qz}$ ,  $\rho_G$  and  $\rho_{HM}$  are the densities of quartz 2.65 g/cm<sup>3</sup>, goethite 4.26 g/cm<sup>3</sup> and hematite/magnetite 5.2 g/cm<sup>3</sup> respectively,  $V_{Qz}$ ,  $\bar{V}_G$  and  $\bar{V}_{HM}$  are the measured volume fractions of quartz, goethite and hematite/magnetite by image analysis. The bars indicate when the measured volume includes porosity.  $M_{Qz}$  is the mass fraction of quartz from

chemical assay and  $P$  is the total porosity (micro- and macro-porosity combined). Results for the feed stream are shown in Table I, and the absolute values of porosity calculated are huge, with micro-porosities ranging from 30% to 50%. This may be the reason why direct reduction in mini-mills is becoming so popular in Brazil during the past few years.

Table I: Calculated micro-porosity from chemical and image analysis assays in hydrocyclone feed samples.

Size ( $\mu\text{m}$ )	Chemical assay			Calculated porosity		Image analysis		
	$M_{Qz}$ (%)	$M_G$ (%)	$M_{Hm}$ (%)	$P_{macro}$ (%)	$P_{micro}$ (%)	$V_{Qz}$ (%)	$V_G$ (%)	$V_{Hm}$ (%)
-53+44	14.30	18.64	67.06	0.99	36.36	16.28	24.11	59.61
-149+105	21.86	26.60	51.54	1.69	29.62	26.29	22.04	51.67
-297+210	15.60	34.67	49.73	2.78	48.63	14.23	27.92	57.85

### Liberation measurement results

Liberation of itabirite is comparatively easy, with most particles completely liberated at about 300  $\mu\text{m}$ . Unliberated particles with sizes larger than 300  $\mu\text{m}$  are mostly particles with high iron bearing minerals content, in the 90÷100% volumetric grade range. Particles of size larger than 600  $\mu\text{m}$  are almost completely unliberated. The complete process of liberation takes place on the 600  $\mu\text{m}$  to 300  $\mu\text{m}$  size range. It is believed that porosity contributes to this quick liberation process, since most macro-pores observed were in the quartz-hematite, quartz-goethite interfaces, probably and likely causing the quartz grains to liberate by detachment, which is a mode of liberation that is never observed in non-lateritic ores. Surely, this property is most advantageous to the itabirite iron industry. The overall liberation spectra for all sizes, after stereological correction, and conversion to weight fractions, in the three hydrocyclone streams is shown in Figure 4, and is represented by the symbols in the figure.

### Hydrocyclone modeling with liberation data

The separation of the feed into a high grade and a low grade product is clearly shown in Figure 4, and this is due to strong concentration effects with respect to particle density in the hydrocyclone. Plitt's model (Plitt, 1976; Flintoff et al., 1987) for the hydrocyclone is used here as implemented in MODSIM™ to simulate this operation. The underlying idea in Plitt's model is to estimate the cut size, sharpness of separation and short circuit to underflow based on the hydrocyclone geometry and the operational conditions. The required variables for Germano's hydrocyclone are listed in Table II. MODSIM™ is liberation ready and the liberation spectra per size can be entered as system data, besides flowrates, solids contents and particle size distributions. The original Plitt model, as published in 1976, embeds particle density in the calculation of the cut size  $d_{50}$ . This is shown in equation (2).

$$d_{50} = \frac{50.5 D_c^{0.46} D_i^{0.6} D_o^{1.21} e^{(0.063 - )}}{D_u^{0.71} h^{0.38} Q^{0.45} (\rho_s - \rho)^{0.5}} \quad (2)$$

In equation 2,  $Q$  is the volume flowrate of slurry in the hydrocyclone feed,  $\rho_s$  is the particle density and  $\rho$  is the density of the liquid (water). All other parameters are specified in Table II (see Plitt, 1976 for the appropriate units). In equation 2,  $d_{50}$  varies

with particle density, and the result is that a different value of  $d_{50}$  must be calculated for each particle composition, or particle type.

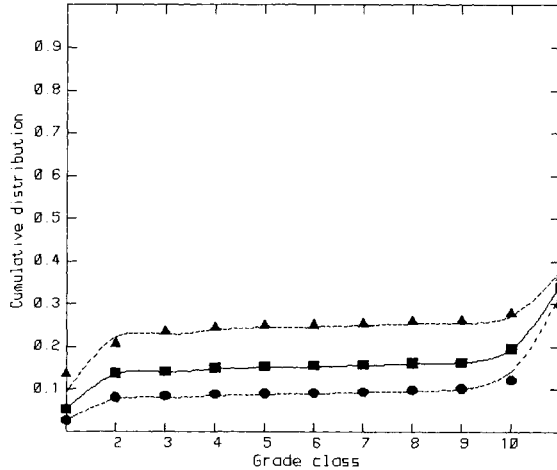


Figure 4: Measured (symbols) and calculated (lines) liberation spectra around the hydrocyclone. ■ = Feed; ▲ = Overflow; ● = Underflow.

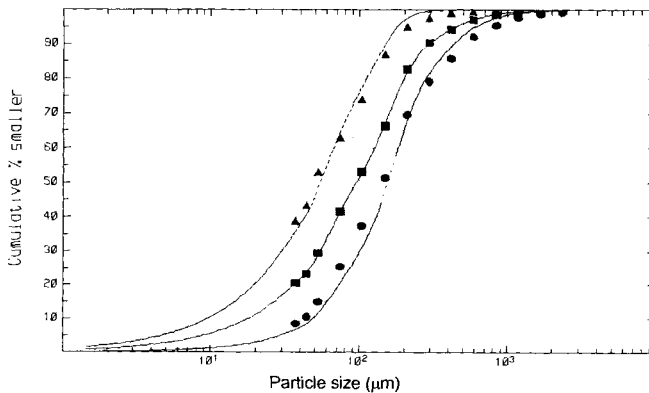


Figure 5: Measured (symbols) and calculated (lines) size distributions in the three sampled hydrocyclone streams. ■ = Feed; ▲ = Overflow; ● = Underflow.

In this work, all iron bearing minerals were considered as a single phase, with average density of  $3.5 \text{ g/cm}^3$ , which is very low when compared to that of pure hematite, but is a good estimate of bulk density based on the high values of porosity encountered in the ore characterization section. The density of pure gangue particles was taken as the density of quartz,  $2.65 \text{ g/cm}^3$ . Ten additional particle types are defined according to the measured liberation spectra, and each of these particle types have a density between  $2.65 \text{ g/cm}^3$  and  $3.5 \text{ g/cm}^3$  as defined by their composition. The problem of applying Plitt's model with liberation information is therefor straight forward, and each particle type will have a characteristic  $d_{50}$ , as calculated in equation 2. The model provides three additional

correction factors, one for the cut size, one for the sharpness of separation and one for the short-circuit to underflow.

Table II: Characteristics of the sampled hydrocyclone cluster.

Geometry		Operational	
Hydrocyclone diameter, $D_c$	0.6604 m	Solids in the feed slurry	58.65 %
Vortex finder diameter, $D_o$	0.2032 m	Solids feed rate	1,640 t/h
Inlet diameter, $D_i$	0.2540 m	Pressure drop across cyclone, $H$	0.1 MPa
Apex diameter, $D_u$	0.1143 m	Number of cyclones in cluster	6
Vortex finder - spigot distance	3.96 m		

These parameters are calculated from the experimental data, under the operational conditions that are required, using an optimization procedure. Normally, only particle size distributions in the three streams are available to estimate the correction factors. In this work, measured grade distributions must also be predicted by the model, simultaneous with the measured size distributions. The three size distributions measured are represented by the symbols in Figure 5. When calculating the correction factors, which is essentially the only modeling work that is required to simulate the hydrocyclone, a lack-of-fit is observed in both predicted size distributions and predicted grade distributions, and the lack-of-fit was particularly high in the predicted grade distributions. The model, as implemented, was clearly not capable of describing the hydrocyclone operation. However, adopting the Plitt suggestion (1976) the optimization procedure was re-implemented to calculate also the regimen exponent and the slurry density in equation (2), besides the three correction factors, to fit simultaneously the size and grade distributions measured. The resulting fit is excellent, and this is represented by the continuous lines in Figures 4 and 5. The parameters for this fit are: correction factor for  $d_{50} = 4.9067$ , correction factor for sharpness = 0.38833, correction factor for solids bypass = 0.70023 and  $d_{50}$  is proportional to:

$$d_{50} \propto (\rho_s - 2.26)^{-0.90} \quad (3)$$

showing that the regimen inside the hydrocyclone is much closer to turbulent than it is to laminar and that the slurry density in the hydrocyclone separation zone should be used instead of the density of the liquid.

## References

- Fandrich, R.G., 1998. Mineral Liberation Through Confined Bed Breakage, PhD. Thesis, Un. Queensland.
- Flintoff, B.C., Plitt, L.R. and Turak, A.A., 1987. Cyclone modeling: a review of present technology, CIMM Bull., Vol. 80, No. 905, pp. 39-50.
- Lynch, A.J., Rao, T., 1975. Modeling and Scale Up of Hydrocyclone Classifiers, Proc. 11<sup>th</sup> Int. Min. Proc. Cong., Cagliari.
- Plitt, L.R., 1976. A Mathematical Model of the Hydrocyclone Classifiers, CIMM Bull., Vol 69, No. 776, pp. 114-123.
- Sampaio, R.S., Souza Neto, A.N., Fujikawa, L.H., Garcia, L.R.A., Pereira, R.O.S. and Reis, J.A.S., 1997. Avaliação de minério de ferro para processos de redução direta em leito fluidizado, Anais do 2<sup>o</sup> Congresso Internacional de Tecnologia Metalúrgica e de Materiais, São Paulo.
- Srivastava, M.P., Pan, S.K., Prasad, N., 1999. Characterization and Processing of Iron Ore Fines of Kiriburu Deposit of India, submitted to the International Journal of Mineral Processing.

## CHEMICAL REACTIVITY OF DIFFERENT PHOSPHATE MINERALS FOR DIRECT APPLICATION AS FERTILIZERS

S.I. Mostafa, T.A. Bibawi, A. A. Yehia, I.A. Ibrahim

CMRDI, P.O. Box 87 Helwan, Cairo, Egypt

### Abstract

Characterization of different phosphates and correlation of their computed unit cell dimensions with the type of ionic substitutions were conducted. Correlation of ASI with the a-axis of synthetic apatites showed two trends for carbonate apatite and for hydroxyapatite and fluoroapatite, signifying close correlation between their chemical reactivity, crystal dimensions and type of substitution. Natural phosphates proved to be apatitic, typically francolite. Higher correlation coefficients with an a-axis of natural apatites and their concentrates were established. The ASI increased linearly with a decrease in the length of the a-axis and an increase in the degree of carbonate substitution, which is the key factor in the chemical reactivity. Higher solubility of concentrates was attributed to physical and crystallographic reasons. Statistical correlation of agronomic measures with maize plants in alluvial soil with phosphates and neutral ammonium citrate solubility endorsed the interrelation between rock reactivity and agronomic response, exhibiting good correlations between greenhouse measures and solubility. The effectiveness of the Egyptian phosphates in supplying available phosphorus depended upon the degree of carbonate substitution and the physical characteristics of the ore. Consequently, correlation between physicochemical characteristics of different phosphates and their crystallographic structures could be correlated with their natural chemical reactivity as direct fertilizers.

*Keywords: crystalline structure, phosphate, fertilizer, solubility*

### Introduction

Direct application of domestic phosphate rocks for fertilizing purposes offers the lowest cost and energy expenditure, and sensitivity to ore quality in processing raw phosphates of marginal quality, since the apatite is the reactive component. The fertilizing efficiency is influenced by the pH and the moisture of the soil, and by phosphate adsorption properties. The technology of partial acidulated-granulated phosphate rock may bridge the gap between direct application of phosphate rocks and water-soluble manufactured chemical phosphates (Lehr, 1976). Direct application of a phosphate rock was found to be technically feasible only if it is reactive enough, properly ground and is used on soils that can transform the poorly soluble phosphate rock into a more soluble one. Correlation of the effectiveness of phosphate rock for direct applications have been made with its physico-chemical properties and the nature of the soil (Khasawneh, 1978). Recent advances in understanding of apatite composition and the use of a new solubility index have clarified its role in correlation of phosphate rock reactivity with its constitution and structure. Direct application of phosphate fertilizers was limited due to the conflicting ways of expressing rock reactivity. In recognition of this problem, rock solubility was expressed in terms of the grade of apatite mineral, which is relatively constant in a given deposit, instead of

the rock grade, by the Absolute Citrate Solubility or Absolute Solubility Index, when using neutral ammonium citrate or any other extractant:

- ACS = (AOAC – soluble P<sub>2</sub>O<sub>5</sub>%) / (theoretical P<sub>2</sub>O<sub>5</sub>% of apatite);
- ASI = (solvent – soluble P<sub>2</sub>O<sub>5</sub>%) / (theoretical P<sub>2</sub>O<sub>5</sub>% of apatite).

The three solvents used, neutral ammonium citrate, citric acid and formic acid, could result in different amounts of the extracted P. This could be solved by the correlation of soluble P of certain phosphates with the unit cell dimensions of their apatites and by conversion of solubility from one solvent to another. This correlation could be used to estimate the value of a phosphate or other rock of agronomic value, from their solubility estimated by the measurement of the unit cell (McClellan, 1976).

Phosphorus reactivity depends on the crystalline structure of the apatite mineral. Francolite, in which some of phosphate ions are substituted by carbonate, has a weak structure, which enhances its reactivity for P uptake by the plant. The adverse effect of F on rock activity has been the subject of many workers (Lehr et al., 1967). A realistic measure for quantitative evaluation of phosphate rock is its reactive agronomic effectiveness, RAE (Peng, 1979). Consequently, the agronomic effectiveness of phosphate rock would increase or decrease, depending on its apatite composition and type of substitution in crystal lattice.

With the latest advancement in the accurate determinations of apatite composition, the degree of the carbonate substitution and the precise reactivity measurements, much wider use of phosphate rock is forecast (Lehr, 1976). Citrate solubility of a phosphate rock was found to be related primarily to the composition of its apatite, and this is independent of its P<sub>2</sub>O<sub>5</sub> content, particle size or surface area. That was the basis of the Absolute Citrate Solubility Index for reactivity measurements.

The main reason for using different solvents in reactivity measurements is their diverse chemical nature in the presence of soluble interferences in phosphate rocks (Soleimani, 1978). Phosphate rocks contain various accessory minerals, but little attention has been given by agronomists to their effect on rock reactivity. Inert quartz increased the solubility of P, due to its diluting effect, whereas soluble silica slightly improved it - presumably a similar effect on F as that of Al, but to a lesser extent. Ca and Mg salts in phosphate rock markedly decreased its solubility in neutral ammonium citrate (Shimshon, 1979).

This work is devoted to correlate chemical reactivity in terms of the ASI of apatite minerals with variations in their physicochemical characteristics and crystallographic structures, for selection of potentially reactive phosphate ore resources for direct application as fertilizers. Agronomic testing of natural apatites was done for a better understanding of this correlation.

### **Experimental procedures**

Characterization of apatite minerals and their computed unit cell dimensions were correlated (Mostafa, 1998). Measurements of the chemical reactivity of these phosphates were employed using neutral ammonium citrate, 2% and 4% citric acid, 2% formic acid and 2% acetic acid, according to the standard method recommended by the Association of Official Analytical Chemists, AOAC (McClellan, 1976). Neutral ammonium citrate solubility was determined by stirring a 1 g sample ground

to <200 mesh for 60 min at 65 °C in 100 ml ammonium citrate solution at pH = 7, followed by determination of P in the filtrate. Solubility measurements of citric, formic or acetic acid were conducted by stirring a mixture of 1 g sample, finely ground to <200 mesh in 100 ml of the solvent for 30 min, followed by determination of P.

The agronomic efficiency of phosphate ores and concentrates for direct application as fertilizers was investigated on one green house pot test. A study was carried out on the response of maize plant grown in an alluvial soil, which was made up of 18.8% clay, 22.3% silt and 51.9% sands at pH = 7.8. pots filled with 5 kg each of this soil and thoroughly mixed with phosphate samples were prepared before planting. Eight samples representing the various crude phosphate ores and their concentrates at 200 ppm available P were employed, in each of which 2 seeds of the maize plant were planted in 3 replicates. The yield of dry matter was determined by drying the green plant at 105 °C until constant weight was reached, and the P was determined.

## Results and discussion

### *Correlation of the reactivity of synthetic apatites with their compositions*

Absolute solubility index (ASI) of synthetic apatites in different organic solvents, after regression analysis with their unit cell a-axis and a regression equation for each, and a correlation coefficient for every apatite mineral are shown in Figure 1 and Table I. Two main trends were identified in correlation – one for carbonate apatite (CA), and one for hydroxyapatite (HA) and fluorapatite (FA).

Table I: Regression equations and maximum correlation coefficients of solubility of synthetic apatites.

Regression equation of every solvent	Correlation coefficient, r	
	CA	HA & FA
ASI (NAC) = 318.3524(9.5405 – a)	- 0.9962	-
ASI (NAC) = - 207.0545 (9.3192 – a)	-	0.9983
ASI (2% Citric) = 57.3456(10.8495 – a)	- 0.9525	-
ASI (2% Citric) = - 692.0263 (9.3468 – a)	-	0.9997
ASI (2% Acetic) = 300.4123 (9.5861 – a)	- 0.9958	-
ASI (2% Acetic) = - 416.6122 (9.3538 – a)	-	0.9965
ASI (4% Citric) = 60.1476 (10.8853 – a)	- 0.9509	-
ASI (4% Citric) = - 910.6568 (9.3411 – a)	-	0.9897

HA showed the maximum solubility, with a unit cell parameter, a-axis, of 9.431 Å higher than that of FA, due to the large ionic radius of the OH group (Le Geros, 1980). By introduction of F into the lattice, a corresponding shrinkage of the a-axis to 9.384 Å occurred, which might affect the crystallite size and morphology deteriorating the solubility of the apatite (Soleimani, 1978). The ASI of CA increases linearly with an increase in carbonate substitution (C/P ratio), a factor which was reached by many workers for synthetic and natural apatites (Young, 1975). Le Geros et al., (1967) showed that carbonate in apatite reduces the crystallite size and changes the morphology, which together with the increase in surface area, increases the solubility and dissolution rate (Soleimani, 1978). Carbonate fluorapatite (CFA) showed much less solubility than that of CA having the same C/P ratio of 10,



confirming the inhibiting effect of F. By introduction of F into the CA lattice, a contraction in the unit cell parameter occurs from a = 9.3365 Å of CA to a = 9.306 Å in CFA, which deteriorates its solubility. The lower ASI of calcined FA is ascribed to physical and crystallographic effects. Consequently, high correlation coefficients obtained with the different synthetic apatites in the different solvents signified the close correlation between the reactivity of these apatites, and their crystal dimensions and the type of substitution in the lattice.

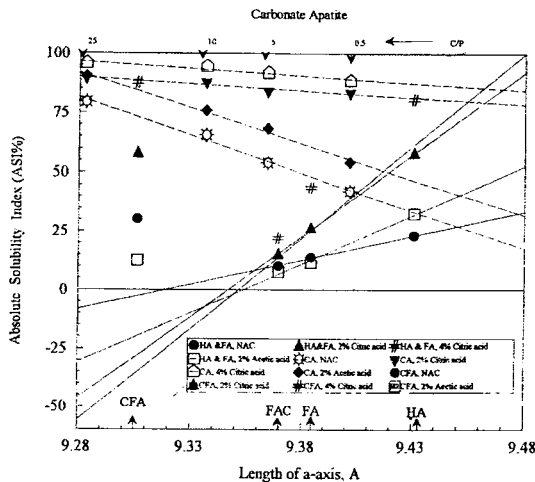


Figure 1: Variation of ASI of synthetic apatites with unit cell parameter a-axis using different organic solvents.

*Correlation of the reactivity of natural phosphates with their compositions*

In case of natural apatites, higher correlation coefficients were obtained for either original ores or concentrates (Figure 2 and 3 and Table II).

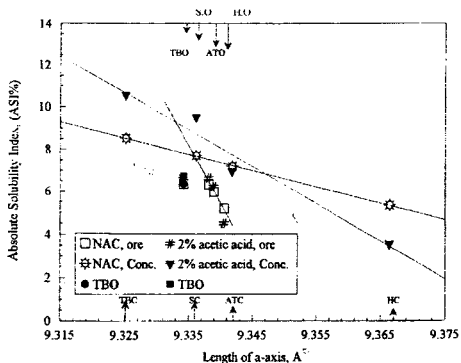


Figure 2: Variation of ASI of natural phosphates and their phosphoconcentrates with their unit cell parameter a-axis in organic solvents.

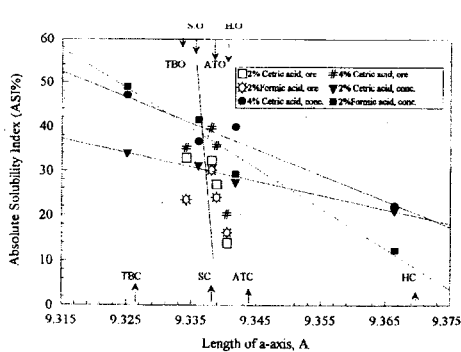


Figure 3: Variation of ASI of natural phosphates with their unit cell parameter a-axis using different organic solvents.

For every group of samples, the ASI increases linearly with the decrease in the length of a-axis, i.e. with the increase in the degree of carbonate substitution in the apatite lattice, which is the key factor in the reactivity of CA.

Higher solubility of most concentrates is attributed to both physical and crystallographic reasons, particularly due to a relative increase in  $\text{CO}_3/\text{PO}_4$  molar ratio as a result of acid leaching. The increase in surface area, coupled with the increase in  $\text{CO}_3/\text{PO}_4$  molar ratio for Hamrawein phosphate (H) and (SE) ores due to acid leaching of concentrates, led to a corresponding increase in their solubility (Table III).

Table II: Regression equations and maximum correlation coefficients of solubility of natural phosphates, and their concentrates in organic solvents.

Regression equation of every solvent	Correlation coefficient, r
ASI (NAC) = 470.1617 (9.35160 - $a_0$ ) ores without TB	- 0.9998
ASI (NAC) = 155.8693 (9.37617 - $a_0$ ) ores with TB	- 0.7769
ASI (NAC) = 77.1612 (9.43550 - $a_0$ ) concentrates	- 0.9998
ASI (2% citric acid) = 7755.74150(9.3423- $a_0$ ) ores without TB	- 0.9987
ASI (2% citric acid) = 2567.20728 (9.3483 - $a_0$ ) ores with TB	- 0.7755
ASI (2% citric acid) = 317.75820 (9.4322 - $a_0$ ) concentrates	- 0.9880
ASI (4% citric acid) = 8346.7460 (9.34299 - $a_0$ ) ores without TB	- 0.9904
ASI (4% citric acid) = 581.2500 (9.40508 - $a_0$ ) concentrates	- 0.9664
ASI (2% formic acid) = 5693.5253 (9.3433 - $a_0$ ) ores without TB	- 0.9920
ASI (2% formic acid) = 901.5956 (9.3790 - $a_0$ ) concentrates	- 0.9819

The Sebaiya East (SE) concentrate, which has the highest solubility, is characterized by substitution in the francolite lattice by many trace elements, resulting in maximum compaction in the a-axis to 9.3251 Å. Concentration leads to a change in the apatite structure or to a decrease in  $\text{CO}_3/\text{PO}_4$  molar ratio like in H. The drastic drop in the surface area from 16.9 to 2.2  $\text{m}^2/\text{g}$  with calcination results in a corresponding decrease in its reactivity. However, higher solubility of this calcine than in the original in citric acid may be due to the adverse effect of chloride ions associated with the latter regarding its behaviour in this solvent. The H ore, which has a high dolomite content in addition to quartz, iron oxide and clays, showed the lowest solubility in all solvents.

Table III: Physico-chemical properties of different phosphate ores and their concentrates, and the corresponding agronomic response of Maize plants.

Sample	Rock properties			Apatite properties				Agronomic response	
	Surf. area ( $\text{m}^2/\text{g}$ )	Tot. $\text{P}_2\text{O}_5$ (%)	a-axis (Å)	$\text{P}_2\text{O}_5$ (%)	$\text{CO}_3/\text{PO}_4$	NAC	2% citric acid	Total "P" uptake (%)	Yield (%)
H ore	16.9	23.20	9.3405	37.31	0.330	5.12	13.89	29.63	11.85
AT ore	25.3	25.90	9.3389	37.10	0.344	5.97	27.01	28.53	12.97
SE ore	16.3	24.20	9.3381	37.00	0.353	6.32	32.32	32.53	13.01
TB ore	14.4	20.30	9.3342	36.50	0.390	6.35	33.00	33.10	12.73
H calcin.	2.2	35.00	9.3664	40.99	0.076	5.34	21.15	29.96	15.77
AT conc.	27.5	30.70	9.3418	37.48	0.317	7.20	27.51	35.14	12.55
H conc.	24.5	27.80	9.3361	36.75	0.371	7.70	31.39	47.36	16.33
SE conc.	19.4	32.40	9.3251	35.43	0.480	8.52	34.10	52.45	16.92

SE and Tersobanko phosphate (TB) ores show high solubility due to the diluting effect of silica on the  $P_2O_5$  concentration of apatite, the denominator in the formula of ASI (Shimshon, 1979). The association of pyrite with the Abu Tartar phosphate (AT) (S = 2.83%) and dolomite ( $CO_2 = 6.4\%$ ) should be responsible for the relatively lower solubility. The abnormal behaviour of TB ore showing a lower correlation coefficient of ASI with a-axis may indicate the unreliability of solubility measurements due to insoluble film formation or any interference due to foreign ions, as it contains iron oxide, clay, silica, dolomite etc. Consequently, measurements of phosphate rock reactivity depending on its physico-chemical characteristics merely predict the rock's ability to supply available "P", but not the efficiency of its utilization by crops under field conditions. Therefore, they could be used as an approximate guide in ranking rocks for further testing. Thus, agronomic evaluation of the rock remains inevitable.

**Agronomic evaluation of phosphate ores and concentrates as fertilizers**

Statistical correlation of the two agronomic measures with maize plants in an alluvial soil, i.e. the P uptake and the yield of dry matter with ASI of Egyptian phosphorite samples, endorsed the interrelation between rock reactivity in terms of apatite composition and agronomic response. A high degree of correlation with the ASI of citric acid and neutral ammonium citrate has a great significance, since its values are based on apatite compositions derived from X-ray data, which shows that the release of available P is controlled primarily by the composition of its apatite component. Two straight-line correlations are identified (Figures 4 and 5) - one for phosphate ores and the other for concentrates - for each of which the increase in P uptake and yield of dry matter run parallel to the decrease in unit cell a-axis of the apatite, i.e with the increase in the  $CO_3/PO_4$  ratio. Consequently, the effectiveness of Egyptian phosphorites in supplying available P, under constant field conditions, proved to be mainly dependent on the degree of carbonate substitution and relatively on characteristics of the ore.

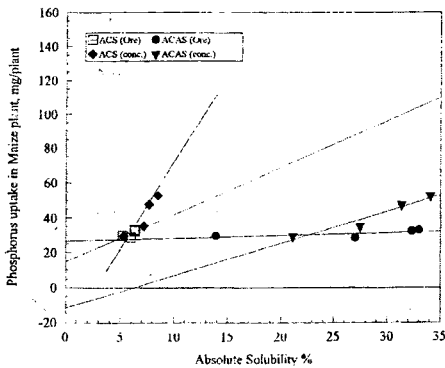


Figure 4: Correlation of "P" uptake of Maize plant for phosphate ores and their concentrates with their ASI in organic solvents.

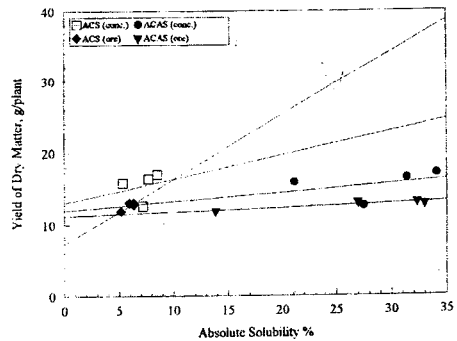


Figure 5: Correlation of the dry matter of maize plant for phosphates ores and their concentrates with their ASI in organic solvents.

**References**

- Khasawneh, F.E. and Doll, E.C., 1978. The use of phosphate rock for direct application to soils, *Adv. Agron.*, 30, 159.
- Le Geros, R.Z., Trauz, O.R., Le Geros, J.P and Klein, E, 1967. Apatite crystalites: effect of carbonate on morphology. *Science*, 155, 1409.
- Le Geros, R.Z., Taheri, M.H., Quirologico, G.B and Le Geros, J.P., 1980. Formation and stability of apatites: effects of some cationic substituents. *Proc. 2nd Int. Congress on Phosphorus Compounds*, Boston, April 21, 89.
- Lehr, J.R., 1976. Phosphate raw materials and fertilizers. *Proc. of Symposium on the Role of Phosphorus*, IFDC, TVA, Alabama, USA, 81.
- Lehr, J.R., McClellan, G.H., Smith, J.P and Frazier, A.W., 1967. Characterization of apatites in commercial phosphate rocks. *Int. Colloq. Solid Inorg. Phos.*, Toulouse, France.
- McClellan, G.H., and Gremillion, L.R., 1976. Evaluation of phosphatic raw materials. *Proc. of Symposium on the Role of Phosphorus*, IFDC, TVA, Alabama, USA, 54.
- Mostafa, S.I., Bibawy, T.A., Abdel-Khalek, N.A., and Abdel-Rahman, E.A., 1998. Characterization of different phosphate ores for direct application as fertilizers. *CIM/CMMI/MIGA*, Montreal '98 Conference, Canada.
- Peng, P. and Hammond, L.L., 1979. Ground and granulated phosphate rock for direct application. *Proc. 17th Tech. Conference*, Univ of Auckland, New Zealand, Fertilizer Manufacturer Research Meeting, Auckland Univ.
- Shimshon, A., and Dahlia, 1979. Phosphate solubility tests: interference of some accessory minerals. *G. J. Sci. Food Agric.*, 30, 153.
- Soleimani, G.B., 1978. Phosphate mineralogy with particular references to carbonate substitution. Ph.D Thesis, Univ. of Leeds, UK.
- Young, R.A., 1975. Some aspects of crystal structure modelling of biological apatites. *Colloques Internationaux C.N.R.S.*, No 230, Paris.

This Page Intentionally Left Blank

## **MINERAL LIBERATION**

This Page Intentionally Left Blank

**Poor Manganese Ore Dressing on the Basis of Mineralogical-Technological Studies**

E.L. Chanturiya, T.V. Bashlykova, N.I. Potkonen, A.R. Makavetskas

C2-1

**Prospective of Electric Impulse Processes for the Study of the Structure and Processing of Mineral Raw Materials**

A. Usov, V. Tsukerman

C2-8



This Page Intentionally Left Blank

## POOR MANGANESE ORE DRESSING ON THE BASIS OF MINERALOGICAL-TECHNOLOGICAL STUDIES

E.L. Chanturiya, T.V. Bashlykova, N.I. Potkonen, A.R. Makavetskas

Scientific Introductory Venture Centre - ESTAgeo,  
Leninsky prospekt, 4, Moscow, Russia

### Abstract

The running characteristics of poor-oxide manganese ores of the Russian deposits are investigated, by complex modern methods of research. Optical microscopy, image analysis, X-ray diffraction, electron microscopy (EPMA), routine chemical analysis, auger electron spectroscopy (AES), scanning electron microscopy (SEM), X-ray radiometric, gravitational-magnetic fractionating and other methods has been used.

There were established mineral and chemical structures of ores, including textural and structural features, and morpho-metrical and physical-mechanical characteristics of main minerals and mineral complexes, the most highly contrasting properties of divided minerals.

With the help of the obtained information, parameters are determined for the disclosure of valuable components and modes of ore preparation. Optimum depth of enrichment (optimum combination of mechanical, chemical and metallurgical limits), limits of possible technological parameters, degree of extraction of accompanying elements (nickel, cobalt, phosphorus, etc.), inevitable technological losses, and optimum sequence of technological operations are pointed out. The particularities of the methodical approach for the investigation of poor oxide manganese ores and the creation of technology for their enrichment were first found and exposed in this work. New principles of "phase technology", in combination with the principles of "non-hard technology" are offered.

Research has allowed for making prognoses regarding mineral processing of manganese ores to evaluate the expediency of their processing. It was established that in a number of cases, the manganese concentrates containing from 42% to 56% manganese, 1÷13.8% iron, and 0.07÷0.29% phosphorus can be obtained from poor-oxide manganese ores containing 14.57÷29.00% manganese, 7.10÷21.25% iron, and 0.12÷0.83% phosphorus. These concentrates are suitable for using in metallurgy, chemical industry and agriculture. Increasing the economic efficiency of processing manganese ores ensures complex use of raw material and reduces volumes of waste.

The technological schemes of the processing of ores are presented.

*Keywords: manganese, technological mineralogy, enrichment scheme*

### Introduction

In connection with the low quality of manganese ores, the problem of creating a profitable, effective technology of processing poor manganese ores in a short space of time has appeared in Russia. The base of the solution for this task is the accelerated, comprehensive, mineralogical-technological investigation of the ore (Chanturiya et al., 1995; Chanturiya et al., 1997; Chanturiya et al., 1999).

Investigation of ores is conducted with help of complex, modern methods of research: optical microscopy, optical-geometric image analysis by the computer system "Video-Master", the X-ray diffraction of method, routine chemical analysis, electron

microscopy (EPMA), Auger electron spectroscopy (AES), scanning electron microscopy (SEM), X-ray radiometry and other methods.

The obtained information is used for determination of parameters for disclosing minerals and the regimes of ore preparation, for choosing enrichment methods and their rational combination, for determination of the optimum required enrichment and maximum-possible technological indexes. In principle, it permits recommendation of an enrichment scheme and necessary technological equipment.

The two-year researches on poor oxide manganese ores (5.33÷29.79% Mn) from ten different fields have allowed for making a prognosis for the enrichment of these ores, and for evaluating the expediency of their processing. The ore characteristics, natural factors and prognosis parameters of their enrichment are determined. In Table I, some parameters for most typically investigated deposits are offered.

### **Research results**

The above-explained ores are characterized by a high content of silica, iron, and phosphorus. Sometimes, the ores have a heightened content of nickel and cobalt. As a rule, the ores in one deposit have a different texture. Such textures are: brecciated, cement, earthy, veined, kolloform, sooty texture, and more rarely, massive types.

Usually, manganese is represented by psilomelane, vernadite, lithiophorite, todorokite, rancieite, and rarely by cryptomelane, pyrolusite, braunite, manganite, and ramsdellite, in different ratios. The structure of mineral aggregates is latent-crystalline, and concentric-zonal.

Because of repeated accumulation, the manganese minerals are in close accretion with one another and with iron hydroxides (Figure 1a and 1b).

For this reason, the traditional approach to ore minerals, as for grain, is possible only in some cases. More often, it is necessary to use such a concept as "ore mineral phase", which means aggregates with close mutual germination and transitional phases of oxide minerals.

Another characteristic feature of the ore is the evolution of ore minerals in the products of weathering of different types of rocks, when quartz and clay minerals are submerged into masses of the ore substance (Figure 1a).

For this reason, it is necessary to consider ore mineral phases from the point of view of the rock-forming minerals in the ores.

Fine, mutual germination of ores and rock-forming minerals stipulates the formation of an "accretion phase" during ore disintegration, which may be represented as some part of a complex union that it is not possible to disclose in the process of grinding and that forms middlings (Figure 1-3).

It was established that in such ores, the part of the accretion phase concerned with reducing the material size remains practically on one level. This is the reason for the low quality of manganese concentrate. Part of quartz is reduced in the "accretion phase", with a decrease in the material's size from 20÷30% in the large class, - 1 + 0.5 mm, and to 10% in class - 0.1 + 0.074 mm.

Kepler analysis of the initial image (Figure 1a and 1b) allows for isolation (Figure 2a and 2b) of transitional zones between mineral aggregates (black outline) of the accretion phase. Their quantity and relatively large width (eroding of boundary

accretion) demonstrates that the structure of the ore mass is very complex and shows the invariability of the texture drawings of particles with the reduction of their size. It indicates the impossibility of selecting mineral disclosure while reducing ore size, as well as the impossibility of their mechanical separation.

Table I: Some parameters for most typically investigated deposits.

Deposit parameters	Cheboldag	Rudnoe	Sungay	Porojinskoe poor-phosphorus	Porojinskoe phosphorus
Mn content (%)	14.57	20.93	18.47	17.39	18.28
Content of some passing component (%)	Fe = 13.87 P = 0.122 SiO <sub>2</sub> = 48.01 Ni = 0.033 Co = 0.052	Fe = 21.25 P = 0.493 SiO <sub>2</sub> = 23.96 Ni = 0.028 Co = 0.042	Fe = 2.23 SiO <sub>2</sub> = 62.80 Ni = 0.069 Co = 0.07	Fe = 9.66 P = 0.166 SiO <sub>2</sub> = 33.75	Fe = 7.77 P = 0.830 SiO <sub>2</sub> = 35.00
Main ore minerals (%)	criptomelane + psilomelane(19) pyrolusite + ramsdellite (5)	criptomelane + hollandite + pyrolusite + psilomelane (38)	criptomelane(20) lithiophorite (5) psilomelane (5)	psilomelane + vernadite (25-30) pyrolusite (3-8)	psilomelane(10) pyrolusite (15) vernadite (11)
Main rock-forming minerals (%)	iron-hydroxide (22) quartz (45.5) clay (6.5) phosphate	iron-hydroxide (38) quartz (19) apatite (2)	quartz (55)	quartz (24) clay (24) iron-hydroxide (15)	quartz (24) clay (22) iron-hydroxide (13) fluorine-apatite(4)
Maximum size of ore minerals (µm)	4	44	250	30	20
Distribution of manganese in size-class +3 mm of initial ore (%)	88.24	47.57	95	62.40	73.99
Contrast coefficient of large-scale radiometric enrichment	0.37	0.48	0.20÷0.50	0.73÷0.75	0.75÷0.90
Prognosis Mn extraction/ Mn content in summary concentrate (%)	70÷75/25÷30	80÷85/30÷35	70÷75/35÷40	80÷90/30÷40	70÷80/30÷36

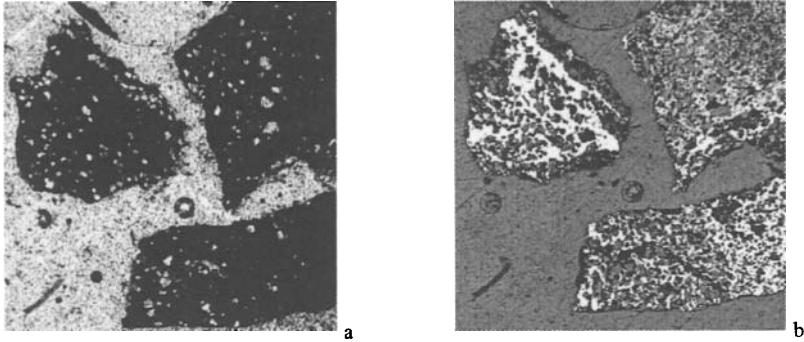


Figure 1: The initial image of mineral aggregates (size  $-1 + 0.5$  mm) in the accretion phase:

- a) light passing through: white = quartz, black = ore minerals;  
 b) reflecting light: white = manganese ore minerals, gray = iron ore minerals.

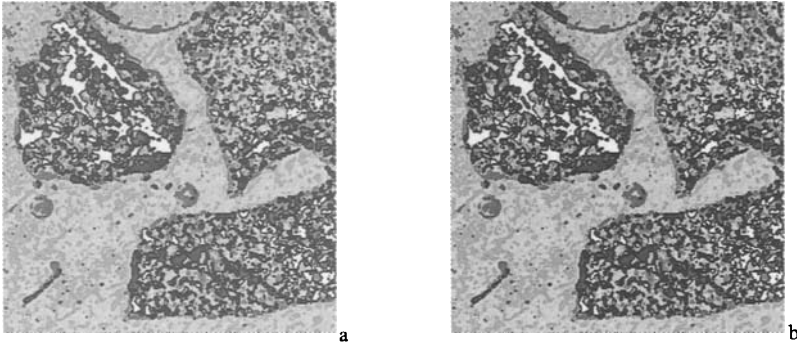


Figure 2: The results of Kepster analysis (a) and of texture-Kepster analysis (b) of the initial image of mineral aggregates (size  $-1 + 0.5$  mm) in the accretion phase:

- white = latent-crystalline ore minerals; black = noncrystalline ore minerals;  
 gray = rock-forming minerals; black line = board of germination.

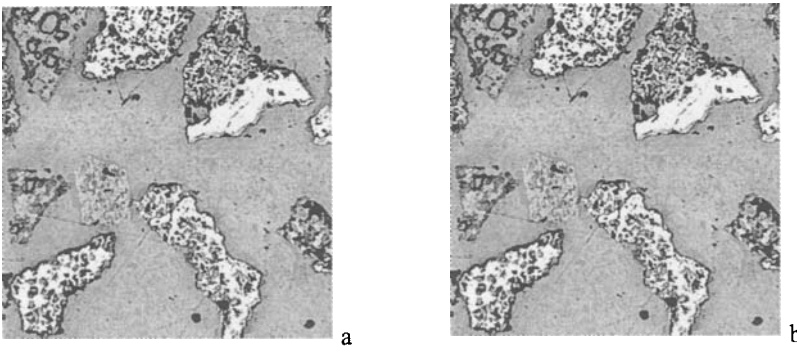


Figure 3: The results of Kepster analysis (a) and of texture-Kepster analysis (b) of the initial image of mineral aggregates (size  $-0.5 + 0.25$  mm) in the accretion phase:

- white = latent-crystalline ore minerals; black = non-crystalline ore minerals;  
 gray = rock-forming minerals; black line = board of germination.

The peculiarity of the represented ores consists of the presence in these ores of compact (heavy), sooty, and porous (light) kinds of ore mineral phases, which do not allow for isolation of a concentrate's required quality by the process of gravitation. For such a reason, it is necessary to conduct an investigation on ore materials and their enrichment in the materials of natural size to avoid the crushing and the grinding of ores. In fact all these operations promote transformation into slime of some part of the sooty mineral type of the ore phase.

For example, heterogeneity was established for the chemical composition of lithiophorite aggregates, which have a complex concentric-zonal structure. Content of  $\text{MnO}_2$  in these zones is modified from 30.7% to 44.4%,  $\text{CoO}$  from 0.4% to 1.3%,  $\text{NiO}$  from 0.00% to 0.36÷0.38%, and  $\text{Fe}_2\text{O}_3$  from 0.2% to 2.2%.

Lithiophorite zones, with the low reflection ability are characterized by maximum content of  $\text{CoO}$  (1.3%), and by increasing thickness at the rim of aggregates. Consequently, during disintegration some part of lithiophorite enriched by cobalt will become slime, lowering the extraction of cobalt.

The main rock-forming minerals of poor-oxide manganese ores are quartz, clay minerals, iron hydroxides, and phosphates.

The peculiarity of rock-forming minerals is their impregnation by hydroxides of manganese and iron. They decrease the level of contrast of the magnetic properties of manganese-containing and rock-forming phases, making its separation by magnetic methods of enrichment difficult. Iron minerals, in the majority of cases, contain phosphorus as an adsorption agent.

Of special significance is the presence of the phosphates in ores, because they are very brittle, and during crushing, they soil the surface of ore- and non-ore phases, hampering the obtaining of qualitative concentrates.

In connection with noted peculiarities of such types of ores, it is necessary to create a technological scheme, for the purpose of extracting from ores of ore mineral phases, but not from individual manganese minerals. We have named this technological principle *phase technology*.

At the level of mineralogical-technological study, it is necessary to diagnose and to determine the quantitative content of the manganese phases, which will differ in behavior from mineral processing. Determination of the content of phases, the disclosing of which is impossible, has an important significance. For example, if the yield of such a phase is significant, we have to take this phase out from the enrichment process and place it directly into hydro-metallurgical processing.

The technology scheme should provide for the enrichment of classified ores of initial size by the methods of enrichment for large-sized particles (>3 mm) and by the methods of enrichment for small-sized particles (<3 mm). Preliminary disintegration has to be conducted only with the use of washing and classification. That allows for reduction of the loss of manganese with manganese minerals that turn into slime easily and that prevail in such type of ores.

This principle is known in the practice of enrichment of manganese ores as *non-hard technology*. Combination of the principles of *phase technology* and *non-hard technology* allows for new ways of solving the problems of difficult processing for enrichment of manganese raw materials.

Specificity of poor oxide manganese ores requires using the large-size particle methods of enrichment, with minimum crushing and grinding. At present, the methods of radiometric enrichment (X-ray-radiometric separation, X-ray-luminescence separation, photometric separation and so on) are the most promising. All presented materials are well illustrated by the results for the determination of the enrichment ability of the few phosphorus ores and of the phosphor ores at the Porojinsky deposit.

It has been discovered that there are a few ore- and non-ore phases in these ores. The behavior of these phases during mineral processing is significantly different. There is a compact, massive kind of mineral of latent and weakly crystallized psilomelane and pyrolusite. It has a particle size of over 1,000  $\mu\text{m}$  and contains single fragments of siliceous tuffite and quartz (dense massive phase). There are particles of the compact-kind of manganese mineral contained in iron siliceous tuffites (*dense, spotted-vein phase*). The thickness of secant veins of manganese minerals are from 10÷20  $\mu\text{m}$  (~50%) to 100÷150  $\mu\text{m}$ . The manganese minerals appears as a light, porous and sooty kind of vernadit-psilomelane - an ore substance that is represented by fragments with a size less than 10  $\mu\text{m}$ , cemented by clay materials impregnated by ore substances (*porous-earthy, sooty*); and two non-ore mineral phases, consisting of siliceous tuffites, which differ from each other in the extent of their pigmentation by ore substances (*siliceous and pigmented*).

The presence of free-manganese mineral phases in a class of size over 1,000  $\mu\text{m}$ , and the radio-physical contrast of manganese mineral phases and rock-formed mineral phases in large pieces, determines the opportunity to successfully use radiometric enrichment for ores.

As a result of a mineralogical-technological investigation, we offered and tested the technological scheme (Figure 4), which provides for phosphorus-containing ore, besides x-ray radiometric and photometric separation, and for usage of x-ray luminescence separation for de-phosphoration of manganese concentrates, in order to isolate phosphate products.

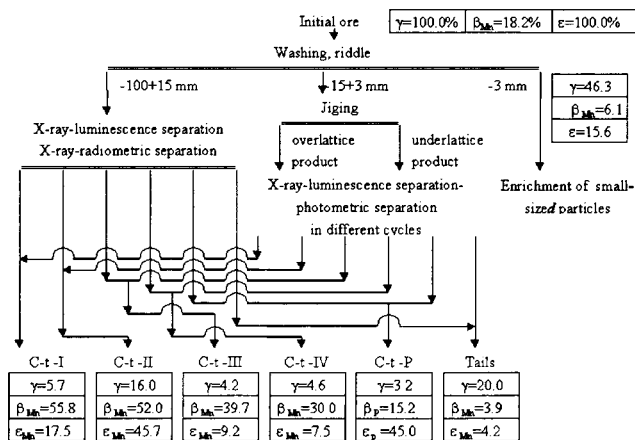


Figure 4: Principal scheme of enriched phosphorus ores of the Porojinsky deposit.

With the help of this scheme, it is possible to obtain a manganese concentrate from the poor-phosphorus ores containing 31.82% Mn, with a recovery of 83%. From the phosphorus ores, the extraction is 80% of the total concentrate, which contains 48% Mn. Phosphorus is isolated from good products containing 35% P<sub>2</sub>O<sub>5</sub>.

On the whole deposit, the average calculated indexes of enriched ores, taking into account the proportional quantity in the few phosphorus ores and phosphorus-containing ores, were as follows: the yield of the manganese concentrate was 33.6%, while the content of Mn is 43.4%, and extraction was 80.7%.

The application of the principle of phase technology allows for the transfer of the Porpjinskoe deposit from the industry category of *non-valuable* to *immediate object for assimilation*.

### Conclusions

It was established that poor manganese ores are characterized by:

- a heightened content of iron, phosphorus, and silica;
- a variety of texture within individual deposits, with earthy and sooty prevailing;
- a wide range of sizes of ore and mineral phases;
- the presence of ore mineral phases with a wide range of density;
- fine, mutual-germination of minerals;
- earthy and sooty ore mineral phases that easily turn into slime ;
- low contrast of gravitational and magnetic properties and high contrast of radio-physical properties of ore and non-ore mineral phases.

New principles of *phase technology* for enrichment, in combination with the principle of *non-hard technology*, have been presented:

- the technological process should be applied only for extraction of ore mineral phases, but not for single fragments of manganese minerals;
- preliminary ore disintegration has to take place only with usage of washing and classification;
- the technological scheme should provide the enrichment of classified ores of initial size by combining the methods of large-size pieces and small-piece enrichment;
- the most effective enrichment method of poor-oxide manganese ores is radiometric, large-piece enrichment.

### References

- Chanturiya, V.A., Bashlykova, T.V. and Chanturiya, E.L., 1995. Predictive evaluation of the dressability of gold-containing mineral resources by means of an image analysis technique (in Russian). *Gornyi zhurnal*, 11, pp.46-50 (in Russian).
- Chanturiya, V.A., Bashlykova, T.V., Chanturiya, E.L. and Amosov, R.A., 1997. Estimation of mineral and technogeneuous raw material amenability using computer image analysis systems and other modern research methods. Proceedings of the XX International Mineral Processing Congress, Aachen, Germany, V.1, pp.121-130.
- Chanturiya, E.L., Bashlykova, T.V. and Amosov, R. A., 1999. The usage of image-analysis in processing the technology of extracting gold from the tails of enrichment. Proceedings of the conference on the complex problems of remaking raw mineral materials and on environmental protection. Moscow, pp. 30-34 (in Russian).



## PROSPECTIVE OF ELECTRIC IMPULSE PROCESSES FOR THE STUDY OF THE STRUCTURE AND PROCESSING OF MINERAL RAW MATERIALS

A. Usov, V. Tsukerman

Kola Science Centre of Russian Academy of Sciences, Apatity, Russia

### Abstract

The prospective use of processes of electric impulse (EI) disintegration of materials in order to study mineral structure for beneficiation of ores, for the processing of mineral raw material, and for the processes of industrial-waste utilization are examined. The principles of EI-destruction have been briefly depicted, and a specific feature of multi-component material disintegration has been explained (a strongly expressed, selective character of destruction). This ensures a high degree of disclosure of useful mineral grains in the process of disintegration and an essential increase in extraction and in improving the quality of concentrates at the next stage of ore beneficiation.

The features and technological efficiency of EI-disintegration of various types of ores, and the spheres of effective use of the method have been determined. In particular, a part from minimizing damage, a high degree of mineral grain disclosure provides a highly effective method for implementing extraction of jewels and mica crystals for the process of artificial mica processing. The possibility of using EI-disintegration in special purposes, such as in deriving pure mono-mineral fractions of a product for geological investigations of mineral raw material, has been shown. Possibilities have been shown for using EI-technology to resolve different ecological problems, while increasing use of integrated raw mineral and industrial waste.

*Keywords: rock, ore, electrical, discharge, disintegration, selective destruction*

### Introduction

The possibilities of mechanical methods for improving destruction of rocks and ores of increased strength are largely exhausted. The process is characterized by high power consumption, and the technology is labor consuming and unproductive. The efficiency of mechanical methods of strong rock destruction has been reduced, mainly due to the low durability of tools and to the impossibility of developing large energy density on a drift, because of the existence of several intermediate cycles of energy transformation leading up to the impact on the rock.

In trying to find methods to avoid these limitations, research is being actively conducted on other physical methods of material destruction. Many new methods of destruction of solid bodies have been proposed, including those that use an explosive operation effect of electrical discharges on solid bodies. The electric impulse (EI) method of destruction belongs to this class, which with the help of high voltage impulses, is achieved by the electrical breakdown of a solid body, with following destruction by the energy of the discharge channel. This manner of material destruction was offered and carefully investigated in Russia (Vorobiev et al., 1971; Kalyatsky et al., 1980; Siomkin et al., 1995), but for some reason, it has not been well known in the West until recently.

**Mechanism of EI-destruction of solids**

The mechanism of EI-destruction of solid bodies consists of two sequential stages. In the first stage, the channel of the discharge is formed in a surface stratum of a solid body. High-voltage impulses, with duration of less than  $10^{-6}$  s are used, which allows for realizing the effect of ratio inversion of the electrical strength of solid dielectrics and liquid substances. For electro-technical devices of DC and AC current, the most general case is when the electrical strength of solid dielectrics is higher than the strength of liquid dielectrics, and to a greater degree of the electrical strength of gases. With a diminution of voltage exposure time, the electrical strength of various media is increased, but to a different degree. It is increased most of all for a liquid, and less for solid dielectrics. The consequence of this is that during the exposition of voltages less than  $10^{-6}$  s, the electrical strength of rocks becomes lower than the strength of dielectric liquids (mineral oil), and during the exposition of voltages less than  $2 \div 3 \cdot 10^{-7}$  s, it becomes lower than the strength of water.

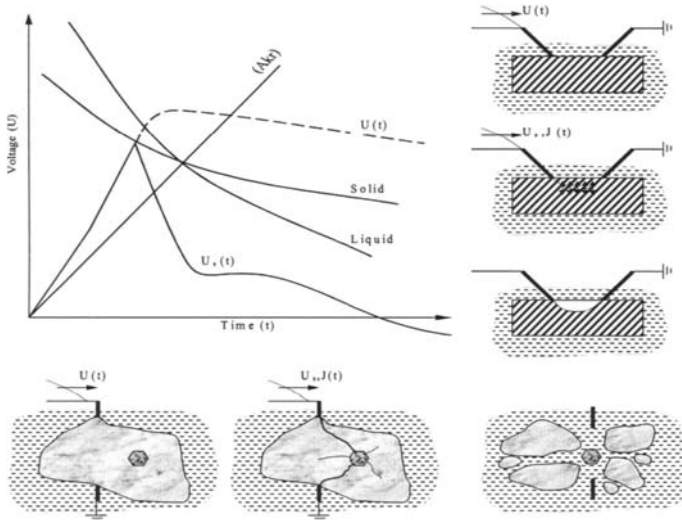


Figure 1: Principle of electric pulse destruction: comparison of volt-second characteristics of various media; consequences of the breakdown processes and destruction of the system, with one free surface; consequences of the breakdown processes and destruction of material fragments.

In Figure 1, a comparison of voltage-time characteristics in an identical discharge gap of a solid body (rock) and in liquid is schematically given. The intersection of voltage-time characteristics corresponds to the equality of strength and the equal probability of an electrical breakdown of compared substances. In the field of the diagram toward the left of intersection  $A_k$ , the electrical breakdown of a solid body predominates. The parameter  $A_k = U/t$ , for a point of equal strength, is a critical parameter for the realization of the EI-process. For impulses with a linear increase in voltage, the parameter is identical to the steepness of the impulse front and is  $200 \div 500$  kV/ $\mu$ s in the

case of breakdown in a dielectric liquid and  $2,000\div 3,000$  kV/ $\mu$ s in the case of breakdown in water.

The application of the media's electrical strength inversion to rock destruction is explained in a Figure 1. The electrodes are installed on the surface of a solid body (rock), and the impulse of voltage  $U(t)$  is sent through them. The electrical breakdown in the gap is formed inside a solid body instead of the shortest way, such as on the surface of the body. This phenomenon has been called an introduction of the discharge into a solid body. The substance surrounding the destroyed material with current from installed electrodes serves as an agent in the process to promote the electrical breakdown of the solid body, and provides the technological function of product destruction by deleting from the zone of process realization. More often, it is a liquid, but also it can be an electrically strong gas, a steam-air mixture under pressure or a vacuum.

At the second stage of the process, the energy of a capacity accumulator is exuded in the discharge channel. The fast energy input provides the hydrodynamic nature of the discharge channel extension and the origin of dynamic mechanical stresses in the solid body. Under the impact of these stresses in the material, the cracks appear and are extended, which result in destruction of the solid body. If the amount of energy is enough, a significant volume of the material (up to tens of  $\text{cm}^3$ ) is involved in the zone of destruction of the single discharge. The method allows for separation of portions of material from a massive or large block and for crushing separate pieces of material.

The electric pulse method of rock and ore destruction is deprived of many defects and limitations that are inherent to mechanical methods of material destruction. An electrical spark is a method of destruction that does not use chisel-destroying agents. The character of loading is an impulse, with a rather simple way of adjusting its parameters over a wide range. Destruction of rocks is carried out mainly at the expense of rupture and shift forces, from inside solid bodies under the impact of the discharge channel. In the process, the only kind of energy used is electrical, and its transformation to cause destruction happens with the greatest possible efficiency. It adds to this method of destruction unique features that provide high technical and economic efficiency and enable the realization of operations that cannot be realized with traditional devices.

### **Energy consumption**

The physical principles of this method provide the possibility of realizing lower energy consumption during destruction, in comparison with traditional methods. The source of loading is the discharge channel, which is in the solid body. The EI-destruction of the solid body happens due to the stress of stretching. It ensures reaching the minimal energy quantity for destruction. The dynamic character of EI-loading ensures fragile destruction of a material without any losses of energy upon plastic deformation. The method of EI-destruction is energetically as effective as rock-destructive use of explosive substances (ES). At the same time, the method is realized with extremely low indicators of energy (equivalent to small shares of ES gram's) for each breakdown. The high productivity of the process is provided by the possibility of

continuously realizing the process with the frequency of breakdown actions - up to tens of times per second. At the same time, if compared with ES, the discharge channel has the advantage that as its energy consumption is provided by a supply of energy from an outside capacity accumulator. This can be adjusted by simple methods of operation over a wide range of magnitude and time, allowing for optimal conditions of loading to achieve the required technological effect.

The important physical phenomenon of the process EI is the automatic distribution of the discharges in a mass of material particles, in such way that it allows for providing continuity of the disintegration process. Since under conditions of realizing the method, the electrical strength of the particles of a solid body is lower than the strength of a liquid medium, an electrical breakdown from all possible directions moves in a gap between electrodes, selecting the one where the solid component predominates. While with the disintegration of different aggregates of particles, the process automatically ensures selective crushing of the largest particles, with the consequential reduction of their size. During the drilling of rock surfaces, it is not required to rotate the electrode devices. It is enough to provide the contact of the tool with the surface, without applying any significant pressure. On the base of the EI-method, effective technologies have been developed for drilling bore-holes, driving tunnels, cutting slots in rock surfaces and large blocks, for aligning a surface stratum of rock or separate blocks, for disintegration of materials and for other processes. The technologies have been experienced on an industrial scale, and now they are used in the practice of scientific research (Siomkin et al., 1995).

The most positive features of the method are realized in the process of drilling and cutting of especially hard rocks and frozen ground. In comparison with mechanical methods, the electrical-impulse method demands less energy, it is more efficient and is a prospective tool for complicated working conditions in limited space, under water, etc. Detailed research has been carried out on a broad range of problems to develop the EI-material disintegration of various natures and areas of use. The electrical and power characteristics of the process, the physical basis of the selectivity of a breakdown, and destruction have been investigated; the electrical and technological means and equipment devices have been developed, the technological efficiency of disintegration of various ores and materials has been determined.

### **Electrical parameters of breakdown**

The research on electrical parameters of a breakdown shows a possibility of describing and forecasting the probability of the breakdown, and the voltage level of a breakdown, for various ores and materials. Regarding the electro-technical aspect, the process of EI-disintegration is easier than drilling slits or cutting rocks. Practically all the technological applications of the method can be realized with a voltage level of 250÷400 kV, with the use of water as an accompanying dielectric medium. Application of the rather simple schemes for generators of impulse voltages, with a correction of the impulse front, allows for receiving demands for the parameters of process realization of impulse voltage. The dominant mass of rocks, ores and artificial materials, excluding only those distinguished by entirely metal conductivity (entirely magnetic and poly-metal ores, etc.) are subjects for electrical-impulse breakdown and

destruction. Another factor, which narrows down the possibilities of the method, is connected with larger sizes of the material particles. With larger sizes of particles being less than 1-2 mm, their open electrical breakdown becomes impossible, and the process passes into an energetically unprofitable mode of destruction, at the expense of the electrical discharges in a liquid.

During the EI-disintegration of the ores, it has not been possible to achieve appreciable reduction of energy consumption, compared with mechanical methods. It is partly connected with the fact that during EI-disintegration of groups of particles, the energy losses in the liquid interlayer between them takes place. The final outcome of special research on this question concerns the area  $Q = 1 \div 50 \text{ cm}^2$ , for which the specific energy consumption is  $0.4 \div 0.05 \text{ J/cm}^2$ , that is comparable to traditional mechanical methods (Figure 2). During fragmentation of large aggregates, the decrease in specific energy consumption is quite noticeable. The possibilities of decreasing the specific energy consumption during EI-disintegration are far from being exhausted, and they are connected to the possibility of increasing the efficiency (c.u.a.) of energy transfers in a discharge circuit from an accumulator in the discharge channel. In the existing schemes of accumulation of impulses the c.u.a. does not exceed  $0.35 \div 0.4$ , and by using special plans and methods, it can be increased by 1.5-2 times.

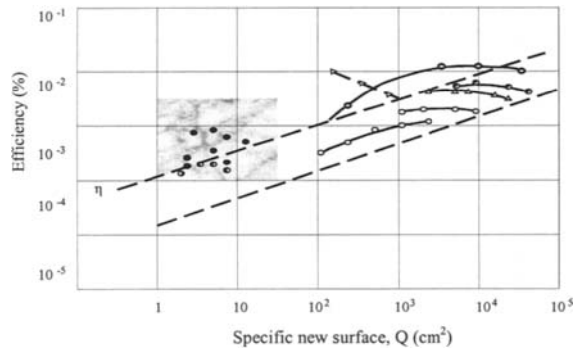


Figure 2: Efficiency of the comminution of crystal by various mechanical methods (curves) and by the EID method (dots within the square).

However, the main premise of EP-disintegration use is connected to a possibly essential increase in technological efficiency. EP-disintegration differs by the following major feature: The destruction of ores has a strongly expressed selective character. It provides a high degree of disclosure for destruction of smaller grains of useful minerals and high safety level for the natural form. This effect is exhibited to a various degree in practically all types of ore, including thin, impregnated types, and is stipulated by the following factors:

- selective direction of the discharge channel regarding inclusion of useful minerals (the inclusions are distinguished by containing rock, matrix, by electroconductivity and by dielectric permeability, and they are at the center of a local amplification of an electrical field in ore - up to triple, compared with the average strength of the digit gap);

- selective electrical breakdown and destruction of a component having lower electrical strength, most often containing rock (the most vivid example of this is in ore with crystals of mica);
- weakening of grains of minerals along the boundaries of their contact with one another, or containing rock under the impact of a highly intense presser wave system (it is especially strongly expressed in cases when the minerals differ on deformation and acoustic properties).

The higher degree of useful mineral grain disclosure, compared with traditional methods, provides the EI-disintegration in the following stage, enrichment of essential ores for an increase in extraction and an improvement in the quality of concentrates.

### **Devices and plants**

The devices of electrical impulse disintegration are proposed for an initially large size, up to 300÷400 mm, at most. This allows for selection from ores of large sizes up to 100 mm, with minimum crystal damage of minerals. During the disintegration of the material, up to 1÷2 mm are effectively opened and selected in a concentrate of the mineral grain, with sizes of inclusion above 0.1÷0.2 mm. Electrical discharge disintegration, as a combination of the EI-process and the consequent effect of the electrical discharges in a liquid is capable of opening inclusions with sizes up to 1 µm. A number of plants have been developed and tested, including 4<sup>th</sup> stage plants for processing raw material with minerals of jewels, plants for selection of mica from rocks, and plants for processing the merging of artificial mica. The compacting plant has been created for geological research (for the study of mineral raw material and for deriving mono-mineral factions).

The high level of safety and useful destruction makes electric impulse destruction especially effective for extraction of large rocks, especially of valuable crystals of minerals such as jewels, crystals of mica, asbestos, and pyeozquartz.

A comparison has been made with a precise manual disclosure of mica aggregates of the technological efficiency of EI-disintegration (Mammsko-Tchuiskeye deposit, East Siberia, Russia). A comparison has been made as well of the output and group structure of the disintegration product and the output of an industrial product at the next stage of processing an intermediate raw product phase (Usov and Rakayev, 1989). The EI-disintegration of mica aggregates in the stage from 250 mm up to 50 mm, by the output of the raw phase, is almost the same as the precise manual disclosure of aggregates, while the existing technology of aggregate disclosure in mechanical crush-machines, in comparison with manual disclosure, produces outcomes 1.2÷1.3 times longer. The main strong-point of the EI-disclosure of the accrete is the high safety of the crystals of mica. Large crystals (more than 50 cm<sup>2</sup>) are saved in a time that is 3÷4 times longer than the manual disclosure, which, in terms of cost, corresponds to an increase in mica output of 20÷25%. Output of small sized mica (>5 mm), as the base mass of the chosen mica, is increased more than 2 times. The intermediate product of the EI-disclosure contains considerably less material of the matrix: frequently, even small mineral inclusions inside crystals can be crumbled out. As a consequence of this, the output of industrial production from an intermediate by EP-disclosure is higher than 47.4%, against 44.3%. Damage of

crystals is practically not observed. On the surface, slices of crystals, traces of electrical categories that look like branching tracks of a depth no more than  $0.1\div 0.2$  mm and measuring up to  $1\div 3$  cm<sup>2</sup> are sometimes visible. The amount of such material totals no more than 1%. It is necessary to note that the depth of damage of the surface stratum from the electrical breakdown is less than from mechanical effects. It is essential less than that, where according to the technology of processing of an intermediate product in an industrial product extracted from crystals in the form of defective material with scratches, cracks, clips and etc., it is also on the average  $1\div 3$  mm. Modifications of mechanical and electrical properties of muscovite under the influence of electrical discharges have not been revealed. The technology of merging processing (a diameter of  $600\div 900$  mm) of artificial mica fluorine-flogipide has been developed. During comparison testing of the method with the technology of processing, which is applied by the enterprise-manufacturer (Alexandrov, Russia), the output of an industrial product (selections of mica) by EI-disintegration of merging, appears 1.3 times higher.

The EI-disintegration use for extraction of jewels is especially effective. In traditional industrial conditions, the selection of stones from radically productive rocks is carried out manually by the processing of pieces of ore in which most often, crystals are revealed visually, or which are chosen on certain indications. Such a method of extraction is expensive and labor consuming and can not be done without essential losses to selected valuable raw materials. During subdivision of rocks in mechanical crushing-machines, the significant part of valuable raw material is destroyed. With various ores (with crystals of emeralds, diamonds, rubies, spinals, garnets) a comparison of the EI-disclosure of rocks has been conducted with careful manual processing (Kurets et al., 1989). The extraction of crystals by the EI-disclosure is increased by  $1.5\div 2$  times with greater safety from destruction.

The technological tests on various poly-metal ores have shown the possibility that the EI-disintegration is the most efficient process for disclosure of useful minerals in all types of ores (Shuloyakov et al., 1995). The technological and economic efficiency of method implementation is highest for ores that are hard to reach, with rather low extraction by existing methods. The increase in extraction, in this case, can reach several percent. As a rule, the disclosure of mineral grains happens in earlier stages of material refinement than during mechanical refinement, and with less damage to a refinement product. It allows for simplifying the process of ore preparation and for reducing the power expeditors. EI-disintegration is the most effective method for deriving a mono-mineral faction of a product from a poly-mineral and from mono-mineral raw material. The branch of harmful impurities (biotite, garnets, iron oxides) happens more effectively and at early stages of refinement in comparison to a mechanical method. EI-disintegration of materials just for the purpose of reducing the sizes of particles energetically is unprofitable, but it can be justified if special requests are presented concerning cleanness, the form of particles, or the granule-metric structure of a product of refinement.

Since the working tool during the electric pulse destruction is the spark, there are no problems with contamination of the refinement product by instrument metal or material of growing shallow bodies, that is peculiar to mechanical methods of a

refinement of materials. Therefore, electrical pulse refinement of highly abrasive materials, especially clean materials is preferable to mechanical refinement. The possibility of the EP-method changing a character of dynamic loading simply and over a wide range allows for regulating the granule-metric structure of the refinement product to receive a narrower class of large products than is possible by mechanical refinement. For example, it is of interest for the technology of deriving quartz glass. Production of electrical impulse refinement is characterized by the large specific surface of grains and larger correspondence of open particles of mineral inclusions, compared to their initial natural condition in rock (morphology). These properties of the crushed material can strongly determine the quality of a product, for example, the luminosity of luminophors, and the reactionary ability in a hydro-metallurgical process, in a concrete mixture etc. The product of electrical pulse refinement better saves (transmits, reflects) mineralogical and pictorial/graphical features of rock, and therefore the reliability of the interpretation of the geological process is higher.

### Conclusions

EI-technologies open additional possibilities for a solution to ecological problems, with an increase in an integrated approach to raw mineral use and industrial waste use. An example of the realization of these possibilities is utilization of sub-standard ferro-concrete items (Zinovyev, 1989). The objects of destruction are the sub-standard ferro-concrete items (the rejects of production or boards that are out of operation). The purpose of their destruction is for utilization in reinforcing metal and concrete. Experimental works on the destruction of ferro-concrete items have shown that the conditions of reinforcement after extraction allow for reuse for specific purposes. After additional refinement, the concrete also can be used for various purposes, for example, as a component for road covers. The utilization of ferro-concrete pylons in electrical power line constructions, and also various electro-technical items (for example, insulators) and electronic breakers containing precious metals can be realized in the same way.

### References

- Kalyatsky, I.I., Kurets, V.I., Finkelstein, G.A. and Tsukerman, V.A., 1980. The principle of electric pulse disintegration and prospects for its application in industry. *Obogashcheniye Rud*, 1, 6-11 (in Russian).
- Kurets, V.I., Usov, A. F., Finkelstein, G.A. et al., 1989. A packaged facility for disintegration and extraction of diamond-cut crystal raw materials from productive bed rock. *Obogashcheniye Rud*, 4, 40-41 (in Russian).
- Siomkin, B.V., Usov, A.F. and Kurets, V.I., 1995. The principle of electric pulse destruction of materials. KSC RAS, Apatity (in Russian).
- Usov, A.F. and Rakayev, A.I., 1989. Electric pulse crushing and weakening of ores and other materials. *Obogashcheniye Rud*, 4, 42-43 (in Russian).
- Shuloyakov, A.D., Finkelstein, G.A., Tsukerman, V.A. and Kurets V.I., 1995. Electric pulse disintegration as the most efficient method for selective destruction of minerals. *Proceedings of the XIX Int. Min. Proc. Congr., San-Francisco, USA*, 147-150.
- Vorobiev, A.A., Vorobiev, G.A., Zavadovskaya, E.K. et al., 1971. Impulse breakdown and destruction of dielectrics and rocks. TGU Publishing house, Tomsk (in Russian).
- Zinovyev, N.T., 1989. Electric pulse fracture of sub-standard concrete. *Obogashcheniye Rud*, 4, 43-45 (in Russian).



This Page Intentionally Left Blank

# **PROCESS SIMULATION AND CONTROL**

This Page Intentionally Left Blank

<b>Pulp-Froth Interface Control in the Flotation Column</b> A.C. Maffei, I.L. de Oliveira Luz	C3-1
<b>Acoustic Emissions from the Impact of Particles and their Application to On-Line Monitoring for Zirconia Micro-Agglomerate Production in Liquids</b> T. Hirajima, M. Tsunekawa	C3-8
<b>Strategies for Fuzzy Control of a Water/Air Column</b> M.T. Carvalho, F. Durão	C3-17
<b>Improving Controllability on Flotation Columns</b> L.G. Bergh, J.B. Yianatos	C3-24
<b>Cost Cutting in Optimizing a Flotation Unit by Use of Statistical Methods</b> H.-C. Haarmann, R. Janitschek, E. Beeker	C3-32
<b>Validation of the Discrete Element Method (DEM) by Comparing Predicted Load Behaviour of a Grinding Mill with Measured Data</b> M.H. Moys, M.A. van Nierop, J.C. van Tonder, G. Glover	C3-39
<b>Design and Implementation of an On-Line Optimizing Control System for Processing the Sadiola Hill Oxidised Gold Ore</b> T. Mulpeter, O. Guyot	C3-45
<b>On-Line Prediction of Transient Phenomena in the Slag Phase during Ilmenite Smelting</b> J.J. Eksteen, M.A. Reuter	C3-55
<b>The Uniform Description of Mineral Processes by Methods of Compound Distributions of Material Features</b> T. Tumidajski	C3-65
<b>Arma Type Model for Copper Ore Flotation</b> K. Trybalski, J. Ciepły	C3-72

This Page Intentionally Left Blank

## PULP-FROTH INTERFACE CONTROL IN THE FLOTATION COLUMN

A.C. Maffei\*, I.L. de Oliveira Luz<sup>o</sup>

\*Fundação Centro Tecnológico de Minas Gerais / CETEC, Av. José Cândido da  
Silveira, 2000, Horto, CEP 31170-000, Belo Horizonte, MG, Brasil

Tel: +5521 489 2363 - e-mail: maffei@cetec.br

<sup>o</sup>RECIL Representações e Consultoria Industrial Ltda, Rua Bambuí, 448, Conj. 302,  
CEP 30310-320, Belo Horizonte, MG, Brasil  
e-mail: ivanluz@microplanet.com.br

### Abstract

Considering the available alternatives for automation of the operation and control of the pulp-froth interface, and aiming at its stabilization, as well as the accomplishment of scale-up parameters, CETEC (Technological Center of Minas Gerais Foundation), located in Belo Horizonte/Minas Gerais/Brazil, developed a computer-control system to vary the pulp-froth interface by varying the flow of non-floated fraction. The chosen alternative to control the flotation column operation aimed to render available an installation, in pilot plant scale, endowed with a control system with faster response and lower cost, compared to what is currently available on the market. In the system which is already in operation, and whose results will be presented here, FIELDBUS technology was used. Besides allowing further implementation of measurements and flow control at a distance, the system presents the basic characteristics of a "network architecture" and has as its main advantages: low installation cost, simple maintenance procedures, options to upgrade, information for quality control, and compatibility with equipment of various manufacturers.

*Keywords: flotation, interface, pilot plant, communication, FIELDBUS*

### Introduction

This paper presents an instrumentation of a flotation column system for process control using digital FIELDBUS communication. The pressure transmitters work with FIELDBUS converters for an intensity of current of 4 mA to 20 mA, which renders possible the link between the conventional part of the pilot plant, the frequency inverters, and the transmitters.

A simple interface connects the field instruments to a Pentium II 300 PC, which contains a software configuration for maintenance and supervision of the system. The more complex system depends on a power intelligent board that executes advanced controls and mathematics functions. This system also includes isolated safety barriers, FIELDBUS feed power, impedance controller and FIELDBUS terminator. The large amount of functional blocks and available mathematical controls in this system provides for engineering processes and a large capacity control. The protocol opened leads entirely to a real open solution that permits the use of the software and hardware of several producers at any time.

This project is in accordance with the ISO/OSI model and the connections are executed by a normal industrial cable. The equipments provide an intrinsic security

for dangerous atmosphere and variables are identified by expressing tags in the engineering units. Functional blocks with input and output standardized parameters, configuration and known algorithm, indicate the variable conditions.

### **Objectives**

The goal is to develop an instrumentation in order to reach complete flotation column process control using digital communication. The flotation column automatization makes for easier control of the pilot plant performance. This automatic system makes it possible to collect all technical parameters in order to make the scale-up of the flotation column.

### **Characterization of the components**

The FIELDBUS net of the flotation column pilot plant in CETEC consists of six pressure transmitters bus powered type, two converters of current to FIELDBUS, four frequency inverters, one feed power, one impedance for FIELDBUS feed power, two terminators and one PCI board.

The AIMAX supervisor program is used and SYSCON is used to configure the system giving a software tool whose requirements consist in:

- hardware: PC Pentium II 300 or similar; Microsoft mouse or similar; 8 MB of RAM; 4 MB of hard disk space; VGA monitor (16 colors) with high resolution or a SVGA monitor is recommended; 3½" floppy-disk drive, 1.44 MB; interface FIELDBUS of SMAR: BC1 (converter FIELDBUS-EIA-232-R) or PCI (Interface of the Process Control),
- software: AIMAX supervisor and SYSCON configuration system work in Microsoft Windows 3.1 or Windows 95 platform, as an application of 16 bits.
- pressure FIELDBUS transmitters: model LD302D21Z-001Z-00-2D/I1; capacitance type (capacitance cell); calibration: 0.0000 to 15.0000 and 0.0000 to 50.0000 kPa; range: 5 inch to 200 inch of H<sub>2</sub>O; material of diaphragm/fluid of filling: inox 316L/silicone; without adaptation body; place of indication: digital; without process connection; electrical connection: ½"-14 NPT; without support; installation: directly to the equipment body; precision: ± 0.07, 5% of span.
- PCI = Interface Process Control: interface FIELDBUS of high performance; multi-canal; ISA card of 16 bits; CPU RISC de 32 bits c/04 channel master FIELDBUS H1 (31.25 Kbps).
- BT302 = FIELDBUS terminator: maximum operation tension: 35 Vdc; impedance of the entrance: 100 Ω±2%@7, 8 KHz.
- PS302 = feed power to FIELDBUS: entrance: AC = 90 a 260 Vac to 47 a 440 Hz; maximum power: 45 Watts; DC:127 to 367 Vdc; exit: tension of 24 Vdc ± 1%; electrical current: 0 to 1.5 A.
- PSI = impedance to the feed of FIELDBUS: feed tension: 24 to 32 Vdc ± 10%; outside electrical current (max.): 340 mA; normal dissipated power: 2.5 Watts @ 24 Vdc (max).

### **The project and its configuration**

Table I synthesizes the main parameters of the process control.

Table I: Flotation column process control.

Item	Parameter discrimination	Symbol	Range	Unit
1	Froth layer height in the column	L	0.0 to 100.0	cm
2	Air flow rate	$Q_g$	4.6 to 13.8	l/min
3	Air superficial velocity	$J_g$	1.0 to 3.0	cm/s
4	Pulp volume of tailings	$Q_t$	100.0 to 2,500.0	ml/min
5	Pulp mass of the feed	$F_m$	100.0 to 3,750.0	g/min
6	Pulp mass of tailings	$F_t$	100.0 to 3,750.0	g/min
7	Mass of ore feed	$M_f$	0.0 to 2,250.0	g/min
8	Mass of tailings	$M_t$	0.0 to 2,250.0	g/min
9	Water weight in the feed	$W_f$	0.0 to 1,500.0	g/min
10	Water weight in the tailings	$W_t$	0.0 to 1,500.0	g/min
11	Clean water flow rate	$W_c$	0.0 to 500.0	ml/min

### Equations of net control configuration of the flotation column

For each one of the three flotation columns, the mathematical algorithms were used to calculate the operational variables:

- Equation to control the froth level, i.e., the pulp froth interface of the flotation column, was cited by Yichausti et al. (1988):

$$L_{cm} = \frac{P_1 \cdot H_2 - P_2 \cdot H_1}{P_1 - P_2 + (H_2 - H_1) \cdot g \cdot 10^{-4} \rho_e} \quad (1)$$

The specification of each variable is presented in Table II;  $\rho_e$  means froth density varies from 0,2 g/cm<sup>3</sup> to 0,3 g/cm<sup>3</sup>.

- Equation to monitor air density (Holdup) in the flotation column was cited by Yianatos and Finch (1990):

$$Eg(\%) = \left( 1 - \frac{P_2 - P_1}{\rho_t \cdot g \cdot (H_2 - H_1) \cdot 10^{-4}} \right) \cdot 10 \quad (2)$$

$\rho_t$  means pulp tailing density.

- Equation of pulp feed flow rate of the flotation column:

$$Q_f = 24.0 \cdot Q(\%), \quad (3)$$

range from 100.0 l/h to 2,500.0 l/h.

- Equation of pulp tailing flow rate of the flotation column:

$$Q_t = 24.0 \cdot Q(\%), \quad (4)$$

range from 100.0 l/h to 2,500.0 l/h.

- Equation of pulp mass in the feed of the flotation column:

$$M_f = Q_f \rho_f, \quad (5)$$

range from 100. 0 to 3,750.0 kg/h.

- Equation of pulp mass tailing of the flotation column:

$$M_t = Q_t \rho_t, \quad (6)$$

in kg/h;  $\rho_t$  in g/cm<sup>3</sup>, varies from 1.0 to 1.5.

- Equation of ore mass flow rate in the feed of the flotation column:

$$M_o = M_f \delta(\%), \quad (7)$$

in kg/h;  $\delta(\%)$  varies from 0% to 60%.



- Equation of water mass flow rate in the feed of the flotation column:

$$M_w = M_f \times (100 - \delta_{(\%)}) \quad (8)$$

in l/h;  $\delta_{(\%)}$  varies from 0 to 60%.

- Equation of pulp mass tailing flow rate in the flotation column:

$$M_t = Q_t \times \rho_t \quad (9)$$

range 100 to 3.750 kg/h;  $\rho_t$  in  $\text{g/cm}^3$  varies from 1.0 to 1.5.

- Equation of ore mass flow rate in the tailing of the flotation column:

$$M_o = M_f \times \delta_{(\%)}, \quad (10)$$

in kg/h;  $\delta_{(\%)}$  varies from 0 to 60%.

- Equation of water mass flow rate in the tailing of the flotation column:

$$W_t = M_o \times (100 - \delta_{(\%)}) \quad (11)$$

in l/h;  $\delta_{(\%)}$  varies from 0 to 60%.

- Bias

Bias is a parameter which refers to the relationship between the water flow in the feed and in the tailings of the flotation column, such as:

$$\text{Bias} = \frac{W_f}{w_t}, \quad (12)$$

When the bias is greater than 1, this means that the water flow rate inside the flotation column is ascendant, otherwise, descendant.

### **General aspects of the CETEC's pilot plant flotation column using FIELDBUS technology**

The researchers of the CETEC's Mineral Technology Sector trying for complete control of the operation of three flotation columns decided to use a FIELDBUS system of industrial instrumentation produced by SMAR. This system is very well adapted to the exigencies of the development technology concentration project.

FIELDBUS system consists of data transmission network to communicate with instrumentation equipments and pilot plant control, such as: transmitters, makers and controllers. It's a digital network because it transmits information by messages according to defined communication layers with the protocol FIELDBUS system; serial because its information is transmitted and received bit to bit; half-duplex because the communication is bi-directional, therefore only in one direction at a time and multidrop because it permits communication among several linked equipment in the network. These can be or not be bus powered type, in other words, they can or cannot be fed by the network communication system. Subsequently, in the FIELDBUS network for bus powered equipment, the communication and feed distribution networks converge to only a unique interlaced pair. In this case, the FIELDBUS network must provide current and continuous tension with the necessary power to feed the equipment and permit the communication signals to overcome the DC feed level.

The model LD302 FIELDBUS pressure transmitters, two in each flotation column at different heights, are responsible for reading the pressure values, inside of each

column, at the point where they are attached. These translate the pressure value to FIELDBUS signs.

This data is used in algorithms for the PCI board (Process Interface Control), that is, a high performance FIELDBUS interface which combines advanced process control with multi-channel communication management. This PCI board is capable of manipulating several complex functional blocks which are responsible for the execution of programmed algorithms.

These algorithms receive as data input the pressure values read by the LD302 pressure transmitters, flotation column feed values, and other data, such as pulp density and the data collected by the AIMAX supervisory program. The output values from these algorithms are sent to the two FI302 model FIELDBUS current converters, which transform the exit algorithm signals to the 4 mA to 20 mA current signal.

Each FI302 converter is capable of communicating with up to three VF-S7 Toshiba frequency inverters which control the pulp flow rate pumps of the feed flotation columns and air flow rate entrance valves in each column. In this way, these algorithms are capable of controlling the pulp-froth interface, the flotation columns feed, the column holdup monitoring, the bubble diameters, carrier capacity of the bubbles, transportation capacity, bias velocity, etc.

SYSCON is the software used for the configuration of this system. It guides all algorithms safely and easily. SYSCON also has the responsibility of all the network instruments used in this system.

The interface between the FIELDBUS network and its pilot plant operator is made by the AIMAX supervisory system. Through this system, the operator is capable not only of doing his work, but also of determining the best operational conditions, by using the right process variables, whereby he can observe graphical analyses of the operational stability conditions of each column individually or in group.

### Results of the pilot plant test using this system

The results are shown in Table II and in Figures 1 and 2. The Table II shows the operational data of the company MANNESMANN MINERAÇÃO, an iron ore pilot plant. Figure 1 shows all the flotation column variables used to obtain the mass and metallurgical balances of Figure 2.

Table II: Operational parameters of the system

Operational parameters	Unit	Rougher	Cleaner	Recleaner
$P_1$ = Superior pressure transmitter	(kPa)	10.34	15.83	6.56
$P_2$ = Inferior pressure transmitter	(kPa)	31.32	25.00	44.39
$H_1$ = Height of the superior transmitter	(cm)	139.09	144.92	135.41
$H_2$ = Depth of inferior transmitter	(cm)	331.27	215.49	335.25
$(H_2 - H_1)$	(cm)	192.18	70.57	199.84
$g$ = Gravity acceleration	( $\text{cm/s}^2$ )	980.6	980.6	980.6
$D_e$ = Froth density	( $\text{g/cm}^3$ )	0.3	0.2	0.2
$D_r$ = Non floated density	( $\text{g/cm}^3$ )	5.2	5.2	5.1
Froth layer height in the column	(cm)	60.0	27.2	19.0
$E_g$ = Gas holdup	(%)	21.2	17.2	16.0

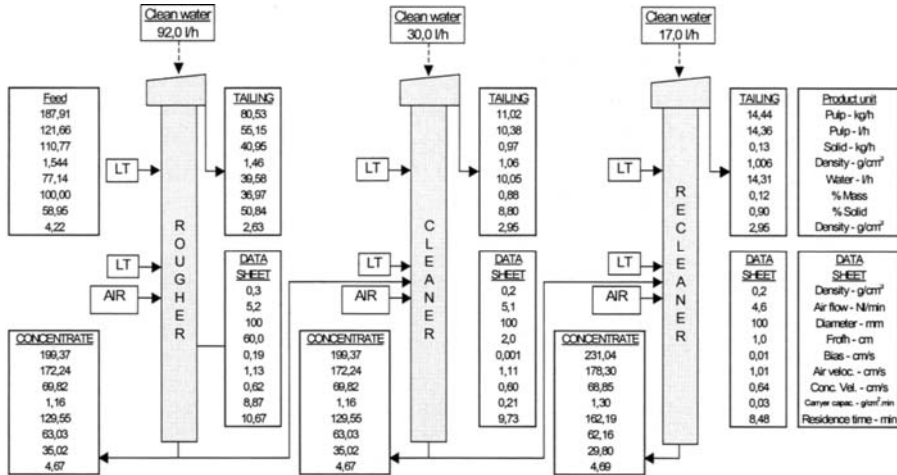
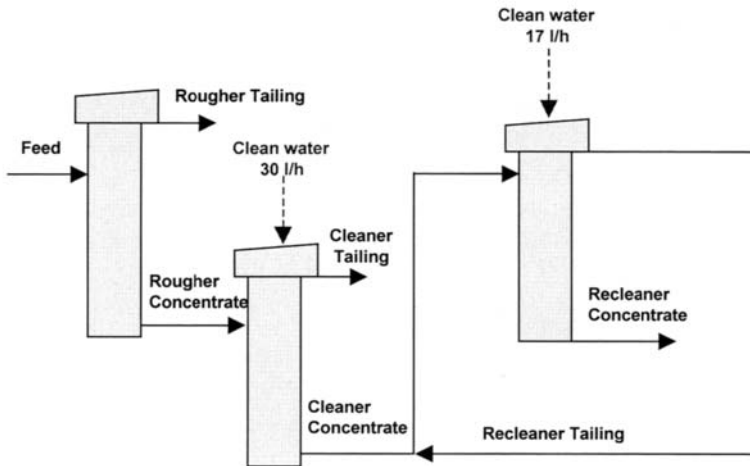


Figure 1: Flotation column operational variables of the FIELD BUS system.



Products	Flow rate		Grade (%)				Recovery (%)		
	(kg/h)	(%)	Fe	SiO <sub>2</sub>	Al <sub>2</sub> O <sub>3</sub>	P	P.F.	Fe	SiO <sub>2</sub>
Column rougher-feed	110.77	100.00	47.06	29.66	0.92	0.0404	2.16	100.00	100.00
Rougher concentrate	69.82	63.03	66.10	1.31	0.98	0.0583	3.01	88.53	2.78
Rougher tailing	40.95	36.97	14.60	78.00	0.83	0.0100	0.70	11.47	97.22
Cleaner concentrate	68.85	62.16	66.10	1.30	0.97	0.0485	3.00	87.30	2.72
Cleaner tailing	0.97	0.88	58.60	10.90	2.03	0.0481	2.74	1.09	0.32
Recleaner concentrate	68.85	62.16	66.10	1.28	0.96	0.0479	3.00	87.30	2.68
Recleaner tailing	0.13	0.12	61.80	25.50	1.78	0.0479	3.89	0.15	0.10

Starch: Rougher column - 378.1 g/t. Amine: rougher column - 55.6 g/t; cleaner column - 12.4 g/t.

Figure 2: Mass and metallurgical balance of the Mannesmann project.

**Conclusions**

The use of this system makes possible the automation of the pulp-froth interface control, and holdup monitoring, to obtain the correct and necessary scale-up parameters. Its main advantages are low-cost operation, simple maintenance procedures, options to upgrade information for quality control, and compatibility with equipments of various producers.

**References**

- Yianatos, J. B. and Finch, J. A., 1990. Gas holdup versus gas rate in the bubbly regime. *International Journal of Mineral Processing*, 29, 141-146.
- Yichausti, R. A., McKay, J. D. and Foot, D.G., 1988. Column flotation parameters; their effects. *Column flotation 88*, Chapter 17.

## ACOUSTIC EMISSIONS FROM THE IMPACT OF PARTICLES AND THEIR APPLICATION TO ON-LINE MONITORING FOR ZIRCONIA MICRO-AGGLOMERATE PRODUCTION IN LIQUIDS

T. Hirajima, M. Tsunekawa

Graduate School of Engineering, Hokkaido University, Sapporo, Japan

### Abstract

Fundamental studies of the mechanism of noise generation, i.e. continuous acoustic signals, were performed by analyzing the noise and burst acoustic signals emitted by the impact of particles on a plate or generated by particles suspended in liquid and agitated in a vessel. High-frequency noise signals exhibited characteristic changes relative to the size and number of particles. An increase in the size or in the number of particles increased the event rate, energy rate, oscillation rate, and frequency power spectra. The fundamental frequencies of vibration were estimated. The calculated frequencies of vibration arising from particle-plate impacts were in good agreement with the measured frequencies. An empirical relation between relative energy of the noise and the diameter and number of particles was also derived. Techniques of agglomeration in liquids were used to produce zirconia microspheres with diameters less than 500  $\mu\text{m}$ . A monitoring system that utilizes changes in turbidity of suspension and noise emitted during the process of agglomeration was developed to repeatedly produce agglomerates with desired properties. The technical feasibility of the on-line monitoring of the agglomerate diameter and recovery was demonstrated by measuring relative energy and laser attenuation.

*Keywords: acoustic emission, on-line monitoring, impact, agglomeration, noise*

### Introduction

Several investigators have used noise or acoustical signals for the determination of particle size or monitoring some processes in powder technology. Leach et al. (1977) utilized the sound originating from the elastic collision of rigid particles for determining the particle size and size distribution. The frequencies of interest were in the range of 50–200 kHz. Wakimoto et al. (1980) reported the application of noise measurements for monitoring the coating process of pharmaceutical products. They used the results of low-frequency amplitude analysis to describe the degree of coating. The acoustic emission (AE) technique was used by Hidaka et al. (1989) to monitor the compaction process of a powder bed. They related the AE count rate and high-frequency components of the AE waves to powder properties and compression conditions. However, no literature is available about the noise generated by a large number of particles suspended in liquid and agitated in a vessel. Consequently, it is necessary to clarify the mechanism of generation of these noises, in order to utilize this technique for monitoring the process of agglomeration in liquids. In this respect, high-frequency noises emitted by suspended model particles in an agitated environment were experimentally investigated in order to verify and fully understand the phenomenon of noise emission during the process of agglomeration in liquid. And

fundamental studies on the mechanism of noise generation were performed by analyzing the noise emitted by the impact of beads on a plate.

A monitoring system that utilizes changes in turbidity of suspension and noise emitted during the process of agglomeration was developed to repeatedly produce agglomerates with desired properties. The technical feasibility of the on-line monitoring of the agglomerate diameter and recovery was demonstrated by measuring relative energy and laser attenuation.

**Experimental**

Paraffin-type organic liquid was used as the suspending medium. Highly spherical glass beads with a density of  $2,500 \text{ kg/m}^3$  and mean sizes of  $255 \mu\text{m}$ ,  $412 \mu\text{m}$  and  $755 \mu\text{m}$  were used. The beads were sieved to remove off-size particles and ensure a sharp size distribution. The device used for agitating the suspension containing the glass beads was a horizontal agitator that was designed for the production of ceramic microspheres by agglomeration in liquid (Guinto et al., 1993a, b). The internal volume of the cylindrical vessel was  $3,000 \text{ cm}^3$ . Agitation of suspensions containing a specific number of beads was carried out at  $1,840 \text{ rpm}$ , which was similar to the rotational speed needed to form agglomerates with good properties.

The diagram of the high-frequency acoustic emission acquisition system is shown in Figure 1. Sound emissions were detected by a sensor (AE-900S-WB, NF Corp.) fixed at the side of the vessel. The envelope and relative energy from the discriminator and the outputs of the four counters, i.e., event rate, event total, oscillation rate and energy rate, were routed to an analog/digital converter (A/D) and stored in the data logger computer.

For an off-line frequency analysis of the emitted noise, waveforms were digitized and temporarily stored in a wave memory (9620, NF Corp.). Data from the wave memory were transferred to a personal computer and recorded in floppy disks. A FFT program was prepared for the power spectrum analysis.

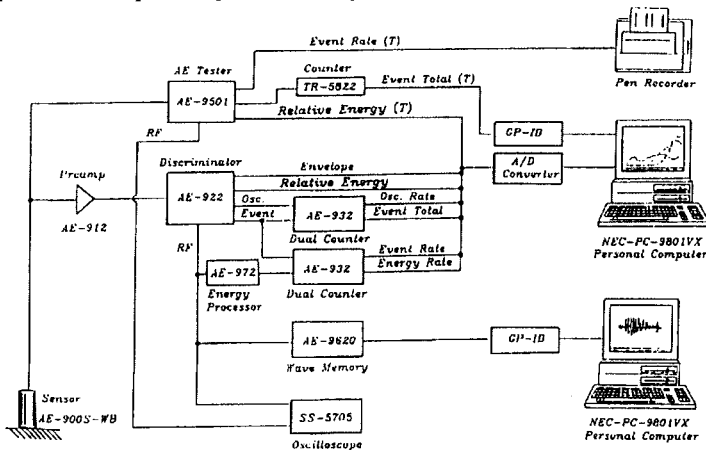


Figure 1: Schematic diagram of the high frequency noise emission acquisition system.

## Results and discussion

Shown in Figure 2 is the log-log plot of the number of beads against event rate. For all bead sizes, increasing the number of beads in the suspension increases event rate. Bigger beads generate noises even in lesser number. The increase in the number of beads increased the number of impingements and collisions, thereby increasing the event rate or the amount of noise emitted per unit time.

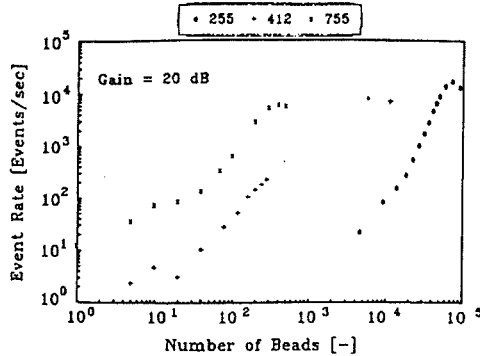


Figure 2: Logarithmic plots of high-frequency noises: event rate against the number of 255  $\mu\text{m}$ , 412  $\mu\text{m}$  and 755  $\mu\text{m}$  beads.

With the increase in noise activity, the energy rate and oscillation rate also increased. These results show that bigger beads have higher impact energy. The impingements of big beads generate noises with amplitudes that exceed the threshold level. This explains Figure 2, where 755  $\mu\text{m}$  beads exhibited higher event rates even in lesser number than 255  $\mu\text{m}$  beads.

Typical noise signal waveforms obtained when 20, 160 and 3,120 pieces of 412  $\mu\text{m}$  glass beads were used are shown in Figure 3. The lines drawn in Figure 3 indicate the discrimination levels. It can be seen that as the number of beads increases the number of waves exceeding the discrimination levels increases. Thus, the event rate and oscillation rate increases with an increase in the number of beads. As the number of beads increases, the initial burst-type emission (Figure 3.a) becomes a pseudo-continuous type emission (Figure 3.c) due to overlapping of events. This explains the increase in the energy rate and the relative energy with increasing number of suspended beads. The power spectrum of the waveforms was obtained for the three bead sizes. In the case of 255  $\mu\text{m}$  beads, three distinct peaks in the spectrum; 264 kHz, 534 kHz and 989 kHz were observed. With 412  $\mu\text{m}$  beads, the peaks in the spectrum were noted at frequencies of 166 kHz, 272 kHz and 532 kHz. With 755  $\mu\text{m}$  beads, peaks at 242 kHz and 533 kHz were observed.

Hertz's law of contact was utilized to approximate the frequency of vibration arising from the impingement of glass beads to the vessel wall. The equation for the duration of contact ( $\tau_{bw}$ ) reported by Goldsmith (1960) for the Hertzian impact of a spherical object of diameter ( $D$ ) and mass ( $m$ ) on a thick plate will be given without proof:

$$\tau_{hw} = 4.53 \left| \frac{(\delta_s + \delta_p)m}{\sqrt{(D/2)v}} \right|^{0.4} \quad (1)$$

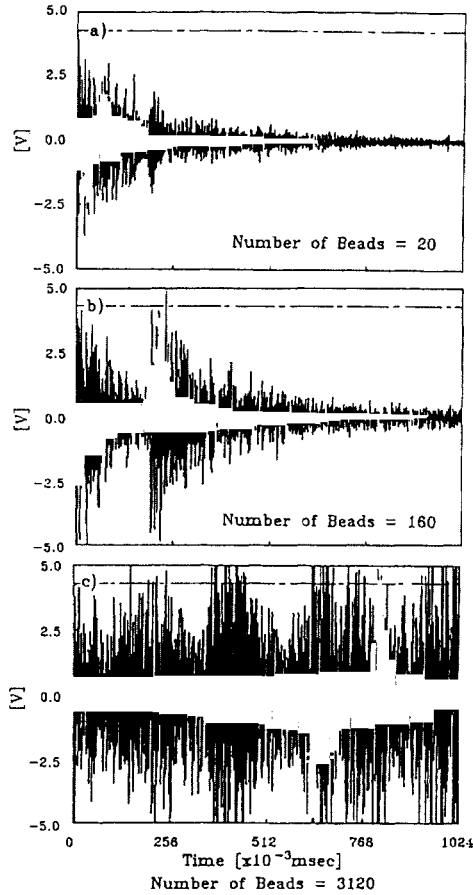


Figure 3: Typical noise waveforms with 412  $\mu\text{m}$  beads.

For two spherical objects impinging on each other, the duration of contact ( $\tau_{bb}$ ) is given as:

$$\tau_{bb} = 4.53(\delta m)^{0.4} \left| \frac{4}{vD} \right|^{0.2} \quad (2)$$

where  $v$  is the relative velocity during collision, and  $\delta_s$  and  $\delta_p$  are the material property constants of the sphere and the plane surface, respectively. It is defined as:

$$\delta = \frac{1 - \mu^2}{E\pi} \quad (3)$$



where,  $\mu$  is the Poisson's ratio and  $E$  the Young's modulus of elasticity. For glass,  $E_g = 6.9 \cdot 10^{11}$  Pa and  $\mu_g = 0.19$ ; while for stainless steel,  $E_s = 2.1 \cdot 10^{11}$  Pa and  $\mu_s = 0.28$  (Goldsmith, 1960).

Approximation of the particle velocity in an agitated environment was carried out by using the empirical equation obtained by Delichatsios and Probst (1975) for eddies larger than the Kolmogorov microscale in a homogeneous isotropic turbulent flow. The magnitude of relative particle velocity is given by:

$$v = 1.37(\xi D)^{1/3} \quad (4)$$

where  $\xi$  is the rate of turbulent energy dissipation per unit mass.

The value for  $\xi$  was obtained by dividing the power input ( $P$ ) by the mass of fluid ( $m_f$ ) in the vessel, i.e.  $\xi = P/m_f$  (Schubert and Muhle, 1990), which gave a value of 0.1634 J/kg.s. The Kolmogorov microscale was calculated to be 62  $\mu\text{m}$ .

In conjunction with the above equations, the fundamental frequency of vibration was calculated to be the reciprocal of twice the duration of contact (Tillet, 1954):

$$F = 1/(2\tau) \quad (5)$$

The calculated frequencies of vibration arising from bead-wall ( $F_{bw}$ ) and bead-bead ( $F_{bb}$ ) impacts for the three beads used are summarized in Table I. In the case of two beads colliding against each other, the velocity was approximately equal to equation (4) multiplied by 2.

Table I: Calculated frequencies.

Bead size ( $\mu\text{m}$ )	$F_{bw}$ (kHz)	$F_{bb}$ (kHz)
255	570	1,012
412	364	647
755	207	368

The order of magnitude of the calculated frequencies for all three beads sizes is in agreement with that of the peak frequencies. The other unaccounted peak frequencies from the results of the FFT analysis are attributable to either the flexural vibration of the vessel wall or to other modes of bead collisions. It is also possible that the other peaks represent the harmonics of the fundamental frequencies of vibration. In our calculations, we assumed the vessel to be a massive thick plate with negligible or minimal flexing. Dimensional analysis by Goodier and Ripperger (1959) showed that the ratio of the thickness of the plate ( $h$ ) over twice the impinging bodies' radius ( $a$ ) must exceed 16, i.e.  $h/2a > 16$ , for a plate to behave as a thick plate or semi-infinite solid. Flexural behavior is not observed in a thick plate, because the time of contact or the duration of impact is less than the time needed for the wave to reflect from the other side of the plate. For thin plates, the contact time exceeds the time needed for a wave to reflect back to the point of contact, and flexural vibrations tend to dominate sound radiation (Takahagi et al., 1980). When compared to the size of impinging beads, the thickness of the vessel wall can be categorized either as a thick plate or a thin plate. Thus, it is probable that the unaccounted for measured frequencies are due to flexural behavior of the walls. However, considering the complicated shape of the

vessel, it is difficult to obtain a good theoretical approximation of this flexural vibration.

Impact experiments of glass, chrome and nylon beads on a thick circular plate of steel were conducted (Hirajima et al., 1999). The initial peak frequency ( $f_p$ ) and the peak height ( $P$ ) of the impact signal were measured. As shown in Figure 4, the frequencies obtained from the experiments were proportional to the theoretical frequencies ( $f_b$ ) from equations (1) and (5). The empirical equation for  $P$  is given as follows:

$$P \propto v^{1.2} D^{2.49} E^{0.07} \rho^{0.91} \quad (6)$$

where  $\rho$  is the particle density.

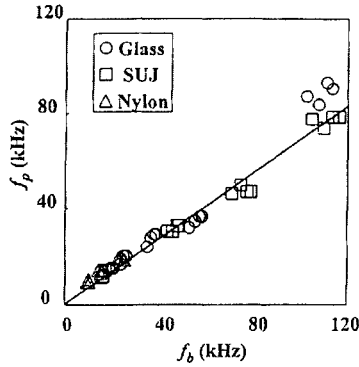


Figure 4: Comparison of  $f_p$  and  $f_b$ .

The event rate and oscillation rates are dependent on the threshold setting and are ideal for burst type signals (Kline, 1983). Noises emitted by large numbers of suspended particles are continuous-type signals, which make adjustments of the amplifier gain and the threshold level very critical. Envelope processing of the signal is independent of the threshold, making it suitable for monitoring noise emission of suspended particles. The envelope of a signal is a fluctuating dc output, whose amplitude is proportional to the energy inherent in the signal. Since noises emitted by suspended particles are attributed to the release of energy due to the impact of particles, the measurement of the parameters related to the energy content of the signal, such as the envelope, is considered to be an indication of the impact energy of the particles. Fluctuation in the envelope is eliminated by passing it through an averaging circuit. In this study, henceforth, the output of the averaging circuit is called the relative energy or  $E_r$ .

The relative energy of the emitted noises plotted against the number of beads in a log-log scale becomes a straight line when the number of beads exceeded 200. This relationship is depicted in Figure 5. The slopes of the lines for all the three bead sizes are similar. The empirical relation between the relative energy and the diameter and number of beads is given as follows:

$$E_r = 1.72 \times 10^{-10} D^{2.80} N^{0.53} \quad (7)$$

where  $E_r$  is the relative energy [V],  $D$  the bead diameter [ $\mu\text{m}$ ] and  $N$  the number of beads. With a constant  $D$ ,  $E_r$  increases with an increase in  $N$ , and with a constant  $N$ ,  $E_r$

also increases with an increase in  $D$ .  $E_r$  is a function of amplitude and considered to be proportional to  $P$  expressed in equation (6). Thus,  $E_r$  is considered to be a function of  $v, D, E, N$  and  $\rho$ .

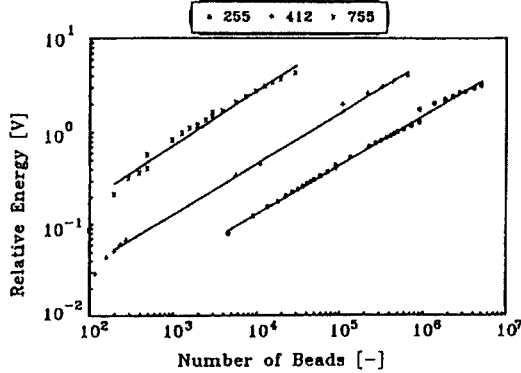


Figure 5: Logarithmic plot of the relative energy of high-frequency noises against the number of 255  $\mu\text{m}$ , 412  $\mu\text{m}$  and 755  $\mu\text{m}$  beads.

In order to establish the relationship between noise emission and mean agglomerate diameter ( $D$ ) and number ( $N$ ), agglomeration experiments with different agglomeration times and bridging liquid dosages were carried out. Figure 6 is a simplified diagram of the semi-continuous agglomeration system, with the noise and laser-attenuation monitoring devices (Hirajima et al., 1994). From the results of the agglomeration experiments, the empirical relation between  $E_r$  and  $D$  and  $N$  was obtained:

$$E_r \propto D^{0.126} N^{0.285} \tag{8}$$

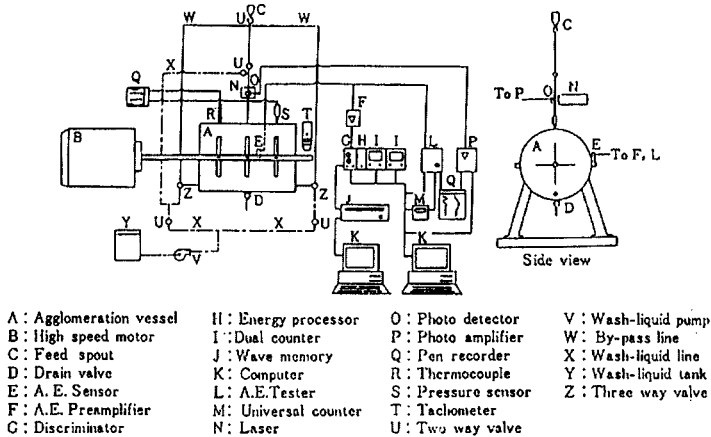


Figure 6: A semi-continuous agglomeration system with on-line monitoring devices.

However, the empirical relations derived from the agitation experiments using glass beads in equation (7) and the impact of glass, chrome and nylon beads on a thick

circular plate of steel in equation (6) showed that  $E_r$  is a function of  $D$  raised to an exponent almost equal to 3. This indicates that the influence of  $D$  on  $E_r$  for beads is greater than that of real agglomerates. It is considered that the reason is that the agglomerates are susceptible to plastic deformation, whereas the rigid beads undergo elastic deformation.

Techniques of agglomeration in liquid were used to produce zirconia microspheres. A monitoring system that utilizes changes in turbidity of suspension and noise emitted during the process of agglomeration was developed to repeatedly produce agglomerates with desired properties (Hirajima et al., 1994). The monitoring result is shown in Figure 7. The measured final agglomerate diameter and recovery are marked by open and closed circles, respectively. The technical feasibility of the on-line monitoring of the agglomerate diameter and recovery was demonstrated by measuring  $E_r$  and laser attenuation.

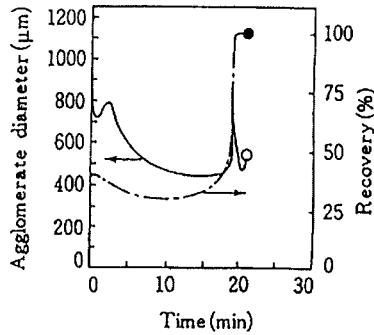


Figure 7: Calculated recovery and agglomerate diameter as a function of lapsed time. Bridging liquid = 115 cm<sup>3</sup>/kg. Measured values are indicated by open and closed circles.

## Conclusions

The noise emission of particles suspended in a liquid medium and agitated in a stirred vessel was studied experimentally. Low-frequency noise signals contain mechanical and hydraulic noises that interfere in monitoring the noise signature of suspended particles. In contrast, high-frequency noise signals exhibited corresponding change relative to the size and number of suspended particles. An increase in the size or in the number of beads increases event rate, energy rate, oscillation rate, relative energy and frequency spectra.

The fundamental frequencies of vibration were estimated based on Hertz's law of contact in conjunction with well-established hydrodynamic equations. The order of the calculated frequencies of vibration arising from bead-wall and bead-bead impacts is in good agreement with the measured frequencies. It can be deduced that the high frequency noises emitted during the agitation of suspension containing model particles are mainly generated by the bead-wall and bead-bead collisions. Relative energy ( $E_r$ ), being independent from threshold level, provides a broader range and simple means of approximating the diameter and number of the suspended particles.

From the impact experiments of glass, chrome and nylon beads on a thick circular plate of steel, it was found that the initial peak frequencies ( $f_p$ ) of the impact signals were proportional to the theoretical frequencies ( $f_b$ ) obtained from equations (1) and (5). The empirical equation of the peak height ( $P$ ) was given by equation (6). Thus,  $E_r$  is considered to be a function of  $v$ ,  $D$ ,  $E$ ,  $N$  and  $\rho$ .

The technical feasibility of the on-line monitoring of the agglomerate diameter and recovery was demonstrated by measuring  $E_r$  and laser attenuation.

### Acknowledgments

The authors express appreciation for support of this research by a Grant-in-Aid for Scientific Research from the Ministry of Education, Science and Culture, and a Grant from Arai Science and Technology Foundation.

### References

- Delichatsios, M. and Probstein, R., 1975. Coagulation in turbulent flow: theory and experiment. *J. of Colloid Interface Science*, 51, 394-405.
- Goldsmith, W., 1960. *Impact*. E. Arnold, London, 82-144.
- Goodier, J. and Ripperger, E., 1959. Response of a slab to impact. Transition from surface wave to flexural behavior. *J. of Applied Mechanics*, 26, 146-147.
- Guinto, W., Hirajima, T., Tsunekawa, M., Nishisu, Y. and Nakamura, M., 1993a. Production of Zirconia microspheres using a newly developed semi-continuous system of agglomeration in liquid. *J. Mining Mater. Proc. Inst., Japan*, 109, 65-71.
- Guinto, W., Hirajima, T., Tsunekawa, M., Tadano, K. and Nakajima, I., 1993b. Noise emission of suspended particles in an agitated environment. *Advanced Powder Technol.*, 4, 143-157.
- Hidaka, J., Kinboshi, T. and Miwa, S., 1989. Parameters of acoustic emission during the copact of a powder. *J. Soc. Powder Technol., Japan*, 26, 238-244 (in Japanese, with English Abstr.).
- Hirajima, T., Guinto, W., Tsunekawa, M., Tadano, K., Nakajima, I. and Nakamura, M., 1994. On-line monitoring for agglomeration in an organic liquid. *Advanced Powder Technol.*, 5, 365-376.
- Hirajima, T., Kataoka, K. and Tsunekawa, M., 1999. Study on particle size and properties from impact sound. Application to PET bottle separation. Preprints of Mining and Materials Processing Institute of Japan, Hokkaido Branch Spring Meeting, 17-18 (in Japanese).
- Kline, R., 1983. Acoustic emission signal characterization. In: J. Matthews (Editor), *Acoustic emission*, Vol. 2. Gordon and Breach Science Pub., New York, 105-138.
- Leach, M., Robin, G. and Williams, J., 1977. Particle size determination from acoustic emissions. *Powder Technol.*, 16, 153-158.
- Schubert, H. and Muhle, K., 1990. The role of turbulence in unit operations of particle technology. *Proc. of 2nd World Congress of Particle Technology*, Society of Powder Technology, Japan, Vol. III, 55-67.
- Takahagi, T., Yokoi, M. and Nakai, M., 1980. The sound by a transverse impact of a ball on a circular plate. *J. of Acoustical Society Japan*, (E)1, 2, 121-132.
- Tillet, J. 1954. A study of the impact on spheres of plates. *Proc. Physics Society*, 67, 677-688.
- Wakimoto, A., Takeda, A. and Otsuka, A., 1980. The utilization of noise emission in monitoring the coating process. *J. Soc. Powder Technol., Japan*, 17, 693-697 (in Japanese, with English Abstr.).

## STRATEGIES FOR FUZZY CONTROL OF A WATER/AIR COLUMN

M.T. Carvalho, F. Durão

CVRM - Instituto Superior Técnico, Av. Rovisco Pais, 1000-049 Lisboa, Portugal  
e-mail: teresa.carvalho@ist.utl.pt

### Abstract

In a fuzzy controller, the control strategy is expressed as a rule base, a set of linguistic rules that express the interrelations between controlled and manipulated variables. When the rule base is based on heuristics, and when the process to be controlled is complex, a certain degree of freedom exists, allowing the formulation of several rule bases with different control strategies.

In this paper, the performance of five different fuzzy control strategies developed to control a flotation column are compared. The controller, working in real time, is based on fuzzy logic inference with Mamdani-type rules. Its aim is stabilization (regulation) of the air holdup in the collection zone, and the command and stabilization of pulp height and bias water-flow rate by manipulation of the underflow, washing water and air-flow rates.

The strategies formulated were all developed heuristically and were: a rule base expressing the equivalent in fuzzy control of the column flotation classical-control strategy (three independent SISO loops), one rule base with only 11 rules, two more complex rule bases, and another, which considers dynamic compensation.

The experimental work was performed on a fully monitored laboratory scale column 9 cm in diameter and 4 m in height. A two-phase system (air and water) was tested.

The main conclusion of this study is that it is possible to adequately control a flotation column using a fuzzy controller with a heuristically developed rule base. The controlled-system performance, using a simple rule base with 11 rules, is comparable to the performance achieved with more complex rule bases. In fact, operators can drive the process based on only a few simple rules.

*Keywords: column flotation, fuzzy control, control strategy, Mamdani rules, heuristic knowledge*

### Introduction

Column flotation is a complex, multi-variable process for which there is not yet an accurate, simple, dynamic mathematical model that can be used for the synthesis of a classical controller. However, the process is successfully controlled by means of fuzzy control (Hirajima et al., 1991; Carvalho et al., 1994; Bergh et al., 1996).

A fuzzy controller of the Mamdani type has the structure depicted in Figure 1. For more details about a fuzzy control refer, for instance, to Lee (1990), Pedrycz (1993) or Lewis (1997).

The rule base expresses a qualitative control strategy, i.e. the relationship between the relative deviations of the process outputs (controller inputs) and the control actions (controlled outputs).

The rule base is a set of linguistic rules described by the following type of propositions:

If  $\varepsilon_c$  is *low*,  $Q_B$  is *medium* and  $H$  is *high*, then  $Q_U$  is *medium*,

where the words in italic describe linguistic attributes that characterize the linguistic variables, and  $\epsilon_c$ ,  $Q_B$ ,  $H$  and  $Q_U$  represent, respectively, air holdup in the collection zone, bias water-flow rate, pulp height and underflow flow rate.

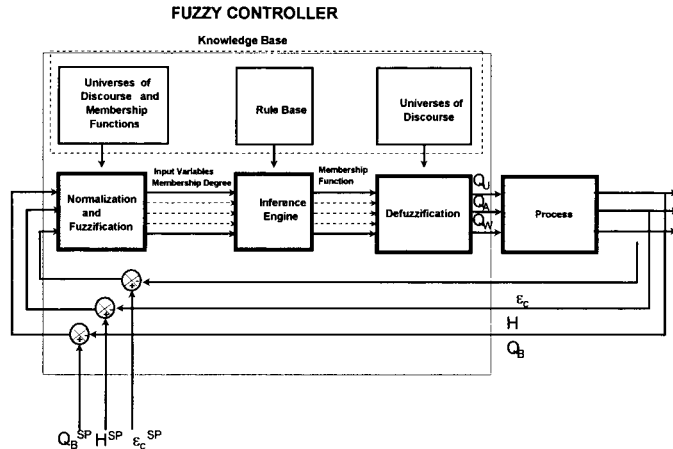


Figure 1: Fuzzy controller structure.

A human operator takes actions using some rules (generally a small number) similar to the one presented above. However, due to the complex nature of column flotation, which permits a certain degree of freedom, some strategies can be heuristically formulated for its control:

- to control the pulp height by manipulating the reject-flow rate and to control the bias water-flow rate by manipulating the washing-water flow rate. Or, on contrary, to control the bias-water flow rate by manipulating the reject-flow rate, and to control the pulp height by manipulating the washing-water flow rate?
- to use only the controlled variable error as the input variable, or to also include its time variation (dynamic compensation)?
- to use simple rule bases (with a small number of rules), or to use more complex ones, using several attributes to characterize the variables?

In IST a flotation column is automatically controlled by means of a controller based on fuzzy logic inference, with Mamdani type rules (Carvalho, 1998). The control objectives are the stabilization (regulation) of the air holdup in the collection zone, and the command (servo control) and stabilization of pulp height and bias water-flow rate by manipulation of the under-flow, washing-water and air-flow rates.

Formulation of the rule bases discussed in this paper was based on the knowledge acquired through bibliographic research, a steady-state simulation study, interrogation of experimented experts/operators, experimental study of the transient state and acquired experience in the manual control of the process.

### Control strategies

Experience has shown that three processing variables: collection zone height ( $H$ ), air holdup (volumetric percentage of air) in the collection zone ( $\epsilon_c$ ), and bias water-flow

rate (net flow of wash water passing through the froth zone) ( $Q_B$ ), are key parameters of the metallurgical column performance and are directly related to grade and recovery (Finch and Dobby, 1990). They are controlled by direct manipulation of wash water ( $Q_W$ ), air ( $Q_A$ ) and under-flow ( $Q_U$ ) flow rates (Table I).

Table I: Fuzzy controller input and output variables.

Input variables		Output variables
controlled variables	controlled variables' set-points	manipulated variables
H	$H^{SP}$	$Q_A$
$Q_B$	$Q_B^{SP}$	$Q_W$
$\varepsilon_c$	$\varepsilon_c^{SP}$	$Q_U$

In the linguistic characterization of the variables, a maximum number of five attributes were considered: *low (L)*, *medium low (ML)*, *medium (M)*, *medium high (MH)* and *high (H)*. A small number of attributes was considered, due to the fact that the rule bases were heuristically developed. A larger number of attributes would not, therefore, reflect an effective knowledge of the variable characterization and their relations.

In each control strategy, the MIMO system (Multiple Input/Multiple Output) is composed of three sub-systems, one for each manipulated variable (controller output), with one rule base formulated for each manipulated variable. The following strategies were developed and experimentally tested.

#### Rule base A

In fuzzy control, this strategy (Table II) is the equivalent of the classical, independent multi-SISO control loops (Finch and Dobby, 1990): control of H manipulating  $Q_U$ , control of  $Q_B$  manipulating  $Q_W$  and control of  $\varepsilon_c$  manipulating  $Q_A$ . It should be pointed out that in this strategy, the control of  $Q_B$  is made independently of the control of H, assuming that it can be estimated in any circumstances (steady or transient states).

Table II: Rule base A.

	Controlled variables		Manipulated variables	Comment
If	H <i>low</i>	then	$Q_U$ <i>low</i> ;	
If	H <i>medium</i>	then	$Q_U$ <i>medium</i> ;	Control of $Q_U$
If	H <i>high</i>	then	$Q_U$ <i>high</i> ;	
If	$Q_B$ <i>low</i>	then	$Q_W$ <i>high</i> ;	
If	$Q_B$ <i>medium</i>	then	$Q_W$ <i>medium</i> ;	Control of $Q_W$
If	$Q_B$ <i>high</i>	then	$Q_W$ <i>low</i> ;	
If	$\varepsilon_c$ <i>low</i>	then	$Q_A$ <i>high</i> ;	
If	$\varepsilon_c$ <i>medium</i>	then	$Q_A$ <i>medium</i> ;	Control of $Q_A$
If	$\varepsilon_c$ <i>high</i>	then	$Q_A$ <i>low</i> ;	

#### Rule base B

In this rule base (Table III), the strategy is to control  $\varepsilon_c$  by manipulating  $Q_A$ , and to control  $Q_B$  by manipulating  $Q_U$ . H is a variable that demands a special accurate control, due mainly to the fact that the other two controlled variables,  $\varepsilon_c$  and  $Q_B$  cannot be correctly estimated (and controlled) when H is not in a steady state.



Strategy B intends to control H with a higher priority than the other controlled variables, using the non-linear characteristics of fuzzy control: if H is nearby its set point (H *medium*), only one manipulated variable is used in the control of H; if H is far from its set point (H *high* or *low*), two manipulated variables ( $Q_U$  and  $Q_W$ ) are manipulated to control H, in order for H to quickly converge in the neighborhood of its set-point.  $Q_B$  is controlled only when H is stabilized (H *medium*).

Table III: Rule base B.

Controlled variables		Manipulated variables		Comment
If	H <i>low</i>	then	$Q_U$ <i>low</i> ;	
If	H <i>medium</i> and $Q_B$ <i>low</i>	then	$Q_U$ <i>high</i> ;	
If	H <i>medium</i> and $Q_B$ <i>medium</i>	then	$Q_U$ <i>medium</i> ;	Control of $Q_U$
If	H <i>medium</i> and $Q_B$ <i>high</i>	then	$Q_U$ <i>low</i> ;	
If	H <i>high</i>	then	$Q_U$ <i>high</i> ;	
If	H <i>low</i>	then	$Q_W$ <i>high</i> ;	
If	H <i>medium</i>	then	$Q_W$ <i>medium</i> ;	Control of $Q_W$
If	H <i>high</i>	then	$Q_W$ <i>low</i> ;	
If	$\epsilon_c$ <i>low</i>	then	$Q_A$ <i>high</i> ;	
If	$\epsilon_c$ <i>medium</i>	then	$Q_A$ <i>medium</i> ;	Control of $Q_A$
If	$\epsilon_c$ <i>high</i>	then	$Q_A$ <i>low</i> ;	

*Rule bases C and D*

Both rule bases C and D are refinements of Rule base B, to which more linguistic attributes characterizing  $Q_U$  and  $Q_W$  (*medium low* and *medium high*) and rules were added (in a total of 81 rules). With these rule bases, the current value of  $\epsilon_c$  in the manipulation of  $Q_U$  and  $Q_W$ , to anticipate the response of H to the manipulation of  $Q_A$  in the control of  $\epsilon_c$ , was considered. When needed, other controlling parameters were also modified.

The difference between these two rule bases is that while in rule base C,  $Q_B$  is controlled only when H is *medium*, in Rule Base D, it is considered that the Universe of Discourse of H is so short that  $Q_B$  can be controlled even when H is *low* or *high*. For the sake of simplicity, and due to the lack of space and increased complexity, these rule bases are not presented.

*Rule base E*

Table IV: Rule base E - Manipulation of  $Q_U$ .

H (past) →		L			M			H		
$Q_B$ (past)	H →	L	M	H	L	M	H	L	M	H
↓	$Q_B$ ↓									
L	L	L	H	M	ML	H	MH	M	H	H
	M	L	M	M	ML	M	MH	M	M	H
	H	L	M	M	ML	M	MH	M	M	H
M	L	L	MH	M	ML	MH	MH	M	MH	H
	M	L	M	M	ML	M	MH	M	M	H
	H	L	ML	M	ML	ML	MH	M	ML	H
H	L	L	M	M	ML	M	MH	M	M	H
	M	L	M	M	ML	M	MH	M	M	H
	H	L	L	M	ML	L	MH	M	L	H

This rule base (Table IV, which presents the table for  $Q_U$  manipulation) is based on rule base B. It includes the equivalent of the derivative term of classical linear controllers. This term is approximated by the difference between the current value of the variable and the value in the last sampling time (past).

### Experimental design and evaluation

Due to the non-existence of mathematical dynamic models that can be used in simulation, an experimental study was undertaken to evaluate the performance of the controlled system for modification of the rule base. In each test, after achieving a steady-state operation, one variable was disturbed, according to the scheme illustrated in Figure 2. The following disturbances were generated:

- load disturbance, i.e. disturbance of an independent variable that is not manipulated by the fuzzy controller; feed-flow rate ( $Q_F$ ) was the independent variable chosen;
- controlled variables' set-point disturbance (servo control). Only the set points of  $H$  ( $H^{SP}$ ) and  $Q_B$  ( $Q_B^{SP}$ ) were modified. Modification of the air-holdup set point was not considered, because the servo control of this variable is not achievable by manipulation of one or more of the manipulated variables, unless a modification of the frother concentration is made.

The frother concentration was kept constant, and the control of  $\varepsilon_c$  refers only to the rejection of load disturbances or other controlled variables' set-point modifications.

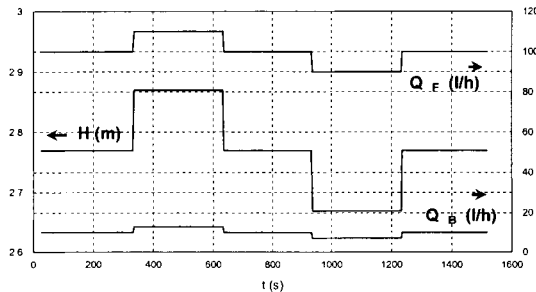


Figure 2: Disturbances introduced.

The evaluation of the controlled system performance is a compromise between the speed of response, stability and accuracy. Depending on the weight that can be given to each one of these criteria, a different controller can be obtained. Three performance parameters, or indices, were considered for evaluation:

- *settling time*, is defined as the time, after the disturbance, that the controlled variable takes to reach a new steady-state value. This parameter is a measure of the speed of response. In each test, four-step changes were performed. Therefore, four settling times were determined, and an arithmetic average, ST, was calculated;
- *stead-state error*, is the average deviation of the controlled variable from its set-point. In each test, five steady-state errors were determined, and an arithmetic average, SSE, was computed;

– *standard deviation*,  $\sigma$ , is defined as follow:

$$\sigma = \sqrt{\frac{\sum e^2(t)}{N-1}} \quad (1)$$

where  $e(t)$  is the deviation of the variable from its set-point and  $N$  is the number of sampling intervals during the test. This parameter can be viewed as a measure of stability.

### Pilot flotation column description

The pilot flotation column is an acrylic tube 80 mm in diameter and 3.2 m in height. The feed is introduced at about 1/3 of the column height from the top, and air is introduced a few centimeters from the bottom.

Controlled variables ( $\epsilon_c$ ,  $H$  and  $Q_B$ ) are not directly measurable. However, they can be estimated or inferred from other measured variables.  $\epsilon_c$  and  $H$  are calculated from measurements of two pressure sensors mounted on the column wall. The value of  $Q_B$  is approximated by the difference between underflow and feed-flow rates (corrected for  $H$  variation).

Manipulated variables ( $Q_A$ ,  $Q_W$  and  $Q_U$ ) are measured with different flow meter types, and their control is achieved by direct manipulation of variable speed pumps and control valves by using local PID controllers.

The work presented here considers only the two-phase system, an air and water mixture. A constant frother concentration of 10 ppm was used for froth stabilization.

### Results and discussion

#### *Response to a load disturbance*

None of the three controlled variables are affected by the load disturbance of  $Q_F$ . This conclusion is independent of the strategy used.

#### *Response to a set-point disturbance of $H$ and $Q_B$*

In all tests performed, it was found that  $\epsilon_c$  is not affected by the disturbance of the set points of  $H$  and  $Q_B$ .  $H$  and  $Q_B$  are only slightly affected by the disturbance of  $H^{SP}$ , but the responses are not sensitive to modification of the control strategy.

Table VI: Maximum values of performance parameters.

Strategy	SSE		ST (s)		$\sigma$
	H (cm)	$Q_B$ (l/h)	H	H (cm)	
A	0.7	0.6	32	2.3	6.2
B	0.5	0.2	31	2.5	6.9
C	0.5	0.9	29	2.4	2.6
D	1.0	0.3	31	2.6	7.0
E	0.5	0.3	27	2.2	6.2

These conclusions can be drawn from Figures 3 to 6, which show the responses of  $H$  and  $Q_B$  to  $H^{SP}$  disturbance. Table VI shows the maximum values of the performance parameters obtained for ST, SSE and  $\sigma$ .

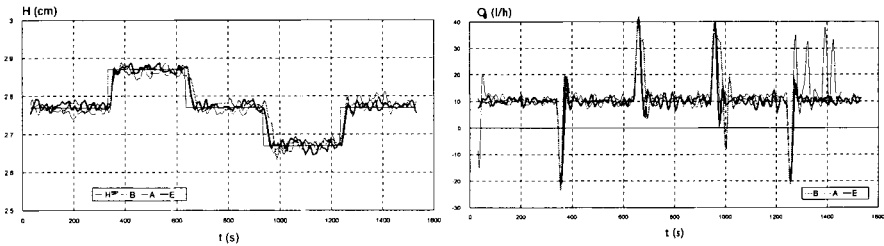


Figure 3: Response of  $H$  and  $Q_B$  to a disturbance in  $H^{SP}$ , when using control strategies A, B and E.

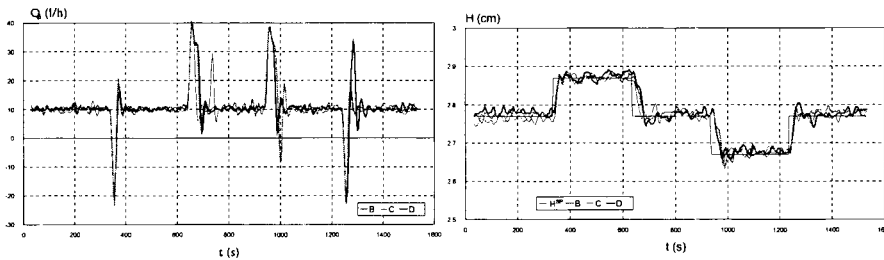


Figure 4: Response of  $H$  and  $Q_B$  to a disturbance in  $H^{SP}$ , when using control strategies B, C and D.

## Conclusions

The main conclusion of this study is that it is possible to adequately control a flotation column using a fuzzy controller with a heuristically developed rule base. The controlled system is robust for reasonable modifications of the control strategies. The performance of the controlled system, using a simple rule base of 11 rules, is comparable to the performance achieved with more complex rule bases. In fact, operators can drive the process based on only a few simple rules.

## References

- Bergh, L.G., Yianatos J.B. and Cartes, F., 1996. Hierarchical Control Strategy in Columns at El Teniente. Proc. of the International Symposium on Column Flotation. C.O. Gomez and J.A. Finch (Editors), Column '96, 369-380.
- Carvalho, M.T., Sousa, J.M., Durão, F.M. and Martins, P.M., 1994. Real Time Fuzzy Control of Column of Flotation Process. A. Crespo and Lorente (Editors), Proceed. Symposium on Artificial Intelligence in Real Time Control, Valencia, Espanha, 87-92.
- Carvalho, M.T., 1998. Aplicação do Controlo Fuzzy a uma Coluna de Flutuação. Ph.D. Thesis.
- Finch, J.A. and Dobby, G.S., 1990. Column Flotation, Pergamon Press, Oxford.
- Hirajima, T., Takamori, T., Tsunekawa, M., Matsubara, T., Oshima, K., Imai, T., Sawaki K. and Kubo, S., 1991. The Application of Fuzzy Logic to Control Concentrate Grade in Column Flotation at Toyoha Mines. Proc. of Int. Conf. On Column Flotation '91, Sudbury, Canada, 2, 375-389.
- Lee, C.C., 1990. Fuzzy Logic in Control Systems: Fuzzy Logic Controller - part I and II. IEEE Transactions on Systems, Man and Cybernetics, 20 (2), 404-435.
- Lewis, H.W., 1997. The Foundations of Fuzzy Control. Plenum Press.
- Pedrycz, W., 1993. Fuzzy Control and Fuzzy Systems, 2<sup>nd</sup> Ed., John Wiley & Sons Inc.

## IMPROVING CONTROLLABILITY ON FLOTATION COLUMNS

L.G. Bergh, J.B. Yianatos

Chemical Engineering Department  
Santa María University, Valparaíso, Chile

### Abstract

Flotation columns are common devices in cleaning circuits in the mineral processing industry. The operation and control of these columns often have the final responsibility for the quality of the concentrate grade and, to a less extent, for the recovery of the cleaning circuit. The use of basic distributed control has frequently led to a large variability in concentrate grade and recovery, as can be observed in many concentrators world-wide. The contribution to this variability usually comes from different sources, severely constraining the performance of conventional control systems. In this paper, the industrial experience in developing supervisory control systems is discussed in order to provide procedures for the diagnosis of instrumentation, calibration and maintenance, prior to the implementation of control schemes on top of the distributed control system. Examples based on control systems developed for El Teniente and Salvador Concentrators, from Codelco-Chile, are used to illustrate how some of the constraints on the controllability of the process can be relaxed.

*Keywords: flotation columns, process control, instrumentation, diagnosis*

### Introduction

Flotation columns are now used worldwide as efficient cleaning processes in a large number of sulfide mineral concentrators. Increasing degrees of freedom in their operating variables have led to large variations in metallurgical performance and therefore to increased scope for improving their control. In this process, stable operation and consequent consistent metallurgical benefits can only be obtained if basic distributed control systems are implemented. In general, wash water and air flowrates and froth depth are measured on line, while tailings, air and wash water flowrates are manipulated. On line analyzers, tailings and feed flow-rates and some other measurements are often incorporated into the system when a supervisory control strategy is implemented on top of a distributed control system.

The primary objectives, as indices of process productivity and product quality, are the recovery and the concentrate grade. Their on-line estimation, however, usually requires a significant amount of work in maintenance and calibration of on-stream analyzers, in order to maintain good accuracy and high availability. It is therefore common practice to control secondary objectives, such as froth depth, gas flowrate and wash water flowrate (Bergh and Yianatos, 1993). This control is known as a stabilizing strategy. Lack of accurate measurements, non-linear dynamics and high interaction among variables are some of the main problems associated with stabilizing control. These characteristics reduce the effectiveness of conventional PID control without a supervisor to co-ordinate the control loops. The use of basic distributed

control has frequently lead to a large variability in concentrate grade and recovery, as can be observed in many concentrators worldwide. This variability is usually due to different factors, such as disturbances entering the process from the column feed, temporal malfunction of water and air distributors, instrumentation problems related to calibration, maintenance and failure, and lack of co-ordination in the use of resources such as froth depth, air flowrate and wash water flowrate.

This paper focuses on highlighting a revision of those limiting aspects in order to relax some of these hard constraints enabling the implementation of a supervisory control that may achieve reasonable performance and large availability over time. The discussion is based on the experience of developing, commissioning and evaluating the SINCO-PRO at Salvador (Bergh et al., 1999) and the El Teniente (Bergh et al., 1996) concentrators in Codelco-Chile.

### Plant installation and results

#### *El Teniente concentrator*

El Teniente Division of Codelco-Chile produces over 340,000 t/y of copper and 1,900 t/y of molybdenum. A general scheme of the circuit is shown in Figure 1.

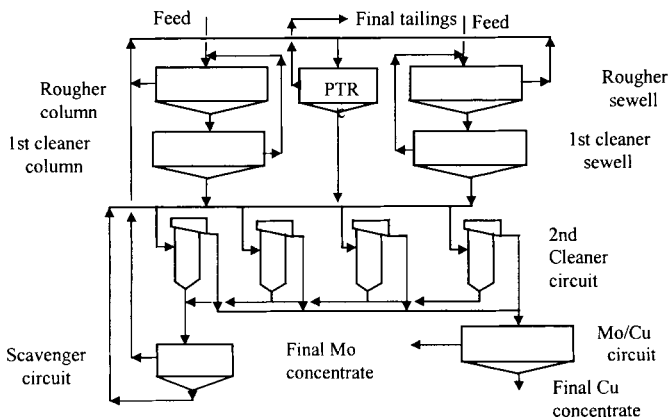


Figure 1: El Teniente Concentrator general flotation circuit.

To obtain this output over 97,000 t/d of ore was mined. The ore from sewell (acid circuit) and column (basic circuit) is floated in separate rougher and cleaning stages. Both concentrates are cleaned in a second common stage by four flotation columns in parallel and feeds the molybdenum/copper separation circuit to obtain the final concentrates. The second cleaner circuit consists of four columns,  $2 \times 8 \text{ m}^2$  for the rectangular section and 14 m in height. The first cleaner concentrates, coming from column and sewell, are mixed and split into two streams, each one feeding a group of two columns. The circuit global head, tailings and concentrate are analyzed by an on-stream X-ray fluorescence analysis system Courier 300 from Outokumpu. The column 1 concentrate and tailings grades in particular are also measured. The feed flowrate every two columns, the global tailings flowrate and column 1 tailings flowrate are

measured by magnetic flow meters. The airflow rate is measured by a combination of orifice plate and dp/cell in each column. The wash water flowrate is measured in each column by magnetic flow meters. Globe type pneumatic control valves are used to regulate the air and wash water flow-rates. Pinch type pneumatic control valves are used to regulate the tailing flowrate in each column. The froth depth is estimated using a pressure measurement under the pulp-froth interface. All sensors and control valves are electrically linked to a TDC-3000 distributed control system from Honeywell. The TDC-3000 system communicates through a CM50S interface to a DEC microVAX 3100/80 computer.

### Salvador Concentrator

The average ore grade was  $0.7 \div 0.75\%$  Cu and  $0.022 \div 0.026\%$  Mo. The circuit tonnage was 34,000 t/d. Figure 2 shows the flotation circuit.

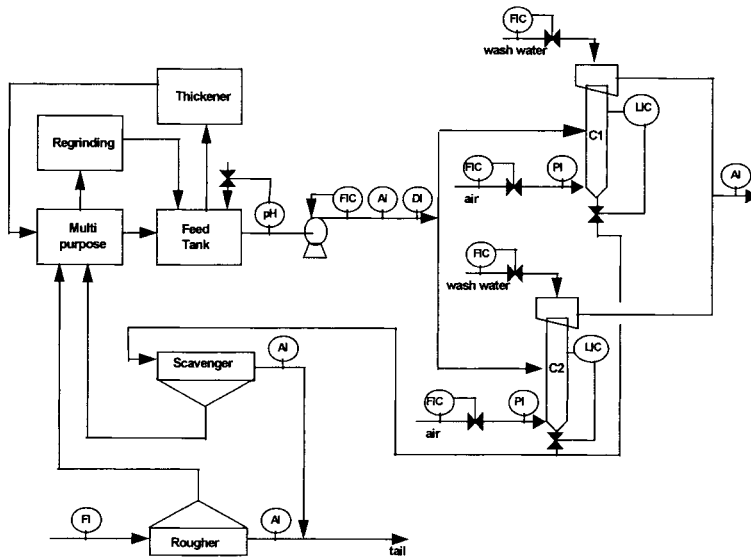


Figure 2: Instrumentation and distributed control system at the Salvador Concentrator.

The flotation feed comes from the hydrocyclone overflow of the grinding circuit. The feed pulp was distributed in four parallel rougher flotation banks. The rougher concentrate is reground and sent to a single cleaning stage or can be partially diverted to a thickener, allowing the control of the feed flowrate to the column circuit. The rougher tailings go to general tails. The single cleaning stage consists of two columns in parallel and produces the Cu-Mo bulk concentrate. The columns are rectangular in cross-section,  $2 \times 6 \text{ m}^2$ , and 13 m in height. Column tailings are distributed in two parallel scavenger banks. The scavenger concentrate was reground and sent to the cleaning columns. The scavenger tails are sent to general tails. The final collective concentrate, about 30% Cu and 0.8% Mo, goes first to a thickener and then on to the molybdenum plant.

The feed flowrate to the columns is regulated using a variable speed pump, and the feed tank is provided with an overflow connected to a thickener allowing for an extra surge capacity. The columns operate with three control loops to regulate the air, wash water and froth depth, as shown in Figure 2. Moreover, four in-line AMDEL analyzers are used to monitor the process. Thus, column feed, concentrate grades, rougher and scavenger tails are continuously monitored. Another control alternative is the addition of reagents, such as frother, to increase column froth recovery, and the addition of lime to regulate pH for iron control.

The supervisor SINCO-PRO was developed in Control Language in the Application Module of a TDC-3000 Honeywell system. All process data is collected and displayed on screen in a TDC-3000 system and sent through a PCNM software interface system to a PC network. The data in the PC is compacted and stored in historical files for further analysis. The operator interface is located at specially designed interactive displays on screen in the TDC-3000 system. Filtered data calculated performance indices, set point values and messages to operators are returned to the system to implement the control actions and to display consistent process variable values, performance indices and messages.

#### *SINCO-PRO evaluation*

Figure 3 shows a sequence of concentrate grade and column recovery differences between column 1 and global circuit at El Teniente Concentrator.

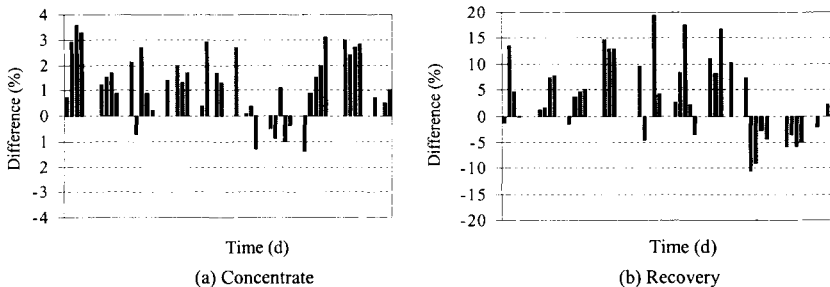


Figure 3: Performance difference between column 1 and global circuit at El Teniente.

At the Salvador Concentrator, a circuit performance comparison was made for a period of two months of operation under supervisory control (November and December 1997), and almost a year before that (August and September 1996) under DCS control. The main results are shown in Figure 4.

The feed grade of the plant remained almost constant, between 0.7% and 0.8%, during both periods of evaluation. The stabilization of the whole cleaning circuit by the supervisor resulted in an average increase of the column feed grade from 8.6% to 10.1% and the standard deviation was reduced from 1.3% to 0.4%. This stabilization decreases the circulating load on the cleaning circuit and help in significantly decreasing the consumption of chemical reagents for pH control. The concentrate copper grade experimented an average increment of 1.2% without loss in process recovery. The circuit stability was improved reducing the standard deviation of the concentrate grade from 0.9% to 0.7%.



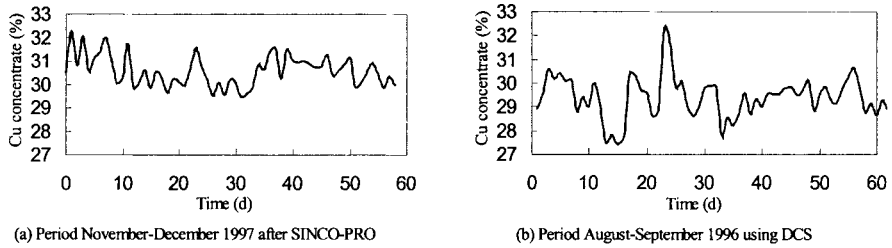


Figure 4: Evaluation at the Salvador Concentrator.

Figure 5 shows the column operation with SINCO-PRO at the Salvador Concentrator, from January 1998 to June 1999. During the first six months the columns operate at conditions similar to those during the evaluation period. Following this period, the temporary shut-down of a large mill, the higher content of oxide copper minerals in the feed and a late decrease in the copper price have contributed to a change in the concentrator grade-recovery policy in order to maintain the copper production. Thus, the mill throughput was increased, the rougher concentrate and the column feed grades decreased (10% to 6%), and the new final concentrate grade was maintained around 30% Cu, also improving the column recovery by 10%. The SINCO-PRO system has been able to manage this operation without any trouble during the last 18 months as shown in Figure 5.

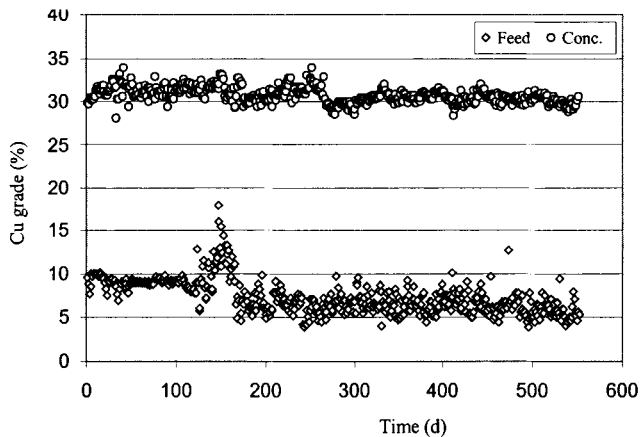


Figure 5: Column operation at the Salvador Concentrator, January 1998 - June 1999.

### Improving controllability

In practice, the extension of the success of any control approach may be severely limited by different constraints, as it is schematically shown in Figure 6. As can be noted, many aspects can affect the performance of a process under control. There are

constraints related to process design, layout, specifications, installation and maintenance of equipment integrating the process.

There are also constraints on the quality (accuracy, repeatability) and availability of the information gathered from the field instrumentation and communicated to a computer interface. In the supervisory control implementation some constraints appear to be related to computer hardware and programming languages, control algorithms, and perhaps the most important of all, lack of process knowledge (Bergh and Yianatos, 1999).

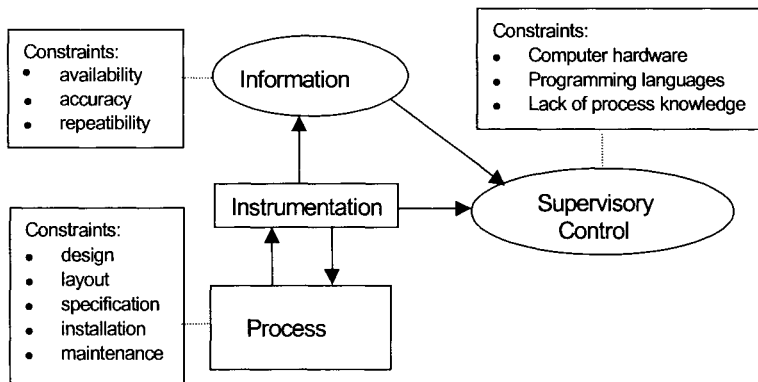


Figure 6: Constraints on supervisory control.

The successful implementation of the SINCO-PRO hierarchical control strategy was made possible by carrying out a complete program before implementing the new control strategy, thus relaxing some of the strict constraints mainly found in the process and instrumentation. Examples of frequently found constraints are:

#### *Process constraints*

- Internal launder design, limiting the carrying capacity and disturbing the froth transport pattern.
- Tailings discharge piping layout and cavitation of pinch valves, limiting froth depth control and feed flowrate distribution to both columns.
- Concentrate spill in the discharging channel, limiting the checking and maintenance of local instrumentation.
- Wash water distributor plugging, limiting proper distribution of water. Lack of appropriate maintenance programs.
- Installed air spargers came from different suppliers and previous comparison studies showed confuse results. Lack of appropriate maintenance programs.

#### *Instrumentation constraints*

- Significant noise on feed flowrate measurement (magnetic flowmeter) leading to loose feed flowrate control and distribution to both columns.
- Pulp level measurement problems in the feeding tank leading to excessive control actions and pulse feed flow and thus creating instability in the operation of both columns.

- Frequent discalibration of froth depth measurement (pressure in an inverted tube) leading to poor froth depth control.
- Control bypass valve opened as a policy to remedial problems on air supply system.
- Plugged pipelines and stacked valves limiting water flowrate supply.
- Calibration problems of magnetic flowmeters.
- Low availability of on stream analyzers.
- Frequent discalibration of on stream analyzers.
- Lack of instrumentation to monitor air pressure in manifolds.
- Pressure regulator malfunction due to poor condition of instrumental air.

#### *Supervisory Control constraints*

- Computer hardware and programming languages.
- Inappropriate computer-operator interface.
- Lack of process knowledge in developing the control strategy and maintaining the system benefits over time.
- Lack of training of field operators, instrumentalist and maintenance personnel.
- Managing problems between operators, instrumentalist and maintenance supervisors.

Appropriate instrument and device calibration and maintenance programs can easily relax some of these constraints. Others may be partially removed by changing and unifying operating practices through extensive training programs. Those still remaining and limiting the process control require to be considered in the supervisory control strategy. Usually this is accomplished by developing special software modules to detect instrumental and operating problems, leading to automatic remediation or messages suggesting actions to operators.

#### **Conclusions**

Hierarchical control is truly an alternative solution to the problem in an integral form, able to manage information obtained on-line (measured directly or by inference) subject to failure and error calibrations, to detect, alarm and sometimes correct operating problems, and to co-ordinate local conventional control loops by using logical rules. In this way, it has been shown as a powerful tool in increasing the operating availability and the product quality of complex processes, such as flotation columns.

The flotation circuit controllability is usually limited because of instrumentation malfunctioning mainly due to inappropriate calibration and maintenance methodologies. Furthermore, constraints on process design, piping layout, equipment specification, installation and maintenance contribute to limit the achievements of any control system. Hence a complete diagnostic program should be carried out before implementing any control strategy. Once the major detected problems are solved, there is a greater opportunity for an appropriate use of the available information.

Distributed control systems are not sufficient in achieving strict metallurgic objectives. In this case a supervisor with different attributes is needed. Supervisory control systems should be adaptable to different computation platforms, and should consider, at very least, modules for: validation and reconciliation of process data,

detection of operation and instrumentation problems and co-ordination of local control loops under an overall strategy.

Other important aspects in the success of a supervisory control system are operator involvement in the project and the ability of the system to continue running even when some of the information is not temporarily available. In our experience, the joint training program for control room and field operators, instrumentalist and maintenance personnel, related to the project on all the aspects, has been extremely helpful in coordinating all the efforts in relaxing different constraints on the process controllability.

#### **Acknowledgements**

This work has been possible thanks to the financial support of Conicyt (Project Fondecyt 1990859) and the Santa Maria University (Project 992723).

#### **References**

- Bergh, L.G. and Yianatos, J.B., 1993. Control Alternatives for Flotation Columns. *Minerals Engineering*, Vol 6, N° 6, 631-642.
- Bergh, L.G. and Yianatos, J.B., 1999. Supervisory Control Experience on Large Industrial Flotation Columns. *Proceedings Control and Optimization in Minerals, Metals and Material Processing Symposium*. Quebec, Canada, August 22-26.
- Bergh, L.G., Yianatos, J.B., Acuña, C.P. and Cartes, F., 1996. SINCO-COL Application to Flotation Columns in El Teniente Concentrator. *Proceedings International Conference Column'96*. Montreal, Canada, August, 583-591.
- Bergh, L.G., Yianatos, J.B., Acuña, C.P., Pérez, H. and López, F., 1999. Supervisory Control at Salvador Flotation Columns. *Minerals Engineering*, Vol 12, N° 7, 733-744.

## **COST CUTTING IN OPTIMIZING A FLOTATION UNIT BY USE OF STATISTICAL METHODS**

H.-C. Haarmann, R. Janitschek, E. Beeker

Geschäftsbereich SysTec, Deutsche Montan Technologie GmbH, Essen,  
Deutsche Steinkohle AG, Herne, Germany

### **Abstract**

In 1997 a pneumatic flotation unit went into operation at the Lohberg/Osterfeld hard coal preparation plant of DSK (Deutsche Steinkohle AG, Herne). Compared to earlier units in Germany the aerating reactor has been modified. The modified aerator uses the kinetic energy of the slurry to suck air into the reactor. The unit is designed to process 750 m<sup>3</sup>/h of slurry at an average solids concentration of 80±20 kg/m<sup>3</sup>. The two-stage unit comprises a rougher and a scavenger stage with a 67 m<sup>3</sup> separating vessel each.

A series of plant investigations have been carried out in order to optimize the operating conditions and to increase unit efficiency. To accelerate the testwork the experiments were set up as a series of fractional factorial experiments. A detailed discussion of the experimental designs and their development is given. The results are presented. Various parameters that could not be controlled within the experimental set-up but show marked effects on process results are discussed and the benefit of statistical experimental designs for the interpretation of the results of plant investigations is shown.

*Keywords: coal-flotation, aeration, fractional factorial experiments, optimization*

### **Introduction**

In 1997 a new pneumatic flotation unit has been commissioned in the Lohberg hard coal preparation plant to meet new, more severe quality demands on the alkali grade of coking coal (Bogenschneider et al., 1998). The initial aim was to produce concentrates of no more than 7.2% ash content at maximum mass recovery.

In the following time contracts have been modified again which opened the opportunity to increase the ash content of the products and therefore to increase the yield of the process by minimizing the loss of combustible material to the tailings. The changed operational background required several sets of experiments to adapt the unit's operational set points. Figure 1 shows a view of the new unit type Pneumoflot™. It consists of two identical flotation tanks of 67 m<sup>3</sup> volume each. The first tank acts as a rougher stage, the second tank (shown in the center part of Figure 1) is used as scavenger. The self-suction aerators of vertical type are designed for a volume flow of 750 m<sup>3</sup>/h each. The tanks are fed by centrifugal pumps of constant speed. To compensate for the volume loss in the first stage's concentrate a part of the final tailings is recycled to the second stage feed tank.

### **General process conditions**

#### *Characteristics of the flotation feed*

The design feed is at a solid mass concentration of 80±20 kg/m<sup>3</sup> and an ash content of around 20% to 22%. The target maximum particle size in the feed is 0.7 mm.

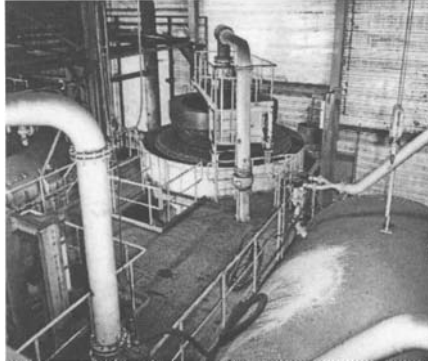


Figure 1: The two-stage pneumatic flotation unit at the Lohberg preparation plant: scavenger stage with feed pipe of rougher stage and pressure vessel of pressurized disc filter.

A part of the feed solids consists of suspended dust. According to the general process lay-out of DSK's-preparation plants (Kubitzae et al., 1987) the fines <0.7 mm are extracted as dust from the fine coal before it is fed to the fine coal jigs. Since the dust's ash content is too high to mix it with the coking coal, in the Lohberg plant the process has been modified and now the dust is suspended, classified in a hydro-cyclone and the fines <0.5 mm are mixed to the flotation feed. This results in an additional parameter, which may be manipulated in operation of the unit.

During one year of operation the actual feed quality of the unit varied considerably. Table I gives some key figures on the feed quality as sampled at several occasions.

Table I: Key-figures on flotation feed characteristics.

Date	11/97	01/98	04/98	11/98	03/99	03/99	07/99
Mass. conc. (kg/m <sup>3</sup> )	56.2	57.2	72.4	86.7	69.8	68.4	67.0
Mean ash (% mf)	22.8	22.7	21.8	23.8	19.4	19.0	17.9
Mass Fraction >0.5 mm (%)	10.7	15.3	9.1	18.6	9.5	10.2	8.8
Mass Fraction <0,063 mm (%)	36.1	32.2	35.4	30.3	34.5	34.3	30.6
Ash of fraction >0.5 mm (% mf)	9.9	10.6	7.0	6.6	4.5	4.4	5.1
Ash of fraction <0.063 mm (% mf)	22.8	35.4	37.2	41.4	33.5	31.3	32.5

Changes in the feed mass concentration are due to modifications in the feed make-up system and to alterations in the suspended dust quantities. Changes in ash content and particle size distribution are due to variations in underground operation and modifications of the feed make up system. The concentration is adjustable and was one of the parameters under investigation. Overall during one year of operation the feed ash content dropped by near 5%. Furthermore the misplaced fraction >0.5 mm showed great variability between different sampling sessions as well in it's mass fraction as in the ash content.

#### *Operating parameters*

The possible parameters to be manipulated are given in Table II. Apart from those parameters known from conventional flotation machines and from Pneumoflot™-cells

with tangential, pressurized aeration, the position of the cone is an additional parameter that has an impact on the froth flow speed in the upper part of the flotation tank.

Table II: Operational parameters of the flotation unit.

Parameter	Comment
Tank level / froth thickness	
Cone position	See Cordes (1997)
Aeration rate	Restricted by suction capacity of reactor
Reagent dosage	Controlled by solids mass feed
Mass concentration solids	Rate of dust suspension / water addition

### Experimental design

To get a rough idea of the interaction of all parameters and to restrict further work to the most important factors following one initial series of sampling without any change of operation conditions the first approach was taken in a fractional factorial design (Box et al., 1978). In this first sampling series only parameters of the first stage were manipulated. Since the aeration rate was suspected to be below the required optimum from the beginning, the system was changed to pressure aeration for the experiment. The low level of aeration was chosen according to the observed self-suction capacity. The plan of the experiment is shown in Table III.

Table III: Set up for the first test series:  $2^{4-1}$  runs.

Run n°	Air rate	Oil	Tank level	Cone position
1	+	+	+	+
2	-	+	+	-
3	+	-	+	-
4	-	-	+	+
5	0	0	0	0
6	+	+	-	-
7	-	+	-	+
8	+	-	-	+
9	-	-	-	-
10	0	0	0	0

Runs 5 and 10 are the center points. In the other runs all possible combinations of the + and - levels of the parameters have been realized. Taking four parameters at two levels each into consideration a number of  $2^4$  or 16 runs would result. To reduce the number of runs and guard a reasonable level of statistical reliability, the design was reduced to  $2^{4-1}$  or 8 runs. Instead of doing all combinations, the "half design" was repeated completely. The loss in information on higher order interactions was regarded to be tolerable since under the rough conditions of the plant tests a high level of noise had to be expected that would complicate the detection of these interactions anyway. All runs except the center points have been carried out in random order. Taking into account the time lag of the unit to reach steady state conditions after manipulation of the parameters it appeared to be possible to do 10 runs per day. The complete test series takes two days of sampling and regarding a

number of 6 material streams to be sampled in each run about two weeks of laboratory work to complete screen and ash analysis.

Doing the same investigation by a conventional experimental design would have resulted in at least one day of sampling per included parameter, without getting any reliable information on possible interactions of parameters. From the first set of experiments feed mass concentration, aeration rate and reagent dosage were retained as most important factors. Consequently a second series of tests was run to proof the results. In this series the second stage was included to improve understanding of the interactions between both stages. Both stages were set on pressurized aeration.

Since it is not envisaged to change the unit to pressurized aeration on a permanent basis, a third series of test was run to test optimal conditions on self-suction with all other parameters set to the previously detected work points. The results of this test were not satisfactory. Consequently the slurry distributor system was altered in order to improve the self-suction capacity of the unit without changing the aeration-system.

For the first set of tests a  $2^{4-1}$  design was chosen. The experiment was repeated once. Additionally to the 16 runs on high and low level for the factors "reagent dosage", "aeration", "froth level" and "cone position" four runs on central points for each factor were included thus giving a total of 20 runs. In the following experiments this design was kept, the included factors, however, were changed. One exception is the last series of tests. Since only one factor was manipulated the unit was sampled for two days before the change was implemented and for two days after the change was completed. The whole series of tests was realized in only 12 days of sampling.

## Results

### *Impact of changing feed quality*

All results showed a marked influence of the changing feed quality that renders it very difficult to compare results of different test sets. Some general results may be retained from the comparison of the different sets, however. Since all manipulations of parameters have been centered around fixed levels within the single experiments, by comparing mean feed characteristics with mean results of experiments, the only remaining impact is the feed quality. Figure 2 shows this analysis done for the mass recovery and the feed ash content. The result shows a good linear relation which is very close to the rule of thumb  $mass\ recovery = (100 - feed\ ash)$ . This rule is valid for many German seams. The relation shows  $R^2 = 81.2\%$ .

In all the experiments it appeared that the tailings' ash content was strongly influenced by the feed mass concentration, the feed content of oversized material and the ash content of this particular fraction. The analysis of all results indicated that the new parameter "t" given by Equation 1 would be appropriate to characterize the impact of the feed quality on tailings ash content.

$$t = \frac{\%(\text{mass}) > 0.5\text{ mm}}{\%(\text{ash}) > 0.5\text{ mm}} \cdot \frac{1}{\text{mass concentration feed}} \quad (1)$$

The result is given in Figure 3. The tailing's ash content shows a linear relation with the t-parameter. The  $R^2$  value is 89%, which is regarded as very good under plant conditions. This result shows the difficulty to make oversized material float at low



feed concentrations. Even almost pure coal particles in this fraction don't float at 100 % recovery. On the other hand few particles of the fraction reporting to the tailings bring down the ash content significantly. In slurry of higher mass concentration apparently the recovery in this fraction is much better.

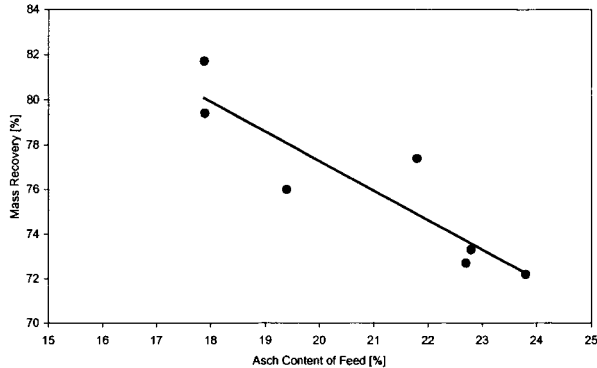


Figure 2: Relation between mean ash content of feed and mean mass recovery.

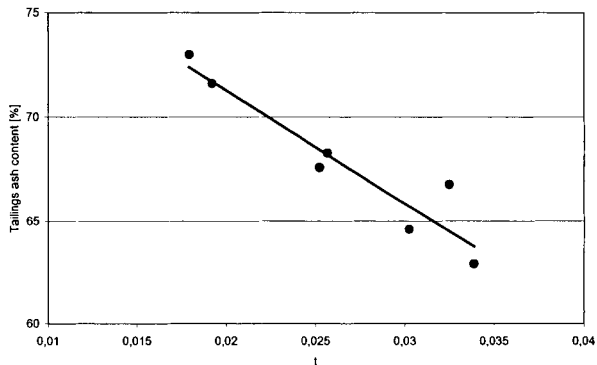


Figure 3: Influence of feed quality on tailing's ash content; parameter  $t$  as given by equation 1.

#### *Effects of the tested parameters*

From laboratory tests in a stirred Wedag flotation cell it appeared that around 200 g/t reagent dosage would be the optimum dosage. First operational experience however showed that optimum results occurred at dosages of 400 g/t, which is within operational experience with other flotation units. It was not clear, however, in which stage the oil would be applied most economically. Table IV gives the results of the tests run to answer this question.

Table IV: Flotation results for different reagent dosages (\*level rougher/level scavenger).

Oil distribution	Dosage (g/t)	Concentrate ash (%)	Tailings ash (%)	Mass recovery (%)	$\eta$ (%)
+/+*	563	7.7	70.0	75.5	66.6
+/-	391	7.2	70.7	74.4	69.6
-/+	338	7.2	63.0	69.7	63.5
-/-	249	7.2	63.5	69.4	64.1

From these results it is evident that the decisive step is the oil dosage in the rougher stage. Whereas an increased dosage from roughly 400 g/t to 560 g/t does not cause significant additional benefits, any dosage below 200 g/t in the first stage (which was realized in the position  $\pm$ ) appears to be insufficient under plant conditions. The concentrate grade is not influenced significantly by the increased oil dosages. The tailings grade and subsequently the mass recovery, however, is increased by almost 5% (abs.) due to increased oil dosage. Second stage oil dosage does not effect tailings grade very much. It's effect becomes more evident from the deterioration of the selectivity parameter  $\eta$ , which is used to describe the yield on correct material in separation processes (Kubitza, 1980). As a conclusion from these results, it may be retained that a reagent dosage of around 400 g/t, applied for the bigger part in the rougher stage, currently gives best achievable results. Apart from the oil dosage the aeration rate and the air/slurry ratio was the most influential factor under investigation. The result for the rougher stage is shown in Figure 4.

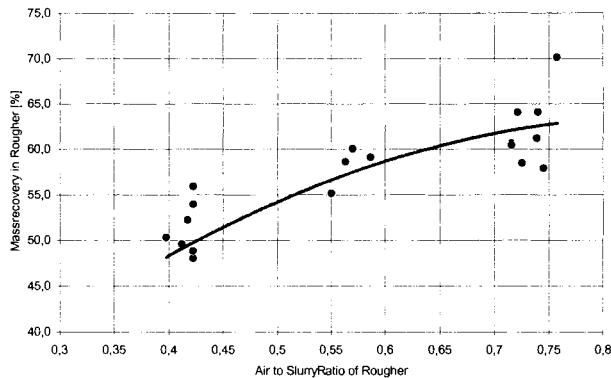


Figure 4: Recovery of rougher over air to slurry ratio of rougher stage.

The results give clear evidence that the original suction capacity ( $0.4 \text{ m}^3/\text{m}^3$ ) of the aerator did not give optimum results under the tested conditions. The results are in fair agreement with data on pneumatic flotation with other reactors that suggest that for coal an air to slurry ratio of around 1 gives optimum results (Bahr et al., 1985). Putting both vessels on pressure aeration at an air-to-slurry ratio of 0.8 resulted in a gain of 1.8% in mean mass recovery compared to the expected value according to Figure 2. Putting them at a rate of 1.1 increased the mean recovery to 77.1% instead of 74.1%, which had to be expected in the experiment. It turned out that, although the scavenger is able to compensate part of the loss in yield due to low aeration rates in the rougher the overall yield could be improved substantially by increasing the suction capacity. This was done by modifying the slurry distributor.

The effect of these changes on the suction capacity was very pronounced. Before the changes in both stages more or less identical air-rates have been observed. The changes in the distributor system of the rougher stage resulted in an increase in air-intake from  $320 \text{ m}^3/\text{h}$  to  $400 \text{ m}^3/\text{h}$  or 25%. This corresponded to an increase in the air

to slurry ratio from 0.45 to 0.6 and a gain in mass recovery of 4.3% (abs.) in the rougher stage and 3.4% (abs.) overall.

The last results of sampling after the changes indicate that after the modification tailings ash contents of over 70% at concentrate ash contents of 6% and overall mass recoveries of around 80% are achieved in normal i.e. none-testing conditions. The selectivity of the process, however, decreased slightly, which does not appear to be a big problem at the moment since currently no very high selectivity is required to ensure product quality.

### **Conclusions**

The aim of the presented work was to identify optimum operating conditions of a new flotation unit and to achieve maximum mass recovery at acceptable product qualities. This task was to be fulfilled at minimum expenses.

Since no physical-chemical model was available which would have allowed to describe the process sufficiently, a statistical approach was used. In a first step the most influential parameters have been identified. In the following work set points have been worked out for oil dosage, feed mass concentration and air to slurry ratios. Changes of the slurry distribution system in the rougher stage helped to improve process results.

Due to the experimental design effects of changes in feed quality could be compensated which allowed to compare results of different test series to a certain degree. The overall effort required for this work was only 12 days of sampling plus the additional laboratory work, compared to at least 20 days of sampling calculated to be necessary with a conventional sampling campaign giving the same degree of reliability in the results. Production went on without perturbations during test work. The approach was used for the first time in a DSK preparation plant. It is regarded as a very successful way and will be used wherever process conditions allow to adjust parameters to fixed values in future optimization work.

### **References**

- Bahr, A., Imhof, R. Lüdke, H. 1985. Application and sizing of a new pneumatic flotation cell. Proc. 15. Min. Proc. Congr., Cannes
- Bogensneider B, Janitschek R., Jung R.G., Haarmann H.-C., Lotzien R., Schwerdtfeger J., 1998. Pneumatic Flotation: an Alternative to conventional Mechanical Flotation machines? Proceedings of the XIII International Coal Preparation Congress, AC Partridge, IR Partridge (Eds) Vol. 1, 427-435
- Box G.E.P., Hunter, W.G., Hunter, J.S., 1978. Statistics for experimenters. John Wiley and Sons, New York
- Cordes, H., 1997. Die Pneumatische Flotation – eine Alternative und Ergänzung zur konventionellen Flotation. Aufbereitungs-Technik., No 2, Februar, 69 - 82
- Kubitzka, K.-H., 1980. Der Anreicherungsgrad des Normalgutaustrags zur Kennzeichnung von Trennungen. Glückauf 116. No 10, 508-513
- Kubitzka, K.-H., Wilczynski, P., Bogensneider, B., 1987. Die Aufbereitung von Steinkohle in der Bundesrepublik Deutschland. Glückauf 123, No 4, 177-182

## VALIDATION OF THE DISCRETE ELEMENT METHOD (DEM) BY COMPARING PREDICTED LOAD BEHAVIOUR OF A GRINDING MILL WITH MEASURED DATA

MH Moys\*, MA van Nierop\*, JC van Tonder<sup>o</sup>, G Glover<sup>o</sup>

\*School of Process and Materials Engineering

University of the Witwatersrand, Johannesburg, P.O. WITS, 2050, South Africa

<sup>o</sup>Eskom Technology Group, Johannesburg, South Africa

<sup>o</sup>Mintek, Randburg, South Africa

### Abstract

The Discrete Element Method (DEM) is a model that is used to simulate the motion of the media in a grinding mill. The sum of the energy that is lost in inter media and media-wall collisions represents the power drawn by the mill. The fact that DEM predicts the power drawn by grinding mills over a large range of diameters has been used to show the validity of DEM. However, the power drawn by a mill is a function only of the *sum* of forces of the load on the shell. A more accurate validation of DEM would involve an assessment of the ability of DEM to predict these forces. DEM should also be able to predict details of the behaviour of the load in the mill (e.g., the tendency of the load to cascade/cataract/centrifuge, the position of the toe and shoulder of the load, etc).

An experimental mill has been developed to reproduce exactly what two-dimensional DEM simulates. The 0.55 m diameter mill has a length of 0.023 m, which is slightly larger than to the diameter of the media used in the mill. One of the lifters in the mill has been instrumented so that the forces on the lifter can be measured as the mill rotates. DEM was used to predict these forces. A high-speed video camera was used to record details of the load behaviour. Reasonable qualitative agreement between predictions and experiment was obtained, but substantial adjustment of the model parameters and perhaps even of DEM algorithm itself (for example, the particle collision model) will be required before adequate quantitative agreement is obtained. This will give experimental evidence of the validity of DEM for rotating grinding mills. This work will also serve as an assessment of the accuracy of the generic DEM algorithm itself, so has implications for other uses of DEM, e.g. in the design of bins, silos, chutes, jigs and other processes.

*Keywords: discrete element method, DEM, comminution, simulation*

### Introduction

The importance of milling has been repeatedly emphasised. Rotary grinding mills are generally expensive to run and at the same time inefficient in the utilisation of energy for breakage. Any improvements in knowledge of mill load behaviour, and therefore potentially efficiency, can have dramatic improvements on the profitability of mineral processing operations.

Discrete Element Method (DEM) simulations are increasingly being applied to the modelling of the load behaviour of grinding mills. DEM simulations have the benefit of visually predicting load motion, as well as the power drawn by the mill. Increasing understanding of the effects of design and operating parameters on mill efficiency is being obtained through its use (Cleary, 1998).

It is essential that DEM predictions will be verified rigorously against experimental data. It is only once DEM has been shown to model the load behaviour adequately that the predictions will be used with confidence in industrial applications.

This paper provides an overview of the work being done to provide experimental data against which DEM predictions can be verified. To describe this work, some background on DEM theory is provided, the experimental apparatus is described, and results are discussed. This discussion includes comparisons of DEM predictions with the measured data.

### **DEM background**

The Discrete Element Method (DEM) is a way of modelling the motions and interactions of a set of individual particles and moving walls, as affected by gravity, models for particle interaction and Newton's Laws of Motion.

The interactions of the particles are modelled by the spring-slider-dashpot model. The particle and wall material properties are taken into account by specifying the coefficients of friction and restitution, as well as the shear and normal stiffness.

It is only due to the recent advances in computer accessibility and speed that it has become viable to calculate the motion of large sets of interacting particles. At first, a two-dimensional slice of the grinding mill, was simulated (2D DEM). This assumed that there was little net motion in the third dimension. With faster computers becoming available at reasonable cost, the developers of DEM software are rapidly turning to three-dimensional simulations (3D DEM).

To date most validation of DEM applied to grinding mills has been to compare the power drawn by mills and overall load motion (Agrawala, 1997; Mishra and Rajamani, 1990, 1992). At a recent (August 1999) DEM workshop held in South Africa, it was felt that more rigorous verification of DEM applied to grinding should be undertaken. Good predictions of mill power do not necessarily imply that the DEM provides a reliable model for mill behaviour. There are a number of possible load behaviour conditions that could result in the same power drawn. However, all energy provided to the load is passed through the mill shell. Thus the forces on a lifter would give a more detailed indication of how power is provided. The DEM simulator should be able to predict these forces accurately.

### **Experimental grinding mills**

An experimental mill (0.55 m diameter) was constructed that could mimic what a two-dimensional DEM model simulates. In other words the length of the mill (0.023 m) was set just fractionally larger than the diameter (0.02224 m) of the balls used. This mill is termed the "2D-mill" below.

In addition to this, there is a second mill (termed the "3D-mill" below) with the same diameter but with variable length. The effect of mill length can be investigated with this mill.

The mills were equipped with 12 square ( $22 \times 22 \text{ mm}^2$ ) lifters. The mills had variable speed drives allowing speeds up to 200% of the critical speed. Accurate torque measurements were obtained. The mill load volume was varied between 20% and 45% of the mill volume.

Load motion was measured using photos (taken through the glass sides) and also by means of infrared probes. Infrared sources were placed at various radial positions on

one side of the mill with matching detectors on the other side plate. These probes indicate the presence or absence of the load as the mill rotates.

An instrumented lifter (Figure 1) measured forces on the lifter of the 2D-mill. One of the lifter bars was mounted on a specially designed load beam so that radial and tangential forces and the bending moment can be measured using strain gauges.

A gap was cut into the shell. Strain gauges were mounted on an aluminium beam with an H cross-section to make available measurements of the radial compression, the transverse shear, and the bending moment suffered by the beam. The lifter is attached to the top of this beam, while the base of the beam is attached to the mill shell as shown.

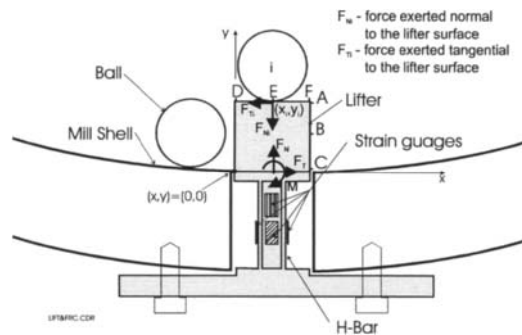


Figure 1: The instrumented lifter bar. Strain gauge bridges were mounted in such a way that compressive and shear forces and moment ( $M$ ) could be measured. A - F indicate points of application of forces used to calibrate the strain gauge bridges. The forces exerted by the ball,  $i$ , are indicated.

Most of the work was done with the 22.24 mm balls. However, it was found that these balls damaged the instrumented lifter in the 2D-mill. A comprehensive set of experiments was thus also undertaken with smaller ( $-9.5 + 5.5$  mm) balls in this mill.

## Results

An initial verification of the DEM is to compare snapshots of load motion. Photos of the 3D Mill were taken where the load is visible through the glass side plate. Figure 2a shows an example of this.

The 'measured' load motion is then compared to that predicted by the DEM. A frame of the load position is also shown in Figure 2c. The DEM qualitatively predicts the load motion of the mill very well.

The infrared probe data gives an estimate of the load shape (Figure 2b). This is useful for quantitative load motion analysis, giving, for example, toe and shoulder positions of the load. This type of data can also be useful in applications where there is no direct visible measurement available. A comparison of Figure 2b with Figure 2a shows that the toe and shoulder positions of the load can be predicted well using the infrared data. The infrared data (Figure 2b) also shows the presence of cataracting material.

The infrared data was used to determine the effect of mill length on load motion. The two-dimensional DEM simulations can only successfully predict three-dimensional

load behavior if the load is not affected by length or end effects. Figure 3 shows the measured shoulder position as a function of length, together with the predicted shoulder positions.

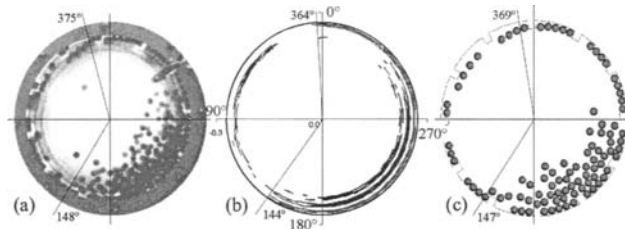


Figure 2: A comparison of the photographed load shape (a) and ball locations predicted by the DEM (c). The mill length was 0.066 m, load volume 20%, mill speed was 90% of the critical speed and 22.24 mm balls. The data from the infrared probes (b) indicates the load shape within the mill.

There is no clear trend of shoulder position with mill length. The shoulder positions at the each length show some scatter, while the positions at the different lengths are relatively close to each other. This enables the two-dimensional DEM simulation to predict the shoulder position with good accuracy.

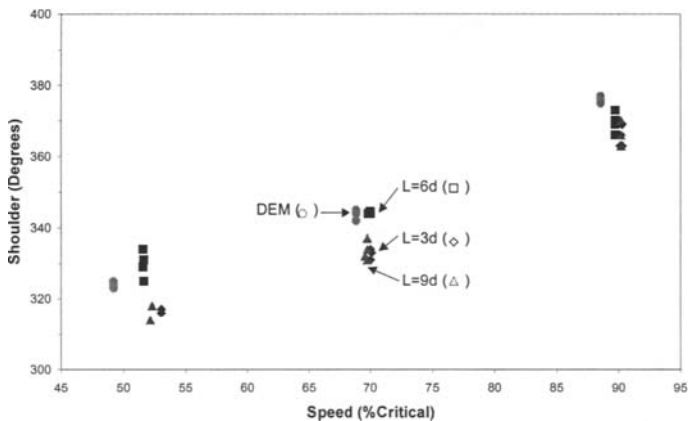


Figure 3: The shoulder positions for the mill operating with 20% load volume, 22.24 mm (d) balls in the variable length mill. The DEM predictions of the shoulder position are also shown. Mill length is given as a multiple of the ball diameter, d.

The torque was accurately measured using a load beam. The mill motor was suspended from the frame with bearings on the motor axis. The motor was only prevented from rotating on its own axis by the load beam. This gave the torque signal. Power was calculated from the torque:

$$P = 2\pi NT/60 \quad (1)$$

where:

P = power (N), T = torque (Nm), N = mill speed (rpm).

The measured power (Figure 4) for the two-dimensional mill with the 22.24 mm balls has the expected pattern. The power increases with mill speed until a maximum between 70% and 80% of the critical speed. The power then falls off until just above the critical speed.

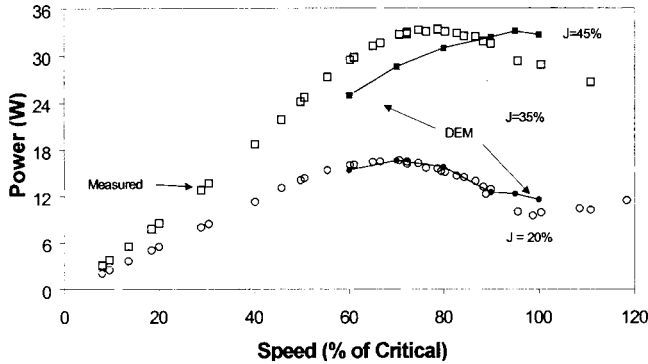


Figure 4: The power measured on the “two-dimensional” experimental mill operating with 22.24 mm balls. The 2D DEM predictions are shown (lines).

The DEM used for this work predicted the mill power from the sum of the calculated tangential forces exerted by particles on the shell. The alternative power prediction method (the sum of the energy expended during inter-particle and particle-wall interactions) was not used here. DEM predicts the power at  $J = 20\%$  well, but tends to under-predict the power at the higher load volumes. DEM also predicts the maximum power at a slightly higher speed than the speed at which the measured maximum occurs. Figure 5 shows an example of the measured and predicted forces on the lifter. The mill was operating with 20% load volume, 30% of the critical speed and 22.24 mm balls.

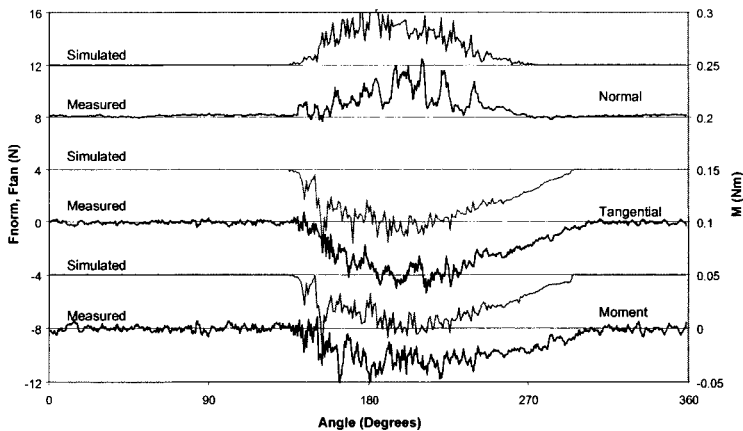


Figure 5: The measured and predicted forces on a lifter for the mill operating with 20% load volume, 30% of the critical speed and 22.24 mm balls.



To take account of particle interactions with the mill end plates the predicted forces were obtained using the 3D DEM, which had become available at this stage of the work. The measured forces shown in the figure are the average over three mill revolutions. The data was also filtered using a 5 point moving average to minimise the noise on the signal. The simulated data is the average of 12 lifters during one revolution. The data has been offset from zero by an appropriate constant to aid visualisation of the data.

Figure 5 shows very good correspondence of the predicted forces with the measured data. The comparison fits well in overall shape and magnitude of the curves. Obviously the detail is different, as is to be expected given the random nature of the interaction between the liner and at most three balls at any particular instant.

### **Conclusions**

The work done to date shows that DEM has great potential for increasing the understanding of load behaviour in grinding mills. Overall load motion and power can be predicted well. This comparison forms the bare essentials for the verification of the Discrete Element Method.

It is felt that for the DEM to be used with more confidence for applications including wear on the lifters (Glover & de Beer, 1997), more rigorous verification needs to be done. The forces on the lifter are a good starting point. All the energy transferred to the load is transmitted through the mill shell. This paper has shown that DEM can indeed predict these forces with reasonable accuracy.

The way forward includes more detailed comparison of various aspects of load motion. Work is being done to compare particle velocity fields and particle densities in the load. These will provide quantitative comparisons rather than the current qualitative comparisons. Also these will provide comparisons within the load, rather than just toe and shoulder positions at the mill shell.

Another important facet that needs to be investigated in future work is particle shape. Particle shape will have dramatic effects on load behaviour. Particle shape is most important in autogenous milling. A conclusion of the DEM workshop (Cape Town, August 1999) was that the ability of DEM in this regard needs to be tested.

The DEM verification discussed in this paper has referred to its application to comminution. However, the DEM can be applied to any unit that processes particles, such as chutes, stockpiles and conveyors. Verification of DEM in the milling environment will have beneficial implications for these other applications.

### **References**

- Agrawala, S., Rajamani, R.K., Songfack, P. and Mishra, B.K., 1997. Mechanics of media motion in tumbling mills with 3D Discrete Element Method. *Minerals Engineering*, 10 (2), 215-227.
- Cleary, P.W., 1998. Predicting charge motion, power draw, segregation and wear in ball mills using discrete element methods, *Minerals Engineering*, 11 (11), 1061-1080.
- Glover, G. and de Beer, J.C.K., 1997. The application of the discrete element method to the optimisation of mill liner systems. *Proc. XX IMPC, Aachen*, 21-26 September, Vol. 2, 219-228.
- Mishra, B.K. and Rajamani, R.K., 1990. Motion analysis in tumbling mills by the discrete element method. *KONA*, 8, 92-98.
- Mishra, B.K. and Rajamani, R.K., 1992. The discrete element method for the simulation of ball mills. *Appl. Math. Modelling*, 16, 598-604.

## DESIGN AND IMPLEMENTATION OF AN ON-LINE OPTIMIZING CONTROL SYSTEM FOR PROCESSING THE SADIOLA HILL OXIDISED GOLD ORE

T. Mulpeter\*, O. Guyot<sup>o</sup>

\*Anglogold, <sup>o</sup>Svedala Cisa, France

### Abstract

Sadiola Hill mine is located in the sub-Saharan part of Mali. In its first two years of operations, Sadiola Hill mine had already exceeded expectations with respect to profitability, plant capacity, metallurgical recovery, cash costs and social integration into the area. The advanced control system installed by the authors has been a major contributor in the substantial throughput of the mill over the design tonnage with no loss of recovery. The run-of-mine ore at Sadiola consists of soft clays with a varying percentage of grit, producing a high viscosity slurry. The percentage of grit fed to the plant varies on an hourly basis. This combination was expected to have a large impact on the milling circuit and determined that the early installation of an expert mill control system would be advantageous. Svedala Cisa OCS<sup>o</sup>, was selected as the most suitable support software. The operational rules and control philosophy are housed in the OCS<sup>o</sup> graphic-oriented fuzzy expert system while a model-based Soft Sensor has the remarkable ability to detect the variations in grit in the feed. Designed during the second half of 1996, commissioning of the system began in March 1997, the OCS was fully on-line by September. With the implementation of the optimising control strategy a throughput of 5.0 million t relative to the target of 4.4 million t was achieved for the 1998-operating year. The Sadiola project confirms that advanced process control techniques are among the most cost-and time-effective methods of improving metallurgical plant performance. The recipe that worked at Sadiola is a mix of metallurgical expertise, proper software selection, adequate design of control philosophy, and excellent plant support and follow-up. The early decision, design and installation of the mill control system have resulted in an enhanced Return on Investment.

*Keywords: optimizing control, expert system, Sadiola, OCS software*

### Introduction

Among Africa's success stories, the Sadiola Hill gold project is a leading case. Sadiola Hill mine is owned by SEMOS, a joint venture between Anglogold (38%) Iamgold (38%) IFC (6%) and the Mali government (18%). Located in the sub-Saharan part of Mali (Figure 1), the Sadiola Hill gold mine started producing in early 1997, with a 1998 production of over 500,000 oz (15 t). In its first two years of operations, Sadiola Hill mine had already exceeded expectations with respect to profitability, plant capacity, metallurgical recovery, cash costs and social integration into the area.

The feasibility study was commenced in 1993 with final approval for the project given in December 1994. Construction was begun in 1995. Despite the logistical problems of shipping equipment from Johannesburg to Dakar then to Sadiola by road/rail, construction was completed in 15 months (first concrete pour to first gold bar) at a capital cost of 280 million US\$. Commissioning began in November 1996 and the first gold bar was produced in December 1996.

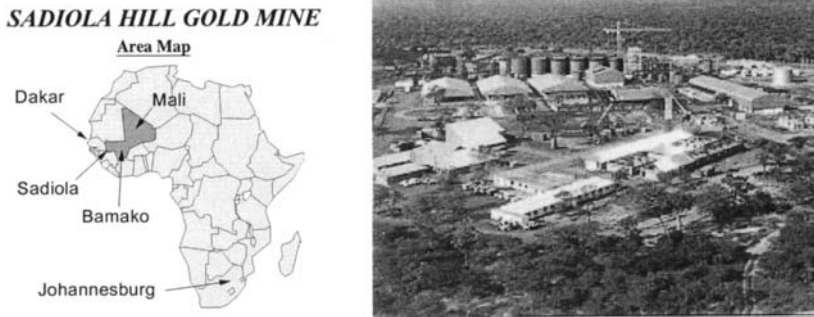


Figure 1: Location map and aerial view of Sadiola Hill Gold Plant.

### The Sadiola ore challenge

The mineralogy of the Sadiola ore deposit shows two major mineral types: decarbonated marble (DCMB) and kaolin diorite. The kaolin diorite contains variable amounts of soft clay mixed with hard siliceous grit.

Tests conducted by Anglo American Research Laboratories (AARL) in South Africa showed a high variability in grit content, hardness and viscosity. The proportion and gold grade of the grit meant that it could not be discarded while viscosity effects from the high clay content caused unfavourable pulp characteristics.

As the percentage of grit/clay fed to the plant was expected to vary on an hourly basis depending on how the ore is blended to meet production targets rapid changes in the behaviour of the milling circuit were expected. Such frequent changes require immediate and well proportioned reactions in a short time span. Therefore to run the plant at high throughput would require the aid of an advanced control system.

### First optimizing control system included in initial plant investment

The Sadiola project unlike previous mining projects is probably the first project for which the Optimising Control System was an integral part of the initial investment and not an add-on generating bonus profit after the routine operation of the plant is established. It is also among the first ones where the Optimising Control System efficiently combines a fuzzy logic expert control strategy with a powerful soft sensor based on a phenomenological model of the process.

The Optimising Control System was installed in March 1997 during plant commissioning, on a monitoring basis to check if the initial control philosophy was valid. In September the same year the Optimising Control System went on-line and immediately turned out to be a major factor in the substantial throughput of the mill over the design tonnage with no loss of recovery. With the implementation of the Optimising Control System a throughput of 5.0 million t relative to the target of 4.4 million t was achieved for the 1998-operating year. The Sadiola project proved that the design addition of an Optimising Control System allowed the operation to obtain early benefits and that it is technically feasible to pre-design such a system from test work before routine operation of the plant is established.

### **Description of the Sadiola Hill process**

The Sadiola Hill gold plant has two parallel streams. The run of mine ore is delivered into the surge bin either from stockpiles or directly from the mining operation. The surge bins are fitted with static grizzlies to reduce the top size of the larger lumps. An apron feeder transports the material directly to a mineral sizer with a gap setting of 300 mm. The sized material discharges directly on to the mill feed conveyor. The two primary milling circuits are identical, comprising a 4.85 m diameter  $\times$  4.88 m length mill. Each circuit is equipped with a cluster arrangement of nine cyclones and can operate in open or closed circuit. When the primary mills are operated in open circuit the underflow from both sets of clusters is combined to form the feed to the secondary milling circuit.

The secondary milling circuit consists of a 4.85 m diameter  $\times$  5 m length regrind ball mill that operates in closed circuit with a cluster arrangement of nine cyclones. The cyclone overflow is fed directly to a distribution box. The box splits the stream and combines it with the cyclone overflow from the primary milling clusters. These streams feed parallel linear screens that remove wood chips and tramp material prior to the material being fed to leach.

Due to the nature of the Sadiola material there is no thickening stage. Therefore the cyclone product flows directly to the leach tanks. Gold dissolution is effected through a 24 h leach followed by a conventional carbon in pulp circuit. The gold is desorbed via the AARL elution process. Recovery is achieved through electrowinning of the eluate solution. The electrowinning product is washed from the cathodes, filtered, dried and smelted.

### **Instrumentation and conventional controls**

The instrumentation installed on the Sadiola milling circuit is comprehensive in order to allow proper stabilising control and effective optimising control (Figure 2).

On both feed streams, a variable speed apron feeder controls the mill feed rate. All three mills are fitted with a variable speed motor capable of varying the speed between 50% and 75% of critical speed. Mill power is available through a dedicated power monitoring PC installed in the control room. Mill discharge pump boxes are equipped with a level transmitter and a variable speed pump.

On all three cyclone feed lines, a volumetric flow meter and density gauge enable control of cyclone feed conditions. The cyclone clusters are fitted with a pressure sensor, and on each cluster, three cyclones were equipped with automatic control valves during 1998.

Slurry dilution is controlled through water flowmeters and control valves on the inlets and discharge of each primary mill. A flow meter on the regrind mill discharge of end water line allows control of density inside the regrind mill through back calculation from the cyclone feed density. Each leach feed stream is equipped with an on line viscosity meter which controls caustic soda and viscosity modifier addition systems for the control of viscosity. The control level consists of Allen Bradley PLCs (Programmable Logic Controllers) and two Operator Workstations running Rockwell Software RSVIEW SCADA (Supervisory Control And Data Acquisition), all devices being connected through a Ethernet LAN.

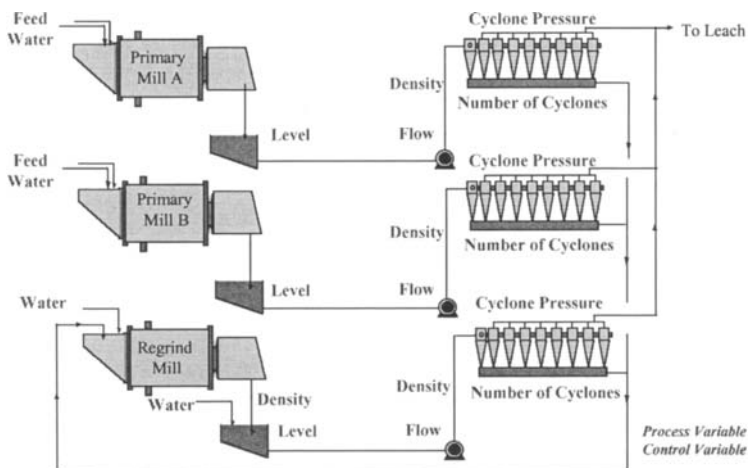


Figure 2: Representation of the current process and control variables.

### Description of the Sadiola mill optimizing control system

#### *Optimizing control systems*

Optimizing control systems are among the most cost- and time-effective methods of improving metallurgical plant performance.

As shown in Figure 3 below, in a mineral processing plant, optimising controls supplement conventional DCSs (Distributed Control Systems) and PLCs and continuously maximise the profitability of plant operation.

Optimising control systems automatically read information from the DCS or PLC data base, and use various advanced techniques to calculate new appropriate set points, typically several times per minute. These set points are established to continuously pursue strategic objectives.

They maintain a required product quality while targeting a technical and economical objective. The set points are automatically applied at DCS or PLC level without involving any action from the operators.

This results in an increase in capacity, product quality and value and/or a decrease in production costs.

In order to effectively provide the expected high profitability, an optimising control system has to be:

- well-accepted: both operators and metallurgists must be confident that the system is their ally, that it increases profitability and does not complicate their life;
- powerful: it must take timely actions. actions have to be sound and generate visible benefits;
- reliable: it must be robust and never make mistakes;
- available: it must be robust to instrumentation failures and remain able to run the plant in all types of situations.

Each of these expectations can only be met by combining an appropriate software platform with a sound methodology for configuring the system.

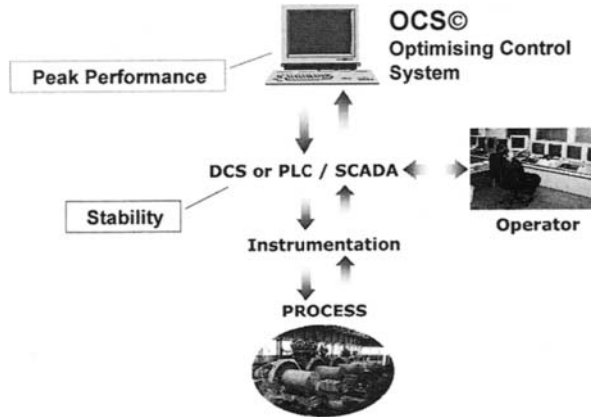


Figure 3: Structure of Optimising Control System.

#### *Hardware platform*

The Mill Control System at Sadiola is installed in the central control room on a dedicated Pentium II PC computer running Microsoft Windows NT (Windows 95 was the initial operating system).

Two software programs are installed on the PC: Svedala Cisa's OCS© software for optimising control and Rockwell's RSVIEW for PLC communication and visualisation duties. The Mill Control System communicates with Allen Bradley PLCs via RSVIEW SCADA.

The communication protocol used here is DDE (Dynamic Data Exchange) which was the only plug-and-play market standard for interprocess communication on Windows platforms when the system was designed. There is one Optimising Control System for the three milling circuits, which makes Expert System decisions based on the status of the three circuits.

The Optimising Control System is fully multitask and not demanding on system resources: it is not slowed down by other applications or operators actions, and it does not slow down other tasks.

The operators normally do not need to interact much with the Optimising Control System which automatically starts, interacts with the plant and implements the most appropriate control actions. However plant operators and metallurgical engineers have permanent access to some features of the system, in order to observe and understand what happens or happened. They can visualise selected information generated by OCS© and modify selected control parameters either directly through OCS© interface or through RSVIEW faceplates.

#### *OCS© software*

Svedala Cisa's OCS© software embeds selected artificial intelligence and other techniques in a uniquely easy-to-use modular, yet integrated structure: an expert system with crisp logic and fuzzy logic reasoning, supplemented with Svedala Cisa self calibrating models based on the physics of the process and soft sensors and, when necessary, neural networks.

OCS© offers the flexibility and safety of a rule-based approach and the powerful ability to combine the fuzzy logic expert system with soft sensors and adaptive phenomenological models to find fully optimised set points. The approach reflects experience in optimising control acquired over more than ten years in Europe and North America.

All modules within OCS© exchange input and output data. There is no set limit to the number of tags and rules manipulated. Rules are entered and displayed using a simple graphical interface, similar to a "Windows Explorer" tree-structured hierarchical window. OCS© is also configurable to automatically read and play voice messages for the operators when it is important to draw their attention.

OCS© builds and displays the inference tree associated with a knowledge base, shows dynamically a graphical status of fuzzy sets, thus allowing for easy logic tracing.

Because OCS© physical models are available for most unit operations encountered in mineral processing, the most powerful approach in a mineral plant usually consists of a model-predictive approach combined with a fuzzy logic expert system. The knowledge about the physics of the process embedded in the models brings numerous advantages over black box approaches such as neural nets, MVC (Multivariable Control), etc.:

By design, model predictions are based on the physics of the process. In comparison, a neural network only models whatever is in the training data set.

It remains valid over time, thanks to its adaptive filter, even when process conditions change drastically. The system more rapidly adjusts model parameters to accommodate changes in process conditions, again because of the adaptive filter, and optimised responses are readily implemented.

By nature, any alternative "learning" system based on techniques such as neural networks is considerably much slower to adapt its response.

It does not overtrain, which is a concern with neural networks.

However OCS© also includes an easy-to-configure Neural Network module which is valuable for processes for which no physical model is available. OCS© control strategies and models are available for mineral processing plants with crushing, grinding, flotation, magnetic separator, etc., as well as for pyro- and hydro-metallurgical operations.

### **OCS© control philosophy at Sadiola**

The objective pursued by OCS© at Sadiola is to maximise the crushed ore feed rate to the milling circuits while maintaining a constant feed – i.e. acceptable viscosity, density and grading - to the leaching section.

The control philosophy based on initial test work was set during preliminary design review meetings in Johannesburg between Anglo American CTO (Central Technical Offices), AARL and Svedala Cisa. It was structured in four conceptual sets of rules devoted to strategic missions to meet the objective:

"Leach Feed Quality" ensures that the milled product meets the requirements for the leaching section.

"Feed Rate Maximisation" increases the feed rate until the mill product quality would be affected by further increases.

"Grit Fraction" monitors the circulating load, adapts operating set points to high grit feed conditions and displays messages as to when the regrind mill should be operated. (in the system installed on site, the "Grit Fraction" module is greatly assisted by the adaptive modelling module of the OCS© software. The grit fraction in the feed is continuously estimated from other process measurements. The OCS© modelling module is therefore acting as a Software Sensor, providing on-line estimate of a physically unmeasured ore characteristic).

"Ore Sticking" monitors the performance of the primary mills to check for ore sticking in the mill due to the clay content.

Three OCS© modules are activated in the Sadiola configuration: the Expert System, with crisp and fuzzy logic inference engine, an advanced Soft Sensor, based on a powerful on-line adaptive predictive physical dynamic model, and a Statistical module.

The control philosophy is reflected in operational crisp and fuzzy logic rules housed in the Expert System module (Figure 4).

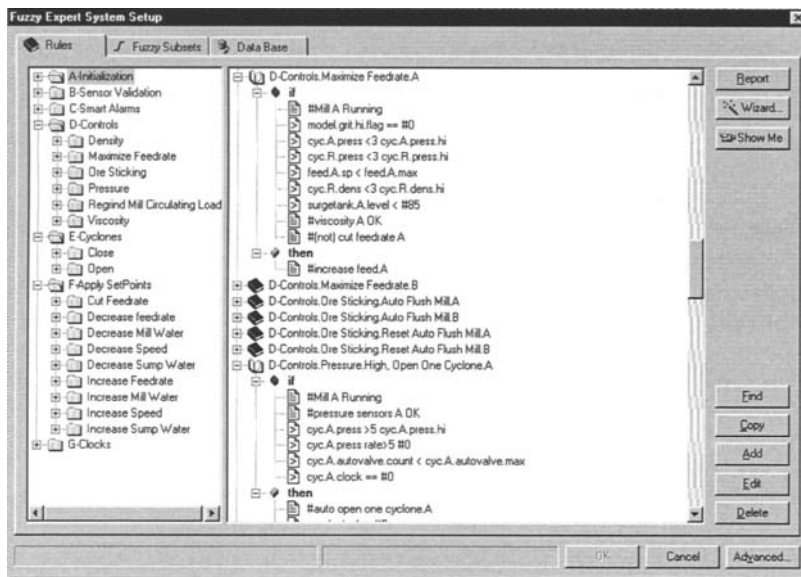


Figure 4: OCS© Rule Base Editor.

The rules use measured process values and estimates computed by the Soft Sensor as inputs. They determine all final set points sent to the process (feed rates, rotation speeds, water additions, cyclone parameters and viscosity controls). Their configuration guarantees that decisions and set points are always realistic and compatible with accepted plant practice. The fact that all model inputs are analyzed by the expert system ensures the realism and relevance of all set points at any time.



The Soft Sensor combines an on-line dynamic phenomenological (physical) population balance model and a filter estimator which continuously calculates the most probable values of process parameters (including grit fraction) from both model predictions and measurements. The remarkable ability of the Soft Sensor to detect the variation of grit in the mill feed, which could obviously not be measured, turned out to be a major strength of the system.

### Evolution of operating and control philosophy

The installation of the mill control system was timed immediately after the plant was initially commissioned. Some parameters could not be determined through test work. The system required some basic knowledge of plant operation so that the control philosophy could be implemented. A project team was assembled consisting of a divisional metallurgist (Anglo American CTO), a commissioning metallurgical engineer (SEMOS) and representatives from Svedala Cisa.

The system was installed in March 1997 on a monitoring basis to check if the initial control philosophy was valid. From commissioning difficulty was encountered maintaining the leach feed density. Through monitoring of the system, it soon became apparent that the problem lay in the control of the primary mill dilution water. The process philosophy was changed so that the primary mills worked as scrubbers with the coarse fraction sent to the regrind mills.

This meant that the regrind mill would not be stopped and started from time to time but would run continuously. Figure 5 below shows the improvement in leach feed density and milling rate achieved after this first change in process philosophy. The milling circuit was stable and the plant was able to achieve the design throughput. During this period a comprehensive study of the milling circuit was undertaken to gain an understanding of how it operated. The results of this study lead to the second change in operating philosophy.

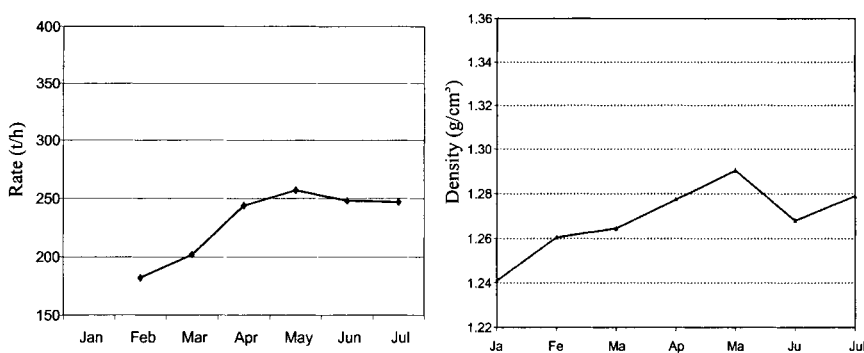


Figure 5: Evolution of throughput (t/h) and leach feed density (g/cm<sup>3</sup>): January to August 1997.

It was found that to achieve a proper control over the mill cyclones, the flowrate to the cyclones would have to be controlled on sump level rather than the density of the cyclone feed. Density control could be achieved by adding all the primary mill process water at the inlet through a ratio controller on the feed rate. The study also

showed that a physical change in the geometry of the cyclones was required. The inlet wedges were found to be too small and larger wedges were installed. These changes were made at the second site visit. The optimising control system entered into operation during the site visit, with among others density control and throughput maximisation philosophy. Figure 6 below shows the improvement in leach feed density and throughput after this second change in philosophy.

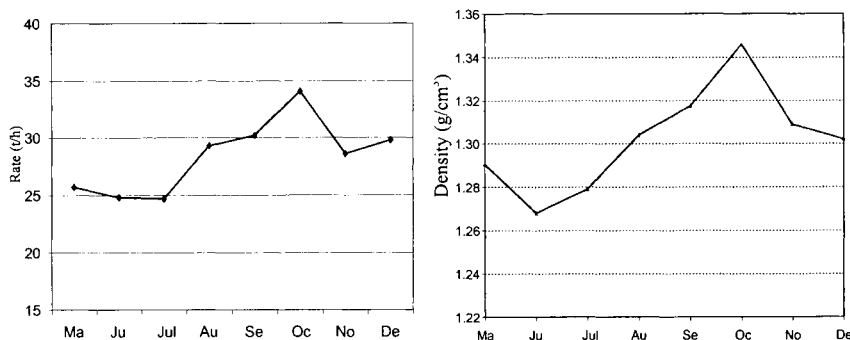


Figure 6: Evolution of throughput (t/h) and leach feed density ( $\text{g}/\text{cm}^3$ ): August to December 1997.

The system was now optimised with the mill circuit throughput increased by 25% without affecting gold recovery.

Sadiola also presented a challenge in that the local labour force was inexperienced in many aspects of plant operation. The system aids the operators by reducing their workload as it checks every parameter once a minute and makes automatic changes to keep the mill performing at its peak for the given ore type. The system was upgraded to deliver voice messages in local language (French) of situations that require their attention and thereby reducing unnecessary losses of throughput. The acceptance of the OCS© by operators is therefore excellent. The system has proved so reliable and gained the trust of the labour force that Sadiola operates with no experienced expatriate labour on shift.

### Maintenance

The system continues to be improved with more rules being added to control the speed of all mills to minimise power requirements. Due to power supply problems this function has still to be fully tested. The capacity of the system has lead to monitoring of other areas of the plant for situations which may cause downtime or affect gold recovery.

This includes the elution area and all plant water tanks. It is planned to add cyanide and pH control to the system to further reduce reagent costs.

The system is reviewed every six months as it has been found that this interval allows to fully evaluate the changes made so that further improvements can be implemented. The control philosophy is also checked to enable any rules no longer required to be deleted, thus keeping the system fully on line. To date the system has proved very reliable with no appreciable downtime associated with the software.

**Conclusions**

The Sadiola project confirms that advanced process control techniques are among the most cost- and time-effective methods of improving metallurgical plant performance. The project achieves a throughput that is more than 25% in excess of design capacity. The recipe that worked at Sadiola is a mix of metallurgical expertise, proper software selection, adequate design of control philosophy, and excellent plant support and follow-up. The early decision, design and installation of the mill control system resulted in an excellent Return On Investment.

**References**

- Broussaud, A., Guyot, O., 1999. Profitability of Optimising Control Systems in Mineral Processing. 3<sup>rd</sup> Processing for Profit Conference, 26-28 April, Antwerp, Belgium.
- Johansson, B., Bergmark, B., Guyot, O., Bouché, C., Broussaud, A., 1998. Model-Based Control of Aitik Bulk Flotation. SME Annual Meeting, March, Orlando, FL, USA.
- Kontopoulos, A., Krallis, K., Koukourakis, E., Denaxas, N., Kostis, N., Broussaud, A., Guyot, O., 1997, A Hybrid, Knowledge-based System as a Process Control "Tool" for Improved Energy Efficiency in Alumina Calcining Furnaces, Applied Thermal Engineering, Vol. 17, No 8-10, Elsevier Science Ltd., 935-945.
- Samskog, P.O., Söderman, P., Storeng, U., Björkman, J., Guyot, O., Broussaud, A., 1996. Model-Based Control of Autogenous and Pebble Mills at LKAB Kiruna KA2 Concentrator – Sweden. Proceedings of the International Conference on Autogenous and Semiautogenous Grinding Technology. October 6-9, Vancouver, Canada, pp. 599-616.

## ON-LINE PREDICTION OF TRANSIENT PHENOMENA IN THE SLAG PHASE DURING ILMENITE SMELTING

J.J. Eksteen\*, M.A. Reuter<sup>o</sup>

\*Department of Chemical Engineering, University of Stellenbosch, Private Bag X1, Matieland, 7602, Stellenbosch, South Africa,

<sup>o</sup>Faculty of Applied Earth Sciences, Technical University of Technology, Delft, The Netherlands

### Abstract

Slag foaming and metal entrainment in high titania slags are complex dynamic phenomena that bears strong non-linear relationships to the slag chemistry and furnace operating conditions. These phenomena are traditionally difficult to predict and control on a feedforward basis. Feedback controls tend to be inefficient due to the large process time constants of industrial furnaces. A system identification technique lends itself to a novel approach for process analysis, when it is used in conjunction with fundamental process and thermodynamic knowledge. This paper presents the results of non-linear, dynamic modelling of transient phenomena such as the chemical causes of slag foaming and entrainment during the carbothermic reduction of ilmenite in open-arc smelting furnaces. The system is characterised using non-linear system identification techniques such as backpropagation neural networks. It will be shown how the outputs of the system characterisation techniques in combination with knowledge of the physico-chemical fundamentals can be used in decision support on a smelter plant. Consequently, feedforward control strategies can be developed to minimise unwanted behaviour. The propensity of slags to foam is a non-linear function of slag viscosity, surface and interfacial tensions, slag density, reaction kinetics and slag inventory, which, in turn, are strongly non-linear functions of the slag chemistry, the type and amount of solid phases present in the slag and the furnace operating conditions. The same factors also influence metal entrainment in the slag phase and consequently metal recovery. This research aims to shed some light on predicting when solid precipitation will take place that may eventually cause severe slag foaming during the carbothermic open-arc smelting of ilmenite.

*Keywords: control strategy, ilmenite, smelting, slag foaming*

### Introduction

Ilmenite ( $\text{FeTiO}_3$ ) concentrates make up 90% of the world titanium feedstock; the rest consists of natural rutile. The ilmenite is concentrated using a combination of magnetic, electrostatic and gravitational mineral separation unit operations to remove most of the gangue minerals that severely impact on both the smelter operation and the subsequent pigment production. In order to prevent excessive reagent consumption and waste products in the subsequent pigment production steps via the sulphating or carbochlorination routes, the titanium grade (measured as the Ti/Fe ratio) has to be upgraded, typically by carbothermic reduction of the ilmenite. During reductive smelting, the ilmenite is upgraded to a high titanium slag (80÷85%  $\text{TiO}_2$ ) and high quality pig iron at slag temperatures between 1,600 °C and 1,750 °C. The high temperatures and extreme reducing conditions lead to partial volatilisation of silicon as silicon monoxide, manganese, sulphur, sodium oxide, phosphorous and

magnesium, which all tend to have high vapour pressures at typical operating temperatures. However, the activities of the metal oxides are reduced in the slag phase due to the formation of stable titanates.

### Reductive smelting of ilmenite

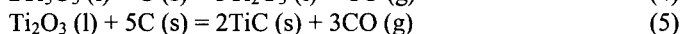
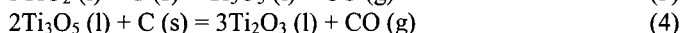
High titanium slags are typically produced in either six-in-line AC open arc furnaces or DC plasma arc furnaces. Open arcs / plasma arcs are required as the high titania slag has a very high electrical conductivity, making power dissipation through resistive heating of the slag infeasible. The feed materials are either introduced into six-in-line open-arc smelter employing multiple feed ports (most of them situated near the side walls of the furnace in order to protect the furnace side walls from refractory erosion) or via a single hollow electrode into the plasma zone of a DC plasma arc furnace. Localised regions of over-reduced slag are periodically produced which gives rise to slag foaming in both types of furnaces. This is regarded as a loss of control and corrective measures which need to be taken, lowers the thermal efficiency and availability of the furnace (Denton and Schoukens, 1993). Moreover, the over-reduced situation is indicative of substantial amounts of slow dissolving carbide and oxycarbide precipitation. These carbides have melting points far above the slag liquidus and the actual slag temperatures. Moreover these carbides not only lead to froth stabilisation due the effect of higher apparent slag viscosity on froth drainage rate, but also lead to metal entrainment in the slag. Severe frothing also leads to erratic electrode behaviour, refractory damage and may even lead to dangerous spillage when the slag foam reaches the furnace roof. Severe slag foaming is therefore indicative of unwanted behaviour, which leads to higher metal-in-slag entrainment, loss of operating stability and unsafe situations. Controlling foaming therefore becomes a priority in the reductive smelting of ilmenite. Due to its impact on slag viscosity and froth stabilisation, it is sensible to limit the amount of titanium carbide formed. As the carbides slowly reoxidises in the slag, and XRD analysis are typically not performed due to time and cost constraints on industrial smelters, the titanium in the metal phase may serve as indicator to infer the level of titanium carbide production. Titanium enters the metal phase as the carbide, as this is the state that is thermodynamically the most feasible. The carbide, however, dissociates into its elements in the metal phase until saturation occurs. The relevant reactions are:



while:



While the reduction of oxide to metal becomes thermodynamically feasible at about 2,041 K, the carbide formation reaction becomes feasible at 1,563 K. Because the temperature dependence of  $\Delta G^\circ$  is so small in the carbide forming reaction, TiC is a very stable compound with respect to Ti and C at all practical temperatures. The actual reduction mechanism probably occurs along the following path (Pesl and Eric, 1997):



As TiC also forms regular solid solutions with TiO to precipitate titanium oxycarbides,  $TiO_xC_{(1-x)}$ , (Coley et al., 1995), the TiC formation is therefore further stabilised by the reduction of TiC activity due to the partial solvation of TiC in TiO. TiC has a melting point of 3,413 K while TiO has a melting point of 2,023 K. Both the carbide and oxycarbides therefore have melting points far above the typical operating slag temperature of 1,973 K. The carbide is wetted by slag and metal, but while insoluble in the slag, it has a limited solubility in the metal. Johnsson (1998) reports that TiC has a solubility of  $0.299 \pm 0.008\%$  wt Ti at graphite saturation in molten iron at 1,873 K, with solubility increasing with temperature. As the titanium level in industrial furnaces typically falls below 0.2% wt, saturation of the metal phase with the carbide is never reached.

The rate of carbide formation is expected to be a function of mixing conditions and turbulence in the slag, the ratio of volatiles in the coal to fixed carbon, the coal particle size and the oxygen and  $TiO_2$  activity in the slag phase. Mixing and turbulence in open arc and plasma arc furnaces occurs due to arc impingement on the slag surface, electrohydrodynamic effects and due to the CO bubbles formed in the slag from the reactions indicated above.

Gibb's free energy minimisation using ideal associated solution modelling for the slag phase at 1,700 °C can be used to estimate the speciation in the melts. Figure 1 illustrates the equilibrium speciation at various carbon additions.

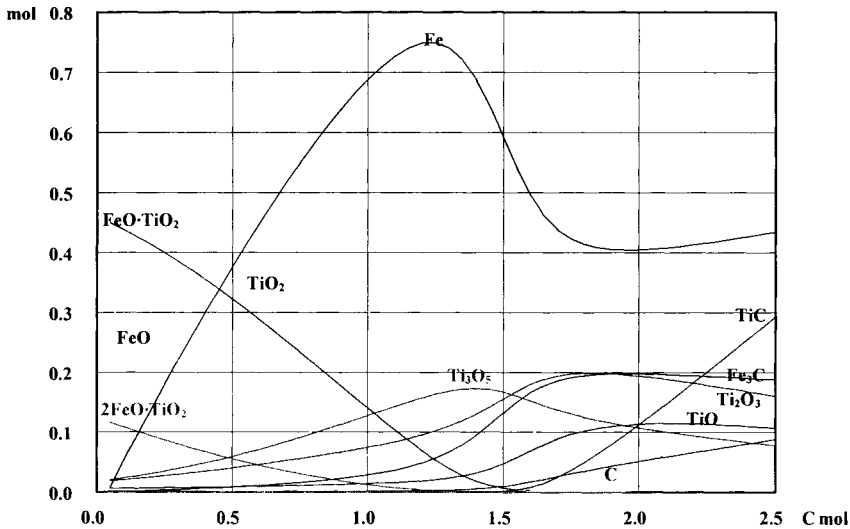


Figure 1: Speciation in high titania slags, based on Gibb's free energy minimisation using ideal associated solution modelling.

### Non-linear system identification and modelling of speciation

As indicated above, it would be sensible to be able to forecast and control the % titanium in the iron melt. Reuter and Moolman (1999) mentions that formulation of a

feedforward control strategy is often extremely difficult, mostly because much of the thermodynamics and kinetics of real coal-slag-gas-metal reactions are still ill-understood, with data lacking to develop a fully integrated model for metallurgical control. Non-linearities are evident from the complex patterns of optima in the systems, making linear techniques unsuitable in many cases. Variable time lags occur, implying the prediction window must adapt to the variable lag. Many of the system characteristics such as feed mineralogy, coal petrology and process conditions change over time, making the system non-stationary as well. It therefore implies that the models should be able to adapt its parameters.

A “Grey Box” approach was followed where metallurgically significant variables have been selected which were obtained by pre-processing the data to build in some level of understanding or higher knowledge into the model. These variables may include stoichiometric ratios, slag basicities, specific energies and dynamic inventories of slag and metal in the furnace. System identification techniques like the Fast Fourier Transform (FFT) of a time series, as well as various time-series analysis techniques plays a significant role in identifying the key process parameters and how their dynamics influences a specified output variable and its behaviour with time. For instance, the FFT is an aid to identify the frequency of underlying cycles in the data. Linear systems analysis for linear time series may be applied in the form of the autoregressive-integrated moving average models, or other non-parametric statistical techniques such as back-propagation and Elman neural networks may be used for non-linear systems identification (Reuter and Moolman, 1999). Once the model has been developed it may be pruned and optimised.

### Analysis and prediction of titanium carbide formation for actual ilmenite smelting furnaces

Figure 2 shows the % Ti (as TiC) in an actual furnace during normal operation. Each point on the graph depicts the titanium assay in the molten metal after each tap.

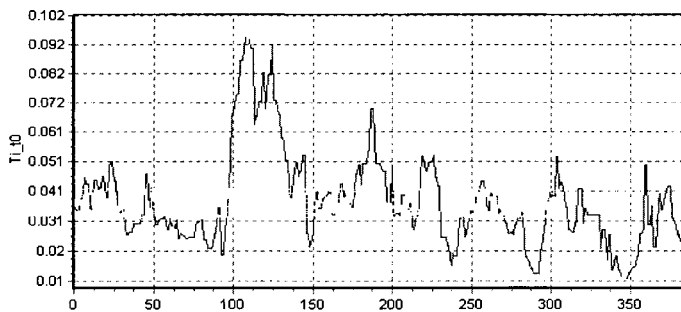


Figure 2: Time series of TiC dissolved in the metal phase for an actual ilmenite smelting furnace: equilibrium speciation during the carbothermic reduction at 1,700 °C, per mole ilmenite feed.

The tap-to-tap time of the metal is variable. As a significant metal and slag heel are always maintained after each tap, the residual melts may effect the metallurgy of future taps quite drastically.

The power spectrum (FFT, Figure 3) shows that most of the energy of the signal is damped long before double of the sampling rate (which takes place every 4 hours). The high frequency component shows that there are low levels of process noise in the data. Furthermore the power spectrum shows that a distribution of cycles of various time constants is present in the data. The metallurgical significance of this observation is that past values of TiC in the iron influences the %Ti of the later assays of metal of subsequent metal taps. This would seem obvious due to the metal heel that remains after tapping, as well as due to the large inventories of these semi-continuous furnaces. Less than 10% of the total inventory of the furnaces is tapped during production runs. This process feature implies that past values of the %Ti (as TiC) may be very significant in dynamically predicting the level of TiC in the metal.

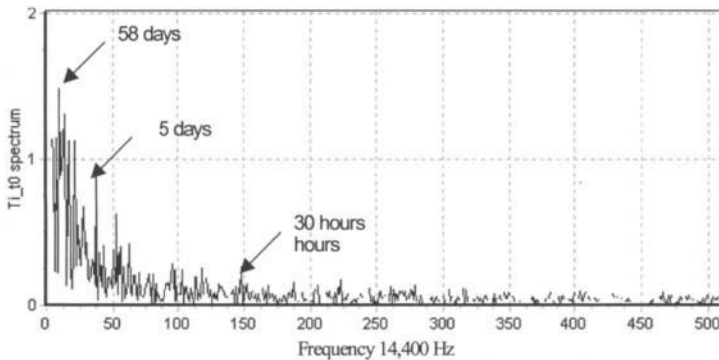


Figure 3: The power spectrum of the TiC time series: FFT of Ti\_t0.

The effect of including the historic values % Ti levels in a backpropagation neural net model is shown in Table I. The model fit ( $R^2$ ) improved from 72% to 91% by including historic values of Ti over and above the operating process parameters. It is interesting to compare the neural net (NN) prediction capability to the prediction capability of a multivariate linear regression (MLR) model. While the NN performs significantly better than the MLR model when historic values of the Ti% are excluded ( $R^2 = 72\%$  for the NN versus 51% for MLR), the models tend to predict with similar accuracy ( $R^2 = 95\div 96\%$ ) when these historic values are included. This shows the overriding effect of historic levels of Titanium in the iron on the model predictions of Titanium in subsequent taps. The dependence of assays of subsequent taps on previous taps is expected to become less as a larger proportion of the furnace inventory is tapped.

A Backpropagation Neural Network (BPNN) has been trained on the available input data (320 training sets and 80 test sets) and pruned until 15 input process parameters were identified as the minimum number of significant process variables to be able to explain more than 90% of the variation of the Ti% time series ( $R^2 > 90\%$ ). An optimum number of 8 primary and no secondary hidden nodes were found after less than 500 epochs, both sets of nodes employing the hyperbolic tangent nodal function. All network weights were randomized to values between  $-0.9$  and  $0.9$ .



Table I: Predictive capabilities of models to predict Ti% assays, using the multiple linear regression model as benchmark.

Model prediction without historical Ti% assays as model variable		
	Correlation coefficient (r)	Explained variance (R <sup>2</sup> )
BPNN	0.83	0.72
MLR	0.70	0.51
Model prediction with historical Ti% assays included as a model variable		
	Correlation coefficient (r)	Explained variance (R <sup>2</sup> )
BPNN	0.95	0.91
MLR	0.96	0.92

The level of TiC in the iron was most sensitive to the following variables, listed in order of descending sensitivity:

- Ti% in metal assay of previous tap;
- average value of the thermocouple temperatures of the furnace shell refractories;
- minimum value of the thermocouple temperatures of the furnace shell refractories;
- maximum value of the thermocouple temperatures of the furnace shell refractories;
- tap-to-tap duration of the slag in the furnace;
- residual sulphur% in the metal of the previous tap;
- total furnace inventory;
- FeO% in the feed;
- FeO% in the residual slag from the previous tap;
- volatiles% in the anthracite fed to the furnace;
- median (D<sub>50</sub>) particle size of the coal;
- CaO% in the feed;
- SiO<sub>2</sub>% in the feed;
- residual carbon in the metal of the previous tap;
- total shell heat loss from the furnace.

The time series of the model prediction versus actual (target) prediction, as shown in Figure 4, indicates that the model predicts the variation of TiC in subsequent taps very well. The variables listed above are used to predict the %Ti in the metal one tap into the future (that is 4 hours into the future). The graph shows the results for the predictions based on unseen data, for which the BPNN was not trained on. A decision support system or closed loop control system may therefore be developed to control the level of TiC formation. It should be noted that most of the TiC would be entrained in the slag as it is wetted by the slag. As indicated by the list of significant model variables, the coal proximate analysis and particle size plays a substantial role in affecting the TiC formation. The non-linear and combined effect of coal particle size and % volatiles in the coal is shown in Figure 5.

Figure 5 clearly illustrates that the formation of TiC is very much controlled by factors related to coal reactivity. The neural network predictions of the points on the figure was made by keeping all the other variables at their average values, while the % volatiles and coal particle size was varied between their typical operating limits.

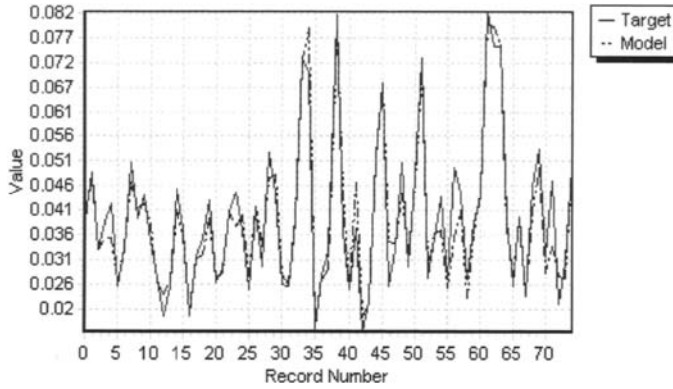


Figure 4: BPNN model predictions versus actual observed levels of %Ti in the molten metal.

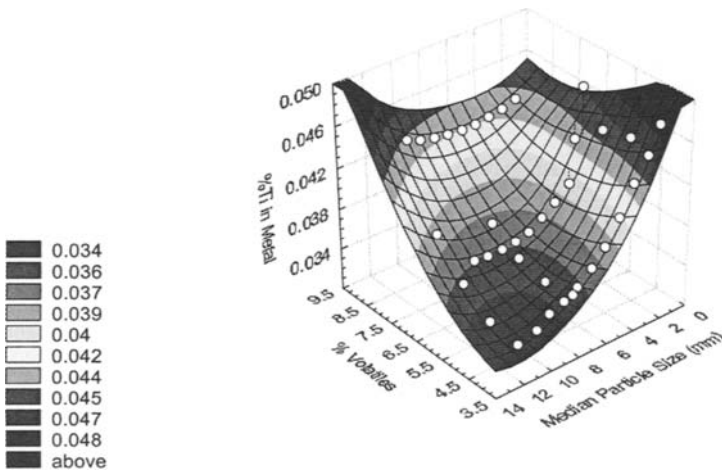


Figure 5: Effect of coal properties on TiC levels as predicted by a neural network.

The actual TiC formation was found to lie far from equilibrium predictions (actual TiC production was found to be as much as one order of magnitude greater than equilibrium predictions). While the amount of reductant fed to the furnace did not feature as a significant model variable, the state of oxidation of the feed and residual slag (measured as the amount of unreduced FeO in the ilmenite or slag) did influence the predicted level of TiC significantly. Variables that tend to influence the rate phenomena, such as particle size, amount of available gaseous reductant, and sulphur concentration (which lowers the slag-metal interfacial tension), featured more pertinently as model variables. The model predictions of the effect of % dissolved residual sulphur in the metal and the residual state of oxidation of the slag (measured as FeO%) is shown on Figure 6. The other model parameters were kept constant at

their average operating values. The residual concentrations refer to the concentrations of materials that were present in the metal or slag heel from the tap previous to the one for which the Ti% is predicted.

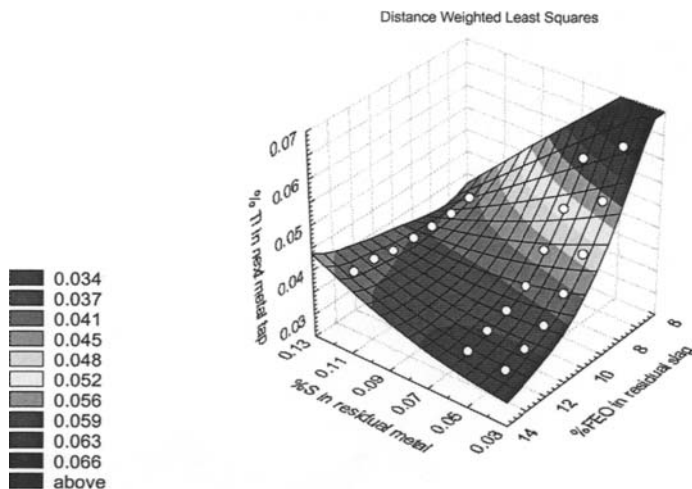


Figure 6: Effect of % dissolved sulphur and % FeO in the residual slag on TiC levels as predicted by a backpropagation neural network.

Figure 6 indicates that high levels of dissolved TiC only occurs when the residual slag was highly reduced (little FeO) and the metal in contact with the slag contained very little sulphur. Increasing the amount of residual sulphur for a less reduced slag, increases the predicted amount of TiC being formed, while increasing the sulphur level for a highly reduced slag, reduces the amount of TiC formed. The extreme non-linearity of the model is apparent from the two figures discussed above. The role of the sulphur is known to reduce the surface tension of molten iron as well as the interfacial tension between metal and slag. For instance, increasing the sulphur activity from 0 to 0.05, reduces the interfacial tension of iron, in contact with a slag containing 50%  $\text{Al}_2\text{O}_3$  and 50%  $\text{CaO}$  at 1,660 °C, from 1,250 to 945 mN/m (Verein Deutscher Eisenhüttenleute, 1995). Although no references to interfacial tensions of molten iron with high titania slags could be found, the trend is expected to be similar than for steelmaking slags.

The effect of the state of reduction of the slag on TiC formation is anticipated if one refers to Figure 1. However, TiC formation starts at a lower state of reduction (more FeO present) than is predicted by the equilibrium relationship. For example, the equilibrium amount of Ti in the iron at a FeO concentration of 8.9% is 0.00123%, while the actual amount found in the metal is 0.0327%. Geldenhuis and Pistorius (1999) have shown how commercial oxygen probes, using zirconia electrolytes, can be used to measure the oxygen potential of high titania slags and show in their paper that equilibrium conditions are not attained during the production of high titania slags. This is in line with our findings, as stated above.

It should be noted that TiC solid precipitation is not the only cause of viscosity increase that may lead to significant foaming, precipitation of  $\text{TiO}_2$  or one of the lower oxides may also occur when the slag temperature drifts to below the system liquidus temperature. This may result from subcooling of the slag due to bank slides of frozen slag from the furnace wall or roof, or operating at too low specific input energies. A positive degree of superheat of the slag should always be maintained. However, a positive degree of superheat was not maintained throughout the production processes, as the furnaces were operated below the liquidus (i.e. negative superheat) for about 24% of the time shown in Figure 7.

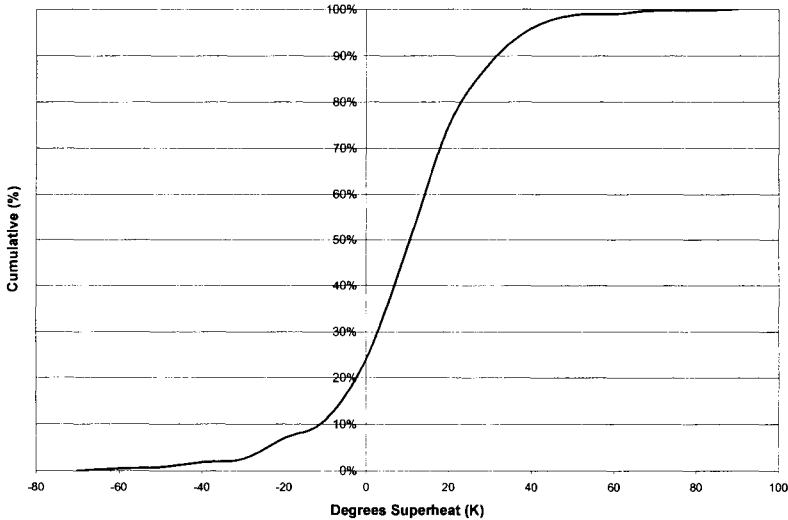


Figure 7: Cumulative frequency of operation below a specified degree of slag superheat.

Zhang and Fruehan (1995) and Jiang and Fruehan (1991) showed that the foaming index of steel making slags is the most sensitive for variations in slag viscosity, followed by slag density and surface tension. The foaming index is a measure of the foam stability and is defined as the steady state foam height per unit superficial gas velocity. Other authors indicated that slag inventory and the two-phase flow regime also plays a role in froth formation. Fruehan has also shown that small carbonaceous particles will tend not to be wetted by the slag and may even destabilise the slag foam. This effect was not observed for lumpy coal. The actual determination of slag foam height at various gas flow rates or coal-slag reaction rates is difficult to simulate in the laboratory, especially at various slag heights and at the temperatures required for ilmenite smelting.

The measurement of foam-heights in an industrial or pilot furnace is made difficult due to the operation of the open arc and the high temperature gases which contains much entrained particles (which may even be partially molten) which are formed during the smelting operation. Innovative solutions still have to be found for the on-line measurement of foam heights during the operation of open-arc furnaces and the measurement of slag foaming of high-titanium slags in the laboratory.

## Conclusions

The causes of slag foaming and metal entrainment in slag can be identified and modelled for ilmenite smelting processes.

System identification techniques prove valuable in assessing the temporal nature of the system. Although the predictions and actual furnace operations lie far from equilibrium, the predictions of TiC parallels the equilibrium trend, with increasing TiC production as the FeO in the slag decreases. It was found that TiC formation starts at an less reduced state (higher FeO% in slag) than predicted by equilibrium.

The significant metal and slag heel (residual inventory) dampens the direct effect of the operating variables, but increases the effect of historic metal and slag assays on future metal and slag compositions. Accurate dynamic predictions of the main species that contribute to viscosity increases (which eventually worsens slag foaming) can be made, using a combination of higher fundamental knowledge and computational intelligence. The % volatiles, coal particle size and % sulphur (as pyrite in the coal), strongly influences the amount of titanium that enters the metal phase.

Foaming due to viscosity increases arises from increases in the total wettable solids content of the slag of fine particle size. Foaming of slags remains a fundamentally ill understood subject of major process significance. Many variables are at play in industrial furnaces that influence slag foaming and one should not ascribe foam formation to any single factor.

## References

- Coley, K.S., Terry, B.S. and Grieveson, P., 1995. Simultaneous Reduction and Carburization of Ilmenite. *Metallurgical and Materials Transactions B*, 26B, June, pp. 485-494.
- Denton, G.M. and Schoukens, A.F.S., 1993. The Production of High Titania Slag from Ilmenite. SA patent 935072, Mintek, South Africa.
- Geldenhuis, J.M.A., and Pistorius, P.C., 1999. The use of commercial oxygen probes during the production of high titania slags. *Journal of the South African Institute of Mining and Metallurgy*, January / February, 99(1), pp. 4-47.
- Jiang, R., and Fruehan, R.J., 1991. Slag Foaming in Bath Smelting. *Metallurgical and Materials Transactions B*, 22B, August, pp. 481-489.
- Johnsson, S., 1998. Assessment of the Fe-Ti-System, Calculation of the Fe-Ti-N System, and Prediction of the Solubility Limit of Ti(C,N) in Liquid Fe, *Metallurgical and Materials Transactions B*, 29B, April, pp. 371-384.
- Pesl, J. and Eric, R.H., 1997. Metal-gas equilibrium pertinent to the smelting reduction of ilmenite: Significance for industrial processes. *Heavy Minerals 1997*, Johannesburg, SAIMM, pp. 143-150.
- Reuter, M.A., and Moolman, D.W., 1999. Feedforward quality control methodology for reactors based on the thermodynamics and system identification techniques. *Erzmetall*, October 1999.
- Verein Deutscher Eisenhüttenleute, 1995. *Slag Atlas*, 2 Edition, Verlag Stahleisen, Dusseldorf, pp.484.
- Zhang, Y, and Fruehan, R., 1995. Effect of Bubble Size and Chemical Reactions on Slag Foaming. *Metallurgical and Materials Transactions B*, 26B, August, pp. 803-812.

## THE UNIFORM DESCRIPTION OF MINERAL PROCESSES BY METHODS OF COMPOUND DISTRIBUTIONS OF MATERIAL FEATURES

T. Tumidajski

Department of Mineral Processing, Environment Protection and Waste Utilisation  
Faculty of Mining, University of Mining and Metallurgy, Kraków, Poland

### Abstract

The basic model describing the separation of grained materials is the following equation

$$g(x) = (1 - \gamma) \cdot h(x) + \gamma \int_D p(w, x) f(w) dw$$

where:  $g(x)$  is the function of distribution density of probability of the feature  $X$ , determining the separation into products,  $h(x)$  is a similar function as  $g(x)$  for the material which constituted the products existing before the process in which the probabilities of transfer from the fraction  $(w, w + dw)$  are determined by  $p(w, x)$ ,  $f(w)$  is the function of density determining the material composition according to the feature  $W$ ; the parameter  $0 < \gamma < 1$  determines the proportion of products existing and formed in the process of separation while  $D$  is the range of changes of values of the random variable  $W$ . In mineral processing data are not available for each conditional distribution separately but only for the overall mixture distribution. Often such situation arise because it is impossible to observe some underlying variable which splits the observations into classes only the combined distribution can be studied. In these circumstances interest often focuses on estimating the mixing proportions and on estimating the mixing proportions and on estimating the parameters in the conditional distributions. The results of such investigations permit to better interpret the course of processes and the behavior of materials.

*Keywords: stochastic models, separation, compound distributions*

### Introduction

The basic feature of mineral processing is constituted by the separation of material into products, which differ from each other by distributions of many features, which characterize the material.

The passage of grains into products is conditioned by the joint action of forces, which make the grains move in the working spaces of machines. It is worth mentioning that in case of enrichment or classification processes the grains are not subjected (a theoretical assumption) to disintegration and are passed to the products unchanged. In case of crushing the products are formed by the division of the grain and by transmission of its fragments into finer classes, which constitute the product of crushing.

In such an approach to mathematical modeling of mineral processing the law of conservation of mass becomes the basic law applied in the form of the balance equation. As it appears, many significant models are based on this law whereas the differences between them consist in the accepted assumptions (interpretations of phenomena) and the applied mathematical methods.

In mineral processing it rarely happens that the feed is significantly homogeneous. As a rule, we deal with grained materials which are mixtures of various types (coals of different deposits, different ore types, e.g. of copper) and, in extreme situations, they are conglomerates of useful minerals and waste rock.

It can be assumed that respective material types will be crushed in different ways and will produce certain types of grain compositions and this will cause further consequences in enrichment processes (separation processes in general).

Let us perform simplified reasoning. Let us assume that from the grained-material we choose the grains of a certain narrow grain class and next we crush them in a certain way. Assuming that these grains are a composition (conglomerate) of smaller grains of two minerals (e.g. useful mineral and waste rock), after crushing we receive a mixture of grains of three types, i. e. waste rock, useful mineral and intergrowths, or two assuming the complete liberation. Assuming that these grain types produce certain grain compositions as a result of crushing we obtain consequently the grain composition of the material which is the mixture of grain compositions of respective types.

With certain assumptions and applying the theory of mixtures of distributions, on the basis of characteristics of the final distribution of grain sizes (i. e. the distribution of grain sizes in the product of crushing) this distribution can be divided into the distributions of mixture components.

### General description of separation processes

Let us assume that we consider one-grain feature  $W$  (size, density, component content, etc.). Let us also assume that there is a separation of elementary fractions  $(w, w + dw)$  into products (fractions)  $(x, x + dx)$  where  $X$  is a continuous variable being the basis of separation into products. In case of crushing  $X$  will be, as a rule, the grain size while the separation of the fraction  $(w, w + dw)$  consists in transferring the grain fragments from the fraction to respective grain classes of the product. At gravitational enrichment these will be density fractions, at flotation it can be assumed, for example, that  $X$  is the height of the overflow edge in the flotation machine, etc. The proposed unification of the description is to show the general structure of mathematical models of separation processes and its detailed analyses will require preparing precise characteristics of the used variables (Tumidajski, 1996).

The random variable  $W$  is characterized by the density function  $f(w)$  and the portion of the elementary fraction  $(w, w + dw)$  is determined by the product  $f(w)dw$ . Let us introduce the function  $p(w, x)$  denoting the probability of transfer of the grain (its fragment) from the fraction  $(w, w + dw)$  to the product  $(x, x + dx)$ .

The amount of material transferring to the product  $(x, x + dx)$  from the fraction  $(w, w + dw)$  is  $p(w, x) dx f(w) dw$  and is in total equal  $g(x)dx$  where  $g(x)$  is the density function for the variable  $X$ . The variable  $X$  can be treated as a random variable due to the random selection of its value by the grain or its fragment. Hence we can write:

$$\int_D p(w, x) f(w) dw = g(x) \quad (1)$$

where  $D$  denotes the area of variability of the variable  $W$ , i. e.  $D = \langle w_{\min}, w_{\max} \rangle$ .

Because of determining the function  $p(w,x)$  we have:

$$\int_{x_{\min}}^{x_{\max}} p(w,x)dx=1 \tag{2}$$

i. e., at the fixed value of  $w$  we can consider the function  $p(w,x)$  to be the density function of the conditional distribution of the random variable  $X$  under the condition of assuming the value  $w$  by the random variable which means that:

$$p(w, x) = p(x | w) \tag{3}$$

for the fixed  $w$ , treated as a parameter.

Therefore equation (1) can be written:

$$\int_{w_{\min}}^{w_{\max}} p(x | w) f(w) dw = g(x) \tag{4}$$

We obtained the equation determining the complex distribution of the conditional distribution of density  $p(w|x)$  with the distribution of the random variable  $W$  of density  $f(w)$ .

Equations (1) and (4) describe the process of origin of a “product” in case of the process of crushing or, in case of an erroneous classification of grains into respective fractions:  $p(w|x)$  is than called a fuzzy function.

In case of real enrichment or classification processes it is assumed that a grain is not subject to degradation and that there is a separation into a few products to the utmost. This corresponds to the division of the area of variability of value  $X$  into a few sub-ranges. Attributing the values  $x_j$  to respective products (average boundaries of ranges, numbers of sub-ranges, etc) we can attribute the probability of transferring to the  $j^{\text{th}}$  product  $p(w, x)$  to each grain of the value of the feature  $w$ . Due to the fact that transfers of the feed grains to the products are mutually exclusive phenomena and that their sum is a certain phenomenon, we can write for the density  $f(w)$ :

$$f(w) = \sum_{j=1}^k p(w, x_j) f(w) \tag{5}$$

Bilateral integration of this dependence in the area of variability of the feature  $W$  results in a relation of balance of product masses and a system of dependencies analogous to equation (1).

$$\int_{w_{\min}}^{w_{\max}} p(w, x_j) f(w) dw = g(x_j) = \gamma_j \tag{6}$$

$$\sum_{j=1}^k \gamma_j = 1 \quad \text{for } j = 1, 2, \dots, k.$$

Dependence (5) can be presented as:

$$f(w) = \sum_{j=1}^k \frac{\gamma_j p(w, x_j) f(w)}{\gamma_j} \tag{7}$$



and by comparing it to the equation of balance:

$$f(w) = \sum_{j=1}^k f_i(w) \gamma_j \quad (8)$$

we receive:

$$f_j(w) = \frac{p(w, x_j) f(w)}{\gamma_j} \quad (9)$$

where  $f_j(w)$  are distribution densities of the random variable  $W$  in the products. From dependence (9) it comes:

$$p(w, x_j) = \gamma_j \frac{f_j(w)}{f(w)} \quad (10)$$

i. e. the probabilities  $p(w, x_j)$  are equivalent to separation functions, defined in the known way. Depending on the assumptions concerning the functions of equation (1), which are connected with the possibilities of obtaining them, also the aim and sense of process modeling is determined. Generally speaking, three types of tasks connected with process modeling can be differentiated. These are forecasting of results, the so-called feed reconstruction and determining the function  $p(w, x)$ .

We have to do with forecasting of results when the functions  $h(x)$ ,  $f(w)$  and  $p(w, x)$  are known. These are tasks concerning balancing of components in material streams. In some processing processes it is not possible to investigate the feed empirical characteristics and, as a rule, there are no premises for its theoretical characterization. From the formal point of view, if the functions  $g(x)$ ,  $h(x)$  and  $p(w, x)$  are known, equation (1) is Fredholm's integer equation of the first type.

### Description of the material grained with distribution mixtures

Passing to the application of theory of distribution mixtures in the description of the composition of grained materials it is worth paying attention to the existing solutions in this respect, i. e. the works by Kolmogorov, Epstein, Gumtz, Meloy and others (Epstein, 1948, Meloy and Gumtz, 1968/69, Brožek et al., 1993a).

Epstein considered the process of crushing as a sequence of consecutive crushing and after accepting assumptions saying that the probability of crushing of a grain of size  $y$  in the  $n^{\text{th}}$  crushing is constant and independent from  $y$  and presence of other grains (whereas it can depend on  $n$ ) and that the obtained distribution function (determined by means of the relation of masses) of distribution of the product grain sizes  $F(x|y)$  is independent from  $y$  in such sense that the mass portion of grains of the size  $< ky$  where  $k \in (0, 1)$ , formed from the unitary mass of grains of size  $y$ , is independent from  $y$ . He proved that after  $n$  crushing actions the distribution function of distribution of the value  $x$  is a distribution function of the asymptotically logarithmic-normal distribution.

In Gumtz-Meloy's model (Meloy and Gumtz, 1968/69) it is assumed that the crushed (in any way) grain can be reconstructed, i. e. put together from the newly formed grains to its primary form. A straight line is led through the reconstructed grain in an arbitrary direction and the cross-section of length  $x_0$  is obtained which is transected  $r$

with newly formed surfaces. It was assumed that the function  $\rho(y)$  is the function of density distribution of probability of occurrence of surface in the section  $(0, x_0)$ . The function  $\rho(y)$  characterizes the process of crushing and depends on many factors connected with physical and chemical properties of the grain and its history.

The observations of crushing of a single grain indicate that in the process of grains chips are formed which form large grains. In relation with the above, the curve of the grain composition is a distribution function of distribution which should be treated as a merge of two distributions; the one describing the distribution of formed fine grains and the other describing the distribution of formed coarse grains. The quoted function (11) is a distribution function of this very distribution. Differentiating the function (11) the following formula is obtained for the density of the above distribution (Brożek 1993b):

$$F'(x) = f(x) = abx^{b-1}e^{kx} + kax^b e^{kx} \quad (11)$$

Therefore this function is a linear combination of two functions.

The premises presented above and concerning the distributions of grain sizes of the products of crushing contribute to formulate a general hypothesis stating that the grained materials are crushed producing a certain type of distribution while their parameters will depend on the type of material and the applied machines (depth of crushing). This hypothesis allows the mixtures of a certain type of distributions to be applied which, consequently, enables their effective separation according to their joint results, i. e. investigating the distribution being, as it is assumed, the mixture of component distributions. Not going into details, the complete mixture of distributions of a certain random variable can be the distribution of this variable whose density function is a weighed sum of density of component distributions, i. e.:

$$f(x) = \sum_{i=1}^n p_i f_i(x), \quad \sum_{i=1}^n p_i = 1 \quad (12)$$

whereas the types of function  $f_i$  are identical and the distributions determined by them have different static moments.

The method of moments and the maximum likelihood method (Everist and Hand, 1984) are the basic methods of determining the component distributions.

This paper will also present some selected solutions in the range of these methods for two types of distributions, i. e. normal (after some slight interpretative change lognormal) and Weibull's. In case of unidimensional distributions the finite mixtures of normal distributions have got long histories. For example, Pearson (1894) obtained estimation of five parameters in the mixture of two normal distributions applying the method of moments. The numerical implementation of the method of moments begins from determining appropriate central moments of a given sample and fixing Pearson's  $a_i$ ,  $i=0, \dots, 9$ . According to the method of moments the negative real root of the equation  $a_9 x^9 + \dots + a_1 x + a_0 = 0$  is used for estimation of component parameters of normal distribution. It can be obtained by means of one of the methods of determining the polynomial roots, e. g. Bairstow's method (Stoer, 1979). The use of Bairstow's method results from the need of determining all real roots of the appropriate polynomial (to select the optimum one) whereas the more traditional methods, for instance Newton's, allow only one root to be calculated (usually the smallest or the largest one as far as modulus is concerned). A possible iterative

application of Newton’s method becomes inconvenient due to the unknown number of real roots. That is why all roots are determined, also the complex ones, which are next rejected (out of the remaining real roots only the optimum one can be chosen).

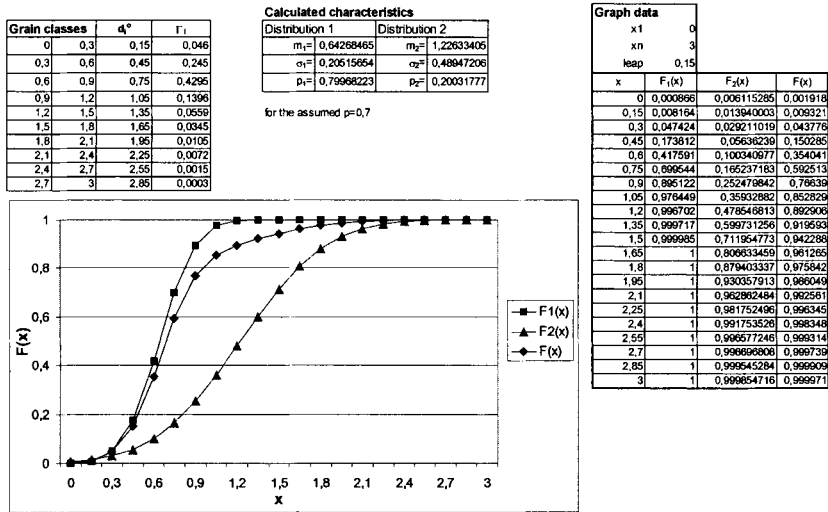


Figure 1: An example of numerical separation of two normal distributions.

Figure 1 shows the results of “reconstruction” of the feed with the given  $F1(x)$  and  $F2(x)$  and the given mixing proportion  $p = 0.7$ . The reconstruction of the feed resulted in the proportion  $p = 0.8$ . This means that the entire algorithm of feed reconstruction requires improvement. For Weibull distributions (RRB) it should draw attention to two methods presented by Kao and Falls.

*1<sup>st</sup> method:* determining the proportions of mixing  $p_1$  (Kao, 1959); this method consists of three stages:

1<sup>st</sup> stage: drawing the distribution function of the investigated random variable on the function paper ( $\ln x, \ln \ln \Phi$ ) and manual adjustment of the smooth curve to the points,

2<sup>nd</sup> stage: drawing tangents to both ends of this curve (these tangents approximate  $p_1 G_1$  and  $p_2 G_2$  where:

$$G_1(x) = 1 - \exp\left(-x^{\beta_1}/\alpha_1\right) \quad x > 0, \quad \alpha_1 > 0, \quad 0 < \beta_1 < 1$$

$$G_2(x) = 1 - \exp\left[-(x - \gamma)^{\beta_2}/\alpha_2\right] \quad x > \gamma, \quad \alpha_2 > 0, \quad \beta_2 > 1$$

3<sup>rd</sup> stage: drawing the vertical line in the point of crossing of the tangent estimating  $p_2 G_2$  with the bottom boundary line (i. e. approximately, where the adjusted curve intersects the boundary line) in order to intersect the other tangent. The co-ordinate of the point of intersection on the percent (ordinate) scale gives  $\hat{p}_1$ , -  $p_1$  estimator.

2<sup>nd</sup> method Falls considered also the mixture of two Weibull's distributions (Falls, 1970). The first five central moments are of the form:

$$\mu_r = p_1 \alpha_1^{r/\beta_1} \Gamma\left(\frac{r}{\beta_1} + 1\right) + p_2 \alpha_2^{r/\beta_2} \Gamma\left(\frac{r}{\beta_2} + 1\right) \quad r = 1, \dots, 5$$

where  $\Gamma$  is the gamma function; according to the rule Falls compared these moments to the moments of sample  $m'_r$  and next, after substitutions:

$$v = \alpha_1^{1/\beta_1}, \quad w = \alpha_2^{1/\beta_2}, \quad \Theta_r = \Gamma\left(\frac{r}{\beta_1} + 1\right), \quad \Psi_r = \Gamma\left(\frac{r}{\beta_2} + 1\right), \quad r = 1, 2, 3$$

reduced the equations for the three first moments to

$$m'_r = p_1 v^r \Theta_r + p_2 w^r \Psi_r, \quad r = 1, 2, 3$$

Solving the first of these equations in relation to  $v$  and substituting to the other one we obtain a square equation because of  $w$ . Solving it and substituting again to the first one we receive  $v$  and  $w$ . Substituting it to the third equation we obtain a single  $p_1$ ,  $\beta_1$  and  $\beta_2$ . Falls suggests determining  $p_1$  with Kao's method and to estimate  $\beta_1$  and  $\beta_2$  with Newton-Ralphson's method.

### Final remarks

The above considerations contribute to a homogeneous description of mineral processing processes and product characteristics by means of complex distributions. The unification of the description allows wider applications of mathematical methods to be introduced in the description, simulation and forecasting of mineral processing.

### References

- Brożek, M., Przybyło, L. and Tumidajski, T., 1993a. The analysis of Meloy-Gumtz's model of fracture of single grains. Arch. Min. Sci., 38, 169-178.
- Brożek, M., Przybyło, L. and Tumidajski, T., 1993b. Charakterystyka rozdrabniania pojedynczych ziarn w prasie hydraulicznej (The character of the single particle comminution in a hydraulic press). Górnictwo, 17, 109-116.
- Epstein, B., 1948. Logarithmic-normal distributions in breakage of solids. Ind.Eng. Chem., 40, 2289-2291.
- Everist, B.S. and Hand, D.J., 1984. Finite Mixture Distributions. Chapman and Hall, London New York.
- Falls, L.W., 1970. Estimation of parameters in compound Weibull distributions. Technometrics, 12, 399-407.
- Kao, J.H.K., 1959. A graphical estimation of mixed Weibull parameters in life-testing electron tubes. Technometrics, 1, 389-407.
- Meloy, T.F. and Gumtz, G.D., 1968/69. The fracture of single, brittle heterogeneous particles - Statistical derivation of the mass distribution equation. Powder Tech., 2, 207-214.
- Stoer, J., 1979. Wstęp do metod numerycznych (The introduction to numerical methods), t. I, PWN, Warszawa.
- Tumidajski, T., 1996. Stochastic models of separation of mineral raw materials. Arch. Min. Sci., 41, 515-530.

## ARMA TYPE MODEL FOR COPPER ORE FLOTATION

K. Trybalski, J. Cieplý

Department of Mineral Processing, Environment Protection and Waste Utilisation  
Faculty of Mining, University of Mining and Metallurgy, Kraków, Poland

### Abstract

The processes of mineral processing can be regarded as discrete processes. Discrete processes can be described using time series. The difference equations derived from the theory of time series dynamics, as well as ARMA and ARMAX models, are used to describe processes of minerals flotation. Several models are attempted ARMAX for rougher flotation of copper, and a bank of cleaning flotation, as well as ARMA, for the stream of flotation concentrate. All models are based on the actual industrial data. The models express the dependence of output quantities from the processes, i.e. copper concentration in products, on input i.e. copper concentration in the feed materials, density of pulp, pulp level in the flotation machines and mass flow rate of feed.

*Keywords: copper, flotation, model, ARMAX*

### Introduction

Although most mineral processing unit operations, in the macroscopic level, are in principle continuous processes, they also comprise discontinuous ones, as for example, those which perform periodical actions, or the product of which is obtained periodically. The majority of continuous processes can be regarded as discontinuous (discrete), because the only accessible characteristic features are the values of signal samples in the products or periodically measured parameter values. These values are measured in discrete time intervals, distant from one another by a sampling period. This situation has been reported in the following cases (Amborski, 1987; Kaczorek, 1983):

- the process of dewatering in a pressure-filter press can be considered a discrete process;
- in numerous mineral processing unit operations, the analysis of product composition is carried out periodically. Sampling time, sample transport and laboratory chemical analysis make the measurements discrete;
- the transmission of data and measurement results, in industrial conditions, occurs usually in a discrete form;
- conversion of analogous signals to digital data;
- during rarely applied manual measurements, e.g. measurements of product density, or sampling and analysis of sample grain composition.

Sampling in time constitutes the characteristic feature of all cases. Sampling is a presentation of a continuous function of time  $y(t)$ , by a sequence of its values  $y(t_1)$ ,  $y(t_2)$ ... in discrete time intervals  $t_1$ ,  $t_2$ ..., whereas the intervals between respective times of sampling are most often equal, and are called sampling time,  $T$ . The discrete values obtained by sampling most describe the continuous function completed. In

order to accomplish this, an appropriate frequency of sampling is required which should be larger than twice the largest frequency occurring in the spectrum of this function (Shannon-Kotelnikov's theorem).

The sequence of discrete values, obtained as a result of sampling in time of a continuous function, i.e. the set of consecutive observations in time, are called time series (Box and Jenkins, 1983). Time series models in the domain of time are a convenient representation of both deterministic and random signals occurring in mineral processing unit operations (Bazin and Hodouin, 1988; Walaszek-Babiszewska and Zapała, 1993).

### Rougher flotation model

The rougher flotation machine is the subject matter of this research. The initial flotation in the considered case is constituted by a flotation cell with three products: concentrate, forwarded to cleaning flotation, and wastes, which, after additional grinding, constitute the feed for main flotation. The feed for rougher flotation is constituted by appropriately ground copper ore, which is characterized by a content of copper  $\alpha$  and a mass flow rate  $Q$ . The content of copper in the feed was measured in discrete moments of time with a sampling time  $T = 10$  min, while the feed flow rate was measured continuously at the onset of the grinding circuit and read at discrete time intervals, with the same sampling time as measurements of copper content in the feed. It was also possible to determine a value of flow rate. The response of flotation can be affected by level of pulp in the flotation machine. This level is maintained by a proper automatic regulating system. A change of this level influences the rate of separation into concentrate and wastes, by changing the yields of these products and consequently, by changing the copper content.

The copper content in the flotation tailings ( $\mathcal{G}_{FW}$ ) was measured in discrete time intervals with the same frequency as formerly described.

A flotation process can be presented by means of a block diagram, as in Figure 1. The respective parameters connected to the process can be qualified as:

- control variables:
  - $Q$  = mass flow rate of the feed (t/h),
  - $L$  = pulp level in the machine (%),
- input function variable:
  - $\alpha$  = copper content in the feed (%),
- output variable:
  - $\mathcal{G}_{FW}$  = copper content in tailings (%).

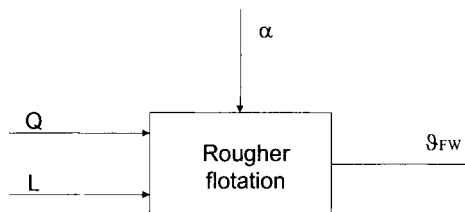


Figure 1: A block diagram for rougher flotation.

The recorded values of the process parameters, for a period of 18 h and 20 min (110 measurements), are presented in Figure 2. The figure shows the time intervals and also presents the following values: average, variance, minimum and maximum values, for each measured parameters.

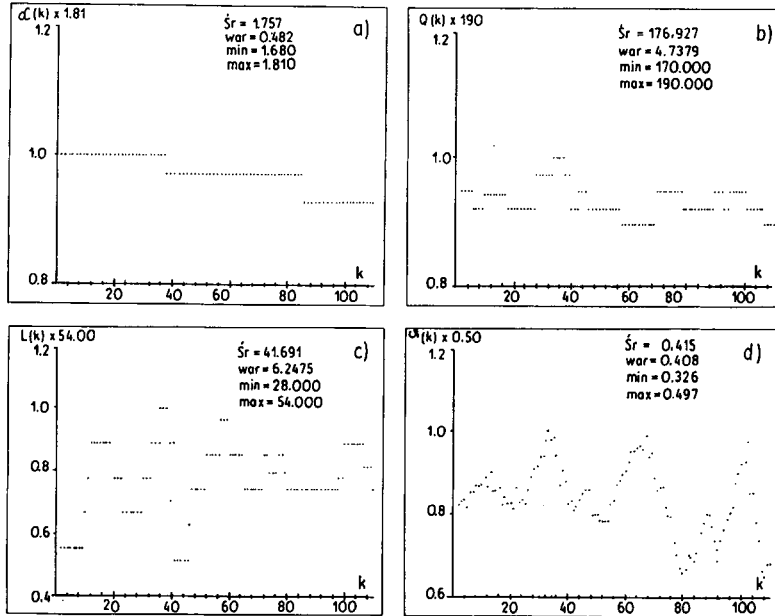


Figure 2: The course of the input and output variables.

The discrete ARMAX model formulates the following dependence.

$$\vartheta_{FW} = f(\alpha, Q, L) \quad (1)$$

This is determined by means of the IDCAD program, which contributes to determining the ARMA or ARMAX dynamic models of objects as a differential equation of the following form.

$$y(k) = \sum_{i=1}^n a_i y(k-i) + \sum_{j=1}^m \sum_{i=1}^n b_{ji} u_j(k-i-d_j) + \sum_{i=1}^n c_i \eta(k-i) \quad (2)$$

where:

- $y(k)$  = model output signal;
- $u(k)$  = input signal;
- $\eta(k)$  = estimated signal of the additive disturbance;
- $n$  = order of the model;
- $m$  = number of input signals;
- $d_j$  = value of delay for the  $j^{\text{th}}$  input.

The model obtained for copper content in the rougher flotation tailings is of the form:

$$\vartheta_{FW}(k) = 1.9745\vartheta_{FW}(k-1) - 0.9929\vartheta_{FW}(k-2) - 0.0018\alpha(k-1) + 0.0055\alpha(k-2) - 0.0002L(k-1) + 0.0002L(k-2) + 0.0734\eta(k-1) + 0.0095\eta(k-2) \quad (3)$$

The parameters of the model obtained are:

- output variance  $= 2.37 \cdot 10^{-4}$
- error variance  $= 9.59 \cdot 10^{-8}$
- FPE coefficient (model estimation criterion)  $= 1.16 \cdot 10^{-7}$
- number of iterations  $= 5$

Figure 3 presents the output from the model. This is a centred time series, i.e. obtained according to the following general dependence (Zapała, 1990):

$$y^* = Y - E\{y\} \quad (4)$$

where:  $E\{y\}$  is the expected value of  $y$ .

The model obtained is a very precise description of the dependency of the measured values for copper content in tailings on the copper contents in the feed, feed flow rate, and pulp level in the flotation machine (Figures 2a and 3). The quality of the model obtained is evidenced by the low values of variance and low values of the model estimation criterion (FPE).

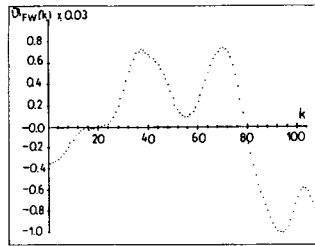


Figure 3: The course of output from the model.

The model obtained is a second order ARMAX type model. It includes a clear and distinct autoregression dependence, i.e. the dependence of the output value  $\vartheta_{FW}$  in its former measurements. On the other hand, the effect of the input values, i.e. the Cu content in the flotation feed (input function) and the level of pulp in the flotation machine is relatively small and the mass flow rate of ore to the rougher flotation has no significant effect on the model output, according to the calculations performed. The effect on the output of the estimated disturbance signal  $\eta$  is slight.

The structure of the model obtained and its numerical shape contribute, above all, to forecasting the value of  $\vartheta_{FM}$ , as a function of its previous values and, to a lesser degree, as a function of the value of input function  $\alpha$ .

This model can be applied to control the process only with very low efficiency, and exclusively by means of the level of pulp in the machine. On the other hand, the mass flow intensity,  $Q$ , was revealed to be unimportant.

### Cleaning flotation process model

As opposed to the previously modeled process of rougher flotation, the considered technological process of cleaning flotation is a process composed of three consecutive cleaning flotation: the first (FC I), the second (FC II) and the third (FC III), are additionally connected by returns of waste material products. The only measured values that were connected with the considered processes were as follows: the levels



of pulp in the machines of successive flotation, and the content of copper in the final concentrate coming from the third cleaning flotation. The values of the levels can be given and maintained by appropriate systems of automatic regulation.

Therefore, for the tested system, we can consider:

- $L_{FC I}$  = pulp level in the machine for the first cleaning flotation (%);
- $L_{FC II}$  = pulp level in the machine for the second cleaning flotation (%);
- $L_{FC III}$  = pulp level in the machine for the third cleaning flotation (%),

as control input variables; and

- $\beta$  = copper content in the final concentrate (%),

as an output variable.

The block diagram of the considered system was presented in Figure 4.

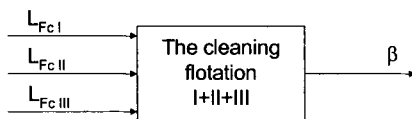


Figure 4: The block diagram of cleaning flotations.

The ARMAX model formulating the dependence:

$$\beta = f(L_{FC I}, L_{FC II}, L_{FC III}) \quad (5)$$

has the numerical form:

$$\begin{aligned} \beta(k) = & 1.992 \beta(k-1) - 1.023 \beta(k-2) \\ & + 0.0027 L_{FC I}(k-1) - 0.0007 L_{FC I}(k-2) \\ & + 0.0209 L_{FC II}(k-1) + 0.0285 L_{FC II}(k-2) \\ & - 0.0433 L_{FC III}(k-1) + 0.0535 L_{FC III}(k-2) \\ & + 0.0039 \eta(k-1) + 0.0081 \eta(k-2) \end{aligned} \quad (6)$$

The model was obtained with the following parameters:

- output variance =  $5.89 \cdot 10^{-1}$
- error variance =  $8.86 \cdot 10^{-5}$
- FPE =  $1.07 \cdot 10^{-4}$
- number of iterations = 4.

The model obtained is of the second order. It reveals a clear autoregressive dependence (AR) for the  $\beta$  parameter. On the other hand, the influence of control values, which are constituted by pulp levels in respective cleaning flotations (part MA of the model) is not very high, and it grows with the increase in a consecutive flotation number. Therefore the highest effect on the value of the quality of the produced concentrate is exerted by the pulp level in the machine of the third cleaning flotation, i.e. that which directly generated this concentrate, while the lowest effect is exerted by the level of the first cleaning flotation, which is most distant from the process output. The influence of the part of the model representing the evaluated signal of the  $\eta$  additive disturbance is very small.

The structure of the obtained model and its numerical form allow us to forecast the  $\beta$  value and to control the quality of this parameter by means of the pulp level in the flotation machines, especially in the third cleaning flotation.

### Model of material stream

For the model of material stream, which is the total final concentrate of the flotation process, the following items were measured during the discrete moments:

- $\beta_{Cu}$  = copper content (%),
- $\beta_{Fe}$  = iron content (%),
- $G$  = mass of solid parts in 1 dm<sup>3</sup> (g).

The ARMA model was determined, which formulated the dependence:

$$\beta_{Cu} = f(\beta_{Fe}, G) \quad (7)$$

while the input values  $\beta_{Fe}$   $G$  were treated as input functions.

A block model for the stream considered in this way can be presented as in Figure 5.

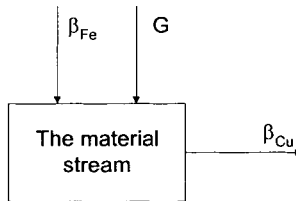


Figure 5: The block diagram of the material stream.

The numerical form of the ARMA model was obtained for the set of 110 measurements:

$$\begin{aligned} \beta_{Cu}(k) = & 2.4755\beta_{Cu}(k-1) - 2.0352\beta_{Cu}(k-2) + 0.5503\beta_{Cu}(k-3) \\ & + 0.2528\beta_{Fe}(k-1) - 1.9953\beta_{Fe}(k-2) + 1.7532\beta_{Fe}(k-3) \\ & - 9.2482G(k-1) + 2.5083G(k-2) + 5.2112G(k-3) \end{aligned} \quad (8)$$

with the following parameters of the model:

- variance =  $3.19 \cdot 10^{-1}$
- variance of error =  $2.92 \cdot 10^{-4}$
- FPE =  $3.46 \cdot 10^{-4}$
- number of iterations = 2.

This is the model of the third order, i.e. formulating the dependence of the initial value on the three values of parameters measured in the moments  $t = 10$  min,  $t = 20$  min and  $t = 30$  min. The copper content in the considered concentrate is strongly dependent on its value in previous measurements (the AR part of this model). The force of this dependency decreases, receding over time from the moment of a present measurement.

It is also strongly dependent on the iron content in this concentrate, and especially on the concentrate density (the MA part).

These dependencies testify to a similar rate of flotation-enrichment capacity of copper and iron minerals, and to a high rate of dependence of the copper-concentrate quality on its density. This second dependence is connected indirectly with the amount of the concentrate yield from flotation; the smaller yield, the higher the concentrate density and the higher the content of copper in it. Knowing this model contributes to a better understanding of the copper ore flotation process and to its better execution.

## **Conclusions**

This work presents a technological description of the copper ore enrichment processes by means of empirical models of the discrete type. Such an approach to modeling justifies the character of available data, by describing the mineral processing processes, the development of computer and calculating techniques and the implementation in processing plants. The technological processes of mineral processing (this work deals only with copper-ore processing) have already been sufficiently measured by means of automatic control-regulating equipment, which allows their automatic computer control to be attempted. Attempts at implementation can be encountered in the Polish copper-ore processing plants (Sztaba and Trybalski, 1987). The construction of computer-control systems, however, depends on whether there are mathematical models that describe the processes.

Taking into account the fact that the industrial measuring data reflecting the technological parameters of processing processes are most often of the discrete data character, it is justified to model these processes by means of discrete models.

The presented examples of models testify to the fact that they can describe respective technological processes (flotation), technological blocks (cleaning flotation) and also individual material streams (concentrate streams). The models of a discrete type can be applied to control the mineral-processing processes or just to forecast the values of parameters.

## **References**

- Amborski, K., 1987. Teoria sterowania podręcznik programowany. PWN, Warszawa, (in Polish).
- Bazin, C. and Hodouin, D., 1988. Off-line and On-line Identification of Empirical Dynamic Models for a Flotation. E. Forssberg (Editor), XVI International Mineral Processing Congress, Amsterdam.
- Box, G.E.P. and Jenkins, G.M., 1983. Analiza szeregów czasowych. WPN, Warszawa, (in Polish).
- Kaczorek, T., 1983. Teoria wielowymiarowych układów dynamicznych liniowych. WNT, Warszawa (in Polish).
- Sztaba, K. and Trybalski, K., 1987. Principles of the Block Control of Copper ore Dressing and Optimization Control of Flotation Block as an Example. Międzynarodowa Konferencja: Copper '87, Chile-Vina del Mar.
- Walaszek-Babiszewska, A. and Zapała, W., 1993. Dyskretne modele stochastyczne zakłóceń w procesie flotacji węgla. Materiały: XXV Krakowskiej Konferencji Naukowo-Technicznej Przeróbki Kopalni. PAN CPPGSMiE Sympozja i Konferencje nr 8, Kraków, (in Polish).
- Zapała, W., 1990. Algorytmy regulacji predykcyjnej maszyn przerobczych. XIX Sympozjum SCwG oraz SWSM KG PAN. Ustronie-Zawodzie, Katowice, (in Polish).

**COMMINUTION, CLASSIFICATION AND  
AGGLOMERATION**

This Page Intentionally Left Blank

<b>Operational Work Index for Grinding Plants</b> G.D. González, C. Pérez, A. Casali, G. Vallebuona, R. Vargas	C4-1
<b>Magotteaux Automatic Ball Charger (Abc)</b> W. Conger, P. Amelynck	C4-8
<b>Breakage Parameters of Chromite and Simulation of the Product-Size Distributions</b> M.Yekeler, U. Ulusoy, I. Akbaba	C4-16
<b>Run-of-Mine Milling Pilot Plant Test Work</b> B. Clermont	C4-22
<b>The Effect of Viscosity on Small-Diameter Hydrocyclones' Performance in Desliming Process</b> M.V. Possa, J.R.B. Lima	C4-29
<b>Drum Granulation of Mineral Raw Materials with Different Particle Size Distributions</b> T. Gluba, A. Obraniak	C4-36
<b>Studies on Comminution Mechanism of the Dry Tower Mill Kd-3</b> A. Shibayama, S. Mori, A. Bissombolo	C4-44
<b>Improvement in Classification Performance of Turbo Classifiers by Reducing the Inertia Counter-Rotating Vortices</b> J. Liu, B. Chen, D. Xu	C4-53
<b>Optimized Production Scale Classifier for Finest Cuts at High Capacities</b> M. Adam, S. Zampini	C4-58
<b>The Influence of Comminution Method to Particle Shape</b> M. Oja, R. Tuunila	C4-64
<b>Maxmill - a Field Report about the Application of a Stirred Ball Mill with Increased Economic Efficiency for Grinding of Minerals</b> J. Sachweh	C4-72
<b>The Kelsey Fine Autogenous Grinding (Fag) Mill</b> B. Kelly, D. Geraghty	C4-80
<b>The Effect of Using Concave Surfaces as Grinding Media</b> F.L. von Krüger, J.D. Donda, M.A.R. Drummond, A.E.C. Peres	C4-86
<b>Studies in Fine Grinding in an Attritor Mill</b> P. Raghuraman, R. Rajiv Raman, B. Pitchumani	C4-94
<b>Role of Particle Microstructure in Comminution</b> L.M. Tavares	C4-99

This Page Intentionally Left Blank

## OPERATIONAL WORK INDEX FOR GRINDING PLANTS

G.D. González\*, C. Pérez\*, A. Casali<sup>o</sup>, G. Vallebuona<sup>o</sup>, R. Vargas<sup>o</sup>\*Electrical Engineering Department, University of Chile, <sup>o</sup>Mining Engineering Department, University of Chile, <sup>o</sup>CODELCO-Chile, Andina Division, Chile

### Abstract

An global operational work index,  $W_{iog}$ , is defined for a conventional grinding plant consisting of a rod mill followed by three inverse hydrocyclone-ball mill grinding circuits and its value is estimated on-line. This global operational work index is based on an equivalent unitary ball mill circuit. The foundation for  $W_{iog}$  is Bond's equation for a grinding circuit, but here it is defined on the basis of measurements performed on the complete grinding plant: solids feed flow to the rod mill,  $f_{80}$  of the feed ore,  $p_{80}$  in the hydrocyclones overflow and the power draft of the mills. The on-line calculation of either the rod mill operational work index or the overall plant operational work index  $W_{iog}$  requires the feed size  $f_{80}$ , which is not measured on-line. A sensitivity analysis is made to assess the influence of  $f_{80}$  and  $p_{80}$  in the determination of the work index. It is found that only a small error is made if the average  $f_{80}$  is used instead of  $f_{80}$  to compute  $W_{iog}$ . However, for the case where the particle size at the hydrocyclones overflow is not measured, it is shown that a soft-sensor is necessary, but using only mill power draft and solids feed flow as inputs. This procedure produces relatively small errors in the calculation of the operational work index. Data collected in a large grinding plant is used here, including laboratory measurements of  $f_{80}$  and  $p_{80}$ , so it is possible to assess the effects of the soft-sensor inference in the on-line calculation of the global work index. The results may be extended to other grinding plants.

*Keywords: grinding plant, work index, operational work index, soft-sensors*

### Introduction

The concept of operating work index,  $W_{iop}$ , has been used to evaluate the efficiency of a grinding circuit (Rowland, 1973). Work indices obtained from operating data on any mill can be compared to grindability test results. The operating work index,  $W_{iop}$ , can be obtained using Bond's equation by defining  $W$  as the specific energy being used (power draw/new feed-rate),  $f_{80}$  and  $p_{80}$  as the actual feed and product 80% passing sizes, and  $W_i$  as the operating work index,  $W_{iop}$ . Once corrected for the particular application and equipment - related factors,  $W_{iopc}$ , can be compared on the same basis to grindability test results. This allows a direct comparison of grinding efficiency. Ideally  $W_i$  should be equal to  $W_{iopc}$  and grinding efficiency should be unity (Napier-Munn et al., 1996). However, results for ball mills in rod - ball mill circuits (Rowland, 1973) show variation of the ratio  $W_{iopc}/W_i$  from 0.78 to 1.29. A mill can be operating efficiently but because of the influences of classifier efficiency, ball size distribution, etc., this ratio can vary from 1.

The operational work index can be used to evaluate the grinding operational efficiency or even to determine the optimal distribution of feed ore among parallel grinding sections. The efficiency evaluation can be performed through the comparison of the operational work index with the ore work index  $W_i$ . Another



option is to observe the trend exhibited by the operational work index. This requires the measurement of the feed and product size distribution, the fresh ore feed-rate and the power draw. The on-line measurements of the fresh ore feed-rate and the power draw are usually available. In some occasions also the product size measurement is available, but almost never the feed size. For this reason, the operational work index is determined only with occasional sampling campaigns and with time delays, which are an impediment for taking opportune corrective actions. For the reasons stated, a global operational work index for a complete grinding plant is defined here, and its on line measurement is addressed, including the required soft-sensors to overcome the measurement problems.

### The global operational work index

Figure 1 shows a schematic diagram of the plant from which the data has been obtained for this paper. It consists of a rod mill followed by three sections in parallel, each one formed by a ball mill in inverse circuit with an hydrocyclone battery.

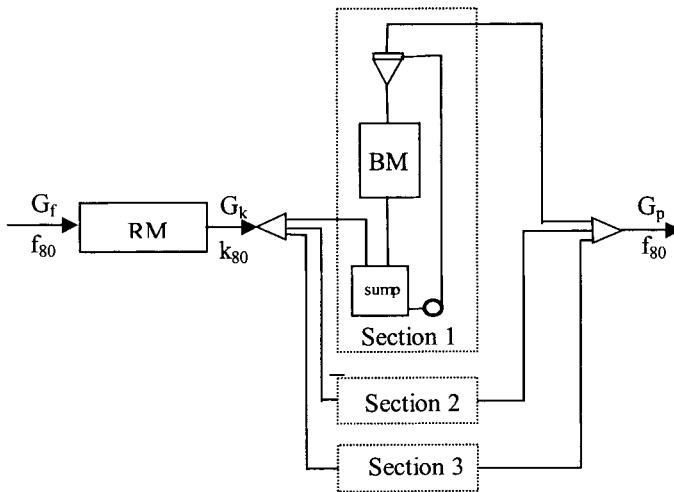


Figure 1: Grinding plant consisting of a rod mill (RM) and three ball mill (BM)-hydrocyclone inverse circuits.

In figure 1, the feed and product ore flows of the rod mill are  $G_f$  and  $G_k$ , with sizes  $f_{80}$  and  $k_{80}$ , respectively. The plant product ore flow is  $G_p$ , with size  $p_{80}$ . ( $f_{80}$ ,  $k_{80}$  and  $p_{80}$  are the sizes for which 80% of the ore has a smaller size, at the places shown). The power draws are  $P_{eR}$  for the rod mill and  $P_{eBj}$  for ball mill  $j$  ( $j = 1, 2$  and  $3$ ).

The operational work indices:  $W_{ioR}$  for the rod mill and  $W_{ioBj}$  for each ball mill – hydrocyclone section are given by (Rowland, 1973):

$$W_{ioR} = \frac{\frac{P_{eR}}{G_f}}{11.02 F_{TR} \left( k_{80}^{-\frac{1}{2}} - p_{80}^{-\frac{1}{2}} \right)}, \quad W_{ioBj} = \frac{\frac{P_{eBj}}{G_{kj}}}{11.02 F_{TB} \left( k_{80j}^{-\frac{1}{2}} - p_{80j}^{-\frac{1}{2}} \right)} \quad (1)$$

Here  $F_{TR}$  and  $F_{TB}$  are particular application and equipment-related factors, depending on the geometry of the mills, the type of grinding and the size reduction range (constant for a given application). For the grinding plant treated here, they are:  $F_{TR} = 1.236$ , and  $F_{TB} = 0.922$ .

*Global operational work index for the complete plant*

A global operational work index  $W_{iog}$  will be defined for the plant shown in Figure 1, assuming a unitary ball mill circuit equivalent (i.e., having one ball mill). Therefore:

$$W_{iog} = \frac{\frac{P_T}{G_f}}{11.02 F_{TG} \left( p_{80}^{-1} - f_{80}^{-1} \right)} \quad (2)$$

where

$$P_T = P_{eR} + \sum_{j=1}^3 P_{eBj} \quad (3)$$

is the total power drawn by the four mills.

Then  $W_{iog}$  considers  $P_T$ , the total ore feed ( $G_f$ , size  $f_{80}$ ) and the total product ( $G_p = G_f$ , size  $p_{80}$ ). The value  $F_{TG}$  for the global case was chosen so that the equivalent global circuit corresponds to one using a unitary ball mill:  $F_{TG} = F_{TBE}$ .

To determine  $F_{TBE}$  6 factors (Rowland, 1973) must be evaluated. Most of them are equal to 1, except those related with the feed size (equal to 1.4) and with the mill diameter. Then, for this case  $F_{TBE}$  is given by:

$$F_{TBE} = 1.4 * \left( \frac{2.44}{D_E} \right)^{0.2} \quad (4)$$

The diameter  $D_E$  in (4) of the equivalent unitary ball is found using the power draw equation for wet grinding ball mills (Rowland, 1982):

$$P_T = 5.7 * D_E^3 + 14.9 * D_E^{3.3} - 0.6 * D_E^4 \quad (5)$$

Using the average power draw of the plant,  $D_E = 5.41$  m, so that  $F_{TBE} = 0.8566$ .

*Measuring the global operational work index  $W_{iog}$*

Of the four variables that determine the global operational work index (equation 2), the power draw  $P_T$  is the sum of reliable on-line electrical measurements. The on-line measurement of the plant throughput,  $G_f$ , is very important for assessing the plant performance, so it is usually a high availability exact and precise measurement.

On the other hand, there is no on-line measurement of  $f_{80}$ , or  $p_{80}$ . But  $p_{80}$  may be correlated with a particle size measurement, such as  $g_{65}$ , the percentage +65# (i.e. the weight percentage of the solids in the plant product having a size greater than 212  $\mu$ m). For this plant the relation between  $p_{80}$  and  $g_{65}$  has been found to be given by:

$$p_{80} = -1.78 + 10.07 g_{65} \quad (6)$$

In some cases a sensor for measuring  $g_{65}$  - or some other mesh size - is installed in a plant, even though its measurement may not have the availability of the power and mineral flow measurements. But the corresponding sensor for measuring particle size at the feed end of the grinding plant is not available. In either case then it becomes

necessary to infer  $f_{80}$  always, and to infer  $p_{80}$  whenever the particle size sensor fails, it is removed for maintenance, or simply because it is not installed. Soft-sensors (González, 1999) for inferring particle size at hydrocyclone overflow have been reported in the literature (Casali et al., 1998).

### Soft-sensors for $f_{80}$ and $p_{80}$

In order to determine the requirements of the soft-sensors that must be used to infer these variables, the sensitivity of the operational work index  $W_{iog}$  with respect to  $f_{80}$  and  $p_{80}$  will be found.

#### Sensitivity of the operational work index

Taking partial derivatives of equation 3,

$$\frac{\partial W_{iog}}{\partial f_{80}} = -\frac{0.5 W_{iog} f_{80}^{-1.5}}{(p_{80}^{-0.5} - f_{80}^{-0.5})} \quad \frac{\partial W_{iog}}{\partial p_{80}} = \frac{0.5 W_{iog} p_{80}^{-1.5}}{(p_{80}^{-0.5} - f_{80}^{-0.5})} \quad (7)$$

so that

$$dW_{iog} = -\frac{0.5 W_{iog} f_{80}^{-1.5}}{(p_{80}^{-0.5} - f_{80}^{-0.5})} df_{80} + \frac{0.5 W_{iog} p_{80}^{-1.5}}{(p_{80}^{-0.5} - f_{80}^{-0.5})} dp_{80} \quad (8)$$

Then, the sensitivities  $S_{Wf}$  and  $S_{Wp}$  of  $W_{iog}$  with respect to  $f_{80}$  and  $p_{80}$ , given by the relation between the relative variations, are:

$$S_{Wf} = \frac{\frac{dW_{iog}}{W_{iog}}}{\frac{df_{80}}{f_{80}}} = -0.5 \frac{1}{\sqrt{r_{80} - 1}} \quad S_{Wp} = \frac{\frac{dW_{iog}}{W_{iog}}}{\frac{dp_{80}}{p_{80}}} = -0.5 \frac{\sqrt{r_{80}}}{\sqrt{r_{80} - 1}} \quad (9)$$

where  $r_{80} = f_{80} / p_{80}$  is an index giving the size reduction performed by the plant. These sensitivities were evaluated using data collected from the CODELCO Andina grinding plant (Figure 1) and the following results were obtained:

$$S_{Wf} = -0.1084 \quad S_{Wp} = 0.608 \quad S_{Wp} / S_{Wf} = -5.61$$

showing a much higher sensitivity with respect to  $p_{80}$  than to  $f_{80}$ .

An analysis of the plant data during a period of 46 months shows the statistics for  $f_{80}$  and  $p_{80}$  given in Table I.

Table I: Statistics for  $f_{80}$  and  $p_{80}$  over a 46 months period.

	Average ( $\mu\text{m}$ )	Std. dev. ( $\mu\text{m}$ )
$f_{80}$	9774	379
$p_{80}$	310	45

If variations of  $f_{80}$  and  $p_{80}$  of  $\pm 3$  times their corresponding standard deviations are considered, the following is noted.

#### Soft-sensor for $f_{80}$

For a change of  $f_{80}$  of 1136  $\mu\text{m}$  (three times its standard deviation) around 9774  $\mu\text{m}$ , using equation 5 it is found that  $W_{iog}$  changes in 0.24 kWh/t about the average  $W_{iog}$  of

19.1 kWh/t. Therefore the change of  $W_{iog}$  is 1.26%, i.e., quite small. As a result, the soft-sensor for  $f_{80}$ , giving  $f_{80est}$  is the simplest of all, since it will only contain the constant ( $C_{dc}$ ) term, equal to the average  $f_{80ave}$  of  $f_{80}$  during the period considered. The  $f_{80}$  will have been determined through laboratory analysis during a given period. Then  $f_{80est} = f_{80ave}$  is used in following periods when  $f_{80}$  is not measured, supposing  $f_{80ave}$  remains fairly fixed, until new laboratory measurement are obtained and  $f_{80ave}$  may be updated.

#### Soft-sensor for $p_{80}$

For changes of  $p_{80}$  of 136  $\mu\text{m}$  (three standard deviations) around 310  $\mu\text{m}$ , using equation 5  $W_{iog}$  is found to change by 5.1 kWh/ton around the average  $W_{iog}$  of 19.1 kWh/ton, i.e., the change in  $W_{iog}$  is 29.4%. This is a rather large change, so that the average  $p_{80}$  may not be an adequate estimator of  $p_{80}$  and a more complex soft-sensor is needed. This fact will be confirmed below.

For the design of a soft-sensor for  $p_{80}$  only the very reliable measurements  $P_T$  (power draft of the mills), and  $G_s$  (the feed ore flow) have been used. This reliability criterion restricts the candidate measurements as opposed to the soft-sensors determined by Casali et al. (1998). The resulting soft-sensor is given by

$$p_{80est}(t) = \theta_1 G_s(t) + \theta_2 P_e(t) + C_{dc}(t) \quad (10)$$

On fitting this model to the 46 month long data, the estimated parameters turned out to be  $\theta_1 = 0.708$ ,  $\theta_2 = -0.0107$ ,  $C_{dc} = -566$ , and the root mean square error of the model fit was 20.7  $\mu\text{m}$ . The relative standard deviations of the parameter determination error was less than 0.5.

Figure 2 shows a test of the prediction capabilities of this soft-sensor. In this case the parameter estimation period was from months 12 to 40, so that the prediction (i.e., using data different from the fitting stage) covers the periods from months 1 to 11 and from 41 to 46.

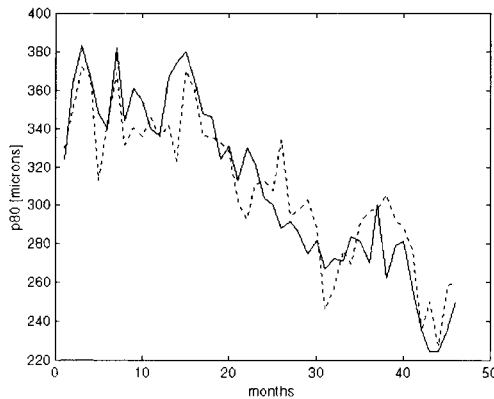


Figure 2: Soft-sensor for  $p_{80}$  (dashed line) compared with actual  $p_{80}$  real (solid). The parameter estimation period is form months 12 to 40 and the prediction period from months 1 to 11 and 41 to 46.

If the measurement of  $g_{65}$  (%+65#) is available then  $p_{80}$  may be found and used in the determination of  $W_{iog}$ . But if there are no measurements of  $f_{80}$ , according to the small sensitivity of the work index with respect to  $f_{80}$ , its average value might be used. This is confirmed by Figure 3, which shows in solid line the actual work index  $W_{iog}$  (computed using the actual measurements of  $f_{80}$  and of  $p_{80}$ ) and the  $W_{iog}$  (computed using the measured value of  $p_{80}$ , but instead of  $f_{80}$ , its average value of  $f_{80} \pm$  three standard deviations of  $f_{80}$  (dotted lines). A good result is obtained. The average value as well as the standard deviation are also those of the period 12÷40 months.

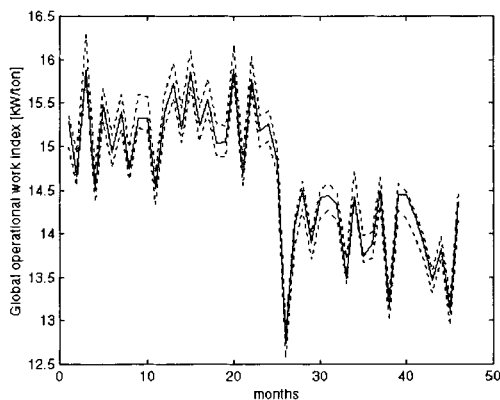


Figure 3: Actual  $W_{iog}$  (solid line) and  $W_{iog}$  computed using the average value of  $f_{80} \pm 3$  standard deviations of  $f_{80}$  (dotted lines) and measured  $p_{80}$ .

In Figure 4 a test of the prediction capability for  $W_{iog}$  is shown using the fixed value (average) for  $f_{80}$  and  $p_{80est}$  given by the soft-sensor determined in the period from months 12 to 40, so that, in periods 1 to 11 and 41 to 46, a prediction for  $W_{iog}$  is obtained.

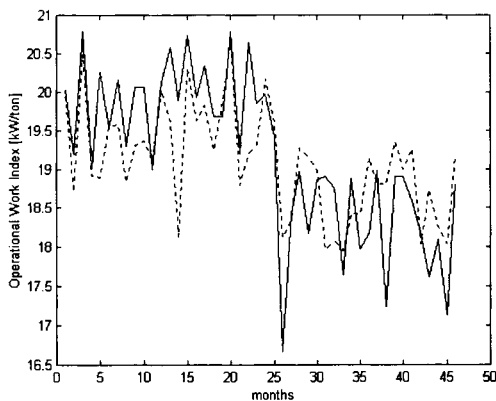


Figure 4: Actual global operational work index  $W_{iog}$  (solid line) and its estimated value  $W_{iogest}$  (dashed line) using the  $p_{80}$  soft-sensor determined in the period 12÷40 months, according to Figure 2, and the average  $f_{80}$ .

## Conclusions

A global operational work index for a grinding plant has been defined using Bond's equation applied to the total feed, total product and total mills power draft of a grinding plant.

Two main problems in the determination of the operational work index were identified. These were:

- an estimation of  $f_{80}$  for the feed ore;
- an estimation of the  $p_{80}$  in the product (hydrocyclones overflow) in the event that no particle size measurement is available (either because the sensor has not been installed or because it has failed or has been removed for maintenance or repairs).

A sensitivity analysis showed that the operational work index had a small sensitivity with respect to  $f_{80}$ , so that its average value could be used with good results. Hence, if the  $g_{65}$  (% >65#) measurement is available a very good estimate of the operational work index is obtained. On the other hand, the sensitivity of the operational work index with respect to  $p_{80}$  was not small, so that an average value of  $p_{80}$  was an inadequate estimation. Therefore a soft-sensor for  $p_{80}$  had to be developed, but restricted by design to be a function only on the reliable measurements provided by the total power draft and the total ore feed measurements. It has been further shown that an acceptable estimation of the global operational work index may be obtained using the average  $f_{80}$  and the estimate of  $p_{80}$  given by the soft-sensor.

It is apparent that the procedure described here for obtaining a global operational work index may be applied to other grinding plants.

## Acknowledgements

This research was funded by CODELCO-Chile under a grant from CODELCO / U. de Chile research agreement. The authors express their thanks to CODELCO - Andina Division for their valuable contribution.

## References

- Casali, A., González, G.D., Torres, F., Vallebuona, G., Castelli, L. and Giménez, P., 1998. Particle size distribution soft-sensor for a grinding circuit. *Powder Technology*, 99, pp. 15 – 20.
- González, G.D., 1999. Soft-sensors for processing plants. *Proc. Second International Conference on Intelligent Processing and Manufacturing of Materials*, vol. 1, pp. 59-70.
- Napier-Munn, T., Morrell, S. et al., 1996. In: *Mineral comminution circuits - their operation and optimization*. JKMR, Queensland, Australia, Chapter 4, pp. 57-66.
- Rowland, C., 1973. Comparison of work indices calculated from operation data with those from laboratory test data. *Proc. X IMPC, IMM, London*, pp. 47-61.
- Rowland, C., 1982. Selection of rod mills, ball mills, pebble mills and regrind mills. In: A. Mular and G.Jergensen, (Editors). *Design and Installation of Comminution Circuits*, Chap. 23. AIME, pp. 415-416.

## MAGOTTEAUX AUTOMATIC BALL CHARGER (ABC)

W. Conger, P. Amelynck

Magotteaux International, Belgium

### Abstract

The Magotteaux Automatic Ball Charger (ABC) optimizes ball mill performance by controlling ball addition. Each ABC consists of a storage hopper, vibrating feeder, load cells, local control electronics and computer link to the grinding process. The system continuously monitors absorbed power, feed rate and ball consumption to calculate the proper ball addition rate to maintain optimum mill power. Advantages of the ABC include optimized grinding through mill power control, reduced operator involvement, and real time adjustment of ball consumption rates relative to the abrasiveness of the current mill feed.

*Keywords: grinding, control, media, wear, process*

### Introduction

Magotteaux International is a group of foundries located worldwide that supply high quality cast grinding media, grinding mill liners and other wear parts to the mining, cement, aggregate and recycling industries. Magotteaux has also developed process control products and grinding expertise to provide customers with cost-effective grinding solutions. The automatic addition of grinding media to mills has been identified as a way to improve the grinding process in the mining industry.

Magotteaux has developed an improved system to automatically add grinding balls to grinding mills, the Magotteaux Automatic Ball Charger (ABC). The ABC adds relatively small weighed increments of balls, typically 100 kg, as required, rather than the large increments, 1,000÷10,000 kg, that are common in manual charging systems. The Magotteaux ABC works with a mixture of ball sizes in the range of ½" to 5", making it possible to customize ball size for optimized mill performance.

The ABC uses a dynamic ball consumption rate to control ball addition. The consumption rate of grinding media is related to the operating conditions of the mill and the characteristics of the ore. Magotteaux relates ball wear to three factors: abrasion, corrosion and impact.

These factors change in normal operation, and the Magotteaux ABC has been designed to use the mill absorbed power to compensate for resulting changes in ball wear rate (BWR). This is an advantage over systems that use a static historical wear rate. Several prototype Magotteaux ABC systems have been successfully operating in the field. The experience gained from these systems has been used to refine the latest standard model, scheduled to begin field-testing in late 1999.

### Physical description

The Magotteaux ABC has been designed as a single structure to simplify installation. The field unit communicates with a remote computer that monitors mill power and calculates charging requirements.

### *Ball storage hopper*

The ball storage hopper is a cylindrical rubber lined steel hopper supported on four legs. The hopper is 7' diameter with a capacity of 10 t, and the capacity can be increased 4.7 t by adding additional one foot high ring segments to the hopper.

### *Vibrating feeder*

The balls are fed from the hopper using a heavy-duty electromagnetic vibrating feeder. The feeder model is specified to handle the specific ball size(s) to be used. The feeder controller is located in the attached electrical enclosure.

### *Weigh hopper and dumping mechanism*

The balls are fed into a rubber lined weighing hopper equipped with a movable gate. The hopper is suspended on three 1,250 lb capacity load cells. An electronic weigh module is used to perform the weighing function.

### *Control electronics*

The ABC's functioning is controlled by a programmable logic controller (PLC). This PLC communicates to the field operator through a local display and with a remote computer used to track mill power and calculate ball addition rate. The software in the remote computer provides the main user interface and database functions. All motor starters, control relays, voltage transformers and other necessary electrical components are located in one electrical enclosure.

## **Operation**

The ABC operates continuously with minimum operator intervention. The operator is only required to periodically replenish the ball supply once the unit is installed and initialized. The remote computer then determines when ball additions are needed and communicates this fact to the field unit. The typical ball addition cycle is as follows:

- the local PLC zeroes the scale;
- the vibrator operates until the weigh hopper detects that the preset target weight of balls has been introduced into the hopper (typically 100 kg);
- a stable weight is recorded in the local PLC,
- the dump gate opens until the weigh hopper is empty, then closes;
- the weight of balls is reported to the remote computer.

There is a system of checks and alarms to detect and correct system faults. Typical faults include foreign material obstructing ball flow and an empty bin condition. The alarms are displayed on the remote computer screen to alert the operator.

The normal operator interface with the ABC is through the remote computer. However, in case of communications failure, the ABC is capable of functioning in a stand-alone mode for an indefinite period of time, storing all actions in the PLC until communications are restored.

## **Control strategy**

Previous ball addition control strategies assume that the ball wear rate (BWR) is constant, however, this is not true in mineral grinding applications. The BWR is related to the metallurgy of the grinding media, the mineralogy of the ore and the



operating conditions in the mill. While the metallurgy of the media is constant, the mineralogy of the ore and the operating conditions in the mill are not. Therefore, it is reasonable to consider that BWR changes with time, and that the rate of ball addition should change to compensate for this. The difficulty lies in evaluating the instantaneous ball wear rate. The straightforward method to control ball addition would be to directly measure the ball volume in the mill and add the balls necessary to return to the desired volume. However, there is no means available to measure the instantaneous ball volume of a grinding mill in operation. This lack of measurement technique requires that the instantaneous ball volume be inferred from other available continuous measurements. The power absorbed by a grinding mill is a function of the ball volume, as well as a number of other factors, including pulp density, mill speed, liner design and life, media density, etc. If all other factors remained constant, then the ball volume could be calculated from the mill absorbed power, providing the instantaneous measure of the ball volume. However, experience shows that the other factors are not constant. One can see on the 24 h trace chart in Figure 1 that the mill power changes for reasons other than ball volume. These changes are related to changes in operating conditions, such as pulp density, ore particle size or circulating load that result from ore changes or operator intervention. This fluctuation in power not related to ball volume makes it dangerous to control based on power alone.

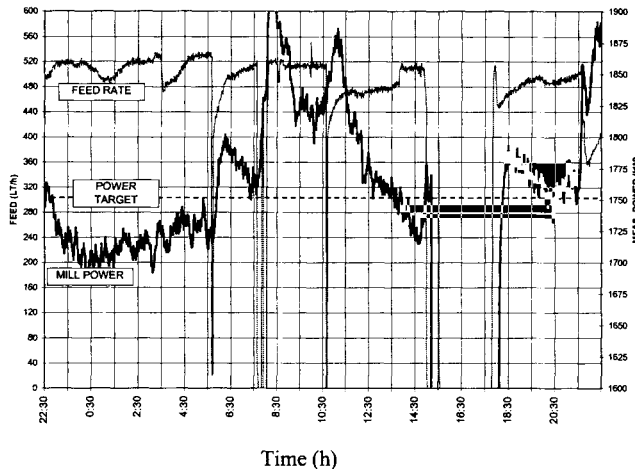


Figure 1: 24 h trace of secondary ball mill power and feedrate.

The control strategy of the Magotteaux ABC accounts for the facts that BWR does change, and that the mill power is related to the ball volume, to provide a dynamic system to control ball addition.

The ABC program uses a BWR (expressed in g/kWh) to calculate the reduction of the mass of the balls in the mill as the mill operates. This reduction in ball mass is tracked as the need in balls required to return to the desired ball volume. When a preset quantity of balls are required, (generally 100 kg), the ABC makes a weighed addition of balls and adjusts the need in balls to reflect the actual addition.

The ABC uses the power reading to continuously adjust the BWR. The power target in the program corresponds to the power expected at the desired ball volume. If the actual power is higher than the target, the program assumes that the ball volume is too high and lowers the BWR, so that less balls are added and the volume decreases. If the actual power is lower than the target, the opposite occurs. The amount of BWR adjustment is related to the amount of power deviation and the duration.

To allow the BWR to change too much or too quickly is dangerous. Since mill power is also related to factors other than ball volume, limits are placed on the magnitude of the BWR and the rate of change in the control program. Experience with prototype installations shows it is critical that the BWR parameters be set correctly.

### Industrial performance

Two prototype units have been successfully operating in the mining industry. These units have demonstrated the reliability of the standard design and the applicability of the control strategy.

#### *Codelco - El Teniente - Colon*

The El Teniente Mine– Colon Convencional Concentrator is an underground copper mine located in Central Chile operated by the Codelco group. The 12 line concentrator is capable of processing 50,000 t/day of ore. The prototype ABC is installed on Line 7 in a section of the concentrator containing eight grinding lines, each line consisting of a 14'×24' overflow ball mills operating in closed circuit with an array of hydrocyclones. See Figure 2.

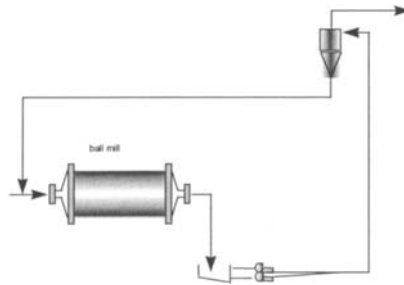


Figure 2: El Teniente - Colon flowsheet.

The ABC unit has been operating reliably with new electrical components and improved software since September 1998.

The mills in this circuit are operated at a fixed feed rate to produce the target fineness (typically 23.5% >150  $\mu\text{m}$ ). The target ball volume is 38%, which translates to a target power of 2,145 kW ( $\pm 32$  kW depending on liner life). The ABC is setup to add 100 kg increments as required, typically 10÷15 times per day. The maximum BWR allowed by the control program is 50 g/kWh and the minimum is 30 g/kWh. Plant operating data collected in the period from September 1998 through June 1999 (10 months) shows that Line 7, equipped with the ABC, when compared to Lines 2-6, has produced an equivalent product while using less balls (Table I).

Table I: El Teniente - Colon plant operating data for the period Sep-98 to Jun-99.

Parameter	Line 7, with ABC	Lines 2-6, without ABC
Power, kW	2,122	2,084
Feed rate, t/h	172.3	170.2
Ball consumption, g/t	484	532
Fineness, % >150 $\mu$	23.54	23.52
Specific power, kWh/t	12.32	12.25

The daily performance of Line 7 as recorded by the remote ABC control computer operating is illustrated in Figure 3. The data plotted is the daily average value. The effect of the variable ball rate can be seen in the plot of the ball consumption.

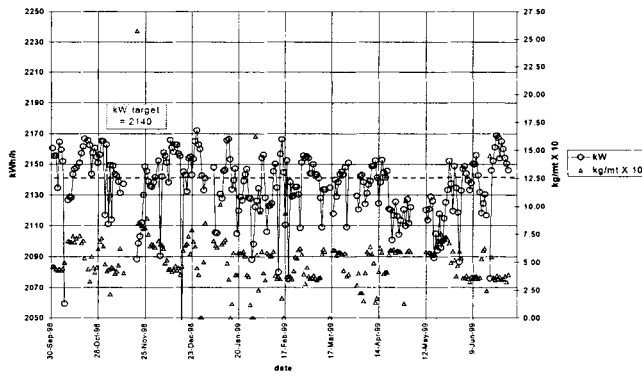


Figure 3: Chart of Line 7 daily operating data at El Teniente - Colon.

Plant personnel routinely measure the % ball volume of the ABC equipped ball mill. These measurements are compared against less frequent measurements of the other ball mills in Figure 4. The standard deviation of the ABC equipped mill is 1.4% while the mean standard deviation of the other lines is 3.0%.

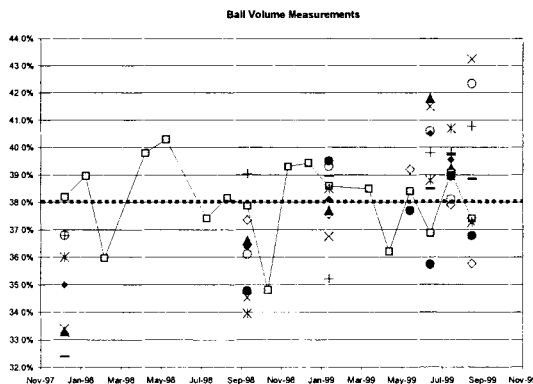


Figure 4: Chart of % ball volume at El Teniente - Colon.

The monthly ball consumption performance of Line 7 versus Lines 2-6 is illustrated in Figure 5.

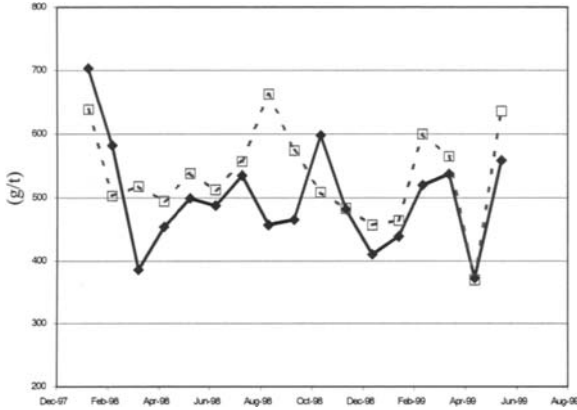


Figure 5: Monthly ball consumption at El Teniente - Colon.

*US Steel – Minnesota ore operations (Minntac)*

Minntac is an iron ore (taconite) mine capable of producing 15,800,000 t of pellets annually operated US Steel in Northern Minnesota, USA. The 16 grinding line concentrator processes approximately 50,000,000 t of ore per year. Each grinding line contains one rod mill, one primary ball mill and one secondary ball mill, with hydrocyclone and vibrating screen classification and three stages of magnetic separation. The final silica grade is achieved through silica flotation (Figure 6).

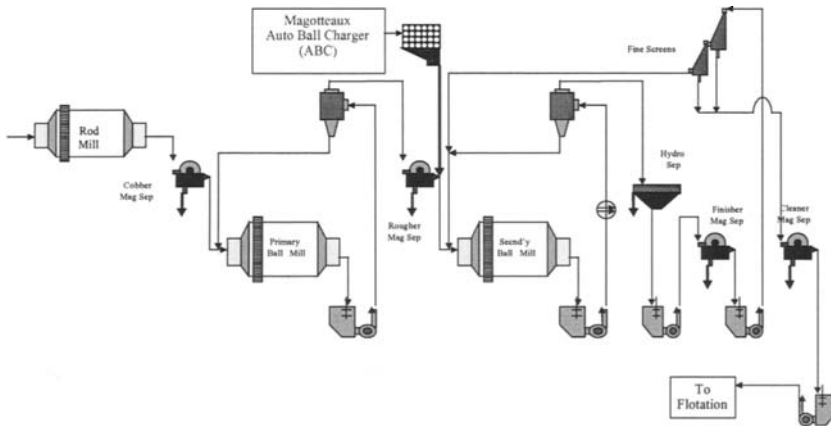


Figure 6: Minntac grinding line flowsheet.

The ABC is installed on the secondary ball mill of line 17, which is one of the six Step 3 grinding lines. Mechanical reliability has been excellent since the unit was upgraded to its present software and hardware configuration in August 1997.

The complexity of the Minntac flowsheet makes it difficult to control the operating conditions in the secondary ball mill. The relationship between ball volume and absorbed power is more variable and unpredictable than in a simpler circuit. The daily values for the period between December 1998 to July 1999 shows the ability of the ABC to maintain the mill power at three different setpoints (Figure 7).

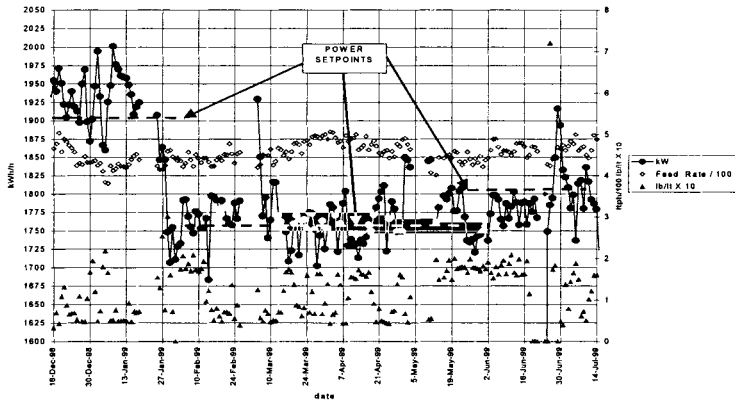


Figure 7: Daily operating data for the Minntac Line 17 secondary ball mill – Dec-98 to Jun-99.

The ABC has been used to maintain several power targets. The testing at different power targets on the secondary ball mill at this plant indicates that throughput has not been significantly effected by operating this mill at lower power. In Figure 8 the plant operating data for line 17 against the other Step 3 lines, not equipped with ABC's, are compared. This data shows that Line 17 can operate at a significantly lower kW without having a negative impact on throughput. This could result in significant savings if all the secondary ball mills can be operated at reduced power.

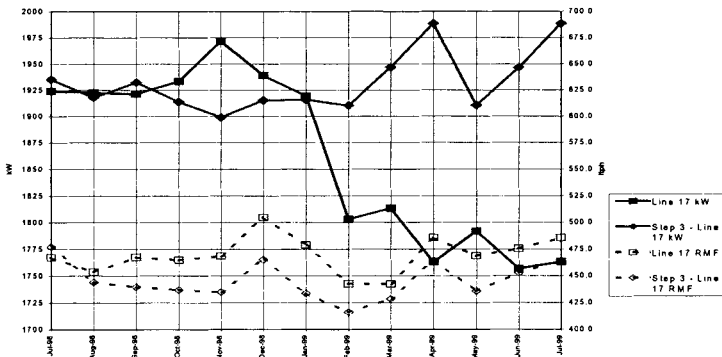


Figure 8: Comparison of secondary ball mill power and grinding line throughput at Minntac Step 3.

The plant operating data for the Step 3 mills for the period from July 98 to June 99 is summarized in Table II.

Table II: Plant operating data at Minntac Step 3.

Parameter.	Line 17 with ABC	Lines 13-18 without ABC
Power (kW)	1,886	1,929
Feed rate (t/h)	460	440
Ball consumption (lb/t)	0.193	0.203*

\* ball consumption lines 13,16 and 18 only

## Conclusions

The Magotteaux Automatic Ball Charger is a device that optimizes ball mill grinding by maintaining the charge of the ball mill within 50 kg of the optimum level at all times. Industrial experience has proven the ABC able to operate with minimum operator effort, requiring only periodic filling of the ball storage hopper. Ball addition rate is controlled to maintain the target power chosen by the mill operator. Data on ball consumption and mill performance is instantaneously available. It is possible to reduce financial losses by reducing the excess ball consumption associated with overcharging the mill and the lost production associated with undercharging the mill, as well as determining the optimum ball volume. Work continues to improve the standard design and prove the benefits of the Magotteaux Automatic Ball Charger.

## Acknowledgements

We would like to acknowledge the following for allowing us to use the data and experience gained in their plants in this paper: Luis Henriquez, Jefe de Unidad Proceso Minco, Codelco, division Teniente-Colon; Scott Vagle, Area Manager, Quality Assurance – Plant, Minnesota Ore Operations, U.S. Steel.

## BREAKAGE PARAMETERS OF CHROMITE AND SIMULATION OF THE PRODUCT-SIZE DISTRIBUTIONS

M.Yekeler, U. Ulusoy, I. Akbaba

Department of Mining Engineering, Cumhuriyet University, 58140 Sivas, Turkey

### Abstract

The breakage parameters of a run of mine chromite for dry and wet ball milling were obtained by means of standard S and B test methods. This method requires a small amount of powder for grinding for different length of time in a laboratory ball mill to obtain the breakage parameters. The single sized fraction of a  $-425 + 250 \mu\text{m}$  feed of material obtained from our laboratories was ground for different lengths of time in a laboratory ball mill. The specific rate of breakage, ( $S_i$ ), for dry milling was determined to be  $0.28 \text{ min}^{-1}$ , while the  $S_i$  value for wet grinding was  $0.56 \text{ min}^{-1}$ . The cumulative breakage-distribution function ( $B_{ij}$ ) values ( $\theta$ ,  $\gamma$  and  $\beta$ ) obtained were the same for dry and wet ball milling. The  $\phi$ ,  $\gamma$  and  $\beta$  values were 0.75, 1.14 and 7.9, respectively. The simulation of the product-size distributions using a "Two-Stage Ball-Mill Circuit Simulator: PSUSIM" was performed by making use of the obtained S and B parameters. The simulated results were in good agreement with the experimental results.

*Keywords: grinding kinetics, chromite, ball milling, simulation*

### Introduction

The size reduction of minerals and solids by crushers and mills is a very important industrial operation. The large amounts of minerals, rocks, coals, cement and plastic raw materials are ground by this means, and a lot of energy is consumed during the size-reduction operations.

On the other hand, fine and ultra-fine grinding consumes a great deal of energy and leads to the highly abrasive wearing of the balls and mills.

It is known that dry grinding of brittle materials in ball mills in order to obtain very fine sizes departs from "normal" grinding behavior (Austin et al., 1984). This is explained in terms of the build up of fine sizes of balls and formation of larger pelletized particles (Opaczky, 1969; Ghigi and Rabottino, 1966) or elimination of Griffith flaws as particles become smaller by fracturing (Evans and Pomeroy, 1958). The effect of surface-active agents (grinding aids) on fine, dry grinding has helped resolve the problems related to these mechanisms.

An analysis of the kinetics of dry grinding in a laboratory ball mill is introduced by a concept called the "slowing-down factor, k," which is the ratio of the specific rates of breakage for long grinding time, and the normal specific rates of breakage (Austin and Bagga, 1981). The concept of the slowing-down factor is also used in wet grinding (Tangsathikulchai and Austin, 1985). At very high slurry concentrations, a steady decrease of mill power caused by the build-up of a deposited layer that sticks to the mill case is seen. This problem reduces the effective mill diameter, and the balls start to adhere to the layer and centrifuge.

The normal breakage rate is defined by first-order breakage, defined as follows by Austin (1971):

$$\text{rate of breakage of size } j = S_j \cdot w_j(t) \cdot W, \quad (1)$$

where  $S_j$  is the specific rate of breakage of size  $j$ , and  $w_j(t)$  is the mass fraction of the total charge,  $W$ , which is of size,  $j$ , at time,  $t$ , of grinding. However, at long grinding times,  $S_j$  decreases as fine material accumulates in the mill. Therefore, this breakage is called non-first order, i.e. the slowing-down breakage rates.

Equation 1 becomes:

$$-\frac{dw_i(t)W}{dt} = S_i w_i(t)W, \quad (2)$$

for the top interval size of the charge. Since  $W$  is constant, the first-order breakage is formulated due to integration:

$$\log\left(\frac{W_i(t)}{W_i(0)}\right) = -\frac{S_i \cdot t}{2.3} \quad (3)$$

For any size interval, a size-mass balance for batch grinding gives the following equation (Austin, 1971):

$$\frac{dw_i(t)}{dt} = -S_i \cdot w_i(t) + \sum_{j=1}^{i-1} b_{i,j} S_j w_j(t), \quad n > i > j > 1 \quad (4)$$

where  $b_{i,j}$  is the fraction of material broken from larger size,  $j$ , which reports to smaller size,  $i$ , on the primary fracture, and  $n$  is the "sink" size interval, defined by the lowest measurable size.

The cumulative primary daughter-fragment distribution  $B_{i,j}$  is defined by:

$$B_{i,j} = \sum_n^i b_{k,j}$$

and it is given in an empirical form (Austin and Luckie, 1971) by:

$$B_{i,j} = \phi_j \left(\frac{x_{i-1}}{x_j}\right)^\gamma + (1 - \phi_j) \left(\frac{x_{i-1}}{x_j}\right)^\beta, \quad n > i > j, \quad (5)$$

where  $x_i$  is the top size, and  $B_{i,j}$  is the weight fraction of primary breakage products. The parameters  $\phi$ ,  $\gamma$  and  $\beta$  define the size distribution of the material being ground. On plotting size versus  $B_{i,j}$  on log paper, the slope of the lower portion of the curve gives the value of  $\gamma$ , the slope of the upper portion of the curve gives the value of  $\beta$ , and  $\phi$  is the intercept (Shah and Austin, 1983).

This paper is aimed at extending the results of this work to dry and wet grinding of chromite using standard S and B test conditions, as applied to one feed-size interval, and also to simulating the product-size distributions with a "one-point fit" approach.

## Materials and method

### Mineral

The run of the mine chromite mineral used for the grinding tests was obtained from the Pınarbaşı, Kayseri location of Turkey. The sample was crushed, ground and sieved to a single sized feed fraction of the interval – 425 + 250  $\mu\text{m}$ .



### Grinding tests

A laboratory ball mill was used to do the standard S and B tests. Dry and wet grinding were carried out in the laboratory ball mill described in Table I:

Table I: Ball mill characteristics and test conditions.

Mill	Inner diameter (mm)	200
	Length (mm)	200
	Volume (cm <sup>3</sup> )	6,284
	Critical speed (rpm)	100.8*
	Operational speed: 70% of critical speed (rpm)	70
	Solid (% by volume)	30
Lifters	Number	6
	Cross-section	semi-circular
	Radius (mm)	10
Media (balls)	Material	Alloy steel
	Diameter (mm)	20 and 25
	Specific gravity (g/cm <sup>3</sup> )	7.8
	Total ball weight (g)	5,875
	Fractional mill filling J <sub>B</sub>	0.20**
Material	Chromite ore	-
	Specific gravity (g/cm <sup>3</sup> )	4.2
	Powder weight (g)	633

\* Calculated from  $N_C = 42.3/(D-d)^{1/2}$  (rpm); D, d (m).

\*\* Calculated from  $J_B = [(mass\ of\ balls/ball\ density)/(mill\ volume)]/[1.0/0.6]$

Tests were done at a low ball load of 20% of the mill volume filled with the ball bed and a low powder load, corresponding to the formal interstitial filling of the space voids of the ball bed of  $U = 0.5$ . These conditions were chosen because it is known that both dry and wet grinding give normal first-order grinding kinetics under such conditions. After each grinding period, the mill was left long enough to allow the particles to settle, the balls were cleaned and removed from the mill one-by-one, and the mixed powder was sampled for size analysis by coning and quartering. The wet ground material was also dumped into a bucket by washing the balls and the mill. After taking a representative sample for size analysis, the material and the balls were returned to the mill for further grinding after each size analysis. After dry screening for 20 min in a stack of standard sieves and a Ro-tap shaker, the material on the screens was washed under a water spray to remove adherent fine powder before drying and weighing.

### Simulation

The simulation of the product-size distribution data was performed by using a Penn State Ball Mill Simulator (Austin et al., 1989).

### Experimental results

Figure 1 shows the initial grinding results plotted in first-order form for dry and wet grinding (Austin et al., 1984):

$$w_1(t) = w_1(0) \cdot \exp(-S_1 \cdot t), \quad (6)$$

where  $w_1(t)$  is the fraction remaining in the feed size interval after time,  $t$ , and  $S_1$  is the specific rate of breakage of that size.

The  $S_i$  value of the  $-425 + 250 \mu\text{m}$  feed fraction for dry grinding is  $0.28 \text{ min}^{-1}$ , and it was  $0.56 \text{ min}^{-1}$  for wet grinding, which indicates that wet grinding is two times faster at breaking the top size particles than dry grinding. The primary breakage-distribution function (Austin et al., 1984) determined using the BII procedure for the shortest grinding time,  $t=1 \text{ min}$ , is:

$$B_{i,j} \cong \frac{\log\left[\frac{(1 - P_i(0))}{(1 - P_i(t))}\right]}{\log\left[\frac{(1 - P_2(0))}{(1 - P_2(t))}\right]}, i > 0, \tag{7}$$

where:  $P_i(0)$  = cumulative weight fraction of time, 0, for size interval,  $i$ ;  $P_2(0)$  = cumulative weight fraction of time, 0, for the second interval;  $P_i(t)$  = cumulative weight fraction of time,  $t$ , for interval,  $i$ ; and  $P_2(t)$  = cumulative weight fraction of time,  $t$ , for the second interval. The BII method fits equation 5 stated before, and is shown in Figure 2. The  $B_{i,j}$  values were obtained as  $\phi = 0.75$ ,  $\gamma = 1.14$  and  $\beta = 7.9$ . Figures 3 and 4 show the particle-size distributions obtained at various times of grinding, respectively.

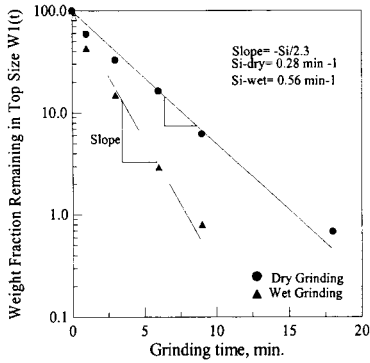


Figure 1: First-order plots of breakage of  $-425 + 250 \mu\text{m}$  feed of chromite ore for dry and wet grinding.

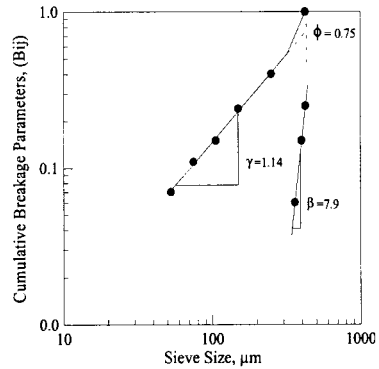


Figure 2: Primary breakage-distribution function of  $-425 + 250 \mu\text{m}$  chromite ore feed (the  $B_{i,j}$  values are the same for wet and dry grinding.).

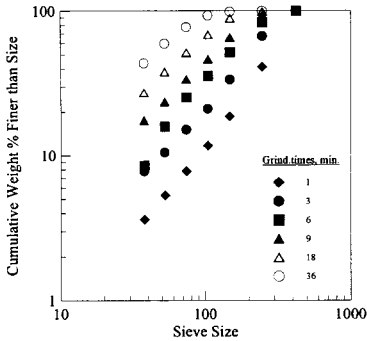


Figure 3: Product-size distributions from dry grinding of  $-425 + 250 \mu\text{m}$  chromite ore in a laboratory ball mill.

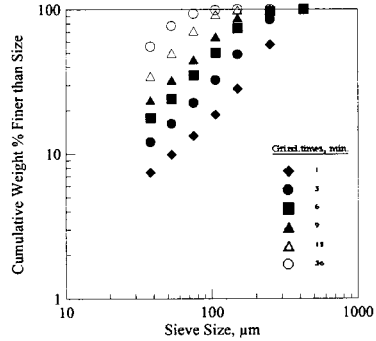


Figure 4: Product-size distributions from wet grinding of  $-425 + 250 \mu\text{m}$  chromite ore in the same laboratory mill as dry grinding.

Figure 5 shows the <106 μm and <38 μm fractions with respect to grinding time to compare the dry grinding to wet grinding to see the net production rates.

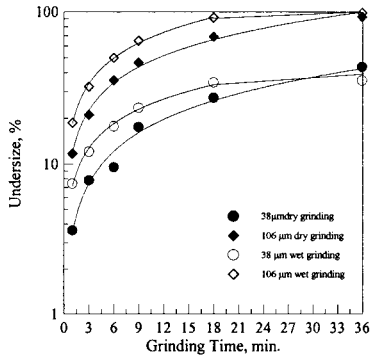


Figure 5: Production of <106 μm and <38 μm fractions for dry and wet grinding of chromite ore.

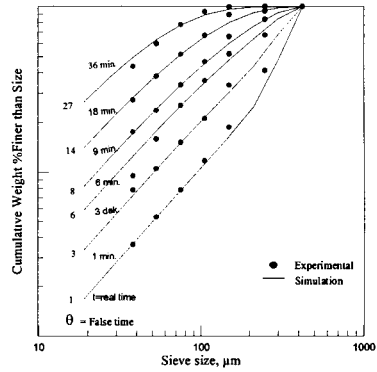


Figure 6: Simulated and experimental product-size distributions of dry grinding of chromite ore.

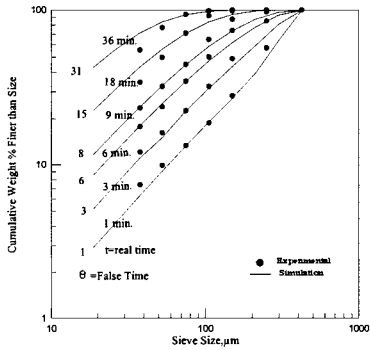


Figure 7: Simulated and experimental product-size distributions of wet grinding of chromite ore.

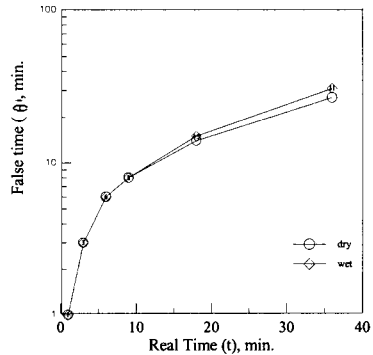


Figure 8: False grinding time (apparent first-order grinding time) versus real grinding time (Figures 6 and 7).

**Simulation results and conclusions**

In order to do the product size distribution simulations, an  $a_T$  value was obtained from the following equation (Austin et al., 1984):

$$S_i = a_T \left( \frac{X_i}{X_0} \right)^\alpha \tag{8}$$

Where:  $S_i$  is the specific rate of breakage ( $\text{min}^{-1}$ );  $a_T$  is the  $S_i$  value at  $X_0 = 1 \text{ mm}$  size; and  $X_i = 425 \text{ μm}$  (top size).

The primary breakage-distribution function values of  $\phi$ ,  $\gamma$  and  $\beta$  values obtained in Figure 2 were used to do the simulations.

The slowing-down region started after 9 min of grinding. The grinding up to 9 min of grinding time was simulated using the characteristic parameters of  $\alpha$ ,  $\mu$ ,  $\lambda$ ,  $\beta$ ,  $\gamma$  and  $\phi$

in a Penn State Ball Mill Simulator (Austin et al., 1989). This simulation is in good agreement with the experimental data up to 9 min of grinding. However, the predicted size distributions at 9 min and longer were finer than those observed experimentally. This was handled by using the false time concept (Austin and Bagga, 1981), making the simulator produce a match to a specified point on the product-size distribution and designating the grinding time necessary to achieve this match as the false time  $\theta$ , where  $\theta \leq t$ .

Figures 6 and 7 show the comparison of simulated and experimental values based on choosing a false time in order to produce a one-point fit of the simulated result up to an experimental fit point that was 75  $\mu\text{m}$ .

Figure 8 shows the relation between the false grinding time and the first-order grinding time. Differentiation of this curve produces the value for the slowing-down factor,  $\kappa$ :

$$\kappa = \frac{d\theta}{dt} \quad (9)$$

A major change in  $\kappa$  can be seen after 9 min or more of grinding time.

#### References

- Austin, L.G., 1971. A review introduction to the mathematical description of grinding as a rate process. *Powder Technology*, 5, 1-17.
- Austin, L.G. and Bagga, P., 1981. *Powder Technology*, 28, 83.
- Austin, L.G. and Luckie, P.T., 1971. Methods for determination of breakage distribution parameters. *Powder Technology*, 5, 215-222.
- Austin, L.G., Klimpel, R.R., and Luckie, P.T., 1984. *Process Engineering of Size Reduction Ball Milling*, SME, New York, U.S.A.
- Austin, L.G., Yildirim, K., Luckie, P.T. and Cho, H.C., 1989. Two Stage Ball Mill Circuit Simulator. The Pennsylvania State University, Univ. Park, PA, U.S.A.
- Evans, I, and Pomeroy, C.D., 1958. The Strengths of Cubes of Coal in Uniaxial Compression. In: W.H. Walton (Editor), *Mechanical Properties of Non-Metallic Brittle Materials*, 5-28.
- Ghigi, G. and Rabottino, L., 1966. Experiments on cement clinker grinding with additives. *Dechama Monograph*, 57, 427-448.
- Opoczky, L., 1969. Effect of surface active agents on the grinding process of cement clinker. *Epitoanyag*, 21, 188-193.
- Shah, I. and Austin, L.G., 1983. Breakage rates and size distributions in dry ball milling for fine sizes. In: S.G. Malghan (Editor), *Ultrafine Grinding and Separation of Industrial Minerals*, AIME, New York, pp. 9-19.
- Tangsathitkulchai, C. and Austin, L.G., 1985. *Powder Technology*, 42, 287.

## RUN-OF-MINE MILLING PILOT PLANT TEST WORK

B. Clermont

Magotteaux International, Belgium

### Abstract

In the run of mine ("ROM") autogenous and semi-autogenous milling process, the influence of a single parameter cannot be determined easily as variations in the size analysis, shape, competence, crushability and grindability of the feed are unavoidable. Magotteaux wished to undertake a project to develop Products for use in this process. The project required the mobile pilot plant be situated adjacent to a gold plant. Our research and development activities were mainly focused on two aspects:

- conducting of ore characterisation test;
- conducting of pilot plant test.

The pilot plant testwork allowed to increase the understanding of the ore grinding and to highlight the main problems and their relative influence on the grinding efficiency. The purpose of this paper is to give an overview of some obtained results:

- effect of the addition of grinding media;
- effect of the pebble ports.

*Keywords: pilot plant, run of mine, milling process, grinding efficiency*

### Introduction

For over 40 years, MAGOTTEAUX has specialised in the industrial grinding process, in both dry and wet environment.

This specialisation enables the company to reach 3 objectives:

- search for the highest quality level;
- development of solutions which meet the customer's specific requirements;
- innovative approach.

Specialization means constant research, either in laboratory or at industry level. Through the integral comminution approach and in order to respond to a demand from the mining industry regarding the possibility of conducting tests with various types of ores at concentrator site, Magotteaux built a mobile laboratory grinding plant. This pilot plant enables Magotteaux to constantly research the grinding parameters. The purpose of this report is to set out some results of the pilot plant test work in the run of mine autogenous and semi-autogenous milling process.

### Pilot plant description

The mobile pilot plant consists of a steel main frame in two parts (the pilot plant itself), a separate control room, a separate workshop and a separate laboratory.

Different mill shells (rod/ball mills, run-of-mine mill) due to a unique drive system can be erected. The overflow or grate discharge configuration can easily be installed and tested. The mill is powered by a variable speed motor and can run at various speeds, ranging from 55% to 110% of the critical speed.

The pilot plant can also be characterised by:

- a multiple feeding system:
  - bin and weigh-feeder for particles smaller than 60 mm,
  - bin and weigh-feeder for pebbles (60 mm to 175 mm);
- variable speed pumps.

The mill can be operated either in open or in closed circuit with a cyclone.

A unique feature of the pilot plant is the high level of instrumentation:

- torquemeter: absorbed power or mill power drawn via a torquemeter installed on the drive shaft;
- load cell: mill mass via load cells under the mill supporting frame;
- weigh-feeder: ore feed rate is controlled by means of weigh-feeder;
- densitometer: slurry specific gravities via densitometers at various points of the circuit;
- magnetic flowmeter: water flow rate at any water inlet points is controlled by the combination of magnetic flowmeters and control valves;
- ultrasonic detector: for closed circuit test, pulp level is measured in the discharge sump by means of an ultrasonic detector.

A programmable logic controller (PLC) supervises the pilot plant operational functions. The intellution based software in the computer provides the main user interface and database functions. All signals are monitored on a continuous basis.

### General test procedure

#### *Ore collection*

During the ore collection, the operating conditions of the industrial mill are recorded. The material is hand sorted and screened. The dried size fractions are stored in big bags and loaded in the two bins according to the following sizes: – 175 mm + 60 mm and – 60 mm.

#### *Pilot plant tests*

The equilibrium is assumed to have been reached when mill power drawn and weight of slurry (therefore slurry hold-up and slurry density) have remained steady for at least three times the mill residence time. Samples are taken from the mill feed, mill discharge, underflow and overflow streams. Each sample is dried to obtain the percentage of solids by weight and screened to obtain the particles size distribution. At the end of each test, the entire mill content is dropped and sized from the top size to 38 $\mu$ m. Two methods will be used to determine the efficiency of the mill:

- the work operating index  $W_{io}$ :

$$W = 10 W_{io} \frac{\sqrt{F_{80}} - \sqrt{P_{80}}}{\sqrt{F_{80}} \cdot \sqrt{P_{80}}} \quad (1)$$

- the required energy to produce 1 t of particles passing on a given screen (75 $\mu$ m).

### Pilot plant testwork

#### *Effect of steel grinding media*

Run of mine (ROM) autogenous milling is a process in which the entire ore streams are fed directly to the grinding mill. The grinding media are generated within the mill from suitably size pieces of ROM ore itself. The grinding media size distribution in

the mill results mainly from the competence of the ore and from the feed size distribution. Pilot tests were conducted on a Gold ore and a Platinum ore to investigate the influence of steel grinding media on the grinding efficiency. As the process of reduction, which occurs in AG/SAG mills is a combination of attrition, abrasion and impacts, it has been an objective of our work to conduct ore characterisation tests in parallel with pilot tests.

The ore characterisation test consists of abrasion tests in a batch mill and single particle breakage tests such as drop weight tests and compression tests.

#### *Abrasion test*

The test materials are pebbles collected in the feed of the industrial mill. These pebbles are classified in a size range between 120 mm and 150 mm. A shape factor (min.diameter/max.diameter) is applied to select the pebbles.

The test material are loaded in a batch mill (1.3 diameter and 0.5 m long) equipped with a smooth lining. The quantity of pebbles is calculated to obtain a filling degree of 33%. The batch mill runs at 90% of critical speed in dry process.

The mill is stopped after 15 min, 45 min and 80 min. At each step, the material is discharged, the pebbles are sieved and the fraction bigger than 60 mm are put back into the mill. The result of the test gives the evolution of the cumulated residues on 60 mm in function of the grinding time (Figure 1).

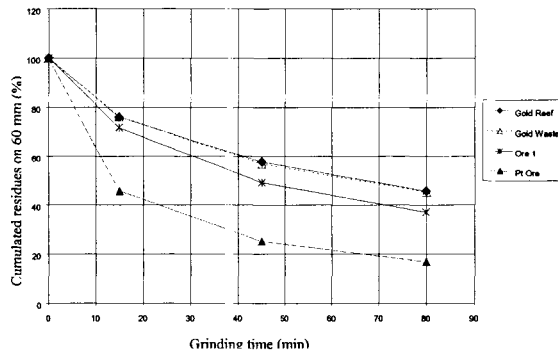


Figure 1: Obtained results on gold ore and platinum ore.

#### *Drop weight tests*

Pebbles in the mass range (4 kg to 6 kg) and a specific ratio (maximum diameter/minimum diameter) is dropped from a known height (3 m). Each pebble is dropped at least 50 times, and is weighed at the start of the test and again every 10 drops. The number of drops to obtain the 50% of the original weight is recorded (Figure 2).

#### *Compression tests*

The ground pebbles coming from the abrasion test and being bigger than 120 mm are collected and weighed. They are then broken by a 100 t press. The compressive strength is recorded when the failure occurs (Figure 3).

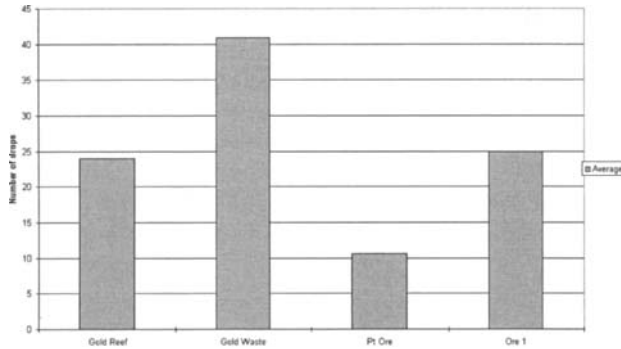


Figure 2: Obtained results on gold ore and platinum ore (drop test).

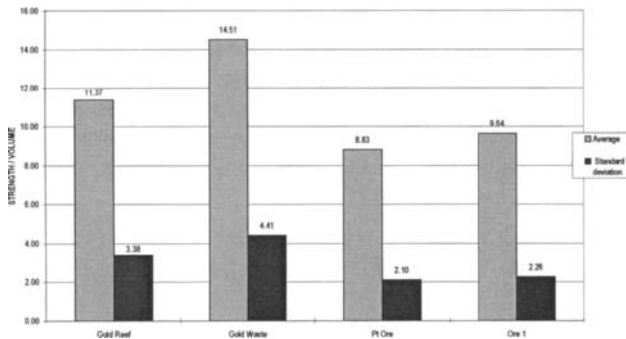


Figure 3: Obtained results on gold ore and platinum ore (compression test).

### Pilot test results

On the platinum (Pt) ore, three tests were conducted to study the influence of the quantity of steel grinding media on the grinding efficiency. On the gold ore, fully autogenous and semi autogenous grinding process are compared (Figure 4) (Table I). Based on the ore characterization, the platinum ore has a very high wear rate in the abrasion test and does not resist to the impact. This ore will not provide rocks grinding media. The feed size distribution is a flat curve and not really suited for ROM fully autogenous process. The tests conducted in the pilot plant show an improvement of  $\pm 11\%$  on the kWh/t  $< 75\mu\text{m}$  and  $\pm 3\%$  on the work-operating index. At the pilot scale, the addition of steel grinding media (10% to 20%) leads to an increase of 25% in the output which is the major improvement (Table II). The ROM feed consists of two different rock types namely Reef and Waste. Based on the ore characterisation, Reef is more subject on the chipping effect from collision with other particles. The mill performance will depend on the percentage of Waste in the feed.

At the pilot scale, the success of steel balls at reducing the amount of rock grinding media leads to an increase of 34% on the output and a coarser product.



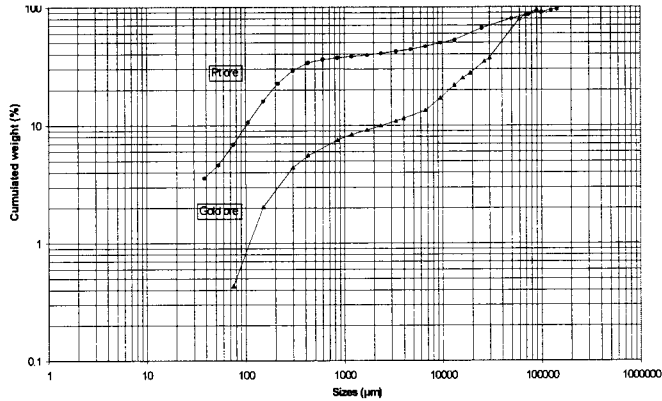


Figure 4: Feed size distribution.

Table I: Results (platinum ore).

Parameter	Filling degree of steel grinding media		
	10%	15%	20%
Feed rate (kg/h)	2,173	2,522	2,983
F <sub>80</sub> (µm)	50,000	50,000	50,000
Total filling degree (%)	24	30	30
Absolute power (kW)	18.07	22.06	24.74
Specific energy (kWh/t)	8.6	8.75	8.29
Product P <sub>80</sub> (µm)	171	168	173
% passing 75 µm	36.8	39.2	39.4
W <sub>io</sub>	11.94	12.03	11.59
kWh/t need for <75 µm	28.77	27.07	25.52
Circulating load	1.514	1.725	1.607

Table II: Results (gold ore).

Parameter	Fully autogenous	13% of steel balls
Feed rate (kg/h)	995	1,338
F <sub>80</sub> (µm)	60,600	61,000
Total filling degree (%)	43.3	33.1
Absolute power (kW)	22.13	25.88
Specific energy (kWh/t)	22.24	19.34
Product P <sub>80</sub> (µm)	105	134
% passing 75 µm	66.6	57.03
W <sub>io</sub>	23.78	23.49
kWh/t need for <75 µm	33.57	34.17
Circulating load	1.31	1.42

To go further in this research work, the influence of the grinding efficiency by decreasing the ball charge volume needs to be investigated.

### Effect of pebble ports

The industrial milling circuit consists of single stage ROM mills, which are controlled on maximum power. Each ROM mill is 4.9 m diameter  $\times$  10 m length and grind the ore to 70%  $<75 \mu\text{m}$ . Each mill is in closed circuit with a primary cyclone.

In the industrial mill, a build-up of pebbles occurs in the 25–50 mm size-fraction. These rocks occupy a volume at about 35% of the load volume.

It was requested to conduct a feasibility study in the pilot plant to quantify the increase on the production, which can be reached and to highlight the requested modifications in the industrial grinding circuit.

One of the industrial mills was equipped with pebble ports without any recirculation of a crushed product. The increase on the output was about 15%.

Tests were conducted in the pilot plant. The pebble ports were designed according to the critical size fraction existing in the mill.

The product coming from the oversize was crushed at a ratio of 1/5 and recirculated in the mill as indicated on the Figure 5.

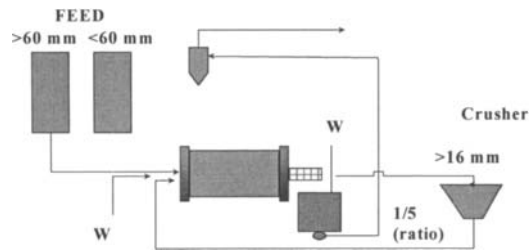


Figure 5: Flow sheet.

Table III: Results.

Parameter	N° pebbles ports	With pebbles ports and crushed product recycled
Feed rate (kg/h)	991	1,084
$F_{80}$ ( $\mu\text{m}$ )	82,000	82,000
Total filling degree (%)	43	39
Absolute power (kW)	21.61	21.25
Specific energy (kWh/t)	21.81	19.6
Product $P_{80}$	115	92
% passing $75 \mu\text{m}$	72.87	64.39
$W_{80}$	21.4	20.83
kWh/t need for $<75 \mu\text{m}$	31.91	32.75
Circulating load	1.336	1.457

At the pilot plant scale, without any recirculation, the increase in the output is estimated at about 13%, which corresponds well with the 15% in the industrial mill (Table III). By recirculating the crushed product using pebble ports, an increase of 9% on the output was obtained at equivalent power. The final product was a little bit coarser on the  $75 \mu\text{m}$  and the circulating load increased marginally (Table III). This

means that only minor modifications on the circuit need to be done. The parameters and operating conditions of the cyclone must be investigated first.

### **Conclusions**

The pilot plant test work conducted in parallel with the ore characterisation gives reliable results by predicting the optimum milling process on different type of ore.

#### *Platinum ore*

Based on the ore characterisation (abrasion, drop and compression tests) this ore is not competent and will not provide rocks grinding media. The feed size distribution is not really suited for ROM fully autogenous process.

The tests conducted in the pilot plant give that the addition of steel grinding media leads to an increase of 25% in the output.

#### *Gold ore*

Based on the ore characterisation, Reef and Waste are really competent and Reef ore is more subject on the chipping effect. The mill performance will depend on the percentage of waste in the feed.

At the pilot scale, the addition of grinding media leads to an increase of 34% in the output and a coarser product. The tests conducted with pebble ports and recirculating of crushed product give an increase of 9% in the output. The parameters and operating conditions of the cyclone need to be investigated.

## THE EFFECT OF VISCOSITY ON SMALL-DIAMETER HYDROCYCLONES' PERFORMANCE IN DESLIMING PROCESS

M.V. Possa\*, J.R.B. Lima<sup>o</sup>

\* Centro de Tecnologia Mineral, CETEM/CNPq, Departamento de Tratamento de Minérios, Rua 4, Quadra D, Ilha do Fundão, 21941-590, Rio de Janeiro, RJ, Brasil

<sup>o</sup>Universidade de São Paulo, EPUSP, Departamento de Engenharia de Minas Av. Prof. Mello Moraes, 2324, Cidade Universitária, 05508-900, São Paulo, SP, Brasil

### Abstract

In recent years, the use of small diameter hydrocyclones, with internal diameters less than 75 mm, is growing in mineral processing for fine particle classification. These hydrocyclones are being used for recovery of kaolin and diatomaceous clay, for desliming of ores, water recovery and processing of old tailing deposits to respect environmental polices. Also, in the chemical and food-processing industries they are used for remission of particles from effluents, starch refinement and recovery of organic crystals.

An important property of slurry flowing is its resistance to shear, or its viscosity. This property is present in many mineral processing systems, but its influence is rarely incorporated into models, analyses or optimisation processes.

This work present a study carried out on slurry phosphate ore from the feed of a desliming circuit, 80% passing the 20  $\mu\text{m}$  size. Tests were conducted adopting two different small-diameter hydrocyclones (25.4 and 50.8 mm internal diameters). The feed pressures ranged from 25+65 psi. The slurry viscosity appeared naturally as 15.25% and 35% solid in weight, and the last one (35% w/w) was changed by a chemical reagent to low and intermediate viscosity.

The usual measurements were made on feed slurry viscosity using a rheometer. Flow rates of the products, inlet feed pressures, solids contents and size distributions of the products were measured using a laser diffraction analyser.

The flow rates were mass balanced by a computer program, and the water was split;  $d_{50c}$  and efficiency parameter,  $\alpha$  (sharpness of separation), were calculated using Whiten equation.

The results have shown that the slurry viscosity influenced the hydrocyclone performance: when the viscosity increases with the solid content, the  $d_{50c}$  increases too; when the viscosity is decreased by a dispersing agent, at high solid content, the  $d_{50c}$  decreases too (thus it is possible to work with slurry at high solid content and to get a  $d_{50c}$  as small as that for low solid content); viscosity had a negligible effect on efficiency parameter,  $\alpha$  (sharpness of the separation), of the reduced partition curves as is observed for larger hydrocyclones; fish hook phenomenon was present in natural and dispersed slurries.

*Keywords: small-diameter hydrocyclone, partition curve, rheology, viscosity, desliming process*

### Introduction

In recent years, there are visible new tendencies in mineral processing. The decrease in the size of particles processed is one of these. It is due to the necessity of grinding at fine sizes for mineral liberation of ores coming from hot and humid countries, where normally there are large amounts of fine mineral particles; and to the necessity of processing old tailing deposits to respect environmental polices.

By decreasing the size of the particles, their behaviour in the fluid (water) deviates from the large ones. This stems from the increase in the participation of the other actions in the balance of forces upon a particle. These forces are mainly those related to the electrical state of the surface of the particle and those connected with the discontinuity of the medium (Sztaba, 1994).

According to Bakshi and Kawatra (1996), establishing relationships between slurry viscosity and process performances has been the aim of many researchers for several years. But these studies have focused on slurries with low solid content and the rheology of most of these slurries show Newtonian-flow properties.

If the solid content increase, mainly in slurry with fine mineral particles, the slurry can deviate from Newtonian behaviour and can be dilatant, pseudoplastic, Bingham plastic and pseudoplastic, and yield-stress behavior can take place.

The solid content is not the only variable that affects the slurry rheology; temperature, size distribution, shape of the particles, and chemical environment of the slurry can also affect the rheology behaviour. The small-diameter hydrocyclones, with an internal diameter less than 75 mm (Lima, 1997), were developed for fine particle classification in the 1950's, but it has been necessary to improve their efficiency (Vallebuona et al., 1995). Most of the classical studies of hydrocyclones have been performed on those with diameters larger than 100 mm (Kelsall, 1952; Bradley and Pulling, 1959; Fahlstrom, 1963; Lynch and Rao, 1975; Plitt, 1976).

The purpose of this work is to present a contribution to small-diameter hydrocyclone studies. The present work was carried out on slurry of a phosphate ore with around 80% solid particles passing the 20  $\mu\text{m}$  size. It was carried out in two small-diameter hydrocyclones (50.8 and 25.4 mm) taking into account the effect of slurry viscosity on cycloning by changing:

- the solid content (15%, 25% and 35% w/w);
- the chemical environment after adding a dispersing agent with high solid content of slurry (35% w/w).

The performances of each test were measured by the effects on  $d_{50c}$  and on the efficiency parameter,  $\alpha$  (sharpness of separation), of Whiten equation.

Table I: Size distribution for the feed of the desliming circuit.

Size ( $\mu\text{m}$ )	% wt passing
35.56	93.54
19.31	83.92
10.48	74.14
5.69	64.84
3.09	56.53
1.68	49.35
0.91	43.12
0.49	32.52

## Methods and materials

### *The sample*

The sample used was a phosphate ore (density = 3.43 t/m<sup>3</sup>) from the feed of the desliming circuit of Fertilizantes SERRANA S.A. - Complexo Industrial Arafertil,

Araxá, Brazil. The size distribution, which was measured using a Malvern Mastersizer Microplus, laser-diffraction instrument, is shown in Table I.

The main mineral contents in the sample ore are apatite (17%), gorceixite (secondary phosphate) (16%), goethite (43%), quartz (4%), mica vermiculite (6%) and barite (8%).

The apparent viscosities and the rheological studies were carried out in a Haake, model RS 100 rheometer at 30 °C temperature, with shear rate up to 1,500 1/s, under the following five different slurry conditions:

- 15% w/w natural with low viscosity;
- 25% w/w natural with intermediate viscosity;
- 35% w/w natural with high viscosity;
- 35% w/w dispersed with Poly Sal A-BASF (946 g/t phosphate) up to intermediate viscosity;
- 35% w/w dispersed with Poly Sal A-BASF (2,610 g/t phosphate) up to low viscosity.

The results are shown in Figure 1.

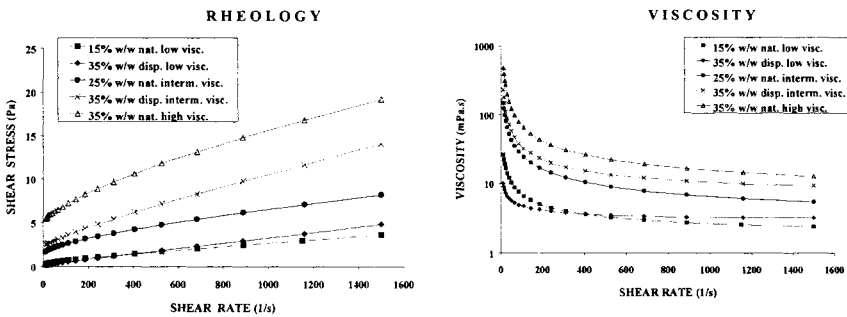


Figure 1: Apparent viscosities and rheological studies of slurries.

All five slurries have shown pseudoplastic behaviour. The 35% w/w slurry, dispersed up to a low viscosity and at a high shear rate (more than 400 1/s), presented practically constant apparent viscosity.

#### Experimental tests

The tests (thirty-five altogether) were conducted on a hydrocyclone test rig, which consisted of a 60 l sump, a slurry pump, a pressure gauge (up to 100 psi), a by-pass gauge and two Krebs hydrocyclones. The usual measurements were: flow rate of the products; inlet pressure; solid content of feed and products; and size distribution of overflow and underflow products, measured by the Malvern Mastersizer Microplus.

The test conditions for five different samples are shown in Table II:

Table II: Test conditions.

% w/w	Viscosity	Pressure (psi)	Hydrocyclone
15	low	25, 35, 45	50.8 mm diameter; 12.70 mm vortex finder
25	intermediate	25, 35, 45	14.33 mm inlet diameter equivalent 9.52 apex diameter
35	high	25, 35, 45, 65	25.4 mm diameter; 9.52 mm vortex finder 6.21 inlet diameter equivalent 9.52 apex diameter

The results are available on the basis of real, corrected and reduced partition curves, water split ( $R_f$ ), corrected cut point ( $d_{50c}$ ), and efficiency parameter,  $\alpha$  (sharpness of the separation), for reduced partition curves, for each one of the five different slurries and for all thirty five tests.

After obtaining the real partition curves, parameters  $R_f$ ,  $\alpha$  and  $d_{50c}$  were calculated using a non-linear regression fitted by a mathematical computer program from Whiten equation for reduced efficiency curves (Napier-Munn et al., 1996):

$$Y_i = R_f + (1 - R_f) \frac{e^{(\alpha x)} - 1}{e^{(\alpha x)} + e^{(\alpha)} - 2} \quad (1)$$

$Y_i$  = percent of particles that report to the underflow;

$R_f$  = water split;

$x = d_i/d_{50c}$ ;

$\alpha$  = efficiency parameter (sharpness of the separation).

By taking  $R_f$  from equation 1, the calculated partition curves were determined by Kelsall's equation (Lima, 1997):

$$Y_{ci} = \frac{Y_i - R_f}{1 - R_f} \quad (2)$$

$Y_{ci}$  = percent of particles that reports to the underflow (calculated partition).

For each one of the tests, the reduced partition curves for the experimental values were determined from  $d_{50c}$  and  $Y_{ci}$ , which were calculated by equations 1 and 2.

## Results and discussion

All flow rates were previously mass balanced by the MATBAL computer program (Laguiton, 1984).

### Water split $R_f$

The correlation curve of the experimental values and the values for  $R_f$ , calculated by equation 1, are shown in Figure 2. It can be remarked that correlation between calculated and experimental values is good, but all calculated values are higher than the experimental ones. This shows a systematic error: Either equation 1 is not good for calculating  $R_f$ , or the assumption that the experimental  $R_f$  equals the ratio of water underflow by water feed is not true.

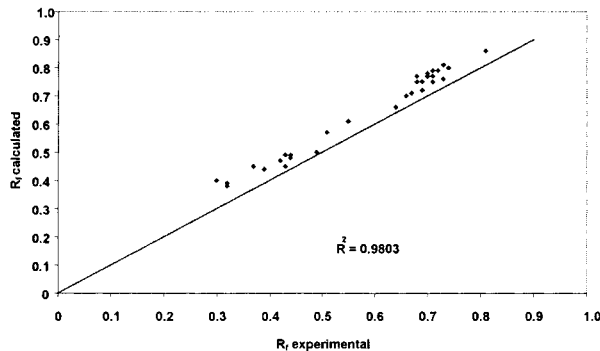


Figure 2: Experimental and calculated  $R_f$  results;  $R^2$  coming from equation 1.

*Corrected cut point  $d_{50c}$  and parameter  $\alpha$*

The effects of viscosity on  $d_{50c}$  for both small-diameter hydrocyclones are shown in Figure 3. It can be seen that as solid content increases in natural slurries  $d_{50c}$  increases too. The viscosity effect on cycloning was also observed by adding the dispersing agent in the slurries. When the slurry at high solid contents (35% w/w) is dispersed up to intermediate and low viscosity, the  $d_{50c}$  decreases. Particularly for low viscosity, the  $d_{50c}$  is as small as at low solid contents (15% w/w).

Table III shows the efficiency parameters,  $\alpha$ , calculated by equation 1 for the five slurries, and, in Figure 4, parameter  $\alpha$  for all thirty-five tests.

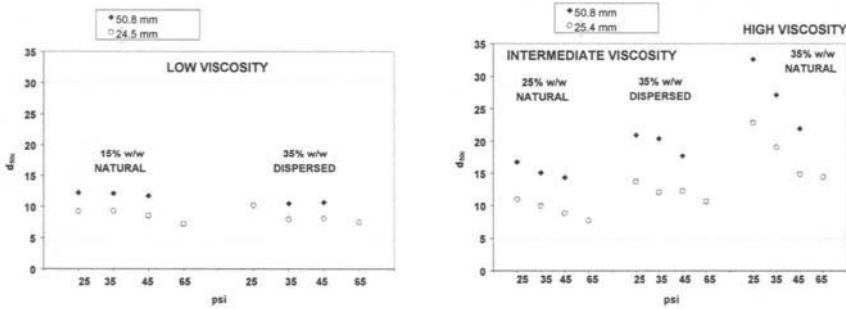


Figure 3:  $d_{50c}$  for different pressures and different slurry viscosities.

Table III: Efficiency parameter  $\alpha$  for the five slurries.

Slurry	Viscosity	$\alpha$	$R^2$
15% w/w natural	low	2.17	0.9862
35% w/w dispersed	low	2.66	0.9726
25% w/w natural	intermediate	2.07	0.9721
35% w/w dispersed	intermediate	2.62	0.9687
35% w/w natural	high	2.55	0.9810

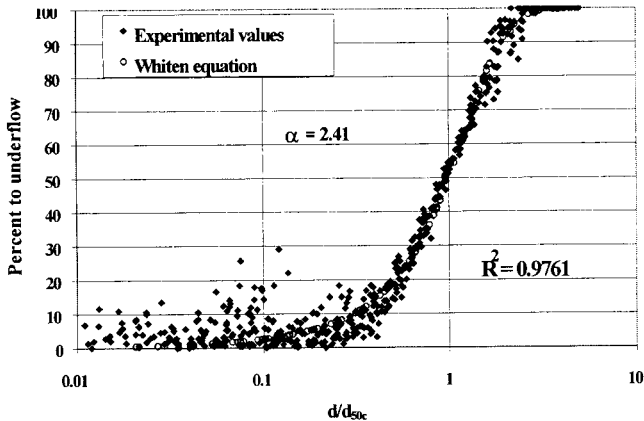


Figure 4: The efficiency parameter  $\alpha$  for all thirty-five tests after partition curve reduction.



The results have shown that the effect of viscosity on the sharpness of separation in reduced partition curves can be considered negligible.

A fishhook for the very fine particles can also be noticed. This phenomenon was observed in all five different slurries. It is difficult to describe the mechanisms for the fishhook. An explanation usually accepted is that before the size distribution analysis (Sedigraph, Malvern, micro-sieves devices) the samples are dispersed, and the very fine particles are detected. But this explanation may be rejected in the present study, because two different slurries were dispersed during the experimental tests, and the fishhook phenomenon was already present. For the same reason, it is unlikely that the shear flocculation event can explain this fact.

Other reason may be that the density difference between the minerals and the internal recycling of the very fine particles, increasing the probability of reporting the apex.

The best explanation is presented by Finch (1983), and del Villar and Finch (1992), who pointed out two mechanisms to account the fishhook. One is the entrainment of the fine particles in the water below a certain size. The particles move less relative to the water. Another reason would be a selective short-circuiting of the underflow, where part of the inner core of slurry is entrained at through the apex. For these reasons, the authors suggested that the water split must be a function of particle size.

## Conclusions

The following conclusions were drawn from this study for small-diameter hydrocyclones:

- fishhook phenomenon was present in natural and dispersed slurries;
- viscosity and rheology of the slurry had a major role in  $d_{50c}$ ;
- when the viscosity increases with the solid content, the  $d_{50c}$  increases too;
- when the viscosity is decreased by a dispersing agent, at high solid content, the  $d_{50c}$  decreases too: thus it is possible to work with slurry at high solid content and to get a  $d_{50c}$  as small as that for low solid content;
- viscosity had a negligible effect on efficiency parameter,  $\alpha$  (sharpness of the separation), of the reduced partition curves as is observed for larger hydrocyclones.

## Acknowledgements

The authors are grateful to CNPq for financial support of this study and to the Fertilizantes Serrana S.A. - Complexo Industrial Arafertil for the sample. They also wish to express gratitude to Prof. Dr. Luis Marcelo Tavares and Leonardo Leite Garcia (Metallurgical Engineering Department of UFRJ) for useful suggestions, to Prof. Dr. Giulio Massarani and Chem. Eng. Marcos Roberto Halasz (Chemical Engineering Department of Coppe/UFRJ) for the Malvern analysis, and to Chem. Eng. Edimir Martins Brandão from Cenpes/Diplot/Setep-Petrobras for the rheological analysis.

## References

- Bakshi, A.K., and Kawatra, S.K., 1996. Rapid determination of non-Newtonian flow behaviour in mineral suspensions. *Minerals and Metallurgical Processing*, 13(4), 165-9.
- Bradley, D. and Pulling, D.J., 1959. Flow patterns in the hydraulic cyclone and their interpretation in terms of performance. *Transaction of the Institution of Chemical Engineers*, 37, 34-45.

- Del Villar, R. and Finch, J. A., 1992. Modelling the cyclone performance with a size dependent entrainment factor. *Minerals Engineering*, 5 (6), 661-9.
- Fahlstrom, P.H., 1963. Studies of hydrocyclone as a classifier. In: 6<sup>th</sup> International Mineral Processing Congress. France, 87-114.
- Finch, J.A., 1983. Modelling a fish-hook in hydrocyclone selectivity curves. *Powder Technology*, 36, 127-9.
- Kelsall, D.F., 1952. A study of the motion of the solid particles in a hydraulic cyclone. *Transaction of the Institution of the Chemical Engineers*, 30 (2), 84-108.
- Laguitton, D., 1984. MATBAL - Computer program for material balance data adjustment. In: *The SPOC Manual*, CANMET, Chapter 3.2, 61 p.
- Lima, J.R.B., 1997. Estudo da modelagem matemática da microciclonação, Tese de Livre Docência, Escola Politécnica da Universidade de São Paulo, EPUSP, Brasil, 162 p.
- Lynch, A.J. and Rao, T.C., 1975. Modelling and scale-up of hydrocyclone classifiers. In: XI International Mineral Processing Congress, Paper 9. Cagliari, Italy.
- Napier-Munn, T.J., Morrell, S., Morrisson, R.D. and Kojovic, T., 1996. Screens and hydrocyclones. In: *Mineral Comminution Circuits Their Operation and Optimisation*. JK/MRC, Chapter 12, 273-330.
- Plitt, L.R., 1976. A mathematical model of the hydrocyclone classifier. *CIM Bulletin*, 114-23.
- Sztaba, K., 1994. The problems of flow classification of very fine grained materials. In: IV Southern Hemisphere Meeting on Mineral Technology, Chile, 135-45.
- Vallebuona, G., Casali, A., and Bevilacqua, P., 1995. Small-diameter hydrocyclones: performance prediction by empirical models. *Minerals and Metallurgical Processing*, 12 (4), 184-8.

## DRUM GRANULATION OF MINERAL RAW MATERIALS WITH DIFFERENT PARTICLE SIZE DISTRIBUTIONS

T. Gluba, A. Obraniak

Faculty of Process and Environmental Engineering; Technical University of Lodz,  
Lodz, Poland

### Abstract

Results of an investigation of drum granulation of dolomite flour of selected grain-size composition, which guaranteed geometrical similarity at different degrees of bed-wetting, are discussed. Taking into account changes in granule porosity, the dependence of agglomerate growth rate in particular raw materials on the liquid saturation degree in the agglomerates was shown. It was found that a necessary condition to initiate the process of agglomerate growth was to reach some required degree of saturation of the liquid in the  $S_{gl}$  granules. After achieving the second boundary value of saturation degree in the  $S_{gl}$  granules, an abrupt growth of agglomerates was observed. It was reported that the values  $S_{gl}$  and  $S_{gl}$  depended on the mean particle size of raw material.

*Keywords: agglomeration, granulation, size distributions, porosity, saturation*

### Introduction

For the majority of fine granular materials, a possibility to form agglomerates depends on adding an appropriate amount of wetting or bonding liquid. During the flow of a wetted bed, there is an interaction between solid particles, droplets of the wetting liquid and air. The size and type of forces acting on material particles depend strictly on the properties of the media participating in the process and on the mutual quantitative interrelations between the solid body and wetting or bonding liquid. The effect of the quantity and properties of wetting liquid on the mechanisms of agglomerate growth and properties was studied by many researchers: Kapur and Fuerstenau (1969), Sastry and Fuerstenau (1973), Gluba et al. (1990), Horvath et al. (1987) Iveson and Litster (1998). These studies, carried out for various solid-wetting liquid systems, confirmed a significant impact of the amount and properties of the liquid on the growth kinetics of agglomerates and their mechanical properties. Another parameter affecting the growth mechanisms, and consequently the properties of the granulated product, is the grain-size composition of the raw material. Forces binding individual grains depend on the grain-to-grain distance in a given system, which in turn depends also on the grain-size composition of the material being granulated. There are a few studies on this subject, and they refer to specific systems. The investigations on the impact of grain-size composition of quartz sand during disk granulation were presented by Horvath et al. (1989). They showed the effect of the mean and the standard deviation of particle-size of a raw material on the properties of the granulated product. The effect of grain-size composition was also described by Linkson et al. (1973), who studied granulation of quartz sand with a narrow and broad

range of grain-size composition, and by Iveson and Litster (1998) during the granulation of glass balls of different sizes.

Due to the variety of applied materials and methods, a comparison of the results of these studies is rather difficult. Further research is required to extend the knowledge on the above-mentioned problems, so it was justified to undertake this study.

## Experimental

### Materials

The raw material to be tested was prepared from four sizes of dolomite flour fractions, with grain sizes ranging from 0 to 15  $\mu\text{m}$ , 0 to 60  $\mu\text{m}$ , 0 to 100  $\mu\text{m}$ , and 0 to 250  $\mu\text{m}$ . The grain size composition of each fraction was determined by a laser particle size analyser Analysette 22.

The particle size distribution was described by statistical moments:

- the ordinary moment of the first order

$$m_1 = \sum_{i=1}^n d_i x_i \quad (1)$$

- the central moment of the second order (variance)

$$m_2 = \sigma^2 = \sum_{i=1}^n (d_i - m_1)^2 x_i \quad (2)$$

where:  $d_i$  = mean diameter of class  $i$ , and  $x_i$  = mass fraction of class  $i$ .

On the basis of central moments of the 2nd to 4th order,

- the concentration coefficient

$$K_1 = \frac{m_4}{m_2^2} \quad (3)$$

- and the asymmetry coefficient

$$K_2 = \frac{m_3}{(m_2)^{3/2}} \quad (4)$$

were determined.

On the basis of data obtained from the laser analyzer, the grain-size compositions of raw material for granulation were calculated numerically, assuming a geometrical similarity of these compositions.

Two parameters:  $\sigma/m_1 = 1.07$  and  $K_2 = 2.30$  were assumed constant for different values of the mean diameter  $m_1$ , ranging from 10.6  $\mu\text{m}$  to 28  $\mu\text{m}$ .

Grain-size compositions of mixtures obtained (denoted by symbols  $M_1$  to  $M_5$ ), which are raw materials for the granulation process, are shown in Figure 1. Such a selection of grain-size compositions enables a preliminary evaluation of the impact of mean particle diameter on the granulation process (specific surface area should be measured in order to obtain a more representative evaluation). For each raw material, basic physical properties, such as specific and bulk density, and porosity of each material, were determined. For bulk density, two values were determined each time: for loose material and for material condensed to its minimum volume on a riddle.

Figure 2-a, -b shows changes in bulk density and porosity of raw materials as a function of the mean diameter of the constituting particles.

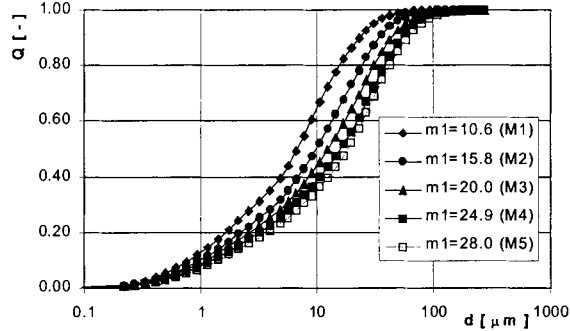


Figure 1: Comparison of particle size distributions of raw materials

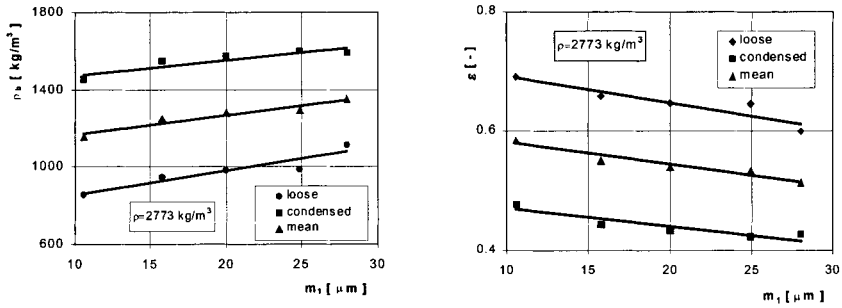


Figure 2-a, -b: Dependence of bulk density and bed porosity on mean particle diameter of raw material.

*Choice of process parameters and methods*

For each raw material, the range of changes of feed moisture content guaranteeing correct granulation was selected. Figure 3 shows values of the bed saturation degree, given as a ratio of the wetting liquid volume to the volume of inter-particle space in reference to loose material, condensed material and mean value.

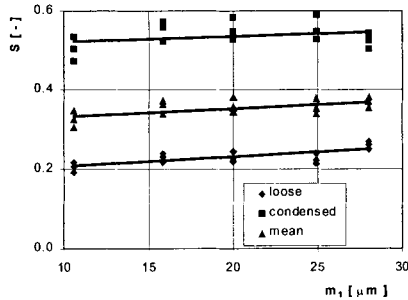


Figure 3: Saturation degree of the feed during investigations.

With an increase in mean particle diameter, the required saturation degree increases. The process of granulation was carried out batch-wise in a drum granulator 0.5 m in volume and 0.4 m long, at a rotational speed of  $0.33 \text{ s}^{-1}$  and constant drum filling,

with the feed  $\varphi = 0.1$ . The feed volume was determined on the basis of the mean bulk density of particular raw materials. On the bed of raw material tumbling in the drum, a wetting liquid (distilled water) was sprayed by two pneumatic nozzles located along the drum and operating at steady feed parameters:

- water-flow rate  $Q_w = 12 \cdot 10^{-6} \text{ m}^3/\text{h}$ ;
- air-flow rate  $Q_a = 2,5 \cdot 10^{-3} \text{ m}^3/\text{h}$ ;
- air pressure  $p_a = 3 \cdot 10^5 \text{ Pa}$ .

After completing the wetting, the process of granulation was continued until the moment when granulated product started sticking to the drum walls, thus preventing any further processing. In determined time intervals, samples representative of the whole feed were taken. On this basis, properties of the product obtained were specified. The first sample was taken immediately after completing the wetting ( $t = 0$ ), while the last one was taken at the end of the process.

### Results

An example of the change in mean diameter  $m_{lg}$  and parameter  $\sigma_g/m_{lg}$  characterizing the range of grain-size composition of granulated product during the process is shown in Figure 4.

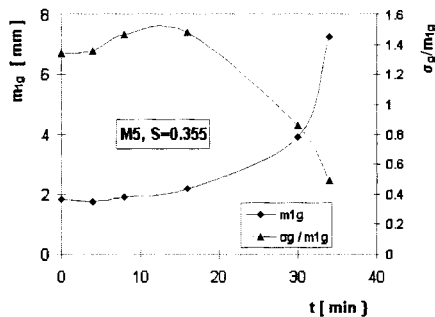


Figure 4: Change of  $m_{lg}$  and  $\sigma_g/m_{lg}$  during granulation.

With an increase in granulation time the mean particle diameter of the raw material increases, and the value of  $\sigma_g/m_{lg}$  decreases, which means that the product is characterized by a decreasing scatter of sizes close to the medium value.

A parameter that determines suitability of a given raw material for granulation and for the process itself is the amount of wetting liquid added, which was characterized by the feed's mean saturation degree,  $S$ . An increase in the saturation degree for each tested raw material leads to a faster run of the process and, most frequently, to a coarser product.

Figure 5-a, -b shows examples of the dependence of changes in mean particle diameters over time, and the growth rate of mean diameter per 1 revolution of the drum, for three values of saturation degree  $S$ .

Changes, taking place in the granulated bed during the process, are confirmed also by the bulk density of the product obtained. Figure 6 shows the dependence of the bulk density of the dried granulated product on the process duration, and compares this with the values of bulk density of the raw material, i.e. loose and condensed material.

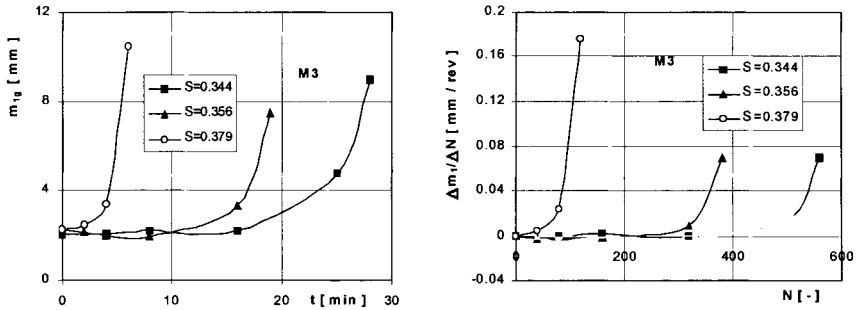


Figure 5-a, -b: Effect of feed saturation on the growth and on the rate of growth of mean particle diameter of the granulated product.

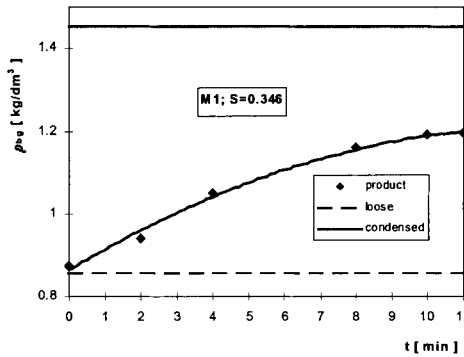


Figure 6: Changes in bulk density of granulated product over time.

For all types of raw material, the bulk density of granulated product increases with granulation time, however in no case does it reach the value obtained for a condensed raw material. The bulk density of granulated product depends both on bed porosity  $\epsilon_b$  and on the porosity of granules  $\epsilon_g$  forming the bed. Total porosity of granulated feed  $\epsilon_t$  can therefore be determined by the relation:

$$\epsilon_t = \epsilon_b \cdot \epsilon_g \tag{5}$$

Bed porosity  $\epsilon_b$  depends on the density of granule packing and is the function of particle size composition of the product, while granule porosity  $\epsilon_g$  depends on packing density of material grains in agglomerates and is the function of particle size distribution of raw material and process conditions.

Figure 7-a shows a change in the inner porosity of granules during the process, at different values of mean feed saturation  $S$ .

Packing of grains in the agglomerates results in a decrease of inter-particle space, which leads in turn to an increase in the degree of liquid saturation in the  $S_g$  granules. Taking into account liquid content and granule porosity, a change in the liquid saturation in agglomerates  $S_g$  during granulation was determined.

An example of the diagram presenting this dependence for various feed saturation degrees ( $S$ ) is shown in Figure 7-b.

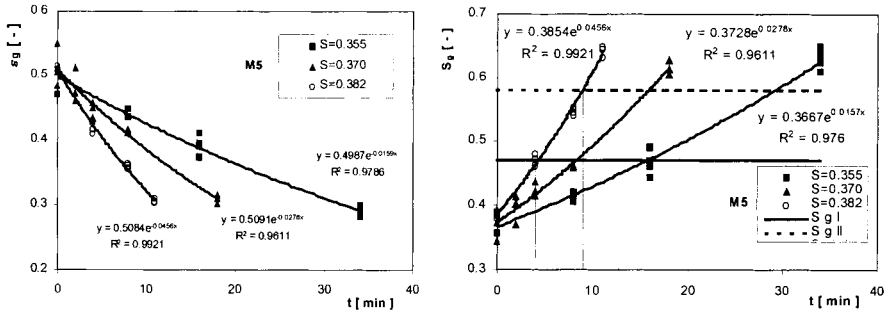


Figure 7-a, -b: Change of granule porosity and liquid saturation degree in the granules during granulation.

To describe the above interrelation, an exponential function was used. The function enables approximation of the obtained results with high accuracy:

$$S_g = A \cdot e^{Bt} \quad (6)$$

When analyzing the functions obtained for a particular granulation processes, it was found that the value  $A$  was in each case close to the mean feed saturation  $S$ , so equation (6) could be written in the form:

$$S_g = S \cdot e^{Bt} \quad (7)$$

Coefficient  $B$  was dependent on feed saturation  $S$  and on the mean particle diameter of the raw material, described by moment  $m_1$ . As a result of power regression, the following equation was obtained:

$$B = 10^{-3} \cdot S^{13.8} \cdot m_1^{-1.7} \quad (8)$$

where correlation coefficient  $R = 0.975$ .

The values of exponents in this equation show that an increase in the amount of wetting liquid added ( $S$ ) has a strong impact on the increase in liquid saturation in granules. A smaller and inversely proportional effect is revealed by the size of raw material particles.

#### Discussion: a model of agglomerate growth

On the basis of an analysis of the curves for saturation growth in granules and their comparison with relationships defining the increase in mean particle diameter of the granulated material over time, or the growth rate of this diameter, it was found that a condition necessary to initiate the process of agglomerate growth was, for a given raw material, to reach some degree of required saturation of the liquid in  $S_{gI}$  granules. The straight line  $S_g = S_{gI}$  intersects curves  $S_g = f(t)$  (Figure 7-b) for particular values of  $S$ , in points whose abscissa determine the process duration needed to start the agglomerate growth. After passing this boundary value, a systematic, initially non-rapid increase in agglomerate size occurs, and along with it, further condensation of particles in the granules takes place, causing an increase in saturation degree  $S_g$ . After achieving the second boundary value of saturation degree in  $S_{gII}$  granules, an abrupt growth of agglomerates is observed, and in a short time water pressed out causes the granules to start clinging to the drum walls, thus preventing any further processing. The straight line  $S_g = S_{gII}$  in the points of intersection with curves  $S_g = f(t)$ , define the duration of the granulation process in which an intensive growth of agglomerates



begins, for particular values of  $S$ . It was reported that values  $S_{gI}$  and  $S_{gII}$  were different for particular materials and appeared to be dependent on the mean particle diameter of the raw material. This relationship is shown in Figure 8.

It follows from this relationship that boundary values of liquid saturation in granules increase with an increase in the mean particle diameter of the material.

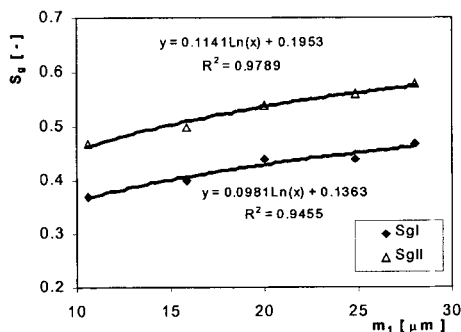


Figure 8: Dependence of the values  $S_{gI}$  and  $S_{gII}$  on the mean particle size of the raw material.

## Conclusions

The results obtained allow us to formulate a general model of growth of agglomerates from raw materials of different grain-size composition. After wetting, the bed consists of granulation nuclei of different sizes. These nuclei are systems of solid grains, liquid droplets and air particles. The porosity of the nuclei formed from individual raw materials is approximately equal to the mean porosity of the dry bed, and the saturation degree of liquid in the nuclei is approximately equal to the mean feed saturation  $S$ . Further processes of granulation depend on the feed saturation degree  $S$  and also on the mean particle diameter of the raw material. In the initial period, whose duration for a given raw material depends on feed saturation  $S$ , no significant changes in agglomerate size occur. The processes of growth (coalescence, build-up) and destruction of agglomerates (crushing, abrasion) occur simultaneously at a similar intensity, and bonding forces are still too weak to form solid agglomerates of a larger size. Due to collisions of particles during bed motion, a constant increase in particle packing in the granules and in the growth of saturation degree  $S_g$  takes place. After achieving the boundary value of saturation  $S_{gI}$  (0.37 to 0.47), the mechanisms of growth prevail, which lead to a systematic increase in agglomerate size. The growth rate increases slowly, with an increase in liquid saturation in the  $S_g$  granules. Because of a relatively slow increase in size during this period, it can be suspected that the most resistant agglomerates of thin layers formed as a result of the destruction of the weakest systems' build-up on the surface. After achieving a degree of saturation in the  $S_{gII}$  granules ranging from 0.48 to 0.58, an abrupt increase in agglomerate growth rate occurs. At this saturation degree, water pressed out from the inside appears on the granule surface. It enables an agglomeration of individual granules into larger clusters. In a parallel manner, further condensation of particles and the pressing of water occur, causing wet and flexible granules to begin adhering to the inner drum surface in a short time, thus preventing any further granulation.

The granulation tests revealed the significant impact of the grain-size composition of the raw material on the agglomerate's process of formation and growth. By choosing grain-size composition (instead of more effective specific surface area, but more difficult to determine) the process can be speedily controlled to some extent, in order to obtain a product of desired parameters and also to reduce costs of the process (shorter granulation time), product classification and drying (lower moisture content).

### Acknowledgments

The work was carried out under research project no. 3T09C 032 12, financed by the State Committee for Scientific Research for the years 1997-2000.

### References

- Gluba, T., Heim, A. and Kochanski, B., 1990. Application of the theory of moments in the estimation of powder granulation of different wettabilities. *Powder Handling and Processing*, 2, 323-326.
- Horvath, E., Pataki, K. and Ormos, Z., 1987. Study of rolling-bed granulation II. *Hung. J. Ind. Chem.*, 15, 121-131.
- Horvath, E., Pataki, K. and Ormos, Z., 1987. Study of rolling-bed granulation III. *Hung. J. Ind. Chem.*, 15, 133-140.
- Horvath, E., Pataki, K. and Ormos, Z., 1989. Study of rolling-bed granulation VII. *Hung. J. Ind. Chem.*, 17, 121-130.
- Iveson, S.M. and Litster, J.D., 1998. Fundamental studies of granule consolidation. Part 2: Quantifying the effects of particle and binder properties. *Powder Technol.*, 99, 243-250.
- Kapur, P.C. and Fuerstenau, D.W., 1969. A coalescence model for granulation. *I&EC Process Design and Development*, 8, 56-62.
- Linkson, P.B., Glastonbury, J. R. and Duffy, G.J., 1973. The mechanism of granule growth in wet pelletising. *Trans. Instn. Chem. Engrs.*, 51, 251-259.
- Sastry, K.V.S. and Fuerstenau, D.W., 1973. Mechanisms of Agglomerate Growth in Green Pelletization. *Powder Technology*, 7, 97-105.

### Symbols

A, B	coefficients
d	particle size of the raw material ( $\mu\text{m}$ )
$m_f$	mean particle size of the raw material, ( $\mu\text{m}$ )
$m_{fg}$	mean particle diameter of granulated product (mm)
N	number of drum revolutions
Q	volume sum distribution
S	degree of feed saturation
$S_g$	degree of liquid saturation in granules
t	granulation time (min)
$\epsilon_b$	granular bed porosity
$\epsilon_g$	granule porosity
$\phi$	drum filling
$\rho$	density of the raw material ( $\text{kg}/\text{m}^3$ )
$\rho_b$	bulk density of the raw material ( $\text{kg}/\text{m}^3$ )
$\rho_{bg}$	bulk density of granulated product ( $\text{kg}/\text{m}^3$ )

## STUDIES ON COMMINUTION MECHANISM OF THE DRY TOWER MILL KD-3

A. Shibayama<sup>\*</sup>, S. Mori<sup>°</sup>, A. Bissombolo<sup>°</sup>

<sup>\*</sup>Department of Recycle Plant Engineering, Kubota Cooperation  
2-35, Jinmucho, Yao, 581-8686, Japan

<sup>°</sup>Department of Earth Resources Engineering, Kyushu University  
6-10-1, Hakozaki, Higashi-ku, Fukuoka 812-8581, Japan

### Abstract

In order to obtain economically lot of fine particles, a dry tower mill KD-3, composed of a comminuting section, a classifying column and a collecting section, has been developed through this study. Grinding tests were carried out on limestone to clarify the comminution mechanism in the KD-3. A particular attention was paid to important factors such as the size of the grinding media (steel balls of  $\phi$  10 mm,  $\phi$  13 mm,  $\phi$  16 mm,  $\phi$  20 mm), the speed of the stirring screw (from  $1.08 \text{ s}^{-1}$  to  $1.58 \text{ s}^{-1}$ ) and the role of the net in the classifying column. The study has revealed an optimum efficiency for steel balls of  $\phi$  20 mm size and a stirring screw rotating at  $1.58 \text{ s}^{-1}$ . Besides, a series of nets settled in the classifying column have improved the efficiency of the classifying operation by reducing the buoyancy of the materials and regulating the maximum size of products collected in the cyclone ( $d_{\max}$  is about  $10 \mu\text{m}$ ). The air flow rate in the duct and the pressure of drops in the column were approximately quadratic curves, but the  $d_{\max}$  of products collected in the cyclone was proportional to the pressure of drops in the classifying column.

*Keywords: dry tower mill, comminution, grinding media, stirring screw, classifying column*

### Introduction

Some industrial mineral producers have extensively used the tower mill through the world as a new type of fine grinding pulverizer. However, few studies have been carried out on the mechanism and conditions to achieve a higher fine grinding performance with this tower mill. Recently, a series of modifications made in the structure of the cyclone and the classifying column have led to some new types of dry tower mill. The latest version of the tower mill (KD-3) gives a product whose maximum particle diameter is smaller than  $10 \mu\text{m}$  (Mori et al., 1997). The present work deals with the influence of the grinding media (steel balls) size and the speed of the stirring screw on the grinding efficiency, the role of the nets settled in the classifying column of the tower mill KD-3. Further development would permit to achieve a higher recovery of fine particles from the pulverized products.

### Experiment and method

The dry tower mill KD-3, illustrated in Figure 1, is a modified version of the commonly used laboratory tower mill. Its comminuting cell (A) is separated from the classifying column (B) to regulate the maximum size of particles in the products collected in the section (C). The inside diameter and length of the comminuting cell

are 0.26 m and 0.6 m respectively and the grinding media is made of steel balls (loading mass: 40.0 kg). Tests were carried out on 1.0 kg of limestone ore (density  $2.70 \cdot 10^3 \text{ kg/m}^3$ ), sizing from 420  $\mu\text{m}$  to 3.36 mm and provided by the Todaka Tsukumi Mine (Japan). The rate of the air circulating inside the tower mill, later referred as the duct air flow rate ( $U_d$ ), is measured through an orifice ⑧ settled inside the duct and the particles size distribution were performed on a sedimentation balance (Hara and Mori, 1995).

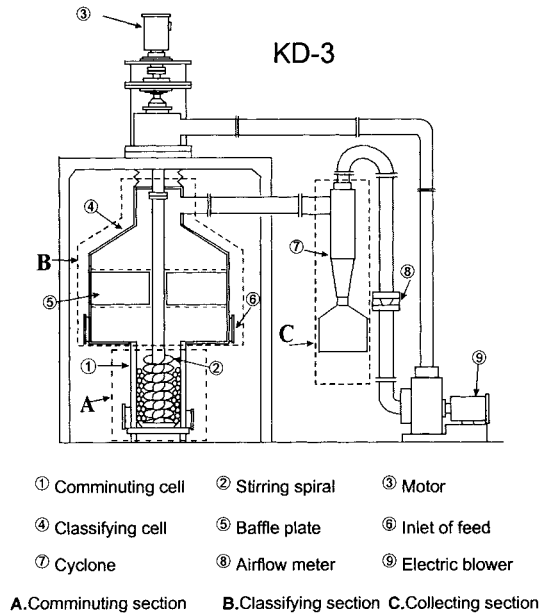


Figure 1: Schematic view of the tower mill KD-3.

The limestone is ground twice for 60 min and the fresh-formed particles are transported upwards to the classifying column ④ and the cyclone ⑦ by a circulating air flow generated inside the mill (by the blower ⑨ through the bottom of the comminuting cell ①).

A sudden increase in the diameter of the classifying column reduces the buoyancy of the materials and allows only fine particles to be collected while coarse particles settle at the bottom of the column. The cyclone C2 is provided with a central spiral ribbon (CSR) that is supposed to increase the centrifugal force of fine particles settling down the spirals.

The firstly investigated parameters were the size of the steel balls ( $\varphi = 10 \text{ mm}$ ,  $\varphi = 13 \text{ mm}$ ,  $\varphi = 16 \text{ mm}$ ,  $\varphi = 20 \text{ mm}$ ) and the speed of the stirring screw (from  $1.08 \text{ s}^{-1}$  to  $1.58 \text{ s}^{-1}$ ). Then, followed the role of the nets (S1, S2, and S3) and the type of columns (CLA0, CLA1, CLA2, and CLA3) used to reduce the air turbulence and improve the classifying efficiency. Table I gives the characteristics of sieves and Figure 2 illustrates different views of columns.

Table I: Kind of sieves using in column of KD-3: S1, S2, S3.

Types of nets	Opening (mm)	Diameter of line (mm)
S1	5.0	0.75
S2	3.5	1.00
S3	1.0	0.20

As seen, the column CLA0 does not have a net, but a baffle plate settled in the column. The CLA1 has two nets: one (S1) is settled downside and the other (S3) upside the baffle plate. In the case of CLA2, S3 is settled above S1 upside the baffle plate. Its diameter is half that of the column. As for CLA3, both S1 and S3 are now settled downside the baffle plate and S3 is the lower net. Upside the plate, S1, S2 and S3 are put in this order from the bottom to the top. Besides, the diameter of S2 is two third and that of S3 is one third of the diameter of the classifying column.

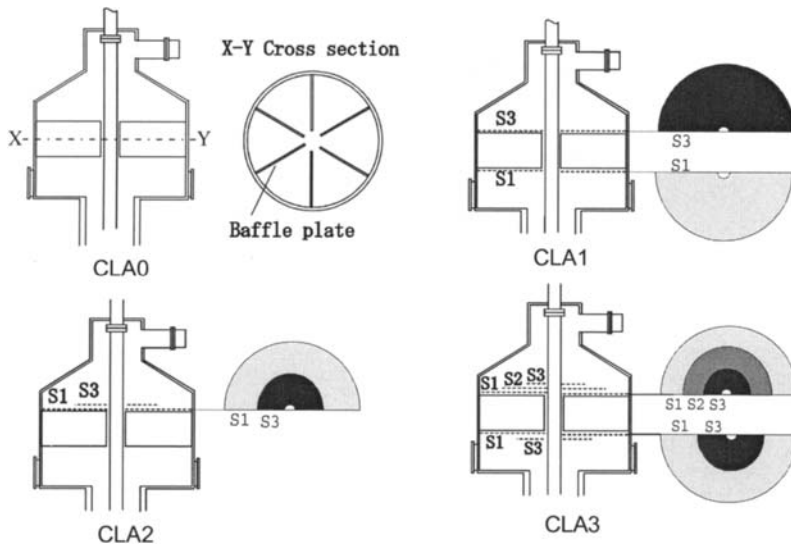


Figure 2: Schematic view of modified columns of KD-3.

## Results and analysis

### *Influence of the air flow rate*

Previous studies carried out on a laboratory tower mill in which the comminution and classification mechanisms occur in the same column have shown an increase in the  $d_{\max}$  value with the airflow rate. At duct airflow of 1.35 m/s for instance, the  $d_{\max}$  was high enough (about 70  $\mu\text{m}$ ). These studies suggested that a better classifying/collecting effect could help producing more fine particles. The following steps have been made with this purpose:

- enlarge the diameter of the classifying column;
- provide the classifying column with a series of nets to separate the classifying and collecting functions, stabilize the air turbulence and increase the process selectivity;

- insert into the cyclone a central spiral ribbon that would increase the centrifugal force of collected particles and improve, in the same way, the air-solid separation process.

These modifications have improved the efficiency of the Tower Mill KD-3: the  $d_{\max}$  value of particles in the cyclone products has dropped to 10  $\mu\text{m}$  (Figure 3) and the product fineness or median size of particles ( $d_{50}$ ) is up to 1.5  $\mu\text{m}$ .

#### *Influence of the grinding media size*

Figure 3 gives the weight of cyclone and column products obtained after pulverization of limestone ore with steel balls of different diameters ( $\varphi = 10$  mm,  $\varphi = 13$  mm,  $\varphi = 16$  mm,  $\varphi = 20$  mm) at increasing duct airflow rates. At lower rates, the weight of products is not influenced by the size of the grinding media. This dependence increases sharply at higher values. So, the weight of cyclone products obtained with 20 mm diameter balls, for example, is four times, and that of column products - fifteen times, as large as that obtained with 10 mm diameter balls. These results are an evidence of the highly comminuting efficiency of 20 mm diameter balls to produce many fine particles (Mori et al., 1995). Figure 4 represents the maximum diameter of particles collected in the cyclone and the column at increasing duct airflow rates. It is shown that the size of the balls is not a major factor in the determination of the maximum diameter of particles in the products.

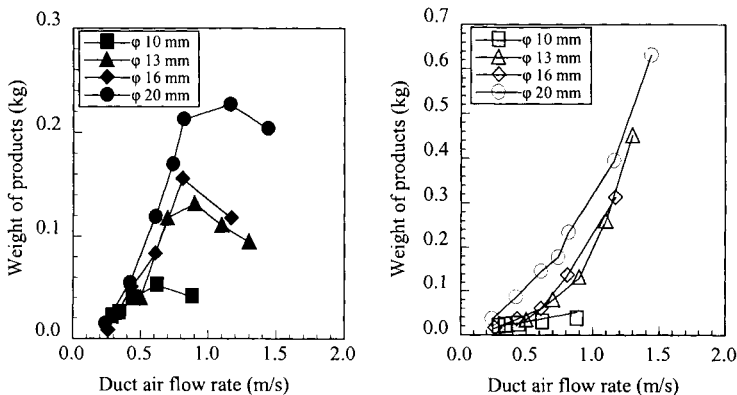


Figure 3: Weight of cyclone products (left) and column products (right) at different airflow rates.

#### *Influence of the stirring screw speed*

Figures 5 and 6 give the results of the tests carried out at various values of the stirring screw speed and the duct airflow rate (Shibayama et al., 1997). The plot in Figure 5 between the specific energy (J/kg) and the duct airflow rate reveals that these two parameters are inversely proportional. Although some differences are observed at lower duct airflow rates, the energy consumption of the KD-3 remains almost constant at higher rates. It is likely to obtain a high grinding efficiency by increasing the speed of the stirring screw without increasing the specific energy. That does not influence the shape of the particles size distributions of products in the cyclone and the column (Figure 6). In these plots, both  $d_{50}$  and  $d_{\max}$  increase with the duct airflow rate independently of the stirring screw speed.

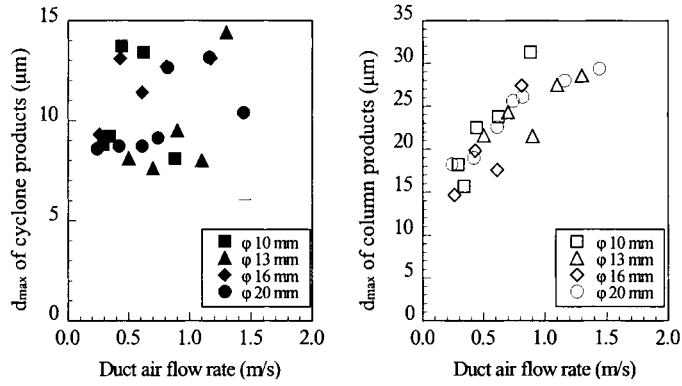


Figure 4: Maximum diameter ( $d_{max}$ ) of cyclone products (left) and column products (right) versus duct air flow rates.

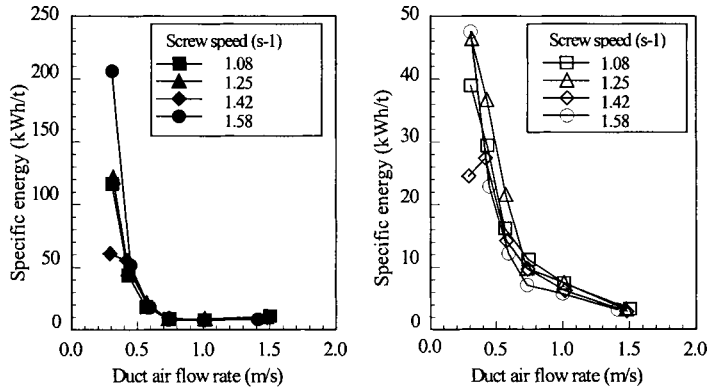


Figure 5: Specific energy ( $\text{kWh/t}$ ) for cyclone products (left) and column products (right) at various duct air flow rates.

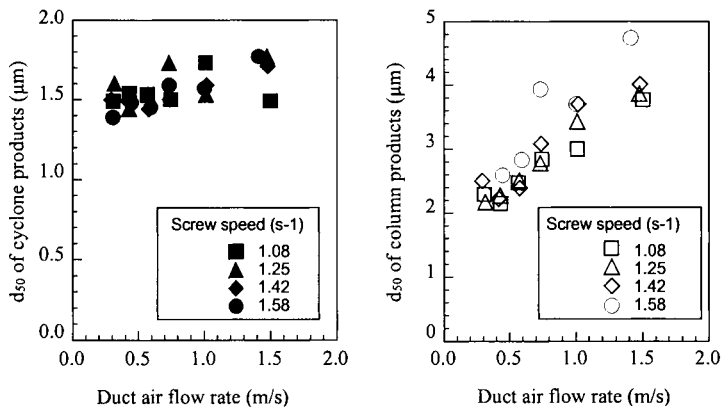


Figure 6: Median size ( $d_{50}$ ) of cyclone products (left) and column products (right) at different duct air flow rate.

### Role of the nets in the classifying column

Fine particles, freshly produced by the grinding motion of the steel balls and the stirred screw in the comminuting cell of the tower mill KD-3, are directly removed by a circulating air flow generated inside the mill. The classifying operation occurs in the column next to the comminuting cell. To understand the behavior of these particles during the classifying action and the role of the nets in the column, a series of experiments was carried out modifying the structure of the column (Figure 2) and assuming that:

- the air flow rates in the classifying column ( $U_{cl}$ ) and the comminuting cell ( $U_{ce}$ ) can be converted from the measured duct air flow rate ( $U_d$ ) in accordance with the calculated cross area of each section of the tower mill KD-3; the relationships between  $U_{cl}$ ,  $U_{ce}$  and  $U_d$  are presented below:

$$U_{cl} = 0.02 U_d \quad (1)$$

$$U_{ce} = 0.19 U_d \quad (2)$$

- the maximum diameter ( $d_{max}$ ) of particles in the cyclone and column products is determined by the column and the cell airflow rates respectively;
- particles in the column and the cell are supposed to be not secondary, but primary particles; besides, the dropping rate ( $U_p$ ) of particles whose diameter is  $D_p$  may have the same value as the column airflow rate ( $U_{cl}$ ).

Therefore, the Stoke's law, applied to the particles inside the column and the cell, gives an estimate of the maximum particles diameter of cyclone ( $d_{max-cy}$ ) and column products ( $d_{max-cl}$ ) as a function of  $U_{cl}$  and  $U_{ce}$  (equations 3 and 4):

$$d_{max-cy} = \left( \sqrt{\frac{18\eta}{g(\rho_m - \rho_a)}} \times U_{cl} \right) \quad (3)$$

$$d_{max-cl} = \left( \sqrt{\frac{18\eta}{g(\rho_m - \rho_a)}} \times U_{ce} \right) \quad (4)$$

The plots of these equations, represented in Figure 7 above, are referred as estimated curve 1 and estimated curve 2 respectively.

The introduction of nets in the classifying column modifies slightly the curves representing the maximum particles diameter of cyclone and column products:

$$d_{max-cy} = \left( \sqrt{\frac{18\eta}{g(\rho_m - \rho_a)}} \times U_{cl} \right) \times C_1 \quad (5)$$

$$d_{max-cl} = \left( \sqrt{\frac{18\eta}{g(\rho_m - \rho_a)}} \times U_{ce} \right) \times C_2 \quad (6)$$

Where:  $C_1 = 0.65 \sim 1.5$  and  $C_2 = 0.6$

The maximum particles diameter ( $d_{max}$ ) of products can be also calculated from the pressure drop ( $P_d$ ) in the duct, using the relationship:

$$P_d = 835.31 U_d^2 + 44.18 U_d \quad (7)$$

Several observations show a relatively high air current in the center area of the column blowing up particles coarser than those of the estimated curve 1 to the cyclone (cases CLA0 and CLA1). For CLA2 and CLA3, many of finely ground



particles, blown up from the comminuting cell through the column and the nets are supposed to cohere and form secondary particles (Shibayama and Mori, 1999).

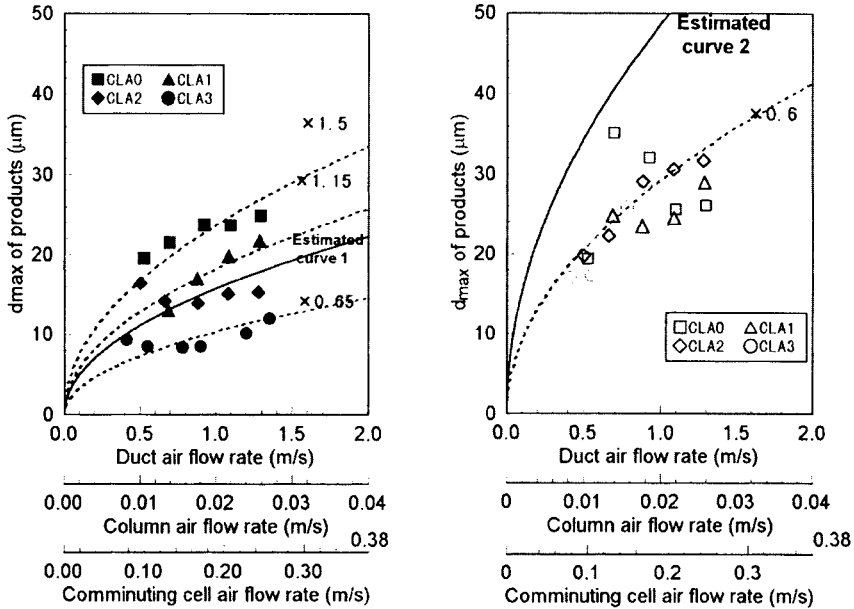


Figure 7: Maximum size ( $d_{max}$ ) of particles collected in the cyclone (left) and column (right) at various duct, column and cell air flow rates.

Figure 8 gives, for each type of column, the relationship between the maximum diameter of particles ( $d_{max}$ ) and the fineness of products ( $d_{50}$ ) in the cyclone and column.

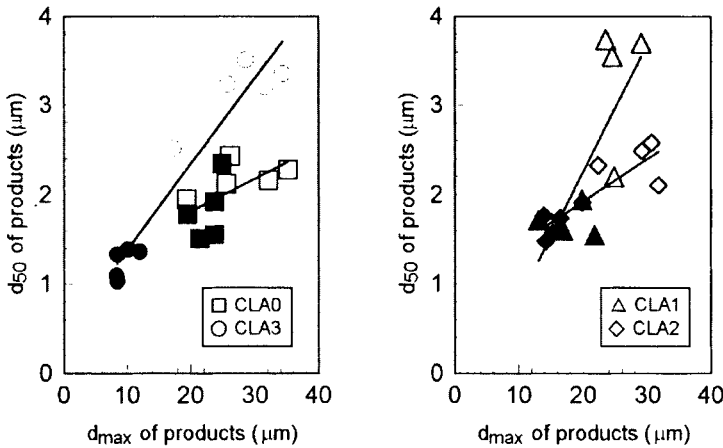


Figure 8: Relationship between  $d_{50}$  and  $d_{max}$  of cyclone (black) and column (white) products.

In the case of CLA0, the overlap of curves in Figure 8, as well as the superposition of the particle-size distributions curves of products in Figure 9 denote a poor efficiency of the classifying structure. As for the columns CLA1, CLA2 and CLA3, the  $d_{max}$  versus  $d_{50}$  charts indicate a sharp classification of products confirmed by the distinct separation of distribution curves in Figure 9 (case of CLA3). It is obvious that settling a sieve to screen the pulverized products in the column reduces the air turbulence and increases the classifying efficiency of the mill. So, the maximum diameter of particles in the products is influenced by the type of the nets and the way they are settled on the baffle plate.

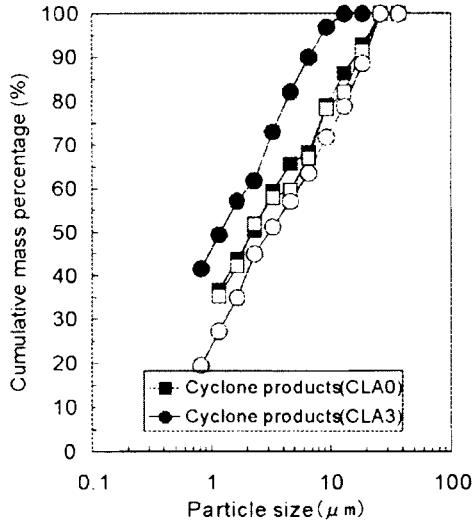


Figure 9: Particle size distribution of cyclone (black) and column (white) products.

## Conclusions

The Tower Mill is a new type of pulverizer specially conceived for a fine grinding. Its efficiency largely depends on the shape and structure of each of the three constituting sections: comminuting, classifying and collecting. In this present study a high recovery of fine particles ( $d_{max}$  smaller than 10 μm) have been achieved on the latest version of the Tower Mill KD-3.

The experimental results of these investigations can be summarized as follows:

- the performance of KD-3 increases with the size of the grinding media: a higher efficiency is observed with 20 mm diameter balls rather than with 10 mm diameter balls;
- the weights of cyclone and column products, as well as the electric consumption of the stirring motor increase with the speed of the stirring screw while the specific energy (J/kg) tends to be constant; besides, the size distribution curves of particles in the cyclone and column products are not influenced by the ball size and the stirring screw speed;
- the maximum particle diameters of pulverized products can be estimated applying

the Stoke's law of sedimentation; the maximum and median particle diameters of products have a proportional relationship; besides, the use of a column provided with a series of "screening" nets (CLA3) decreases the air turbulence and improves the efficiency of the classification of products.

**References**

- Hara, T. and Mori, S., 1995. Application of Ultrasonic Waves in the Preparation of Suspension for a Particle Size Distribution Analysis of Powder by Sedimentation: Kyushu Daigaku Kougaku Syuuhou (Technology Reports of Kyushu University, Japan), 68. 211-216.
- Mori, S., Shibayama, A. and Hara, T., 1997. Development of a Tower Mill for Fine Grinding. Proceedings of the XX International Mineral Processing Congress, 2. Aachen, Germany, 61-69.
- Mori, S., Hara, T., Hamada, K., Okada, Y., Izumi, T. and Shibayama, A., 1995. The Effect of Ball Size on Limestone Pulverization by the Tower Mill KD-3: Kyushu Daigaku Kougaku Syuuhou (Technology Reports of Kyushu University, Japan), 68. 577-582.
- Shibayama, A. and Mori, S., 1999. Roles of the Net in the Column on Tower Mill KD-3: Shigen-to-Sozai (Journal of the Mining and Materials Processing Institute of Japan), 115. 83-88.
- Shibayama, A., Mori, S., Hara, T., Izumi, T. and Nagatome, S., 1997. Influence of Stirring Screw Speed on Grinding Efficiency of the Tower Mill KD-3: Shigen-to-Sozai (Journal of the Mining and Materials Processing Institute of Japan), 113. 842-846.

## IMPROVEMENT IN CLASSIFICATION PERFORMANCE OF TURBO CLASSIFIERS BY REDUCING THE INERTIA COUNTER-ROTATING VORTICES

J. Liu, B. Chen, D. Xu

Xi'an University of Architecture & Technology, Xi'an Shaanxi, 710055 P.R. China,  
Northeastern University, Shenyang Liaoning, 110006, P.R. China

### Abstract

For the purpose of improving the performance of a model of turbo classifiers, a certain type of narrow plates were fitted into the passages of its impeller. Experiments of powder-material classification with the model classifier indicated that a degree of reduction of the particle size of the products and an increase in classification precision resulted from the modification, and that the effects were more appreciable for the impeller with wider passages than for that with narrow passages.

*Keywords: turbo classifier, structure parameter, classifying index, counter-rotating vortex*

### Introduction

For some kinds of fluid machines, such as centrifugal pumps, fans and air classifiers, an impeller is an important component. This movable device consists of a number of air passages formed by arranging blades in a radial direction between two parallel disks. As reported by a number of researchers, the so-called inertia counter-rotating vortices always exist in the fluid flow passing through the impeller passages when operating the machine (Lakshminarayana B., 1980; Cohen et al., 1972; Ito et al., 1006; Richard and Hartman, 1981). The fluid flow is in a superimposed pattern: radial converging or diverging, and circulating backward relative to the impeller motion. In Figure 1 the later is shown.

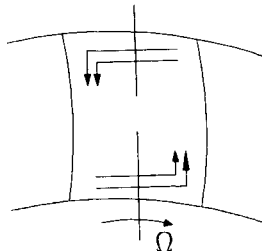


Figure 1: The diagrammatic sketch of inertia counter-rotating vortices in the passage between two blades.

This rotational flow is usually called the inertia counter-rotating vortices. Existence of the inertia counter-rotating vortices detrimentally effect performance of some fluid machines at the outlet of the impeller of the centrifugal pumps and fans. The vortices cause a decrease in the tangential velocity of fluid particles and, consequently, in the total head of the pumps or fans. For turbo air classifiers, the inertia counter-rotating

vortices must effect the radial velocity distribution in the impeller passages. In the region adjacent to the surface of the blades going forward, the radial component of flow velocity increases. In contrast, in the region near the surface going backward, it decreases. This causes dispersion in the cut size and a decrease in classifying efficiency and precision. The author (Jiaxiang et al., 1998) pointed out that the strength of the inertia counter-rotating vortices would be equal to twice the angular velocity of the impeller multiplied by the passage area, and its rotating would be in an opposite direction to that of the impeller:

$$S = -2\Omega\sigma \quad (1)$$

Where

$S$  = strength of inertia-counter-rotating vortices;

$\Omega$  = angular velocity of impeller;

$\sigma$  = passage area.

An equation for estimating the average deviation in radial velocity at the inlet of the passage from the mean radial velocity is suggested by the author as follows:

$$\overline{\Delta V_r} = \frac{2\pi r_z \Omega}{n} \quad (2)$$

where:

$\Delta V_r$  = average deviation of radial velocity;

$n$  = number of rotating blades;

$r_z$  = inlet radius of the blades.

A series of experiments have been carried out to search for measures for reducing the counter-rotating vortices. The authors of this paper have experimented with the measures of reducing counter-rotating vortices and have determined the effect of improving classifying precision from these measures.

## Experimental

The diagrammatic sketch of the experimental device is shown in Figure 2.

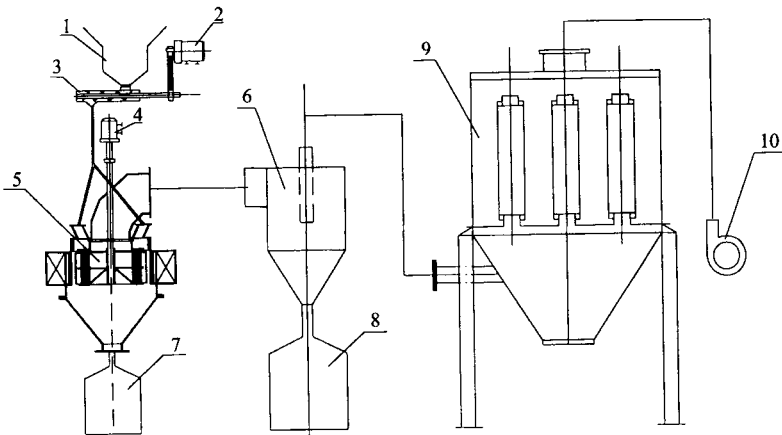


Figure 2: The experimental device: 1. Feed storehouse. 2. Rotational speed-modulation motor. 3. Spiral feed machine. 4. Rotational speed-modulation motor. 5. Vortex air classifier. 6. Cyclone dust collector machine. 7 and 8. Barrel of collector powder. 9. Cloth bag-type collector. 10. Centrifugal ventilator.

The impellers used in the experiment involve fan-shaped passages. The number of blades in the impeller is 16 and 24, respectively. The unit for reducing the inertia's counter-rotation vortices is the narrow blades, with a 10 cm width fitted into the middle of the passages between every two neighboring blades.

The impeller of 16 blades is called No.1, the 24 blade one is called No. 2. For the diagrammatic sketch for fitting narrow blades, see literature (Jiaxiang, 1997). The impellers with fitted, narrow blades are called n° 3 and n° 4, respectively.

The classified raw materials were taken from the exit of a tube mill in a cement plant. The size distribution of raw materials tested is listed in Table I. The wind speed of the entrance in the classifier is 20 m/s. The test conditions are listed in Table II.

Table I: Size distribution of raw material tested.

Size class (mm)	+0.220	-0.220	0.154	-0.105	-0.080	-0.063	-0.055	-0.040
Weight (%)	0.6	2.0	5.2	11.6	11.4	7.0	7.0	14.6
Size class (mm)	-0.030	-0.022	-0.015	-0.011	-0.007	-0.003		
Weight (%)	4.53	14.07	8.13	4.45	1.54	7.88		

Note: The sizes larger than 0.080 mm were measured by dry screen. The sizes from 30  $\mu\text{m}$  to 80  $\mu\text{m}$  were measured by wet screen. The sizes smaller than 30  $\mu\text{m}$  were measured by light size instrument. The sum of the sizes larger than 30  $\mu\text{m}$  and smaller than 30  $\mu\text{m}$  has still been listed according to 1%

Table II: The experimental conditions.

Test order	Type of impeller	Rot. speed of impeller ( $\text{r}\cdot\text{min}^{-1}$ )	Rot. speed of feed machine ( $\text{r}\cdot\text{min}^{-1}$ )	Feed (kg)	Temperature ( $^{\circ}\text{C}$ )	Solid density ( $\text{g}/\text{cm}^3$ )	Resistance loss (Pa)	
							Bef. feed	feed
L-1	1	700	400	45.64	8	1.71	612	692
L-2	1	700	200	48.96	8	0.92	612	692
L-3	3	550	400	43.64	12	1.64	622	840
L-4	3	700	400	44.46	12	1.67	622	790
L-5	2	550	400	45.14	19	1.69	578	778
L-6	2	700	400	45.40	18	1.70	578	758
L-7	4	550	400	42.92	12	1.61	590	840
L-8	4	700	400	45.22	12	1.70	590	780

The coarse powder size distribution of each experiment is listed in Table III and Table IV, respectively.

Table III: The coarse powder size distribution of each experiment (%).

Test order	Size class (mm)								
	+0.220	-0.220	-0.154	-0.105	-0.080	-0.063	-0.055	-0.040	-0.030
L-1	1.2	6.6	12.0	22.6	20.6	10.8	7.4	6.8	12.0
L-2	1.2	4.3	11.0	24.0	23.4	13.8	8.8	5.4	8.1
L-3	1.4	4.4	10.7	23.5	22.1	12.8	7.9	6.0	11.2
L-4	1.2	4.0	9.1	20.2	19.8	11.6	11.0	8.1	15.0
L-5	1.1	4.0	10.5	22.1	20.8	12.0	10.2	7.4	11.9
L-6	1.1	3.4	8.9	19.8	19.5	12.0	11.9	8.8	14.6
L-7	1.1	3.7	9.7	21.4	21.0	12.8	10.4	6.9	13.0
L-8	1.0	4.0	9.3	20.0	19.6	12.0	11.9	7.3	14.9

Table IV: The coarse powder size distribution of each experiment (%).

Test order	Size class (mm)					
	-0.030 +0.022	-0.022 +0.015	-0.015 +0.011	-0.011 +0.007	-0.007 +0.003	-0.003
L-1	18.07	29.24	18.06	7.23	3.96	23.43
L-2	23.12	38.02	12.67	6.74	0.69	18.50
L-3	7.91	36.75	22.90	8.64	1.66	22.13
L-4	19.49	35.93	10.02	14.61	2.53	17.42
L-5	14.22	28.47	19.72	15.00	4.40	18.19
L-6	18.52	20.38	10.44	26.20	1.00	23.46
L-7	13.81	31.22	28.75	10.82	1.01	14.39
L-8	15.00	34.77	15.33	13.84	3.20	17.86

The experiment's results are listed in Table V. For the coarse powder's parts classification efficiency curves of L-1 and L-2, see Figure 3 and Figure 4, respectively. In Figure 3 and 4, the ordinate  $E_1$  is the classification efficiency of parts of every sized feed in the coarse powder. The classification efficiency curve of the coarse powder part is from L-3 to L-8 (Jiaxiang, 1997).

Table V: Test results.

Test order	Coarse powder weight (kg)	Coarse powder yield (%)	Fine powder weight (kg)	Classification efficiency (%)		Feature size ( $\mu\text{m}$ )			Classification precision index		
				<0.03 mm	<0.08 mm	$d_{25}$	$d_{50}$	$d_{75}$	$K=d_{25}/d_{75}$	$K=d_{25}/d_{50}$	$K=d_{50}/d_{75}$
L-1	23.46	51.40	10.22	84.81	63.27	35.3	46.0	57.0	0.62	0.77	0.81
L-2	23.12	47.22	23.60	90.58	65.14	37.3	44.7	52.7	0.71	0.83	0.85
L-3	19.72	45.19	22.76	87.54	66.36	37.6	47.3	56.1	0.67	0.79	0.84
L-4	25.44	57.22	18.10	78.86	53.50	29.3	38.6	44.4	0.66	0.76	0.87
L-5	22.44	49.71	21.66	85.43	61.57	35.0	41.6	50.0	0.70	0.84	0.83
L-6	26.58	58.54	17.92	78.95	51.48	23.5	37.6	42.6	0.55	0.63	0.88
L-7	22.98	53.46	18.74	82.64	59.41	34.0	40.5	46.5	0.73	0.84	0.87
L-8	26.32	58.20	17.82	78.64	52.56	24.2	38.5	43.2	0.56	0.63	0.89

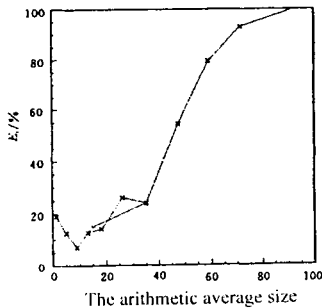


Fig. 3: The coarse powder's parts classification efficiency curve of L-1.

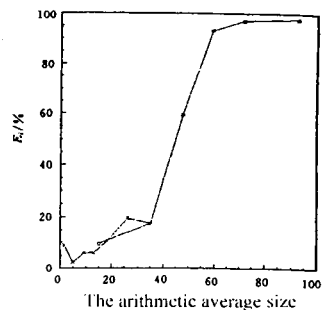


Fig. 4: The coarse powder's parts classification efficiency curve of L-2.

○— Particle sizes smaller than 30  $\mu\text{m}$  with regard to average size of 15  $\mu\text{m}$  in the drawing.

×— Particle size smaller than 30  $\mu\text{m}$  in the drawing.

### Analyses of the experimental results

The analysis of the L-1 and L-2 tests in Table II and the Table V, shows as the solid density is  $0.92 \text{ g/cm}^3$ , the cut size is smaller and the classification precision index higher than the solid density of  $1.71 \text{ g/cm}^3$ . Figure 3 and Figure 4 demonstrate that when the solid density is  $0.92 \text{ g/cm}^3$ , the missing proportion of fine powder is smaller than that when the solid density is  $1.71 \text{ g/cm}^3$ . By comparing L-1 and L-4 in Table II and Table V, it can be shown (for the impeller possessing 16-piece blades with fitted narrow blades) that the cut size is reduced from  $46.0 \text{ }\mu\text{m}$  to  $38.6 \text{ }\mu\text{m}$ , and the classification precision index increases from 0.62 to 0.66. Relatives increase by 6.5%, with a slight reduction in the missing proportion of fine powder, has been observed. These results illustrate that, in the case of the narrow, fitted blades, the inertia counter-rotating vortices inside passages are reduced, and this causes the cut size to be reduced and an improved classification precision index. By comparing the L-5 and L-6 in Table II and Table V, it can be evidenced as the cut size reduces, and the classification precision index cuts down from 0.70 to 0.50 when the rotational speed of impeller increases from 550 rpm to 700 rpm. These results illustrate that the inertia counter-rotating vortices increase with increases in the rotational speed of impeller. Finally, by comparing L-5 to L-8 tests (Table II and Table V), the cut sizes result almost unchanged, and the classification precision indexes just slightly increase (from 0.70 to 0.73, and from 0.55 to 0.56, respectively) for the narrow blades being fitted into the passage center in one impeller of 24-piece blades. Therefore, this concludes that when the number of radial blades is much greater, the function of the narrow blades reducing the inertia counter-rotating vortices is not remarkable.

### Conclusions

The experiments test and verify that the intensity of inertia counter-rotating vortices and the deviation of radius velocity are proportional to the rotational speed of the rotor impeller. With the rotational speed of the rotor cage being increased, the intensity of inertia counter-rotation vortices increases, and the classification precision index reduces. The device of fitted, narrow blades can indeed reduce the inertia counter-rotating vortices and increase the classification precision index. This effect is more obvious for those impellers with fewer blades than for with more fitted blades.

### Acknowledgments

Thanks have to be addressed to Natural Science Foundation of Shaanxi Province for supporting (N<sup>o</sup> 98c08).

### References

- Cohen, H., Rogers G.F.C., Saravanamuttoo H.I.H, 1972. Gas Turbine Theory. Longman Group Ltd.
- Harman, R.T.C., 1981. Gas Turbine Engineering. Applications, Cycles and Characteristics. Landon and Basingstoke, The Macmillan Press Ltd.
- Ito M., Sutoh K., Matsuda T., 1996. Classification efficiency of cage-type air classifier. ZKG Int. 49, 134-144.
- Lakshminarayana, B., 1980. Measurement Methods in Rotating Components of Turbomachinery.
- Lakshminarayana, B., The Pennsylvania State University, Pennsylvania and P. Runstadler, Jr., Creare Incorporated, Hanover, New Hampshire, The American Society of Mechanical Engineers.
- Liu Jiexiang, 1997. A Study on the vortex classifier's classifying characteristics and its improvement. PhD thesis, Eastnorthern University, China.
- Liu, Jiexiang, Xu, Delong, Zhao, Jiangping, and Xu, Yusheng, 1998. The effects of inertia counter rotating vortices in a vortex classifier on particle classification. Journal of Xian University of Architecture & Technology, 30, 63-66.



## OPTIMIZED PRODUCTION SCALE CLASSIFIER FOR FINEST CUTS AT HIGH CAPACITIES

M. Adam, S. Zampini

Technical Division  
HOSOKAWA ALPINE AG & Co. OHG, Augsburg, Germany

### Abstract

The demand for ultrafine materials in the mineral industry is presently met by Hosokawa Alpine with the patented multiwheel classifiers. Since this type of machine is not always suitable for mass products a new classifier for the production of finest minerals has been developed. The Alpine TurboTwin combines low energy costs with fine cutpoints and high yields.

The paper presents the fundamentals of classification, the requirements for a modern production classifier and the current solutions. The newly designed TurboTwin is introduced and the considerations of its development are presented. Test results show the advantages and possibilities of the new machine.

*Keywords: classifier, pressure drop, minerals, production, energy costs*

### Introduction

Regardless of the field of operation, may it be the chemical, pharmaceutical, mineral or ceramic industry, the demand for fine powders is almost omnipresent. Toners, in the chemical industry, are ground and then classified to remove particles below 5  $\mu\text{m}$ . Penicillin for pharmaceutical applications is ground to 97% <5  $\mu\text{m}$ . Fillers for the paper industry often require a  $d_{50} \leq 1.5 \mu\text{m}$  and High Tech Ceramics frequently are ground to a  $d_{99} < 6 \mu\text{m}$ .

The mineral industry has its specific requirements regarding the machines used for the production of fine powders. Although there are certain products produced only for a small market in relatively small amounts most materials are produced for a mass market. Moreover the price per kilogram achieved for the materials in question often is not very high, regardless of the high quality demands.

Thus the requirements of the mineral industry are high capacities, low investment and energy costs and a high quality product. High quality in this case means very fine top sizes, steep particle size distribution, no oversized particles etc.

For the machines and here the classifier in particular this means:

- the classifier must be able to handle high throughputs and at the same time require as less air flow as possible to keep the energy costs low;
- the machines must require small maintenance;
- low energy costs require a low pressure drop of the classifier since it is direct proportional to the required fan power;
- high yields at fine cutpoints, reducing the amount of recirculated material, are desired. Fine cutpoints in this case meaning a  $d_{97}$  in the range of 2÷5  $\mu\text{m}$ .

Easy access and good cleanability, highly polished surfaces and stainless steel design are features of lesser interest, although these features are highly valued and essential to other industries.

This paper presents the new optimized production-scale classifier TurboTwin TTC by Hosokawa Alpine AG & Co. OHG, Augsburg. In the first part the principles of classification in wheel type air classifiers are presented followed by a brief description of the technical status quo of air classification in the mineral industry.

Proceeding from the above mentioned requirements for a machine in the field of fine classification of minerals the second part explains the new machine and shows experimental results of an TTC test unit and an operating commercial installation. The results of various tests are compared to another machine by Alpine.

## Fundamentals

### Theoretical cutpoint

When classified the particles are submitted mainly to the centrifugal force and the drag force, which are opposed to each other and -for steady state- equal (figure 1).

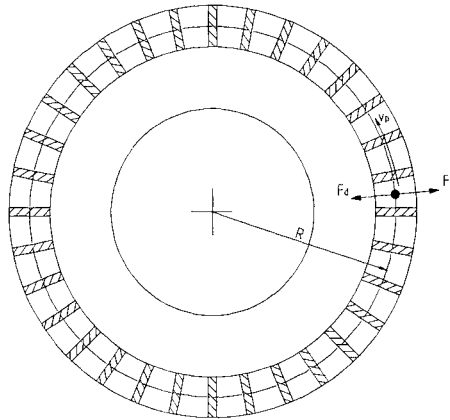


Figure 1: Forces on the particle.

The centrifugal force  $F_C$  is a function of the particle density  $\rho_p$ , of the radius of the circle of motion  $R$ , of the particle size  $x$  and of the circumferential velocity  $u$ :

$$F_C = \rho_p \cdot \frac{\pi}{6} \cdot x^3 \cdot \frac{u^2}{R} \quad (1)$$

The drag force of the fluid  $F_D$  is defined by:

$$F_D = c_w(\text{Re}) \cdot \frac{\pi}{4} \cdot x^2 \cdot \frac{\rho_L}{2} \cdot w_{\text{rel}}^2 \quad (2)$$

where  $c_w(\text{Re})$  is the drag coefficient of the particle and  $w_{\text{rel}}$  is the relative velocity of fluid and particle:

$$w_{\text{rel}} = w_L - w_p \quad (3)$$

At low Reynolds numbers (Stokes law is applicable) the drag force can be written as

$$F_D = 3 \cdot \pi \cdot \eta_L \cdot x \cdot w_{rel} \quad \text{for} \quad Re < 1 \quad (4)$$

A particle with the particle size  $x_T$ , called the cutpoint, has no radial velocity, i.e.  $w_p = 0$ . Consequently the particle theoretically is neither coarse nor fine fraction but circles on an orbit. From the radial equilibrium of the effective forces the particle size  $x_T$  can be calculated as

$$x_T = \text{Konst} \cdot \sqrt{\frac{\eta_L}{\rho_p} \cdot \frac{w_L}{u^2}} \cdot R \quad \text{for} \quad Re < 1 \quad (5)$$

As one can see the cutpoint  $x_T$  is dependent on the material properties dynamic viscosity of the fluid  $\eta_L$  and particle density  $\rho_p$ , on the operational parameters circumferential speed  $u$  and radial velocity of the fluid  $w_L$  as well as on the geometric parameter radius  $R$ .

There are of course other important aspects of the classification that are not accounted for in the calculation. Some of these are described briefly in the following.

#### *Deviation to theory*

There are numerous factors that lead to a deviation between the calculated cutpoint and the actual result of a classification. The solids loading of the fluid, the fineness of the feed material and the surrounding flow pattern are not accounted for in the calculation. Moreover, turbulence and inertia forces are neglected. In addition, an even flow distribution in the classification zone is assumed. The effects of uneven flow distribution and turbulence will be shown in more detail later on.

The deviation is expressed as the ratio  $F$  of the measured value  $x_T$  and the calculated cutpoint  $x_{T,theo}$ :

$$F = \frac{x_T}{x_{T,theo}} \quad (6)$$

A higher ratio  $F$  always has to be compensated by either a higher circumferential velocity  $u$  or a smaller airflow and therefore smaller radial fluid velocity  $w_L$  (see equation 5). The smaller the ratio  $F$  the smaller is the cutpoint that can be achieved at otherwise equal conditions.

#### *Wheel types*

Basically there are two wheel types that are used in classifiers: potential vortex wheels and solid body rotation vortex wheels. The two types display completely different flow and classification characteristics.

Figure 2 shows the cutpoint as a function of the radius for the two wheel types. Between the blades of the classifier wheel the cutpoint increases with decreasing radius. In the solid body rotation wheel the air outlet is situated directly at the inner periphery of the blades whereas in the potential vortex wheel the air outlet is situated further inward allowing a potential vortex to form in the inner section of the wheel. In this region the cutpoint is proportional to the radius. This characteristic has been described by Rumpf and Leschonski (1968/69).

It can be seen that the solid body rotation-vortex wheel theoretically yields a coarser cutpoint if operated at the same rotation-speed as the potential vortex wheel.

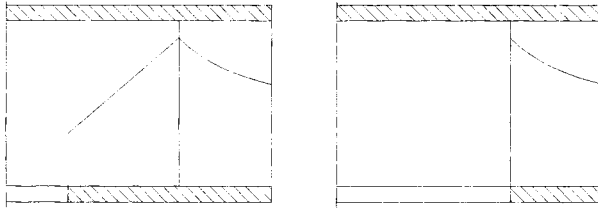


Figure 2: Cutpoint as a function of the radius for potential vortex and solid body rotation vortex type wheels.

Consequently, with a solid body rotation wheel higher speeds are necessary to obtain the same result as with a potential vortex. However, as the ratio  $F$  can be different for the two wheel types this difference may not be as big as calculated. Another effect that is not taken into consideration in the calculation of the cutpoint in equation 5 is the secondary vortex between the deflection blades of the classifier. This secondary vortex as shown in Figure 3 has already been described by Legenhausen (1991).

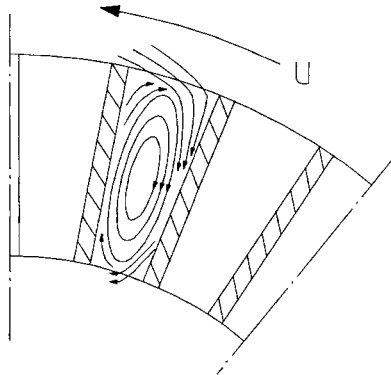


Figure 3: Flow pattern between conventional rotor blades.

It can be seen that, due to the vortex, the actual radial velocity is higher than calculated because the area where the fluid flow is directed inward is extremely reduced which results in higher cutpoints than calculated. The secondary vortex can be observed in both wheel types. However, the negative effect on the cutpoint is more severe in the solid body rotation wheels since the air and product outlet is situated directly behind the vanes.

### Status quo of fine classification

The Alpine TurboPlex<sup>®</sup> (ATP) can be considered one of the best classifiers for fine and ultrafine classification. It achieves fine cutpoints at high yields, which can be further improved by using the patented multiwheel principle.

The patented multiwheel classifiers use several wheels in one housing in order to maximize yields at fineness, which can only be achieved with small rotor sizes.

However, a further improvement of fineness could only be achieved by higher rotor speeds, i.e. higher peripheral velocities. Since the ATP uses a wheel with a potential

vortex an augmentation of the rotor speed would result in an increase of the pressure drop. Due to the relation between pressure drop and operational costs this increase has to be avoided. On the other hand the number of wheels that can be incorporated in one multiwheel classifier is not infinite. Space and costs have to be considered and limit the number of wheels to six to eight in one housing.

A different classifier is the Alpine StratoPlex<sup>®</sup> (ASP) which uses a solid body rotation wheel and has an extremely low-pressure drop. The disadvantage of this machine in respect to finest classification is the limitation to cutpoints in the 10  $\mu\text{m}$  region.

The design of the new classifier for finest cuts therefore had to be a combination of the advantageous features of the ATP and the ASP together with new developments to achieve even lower cutpoint diameters.

### **The new design**

The basic design of the classifier housing is the well proved design of the ATP, i.e. the wheel in the head of the machine and a coarse classification zone with spiral air inlet at the bottom of the classifier. This allows a recirculation of material within the classifier in order to achieve multiple chances of classification and therefore a high recovery of final product.

In order to achieve the necessary small pressure drop a solid body rotation-vortex wheel as in an ASP is used. The wheel has a special design (patent pending) to assure the even distribution of air throughout the whole height of the wheel and to overcome the undesired effects of the secondary vortices in such a wheel design.

One key for higher fineness is the circumferential speed of the wheel and the radial velocity of the fluid as shown in equation 5. In order to reduce the radial velocity the wheel height was increased and to achieve higher rotation speeds the wheel now has a bearing on each side in contrast to the ATP, which has the whole bearing unit on one side of the wheel. Consequently, the rotor of the TurboTwin has a horizontal orientation in order to avoid bearings in the material chamber of the classifier. The circumferential speed of the classifier is now in the range of 100 m/s. The lower radial velocity allows the use of higher air flows and thus enables the classifier to handle higher mass flows. When using lower airflows the cutpoint is further reduced.

The coarse classification zone with the spiral air inlet has been modified for a lesser pressure drop without losing the recirculation effect.

Thus the TurboTwin is able to replace some multiwheel classifiers in respect to capacity and fineness while operating at lower pressure drops.

### **Experimental results**

Comparison tests with the TurboTwin and the ATP show the advantages of the new concept. A higher fineness was achieved while maintaining the high recovery of final product that is known from the ATP. The finest cutpoint could even be reduced while operating at less than half of the pressure drop. This is illustrated in Figure 4 where the pressure drop in daPa is shown versus the  $d_{97}$  of the fine material.

With the new classifier it is possible to produce material with a  $d_{95}$  of 2  $\mu\text{m}$  and a  $d_{50}$  below 0.8  $\mu\text{m}$  measured on a Sedigraph as shown in Figure 5. This kind of material is widely used in the filler industry.

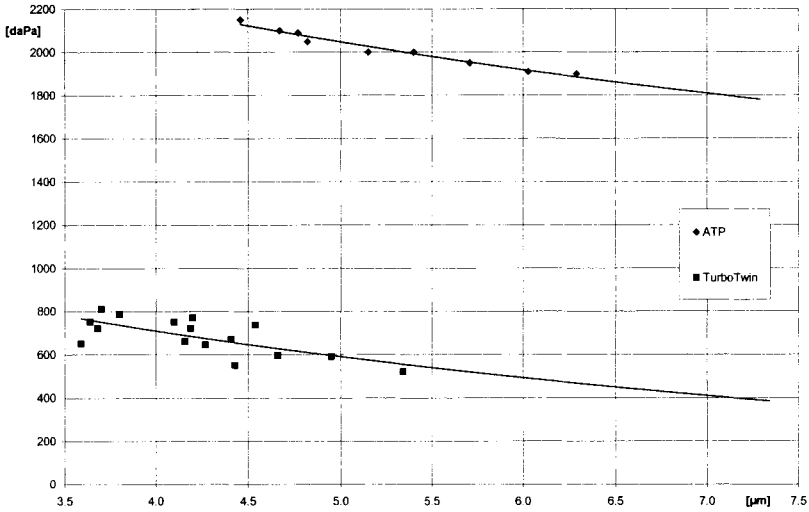


Figure 4: Pressure drop across the classifier versus the top size  $d_{97}$  of the fine material.

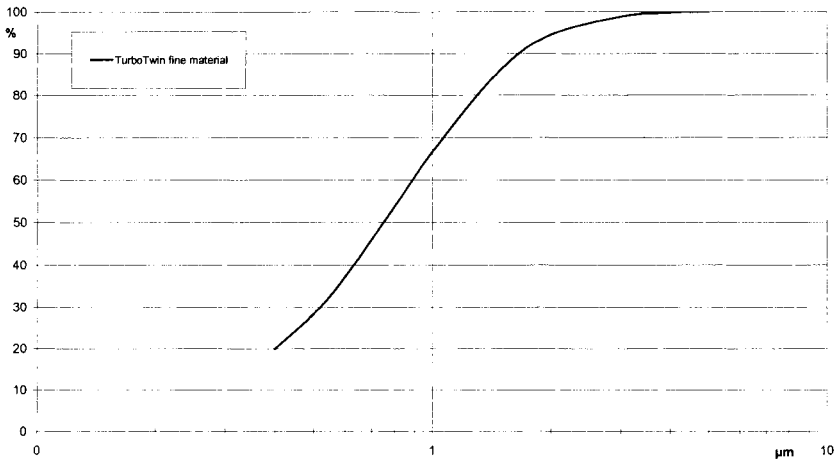


Figure 5: Fine material (calcium carbonate) produced on a TurboTwin.

With a TurboTwin a multiwheel classifier can be replaced. While achieving the same throughput it is possible to reduce the fineness and to operate at a considerably lower pressure drop thus eliminating the need for multi-stage fans and reducing investment costs as well as operating costs.

#### References

- Legenhausen, K. 1991. Untersuchung der Strömungsverhältnisse in einem Abweiseradsichter, Dissertation, TU Clausthal.
- Rumpf, H. and Leschonski, K. 1968/69. Principle and Construction of Two New Air Classifiers for Size Analysis, Powder Technology 2, 175-185.

## THE INFLUENCE OF COMMINUTION METHOD TO PARTICLE SHAPE

M. Oja, R. Tuunila

Lappeenranta University of Technology, Department of Chemical Technology  
P.O. Box 20, FIN-53851 Lappeenranta, Finland

### Abstract

The different applications of fine powders need different physical characteristics of the solids. This study presents the influence of the comminution method to the shape of the product particles. The types of mill were a ball mill, an attrition bead mill and a jet mill. The test minerals were limestone, FGD (Flue Gas Desulfurisation) gypsum and waste gypsum from phosphoric acid plant. The size and the shape of the ground particles were measured with an image analyzer. The relevant shape features of the ground products were extracted by self-organizing maps (SOM) and then the particles were clustered with the SOM. The different mill products were clustered differently showing that the fraction of concave particles is a relevant shape feature.

*Keywords: comminution, particle shape analysis, self-organizing map, SOM*

### Introduction

The importance of particle shape on the behavior of the powders and slurries is well known, but there is no general method for the shape characterization and therefore the influence of shape is often neglected. The different applications of fine powders need different physical characteristics from solids. Holt (1981) pointed out in the beginning of 80's that in comminution literature the shape of the comminuted particles is presented only as a secondary topic. He hoped that the advanced particle shape measurement techniques are applied to explain the role of particle shape in comminution. However, only few studies have tried to find out the answer to this question (Meloy, 1985). Recently Trass et al., (1995) performed a qualitative study of particle shapes in coal products obtained in different operation condition of the Szego mill. It is known that the character of the material determines the shape of the product particles but the type of mill may have even more marked effect. In this study these effects were tested using three materials and three types of mill. The types were a ball mill, an attrition bead mill and a jet mill. The test minerals were limestone, flue gas desulfurization (FGD) gypsum and waste gypsum from phosphoric acid plant. The size and the shape of the product particles were measured with an image analyzer. The shape of a particle was characterized using six different shape factors. The relevant shape features of the product particles were extracted by self-organizing maps (SOM) and then the particles were clustered with the SOM.

### Materials

Limestone was a general reference material. The feed limestone was dry Parfill limestone from Partek Oy, Lappeenranta. The median particle size was 28  $\mu\text{m}$ .

Gypsum products were selected due to their different crystalline structures and original particle shape (Figure 1).

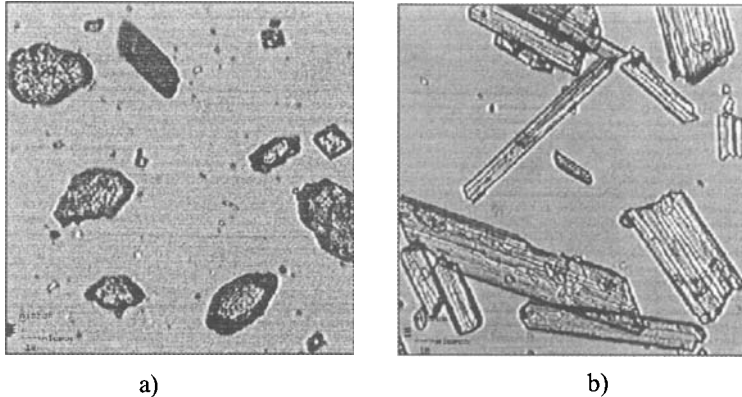


Figure 1: Feed particles a) FGD gypsum b) waste gypsum.

FGD gypsum was the product of flue gas desulfurization process of Meripori power plant. This FGD gypsum is moist crystalline high purity calcium sulfate dehydrate ( $\text{CaSO}_4 \cdot 2\text{H}_2\text{O}$ ) (Wirching 1994). The moisture of used FGD gypsum was 26%, and the median particle size was 36  $\mu\text{m}$ . The waste gypsum was obtained from Siilinjärvi phosphoric acid plant of Kemira Oy. This phosphogypsum is formed when raw phosphate reacts with sulfuric acid. This waste gypsum may contain phosphate residues and small amounts of sodium and fluorine compounds (Lutz 1995). The moisture of the waste gypsum was 29% and the median particle size was 32  $\mu\text{m}$ . Gypsum samples were dried before grinding in the ball, and in the jet mill.

### Size reduction equipment

The gypsum samples and limestone were ground in the laboratory with a ball mill, with an attrition bead mill, and with a jet mill. The breakage mechanism of a bead mill is mainly by attrition and in a jet mill it is by mainly impact. In a ball mill both previous mechanism are present. Minerals were ground as dry with the ball mill and with the jet mill and as wet with the attrition bead mill.

The ball mill was Bond test mill with the volume of 8.9  $\text{dm}^3$  (305×305  $\text{mm}^2$ ). The ball charge was specified numbers of balls from 15 mm to 40 mm in diameter, with a total weight of 20.13 kg. One kilogram of the material was ground 100 rounds with the rotational speed of 70 rpm that is 85% of the critical speed.

The attrition bead mill was a five liters vertical cylinder with the diameter of 160 mm and with the height of 250 mm. 3 kg of 2 mm glass beads formed the grinding media. The charge of 600 g of dry material was ground for ten minutes with the stirring speed of 500 rpm. The pin stirrer has 12 pair of pins that were 40 mm apart from each other. The rotational diameter of the stirrer is 120 mm. The concentration of the suspension was 30% by weight and 6 g of CMC (carboxy methylcellulose) was used in each batch as grinding additive.

The spiral type jet mill is used for fluid energy grinding of the materials. The particles



are forced to hit each other and the violent impacts reduce the size. The diameter of grinding chamber of the jet mill was 100 mm and the height was 15 mm. The material was fed into the chamber from one point and the compressed grinding air was fed with high speed through six nozzles. The diameter of the nozzles was 1.5 mm and the entering angle was  $43^\circ$ . The center outlet enhances the separation due to the centrifugal force. The diameter of the vortex finder was 45.8 mm. Product was collected into the filter bag through which the air exits the system. The pressure was 450 kPa.

### Measurement particle size and shape

Particle size distributions of the samples were analyzed in 0.2% NaHMP-water solution with the Sedigraph 1,500 particle size analyzer. For gypsum analysis the solutions were saturated with the gypsum to be analyzed to prevent gypsum from dissolving in the water. Figure 2 gives the measured size distributions for the feed materials.

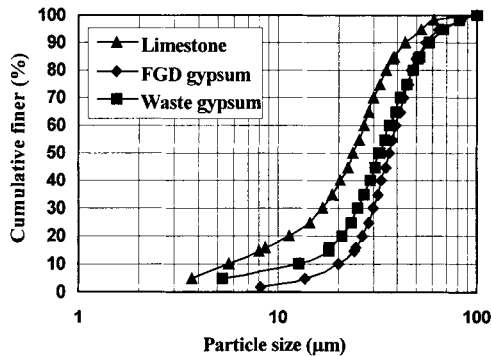


Figure 2: Particle size distributions of the test materials.

The shape and size of the product particles were measured with an image analyzer with an optical microscope. The shape of the particle was characterized by six shape factors that are the ratios of characteristic diameters of a particle (Oja et al., 1997). The image fields for the analysis were selected manually so that the fields contained only whole single particles. In the analysis of a product the size and shape of 500 particles was measured.

### Shape quantification

In particle technology Drescher et al., (1990) used clustering for shape connected to size and showed that technically relevant features can be extracted. In visual inspection of particle samples, it is easily seen that shape changes gradually in a process. SOM gives spatial order to the clusters and therefore is a suitable clustering method for particle technology. In this study each particle was described by seven variables, its size and six shape factors. For a sphere the value of all shape factors is one. Four shape factors characterize the elongation of the particle. One is a general shape factor and one of the shape factors characterizes concavities selectively.

For scaling, the variance of each variable was normalized over the selected training data and the scaled data was used for the SOM training (Oja et al., 1997). The shape and the size of the product particles can be evaluated when the particles used for training are clustered with the SOM.

## Results

The efficiency of the size reduction method can be evaluated with the reduction ratio ( $R = x_f/x_p$ ). In the attrition mill, the rotating stirrer sets the beads and the suspended particles in motion. The size reduction is caused mainly by attrition but also by impact (Becker, 1987). A jet mill does not have moving parts and the particles are accelerated in a fast gas stream and reduced by impact against each other and against the chamber wall (Hixon et al., 1990). In a ball the speed of the mill defines the reduction mechanism. When the rotational speed is 85% of the critical speed attrition and impact reduction are almost in balance. The aim was to obtain nearly the same size range for the ground particles.

Table I: Reduction ratios.

	Limestone		FGD gypsum		Waste gypsum	
	50%	80%	50%	80%	50%	80%
Ball mill	1.9	1.1	1.3	1.3	1.9	1.7
Bead mill	5.7	3.5	8.5	4.2	7.5	1.8
Jet Mill	3.5	2.5	1.7	1.7	2.6	3.0

Table I gives the reduction ratios for the studied cases. Bead mill was efficient reduction equipment for all materials. The reduction ratios for ball mill are small for all materials. For grainy crystalline FGD gypsum also jet mill has given low reduction ratio. However, all obtained products are in the measurement range of the image analysis. The effect of the mill type on the particle shape was tested separately for each material. The training data of SOM contained 1,500 particles for each material. Before the map training the size, topology and neighborhood type are selected. The size of the map depends on the application. In this study the map size was  $12 \times 10$ , topology was hexagonal and neighborhood type was the step function nicknamed 'bubble'. One unique feature of SOM is that each unit has fixed values for the parameters that can be visualized as SOM-surfaces. Figure 3a shows an example of the particle size SOM-surface for waste gypsum. Figure 3b gives the SOM-surface for the shape factor that characterizes concavities selectively. Figure 3c gives one of the elongation surfaces for waste gypsum. The other three elongation surfaces look almost the same. In these Figures the zero marks the mean value and the other values give distance from the mean divided with the standard deviation of the parameter.

Figure 3a shows that about 40% of the units are reserved for the particles larger than the mean particle size of the image analysis ( $43.7 \mu\text{m}$ ). Particles in these units are called large particles. Figure 3b shows that particles of these units have concavity shape factor smaller than the mean value (0.81). This means that these particles are more concave than most of the smaller particles. Some of these units are reserved for the larger particles that have similar concavity shape factor values as the smaller particles.

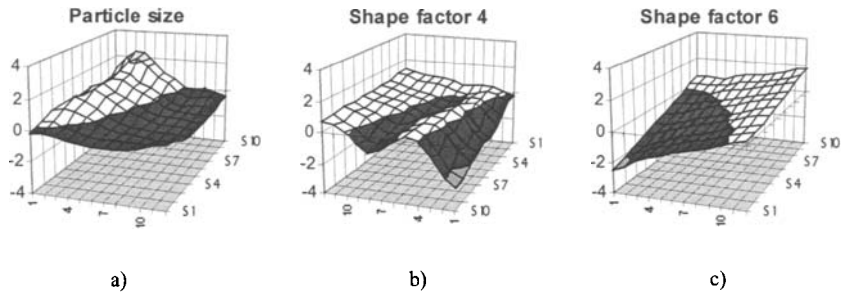


Figure 3: SOM-surface visualization of the SOM trained by 1,500 waste gypsum particles. x- and y-axis are the codes for the SOM-unit, and z-axis is the normalized value of the parameter.

These units are situated on the ridge seen in the Figure 3b. Please note that the view in the Figure 3b is from the opposite corner than in the Figures 3a and 3c. The SOM-surface of elongation (Figure 3c) divides the units into two parts around the mean value (0.72). The shape and size of the sample particles can be evaluated when the particles used in training are clustered with the SOM. When the waste gypsum particles of the ball mill are placed in the SOM units (Figure 4), they are distributed quite evenly throughout the SOM.

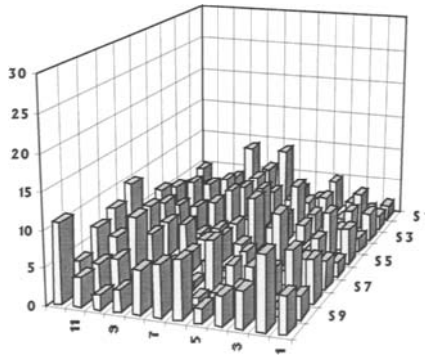


Figure 4: Waste gypsum particles ground with ball mill placed in the SOM units. The number of the particles in the sample was 500. x- and y-axis are the codes for the SOM-unit and z-axis is the number of particles in unit.

Only the units reserved for elongated particles have smaller number of particles. The feed particles of waste gypsum are needlelike particles that break into parts giving shorter particles than the feed particles. When the ground waste gypsum particles of the attrition bead mill are clustered with the SOM (Figure 5), most of small and large particles are placed in the units where the concavity shape values are larger than the mean value. These particles are called rounded particles. Also in this mill the number of particles placed in the units reserved for elongated particles is small.

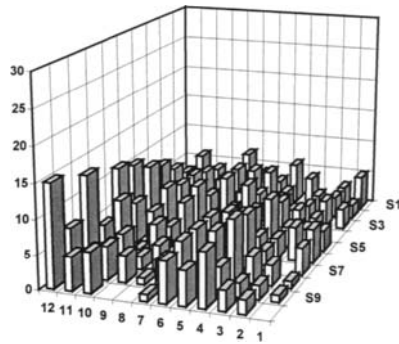


Figure 5: Waste gypsum particles ground with attrition bead mill placed in the SOM units. The number of the particles in the sample was 500. x- and y- axis are the codes for the SOM-unit and z-axis is the number of particles in unit.

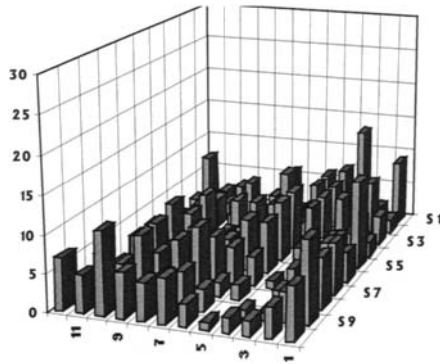


Figure 6: Waste gypsum particles ground with jet mill placed in the SOM units. The number of the particles in the sample was 500. x- and y- axis are the codes for the SOM-unit and z-axis is the number of particles in unit.

When the ground waste gypsum particles of the jet mill product are clustered with the SOM (Figure 6), the units reserved for rounded large particles are empty or almost empty. The units reserved for elongated or concave particles are filled. Same analysis was made for limestone and FGD gypsum particles. The SOM-surfaces and the clustering histograms of limestone are presented elsewhere (Tuunila et al., 1998). The results showed that with limestone the influence of the grinding method is significant. The particles of the jet mill product were clustered in units for concave particles. Both ball mill and attrition bead mill produced small and rounded particles. Especially with the attrition bead mill the portion of small particles in the product was significant. In the ball mill product the concave particles were totally missing.

For the FGD gypsum the differences in concavity shape factor values in the SOM units were very small and therefore the SOM-surface for concavity shape factor was flat. However, the jet mill produced the most concave particles.

## Conclusions

Particle shapes of three milling products for three different minerals were measured by image analysis system. The mills were an attrition bead mill, a ball mill and a jet mill. Limestone, FGD-gypsum and waste gypsum were the test minerals. The product particles were characterized by size and six shape factors, which were ratios of different characteristic diameters of particles. One shape factor is a general shape factor. Four shape factors characterize the elongation of the particle. One shape factor characterizes the concavities selectively.

Feature extraction methods based on the particle shape without size do not give technically relevant information about minerals and their behavior in a process. The typical features of mineral products were extracted by Self-Organizing Map (SOM) that gives spatial order the clusters. In this application a specific shape was not connected to a specific size, all size ranges had elongated and round particles as well as rough and smooth particles. Different mill products were clustered differently showing that the fraction of concave particles is a relevant shape feature for the grinding method. The concavities of the particles were characterized with the basic shape factor; the ratio between the convex perimeter and actual perimeter. The analysis showed that size reduction caused by impacts produce concave particles and size reduction caused by attrition produce rounded particles.

In generally it can be said, that there is a clear difference in the particle shape of different grinding methods, and that SOM method is useful in evaluation of particle size and especially shape data of ground material.

## References

- Becker, J.E., 1987. Attrition mill fine grinding of advanced ceramic powders. *Interceram* 6(1987), 55-57
- Drescher, S., Heidenreich, E. and Müller, G., 1990. Technologically relevant particle shape analysis. Part. Part. Syst. Charact. 7, 30-35.
- Hixon, L., Prior, M., Prem, H., Van Cleef, J., 1990. Sizing materials by crushing and grinding. *Chem. Eng.*, Nov. 1990, 94-103
- Holt, C.B., 1981. The shape of particles produced by comminution. *Powder Technology* 28, 59-63
- Lutz, R., 1995, Preparation of phosphoric acid waste gypsum for further processing to make building materials. *ZKG International* 2, 98-102
- Meloy, T.P., 1985. Distribution of original surface features during comminution. *Powd. Tech.* 41 (2), 197-202
- Oja, M. and Nyström, L., 1997. The Use of Self-Organizing Maps in Particle Shape Quantification. *XX International Mineral Processing Congress, GDMB, Aachen, Germany*, 141-150
- Trass, O., Koka, R., Papachristodoulou, G., 1995. Particle shapes produced in the Szego mill. Part. Syst. Charact. 12, 158-165
- Tuunila, R., Oja, M., and Nyström, L., 1998. The Relevant Shape Features of Ground Particulate Materials. *PARTEC 98, 7<sup>th</sup> European Symposium Particle characterization, Preprints III, NürnbergMesse GmbH, Nürnberg, Germany, (1998)*, 1167-1174.
- Wirching, F., Hüller, R., Olejnik, R., 1994. Gypsum from the flue gas desulphurisation plants - definitions and legislation in the European Communities in the OECD and in the Germany. *ZKG* 2, 65-69.

## **MAXXMILL - A FIELD REPORT ABOUT THE APPLICATION OF A STIRRED BALL MILL WITH INCREASED ECONOMIC EFFICIENCY FOR GRINDING OF MINERALS**

J. Sachweh

Maschinenfabrik Gustav Eirich GmbH & Co KG, D-74736 Hardheim, Germany,  
fax +49.06283.51325, e-mail: eirich@eirich.de

### **Abstract**

The MaxxMill is a newly developed agitated media mill, which differs essentially from stirred bead mills well-known already and used for many applications. Taking advantage of the performing principle of the stirred bead mills and by modification of the energy introduction into the grinding chamber, applications are now possible with this new mill, which remain inaccessible up to now for conventional stirred bead mills. The MaxxMill is now being used in fields where up to now the drum - type mill dominated. A much more flexible and low-cost production is allowed by the enlargement of the range of stirred ball mills respectively the replacement of drum-type mills. Above all, savings are possible by lower investment and operating costs. Moreover, higher product qualities can be achieved with the MaxxMill, frequently enabling an essential economic advantage.

*Keywords: grinding, agitator, mill, media mill, continuous, dry, wet*

### **Introduction**

In the past decades the agitated media mills succeeded more and more in comparison with the conventional grinding aggregates. If the production of very fine-grained products in a grain size range  $<1\div 100\ \mu\text{m}$  is concerned, this grinding method can be advantageously applied in many cases. Only few industries can manage without agitated media mill because by applying this mill type, highest product qualities can be achieved. As an example, the printing ink industry can be mentioned. In former times, nearly exclusively drum-type mills were used. However, nowadays the demands on the product increased in such a way that no competitive product can be obtained without agitated media mill. For this range of application, drum-type mills are no longer used with some exceptions only. Nowadays, the share of the market for drum-type mills has considerably decreased and will even more decrease in the coming years due to the development of the grinding technology.

### **Objective**

The worldwide pressure of cost reduction in production also requires numerous technical innovations as to crushing processes. In addition to the pressure of cost reduction, the environmental awareness becomes more and more important in the highly developed industrial countries. In particular, the decrease of energy requirement and emission of harmful substances and noise are concerned. Moreover, the increasing quality demand on the grinding processes is of great importance. The development of new products inevitably requires a higher demand on the raw

materials with regard to grain size and grain size distribution. Even if very conventional products are concerned such as floor tiles, requirements change in such a way that new grinding processes must be envisaged. Therefore, it is very important for the producer not to fixate on a certain product by selecting an inflexible grinding process. Even an universally planned grinding plant which seems to be somewhat more expensive for the moment will add up very rapidly if such a plant can be modified in case of new product requirements i.e. it is not necessary to build a completely new plant.

If new grinding processes are developed, the objectives can be combined as follows:

- reduction of investment costs:
  - favorable price of mill;
  - uncomplicated peripheral units;
  - low space requirement (building costs);
  - unproblematic integration in existing plants;
- reduction of operating costs:
  - low energy requirement;
  - reduced personnel costs;
  - low wear;
- facility for a flexible production:
  - simple change of product;
  - easy cleaning facilities;
  - adaptability of mill to different products and/or product requirements;
- reliable adherence to quality standards:
  - reproducible results;
  - defined and controllable grain size distributions;
  - fully automatic monitoring of product quality;
- high operational safety:
  - avoidance of disturbing sources;
  - automatic fault managing;
  - construction for easy servicing;
  - preventive plant maintenance;
- fully automatic control and monitoring.

The basic demand on an optimum crushing machine is the suitable energy transfer from drive of machine onto the grinding material. The energy flow should be carried out in a way that there will be only few transfer losses, that means the portion of the energy absorbed by the grinding material must be maximized (= degree of action).

The energy should be introduced into the grinding chamber so that the energy is changed into crushing energy as a matter of priority and not into heat. Therefore, the mill operation varies for each product. For example, a soft product requires less energy compared with a hard material. At the moment, the grinding balls touch each other, the energy must just be sufficient to crush the product. If more energy is introduced, wear and energy consumption will be higher because this energy excess will be changed into heat. This would induce unnecessary costs of the process. A too low energy introduction can be just as harmful because no grinding effect will be achieved when the grinding balls touch each other.

### Conventional technology

The drum-type mill is still widely held nowadays. Important application fields are, for example, grinding of ores, cement, carbon and ceramic raw materials.

Although drum-type mills are still frequently used, the fact cannot be hidden that an outdated technology is concerned with considerable disadvantages. These disadvantages are a result of the functioning mode of this mill.

Figure 1 shows a representation in diagrams of a drum-type mill. Energy introduction into the grinding chamber is made by the rotation of the grinding drum inducing the movement of the grinding balls in the grinding chamber.

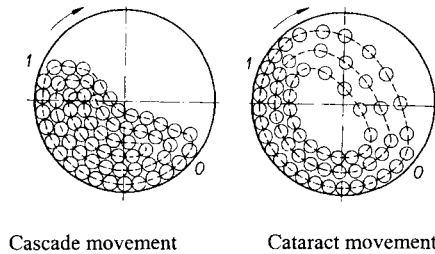


Figure 1: Ball movement in ball mills.

One distinguishes between the cataract and the cascade effect and in this way the moving behavior of the grinding balls is roughly described; the moving behavior mainly depends on the speed. In certain limits, the portion of knocking and rubbing stress can be controlled through the rotational speed of the grinding drum. However, the energy density in the grinding chamber can be hardly influenced because density is only determined by energy release at the moment the grinding balls fall down. According to equation (1), the energy of the grinding ball only depends on the height of fall and the ball weight. As both are generally fixed by the mill geometry, no free parameter (which can be influenced) remains.

$$E_{MK} = m_{MK} \cdot g \cdot \Delta h = \frac{m_{MK}}{2} v^2 \quad (1)$$

Even by increasing the rotational speed of the grinding drum, no more energy can be introduced into the grinding chamber because the mill content would be pushed against the mill walls by the centrifugal forces and crushing would stop completely. Equation (2) is applicable.

$$n_{krit} = \sqrt{\frac{g}{2\pi^2 D}} \quad (2)$$

Consequently, only the retention time of the grinding material in the grinding chamber remains to control the grinding result. Another disadvantage is that this retention time can last several hours or even several days due to the ineffective energy introduction.

A further consequence of this active principle is that no small grinding balls are allowed because they do not have the required minimum energy to crush the grinding material.



### MaxxMill agitated media mill for enlarged fields of application

Agitated media mills transfer the energy by an agitator to the grinding balls, thereby the height of the energy density can be controlled to a large extent via the rotational speed of the agitator. That means, a lot of energy can be introduced into the grinding material on a minimum space. In addition, the energy density can be adapted very easily to the grinding material and/or to the grinding task.

Contrary to drum-type mills, much more grinding balls of a smaller size can be used now. Conditioned by the agitator movement, even a very small ball receives a sufficient energy potential to cause a crushing effect in the grinding material. In this way, the effectivity of grinding (grinding time, energy requirement) and the achievable fineness of product will be decisively improved.

With the conventional agitated media mills - being used for approx. 50 years in industry - it was rendered possible to achieve many envisaged objectives.

However, up to now some tasks could not yet be solved in a satisfactory way with the conventional agitated media mills. Up to the present, the range of application is limited to raw materials having a grain size  $<200 \mu\text{m}$ . Coarser raw materials can be hardly processed. Moreover, it is a problem that the conventional agitated media mills can scarcely be applied for dry grinding up to now. Now it is intended to solve these tasks to be performed with the MaxxMill so that the advantages of the agitated ball mills can be utilized in further fields.

In the course of development of MaxxMill the objective is the extension of application of agitated media mills, that means problems should become solvable that were not overcome till now with the agitated media mills. In particular, tasks are concerned, in which dry grinding or fine grinding of coarse particles are requested. Therefore, we are not in direct competition with the conventional agitated media mills. In contrary, an intensive cooperation is intended in which the MaxxMill will be applied for grinding coarse materials so that a suitable basic material can be made available for final grinding in the standard agitated media mill.

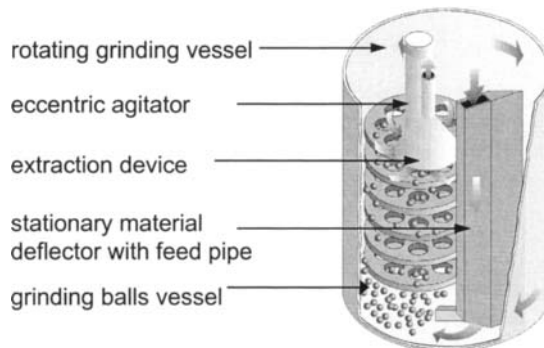


Figure 2: Functioning principle of MaxxMill.

Figure 2 shows the principal structure of the MaxxMill. The main components are the rotating grinding vessel, the agitator and the stationary material deflector with

integrated feed pipe. The agitator is eccentrically arranged to the grinding vessel center. Depending on the crushing problem, the rotational speed of the agitator can be concurrent or countercurrent to the grinding vessel rotation.

The grinding vessel is fed with grinding balls of size 3 mm to 10 mm up to a volume of max 90% (bulk volume). The used grinding ball size depends on the grain size of the grinding material and on the required fineness of product.

In wet and dry processes, the MaxxMill works continuously. The material to be ground enters the machine together with the carrier flow - that can for example be air or water - through the feed pipe near the vessel bottom. There, the material is drawn into the grinding chamber by the vessel rotation and mixed with the grinding balls.

The grinding effect in the grinding chamber is a result of the energy introduction via the agitator, the variable compression of the grinding ball filling in the agitator area, the force in the bottom area and the generation of shearing forces in front of the material deflector. The crushed product is continuously extracted from the upper ball layer by using the extraction device. Normally, the grinding balls are not extracted due to their force of gravity. However, in case of higher product viscosity, a protective sieve must be installed at the outlet for retaining the balls.

According to the demands regarding wear and product contamination, machines are available with different lining variants. The parts coming into contact with the process material can be alternatively equipped with wear elements out of steel, polyurethane or ceramics. Balls out of steel or ceramics are used as grinding media.

By combination of the stress mechanisms there are considerable advantages compared with conventional crushing plants as mentioned hereafter:

- high capacities yet small space requirement for the plant;
- advantageous energy distribution in the grinding chamber by the rotating vessel;
- optimum adjusting facilities of grinding conditions by variation of rotational speeds for agitator and grinding vessel resulting in low energy consumption;
- no danger of ball blocking even if densely packed and hence improved crushing effect and high operational safety;
- even very coarse grinding particles are permitted - these particles cannot deposit or get jammed in the mill;
- no dead spaces;
- combination of grinding and mixing processes;
- solid and liquid components can be added without premixing;
- material caking at wall and bottom are prevented.

### **Fields of application**

The application of MaxxMill is always useful if the following tasks must be performed:

- dry or wet grinding:
  - raw materials  $<2\div 5$  mm;
  - product size  $<20\div 500$   $\mu\text{m}$ ;
- combined grinding and mixing processes;
- disagglomeration and dispersing;
- activation of grain surfaces.

Prior to introduction on the market, the MaxxxMill was intensively investigated and assessed in the factory's own test center. Production tests with the most different materials were performed so that it has been possible in the meantime to fall back on extensive experiences if dimensioning of a grinding plant is desired. Nevertheless, it is recommended to perform a test in the test center for each application and thus to back up the made thesis.

In the industrial scale as well, a multitude of experiences is available. After having mounted some pilot plants and having performed extensive production, very valuable long-term experiences could be gained. It was confirmed by customers that the MaxxMill represents a serious alternative compared with the conventional process.

In the present phase, production is still performed with smaller machine sizes having a throughput of 4-6 t/h; in this phase potential customers are wanted especially in the ceramic industry. However, for the future, larger mill sizes up to 25 t/h are planned enabling the development of even more application fields.

## Examples

### *Building materials*

The first MaxxMill for the building industry has been sold to an Italian company and runs very successfully since 1997. In this case, a relatively small agitated media mill is concerned with a grinding chamber volume of 160 l. Milk of lime is to be ground which is available as pumpable suspension. It is aimed to reduce the grain size portion  $>0.2$  mm, ranging between 8% and 10%, to a value  $<1\%$ . Grain-size distributions of raw material and of the product are shown in Figure 3.

The material is continuously pumped into the mill and drawn off in the same way from the mill so that a constant filling level in the mill is guaranteed.

At the present, the mill is run with a throughput of 3 m<sup>3</sup>/h and the operating time ranges over 22 h/day.

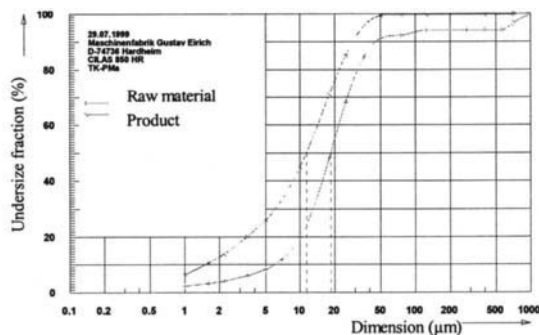


Figure 3: Grinding of milk of lime.

There also exist many promising first signs regarding dry grinding of fly ash which can be used - in finely ground state - as cement substitute. For grinding cullets to  $<40$  µm the MaxxMill has already shown good results. In ground state, this material is used for the production of insulation boards. Grinding of cement can also be carried out very well. However, in most cases the required throughput is so high that in

exceptional cases only the MaxxMill can be used. It is however quite possible to apply the MaxxMill for special applications if the throughput ranges below 15 t/h.

### Ceramics

In this connection the task of a company from sanitary engineering is presented as an example. A white glaze was to grind down to a  $d_{50}$ -value of approx. 4  $\mu\text{m}$ . No residues were allowed in the range  $>63 \mu\text{m}$  and it was only permitted to slightly raise the portion of grains  $<1 \mu\text{m}$ . The glaze material mainly consisted of quartz powder, kaolin, feldspar and dolomite. Pre-ground raw materials were used, the grain size of which already ranged mostly below 100  $\mu\text{m}$  (Figure 4). By adding water a density of approx. 1.9 kg/l was adjusted. During voluminous tests it was confirmed that the envisaged target can be achieved and even a higher fineness of product can be obtained.

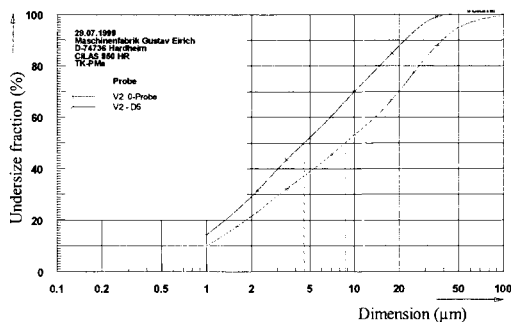


Figure 4: Glaze grinding: size distribution.

The grain size of the product is shown in Figure 4. There it can be recognized that the grain size distribution can be achieved without any problems for which the wet drum-type mill requires 8 h. Moreover, for the following processes it is of advantage that the MaxxMill works continuously and the product can be further processed immediately. In principle, an online grain size analysis could be applied enabling a production with stable product parameters, that means the plant parameters can be automatically readjusted if the product quality is to be changed. As a further advantage it can be mentioned that the specific energy consumption of 16 kWh/t is very low. The following Figure 5 shows the comparison of space requirement of MaxxMill compared with the presently used drum-type mills. It can be seen very well that the MaxxMill requires much less space and consequently smaller production space is occupied. This advantage is of great importance in cases where existing plants are to be extended and the production building size is limited.

Grinding glaze bodies with the MaxxMill is very interesting in cases in which less high-quality raw materials are used as in the presented example.

It is imaginable to use raw materials with an initial grain size of 1÷2 mm that means there would be savings in supplying the glaze raw materials. For manufacturers of glaze bodies (there normally larger quantities are occurring) dry grinding of frits is for example very interesting so that these companies can produce ready glazes, which must not be ground or very shortly only by the ultimate consumer. In addition to glaze grinding, grinding of ceramic bodies is very profitable.

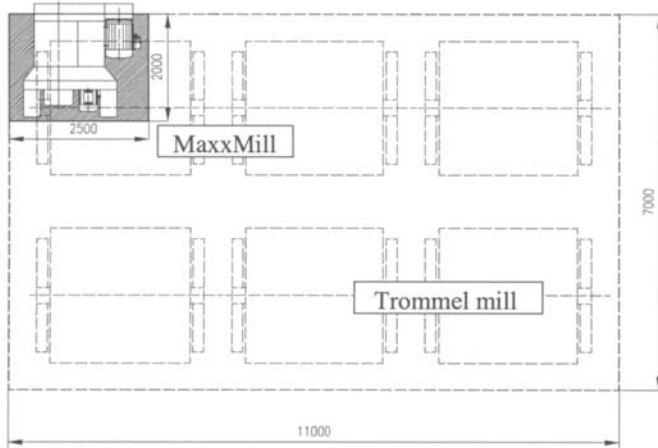
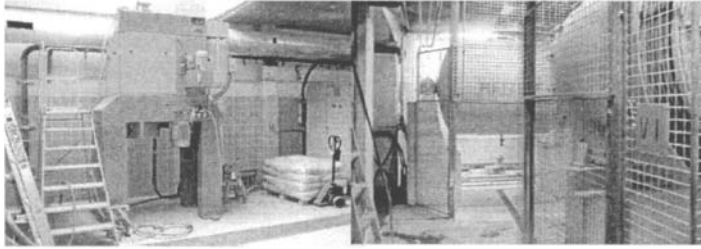


Figure 5: Comparison of space requirement drum-type mill and MaxxMill, example of a glazing process.

Because of their higher throughput, larger mills are used resulting in a higher saving potential. It is possible to grind the solids separately or together with the clay; the selected course depends on the required destination of process. Another possibility is the separate grinding of clay, which must be dissolved prior to grinding. If the clay still contains organic impurities it will be useful to screen the material prior to treatment in the MaxxMill, so that these foreign matters will not be crushed in the following grinding process.

#### *Sundries*

In addition to the before mentioned examples of application there exist many other applications. However, only some of these applications are mentioned at this point which have proved to be suitable after having performed tests in the test center. Hereafter some examples:

- grinding of raw materials for the production of ferrite;
- grinding of magnesium hydroxide for the production of feeding stuff;
- making cement hydrophobic;
- mixing and disagglomeration of pigments;
- grinding and delamination of mica;
- grinding of coke.

## THE KELSEY FINE AUTOGENOUS GRINDING (FAG) MILL

B. Kelly, D. Geraghty

Geologics Pty. Lt. 34 Aldershot Rd. 5160, Lonsdale, Australia

### Abstract

Geologics Pty. Lt. with headquarters in Adelaide, South Australia, are widely known for incorporating innovative engineering concepts in development of mineral processing equipment such as the Kelsey Centrifugal Jig. Geologics engineers have recently turned their attention to fine particle breakage technology, leading to the development of the Kelsey Fine Autogenous Grinding (FAG) Mill.

The Kelsey FAG Mill offers a unique particle fracture environment, which concentrates the localised strain energy necessary to induce breakage by simultaneously compressing and mobilising particles under the influence of a high acceleration field in a vertically oriented cylindrical grinding chamber.

The high acceleration field is produced by spinning the chamber about its vertical axis.

Intense inter-particle breakage stresses are generated within the compressed particle bed by the mobilizing action of a static disc placed co-axially within the grinding chamber and fixed in the horizontal plane. The rotational speed and diameter of the chamber determines the centrifugal force applied in compressing the particle bed.

The exceptionally high rate of comminution, which characterizes the mill, is achieved primarily by inducing high shear forces and rapid shear rates, which transfer a relatively large proportion of the available input energy directly to the particles as fracture promoting stress.

A further unique feature of the FAG mill is that in contrast to other fine and ultra-fine grinding systems no separate medium is required to transfer strain energy to particles.

Pilot mill performance data presented for mineral slurries with a range of hardness and textural characteristics indicates that the mill has the potential to significantly extend the present practical and economic boundaries of fine particle comminution.

*Keywords: autogenous, grinding, ultra fine, mill, efficiency*

### Introduction

The Kelsey Fine Autogenous Grinding (FAG) Mill offers the minerals industry a new fine grinding environment which drives inter-particle shear and abrasion fracture rates to unprecedented levels. This paper introduces the mill at pilot stage. Presents results indicating that the mill has the potential to significantly extend the present practical and economic boundaries of fine particle comminution with respect to capital and operating costs, maximum feed size, reduction ratios, specific energy consumption, throughput per unit volume and energy utilization.

### Pilot mill description

The pilot mill illustrated in figure 1 consists of a 440 mm internal diameter by 83 mm deep fabricated mild steel grinding chamber with a volume of 12.5 dm<sup>3</sup>. The chamber carries a 6 vein feed inlet impeller and a 175 mm diameter product discharge ring. The chamber rotates about its vertical axis and is driven by a 22 kW motor over a speed range of 800 to 1,200 rpm. Acceleration fields generated over this range vary from 100·g to 400·g.

The fixed feed pipe concentric with the drive shaft carries a fixed 10 mm thick mild steel disc which is suspended within the grinding chamber, 25 mm above the product discharge ring. The fixed disc has two 10 mm diameter water by-pass ports. The mill is suspended from the drive shaft assembly and supported by a free standing 75 mm RHS steel frame. The mill has an interchangeable 22 dm<sup>3</sup> grinding chamber capable of housing up to four discs.

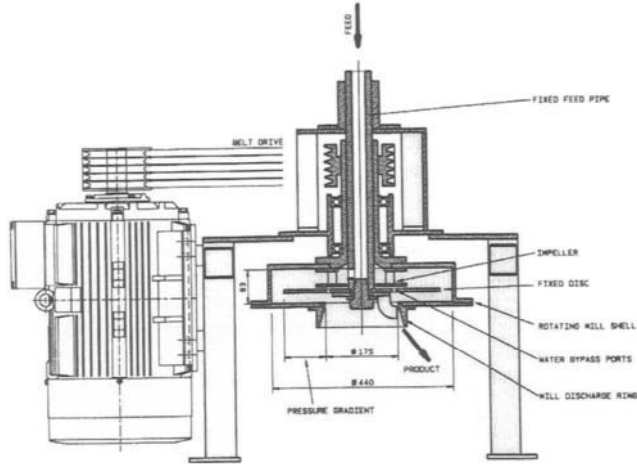


Figure 1: Pilot mill.

### Concept

The concept, which led to the development of the mill, involves the creation of a unique particle fracture environment, which concentrates the localized strain energy necessary to induce breakage by simultaneously compressing and mobilising particles in a cylindrical grinding chamber under the influence of a high acceleration field. The rotational speed and diameter of the grinding chamber determines the centrifugal force applied in compressing the particle bed. The intense inter-particle breakage stresses generated by this action induce high shear forces and rapid shear rates, which transfer most of the input energy directly to the particles as fracture promoting stress.

### Pilot mill operation

Mineral slurry is fed through the fixed vertical feed pipe and discharges into the grinding chamber through a port in the drive shaft. The feed inlet impeller integral with the grinding chamber picks up and accelerates feed particles into the packed particle bed which lines the inside of the grinding chamber.

Most of the water separates from the feed slurry and is diverted through by-pass ports in the fixed disc. The finest product particles are progressively displaced from the active zone of the compressed particle bed and carried to the mill discharge ring with the displaced water.

### **Breakage mechanisms**

The dominant breakage mechanisms are shear and abrasion fracture. These mechanisms occur in an environment, which enables the strain energy causing fracture to be applied to the total population of mobilized particles. A key feature of this environment is its capacity to sustain effective fracture by the same mechanisms at high expansion rates of particle population. As well as inducing shear and abrasion, the compressive and tensile stresses exerted also induce some brittle type fracture. The combination of these mechanisms enables comminution to progress from relatively coarse sizes through to ultra-fine sizes within a single pass of the mill.

### **Test procedure**

The test program was conducted using pilot facilities at Geo Logics Pty Ltd Manufacturing and Development Plant in Lonsdale, South Australia.

A 200 l capacity pulp storage agitator was used to provide a homogenous feed for each of the tests.

A peristaltic pump provided an accurate and constant feed rate of mineral slurry to the mill.

Product samples were taken at 1 minute intervals together with pulp temperature and mill motor amperage measurements.

Depending on mass flow rates, steady state conditions were reached within two to three minutes. Constant power-draw and discharge pulp-temperature confirmed steady state. Test runs were limited to ten minutes duration due to the limited sample size and high feed rate demands.

Particle-size distributions were measured using an in-house Coulter LS130 particle size analyzer. Each result was determined from the average of three measurements.

A Malvern particle size analyzer at an external laboratory was used on a selection of samples to validate the accuracy of the Coulter.

### **Test results**

#### *Pilot mill performance*

Table I presents the results of pilot tests on silica, magnetite, pyrite and sphalerite mineral slurries over a range of feed sizes and operating conditions.

A single disc 12.5 l chamber was used for the coarser silica and magnetite feed slurries while a four disc 22 dm<sup>3</sup> chamber was used to provide additional residence time for the finer pyrite and sphalerite feeds.

The silica result was outstanding with high throughput at 425 kg/h and a size reduction from 270 µm to 5 µm. for a specific energy consumption of 16.5 kWh/t.

Magnetite size-reduction from 293 µm to 50 µm for a similar specific energy consumption was less dramatic but still impressive for single pass open circuit operation.

The obvious differences in operating conditions which partly account for the lower magnetite reduction ratio include; the 12% higher throughput of 470 kg/h, the 33% reduction in acceleration field strength from 215 g's to 145 g's and the 11% reduction in disc diameter from 420 mm to 375 mm.



Table I: Pilot mill performance for different minerals.

		Silica	Magnetite	Pyrite	Sphalerite
Feed size ( $F_{80}$ )	( $\mu\text{m}$ )	270	293	18	16
Prod. size ( $P_{80}$ )	( $\mu\text{m}$ )	5	50	7	10
Specific energy	(kWh/t)	16.5	16.9	25.1	10.3
Throughput	(kg/h)	425	470	231	396
Reduction ratio		54	6	2.6	1.6
Residence time	(s)	32	40	80	48
$\Delta\text{Temp}$	( $^{\circ}\text{C}$ )	10	17	22	9
Acceleration field	( $\text{g}'\text{s}$ )	215	145	100	100
Solids in feed	(%)	45	52	52	52
Power intensity	( $\text{kW}/\text{m}^3$ )	1750	1750	1000	1000
Bond work index	(Wi)	4.5	23	17.6	14.7
Disc diameter	(mm)	420	375	420	420
Number of discs		1	1	4	4

Although mineral characteristics such as size hardness and texture can also become critical variables the selection of test operating conditions was largely influenced by available power.

It became clear during testing that a significant increase in power above the 22 kW available would be necessary to optimize mill performance with respect to both reduction ratio and throughput.

Autogenous grinding of pyrite from 19  $\mu\text{m}$  to 7  $\mu\text{m}$  at 231 kg/h in a 22 dm<sup>3</sup> chamber for a specific power consumption of 25 kWh/t presents a highly competitive ultra fine grinding option. However, the result is typical of the increasing residence time and power required for grinding fine feed (in this case, less than 20  $\mu\text{m}$ ) to product sizes below 10  $\mu\text{m}$ .

It became necessary to induce greater particle mobilization and create a broader active zone within the mill by using discs with radial pins while operating at relatively low acceleration field strengths of 100-g.

Although these conditions enable the finer feeds with wider particle size distributions to more effectively displace the finest product particles from the active zone, the reduced particle bed compression decreases inter-particle energy transfer and hence breakage rates.

Disc and chamber design modifications currently being assessed will minimize the inefficiencies associated with finer feeds by establishing more effective particle bed mobilization at higher acceleration field strengths.

The sphalerite result achieved under operating conditions similar to those for pyrite illustrates the throughput and specific power consumption gains that can be balanced against more modest reduction ratios.

#### *Mass flow-rate tests*

Further tests were carried out on fine (40  $\mu\text{m}$ ) pyrite feed to examine the effect of mass flow rate changes on mill performance at constant acceleration field strength. The results are presented in table II.

Table II: Pyrite - Constant (g) force, varying feed rate.

F <sub>80</sub> ( $\mu\text{m}$ )	P <sub>80</sub> ( $\mu\text{m}$ )	Throughput (kg/h)	Reduction ratio	Specific energy (kWh/t)	Calc. Bond (Wi) (kWh/t)
39	12	187	3.2	34.5	27.1
41	25	570	1.6	9.2	22.4

The results show that the mill remains capable of delivering a high level of operational flexibility even when dealing with the more demanding fine feed duties. Although the mill returned a modest reduction ratio of 1.6, the three fold increase in mass flow rate from 187 kg/h to 570 kg/h was effectively accommodated at the same field strength with a compensating reduction in specific power consumption from 34.5 kWh/t to 9.2 kWh/t.

The capacity of the mill to sustain a predictable balance between product size and power consumption under the above conditions is largely a function of the intrinsic particle classification process that occurs due to the high centrifugal force exerted. Similar mass flow rate tests at constant acceleration field strengths were carried out on the finer (22 to 24  $\mu\text{m}$ ) sphalerite feed and the results are presented in Table III.

Table III: Sphalerite - Constant (g) force, varying feed rate.

F <sub>80</sub> ( $\mu\text{m}$ )	P <sub>80</sub> ( $\mu\text{m}$ )	Throughput (kg/h)	Reduction ratio	Specific energy (kWh/t)	Calc. Wi (kWh/t)
22	9	252	2.5	24.6	19.6
24	10	281	2.3	17.9	17.2

Although the increase in mass flow rate of 12% from 252 kg/h to 281 kg/h was small relative to the pyrite tests, the response pattern was similar.

#### Breakage efficiency

A selection of results from magnetite pyrite and sphalerite tests presented in tables IV, V and VI respectively.

The tables illustrate the capacity of the mill to maintain relatively constant levels of breakage efficiency for a specific mineral over a range of fine grinding duties.

Table IV: Magnetite test results.

F <sub>80</sub> ( $\mu\text{m}$ )	P <sub>80</sub> ( $\mu\text{m}$ )	Throughput (kg/h)	Rate of reduction	Specific energy (kWh/t)	Calc. Wi (kWh/t)
22	7	195	3.4	46.2	26
293	50	470	5.9	19.2	23

Table V: Pyrite test results.

F <sub>80</sub> ( $\mu\text{m}$ )	P <sub>80</sub> ( $\mu\text{m}$ )	Throughput (kg/h)	Rate of reduction	Specific energy (kWh/t)	Calc. Wi (kWh/t)
19	7	231	2.7	31.2	21.0
41	26	570	1.6	9.2	22.4

Table VI: Sphalerite test results.

F <sub>80</sub> ( $\mu\text{m}$ )	P <sub>80</sub> ( $\mu\text{m}$ )	Throughput (kg/h)	Rate of reduction	Specific energy (kWh/t)	Calc. Wi (kWh/t)
29	18	379	1.6	8.0	16.4
31	10	288	3	22.4	16.9

Adopting the Bond work index (Wi) calculated from specific energy consumption as a breakage efficiency indicator, it can be seen that the indices remain reasonably steady over the range of duties covered for specific minerals. Inefficiencies experienced with finer feeds and products are less significant than those associated with conventional fine grinding systems. The high 'g' environment promotes the more effective shear and abrasion fracture mechanisms as well as inducing separation and displacement of the finer size fractions to product. Input energy transfer is therefore mainly via the coarser size fractions.

#### Product size-distribution

Feed and product particle-size distributions for the silica tests, detailed in Table I, are shown in Figure 2.

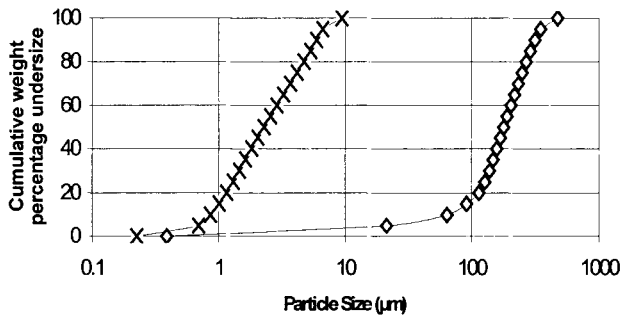


Figure 2: Particle size-distribution for silica.

The size distributions illustrate that under favorable conditions the mill will characteristically return narrow product particle size distributions. The silica product was all minus 10  $\mu\text{m}$  with a  $p_{80}$  of 5  $\mu\text{m}$  and a  $p_{50}$  of 2.3  $\mu\text{m}$ . Only 15% by weight were less than 1  $\mu\text{m}$ . The narrow size-distribution is a function of the intrinsic particle classification process that occurs due to the high centrifugal force exerted. The finest particles are progressively displaced to product by the incoming feed.

#### Effect of fine feed

Feed and product particle size distributions from a further pyrite test are shown in Figure 3. The pyrite feed size distribution, in contrast to the silica feed, is wide and fine with a  $p_{80}$  of 40  $\mu\text{m}$  and a  $p_{50}$  of only 12  $\mu\text{m}$ .

The combination of relatively low g's and a disc with radial pins was used to assist displacement of the finest product particles by creating a broader active zone within the chamber.

Despite the lower particle bed compression and reduced inter-particle energy transfer under these conditions, single pass performance remained impressive with a reduction ratio of 3.9 for a throughput of 313 kg/h and a calculated Bond  $W_i$  of 23.5.

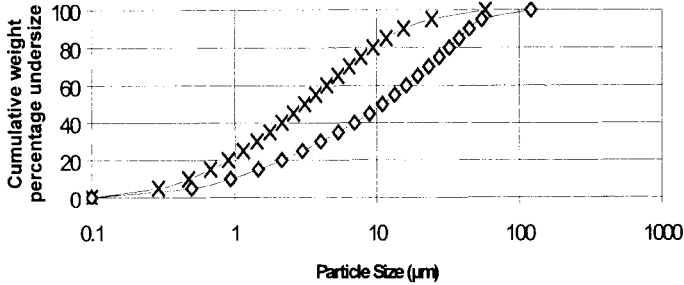


Figure 3: Particle size-distribution for pyrite.

Splitting out of the  $<5 \mu\text{m}$  feed fraction ahead of the mill is expected to significantly improve performance by enabling operation at higher  $g$ 's.

## Conclusions

Results of the pilot work support the assertion that a unique breakage environment has been established and that, it is this environment which enables fine and ultra fine grinding to proceed autogenously at high breakage rates and high levels of power efficiency.

Present indications are that the mill has the potential to efficiently span duties ranging from conventional secondary through to ultra fine.

The autogenous feature of the technology, in particular at fine and ultra fine sizes, can reduce operating costs for grinding by as much as 50%.

The new technology has far reaching flow sheet design implications. Grinding plants can be simple open circuit, very compact in size and yet capable of high throughputs, high reduction ratios and high power efficiencies. These advantages along with the absence of grinding media will enable demanding product specifications to be met at low capital and operating costs.

Engineers will be provided with an additional design dimension within which existing flow sheets can be economically expanded and new flow sheet design options broadened to include processing stages, which would otherwise be considered uneconomical.

## THE EFFECT OF USING CONCAVE SURFACES AS GRINDING MEDIA

F.L. von Krüger\*, J.D. Donda<sup>o</sup>, M.A.R. Drummond\*, A.E.C. Peres<sup>o</sup>

\*Escola de Minas, UFOP, Ouro Preto, Brasil,

<sup>o</sup>Samarco Mineração, Mariana, Brasil,

<sup>o</sup>Escola de Engenharia, UFMG, Belo Horizonte, Brasil

### Abstract

This paper presents an analysis of the effect of utilizing crushing bodies of special shapes as grinding medium. The crushing bodies utilized in this study were modified spheres with a concave portion.

Grinding efficiency is expected to increase with the increasing available surface area of the grinding medium. A grinding ball with concavity has a smaller volume than a sphere of the same radius. Therefore, the convex-concave ball has a smaller mass with the same surface area, providing a larger specific surface area and a greater charge density. In the case of contact between the convex and concave surfaces, the probability of a crushing action over larger particles is higher than for smaller particles, causing preferential grinding of larger particles.

Experiments were carried out in laboratory and consisted of batches of the same feed, ground first with conventional grinding balls. Part of the grinding medium of conventional grinding balls was then replaced by special concave-convex balls, increasing the specific surface area of the grinding balls. The results of the grinding experiments showed an effective selectivity of the grind, and in some cases, an increase in the fineness of the ground product, for a percentage of the concave area in the charge up to about 10%. Increasing the percentage of the concave bodies, the relative motion of the charge units became more irregular, causing a negative impact on grinding efficiency.

*Keywords: grinding, crushing bodies, concave surfaces, grinding efficiency, grinding selectivity*

### Introduction

The grinding media most often employed in fine grinding are spheres and truncated cones (Cylpebs). Other shapes, like cylinders, cones, cubes and hexagons, were studied. This paper analyzes the effect of utilizing crushing bodies of special shapes as a grinding medium. The crushing bodies utilized in this study were modified spheres with a concave portion.

This shape, the new concave bodies, when compared with the spheres, presents a larger specific surface area.

The consequence of this higher specific surface area could be an increase in the grinding efficiency. Another feature that should be put in consideration is the grinding selectivity that arises from the area of contact between concave and convex surfaces. The large particles protect the small ones, similar to the action of the rods in the rod mills.

The comparison between the concave bodies and the spherical bodies can be done in the same fashion as the comparison between spheres and Cylpebs. Grinding tests were carried out with balls and concave bodies, varying the percentage of concave area in the mill charge.

**Background on grinding media**

Wills (1997) says: "grinding within a tumbling mill is influenced by the size, quantity, the type of motion and space between the individual pieces of the medium in the mill." Grinding is a random process subject to the laws of probability. The degree of grinding of a particle depends on its probability of entering a zone between pieces of grinding media, and the probability of contact with the grinding media after entry. Grinding takes place by several mechanisms, including impact or compression, due to forces applied almost normally to the particle surface, chipping due to oblique forces, and abrasion due to forces acting parallel to the surfaces. These mechanisms deform the particles and change their shape, beyond certain limits determined by their degree of elasticity, to achieve breaking.

MINTEK (1991) reports that non-spherical grinding media, such as cones or Cylpebs, have been manufactured and marketed on the basis of a number of claimed advantages over spheres. A substantial reduction in foundry costs is possible, as a result of the high yield of metal in finished castings. For an equal mass of grinding charge, such shapes provide a higher grinding surface area, hence, it is claimed, more efficient grinding is attained.

While testing cones and Cylpebs against balls, it was found that all three types of grinding media performed well, if the feed rate of the ore was kept relatively low. It was further found that neither cones nor Cylpebs achieved the same fineness of grind as an equal charge of balls, even though the surface-area of the non-spherical media was larger, casting doubt on the previously held assumption in this regard.

Relative movement of units in a grinding charge plays an important role in grinding, particularly when conditions are predominantly abrasive. Such relative motion is expected to be easier with spherical media than non-spherical media, and to play a dominant role in the fineness of the grind.

According to Cloos (1983), the grinding media should have the largest possible surface area, to provide a suitable contact surface with the material being ground, and be the heaviest possible, in order to have the necessary energy for breaking the ore particles. These requirements must be balanced, since the heavier the individual grinding media, the smaller the specific surface developed.

The advantage of Cylpebs over balls lies in the surface area, and linear and point contact, which happens to Cylpebs, versus point contact only, which happens to spheres. As a result, the product will have a narrower-size spectrum than that verified by analogous rod mill grinding.

By studying the geometrical attributes of balls versus Cylpebs, other advantages become clear.

If we examine the two shapes, both made of the same material and having an equal diameter, the Cylpebs will have 50% greater surface area, 50% more weight and 50% more volume.

It follows that for a specific diameter, the specific surface of the areas is the same. Further advantages of media surface area result from density and packing comparisons of the two shapes.

Donda (1998) compared balls and Cylpebs of the same weight. Cylpebs have 15% more surface area than balls.

The Cylpebs have a lower cost, and it was assumed that they have a larger grinding efficiency, due to their larger surface area.

Laboratory tests show that, in spite of the larger surface area of the Cylpebs, the BSA (Blaine surface area) of the product was 7.5% less for the Cylpebs of the same weight as 30 mm diameter balls, and 11% less for the Cylpebs of same weight as 25 mm balls. In spite of the 15% larger surface area of the Cylpebs, that difference did not result in a larger surface generation in the product.

Sepulveda (1990) states that the critical, controlling variable for ball charge optimization is the specific area exposed to impact by the charge. There is an optimum specific charge area exposed, which maximizes the grindability of any particular ore under consideration.

### Assumptions

Grinding efficiency increases with an increase in the available surface area of grinding medium. A grinding ball with a concavity has a smaller volume than a sphere of same radius.

Therefore, the convex-concave ball has a smaller mass with the same surface area, providing a larger specific surface area.

A concave surface allows a larger contact area with convex surfaces than the contact area between two convex surfaces; therefore, a concavity may simultaneously exert stress on a larger number of particles than a convex surface.

The particles that are caught between the convex portion of a grinding ball, and the concave portion of another, would be trapped under the crushing action of the grinding medium for a longer time than in the case of two convex surfaces, where the particle would be under crushing action for a shorter contact time.

In the case of contact between convex and concave surfaces, the probability of crushing action over larger particles is greater than for smaller particles, causing preferential grinding of larger particles.

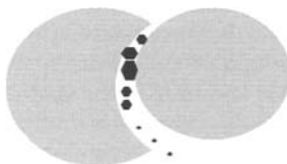


Figure 1: Action of the concave grinding bodies.

### Design of experiments

Experiments were carried out in a laboratory and consisted of batches of the same feed that was first ground with conventional grinding balls. Then, part of the grinding medium balls was replaced by concave-convex balls, increasing the specific surface area of the grinding charge.

The ore used was an iron ore concentrate from a commercial plant.

Two types of concave balls made of cast iron were used, as sketched in Figure 2.

The main characteristics of these bodies are presented in Table I.



Figure 2: Concave grinding bodies.

Table I: Concave crushing bodies.

Crushing bodies	Diameter (mm)	Weight (g)	Overall area (cm <sup>2</sup> )	Concave area (cm <sup>2</sup> )
Type I	38.8	181	47.3	9.8
Type II	38.8	148	47.3	13.4

The radius of the concavities is the same as the sphere radius.

The harmonic mean size (HMS) is defined as the harmonic mean of the size fractions, weighted according to their mass and expressed approximately as:

$$HMS = \frac{\sum_{i=1}^{n+1} m_i}{\sum_{i=1}^{n+1} m_i / x_i} \quad (1)$$

where:

- $m_i$  is the mass fraction of the  $i_{th}$  screen fraction;
- $x_i$  is the arithmetic mean of the size limits of the  $i_{th}$  screen fraction.

The harmonic mean size is a single value that provides an indication of the relative fineness of the grind obtained from a mill operating under different conditions, or using different types of grinding media under the same milling conditions.

#### First round of experiments

The following parameters were adopted for the first round of experiments: mill dimensions, 20×30 cm<sup>2</sup>, 67 rpm (72.0% of critical speed), 38% filling, 17.5 kg ball charge, 2.975 kg ore charge, 697 ml water (81% solids), 20 min, 40 min and 60 min grinding time.

In this round of experiments, only the Type I concave was used, and just one size of balls, with the same weight as the Type I concave, as seen in Table II.

Table II: Charge composition for the first round of tests.

Test	Crushing bodies of the charge (% wt)					
	1A	2A	3A	4A	5A	6A
Sphere 36.2 mm diameter	100	80	60	40	20	0
Type I concave	0	20	40	60	80	100
Total charge area (cm <sup>2</sup> )	3,787	3,945	4,102	4,313	4,430	4,587
Concave area of the charge (%)	0.0	4.7	9.1	13.5	17.3	20.8



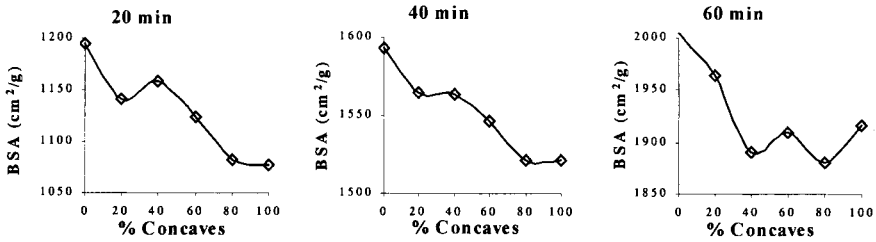


Figure 3: Blaine surface area (BSA) for the first round of tests, as a function of the percentage of type I concave crushing bodies in the charge.

The Blaine surface area (BSA) data for the ground products, as seen in Figure 3, have a clear tendency to be reduced with an increase in the concave bodies of the charge.

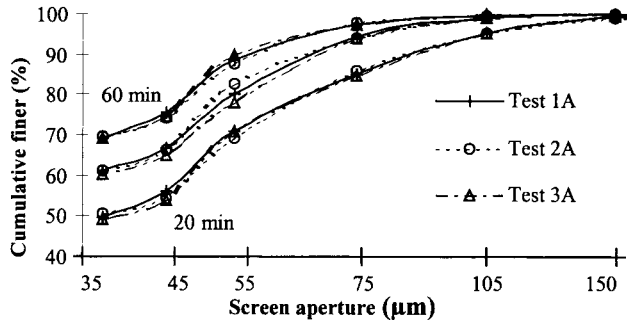


Figure 4: Size distribution of the first round of tests. The curves for the other tests are not plotted.

Table III: Harmonic mean size (HMS) for the ground product of the first round of tests.

Test	Feed	1A	2A	3A	4A	5A	6A
20 min grinding							
HMS total	36.30	28.37	28.31	28.54	29.01	28.83	28.66
HMS >37 µm	70.67	60.19	61.46	60.63	61.68	60.45	60.61
40 min grinding							
HMS total	36.30	24.94	24.93	25.29	25.17	25.26	25.23
HMS >37 µm	70.67	55.67	54.94	56.81	55.59	55.71	56.51
60 min grinding							
HMS total	36.30	23.06	23.08	23.10	23.32	23.28	23.38
HMS >37 µm	70.67	52.00	52.90	51.72	52.75	52.56	52.71

In most cases, the larger the concave area in the charge, the coarser is the ground product.

#### Second round of experiments

The second round of experiments was carried out under the following operating condition: the same mill and body charge as the first round of tests was used, with the exception that grinding time was only 40 min.

Table IV: Charge composition for the second round of tests.

Test	Crushing bodies of the charge (% weight)					
	1B	2B	3B	4B	5B	6B
Sphere 36.2 mm diameter	100	80	60	40	20	0
Type I concave	0	20	40	60	80	100
Total charge area (cm <sup>2</sup> )	3,787	3,945	4,102	4,313	4,430	4,587
Concave area of the charge (%)	0.0	4.7	9.1	13.5	17.3	20.8

The previous round of tests did not show a reduction of the fineness in the product with the introduction of the concave bodies. In order to highlight the selectivity effect, the second set of tests was performed on the coarsest possible ore, in relation to the size of the concave bodies.

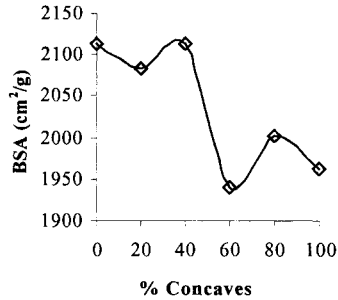


Figure 5: Blaine surface area (BSA) for the second round of tests, as a function of the percentage of Type I concave crushing bodies in the charge.

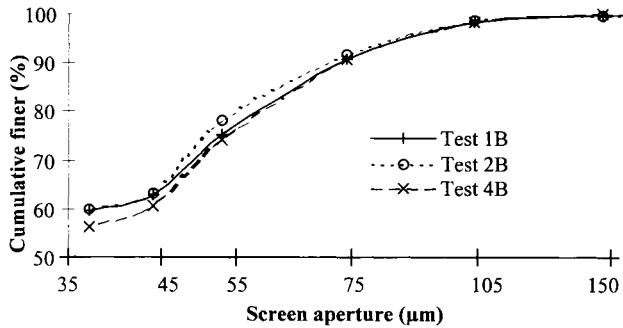


Figure 6: Size distribution of the second round of tests. The other tests are not plotted.

Table V: Harmonic mean size (HMS) for the ground product of the second round of tests.

Test	Feed	1B	2B	3B	4B	5B	6B
HMS total	77.63	25.66	25.46	25.63	26.43	25.95	25.91
HMS >37 µm	103.89	59.50	57.98	57.62	58.64	58.81	58.56

With a coarser feed, the product is finer, in the range between 37 µm to 150 µm, for all percentages of concave areas in the charge, confirming the selectivity effect.

### Third round of experiments

The third round of experiments was performed with the following operating parameters: mill dimensions, 20×20 cm<sup>2</sup>, 68 rpm (72.4% of critical speed), % filling, 12 kg ball charge, 1.9 kg ore charge, 630 ml water (75% solids), and 40 min. grinding time. In this round of experiments, we first tested only balls. Three other tests were done with concave bodies substituting balls with the same weight. To improve the use of the concave surfaces, different sizes of balls were used.

The ball distribution follows Bond's charge equilibrium equation,

$$Y = (X/B)^{3.8} \quad (2)$$

where Y is the percentage of the total equilibrium charge passing any size X, and B is the diameter of the larger ball.

Table VI: Charge composition for the third round of tests.

Test	Crushing bodies in the charge (% weight)			
	1C	2C	3C	4C
Sphere 35.5 mm diameter	24.2			24.2
Sphere 33 mm diameter	35.2	35.2		
Sphere 28 mm diameter	21.4	21.4	21.4	21.4
Sphere 23 mm diameter	11.6	11.6	11.6	11.6
Sphere 18 mm diameter	5.4	5.4	5.4	5.4
Sphere 13 mm diameter	2.2	2.2	2.2	2.2
Type I concave		24.2	24.2	
Type II concave			35.2	35.2
Total charge area (cm <sup>2</sup> )	3341.4	3449.1	3817.2	3700.8
Concave area in the charge (%)	0.0	4.8	14.5	10.5

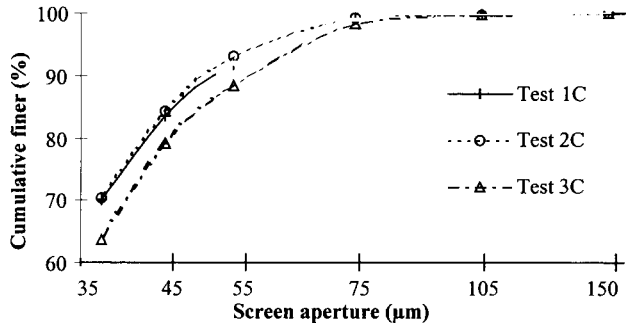


Figure 7: Size distribution of the third set of tests. Test 4 is not plotted.

Table VII: Harmonic mean size (HMS) for the ground product of the third round of tests.

Test	Feed	1C	2C	3C	4C
HMS total	29.77	22.65	22.57	23.90	22.69
HMS >37 µm	77.46	47.79	47.14	48.71	47.19

Figure 7 shows that a finer product was obtained with a 5% concave area of Type I bodies in the charge, for the size range between 35 µm and 150 µm. Test 3, with almost 15% of concave area of both types, produced a coarser product. Test 4, with

about 10% of concave area of Type II bodies, did not produce any significant difference in the fineness of the product. The curve for test 4 lies in between the curves for tests 1 and 2 and is not plotted.

There was a better use of the grinding surface: the 40 min grinding time in the third round of tests is almost the same as the 60 min grinding time in the first round of tests, with a similar feed.

### **Conclusions**

The initial assumption of increasing grinding efficiency with an increase in specific charge area was not proven. In all tests, there was a reduction of the product BSA (Blaine surface area) for increasing concave surface area and total surface area.

For up to about 10% of the concave area of the charge, there was a trend toward a finer ground product.

Apparently, the increase in the proportion of concave bodies with a less regular shape causes the charge to have less smooth movement, causing a negative impact on the grinding efficiency.

The expected increase on Cylpebs grinding efficiency related to their larger specific surface area does not occur, perhaps for the same reason.

On other hand, the selectivity of the grinding was proven to be effective, as highlighted in the second round of tests.

When grinding coarse feeds, for instance, to feed a flotation plant, this selectivity effect may cause a positive impact on flotation recoveries, due to the reduction of fines lost in de-sliming.

### **References**

- Cloos, U., 1983. Cylpebs: an alternative to balls as grinding media. *World Mining*, 10/83, 59.
- Donda, J.D., 1998. Estudo do Comportamento de um Itabirito do Quadrilátero Ferrífero Quanto à Superfície. MSc. Thesis, Universidade de São Paulo, São Paulo, Brasil.
- MINTEK, 1991. The selection of grinding balls for specific ores and the development of a suitable theory of ball wear. Application Report No. 10, MINTEK, Randburg, South Africa.
- Sepúlveda, J.E., 1990. Ball Mill Grinding: 40 Years After Bond, Proceedings. VI Simposium sobre Molienda, Armco Chile Procesamiento de Minerales S.A., Viña del Mar, Chile, 13-32.
- Wills, BA, 1997. *Mineral Processing Technology*. Butterworth-Heineman, Oxford, England.

## STUDIES IN FINE GRINDING IN AN ATTRITOR MILL

P. Raghuraman\*, R. Rajiv Raman<sup>o</sup>, B. Pitchumani\*

\*Particle Science and Technology Laboratory, Department of Chemical Engineering,  
Indian Institute of Technology New Delhi, India

<sup>o</sup>ADITI Consultants Greater Kailash-II, New Delhi, India

### Abstract

Ultra-fine grinding has proved to be a major attraction for industries for use in improving the quality of products. An attritor mill has a specific advantage over other conventional milling equipment, such as a fluid energy mill, due to energy saving during the comminution process. Experiments were conducted to study the performance of grinding in a laboratory attritor mill. This consists of a mild steel vessel with an interior lining of stainless steel, 4 mm thick. A stainless steel impeller of 82 mm diameter fitted with 10 mm diameter pins in pairs, at four different axial positions, is held in the central position of the mill by a sealed bearing. The shaft is belt-driven with an AC motor of 1 horsepower using a 440 V supply. The grinding of calcite is studied under wet conditions using zirconium balls. The mill feed has a very wide size distribution, with a maximum particle size of 35  $\mu\text{m}$ . The balls used are of two sizes, with average diameters of 3 mm and 1 mm and are added in different proportions. The aim of this study is to reduce the time of grinding and simultaneously obtain a narrow distribution. Preliminary investigation shows that a single size of large balls increases the grinding rate but reaches a constant value within a short time. Hence, there is no further decrease in the particle size of the product. The larger grinding media is then replaced by a smaller one. This decreases the product size considerably. Alternatively, grinding media consisting of a mixture of different ball sizes results in finer product size than that from single-sized grinding media. The breakage and selection functions, which are used for prediction of product-size distribution, are estimated.

*Keywords: calcite, fine grinding, attritor, comminution*

### Introduction

Ultrafine powders have wide applications in new high technology materials and in the manufacture of tyres, high quality paper, as well as fillers in high performance polymers. The fine powders have to be of very small size, with a narrow size distribution. The conventional method of grinding for a long time gives the desired average size, but the size distribution widens. This affects the quality of the final product. In most industries, attempts are made to get fine powder from attritor mills by trial and error. Often this effort is fruitless and frustrating, and one is forced to compromise with the wide distribution of the powder sizes obtained.

Viswanathan and Pitchumani (1982, 1984), and Pitchumani (1995) studied the grinding process in ball mills and other size-reduction processes. Viswanathan and Pitchumani (1984) studied attrition during pneumatic conveying of solids. Rama Ratnam et al. (1984) studied attrition of particles in fluidized beds. Grinding circuit analysis reported by Luckie and Austin (1972), Shishodia et al. (1992) and Ramian et al. (1990, 1992), explained the energy-saving method in grinding and carried preliminary experiments on an attritor mill. Ramanan and Pitchumani (1996) have shown that the attritor mill has a considerable advantage over the conventional ball

mill. It has been concluded that the size distribution obtained from the ball mill after about 8 h can be achieved within 30 min by using the attritor mill. The main aim of this study is to reduce the time of grinding and to simultaneously obtain a narrow distribution from an attritor mill.

### Experimental set-up and procedure

Experiments are conducted in a vertical-type laboratory attritor mill. This consists of a mild steel vessel of one litre capacity with a 106 mm ID and 114 mm height. It has a 4-mm thick, stainless steel interior lining and a 40 mm, hollow outer jacket for cooling the vessel. A stainless steel impeller of 82 mm diameter fitted with 10 mm diameter pins, in pairs at four different axial positions, is held in the central position of the mill by a sealed bearing. The shaft is belt-driven with a motor of 745.7 W.

The grinding of calcite was performed under wet conditions using zirconium balls. Feed for the mill has a very wide size distribution, with a maximum particle size of 35  $\mu\text{m}$ . The feed size distribution is shown in Figure 1. The zirconium balls used are of two 3 mm and 1 mm diameters. The experiments are performed under the conditions given in Table I.

Table I: Operating conditions for attritor grinding of calcite.

Material loading, volume of powder/mill volume	$f_c$	(-)	0.27
Ball loading, volume of balls/mill volume	J	(-)	0.4
Rotational speed of the mill shaft	n	(rad/s)	60.7
Impeller tip velocity	v	(m/s)	2.5
Concentration of material in water	c	( $\text{kg}/\text{m}^3$ )	400

The experiment is carried out for a total time of 30 min under the operating conditions given in Table I. The sample is taken at intervals of 5 min to measure size distribution. The powder-size analysis is measured in a laser particle size analyser. It can be observed that after 5 min of grinding, the slurry becomes highly viscous. On continuing grinding, a thick cake with a large number of balls entrapped is formed. To run the mill continuously, the viscosity of the slurry is reduced by adding 5% vol. of plasticizer GRAID-2000.

### Results and discussion

Experiments are carried out by grinding calcite with 3 mm diameter, zirconium grinding balls as grinding media. The results of these measurements are shown in Figure 1.

It can be observed from Figure 1 that with an increase in grinding time, there is a decrease in the particle size.

However, with a longer grinding time, there is not much variation in the average particle size.

It can be seen from Figure 1 that the width of size distribution narrows with an increase in grinding time. The above observation can be explained by the fact that as the particle size decreases, the number of particles increases, and the number of contact points between balls and particles decreases. Thus, the ratio of ball to particle decreases, and the grinding rate decreases.

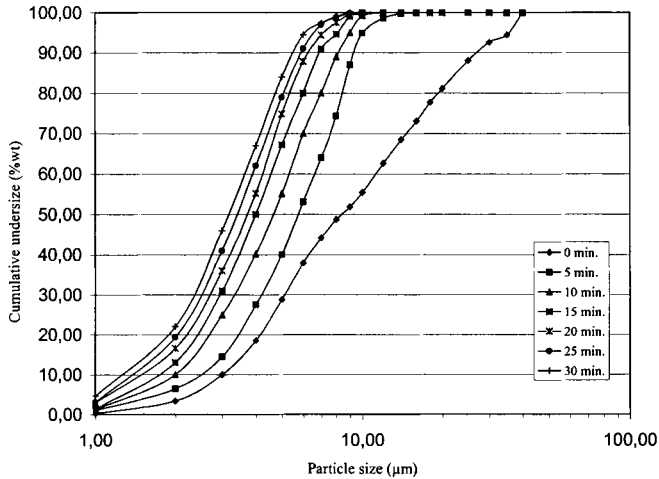


Figure 1: Effect of grinding time on product size distribution.

It can be concluded that when single-sized balls are used, the grinding rate decreases over time, and product size does not decrease after a long grinding time. It is difficult to produce fine particles with single-sized ball loading.

#### *Effect of ball size distribution*

Experiments were performed with various ball size distributions, as given in Table II. The results of the size analysis are used to calculate cumulative weight less than 50% (average diameter  $d_{50}$ ), cumulative weight less than 84%,  $d_{84}$ , and cumulative weight less than 16%,  $d_{16}$ .

The width of distribution is characterised as the ratio of size,  $d_{84}/d_{16}$ . The variation of  $d_{50}$  and the ratio  $d_{84}/d_{16}$  obtained at various grinding times are studied.

Table II: Ball size distribution.

Run n°	Ball size 1 mm (%) vol	Ball size 3 mm (%) vol
1	0	100
2	30	70
3	50	50
4	70	30

#### *Average diameter, $d_{50}$*

Figure 2 shows the variation in the average particle size,  $d_{50}$ , over time for different ball size distributions.

It can be observed from Figure 2 that for up to 5 min, the rate of production (the slope) of the average diameter for the ball size distribution of (70:30) is lower than that for (50:50) and (30:70).

The rate of grinding starts decreasing after 5 min of grinding time. It can be seen that, for the ball size distribution of (70:30), the rate of grinding increases after 20 min of grinding time, as compared to that of the ball distributions (50:50) and (30:70).

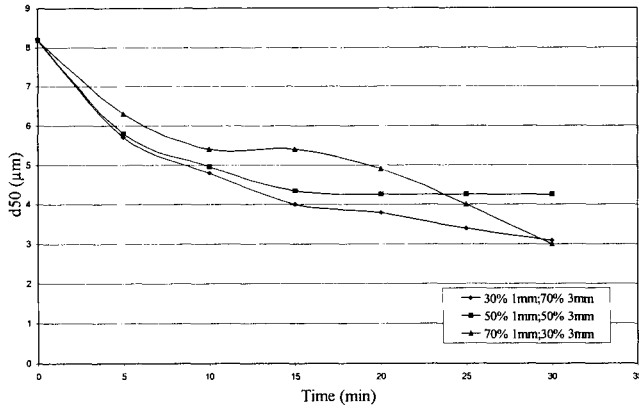


Figure 2: Effect of grinding on average particle diameter,  $d_{50}$ , for different ball loadings.

This may be due to a lower ratio of ball to particle size. The ratio of ball to particle size is relatively less, and hence breakage particles are few.

As the proportion of larger 3 mm balls is increased (30:70), the rate of grinding (slope) increases.

It may be explained that with an increase in grinding time, there will be an increase in the production of smaller particles.

Ramanan et al. (1996) has observed that there is an optimum ratio of ball diameter to particle diameter for the maximum specific rate of grinding. It can be inferred from the present study that at 20 min of grinding time, the particle size produced is small enough, and further grinding will not produce fines.

#### Width of size distribution, $d_{84}/d_{16}$

The ratio  $d_{84}/d_{16}$  is estimated from the size distribution measured. The estimated values of  $d_{84}/d_{16}$  are plotted against the grinding time in Figure 3.

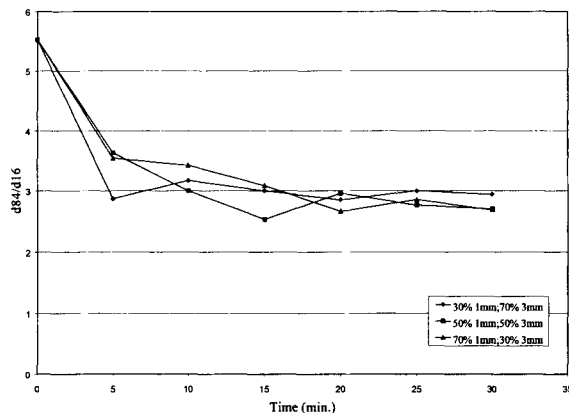


Figure 3: Effect of grinding time on width of size distribution  $d_{84}/d_{16}$  for different all loadings.



It can be seen from Figure 3 that  $d_{84}/d_{16}$  decreases over time up to 5 min of grinding. There is a small variation up to 20 min of grinding time, and after 20 min, there is not much variation in  $d_{84}/d_{16}$ .

It can be concluded that the attritor product will have a narrow distribution. This is due to the short grinding time.

### **Conclusions**

It can be concluded that with an increase in grinding time, the average diameter decreases, but the decrease is less after a long grinding time. The width of the distribution decreases with an increase in grinding time. The grinding rate decreases and becomes negligible after 5 min of grinding time. The particle size distribution obtained is narrow.

### **References**

- Luckie, P.T. and Austin, L.G., 1972. Methods for Determination of Breakage Distribution Parameters. *Powder Technology*, 215-222.
- Pitchumani, B., 1995. Studies on coal grinding in a Bowl Mill in thermal power plant. *Int. Conf. on Mineral Processing: Recent Advances and Future Trends*. Jamshepur, India.
- Rama Ratnam, S., Viswanathan, K. and Pitchumani, B., 1984. Studies on Attrition in Fluidized Beds. *Int. J. of Powder and Bulk Solids Technology*, 4, 1-9.
- Ramanan, P., Ramian, M.H. and Pitchumani, B., 1996. Control of Particle size distribution in an Attritor Mill. *Proc. Int. Symp. on Grinding Process*. Toulouse, France.
- Ramanan, P. and Pitchumani, B., 1996. Comparison of Fine Grinding of Metal Oxide Powder in Ball Mill and Attritor Mill. *Proc. of Int. Conf. on Advances in Chemical Engineering*, IIT Madras.
- Ramian, M.H., Amar, O.P. and Pitchumani, B., 1992. An Approach to Study Comminution in an Attritor Mill. *Int. J. of Powder & Bulk Solids*, 27-30.
- Ramian, M.H. and Pitchumani, B., 1990. Strategy for Energy Saving in Cement Plant. *Cement Industry-Annual review*, 129-134.
- Shishodia, V., Behl, R. and Pitchumani, B., 1992. Effect of Ball Size Distribution on Ball Milled Product Size Distribution. *Proc. CHEMCON Annual Session*, Institute of Chemical Engineering, Kalpakkam, India.
- Viswanathan, K. and Pitchumani, B., 1984. Analysis of Closed Grinding Circuit. *Int. J. Powder & Bulk Solids Technology*, 2, 25-28.
- Viswanathan, K. and Pitchumani, B., 1984. Attrition in a Pneumatic Pipeline. *Int. J. of Pipeline*, 252-258.
- Viswanathan, K. and Pitchumani, B., 1984. Optimum method of calculation of product size distribution from distribution fracture model. *Int. J. of Mineral Processing*, 11, 155.
- Viswanathan, K. and Pitchumani, B., 1982. Determination of Product Size Distribution from Distribution Fracture Model. *Proceedings Paper B1*, *Proc. Int. Symposium on Particle Science and Technology*, IIT Madras.
- Viswanathan, K. and Pitchumani, B., 1982. Distribution Function of Comminution Kinetics-Modelling and Experimental Study. *Int. J. of Mineral Processing*, 9, 385-392.

## ROLE OF PARTICLE MICROSTRUCTURE IN COMMINATION

L.M. Tavares

Department of Metallurgical and Materials Engineering  
Universidade Federal do Rio de Janeiro, COPPE/UFRJ  
Cx. Postal 68505, CEP 21945-130, Rio de Janeiro, RJ, Brazil

### Abstract

Microstructure affects significantly all mechanical properties of materials. While the effect of microstructure on the deformation and failure behavior is well known for steels, alloys and ceramics, this is not the case for the breakage behavior of geological materials inside comminution equipment. Taking advantage of the great progress made in recent years in measuring fundamental data that characterize the deformation, primary fracture and fragmentation behavior of single particles, a detailed analysis was carried out in the present study. Experimental work was conducted using both the Dual-Impact Load Cell and the Ultrafast Load Cell on a variety of single- and multiphase materials. Single-phase particles usually exhibited brittle fracture and their fracture energy decreases continuously with an increase in particle size. On the other hand, ores and rocks more often showed a tendency towards accumulation of damage prior to fracture and their primary fracture energy often became independent of size above a particle size of a millimeters or so. It was also shown that breakage of multiphase particles (particularly those that appear to exhibit low intergranular bonding) produced more intense fragmentation than of single-phase mineral particles. This is discussed in light of the deformation and fracture differences that were measured.

*Keywords: ore microstructure, particle breakage, comminution*

### Introduction

In industrial comminution, covering crushing and grinding, particles of a very wide range of sizes are subject to size reduction. Particle microstructures vary enormously from highly polycrystalline rock lumps, to fine powders composed of single mineral grains. In addition to that, rock and ore particles can exhibit widely differing microstructures even in the same mineral deposit, due to local variations of the geological processes that take place during its formation. Understanding and quantitatively describing this effect can be very useful in the modeling of the breakage process in crushers and mills (King and Bourgeois, 1993).

The relationship between microstructure and the mechanical properties of material such as steels, alloys, ceramics and even geological materials (Atkinson, 1987; Dieter, 1986; Dukino et al., 1995) is fairly well known. Little, however, is the amount of data that indubitably show the relationship between microstructure and the breakage characteristics of particles. This, in part, could be explained by the fact that the measures of comminutive behavior of materials, that are either based on a single parameter (such as Bond's work index) or a function (such as the breakage function), are actually also influenced by the operating conditions of the equipment. In order to overcome this, single-particle breakage experiments were used to carefully study the various stages of particle loading inside comminution machines: their deformation,

primary fracture and fragmentation producing progeny particles. It takes advantage of the recent advances in experimental techniques used to study compressive loading of single-particles at moderate speeds in studying the role of particle microstructure in comminution.

## Experimental

Samples of over 30 minerals, rocks and ores have been collected and prepared by screening to produce narrow-size fractions. These samples were then subject to single-particle breakage in the Ultrafast Load Cell (UFLC) and a modified apparatus, called Dual-Impact Load Cell (DILC). These are instrumented drop-weight apparatuses used for particle-breakage studies. Particle deformation studies were conducted in the DILC and fracture and fragmentation studies in the UFLC. Detailed descriptions of the samples characteristics, as well as of experimental equipment and procedure are available elsewhere (Tavares, 1997; Tavares and King, 1998). Impact energies used in the experiments were chosen by adequately selecting weight and height of fall of the steel ball. Size distributions of the progeny were determined by wet-dry sieving.

### Single-particle breakage characteristics

#### *Particle deformation*

Force versus deformation curves for various materials were measured using the DILC (Figure 1). In order to extract some information regarding their deformation behavior up to the instant of primary fracture (observed by a sharp drop in the force exerted on the particle), it is necessary to fit the force-deformation response to an appropriate model. An expression that relates the load ( $F$ ) and the deformation ( $\alpha$ ) in a spherical or nearly spherical particle of size  $d_p$  compressed between a falling ball and a rod is given:

$$F = \frac{k_p d_p^{1/2}}{3} \alpha^{3/2} \quad (1)$$

where  $k_p$  is the particle stiffness (Tavares and King, 1998), which is given by the ratio between the modulus of elasticity and one minus the square of the Poisson's ratio.

Equation (1) assumes that both the diameter and the stiffness of the falling ball and the rod are substantially greater than the particle's. A more rigorous analysis of this problem is given elsewhere (Tavares, 1997). For  $k_p$  constant, equation (1) becomes the Hertzian model, which describes the deformation behavior of perfectly elastic brittle solids. In practice, however, some materials seem to exhibit non-linear deformations prior to fracture. This can be addressed by changing  $k_p$  in equation (1) by an effective stiffness  $\tilde{k}_p$ , given by (Kachanov, 1958):

$$\tilde{k}_p = k_p (1 - D) \quad (2)$$

where the damage variable  $D$  can be expressed by (Atkinson, 1987; Loland, 1980):

$$D = (\alpha / \alpha_c)^\gamma \quad (3)$$

where  $\alpha_c$  and  $\gamma$  are parameters that must be determined experimentally. Model fitting results are given in Figure 1 and Table I. An efficient model fitting procedure is described elsewhere (Tavares, 1997). Brittleness is here defined as the ratio between the area below the force-deformation profile assuming elastic behavior (equation 1

with constant  $k_p$ ) and the area below the force-deformation profile resulting from both elastic and inelastic deformations.

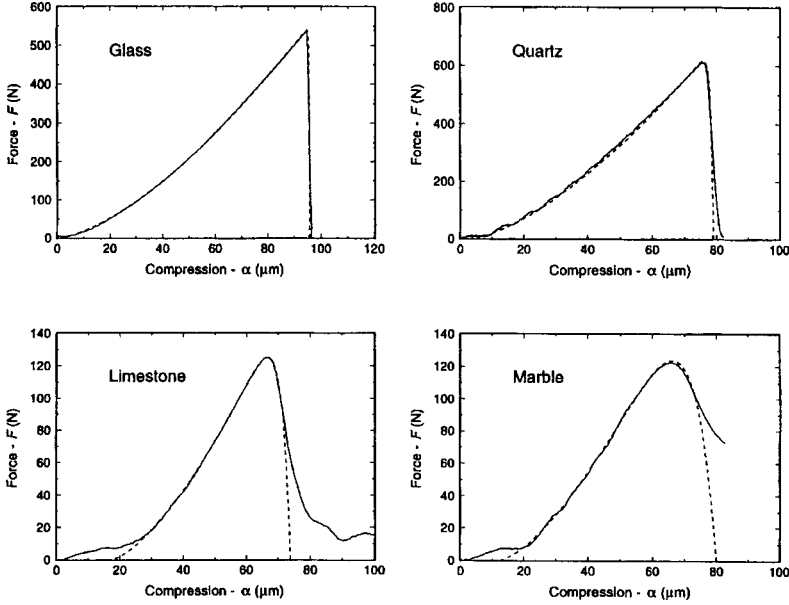


Figure 1: Typical force-compression profiles of particles tested. Solid lines are experimental results and dashed lines correspond to equations (1-3).

Table I: Parameters of the damage model of particle fracture (mean/standard deviation). Particle sizes are  $4.00 \pm 4.75$  mm, except for glass, which is  $1.00 \pm 1.18$  mm. \* Calculated using equation (4)

Material	Particle stiffness, $k_p$ (GPa)	$\alpha_c$ ( $\mu\text{m}$ )	$\gamma$	Brittleness number, $\chi^*$
Glass	73.1 (9.8)	91.3 (16.5)	500	1.00
Quartz	84.8 (28.2)	63.7 (14.9)	89.4 (49.3)	0.97
Cement clinker	14.4 (6.2)	139.3 (41.8)	55.8 (30.3)	0.96
Limestone	18.0 (7.1)	76.1 (11.8)	35.3 (17.0)	0.94
Iron ore	11.5 (6.6)	116.0 (29.0)	19.0 (13.4)	0.89
Marble	19.7 (7.5)	68.1 (8.4)	8.9 (3.2)	0.80

From this, it is straightforward to show that:

$$\chi = \sqrt[3]{2} \left( \frac{2\gamma + 5}{\gamma + 4} \right) \left( \frac{\gamma}{2\gamma + 3} \right)^{2/3} \quad (4)$$

The results show that glass and quartz exhibit more rapid damage accumulation (high values of  $\gamma$ ) than the other materials studied. This suggests a relationship between damage accumulation behavior and microstructure: the amenability of a material to accumulate damage is related to the ability of its microstructure to sustaining local damage without catastrophic failure. Along with cracks, other microstructure features such as pores, inclusions and weak grain-boundaries can also prevent rapid crack

growth and favor crack propagation through pre-existing discontinuities, thus creating tortuous paths and higher crack density that drain crack energy, and also by arresting propagating cracks, given its dissipative effect. Some of these microstructural features were found during microscopic examination of the samples studied. Indeed, the particularly gradual damage accumulation that was shown by marble and iron ore particles can be attributed to weak intergranular bonding. Detailed analysis of the indentation fracture characteristics in the iron ore by Middlemiss and King (1996) supports this observation.

#### *Particle primary fracture*

One important measurement using the UFLC is the mass-specific fracture energy, which is the area between the force-deformation profile until the point of first fracture. It has a particular significance in comminution as it represents the minimum energy required to fracture a brittle particle. The variation of the mean particle fracture energy with particle size for various materials and results are given in Figure 2. Mean fracture energies of single-phase crystalline materials are always reduced with an increase in particle size. However, it was observed that the mean fracture energies of multiphase materials become fairly constant above a particle-size of about 1 mm.

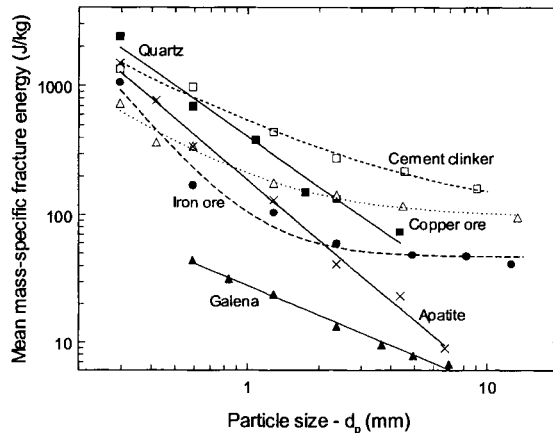


Figure 2. Variation of mean volume-specific fracture energy with particle size for selected materials.

#### *Particle fragmentation*

Single-particle fragmentation data for selected materials are given in Figure 3, which show the effect of material type and impact energy on the size distribution of the progeny. For most materials studied, fragmentation results resemble those from hematite (Figure 3 left), which allows normalization in respect to size, given the scale-invariance of the data. For some materials (Figure 3 right) such scale invariance seemed to be absent. These abnormal size distributions have often been associated with the breakage of heterogeneous materials that have a tendency towards grain-boundary fracturing (Gaudin, 1939; Wen et al., 1998). Measurements of the average grain-size (Figure 3 right), which closely match the points of inflection of the size distribution curves, support that observation. For these materials, the size

distributions cannot be normalized below the ore grain-size. Scale-invariant size distributions of the progeny resulting from single-particle breakage can be represented using a normalized size axis. The shift of the size distribution toward finer size resulting from higher impact energies can be described essentially by the variation of a single point from the curve, which corresponds to a normalized size of 10. This is the basis of the procedure originally proposed by Narayanan and Whiten (1983). The parameter, called  $t_{10}$ , gives the cumulative percent passing in one-tenth of the parent particle size (Figure 3 left), which must be related to the impact energy. Plotting the  $t_{10}$ s for the various materials studied as a function of the ratio between the impact energy and the mean particle fracture energy of the appropriate size of the parent particle (Figure 2), called relative impact energy  $E^*$ , then a remarkable clustering of the data in respect to material type appears (Figure 4).

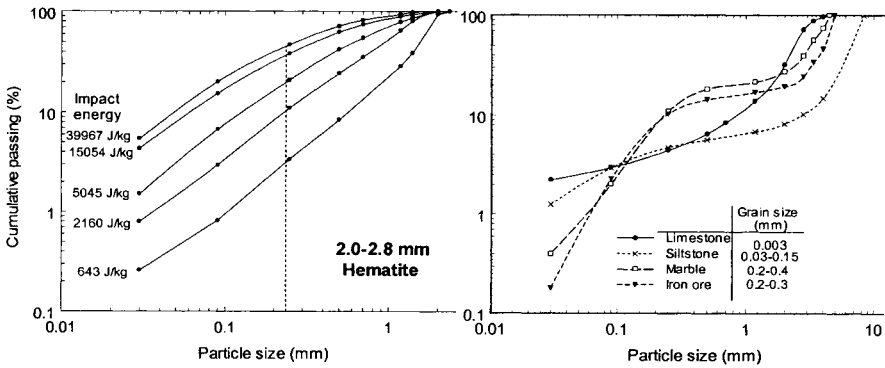


Figure 3. Progeny size distributions from breakage of single particles of hematite (left) and selected ores and selected rocks and ores that show non-normalizable breakage patterns (right).

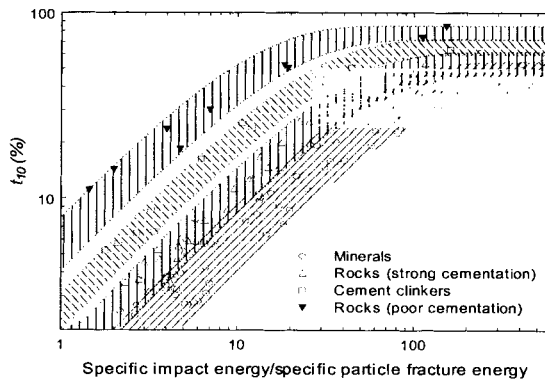


Figure 4. Variation of the parameter  $t_{10}$  with relative impact energy for selected materials. The lower first band groups single-phase crystalline materials, the following band groups polycrystalline rocks and ores, then cement clinkers, and finally polycrystalline rocks with poor intergranular bonding.

The data has been fit to the empirical model given by:

$$t_{10} = t_{10,max} [1 - \exp(-\eta E^*)] \tag{5}$$

Values of the model parameters  $t_{10,\max}$  and  $\eta$  determined by fitting the model to the experimental data are given in Table II.

The product  $t_{10,\max} \eta$ , that gives the amenability of the material, in respect to multiple fracture, shows a relationship to material type.

In order to illustrate the effect of material on fragmentation, progeny size distributions (here called breakage functions) were estimated for several materials using a value of  $E^* = 3$ , which approximately corresponds to the minimum impact energy that is required to break all particles in a monosize sample. The results show again a remarkable clustering of the data according to material type. Breakage functions of minerals approach straight lines in log-log coordinates, with slopes from 0.4 and 0.5, whereas data for the other materials could be better fitted using the two-sloped breakage function traditionally used to model mills and crushers (Austin et al., 1984). Indeed, some scattered evidence of material type on the breakage function of mills can also be found in the literature (Austin et al., 1984).

## Discussion

Monolithic materials such as mineral crystals and glass typically exhibit very rapid damage accumulation and therefore brittle fracture. Fracture of these brittle materials is primarily controlled by fracture initiation, which results in a strong dependence of particle strength and particle fracture energy on size. During the experiments it was also observed that fragments produced by breakage of crystalline materials and glass are often scattered over a wide area after fracture, because of the high velocity of the fragments. This spatial distribution of the fragments often resulted in lower efficiencies of transfer of kinetic energy of the ball to particle breakage energy (Tavares, 1999). This, along with the smaller proportion of fragments produced by each fracture event because of the limited crack bifurcation that occurs in fracture of crystalline materials, resulted in less fragmentation when compared to polycrystalline materials at comparable relative impact energy levels. Polycrystalline materials showed in general more gradual damage accumulation behavior and presence of inelastic deformations prior to fracture. The abundance of micro-structural features (grain-boundaries), which promote damage accumulation and crack This, along with the greater bifurcation, result of the greater accumulation of damage, produced greater breakage in comparison to crystalline materials.

Table II. Parameters of  $t_{10}$  model for various materials.

Material	$t_{10,\max}$ (%)	$\eta$	$t_{10,\max} \eta$
Apatite	45.4	0.0115	0.522
Quartz	38.8	0.0176	0.683
Hematite	45.6	0.0164	0.748
Galena	44.5	0.0176	0.783
Copper ore 1	44.8	0.0263	1.178
Copper ore 2	58.9	0.0204	1.202
Titanium ore	51.0	0.0269	1.372
Cement clinker	69.2	0.0276	1.910
Marble	76.3	0.0792	6.043
Iron ore	65.4	0.0932	6.095

The nature of the intergranular bonding also affects particle breakage. Poor intergranular bonding has been responsible for the gradual damage accumulation of materials such as marble and iron ore as well as for the appearance of non-normalizable progeny size distributions (Figure 3 right).

The nature of the intergranular bonding also affects particle breakage. Poor intergranular bonding has been responsible for the gradual damage accumulation of materials such as marble and iron ore as well as for the appearance of non-normalizable progeny size distributions (Figure 3 right).

The amount of fragmentation produced from impact, at comparable relative impact energies, of polycrystalline materials with weak intergranular bonding was greater than that of impact of materials with strong bonding.

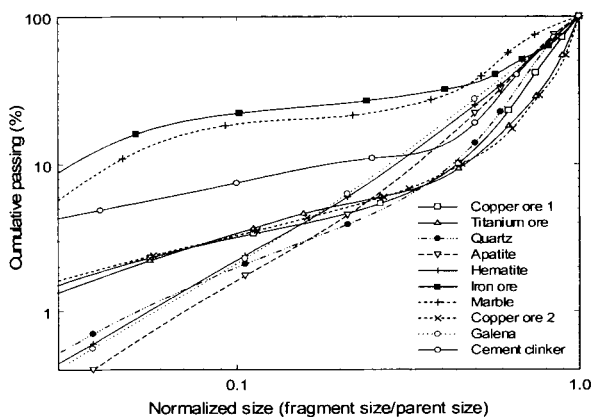


Figure 5. Single-particle progeny distributions predicted for impact of selected materials at an impact energy of three times the mean fracture energy of the particles ( $E^* = 3$ ).

## Conclusions

Material microstructure affects nearly all aspects of particle breakage. Fracture of single-phase crystalline and glassy materials often results in brittle fracture, as no distinct period of damage accumulation can be identified. Fracture of single-phase materials appears to be controlled primarily by crack initiation, which results in strong dependence of particle fracture energy on particle size. Also, less fragmentation is observed, when compared to multiphase materials, when both are impacted at comparable relative impact energies. Fracture of multiphase materials, on the other hand, was often found to result from a more gradual period of accumulation of damage. Fracture appears to be controlled by crack propagation, thus resulting in the nearly-independence of particle fracture energy on particle size.

## Acknowledgements

This work was undertaken as part of the author's Ph.D. at the Utah Comminution Center under the supervision of professor R.P. King. His guidance and the financial support from the Conselho Nacional de Desenvolvimento Científico e Tecnológico (CNPq), and the U.S. Bureau of Mines through the Comminution Center are greatly appreciated.



**References**

- Atkinson, B.K., 1987. *Fracture Mechanics of Rock*. Academic, London.
- Austin, L.G, Klimpel, R.R and Luckie, P.T., 1984. *The Process Engineering of Size Reduction*. Society of Mining Engineers, New York.
- Dieter, G.E., 1986. *Mechanical Metallurgy*, 3<sup>rd</sup> edn. McGraw-Hill, New York.
- Dukino, R.D., Swain, M.V., Loo, C.E., Bristow, N. and England, B.M., 1995. Fracture behavior of three Australian iron ores. *Trans. Instn. Min. Metall. (Sect. C)*, 104, C11-C19.
- Gaudin, A.M., 1939. *Principles of Mineral Dressing*. McGraw Hill, New York.
- Kachanov, L.M., 1958. Time of the Rupture Process under Creep Conditions (in Russian). *Izv. Akad. Nauk AN SSSR*, 8, 26-31.
- King, R.P. and Bourgeois, F., 1993. A new conceptual model for ball milling. *Proc. XVIII Int. Miner. Process. Cong.*, Vol. 1, Sydney, 81-86.
- Loland, K.E., 1980. Continuous damage model for load-response estimation of concrete. *Cem. Concr. Res.*, 10, 395-402.
- Middlemiss, S. and King, R.P., 1996. Microscale fracture measurements with application to comminution. *Int. J. Miner. Process.*, 44-45, 43-58.
- Narayanan, S.S. and Whiten, W.J., 1983. Breakage characteristics for ores for ball mill modeling. *Proc. Australas. Inst. Min. Metall.*, 286, 31-39.
- Tavares, L.M., 1997. Microscale investigation of particle breakage applied to the study of thermal and mechanical predamage. Ph.D. Thesis, University of Utah.
- Tavares, L.M., 1999. Energy absorbed in breakage of single particles in drop weight testing. *Min.Eng.*, 12, 43-50.
- Tavares, L.M. and King, R.P., 1998. Single-particle fracture under impact loading. *Int. J. Min. Proc.*, 54, 1-28.
- Wen, S.B., Yang, C.S. and Hsieh, C.S., 1998. The abnormal size distribution of comminuted heterogeneous ores due to detachment of grain boundaries fracturing. *Int. J. Min. Process.*, 53, 183-200.

# **FINE PARTICLE PROCESSING**

This Page Intentionally Left Blank

<b>Formation of Fine Particles with Compressed Gases</b> U. Teipel, U. Foerter-Barth	C5-1
<b>Dewatering of Fine Granular Materials by Vibrating Screens with Superposed Capillary Suction</b> A. Ettmayr, W. Stahl, K. Keller, G. Sauer	C5-8
<b>Production of Rheological Additives for Solvent Based Paint from Turkish Bentonite</b> K. Cinku, B. Ipekoglu, Y. Bilge	C5-16
<b>Flocculation and Adsorption-Desorption Mechanism of Polymers on Albite</b> I. Kurşun, B. Ipekoğlu, M.S. Çelik, Y. Kaytaz	C5-24
<b>TheoRy and Applications of Hydrophobic Flocculation Technology</b> S. Song, S. Lu	C5-31

This Page Intentionally Left Blank

## FORMATION OF FINE PARTICLES WITH COMPRESSED GASES

U.Teipel, U. Foerter-Barth

Fraunhofer Institut fuer Chemische Technologie (ICT)  
Pfinztal, Germany

### Abstract

The application of supercritical fluids has been introduced in the near past, especially in the field of material separation. For the large-scale production, the supercritical extraction of caffeine from raw coffee and hop with carbon dioxide as solvent was established.

A new application of supercritical fluids is the formation of fine particles with a narrow particle size distribution. In this field, two different processes are available.

For the RESS-process (Rapid Expansion of Supercritical Solutions), the first step is the supercritical extraction of the solid, and the second one the expansion of the loaded supercritical solution through a nozzle. The expansion causes a locally high supersaturating and thus nucleation within the free jet.

Another application of supercritical fluids is their use as anti-solvent. For the GAS-process (Gas Anti-Solvent), the solid is dissolved in a common solvent. The addition of a high-compressed gas as anti-solvent results in a volumetric expansion of the solution leading to the precipitation of the solid.

*Keywords: compressed gases, supercritical fluids, fine particles, RESS-process, GAS-process*

### Introduction

If a gas or a liquid is compressed above its critical pressure  $p_c$  and heated above its critical temperature  $T_c$ , the fluid becomes supercritical. Figure 1 shows the systematic pressure-temperature ( $p$ ,  $T$ ) diagram of  $\text{CO}_2$  that is very often used in technical processes.

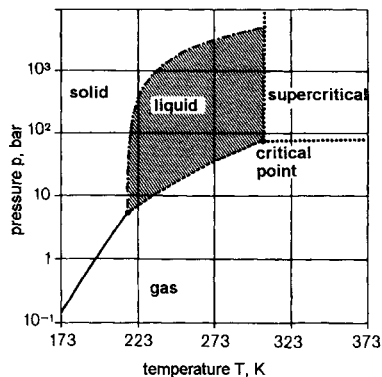


Figure 1: Pressure-temperature ( $p$ ,  $T$ ) diagram of  $\text{CO}_2$  (Eigenschaften der Kohlensäure, 1992).

Passing over the critical parameters by compressing and heating, the fluid gets some favorable properties. In comparison to liquids, supercritical fluids have a liquid like

density, but the dynamic viscosity is that of gases at standard conditions. The diffusion coefficient of compressed gases is near the critical point, ten times higher than that of liquids (see Table I). This causes a rapid mass transfer in supercritical fluids, and therefore supercritical fluids are well suitable for their use as solvents, i.e. as substitute for common solvents.

Table I: Comparison of physical properties of gases, compressed gases and liquids (Stahl et al., 1987).

	$\rho$ (kg/m <sup>3</sup> )	$\eta$ (Pas · 10 <sup>3</sup> )	$D^*$ (m <sup>2</sup> /s)
gases at 1 bar, $\vartheta = 25^\circ\text{C}$	0.6÷2.0	0.01÷0.03	$1\div 4\cdot 10^{-5}$
supercritical fluids	200÷500	0.01÷0.03	$7\cdot 10^{-8}$
liquids at $\vartheta = 25^\circ\text{C}$	600÷1600	0.2÷3.0	$0.2\div 2\cdot 10^{-9}$

\*self-diffusion for gases and compressed gases, binary mixtures for liquids.

For the application of a supercritical fluid as solvent, it is very useful that the fluid has low critical parameters (pressure, temperature) and simultaneously a high solvent power concerning the solid to be extracted. Table II gives an overview about the critical temperatures and pressures of different fluids.

Table II: Critical parameters of different fluids (Span, 1993).

Fluid	$\vartheta_c$ (°C)	$p_c$ (bar)
n - pentane	196.5	33.7
n - butane	152.0	38.0
propane	96.8	42.5
methane	-82.8	46.0
ethylene	9.2	50.4
carbon dioxide	30.9	73.7
toluene	320.8	41.6
methanol	239.4	80.9
ammonia	132.3	113.5

Low critical parameters are not only advantageous for the construction of a plant (i.e. the investment costs), but also for the safety of a plant and a process. The toxicity, availability, material costs, flammability, corrosiveness etc. are also important characteristics, which have to be considered.

Regarding these characteristics, carbon dioxide is a suitable solvent for many applications. The solvent power of a supercritical fluid can be essentially increased by the addition of an entrainer. An important advantage of supercritical CO<sub>2</sub> as solvent in many technical applications, especially for the formation of particles with supercritical fluids, is the easy way to separate the solid from the solvent.

### The RESS-process

When a solution is rapidly depressurized, the dissolved solid becomes insoluble in the low-pressure gas. The rapid expansion of supercritical solutions (RESS) exploits this phenomenon. During the process, a loaded supercritical fluid is expanded through a nozzle creating high supersaturating in the jet. Fast nucleation and growth of the crystalline particle occurs. If carbon dioxide is used as a supercritical fluid, the RESS-process offers advantages over conventional size

reduction methods. Heat sensitive and solvent free products can be achieved with this process.

With the pilot plant, which was built in co-operation with SITEC AG (Switzerland), it is possible to carry out extractions up to 80 °C and 300 bar. The maximum mass flow of carbon dioxide is limited to 20 kg CO<sub>2</sub>/h. Figure 2 shows the scheme of the pilot plant.

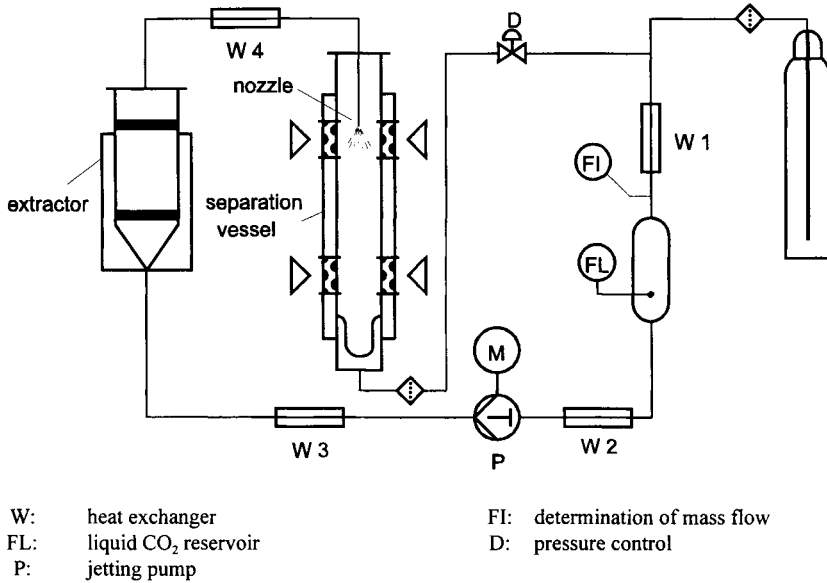


Figure 2: Scheme of the experimental apparatus.

Liquid carbon dioxide (purity 99.95 Vol %) was undercooled (W2) to avoid cavitation in the membrane pump (P).

After the compression to pre-expansion pressure, the fluid is heated to the extraction temperature (W3).

The supercritical fluid, loaded with the solid, leaves the extractor ( $V = 0.6$  l).

With an additional heat exchanger (W4), the solution is heated to pre-expansion temperature. In the separation vessel, the supercritical solution is expanded through a nozzle.

The expanded gas will be condensed (W1) and recompressed or let off. After the experiment, the separation vessel is opened and the particles were collected.

The particle size is measured by laser diffraction spectroscopy (Malvern Master Sizer X).

Parameters, which strongly influence the RESS-process, are: pressure, temperature, geometry of the nozzle and mass flow. The target of the process is the particle size and the particle size distribution.

Exemplary for the experimental results, Figure 3 shows the particle size distribution of anthracene detected by laser light diffraction spectroscopy.



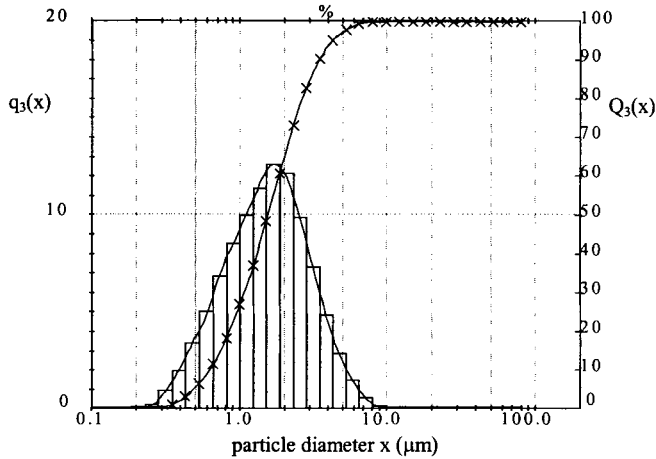


Figure 3: Volume sum distribution  $Q_3(x)$  and volume density distribution  $q_3(x)$  of anthracene;  $x_{10,3} = 0.6 \mu\text{m}$ ,  $x_{50,3} = 1.5 \mu\text{m}$ ,  $x_{90,3} = 3.5 \mu\text{m}$ .

### The GAS-process

While a supercritical fluid is used as a solvent in the RESS-process, a high compressed gas is used as an anti-solvent in the GAS-process to precipitate a dissolved solid from a common solvent. This process is applied for the crystallization of solids, which cannot be dissolved in supercritical fluids.

Many organic solvents are at least partially miscible with compressed gases. The absorption of the gas into the solvent causes a volumetric expansion of the liquid phase. The increase in the specific volume of the solution, i.e. the decrease in the density, effects the lowering of the solvent power of the solvent, and thus precipitation of solid particles occurs. Crystallization, using a compressed gas as anti-solvent, is realized in two different ways:

The solution is put into the crystallization vessel, and afterwards the compressed gas is supplied (Batch-process). The solution and the compressed gas are simultaneously, preferably in reverse direction flow injected into the crystallizer. This process is called PCA-process (Precipitation with a Compressed Fluid Anti-Solvent). It is a semi-continuous process.

#### *The Batch-process*

Figure 4 shows the scheme of the Batch-process. The gas from the supply bottle is liquefied in the heat exchanger (W1) and comes into the store tank. The store tank takes care of the steady supply of the gas into the crystallization vessel to avoid pressure fluctuation. In the heat exchanger (W2), the gas is undercooled to avoid cavitation in the pump. A third heat exchanger (W3) heats the gas up to the correct temperature for the process. A stirrer inside the crystallization vessel achieves a good mixture of the solution and the compressed gas. After the precipitation, the loaded solvent comes to the separator where the solvent and the gas are separated.

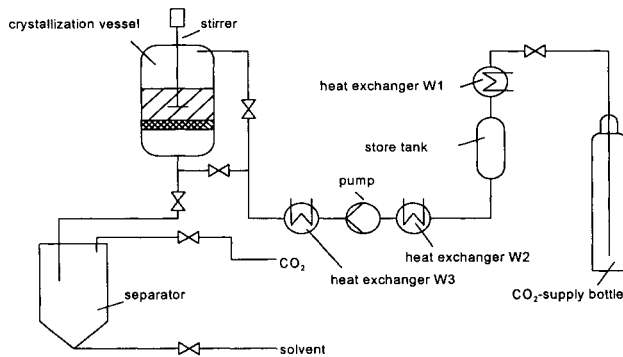


Figure 4: Scheme of the Batch-process.

### The PCA-process

The scheme of the PCA-process is shown in Figure 5. Via the top of the crystallizer, the solution is sprayed through a nozzle while the compressed gas is delivered in reverse direction flow. This procedure enables a rapid diffusion of the gas into the solution and hence the precipitation of very fine solid particles.

The volumetric expansion is significantly influenced by the parameters pressure, temperature and the time needed to build up the pressure in the crystallizer. Generally, higher temperatures request higher pressures to get the same amount of volumetric expansion (Gallagher et al., 1989).

Furthermore, the expansion is dependent on the solid concentration in the solution. If the solid content is high, a lower volumetric expansion is necessary to reach that rate of supersaturation that nucleation occurs. Even a saturated solution must be expanded to start the formation of nuclei (Gallagher et al., 1992).

The crystal form of the recrystallized solid is also influenced by the solvent, which is used for the dissolution of the solid material.

Exemplary for the experimental results, Figure 6 shows the particle size distribution of cyclotetramethylene tetranitramine (HMX) detected by laser light diffraction spectroscopy.

For raw HMX, the mean volume diameter  $x_{50,3} = 200 \mu\text{m}$ ; for HMX from acetone,  $x_{50,3} = 65 \mu\text{m}$ ; for HMX from  $\gamma$ -butyrolactone,  $x_{50,3} = 90 \mu\text{m}$ . It has to be considered that the particle size distribution of HMX from  $\gamma$ -butyrolactone is more spread compared to the distribution of HMX from acetone. The raw material has the broadest size distribution.

The Figures 7 and 8 show the results in comparison to the raw material. Note that the figures are on the same scale. The pictures give an impression of the particle size reduction received by the GAS-recrystallization.

The particles precipitated from acetone are more regular shaped and of more uniform size than the particles from  $\gamma$ -butyrolactone. It is noticed that long, rectangular crystals appear when  $\gamma$ -butyrolactone was used as solvent.

Maintaining process conditions (amount of HMX in the solution, pressure, temperature and time to build up pressure), the supersaturation gained is different for the two

solvents due to their different solvent capacity towards the solid. The supersaturation for the HMX -  $\gamma$ -butyrolactone solution is high enough to start nucleation. But, for the HMX - acetone solution, the rate of nucleation is higher due to the higher supersaturation.

The nuclei grow until the solution is depleted of the solute, and, due to the larger number of nuclei, smaller and more regular-shaped particles are formed in comparison to the HMX -  $\gamma$ -butyrolactone solution.

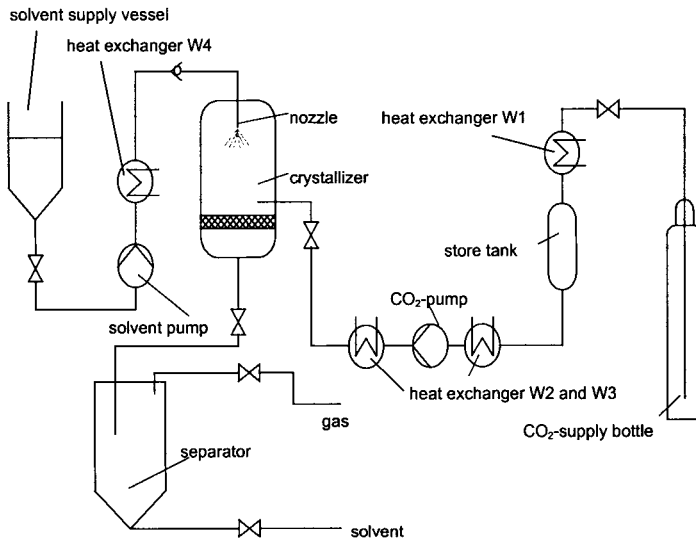


Figure 5: Scheme of the semi-continuous process.

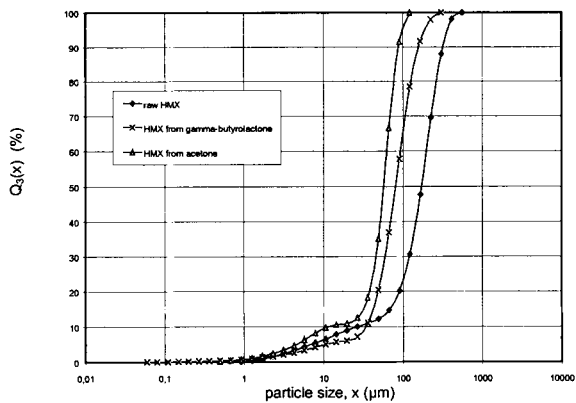


Figure 6: Volume sum distribution  $Q_3(x)$ .

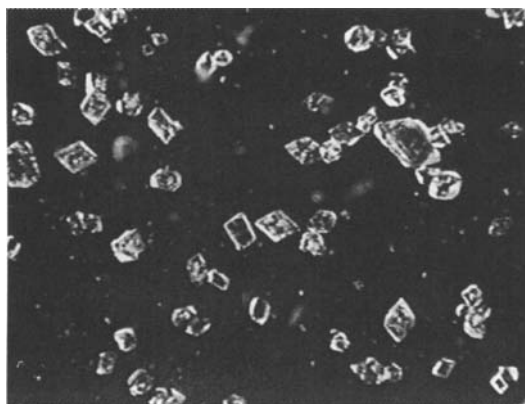


Figure 8: Light-optical microscopy of HMX from acetone.

#### References

- Eigenschaften der Kohlensäure, Fachverband Kohlensäure - Industrie e. V., 1992.
- Gallagher, P.M., Coffey, M.P. and Krukonis, V.J., 1992. Gas Anti-Solvent Recrystallization of RDX: Formation of Ultra-fine Particles of a Difficult-to-Comminute Explosive. *The Journal of Supercritical Fluids*, 5, pp. 130 - 142.
- Gallagher, P.M., Coffey, M.P., Krukonis, V.J. and Klasutis, N., 1989. Gas Anti-Solvent Recrystallization: A New Process to Recrystallize Compounds Insoluble in Supercritical Fluids, In: Johnston K. P., Penninger J. M. L.: *Supercritical Fluid Science and Technology*. ACS Symposium Series 406, American Chemical Society, Washington DC, Chapter 22.
- Span, R., 1993. Eine neue Fundamentalgleichung für das fluide Zustandsgebiet von Kohlendioxid bei Temperaturen bis zu 1100 K und Drücken bis zu 800 MPa. *Fortschr. Ber. VDI Reihe 6 Nr. 285*, Düsseldorf.
- Stahl, E., Quirin K. W. and Gerard D., 1987. *Verdichtete Gase zur Extraktion und Raffination*. Springer - Verlag, Berlin.

## DEWATERING OF FINE GRANULAR MATERIALS BY VIBRATING SCREENS WITH SUPERPOSED CAPILLARY SUCTION

A. Ettmayr\*, W. Stahl\*, K. Keller<sup>°</sup>, G. Sauer<sup>◇</sup>

\*Institut für Mechanische Verfahrenstechnik und Mechanik

Universität Karlsruhe (TH), Karlsruhe, Germany

<sup>°</sup>DuPont, Wilmington, Delaware, USA

<sup>◇</sup>Jöst GmbH+Co KG, Dülmen, Germany

### Abstract

Vibrating screens are widely used for dewatering bulk materials in the mineral-processing industries. Advantages are high throughput and low capital costs. However, the residual moisture of bulk materials after conventional vibrational dewatering often turns out to be only a little lower than the moisture achievable by stationary draining. There is strong evidence that the mechanism of drop formation and dripping off the screen is usually the limiting factor of dewatering kinetics on vibrating screens. Pilot scale studies at the Institut für Mechanische Verfahrenstechnik und Mechanik have shown that the additional use of capillary suction media can considerably lower residual moisture, compared to conventional vibrational dewatering. The suction medium is designed as an endless textile belt, which is constantly moved in a counterflow mode along the underside of the screen of a modified vibrating screen. All water that has left the bulk due to vibrational acceleration gets immediately absorbed by the porous belt, thus being removed by active transport, instead of having to drip off. In addition, the capillary suction caused by the fine pores of the suction media acts as a superposed driving force on the water in the bulk, resulting in further dewatering. In the work presented, this modified pilot scale vibrating screen has been used for dewatering quartz sand. The influence of bulk height, residence time, frequency of vibration and acceleration on dewatering have been studied with throughputs ranging up to 5 t/h. By comparison with lab-scale batch experiments, methods for scale up calculations have been developed and verified. Possible fields of application for the process presented can be found in processing industries, as well as in chemical industries.

*Keywords: dewatering, vibrating screen, suction media, pilot scale studies*

### Introduction

Vibrating screens are widely used for dewatering bulk materials, such as coal, sand, ores, raw materials in the ceramics industries, granular plastics and intermediate products in the chemical industries. Typical throughputs range up to more than 100 t/h. Machines are generally simple and robust, thus keeping rather low capital cost, downtimes and maintenance costs. However, the residual moisture of bulk materials after conventional vibrational dewatering often turns out to be only a little lower than the moisture achievable by gravitational dewatering, as experimental studies on sand dewatering by Helfricht (1966) indicate.

Keller (1997) and Keller and Stahl (1995) describe the kinetics of vibratory dewatering by introducing a physical model, which is derived analogously from the centrifugal dewatering theory of capillary plug and film flows, additionally

considering the process of drop formation and dripping-off. Since no continuous filtrate flow emerges from the bulk, the water being removed has to form drops at the underside of the screen. If during one period of vibration such a drop does not reach a certain critical volume, the water will reenter the bulk, instead of dripping off. This critical volume is a function of the effective acceleration. Since drop size depends on the hydraulic diameter of the bulk pores being dewatered, especially fine granular material often does not reach satisfactory residual moistures on vibrating screens, because the effective acceleration necessary to meet the drip-off condition would be too high to actually get applied. Thus, considerable amounts of water merely oscillate back and forth, instead of being removed. Keller's (1997) and Keller and Stahl's (1995) studies include both theoretical and experimental approaches to describe the phenomenon.

### Equipment

To avoid the limitations described above, the water that has left the bulk due to vibrational acceleration should be removed by active transport, instead of having to drip off. A way to achieve this is by the combination of vibration dewatering and capillary suction. For the first time, this principle has been implemented for continuous operation on a pilot scale at the Institut für Mechanische Verfahrenstechnik und Mechanik, Karlsruhe, although Batel (1954) has already suggested absorbing water from bulk material being conveyed across a vibrating screen by using a fleece belt moving along the underside of the screen.

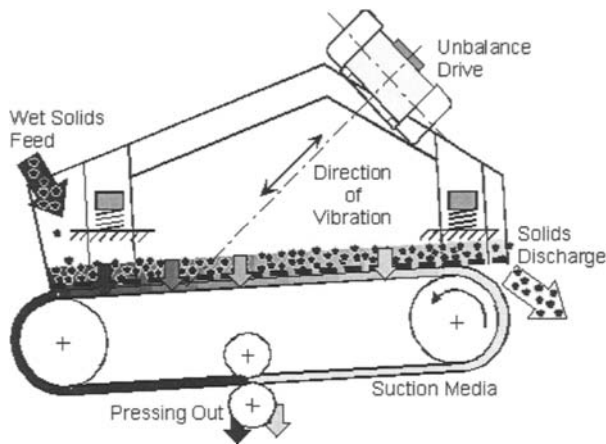


Figure 1: Schematical sketch of continuously operated vibrating screen with belt assembly to apply superposed capillary suction.

As schematically shown in Figure 1, the novel machine basically consists of a vibrating screen frame, powered by two 2.8 kW unbalanced drives with adjustable balances and angular adjustability for an infinitely variable direction of vibration, and a suction belt assembly-mounted within the vibrating system. The endless porous belt, which constantly moves in a counterflow mode along the underside of the screen,

immediately absorbs the water after leaving the bulk, due to vibrational acceleration. Press rolls continuously regenerate the suction media by squeezing out water. In addition, water and compressed air nozzles can be used to clean or dewater the belt, respectively. The exchangeable screen consists of monofilament polyamid fabrics thin enough to allow good hydraulic contact between the bulk and suction media. For the work presented, a mesh width of approximately 330  $\mu\text{m}$  was applied. The screen area is 1.4  $\text{m}^2$ .

Among the different belt layouts tested were a WFG felt band, a WFG needled spiralflex belt, and a Freudenberg non-woven fabric attached to a carrier belt, necessary for mechanic stability. For the results presented, seven layers of Freudenberg non-woven fabric were sewn onto a WFG spiralflex belt.

### Test material

The test material used is quartz sand with a mass-related median of the particle-size distribution of about 850  $\mu\text{m}$ . Figure 2 shows the cumulative particle size distribution by mass.

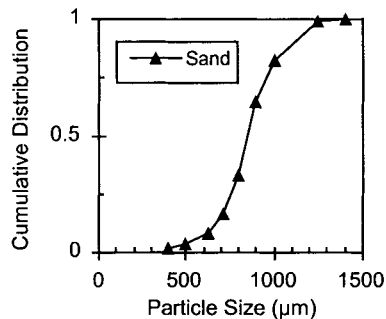


Figure 2: Cumulative particle-size distributions of the test material used.

### Effective bulk accelerations

Although the unbalanced drives cause vibratory excitation following a sine function of the screen frame, the acceleration pattern effective in the bulk is quite different because of bouncing. Figure 3 shows such a typical pattern with short acceleration peaks. Since efficiency of dewatering will depend on the actual acceleration in the bulk, the acceleration values were measured by piezoelectric sensors for several amplitude and frequency settings.

The sensors are mounted to small pieces of aluminium sheets, which are three dimensionally beaded, to ensure that the sensor keeps its orientation relative to the screen and are held by a thread in order not to get conveyed off the screen. After the sensor has been placed into the bulk, only the first few seconds yield useable acceleration readings, because by-and-by, the sensor separates from the bulk.

At higher screen amplitude settings, no useable acceleration readings could be achieved. Additional bulk accelerations have been determined on a lab scale vibrating bench for batch dewatering. The corresponding accelerations of the screen frame have been measured in parallel.

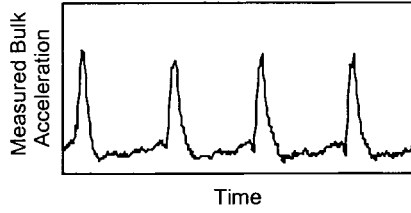


Figure 3: Typical pattern of acceleration peaks measured in the bulk.

Plotting the actual peak accelerations in the bulk against the acceleration maximum of the screen frame, as shown in Figure 4 (left), does not yield a uniform relation. A simple kinematic consideration can explain this. The higher the impact velocity, i.e. the orthogonal velocity of the bulk relative to the screen, the higher the peak acceleration will be in the bulk. Figure 4 (right) confirming the correlation of the theoretical impact velocity and the measured bulk accelerations.

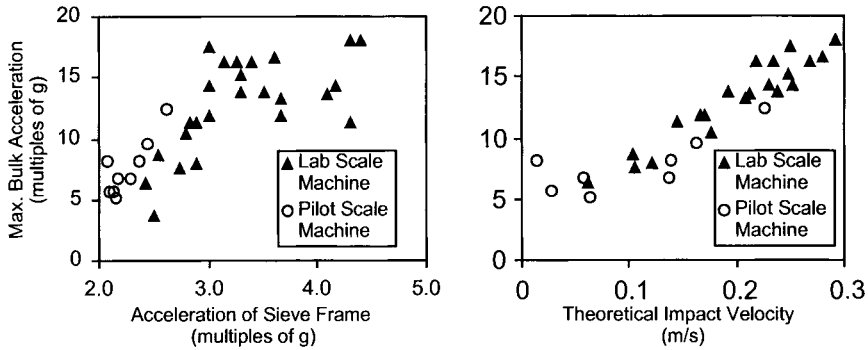


Figure 4: Measured bulk accelerations plotted against acceleration maximum of the screen frame (left) and the theoretical impact velocity (right).

The theoretical impact velocity has been calculated (analogously to Böttcher’s (1958) calculation to determine bulk transport velocity), as described below, and used as a measure of the driving force of dewatering. For the following, it is assumed that bulk and screen behave as rigid bodies, that air resistance is neglected and that the screen is horizontal. The vertical space coordinate of the screen  $z_S$  is:

$$z_S(t) = A \cdot \sin(2\pi ft) \cdot \sin\beta, \tag{1}$$

with amplitude  $A$ , frequency  $f$  and the angle  $\beta$  between the direction of the excitation and the horizontal.

When acceleration of the screen reaches  $\ddot{z}_S(t) = -g$ , with gravity acceleration  $g$ , the bulk will lift off the screen. This yields the time of lift-off  $t_L$  and the vertical “launch” velocity  $v_B(t_L)$  of the bulk:

$$t_L = \frac{1}{2\pi f} \arcsin \frac{g}{4A\pi^2 f^2 \sin\beta} = \frac{1}{2\pi f} \arcsin \frac{1}{C_S} \tag{2}$$

$$v_B(t_L) = \dot{z}_S(t_L) = 2A\pi f \sin\beta \cos(2\pi ft_L) = 2A\pi f \sin\beta \cos(\arcsin \frac{1}{C_S}), \tag{3}$$



with  $C_s$  expressing the vertical acceleration amplitude of the screen as a multiple of gravity acceleration,  $g$ . After lift-off, the vertical space coordinate of the bulk  $z_B$  is:

$$z_B(t) = z_B(t_L) + \int_{t_L}^t [v_B(t_L) - g(t - t_L)] dt = z_s(t_L) + (t - t_L) \cdot v_B(t_L) - \frac{g}{2}(t - t_L)^2 \quad (4)$$

By equating (4) with (1) and solving numerically, the time of collision of the bulk and of the screen  $t_C$  can be calculated. The theoretical impact velocity  $\Delta v$  results as:

$$\Delta v_C = \dot{z}_s(t_C) - \dot{z}_B(t_C) = 2A\pi f \sin\beta [\cos(2\pi f t_C) - \cos(2\pi f t_L)] + g(t_C - t_L) \quad (5)$$

### Dewatering results

All the dewatering results are presented as residual moistures, i.e. the quotient of the mass of liquid  $M_L$  and the total mass of the sample (with mass of solids  $M_S$ ) is:

$$RM = \frac{M_L}{M_L + M_S} \quad (6)$$

All residual moistures are mean values of three independently taken samples, unless indicated otherwise. The feed product enters the machine fully saturated with water. Thus the initial residual moisture was always about 21%.

Throughputs have been obtained as mean values of two cumulative measurements. For determining residence times, colored sand of the same particle size was added to the feed, and the time was taken until the first and the last colored grains became visible in the solids discharge. For each data point, the mean value obtained from three measurements was used. Residence times are expressed in a dimensionless form as the theoretical number of impacts, i.e. the product of residence time and frequency of vibration. As shown later, it turned out to be a practical method to compare results obtained with lab and pilot scale machines, each working in a different frequency range.

Figure 5 shows the residual moistures achieved for different throughputs, whereas residence time was kept constant at about one minute (900 impacts at 14.35 Hz) by slight adjustment of the angle of excitation. Thus, every throughput represents a certain theoretical bed height, which is written next to the corresponding data point (black diamonds). Actual bed heights are space-variant on the screen. Theoretical impact velocity was kept constant at about 640 mm/s. Although residual moistures are lower for small bed heights, the difference appears to be not very high for the selected combination of parameters. For comparison, data of vibrating dewatering without capillary suction are also included in the diagram (squares). They were achieved after removing the suction media from the vibrating screen. The positive effect of the suction media is evident.

Figure 6 shows residual moistures resulting for different outputs with similar bed height of about 50 to 60 mm and thus varying residence times, ranging from 65 to 390 seconds. In the diagram, residence times are expressed in the dimensionless form described above. Theoretical impact velocity was kept constant at about 450 mm/s.

Obviously, dewatering kinetics are slow enough to lead to considerably higher residual moistures for shorter residence times. As Figure 7 indicates, it is better, in terms of dewatering, to achieve a certain throughput by increasing bed height than by reducing residence time.

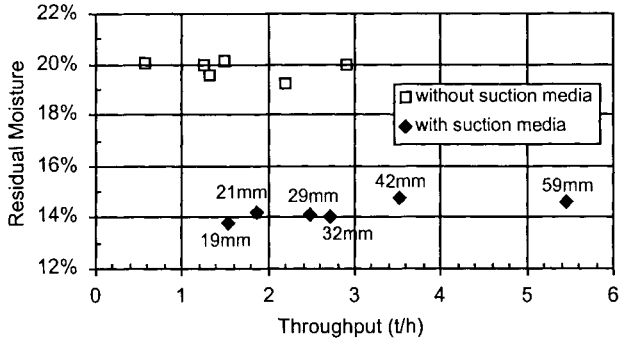


Figure 5: Comparison of vibratory dewatering with and without superposed capillary suction. Residual moisture is plotted against output, about 900 impacts at 640 mm/s ( $f = 14.35$  Hz,  $C_s = 2.8$ ). Data points are labeled with bed heights.

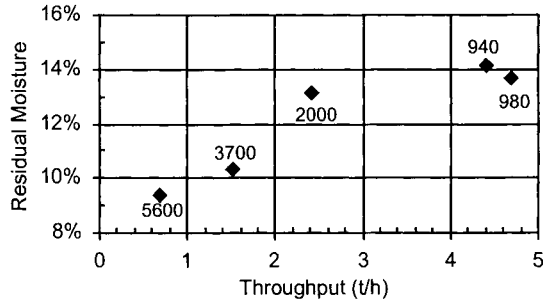


Figure 6: Residual moisture plotted against throughput. Theoretical impact velocity, 450 mm/s ( $f = 14.35$  Hz,  $C_s = 2.1$ ), bed height at about 50-60 mm. Data points are labeled with the theoretical number of impacts.

The diagram includes residual moistures resulting for outputs of 2.7 t/h and 3.6 t/h, respectively, with different combinations of bed heights and residence times.

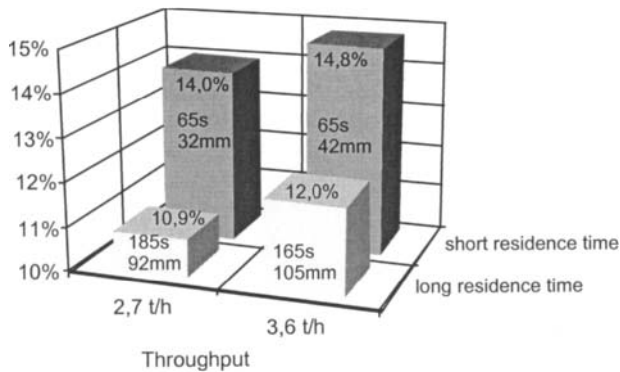


Figure 7: Residual moisture resulting for different parameter combinations. Theoretical impact velocity, 640 mm/s ( $f = 14.35$  Hz,  $C_s = 2.8$ ).

### Scale up considerations

For scale up, three parameters have to be kept constant in order to achieve about the same residual moisture:

- the theoretical impact velocity between the bulk and screen characterizing the actual acceleration peaks in the bulk;
- the product of frequency and residence time, i.e. the number of actual impacts between the bulk and screen;
- the bed height of the bulk.

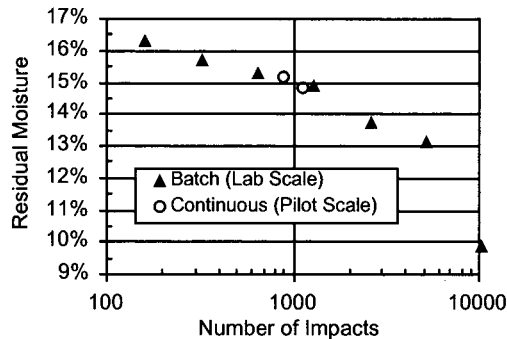


Figure 8: Comparison of dewatering results between lab-scale batch vibrating screen and continuously operated, pilot-scale vibrating screen, both with suction media (non-woven fabric). Theoretical impact velocity, about 400 mm/s ( $f = 27.2$  Hz,  $C_s = 3$  and  $f = 13.55$  Hz,  $C_s = 1.9$ ). Bed height,  $20 \pm 30$  mm.

In Figure 8, residual moistures obtained with lab-scale and pilot-scale experiments are plotted against the number of impacts. Bed height and theoretical impact velocity have been kept constant. The batch test results are mean values of two independent measurement series with a maximal difference of 0.36% residual moisture.

Figure 8 indicates the transferability of results from lab scale batch experiments to pilot scale dewatering. By using the three characteristic parameters listed above, this comparison makes sense, although the batch experiments were performed with less than 1 kg of sand, and the amplitude and frequency ranges of the two machines do not even overlap.

However, it is required for batch tests that enough suction medium is supplied in order not to become saturated during the course of the experiment, and it has to be kept in mind that no true counter-flow mode can be simulated.

If the three characteristic parameters relevant for dewatering are kept constant, to scale up, the screen area in contact with the suction media has to be increased proportionally with the throughput desired. Since thickness of the suction media is limited, belt velocity has to be high enough to prevent the fabrics from getting saturated.

To roughly estimate the bulk transport velocity  $v_T$ , equation (7) derived by Böttcher (1958) can be used:

$$v_T = \frac{g(t_C - t_L)^2}{2f} \cot \beta \quad (7)$$

For relevant bed heights, however, transport velocity will be slower (Peschl, 1970). In order to achieve the residence time desired, the angle of excitation should be adjustable.

**Acknowledgments**

The authors would like to thank the German Bundesministerium für Bildung und Forschung (BMBF) for financial support.

**References**

- Batel, W., 1954. Vorgänge bei der mechanischen Entwässerung. *Chem.-Ing.-Tech*, 26(8/9): 497–502.
- Böttcher, K.H., 1958. Beitrag zur Klärung der Gutbewegung auf Schwingrinnen. *Fördern und Heben* 8, 127–131, 235–240, 307–315.
- Helfricht, R., 1966. Zu einigen Fragen der Entwässerung von Sand und Kies. *Bergakademie*, 10, 621–628.
- Keller, K. 1997. Schwingentwässerung von Körnigen Produkten. Dissertation, Universität Karlsruhe (TH), Karlsruhe, Germany.
- Keller, K. and Stahl, W. 1995. Vibration screens for dewatering of minerals – theory and practice. *Proc. 19th Int. Min. Proc. Congr.*, San Francisco, Vol. 2, 117-124.
- Peschl, J., 1970. Effect of material properties on the handling speed of vibratory feeders. *Fördern und Heben*, 20, 442-447.

## PRODUCTION OF RHEOLOGICAL ADDITIVES FOR SOLVENT BASED PAINT FROM TURKISH BENTONITE

K. Cinku\*, B. Ipekoglu\*, Y. Bilge°

\*Istanbul University Mining Engineering Department, Avcılar-Istanbul, Turkey

°Bensan C.o. Kadıköy-Istanbul, Turkey

### Abstract

Bentonite is a clay mineral, which can be used in many industries due to its unique chemical and physical properties. In this study, a rheological agent was obtained from Yazır region bentonite in order to produce solvent-based paint. This material is a mixed type bentonite (Na/Ca ratio is about 0.35) which consists of 86% montmorillonite and some impurities such as quartz, calcite, feldspar and biotite. Different techniques such as agitation, classification and decantation were applied to remove the impurities from the sample for obtaining the pure Na-bentonite. Then, ion exchange process was applied to the material with the quaternary ammonium salts at certain temperature and period. At the end of these tests, a specific organo-clay (rheological agent) was obtained. The properties of the obtained product was compared to other industrial trade mark products.

*Keywords: bentonite, rheological additive, paint, organo-clay, ion exchange*

### Introduction

Bentonite is clay of volcanic origin, it contains montmorillonite as a major mineral and impurities such as quartz, calcite, mica and feldspar etc. (Grim, 1968; Grim and ve Güven, 1978; İpekoğlu and Bilge, 1997; Süd-Chemie, 1996).

Bentonite has a variety of industrial, engineering, agricultural and other uses including the clarification of beverages, water and decoloring of oil. It is also used as rheological agent in the paint industry, cat litter and storing nuclear waste because of its colloidal property, high ion exchange capacity, swelling in water and having high plasticity (Baxter, 1997; House, 1983; McMurry, 1992; Reynolds et al., 1995; Tixogel, 1996).

Turkey is among the first ten countries in terms of the world bentonite reserves. The important bentonite deposits in Turkey are Ordu-Ünye, Tokat-Reşadiye, Eskişehir-Mihallıçık, Ankara-Kalecik, Edirne-Enez. In this study, the bentonite deposit in Edirne-Enez is investigated.

The Enez bentonite deposit is operated by Bensan Co. for production of bleaching earth for edible and mineral oils, drilling bentonite, foundry bentonite, desiccant clay, cat litter, animal feed additive and etc. (Akbulut, 1996; İpekoğlu and Bilge, 1997; Keegan, 1998).

### Experimental studies

The aim of this study was to obtain economically rheological additive material from the Trace/Yazır bentonite, which is used in the paint industry. Wyoming (USA), Ipsala and Raner Co. (Trace) bentonites were simultaneously used for comparison.

*Samples used in the experiments*

Representative samples were taken (500 kg) from the stockpile of Bensan Co. in Edirne-Enez (Yazır bentonite). It was reduced in size by coning-quartering and riffler in corresponding quantities for preparing chemical, mineralogical and size analyses, humidity, swelling, pH tests and for processing. The properties of the Yazır, Raner Co., Ipsala and Wyoming bentonites were given in Table I.

Table I: Chemical analysis of bentonite samples.

Component	Weight (%)			
	Yazır	Raner	Ipsala	Wyoming
Montmorillonite	82	-	-	-
Na <sub>2</sub> O	0.91	0.24	0.19	1.53
K <sub>2</sub> O	2.23	0.29	-	0.53
MgO	2.41	1.69	18.33	3.05
SiO <sub>2</sub>	58.37	73.79	33.42	62.90
Al <sub>2</sub> O <sub>3</sub>	18.59	14.58	3.38	19.60
CaO	2.55	2.51	16.12	1.68
Fe <sub>2</sub> O <sub>3</sub>	5.24	0.99	1.17	3.35
LOI	8.7	5.6	27.19	1.59
SiO <sub>2</sub> /Al <sub>2</sub> O <sub>3</sub> ratio	3.14	5.06	9.88	3.20
Na/Ca ratio	0.35	0.09	0.01	0.91

The mineralogical analysis was carried out by the use of electron microscope and the X-Ray Diffraction method. These tests revealed quartz, calcite, biotite and feldspar as well as montmorillonite, as shown in Figure 1. The size-distribution of the sample was made by using the sieve system and the Scanning Photo Sedimentograph ( $2 \div 100 \mu\text{m}$ ) together. The results were given in Table II and in Figure 2.

As shown in Table II and Figure 2, 86% of the raw Yazır bentonite, that was under  $38 \mu\text{m}$ , has a main particle-size of about  $25 \mu\text{m}$ , 92.2% of the material under  $106 \mu\text{m}$  and a main particle size of about  $7 \mu\text{m}$ .

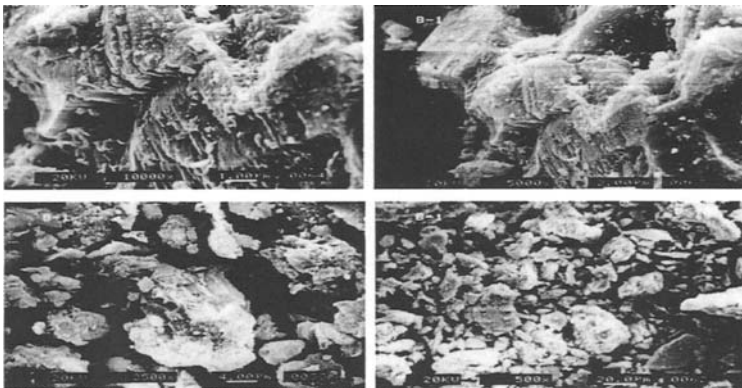


Figure 1: The view of the Yazır bentonite in the electron microscope.

Yazır bentonite is also analyzed for humidity (16%), pH (9.3), swelling proportion (6 times its own volume), surface area (72.96 m<sup>2</sup>/g with BET) and cation exchange capacity (CEC = 81÷87 meq/100 g).

Hydrocyclone and decantation techniques were applied to remove the impurities from the sample.

Table II: Size distribution of Yazır bentonite.

Size fraction (μm)	Yield (% wt)
- 1000+500	2.6
- 500+300	1.0
- 300+212	1.0
- 212+150	1.4
- 150+106	1.8
- 106+75	2.8
- 75+53	2.0
- 53+38	1.4
- 38	86.0

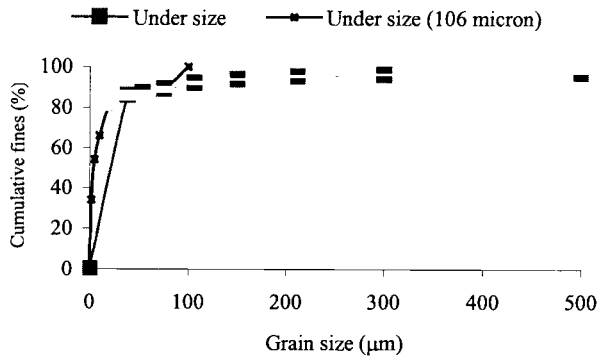


Figure 2: Particle size distribution of Yazır bentonite.

### Hydrocyclone tests

The purpose of the hydrocyclone tests was the removal of impurities (calcite, biotite, feldspar and quartz) from the sample. The effects of the apex (A) and vortex diameters (V) and feed pressure (P) on the separation efficiency were investigated.

The Yazır bentonite, was completely dispersed in water with the “Gieves Mixer” before processing in hydrocyclone. Table III shows the classification results in hydrocyclone obtained from the experiments.

As it is seen, the best results in the hydrocyclone were obtained at vortex diameter: 25 mm, apex diameter 10 mm and a pressure of 3 bar as shown in Table IV.

The quantity of the montmorillonite, in the hydrocyclone overflow products was determined by using the XRD method. The impurities from the Yazır bentonite were completely removed, however, Ca-bentonite could not be separated from the Na-bentonite. For this reason, before the ion exchange process the overflow products obtained from the hydrocyclone were decanted to further purify bentonite.

Table III: Results of hydrocycloning of Yazır bentonite (pulp density 10%).

Diameter (mm)	Pressure (bar)	Overflow (% wt)	Underflow (% wt)
Vortex: 25 Apex: 10	1	75.30	24.70
	2	75.00	25.00
	3	70.80	29.20
Vortex: 25 Apex : 15	1	65.50	34.50
	2	63.60	36.40
	3	58.05	41.95
Vortex: 25 Apex: 20	1	50.24	49.76
	2	49.26	50.74
	3	45.35	54.65
Vortex: 18 Apex: 10	1	65.04	34.96
	2	61.99	38.01
	3	58.50	41.50
Vortex: 18 Apex: 15	1	43.60	56.40
	2	36.48	63.52
	3	63.52	36.48
Vortex: 18 Apex: 20	1	22.22	77.78
	2	24.34	75.66
	3	25.45	75.55

Table IV: Size distribution of hydrocyclone products at Vortex=25 mm, Apex=10 mm, Pressure=3 bar.

Grain size ( $\mu\text{m}$ )	Under flow (% wt)	Over flow (% wt)	Yield of underflow (% wt)	Yield of overflow (% wt)	Mathematical feeding (%)	Average of grain-size (%)	Feed according to passing under flow (% wt)
+50	20	0	5.84	0	5.84	50	100
- 50 + 38	10	0	2.92	0	2.92	44	100
- 38 + 20	24	0	7.01	0	7.01	29	100
- 20 + 10	17	0	4.96	0	4.96	15	100
- 10 + 5	6	0	1.75	0	1.75	7.50	100
- 5 + 2	11	36	3.21	25.49	28.71	3.50	11.19
- 2	12	64	3.51	45.31	48.81	1	7.18
Total	100	100	29.20	70.80	100.00		

### Decantation tests

The decantation process was utilized to obtain rich Na-bentonite product from the Yazır bentonite. In comparison with Ca-bentonite, Na-bentonite remains completely suspended when it was in water because of its larger swelling capacity, whereas Ca-bentonite does not form a colloidal system. Different pulp densities, decantation periods and different decantation stages were investigated and the decantation results were given in Table V.

Table V: Decantation results of Yazır bentonite.

Time between decantation steps (min*)	Suspended product eight (%)	Settled product (% wt)
30	61.3	38.7
60	57.3	42.7
120	56.7	43.3

\*After 4 decantation steps.



The following optimum conditions were determined as 4% pulp density, decantation period of 2 h and a total of 7 decantation steps. At the end of the decantation process, the surface area of the best product was determined as 90.28 m<sup>2</sup>/g and the main particle size was 3 µm.

#### *Ion exchange tests*

The product with relatively high Na content was additionally activated with sodium carbonate (Na<sub>2</sub>CO<sub>3</sub>) in order to reduce the Ca<sup>+2</sup> ions content and obtain a rich Na-bentonite.

In order to produce the organo-clay, the rich Na-bentonite product obtained after the hydrocycloning and decantation experiments was in reaction with quaternary ammonium salts. Thus the variable Na cations, which exist in the Na-bentonite structure have changed place with the organo-molecules existing in the structure of the quaternary ammonium salts.

At the ion exchange experiments corresponding conditions were determined a 1% pulp density, boiling period of 2 h, using disterile dimethyl ammonium chloride in 35% of solid proportion and 2.5 h ion exchange process. The organo-clays obtained, were treated for whitening and then subjected to filtering, drying and grinding. After these processes, viscosity of the product was measured.

#### *Whitening process*

Color of rheological agents is an important parameter for paint industry. If the color is not white, it causes color problems for paint. The obtained organo-clay has a yellow and light brown color, which would not be appreciated as a rheological additive. In order to obtain the white color as Tixogel, the product was firstly washed at least four times in order remove the Na-salts and non-reacted quaternary ammonium salts and then treated with H<sub>2</sub>SO<sub>4</sub> solution which has a pH value of 2.5 before filtering of organo-clay cake.

#### *Filtering-washing and drying*

Conductivity measurements were made with the "Hanna" conductivity measurement equipment with the filtered products which were obtained by filtering-washing after the ion exchange processing that was applied to the Yazır bentonite (Table VI).

Table VI: Conductivity measurement results.

Water type	Conductivity (µS/cm)		
	Yazır	Wyoming	Activated Yazır
Filtered	640	710	2,680
Washing 1	130	80	520
Washing 2	50	70	230
Washing 3	20	60	190
Washing 4	10	20	100
Deionized		0÷10	
Distilled		10÷20	

As shown in Table VI, the conductivity of the aqueous solution, which was obtained after filtering, shows a high value like 640 µS/cm. After washing this value was

reduced to 10  $\mu\text{S}/\text{cm}$ . This indicates that the sodium salts, which exist after filtering-washing, were successfully removed from the clay structure.

To provide the quality of the organo-clays, which were obtained through the experiments, a comparison was made with commercial rheological additive material called Tixogel that was used in solvent based paint.

The results of the viscosity measurement and surface areas (with BET) of the organo-clays that were obtained from the Yazır (Trace), Wyoming (USA), alkaline activated Yazır, Ipsala, Raner bentonites and commercial product Tixogel were shown in Table VII. The whole experimental works were shown in Figure 3.

Table VII: BET surface area and viscosity measurements of organo clays.

Name of bentonite	Surface area ( $\text{m}^2/\text{g}$ )			Viscosity (cP)
	Before ion exchange	After ion exchange with coconut alkylmethyl ammonium chloride	After ion exchange with distrerile dimethyl ammonium chloride	
Yazır	90.28	34.79	11.41	95
Activated Yazır	60.35	-	16.11	80
Wyoming	140.60	25.41	17.50	95
Ipsala	93.22	27.12	8.12	70
Raner	99.70	48.06	24.33	75
Tixogel		5.8		132

## Conclusions and discussion

The particle size distribution experiments, which were made with the sieve analysis and Scanning Photo Sedimentograph equipment, show that 92.2% of the raw Yazır bentonite was under 106  $\mu\text{m}$  and that the main particle size of this fraction was 7  $\mu\text{m}$ . The analysis of the Yazır bentonite shows the following values: humidity 16%, pH 9.3, swelling proportion was 6 times at its own volume, surface area 72.96  $\text{m}^2/\text{g}$  and cation exchange capacity (cec) 81÷87 meq/100 g.

Hydrocycloning and decantation techniques were applied to remove the impurities exist in the bentonite. Following the hydrocyclone tests it was found that the best results were obtained with vortex diameter of 25 mm, apex diameter of 10 mm and pressure of 3 bar. It has been determined that the impurities were completely removed, also very high percentage of Ca-bentonite could be removed from the bentonite. Before the ion exchange process, the overflow products, which were obtained by hydrocycloning, were subjected to decantation.

After the decantation experiments the corresponding conditions were determined as 4% pulp density, decantation period of 2 h and a total of 7 decantation steps. At the end of the decantation process, the surface area of the best product was determined as 90.28  $\text{m}^2/\text{g}$  and the main particle size was obtained as 3  $\mu\text{m}$ .

For obtaining fully riched Na-bentonite,  $\text{Na}_2\text{CO}_3$  activation process was applied to the product before the ion exchange process. After the ion exchange experiments, the corresponding conditions were determined as 1% pulp density, boiling period of 2 h, using distrerile dimethyl ammonium chloride in 35% of solid proportion and the period was 2.5 h.

The conductivity value of the filtrate which was warm and softened water, that was obtained as a result of the filtering-washing which was made after the ion exchange, decreasing from 640  $\mu\text{S}/\text{cm}$  to 10  $\mu\text{S}/\text{cm}$ . This decrease indicates that the sodium salts were successfully removed from the clay structure.

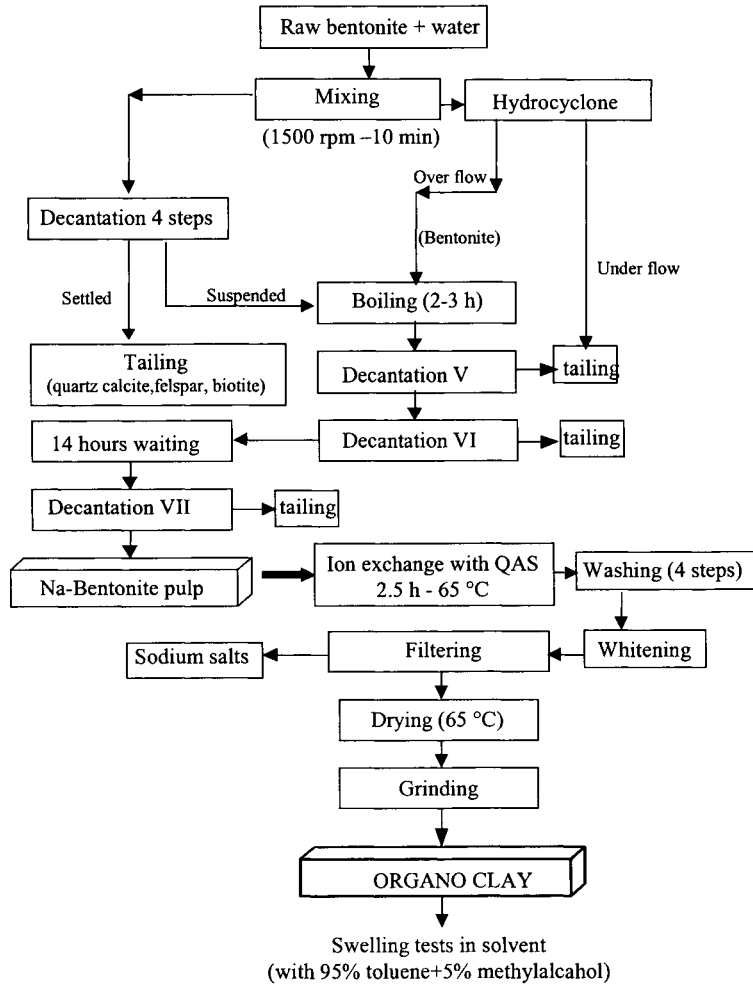


Figure 3: Flowsheet of tests.

The quality of the organo-clays, which were obtained in the reported experiments, compared with Tixogel. The viscosity of Tixogel shows a value of 132 cP whereas the viscosity of the Yazır bentonite remains at 95 cP in solvent. The Na content of the raw Yazır bentonite could be low, need some changes in ion exchange conditions, and to use a different quaternary ammonium salts, to solve the problem.

**References**

- Akbulut, A., 1996. Bentonit, M.T.A. Eğitim serisi no 32, Ankara.
- Baxter, P., 1997. European Markets for U. S. Bentonites, *Industrial Minerals* No 361, 43-49.
- Grim, R.E. and ve Güven, N., 1978. Bentonites, *Geology, Mineralogy, Properties and Uses*. Elsevier, 256.
- Grim, R.E., 1968. *Clay Mineralogy*, 2<sup>nd</sup> ed., McGraw-Hill, New York.
- House, R.F., 1983. Organophilic Clay Gellants. U. S. A Patent Office, Patent number 4382868.
- İpekoğlu, B. and Bilge, Y., 1997. Improvement of the Bentonite Acid Activation Process. *Proceedings of the XX International Mineral Processing Congress, Aachen/Germany*, 249-256.
- Keegan, N., 1998. Bentonite Production. *Industrial Minerals*, No 370, 33-39.
- McMurry, R.C., 1992. *Organic Chemistry*, Cornell University, U.S.A.
- Reynolds, W., Doren, R.V. and Cody, C.A., 1995. Thixotropic Organoclay Additive for Highly Viscous Systems. U. S. A Patent Office, Patent number 5407477.
- Süd-Chemie, 1996. *What is Bentonite?* Catalogue, München, Germany.
- Tixogel, 1996. *Gellants for organic media*. Catalogue, Germany.

## FLOCCULATION AND ADSORPTION-DESORPTION MECHANISM OF POLYMERS ON ALBITE

I. Kurşun\*, B. Ipekoğlu\*, M.S. Çelik<sup>o</sup>, Y. Kaytaç<sup>o</sup>

\*Istanbul University, Mining Engineering Department, Istanbul, Turkey

<sup>o</sup>Istanbul Technical University, Mineral And Coal Processing Sect., Istanbul, Turkey

### Abstract

For several decades, inorganic electrolytes, natural polymers and synthetic, high molecular weight polymers have been used as coagulants or flocculants for clarification of effluents, acid mine drainage and treatment of paper, textile, sugar and other industrial waste water processing applications. Research has shown that interactions between the functional groups on particulate surfaces and those on polymers are responsible for adsorption and subsequent flocculation, and can be appropriately controlled by tailoring polymers with specific functional groups suitable for particular applications. The effectiveness of a polymer for a given flocculation system depends on several parameters, e.g. the polymer dosage, amount adsorbed on the solid surfaces, molecular weight of the polymer, particle size, shape, porosity, ionic strength of the system, electrokinetic properties and more importantly, conformation of the polymer at the solid-liquid interface.

Electrokinetic studies on pure albite show that it is negatively charged throughout the entire pH, and the isoelectric point of the mineral is below pH = 2. Adsorption of the non-ionic polymer (N-300) is found to increase with increasing the pH and concentration of the polymer. A hydrogen-bonding mechanism between the polymer carbonyl (-C=O) or the amide (-NH<sub>2</sub>) groups and the surface oxygen species is proposed to be responsible for the adsorption of non-ionic polymer onto albite. According to desorption tests, no significant change was observed for the albite-non-ionic polymer system.

*Keywords: polymer, adsorption, desorption, flocculation*

### Introduction

Polymer molecules can be made to selectively adsorb onto particles:

- by adjusting the chemical composition of the suspending media;
- by introducing into polymer, active functional groups that will form complexes or salts with the metal atoms on the surfaces of the desired minerals
- by using depressants, such as sodium silicate, that would adsorb on the undesired mineral surface, thereby preventing adsorption of the polymer;
- by using activators that induce adsorption of polymers on desired minerals (Akers, 1975).

Adsorption of polymers on solid surfaces is dependent on polymer properties, such as molecular weight and configuration, distribution of functional groups, solid properties, such as surface charge and oxidation states, and solution properties such as ionic strength, temperature and solvent power for the polymer. The various forces responsible for the adsorption of the polymers on the mineral surfaces result primarily from three types of bonding, namely electrostatic, hydrogen and covalent bonding. The solution-chemistry conditions, the rheology of the solid suspension and the polymer properties dictate the nature of interactions (Chou and Wollast, 1985). Often

several mechanisms may be operating at the same time in controlling the adsorption/flocculation behavior system.

Long chained polymers can be adsorbed onto the grains from several locations along the chain in a single polymer molecule and can also be adsorbed onto more than one grain. In such cases, the grains are bridged by the adsorbed polymers. This mechanism plays an important role in a number of applications. In order for the bridging flocculation to form, the polymer should be of large molecular weight, and a large part of the polymer chain should be adsorbed without interaction with the grain surface. Moreover, the adsorbed amount should not be high, so that a larger part of the grain surface remains free (Çelik et al., 1991). Only in such a case, the free part of the grain surface and extended part of the polymer that is adsorbed onto another grain come into mutual contact. When over-adsorption of a polymer occurs, there remains no free surface for bridging to take place, and bridging is further prevented because of steric impulsion. Therefore, in order for bridging flocculation to occur, there is an optimum polymer dosage, the value of which depends generally on grain concentration.

## **Experimental**

### *Materials*

Ultrapure albite crystals were ground in an agate mortar to obtain a sample  $<74 \mu\text{m}$  in size. This sample was used for both adsorption, desorption and zeta potential measurements, while experiments associated with pure albite were conducted in distilled water. Three non-ionic (N-300) flocculants were received from Cytec Chemical Co. It has been specified that they had molecular weights of  $3 \div 15 \cdot 10^6$ ,  $3 \div 4 \cdot 10^5$ , and  $3 \div 4 \cdot 10^6$ , respectively. Tannic acid, NaCl, NaOH and HCl were certified by Fluka.

### *Methods*

Zeta potential measurements were conducted by means of a Zeta Meter 3.0, which is equipped with a microprocessor unit capable of directly measuring the average zeta potential and its standard deviation. 100 mg of  $<20 \mu\text{m}$  pure albite was added to 100 ml of distilled water and conditioned for 10 min. The suspension was kept stationary for 3 min and the average zeta potential relieved on ten particles was taken as result. Adsorption tests were carried out in 20 ml glass scintillation vials. 1 g of  $<20 \mu\text{m}$  pure albite was added to 15 ml of polymer solution of the desired concentration. The suspension was conditioned for 1 h, and the solids were filtered out. The supernatant was subjected to polymer analysis.

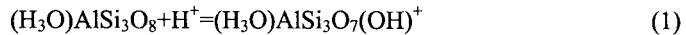
Polymer analysis was made by a nephelometric method developed for low concentrations of polyethylene oxide and polyacrylamide flocculants. A series of samples (5 ml each) of non-ionic polymer solutions of known concentrations in the range of 0–3 ppm was treated with 40 ml of 0.1 M NaCl solution and 5 ml of 0.1 % tannic acid solution in a 50 ml volumetric flask. The mixture was shaken for 1 h, and the turbidity of the resultant solution was measured by a Shimadzu UV/Vis spectrophotometer at a wavelength of 625 nm. The linear portion of the calibration curve, in the range of 0.5–2.5 mg/kg, was used for calculating the residual polymer concentrations.

## Results and discussion

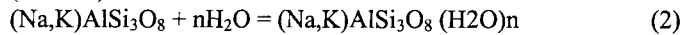
### *Equilibration of albite in water*

The plagioclase feldspars form a complete solid-solution series from pure albite ( $\text{NaAlSi}_3\text{O}_8$ ) to pure anorthite ( $\text{CaAl}_2\text{Si}_2\text{O}_8$ ). Considerable potassium may be present toward the albite end of the series. Therefore, it is more likely that albite should be written as  $(\text{Na,K})\text{AlSi}_3\text{O}_8$ . The dissolution behavior of albite has been systematically studied, showing that the rate of hydrolysis of feldspar is highly pH dependent and results from the following reactions:

- at low pH (<2.9):



- at intermediate pH (2.9÷8.0):



- at high pH (>8.0):



On the basis of coordination chemistry it has been suggested that the factorial orders on  $\text{H}^+$  and ligands given in Equation 3 are compatible with a direct dependence on the degree of surface protonation or on the concentration of ligand surface complexes. It has been also proposed the existence of charged complexes at mineral surfaces. In both equations 1 and 2, hydronium ( $\text{H}_3\text{O}^+$ ) ions can replace  $\text{Na}^+$  or  $\text{K}^+$ . It has been demonstrated that the alkali ions are replaced by  $\text{H}^+$  rather than  $\text{H}_3\text{O}^+$ . This hypothesis is further supported by the fact that the volume occupied by alkali ions in albite is rather small compared to the large  $\text{H}_3\text{O}^+$  (Chou and Wollast, 1985). The most important factors affecting the rate of dissolution of albite are pH and the concentration of dissolved Al. The rate dependence on pH exhibited remarkable similarities to the solubility curves of Al compounds and also, Al showed the largest inhibiting effect on the dissolution rate. Chou and Wollast (1985) thus suggest the formation of surface complexes involving both  $\text{H}^+$  and Al.

### *Dissolution behavior of albite*

Figure 1 presents the dissolution kinetics of albite in water as a function time at initial pH values of 3 and 11, and at natural pH = 6, obtained after introducing the mineral in distilled water.

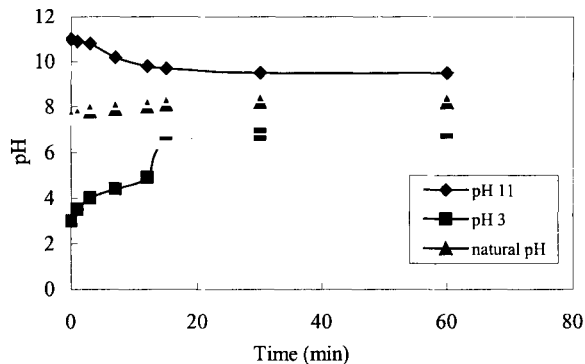


Figure 1: Dissolution kinetics of pure albite in water at different pH values.

It takes approximately 15 min to reach equilibrium pH of 8.1. When the initial pH is adjusted to 3 or 11, it takes about 15 min to approach one pH unit to the natural pH, but several additional hours to reach its equilibrium pH. In other words, albite suspensions are buffered relatively strongly in both acidic and alkali media. It is known that albite dissolution rate is extremely slow under ambient conditions and at a pH close to neutral.

*Electrokinetic behavior of albite*

Albite, as most other silicate minerals, exhibits negative zeta potentials throughout the practical pH range of 2 to 12. The zero point charge (zpc) of albite is roughly between 1 and 2, as shown in Figure 2. This is in line with the zpc of many silicate minerals, including quartz. However, no electrokinetic data on albite was found in the literature. The zeta potential of albite as a function of N-300 non-ionic polymer concentration is given in Figure 3.

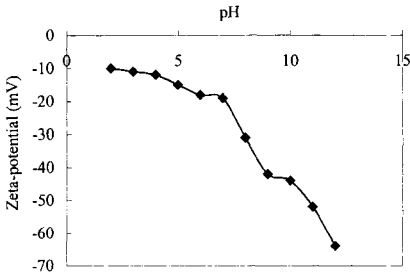


Figure 2: Zeta potential of albite as a function of pH in water.

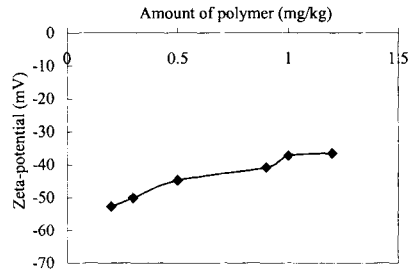


Figure 3: Variation of zeta potential with concentration of N-300.

The zeta potential gradually decreases with increasing N-300 concentration, i.e. it becomes less negative. The albite suspension was found to flocculate at 1 mg/kg N 300 concentration, and measurements became increasingly difficult above this value. The dependence of pH on zeta potential of albite in the presence and absence of different non-ionic polymers is presented in Figure 4. It is clear that the addition of polymer makes the surface of albite less negative at all pH values, with N-300 being the most effective.

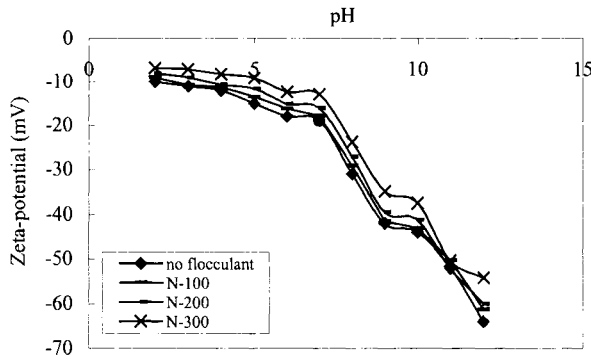


Figure 4: Zeta potential versus pH profile for albite with 1 mg/kg and without polymer addition.



This indicates that as the non-ionicity increases, more of negative charges on the albite surface are tied up with the polymer.

Figure 3 exhibits the settling behavior of albite in the absence and presence of polymer as a function of pH. It is clear that due to scattering, no significant effect of pH is apparent either in the presence or absence of polymer.

#### *Adsorption of polymer on albite*

Adsorption is a rate-dependent phenomenon. Polymers, unlike low molecular weight compounds, are made up of thousands of units. Adsorption kinetics is therefore not only dependent on the surface properties of minerals, but on those of chemicals as well. For a polymer to adsorb, it is sufficient to attach one or more segments to the solid. The dependence of adsorption on conditioning time at the natural pH of albite is given in Figure 5. The equilibrium was attained in about 1 h, and this was used in the subsequent adsorption experiments.

Flocculation and adsorption are both dependent on solid concentration. In flocculation experiments, flocculation was shown to drastically change with the amounts of solid in solution. Similarly, adsorption also changes with solid concentration, as shown in Figure 6. It is seen that adsorption decreases with increasing the solid concentration, and the curve flattens out at above about 0.05 g/ml. For the sake of convenience, all adsorption tests were thus conducted at 0.066 g/ml solid concentration.

Since pH was pointed out as an important parameter in the dissolution of albite, the dependence of adsorption of N-300 was studied as a function of pH. This is shown in Figure 7. Evidently, the adsorption density increases with increasing pH and reaches a constant value above pH = 9, where it becomes difficult to adjust pH. Adjusting the initial pH of the solution to pH = 12 resulted in a pH = 9.3. High adsorption density, neutral and high pH correlate well with the flocculation and settling tests discussed previously.

Adsorption of an isotherm of N-300 onto albite is presented in Figure 8, where the adsorption density is plotted against the residual polymer concentration. Adsorption is found to increase with an increase in polymer concentration and reaches a plateau value at about 30 mg/kg N-300 concentration.

#### *Desorption experiments*

Desorption tests were carried out by replacing the removed portion of the supernatant (2÷4 ml) with a supernatant solution of the same salinity and adjusted pH to match the original supernatant. The desorption cycle was continued until the polymer concentration was below detection limit of the polymer analyses technique. As a result of desorption tests, no significant change was observed for the albite–non-ionic polymer system.

#### *Adsorption mechanism of non-ionic polymer onto albite*

Several mechanisms of polymer adsorption have been suggested, including electrostatic interaction, hydrogen bonding, chemical interactions and hydrophobic bonding.

Since the polymer under discussion is non-ionic in nature, the electrostatic mechanism can be ruled out. Hydrophobic bonding requires that the surface on a mineral be modified by a non-polymeric surfactant and thus, can be excluded as well.

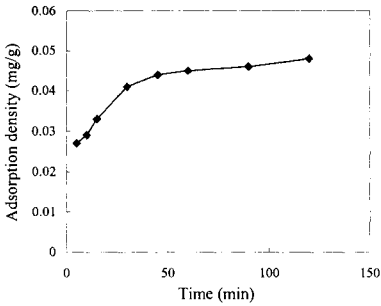


Figure 5: Dependence of adsorption of 10 mg/kg N-300 on albite against conditioning time.

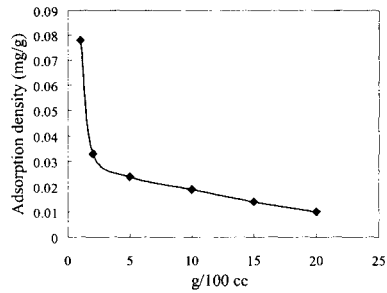


Figure 6: Adsorption density as a function of solid concentration at 10 mg/kg N-300 concentration.

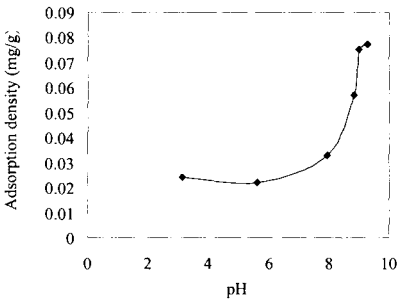


Figure 7: Effect of pH on the adsorption of 10 mg/kg N-300 onto albite.

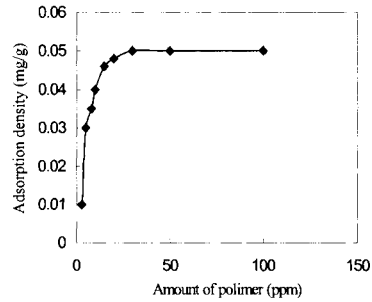


Figure 8: Adsorption of N-300 onto albite at natural pH.

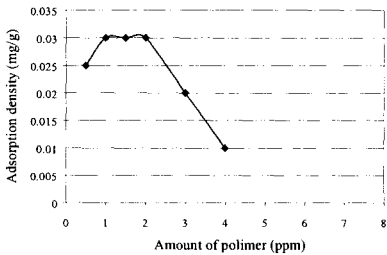


Figure 9: Desorption of 5 ppm polymer concentration.

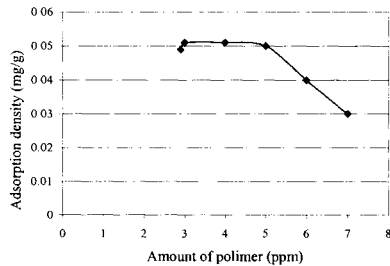


Figure 10: Desorption of 5 ppm polymer concentration.

The latter two mechanisms are therefore possible candidates. Hydrogen bondings occur through binding hydrogen to electronegative elements, such as F, N, S and O. This is a widely accepted mechanism for freshly ground natural silica (Griot and Kitchener, 1965) and clays with non-ionic polymers. Hydrogen bonding can occur between the polymer karbonyl (-C=O) or the amide (-NH<sub>2</sub>) groups and the surface oxygen species. The sharing of the hydrogen bonding between the two electronegative oxygen species induces the adsorption. Flocculation then follows by interparticle

bridging, if the electrostatic repulsion between the particles is not strong. Since albite is a sodium form of silicate mineral, and the polymer is non-ionic, it appears that hydrogen bonding is the only plausible mechanism in the system. As shown in Equations 1 through 3, albite acquires a positive charge below pH = 2.9, and thus is not as very amenable to adsorption of N-300. Above pH = 3, adsorption progressively increases, due to formation of silanol groups, and reaches its highest level above pH = 8, where additional negatively charged surface complexes form. The decrease in the zeta potential of the surface with the addition of polymer shown in Figures 6 and 7 is in agreement with the above explanation. It appears that positive sites are depleted upon addition of the polymer.

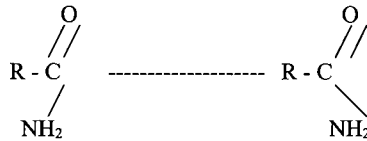


Figure 11: Change of amide groups.

## Conclusions

Electrokinetic studies conducted with pure albite show that albite is negatively charged throughout the entire pH, and the isoelectric point of the mineral is below pH = 2. Adsorption of the non-ionic polymer is found to increase with increasing the pH and concentration of the polymer. A hydrogen-bonding mechanism between the polymer carbonyl or the amide groups and the surface oxygen species is proposed to be responsible for the adsorption of non-ionic polymer onto albite. According to desorption tests, no significant change was observed in the system.

## References

- Akers, R.J., 1975. Flocculation. I Chem. Services, London.
- Çelik, M.S., Ahmad, S. and Al-Hasim, S., 1991. Adsorption/desorption of polymers from Saudi Arabian limestone. *J. Petroleum Sci. and Engineering*, 6, 213-223.
- Chou and Wollast, 1985. Steady-State kinetics and dissolution mechanism of albite. *Amer. J. Sci.*, 285, 963-993.
- Griot, O., Kitchener, J.A., 1965. Role of surface silanol groups in the flocculation of silica suspensions by polyacrilamide. *Trans. Faraday Soc.*, 61, 1026-1038.

## THEORY AND APPLICATIONS OF HYDROPHOBIC FLOCCULATION TECHNOLOGY

S. Song\*, S. Lu<sup>o</sup>

\*Instituto de Metalurgia, Universidad Autónoma de San Luis Potosí  
Av. Sierra Leona 550, San Luis Potosí, S.L.P., C.P.78210, Mexico

<sup>o</sup>Resources Eng. School, University of Science and Technology Beijing  
Xueyuan Road 40, Beijing, 100083, China

### Abstract

The hydrophobic flocculation technology applied to fine minerals and coals beneficiation is described in this paper on the basis of the investigations in laboratory. Initially, a brief description to this process is made. Then, the three important factors of hydrophobic flocculation, namely particle hydrophobicity, kinetic energy input and non-polar oil, are theoretically discussed. Finally, the examples of this process applied to the beneficiation of hematite, sulfide minerals and coal in fine size range are presented. The experimental results suggest that hydrophobic flocculation technology is a promising mean to efficiently recover valuable minerals in the form of fine dissemination.

*Keywords: hydrophobic flocculation, fine particle processing, flocculation kinetics, non-polar oil*

### Introduction

Hydrophobic flocculation arises as a result of hydrophobic interaction between particles in aqueous suspensions and kinetic energy of sufficient magnitude. Because of its high selectivity, it was applied early to mineral beneficiation and can be traced back to the 1950s, when emulsion flotation was presented to treat manganese ore (McCarrol, 1954). In this technique, proper collectors and fuel oil are added to induce the aggregation of valuable mineral fines, while a strong mechanical stirring is applied to the slurry. Later, carrier flotation (Green and Duke, 1962), spherical agglomeration (Capes and Germain, 1982) and shear flocculation flotation (Koh and Warren, 1977) were developed to beneficiate valuable minerals, in form of fine dissemination and slimes. During last two decades, the hydrophobic flocculation technology has been attracted more attentions not only in mineral beneficiation, but also in environmental engineering.

Hydrophobic flocculation technology is coined for the all separation methods based on hydrophobic flocculation of fine particles. It consists of two steps, the selective hydrophobic flocculation and the separation of the flocs from dispersed particles (Song and Lopez-Valdivieso, 1998). The former one includes dispersion, selective hydrophobization and hydrophobic flocculation, which are schematically represented in Figure 1 and depicted as follows. Dispersion is realized by dispersants together with pH adjustment to prevent mineral fines from hetero-coagulation that would be detrimental to separation efficiency. Selective hydrophobization is achieved by special collectors upon their adsorption on desired minerals, which is not unfamiliar to flotation scientists and engineers. Hydrophobic flocculation is usually realized in

mixing tanks, through which the kinetic energy is provided mechanically to hydrophobic particles to overcome the energy barrier. It could be greatly enhanced by introducing various additives such as non-polar oil, force fields, etc. The separation of hydrophobic flocs is usually achieved using froth flotation because of the hydrophobic surfaces. Also, screening and magnetic separation are used for the big and compact flocs and magnetic flocs, respectively.

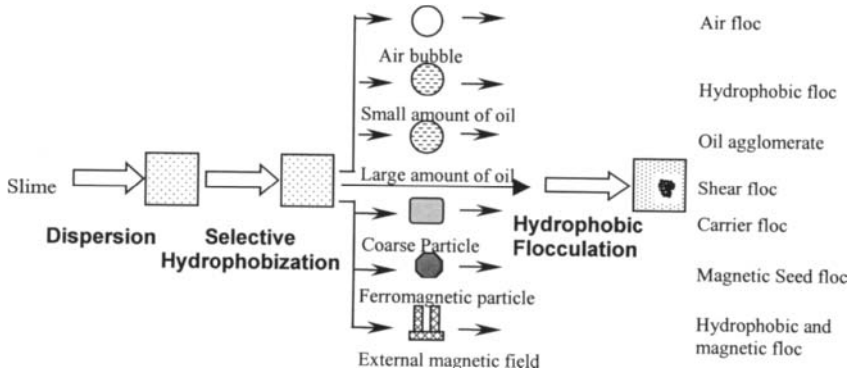


Figure 1: Schematic representation of hydrophobic flocculation of fine particles.

Hydrophobic flocculation and its application to mineral and coal beneficiation have been the authors research interests since the 1980s (Lu et al., 1988; Song and Lu, 1990, 1994; Lu et al., 1998). This paper attempts to highlight what has been achieved on this subject. Some experimental results are presented to show the theoretical characterizations and to illustrate how the beneficiation of mineral and coal fines is improved due to the hydrophobic flocculation.

### Theory of hydrophobic flocculation

#### *Particle hydrophobicity*

Particle hydrophobicity is of foremost importance in hydrophobic flocculation. This characteristic can be made clearer by the experimental results on rhodochrosite fines shown in Figure 2, in which the aggregation efficiency was estimated by sedimentation as described elsewhere (Song and Lu, 1994). As it is noted, no aggregation happened to hydrophilic particles (zero contact angle) even though a strong shear field was applied to the suspension. However, strong aggregations happened to the hydrophobic particles (contact angle of  $33^\circ$  to  $51^\circ$ ). The aggregation efficiency strongly increased with increasing the stirring time, until reaching a maximum and then flatten out. The maximum closely correlated with the contact angle. The more hydrophobic the particles, the more powerful the hydrophobic flocculation was. According to the direct surface forces measurements (Parker et al., 1993; Pashley et al., 1985), the hydrophobic force between hydrophobic surfaces in aqueous solutions is one or two orders of magnitude larger than the DLVO forces in some separation range. Also, the hydrophobic force increases with increasing the

contact angle of the surfaces (Rabinovich and Yoon, 1994). Hence, it is clear that the particle hydrophobicity plays a dominant role in hydrophobic flocculation.

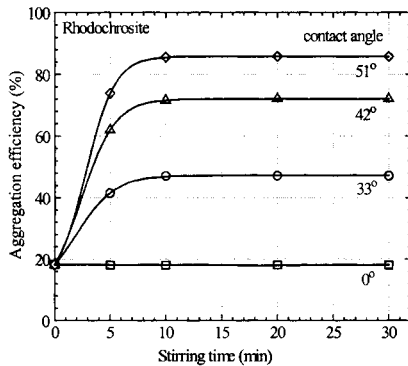


Figure 2: Dependence of the hydrophobic flocculation of rhodochrosite fines ( $d_{50} = 1.79 \mu\text{m}$ ) on particle hydrophobicity (represented by contact angle, and adjusted through varying the sodium oleate concentrations). Other test conditions: pH = 7.8, suspension stirring speed 1,480 rpm.

Because of this characteristic, hydrophobic flocculation features high selectivity, which is ideal for separation technologies. Through adjusting the hydrophobicity of various minerals by using special collectors and depressants, as practiced in froth flotation, the hydrophobic flocculation could only happen to desired minerals, remaining other minerals in dispersion.

#### *Kinetic energy input*

As already stated, in order to prevent various kinds of mineral fines from hetero-coagulation, sufficient surface charges have to be imparted to all the particles, due to which the energy barrier arises. In the case of hydrophobic mineral fines induced by collectors upon their adsorption, the hydrophobic interaction between the particles usually is not strong enough to destroy the energy barrier. Hence, a sufficient kinetic energy input is needed to be provided to the particles to overcome the barrier. This conclusion is supported by the experimental results on the hydrophobic flocculation of quartz fines induced by dodecylamine (DCA), as shown in Figure 3. In this graph, the aggregation degree that is expressed by the change of the particle number concentration before and after the aggregation were measured using a computerized laser turbidity meter, as described elsewhere (Song et al., 1999). As it is noted, the aggregation degree substantially increased with increasing the stirring speed until reaching a maximum around 1,000 rpm, after which it decreased, indicating that a sufficient stirring strength is necessary to achieve the maximum flocculation. The higher stirring speeds yield greater floc-rupture forces in the turbulent flows, breaking the flocs into small pieces and thereby decreasing the aggregation degree.

The hydrophobic flocculation is characterized by the kinetics (Lu et al., 1998). At beginning of hydrophobic flocculation process, in which turbulence appears in the viscous subrange, no floc-rupture occurs and the process is solely dominated by floc formation and the flocs keep growing up. Then, when the flocs grow up to be so large

that the turbulence comes in the inertial subrange, the floc-rupture arises against the floc formation. The flocculation enters an equilibrium state when the rate of floc formation and floc-rupture is balanced. Hydrophobic flocs are ruptured in the form of fragment. However, for electrolytic coagulation, the formation and rupture of coagulates occur simultaneously in the viscous subrange, leaving a much weaker equilibrium aggregation degree. The kinetic characterization of hydrophobic flocculation is mainly due to the deep primary energy valley, and thereby the high floc-strength. The theoretical computation found that for the same surface charge, hydrophobic flocs of quartz have a floc-strength with an order of magnitude two times larger than coagulates (Lu et al., 1998). It is because of the high floc-strength that hydrophobic flocculation can be yielded in strong shear fields, in which no electrolytic coagulates or polymer flocs exist as a result of aggregate rupture.

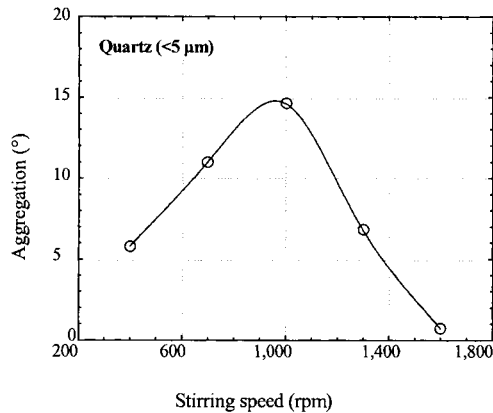


Figure 3: The aggregation degree of the hydrophobic flocculation of quartz fines induced by dodecylamine as a function of stirring speed. Other test conditions: pH=7, T=35 °C.

Hydrophobic flocculation needs high kinetic energy input, and can withstand the strong floc-rupture forces from it. In addition, because of high kinetic energy input, hydrophobic flocs could be more compact as floc porosity is reduced by extrusion, and be purer as impure particles entrained and adhered into the flocs are rejected due to shear and strain forces.

#### *Non-polar oil enhancement*

Non-polar oil such as kerosene and fuel oil was early found to greatly enhance hydrophobic flocculation. This effect mostly originated from two aspects, namely particle hydrophobicity increase and oil bridge. Oil droplets in aqueous suspensions always spread on hydrophobic surfaces due to hydrophobic attraction, resulting in an oil coverage on hydrophobic particles and thus the hydrophobicity increase, which certainly enhances the hydrophobic flocculation. The formation of oil bridges that connect hydrophobic particles involved in flocs strongly increases the floc-strength, resulting in a much more powerful flocculation. Force measurements found that the hydrophobic adhesion force of rhodochrosite particles rendered hydrophobic by

sodium oleate adsorption increased by about 280-fold due to oil bridge in comparison to that without oil (Song et al., 1999).

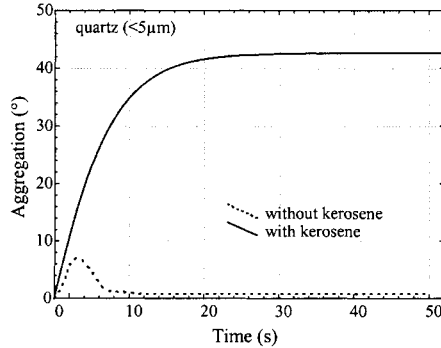


Figure 4: Hydrophobic flocculation process of quartz fines induced by dodecylamine in the presence or absence of kerosene. Other test conditions: pH = 7, T = 35 °C, 1,600 rpm stirring speed.

Non-polar oil enhancement of hydrophobic flocculation can be observed from the experimental results on the hydrophobic flocculation of quartz fines induced by DCA, as shown in Figure 4. It can be seen from this graph that in the presence of kerosene, the aggregation degree strongly increased with increasing the stirring time until reaching a maximum and then flatten out. Without kerosene, however, the aggregation degree reached a small peak as increasing the stirring time, followed by a decline until an equilibrium value was reached. The aggregation degree was much larger in the presence of kerosene than in the absence of kerosene. This increase is mainly due to that the kerosene addition greatly increased the floc-strength, resulting in that the flocs can sustain much stronger floc-rupture forces from turbulent flows. From the point of view of flocculation kinetics, the kerosene addition substantially increased the rate of floc formation, leading to the equilibrium was reached at the much higher aggregation degree.

### Application to fine mineral and coal processing

#### *Beneficiation of Donganshan hematite ore*

Donganshan hematite ore from the Liaoning province of China, is a typical iron ore rich in silica (55% SiO<sub>2</sub>) and poor in iron (30% Fe), in which part of the hematite is finely disseminated. Froth flotation is currently run in the Donganshan concentration plant, producing a concentrate assaying 60% Fe with a recovery of 60%. The majority of the iron loss is found in the form of hematite fines and locked particles. Hydrophobic flocculation technology was tested on this ore in laboratory. First, the head ore was finely ground to 81% minus 10 μm in size, while water glass was added as dispersant. After that, selective hydrophobic flocculation was induced by sodium oleate and a small amount of kerosene was applied to hematite fines, followed by one-step desliming, leaving the overflows as final tailings (desliming was used because of poor iron in the head ore). The sediments then past a high-intensity magnetic separator to obtain a concentrate (hematite flocs) and a middling. An iron



concentrate assaying 65.7% Fe was produced, with a recovery of 76.6%, as shown in Table I. For the concentrate assaying 62.7% Fe, the recovery could increase to 87%. It is clear that hydrophobic flocculation technology is an effective method for the recovery of the hematite fines.

Table I: The beneficiation results of Donganshan hematite ore processed by hydrophobic flocculation technology.

Test N°		Head	Concentrate	Middling	Tailings
E-72	Weight (%)	100.00	35.97	15.49	49.04
	Fe grade (%)	30.85	65.71	24.88	6.58
	Fe recovery (%)	100.00	76.63	12.90	10.47
E-68	Weight (%)	100.00	42.33	11.74	45.93
	Fe grade (%)	30.41	62.70	9.60	6.00
	Fe recovery (%)	100.00	87.27	3.69	9.04

Test conditions: pH=9.5; 20% solid slurry; 0.9 kg/t and 0.7 kg/t water glass for E-72 and E-68; 1 kg/t and 1.5 kg/t sodium oleate for E-72 and E-68; 2.5 kg/t kerosene; 1,200 rpm slurry stirring for 20 min in hydrophobic flocculation step; 1 T field strength for high-intensity magnetic separator.

#### *Beneficiation of sulfide minerals from Rey de Plata ore*

Hydrophobic flocculation flotation was tested on the Rey de Plata ore from Guerrero of Mexico in laboratory. This ore contains silver, gold and sulfide minerals of lead (galena), zinc (sphalerite) and copper (chalcopyrite), which are finely disseminated with pyrite, baryte and quartz. For the test, the head ore was first ground to 87.5% minus 400 mesh, while zinc sulfate, sodium sulfite and sodium cyanide were added as depressants for pyrite and sphalerite. Then, the slurry was intensively conditioned in a mixing tank while lime as pH-regulating reagent, and Aerofloat-242, Aerofloat-3418 and kerosene as collectors were added.

The hydrophobic flocs of galena and chalcopyrite generated from this conditioning, followed by the rougher and three-step cleaner flotation to float the flocs and obtain the lead concentrate. After that, the rougher tailings from lead flotation were strongly stirred while lime as pH-regulating reagent, copper sulfate as activator, and amyl xanthate and kerosene as collectors were added, in order to produce the hydrophobic flocs of sphalerite.

Next, the rougher and three-step cleaner flotation were followed to obtain zinc concentrate. Part of the beneficiation results is illustrated in Figure 5.

The results from the conventional flotation that followed the same flowsheet and reagents as the hydrophobic flocculation flotation but under intensive conditionings and kerosene addition are also presented. It is noted from the graph that the beneficiation of the Rey de Plata ores was greatly improved due to the hydrophobic flocculation.

At the same concentrate grades, the hydrophobic flocculation flotation increased the recoveries of lead, silver and copper in lead concentrate to about 11%, 4% and 22%, respectively, and the recovery of zinc in zinc concentrate to about 16%, in comparison to the conventional flotation. It is clear that this process is a promising mean to beneficiate sulfide mineral fines.

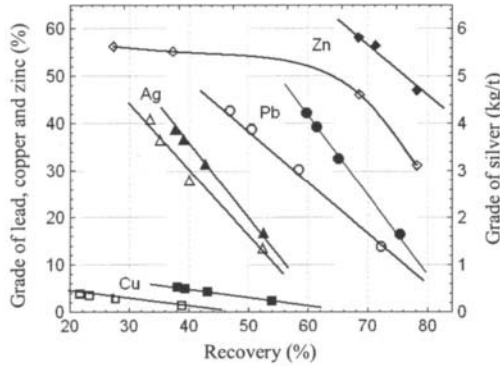


Figure 5: Cumulative grade vs. recovery for the concentrates from the beneficiation of Rey de Plata ore with hydrophobic flocculation flotation (solid symbols) or conventional flotation (open symbols) (triangle: silver in lead concentrate; circle: lead in lead concentrate; diamond: zinc in zinc concentrate; rectangle: copper in lead concentrate).

*Preparation of ultra-clean coal from Bayi bituminous*

Hydrophobic flocculation flotation was tested on the Bayi bituminous from the Shandong province of China for preparing an ultra-clean coal (less than 1% ash remaining). The head coal, with 11.86% ash, taken from the flotation concentrate of the Bayi coal cleaning plant, was first finely ground to 4.2 μm volumetric mean diameter (d<sub>50</sub>) using a ball mill while 1.0 kg/t tannic acid was added as dispersant. Then, the slurry was strongly conditioned at 1,800 rpm for 40 min together with 20 kg/t of kerosene, followed by flotation to recover the coal flocs. Through rougher and two-step cleaner flotation, the ultra-clean coal with 0.6% ash remaining was produced, with 65.5% Btu recovery and 97% ash rejection, as shown in Table II. With techniques other than the chemical processing method, it is hard to produce such ultra-clean coal.

Table II: The beneficiation results of Bayi bituminous for the preparation of ultra-clean coal with hydrophobic flocculation flotation. Test Conditions: pH = 8.8; 20% solid slurry; 1 kg/t tannic acid; 20 kg/t kerosene; slurry stirring in 1,800 rpm for 40 min in the flocculation step.

Products	Head coal	Clean coal	Middling I	Middling II	Tailings
Weight (%)	100.00	58.02	6.46	10.14	25.38
Ash content (%)	11.86	0.62	4.42	15.42	38.04
Btu recovery (%)	100.00	65.42	7.01	9.73	17.84
Ash rejection (%)		96.97			

**Conclusions**

From the experimental results presented in this paper, the hydrophobic flocculation technology is pointed out as a promising mean for the beneficiation of valuable minerals from finely disseminated ores and slimes, and for the deep rejection of minerals fines from coal. The key to this process is the selective hydrophobic flocculation, which is realized through the adsorption of special collectors and depressants and the kinetic energy input of sufficient magnitude. The separation of

hydrophobic flocs from dispersed particles can be realized not only by froth flotation, but also magnetic separation and other techniques.

The dominant factors of the hydrophobic flocculation are particle hydrophobicity and kinetic energy input. By adjusting the two parameters, not only a powerful hydrophobic flocculation, but also high selectivity and compact and pure flocs can be obtained. The another important factor is non-polar oil addition, which enhances the hydrophobic flocculation owing to increasing the floc-strength.

#### Acknowledgements

S. S. gratefully acknowledges the Consejo Nacional de Ciencia y Tecnologia (CONACyT) of Mexico for his financial supports to this work under the grant #485100-5-25840A and the Servicios Industriales Peñoles, S.A. de C.V. of Mexico for the permission to publish the data.

#### References

- Capes, C.E. and Germain, R.F., 1982. Selective oil agglomeration in fine coal beneficiation. Y.A. Liu (ed.), *Physical Cleaning of Coal*, Dekker, New York, 293-352.
- Green, E.W. and Duke, J.B., 1962. Selective froth flotation of ultrafine minerals or slimes. *Trans. AIME*, 233, 389-395.
- Koh, P.T.L. and Warren, L.J., 1977. Flotation of flocs of ultrafine scheelite. *Trans. Inst. Min. Metall., Sect. C*, 86, 94-95.
- Lu, S., Ding, Y. and Guo, J., 1998. Kinetics of fine particle aggregation in turbulence. *Adv. Colloid Interface Sci.*, 78, 197-235.
- Lu, S., Song, S. and Dai, Z., 1988. The hydrophobic and magnetic combined aggregation of paramagnetic minerals, a new way of fine particles separation. *Proceedings of XVI International Mineral Processing Congress*, E. Forssberg (ed.), Elsevier, Amsterdam, 999-1009.
- McCarroll, S.J., 1954. Upgrading manganese ore. *Trans. AIME*, 199, 289-293.
- Parker, J.L., Yaminsky, V.V. and Claesson, P.M., 1993. Surface forces between glass surfaces in cetyltrimethylammonium bromide solution. *J. Phys. Chem.*, 97, 7706-7710.
- Pashley, R.M., McGuiggan, P.M. and Ninham, B.W., 1985. Attractive forces between uncharged hydrophobic surfaces: direct measurements in aqueous solution. *Science*, 229, 1088-1089.
- Rabinovich, Y.I. and Yoon, R.-H., 1994. Use of atomic force microscope for the measurements of hydrophobic forces between silanated silica plate and glass sphere. *Langmuir*, 10, 1903-1909.
- Song, S. and Lopez-Valdivieso, A., 1998. Hydrophobic flocculation flotation for beneficiating fine coal and minerals. *Sep. Sci. Technol.*, 33, 1195-1212.
- Song, S., Lopez-Valdivieso, A. and Ding, Y., 1999. Effects of nonpolar oil on hydrophobic flocculation of hematite and rhodochrosite fines. *Powder Technol.*, 101, 73-80.
- Song, S. and Lu, S., 1990. Hydrophobic aggregation flotation of rutile particles. *Advances in Fine Particles Processing*, J. Hanna and Y.A. Attia (eds.), Elsevier, New York, 279-283.
- Song, S. and Lu, S., 1994. Hydrophobic flocculation of fine hematite, siderite and rhodochrosite particles in aqueous solution. *J. Colloid Interface Sci.*, 166, 35-42.

## **HYDRO AND BIOHYDROMETALLURGY**

This Page Intentionally Left Blank

<b>The Dissolution and Interactions of Gibbsite Particles in Alkaline Media</b> J. Addai-Mensah, J. Dawe, J. Ralston	C6-1
<b>Evaluation of an HCl Process for Leaching of Low-Grade Highly Siliceous Bauxite Ore from Khushab, Pakistan</b> S.A. Hussain, R. Jamal	C6-8
<b>Application of Solvent Impregnated Resin to the Treatment of Heavier Rare Earth Residue</b> J. Shibata, S. Matsumoto, H. Yamamoto	C6-15
<b>Gold Extraction from Kaymaz Gold Ore by Thiourea Leaching</b> S. Örgül, Ü. Atalay	C6-22
<b>Synthesis of Aragonite by the Carbonation Process Using Stainless Refining Dust in Iron &amp; Steel Plants</b> J.H. Ahn, K.S. Choi, H. Kim, S.H. Yoon, J.S. Kim, G.W. Sung, K.H. Lee	C6-29
<b>Development of an Iron Removal Process from Kaolin by Thiourea Leaching: Kinetic and Related Statistical Analysis</b> F. Vegliò, F. Beolchini	C6-36
<b>Application of Thiobacillus Ferrooxidans by Bacterial Desulfurization of Coal</b> P. Fečko, V. Sedláčková	C6-43
<b>The Adsorption of Precious and Base Metals on Xad7 Ion Exchange Resin</b> E.R. Els, L. Lorenzen, C. Aldrich	C6-50
<b>The Influence of Precipitation Variables on the Aggregation and Crystalline Structure of Stabilized Zirconia Powders</b> A.P.A. Oliveira, M.L. Torem	C6-57
<b>Solvent Extraction of Cu (Ii) and Fe (Iii) using Lix 1104sm</b> P. Navarro, J. Simpson, F.J. Alguacil	C6-64
<b>A Comparison of Lix984® and Non-Conventional Reagents as Copper Extractants</b> J.B.A. Paulo, J.Y.P. Leite	C6-70
<b>Development and Application of Filblast Mass Transfer Technology in Hydrometallurgical Processing</b> B.J. Sceresini, G. Nguyen	C6-77
<b>Selective Separation of Yttrium from Chemical Concentrate of Rare Earth</b> E. Panturu, D.P. Georgescu, F. Aurelian, N. Udrea	C6-84

This Page Intentionally Left Blank

## THE DISSOLUTION AND INTERACTIONS OF GIBBSITE PARTICLES IN ALKALINE MEDIA

J. Addai-Mensah, J. Dawe, J. Ralston

Ian Wark Research Institute, University of South Australia  
Mawson Lakes, Adelaide, 5095, Australia

### Abstract

Gibbsite-solution interfacial reactions are important in the Bayer process used for alumina extraction from caustic soda-digested bauxite ores.

The dissolution and the interaction forces of gibbsite particles dispersed in undersaturated NaOH solutions have been investigated to characterize the kinetic behavior and elucidate the existence of gibbsite colloid stability at high ionic strength and pH >13.

The results showed that the dissolution of pure, colloidal size gibbsite crystals increases rapidly with increasing temperature and total surface area of crystal but was independent of the rate of agitation and NaOH concentration >1 M.

The dissolution rate depended upon the concentration of  $Al^{III}$  released in solution to the power of 2, with an activation energy  $90 \text{ kJmol}^{-1}$  estimated for the dissolution process. At near  $Al^{III}$  saturation and high ionic strength >2 M, the gibbsite dispersion showed an unusual colloid stability. Under this solution condition, colloid probe atomic force microscopy (AFM) measurements indicated the presence of long-range, monotonically repulsive forces between the gibbsite particles. A surface, chemical reaction-controlled model derived for the dissolution kinetics and the AFM force data together suggest that a structured, interfacial layer whose formation possibly involves dimeric  $Al^{III}$ -containing species may be responsible for the observed colloidal stability.

*Keywords: gibbsite, dissolution, kinetics interaction forces, colloid stability*

### Introduction

Interactions between octahedrally-coordinated gibbsite ( $\gamma\text{-Al}(\text{OH})_3$ ) particles and tetrahydroxo  $Al(\text{OH})_4^-$  species in caustic aluminate solutions at high ionic strength are of fundamental importance to the production of alumina from bauxite by the Bayer process. Gibbsite dissolution occurs during bauxite digestion in concentrated caustic soda whilst its subsequent separation is achieved by recrystallization from supersaturated caustic aluminate liquor. Due to the high activation energy involved energy ( $90\div 120 \text{ kJmol}^{-1}$ ) high dissolution rates are only achieved at elevated temperatures (>150 °C) (Roach, 1985; Scotford and Glastonbury, 1972). Crystal growth is also slow even at high temperatures (>60 °C) and high  $Al^{III}$  supersaturation. To date, only limited number of fundamental studies of gibbsite dissolution in alkaline media have been reported (Roach, 1985; Packter and Dhillon, 1973; Scotford and Glastonbury, 1972; Lundquist and Leitch, 1964). The mechanisms and kinetics of dissolution were revealed to be dependent upon solution pH,  $Al^{III}$  undersaturation, water activity, mean ionic activity of NaOH, temperature, particle size and active surface area. Although our understanding of both gibbsite dissolution and crystallization processes is fairly advanced, there is a paucity of knowledge on



gibbsite-solution interfacial chemistry underpinning particle interactions, particularly in undersaturated/saturated solution environment at high pH (>13). Our previous coagulation rate and rheological studies indicated the existence of unusual gibbsite colloid stability at low ionic strength ( $<10^{-2}$  M) and high pH (Addai-Mensah et al., 1998). The nature of the structure of the interfacial layer structure, linked with the gibbsite dissolution process and the consequent impact on colloid stability in dispersions of high alkalinity, is of particular interest. Therefore, the focus of the present work is to investigate the gibbsite dissolution behavior and measure particle interaction forces in high ionic strength NaOH solutions at near  $\text{Al}^{\text{III}}$  saturation conditions. The effect of caustic concentration, temperature, seed charge/surface area and agitation rate was probed.

### Experimental section

Pure, synthetic gibbsite crystals (Hydral-710, Alcoa, USA) with sizes in the range  $0.3\div 2\ \mu\text{m}$  with specific surface of  $7.2\ \text{m}^2\text{g}^{-1}$ , were used in isothermal, batch dissolution studies. Caustic solutions containing 0.1 to 8.0 M NaOH were prepared from NaOH (99.0% wt, 1.0% wt  $\text{Na}_2\text{CO}_3$ ; Merck, Australia) and Milli-Q water (specific conductivity  $<0.5\ \mu\text{Scm}^{-1}$ , surface tension at  $20\ ^\circ\text{C}$  of  $72.8\ \text{mNm}^{-1}$  and  $\text{pH} = 5.6$ ). A stirred, well-sealed,  $1\ \text{dm}^3$  polymethylpentane vessel maintained at constant temperature by a thermostatically controlled oil-bath served as the reaction vessel. Dissolution was studied at  $30\div 70\ ^\circ\text{C}$  and seed charge  $3\div 30\ \text{g/dm}^3$  solution. An agitation rate of 180 rpm was used unless stated otherwise. Slurry samples were periodically removed from the dissolver to determine their solids content, BET surface area of undissolved crystals and concentration of  $\text{Al}^{\text{III}}$  in solution. The latter was measured by atomic absorption spectroscopy (GBC 9066AA). Gibbsite interparticle force measurements were conducted at  $30\ ^\circ\text{C}$  using coarse, monocrystalline gibbsite crystal (Pechiney/Queensland Alumina), a hydrated alumina sphere (Union Carbide, USA) and a Digital Instruments Nanoscope III, USA, equipped with an E-head and a fluid cell as well as the colloid probe AFM methodology described elsewhere (Addai-Mensah et al., 1998; 1999a). The hydrated sphere, shown by XPS analysis to have gibbsite-like surface structure, was glued to the tip of an AFM cantilever and used as *colloid probe*.

### Results and discussion

#### *The effect ionic strength and agitation rate on dissolution*

The effect of  $\text{OH}^-$  ion concentration on the dissolution rate was investigated by varying the ionic strength of NaOH ( $0.1\div 8.0$  M). Figure 1 shows typical solution  $\text{Al}^{\text{III}}$  concentration profile as function of time at  $30\ ^\circ\text{C}$  and seed charge of  $9\ \text{g/dm}^3$  solution, indicating that the dissolution rate was NaOH concentration independent at  $>1$  M. This result is contradictory to the hydroxide ion concentration dependence reported by Scotford and Glastonbury (1972) and Packter and Dhillon (1973) for the dissolution of coarse gibbsite crystals. Apart from the difference in particle sizes/surface area, the exact reason for the lack of agreement is not clear. Furthermore, fast and slow dissolution regimes were observed at the initial ( $<50$  min)

and later stages, respectively. After 72 h, the rate was negligibly small, approaching a 'pseudo equilibrium' state, although >20% of the initial mass of crystals remained undissolved. This is believed to be due to the loss of the active sites (e.g. kinks and steps) at the crystal surface. Similar trends but faster kinetics were obtained at a seed charge of 30 g/dm<sup>3</sup> solution and at 50 and 70 °C.

The investigation of the influence on agitation rate on the dissolution showed that stirring enhanced the kinetics but increasing impeller speed above 100 rpm did not have any noticeable effect (Figure 2). This suggests that volume diffusion did not play any significant role in the mechanism of dissolution at the agitation rate (180 rpm) used in this study.

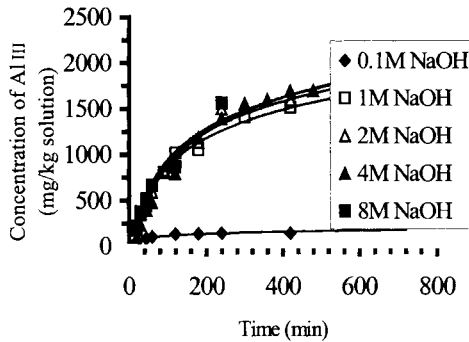


Figure 1: The concentration of Al<sup>III</sup> released during gibbsite dissolution in NaOH solutions of different molarities at 30 °C as a function of time.

#### *Effect of crystal surface area and temperature*

The amount of Al<sup>III</sup> released in solution was observed to increase proportionally with increasing initial crystal surface area (22 m<sup>2</sup>/dm<sup>3</sup> to 194 m<sup>2</sup>/dm<sup>3</sup> and 216 m<sup>2</sup>/dm<sup>3</sup> solution). A linear increase of specific surface area and a concomitant, non-linear decrease in slurry solids content and hence, total surface area of crystals were noticed with time.

The effect temperature was investigated at 30 °C, 50 °C and 70 °C and in 2.0 and 4.0 M NaOH solutions. The flux of Al<sup>III</sup> released was determined from the instantaneous Al<sup>III</sup> concentration and total surface area of crystals in suspension. The initial fluxes estimated from the fast regime at <50 min showed that a 20 °C temperature increase resulted in 8÷10 fold increase in the dissolution kinetics. The rate constants estimated from the initial rate data showed Arrhenius temperature-dependency as indicated by Figure 3. Activation energies ( $E_a$ ) 85 ± 10 kJmol<sup>-1</sup> and 91 ± 10 kJmol<sup>-1</sup> were respectively estimated for the 2 and 4 M NaOH solutions, which thus indicate the lack of ionic strength dependency. The observed  $E_a$  show strong agreement with 90÷120 kJmol<sup>-1</sup> reported (Scotford and Glastonbury, 1972; Packter and Dhillon, 1973). The high activation energy also suggests that the dissolution process is distinctly, surface chemical reaction-controlled, and concurs with the lack of influence of agitation.

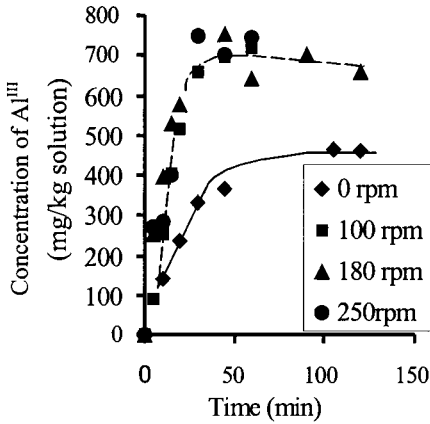


Figure 2: The Effect of agitation rate on the concentration  $Al^{III}$  released as a function of time, in the dissolution of Hydral 710 ( $3 \text{ g/dm}^3$ ) in 4 M NaOH at  $30^\circ\text{C}$ .

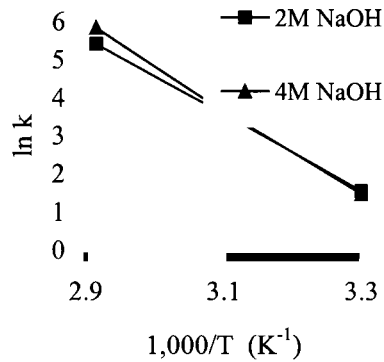


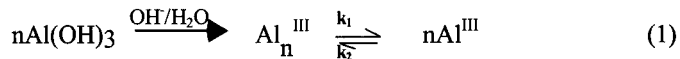
Figure 3: Arrhenius plot of  $\ln(k)$  versus reciprocal temperature for gibbsite dissolution in 2 M and 4 M.

#### *Gibbsite particle interaction forces*

The dissolution process was marked by a fast phase initially followed by a perennially slow regime where pseudo-equilibrium existed (typically after 72 h). For the latter, solution  $Al^{III}$  concentration of  $0.2 \div 0.3 \text{ M}$  (25% lower than the equilibrium solubilities achieved after 14 days) was observed in dispersions of ~2% wt solids (from initial 3% wt solids) for 2 and 4 M NaOH solutions at  $30^\circ\text{C}$ . The analysis of the turbidity of the slow dissolving dispersions, performed by UV-Vis spectrophotometry in the manner of Addai-Mensah et al., (1998) showed clear evidence of an usual colloid stability. Colloid probe AFM investigation of the interparticle forces was carried out under similar solution conditions at  $30^\circ\text{C}$ . Sphere radius-normalized force ( $F/R$ ) versus interparticle separation distance data extracted from the cantilever-piezoelectric data is given in Figure 4. The results for gibbsite (001) face-sphere interactions show monotonic repulsion over a 40 nm range with no jump into contact in both caustic media and Milli-Q water. The forces were 3 to 4 times higher in the caustic media than in Milli-Q water and more pronounced in 4 M than in 2 M solution. The existence of such long-range, repulsive forces at high ionic strength is contrary to the expectations of DLVO theory.

#### *Modelling the mechanism and kinetics of dissolution*

Gibbsite dissolution in caustic solution may be generically described by a system of tetrahedral,  $Al^{III}$ -containing species in dynamic equilibrium as in equation 1. In the initial stages where faster dissolution occurs due to the high  $Al^{III}$  under saturation, the equilibrium is largely shifted to the right in favor of the forward reaction.



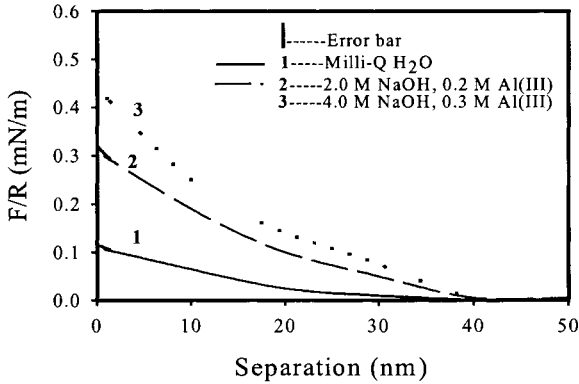


Figure 4:  $F/R$  as a function of separation distance measured at gibbsite (001) crystal face in Milli-Q water, undersaturated sodium aluminate solutions at 30 °C and scan rate of 0.49 Hz.

The kinetics data showed that above 1 M NaOH, gibbsite was the only rate limiting reactant. Thus, the  $\text{OH}^-$  ion being an excess reactant was not considered a variable for modelling the dissolution kinetics at high caustic concentrations. Furthermore, in the absence of volume diffusion and the observation of high activation energy, we consider only the models applicable to surface reaction-controlled dissolution. Two basic kinetic expressions, one based on empirical power law approach (equation 2) and the other derived on the basis of conventional kinetic arguments (equation 3) were examined.

$$\frac{1}{A} \frac{d(C^* - C)}{dt} = k(C^* - C)^n \quad (2)$$

$$\frac{1}{A} \frac{dC}{dt} = k((C^*)^n - C^n) \quad (3)$$

Where  $A$  is total crystal surface area at time  $t$ ,  $C$  instantaneous  $\text{Al}^{\text{III}}$  concentration,  $C^*$  equilibrium gibbsite solubility,  $k$  is a rate constant and  $n$  is the “reaction order”. We note that the reaction order  $n$  neither has a simple theoretical basis nor a direct relationship with the number of species ( $= 4$ ) obtained by gibbsite dissociation  $\text{Al}(\text{OH})_3 \rightarrow \text{Al}^{\text{III}} + 3(\text{OH})^-$  as proposed by Davies and Jones (1955). Analysis of the log-log plots of the kinetic data using equation 2 indicated  $n$  to be  $2.1 \pm 0.2$ . Hence, a second order rate law was assumed as a basis for equation 3, which as a consequence, leads to a bimolecular dissolution reaction mechanism (for  $n = 2$  in equation 1). Upon integration with  $n = 2$ , equation 3 becomes:

$$\frac{1}{2AC^*} \log \frac{C^* + C}{C^* - C} = kt \quad (4)$$

The goodness of fit of the kinetics data to equation 4 is exemplified by the strong, linear relationship between  $\frac{1}{A} \log \frac{C^* + C}{C^* - C}$ , and time  $t$  shown in Figure 5 for a typical

run carried out at 30 °C in 4 M NaOH. The discrimination between the 2 models (equations 2 and 3) carried out on the basis of the minimum predictive variance and minimum bias criteria showed that the kinetics of dissolution were better represented by equation 3 than 2. Consequently, it may be contended that the dissolution process possibly involves rate-determining,  $\text{Al}^{\text{III}}$ -containing dimer formation and saturation at the crystal-solution interface, which may lead to  $2 \text{Al}(\text{OH})_4^-$  monomers release into solution. The simplified process is schematically is described in Figure 6.

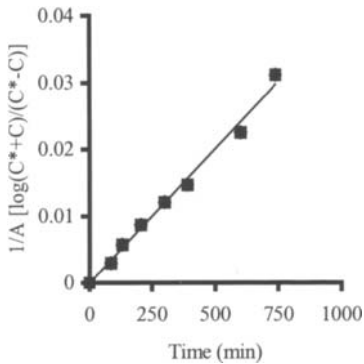


Figure 5: The plot of  $1/A[\log(C^*+C)/(C^*-C)]$  and dissolution time determined according to equation 3 by assuming a 2<sup>nd</sup> order rate law, using the data obtained at 30 °C, 4 M NaOH and 30 g/dm<sup>3</sup> seed.

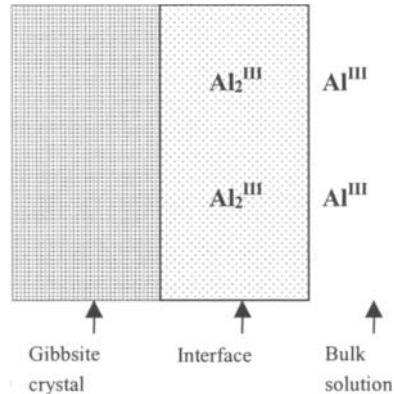


Figure 6: A schematic representation of the proposed  $\text{Al}^{\text{III}}$ -containing, "structured" layer present at the gibbsite-solution interface.

The formation of dimeric and polycondensed aluminate species at the surface of each gibbsite particle may be part of the mechanism responsible for the build-up of repulsive, 'structured', interfacial layers (Addai-Mensah and Ralston, 1999). Unequivocal evidence for the formation of tetrahedrally-coordinated,  $\text{Al}^{\text{III}}$ -containing dimers and polycondensed species in caustic aluminate solutions has been provided by several studies (Watling, 1998; Watling et al., 1998; Buvari-Barcza et al., 1998; Baes and Mesmer, 1976). The existence of long-range, repulsive forces is believed to be linked to an interfacial structure developed from the  $\text{Al}^{\text{III}}$ -containing dissolution products. Similar structured layers have been reported to be responsible for the repulsion between gibbsite particles in metastable caustic aluminate solutions (Addai-Mensah et al., 1998; 1999a and b).

## Conclusions

The kinetics of dissolution and interaction forces of gibbsite particles have been investigated in undersaturated NaOH solutions at ionic strength  $>1$  M. The results showed that the dissolution of pure, colloidal size gibbsite crystals occurred at a rate which increased rapidly with increasing temperature and total surface area of crystal solution but independent of agitation rate and caustic concentration. The dissolution

rate depended upon solution  $\text{Al}^{\text{III}}$  concentration to the power of 2 and involved an activation energy of  $90 \text{ kJmol}^{-1}$ . Under near saturation conditions and high ionic strength ( $>2 \text{ M}$ ), anomalous colloid stability was evident. AFM colloid probe measurements indicated the presence of monotonically repulsive interaction forces between the gibbsite particles. A surface, chemical reaction-limited model derived for the dissolution kinetics and the interaction force data together suggest that an interfacial layer whose formation possibly involves dimeric/polymeric  $\text{Al}^{\text{III}}$ -containing species in solution is believed to be responsible for the observed colloid stability.

### References

- Addai-Mensah J., Dawe, J., Hayes, R., Prestidge, C.A. and Ralston, J., 1998. The unusual colloid stability of gibbsite at high pH. *J. Colloid and Interface Science*, 203, 115-121.
- Addai-Mensah, J., Prestidge, C.A. and Ralston, J., 1999. Interparticle forces, interfacial structure development and agglomeration of gibbsite particles in synthetic Bayer liquor. *Min. Eng.*, 655-669.
- Addai-Mensah, J. and Ralston, J., 1999. The influence of interfacial structuring and forces on gibbsite interactions in Bayer liquors. *J. Colloid. and Interface Science*, 215, 124-130.
- Baes, C.F and Mesmer, R.E., 1976. The hydrolysis of cations: Boron, Aluminium and scandium. A Wiley-Interscience Publication, John Wiley and Sons. New York, 112-122.
- Buvari-Barcza, A., Rozsahegyi, M. and Barcza, L., 1998. Hydrogen bonded associates in the Bayer process (in concentrated lyes): the mechanism of dissolution. *J. Mater. Chem.*, 8(2), 451-455.
- Davies, C.W. and Jones, A.L., 1955. Inadequacy of theories of crystal dissolution. *Trans. Faraday Soc.* 5, 812-818.
- Lundquist, R.V. and Leitch, H., 1964. Solubility characteristics of sodium aluminate. United States Dept. of Interior Report 6504.
- Packter, A. and Dhillon, H.S., 1973. The kinetics and mechanism of the heterogeneous reactions of crystallized gibbsite powders with aqueous NaOH solutions. *J. Phy. Chem.*, 77(25), 2942-2947.
- Roach, G.I.D., 1985. The influence of mineralogy on the dissolution kinetics of gibbsite. *Light Metals TMS publication USA.*, 183-196.
- Scotford, R.F. and Glastonbury, J.R., 1972. The effect of concentration on the rates of dissolution of gibbsite and boehmite. *The Canadian Journal of Chem. Eng.*, 50, 754-758.
- Watling, H., 1998. Spectroscopy of concentrated sodium aluminate solutions. *Applied Spectroscopy*. 52(2), 250-258.
- Watling, H.R, Fleming, S.D. Bronswijk, W.V and Rohl, A.L., 1998. Ionic structure in caustic aluminate solutions and gibbsite precipitation. *J. Chem. Soc. Dalton Trans*, 3911-3917.

## EVALUATION OF AN HCL PROCESS FOR LEACHING OF LOW-GRADE HIGHLY SILICEOUS BAUXITE ORE

S.A. Hussain, R. Jamal

Department of Mining Engineering, University of Engineering and Technology,  
Lahore-54890, Pakistan

### Abstract

This paper presents the results of the experimental work done to find out the extraction percentage of alumina content in ore samples of bauxite from four mines of Khushab (the Sultan Mehdi, Chamil More, Nadi and Niaz mines), after they were subjected to leaching with hydrochloric acid (HCl). The alumina ( $\text{Al}_2\text{O}_3$ ) content of the raw ore samples was 39.51%, 38.23%, 45.01% and 37.17%, whereas silica content was 40.64%, 42.26%, 36.50% and 44.41%, respectively. The petrographic study showed that there are fine-grained dissemination of goethite. A minor amount of quartz was also present in the ore. X-ray diffraction (XRD) studies and photo-micrographs of thin sections showed that all four samples were mainly mono-hydrate boehmite ( $\text{Al}_2\text{O}_3 \cdot \text{H}_2\text{O}$ ), with kaolinite and quartz as main impurities.

Results showed that the ore samples from the Niaz mine had lowest leaching recovery of alumina, due to the lowest alumina content in the ore, despite their better response to leaching. On the other hand, Nadi mine samples containing the lowest silica and highest alumina content showed lower recoveries of  $\text{Al}_2\text{O}_3$ . It was observed that with the exception of Nadi, all the samples from highly siliceous low grade Khushab bauxite ore were quite reasonably amenable to HCl leaching, making the acid process suitable to leaching most of this ore at atmospheric pressure. An overall average of 72.06% alumina extraction and 42.27% recovery is possible from the samples of ore from the Sultan Mehdi, Chamil More and Niaz mines, excluding the Nadi mine, which was considered unsuitable for leaching.

*Keywords: bauxite, HCl process, extraction of alumina, chemical analysis*

### Introduction

Bauxite is a heterogeneous material composed principally of aluminum oxide minerals, especially the trihydrate, gibbsite ( $\text{Al}_2\text{O}_3 \cdot 3\text{H}_2\text{O}$ ) and the monohydrate, boehmite and diaspor ( $\text{Al}_2\text{O}_3 \cdot \text{H}_2\text{O}$ ) (Ahmad and Siddiqi, 1991). Bauxite deposits exist in various locations of the Sargodha District of Tehsil Khushab. These deposits are of low grade and have been under investigation for many years. There are small pockets containing high-grade ore, (Ashraf, 1979) but large deposits are of low-grade siliceous ore, so on this basis, the alumina industry could not count on these deposits. Although the bauxite/laterite-bearing area is very vast, Chumbalwala-Mohar and Sultan Mehdi areas have proven to be most promising.

The initial investigation put the total estimation at 0.3 million t, assaying  $\text{Al}_2\text{O}_3$  40% min,  $\text{SiO}_2 = 15\%$  max.

Huge deposits (190 million tons) of low-grade bauxite ore are in the Khushab area, and along with it, lateritic bauxites are also located in this area in vast quantities. Some work on the extraction of alumina from Khushab bauxite has been carried out on high-grade ore (Farooq et al., 1978), but low-grade siliceous ore

(SiO<sub>2</sub> = 36.5÷44.1%) has not been tested with HCl (Hussain and Bashir, 1996) before for extraction.

### Scope of this work

Alumina can be extracted from calcined clays with acids, resulting in highly exothermic reactions and good yields that depend on the type of clay and the temperature of calcination. An acid process using HCl is sometimes used commercially and is considered in this report. The Bureau of Mines (Peters et al., 1962) procedure for extracting alumina by using HCl was adopted. The process was designed to extract alumina as aluminum chloride from calcined bauxite ore, by leaching with HCl to remove silica residue by filtration. Some of the more important advantages of using HCl over other acids for leaching alumina are that no separate iron-removal section is required; the temperature at which aluminum chloride crystals can be decomposed is low, compared to the higher temperature of other acid processes; the process can be done at atmospheric pressure; and the price of HCl is cheap, compared to other acids in the market, as it is a by-product in many chemical industries.

### Selection and procurement of material for analysis

Samples from four different sites of the Khushab mines, each weighing about 60 kg, was packed separately in airtight bags and labeled. It was ensured that the material arriving in the laboratory was representative of the deposit from which it was taken (Jeffery and Hutchison, 1981).

### Mineralogical appraisal of the sample

#### *X-Ray diffraction and mineral identification*

The X-Ray diffraction studies were undertaken using a Siemens Diffractometer. The ASTM crystallographic data was used to interpret the mineral phases present in the samples. The results are summarized below in Table I (Hussain and Bashir, 1996), which shows that all samples are boehmite (Al<sub>2</sub>O<sub>3</sub>·H<sub>2</sub>O), with kaolinite (clay) and quartz as main impurities.

Table I: Results of X-Ray diffraction studies.

Mine locations	Mineral present	Remarks
Sultan Mehdi	boehmite + kaolinite	peaks of quartz, calcite and
Chamil More	boehmite + kaolinite + geothite	diaspore not detected or in traces.
Nadi	boehmite + kaolinite + geothite	
Niaz	boehmite + kaolinite	

#### *Petrographic studies*

The Petrographic study shows that there are fine-grained disseminations of geothite in the samples, except in the Niaz mine, where it is seen as an aggregate. The grain size of geothite ranges from 10 µm to 200 µm. Minor amounts of quartz are present in the Sultan Mehdi, Niaz and Nadi mines but the amount of quartz present in the Chamil More sample is prominent. Quartz grains of the 100÷200 µm size were observed in the samples. Minerals in the four site samples were reddish-brown colored, due to staining by iron oxide.



### Sample preparation and chemical analysis of Khushab bauxite ore

#### *Crushing and grinding*

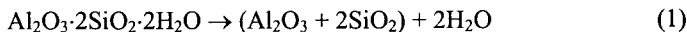
Approximately 40 kg of representative samples of bauxite ore from the bulk samples of the four sites were weighed. Primary crushing was carried out in a Jaw Crusher set at 0.64 cm. as the minimum, with the maximum at 2.54 cm. The throw of the movable jaw was 1.9 cm. The product of the Jaw crusher was fed to the Jone's Riffler, in order to take out the representative sample for further processing. As the first step, the total crushed material was passed through the Riffler (40 kg), dividing it into two parts. One part was preserved and the other re-fed to the Riffler (20 kg) which was again split into 2 parts. One part was again preserved, and one (10 kg) was fed to the Riffler with the resulting two parts, about 5 kg each, representing the whole sample received, and one of them was taken for further processing. The product from the Jone's Riffler was fed to the Rolls Crusher. The crushing was effected through the rolls set at 0.16 cm. The product of the Roll Crusher was passed through the Disc crusher, which was adjusted to obtain the maximum product for the -100 +200 mesh size-range. Chemical analysis of the Khushab bauxite ore is shown in the Table II (Jamal, 1998):

Table-II: Chemical analysis of samples from the Khushab mines.

	Sultan Mehdi	Chamil More	Nadi	Niaz
SiO <sub>2</sub> %	40.64	42.26	36.50	44.41
Al <sub>2</sub> O <sub>3</sub> %	39.51	38.23	45.01	37.17
Fe <sub>2</sub> O <sub>3</sub> %	0.23	2.14	0.30	0.15
Others	4.63	5.77	4.00	4.38
Total	98.74	99.79	99.30	99.22

#### *Moisture removal*

The crushed bauxite ore, which was in the form of hydrous aluminum silicate, was dehydrated at 100 °C for one hour in Fisher's electric oven, to remove both moisture and combined water. This was done in order to facilitate the process of sieving, i.e. to prevent clogging of the sieve holes:



#### *Sieving*

The material was sieved through a set of three Tyler series sieves (35, 100 and 200 mesh). The fractions obtained are shown in Table III. Sieve product -100 +200 mesh, of each sample was chosen for further processing, because of optimum grain-surface area for leaching purposes, and were labeled separately for further use in airtight plastic bags.

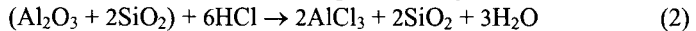
Table III: Results of sieve analysis.

Size-class (mesh n°)	Weight (%)
+ 35	0
-35 + 100	30
-100 + 200	56
-200	14
Total	100

## Experimental procedure

### *Sample used and procedure for extraction of alumina using the HCl process*

A sample of the Sultan Mehdi mine was selected randomly to find the optimum conditions for leaching, which was later applied to samples of three other sites (Jamal, 1998). The first step in the HCl process before leaching was to dehydrate the hydrous aluminum silicates, which are not readily soluble in dilute acids. This was done in an electric furnace for 6 h at 705 °C. To start the leaching, the dehydrated bauxite sample was digested with HCl at atmospheric pressure. The reaction of alumina with HCl, forming aluminum chloride, is represented by:



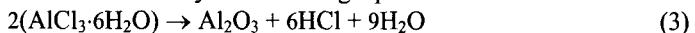
### *Procedure for selection of optimum conditions for leaching and chemical analysis*

To find the optimum conditions for the best/economical leaching, the particle size, weight of the sample, quantity of HCl and temperature of leaching were fixed as -100 +200 mesh, 40 g, 152 ml and 100 °C, respectively. The effects of varying the concentration of HCl to 10%, 20% and 35.4%, with 1, 2 and 4 h of leaching time applied to each concentration of HCl at atmospheric pressure, were obtained (Jamal, 1998).

During the research it was observed that:

- as the concentration of HCl was raised from 10% to 20% and finally to 35.4% (commercial grade), the percentage extraction raised up to the 20% mark, and then tapered off towards 35.4%, with the time of extraction being 1, 2 and 4 h (concentration of HCl vs. extraction %).
- for 20% HCl, the percentage of extraction raised up to 2 h and then tapered off towards the 4<sup>th</sup> hour mark; 35.4% HCl is not economical and safe to use (time of leaching vs. extraction %).

The leached slurry obtained in each of the cases through digestion with HCl was cooled to room temperature. Then the residue containing silica and iron was easily separated from the solution of aluminum chloride by filtration. The wash water was used for washing the filter paper. The filtrate containing dissolved alumina was concentrated by evaporation in a china crucible on a sand bath, precipitating aluminum chloride ( $\text{AlCl}_3$ ) and iron chlorides ( $\text{FeCl}_3$ ). The concentrate obtained was then placed in an electric oven for drying at 100 °C for 8 h. After dehydration, the solution was in the form of dirty white powder. The residue obtained after filtration was also dried at 100 °C in the electric furnace for 8 h, and its weight was recorded. The material obtained after dehydration/concentration was calcined at 540 °C by placing it in a china crucible in the electric furnace for 8 h. The formation of alumina from aluminum chloride is indicated by the following equation:



The product was cooled and the weight was carefully recorded after the above process. The optimum conditions found from the above work were concentration of HCl = 20%, time of leaching = 2 h. These conditions were applied to the Sultan Mehdi mine sample four times, and the results were recorded and the average taken. Similar parameters were applied to the samples from three other sites, and the results were recorded and their average was taken. Chemical analysis of the filtrate and residue was carried out as shown in Table IV (Jamal, 1998):

Table IV: Chemical analysis of filtrate and residue of all four mine samples.

Mine locations	SiO <sub>2</sub> (%)		Al <sub>2</sub> O <sub>3</sub> (%)		Fe <sub>2</sub> O <sub>3</sub> (%)		Others (%)	
	Filtrate	Residue	Filtrate	Residue	Filtrate	Residue	Filtrate	Residue
Sultan Mehdi	1.60	35.50	59.80	33.10	2.00	0.10	36.60	31.30
Chamil More	1.80	34.90	67.50	31.50	1.60	0.11	29.10	33.49
Nadi	1.50	35.00	66.30	35.20	1.20	0.12	31.00	29.68
Niaz	2.10	32.90	69.10	34.80	1.70	0.13	27.10	32.17

### Experimental results and recovery of Al<sub>2</sub>O<sub>3</sub>

The average extraction and recovery of Al<sub>2</sub>O<sub>3</sub> from all four sites' samples (40 g) are shown in Table V (Jamal, 1998).

Table V: Average extraction percentage and recovery of all four sites of Khushab bauxite ore.

Mine locations	HCl		Leaching		Calcination		Weight of residue (g)	Weight of leached sample (g)	Extraction (%)	Al <sub>2</sub> O <sub>3</sub>	
	conc. (%)	Q.ty (ml)	time (h)	temp (°C)	time (h)	temp (°C)				grade (%)	recovery (%)
Sultan Mehdi	20	152	2	100	8	540	29.25	10.80	68.34	(%)	(%)
Chamil More	20	152	2	100	8	540	28.88	11.50	75.20	59.80	45.15
Nadi	20	152	2	100	8	540	29.00	11.00	61.10	67.50	42.59
Niaz Mine	20	152	2	100	8	540	29.25	10.80	72.64	66.30	41.48
Average									69.32	69.10	39.07

### Discussion of results

The Table V shows that Chamil More has the best extraction response to HCl leaching, followed by ores from the Niaz, Sultan Mehdi and Nadi mines, in descending order. The extraction rate of the Chamil More ore includes leached-iron content (2.14%) as well, which is not present in the mineral samples of the other three sites. Therefore, the response to leaching of the Niaz mine ore is comparable to the Chamil More ore as well. As the alumina content of ore is different in the samples from the four sites, the recovery of Al<sub>2</sub>O<sub>3</sub> may not be in this order. Also, maximum recovery of alumina obtained from the Sultan Mehdi ore samples showed its greater amenability to leaching with HCl, in terms of recovery, followed by the Chamil More and Nadi mine samples, with slightly lower results.

This indicates their response to leaching in descending order. However, the Niaz mine ore samples showed the lowest leaching recovery, despite a better response to leaching, because they had the lowest alumina content. It shows that higher content of silica does not pose a great problem for extraction.

The lowest recovery only appears to be due to the lower alumina content in the Niaz mine ore. It is interesting to note that the Nadi mine's ore, unlike other ores, showed the lowest extraction rates, despite its lowest silica content and highest alumina content, and hence, lower recoveries.

This indicates that the Nadi mine ore is not suitable for leaching.

The silica in the ore is not in a free state, and therefore hampers the leaching reaction to a great extent. Figure 1 shows the percentages of extraction and recovery of all four sites, respectively, in bar and line graphs.

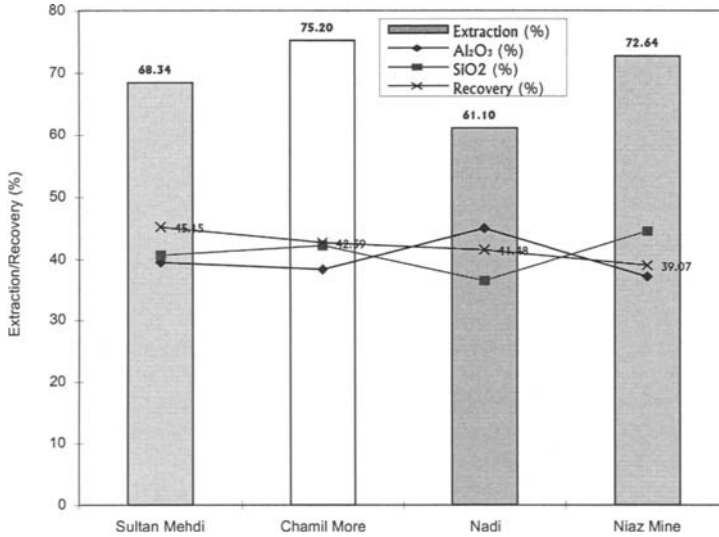


Figure 1: Graph showing percentages of extraction and recovery of all 4 sites, respectively, in Bar & Line graphs. The  $\text{Al}_2\text{O}_3$  and  $\text{SiO}_2$  content of the ore is also shown in the Line graph.

## Conclusions

The raw samples of bauxite ore from the four different sites of the Khushab mines were earthy yellow in color, resembling Kaolinite clay. The Khushab bauxite samples' chemical analysis showed that Sultan Mehdi, Chamil More, Nadi and Niaz mines contain alumina 39.51%, 38.23%, 45.01% and 37.17%, respectively, while each sample contains high silica content, i.e. 40.64%, 42.26%, 36.50% and 44.41%, respectively. These samples of ore are, therefore, low grade and highly siliceous, with low iron contents varying from 0.15% to 2.14%. X-ray diffraction studies and photomicrographs of the thin section further confirmed that all four samples, namely the Chamil More, Sultan Mehdi, Nadi and Niaz mines, are mainly mono-hydrate boehmite ( $\text{Al}_2\text{O}_3 \cdot \text{H}_2\text{O}$ ), with kaolinite and quartz as main impurities. The particle size-range of the samples used in this study was from  $-100$  to  $+200$  mesh, because this size-range gives the best results in the HCl process. During the research, the optimized parameters for maximum extraction by HCl leaching, while keeping particle size at  $-100$   $+200$  mesh and a temperature of leaching at  $100$  °C at atmospheric pressure, were weight of sample = 40 g, concentration of HCl = 20%, quantity of HCl = 152 ml and time for leaching = 2 h. Decomposition of  $\text{AlCl}_3$  to  $\text{Al}_2\text{O}_3$  was done at a temperature of  $540$  °C, at atmospheric pressure, for 8 h.

The leaching of the Sultan Mehdi, Chamil More, Nadi and Niaz Mine samples by the HCl process shows an extraction percentage of 61.10% to 75.20%. The Chamil More mine sample showed the highest extraction rate (75.20%), which includes iron as well, whereas the Niaz mine sample without iron also showed comparable results (72.64%). The Nadi mine had the lowest rate of alumina extraction (61.10%). The Sultan Mehdi sample had the alumina extraction percentage of 68.34. The average

alumina extraction amounts to 69.32% from four different sites, namely the Sultan Mehdi, Chamil More, Nadi and Niaz mines. The overall recovery of  $\text{Al}_2\text{O}_3$  from four different mine site samples of ore varies from 39.07% to 45.15%, depending on their alumina content. Sultan Mehdi ore samples showed maximum alumina recovery of 45.15%, as compared to the Chamil More (42.59%) and Nadi samples (41.48%). However, Niaz mine samples indicated lowest leaching recovery of alumina, i.e. 39.07%. The average recovery of  $\text{Al}_2\text{O}_3$  is 42.07% from all four mine-sites.

To conclude, ore samples from the Sultan Mehdi, Chamil More and Niaz mines yield an average alumina of 72.06% after leaching with HCl, and hence an average recovery of 42.27% alumina, aside from the sample from the Nadi mine, which is considered unsuitable for leaching due to its texture. Therefore the HCl process of leaching can be applied to most of the ore from Khushab Areas.

The Nadi mine ore was found unsuitable for HCl leaching due to its texture, and can be further investigated in order to discover its suitability for leaching.

#### **References**

- Ahmad, A. and Siddiqi, R.A., 1991. Minerals and Rocks for Industry. Geological Survey of Pakistan Vol.1.
- Ashraf, A., 1979. Bauxite and Laterite Clay Deposits of Punjab. A paper presented at International Seminar on Mineral Exploitation Technology. Peshawar, Pakistan. 26th March to 2nd April.
- Farooq, K., Aqil, M.R.K., Naqvi, A.A. and Safdar M., 1978. Utilization of Indigenous Bauxite for the Production of Alumina. National Seminar on Development of Mineral Resources, Lahore, Pakistan, March 6-9.
- Hussain, S.A. and Bashir, A., 1996. Preliminary Investigation Report on Processing of Khushab Bauxite. Mining Engineering Department, University of Engineering and Technology, Lahore, Pakistan.
- Jamal, R., 1998. An Evaluation of HCl Process for Leaching of Low Grade Highly Siliceous Bauxite Ore from Khushab, Pakistan. M.Sc. Thesis, University of Engineering and Technology, Lahore, Pakistan.
- Jeffery, P.G. and Hutchison, D., 1981. Chemical Methods of Rock Analysis. 3rd. edition, Pergamon Press.
- Peters, F.A., Johnson P.W. and Kirby R.C., 1962. Methods for Producing Alumina from Clay: An Evaluation of Five Hydrochloric Acid Processes. U.S. Bureau of Mines No. R.I. 6133, 68.

## APPLICATION OF SOLVENT IMPREGNATED RESIN TO THE TREATMENT OF HEAVIER RARE EARTH RESIDUE

J. Shibata, S. Matsumoto, H. Yamamoto

Faculty of Engineering, Kansai University, Suita, Osaka 564-8680, Japan  
Fax +81.6.6388.8869, e-mail: shibata@kansai-u.ac.jp

### Abstract

Heavier rare earths contained in a small amount in ores such as bastnesite and monazite have been piled up as heavier rare earth residue without doing separation and purification after extraction of required elements. The heavier rare earth residue; Tb, Dy, Ho, Y, Er, Tm and Yb, which have some beneficial uses as industrial materials. In this study, separation and recovery process of Dy, Y, Tm and Yb from leached solution of the heavier rare earth residue was investigated by using a column method with solvent impregnated resin prepared by impregnation of organophosphorus extractant whose trade name is PC-88A into macro porous resin, Amberlite XAD-7. In the batch sorption test for rare earth elements, sorption takes place in the pH region 0-2.0 and the sorption-pH curves are closely located. This means the difficulty in the rare earth separation. The heavier rare earth is adsorbed on the solvent impregnated resin at the lower pH, since the affinity of the extractant PC-88A for heavier rare earth is stronger than for lighter rare earth. It was clarified to be almost impossible to separate them in simple sorption and elution steps. However, we accomplished to individually separate them with high purity and yield from the leached solution in elution step, first by changing eluent HCl concentration gradually from pH = 2 to 2 mol/dm<sup>3</sup>, and secondly by application of a development column and changing eluent concentration. The purity of Dy, Y, Tm and Yb were 94.3%, 82.4%, 99.7% and 99.9% respectively and the yield were 73.5%, 74.1%, 81.3% and 82.6%, respectively. Finally, we established the novel process combining the solvent impregnated resin method and solvent extraction method in order to separate and recover all the seven rare earth elements.

*Keywords: solvent impregnated resin, rare earth residue, separation, sorption, column method*

### Introduction

Rare earth elements, which comprise lanthanides from, scandium and yttrium, are used as fluorescent materials and magnetic materials. Since these elements have similar chemical properties, their separation is extremely difficult. The typical separation process consists of solvent extraction or ion exchange resin methods. In the solvent extraction process, the separation factors between adjacent elements are not great, and so the countercurrent multistage extraction with many stages has to be employed to achieve high purity products. On the other hand, in the ion exchange resin process rare earth elements are sorbed together in a cation exchange sorption column, and the separation is carried out in a series of sorption and elution columns by using chelating agents such as EDTA and citric acid (Vickery, 1952).

A solvent impregnated resin (abbreviated as SIR henceforth) that was developed about 15 years ago (Warshawsky, 1974, 1976, 1981), is produced by adsorbing extractants such as D2EHPA and TBP on a macro porous resin without any functional group. We can make a different type of highly selective resin by adsorbing various extractants. The research was continued for several years after the

development of SIR (Akita et al., 1990, Flett, 1977, Kanosato et al., 1992, Matsunaga et al., 1988,1989), but the investigations on SIR declined afterwards. This may have been due to a smaller sorption capacity and a shorter life of SIR compared with the usual ion exchange resins. If we select a suitable application, however, SIR can be applied to the aqueous solution with the aim of separating individual elements.

In this study, we applied SIR to separate Dy, Y, Tm and Yb from a heavier rare earth residue. The heavier rare earth is accumulated as a residue after separating the lighter and middle rare earths. For this purpose, we used the SIR, which was produced from a macro porous resin, Amberlite XAD-7 and organophosphorus extractant, PC-88A (trade name of Daihachi Chemical Industry Co., 2-ethylhexyl phosphonic acid mono-2-ethylhexyl ester).

### Experimental

The extractant, PC-88A was obtained from Daihachi Chemical Industry Co. and used without further purification. The aqueous solution was prepared by dissolving rare earth oxides or a residue with hydrochloric acid at 373K. The composition of the heavier rare earth residue is shown in Table I. Amberlite XAD-7 (Rohm and Haas) was used as a macro porous resin for impregnation.

Amberlite XAD-7 was washed with ethanol and then distilled water. After washing, the resin was dried under a vacuum at 323 K. Fixed amounts of Amberlite XAD-7 and PC-88A diluted in chloroform were mixed in a beaker for 86.4 ks. The mixture was transferred to a rotating evaporator, and then chloroform was removed under a vacuum at 343 K. By the above operation, PC-88A was impregnated in the micro pores of Amberlite XAD-7.

The solvent impregnated resin produced by the above method was a white colored resin with good fluidity and hydrophobicity. In order to make the SIR hydrophilic, the SIR was treated by 0.1% wt sodium lauryl sulfate solution.

The impregnation percent was defined as the weight ratio of impregnated extractant to the produced SIR (Mashimo, Nagasaka et al., 1994; Mashimo, Matsumoto et al., 1996).

Batch sorption test was carried out in an erlenmeyer flask using 1 g of SIR and 30 cm<sup>3</sup> of aqueous solution containing 5·10<sup>-3</sup> kmol/m<sup>3</sup> rare earth. The flask was shaken for 7.2 ks at 297 K and the equilibrium pH and metal concentration were measured after filtration.

Table I: Composition of heavier rare earth residue.

Rare earth (% wt)	Tb	Dy	Ho	Y	Er	Tm	Yb
	2.09	33.2	6.63	25.0	17.4	2.21	13.5

A glass column of 10 mm diameter and 1 m length was used in a column test. In the case of 2÷3 m bed height, two or three 1 m columns were connected in series. In an elution test, hydrochloric acid solution of various concentrations was passed through the column. The effluent solution from the column was fed to an ICP spectrophotometer and then the metal concentration was determined.

## Results and discussion

The solvent impregnated resin with impregnation percent less than 55% was produced by the method described in this study. It was confirmed that the calculated value of impregnation percent is almost equal to the measured value. Figure 1 shows the results of the batch sorption test for 13 rare earth elements. Sorption of rare earth from La to Yb takes place in the pH region 0-2.0. The sorption-pH curves are closely located one another, which means difficulty in their separation. The rare earth of greater atomic number is sorbed on SIR at lower pH. That is, the affinity of heavier rare earth for PC-88A is stronger than that of lighter rare earth. Table 2 shows the pH for rare earth elements at 50% sorption ( $pH_{50}$ ) and the pH difference for adjacent rare earth elements at 50% sorption ( $\Delta pH_{50}$ ). It is considered that unless  $\Delta pH_{50}$  is great, we cannot obtain good separation. For example, the realization of separation of Sm/Nd and Tb/Ho systems with the SIR column method is caused by some largeness of  $\Delta pH_{50}$  values, 0.19 and 0.19, respectively.

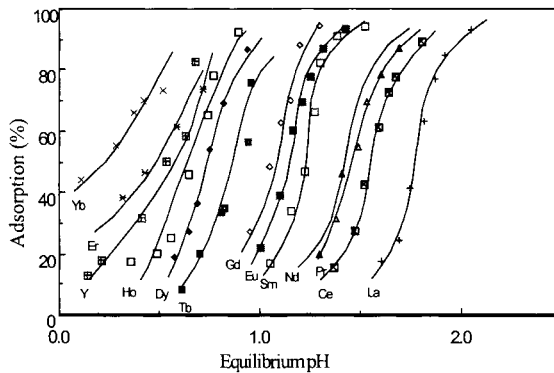


Figure 1: Sorption of rare earth with 50% PC-88A impregnated resin as a function of pH.

Table II: Values of  $pH_{50}$  and  $\Delta pH_{50}$ .

	La	Ce	Pr	Nd	Sm	Eu	Gd	Tb	Dy	Ho	Y	Er	Yb
$pH_{50}$	1.76	1.54	1.45	1.39	1.20	1.12	1.06	0.87	0.75	0.68	0.56	0.47	0.22
$\Delta pH_{50}$		0.22	0.09	0.06	0.19	0.08	0.06	0.19	0.12	0.07	0.12	0.09	0.25

According to our previous papers, if  $\Delta pH_{50}$  value is larger than 0.19, like  $\Delta pH_{50}$  between Nd and Sm, it is easy to separate two adjacent elements using the usual SIR column method. The sorption rate measured in a batch test is quite fast; for example 80% sorption of rare earth takes place within 600 s and 2.4 ks is required for equilibrium. As the sorption rate is similar to the rate of sorption for normal cation and anion exchange resins, there is no difficulty in the sorption rate in use of SIR in a column method (Shibata, 1995, Matsumoto et al., 1995).

The column sorption tests for Y and Er, Y and Ho, Dy and Ho, and Tb and Dy were carried out using a 1 m column of 50% SIR. The breakthrough curves are shown in



Figure 2. The concentrations of rare earth elements in the feed solution are determined according to the composition of the heavier rare earth residue. The  $\Delta\text{pH}_{50}$  values for Y and Er, Y and Ho, Dy and Ho, and Tb and Dy are 0.09, 0.12, 0.07 and 0.12 respectively. As expected from the  $\Delta\text{pH}_{50}$  value, the breakthrough point for each element appears at the same effluent volume and rare earth elements cannot be separated in the sorption step. The column sorption and elution tests were carried out for the leached solution of the heavier rare earth residue.

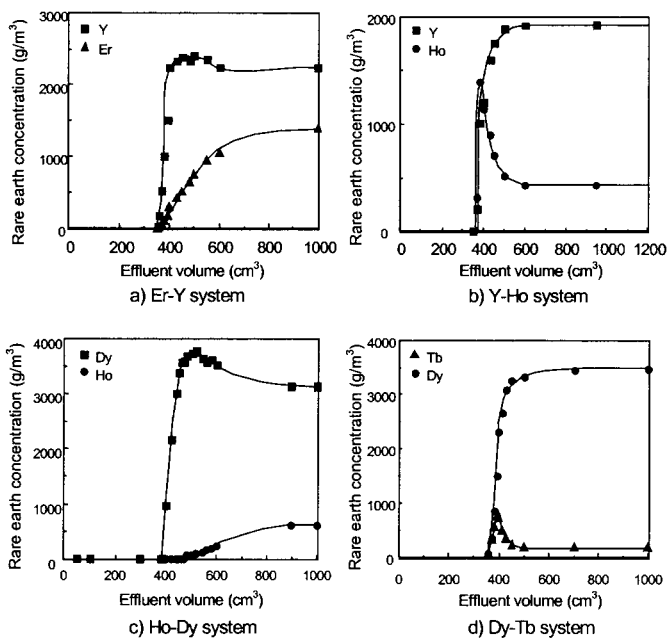


Figure 2: Breakthrough curves for several binary systems (Bed Height 1.0 m, S.V.1.0).

Table III: Composition of leached solution from heavier rare earth residue.

		Tb	Dy	Ho	Y	Er	Tm	Yb
Feed	(mol/dm <sup>3</sup> )	1.29	20.1	3.83	28.1	9.79	1.37	5.41
Concentration	(g/m <sup>3</sup> )	204	3,280	632	2,500	1,640	230	935

The residue was dissolved with hydrochloric acid. The obtained solution contains 7 elements such as Yb, Tm, Er, Y, Ho, Dy and Tb at the concentrations shown in Table III. The objective elements for recovery are Dy, Y, Tm and Yb, because they have a high concentration and they are known to be in industrial use. An example of column sorption and elution test is shown in Figure 3. The breakthrough point appears in turn for the element which has a smaller atomic number, namely weaker affinity to SIR. The heavier rare earth elements like Tm and Yb leak from the column in the latter

part of effluent volume of 500 and 700 cm<sup>3</sup> respectively. It seems to be impossible to separate each element in the sorption step.

The sorption column shown in Figure 3 was used for the elution test. The eluent passed through the column is 2 kmol/m<sup>3</sup> HCl solution. The results obtained are shown in Figure 4. As is apparent from the figure, most of elements flow out of the column at the same time. The above results are predicted from the batch sorption experiment shown in Figure 1, which gives the quantitative elution with 0.1 kmol/m<sup>3</sup> solution. The heavier rare earth elements like Tm and Yb having a stronger affinity with SIR slowly flow out of the column and then the elution curve exhibits a tailing. The specific elements in the heavier rare earth residue cannot be separated in such a simple elution. Figure 5 shows the elution results where the eluent is changed from the dilute HCl solution with pH=2 to 2 kmol/m<sup>3</sup> HCl solution. The measured and calculated pH change in eluent output is shown in the figure. Since the rare earth element, which has a smaller atomic number, is easy to desorb with dilute HCl solution, while the element, which has a larger atomic number, is eluted with the concentrated HCl solution, the change in eluent HCl concentration is adopted.

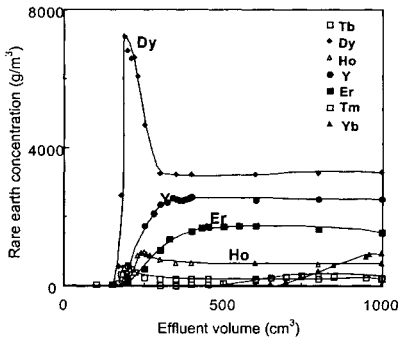


Figure 3: Column sorption test of 7 elements from leached solution of heavier rare earth residue. (Bed height = 1 m, S.V.= 1.0, Feed pH = 1.0).

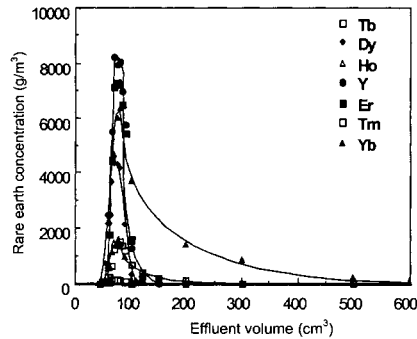


Figure 4: Column elution test of 7 elements with 2 mol/dm<sup>3</sup> HCl. (Bed height = 1 m, S.V.= 1.0, Feed pH = 1.0).

Table IV: Purity and yield of Dy, Y, Tm and Yb obtained from Figure 5.

	Dy	Y	Tm	Yb
Purity (%)	82.0	69.9	32.3	99.9
Yield (%)	76.7	76.9	77.4	74.2

The results in Figure 5 are completely different from the Figure 4. We can recognize the effect of the change in eluent HCl concentration. In the first part of elution, the elements having a smaller atomic number such as Tb, Dy and Ho are eluted from the column, then the elements like Y and Er are eluted with the higher HCl solution and finally Tm and Yb are washed out with 1 kmol/m<sup>3</sup> and 2 kmol/m<sup>3</sup> HCl solution respectively. The purity and yield of Dy, Y, Tm and Yb obtained by the above operation are shown in Table IV.

To get better separation, purity, and yield, both the development column and the change in eluent HCl concentration were employed for elution. The results for elution are shown in Figure 6. The effluent from Figure 5 passes through the development column, which is 3 m length with the new SIR and then each element possesses different retention time in the development column due to the difference in affinity between the element and SIR. As the results, good separation of Dy, Y, Tm and Yb from the residue containing heavier rare earth is obtained. The elution curves for the objective elements of Dy, Y, Tm and Yb have a peak at a different effluent volume. Table V shows the purity and yield for Dy, Y, Tm and Yb attained from Figure 6.

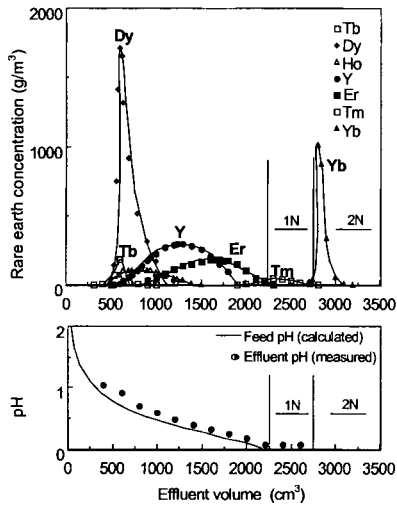


Figure 5: Column elution test with eluent having various HCl concentrations.

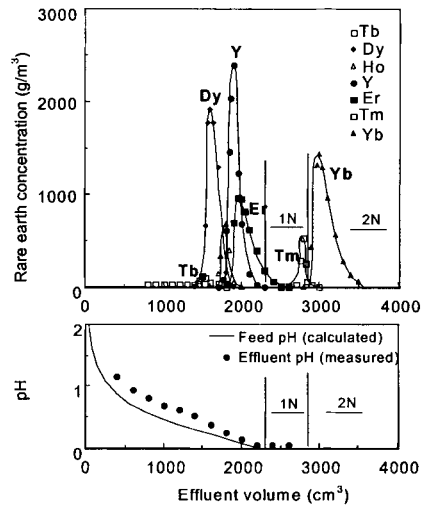


Figure 6: Column elution test with development column (Adsorption column = 0.5 m, Development column = 3 m).

Table V: Purity and yield of Dy, Y, Tm and Yb obtained from Figure 6.

	Dy	Y	Tm	Yb
Purity (%)	94.3	82.4	99.7	99.9
Yield (%)	73.5	74.1	81.3	82.6

The separation is much improved by using the development column and the change in eluent HCl concentration. Figure 7 shows the proposed flowsheet for the separation of rare earth elements from the raw material and the heavier rare earth residue. In the figure, several methods including precipitation, solvent extraction and solvent impregnated resin are effectively combined. The raw material is leached with dilute hydrochloric acid after oxidation roasting, where most of the Ce is removed as  $Ce(OH)_4$ . Cerium and europium have different oxidation states, namely tetravalent and divalent respectively. These elements are removed from the solution as  $Ce(OH)_4$  and  $EuSO_4$ . Solvent extraction is applied for the separation of lighter rare earths such as La, Ce, Pr, Nd, Sm, Eu and Gd. The SIR method is applied for the separation of Sm and Gd, and the heavier rare earths such as Dy, Y, Tm and Yb.

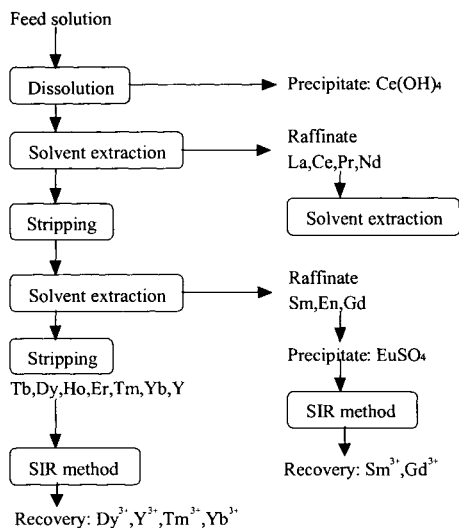


Figure 7: New separation process of rare earth.

## Conclusions

The new separation technology for heavier rare earth was tried to be establishing with SIR. We accomplished the separation and recovery of valuable elements from leached solution of a heavier rare earth residue by using this technique. The batch sorption behavior of heavier rare earths on the impregnated resin has a similarity when PC-88A is used in solvent extraction. In a column method, it is difficult to separate the rare earth sharply, because almost every rare earth element is adsorbed and eluted at the same time. Good separation between them was attained by gradually changing the eluent HCl concentration. In addition, quantitative separation of Dy, Y, Tm and Yb was attained by using a development column.

## References

- Akita, S. and Takeuchi, H., 1990. *J. Chem. Eng. Japan*, 439-443. (in Japanese, with English Abstract)
- Flett, D.S., 1977. *Chemistry and Industry*, 6 August, 641-646.
- Kanesato, M., Kobayashi, S., Matsunaga, H., Suzuki, T.M. and Wakui, Y., 1992. *Analytical Chimica Acta*, 262, 161-166.
- Mashimo, M., Nagasaka, T. and Shibata, J., 1994. *J. Min. Mat. Proc. Inst. Japan*, 110, 191-194, 613-617. (in Japanese, with English Abstract)
- Mashimo, M., Matsumoto, S., Nakayama, N., Shibata, J. and Yamamoto, H., 1996. *J. Min. Materials Processing Inst. Japan*, 112, 873-878. (in Japanese, with English Abstract)
- Matsumoto, S., Shibata, J. and Yamamoto, H., 1995. *Mineral Processing Recent Advances and Future Trends*, Kanpur, India, 548-554.
- Matsunaga, H., Suzuki, T.M. and Wakui, Y., 1989. *Analytical Science*, 5, 189-193.
- Matsunaga, H., Suzuki, T.M. and Wakui, Y., 1988. *Analytical Science*, 4, 325-327.
- Shibata, J., 1995. *Proc. 19th Int. Min. Proc. Congr., San Francisco*, Vol. 2, 233-236.
- Vickery, R.C., 1952. *Journal of Chemical Society*, 4357-4363.
- Warshawsky, A., 1981. *Ion Exchange and Solvent Extraction*. Vol. 8, Marcel Dekker Editor, 229-310.
- Warshawsky, A., 1974. *Trans. Inst. Min. Metal.*, 83, C101.
- Warshawsky, A., 1976. *The Theory and Practice of Ion Exchange*, Society of Chem. Ind., 38-1-38-7.

## GOLD EXTRACTION FROM KAYMAZ GOLD ORE BY THIOUREA LEACHING

S. Örgül, Ü. Atalay

Mining Engineering Department, Middle East Technical University, Ankara, Turkey

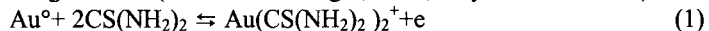
### Abstract

For over one hundred years, gold has traditionally been extracted from ores by cyanide leaching. In recent years, due to pressure by environmentalists and to certain disadvantages of the cyanidation process, investigations were directed towards alternative gold lixivants. The most promising results in gold leaching were obtained by use of thiourea, a complexing/extracting agent, together with ferric sulfate as an oxidizing agent. The study was carried out on finely disseminated Kaymaz gold ore from Turkey (4.0 g/t Au). The effect of various leaching parameters on gold extraction was examined, such as the concentration of thiourea, concentration of ferric sulfate, molar ratio of ferric sulfate/thiourea, leaching duration and particle size. The investigations indicated that at room temperature, with a 15.96 kg/t consumption of thiourea at pH 1.35, it was possible to obtain gold extraction at 80.5%, for a 100%, 106 µm feed in 6 h. Higher extractions such as 92.5% were also possible, with a finer feed and lower pH values. Thiourea consumption for different leaching conditions was also examined.

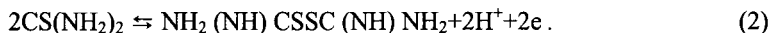
*Keywords: gold, leaching, thiourea, and ferric sulfate*

### Introduction

Gold has always been in demand for decorative and ornamental purposes. Increases in gold metal prices and demands for gold have prompted increased activity in all aspects of gold metallurgy. Traditionally, gold has been recovered from ores by leaching with aqueous cyanide solutions. In recent years, the interest in alternative lixivants, such as thiourea, halogens, and thiosulfate, have been revived concerning the continual gold price increase in the gold market, which stimulated new innovations in extraction technology and a greater degree of environmental concern. Thiourea ( $\text{H}_2\text{NCSNH}_2$ ) is an organic compound, the crystals of which dissolve in water to yield an aqueous form stable in acidic solutions. In an acidic medium, thiourea forms a single cationic species with Au according to the following dissolution/complexing reaction (Preisler and Berger, 1947; Huyhua et al., 1989):



In the presence of an oxidizing agent, such as ferric ions or hydrogen peroxide, thiourea will oxidize in successive stages to a number of products. The first oxidizing product of thiourea is formamidine disulfide, which serves as a selective oxidant for Au:



Formamidine disulfide oxidizes over time to produce cyanamide, hydrogen sulfide and elemental sulfur by irreversible reactions, and thus increases consumption of thiourea (TU) (Groenewald, 1976):



The overall equations for dissolution of Au, in the case of  $\text{Fe}^{3+}$  as an oxidant, is as follows:



The literature contains many studies concerning different aspects of thiourea leaching parameters (Pyper and Hendrix, 1981; Caldeira and Ciminelli, 1993; Deschenes, 1986; Ubaldini et al., 1998). In this study, some of them were investigated. In addition, high reagent consumption is the main handicap in the use of thiourea. Excessive reagent consumption and low leaching efficiency have limited commercial development to thiourea processes for gold. Due to these reasons, this study is also focused on thiourea consumption and its variations under different leaching conditions.

## Experimental procedure

### Materials

The gold ore sample used was obtained from the Kaymaz gold deposit, which exist in the Middle Anatolia region in Turkey. Finely disseminated Kaymaz gold ore has a 4.0 g/t gold grade. Chemical analysis of the representative sample is given in Table I.

Table I: Chemical analysis of sample by semi-quantitative optical spectrophotometer.

Element	%
Si	>10
Ba	0.3
Cr	0.3
Ca	0.07
Fe	7
Mg	0.15
Cu	0.015
Al	0.4
Ni	0.1
Ti	0.007

Under mineralogical analysis, two types of gold inclusions were identified: native gold and electrum. Quartz, serpentine, ankerite, and dolomite were the main gangue minerals. Most of the gold was deposited in silicified serpentine and was characterized by very fine grain size in the range of 1–4  $\mu\text{m}$ . The rest of the gold particles were electrum particles, which exist in the sample as inclusions in the gangue matrix.

### Leaching

Agitating leach experiments were performed in a glass beaker at room temperature and atmospheric pressure. Analytical-grade thiourea ( $\text{CS}(\text{NH}_2)_2$ ) and ferric sulfate ( $\text{Fe}_2(\text{SO}_4)_3$ ) were used as the lixiviant and oxidant, respectively. The pH of the medium was adjusted with  $\text{H}_2\text{SO}_4$ . A magnetic stirrer agitated the slurry, constituted from the ground ore, chemicals and distilled water. During the leaching tests, samples of solution were pipetted out at predetermined times to investigate the consumption of thiourea. At the end of the tests, the pulp was filtered and washed with water, and the filter cake was submitted to gold analysis.

## Results and discussion

The effects of leaching parameters in agitating leaching were analyzed by varying leaching conditions. The main aspects discussed here include the effect of the concentration of thiourea, concentration of ferric sulfate, molar ratio of ferric sulfate/thiourea, leaching duration and particle size (Örgül, 1999). All tests were carried out at pH = 1.35, with a solid/liquid ratio of 1:4.

### *The effect of thiourea concentration*

Thiourea concentration has one of the most powerful effects on gold dissolution. At the same time, keeping the thiourea concentration as low as possible to extract enough gold recovery leads to a decrease in the cost of the leaching process. As is known, the economics of thiourea leaching for gold is limited to the use of thiourea. Accordingly, the effect of the thiourea concentration was investigated in the range of thiourea concentrations of 1.25÷20 g/l. The addition of oxidant ( $\text{Fe}_2(\text{SO}_4)_3$ ) was done to keep the  $\text{Fe}_2(\text{SO}_4)_3$ /thiourea molar ratio as 1/2 and 1/1. Figure 1 shows the relationship between thiourea concentration and gold extraction. Gold extraction increases with the increasing concentration of thiourea and the additions in excess of a concentration of 5 g/l thiourea do not improve gold extraction significantly.

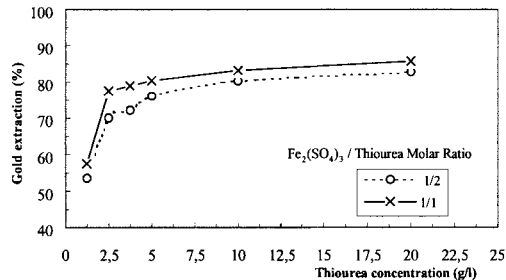


Figure 1: Effect of thiourea concentration on gold extraction.

### *The effect of ferric sulfate concentration*

One series of experiments were performed independent of ferric sulfate/thiourea molar ratio at three levels of thiourea concentration. Figure 2 shows the variations of gold extraction with respect to the ferric sulfate concentration.

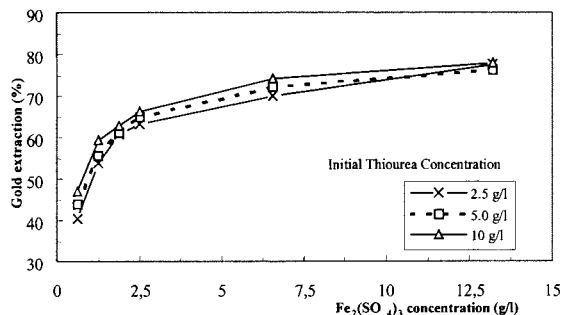


Figure 2: Effect of  $\text{Fe}_2(\text{SO}_4)_3$  concentration on gold extraction.

Figure 2 demonstrated that  $\text{Fe}_2(\text{SO}_4)_3$  has a positive effect on gold extraction. For the above given the leaching conditions, it was not possible to reach 80% gold extraction.

#### The effect of $\text{Fe}_2(\text{SO}_4)_3$ /thiourea molar ratio

The initial concentration of thiourea, with respect to the initial oxidant ( $\text{Fe}_2(\text{SO}_4)_3$ ) concentration and the kinetics of thiourea oxidation, is the most influential factor affecting the dissolution of gold. This time, initial thiourea concentration was kept constant as 2.5 g/l, and the pre-calculated amount of  $\text{Fe}_2(\text{SO}_4)_3$  was added by maintaining the required  $\text{Fe}_2(\text{SO}_4)_3$ /thiourea molar ratio of 1/2, 1/1 and 2/1. In order to assess the necessity of oxidant in gold dissolution, one leaching test was done without using any oxidizing agent. Table II provides data on gold extraction versus the molar ratio of  $\text{Fe}_2(\text{SO}_4)_3$  /thiourea. The results are shown graphically in Figure 3.

Table II: Results of scouting leaching tests.

$\text{Fe}_2(\text{SO}_4)_3$ /Thiourea (molar ratio)	Gold extraction (%)					
	leaching duration, h					
	1	2	4	6	8	18
0	24.90	35.30	37.00	37.28	36.90	33.75
1/2	38.20	68.20	69.20	70.00	69.10	69.00
1/1	40.30	76.40	77.00	77.50	76.80	71.20
2/1	30.50	53.70	60.10	62.50	63.70	65.00

\* Leaching test conditions: initial thiourea concentration = 2.5 g/l; pH = 1.35; pulp density = 20%; particle size = 80% passing 74  $\mu\text{m}$

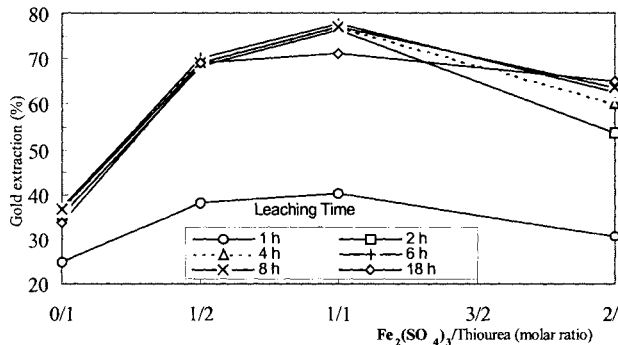


Figure 3: Effect of  $\text{Fe}_2(\text{SO}_4)_3$ /thiourea molar ratio on gold extraction.

As it is seen in Figure 3, without oxidizing agent ( $\text{Fe}_2(\text{SO}_4)_3$ ), the thiourea solution provides very low gold extraction. Figure 3 also shows that gold extraction increases with an increasing  $\text{Fe}_2(\text{SO}_4)_3$ /thiourea molar ratio and reaches a maximum value at the  $\text{Fe}_2(\text{SO}_4)_3$ /thiourea ratio of 1/1. Further,  $\text{Fe}_2(\text{SO}_4)_3$  addition results in a decrease in gold extraction. This could be due to the rapid decomposition of thiourea and to the breakdown of formamidine disulfide [ $\text{NH}_2(\text{NH})\text{CSSC}(\text{NH})\text{NH}_2$ ] to sulfur and other secondary reaction products, which are known to passivate gold surfaces.

#### The effect of leaching time

In order to investigate the effect of leaching time on gold dissolution, the data obtained in the experiments for varying  $\text{Fe}_2(\text{SO}_4)_3$ /thiourea molar ratios were used



(Table II). It can be seen easily from Figure 4 that the rate of gold dissolution was very rapid in the first two h leaching that it increased gradually with longer leaching time and flattened off after 6 h.

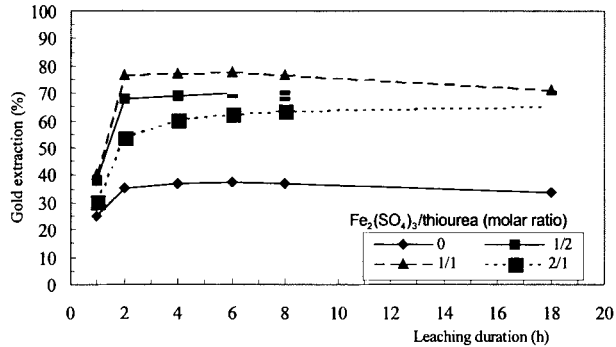


Figure 4: Variation of gold extraction amount.

This can be explained by the decrease in the stability of thiourea over time and production of elemental sulfur, the decomposition product of thiourea, to form a stable film on the gold particle surface. This produced the conclusion that little or no advantages are to be gained by extending the conventional cyanidation leaching time to the standard 16 h or longer.

#### *The effect of particle size*

The particle size of the feed is an important factor to be considered in a leaching operation, because it is directly related to liberating and exposing gold to the thiourea solution. Figure 5 showed that gold extraction increases with decreasing particle size and that maximum gold extraction was obtained with the <math><53 \mu\text{m}</math> feed size. This is due to the fact that with a finer particle size, a greater surface area is obtained, which facilitates the diffusion of thiourea to

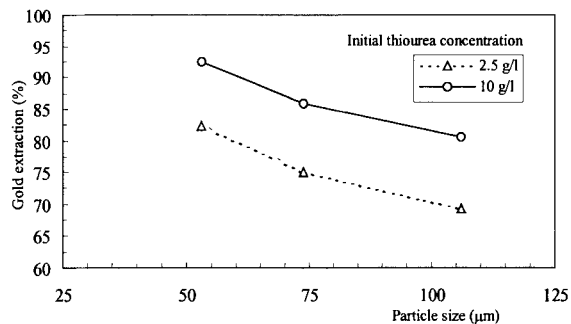


Figure 5: Effect of particle size on gold extraction.

#### *Thiourea consumption*

Throughout the study, samples of solution were pipetted out from the pregnant solution to determine the consumption of thiourea. As demonstrated in Figures 6 to 8,

thiourea consumption is directly proportional to the increase in initial thiourea concentration, and to  $\text{Fe}_2(\text{SO}_4)_3$ /thiourea molar ratio and particle size. The decomposition of thiourea to formamidine disulfide and complexing of thiourea with the ferric sulfate are the main reasons for the high consumption of thiourea. On the other hand, addition of excess amounts of thiourea was necessary to stabilize the weak thiourea-gold complex in the aqueous leaching medium.

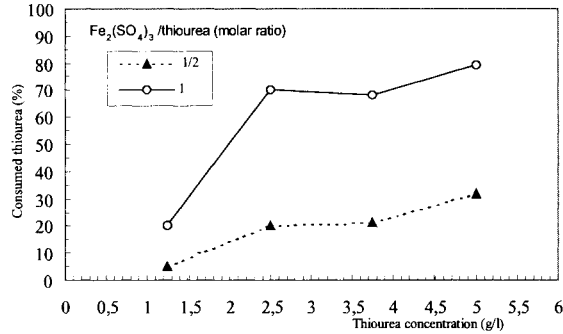


Figure 6: Variation of thiourea consumption with initial thiourea concentration.

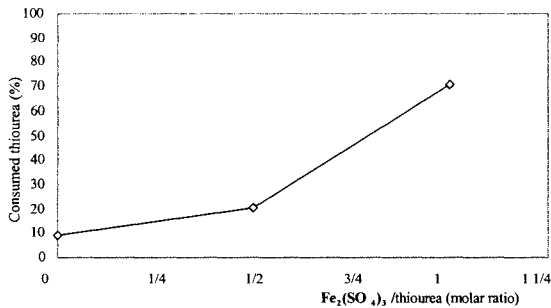


Figure 7: Variation of thiourea consumption with  $\text{Fe}_2(\text{SO}_4)_3$ /thiourea molar ratio.

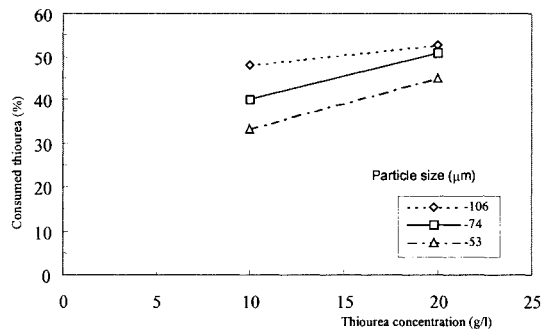


Figure 8: Variation of thiourea consumption with particle size.

## **Conclusions**

Leaching tests under different conditions have provided conclusions that future adoption of thiourea for gold leaching to replace the traditional cyanidation method looks very promising. The kinetics of thiourea oxidation and the concentration of ferric sulfate with respect to thiourea concentration are the most important factors affecting the dissolution of gold in an acidic medium. Although thiourea leaching has the drawback of a high thiourea consumption, thiourea leaching of Kaymaz gold ore was technically possible with 92.5% gold extraction.

## **References**

- Caldeira, C.L. and Ciminelli, S.T., 1993. Thiourea leaching of a refractory gold ore. *Proceedings of the XVIII Int. Min. Proc. Cong.*, Sydney, 5, 1123-1128.
- Deschenes, G., 1986. Literature survey on the recovery of gold from thiourea solutions and the comparison with cyanidation. *CIM Bulletin*, 895, 76-83.
- Groenewald, T., 1976. The dissolution of gold in acidic solutions of thiourea. *Hyrometallurgy*, 1, 277-290.
- Huyhua, J.C., Zegarra, C.R. and Gundiler, İ.H., 1989. A comparative study of oxidants on gold and Silver Dissolution in Acidic Thiourea Solutions. *Precious Metals '89*, M.C. Jha and S.D. Hill (Editors), The Minerals, Metals and Materials Society, 287-299.
- Örgül, S., 1999. Gold Extraction from Kaymaz Gold Ore by Thiourea Leaching. M.Sc. Thesis, METU, Ankara, Turkey.
- Preisler, P.W. and Berger, L., 1947. Oxidation-reduction potentials of thiol-dithio systems: thiourea-formamidine disulfide. *Journal of American and Chemical Society*, 69, 322-325.
- Pyper, R.A. and Hendrix, J.L., 1981. Extraction of gold from finely disseminated gold ores by use of acidic thiourea solution. *The IMM, Extractive Metallurgy*, '81, 57-75.
- Ubal dini, S., Fornari, P., Massida, R. and Abbruzzese, C., 1998. An innovative thiourea gold leaching process. *Hydrometallurgy*, 48, 113-124.

## SYNTHESIS OF ARAGONITE BY THE CARBONATION PROCESS USING STAINLESS REFINING DUST IN IRON & STEEL PLANTS

J.H. Ahn\*, K.S. Choi\*, H. Kim<sup>°</sup>, S.H. Yoon<sup>°</sup>, J.S. Kim<sup>°</sup>, G.W. Sung<sup>◇</sup>, K.H. Lee<sup>◇</sup>

\*Minerals Utilization & Materials Development Division, Korea Institute of Geology, Mining & Materials, Taejeon, Korea

<sup>°</sup>School of Materials Science & Engineering, Seoul National University, Seoul 151-742, Korea

<sup>◇</sup>Waste Recycling Planning Team, Pohang Iron & Steel Co. Ltd, Pohang, Korea

### Abstract

The conditions for the synthesis of aragonite by the carbonation process were investigated, and these results were applied to the recycling of stainless refining dust in iron & steel plants. The formation of aragonite has no relation to the pH value, the mole ratio of  $MgCl_2/Ca(OH)_2$  and Mg/Ca ion concentration in solution. The condition for the synthesis of aragonite requires that the concentration of Mg ions should be in an appropriate range (about 0.1÷0.26 mol/l) and the concentration of Ca ions below a certain range (less than about 0.16÷0.25 mol/l). Too many Ca ions or Mg ions favor the formation of calcite. Needle-like aragonite was successively synthesized using dusts and thus, effective recycling of dusts can be expected.

*Keywords: CaCO<sub>3</sub>, aragonite, carbonation process, recycling, dusts*

### Introduction

There are three kinds of polymorphism in calcium carbonate, and these are calcite, aragonite and vaterite. Among these materials, calcite is the only stable phase at room temperature and pressure, and it is easily synthesized and generally used. Aragonite and vaterite are metastable phases in a natural state, and thus it is difficult to synthesize them. Recently, a needle-like aragonite phase with a high aspect ratio is expected for many applications, such as improvement of the mechanical properties of polymers and rubber materials, or reinforcing materials in the paper industry.

It is generally known that Mg ions inhibit the growth of calcite, and thus relatively enhance the formation of aragonite in the precipitation of calcium carbonate in solution. There are many reports about the effects of Mg ions on the phase formation and crystal growth of calcium carbonate (Bischoff, 1968; Nancollas and Sawada, 1982; Gutjahr et al., 1996; Ota et al., 1983-1984; Sasaki et al., 1998). The aragonite phase can be synthesized using these effects. The crystal can be prepared either by the reaction of solutions containing calcium ions and carbonate ions, or by the carbonation process, in which CO<sub>2</sub> gas is blown into a Ca(OH)<sub>2</sub> slurry. In the case of the former, aragonite can be obtained easily only if the reported condition of synthesis is met. But in the case of the latter, the reports are insufficient, and further, each reported experimental conditions regarding the synthesis of aragonite which were different and somewhat inconsistent (Ota et al., 1983-1984; Sasaki et al., 1998).

Ota et al. reported that aragonite can be synthesized by blowing CO<sub>2</sub> gas into the mixture of Ca(OH)<sub>2</sub> slurry and MgCl<sub>2</sub> solution, with an initial pH value of 9 at a temperature of 80 °C (Ota et al., 1983-1984). He emphasized that the initial pH value of the reaction mixture solution determines the formation of aragonite. But in our experiment, if the total amount of batch or starting materials varied, the precipitated phase was aragonite in one case or calcite in the other, although the initial pH values were the same. Thus we cannot conclude that the initial pH value of the mixture solution necessarily determines the formation of aragonite. Sasaki et al. reported that the important factors to obtain aragonite were the mole ratio of the starting material's MgCl<sub>2</sub>/CaO, flow rate of CO<sub>2</sub>, reaction time, pH and temperature (Sasaki et al., 1998). In the case of the mole ratio of MgCl<sub>2</sub>/CaO, they mentioned that the aragonite phase was dominantly formed when the mole ratio of MgCl<sub>2</sub>/CaO was 1.6, under the condition of a temperature of 35 °C and a CO<sub>2</sub> flow rate of 50 cm<sup>3</sup>/min. But in their data, the major phase was different for each case when the amount of starting material CaO was 5 g and 20 g, although the mole ratio of MgCl<sub>2</sub>/CaO is 1.6. Thus the value of the mole ratio of starting materials cannot necessarily define the condition of the formation of aragonite.

Considering these points, the suggested conditions for the synthesis of aragonite can be applied only to their specific reaction system and thus, cannot be applied perfectly if the amount of batch or starting materials changes. So it is necessary to find the synthesis condition that is consistent and generally applicable, irrespective of the amount of batch. In this study, we intended to define the conditions for the synthesis of aragonite which are generally applicable to any reaction system and to apply these results to the recycling area. Annually, a large quantity of dusts in iron and steel plants, of which the major composition is a CaO-Ca(OH)<sub>2</sub> type mixture, is a stainless refining dust. For example, the amount of dusts from a Korean steel company named POSCO (Pohang Iron & Steel Co., Ltd.) is 6 t/day, and these dusts have not been reused effectively yet. For the recycling of dusts, synthesis of calcium carbonate can be considered, and it would be far better if the high-value, added-aragonite phase can be obtained. Thus, in this study we discuss the condition of the synthesis of aragonite and its application to dusts.

### **Experimental procedures**

In the experiments for defining the synthesis condition of aragonite, the starting materials are reagent grade Ca(OH)<sub>2</sub> and MgCl<sub>2</sub>. Ca(OH)<sub>2</sub> slurry was added to a MgCl<sub>2</sub> aqueous solution, and the total volume of the reaction solution was fixed to 1 liter. The amount of Ca(OH)<sub>2</sub> was varied in the range of 0.05÷0.4 mol, and that of MgCl<sub>2</sub> was varied in the range that sets the pH value of the reaction solution from 11 to 7.5. The reaction temperature was 80 °C, or room temperature, and the CO<sub>2</sub> flow rate was fixed to 100 cm<sup>3</sup>/min. The completion of the reaction was identified by observing the constancy after the decrease in the pH value, and the precipitates were sampled, washed and dried. In this kind of experiment, we should be aware that all of the added MgCl<sub>2</sub> does not contribute to Mg<sup>2+</sup> ion formation in the reaction solution, and part of it exists in the form of Mg(OH)<sub>2</sub>. And as the amount of MgCl<sub>2</sub> increases, the pH value of the reaction solution decreases, which accompanies the increase in

$\text{Ca}^{2+}$  ion, due to enhanced  $\text{Ca}(\text{OH})_2$  dissolution. Thus, if the total amount of starting materials changes, the amount of Ca and Mg ion also changes, although the pH value of the reaction solution is the same, or the mole ratio of  $\text{MgCl}_2/\text{Ca}(\text{OH})_2$  is the same. From these points, we can expect that the concentration of each ion or its ratio determine the formation of aragonite. Thus the concentration of Ca and Mg ions in the initial reaction solution was analyzed by ICP (Inductively Coupled Plasma Spectrometry) analysis, and the effects of the concentration or ratio of each ion in the phase formation was investigated. X-ray diffraction (XRD) analysis was performed to identify the crystalline phase, and morphologies were examined using scanning electron microscopy (SEM). The induced conditions for the synthesis of aragonite were applied to CaO- $\text{Ca}(\text{OH})_2$  type mixtures of dusts. The dusts used in this study are wastes generated from steel works (POSCO), and the major weight-compositions analyzed by XRF (X-Ray Fluorescence Spectrometry) are  $\text{CaO} = 78.6\%$ ,  $\text{Fe}_2\text{O}_3 = 9.9\%$ ,  $\text{Al}_2\text{O}_3 = 6.4\%$ ,  $\text{SiO}_2 = 3.3\%$  and  $\text{MgO} = 1.8\%$ . These dusts were pre-treated with such processes as wet sieving, gravity separation and magnetic separation, and then the synthesis of aragonite was performed.

## Results and discussion

Table I shows experimental conditions and ion concentrations when the amount of  $\text{Ca}(\text{OH})_2$  is fixed to 0.2 mol, and the pH value is adjusted by the amount of  $\text{MgCl}_2$  in the total reaction solution of 1 liter. As compared with the case of no  $\text{MgCl}_2$  addition, the concentration of Ca ion increases about 10 times under the condition of the pH value 10 and increases very slightly with a further decrease in the pH value. The concentration of Mg ion is very low compared with the amount of  $\text{MgCl}_2$  under conditions of pH value 10. As the pH value decreases with an increase in the amount of  $\text{MgCl}_2$ , the concentration of Mg ions increases abruptly and becomes of the same amount of  $\text{MgCl}_2$  as in cases when the pH value is 8.1 and 7.3 at 80 °C. When the amount of  $\text{MgCl}_2$  is small, most Mg ions react with  $\text{OH}^-$  ions, forming  $\text{Mg}(\text{OH})_2$ , and this  $\text{Mg}(\text{OH})_2$  phase was identified by XRD data in our experiment. As the precipitation of  $\text{CaCO}_3$  proceeds and is completed, the pH value of the reaction solution decreases, and this accompanies  $\text{Mg}(\text{OH})_2$  dissolution. As the amount of  $\text{MgCl}_2$  increases, its portion that contributes to Mg ions in the solution increases.

Figure 1 shows the XRD results, corresponding to the experimental conditions in Table I. At the reaction temperature of 80 °C, the calcite phase is mainly formed at pH values of 11.7, 10 and 9, and the aragonite phase is mainly formed at the pH value of 8.1. Ota et al. reported that aragonite was synthesized when the pH value of the reaction solution was 9, but in our study aragonite was synthesized at the pH value of 8.1 under the experimental condition in Table I-(4), and thus some discrepancies exist between the two. In case the pH value is 8.1, the ion concentrations of Ca and Mg in the reaction solution are 0.162 mol and 0.255 mol respectively. That is, the concentration of each ion is similar, compared with the cases of other pH values. It is generally known that Mg ions inhibit the growth of calcite, and thus, relatively enhance the formation of aragonite in the precipitation of calcium carbonate in solution.

Table I: Experimental conditions and ion concentrations when the amount of  $\text{Ca}(\text{OH})_2$  is fixed to 0.2 mol.

Batch number	T(°C)	pH	Starting materials (mol)		Ion concentration (mol/l)	
			$\text{Ca}(\text{OH})_2$	$\text{MgCl}_2$	Ca	Mg
(1)	80	11.7	0.2	0	0.015	0
(2)	80	10.0	0.2	0.15	0.150	0.00016
(3)	80	9.0	0.2	0.17	0.140	0.005
(4)	80	8.1	0.2	0.4	0.162	0.255
(5)	80	7.3	0.2	0.8	0.170	0.502
(6)	27	8.9	0.2	0.4	0.144	0.189
(7)	27	8.7	0.2	0.8	0.146	0.585
(8)	27	8.1	0.2	1.36	0.140	1.160

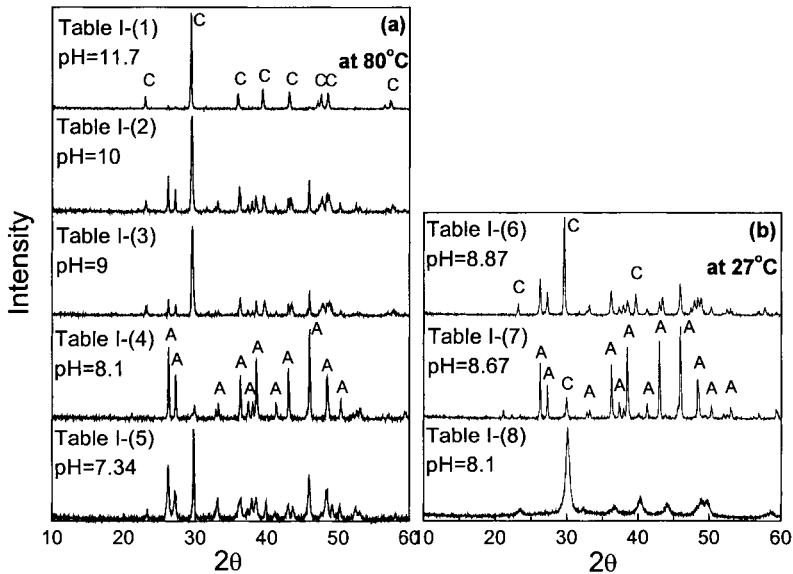


Figure 1: XRD results of precipitates at the reaction temperatures of (a) 80 °C, (b) room temperature, for the experimental condition in Table I.

But from Figure 1 (a) and (b), we can notice that too many Mg ions, on the contrary, inhibit the formation of aragonite and enhance that of calcite. Thus, it seems that there are some ranges of concentrations of Mg ions in which the formation of aragonite is dominant. The reason why the formation of calcite is dominant under the condition of too much Mg ion concentration is not clear. But the main peak of calcite in case of an Mg ion-excess condition (Table I-5) in Figure 1-(a) and Table I-8) in Figure 1-(b),  $2\theta = 29.80^\circ$  and  $30.12^\circ$ , respectively) shifted to higher angle compared with that of a Mg ion-deficient condition (Table I-1) in Figure 1-(a) and Table I-6) in Figure 1-(b),  $2\theta = 29.40^\circ$  and  $29.62^\circ$ , respectively). When the concentration of Mg ions is too high, Mg ions also precipitate, with Ca ions forming a calcite structure  $(\text{Ca},\text{Mg})\text{CO}_3$  solid solution, and these precipitates become the major phase. Then, in order to confirm whether the pH value of the reaction solution determines the formation of aragonite,

as mentioned by Ota et al., experiments for the condition in Table II were performed, and XRD results are shown in Figure 2.

Table II: Experimental conditions and ion concentrations for several fixed pH values.

Batch number	T(°C)	pH	Starting materials (mol)		Ion concentration (mol/l)	
			Ca(OH) <sub>2</sub>	MgCl <sub>2</sub>	Ca	Mg
(1)	80	9.0	0.05	0.05	0.035	0.0064
(2)	80	9.0	0.12	0.17	0.13	0.0051
(3)	80	9.0	0.4	0.35	0.3	0.0022
(4)	80	8.1	0.05	0.15	0.035	0.115
(5)	80	8.1	0.2	0.40	0.162	0.255
(6)	80	8.1	0.4	0.48	0.253	0.079
(7)	80	7.7	0.4	0.6	0.242	0.152
(8)	80	7.4	0.4	0.8	0.26	0.41

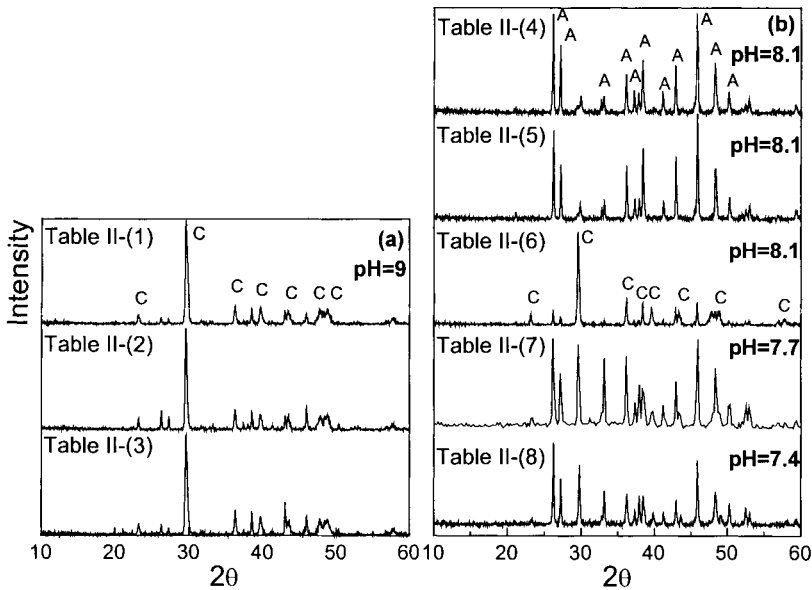


Figure 2: XRD results of the precipitates when the pH value of the reaction solution is (a) 9, (b) below 8.1, under the experimental condition in Table II.

Table III: Experimental conditions in the case of using dusts.

Batch number	T(°C)	pH	Starting materials (mol)		Ion concentration (mol/l)	
			Dust	MgCl <sub>2</sub>	Ca	Mg
(1)	80	8.1	0.05	0.12	0.023	0.088
(2)	80	8.01	0.05	0.17	0.026	0.13
(3)	80	8.1	0.2	0.23	0.1	0.009
(4)	80	7.94	0.2	0.4	0.1	0.15



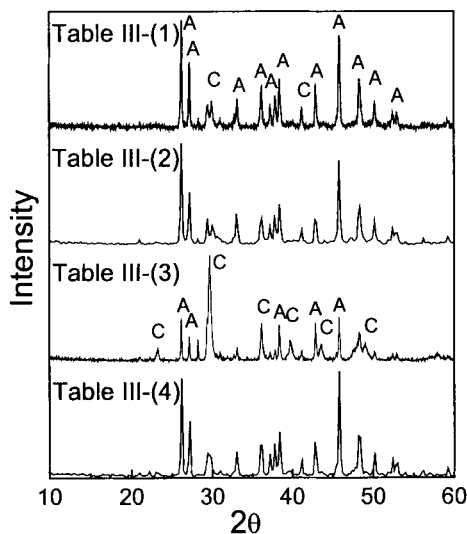


Figure 3: XRD results of the precipitates when the starting materials are dusts under the experimental conditions in Table III.

When the pH value is 9, the major precipitated phase is calcite in all cases. When the pH value is 8.1, the major precipitated phase is aragonite in cases when the amount of  $\text{Ca}(\text{OH})_2$  is 0.05 mol and 0.2 mol (Table II-(4) and Table II-(5)). But in cases when the amount of  $\text{Ca}(\text{OH})_2$  is 0.4 mol (Table II-(6)), the major precipitated phase is calcite, although the pH value is 8.1. When the amount of  $\text{Ca}(\text{OH})_2$  increased to 0.4 mol, the amount of  $\text{MgCl}_2$  also increased to set the pH value to 8.1, but the amount of Mg ions, on the contrary, decreased compared with the case when the amount of  $\text{Ca}(\text{OH})_2$  was 0.2 mol. Thus, although the pH value is the same, the concentration of Ca and Mg ions or their ratio varies with changes in the amount of batch or starting materials, and this phenomenon causes differences in the phase of precipitates.

From these data (Table II and Figure 2), several facts can be induced. The formation of aragonite has no relation to the pH value from the data of Table II-(4), Table II-(5) and Table II-(6). In addition, the mole ratio of  $\text{MgCl}_2/\text{Ca}(\text{OH})_2$  cannot necessarily define the condition of aragonite formation, because the results can be different from the data of Table II-(5) and Table II-(8), in spite of the same mole ratio of  $\text{MgCl}_2/\text{Ca}(\text{OH})_2$ . The mole ratio of Mg/Ca ion concentration in solution also can not define the condition of aragonite formation, because the portion of the aragonite phase is small, although the Mg/Ca ion concentration ratio is high from the data of Table II-(5) and Table II-(8). From the data in Table I and Figure 1, we noticed that too much of the Mg ion inhibited the formation of aragonite and enhanced that of calcite. From the data in Table II and Figure 2, the condition of high Ca ion concentration in solution also favors the formation of calcite, although the Mg ion concentration is high (Table II-(8)). Thus, the condition for the synthesis of aragonite requires that the concentration of the Mg ions should be in an appropriate range (about  $0.1 \div 0.26$  mol/l), and the concentration of the Ca ions below a certain range

(about less than  $0.16\div 0.25$  mol/l). Too many Ca ions or Mg ions favors the formation of calcite. Table III shows experimental conditions in the case of using dusts, and the XRD results are shown in Figure 3. We can also confirm that the formation of aragonite has no relation to the pH value from Table III-(1) and Table III-(3) data, or to the ratio of starting materials or Mg/Ca ion concentration from Table III-(1) and Table III-(4) data, because the portion of aragonite is slightly higher. The ratio of  $\text{MgCl}_2/\text{Dust}$  or Mg/Ca ion concentration is lower in the case of Table III-(4) than in that of Table III-(1), though. Figure 4 shows morphologies of aragonite precipitated under the conditions in Table I-(4) and Table III-(4). Needle-like precipitates with a high aspect ratio can be obtained.

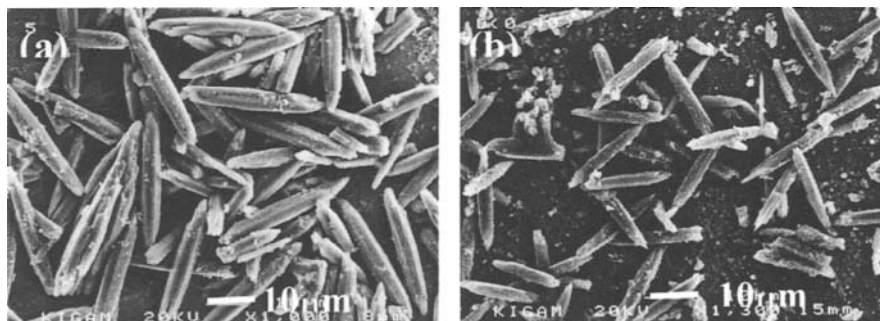


Figure 4: SEM photographs of the aragonite for conditions (a) in Table I-(4): the starting materials are reagent grade  $\text{Ca}(\text{OH})_2$ , and (b) in Table III-(4): the starting materials are dusts.

## Conclusions

The conditions for the synthesis of aragonite were investigated. The formation of aragonite has no relation to the pH value, the mole ratio of  $\text{MgCl}_2/\text{Ca}(\text{OH})_2$ , or Mg/Ca ion concentration in the reaction solution. The condition for the synthesis of aragonite requires that the concentration of Mg ions should be in the appropriate range (about  $0.1\div 0.26$  mol/l) and the concentration of Ca ions below a certain range (about less than  $0.16\div 0.25$  mol/l). Too many Ca ions or Mg ions favor the formation of calcite. These results were applied to dusts, and needle-like aragonite was successively synthesized. Therefore effective recycling of dusts can be expected.

## References

- Bischoff, J.L., 1968. Kinetics of calcite nucleation: magnesium ion inhibition and ionic strength catalysis. *J. Geophysical Research*, 73(10), 3315-3322.
- Gutjahr, A, Dabringhaus, H. and Lacmann, R., 1996. Studies of the growth and dissolution kinetics of the  $\text{CaCO}_3$  polymorphs calcite and aragonite. The influence of divalent cation additives. *Growth and Dissolution Rates. J. Cryst. Growth*, 158, 310-315.
- Nancollas, G.H. and Sawada, K., 1982. Formation of scale of calcium carbonate polymorphs: the influence of magnesium ion and inhibitors. *J. Pet. Technol.*, 645-652.
- Ota, Y., Inui, S., Iwashita, T., Kasuga, T. and Abe, Y., 1995. Preparation of aragonite whiskers. *J. Am. Ceram. Soc.*, 78(7), 1983-1984.
- Sasaki, K., Hongo, M. and Tsunekawa, M., 1998. Synthesis of aragonite-type of calcium carbonate from calcined scallop shell (3rd report). *Shigen-to-Sozai*, 114, 715-720. (in Japanese)

## DEVELOPMENT OF AN IRON REMOVAL PROCESS FROM KAOLIN BY THIOUREA LEACHING: KINETIC AND RELATED STATISTICAL ANALYSIS

F. Vegliò\*, F. Beolchini<sup>o</sup>

\*Dipartimento di Ingegneria Chimica e di Processo "G.B. Bonino", University of Genoa, via Opera Pia, 15, 16145 Genoa, Italy

<sup>o</sup>Dipartimento di Chimica, Ingegneria Chimica e Materiali, Università degli Studi de L'Aquila, 67040 Monteluco di Roio, L'Aquila, Italy

### Abstract

In the present paper an iron removal process by leaching of kaolin using thiourea as a leachant agent in the presence of H<sub>2</sub>SO<sub>4</sub> was studied. The leaching process can improve its economic value and its utilisation in the ceramic and paper industry becomes possible. The effect of thiourea was investigated together with other factors such as sulphuric acid concentration, temperature and different treatment times. The largest iron extraction yield (94.1%) was obtained after 150 min of treatment at 90 °C, H<sub>2</sub>SO<sub>4</sub> 0.25 M and with 10 g/l of thiourea. At the same temperature the iron extraction yield was of 68.4% after 120 min of treatment with H<sub>2</sub>SO<sub>4</sub> 0.1 M and thiourea 1 g/l.

A kinetic analysis indicates that the chemical reaction is the limiting step in the leaching process (Activation energy 74±9 kJ/mole). The overall kinetic model that describes the iron extraction yield vs. time has been pointed taking into consideration iron extraction yield, acid concentration, thiourea concentration and leaching time. From the analysis of the literature the use of thiourea in the iron removal from industrial minerals was found to be original and technically feasible.

*Keywords: kaolin, iron removal, thiourea, factorial experiments, kinetic analysis*

### Introduction

Industrial minerals, such as kaolins, feldspatic and quartziferous sands, are often associated with several impurities that lower their economical value and hinder their application in the ceramic and paper industry. The main impurity that decreases the economical value of these minerals is iron oxides because they lower the degree of whiteness of the obtained product, which is an important technological factor (Abbruzzese et al., 1999). These impurities can be removed by a number of physical or chemical processes (Vegliò et al., 1996). In the last ten years, interest has been directed in finding alternative chemical processes, which would be more efficient with respect to the iron removal process and more environmentally friendly. This interest is shown by some studies reported in the literature and by the financial supports supplied by the E.U. in this sector, in which the main European industries are also involved (Abbruzzese et al., 1999).

Particular attention has been paid to the use of organic acids, such as oxalic, citric and ascorbic acids, as complexing or reducing agents in the iron removal process (Vegliò et al., 1996, 1998). The use of reducing and/or complexing compounds is linked to the fact that oxide dissolution is generally strongly influenced by the presence of

reductive compounds when the oxide dissolution can produce two species in solution with different oxidation levels (Chiarizia and Hortwiz, 1991).

Most papers reported in the literature deal with the iron oxide dissolution of the pure iron compound. For this reason there is greater interest in the study of the leaching of industrial minerals for their beneficiation, because the kinetics of iron dissolution is linked to the siliceous matrix in which the impurity is generally placed.

An analysis of the available literature reveals that the use of thiourea as a leaching agent seems to be original. Moreover, there are some studies, in which the oxidative action of  $\text{Fe}^{3+}$  on thiourea have been carried out, but only for applications linked to the recovery of gold from auriferous minerals by means of thiourea (Zhu, 1992). The only papers reported in the literature which involve compounds similar to thiourea (thiourea dioxide) are those related to a Russian patent (Danilova et al., 1982) and a bleaching wool treatment process (Cegarra et al., 1988).

The results reported in the literature on the reactions which involve the Fe(III) and thiourea show that in solutions of weak mixed sulphate-thiourea medium, a complex  $\text{Fe(III)SO}_4\text{Tu}^+$  is formed (Zhu, 1992). In more concentrated solutions, in the presence of Fe(III), the complex  $(\text{Fe(II)Tu}_2)\text{SO}_4$  is formed, indicating a reductive reaction of Fe(III) with thiourea (Zhu, 1992). The stoichiometry of the reaction under study is 1 mole of ferric with 1 mole of thiourea. Regarding the possible products of reaction, the first oxidation product of thiourea is formamidine disulphide (FDS) (Zhu, 1992).

Starting from these observations, previous work has been performed in order to evaluate the thiourea utilisation in the iron removal process from a kaolin of industrial interest (Vegliò, 1997). From the analysis of the experimental results it was possible to determine the main and interaction effects of the investigated factors such as thiourea and sulphuric acid concentration, temperature and time of treatment. Thiourea has a positive effect on the iron removal process. The action of iron dissolution from the mineral in question is, however, also carried out by effect of the  $\text{H}_2\text{SO}_4$  alone, which also acts with a synergetic action on the extractive process in the presence of thiourea evaluated by factorial experiments. After these studies, aim of this paper is the study of the iron dissolution kinetic modelling in the leaching process.

### Materials and methods

A sample of kaolin from S. Severa (North Latium - Italy) was used in the leaching tests for iron removal. This is the largest kaolin deposit in central Italy, with a hydrothermal origin. A complete and detailed chemical and mineralogical analysis is reported elsewhere (Matiasand and Caneva, 1979), (Vegliò et al., 1993, 1994, 1997). The iron content in the mineral is  $1.08 \pm 0.1\%$  (as  $\text{Fe}_2\text{O}_3$ ). The particle-size analysis shows that 75% of the mineral is larger than 2  $\mu\text{m}$ .

The leaching tests were carried out in shaken flasks placed in a mechanically stirred thermostated bath (Dubnoff): a quantity of mineral (30 g) was suspended in 100 ml of solution containing thiourea and/or  $\text{H}_2\text{SO}_4$ . All chemicals were of reagent grade. Several samples were collected at different times of leaching treatment for the analysis of the liquor leach after centrifugation (5 min at 5,000 rpm). The chemical analyses were performed using a UV spectrophotometer (Varian Cary 1). The total

iron dissolved was monitored using the potassium thiocyanate method at 480 nm (Koltoff, 1974) after the complete oxidation of  $\text{Fe}^{2+}$  with  $\text{KMnO}_4$ .

The leaching tests were performed to mainly investigate the effect of the investigated factors on the iron removal process. Four factors were taken into consideration in the experimental planning:  $\text{H}_2\text{SO}_4$ , thiourea, temperature and time of treatment. All tests were randomised (Montgomery, 1991).

## Results

Considering the experimental results reported elsewhere (Vegliò, 1997), a kinetic analysis was performed to determine the most effective kinetic model to describe the iron removal process. The shrinking core model (Levenspiel, 1972) was employed in the data fitting, considering the following aspects (Vegliò, 1997):

- 1) the temperature plays an important role in the iron dissolution process, as obtained from a previous statistical analysis by factorial experiments;
- 2) the mixing of the solid-liquid system was brought in order to minimise the effect of the mass transfer rate due to the diffusion in the film layer around the ore particles.

From these experimental evidences it is possible to hypothesise that the kinetic model that can represent the leaching process must contain the chemical reaction as kinetic limiting step. The kinetic model is:

$$\frac{t}{\tau} = 1 - (1 - X)^{1/3} \quad (1)$$

in which:

$$\tau = \frac{b}{k \cdot C_a^{n_1} \cdot C_t^{n_2}} \quad (2)$$

$$k = e^{\frac{-E_a}{RT}} \quad (3)$$

where:

X = iron extraction yield	(%)
$C_a$ = sulphuric acid concentration	(M)
$C_t$ = thiourea concentration	(M)
$\tau$ = time to reach the complete iron removal from the kaolin particle	(min)
K = kinetic constant	( $\text{min}^{-1}$ )
$E_a$ = activation energy	(kJ/mol)
T = temperature	(K)
t = time of treatment	(min)
$n_1$ = reaction order for sulphuric acid	
$n_2$ = reaction order for thiourea	
b = constant of the model	( $\text{M}^{n_1} \text{M}^{n_2}$ )

The experimental conditions tested are reported in Table I.

Figures 1 and 2 show some of the main experimental results as an example.

Figure 3 reports the results of the data fitting for some leaching tests carried out in the presence of thiourea using equation (1) as an example. From the analysis of these results, it is possible to observe the optimal adaptation of the experimental results to the model. This confirms the above hypothesis of the chemical reaction as a limiting step. The values of the  $\tau$ 's obtained from this data fitting are reported in Table II.

Considering the tests carried out at two different temperatures (70 °C and 90 °C) it is possible to estimate the activation energy ( $E_a$ ) of the iron dissolution process. The average value of  $E_a$  was of  $70 \pm 9$  kJ/mole. Regarding the thiourea concentration, the average reaction order appears to be  $0.373 \pm 0.054$  (Figure 4) while for  $H_2SO_4$  an average value of  $0.855 \pm 0.12$  was estimated.

Table I: Factors and parameter settings investigated in the leaching test: 30% (wt/vol) mineral concentration; 200 rpm mixing conditions.

Treatment	$H_2SO_4$ (M)	Thiourea (g/l)	Temperature (°C)
1	0.10	1.0	70
2	0.25	1.0	70
3	0.10	3.0	70
4	0.25	3.0	70
5	0.10	1.0	90
6	0.25	1.0	90
7	0.10	3.0	90
8	0.25	3.0	90
9	0.10	5.0	70
10	0.25	5.0	70
11	0.10	10.0	70
12	0.25	10.0	70
13	0.10	5.0	90
14	0.25	5.0	90
15	0.10	10.0	90
16	0.25	10.0	90
17	0.18	5.0	80

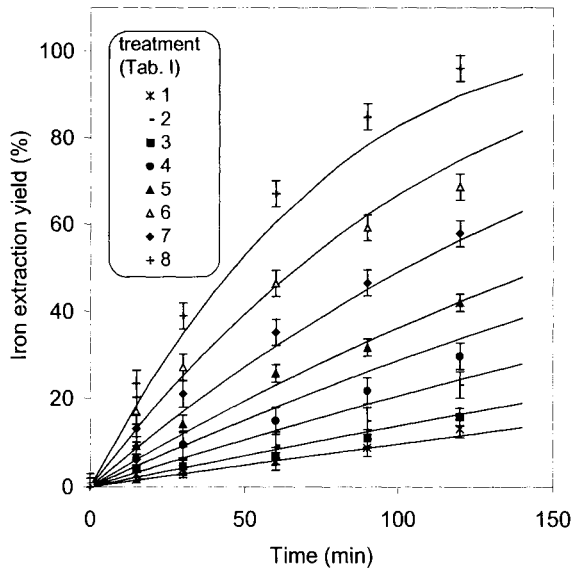


Figure 1: Experimental and calculated iron extraction yield vs. time. The full lines represent calculated yield curves.

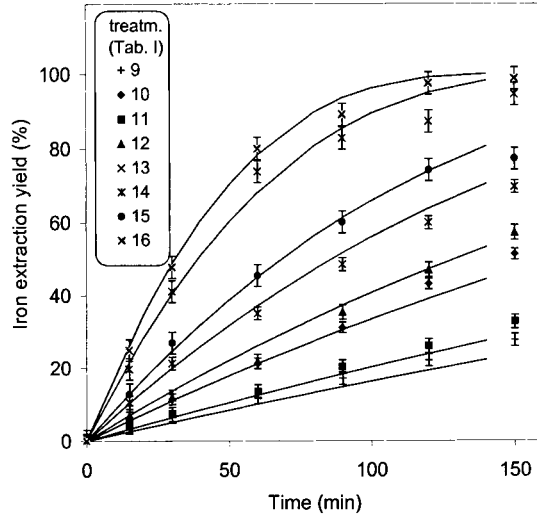


Figure 2: Experimental and calculated iron extraction yield vs. time.

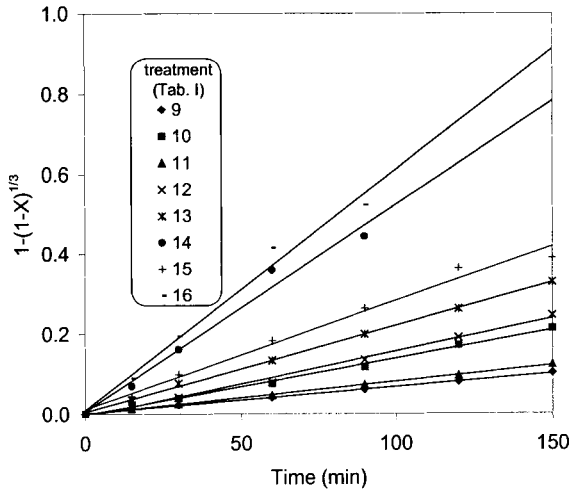


Figure 3: Fitting of the experimental results by a shrinking core model: chemical reaction as limiting step (temperature = 90 °C).

Table II: Some values of  $\tau$ 's (min) obtained from data fitting using equation (1).

Thiourea conc. (g/l)	H <sub>2</sub> SO <sub>4</sub>		H <sub>2</sub> SO <sub>4</sub>	
	0.1 M, 70 °C	0.1 M, 90 °C	0.25 M, 70 °C	0.25 M, 90 °C
1	55.6	12.8	23.8	6.4
3	33.3	8.3	16.7	3.1
5	23.8	7.6	11.9	3.2
10	20.8	6.2	10.4	2.7

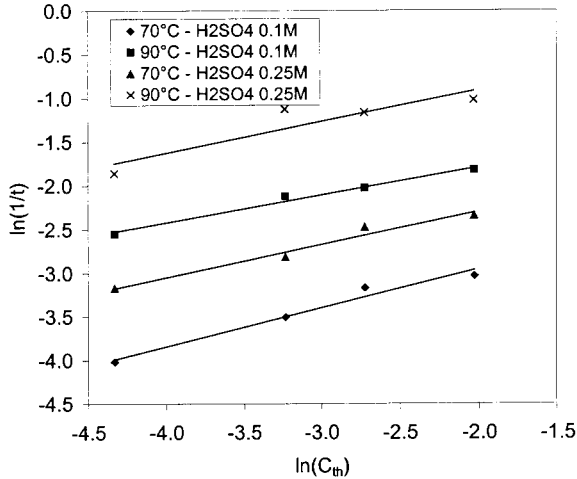


Figure 4: Estimation of thiourea reaction order in equation (2).

A further elaboration of the kinetic analysis was then carried out with all experimental data considering the equation (1), (2) and (3) evaluating the parameters of the following model:

$$X = 1 - \left(1 - \frac{t}{b} \cdot e^{\frac{E_a}{RT}} \cdot C_a^{n_1} \cdot C_t^{n_2}\right)^3 \quad (5)$$

The four parameters of model (5) were found minimising the sum of square of the difference of iron extraction yield experimental ( $X_{exp}$ ) minus that calculated ( $X_{calc}$ ) by equation (5). In other words the minimum of the following function was found by numerical methods:

$$\Phi = \sum (X_{exp} - X_{calc})^2 \quad (6)$$

The initial values of the research were found by the preliminary kinetic analysis above reported. The parameters found by the minimisation of function  $\Phi$  are:

$E_a = 73.8$  kJ/mol;  $b = 5.55 \cdot 10^{-10}$ ;  $n_1 = 0.865$ ;  $n_2 = 0.334$ .

Figures 1 and 2 show the quite good fitting of the experimental results. Regarding the activation energy, Zhu (1992) reports a value of 73 kJ/mole for the reduction of Fe (III) and that under low pH values, the reductive pathway reduction is favoured.

## Conclusions

The positive effect of temperature on the extraction process and the value of  $E_a$  ( $74 \pm 9$  kJ/mole) found in the fitting of the experimental data with the shrinking core model (with chemical reaction control) highlight that the phenomenon is controlled by the chemical reaction. The result obtained for  $E_a$  is in agreement with those reported in the literature (Zhu, 1992). As well as the modelling of the process with typical models of non-catalytic reactions, an empirical model data fitting was used in order to evaluate the optimal conditions of the process, considering the treatment time and the thiourea concentration as factors. The experimental results show the technical



feasibility of this process for the removal of iron from kaolin used in the experimental tests. We intend to continue our study by investigating both the effect of thiourea on other types of minerals and the environmental impact linked to the treatment of the waste products during the process.

#### **Acknowledgements**

The Authors are grateful to Mr. M. Centofanti and Dr. J. Di Pasquale for the leaching tests and chemical analysis. This research has been financially supported by MURST 60%.

#### **References**

- Abbruzzese, C., Bonney, C.F., Criscuoli P., Cucca, P., Dudeney, A.W.L., De Hoop, K., Kaloidas, V., Paspaliaris, I., Petrakakis, M., Ullu, F. and Vegliò, F., 1999. Removal of iron from quartz: development of a continuous organic acid leach/effluent treatment system "QUARTZTREAT", In: I. Paspaliaris, M. Taxiarchou, A. Adjemian, and G. Katalagarianakis (Editors), *Proceeding of the Second Annual Workshop (Eurothen '99)*, Cagliari, Italy.
- Cegarra, J., Gacèn, J., Caro, M. and Pepiò M., 1988. Wool bleaching with thiourea dioxide. *JSDC*, 104, July/August, 273-279.
- Chiarizia, R. and Hortwiz, E.P., 1991. New formulations for iron oxides dissolution. *Hydrometallurgy*, 27, 339-360.
- Danilova, D.A., Tkacheva, L.P., Lapin, V.V. and Ermolaeva, Z.I., 1982. Bleaching of kaolin. U.R.S.S. patent N°937410.
- Koltoff, I. M., 1974. *Analisi Chimica Quantitativa*. Piccin, Padova, Italy.
- Levenspiel, O., 1972. *Chemical Reaction Engineering*. J.Wiley & S., New York.
- Matiasand, P.P. and Caneva, C., 1979. Mineralogia del giacimento di caolino di Monte Sughereto, Santa Severa (Roma). *Rend. Soc. Ital. Mineral. Petrol.* 35 (2), 721-753.
- Montgomery, D.C., 1991. *Design and Analysis of Experiments*. J.Wiley & S., New York.
- Vegliò, F., Passariello, B., Toro, L. and Marabini, A.M., 1996. The development of a bleaching process for a kaolin of industrial interest by oxalic, ascorbic and sulphuric acid: a preliminary study using statistical methods of experimental design. *Industrial Engineering Chemistry and Research*, 35, 5, 1680-1687.
- Vegliò, F., Passariello, B., Barbaro, M., Plescia, P. and Marabini, A.M., 1998. Drum leaching tests in iron removal from quartz using oxalic and sulphuric acids. *International Journal of Mineral Processing*, 54, 183-200.
- Zhu, T., 1992. The redox reaction between thiourea and ferric iron catalysis of sulphide ores. *Hydrometallurgy*, 28, 381-397.

## APPLICATION OF THIOBACILLUS FERROOXIDANS BY BACTERIAL DESULFURIZATION OF COAL

P.Fečko\*, V.Sedláčková<sup>o</sup>

\*Department of Mineral Dressing, VŠB-Tech. University of Ostrava, Czech Republic  
<sup>o</sup>MUS, a.s., Most, Czech Republic

### Abstract

The aim of this paper was an evaluation of the suitability of bacterial leaching as applied to a coal sample from the Northern Bohemian brown coal basin of Merkur. The results of this work show that use of clean cultures of *Thiobacillus ferrooxidans* worked well in this case, if we evaluate desulfurization from the point of view of pyrite sulfur. After one month of leaching, the pyrite sulfur was almost gone from the sample, which contained a large quantity of organic sulfur produced and slightly degraded by the bacteria *Thiobacillus ferrooxidans*. Total desulfurization of coal was about 48%. Perfect adaptability of the *Thiobacillus ferrooxidans* bacteria on coal pyrite is proven by this work, and it is suggested as one of the possible uses of bacteria in mineral processing.

*Keywords: leaching, thiobacillus ferrooxidans, brown coal, desulfurization, mineral processing*

### Introduction

Desulfurization of fuel is the problem. Although considerable effort has been made, the world has not yet been able to keep SO<sub>2</sub> from leaking into the air. The high content of sulfur in coal has an unfavorable effect on its use and on the environment. In direct combustion of coal, a high content of sulfur in SO<sub>2</sub> escapes into the atmosphere, which pollutes the environment and causes acid rain.

#### *Distribution of sulfur in coal*

Sulfur is present in organic and inorganic forms in coal from the above mentioned locality. Free sulfur is present only sporadically. Pyrite and marcasite are present in large quantities, but their proportions vary. Sulfates, mainly gypsum, originate primarily during the carbonization process and secondarily during weathering of iron disulfides. Organic sulfur is mainly bound to the structures of dibenzenethiophene, benzenethiophene and thiols. Iron disulfides are present in epigenetic and syngenetic forms. Syngenetic pyrite was formed during the first phase of the coal-formation process, and that is why these are interspersed during this process. From this, it follows that they were interspersed within the coal substance. Epigenetic pyrite is geologically younger. Therefore, it acts as filling materials in the joints and fissures, it is less interwoven within the coal substance, forms large crystals and is easier to eliminate by suitable coal-processing methods. The integral group of chemical techniques used to separate pyrite from coal and also some microbiology techniques confirmed this. The chemical techniques of desulfurization can be realized for relatively non-specific consumption of chemicals. Microbiology methods have advantages for very specific reactions in a simple reactor at ambient temperature and normal pressure, but they need longer leaching time.

The aim of this work is to confirm the appropriate applications of bacterial leaching for samples of coal from the Merkur locality in the Czech Republic.

### **Methods of bacterial leaching**

For bacterial leaching, a 5 l airlift glass bioreactor, adjusted according to the research of the Deutsche Montan Technologie Company - Essen (Beyer, 1988), was used. After sterilization of the reactor, the prepared samples of coal were placed in it, together with the 9K medium without  $\text{FeSO}_4$ . After one hour of mixing and homogenizing of the suspension, the bacterial culture, *Thiobacillus ferrooxidans* was introduced into the reactor in the amount of 500 ml. For bacterial leaching, a clean bacterial culture of *Thiobacillus ferrooxidans* from the Czechoslovak Collection of Microorganism in Brno was used. The concentration of bacteria introduced in the process of bacterial leaching was  $10^9$  in 1 ml of bacterial solution. Bioreactors were connected to the water engines of aquariums, which supplied the reactor with air. The air was cleaned in washers of 1 M  $\text{H}_2\text{SO}_4$  to clean it from bacteria present in the air. Mixing of 5% suspension was done by air. The pH was measured by a "Radelkis" laboratory pH-meter, and the pH was kept at the optimal value  $1.5 \pm 2.0$  for the whole experiment (28 days) to prevent formation of unwanted jarosite. The temperature was also kept in the range of  $26 \pm 30$  °C for the full experiment. During the leaching, after 1, 2, 3 and 4 weeks, samples were taken from the bioreactor in amounts of approximately 50 ml for analyses. From this sample, part of a suspension for measuring the biomass growth by the MPN method was used, and the rest was filtered in a Buchner funnel. The filtrate and the filtrate cake were taken for other analyses. In the filtrate,  $\text{Fe}^{2+}$  was determined by titration, and the content of total sulfur and separate forms of sulfur were determined in the filtrate cake. The cake was washed in 100 ml of 1 N HCl and in 200 ml of distilled water before determination.

### **Petrographical analyses**

Petrographical analyses were done at the Institute of Geotechnics Czech Academy of Science in Praha. The samples were milled to grains smaller than 1 mm, and from such prepared coal, the grain's thin sections were prepared. The light reflection ( $R_o$ ) of jelled macerates of huminite and the macerated composition were measured on a UMSP 30 Petro fy Opton-Zeis Jena microscope. Monochromatic light with a  $\lambda = 546$  nm wavelength, and a 25× objective for magnification and immersion in oil with a reflection index of  $n = 1.518$  were used. The amount of liptinite was determined by fluorescent analysis on the same instrument and with the same enlargement. As the source of light, a mercury discharge lamp was used.

### **Determination of sulfur and its forms**

Sulfur was determined at the Research Coal Institute in Ostrava-Radvanice on a LECO SC 132 instrument directed by a microprocessor, with detection of  $\text{SO}_2$  using an infrared detector. Different forms of sulfur were determined by thermal phase analyses at temperatures of 420 °C (organic sulfur), 820 °C (pyrite sulfur) and 1370

°C (total sulfur), under constant program conditions. The sulfate sulfur was calculated.

### Result of petrographical analyses

The light reflection ( $R_o$ ) of coal from the Merkur mine was ( $R_o = 0.708\%$ ). Humodetrinite was prevalent over humotelinite. Humodetrinite resulted in the form of jelled denzinite, with gently scattered clay masses that generated a small lens (from over  $5\ \mu\text{m}$ , approximately). Denzinite fluently changed to carbargilite at higher concentrations of clay components. Humotelinite was represented by ulminite, namely as eulminite, and as textoulmenite, which occurred rarely. The wall of the ulminite cell was swollen and highly jelled. The corpuscle of corpohuminitite and rarely, of sclerotinitite, also occurred in denzinite and ulminite.

Sulfide Fe is very numerous and was ascertained in most coal grains. Framboids are an overweight type of sulfide Fe. Their size did not exceed  $10\ \mu\text{m}$ , but larger forms were also observed. Other models of sulfide were also represented in the sample, such as numerous euhedral sulfides and sporadic massive sulfides. Clusters of framboids with euhedrals were frequent (Figure 1). Clusters of sulfides were sporadic. In practice, secondary sulfides were not sighted in crack panes. It was possible to classify coal grains with over 5% sulfides as a carbopyrite (Figure 2). In cases when the content of sulphides was higher then 20%, this was due to minerite (Figure 2). In the sample, carbonate was found in slight amounts. The presence of ulminite and denzinite illustrates the role of the highly quadratic jelled coal masses in reducing the atmosphere in the low water sedimentary basin plane.

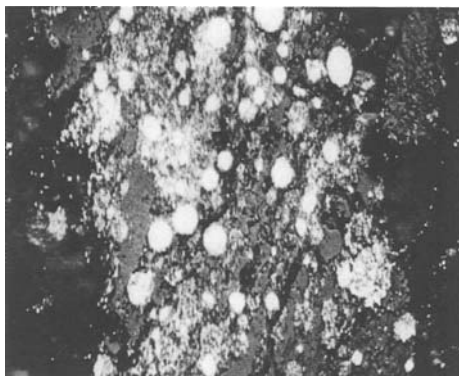


Figure 1: The clusters of framboidal and euhedral framboids in carbominerite.

### Result of bacterial leaching

The coal from the Merkur locality has a high content of sulfur. Sulfur, however, occurs mostly as organic and elementary sulfur, and of the total sulfur content of 9.55%, pyritic sulfur represents only 3.94%. Nevertheless, it was interesting to determine the rate by which the bacteria *Thiobacillus ferrooxidans* removes organic and elementary sulfur, because the references differ greatly. Some research shows that

these bacteria are incapable of removing organic sulfur, (Volšický et al., 1976; Fečko et al., 1991; Fečko, 1997a, 1997b and 1997c). The results of bacterial leaching by the bacteria *Thiobacillus ferrooxidans* are given in Table I.

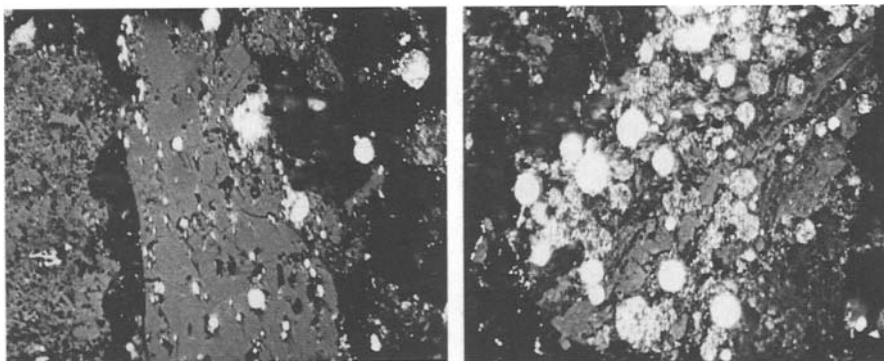


Figure 2: Carbopyrite (left). Clusters of framboidal and euhedral framboids in denzinite (right): the content of sulfide is higher than 20%, and it is minerite.

Table I: The results of bacterial leaching.

Duration after leaching start, days	Fe <sup>2+</sup> (mg/l)	S <sub>total</sub> (%)	Amount of bacteria (n°/ml)
	-	9.55	-
7	2211	-	90.10 <sup>8</sup>
14	125.63	-	160.10 <sup>8</sup>
21	50.25	-	25.10 <sup>9</sup>
28	8.38	4.96	60.10 <sup>9</sup>
Sulfur	Before leaching (%)	After leaching (%)	Rate of desulfurization (%)
S <sub>total</sub>	9.55	4.96	48.06
S <sub>pyritic</sub>	3.94	0.37	90.61
S <sub>organic</sub>	4.31	3.55	17.63
S <sub>sulfate</sub>	1.3	1.04	20
S <sub>sulfide</sub>	0	0	0

The sample of coal from the locality of Merkur contained 9.55% of the total sulfur on input, and after 1 month of leaching by the bacteria *Thiobacillus ferrooxidans*, the total content of sulphur fell by 4.96%, and the desulfurization rate reached 60.12%. Because bacteria mainly oxidizes pyrite, desulfurization of coal is interesting and represented 90.61% in this case. From these results, it follows that coal from the Merkur locality is preferable for bacterial leaching. After 1 month of the leaching method, the amount of bacteria measured by the MPN method in 1 ml of solution reached 60·10<sup>9</sup>.

#### *Character of coal after one week of leaching*

After 1 week of leaching, the sample contained numerous sulfides of Fe. The dominant type of sulfide was framboids, which often occurred in forms of clusters (Figure 3). The euhedral sulfide was sporadic and generally had a dispersive character. The clusters of euhedral sulfide were a unique sighting (Figure 3).

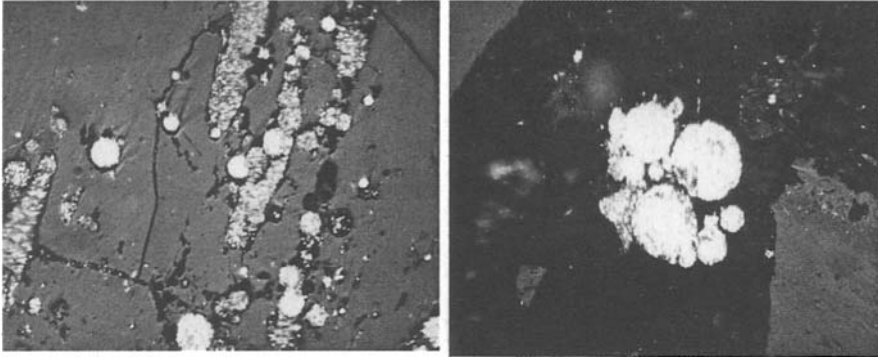


Figure 3: Euhedral and framboidal sulphide in the form of clusters (left).  
Clusters of framboidal sulfide (right).

#### *Character of coal after 2 weeks of leaching*

The content of sulfide Fe essentially decreased in comparison with the sample after 1 week of leaching, and sulfide wasn't found in most coal grains. In this type of sample, the framboidal sulfides dominates (separate frambooids and clusters of frambooids). The grains with a higher concentration of framboidal sulfide can be classified as carbopyrite (Figure 4). Euhedral sulfide is substituted in slight amounts. Dark gaps are evident in coal grains, and there is a larger surface after removed of sulfide.

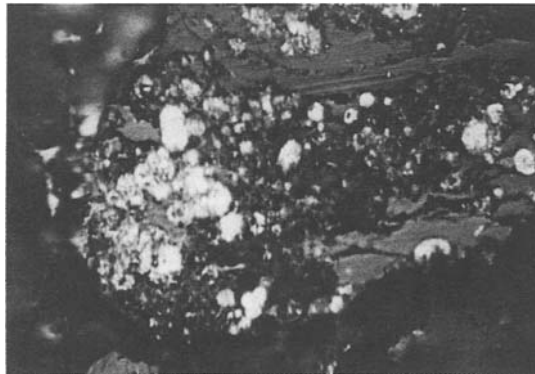


Figure 4 : The grain of carbargilite.

#### *Character of coal after 3 weeks of leaching*

The sample has a lower content of sulfide in comparison with the sample after 2 weeks of leaching. Most of the original sulfide was removed, only in some grains frambooids are evident at different rates of alteration. This lack of sulfide is documented (Figure 5). In the sample, numerous grains occurred with dark gaps and larger areas after sulfide was removed (Figure 5).

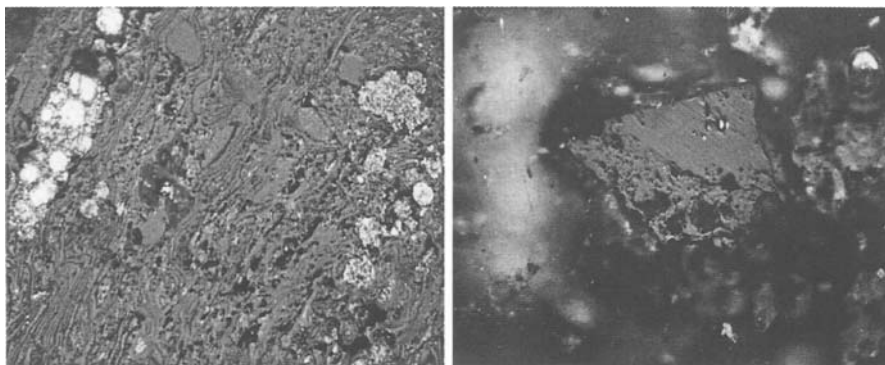


Figure 5: Humotelinite with framboidal and euhedral sulfide (left).  
Dark grain gaps from altered sulfide (right).

#### *Character of coal after 4 weeks of leaching*

After 4 weeks of leaching, complete degradation of sulfide occurs, except for a reserve. The grains with relicts of frambooids or grains with gently scattered euhedral sulfides are sporadically found. In the second case, this regards euhedral sulfide covered with hard vegetative gauze, which probably is more resistant against bacteria than framboidal sulfide. There are numerous grains with gaps and areas after sulfide removal (Figure 6).

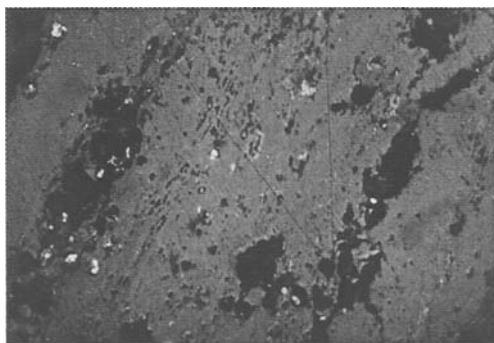


Figure 6: Denzinite: the dark gaps from clusters of frambooids.

#### **Conclusions**

From the results of the research, it follows that the application of a clean bacterial culture of *Thiobacillus ferrooxidans* to coal samples from Merkur in the Czech Republic is a successful method for their desulfurization.

After one month of treatment, 48.06% of sulfur was removed, whereas desulfurization of pyrite, sulfur reached 90.61%.

It is possible to improve results by means of extending leaching time for finer grained coal matter.

**References**

- Beyer, M., 1988. Mikrobielle kohleentschwefelung. Forschungsbericht, DMT Essen.
- Fečko, P., 1997a. Bacterial Desulphurization of coal from the Michal open pit mine. 5<sup>th</sup> Southern Hemisphere Meeting on Mineral Technology, Intemin, Buenos Aires, 249-252.
- Fečko, P., 1997b. Bacterial desulphurization of coal from the Nováky mine. 7<sup>th</sup> Balcan Conference on Mineral Processing, Vatra Domei, Romania, 1, 36-41.
- Fečko, P., 1997c. Bacterial desulphurization of coal from the Sokolov lignite basin. XX IMPC, Aachen, BRD, 4, 573-584.
- Fečko, P., Raclavská, H. and Malysiak, 1991. Desulphurization of coal from the Northern Bohemian brown coal basin by bacterial leaching. FUEL. 70, 1187-1191.
- Volšický, Z. et al., 1976. Bacterielles laugen feinverwachsenen schwefels in der kohle und seine besonderheiten. 7<sup>th</sup> International Coal Preparation Congress, Cracow.



## THE ADSORPTION OF PRECIOUS AND BASE METALS ON XAD7 ION EXCHANGE RESIN

E.R. Els, L. Lorenzen, C. Aldrich

Institute of Mineral Processing and Intelligent Process Systems, Department of Chemical Engineering, University of Stellenbosch, e-mail: rels@ing.sun.ac.za  
Private Bag X1, Matieland, 7602, South Africa

### Abstract

The adsorption characteristics of XAD7 ion exchange resin have been established for precious metals and base metals. Synthetic single precious metal solutions as well as mixed solutions containing base metals were tested for adsorption. The effect of chloride strength on equilibrium adsorption was determined for 10.8%, 14% and 17.2% free HCl in the solution.

*Keywords: adsorption, resin, precious metals, base metals*

### Introduction

Selective recovery of precious group metals (PGM's) from chloride solutions has long been a major challenge to chemists trying to selectively isolate single metal compounds of high purity. Recently the focus has moved towards ion exchange technology and the use of active groups on a resin, which can selectively extract specific species from a solution.

Due to the tendency of PGM ions to form anionic complexes, the focus for PGM recovery with ion exchange is more directed towards anion exchange resins. The PGM industry is refining the chloride complexes of the precious metals as these are the solution products resulting from aqua regia leaching, used for dissolution of the metal sulphides in the ore. The dissolved PGM's form anionic complexes with the general formula  $[MCl_x]^{n-}$ . The base metals tend to dissolve as cations in these solutions. The thermodynamics and kinetics of aqueous solutions containing PGM's and base metals are not always well understood and therefore, remained tenaciously elusive (Dhara and Sudhir, 1993).

To study the adsorption of PGM ions in an industrial solution containing a variety of PGM and base metal ions will therefore be difficult as there are too many species interacting in the solution.

For this reason single component solutions of the precious metals were prepared by using pure metal, and in some cases pure metal salts. These solutions served as mother solution from which further dilution to test concentrations were done. A base metal solution, including the PGM's, was prepared by adding all the individual components to match an industry base metal solution composition.

The adsorption characteristics of a single metal were established and thereafter adsorption from a solution was studied to determine the effect of other ions competing for the adsorption sites on the resin. The effect of chloride strength on equilibrium adsorption was determined.

### XAD7 resin

The resin used was Amberlite XAD7. The resin is a polymeric adsorbent. It is a non-ionic aliphatic acrylic polymer, which derives its adsorptive properties from its patented macroreticular structure (containing both a continuous polymer phase and a continuous pore phase). The adsorption is therefore not ion exchange as such. The macroreticular structure of the resin gives it excellent physical and thermal stability. Due to its aliphatic nature the resin can adsorb non polar compounds from aqueous systems, and can also adsorb polar compounds from non-polar solvents. It has been reported that the resin is ion specific towards gold (Fritz and Miller, 1973).

The resin was supplied wetted with NaCl and Na<sub>2</sub>CO<sub>3</sub> salts to prevent bacterial growth. The resin was prepared in glass columns with upward flow of solution. The solution was pumped with a variable speed peristaltic pump. The upward flow of solution has to be very slow to allow displacement of the air from the resin bed and the connecting tubes as air pockets tend to lift the resin upwards and out of the column. The resin was firstly washed with distilled water to remove all foreign ions entrapped from the factory floor. The resin was then washed with 14% HCl to prepare the resin for adsorption. The resin was then taken out of the column and put in a 5 litre plastic drum from where small amounts were taken for adsorption tests.

### Solution preparation

Platinum, palladium and gold solutions were prepared by dissolution of the pure metals in aqua regia. Ruthenium, iridium, and rhodium were dissolved from pure salts. The salts were used in instances where the dissolution of the metals are very difficult. Ruthenium was dissolved from the (NH<sub>4</sub>)<sub>2</sub>(RuNOCl<sub>5</sub>) salt, iridium from (NH<sub>4</sub>)<sub>2</sub>(IrCl<sub>6</sub>) salt, and rhodium from the DETA salt (DETAH<sub>3</sub>)(RhCl<sub>6</sub>). DETA being the C<sub>4</sub>N<sub>3</sub>H<sub>10</sub> chain. The mass required for a 2,000 ppm stock solution was weighed off and boiled in aqua regia until dissolved. More HCl was added, and the solution was boiled further to drive off all the nitric acid as NO<sub>x</sub> fumes. The resulting free HCl in the solution was determined by titration. The solution was then diluted with the correct amounts of water and acid to achieve the desired final free acid and metal concentration. From this 2,000 ppm stock solutions further dilution to the actual test concentrations, ranging from 25 ppm to 300 and 10.8% to 17.2% HCl, were done.

### Base metal solution

The composition of an industrial base metal solution was matched by adding all the required components in the correct quantities. Ruthenium, rhodium and iridium were added from the already prepared pure stock solutions. The composition of the base metal solution can be seen in Table I. The concentration is reported as ppm metal. Aqua regia was added to dissolve all the solid components. All nitric was boiled off from the solution. The solution was then diluted to the required acid concentration and 2,000 ppm PGM plus base metal concentration.

Table I: Base-metal solution composition.

Comp.	Pt	Pd	Au	Rh	Ru	Ir	Ag	Ni	Cu	Fe	Pb	As	Se	Te	Total	Base metals
ppm	845	423	28	99	127	42	70	28	56	56	85	14	42	85	2,000	437

## **Experimental**

To determine equilibrium points at a specific PGM concentration, the adsorption from the solution was established by varying the amount of resin added to the same solution concentration. The volume of solution used for each test was either 500 or 1,000 ml. Seven different quantities of resin were added to a specific solution concentration ranging between 0.5 ml to 100 ml resin. The amount of resin added to the solution was varied to achieve a low as well as a high total loading on the resin. In batch experimentation the final solution concentration is unknown and it is therefore difficult to predict the eventual equilibrium concentration beforehand.

The resin was measured out in a small plastic measuring cylinder, which was tapped against the bench for settlement of the resin beads. The test solution was prepared by dilution from the 2,000 ppm stock solution to the required metal and free acid concentrations. A sample of the test solution was taken as reference before addition of the resin beads. All analyses were done by inductively coupled plasma (ICP). The reference sample was titrated to check that the targeted free HCl concentration was correct. The resin was added to the solution and rolled in bottles for 24 hours to ensure equilibrium was attained. The bottles were rolled on a roller bench, which facilitate multiple simultaneous tests. After exposure a sample of the solution was taken and analysed by ICP. The adsorption was calculated by difference to the reference sample concentration. IUPAC Recommendations on ion exchange nomenclature define "theoretical specific capacity" as the milliequivalents of ionogenic group per gram of dry ion exchanger (Lehto and Harjula, 1995). The ionogenic group holds the ions capable of exchanging for other ions in the external solution. The IUPAC recommendations also include the "practical specific capacity" of an ion exchanger. This is the total amount of ions expressed in milliequivalents taken up per gram of ion exchanger under specific conditions, which should always be given. The actual uptake will not reach the theoretical stated capacity, for example, when there are exchange sites to which various ions have different accessibility. Some sites may be entirely inaccessible to larger ions. The usual way to present adsorption isotherms is to plot on the Y axis the amount of say  $x$  adsorbed / capacity of the resin for  $x$  against the concentration of  $x$  in the solution / total concentration of  $x$ . In this case  $x$  will be one of the PGM's or base metals. For this graph the maximum capacity must be known. From the above definition it is evident that the practical capacity depends on the experimental conditions. All the experimental work done was done by batch experimentation. To determine the maximum resin uptake of an specific ion, the practical capacity, the counter ion which is displaced from the resin must be continuously removed, such as in a column. The batch equivalent should be a large number of successive batch equilibrations in series.

## **Results**

From the experimental data analysis it became evident that, instead of the usual representation, effective visualisation of the quantitative adsorption data can be obtained by combining the variable parameters like solution concentration and quantity of resin used into a single ratio and to plot this ratio against the gram adsorbed per litre of resin. It is also evident that for each solution concentration the

adsorption, expressed as gram/litre resin, increase as the amount of resin used decrease. This is due to the ratio of exchangeable ions in solution divided by the number of potential adsorption sites on the resin. Therefore the ratio used for the graphs is the initial concentration of precious metal in solution (which determines the potential quantity of ions to be adsorbed onto the resin) divided by the amount of resin used (which determines the total amount of adsorption sites available for adsorption). The graphs presented are therefore presented as such. It is evident that where the resin has a high preference for the ion to be exchanged the initial slope of the graph that is for small ppm/ml resin will be high. This indicates that the resin has a high affinity for the ion to be exchanged and that high loading will be attained in dilute solutions.

#### *Single component PGM adsorption*

Adsorption data points were determined for each test solution concentration used to establish the adsorption characteristics. It should be noted that inaccuracies occur for the very small resin volumes that are where the ratio *start ppm / ml resin* is large. Solution potential was measured with a platinum redox electrode with reference to Ag/AgCl. All single component graphs were determined at 14% free HCl concentration. It is important to note that although the adsorption graphs, presented in Figure 1, are all presented in a single figure they were determined individually from single precious metal solutions. The start PGM concentrations used for the adsorption tests ranged between 50 ppm to 100 ppm as metal. Gold is in solution as the  $\text{AuCl}_4^-$  ion: the solution potential was 670 mV. The iridium ion is present as  $\text{IrCl}_6^{3-}$  at 890 mV. Palladium is in solution as the  $\text{PdCl}_4^{2-}$  ion at 930 mV. Platinum is solution as the  $\text{PtCl}_4^{2-}$  ion at 900 mV. Rhodium is in solution as one of the following chlorocomplexes (Dhara and Sudhir, 1993),  $\text{RhCl}_4(\text{H}_2\text{O})^-$ ,  $\text{RhCl}_5(\text{H}_2\text{O})^{2-}$ , or the  $\text{RhCl}_6^{3-}$  ion, depending on the equilibrium between these species, the solution potential was 910 mV. Ruthenium is solution as one of the following chlorocomplexes (Dhara and Sudhir, 1993),  $\text{RuCl}_5(\text{H}_2\text{O})^{2-}$ , or the  $\text{RuCl}_6^{3-}$  ion, depending on the equilibrium between these species at 929 mV. Many data points were determined for gold at various solution strengths, as it is known that the resin is selective towards gold. The PGM's not seen in the graph is due to negligible adsorption. It is evident that some sorption of ruthenium and iridium does occur. These ions can penetrate the resin, but are not necessary adsorbed by the resin. It is noted that the adsorption quantities for PGM's other than gold are very low.

#### *Effect of additional PGM's in the solution*

A mixed solution containing all the PGM's, excluding gold, was tested for adsorption.

The mixed solution also included the base metals solution. The base metals are added together and treated as a total base metals content. The purpose of this test was to determine the next strongest bonder to gold. From Figure 2 it is evident that very little adsorption of any of the other ions in solution occur.

Ruthenium was selected as the next strongest bonder to gold. A mixed solution containing gold and ruthenium was tested to establish the selectivity of the resin for gold, see Figure 3. It is evident that hardly any adsorption of ruthenium is noticeable. The resin is very specific for gold.

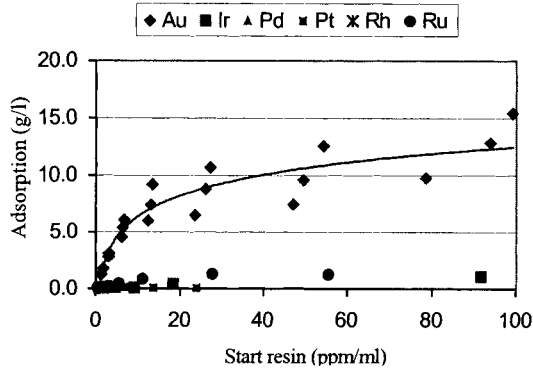


Figure 1: Individual PGM adsorption.

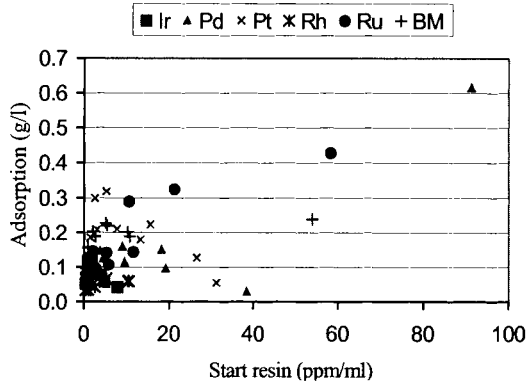


Figure 2: Adsorption from mixed solution excluding gold.

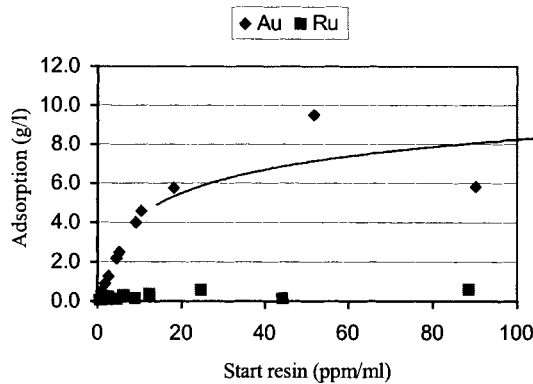


Figure 3: Adsorption from a gold plus ruthenium solution.

*Effect of different Cl<sup>-</sup> concentration (pH) on adsorption*

The effect of HCl concentration on the adsorption was determined for 10.8%, 14%, and 17.2% free HCl in the solution. For each of the three chloride strengths test

solutions were prepared with gold concentrations in the range of 50 ppm to 100 ppm. The solution potential ranged from 630 mV to 680 mV. The adsorption characteristic can be seen in Figure 4.

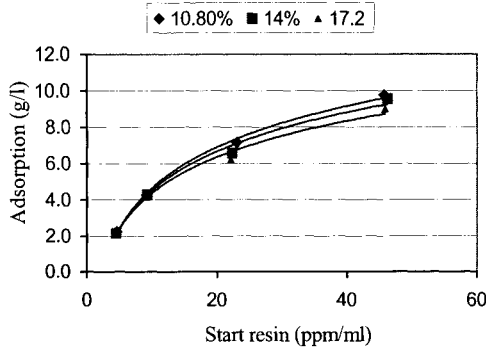


Figure 4: Gold adsorption with different acidity.

The free HCl concentration has very little effect on the adsorption of gold. Lower acid concentrations tend to improve the adsorption quantity. To investigate the effect of different free chloride concentrations on the adsorption of other ions from a mixed solution the adsorption was tested for mixed solutions at 10.8% as well as for 17.2% free HCl, see Figures 5 and 6.

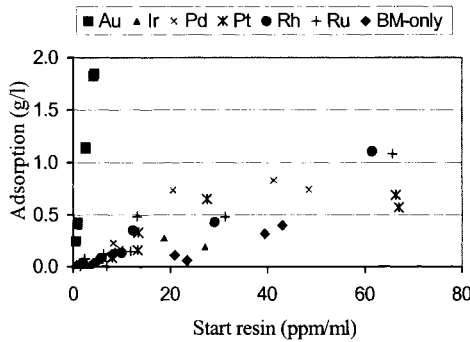


Figure 5: Adsorption from a mixed solution at 10.8% HCl.

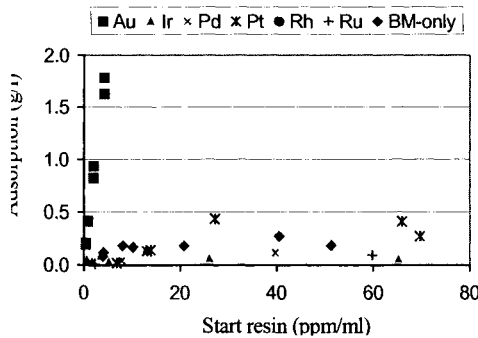


Figure 6: Adsorption from a mixed solution at 17.2% HCl.

It is evident from Figures 5 and 6 that sorption of ions other than gold is very little. The sorption of other ions decrease with increased free chloride concentration.

### **Conclusions**

From the above it is evident that very little sorption of base metals and precious metals other than gold occur. The resin is very specific for gold even from mixed solutions. The concentration of free chloride in the solution does not effect the adsorption much.

### **Acknowledgements**

The authors wish to express their sincere thanks to Mrs H Tan for her help with the experimental work. The contribution from Impala Platinum Refineries is also highly appreciated.

### **References**

- Dhara, C. and Sudhir, D., 1993. The application of ion exchangers in the precious metals technology. *Precious Metals*, vol.17, 375-410.
- Fritz, J.J. and Miller, W.G., 1973. Gold recovery from aqueous solutions. US Pat. 3,736,126.
- Lehto, J. and Harjula, R., 1995. Experimentation in ion exchange studies – the problem of getting reliable and comparable results. *Reactive & Functional Polymers*, 27, 121-146.

## THE INFLUENCE OF PRECIPITATION VARIABLES ON THE AGGREGATION AND CRYSTALLINE STRUCTURE OF STABILIZED ZIRCONIA POWDERS

A.P.A. Oliveira\*, M.L. Torem<sup>o</sup>

\*Department of Metallurgical and Materials Engineering, COPPE/UFRJ, Rio de Janeiro, Brazil

<sup>o</sup>Department of Materials Science and Metallurgical Engineering, Catholic University of Rio de Janeiro, Rio de Janeiro, Brazil

### Abstract

The scope of this work consisted of producing stabilized yttrium-zirconium oxide powders from zirconium oxychloride and yttrium chloride using urea as a precipitating agent and polyacrylic acid as dispersing agent.

A factorial analysis was designed to study the effect of some precipitation variables (temperature, precipitation time, urea concentration, yttrium chloride concentration and polyacrylic acid concentration) on some characteristics of the aggregates (size and electrophoretic mobility) and of the zirconium oxide powders (crystalline structure).

It is suggested that the structure of the dispersion species strongly influenced the crystalline structure of calcined zirconium oxide powders. These species are zirconium polymers that can assume a tridimensional structure similar to fluorite favoring the retention of high temperature polymorphic phases. The decomposition of urea supplied the solution with OH<sup>-</sup> ions at a slow rate enabling the formation of the tridimensional structured zirconium polymers. On the other hand, polyacrylic acid prevented the formation of these tridimensional structures possibly because polyacrylate ions remain in the sites of the zirconium polymeric structure previously available for polymerization reactions. For higher concentrations of urea and polyacrylic acid, an increase in precipitation time implied the predominance of the mechanism ruled by urea over that related to polyacrylic acid.

The role of polyacrylic acid as dispersing agent was evaluated regarding DLVO and extended DLVO theory. In a zirconium-yttrium system, electrosteric repulsion mechanisms would be responsible for a better dispersion.

*Keywords: zirconium oxide powders, precipitation variables, precipitation mechanisms, aggregation, crystalline structure*

### Introduction

Pure zirconium oxide may occur in three crystallographic structures: monoclinic (until 1,170 °C), tetragonal (between 1,170 °C and 2,370 °C) and cubic (above 2,370 °C). The transformation of zirconium from tetragonal to monoclinic structure must be avoided because it can lead to external tensions that may cause material fracture (Heathcote, 1993; Birkby & Hodgson, 1991). The controlled addition of stabilizing oxides, such as yttrium, cerium, magnesium, calcium and rare earth oxides, may retain high temperature polymorphic phases at room temperature. The presence of tetragonal phase is an essential condition for zirconium toughening besides hindering or interrupting crack propagation. The literature reviewed did not present any investigations concerning the utilization of urea as precipitating agent for



zirconium oxide powders and the addition of a dispersing agent during the precipitation process.

In this context, pure zirconium, stabilized yttrium-zirconium and stabilized cerium-zirconium oxides were produced by homogeneous precipitation using urea as precipitating agent and polyacrylic acid as dispersing agent. The aim of this paper is to study the influence of some precipitation variables (temperature, time, urea concentration, stabilizing oxide concentration and polyacrylic acid concentration) on the size of the aggregates and their electrophoretic mobilities in dispersion and on the crystalline structure of zirconium oxide powders.

### Literature review

Considering the structure of precipitated zirconium oxide species, Mamott et al., (1991) reported that a very stable zirconium tetramer occurred at solid octa-hydrated zirconium oxychloride ( $ZrOCl_2 \cdot 8H_2O$ ), maintaining its structure unchanged as a complex ion in solution during hydrolysis. As a result of hydrolysis, the polymerization of these tetramers occurs by the formation of hydroxyl bridges. Along slow polymerization, the tetramers combine to each other to form initially a bidimensional structure. The formation of new hydroxyl bridges between these planes eliminates half of oxygen atoms from hydroxyl groups producing a tridimensional structure similar to fluorite structure. On the other hand, during rapid polymerization, a random structure is formed.

It is well known that urea can be used as precipitating agent to promote a uniform variation of pH that favors a slow polymerization, besides avoiding typical problems of localized precipitation such as wide particle size distribution. Matijevic (1994) produced several monodispersed colloids from single component systems using urea. It can be remarked that yttrium carbonate with a particle size of 300 nm was obtained by heating a solution of yttrium nitrate and urea at 85 °C for 25 min.

Investigations (Balmori et al., 1994; Il'icheva et al., 1996) on the utilization of polymers as dispersing agent for ceramic powder production were done by mixing the powder previously precipitated in a solution of the dispersing agent. Polyacrylic acid is one of the most employed dispersing agents. In aqueous solutions, the dissociation reaction of polyacrylic acid starts at pH >3,5 and ends at pH >8,5 (Balmori et al., 1994). Some studies correlated electrophoretic mobilities and aggregate size in order to evaluate the mechanisms associated to dispersion stability. A correspondence between minimum aggregate size and maximum electrophoretic mobility, in modulus, characterized an electrostatic repulsion mechanism. Otherwise, a steric repulsion mechanism may be acting on the system favoring dispersion stability. When both repulsive forces are acting on the system, an electrosteric repulsion mechanism is responsible for the improvement of colloid stability.

### Experimental procedure

#### *Precipitation experiments and material characterization*

Pure zirconium oxide, stabilized yttrium-zirconium oxide (6% mol  $Y_2O_3 \cdot ZrO_2$ ) and stabilized cerium-zirconium oxide (22% mol  $CeO_2 \cdot ZrO_2$ ) were obtained by precipitating/coprecipitating the hydroxides from a vigorously stirred aqueous

solution of zirconium oxychloride ( $5 \cdot 10^{-2} \text{ mol} \cdot \text{dm}^{-3}$ ), urea, yttrium ( $6 \cdot 10^{-3} \text{ mol} \cdot \text{dm}^{-3}$ ) and cerium ( $1.1 \cdot 10^{-2} \text{ mol} \cdot \text{dm}^{-3}$ ) chlorides. Some experiments used polyacrylic acid (MW = 750,000, concentration =  $6.25 \cdot 10^{-2} \text{ g} \cdot \text{dm}^{-3}$ ) as dispersing agent.

Precipitation temperatures employed were 85 °C and 95 °C with an accuracy of  $\pm 1$  °C. Precipitation times established were 30 min and 120 min. The pH value of all experiments were maintained between 7.5 and 8.0. A detailed explanation of precipitation experiments is accessible elsewhere (Oliveira, 1997). After precipitation, a small aliquot of the dispersion was taken for electrophoretic mobility measurements. The remaining precipitated material was filtrated and the liquor was analyzed by atomic emission spectroscopy using inductively coupled plasma. This procedure aimed to evaluate the zirconium, yttrium and cerium ions concentration. Then, the material was exhaustively washed with distilled and deionized water followed by one stage of ethanol washing and filtration.

Aggregate size analysis was carried out at Mastersizer Microplus (Malvern Instrument Ltd.). An amount of zirconium oxide powder is dispersed in deionized and distilled water and submitted to aggregate size evaluation.

A Rank Brothers Mark II apparatus using two palladium electrodes and a flat quartz cell was used to measure electrophoretic mobility of particles in dispersion.

Investigations on crystalline structure of zirconium oxide powders calcined at 650 °C for 2 h were conducted using CuK $\alpha$  by X-ray diffraction (Siemens, model D5000).

#### *Statistical design of precipitation experiments*

Considering the diversity of precipitation variables to be investigated, a statistical design of precipitation experiments was chosen. Basically, the precipitation experiments were separated in two systems, ZrO<sub>2</sub>·Y<sub>2</sub>O<sub>3</sub> and ZrO<sub>2</sub>·CeO<sub>2</sub>, where each variable (precipitation temperature =  $t$ , precipitation time =  $h$ , urea concentration =  $u$ , yttrium oxide concentration =  $y$ , cerium oxide concentration =  $c$ , polyacrylic acid concentration =  $p$ ) assumed a minimum and a maximum value. This procedure aimed to evaluate the variables that particularly affected some characteristics of precipitated zirconium oxide particles, such as aggregate size and electrophoretic mobility, and the volumetric fraction of monoclinic phase of calcined zirconium oxide powders. These effects, interactions and average were calculated using Yate's algorithm, extensively adopted at factorial analysis of experiments (Box et al., 1978).

Table I: Experimental conditions at minimum (-) and maximum (+) levels for zirconium-yttrium oxide system.

Level	Temperature (°C)	Time (min)	Urea concentration (mol·dm <sup>-3</sup> )	Yttrium chloride concentration (mol·dm <sup>-3</sup> )	Polyacrylic acid concentration (g·dm <sup>-3</sup> )
-	85	30	2	0	0
+	95	120	6	$6.0 \cdot 10^{-3}$	$6.25 \cdot 10^{-2}$

At this study, the confidence level was 95% and the degree of freedom was 31, resulting in a critical value of  $t$ -Student distribution ( $t_{crit}$ ) of 1.696. Comparing  $t_{crit}$  with  $t$ -Student values obtained for each effect and interaction investigated, their significance was evaluated. The notation used for the effects is discussed elsewhere (Box et al., 1978) and it represented that the indicated variables were employed at

their maximum levels and the others were adopted at their minimum levels. Table I indicates experimental conditions for both levels for zirconium-yttrium oxide.

## Results and discussion

### *Zirconium-yttrium oxide system*

Results obtained from characterization experiments for  $ZrO_2 \cdot Y_2O_3$  system are summarized at Table II. All analysis performed at inductively coupled plasma for this system confirmed that the synthesized powder was 6% mol  $Y_2O_3 \cdot ZrO_2$  for all experiments.

Table II: Summary of the results obtained from statistical design for  $ZrO_2 \cdot Y_2O_3$  system.

Test	Identification of the effects	Volumetric fraction of monoclinic phase (%)	Mean volume diameter of aggregate ( $\mu\text{m}$ )	Electrophoretic mobility ( $\mu\text{m}\cdot\text{s}^{-1}\cdot\text{V}^{-1}\cdot\text{cm}$ )
1	average	31.31	57.14	1.47
2	t	29.47	37.24	1.42
3	h	33.51	49.11	1.20
4	th	25.81	30.26	1.33
5	u	38.84	45.57	1.18
6	tu	36.74	58.06	1.08
7	hu	44.53	33.30	0.91
8	thu	41.07	49.24	-1.44
9	y	38.29	71.69	1.18
10	ty	44.49	33.70	1.43
11	hy	28.22	68.87	1.29
12	thy	27.95	35.28	1.21
13	uy	39.29	47.27	1.23
14	tuy	46.69	49.32	1.15
15	huy	41.77	43.01	1.09
16	thuy	28.04	40.33	-2.76
17	p	73.88	42.19	-4.37
18	tp	49.08	34.83	-2.85
19	hp	40.00	27.73	-4.85
20	thp	48.59	27.38	-3.55
21	up	58.77	16.12	-3.88
22	tup	49.61	23.42	-1.72
23	hup	43.51	39.61	-3.08
24	thup	39.44	27.39	-2.64
25	yp	35.94	50.84	-2.97
26	typ	32.34	46.41	-1.66
27	hyp	27.37	47.57	-2.82
28	thyp	26.43	49.24	-4.59
29	uyp	37.45	39.26	-1.90
30	tuy	40.17	42.35	-2.56
31	huyp	38.43	34.80	-4.21
32	thuy	23.96	43.00	-3.61

X-ray diffratograms of zirconium oxide powders are very difficult to examine, since most of cubic and tetragonal peaks are coincident. Srinivasan et al., (1991) noted that, for  $2\theta$  range containing planes (004) and (400), that is 71 °C to 76 °C, tetragonal peaks related to (004) and (400) planes could be clearly observed and cubic peak

related to (400) plane was remarkably sharp. Using this procedure, it was observed that, for all samples investigated in this work, only monoclinic and tetragonal phases were stable.

Table III presents the significant effects calculated from significance test of *t*-Student for volumetric fraction of monoclinic phase of stabilized yttrium-zirconium powders. The statistical analysis for  $ZrO_2 \cdot Y_2O_3$  system shown at Table III indicated that an increase in yttrium chloride concentration (*y* factor) caused the reduction in volumetric fraction of monoclinic phase. The effect of yttrium oxide as stabilizing agent of tetragonal phase at room temperature has been remarked by several works (Srinivasan, 1993; Belous, 1997).

Due to the significance of precipitation time-urea concentration-polyacrylic acid concentration interaction (*hup* factor), these variables were analyzed together, in spite of the relevance of precipitation time (*h* factor) and polyacrylic acid concentration (*p* factor). The *hup* factor showed that the combined effect of these variables resulted in a reduction in volumetric fraction of monoclinic phase.

Table III: Significant effects calculated from significance test of *t*-Student for volumetric fraction of monoclinic phase for  $ZrO_2 \cdot Y_2O_3$  system (confidence level = 95%).

	Volumetric fraction of monoclinic phase effects (%)	<i>t</i> -Student value	Significance of the effects (confidence level = 95%)
Average	38.78		$t_{crit} = 1.696$
Main effects			
h	-7.73	-2.42	significant
y	-7.96	-2.50	significant
p	5.56	1.74	significant
Three-variable interactions			
hup	-9.64	-3.02	significant

The slow polymerization due to the presence of urea improved the stabilization of tetragonal phase at room temperature. On the other hand, polyacrylate ions ( $RCOO^-$ ), formed by polyacrylic acid dissociation, might react with surface sites previously available for polymerization reactions.

Consequently, a random structure should be formed, making the stabilization of tetragonal phase more difficult. Combining these mechanisms, it can be suggested that *hup* factor reflected the predominance of urea action over polyacrylic acid effect. Furthermore, increasing time would make urea action more effective, considering that more  $OH^-$  ions would be provided to the system. This behavior was reflected on the reduction of volumetric fraction of monoclinic phase associated to *hup* factor.

Table IV presents the significant effects calculated from significance test of *t*-Student for aggregate size of stabilized yttrium-zirconium oxide powders.

The unique relevant factor for aggregate size was polyacrylic acid concentration (*p* factor). This result reinforces the dispersing character of polyacrylic acid in this system, according to previously observed by Balmori et al. (1994), for  $ZrO_2 \cdot Y_2O_3$  system, and by Rogan et al. (1994), for calcite. Mechanisms related to dispersing action of polyacrylic acid maybe associated to electrostatic forces, steric forces or to a combination of both resulting in electrosteric forces.

Table IV: Significant effects calculated from significance test of *t*-Student for aggregate size for ZrO<sub>2</sub>-Y<sub>2</sub>O<sub>3</sub> system (confidence level = 95%).

	Aggregate size effects (μm)	<i>t</i> -Student value	Significance of the effects (confidence level = 95%)
Average	41.92		$t_{crit} = 1.696$
Main effects			
<i>p</i>	- 9.83	- 1.70	significant

Electrophoretic mobility measurements were necessary to a more consistent evaluation of the repulsive forces that were acting on the system. It allows to make an estimation of agglomeration degree, since it furnishes data about electrostatic forces present at the system. The significant effects on the electrophoretic mobility, as it is shown in Table V.

Table V: Significant effects calculated from significance test of *t*-Student for electrophoretic mobility for ZrO<sub>2</sub>-Y<sub>2</sub>O<sub>3</sub> system (confidence level = 95%).

	Electrophoretic mobility (μm·s <sup>-1</sup> ·V <sup>-1</sup> ·cm)	<i>t</i> -Student value	Significance of the effects (confidence level = 95%)
Average			$t_{crit} = 1.696$
Main effects			
<i>h</i>	- 0.92	- 1.91	significant
<i>p</i>	- 4.01	- 8.31	significant

The main effects related to precipitation time (*h* factor) and to polyacrylic acid concentration (*p* factor) were significant to the electrophoretic mobility of dispersed particles. An increase on precipitation time resulted in more negative electrophoretic mobility values, indicating higher electrostatic repulsive forces. It was suggested that the aging of the dispersed particles in the solution possibly modified surface characteristics of the precipitates, reducing their electrophoretic mobility. It must be pointed out that this reduction was not sufficient to promote a decrease on aggregate size, as observed on Table IV.

On the other hand, the addition of polyacrylic acid resulted in a decrease in aggregate size and electrophoretic mobility, indicating that electrosteric repulsive forces could be acting on zirconium-yttrium oxide system.

## Conclusions

Experimental results indicated that the decrease in volumetric fraction of monoclinic phase was probably associated to the formation of an ordered tridimensional polymeric structure of zirconium in dispersion. It was suggested that urea supplied solution with OH<sup>-</sup> ions at a slow rate which favored the ordering of those structures. On the other hand, polyacrylate ions, resulted from polyacrylic acid dissociation, might react on surface sites of zirconium polymers available for tetramers hydrolysis (polymerization reaction), randomizing polymer structure.

For zirconium-yttrium oxide system, the reduction in volumetric fraction of monoclinic phase might be related to the predominance of the mechanism associated to urea over that described for polyacrylic acid. This effect was emphasized by a

simultaneous increase in precipitation time, urea concentration and polyacrylic acid concentration. Addition of yttrium chloride was also important for tetragonal phase stabilization.

The addition of polyacrylic acid resulted in a decrease in aggregate size and electrophoretic mobility, indicating that electrosteric repulsive forces could be acting on zirconium-yttrium oxide system. Best results (volumetric fraction of monoclinic phase = 23.17% and mean volume diameter of aggregates = 21.87  $\mu\text{m}$ ) were obtained for temperature = 95  $^{\circ}\text{C}$ , precipitation time = 120 min, urea concentration = 1  $\text{mol}\cdot\text{dm}^{-3}$ , yttrium chloride concentration =  $3\cdot 10^{-3}$   $\text{mol}\cdot\text{dm}^{-3}$  and polyacrylic acid concentration =  $6.25\cdot 10^{-3}$   $\text{g}\cdot\text{dm}^{-3}$ .

#### Acknowledgements

The authors gratefully acknowledge Prof. José Carlos D'Abreu, Prof. Olavo Barbosa Filho and Prof. Roberto Avillez, who are responsible for some equipments employed in this research, Eng. Sandra Decourt de Barros for her collaboration and CAPES for financial support.

#### References

- Balmori, H., Hernández, F., Jamarillo, D., 1994. Electrokinetic Behavior of Aqueous  $\text{ZrO}_2(\text{Y}_2\text{O}_3)$  Suspensions with Ammonium Polyacrylate. *Ceramic Processing Science and Technology*, 55, 367-371.
- Belous, A.G., Pashkova, E.V., Makarenko, A.N., Khomenko, B.S., 1997. Polymorphic Transformations in Heat-Treated Precipitates of Zirconium and Yttrium Hydroxides. *Inorganic Materials*, 33 (1), 44-47.
- Birkby, T., Hodgson, H., 1991. Progress with Zirconia Ceramics. *Eur. Symp. Ceram. (Proc.)*, 167-198.
- Box, G.E.P., Hunter, W.G., Hunter, J.S., 1978. *Statistics for Experimenters: An Introduction to Design, Data Analysis and Model Building*. John Wiley & Sons, New York, 653.
- Heathcote, R., 1993. Zirconia. *Am. Ceram. Soc. Bulletin*, 72 (6), 123-124.
- Il'icheva, A.A., Olenin, A.Yu., Podzorova, L.I., Shevchenko, V.Ya., Lazarev, V.B., Izotov, A.D., 1996. Surfactant Effects on the Aggregation and Structure of Stabilized Zirconia Prepared by Sol-Gel Processing. *Inorganic Materials*, 32 (7), 736-740.
- Mamott, G.T., Barnes, P., Tarling, S.E., Jones, S.L., Norman, C.J., 1991. Dynamic Studies of Zirconia Crystallization. 26, 4054-4061.
- Matijevic, E. Formation of Monodisperse Inorganic Particulates. In: Wedlock, D.J., 1994. *Controlled Particle, Droplet and Bubble Formation*, Butterworth Heinemann, Oxford.
- Oliveira, A.P. Influence of Physico-Chemical Factors on the Precipitation of Zirconia Powders (in Portuguese), 1997. D.Sc. Thesis, Catholic University of Rio de Janeiro, 143.
- Rogan, K.R., Bethan, A.C., Skuse, D.R., 1994. Colloidal Stability of Calcite Dispersion Treated with Sodium Polyacrylate. *Colloid Polym. Science*, 272, 1175-1189.
- Srinivasan, R., De Angelis, R.J., Ice, G., Davis, B.H., 1991. Identification of Tetragonal and Cubic Structures of Zirconia Using Synchrotron X-Radiation Source. *J. of Materials Research*, 6 (6), 1287-1292.
- Srinivasan, R., Hubbard, C.R., Cavin, O.B., Davis, B.H., 1993. Factors Determining the Crystal Phases of Zirconia Powders: A New Outlook. *Chemical Materials*, 5 (1), 27-31.

## SOLVENT EXTRACTION OF $\text{Cu}^{\text{II}}$ AND $\text{Fe}^{\text{III}}$ USING LIX 1104SM

P. Navarro\*, J. Simpson\*, F.J. Alguacil<sup>o</sup>

\*Departamento de Ingenieria Metalúrgica, Facultad de Ingenieria, Universidad de Santiago de Chile, Avda. L.B.O'Higgins 3363, casilla 10233, Santiago, Chile  
<sup>o</sup>Centro Nacional de Investigaciones Metalúrgicas (CSIC), Av. Gregorio del Amo, 8, Ciudad Universitaria, 28040 Madrid, Spain

### Abstract

The extraction of  $\text{Cu}^{\text{II}}$  and  $\text{Fe}^{\text{III}}$  from sulfate media by LIX 1104SM (a modified hydroxamic acid) has been investigated at various experimental conditions: temperature, aqueous pH value, metal concentration, etc.; the extraction order is  $\text{Fe}^{\text{III}} > \text{Cu}^{\text{II}}$ .

Slope analysis of experimental data showed that LIX 1104SM formed species of the nature  $\text{MeL}_2(\text{HL})$  with copper. The stripping of copper is accomplished using sulfuric acid solutions, whereas  $\text{Fe}^{\text{III}}$  is not stripped in these conditions but using hydrochloric acid solutions.

Since LIX 1104SM extracts these two elements from acidic solutions, it seems useful for the removal of  $\text{Fe}^{\text{III}}$  and/or  $\text{Cu}^{\text{II}}$  from other base metals. Iron and copper can be separated by co-extraction and selective stripping.

*Keywords: solvent extraction, LIX 1104SM, iron, copper*

### Introduction

Hydrometallurgy deals with the processing of different metal-containing materials in wet processes associated with the dissolution of some components.

Dissolved metals can be separated and purified using various procedures, e.g. cementation, precipitation, ion exchange, solvent extraction, etc.

In the case of solvent extraction, some landmarks in the application of the procedure for metal treatment are:

- extraction of uranium and plutonium (1940);
- extraction of zirconium, hafnium, rare earths and vanadium (1959);
- extraction of cobalt and nickel (1965);
- extraction of copper (1975).

It is recognized that the application of solvent extraction and processing of waste oxide ores supplies the most economical copper in the world (Szymanowski, 1993). On the other hand, it is known that hydroxamic acid extractants form stable chelates with a number of metal ions; however, aliphatic hydroxamic acids tend to be water-soluble.

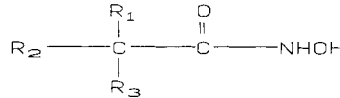
One of these acids, LIX 1104SM, had been developed to obtain high solubility in organic phases and adequate chemical stability in strong sulfuric acid medium, thus allowing its uses to control metal impurity levels in copper tank house electrolytes.

The present work investigates the behavior of LIX 1104SM in the extraction-stripping of  $\text{Cu}^{\text{II}}$  and  $\text{Fe}^{\text{III}}$  from acidic sulfate solutions.

## Experimental

LIX 1104SM extractant was kindly supplied by Henkel Corp., and was used without further purification.

The active substance of the reagent has the following:



where  $R_1$ ,  $R_2$  and  $R_3$  are mixtures of  $C_{10}$ - $C_{19}$  branched chains. Organic diluents Escaid 103 (10% aromatics) and Orform SX12 (> 95% aromatics) were used to dissolve the extractant.

All other chemicals were of AR grade. Extraction and stripping experiments were carried out by the following procedure: equal volumes of organic and aqueous phases were placed in separatory funnels, heated to a thermostatically controlled temperature and mechanically shaken (700 rpm) at the temperature for the time required. Copper and iron were analyzed by AAS.

## Results and discussion

### Copper extraction

In the present work, the use of two types of diluents (mainly aliphatic or aromatic), for the LIX 1104SM-copper extraction system, was investigated to study both kinetics and the effect of temperature for copper extraction carried out with solutions of 2.0 g/l Cu (pH = 2) and 10% v/v LIX 1104SM in Orform SX12 or 1.0 g/l Cu (pH = 2), and organic solutions of 10% v/v LIX 1104SM in Escaid 103.

The results obtained are shown in Figure 1, in which the percent of copper extraction is plotted against the equilibration time. The results show that the change of the diluent influenced the percentage of copper extraction by LIX 1104SM in the order aromatic > aliphatic, but had no influence on copper extraction kinetics. In both cases copper equilibrium was reached within 3-5 min and no further improvement was found at longer contact times.

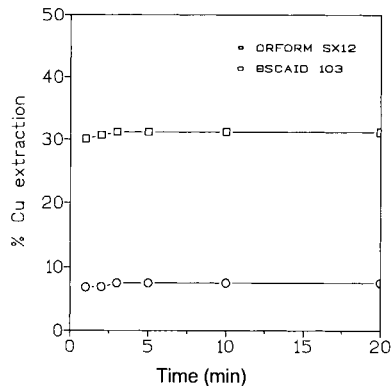


Figure 1: Kinetics of copper extraction using LIX 1104SM; temperature = 25 °C.



Figure 2 shows Arrhenius plot for copper extraction. In both cases, copper extraction increased with increasing temperature, from the experimental data the values of  $\Delta H^\circ$  obtained were of 3.9 kJ/mol (Orform SX12) and 1.3 kJ/mol (Escaid 103).

In Figure 3 the variation in the percentage of copper extracted against pH at various extractant concentrations is shown. Experiments were carried out with aqueous solutions of 1.0 g/l Cu and organic phases of LIX 1104SM 10%, 20%, 25% and 30% v/v in Escaid 103.

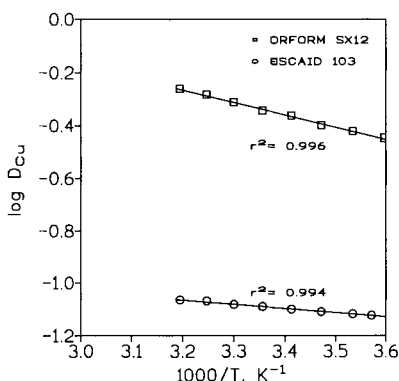


Figure 2: Arrhenius plot for copper extraction by LIX 1104 SM; equilibration time = 15 min.

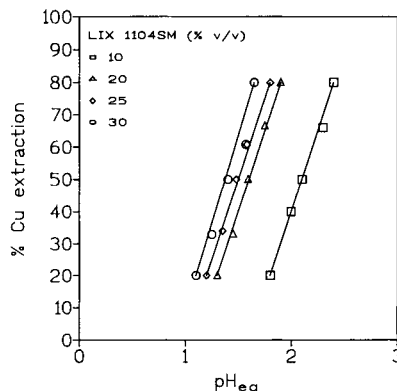
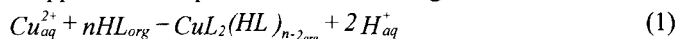


Figure 3: Copper extraction by various LIX 1104SM concentrations in Escaid 103; equilibration time = 15 min; temperature = 25°C.

The figure demonstrates that copper extraction is pH dependent and thus the extraction reaction can be related to a cation exchange reaction: the extraction of the metal releases hydrogen ions from the organic extractant to the aqueous solution. Results also show that the variation in the initial extractant concentration has a significant influence on copper extraction, shifting the extraction curves to the left, that is, to a more acidic pH value, as the extractant concentration increases.

The influence of the initial copper concentration in the extraction of this metal by LIX 1104SM in Escaid 103 was also investigated using various initial copper concentrations (0.01÷1.0 g/l) and extractant (10÷30% v/v) concentrations. Results obtained showed that in the concentration range studied, there was no influence on copper extraction when the copper concentration in the feed solution is varied. Thus should also be considered evidence about the non-formation of copper polynuclear species in the organic solution.

Hydroxamic acid is considered to be a monomer (Ceccione, 1987), thus the cation exchange reaction for copper can be expressed as the following:



$$K_{ext} = \frac{[\text{CuL}_2(\text{HL})_{n-2}]_{org} [\text{H}^+]_{aq}^2}{[\text{Cu}^{2+}]_{aq} [\text{HL}]_{org}^n} \quad (2)$$

where *HL* represents the active substance of LIX 1104SM and *aq* and *org* to the aqueous and organic phases, respectively.

If the definition of the copper distribution coefficient is considered as:

$$D_{Cu} = \frac{[Cu^{II}]_{org}}{[Cu^{II}]_{aq}} \quad (3)$$

by substitution of equation (3) in equation (2), taking log and rearranging, the next expression is obtained:

$$\log D_{Cu} = \log K_{ext} + n \log [HL]_{org} + 2 pH \quad (4)$$

At pH<sub>50</sub> (50% of copper extraction), D<sub>Cu</sub> = 1 and:

$$pH_{50} = -\frac{1}{2} \log K_{ext} - \frac{n}{2} \log [HL]_{org} \quad (5)$$

Thus, a plot of pH<sub>50</sub> values versus log [HL] should yield a straight line with a slope of  $-n/2$ . Figure 4 represents the results obtained from the present investigation (organic phase: various LIX 1104SM concentrations in Escaid 103, aqueous phase: 0.01 g/l Cu), accordingly a stoichiometric factor (n) of 3 was obtained.

#### Iron Extraction

Previous tests have shown that Fe<sup>III</sup> extraction equilibrium was also accomplished within 5 min of contact.

The influence of the initial extractant concentration on Fe<sup>III</sup> extraction was studied using organic phases of 5%, 15% and 30% v/v LIX 1104SM in Escaid 103 and aqueous solutions of 1.0 g/l Fe (III).

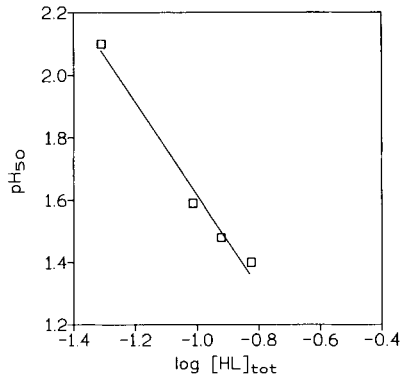


Figure 4: Variation of pH<sub>50</sub> versus log [HL] for copper extraction; equilibration time: 15 min; temperature = 25°C.

Results obtained are shown in Figure 5. As expected, the increase in the extractant concentration allowed to the extraction of iron at more acidic pH values.

The effect of the influence of different initial iron concentrations on the extraction of this element by LIX 1104SM was examined with organic phases of 15% v/v LIX 1104SM in Escaid 103 and aqueous solutions of 0.3 g/l, 1.0 g/l and 2.0 g/l iron.

Results are represented in Figure 6, which demonstrate that the effect of the variation of initial iron concentration is to shift the corresponding extraction to more acidic pH values as the initial metal concentration decreases.

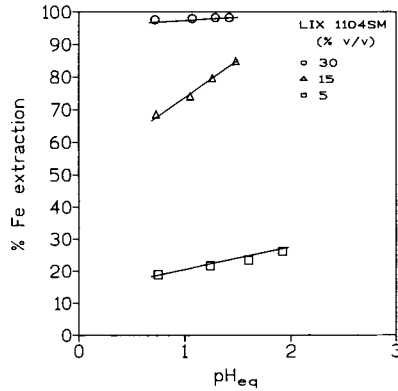


Figure 5: Iron extraction at various LIX 1104SM concentrations; equilibration time = 15 min; temperature = 25°C.

### Stripping

According to equation (1), copper stripping can be accomplished by shifting the equilibrium using acidic solutions, thus the effect of sulfuric acid concentration on copper stripping was studied, and results obtained are shown in Table I.

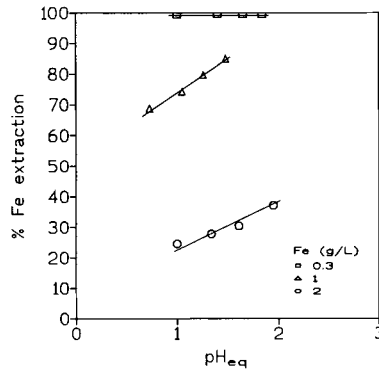


Figure 6: Influence of initial iron concentration on the metal extraction by LIX 1104SM; equilibration time = 15 min; temperature = 25°C.

Copper can be more easily stripped from loaded organic solutions when the organic diluent is mainly aliphatic (e.g. Escaid 103).

However, in both cases, the percentage of copper stripped tends to increase with the increase of sulfuric acid concentration.

It also should be noted that copper stripping is always reached within 5 min. of contact between the phases. Fe<sup>III</sup> is not easily stripped using sulfuric acid solutions, but by using HCl solutions, increasing the percentage of iron stripping by increasing the concentration of the acid. Thus, copper and iron can be separated by selective stripping as indicated in the results shown in table II.

Table I: Copper stripping using sulfuric acid solutions; equilibration time = 10 min; temperature = 25°C; a: organic phase = 10% v/v LIX 1104SM in Escaid 103 loaded with 0.7 g/l Cu; b: organic phase = 10% v/v LIX 1104SM in Orform SX12 loaded with 0.6 g/l Cu.

H <sub>2</sub> SO <sub>4</sub> (g/l)	Test conditions: a	Test conditions: b
	Cu stripped <sup>a</sup> (%)	Cu stripped <sup>b</sup> (%)
100	89.2	66.4
150	93.9	72.4
180	94.9	75.0
200	95.0	80.0
220	95.4	80.5
250	97.0	81.3

Table II: Cu<sup>II</sup>-Fe<sup>III</sup> separation by acidic selective stripping; equilibration time= 10 min; temperature = 25°C; organic phase = 30% v/v LIX 1104SM in Escaid 103, loaded with 0.6 g/l Cu and 0.2 g/l Fe.

Stripping step	H <sub>2</sub> SO <sub>4</sub> (g/l)	HCl (mol/l)	Cu stripped (%)	Fe stripped (%)
1	220	-	98.3	-
2	220	-	quant.	9.0
3	-	7	-	89.5

The greatest potential of LIX 1104SM in respect to base metal extraction lies in the co-extraction of Fe<sup>III</sup> and Cu<sup>II</sup> from relatively high acidic media and in the separation of both elements by selective stripping.

#### References

- Ceccione, T., Hojjatie, M. and Freiser, H., 1987. *Anal. Chim. Acta*, 193, 247-254.  
 Szymanowski, J., 1993. *Hydroxoximes and Copper Hydrometallurgy*. CRC Press, Boca Raton.

## A COMPARISON OF LIX984<sup>®</sup> AND NON-CONVENTIONAL REAGENTS AS COPPER EXTRACTANTS

J.B.A. Paulo\*, J.Y.P. Leite<sup>°</sup>

\*Graduate Program of Chemical Eng., Federal University of R.G. Norte, Natal, Brazil

<sup>°</sup>Technological Formation Centre of R.G. Norte, Natal, Brazil

### Abstract

Various types of vegetable oils found in the Northeast of Brazil have not been properly studied as metal extractants. These oils normally show little solubility in water, besides being biodegradable, which is an important characteristic regarding the environment. In this work, coconut, castor and palm oils are being studied as alternative reagents, like LIX-984<sup>®</sup>, for copper extraction. Results indicate that vegetable oils can be an alternative to conventional reagents, mainly for applications where no selectivity for heavy metals is imposed, for example, in the treatment of industrial-waste water.

*Keywords: extractive metallurgy, hydrometallurgy, solvent extraction, non-conventional extractants*

### Introduction

The fatty acids from natural oils are formed from a long chain of hydrocarbons which are non-polar, with a terminal polar carboxylic group. The fatty acids differ from one another by their chain lengths, as well as by the position of the double bonds in the chain. Fatty acids possessing at least two hydrogen atoms connected to the carbon atom in the chain are classified as *saturated*. When one or more double bonds are present in the main chain, generating carbons associated with only one hydrogen atom, we have an *unsaturated fat*.

A fatty acid is represented by the formula: R-COOH, where R stands for the hydrocarbon chain. Individually, the acids could be described as numerical symbols, for example: lauric acid C12:0; oleic acid C18:1. In this representation, the number after C indicates the number of carbon atoms and the second number is the number of double bonds. The positions of the double bonds are indicated by the numbers between brackets, which in turn identify the carbon involved in the saturation closest to the carboxyl group. In general, the fatty acids of natural occurrence contain a certain number of carbon atoms in pairs and show a hydrocarbon chain without any lateral chains (Moretto and Fett, 1989).

Gindin et al. (1962), Kopatch and Shantulya (1978), Angelova et al. (1981) and Kyuchoukov and Hadjiev (1982) have studied the use of mixtures of fatty acids for the extraction of metallic cations from aqueous solutions. These researchers emphasize that the fatty acids show appropriate physical properties as extracting agents, mainly regarding environmental aspects. These acids are usually described as non-toxic, biodegradable and easily regenerated.

The use of fatty acids as extractants in the recovery of heavy metals contained in industrial effluents has been reported by authors such as Kyuchoukov and Hadjiev (1982), Rice (1978) and others. In this type of application, the extractant charge is

considered as prior to the extractant selectivity. The Northern States of Brazil have a great diversity of vegetable oils. In this work, the extraction of copper by conventional extractants is compared with extraction where non-conventional reagents obtained from coconut, castor and palm oils are used. The preliminary results obtained are encouraging.

### Literature survey

The technique of solvent extraction requires a more intimate contact between the aqueous solution containing the metal to be extracted and the solvent containing the extractant. In practice, this contact is obtained by dispersing one of the liquid phases into the other. On an industrial scale, dispersion is carried out in mixer-settlers, extracting columns fitted with devices such as perforated plates, discs, crowns, etc. On a batch level, dispersion is carried out manually in separation funnels. The contact between the pregnant solution and the solvent allows the desired species to be distributed into two phases. The nature of this distribution could be chemical or physical, according to the system used. In most cases, the process of metal extraction involves chemical interactions between the metallic species and the extractant (Asbrook, 1979).

The extractants normally used in hydrometallurgy are classified according to the way they transform the metallic ion into a solution. There are three main groups of extractants: the acidic extractants and the complex agents, which act upon the metallic ion, thus forming a compound; the amines, which cause the formation of a pair of ions; the neutral extractants which promote dissolving of the metallic cation. The acidic extractants are the carboxylic acids, sulfonic acids and phosphoric acids. The complex agents are compounds essentially containing the hydroxyl functional groups (-OH) and oxyme (=N-OH). These agents form complex ions, or chelates, with the metal to be extracted.

In the present work, the process of extraction of copper using a complex agent usually utilized in the hydrometallurgical industry (LIX984) is compared with the extraction of this metal by fatty acids found in coconut, castor and palm oils. Extraction of a metallic ion in a solution, carried out by an acid extractant or by a complex agent, can be represented by the following equation:



where the species with the bar are present in the organic phase, and the species without the bar are found in the aqueous phase. In equation (1),  $M^{n+}$  represents the metallic cation with valences of "n" and R, the hydrocarbon chain capable of offering the *donating* part of the coordinated link in the organo-metallic complex extracted from the organic phase (Lorrain, 1993). The reversible reaction, represented by equation (1) shows the influence of pH on the aqueous equilibrium phase of the metal extraction. In fact, if the  $H^+$  ion concentration increases, which corresponds to a lowering of the pH, the equilibrium is favored to the left, resulting in a low extraction. On the contrary, if the  $H^+$  ion concentration diminishes, which corresponds to an increase in the pH, the equilibrium will be pushed to the right, favoring the extraction. The limits that are being imposed on this tendency are related to the metal hydrolysis

from a certain pH. When greater quantities of metal are being extracted, the extraction process will also produce  $H^+$  ions in bigger quantities.

The extraction depends also on the stability of the species at equilibrium. If the metal in aqueous phase forms a more stable compound than the organo-metallic complex, it will not be possible to extract it.

In hydro-metallic systems, we normally have a low solubility of the extractor in the aqueous phase, very low solubility of the aqueous phase ions in the organic phase and a greater solubility of the organo-metallic complex in the organic phase. Thus, the extraction mechanism of the metallic ion can reasonably be described by the chemical model presented in equation (1). It is important to remember that in this type of model, correlating phenomena that are very common are not expected, such as:

- metal complexing by other anionic compounds normally present in the aqueous phase, or, in other words, the metal is considered as being totally dissociated;
- parallel hydrolysis reactions;
- formation of intermediate metal complexes;
- association of the organo-metallic complex with a non-dissociated extractant or diluter;
- polymerisation of the constituents in the organic phase.

It can be concluded that the proposed chemical model for the chemical reactions in reaction (1) is only valid under the same conditions. A study of the chemical equilibrium at the bench stage is highly recommended, before passing to pilots or to industrial plants (Lorrain, 1993). By definition, the distribution coefficient,  $D$ , is given by the relation between the concentration of the metal in the organic phase and its concentration in the aqueous phase:

$$D = \frac{[M^{n+}]_{org}}{[M^{n+}]_{aq}} \quad (2)$$

The concentrations of the metal are determined by chemical analysis. In equation (2), the total concentration of the metal in each phase is taken into consideration, as well as all the forms of the metal for these phases. In practice, metal is mainly analyzed during aqueous phases, as well as during feeding or in the refined solution. The metal concentration of the extract is obtained by the mass balance.

For the system described in equation (2), the equilibrium constant,  $K_E$ , is given by:

$$K_E = \frac{[MR_n][H^+]^n}{[M^{n+}][HR]^n} \quad (3)$$

By combining equation (3) with equation (2), we have,

$$K_E = D \left[ \frac{H^+}{HR} \right]^n \quad \text{or} \quad D = K_E \left[ \frac{HR}{H^+} \right]^n \quad (4)$$

It can be observed that  $D$ , which could be determined experimentally, is directly proportional to the equilibrium constant and the  $n^{\text{th}}$  power of the concentration of the extractant, and inversely proportional to the  $n^{\text{th}}$  power of hydrogen ion concentration

in the aqueous phase. Still, it is possible to obtain  $K_E$  from the experimental results. Using the decimal log of (4) and the definition of  $\text{pH} = -\log[\text{H}^+]$  we obtain:

$$\log D = \log K_E + n(\log[\text{HR}] + \text{pH}) \quad (5)$$

According to equation (5), the distribution coefficient of the metal is a linear function of pH and the concentration of the extractant. Thus, a graphical representation of  $\log D$  against  $(\log[\text{HR}] + \text{pH})$  is a straight line with an inclination  $n$  and is ordered at the origin equivalent to  $\log K_E$ .

### Experimental

The extractants used in this work are LIX984<sup>®</sup>, coconut, castor and palm oils. The LIX984<sup>®</sup> is an equivolometric mixture of ketoxime and aldoxime produced by Henkel Corp. (1991). These hydroxyoximes are extensively used in analytical chemistry for the precipitation of metals in the aqueous phase. In the hydrometallurgical industry, these reagents have been used commercially in the extraction of copper from diluted solutions. According to the manufacturer, the new family of LIX reagents bears the excellent extraction properties and the quick kinetics of aldoximes, besides showing the good physical performance and greater chemical stability of the ketoximes.

The vegetable oils were obtained by acidification of their respective soaps with analar concentrated sulfuric acid. In the case of coconut oil, for every 100 g of the commercial soap, 12.5 ml of oil was obtained, after successive washings with distilled water. Table I presents the average chemical composition of the vegetable oils studied:

Table I: Average composition of the vegetable oils studied.

Oil	Fatty acid	Number of C atoms	Composition (%)
Coconut oil	Lauric	C12:0	18.0
	Myristic	C14:0	11.0
	Palmitic	C16:0	6.0
	Capric	C10:0	44.0
	Caproic	C6:0	6.0
	Caprylic	C8:0	6.0
	Erucic	C22:1(13)	2.0
	Palmitoleic	C16:1(9)	7.0
Castor oil	Ricinoleic	C18:1(7)	86.0
	Oleic	C18:1(9)	8.0
	Linoleic	C18:2(9),(12)	3.0
	Stearic	C18:0	3.0
Palm oil	not yet determined	-	-

The organic solutions of LIX984<sup>®</sup>, coconut and palm oils were prepared with kerosene, and the castor oil was prepared with cyclehexane, as the castor oil was insoluble in kerosene. The pregnant copper solution was prepared from analar copper sulphate pentahydrate. Extraction tests were carried out by simple contact between the aqueous and organic solutions in a separation funnel.

The solutions were agitated for a period sufficient enough to attain equilibrium and were kept for 24 h for complete separation of the phases. The efficiency of the extraction was determined through mass balance by dosing with copper in the initial



and final aqueous solutions. Chemical analysis of copper in these phases was done by titration with EDTA and by atomic absorption.

## Results and discussion

Figure 1 shows copper extraction as function of pH for the following systems: LIX-984<sup>®</sup>, coconut and palm oils in kerosene, castor oil in cyclehexane. The concentrations on a volume basis of extractants in the diluents were as follows: LIX984<sup>®</sup> (5.2%), coconut oil (10%), palm and castor oil (20%). The concentration of copper in the pregnant solutions was 3.5 g/l for the LIX-Cu and vegetable oil-Cu systems. It can be seen from Figure 1 that some non-conventional extractants could extract copper. Among these vegetable oils, castor oil extracts copper practically at the same level as LIX984<sup>®</sup> (see also Figure 2). Coconut oil comes into second place, also showing good extraction. Lastly, palm oil does not present significant extraction. This is remarkable, as non-conventional reagents extract copper at a pH level that is less acidic than the conventional one. Using castor oil, for example, good extraction is obtained at pH equal to 4.8. For the same extraction using LIX984<sup>®</sup>, we must use pH equal to 2.3. This offers an advantage over using vegetable oils, due to the reduction of equipment corrosion, as well as to the lower cost of the process.

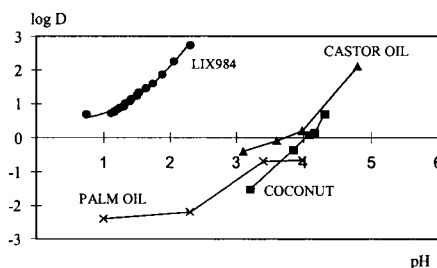


Figure 1: Extraction of copper from aqueous sulfate solution (LIX-984, coconut and palm oil in kerosene, castor oil in cyclehexane ), as a function of pH.

Figure 2 shows the efficiency of extraction as a function of pH under the same conditions carried out in Figure 1. Results show that LIX984<sup>®</sup> is less sensitive to pH variation than the non-conventional reagents studied. From pH = 1.0, the extractions are above 80%, reaching 100% at pH = 2.3. With regard to the vegetable oils, it can be seen by the greater inclination of the extraction curve that coconut oil is more sensitive to pH variation.

It is important to observe that castor oil extracted 100% of the copper at pH = 4.8. It is worth mentioning that until now, coconut oil was tested at concentrations of 10% v/v, while castor and palm oils were tested at 20% v/v.

By comparing the performance of coconut and castor oil, it could be confirmed that the capacity of the charge in coconut oil is highly superior to that of castor oil, which justifies further research on this oil. Extraction of isotherms for LIX984<sup>®</sup> and castor oil shows that the vegetable oil extracts 100% of the copper from aqueous solutions containing 1.5 g/l of the metal.

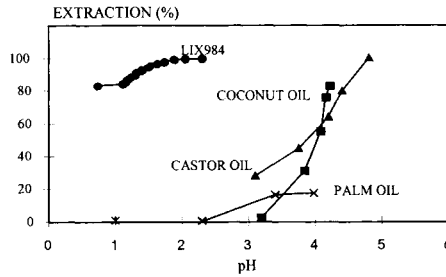
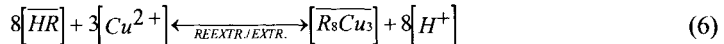


Figure 2: Efficiency of the extraction of copper as a function of pH.

Considering that we used almost four times more castor oil than LIX, it could be concluded that the power of the charge of LIX984<sup>®</sup> is much higher than that of castor oil. Nevertheless, vegetable oil is cheaper than the conventional extractant.

Plotting isotherms of the LIX-Cu system on a volume basis of 2.6%, 4.0% and 5.2%, and taking in account our experimental data of pH and D, we can plot Figure 3, which represents a graphic method for determining  $K_E = 10^{+4}$  and a stoichiometric coefficient for [HR] of 2.68.

Thus, we can propose the following mechanism (Paulo, 1996):



The mechanisms involving vegetable oils were not yet established. We need to carry out a complete characterization of these oils, in order to determine their mechanisms of extraction.

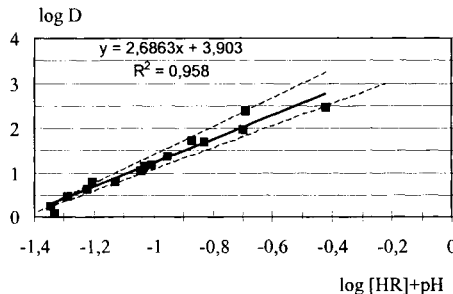


Figure 3: Graphic method for determination of the mechanism of equation (5).

### Conclusions

The results obtained indicate that vegetable oil, especially coconut oil, can be used as an alternative to conventional reagents in applications where the selectivity of the heavy metals is not so important, as, for example, in the treatment of industrial waste. In the Northeast of Brazil, great attention is being directed to the leather and textile industries. It is known that waste-water produced by these industries contains metals such as chrome, cadmium, zinc, etc., often at concentrations detrimental to the environment. This study represents a potential application for vegetable oils as extractants of heavy metals, since selectivity is unimportant. With regard to copper

extraction, the results obtained for coconut oil at 10% v/v in kerosene made it possible to extract up to 80% copper from aqueous solutions containing the metal up to 2.5 g/l. Another advantage of the vegetable oils is their low cost and their availability in greater quantity in the North Eastern States of Brazil.

#### **References**

- Angelova, V., Ilcheva, L. and Mareva, ST., 1981. Extraction of metals with fatty acids (translated title). *Khimia i industrija*, Vol. 154.
- Asbrook, A.W., 1979. Extraction: theory and practice. In: Edit for the University of Utah, Dept. of Met. Eng., Salt Lake City, 210.
- Gindin, L.M., Bobikov, P.L., Patjukov, G.M., Rosen, A.M., Kouba, E.F. and Bugaeva, A.V., 1962. Separation of metals using exchange extraction with carboxylic acids (translated title). *Estrakziavip.2. Gosatomizdat*, Vol. 87.
- Henkel Corp., 1991. The chemistry of metals recovery using LIX reagents. In: Contributions of the Min. Ind. Div.
- Kopach, S., Shantulya, Y., 1978. Extraction of Co(II) with a mixture of fatty acids. *Zh. Neorg. Khim.*, 23, 468.
- Kyuchoukov, G., Hadjiev, D., 1982. On the extraction of metals with carboxylic acids. *Bulg. Acad. of Sci. Commun. of the Dept. of Chem.*, 13, 192. (in Bulgarian)
- Lorrain, C., 1993. Opérations chimiques unitaires: extraction liquide-liquide. In: J. Tome (Editor), *Techniques de l'Ingénieur*, Fasc. 2755, 1-13.
- Moretto, E., Fett, R., 1989. Oils and Vegetable fats - Processing and Analyses (translated title). 2<sup>a</sup> Ed. UFSC Editions, Florianópolis, Brazil.
- Paulo, J.B.A., 1996. Mise au point d'un nouveau mélangeur-décanteur à inversion de phase. Application à l'extraction du cuivre. INPT-Toulouse-France, Thèse de Doct.
- Rice, N.M., 1978. Recent Developments and Potential Uses for Carboxylic Acid Extractants - a Review. *Hydrometallurgy, Elsevier Sc. Publ. Comp.*, 3, 111-133.

## DEVELOPMENT AND APPLICATION OF FILBLAST MASS TRANSFER TECHNOLOGY IN HYDROMETALLURGICAL PROCESSING

B.J. Sceresini, G. Nguyen

Atomaer Pty Ltd, 14 Bell Street, Canning Vale, 6155 W.A., Australia

### Abstract

Development and application of Filblast mass transfer technology for the reaction of gases with liquids and slurries resulted from research into the dispersion of gases in liquid and slurry phases for the purpose of generating controlled bubble size for application in pneumatic froth flotation. The principle was demonstrated in bench scale and pilot scale machines.

Experience gained in the development of the low-pressure flotation machine aerator led to the realisation that the principle of the invention could be applied over a wider pressure range for the enhancement of chemical processing reactions involving mass transfer reactions.

Bench scale tests of a single stage Filblast for aeration of water, using both air and gaseous oxygen, yielded excellent results with faster oxygen up-take rate, higher final DO concentration and increased oxygen utilisation than other devices. Similar enhancements noted when oxygenating a variety of gold ore slurries, led to the development of multi-staged high pressure reactors capable of operating at elevated temperature and in aggressive chemical environments.

Over 100 Filblast devices have been built and deployed in fourteen countries. They range in size from 60 l/min laboratory units to 125 l/s industrial units.

While the major application of the Filblast has been in the cyanidation process, significant progress has been made in base metal leaching using oxygen and ferric sulphate. The high shear effect prevents the development of passivating films such as elemental sulphur and virtually complete leaching of copper from chalcopyrite has been achieved in less than 12 h.

A side benefit of the high shear environment generated within the Filblast reactor is significant shear thinning when treating viscous, thixotropic slurries. Carbonation of red mud residue from the Bayer Process that could not be agitated with a triple impeller mixer resulted in a fluid pulp after passage through the Filblast.

Other successful pilot scale test work has been demonstrated in the oxidation of black liquor in the paper industry and in water treatment.

Successful oxygenation trials for the control of algal growth in stagnant river water was undertaken in conjunction with the Western Australian Water and Rivers Commission in the summer of 1998/99.

*Keywords: Filblast, mass transfer, enhanced kinetics, gas-shear reactor, shear thinning*

### Introduction

The Filblast gas shear reactor is a static in-line or end of line submersed reactor which employs a patented gas/liquid or gas/slurry mixing system, which causes the slurry phase to repeatedly interact with the gas phase resulting in the atomisation of the gas and rapid dissolution into the liquid. The undissolved or free gas causes rapid acceleration of the mixture within the reactor as the material travels towards the lower pressure discharge end.

This action generates a very high velocity gradient and results in shear rates greatly in excess of shear rates that can be generated hydraulically by simply pumping the slurry at a high rate. Furthermore the hydraulic characteristics of the Filblast are quite surprising in that the flow capacity is significantly greater than one might predict by applying typical flow-pressure calculations.

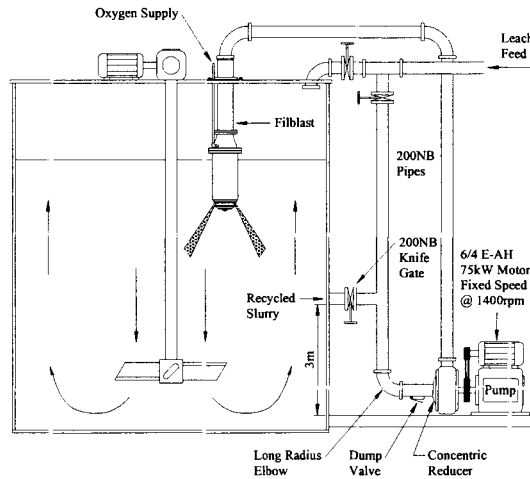


Figure 1: Typical Filblast installation

The application of the Filblast is depicted in Figure 1. The schematic shows the Filblast feed pump recycles slurry from the first vessel in the circuit together with the new feed, which is fed into the pump suction. This configuration ensures zero by-pass of new feed and enables a fixed speed pump to be used. This is an important factor as it ensures a constant feed rate and feed pressure to the Filblast irrespective of variations in plant throughput. The recycle rate is variable and depends upon the degree of leaching required from the Filblast. Typically the recycle rate is 25÷100%.

#### *Fluid mechanics of the Filblast*

The modified particle Reynolds number, to which the particles are subjected, is very high and is typically in the range of 12,000÷15,000, which categorizes the Filblast as a high turbulent flow regime. Whereas the Reynolds Number for an agitated tank as used in the cyanidation process, where the impeller operates at a shear rate of around  $5 \text{ s}^{-1}$ , is typically in the range of 0.5÷1.5, which is in the laminar flow region.

These numbers may be put into perspective by the following comparison of the energy dissipated in the Filblast with the energy dissipated in a typical gold cyanidation tank.

Table I: Comparison of power in-put of Filblast reactor with agitated cyanidation tank.

Filblast	Internal volume l	Capacity (l/min)	Power input (kW)	Slurry residence (ms)	Power input (kW/l)
Typical leach tank	1,000,000	4,167	45	4 h	0.000045
450	43.0	7,500	112	344	2.61

Table I clearly demonstrates that the Filblast reactor is capable of adsorbing a great deal of energy and that it can effectively utilise the energy as the supporting evidence in Tables II and III, clearly demonstrates. Indeed, apart from the economic impracticality of using several times more power in agitated tanks, it has been found in the course of research conducted at the Curtin University of Technology in Western Australia, that beyond a certain power input, the mixing action in an agitated tank resulted in stratification of the suspended particles in the upper region of the tank. This means if the mixing intensity were too intense in a continuous flow application, the solids residence time would be significantly less than the tank volume would suggest.

### Practical demonstration

The ability of the Filblast to utilize high power input to achieve high mass transfer efficiency and high shear is depicted in Table II, which demonstrates the intensity of the shear rate by its effect on particle degradation and the effectiveness of the Filblast in dissolving oxygen is shown in Table III.

Table II: Particle degradation.

Site	Feed $D_{80}$ ( $\mu\text{m}$ )	Product $D_{80}$ ( $\mu\text{m}$ )
Western Australia	~130	~112
Zimbabwe	130	97
Laboratory tests: oxide ore	425	350
Laboratory tests: sulphide ore	260	200

Table III: Effect of Filblast on oxygen consumption.

Site	Oxygen addition or consumption		[DO] (ppm)	
	no Filblast	with Filblast	no Filblast	with Filblast
A	180 m <sup>3</sup> /h	60 m <sup>3</sup> /h	3÷5	33÷35
B	150 m <sup>3</sup> /h	80 m <sup>3</sup> /h	4-6 Tk1 & 1.5-2 Tk2	>17* CIL 1 & 2
C	0.55 kg/t	0.55 kg/t	4÷5	>25
D	290 m <sup>3</sup> /h	40 m <sup>3</sup> /h	8÷10	38
E	45 m <sup>3</sup> /h	15 m <sup>3</sup> /h	17÷18	44
F	0.21 m <sup>3</sup> /t	0.07 m <sup>3</sup> /t	17÷18	22÷25
G	0.5 kg/t	0.2 kg/t	13÷14	27÷28
H	0.79 m <sup>3</sup> /t	0.53 m <sup>3</sup> /t	25	25
I	25% valve set	3% valve set	25	34
J	14 kg/t + 2 kg H <sub>2</sub> O <sub>2</sub>	7 kg/t	Nil 4 h pre-aeration	1-2 no pre-aeration

\*limit of DO meter

The data presented in Figure 2 is particularly revealing of the magnitude of the high-mass transfer rate on oxygen uptake rate and utilisation efficiency. The graph shows the effectiveness of the Filblast reactor in processing an extremely reactive sulphide ore, which had very high oxygen demand and cyanide consumption rates. The data is for the Southern Cross Mill in Western Australia.

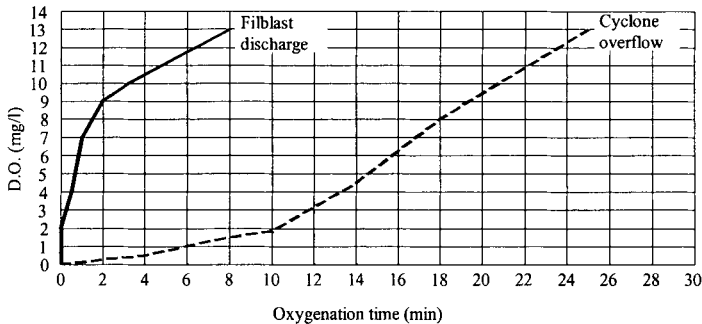


Figure 2: Oxygen up-take rate for Filblast discharge and Filblast feed pulp.

An in-line Filblast reactor was installed and immediately the [DO] in the slurry discharge from the pipeline was off scale (>20 ppm) for the DO meter used. A single pass through the Filblast lasting less than 250 ms, satisfied over 70% of the oxygen demand of a very reactive gold ore consisting of 40% by weight sulphide minerals principally pyrrhotite, arsenopyrite and marcasite. 4 h pre-aeration using up to 14 kg/t of liquid oxygen and 2 kg/t of hydrogen peroxide had resulted in less than 1 ppm [DO]. Cyanide consumption was about of 14 kg/t and gold recovery averaged 73%. Gold extraction increased by approximately 10% and the combined effect of lower reagent consumption and higher gold recovery resulted in 120-130 A\$/oz reduction in treatment costs.

When cyanide was introduced via the Filblast feed pump, the high [DO] in the Filblast increased the leaching kinetics and overall gold extraction was increased. Diagnostic leach studies revealed no free gold in the plant cyanidation residue; only silicate occluded gold and gold in solid solution in the arsenopyrite.

### Effect of the Filblast in cyanidation

A large amount of plant data has been accumulated since the first Filblast was commissioned in 1993. Some of the effects were predictable while others were unexpected, but nevertheless very beneficial. This paper does not permit a detailed review of individual applications, but an over-view of the Filblast cyanidation process is as follows. The factors controlling cyanidation of gold include mixing intensity, oxygen and cyanide concentration, temperature, pressure and surface passivating films. The Filblast concept optimizes these factors and achieves consistently high levels of efficiency by increasing the concentration of dissolved oxygen in the slurry, the mixing intensity and the process pressure, all under conditions of high shear.

The Filblast cyanidation process applies all of these factors in a simple, robust device that increases the cyanidation kinetics and the ultimate gold extraction. It is these characteristics of the process that Atomaer has addressed with outstanding results.

In simple terms, the Filblast acts like a carburettor, the more dissolved oxygen, the more cyanide can be effectively utilised and the quicker and more efficiently the gold is extracted. Higher efficiency translates to higher gold recovery.

*Higher gold recovery*

In addition to the faster reaction kinetics and the elimination of spikes in the tailing residue loss, the faster leaching kinetics reduce solution losses due to steepening of the adsorption profile. This effect is shown in the results from a recent plant trial depicted in Figure 3. The graph plots the tails solution figures for a 12-month period during which the plant converted from air to oxygen to oxygen with Filblast. The steady operating state is clearly reflected in these graphs.

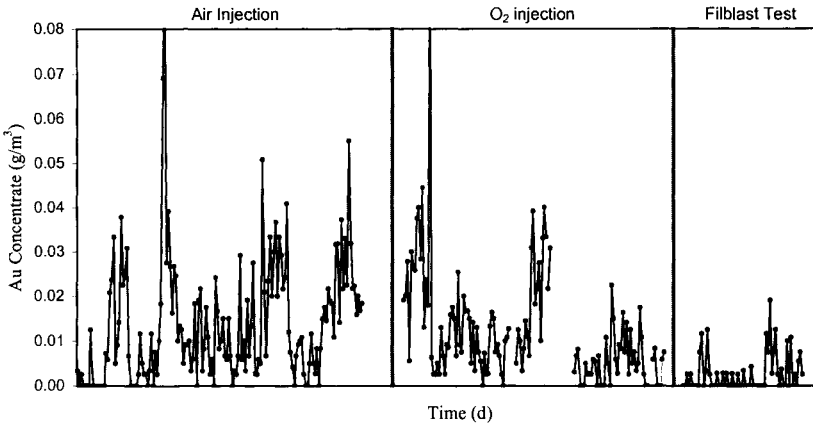


Figure 3: Example of steady-state plant operation with Filblast.

*Increased dissolved oxygen concentration*

The improvement in dissolved oxygen levels is the most visual benefit of the Filblast system. In successfully achieving high shear and micro bubble dispersion, the slurry reaches an almost champagne consistency. As the results in Table III indicate, Atomaer’s oxygen dissolution technology is the most advanced in the market, providing higher [DO] and lower oxygen consumption.

*Reduced cyanide consumption*

Cyanide injection via the Filblast feed pump results in higher free cyanide concentration in the unit and in accelerated leach kinetics while simultaneously reducing overall cyanide consumption (Table IV).

Table IV: Cyanide consumption.

Site	Cyanide consumption (k/t)	
	no Filblast	with Filblast
A	1.13	0.91
B	0.68	0.59
C	0.896	0.823
D	0.83	0.79
E (Site 10 Table I)	12÷16	6.5

*Reduced pulp viscosity*

Significant slurry shear thinning has been noted on a number of sites with viscosity problems. The resultant benefits include an increase in pulp flow through inter-stage



screens and increased adsorption kinetics. At one site the viscosity was reduced by 30% and the effectiveness of viscosity modifier increased by a factor of four. A second site was able to reduce viscosity modifier addition by two thirds.

#### *Particle degradation*

Laboratory tests and plant measurements have been carried out on particle degradation that produced the results shown in Table II. This effect is particularly beneficial in leaching coarse gold particles or gold-silver alloys, which are generally very slow to leach.

#### *Improved adsorption efficiency and carbon loading*

Improved adsorption efficiency and increased gold loading is achieved by a number of synergistic effects caused by the Filblast. The faster leaching kinetics, less gold leached in the adsorption circuit, less competition from base metal cyanides, notably copper, but also nickel, lower pulp viscosity and lower free cyanide plus lower adsorption circuit pH all favour improved adsorption efficiency.

#### *Higher throughput*

Plants that have adequate ore supply have been able to increase throughput using the Filblast. One plant has increased throughput by over 60% by coarsening the grind size, yet recovery increased by ~2%. Some cases are shown in Table V, while other plants have noted the increased leaching kinetics, but have not been able to exploit the faster leaching rate due to ore supply. Still other sites have maintained throughput and increased recovery despite coarser grind size due to harder ore.

Table V: Increased plant throughput.

Site	Throughput (t/h)		Comments
	pre-Filblast	with Filblast	
a	55	105	$P_{80} = 106 \rightarrow 160 \mu\text{m}$
b	100	120	added low grade ore
c	1,050	1,500	limited by interstage screens
d	120	135	tailing retreatment

#### *Consistent results and plant control*

The degree to which any of the above benefits may apply to a particular plant depends on a number of factors such as ore type, grind sensitivity, water quality and general metallurgical efficiency through the plant. However the consistent results as shown in Figure 3, allows the operator to measure the effect of imposed changes and this allows fine tuning to a degree that is unattainable without the Filblast.

### **Base metals applications**

#### *Copper, cobalt and uranium*

The application of the Filblast in base metals extraction is still in the developmental stage. However to date the reactor has been successfully applied in large scale batch leaching operations for various copper concentrates, copper-cobalt bearing tailing and uranium ore. Chalcopyrite concentrates require fine grinding to  $P_{80} \cong 20 \mu\text{m}$  and the addition of 100 g/t of silver to act as a catalyst in order to achieve >98% copper

extraction in 11÷12 h. A 50:50 chalcopyrite/bornite concentrate ground to  $P_{80} \cong 63 \mu\text{m}$  was leached without catalyst and achieved >95% extraction in about 6 h. All the leaching tests were conducted at temperatures between 70 °C to 85 °C.

At the time of writing this paper, a 4-stage continuous pilot plant trial is under way at a major Australian mine using oxygen with the Filblast system as an alternative to the more expensive chemical reagent currently used to oxidise ferrous sulphate to ferric sulphate. This pilot scale trial follows a series of successful batch oxidation and leaching trials for the conversion of ferrous to ferric and the extraction of copper and uranium from flotation tailing.

Results have been encouraging with the ferrous conversion rate being approximately double the target rate.

#### *Bayer process*

Neutralizing Bayer process residue, commonly known as red mud, with carbon dioxide to produce dryable slurry for safe disposal is of significant importance to the alumina industry. However, injection of carbon dioxide by conventional means has been ineffective and inefficient due to the high viscosity of red mud.

The results obtained from a pilot test program conducted at a residue site in Australia indicate that effective and efficient neutralisation of the red mud can be achieved by using the Filblast gas shear reactor.

Based on the pilot plant results, a 3-stage process has been designed for a full-scale continuous carbonation operation. The projected plant, with a maximum capacity of 600 kl/h of red mud at 50% solids, would incorporate 3 treatment tanks, each equipped with a pair of 450 m<sup>3</sup>/h Filblast reactors and a pump for mud recirculation through the Filblast units. Stand-by stage and bypass facilities have been provided to facilitate individual tank maintenance shut down without disruption to the operation.

Preliminary estimates indicate that the proposed plant would cost approximately 2 million US\$ to install, but this depends on local materials and labour costs.

The operating costs have been projected at approximately 0.91 US\$/m<sup>3</sup> assuming power supply cost of 0.05 US\$/kWh and carbon dioxide cost of 30 US\$/t. Efforts have been made to reuse the red mud, but to date no economically viable options have been found. As such the Filblast process has the potential to provide a cost-effective solution to a significant environmental problem.

## SELECTIVE SEPARATION OF YTTRIUM FROM CHEMICAL CONCENTRATE OF RARE EARTH

E. Panturu, D. P. Georgescu, F. Aurelian, N. Udrea

Uranium National Company R&D Center for Rare and Radioactive Metals  
Bd. Carol I, 70132, Bucharest, Romania

### Abstract

The problem of separation of elements from rare earth is one of the most difficult methods in inorganic chemistry. In this paper we used for yttrium separation a chemical concentrate of 83.5% rare earth with a percent content of 51% yttrium. The most useful method for lanthanides separation is liquid-liquid extraction using different types of organic extractants. We used di-(2ethylhexyl)phosphoric acid (D2EHPA) and the complexing agent was diethyltriamine-penta-acetic (DTPA). We obtained the yields with high purity using a process with minimal number of operations.

*Keywords: rare earth, yttrium, liquid-liquid extraction*

### Introduction

Rare earths (lanthanides) include a 15-elements series with the similar chemical properties, having the atomic number 57 to 71. This series include also yttrium with the atomic number 39, because it has an approximately same chemical behavior with the 15 elements presented and it has a geochemical affinity unto the rare earth with high atomic number (Bednarczyk, 1989). The first 7 elements from the rare earth series (La, Ce, Pr, Nd, Pm, Sm, Eu) are known as light elements group. The other eight elements (Gd, Tb, Dy, Mo, Er, Tm, Yb, Lu) together with yttrium, constitute the heavy rare earth group. The researches regarding the use for the nuclear energy brunch of the uranium and ammonium difluoride which results from the phosphoric acid industry, like a byproduct material (Berry, 1989) provide the possibility to separate in the some time a chemical rare earth concentrate with high yttrium content. Liquid-liquid extraction is the most important method for the element separation (Makriliik and Vanura, 1996; Sato and Sato, 1988). In this paper, the researches were carried out based on Japanese patent (Reynolds and Holdings, 1994) proposing the di-(2ethylhexy)phosphoric acid (D2EHPA) acid extractant and a rare earth complexing agent diethyltriamine-penta-acetic (DTPA) (Slovetski, 1989; Berry, 1989).

### Experimental

The research workings for yttrium oxide obtaining were performed using rare earth concentrates as raw material. These concentrates were obtained as byproducts from the uranium and ammonium difluoride conversion technology, when sodium diuranate was the ultimate product. These double fluoride results as byproducts from the phosphoric acid industry, phosphorite materials processing respectively. Chemical concentrates obtained as described are mainly rare earth hydroxides, having the structure reported in Table I. Rare earth contents are reported in Table II.

Table I: Chemical composition of rare earth (RE) concentrates used as raw material.

RE <sub>2</sub> O <sub>3</sub> (%)	Fe <sub>2</sub> O <sub>3</sub> (%)	Al <sub>2</sub> O <sub>3</sub> (%)	CaO (%)	U (%)	ThO <sub>2</sub> (%)
69.11	6.56	2.46	0.43	0.15	0.10

Table II: Detailed rare earth contents (%) in the concentrates.

Element	Content (%)	Element	Content (%)
Y <sub>2</sub> O <sub>3</sub>	35.69%	Sm <sub>2</sub> O <sub>3</sub>	0.20%
Dy <sub>2</sub> O <sub>3</sub>	1.0%	Lu <sub>2</sub> O <sub>3</sub>	8.0%
Gd <sub>2</sub> O <sub>3</sub>	0.08%	Er <sub>2</sub> O <sub>3</sub>	10.0%
Sc <sub>2</sub> O <sub>3</sub>	1.60%	La <sub>2</sub> O <sub>3</sub>	0.05%
Ho <sub>2</sub> O <sub>3</sub>	0.204%	Nd <sub>2</sub> O <sub>3</sub>	0.046%
Yb <sub>2</sub> O <sub>3</sub>	12.0%	Tb <sub>2</sub> O <sub>3</sub>	0.06%
CeO <sub>2</sub>	0.18%		

#### *Rare earth concentrates solubilization*

For performing the necessary aqueous solution for the yttrium extraction stage, the solubilization is carried out using 31.5% nitric acid.

The optimal dissolution conditions are the following:

- temperature: 70 °C;
- duration: 2 h;
- solid/liquid ratio: 1/3.

Solubilization was 99.9%. When the solubilization process ended a rare earth nitrates solution was obtained, having 209 g/l TR<sub>2</sub>O<sub>3</sub> content and a 1 N HNO<sub>3</sub> free acidity.

The Y<sub>2</sub>O<sub>3</sub> content in solution was 108 g/l, for Yb<sub>2</sub>O<sub>3</sub> it was 36.29 g/l and for Er<sub>2</sub>O<sub>3</sub> it was 30.2 g/l.

#### *Yttrium separation-purification by D2EHPA extraction-re-extraction process*

The experiments for yttrium separation-purification using D2EHPA and DTPA extraction-re-extraction process were performed the following conditions:

- organic aqueous extraction ratio: O/A = 3/1;
- time for phase contact: 15 min;
- solution pH: 7.5÷8;
- extractant: D2EHPA 2 M diluted in kerosene;
- re-extraction ratio: O/A = 2/1;
- Re-extractant: HCl = 6M solution on HNO<sub>3</sub> 6 M solution;
- complexant: DTPA = 120 g/l;
- stillness time: 20 min.

After each re-extraction experiment was performed the aqueous phase conditioning by pH adjusting and DTPA adding and after sampling of solution volume for yttrium-ytterbium content analysis the condition aqueous phase was processed in another extraction-re-extraction cycle.

For the organic phase rare earth discharging, there was performed re-extraction in different stages. This re-extraction solution was not further used for another separation cycle. The chloride solution obtained by calcinated oxalates dissolution

had a high calcium content, that way it was necessary to study the extraction mechanism and its influence within the purification process.

In this propose, two experiments were performed using two aqueous solution: a rare earth solution impurified with calcium and a synthetically rare earth chloride solution without calcium.

### Results and discussion

The experimental results were performed using the unprocessed solution and these were presented in Tables III and IV.

Table III: Solutions with calcium in aqueous phase and organic phase.

Test n°	Type of sample	Aqueous phase			Organic phase		
		Y <sub>2</sub> O <sub>3</sub> (g/l)	Yb <sub>2</sub> O <sub>3</sub> (g/l)	Y/Yb	Y <sub>2</sub> O <sub>3</sub> (g/l)	Yb <sub>2</sub> O <sub>3</sub> (g/l)	Y/Yb
I	Initial	3.797	0.6160	6.2			
	Rafinate	0.027	0.0054	5.0	1.257	0.1980	6.0
	Re-extract 1	0.503	0.0470	10.7	0.287	0.1690	4.9
	Re-extract 2	1.239	0.1170	105.9	0.414	0.1660	2.5
	Re-extract 3	0.976	0.0970	10.1	0.251	0.1490	1.7
II	Rafinate	0.070	0.0100	7.0	0.212	0.0180	11.8
	Re-extract 1	0.084	0.0060	14.0	0.178	0.0156	11.4
	Re-extract 2	0.257	0.0010	257.0	0.114	0.0153	7.5
III	Rafinate	0.016	0.1003	7.3	0.029	0.0100	2.9
	Re-extract	0.023	0.0009	25.6	0.150	0.0140	1.0

Table IV: Coefficients of the solution with calcium.

Test n°	Type of sample	D	D	E (%)	E (%)	S
		Y	Yb	Y	Yb	Y/Yb
I	Initial					
	Rafinate	145	113	99.3	99.1	1.3
	Re-extract 1	0.17	0.08	145	7.4	1.9
	Re-extract 2	1.0	0.02	50	2	50
	Re-extract 3	0.6	0.11	63	37.5	5.5
II	Rafinate	6.2	3.70	86.1	78.7	1.7
	Re-extract 1	0.2	0.16	16.7	13.8	1.3
	Re-extract 2	0.4	0.02	28.6	2.0	20
III	Rafinate	3.7	2.10	78.7	67.6	1.8
	Re-extract	0.2	0.15	16.7	13.0	1.3

The results obtained in the processing of solution without calcium, using the extraction-re-extraction process were presented in Tables V and VI.

In Figures 1a and 1b were drawn the extraction results for yttrium and ytterbium, as a function of the number of extraction-re-extraction stages from the data presented in Tables III and IV.

It is concluded that during the extraction step took place a low yttrium content decrease, in the aqueous phase, with the Y/Yb ratio decreasing also, from 6÷6.2 to 4.8÷5 in unprocessed solution.

The yttrium extractability increased during the second and the third cycles.

Table V: Solutions without calcium in aqueous phase and organic phase.

Test n°	Type of sample	Aqueous phase			Organic phase		
		Y <sub>2</sub> O <sub>3</sub> (g/l)	Yb <sub>2</sub> O <sub>3</sub> (g/l)	Y/Yb	Y <sub>2</sub> O <sub>3</sub> (g/l)	Yb <sub>2</sub> O <sub>3</sub> (g/l)	Y/Yb
	Initial	4.378	0.729	6.0			
I	Rafinate	0.019	0.004	4.8	1.4590	0.2030	7.2
	Re-extract 1	0.110	0.011	10.0	1.3460	0.1800	7.5
	Re-extract 2	0.851	0.007	121.6	1.0600	0.1700	6.2
	Re-extract 3	0.726	0.006	121.0	0.9400	0.1600	5.8
	Re-extract 4	0.461	0.005	92.0	0.1600	0.1500	5.7
II	Rafinate	0.039	0.008	4.8	0.0350	0.0040	8.2
	Re-extract 1	0.075	0.005	15.0	0.0100	0.0023	4.3
	Re-extract 2	0.114	0.002	57.0	0.0020	0.0020	1.0
III	Rafinate	0.006	0.002	4.0	0.0009	0.0002	4.5

Table VI: Coefficients of the solution without calcium.

Test n°	Type of sample	D	D	E (%)	E (%)	S
		Y	Yb	Y	Yb	Y/Yb
	Initial					
I	Rafinate	242	229	99.6	99.5	1.1
	Re-extract 1	0.08	0.05	7.4	4.8	1.6
	Re-extract 2	0.27	0.03	21.3	1.0	27.0
	Re-extract 3	0.13	0.004	11.5	0.4	32.5
	Re-extract 4	0.09	0.003	8.3	30.0	
II	Rafinate	3.5	1.8	77.8	64.3	1.9
	Re-extract 1	2.5	0.72	71.4	41.8	3.5
	Re-extract 2	3.1	0.04	75.6	3.8	77.5
III	Rafinate	0.8	0.4	44.4	28.5	2.0

The calcium ions content in solution had not an important influence on the yttrium purification process. Both extraction rates and distribution coefficients were not mostly influenced by initial Y and Yb concentrations in solution.

Thus, in the first extraction cycle it were obtained Y extractability of 99% and for the further cycles were decreased until 44%, keeping the some RE/DTPA ratio. In all the extraction cycle were observed that, in the first re-extraction step, was not performed a suitable Y and Yb separation due to a partial destroying of the Ln<sup>3+</sup>DTPA complex in the solution. In the following re-extraction steps it was provides a high increase of Y/Yb ratio in the aqueous phase (approximately 10 times) and the selectivity coefficient increase for 25 times. In Figure 2a it were shown the extraction variation and the selectivity factors (S) as a function of the re-extraction steps number.

From the data presented in Table III one can see that within the extraction stage was produced a low yttrium content decrease (see Table VII). It was found that the product obtained following the D2EHPA extraction-re-extraction process in presence of DTPA complexant had a very low ytterbium content (420 times decrease).

Table VII: Yttrium content before and after the extraction stage.

Products	Y <sub>2</sub> O <sub>3</sub> (%)	Yb <sub>2</sub> O <sub>3</sub> (%)
Initial	36.0	6.0
Re-extract	51.0	0.02

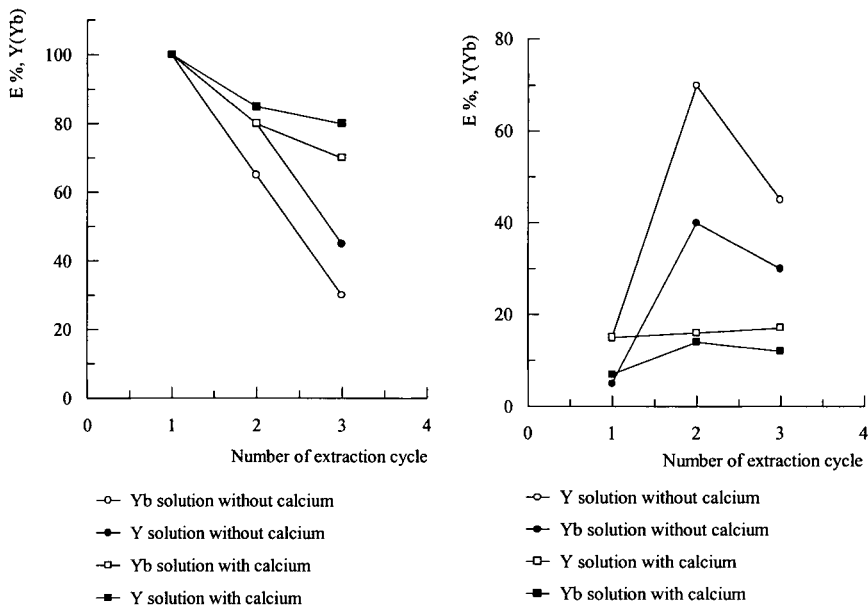


Figure 1: a (left): Y, Yb extraction with D2EHPA by DTPA; b (right): Y, Yb re-extraction with HCl 5 M from organic phase by DT.

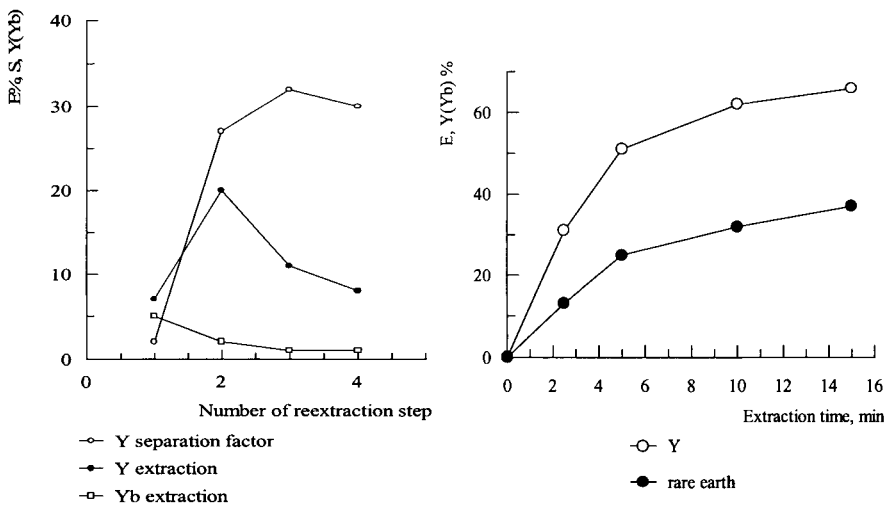


Figure 2: a (left): Y and Yb extraction and separation factor; b (right): the influence of the extraction time.

It was found that the product obtained following the D2EHPA extraction-re-extraction process in presence of DTPA complexant had a very low ytterbium content (420 times decrease). The calcined product had a 98.10%  $Y_2O_3$  content and only 0.04%  $Yb_2O_3$ , so one might consider that the above extraction process led two excellent purification results.

## Conclusions

The yttrium extraction is conditioned by the following factors:

- the yttrium ion concentration and other lanthanide ions concentrations in the raw aqueous solutions is limited to the 0.05÷2 mol/l range, 0.05 mol/l being preferred. This limitation is imposed by the third phase appearance during extraction, for higher ions concentration, followed by a difficult phase separation;
- the quantity for the chelating agent (DTPA or EDTA) is usually greater than the equivalent quantity required for the complex formation a 1.50 times higher content being preferred;
- the nitric solution pH conditioned using the complexing agent must be adjusted in the 7.5÷8.5 range;
- the organic phase used was diluted in aliphatic compounds (odorless kerosene) or aromatic compounds (xylene), having the same 2 M D2EHPA content;
- the O/A ratio must be at least 3/1, smaller value ratio leading to the third phase (organic gel) appearance during extraction;
- the experiments have shown the importance of the concentration time (Figure 2b), so after 5 min the extraction rate is 52% from yttrium and 25% from other lanthanides, but after 15 min extraction rate of yttrium is 65% and for lanthanides the ratio become 37%.

## References

- Bednarczyk, L., 1989. *Solvent Extraction Ion Erch.*, 7, 2, 273-87.
- Berry, W.W., 1989. *Europ. Pat. Appl. Patent No 335.538.*
- Makrilič, E., Vanura, P., 1996. *Collect. Czech. Chem. Commun.*, 51, 3, 489-515.
- Reynolds, W.I., Holdings Ltd, 1994. *Fr., Patent No 1.555.149 and 1.555.148.*
- Sato, T., Sato, K., 1988. *Proc. Symp. Solvent Extr.*, 25-30
- Slovetski, A.I., 1989. *Radiokimia*, 31, 4, 90-3



This Page Intentionally Left Blank

# **PHYSICAL SEPARATION PROCESSING**

This Page Intentionally Left Blank

<b>The Separation of Coarse Particles by a Moving Froth Bed</b> J.S.J. van Deventer, W.A. van Dyk, L. Lorenzen	C7-1
<b>A New Magnetic Separator and Classifier: Case Study</b> P.A. Augusto, J.P. Martins	C7-9
<b>Removal of Sulfur and Mineral Matter from Coal Slurry by a Pilot Scale Wet Magnetic Separator</b> H. Dinçer, G. Ateşok, M.Z. Doğan, Ş. Girgin, F. Boylu, Ö. Yüksel	C7-15
<b>Study of Separation of Refractory Sulfide Minerals by Hgms</b> Y. Zhang, S. Liu, W. Fu	C7-22
<b>Electrostatic Feldspar/Quartz Separation without Hydrofluoric Acid Reduces Pollution</b> S. Dorfner, H. Tröndle, U. Jakobs	C7-30
<b>Assessment of Multistage Turbulent Cross-Flow Aeroseparation of Building Rubble</b> J. Tomas, T. Gröger	C7-34
<b>Separation Technology Based on Segregation Effects in Fast Gravity Flows</b> V. Dolgunin, A. Ukolov, A. Romanov, A. Kudy, A. Klimov	C7-44
<b>Trapped Vortex Magnetic Separation (Tvms)</b> Z. Li, J.H.P. Watson	C7-50
<b>General Trends of Gravity Separation</b> M. Barsky, E. Barsky	C7-57

This Page Intentionally Left Blank

## THE SEPARATION OF COARSE PARTICLES BY A MOVING FROTH BED

J.S.J. van Deventer\*, W.A. van Dyk°, L. Lorenzen°

\*Department of Chemical Engineering, The University of Melbourne, Parkville,  
Victoria 3052, Australia. e-mail: jsj.van\_deventer@chemeng.unimelb.edu.au

°Department of Chemical Engineering, University of Stellenbosch, Private Bag X2,  
Matieland, 7602, South Africa. e-mail: LL1@ing.sun.ac.za

### Abstract

The behaviour of coarse particles in a moving bed of froth was investigated as a potential flotation technique. The technique is based on the fact that coarse particles, if they are selectively rendered hydrophobic, would act as bubble film breakers if the feed is introduced onto the surface of the froth. Such particles would settle through the froth under gravity to be recovered as the underflow product, while the hydrophilic gangue would be supported by the bubble films and be recovered as a float product. The efficiency of separation is primarily dependent on the ratio of particle mass to projected area, while the contact angle has only a secondary effect on the particle trajectory. Large, high density particles and also small, low density particles cannot be separated on the basis of hydrophobicity. This means that particles to be separated on the basis of contact angle should have a mass between an upper and lower critical value. In this study both artificially coated tracer particles and a pyritic ore were used.

*Keywords: flotation, froth, hydrophobicity, film breakage*

### Introduction

Although the flotation of coarse particles has received little attention in comparison with fine particles, it is certainly an important problem in the mineral industry. In the conventional coal preparation process the minus 0.5 mm particles are normally recovered by flotation, but particles up to 2 mm may be present owing to poor upstream classification. These large particles are difficult to recover with conventional techniques, which has led to studies aimed at the use of alternative flotation reagents to improve the yield of coarse coal particles (Moxon and Keast-Jones, 1986; Moxon et al., 1988). Although some degree of success was achieved, this size fraction could still account for the largest losses during coal preparation. A system was proposed (Lloyd, 1987) in which gold and other valuable minerals could be concentrated underground by coarse milling and flotation. However, the flotation step was able to recover only 75% of the valuable minerals owing to the large losses in the coarser particle-sizes.

Schubert (1989) investigated the development of an impeller type and impeller-stator flotation system that would recover coarse particles in the treatment of quartz sands and sylvanite. The aim was to suspend coarse particles in the pulp phase without having to agitate the pulp phase to such an extent that would impose unnecessary turbulent stresses on the bubble-particle aggregates. The design resulted in lower

power consumption, but although it appeared successful for particles up to 0.4 mm, difficulties were encountered at the coarser size ranges.

These investigations have shown that a need exists for a coarse particle separation technique with low operating costs. De Beers in South Africa developed a novel flotation technique for the recovery of coarse hydrophobic particles by reverse flotation in the froth phase of a pneumatic type of flotation cell (Ross, 1993). Although the technique was originally intended to solve the grease belt problem in the diamond industry, various other applications became evident. The De Beers technique is based on the fact that coarse particles, if they are selectively rendered hydrophobic by conditioning, would act as bubble film breakers if the feed is introduced onto the surface of the froth. Such particles would settle through the froth under gravity to be recovered as an underflow product, while the gangue would be supported by the bubble films and therefore be recovered as a float product. This process differs from conventional reverse flotation (in which the valuable mineral is depressed in the pulp phase) in that the separation is effected in the froth phase only. It could therefore be called "reverse froth flotation". The AFT SPRAYFLOT™ cell proposed a number of years ago has similar features in the sense that the ore is fed onto the froth, but it still involves conventional flotation processes such as attachment instead of film breakage as is the case here. The mechanisms of film breakage and their effect on froth stability (Dippenaar, 1982a, 1982b) will not be discussed here, as a previous paper (Van Dyk et al., 1995) explained the relevance to the moving froth bed system.

It is the aim of this paper to discuss the main variables affecting the behaviour of coarse particles in the moving froth bed. Governing parameters of the particles in the feed include density, shape, surface characteristics (wettability and roughness) and size. The bubble size, residence time of the bubbles in the flotation cell, and rigidity and thickness of the bubble films, are important froth characteristics.

### **Experimental methods**

Figure 1 depicts schematically the cell design. The cell made from PVC sheeting allowed visual observation of the froth structure and movement of particles. Air is sparged at the bottom of compartments 1A and 1B (1<sup>st</sup> concentrate), which generates a froth which rises and moves across compartment 2 (2<sup>nd</sup> concentrate) into the tailings compartment. As shown, the positioning of guiding baffles is important to give the right disturbance of froth in the middle of the moving bed in order to decide on the split between the compartments. The water from the bottom products was recycled in some experiments. The height of the cell was adjusted in some experiments in order to improve the distribution of air.

Density tracers (made from inert plastic) of various sizes, specific gravities and shapes were used. Of the numerous surface coatings attempted, only three paints, an adhesive and candle wax were found to give stable coatings on the tracer particles with equilibrium contact angles ranging from 44 to 98 degrees. Although these surfaces were reasonably stable, it was found that most hydrophobic surfaces became hydrophilic with time. Various tests were also conducted using 100 g of gold containing pyritic ore (density = 2,760 kg/m<sup>3</sup>) from the Harmony Gold Mine in South

Africa. Density tracers and ore particles were fed manually onto the froth bed at the end of the first bent weir of compartment 1A.

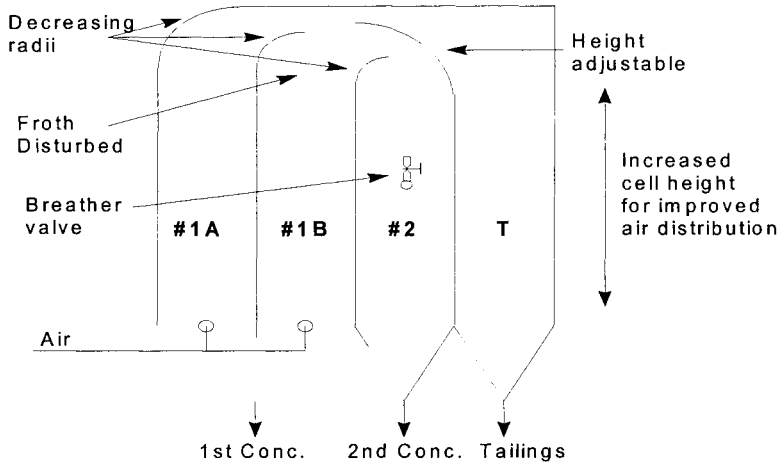


Figure 1: Flotation cell design.

Table I: Operating conditions used.

Variables	Operating conditions				
	1	2	3	4	5
Air flow rate in 1A (l/min)	23.8	23.8	23.8	23.8	29.5
Air flow rate in 1B (l/min)	18.4	18.4	18.4	23.8	18.4
Liquid level from top (mm)	290	265	240	240	240
Froth height over splitter (mm)	20	15	10	5	10
Bubble diameter at interface (mm)	1.07	1.08	1.09	1.17	1.01
Liquid flow to 2nd concentrate (ml/s)	16.7	20.6	47.2	31.2	56.1
Liquid flow to tailings (ml/s)	14.47	17.7	31.6	31.0	33.7

Table II: Mass (mg) and mass/projected area ( $\text{mg}/\text{mm}^2$ ) for various shapes of particles with measurements given in mm, having different densities ( $\text{kg}/\text{m}^3$ ).

Density	Cube		Rod		Flat		Disc		Cube		Flat		Rod	
	3.05	3.38×1.04	3.5×1.52	0.65×1.1	2.1	2.1×1.05	1.98×1.04							
$\text{kg}/\text{m}^3$	M	M/A	M	M/A	M	M/A	M	M/A	M	M/A	M	M/A	M	M/A
3,500	99.30	10.68	40.20	11.83	49.65	10.68			32.41	7.35	16.21	7.35	23.35	6.93
3,300	93.63	10.07			46.81	10.07			30.56	6.93	15.28	6.93		
3,100	87.96	9.46	35.60	10.48	43.98	9.46	33.10	7.28	28.71	6.51	14.35	6.51	20.86	6.14
2,900	82.28	8.85	33.31	9.80	41.14	8.85	30.97	6.81	26.86	6.09	13.43	6.09	19.51	5.74
2,700	76.71	8.24	31.01	9.13	38.30	8.24			25.00	5.67	12.50	5.67	18.17	5.35
2,600	73.71	7.93			36.88	7.93			24.08	5.46	12.04	5.46		

Different operating conditions, as outlined in Table I, were used. By manipulating the air flow rate into the various compartments the trajectory of particles in the cell could be manipulated. This was mainly due to manipulating the froth velocity in the various



froth areas, and subsequently affecting the force balance exerted on the particles in the froth. Table II shows the properties of the density tracer particles used with different coatings.

### Results using coated particles

The limited scope of this paper does not allow the presentation of all relevant experimental results. Therefore, only selected results will be shown, but more general conclusions will be drawn using the particles described in Table II with various coatings of different contact angles. A rigorous mathematical model was also formulated for the process in order to investigate the sensitivity of recovery to changes in a particular variable.

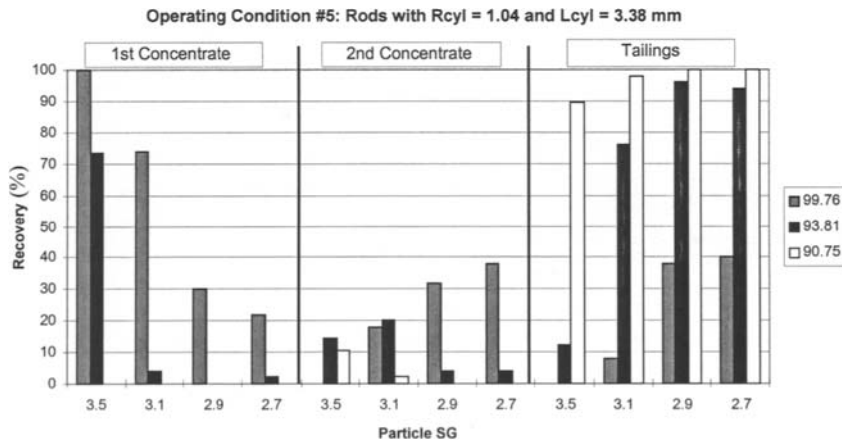


Figure 2: Behaviour of  $3.38 \times 1.04$  mm<sup>2</sup> rods under operating condition #5, using contact angles between  $90.75^\circ$  and  $99.76^\circ$ .

If the particle recovery was purely based on the particle mass, the particle trajectories in the cell (and subsequent recovery to the tailings) would have been in the order of:

1. Cubic particles, where  $S_{cube} = 3.05$  mm
2. Flat shaped particles, where  $L_f = W_f = 3.05$  mm and  $H_f = 1.52$  mm
3. Cylindrical particles, where  $R_{cyl} = 1.04$  mm and  $L_{cyl} = 3.38$  mm
4. Disc-shaped particles, with  $R_s = 0.65$  mm and  $R_d = 1.1$  mm
5. Cubic particles, where  $S_{cube} = 2.1$  mm
6. Cylindrical particles, where  $R_{cyl} = 1.04$  mm and  $L_{cyl} = 1.98$  mm
7. Flat shaped particles, where  $L_f = W_f = 2.1$  mm and  $H_f = 1.05$  mm

The 3.05 mm cubical particles would have had the lowest trajectory and recovery to the tailings, and the  $2.1 \times 1.05$  mm<sup>2</sup> flat shaped particle would have had the highest trajectory and recovery to the tailings.

Similarly, if the particle recovery was purely based on the ratio of mass to projected area (M/A), the particle trajectories in the cell (and subsequent recovery to the tailings) would have been in the order of:

1. Cylindrical particles, where  $R_{cyl} = 1.04$  mm and  $L_{cyl} = 3.38$  mm
  2. Cubic particles, where  $S_{cube} = 3.05$  mm and  
Flat shaped particles, where  $L_f = W_f = 3.05$  mm and  $H_f = 1.52$  mm
  3. Disc-shaped particles, with  $R_s = 0.65$  mm and  $R_d = 1.1$  mm
  4. Cubic particles, where  $S_{cube} = 2.1$  mm and  
Flat shaped particles, where  $L_f = W_f = 2.1$  mm and  $H_f = 1.05$  mm
  5. Cylindrical particles, where  $R_{cyl} = 1.04$  mm and  $L_{cyl} = 1.98$  mm
- The  $3.38 \times 1.04$  mm<sup>2</sup> cylindrical particles would have had the lowest trajectory and recovery to the tailings, and the  $1.98 \times 1.04$  mm<sup>2</sup> cylindrical particles would have had the highest trajectory and recovery to the tailings. Figures 2 to 4 depict the actual results for selected cases.

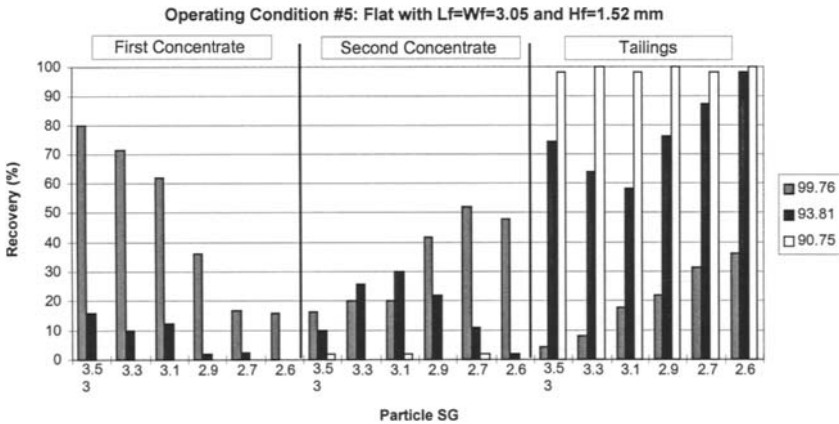


Figure 3: Behaviour of  $3.05 \times 3.05 \times 1.52$  mm<sup>3</sup> flat plates under operating condition #5, using contact angles between  $90.75^\circ$  and  $99.76^\circ$ .

Based on the respective experimental results for operating condition #5, the particles float in the order of:

1. Cubic particles, where  $S_{cube} = 3.05$  mm
2. Cylindrical particles, where  $R_{cyl} = 1.04$  mm and  $L_{cyl} = 3.38$  mm
3. Flat shaped particles, where  $L_f = W_f = 3.05$  mm and  $H_f = 1.52$  mm
4. Disc-shaped particles, with  $R_s = 0.65$  mm and  $R_d = 1.1$  mm
5. Cubical particles, where  $S_{cube} = 2.1$  mm
6. Flat shaped particles, where  $L_f = W_f = 2.1$  mm and  $H_f = 1.05$  mm
7. Cylindrical particles, where  $R_{cyl} = 1.04$  mm and  $L_{cyl} = 1.98$  mm

The 3.05 mm cubic particles have the lowest trajectory and recovery to the tailings, while the  $1.04 \times 1.98$  mm<sup>2</sup> rod shaped particles have the highest trajectory and recovery to the tailings. It is therefore clear that the particle recovery is not purely based on the particle mass, nor purely on the M/A ratios, but rather a combination of these two parameters, coupled with the rate of bubble film rupture per particle shape. The mass of the 3.05 mm cubes is at least twice the mass of any other particle. It can therefore be expected that the gravitational force component exerted on the particles will dominate the force balance.

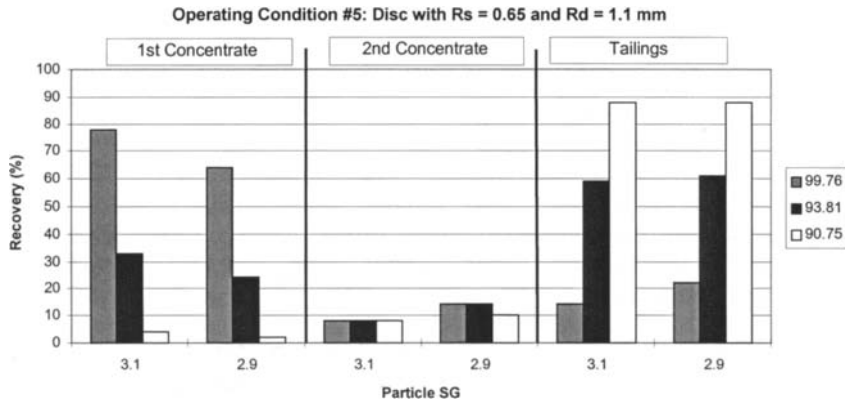


Figure 4: Behaviour of disc shaped particles under operating condition #5, using contact angles between  $90.75^\circ$  and  $99.76^\circ$ .

The 3.05 mm cubes therefore have the lowest recovery to the tailings. Although the mass of the  $3.38 \times 1.04$  mm<sup>2</sup> rod-shaped particles is less than that of the  $3.05 \times 1.52$  mm<sup>2</sup> flat-shaped particles, the M/A ratio is significantly higher. The net force downward would therefore be greater for the rod-shaped particles than for the flat-shaped particles. The rod-shaped particles therefore float at a lower level in the froth, resulting in a higher recovery to the first concentrate than the flat-shaped particles. The disc-shaped particles will recover between the  $3.05 \times 1.52$  mm<sup>2</sup> flat-shaped particles and the 2.1 mm cubes due to their mass, as well as their M/A ratio being between that of the  $3.05 \times 1.52$  mm<sup>2</sup> flat-shaped particles and the 2.1 mm cubes. Both the mass and M/A ratio of the 2.1 mm cubes and  $2.1 \times 1.05$  mm<sup>2</sup> flat-shaped particles result in the particles being recovered as number 5 and 6 respectively in the list. From Table II the mass of the  $1.98 \times 1.04$  mm<sup>2</sup> rod-shaped particles is more than that of the  $2.1 \times 1.05$  mm<sup>2</sup> flat-shaped particles. However, the M/A ratio of these rod-shaped particles is significantly less than that of the flat-shaped particles. It can therefore be expected that the rod-shaped particles would be recovered more to the tailings than the flat-shaped particles.

### Results using pyritic ore

Table III gives the recoveries with and without the use of sodium ethyl xanthate for four sets of operating conditions. An increase in the liquid-froth interface level results in an increase in the mass recovery to the first concentrate. This is in accordance with the results obtained for density tracers of various shapes and sizes. This effect is mainly due to an increase in the bubble size together with a decrease in the bubble film thickness. The froth is therefore incapable of supporting the particles, and the particles will fall through the froth under the influence of gravity. An increase in the air flow rates through the spargers located in compartment 1A (operating condition #5) and compartment 1B (operating condition #4) results in the mass recovery to the first concentrate to decrease in comparison with operating conditions #1 and #3. This

is to be expected due to the increase in the horizontal bubble velocity in the various cell compartments, as well as the increase in the upward force component of the force balance (due to the increase in the vertical velocity component). The components of the force balance, exerted by the bubble films on a particle, are dependent on the operating condition. Since the mass % recovery varies with the operating condition, it must be concluded that a distribution of particle masses exists in the feed sample. With an increase in the mass % recovery to the first concentrate, the associated % sulphur recovery increases as well. However, the increase in % sulphur is not directly proportional to the increase in mass %. Therefore, a distribution of sulphur per particle mass fraction exists.

Table III: Experimental results for the +2.8 mm –3.35 mm fraction of pyritic ore.

Operating Condition	Recovery to:	No Xanthate addition		500 g/t Xanthate addition	
		Yield (%)	S recovery (%)	Yield (%)	S recovery (%)
Op Con #3	first concentrate	51.40	70.15	57.62	87.45
	second concentrate	16.53	8.63	15.83	7.48
	tailings	32.06	21.21	26.55	5.07
Op Con #1	first concentrate	42.38	62.35	48.49	75.63
	second concentrate	11.22	5.80	10.14	3.89
	tailings	46.39	31.85	41.37	20.48
Op Con #4	first concentrate	31.43	49.62	36.07	57.03
	second concentrate	9.11	8.66	8.82	7.54
	tailings	59.46	41.72	55.11	35.43
Op Con #5	first concentrate	29.29	45.31	32.93	49.48
	second concentrate	7.52	8.64	5.45	6.00
	tailings	63.19	46.05	61.62	44.52

With the addition of xanthate the sulphide present on the particle surface will be rendered hydrophobic. Since hydrophobic particles act as bubble film breakers, it is expected that the sulphur recovery to the first concentrate will increase. If particle mass is the main factor determining the separation of particles, there should be no change due to the addition of xanthate. However, a particle with sulphide on its surface that reported to the second concentrate or tailings in the absence of xanthate can now act as a bubble film breaker and report to the first concentrate. The increase in sulphur recovery will then cause an increase in the mass % recovery. However, there was a more selective recovery of sulphide particles in the first concentrate. Even without optimisation of operating conditions it can be concluded that this technique holds some promise for the separation of coarse sulphidic particles from gangue.

## Conclusions

The behaviour of particles in the froth phase of the reverse froth flotation cell is primarily dependent on the ratio of particle mass to projected area. The lower this ratio, the higher the particle would float in the froth, which results in increased recovery to the tailings or second concentrate. Consequently, the contact angle has only a secondary effect on the overall particle trajectory, in that a decrease in the equilibrium contact angle will result in an increased recovery to the tailings. However,

the particle contact angle has very little effect on the behaviour of large, high density particles, as well as small, low density particles. Particles will therefore only separate on the basis of contact angle as long as the particle mass is between an upper and lower critical value. Nevertheless, for a pyritic ore the addition of xanthate significantly improved the grade and recovery of sulphides in the first compartment. These results were very promising in terms of finding a coarse particle flotation technique. However, several potential problems might exist with the technique, for example:

- the pre-concentration of coarse sulphide bearing minerals is dependent on the liberation of sulphide, as well as the distribution of sulphide between the various particle mass fractions;
- separation in the reverse froth flotation cell is based primarily on the ratio of the mass to projected area of a particle rather than the contact angle.

#### **Acknowledgements**

The financial support of De Beers and the technical contribution of Dr Victor Ross are gratefully acknowledged.

#### **References**

- Dippenaar, A., 1982a. The destabilization of froth by solids. I. The mechanism of film rupture. *Int. J. Miner. Process.*, 9, 1-14.
- Dippenaar, A., 1982b. The destabilization of froth by solids. II. The rate determining step. *Int. J. Miner. Process.*, 9, 15-27.
- Lloyd, P.J.D., 1987. The potential of integrating mining and extraction systems on the Witwatersrand. *Proc. 11th Commonwealth Mining & Metallurgical Congress. IMM. Hong Kong*, 631-643.
- Moxon, N.T. and Keast-Jones, R., 1986. The effect of collector emulsification using non-ionic surfactants on the flotation of coarse coal particles. *Int. J. Miner. Process.*, 18, 21-32.
- Moxon, N.T., Keast-Jones, R. and Aston, J.R., 1988. Increased coarse coal yield from flotation using non-ionic frothers. *Int. J. Miner. Process.*, 24, 295-305.
- Ross, V.E., 1993. Separation Method and Apparatus. SA Patent 93/5367.
- Schubert, H., 1989. On optimum hydrodynamics of coarse particle flotation. *Aufbereitungstechnik*, 30(11), 657-663.
- Van Dyk, W.A., Van Deventer, J.S.J. and Lorenzen, L., 1995. The dynamic behaviour of coarse particles in flotation froths. *Proc. XIX Int. Miner. Process. Congr. (XIX IMPC), Soc. Min. Metall. Expl. (AIME). Littleton, Co., vol. 3, Chapter 16*, 99-103.

## A NEW MAGNETIC SEPARATOR AND CLASSIFIER: CASE STUDY

P.A. Augusto, J.P. Martins

Laboratório de Catálise e Materiais II, Dep. de Eng. Química  
Faculdade de Engenharia da Universidade do Porto, Porto, Portugal

### Abstract

Magnetic separation is a very well developed area. However the conventional magnetic separation methods do not have the ability to classify the particles as they are being separated. We have designed a new magnetic separator and classifier, which (besides the new magnetic separation process) enables the classification of the magnetic particles as they are being separated. In this paper, this new magnetic separator and classifier is presented, and its operation principles are described. As the mode of operation depends on the goal selected, two typical cases are analysed: separation and classification of paramagnetic materials of the same nature (constitution) but with different degrees of purity, and separation-classification of paramagnetic materials by material constitution. Finally, some of the economical advantages of using the new magnetic separator and classifier, and the two different case studies, are pointed out.

*Keywords: magnetic separation, magnetic classification, simulation, industrial application*

### Introduction

Since two or three decades ago, mineral processing industries rely on magnetic separation as a valuable method to attain the separation of minerals. Consequently, several magnetic separators have been developed, a great number of patents on magnetic separation has been submitted, and nowadays we may surely say that the separation of magnetic particles is fulfilled with high accuracy.

The magnetic separators developed so far may be divided into two main categories:

- the ones achieving separation purposes by deflecting the magnetic particles from the main stream (e.g. open gradient magnetic separators - OGMS - Boehm, 1990; Stradling, 1993; Svoboda, 1987);
- the ones achieving separation purposes by collecting the magnetic particles (usually) in matrices (e.g. high gradient magnetic separators - HGMS - Gerber and Birss, 1983; Svoboda, 1987).

Despite all this progress, magnetic separation was still lacking the development of a magnetic separator-classifier that enabled classification of the magnetic particles as they were being separated. Actually, there are some separators already presenting some classification principles (namely achieving some sort of selectivity), but the classification process needed is only partially fulfilled invariably by a cascade flowsheet procedure (Augusto and Martins, 1999b). Bearing this gap in mind, a new magnetic separator and classifier was developed. This new magnetic separator-classifier achieves a differential magnetic classification, allied to a magnetic separation, in a single step and on the same machine. It will be briefly presented next.

### The new magnetic separator-classifier (Augusto, 1999)

The design of the new magnetic separator-classifier is presented in detail in Augusto, (2000) and Augusto and Martins (1999a). The description of the separator-classifier working principles, as well as the support theory, may be found in Augusto (2000); Augusto and Martins (1995); Augusto et al. (1998). Only a brief description will be given here.

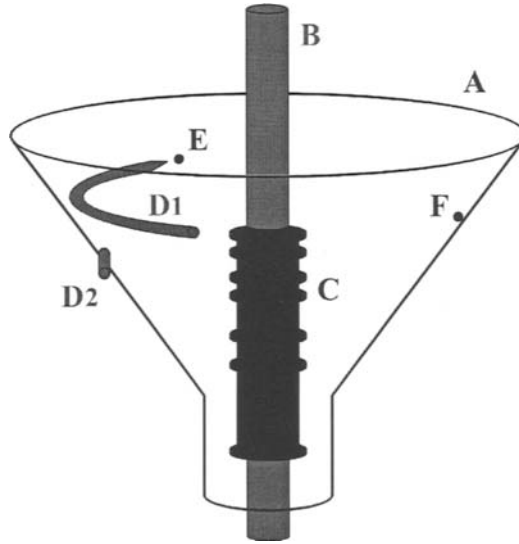


Figure 1: Schematic diagram of the new magnetic separator and classifier. A = funnel-like trunk (which may spin or not); B = superconducting straight wire cable; C = central collector designed to collect magnetic particles by classes; D1 and D2 = feeding systems; E = particle fed at an initial radius  $r_i$ ; F = particle being separated (after Augusto and Martins, 1999a).

A schematic representation of the new magnetic-separator-classifier is depicted in Figure 1. Being composed by a spinning or non-spinning trunk, a feeding system, (which injects the particles tangentially to the surface of the trunk), and a central collector attached to the central superconducting cable, the magnetic separator-classifier achieves the differential classification desired by taking advantage of a wire-configuration system. It is due to the central superconducting magnet which generates a concentric radial decreasing field (Augusto and Martins, 1999a; Jaraíz et al., 1983). This wire-configuration system will give a radial inward direction to the magnetic force defined by (Stradling, 1993):

$$F_m = \frac{m\chi}{\mu_0} B \nabla B \quad (1)$$

(valid for small paramagnetic particles within a media of negligible susceptibility), thus opposing this force to the centrifugal force on the magnetic particles.

Hence, when the magnetic particles are fed to the system, they suffer this force balance between the centrifugal and the magnetic force. If the magnetic susceptibility

of the particles is high enough for the magnitude of the magnetic force to surpass the magnitude of the centrifugal force, the magnetic particles will not move upwards like the other non-magnetic ones, but downwards upon the surface of the trunk. As the magnetic particles descend upon the surface of the separator-classifier, there eventually will be a radius at which the magnetic force (which increases radial inwards) will have such a magnitude that the magnetic particles will depart towards the central collector. Different magnetic susceptibilities imply different take-off radii, thus different heights of arrival at the central collector. Hence, with a central collector properly designed, we obtain the classification of magnetic particles by classes of magnetic susceptibility. The magnetic particles whose magnetic susceptibility magnitude is not high enough for the take-off action will fall at a central base collector.

### Case study

Presented here are the simulations of the separation-classification for two typical cases. They were selected among all the possible ones, because they clearly elucidate two different industrial applications of the new magnetic separator and classifier.

#### *Classification by degree of purity*

The feed is composed of wolframite in several degrees of purity, and also of other diamagnetic, ferromagnetic and paramagnetic particles, whose magnetic susceptibilities are lower than  $4E-7 \text{ m}^3/\text{kg}$  and higher than  $12E-7 \text{ m}^3/\text{kg}$ . The goal is to separate and classify wolframite by degree of purity between 33.24% and 100%. The values of the manipulated variables presented in Table I are set according to this goal, and the simulation of the separation-classification process is depicted in Figure 2.

Table I: Values for the manipulated variables.

Particle	Separator-Classifer
$C_d=0.27$	$\alpha=30^\circ$
$r_{\text{part}}=100 \mu\text{m}$	$\omega=6 \text{ rads}^{-1}$
$\rho_p=7510 \text{ kg/m}^3$	$\mu=0.2$
$\rho_f=1.24 \text{ kg/m}^3$	$r_i=0.3 \text{ m}$
$\chi$ (wolframite 100%) = $12E-7 \text{ m}^3/\text{kg}$	$r_a=0.12 \text{ m}$
	$r_c=0.09 \text{ m}$
	$T_{CG2}=1.05$
	$I=4.44E6 \text{ A}$

Figure 3 schematically sums up all the trajectories followed by the different particles presented in the feed selected for this case (notice also the presence of the trajectories of the diamagnetic, weak paramagnetic and ferromagnetic particles).

#### *Classification by material constitution (selectivity)*

The feed is composed of wolframite, hematite, cromite, rodonite (all 100% pure), and also by other diamagnetic, ferromagnetic and paramagnetic particles whose magnetic susceptibilities are lower than  $3.8E-7 \text{ m}^3/\text{kg}$  and higher than  $26.6E-7 \text{ m}^3/\text{kg}$ .



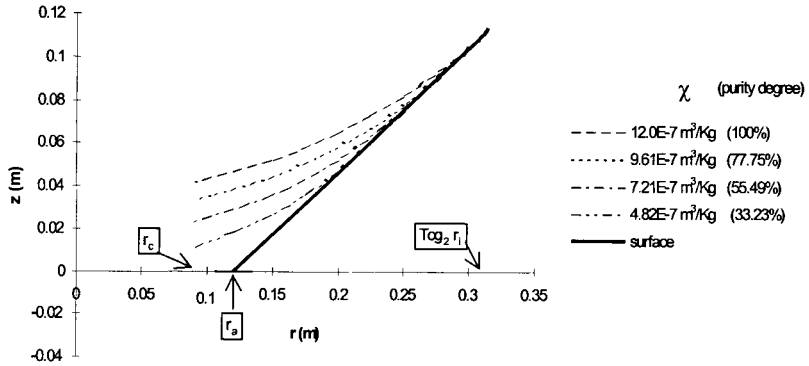


Figure 2: Simulations of the paths followed by wolframite particles of different degrees of purity.

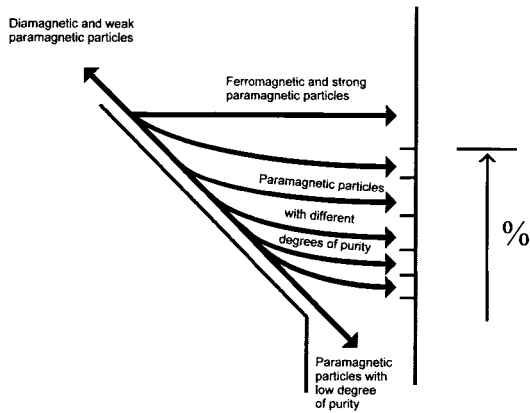


Figure 3: Schematic representation of the trajectories followed by all types of particles fed to the system.

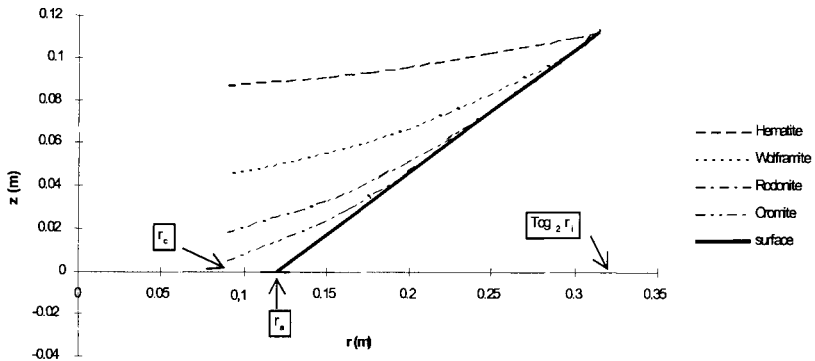


Figure 4: Simulations of the paths followed by particles of different paramagnetic materials (100% pure).

The goal is to separate and classify the four classes of paramagnetic materials by material constitution.

The values of the manipulated variables presented in Table II are set according to this goal, and the simulation of the separation-classification process is depicted in Figure 4.

Figure 5 schematically sums up all the trajectories followed by the different particles presented in the feed selected for this case (to notice also the presence of the trajectories of the diamagnetic, weak paramagnetic and ferromagnetic particles).

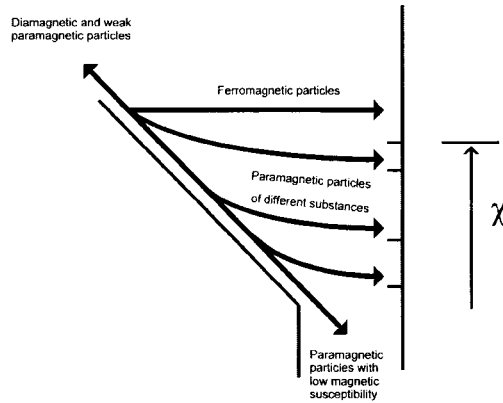


Figure 5: Schematic representation of the trajectories followed by all types of particles fed to the system.

Table II: Values for the manipulated variables.

Particles				Separator-Classifier
$C_d = 0.27; r_{part} = 100 \mu\text{m}; \rho_f = 1.24 \text{ kg/m}^3$				$\alpha = 30^\circ; \omega = 6 \text{ rads}^{-1}$
Hematite	Wolframite	Rodonite	Cromite	$\mu = 0.2; r_i = 0.3 \text{ m}$
$\rho_p = 5,260 \text{ kg/m}^3$	$\rho_p = 7,510 \text{ kg/m}^3$	$\rho_p = 3,760 \text{ kg/m}^3$	$\rho_p = 5,100 \text{ kg/m}^3$	$r_a = 0.12 \text{ m}; r_c = 0.09 \text{ m}$
$\chi = 26.6\text{E-}7 \text{ m}^3/\text{kg}$	$\chi = 12\text{E-}7 \text{ m}^3/\text{kg}$	$\chi = 6.7\text{E-}7 \text{ m}^3/\text{kg}$	$\chi = 3.8\text{E-}7 \text{ m}^3/\text{kg}$	$T_{CG2} = 1.05; I = 4.44\text{E}6 \text{ A}$

## Discussion and conclusions

For a long time, magnetic separation has been pursuing a magnetic separator, which can also perform as a magnetic classifier. The new magnetic separator and classifier developed and presented here is intended to fulfil this objective.

There are many ways to operate this new magnetic separator and classifier, which will vary according to the objective we bear in mind. Two typical cases were studied representing two different goals: the separation and classification of paramagnetic materials of the same nature (constitution) but with different degrees of purity (case A), and the separation-classification of paramagnetic materials by class of material constitution (case B).

Relating to other separation techniques and devices, the operation on the case A mode, will improve the costs associated, namely with solvent expenditures, while the operation on the case B mode will lower the overall costs, by offering a separation

and classification of several paramagnetic materials at the same step, avoiding the several cycles needed on other separating devices to fulfil this goal. Regardless of the operation mode, the new magnetic separator and classifier will also improve the economics, as it uses the same machine and the same stage to achieve the separation and classification of magnetic particles.

### **References**

- Augusto, P.A., 1999. Separador e classificador magnético. Submitted Patent Nr. 102326-B.
- Augusto, P.A., 2000. Separação de partículas em meios fluidos sob a acção simultânea dum campo centrífugo e magnético ou eléctrico. Ph.D.Thesis, Faculdade de Engenharia da Universidade do Porto, Porto, Portugal.
- Augusto, P.A. and Martins, J.P., 1995. A new prototype to separate solid particles by centrifugal and magnetic forces. Filtration and Separation: International Symposium, A. Macías-Machín, A. Estevez and E. Jaraíz (Editors), Salamanca, Spain, 174-183.
- Augusto, P.A. and Martins, J.P., 1999a. A new magnetic separator and classifier: prototype design. Minerals Engineering, 12 (7), 799-807.
- Augusto, P.A. and Martins, J. P., 1999b. Innovation features of a new magnetic separator and classifier. Paper submitted to ICRM'98 – India to be published in Minerals Processing and Extractive Metallurgy Review.
- Augusto, P.A., Martins, J.P. and Villate, J., 1998. A new prototype to separate solid particles by centrifugal and magnetic forces: further developments. Filtration and Separation II: International Symposium. A. Macías-Machín and A. Estevez (Editors), Las Palmas de Gran Canaria, Spain, 339-348.
- Boehm, J., 1990. A study of the open gradient magnetic separation method. Ph.D. Thesis, University of Salford, Salford, UK.
- Gerber, R. and Birss, R.R., 1983. High gradient magnetic separation. Research Studies Press, John Wiley and Sons Ltd., Letchworth.
- Jaraíz-M., E., Levenspiel, O. and Fitzgerald, T. J., 1983. The uses of magnetized fields in the processing of solids. Chemical engineering Science, 38 (1), 107-114.
- Stradling, A.W., 1993. The physics of open-gradient dry magnetic separation. International Journal of Mineral Processing, 39, 1-18.
- Svoboda, J., 1987. Magnetic methods for the treatment of minerals. Elsevier Science Publishers, Amsterdam.

## REMOVAL OF SULFUR AND MINERAL MATTER FROM COAL SLURRY BY A PILOT SCALE WET MAGNETIC SEPARATOR

H. Dinçer, G. Ateşok, M. Z. Doğan, Ş. Girgin, F. Boylu, Ö. Yüksel

Istanbul Technical University, Mining Faculty,  
Mineral Processing Department, Turkey

### Abstract

In order to remove sulfur and inorganic matter content of coal, high intensity magnetic separation tests were carried out, where % solids in the pulp, current intensity in ampere, feed rate and middling wash water were investigated. Under optimum conditions, a clean coal was obtained having 8.10% ash, 1.56% total sulfur, with a combustible recovery of almost 50% from coal, with 12.70% ash and 2.82% total sulfur.

*Keywords: clean coal, ash, sulfur, magnetic separation, Jones magnetic separator*

### Introduction

High-intensity wet magnetic separation (HIWMS) is a relatively new technology, which promises to be a practical method for separating micrometer-sized, weakly magnetic materials on a large scale. The technology is also applicable to separating nonmagnetic materials, which can be made to associate with magnetic seeding materials, such as magnetite.

A promising application of HIWMS is the magnetic removal of inorganic sulfur and ash-forming minerals from coal. Previous experimental investigations have indicated clearly that most of the mineral impurities in coal, which contribute to its pyritic sulfur and ash content, are weakly magnetic (called paramagnetic). Those sulfur-bearing and ash-forming minerals, if sufficiently liberated as discrete particles, can be separated normally from the pulverized diamagnetic or practically non-magnetic coal by magnetic separation (Dinçer et al., 1997; Lua and Boucher, 1990; Özbayoğlu, 1986; Hall and Finch, 1984). Indeed, HIWMS was successfully adopted in 1973 in a bench-scale study to remove sulfur and ash from a finely pulverized Brazilian coal suspended in water (Trinolade and Kolm, 1973; Trinolade and Howard, 1974).

Since then, the technical feasibility of utilizing cyclic and continuous HIWMS units for the magnetic separation of sulfur and ash from water slurries of pulverized United States coals has been demonstrated in a number of experimental studies. Substantial amounts of sulfur and ash removal have been achieved (Lin et al., 1976; Stekly et al., 1980; Wescher et al., 1980). There are many successful studies and applications of HGMS to dry coal desulfurization (Dinçer et al., 1997; Lua and Boucher, 1990; Özbayoğlu, 1986; Arvidson and Bainbrigge, 1992; Arvidson, 1988). The thermal treatment and microwave radiation (dielectric heating) have been used to convert pyrite to more magnetic compounds of iron, thereby increasing the efficiency of the subsequent magnetic beneficiation (Ateşok et al., 1999; Yıldırım et al., 1996; Akoto,

1976; Ergun and Beam, 1968). Also several chemical methods have been investigated for converting pyrite and ash forming minerals in coal to strongly magnetic forms (Wescher. et al., 1980). One new method is the Magnex process, which exposes a dry pulverized coal to gaseous iron carbonyl  $[\text{Fe}(\text{CO})_5]$  under conditions whereby the pyrite and ash become strongly magnetic and can be efficiently removed from coal by magnetic separation (Kinding and Turner, 1976; Kinding, 1979; Porter, 1978). In this study, a large scale electromagnetic Jones HIWMS was used. Effects of field intensity, coal particle size, coal slurry concentration, slurry flow velocity (residence time) and characteristics of separator matrix were investigated to remove sulfur and mineral matter from coal slurry. The coal sample, which was used in this study, was coming from the lignite district in Istanbul, Turkey.

## Experimental

### Materials

High-intensity wet magnetic separation tests were carried out on lignite samples taken from a disposal site in the Istanbul region. The lignite samples were –100 mm in size and contained 12.70% ash and 2.82% sulfur. This coal sample was subjected to crushing to reduce the sample to minus 6 mm. After that, the <6.0 mm coal sample was ground to minus 0.2 mm and 0.1 mm sizes by using a ball mill. Magnetic separation tests were conducted with <0.2 mm and <0.1 mm fractions. The complete analysis of the sample on dry basis is presented in Table I.

Table I. Analysis of the lignite sample.

Item		Dry Coal
Ash	(%)	12.70
Total sulfur	(%)	2.82
Pyritic sulfur	(%)	1.12
Organic sulfur	(%)	1.45
Volatile matter	(%)	45.00
Upper calorific value	(kcal/kg)	5,780
Lower calorific value	(kcal/kg)	5,455

### Methods

Magnetic separation tests were carried out by a High-intensity wet magnetic separator, namely, JONES P 40. In the P 40 Jones magnetic separator, magnetic field intensity can be increased to 16,000 G. With this separator, separation can be made with ores in fine size and high capacities up to 250 kg/h. The P 40 Jones magnetic separator has 2 rotors. Each rotor has a 400 mm diameter with 11 sections. There are 5 plates in each section. Plates have gap distances of 1.25 mm, 1.0 mm, 0.8 mm, 0.6 mm, 0.45 mm and 0.3 mm. These gaps are formed by wires with diameters of 2.1 mm, 2.0 mm, 1.8 mm, 1.7 mm, 1.6 mm and 1.5 mm. Ore is fed to the Jones magnetic separator in pulp form through a plate chamber. These chambers are placed between the magnetic poles. Magnetic particles in the ore pulp will stick to the corrugated plates. Non-magnetic particles are taken below the feed. When the rotor moves in magnetic field, wash water is sent onto the corrugated plates to wash the particles, so

that non-magnetic particles (middlings) are separated. Magnetic particles on the corrugated plates are washed with wash water under pressure, so that they are taken outside the separator. The qualities of the products, namely, magnetic, non-magnetic and middling, can be adjusted through knives below the separation chambers. The effective separation of sulfur and mineral matter from coal can be realized by the use of the P 40 Jones magnetic separator. This high-intensity magnetic separator was manufactured by German V-HD Humbolt Wedag ACo Company in order to apply concentration of ores with low magnetic susceptibility.

All the tests in Jones separator were executed in single stage. In each test, a 1.0 kg sample was fed, and the magnetic, middling and non-magnetic fractions were collected and analyzed for sulfur and ash. Gap distances were adjusted to 0.3 mm during the tests, and the feed with the specified percent of solids was placed in the feeder with a specified feed rate, middling wash water rate, and current in amperes. In order to reach a stable state of separation, a certain time period is needed. Samples from the products were taken at 5 s intervals four times.

During grinding and test runs, no oxidation was allowed. Total sulfur and calorific values were determined by a MET carbon-sulfur analyzer and IKA Isoperibolic Calorimeter, respectively. Ash content was determined by ASTM standards and sulfatic sulfur by a gravimetric method, using  $\text{BaCl}_2$  and pyritic sulfur, dissolving it in HCl, and analyzing the insoluble for iron by an atomic absorption spectrophotometer. Organic sulfur was calculated as the difference.

### Results and discussion

Parameters were changed in the magnetic separation tests, as shown in Table II, where the coal sample was <0.2 mm in size.

Table II. Values of the parameters adopted for the Jones magnetic separator.

Feed rate (l/h)	Solids in pulp (%)	Middling wash water (l/h)	Current (A)
120	5	100	3.0
140	10	120	4.5
160	15	140	6.8

#### *Effect of solids in the pulp*

Magnetic field intensity was at 6.8 A, with a 140 l/h feed rate and 120 l/h middling wash water. Tests were made with solids at 5%, 10%, and 15%. The results are shown in Figure 1. As it can be seen from Figure 1, when the 5% of solids in the pulp are increased, the ash and total sulfur of clean coal are increased as well. Combustible recovery of clean coal shows an increase of 9% when the % of solids is increased from 5% to 10%. The combustible recovery increase is only 1% when the % of solids is increased from 10% to 15%.

#### *Effect of current intensity*

The results of tests where current intensity is changed as 3.0 A, 4.5 A and 6.8 A at 10% solids in pulp, 140 l/h feed rate and 120 l/h middling wash water are shown in Figure 2. As it is seen from Figure 2, ash and total sulfur of clean coal is decreased

when current intensity is increased. On the other hand, combustible recovery is diminished linearly when current intensity is raised.

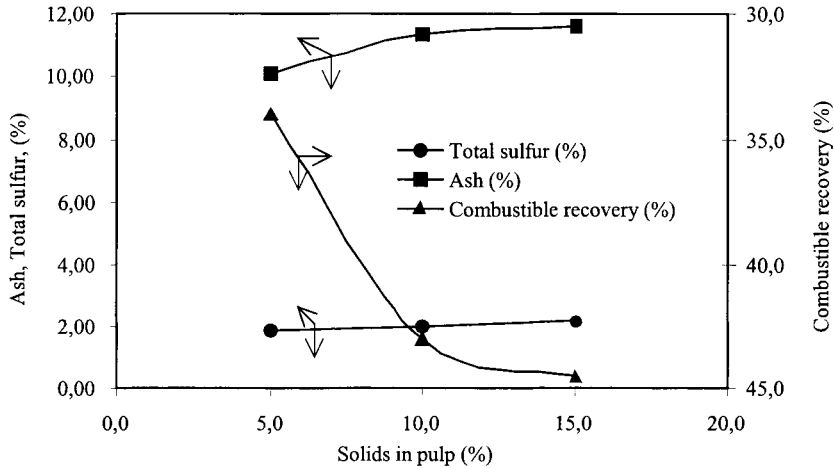


Figure 1. Ash, total sulfur and combustible recovery of clean coal by changing % of solids in the pulp.

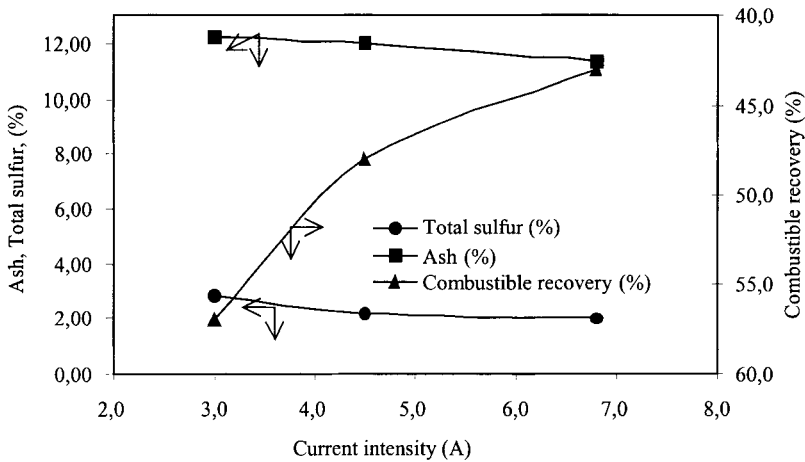


Figure 2. Ash, total sulfur and combustible recovery of clean coal by changing magnetic field intensity.

*Effect of feed rate*

Feed rate was investigated at 120 l/h, 140 l/h and 160 l/h by keeping the % of solids in the pulp at 10% by weight, the currency as 6.8 A and the middling wash water rate at 120 l/h. The results are shown in Figure 3. As it is seen in Figure 3, the lowest ash and total sulfur were achieved at the 140 l/h feed rate. On the other hand, combustible recovery increased when feed rate was raised.

*Effect of middling wash water*

The 10% of solids in the pulp, 6.8 A current intensity and feed rate of 140 l/h were kept constant. The middling wash water rate was changed to 100 l/h, 120 l/h and 140 l/h. The results are shown in Figure 4. As seen in the figure, the lowest ash and total sulfur values of clean coal were obtained at a 140 l/h wash water rate, whereas combustible recovery decreased when middling wash water rate was increased.

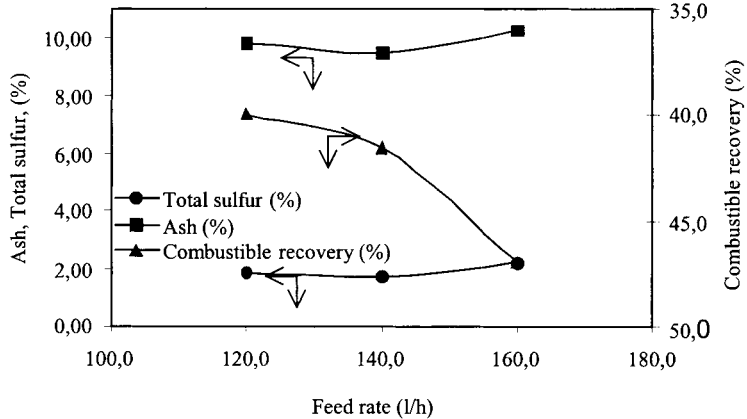


Figure 3. Ash, total sulfur and combustible recovery of clean coal by changing feed rate.

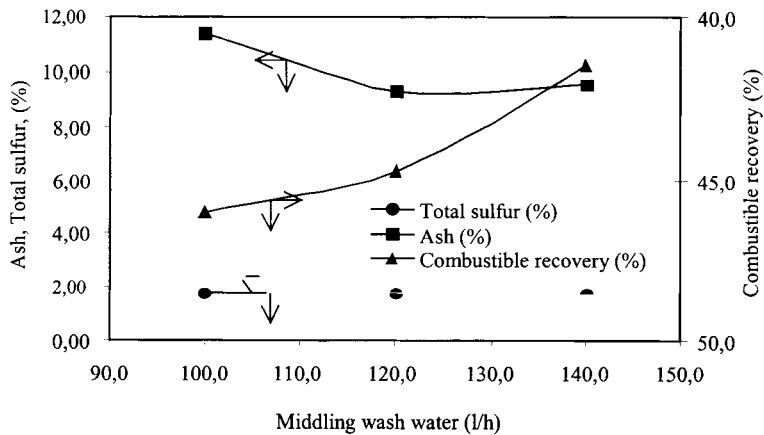


Figure 4. Ash, total sulfur and combustible recovery of clean coal by changing middling wash water.

*Magnetic separation tests in stages under optimum conditions*

Optimum conditions were determined previously, and magnetic separation tests were executed in stages;

- solids in the pulp = 10%
- feed rate = 140 l/h
- middling ash water = 140 l/h



The whole coal was reduced to 0.2 mm and 0.1 mm, and then the Jones magnetic separation tests were carried out in stages. The flowsheet is shown in Figure 5 and test results in Table III.

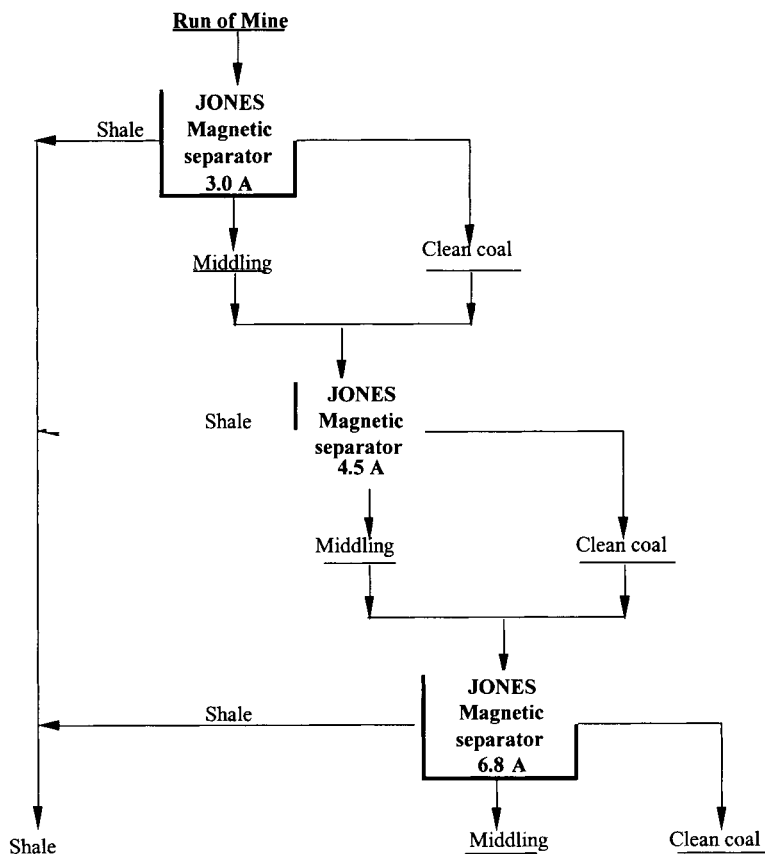


Figure 5. Magnetic separation flowsheet for coal in 0.2 mm and 0.1 mm, beneficiated on Jones magnetic separator.

As is seen in Table III, clean coal obtained from a minus 0.2 mm coal sample has an ash content of 8.61%, with a total sulfur content of 1.74% when the whole coal sample was reduced in size to minus 0.1 mm.

Then clean coal was obtained, with 8.10% ash, 1.56% total sulfur and combustible recovery of 48.16%, against 45.26% combustible recovery in the minus 0.2 mm coal sample.

Better results were obtained with the minus 0.1 mm coal sample, due to better liberation, as far as pyritic sulfur and ash-forming minerals were concerned.

With a Jones magnetic separator, clean coal, with 1.5% total sulfur, 8.0% ash and 50% combustible recovery was obtained.

Table III. Test results of magnetic separation carried out under optimum conditions.

Size (mm)	Product	Weight (%)	Total sulfur (%)	Ash (%)	Combustible recovery (%)
0.2	Clean Coal	42.3	1.74	8.61	45.26
	Middling	36.6	1.83	9.02	45.60
	Shale	20.1	6.94	28.20	9.14
	Total	100.0	2.82	12.70	100.0
0.1	Clean Coal	45.8	1.56	8.10	48.16
	Middling	26.8	1.80	8.87	27.95
	Shale	27.4	5.85	23.89	23.89
	Total	100.0	2.82	12.70	100.0

### References

- Akoto, I.Y., 1976. High gradient magnetic separation: effect of temperature on performance. IEEE Trans. Magn., MAG-12, 511.
- Arvidson, B.R. and Bainbrigg, I., 1992. New Rare-Earth Magnetic Roll Separator Developments. In proceedings of the 10<sup>th</sup> Industrial Minerals Int. Cong., USA, 179-183.
- Arvidson, B.R., 1988. Advances in Fine Particle Dry High-Intensity Magnetic Separation. In: Proceedings of the 27<sup>th</sup> Annual Conf. of Metall. of CIM. Quebec, Canada, Paper No, 13.4.
- Ateşok, G., Perek, K.T., Dinçer H. and Çelik M.S., 1999. Reduction of Ash and Sulfur Contents of Low-Rank Turkish Semicoked Lignite by High Intensity Dry Magnetic Separation. Coal Preparation, 20,3-4.
- Dinçer, H., Önal, G., Ateşok, G. and Yıldırım, İ., 1997. Concentration of Coal by REMS High Intensity Magnetic Separator. 7<sup>th</sup> Balkan Conf. on Mineral Processing, Romania, May, Vol.II, 69-74.
- Ergun, S. and Beam, E.H., 1968. Magnetic Separation of Pyrite from Coals. U.S. Bureau of Mines, Report of Investigation, No 7181.
- Hall, S.T. and Finch, J.A., 1984. Enhanced Magnetic Desulphurization of Coal, Minerals and Metallurgical Processing. Nov., Vol. I.
- Kinding, J.K. and Turner, R.L., 1976. Process for Improving Coal. U.S. Patent3, 938,966
- Kinding, J.K., 1979. The Magnex Process, Review and Current Status in Industrial Applications of Magnetic Separation. IEEE Publ. No. 78CH447-2 MAG, Institute of Electrical and Electronic Engineering, U.S.A., 99-104.
- Lin, C.J., Liu, Y.A., Vives, D.L., Oak, M.J., Crow, G.E. and Hauffman, E.L., 1976. Pilot-Scale Studies of Ash and Sulfur Removal from Coals by High Gradient Magnetic Separation. IEEE Trans. Magn., MAG-12, 513.
- Lua, A.C. and Boucher, R.F., 1990. Sulfur and Ash Reduction in Coal by HGMS. Coal preparation, Vol. 8, 61-71.
- Özbayoglu, G., 1986. Desulfurization of Lignites by High Gradient Magnetic Separation. The First Int. Min. Process. Symp., Vol. 2, Türkiye, 635-645.
- Porter, C.R., 1978. The Magnex Process. Coal Conference and Expo V, Louisville, Ky.
- Stekly, Z.J.J., Mallary, M.L. and Segal, H.R., 1980. Coal Preparation Using Magnetic Separation. EPRI Report No: CS-1517, Vol. 2, Electric Power Research Institute, USA.
- Trinolade, S.C. and Kolm, H.H., 1973. Magnetic Desulfurization of Coal. IEEE Trans. Magn, MAG-9, 310.
- Trinolade, S.C. and Howard, J.B., 1974. Magnetic Desulfurization of Coal. Fuel, 53, 178.
- Wescher, I., Doulin, J. and Eddy, R., 1980. Coal Preparation Using Magnetic Separation. EPRI Report No, CS-1517, Vol. 3, Electric Power Research Institute, USA.
- Yıldırım, I., Dinçer, H., Önal, G. and Çelik M.S. 1996. Upgrading of a Low-Rank Semicoked Lignite by High Intensity Dry Magnetic Separator. 6<sup>th</sup> Int. Min. Proc. Sym., Kuşadası-Türkiye, 137-143.

## STUDY OF SEPARATION OF REFRACTORY SULFIDE MINERALS BY HGMS

Y. Zhang, S. Liu, W. Fu

Mineral Processing Department, Institute of Multipurpose Utilization of Mineral Resources, Fax 0086-28-5594582; e-mail dkbzhs@mail.sc.cninfo.net  
MGMR, 5 Section 3 South Ring Road 2, Chengdu, Sichuan, 610041, P.R. China

### Abstract

The separation efficiency and separation principles for Cu-Pb and Cu-Zn sulfide concentrates with conventional non-vibrating and non-pulsating HGMS, single vibrating HGMS, single pulsating HGMS, and complex vibrating-pulsating HGMS have been investigated. The experimental results show that each HGMS technology can achieve a better separation efficiency for Cu-Pb and Cu-Zn sulfide minerals. Especially by use of complex vibrating-pulsating HGMS, optimal separation efficiency could be attained.

*Keywords: magnetic separation, Cu-Pb sulfide mineral, Cu-Zn sulfide mineral, vibrating HGMS, pulsating HGMS, complex vibrating-pulsating HGMS*

### Introduction

At present, flotation separation is an important process for separation of non-ferrous sulfide minerals. With an increase in the mining production and floatability of, complex sulfide ores or mutually activated metallic ions (such as Cu-Pb or Cu-Zn sulfide minerals), the flotation separation for these bulk concentrates becomes problematic. For instance, there is poor separation efficiency, overdosage, high cost, environmental pollution, and so on. However, sulfide minerals show large differences in their magnetic properties. For example, the average value of the specific susceptibility of pure chalcopyrite is  $0.84 \cdot 10^{-6} \text{ m}^3/\text{kg}$ , which is a paramagnetic mineral. But the specific susceptibility of pure sphalerite and pure galena, which are diamagnetic minerals, is  $-0.026 \cdot 10^{-6} \text{ m}^3/\text{kg}$  and  $-0.62 \cdot 10^{-6} \text{ m}^3/\text{kg}$ , respectively. Therefore, a combined magnetic flotation-separation flowsheet is adapted for treating these complex, refractory, non-ferrous sulfides. Maximum economic benefits and social effects can be gained. Thus, in recent years, many researchers have been engaged in investigation of magnetic separation of Cu-Pb or Cu-Zn bulk sulfide flotation concentrates, and obvious progress has been achieved. Along with the rapid development of magnetic separation technology, in particular, the complex vibrating-pulsating HGMS method, which is the basic process of the magnetic separation of sulfide minerals, has been developed. Thus, further research in this field is necessary.

### Experimental device

The laboratory equipment of a complex vibrating-pulsating HGMS device is shown in Figure 1. It mainly consists of T-type magnetic systems, a separation box, a vibrating coil, a pulsating mechanism, and so on. Its maximum background magnetic

field strength is 1,400 kA/m. The separation box is specialized to ensure the magnetic matrix which is consistently submerged in the pulp during the course of separation. The vibrating coil is fixed on the separation box above the magnetic head. When inputting a 1÷3 A alternating current, the effect of variable magnetic moment on the coil in the background magnetic field enables the separation box to produce vibration. The vibrating frequency of the coil is 50 Hz. The amplitude adjustment is dependent upon the gap between the separation box and the magnetic head; this is 2 mm in both cases. The pulsating mechanism consists of an eccentric connecting-rod mechanism, by which a rubber diaphragm of a cone-shaped compartment is driven in an up-and-down movement through the connecting tube that makes the pulp pulse up-and-down in the separation compartment. The pulsating frequency can be continuously adjusted within the range of 0÷500 r/min, the pulsating stroke of the pulp is in the range of 0÷20 mm, and decreases with an increase in frequency. The magnetic matrix is a meshed plate of stainless steel; the loading ratio of matrix is 7%.

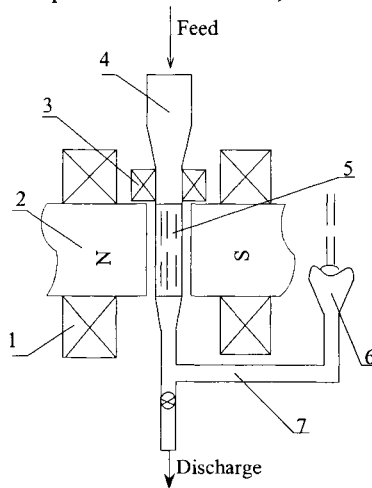


Figure 1: Complex vibrating-pulsating HGMS device: 1 = Energizing coil; 2 = Magnetic core; 3 = Vibrating coil; 4 = Separation box; 5 = Magnetic matrix; 6 = Pulsating mechanism; 7 = Tube.

## Material

The material used is a Cu-Pb-Zn bulk-flotation concentrate from a polymetallic sulfide ore. Its mineral composition is: sphalerite = 60.2%, chalcocopyrite = 26.1%, galena = 4.2%, pyrite and quartz, and other gangue minerals = 9.5%. The sample assays are: Zn = 40.32%, Cu = 8.97% and Pb = 3.60%. The degrees of liberation of the valuable minerals are: sphalerite = 88.82%, chalcocopyrite = 77.10% and galena = 94.94%; others are Cu, Pb, Zn, pyrite, and a gangue of locked-middling grain. The average specific susceptibilities of the valuable minerals are: sphalerite =  $-0.0018 \cdot 10^6$  m<sup>3</sup>/kg, chalcocopyrite =  $0.68 \cdot 10^{-6}$  m<sup>3</sup>/kg and galena =  $-0.068 \cdot 10^{-6}$  m<sup>3</sup>/kg. The particle size distribution is shown in Table I. Before the magnetic separation tests, the removal of the reagents from the samples and dispersion of the samples have been accomplished.

Table I: Size fraction analysis of samples.

Size fraction ( $\mu\text{m}$ )	Yield (%)	Grade (%)			Distribution (%)		
		Zn	Cu	Pb	Zn	Cu	Pb
+74	17.28	37.93	8.64	3.59	16.29	16.60	17.25
-74+38	35.40	41.69	9.31	3.70	36.68	36.66	36.43
-38	47.32	39.98	8.88	3.52	47.03	46.74	46.32
Total	100.00	40.23	8.99	3.60	100.00	100.00	100.00

## Results and discussion

In the tests, the magnetic product is a Cu concentrate; the non-magnetic product is a Pb-Zn concentrate. During each test, 900 g/t sodium hexametaphosphate and 250 g/t sodium carbonate were added to enhance the dispersing efficiency.

### Magnetic field strength (H) tests

Fixed experimental conditions: pulsating frequency (fp) = 150 r/min, vibrating current (Iv) = 0.5 A, flow velocity of pulp ( $V_0$ ) = 2.5 cm/s, loading ratio (RI) = 0.286. Experimental results obtained under different magnetic field strengths are shown in Figure 2 (from Figure 2 to Figure 6, the following symbols have been used:  $\beta_{\text{Cu}}$  = Cu content of magnetic product, %;  $\varepsilon_{\text{Cu}}$  = decoppering rate of non-magnetic product, %;  $\varepsilon_{\text{Zn}}$  = Zn recovery of non-magnetic products, %;  $\varepsilon_{\text{Pb}}$  = Pb recovery of non-magnetic product, %).

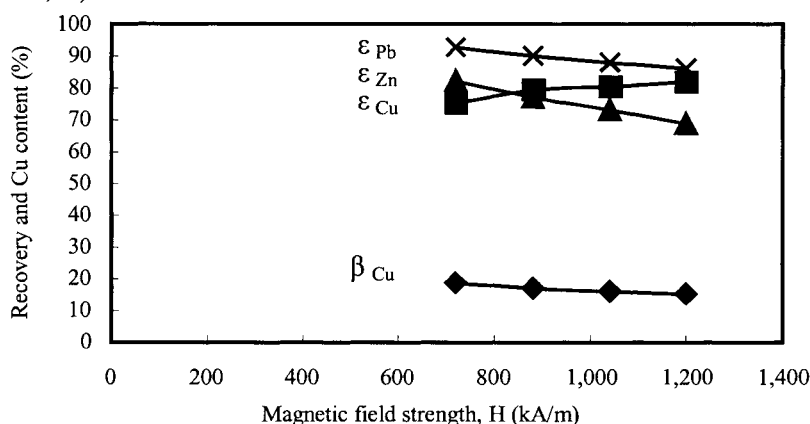


Figure 2: Relation of magnetic field strength and separation index.

The experimental results show that an increase in the background magnetic field strength can effect that the Cu content of the magnetic product and Pb-Zn recovery of the non-magnetic product to gradually fall, and the decoppering rate to gradually rise. After overall evaluation of the corresponding index, the magnetic field strength of 880 kA/m was finally chosen. The separation results obtained are: Cu concentrate grade = 17.02% Cu; Pb-Zn concentrate grade = 3.13% Cu, decoppering rate = 79.77%, Zn recovery = 77.08%, Pb recovery = 90.30%.

*Vibrating current (Iv) tests*

Fixed experimental conditions:  $H = 880 \text{ kA/m}$ ,  $f_p = 1,500 \text{ r/min}$ ,  $V_0 = 2.5 \text{ cm/s}$ ,  $RI = 0.286$ . The experimental results obtained under different vibrating currents are shown in Figure 3.

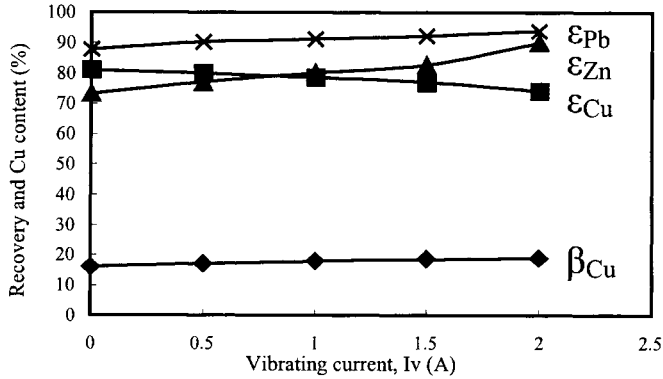


Figure 3: Relation of vibrating current and separation index.

The experimental results indicate that the increase in the vibrating current caused a gradual rise in the Cu content of the magnetic product and Pb-Zn recovery of the non-magnetic product, and a gradual fall in the decoppering rate. After overall consideration of the corresponding index, a vibrating current of 1.0 A was chosen. The separation results obtained under these conditions are as follows: Cu recovery = 78.49%; Zn recovery = 80.54%; and Pb recovery = 91.57%.

*Pulsating frequency (fp) tests*

Fixed experimental conditions:  $H = 880 \text{ kA/m}$ ,  $I_v = 1.0 \text{ A}$ ,  $V_0 = 2.5 \text{ cm/s}$ ,  $RI = 0.286$ . The experimental results obtained under different pulsating frequencies are shown in Figure 4.

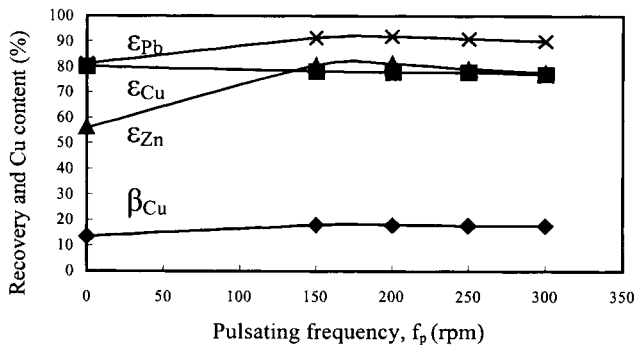


Figure 4: Relation of pulsating frequency and separation index.

The experimental results show that after the addition of a pulse, the Cu content of the magnetic product and Pb-Zn recovery of the non-magnetic product may significantly increase. However, a pulsating frequency that is too high could cause a negative effect on the separation process. This is mainly due to the fact that too high pulsating frequencies can result in a decrease in the corresponding stroke. Thus the pulsating force produced will be greatly decreased, so that the elimination of non-magnetic products from magnetic products becomes difficult. From this figure, it is obvious that the optimal pulsating frequency is in the range of 150÷200 r/min.

#### *Pulp-flow velocity ( $V_0$ ) tests*

Fixed experimental conditions:  $H = 880$  kA/m,  $I_v = 1.0$  A,  $f_p = 160$  r/min,  $R1 = 0.286$ . The experimental results obtained under different pulp-flow velocity are shown in Figure 5.

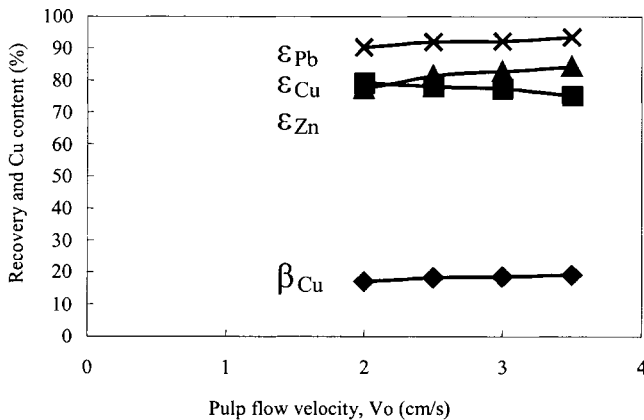


Figure 5: Relation of pulp-flow velocity and separation index.

The results obtained indicate that the pulp-flow velocity does not only have an effect on the capacity of the equipment, but also on the capture ability of magnetic minerals. After an analysis in more detail, the pulp-flow velocity of 3.0 cm/s was chosen.

The separation results obtained in this situation are the following:

Cu grade of Cu concentrate = 18.57%, Cu grade of Pb-Zn concentrate = 3.23%, decoppering rate = 77.47%, recoveries for Zn concentrate = 82.88% Zn and for Pb concentrate = 92.50% Pb.

#### *Loading ratio (Rl) tests*

Fixed experimental conditions:  $H = 880$  kA/m,  $I_v = 1.0$  A,  $f_p = 160$  r/min,  $V_0 = 3.0$  cm/s. The separation results obtained under different loading ratio are shown in Figure 6. The Loading ratio is the feed rate that can load the unit mass magnetic matrix. Its magnitude has direct influence on the capacity of the equipment. However, for any given amount of magnetic matrix, the capture ability also has definite limitations, and when in excess of this boundary, effective separation cannot be accomplished. The experimental results indicate that a better separation index can be

obtained when the loading ratio is in the range of  $0.143 \div 0.3$ . In the interest of safety, the loading ratio of 0.286 was finally chosen.

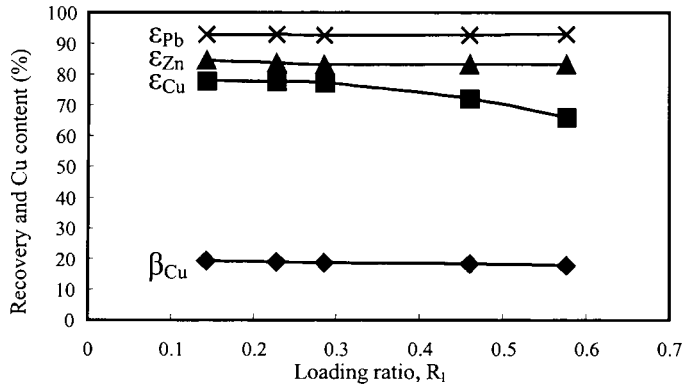


Figure 6: Relation of loading ratio and separation index.

#### *Comparative tests of HGMS in different composite force fields*

Up to now, there have been four kinds of HGMS in different composite force fields, namely: conventional, non-vibrating and non-pulsating HGMS; single vibrating HGMS; single pulsating HGMS; and complex, vibrating-pulsating HGMS. For a comparison of the effect of the magnetic separation on the separation index for different composite force fields, optimal conditions were selected, based on extensive tests. The fixed test conditions were listed in Table II, and the comparative test results were summarized in Table III.

Table II: Fixed conditions of comparative tests for magnetic separation HGMS for different composite force fields.

Name of composite force field	H	Iv	fp	$V_0$	Rl	$(NaPO_3)_6$	$Na_2CO_3$
	(kA/m)	(A)	(r/min)	(cm/s)		(g/t)	(g/t)
Non-V and Non-P	1,040	/	/	3.0	0.143	900	250
Single vibrating	1,040	1.5	/	3.0	0.143	900	250
Single pulsating	960	/	200	2.5	0.228	900	250
Complex V-P	840	1.0	160	2.5	0.286	900	250

Preliminary survey of separation principles of HGMS for different composite force fields.

The separation process' schematic diagram of HGMS for different composite force fields is shown in Figure 7.

Generally, fine particle sizes are separated by HGMS. According to the theory of electromagnetism and surface chemistry, in the magnetic separation system based on fluid medium, the mineral particles suffer from the combined forces of the electrical double-layer force, the London-Van der Waals force, the remaining magnetic force and the fluid shear stress, which favors coagulation and adhesion between mineral



particles separating one another, and in between mineral particles and the magnetic matrix.

Table III: Results of comparative tests for HGMS in different composite force fields.

Name of composite force field	Name of product	Yield (%)	Grade (%)			Recovery (%)		
			Cu	Pb	Zn	Cu	Pb	Zn
Non-V and Non-P	Magnetic	50.97	13.82	1.39	28.66	78.69	19.46	36.22
	Non-magnetic	49.03	3.89	5.98	52.46	21.31	80.54	63.78
	Feed	100.00	8.95	3.64	40.33	100.00	100.00	100.00
Single vibrating	Magnetic	45.60	15.26	0.84	26.53	77.84	10.58	30.03
	Non-magnetic	54.40	3.64	5.99	51.81	22.16	89.48	69.97
	Feed	100.00	8.94	3.64	40.28	100.00	100.00	100.00
Single pulsating	Magnetic	42.98	16.15	0.75	22.45	77.47	8.88	23.94
	Non-magnetic	57.02	3.54	5.80	53.75	22.53	91.12	76.06
	Feed	100.00	8.96	3.63	40.30	100.00	100.00	100.00
Complex V-P	Magnetic	37.11	18.68	0.72	18.47	77.28	7.34	17.01
	Non-magnetic	62.89	3.24	5.36	53.18	22.72	92.66	82.99
	Feed	100.00	8.97	3.64	40.30	100.00	100.00	100.00

As shown in Figure 7(a), in the conventional HGMS, flocculation of the magnetic particles can enlarge the apparent size of particles, thus favoring capture with the magnetic matrix and achieving better recovery of the magnetic minerals.

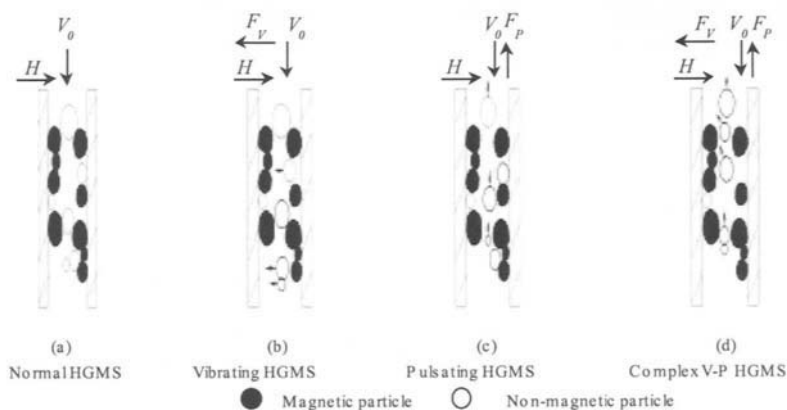


Figure 7: Separation process' schematic diagram of HGMS for different composite force fields.

However, the flocculation of the particles, due to the coagulation between non-magnetic particles and adhesion between the magnetic particles and the magnetic matrix, will cause a mix and form a "bridge frame" in the concentrated magnetic-matrix wire or grid steel plate. Sometimes, this will cause blockage of the pulp. In the single-direction flow (from up to down) and in the cross-magnetic field, these adhesion forms of non-magnetic particles are difficult. This is an important reason why effective magnetic separation using conventional HGMS cannot be accomplished. Just as shown in Figure 7(b), due to the addition of vibrating fluid in the cross-vibrating HGMS, shear stress and inertial forces, "displacement" and "dispersion" may easily appear, so that effective separation can be achieved.

However, in the separation system, the restriction of “bridge frame”-type adhesion is still more difficult to relieve, so the desired separation efficiency was still difficult to obtain. As shown in Figure 7(c), in the pulsating HGMS, due to the periodic up and down pulsating action of fluid in the separation cavity exerting a pulsating force on the mineral particles, the direction and magnitude of these particles were continuously changed. Hence, the particle group was loosened, and the restriction of the “bridge-frame” type of adhesion could also be loosened so effective separation can be accomplished. But this kind of separation structure cannot effectively eliminate inclusion between the up and down particles of non-magnetic materials.

On the one hand, the included non-magnetic particles could be unadhered during the course of magnetic separation by simultaneous addition of a vibrating force and vertical pulsating, using a complex vibrating-pulsating HGMS, as shown in Figure 7(d). Thus, effective separation was attained by means of continuous “displacement” and “dispersion” between non-magnetic and magnetic particles. On the other hand, in the course of this continuous “rinsing” process, not only the adhesion of non-magnetic particles on the magnetic matrix surface was reduced, but the effective adsorption area of magnetic particles was also increased, and the collision probability between the magnetic particles and the magnetic matrix increased. This favored collection of magnetic minerals and achieved a high recovery of magnetic minerals.

## Conclusions

For removal of Cu minerals from sulfide-flotation concentrates, the HGMS is a feasible method. The comparative test results of magnetic separation in different composite force fields have confirmed that the separation efficiency of the complex vibrating-pulsating HGMS is optimal. By means of this method, after one magnetic separation, satisfactory results can be achieved: Pb recovery is 92.66%, Zn recovery is 82.98% and the decoppering rate is 77.28%.

From the investigation of separation principles of HGMS in different composite force fields, “displacement” and “dispersion” of mineral particles that continuously appear in separation cavities, are important conditions for increasing the grade of magnetic products. Pulsating the pulp and vibrating the magnetic matrix can increase the effective capture area and collision probability between the particles and the magnetic matrix, thus increasing recovery of the magnetic particles.

## ELECTROSTATIC FELDSPAR/QUARTZ SEPARATION WITHOUT HYDROFLUORIC ACID REDUCES POLLUTION

S. Dorfner, H. Tröndle, U. Jakobs

Gebrüder Dorfner GmbH Co., Germany

### Abstract

Years ago the electrostatic drum separators are replaced by a freefall separator. The setting and maintenance of the freefall separator is easier and it is cheaper to manufacture. It is somewhat more sensitive to the grain size distribution, compared to the drum separator. Moreover we still need an activation by hydrofluoric acid and elevated temperature.

Looking for a possibility to avoid the hydrofluoric acid, to reduce pollution and the environmental risk, it was proposed to activate the feed with other organic and inorganic reagents. Tests with different polyelectrolytes are carried out. Just as much we studied the effect of pH, temperature, polarity, voltage, the material of the feeder, the electrode shape and configuration and the splitter settings.

The target was a feldspar concentrate with >80% feldspar and a quartz product with <5% feldspar. The feed grain size was 0.1 mm to 0.5 mm. The latest results are a feldspar concentrate with 85% feldspar grade and 27% wt and a quartz product with 4.4% feldspar grade and 40% wt of the feed.

*Keywords: feldspar, quartz, electrostatic, polyelectrolytes, pollution, environment*

### Introduction

In the electrostatic feldspar-quartz separation an activation is done by heating and treatment with hydrofluoric acid. By that means a feldspar concentrate with >90% grade and a quartz with <5% feldspar is produced. The specific capacity is 2.5 t/h·m in the freefall separator compared to 1 t/h·m in the drum separator. Looking for a substitute for the hydrofluoric acid the idea of cationic reagents came in.

### Experimental

A 50% wt mix of feed and water is conditioned with H<sub>2</sub>SO<sub>4</sub> added with polyelectrolyte and stirred during 10 min (which patent is applying together with Inprosys-USA). After dewatering and drying the material runs over a stainless steel vibrating feeder to the slot on top of the separator. The aluminum electrodes measure 0.6×1.9 m<sup>2</sup> and can be charged up to 35 kV negative and positive. The distances of the electrodes on top and at the bottom are changeable. Two splitters below can be set on every position, allowing three products to be taken.

### Results and discussion

Effect of pH was studied in the range of 2 to 7; the reagent concentration within 125 g/t to 1,500 g/t. The best results were obtained at pH = 2.8 using 500 g/t polyelectrolyte (Table I) at a feed rate of 150 kg/h·m. The tension applied was -35 kV and + 35 kV, the distance of the electrodes was 19 cm on top and 33 cm at the bottom. The relative humidity inside the separator was <25%.

Table I: Mass distribution and grade at pH = 2.8 using 500 g/t reagent.

Product	Feldspar	Middlings	Quartz	Feed
Weight (%)	25	40	35	100.0
Feldspar grade (%)	82.9	27.4	4.3	33.2

The middlings consisted mostly of the coarse grain size. Trials to separate the middlings showed only few differences in grade of the two electrode products and the new middlings. Thus we looked for a way to reduce the yield of the middlings and to bring the coarser grains closer to the electrodes.

Increasing the reagent concentration lead to a lesser selectivity, in the extreme to the fact that all material was attracted to the positive electrode. This happened especially with -60 kV against ground. Further tests were done with 375 g/t polyelectrolyte and -25 kV/+35 kV. To prevent bigger quartz grains to be fast attracted to the positive electrode and then mechanically reflected to the adverse side, we increased the electrode distance below to 60 cm. Additionally we exchanged the straight sheet electrodes against flared ones (Ralston, 1961), (Table II). The positive aspects are the increase in the quartz yield and the decrease in the middlings yield. The grades however changed to less feldspar in the feldspar and more feldspar in the quartz.

Table II: Feldspar - quartz separation.

Feed slot 7.5 cm to +E and 7.5 cm to -E (symmetric); electrode distance on top 15.0 cm, bottom 60.0 cm; splitter 27 cm to +E and 29 cm to -E; -25 kV/+35 kV; both electrodes flared.								
1 <sup>th</sup> separation								
	Feldspar		Middlings		Quartz		Feed	
	-E	+E	-E	+E	-E	+E	-E	+E
Weight (%)	27.2	16.9	55.9	100.0				
Feldspar grade (%)	76.8	29.0	7.9	30.2				

Feed slot 7.5 cm to +E and 7.5 cm to -E (symmetric); splitter 27 cm to +E and 29 cm to -E.					Feed slot 7.5 cm to +E and 7.5 cm to -E (symmetric); splitter 27 cm to +E and 29 cm to -E.				
Feldspar cleaning					Quartz cleaning				
	product	middlings	quartz	feed	product	middlings	quartz	feed	
	-E	FS	+E		-E	Q	+E		
Weight (%)	4.3	20.3	2.6	27.2	32.9	33.9	18.8	55.9	
Feldspar grade (%)	89.1	72.3	53.5	73.2	45.6	7.1	5.0	8.6	

Only with an unsymmetric arrangement of the electrodes on top, we got better results (Table III). The middlings were regarded as tailings with 15% wt. But to fit the target both products from the electrodes had to be cleaned; at the same time the splitter setting was optimized (Table IV). With reference to research from Manouchehri et al. (1997), including tests with different contact materials for the tribo-charging we used copper besides steel (Table V). But there was no significant difference to be seen. Finally the optimization resulted with: 19.1% wt feldspar cleaner concentrate with 84.4% feldspar, 39.2% wt quartz with 3.9% feldspar i.e. a total yield of 58.3% (Table VI). The feed rates were about 300 kg/h-m.

Table III: Feldspar-quartz separation.

Feed slot 13.5 cm to +E and 3.5 cm to -E (unsymmetric); electrode distance on top 17.5 cm, bottom 55.0 cm; splitter 26 cm to +E and 17 cm to -E; -25 kV/+35 kV; both electrodes flared.							
	1 <sup>th</sup> separation						
	Feldspar -E		Middlings +E	Quartz +E	Feed		
Weight (%)	24.0	15.6	60.4	100.0			
Feldspar grade (%)	79.2	45.3	7.1	30.4			

Feed slot 13.5 cm to +E and 3.5 cm to -E (unsymmetric); splitter 13 cm to +E; 21.5 cm to -E.				Feed slot 13.5 cm to +E and 3.5 cm to -E (unsymmetric); splitter 26 cm to +E and 12 cm to -E..				
	Feldspar cleaning			Quartz cleaning				
	Product -E	Middlings FS	Quartz +E	Feed	Product -E	Middlings Q	Quartz +E	Feed
Weight (%)	12.7	4.8	6.5	24.0	3.2	30.3	26.9	60.4
Feldspar grade (%)	87.9	81.7	72.7	82.5	20.5	9.1	4.6	7.7

Table IV: Electrode distance on top 17.5 cm, bottom 52.5 cm; feed slot 14 cm to +E and 3.5 cm to -E; Splitter 27 cm to +E and 15 cm to -E; -25 kV/+ 35 kV; both electrodes flared.

	Splitter 24.5 cm to +E and 21 cm to -E.				Splitter 27 cm to +E and 15 cm to -E.			
	Product -E	Middlings FS	Product +E	Feed	Product -E	Middlings Q	Product +E	Feed
Weight (%)	27.5	13.4	59.1	100.0	20.0	17.3	62.7	100.0
Feldspar grade (%)	78.9	38.3	5.8	30.3	82.4	48.5	9.2	30.6

Table V: Electrode distance on top 17.5 cm, bottom 52.5 cm; feed slot 14 cm to +E and 3.5 cm to -E; Splitter 27 cm to +E and 15 cm to -E; -25 kV/+35 kV; both electrodes flared.

	Steel-contact: splitter 24.5 cm to +E and 21 cm to -E.				Copper contact: splitter 27 cm to +E and 15 cm to -E.			
	Product -E	Middlings FS	Product +E	Feed	Product -E	Middlings Q	Product +E	Feed
Weight (%)	27.5	13.4	59.1	100.0	25.4	14.7	59.9	100.0
Feldspar grade (%)	78.9	38.3	5.8	30.3	79.4	29.2	5.5	27.8

Although the fine grained feldspar being fast attracted to the negative electrode, a non neglectable part was still found in the middlings.

Therefore we replaced the flared electrodes by straight ones added with modifications on the inner side. By these means the feldspar concentrate could be improved to 26.9% wt at 85.4% feldspar (Table VII).

On the other hand there was no change on the quartz side.

With increasing feed rates up to 860 kg/h·m there was only a light decrease in yield and grade.

Table VI: Feldspar-quartz separation.

Feed slot 14 cm to +E and 3–5 cm to –E (unsymmetric); electrode distance on top 17.5 cm, bottom 52.5 cm; Splitter 27 cm to +E and 15 cm to –E; –25 kV/+35 kV; both electrodes flared.								
1 <sup>th</sup> separation								
	Feldspar		Middlings	Quartz	Feed			
	–E			+E				
Weight (%)	25.3		14.5		60.2	100.0		
Feldspar grade (%)	77.2		48.5		6.1	30.2		

Feed slot 6 cm to +E and 11 cm to – E (unsymmetric); splitter 32 cm to +E; 9 cm to –E.				Feed slot 6 cm to +E and 11 cm to –E (unsymmetric); splitter 33 cm to +E and 7 cm to –E..				
Feldspar cleaning				Quartz cleaning				
Product	Middlings	Quartz	Feed	Product	Middlings	Quartz	Feed	
–E	FS	+E		–E	FS	+E		
Weight (%)	12.0	7.1	6.2	25.3	1.2	19.8	39.2	60.2
Feldspar grade (%)	88.3	78.9	60.0	78.7	35.9	13.9	3.9	7.8

Table VII: Feed slot 7.5 cm to +E and 7.5 cm to –E (symmetric); electrode distance on top 17.5 cm, bottom 50.5 cm; Splitter 29 cm to +E and 18 cm to –E; –25 kV/+35 kV; both electrodes straight with modifications.

1 <sup>th</sup> separation								
	Feldspar		Middlings	Quartz	Feed			
	–E			+E				
Weight (%)	29.9		9.1		61.0	100.0		
Feldspar grade (%)	79.2		30.6		8.4	31.6		

Feldspar cleaning				Quartz cleaning				
Product	Middlings	Quartz	Feed	Product	Middlings	Quartz	Feed	
–E	FS	+E		–E	FS	+E		
Weight (%)	15.9	11.0	3.0	29.9	3.0	18.4	39.6	61.0
Feldspar grade (%)	91.4	76.8	48.9	81.8	36.5	10.5	4.4	10.2

## Conclusions

It could be shown that electrostatic feldspar/quartz separation using polyelectrolytes is possible. The accuracy of the separation however is less, compared to the activation with hydrofluoric acid. In a three-stage separation an overall yield of 66.5% wt can be achieved with a feldspar grade of 85% in the feldspar and 4.4% in the quartz. These results are mainly affected by modified straight electrodes that keep the fine feldspar out of the field once it reached the negative electrode. Even though this minor results with polyelectrolytes they should not be valued little, especially in view of the health hazards and the environmental risks of hydrofluoric acid.

## References

- Manouchehri, H.R., Hanumantha Rao, K., Forssberg, K.S.E., 1997. Triboelectric separation of chemically treated minerals. MinFo Project 239; Swedish Mineral Processing Research Association.
- Ralston, O.C., 1961. Electrostatic separation of mixed granular solids. Elsevier Amsterdam.

## ASSESSMENT OF MULTISTAGE TURBULENT CROSS-FLOW AEROSEPARATION OF BUILDING RUBBLE

J. Tomas, T. Gröger

Mechanical Process Engineering, Process Engineering Department, Faculty of  
Process Engineering and System Engineering,  
The Otto-von-Guericke-University Magdeburg, Germany

### Abstract

The liberation of building rubble by comminution produces a predominately mineral mixture with a density distribution of  $\rho_s = 1.8\div 2.7 \text{ g/cm}^3$ . As a result of the relatively narrow density range, the requirements regarding the sharpness of the process employed for the separation of partially liberated aggregate and concrete-brick rubble are very high. For the gravity separation a test rig was built consisting of zigzag channel, fan, air cyclone, filter and particle feeding system. Specific mass flow rates  $3 \text{ t/m}^2\text{h}$  to  $16 \text{ t/m}^2\text{h}$  related to apparatus cross-sectional area and mass related energy consumption  $0.2 \text{ kWh/t}$  to  $8 \text{ kWh/t}$  were obtained. To assess the efficiency, the separation function is determined and compared with a theoretical model of multistage turbulent cross-flow separation. On the basis of the well-known separation sharpness as well as geometrical variability of a zigzag apparatus, it could be shown that this separation principle is well suited for the gravity separation of mineral materials.

*Keywords: cross-flow gravity separation model, separation efficiency, building rubble recycling*

### Introduction

The liberation of building rubble by comminution produces a predominately mineral mixture with a density distribution of  $\rho_s = 1.8\div 2.7 \text{ g/cm}^3$  (Tomas et al., 1998). As a result of the relatively narrow density range, the requirements regarding the sharpness of the process employed for the separation of partially liberated aggregate and concrete-brick rubble are very high.

Table I: Selected separation processes for the recycling of building and domestic waste.

Wet separation	Dry separation
<ul style="list-style-type: none"> <li>- Float and sink cleaning (Rohr, 1987, Schütze, 1987)</li> <li>- Upward flow (Kalck and Werther, 1990)</li> <li>- Jig (Breuer, 1988, Kellerwessel, 1993)</li> <li>- Washing drum (Hentzschel, 1990)</li> </ul>	<ul style="list-style-type: none"> <li>- Classification (Greschner, 1994)</li> <li>- Hand sorting (Hanisch et al., 1991)</li> <li>- Automatic sorting (Schubert, 1996)</li> <li>- Counter- and cross-flow aeroclassification (Friedrichs and Tomas, 1996)</li> <li>- Pneumatic table (Güldenpfennig and Löhr, 1995)</li> <li>- Sloping separating belt (Schubert, 1996)</li> <li>- Slinger (Hanisch et al., 1991)</li> <li>- Eddy current separator (Schubert, 1996)</li> </ul>

The separation processes currently employed in the recycling of building materials remove mainly the lightweight impurities such as paper, wood, films, insulating materials and pieces of plastic ( $\rho_s = 0.1\div 1.2 \text{ g/cm}^3$ ) by wet or dry separation. In such cases,

the range of unsharpness of the cut-point can be defined in the intermediate range ( $\rho_s = 1.2\div 1.8 \text{ g/cm}^3$ ), so that equipment with relatively low separation efficiency is still adequate for these applications. Table I provides an overview of the state-of-the-art in respect of separation for recycling building materials (Bilitewski, 1995; Bilitewski and Weltin, 1995; Friedrichs and Tomas, 1996; Hanisch et al., 1991; Kellerwessel, 1993; Melchiorre et al., 1994; Tränkler, 1992).

Wet and dry separation techniques have different advantages and disadvantages. Dry separation is more cost-effective in terms of its energy requirement as problems regarding the treatment of process water and its disposal do need to be considered, and is especially suitable for mobile and semi-mobile processing plants. Wet separation is useful for the removal of pollutants from contaminated building waste (Kalck, 1990).

For the separation of building rubble, mainly classifiers are used in practice. The upward flow or single-stage cross-flow separators commonly employed for dry separation in an air flow separate the material feed according to the respective settling velocities of the different components. The separation behavior is influenced decisively by the particle size, particle shape and particle density of the components to be separated. An air classifier can separate the material according to one of these parameters providing the influence of the other two variables is minimized.

The separation of totally or partially liberated aggregate particles in the size range from  $d = 2\div 16 \text{ mm}$  therefore presents a challenge to the separation sharpness and the efficiency of the equipment. Tests were carried out in a zigzag channel to establish whether the high separation sharpness required can be achieved in a multistage turbulent cross-flow separation apparatus.

### Fundamentals of the aeroseparation of building rubble

The basis for studying a separation process in a fluid cross-flow is the balance of the forces of buoyancy, weight and fluid resistance of a particle. With this balance, it is possible to obtain a correlation between particle size and the quasi-stationary settling velocity  $v_{\text{sink}}$  in the field of gravity  $g$ :

$$v_{\text{sink}}^2 = \frac{2}{c_w} \cdot \frac{\rho_s - \rho_f}{\rho_f} \cdot \frac{V_p}{A_p} \cdot g \quad (1)$$

Here  $A_p$  is the side-fed cross-sectional area,  $c_w$  the drag coefficient of the fluid flow pattern around the particles,  $V_p$  the particle volume and  $\rho_f$  the fluid density. The density of the solid particles  $\rho_s$  is dependent on the inner porosity of the particles (up to 95% for insulating materials), on the particle density and pore saturation with a liquid. In the separation of particles of varying density  $\rho_s$  the principle of what is termed *equivalent falling classes* (Schubert, 1989), i.e. classes with equal settling velocity, can be formulated as follows. If the particle shape is constant, *large* and *lightweight* particles settle just as fast as *small* and *heavy* particles.

With  $d_i$  to  $d_{i+1}$  as the particle size of the class  $i$  to  $i+1$  as well as  $\rho_{s,S}$  and  $\rho_{s,L}$  as the particle densities of the heavy fraction (index S) and the lightweight fraction (index L), the following applies:

$$v_{\text{sink}}(d_{i+1}, \rho_{s,L}) = v_{\text{sink}}(d_i, \rho_{s,S}) \quad (2)$$



Depending on the particle flow-around conditions as in Table II (with  $c_w = f(\text{Re})$ , Reynolds number  $\text{Re} = v_{\text{sink}} \cdot d \cdot \rho_f / \eta_f$  and  $\eta_f$  expressed as the dynamic viscosity of the fluid) it then follows:

$$\frac{d_{i+1}}{d_i} = \left( \frac{\rho_{s,S} - \rho_f}{\rho_{s,L} - \rho_f} \right)^{1/n} \quad (3)$$

Table II: Equivalent-falling condition in dependence of the particle flow-around pattern.

Exponent	Flow pattern	Reynolds number	Drag coefficient
$n = 2$	laminar	$\text{Re} < 1$	$c_w \propto \text{Re}^{-1}$
$1 < n < 2$	transition	$1 < \text{Re} < 10^3$	$c_w \propto \text{Re}^{-1 \dots 0}$
$n = 1$	turbulent	$10^3 < \text{Re} < (2 \div 4) \cdot 10^5$	$c_w \propto \text{Re}^0$

The models of counter-current separations drawn up so far (Gorwitzke, 1982, Böhme, 1989) have proven unsuitable or too complex (Senden, 1979). Therefore, for the evaluation of the multistage cross-flow separation studied here, in order to describe the process efficiency, the separation model of a turbulent cross-flow hydroclassification - developed by Schubert and Neeße (1973), Neeße and Schubert (1975) and Neeße (1969, 1978) - was supplemented with a model for multistage turbulent cross-flow aereoseparation (Tomas and Gröger, 1999). If the turbulent particle flow-around pattern is taken into account the normalized separation function of a separation stage of the overflow  $z_L$  or the underflow  $z_S$  results as follows ( $V_L, V_S$  total volume flow rates over- and underflow):

$$T_{z_L, z_S} \left( \frac{\rho_{s,j} - \rho_f}{\rho_{s,T} - \rho_f} \right) \Big|_{d=\text{const.}} = \frac{1}{1 + \left( \frac{\dot{V}_L}{\dot{V}_S} \right)^{1-n} \sqrt{\frac{\rho_{s,j} - \rho_f}{\rho_{s,T} - \rho_f}}} \quad (4)$$

This fractional grade function equation (4) corresponds to a probability distribution of class  $j$  of the measured density of the porous particles  $\rho_{s,j}$  (the pore space in hardened cement paste measures around 20-30%) being discharged in the heavy fraction  $S$ .

In his case, the cut point (average separation density) is defined with  $T_{z_L, z_S}(\rho_{s,T}) = 0.5$  probability.

For equal fractional grade efficiencies of the  $z_L$  lightweight fraction separation stages and  $z_S$  heavy fraction separation stages, the component mass balance returns the total separation probability (feed index  $A$ , Tomas et al., 1999):

$$T_{\text{tot},j} = \frac{\dot{m}_{S,j}}{\dot{m}_{A,j}} = R_{m,S} \cdot \frac{q_S(\rho_s)}{q_A(\rho_s)} = \frac{1}{1 + \frac{(1 - T_{z_L,j})^{z_L}}{(T_{z_S,j})^{z_S}}} \quad (5)$$

For a symmetrical separation with the same number of stages in the over- and underflow ( $z_L = z_S = z$ ), the total separation function can be simplified with equations (4) and (5) to (Gröger and Tomas, 1999):

$$T_{\text{tot}j} = \frac{1}{1 + \left( \frac{\dot{V}_L}{\dot{V}_S} \right) \left( 1 - \sqrt{\frac{\rho_{s,j} - \rho_f}{\rho_{s,T} - \rho_f}} \right)^z} \quad (6)$$

Hence, the slope of the separation function can be characterized by an elegant analytical formulation of the overall separation sharpness:

$$\kappa = \frac{\rho_{s,25}}{\rho_{s,75}} = \left[ \frac{z \cdot \ln(\dot{V}_L / \dot{V}_S) - \ln 3}{z \cdot \ln(\dot{V}_L / \dot{V}_S) + \ln 3} \right]^2 \leq 1 \quad (7)$$

Separation in the turbulent particle flow pattern can only be achieved with appropriate separation sharpness if the separator has a high number of separation stages and if a sufficiently high ratio between the lightweight and heavy material volume flow rates  $\dot{V}_L / \dot{V}_S$  can be maintained. This is commensurate with practical experience gained with classification, e.g. Kaiser (1963).

With the effective total number of separation stages  $n_e$

$$n_e = 2 \cdot z - 1 \quad (8)$$

(the feed separation stage both in the overflow and the underflow is included in this number), an additional degree of freedom is obtained, which, on the one hand, can be used to fit the measured values to a physically valid separation function equation (6). On the other hand, the so-called separation stage utilization coefficient represents an additional parameter to assess separation efficiency in case of small density differences:

$$\eta_{Tr} = n_e / n \quad (9)$$

### Set-up of the test rig

For the separation of mineral materials, a test rig, consisting of a zigzag channel measuring 173×200 mm<sup>2</sup>, a feed unit, a fan, a cyclone and cloth filter, was set up (Figure 1). The separation process can be observed through the glass side walls of the channel. The mass flow rates of the feed materials and the separation products are determined by means of weight cells. In addition, during the tests, the air volume flow rate, the average channel velocity, the pressure drop versus the zigzag apparatus, the pressure drop versus the filter and the temperature and relative humidity at significant points can be measured (Figure 2) (Friedrichs and Tomas, 1996).

Zigzag classifiers are usually classed as counter-current classifiers (Böhme, 1989). The separation process in the zigzag channel can, however, also be understood as a series arrangement of cross-flow separation stages (Schubert, 1989).

In each stage, so-called vortex rolls are formed, to which one fractional grade can be assigned respectively in the ideal case (Senden, 1979). The characteristic turbulence variables can be calculated from the separation results described in the following, namely the channel Reynolds number  $Re = u \cdot b / \nu \sim 10^4 \div 6 \cdot 10^5$ ; degree of turbulence  $Tu \sim 0.11 \div 0.13$ ; turbulent diffusion coefficient  $D_t \sim 45 \div 63 \text{ cm}^2/\text{s}$ ; Bodenstein number  $Bo = u \cdot b / D_t \sim 1 \div 15$ . Usually the feed material is added to the separation process at the centre, relative to the number of stages in the zigzag channel. In each stage of the apparatus, separation into a lightweight and heavy fraction takes place.

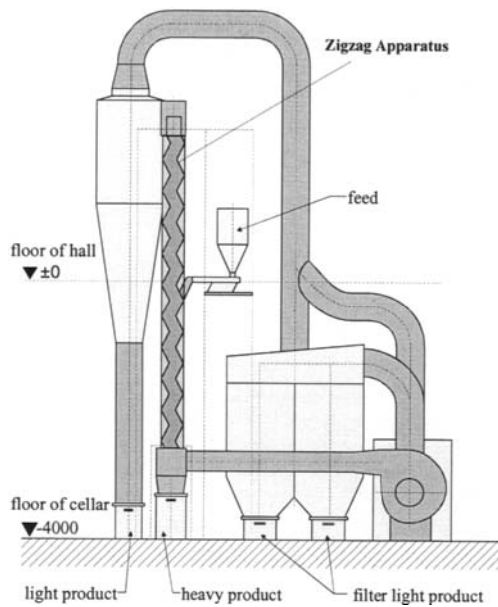


Figure 1: Set-up of the test rig.

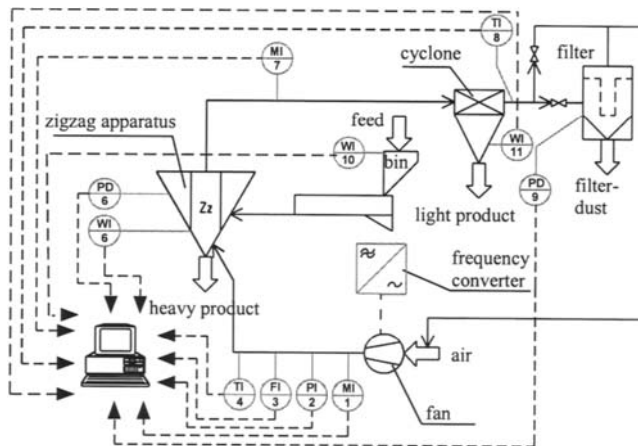


Figure 2: PI-flow chart of the test rig.

The heavy particles slide down the downward sloping channel walls and the light-weight particles are swept up with the airflow at the two upwards sloping channel walls. At the bends of the zigzag channel, these two currents cross the channel so that a cross-flow separation takes place. The good separation characteristics of a zigzag separator are based on the series arrangement of several such stages (Kaiser, 1963; Senden, 1979; Gorzitzke, 1982; Böhme, 1989; Friedrichs and Tomas, 1996; Tomas and Friedrichs, 1997).

### Verifying the separation model for air classification

As part of preliminary studies, the separation model in equation (6) was applied for the classification of sand/split and gravel. In Figure 3 and Table III, the measured values for the three separation experiments with the cut particle size  $d_T = 2.1$  mm, 4.6 mm and 6.7 mm are shown.

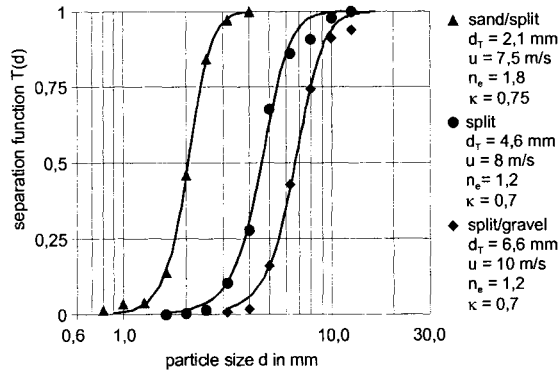


Figure 3: Comparison of the classification results with the separation model according to equation (6).

For the purpose of comparison, the corresponding model curves with fitted, i.e. effective, stage numbers  $z_L = z_S = z = 1.4, 1.1$  and  $1.1$  are also plotted. With this additional degree of freedom  $z$ , the experimental separation processes with the S-shaped curves typical of air classification ( $\rho_s = \text{constant}$ ) can be reproduced very well.

From these, separation efficiencies of  $\kappa = 0.7 \div 0.75$  can be read, which can be considered as good (range  $\kappa = 0.6 \div 0.8$ , Rumpf, 1975). However, for this classification, effective stage number in the range  $n_e = 1.2 \div 1.8$  results.

This means that the seven separation stages of the apparatus are only utilized to a satisfactory extent at  $\eta_{Tr} = n_e/n = 17 \div 26\%$ . Remarkable in technical terms are also the mass flow rates of  $3 \div 8.5$  t/m<sup>2</sup>h related to the apparatus cross-sectional area and the mass related energy consumption of only  $0.4 \div 1.7$  kWh/t.

Table III: Comparison of classification results with the separation model according to equation (6).

Parameters according to Figure 3		▲	●	◆
channel velocity $u$	(m/s)	7.5	8	10
air flow rate $\dot{V}_g$	(m <sup>3</sup> /s)	0.3	0.32	0.38
particle settling velocity $v_{sT}(d_T)$	(m/s)	11.5	15.6	18.7
mass flow rate $\dot{m}_s$	(t/h)	0.34	0.12	0.16
specific mass flow rate $\dot{m}_{s,A}$	(t/m <sup>2</sup> h)	8.5	3	4
particle concentration $\mu_{s,g}$	(g/kg)	262	82	94
cut size $d_T$	(mm)	2.1	4.6	6.6
separation sharpness $\kappa$		0.75	0.7	0.7
effective separation stages $n_e$		1.8	1.2	1.2
utilization of separation stages $\eta_{Tr}$	(%)	26	17	17
pressure drop $\Delta p_{ZZ}$	(Pa)	440	440	700
specific energy consumption $W_{m,ZZ}$	(kWh/t)	0.39	1.25	1.72

### Results of gravity aeroseparation

Tests on the separation of concrete-brick mixtures were carried out. Figure 4 shows the reproducibility of the separation efficiency on the basis of the results of four tests with a 15-stage unit, all conducted under identical conditions ( $d = 8 \div 12$  mm).

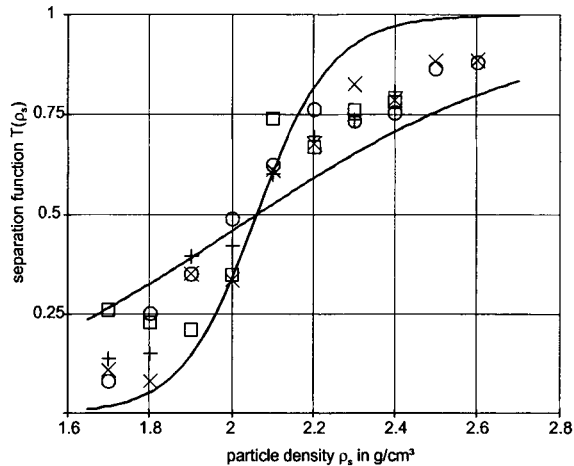


Figure 4: Results for the separation of concrete-brick rubble,  $d = 8 \div 12$  mm,  $n = 15$ .

It can be seen that the separation results demonstrate considerable scattering in comparison with classification according to Figure 3. The plotted model curves limit the range of separation efficiency from  $\kappa = 0.67 \div 0.91$  for  $n_e = 1 \div 7$ .

From a comparison of the separation experiments with narrowly fractionated concrete-brick mixtures  $d = 8 \div 10$  mm (Figure 5), it can be concluded that this scattering is caused by the influence of the particle size.

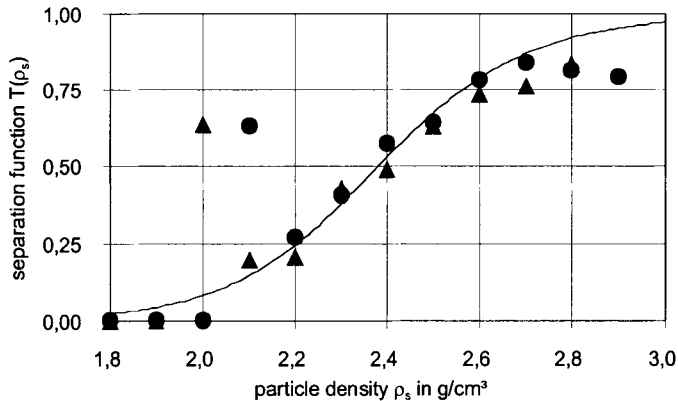


Figure 5: Separation of concrete-brick rubble,  $d = 8 \div 10$  mm,  $n = 7$ .

Representative for the other tests, Figure 5 shows that the separation model equation (6) can be fitted very well to the measurement results for narrow particle size ranges. The sharpness of this separation with the 7-stage unit can be rated as very good with  $\kappa = 0.86$ . The utilization of the seven apparatus stages  $\eta_{Tr} = 54\%$  at an effective number of stages of  $n_e = 3.8$  must be rated as satisfactory to good (Table IV).

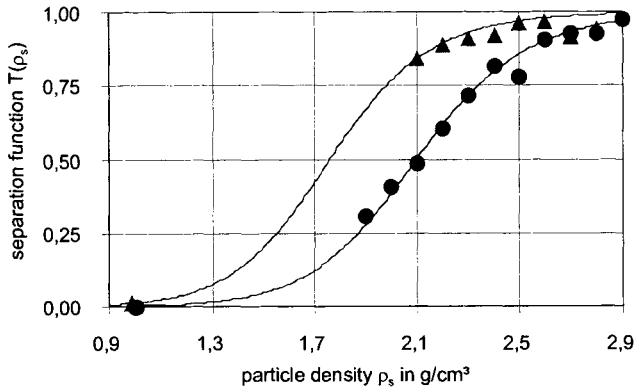


Figure 6: Separation of concrete-brick rubble with rubber granulate, ●  $d = 4\text{-}5$  mm, ▲  $d = 5\text{-}6.3$  mm.

On this basis, the layout for the separation of a lightweight fraction (here rubber granulate  $\rho_s \sim 1.0$  g/cm<sup>3</sup>) is relatively unproblematic (Figure 6). Because of high particle concentration  $\mu_{s,g} = 417$  g/kg adjusted here, a comparably small specific energy consumption  $W_{m,ZZ} = 0.19$  kWh/t is generally obtained for the good separation efficiency (Table IV). Satisfactory to very good results were also achieved in the difficult separation of a partially liberated aggregate consisting of hardened cement paste rubble,  $\kappa = 0.66\text{-}0.94$  (Tomas and Friedrichs, 1997, Tomas et al., 1999) at utilization coefficients of  $\eta_{Tr} = 7\text{-}87\%$ .

Table IV: Technical assessment of the separation results.

		concrete-brick rubble		Concrete, rubber	
		(Figure 4)	(Figure 5)	(Figure 6)	
Particle fraction $d_{u,i} + d_{o,i}$	(mm)	8÷12	8÷10	4÷5	5÷6.3
channel velocity $u$	(m/s)	14	12.5	8.5	8.5
air flow rate $\dot{V}_g$	(m <sup>3</sup> /s)	0.56	0.51	0.35	0.35
particle settling velocity $v_{s,T}(d_T)$	(m/s)	20.3	21.7	14.3	14.9
mass flow rate $\dot{m}_s$	(t/h)	0.12	0.15	0.15	0.63
specific mass flow rate $\dot{m}_{s,A}$	(t/m <sup>2</sup> h)	3.0	3.7	3.7	15.8
particle concentration $\mu_{s,g}$	(g/kg)	50	68	98	417
cut density $\rho_{s,T}$	(g/cm <sup>3</sup> )	2.1	2.4	2.1	1.8
separation sharpness $\kappa$		0.7 - 0.9	0.86	0.80	0.78
effective separation stages $n_e$		1÷7	3.8	3	3.4
utilization of separation stages $\eta_{Tr}$	(%)	7 - 47	54	43	49
pressure drop $\Delta p_{ZZ}$	(Pa)	1600	815	350	350
specific energy consumption $W_{m,ZZ}$	(kWh/t)	8.0	2.75	0.83	0.19

## Conclusions

To assess the efficiency of the separation of liberated aggregate particles of concrete rubble fragments, the separation functions were determined and compared with a theoretical model of multistage turbulent cross-flow separation. Specific mass flow rates 3 t/m<sup>2</sup>h to 16 t/m<sup>2</sup>h and mass related energy consumption 0.2 kWh/t to 8 kWh/t were obtained. On the basis of the well-known separation sharpness as well as geometrical variability of a zigzag apparatus, it could be shown that this multistage cross-flow separation principle is well suited for the gravity separation of mineral materials.

## References

- Bilitewski, B., 1995. Vermeidung und Verwertung von Reststoffen. In: Der Bauwirtschaft, Beihefte zu Müll und Abfall, 30, 40 – 63.
- Bilitewski, B. and Weltin, B., 1995. Trennleistung eines Querstromsichters bei der Aufbereitung von Baustellenabfällen. Vortrag Berg- und Hüttenmänn. Tag, Freiberg.
- Böhme, S., 1989. Zur Stromtrennung zerkleinerter metallischer Sekundärrohstoffe. Freiburger Forschungsheft A 785.
- Breuer, H., 1988. Betriebserfahrungen mit einer luftgepulsten Alljig-Kiessetzmaschine zur Abtrennung von organischen Verunreinigungen aus Sand und Kies. Aufbereitungs-Technik 29, 324-330.
- Friedrichs, J. and Tomas, J., 1996. Aerosortierung von Bauschutt. In: Arbeits- und Ergebnisbericht des Sonderforschungsbereiches 385, Baustoffrecycling Otto-von-Guericke-Univ. Magdeburg, 197-250.
- Goritzke, W., 1982. Trockenes Sortieren grober disperser Feststoffe durch Kombination von Siebung und Windsichtung. Diss. TU Clausthal-Zellerfeld.
- Greschner, J., 1994. Möglichkeiten des Recyclings von Bauschutt, innerstädtischen Aushubmaterialien und kohäsiven Stoffgemischen mit neuentwickelten Vibrationsrosten. Aufber.-Tech. 35, 13-24.
- Gröger, T. and Tomas, J., 1999. Verfahrenstechnische Bewertung einer mehrstufigen turbulenten Querstrom-Aerosortierung. Preprint, OVGU Magdeburg (in preparation).
- Güldenpfennig, M. and Löhr, K., 1995. Sortierung vermischter Reststoffe gleicher Dichte auf dem Luftherd. Aufbereitungs-Technik 36, 314-320.
- Hanisch, J., Jäckel, H.G. and Eibs, M., 1991. Zu aufbereitungstechnischen Aspekten des Baustoffrecyclings. Aufbereitungs-Technik 32, 10-17.
- Hentzschel, W., 1990. Waschen und Läutern – zum gegenwärtigen Stand der wissenschaftlichen Kenntnisse und deren Anwendung. Aufbereitungs-Technik 31, 126 – 130.
- Kaiser, F., 1963. Der Zick-Zack-Sichter-Ein Windsichter nach neuem Prinzip. Chemie Ing. Technik 35, 273-282.
- Kalck, U. and Werther, J., 1990. Zum Einsatz von Aufstromklassierern für die Aufbereitung kontaminierter Baggerschlämme. Aufbereitungs-Technik 31, 593 – 601.
- Kellerwessel, H., 1993. Setzmaschinen, besonders für Recyclingaufgaben. Möglichkeiten, Grenzen, Bauarten-, Aufbereitungstechnik 34, 521-530.
- Melchiorre, M., Güldenpfennig, M., Löhr, K. and Zürn, J., 1994. Teilen und Trennen im Recycling-Prozeß. Chem.-Ing.-Technik 66, 661 – 670.
- Neeße, Th. and Schubert, H., 1975. Modellierung und verfahrenstechnische Dimensionierung der turbulenten Querstromklassierung. part I: Chem. Techn. 27, 529-533; part II: Chem. Techn. 28, 80 – 83; part III: Chem. Techn. 28, S. 273 – 278; part IV: Chem. Techn. 29, 14 – 18.
- Neeße, Th., 1969. Der aufbereitungstechnische Klassiervorgang im turbulenten wässrigen Medium. Freiburger-Forsch.-H. A 465, 9 – 50.
- Neeße, Th., 1978. Modellierung der turbulenten Querstromhydroklassierung. Dissertation B, Bergakademie Freiberg.
- Rohr, W., 1987. Entwicklung und Betriebsergebnisse auf dem Gebiet der Sortierung und Klassierung mit dem Aquamator. Aufbereitungs-Technik 28, 32.
- Rumpf, H., 1975. Mechanische Verfahrenstechnik. München: Carl-Hanser Verlag.

- Schubert, H. and Neeße, Th., 1973. The role of turbulence in wet classification. Proceedings 10<sup>th</sup> Intern. Mineral Processing Congress, London, 213 – 239.
- Schubert, H., 1996. Aufbereitung fester Stoffe, Band II Sortierprozesse. Deutscher Verlag für Grundstoffindustrie, Stuttgart.
- Schubert, H., 1989. Aufbereitung mineralischer Rohstoffe. Band I, Deutscher Verlag für Grundstoffindustrie, Leipzig.
- Schütze, H.J., 1987. Naßaufbereitung von Bauschutt im Aquamator. *Aufber.-Tech.* 28, 463 – 469.
- Senden, M.M.G., 1979. Stochastic model for individual particle behaviour in straight and zig-zag air classifier. PhD Thesis, Eindhoven University.
- Tomas, J., Schreier, M. and Gröger, T., 1999. Liberation and Separation of Valuables from Building Material Waste. *Global Sym on Recycling, Waste Treat. and Clean Technology*, San Sebastian.
- Tomas, J., Ehlers, S. and Schreier, M., 1998. Impact crushing of concrete for liberation and recycling. 9<sup>th</sup> Euro Sym on Comminution, Albi, 57 – 70.
- Tomas, J. and Friedrichs, J., 1997. Waste building material separation in a zigzag air apparatus. *Erzmetall* 50, 562 – 571.
- Tomas, J. and Gröger, T., 1999. Mehrstufige turbulente Aerosortierung von Bauschutt. *Aufbereitungs-Technik* 40, 379 – 386.
- Tränkler, J., 1992. Verbesserung der Produktqualität bei der Bauschutt-aufbereitung durch nasse oder trockene Behandlung. *Aufbereitungs-Technik* 33, 194 – 202.



## SEPARATION TECHNOLOGY BASED ON SEGREGATION EFFECTS IN FAST GRAVITY FLOWS

V. Dolgunin, A. Ukolov, A. Romanov, A. Kudy, A. Klimov

Department of Machines and Apparatus, Tambov State Technical University  
Tambov, Russia

### Abstract

Separation technology of particulate materials, which differ in density and consist of particles of non-uniform sizes, is suggested. The technology is based on a combined application of the two different segregation effects taking place in a fast gravity flow of particulate solids, in the volume of a single moving bed on a rough chute.

*Keywords: separation, segregation, migration, fast gravity flow*

### Introduction

Traditional technologies of ore and raw material concentration are multi-stage, and demand the application of a sieve classification, and of separation processes using gas and liquid flows, such as flotation and sedimentation. Thus, these technologies lead to enlarged air and water consumption and to use of a powerful source of vibration, and they pollute the environment. For example, after mica ore mining the raw material is classified by size for a number of fractions. The mica chip's extraction from the coarse ore fraction (>5 mm) is carried out with the help of special machines. The process of mica extraction from the fine ore fraction (<5 mm) is carried out by the flotation method. The employment of flotation requires a high consumption of water and flotation reagents, and causes serious regional ecological problems. The separation of the particulate solids, consisting of particles differing in size and density, is the problem of special interest. Usually, such a technological problem is solved by preliminary sieve classification of the mixture into a certain number of classes according to particle size. Then, the particles of each class are separated by their density. This problem is more complicated if the mixture contains abrasive particles of angular shape: due to intensive abrasive wear, it is necessary to use rather thick sieves, whose meshes are blocked very quickly. To increase separation reliability of such particulate materials and to decrease environmental pollution, a dry-separation technology, suggested by Dolgunin et al. (1990), may be developed. In the present paper, the separation technology of the particulate solids, which differ in size and density, is being discussed. The technology is based on the complex segregation effects taking place in fast gravity flows of non-uniform particles on a rough chute.

### Segregation effects

The greatest segregation effects of non-uniform particles appear in fast, shear flows of particulate mixtures. Obviously, it is a result of intensive particle interaction in such

kinds of flows. Our research (Dolgunin et al., 1998) shows that segregation in fast, shear flows appears due to the local, as well as spatial, non-uniformity of particulate media. The total flow of segregation is defined as the sum of the flows of hydromechanical segregation,  $J_s$ , and migration,  $J_m$ , caused by local and spatial non-uniformity of particulate media, respectively:

$$J = J_s + J_m \quad (1)$$

In previous investigation (Dolgunin and Ukolov, 1995), it was found that the flow of hydromechanical segregation is proportional to the degree of local non-uniformity of a medium. The non-uniformity parameter is a moment of total excess of friction forces,  $\Delta M_f$ , gravity forces,  $\Delta M_g$ , and impact momentum,  $\Delta M_c$ , acting on a test particle in a conventionally homogeneous medium, relative to a certain instantaneous axis of rotation:

$$J_s = k \cdot \Delta M \cdot c \cdot (1 - c) \quad (2)$$

where:

- $k$  is the kinetic constant of segregation, defined by the experimental method;
- $c$  is the concentration of test particles;
- $\Delta M = \Delta M_f + \Delta M_g + \Delta M_c$  is the sum of moments of total excess of frictional gravity forces and impact momentum.

When the  $\Delta M$  value is positive, the particle is more likely moved towards overlaying layers of the bed. On the other hand, if the value of  $\Delta M$  is negative, the particle is more likely to descent to the underlying bed.

The flow value of migration, caused by the spatial non-uniformity of a particulate medium, is defined as a relative velocity of the quasi-diffusion displacement of non-uniform particles. The migration flow is proportional to the degree of spatial non-uniformity of particulate media. Such a degree of non-uniformity is defined as the rate of change of the mean distance between particles in the migration flow direction:

$$J_m = D_m \cdot \frac{\partial \ln S}{\partial y} \quad (3)$$

where ( $D_m$ ) is the migration coefficient, calculated by analytical methods using the traditional physical and mechanical constants of particles and shear flow parameters.

The migration coefficient for spherical cohesionless particles, having diameters  $d_1$  and  $d_2$ , and densities  $\rho_1$  and  $\rho_2$ , respectively, is defined as:

$$D_m = \frac{\bar{m}(c) \cdot (\bar{V}')^2}{4 \cdot F} \cdot \left( \frac{d_1^2}{m_1 \bar{d}^2} - \frac{d_2^2}{m_2 \bar{d}^2} \right) \quad (4)$$

where:

- $\bar{m}(c)$  is the mean particle mass;
- $F, V'$  are the mean collision frequency and the mean fluctuation velocity.

In the course of migration, the heavier particles move towards the gradient of fraction volume of the solid phase, whereas the light particles are forced into the area with a greater fraction of void volume.

The (2) and (3) kinetic equations of the above-mentioned segregation effects show that the hydro-mechanical segregation flow mainly depends on the difference between the size of the particles. The density difference between the particles is insignificant in such a case, because the value of the non-uniformity parameter,  $\Delta M$ , in equation

(2) mostly depends on the size of particles, rather than on their density. The gravity component in the force balance and its momentum acting on a test particle in a rapid, shear flow is insignificant in comparison with other force components. All these statements are confirmed by experimental analysis and by calculated results of the non-uniformity parameter used in equation (2) for the test particle, which differs from bulk particles of medium size or density (Figure 1).

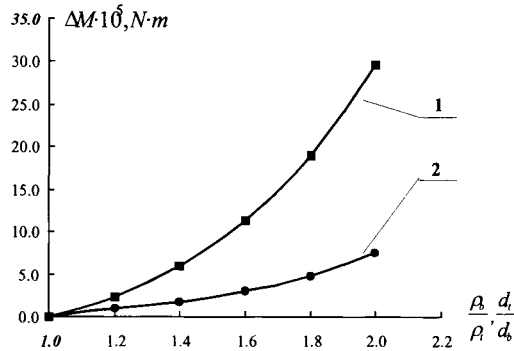


Figure 1: The nonuniformity parameter,  $\Delta M$ , as a dependent of the size,  $d$ , (1) and density,  $\rho$ , (2), of test particles (for bulk particles:  $d_b = 6.6$  mm,  $\rho_b = 2,084.45$  kg·m<sup>-3</sup>).

Analysis of (3) and (4) kinetic equations of migration shows that separation depends equally on size and density of particles. That is the main difference between migration kinetics and hydro-mechanical segregation kinetics when particle size is the only dominant distinctive parameter.

### Separation technology based on segregation effects in rapid gravity flows

In accordance with discussed features of segregation phenomena in a rapid, shear flow, it may be assumed that due to rational combined application of hydro-mechanical segregation and migration effects, the process of particle separation might be organised on size and density simultaneously. This assertion may be substantiated by the fact, that the hydro-mechanical segregation effect has a functional analogy with sieve separation, whereas the functional features of migration effects are adequate for pneumatic and hydraulic separation of particulate solids.

The most acceptable basis for organising the separation process in the mode of shear flow is for a rapid gravity flow on a rough chute. These flows exist on a rough chute at angles of a slope that are equal or exceed the angle of the material at rest. There are several flow modes that may be observed, depending on the slope angle (see Savage, 1983). Each has specific profiles of velocity and of fractions of void volume.

Thus the problem of complex use of hydro-mechanical segregation and migration effects assumes the definition of flow modes, when the flow parameters are favourable for both the first and the second effect.

The analysis of (2) and (3) kinetic equations shows that migration, as well as hydro-mechanical segregation intensity, increase proportionally to the shear rate ( $du/dy$ ). But to support the high intensity of these effects, different flow conditions are re-

quired. So to intensify hydro-mechanical segregation, a shear flow with a minimum fraction of void volume,  $\epsilon$ , is necessary. This conclusion is proven by the fact that with an increase in the fraction of void volume, the value of non-uniformity parameter  $\Delta M$  rapidly decreases (Figure 2).

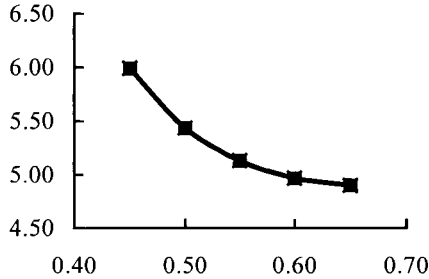


Figure 2: Nonuniformity parameter,  $\Delta M$  (ordinates in  $10^5$  Nm) versus fraction of void volume,  $\epsilon$  (abscisses), of rapid gravity flow at flow parameters:  $d/d_b = 1.4$ ;  $d_b = 6.6$  mm;  $dU/dy = \text{constant}$ , where  $d$  and  $d_b$  are the test and bulk particle diameters, respectively.

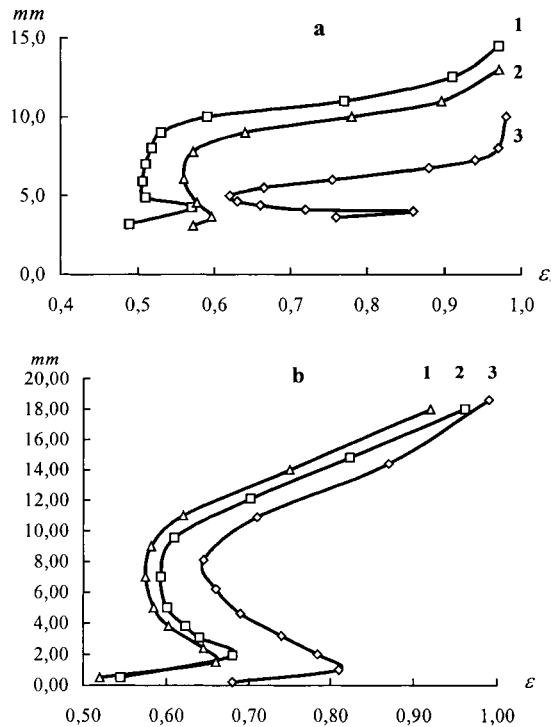


Figure 3: Profiles of the fraction of void volume in the gravity flow on a rough chute at:  
**a)** various flow depths  $h$  (1, 2 and 3 corresponding to  $h = 14$  mm; 12 mm and 1 mm respectively)  
**b)** various chute angles  $\alpha$  (1, 2 and 3 corresponding to  $\alpha = 34.5^\circ$ ;  $35.5^\circ$  and  $41^\circ$  respectively).

Conversely, in order to intensify particle migration, high values of the fraction of void volume and of the concentration gradient of solid fraction are needed. It happens because the value of migration coefficient,  $D_s$ , is proportional to the mean particle-distance,  $S = \bar{V}' / \bar{F}$ , and the rate of change of this distance,  $\partial \ln S / \partial y$ , in the direction of the migration flow,  $y$ .

Figure 3 shows the results of experimental determination of the fraction of void volume in a rapid gravity flow of silica-manganese slugs on a rough chute. These results lead to the conclusion that a decrease in the slope angle and increase in the flow value cause an intensification of hydro-mechanical segregation. And vice versa, an increase in the slope angle and decrease in the flow value (the bed depth) make the migration predominant over hydro-mechanical segregation. Consequently, we can assume that there are some optimal values for the slope angle and that the value of the flow when migration and hydro-mechanical segregation intensities are equal, and simultaneously provide maximum effectiveness of particle separation by size and density. These conditions, favourable for hydro-mechanical segregation, as well as for migration, have been defined by generalisation of the experimental data. Figure 4 shows the typical profiles of the fraction of void volume and light particle distribution in a rapid gravity flow of particles differing in size and density. Such profiles may be observed on a rough chute, under flow conditions corresponding to the conditions of high intensity of both migration and hydro-mechanical segregation effects.

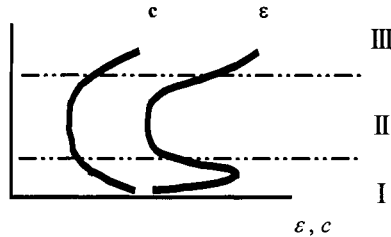


Figure 4: Typical profiles of the fraction of void volume ( $\epsilon$ ) and light particle distribution ( $c$ ) in gravity flows of particles differing in size and density on a rough chute.

This flow may be divided into three zones, depending on the solid phase and the test component distribution. zones I and III, situated near the bottom and the free surface of the flow, have large values for the fraction of void volume and its gradients. Consequently, these zones have favourable conditions for migration effects.

On the other hand, the central zone of the flow, zone II, has minimum values for the fraction of void volume and its gradients, which create favourable conditions for hydro-mechanical segregation. Thus, zone II, situated in the centre of the flow, functions as a sieve separator, so the large particles in this zone move upward to zone III, and small particles move downward to zone I. In the top zone III and in the bottom zone I particles, sorted on size, are separated mainly by density. According to the migration mechanism, taking place in these zones, dense particles move towards the gradient of the fraction of solid volume, i.e. to zone II. As a consequence of the complex act of migration and hydro-mechanical segregation effects, the dense component will be

concentrated in the central zone II, and the light component will be forced to the peripheral zones I and III. Usually, there are not enough migration and hydro-mechanical segregation effects in a rapid gravity flow to provide the necessary effectiveness of the mixture's separation. In this case, it may be recommended to use the principle of multi-stage separation with the counter-current of the non-uniform particles (see Dolgunin et al., 1990). Some results of experimental and industrial tests of the developed technology are shown in Table I.

Table I: Some technological parameters of the gravity separation, based on segregation effects.

Raw material	Admixture concentration in raw materials (%)	Finished product	Admixture concentration in finished product (%)	Yield (%)
Mica shales	70	Mica	4	94
Silica-manganese slag	87	Silica-manganese	19	96

### Conclusions

To minimize environmental pollution and increase the reliability of traditional separation technologies of solid particles differing simultaneously in size and density, dry gravity-separation technology is suggested. This technology is based on the combined application of segregation effects in rapid gravity flows of particulate mixtures. Such flows are performed on a rough chute, installed at an angle to the horizon that is greater than the angle of the material at rest.

Three zones differing from each other according to fractions of void volume appear in the moving bed of particles under certain flow conditions. Two basic segregation effects - hydro-mechanical segregation and migration - take place in such zones. During the hydro-mechanical segregation effect, separation of particles on size prevails, whereas the migration effect leads to separation on density and size.

Such special features of gravity-flow dynamics on a rough chute were used to provide separation of particles differing in size and density into the volume of a single moving bed of particulate mixtures.

### References

- Dolgunin, V.N., Ukolov, A.A. and Borschov, V.J., 1990. Model of segregation in shear flow of particulate solids and multifunctional modules for processes with separation. *Int. Congress of Chemical Engineering, Chemical Equipment Design and Automation, CHISA-90, Prague*, 36.
- Dolgunin, V.N., and Ukolov, A.A., 1995. Segregation modeling of particle rapid gravity flow. *PowderTechnology*, 83, 95-103.
- Dolgunin, V.N., Kudy, A.N. and Ukolov, A.A., 1998. Development of the model of segregation of particles undergoing granular flow down on inclined chute. *Powder technology*, 96, 211-218.
- Savage, S.B., 1983. Granular flows down rough inclines – Review and Extension. In: J.I. Jenkins and M. Satake (Editors), *Mechanics of Granular Materials*, Elsevier Science Publishers, Amsterdam, 261–282.

## TRAPPED VORTEX MAGNETIC SEPARATION (TVMS)

Z. Li, J.H.P. Watson

Department of Physics & Astronomy, University of Southampton, Southampton  
SO16 3PU, United Kingdom

### Abstract

This paper is to present the study on the mechanism involved in Trapped Vortex Magnetic Separation (TVMS). In a single wire system, a pair of stable and symmetrical eddies can be induced behind the wire only when Reynolds number is between 6 and 40. This study used a CFX software package and a high-speed video camera system to investigate the hydrodynamic behavior in a multi-wire system. It was revealed that a pair of stable and symmetrical vortices can be trapped between two cylinders even when Reynolds number reached 300. Magnetic particles can be captured in the trapped vortex regions in TVMS system. It can produce not only the higher selectivity, but also the higher processing rate. The experimental results of some industrial ores obtained with TVMS system demonstrated the advantages of TVMS over High Gradient Magnetic Separation (HGMS).

*Keywords: magnetic separation, vortex, TVMS*

### Introduction

Selectivity has been the main problem in magnetic separation technology. Current High Gradient Magnetic Separation (HGMS) technology can capture from the slurry the magnetic particles with the size down to sub-microns. In order to provide high magnetic force, stainless steel wool is often used as matrix in HGMS, which is placed at random in a canister. There are two disadvantages for HGMS technology. Firstly, it is not suitable for the samples with size distribution above 20  $\mu\text{m}$  because the coarse particles will cause blockage in the matrix. Secondly, the severe mechanical entrapment in HGMS reduces the selectivity of the process. This is the main reason preventing HGMS from wide industrial applications. It was found in our study that when the slurry runs through the canister in HGMS, the magnetic particles are captured on the upstream side of the matrix with the magnetic deposit intruding in the slurry flow. This inevitably results in that the non-magnetic particles are easily mechanically trapped in the magnetic deposits on the matrix.

In our previous work using a single wire microscope system in conjunction with a high-speed video camera, it was revealed that when separation process is run at certain Reynolds number, i.e.  $6 < \text{Re} < 40$ , a pair of stable and symmetrical vortices can be induced behind the matrix. The magnetic particles can be brought into the vortex region and captured on the downstream side of the matrix. It was demonstrated that downstream capture, vortex magnetic capture, can produce much higher selectivity than HGMS, which means both the quality of the magnetic product and the recovery of the non-magnetic product are improved. Besides, because the process is carried out under higher Reynolds number, the throughput of the process is increased.

This paper describes the further study on the mechanism involved in the vortex

magnetic capture in a multi-wire system. A CFX Software package and a high-speed video camera system were used to study the hydrodynamic behaviour of the particles. It was revealed that in a multi-wire system a pair of stable and symmetrical eddies can be formed and trapped between the two wires even when the Reynolds number reaches 300. This can provide much higher throughput for a system of Trapped vortex Magnetic Separation (TVMS).

### Study on hydrodynamic mechanism in TVMS system

When fluid flows around a blunt body, e.g. a circular cylinder wire, the flow pattern depends on the Reynolds number. The Reynolds number is the ratio of inertia force to viscous force and is given by

$$Re = \rho V_0 d / \eta \quad (1)$$

Where  $\rho$  and  $\eta$  are the density and the viscosity of the fluid, respectively.  $d$  is the diameter of the cylinder wire and  $V_0$  is the velocity of the fluid. According to the classical hydrodynamic theory, when  $6 < Re < 40$ , two symmetrical eddies, rotating in opposition to each other, are formed behind the cylinder wire. When  $Re > 40$ , the eddies become more volatile and unsymmetrical.

In our study, a CFX software package was used to analyze hydrodynamic behavior when water flows through a multi-wire system in a rectangular arrangement, where three columns of cylinders were placed in a tube with four cylinders in each column. The diameter of a cylinder was  $d$  cm. The gaps between two rows were  $d$  cm and the gaps between the two columns were  $d/3$  cm. Figure 1 shows the flow pattern at  $Re = 90$ . It was assumed that the length of the cylinders was long enough so that the effect from the third dimension was ignored. In a TVMS system, the gaps between the columns serve as passenger ways for the feed slurry. The gaps between the rows, where vortices are trapped, serve as magnetically collecting area. It can be seen from Figure 1 that the vortices formed in the central column (the left column in the figure) are symmetrical and stable. The wall effect can be seen in the other two columns (the right column in the figure) where the vortices formed between the two cylinders were unsymmetrical.

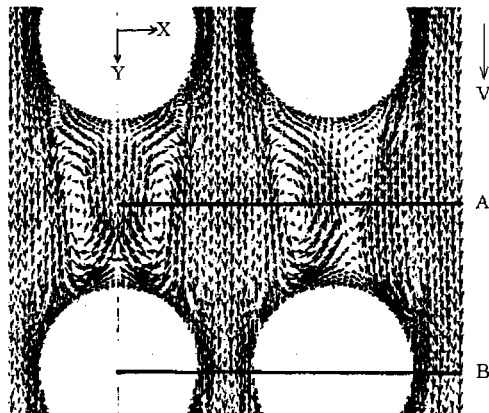


Figure 1: Flow pattern at  $Re = 90$  with the gaps between the cylinders in vertical direction being the diameter of the cylinder.



Figure 2 shows the distribution of  $V_y/V_0$  along the line A, indicated in Figure 1. It can be seen that  $V_y/V_0$  varies dramatically along the line A. The negative values of  $V_y/V_0$  show the velocity of the returning flow in vortices. The zero values of  $V_y/V_0$  show zero velocity at the stagnation points of vortices except the point at  $x = 6.5$  which is on the wall of the tube. The maximum of  $V_y/V_0$  is about 4.6, which appears approximately on the central line in the passenger ways between the two columns of cylinders. As shown by the streamlines in the passenger ways, it can be seen that only the boundary layer flow on the both sides of the cylinders in the passenger ways are involved in the vortices forming between the cylinders in the vertical direction. This means that magnetic particles have to be kept in the boundary layers to enter the vortex regions. The distribution of the magnetic field in TVMS system should always be designed so that it is in favour of attracting magnetic particles into the boundary layer flow.

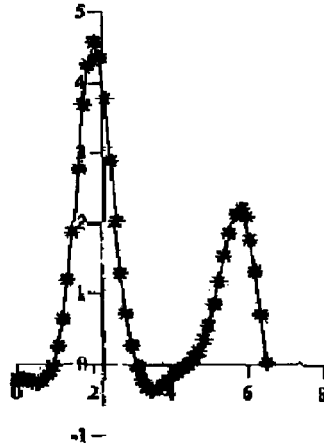


Figure 2: The distribution of  $V_y/V_0$  along the line A as indicated in Figure 1.

Coutanceau and Bouard studied the returning flow encountered in vortices behind a single cylinder at  $6 < Re < 40$  and pointed out that the velocity of the returning flow in the corresponding recirculating region is much smaller than the velocity of the main flow  $V_0$  and it increases with  $Re$ . In the case as shown in Figure 1, where the vortices are located between two cylinders with a much larger  $Re$ ,  $(-V_y/V_0)_{\max} = 0.2$  on the central line of the returning flow at  $x = 0$ . As we know, hydrodynamic force is the main competing force against magnetic force in magnetic capture. In HGMS, magnetic particles are captured in the upstream side of the matrix, which intrude in the slurry. So magnetic force produced by the matrix has to overcome the competing force due to  $V_0$ . In TVMS system, the competing force is much smaller in the vortex regions because  $(-V_y)_{\max} = 0.2V_0$ . This explains why TVMS system can provide higher processing rate without reducing the capture of the magnetic particles.

Figure 3 shows the distribution of  $V_y/V_0$  along the line B, as indicated in Figure 1. The maximum of  $V_y/V_0$  reaches 5.9, which could help preventing blockage in the

passenger ways. That the peak value of  $V_y/V_0$  reduced to about 3.2 at  $X = 6$  is obviously because of the wall effect.

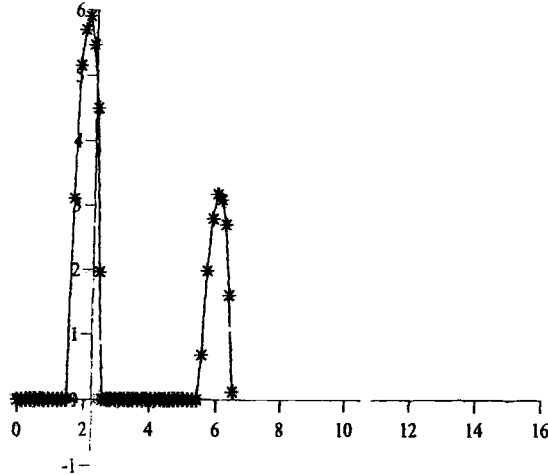


Figure 3: The distribution of  $V_y/V_0$  along the line B, as shown in Figure 1.

Figure 4 shows the flow pattern at  $Re = 90$  when the gaps between the cylinders in the vertical direction are reduced to half of the diameter of the cylinder. Again, we see stable and symmetrical vortices formed between the cylinders in the vertical direction.

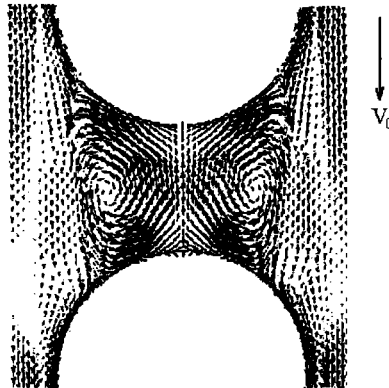


Figure 4: Flow pattern at  $Re = 90$  with the gap between the cylinders being half the diameter of the cylinder.

### The analysis of the particle trajectories with a high-speed video camera

A high-speed video camera together with a cylinder cell was used to record the overall process in the trapped vortex region between the cylinders. The cylinder cell, in which 12 cylinders of 0.3 cm in diameter are mounted in  $3 \times 4$  rectangular

arrangement and in the configuration known as the longitudinal configuration, is placed centrally between poles of an electromagnet. The gaps between the cylinders in the vertical direction are 0.3 cm and the gaps between the cylinders in the horizontal direction are 0.1 cm. The flow velocity in the cell is controlled by adjusting the size of an outlet orifice.

The high-speed video camera system provides operating speeds from 30 to 1,000 frames/s at full aspect ratio pictures. An image processing software package was used to analyze the trajectories of the particles trapped in the vortices region between the two cylinders located in the central column in the cell. The other two columns of cylinders were used to reduce the effect the cell walls. The sample used was synthetic diamond, of which the size was about 0.4 mm.

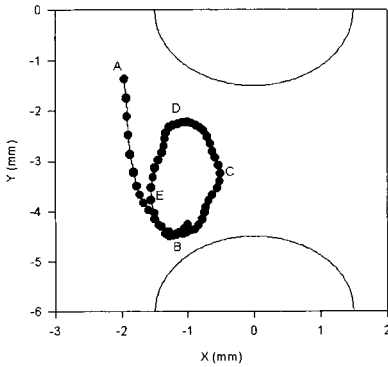


Figure 5a: The trajectory of a particle in the vortex region between two cylinders at  $V_0 = 12.5$  cm/s and  $H_0 = 0$ .

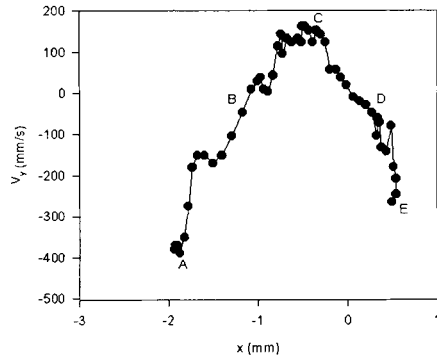


Figure 5b: The variation of  $V_y$  of the particle at different position in the trajectory in Figure 5a (to make the curve clearer the positions of points from C to E on x axis were adjusted).

Figure 5a and Figure 6a show the trajectories of two particles in the vortices region between two cylinders. The trajectory was obtained with the high-speed video system running at 1000 frames/s and the slurry passing through the cell at  $V_0 = 12.5$  cm/s and  $H_0 = 0$ . The velocity of the particle,  $V_y$ , at the different positions in the trajectory was shown in Figure 5b and Figure 6b, respectively. In Figure 5b, in order to avoid the overlap of the curve, the positions of the points from C to E on X axis were adjusted, e.g.  $x_E = x_C + |x_E - x_C|$ . It can be seen that the point A with  $x = -2$  is located near the central line of the passenger way. The corresponding  $V_y/V_0 = 400/125 = 3.2$ . The theoretically calculated result is about 4.6, as shown in Figure 2. At the stagnation points B and D,  $V_y$  dropped to zero. The points from B to D through C form the returning flow in the vortex.  $V_y/V_0$  at those points varied from 0 to about 1. The maximum of  $V_y/V_0$  in the returning flow appeared at the point C where  $V_y/V_0$  was about 1. It dropped quickly and became zero at the point D. It was very difficult to find two particles appearing in a pair of vortices at the same time. But, it was clearly observed from the monitor that the stable and symmetrical vortices formed between the cylinders in this experiment, in which  $Re = 375$ . This can also be seen from the trajectories shown in Figure 5a and Figure 6a, which can be reasonably seen as half of

a pair of vortices. As discussed above, a pair of stable and symmetrical vortices formed behind a single cylinder only when  $6 < Re < 40$ . In multi-wire system, it was demonstrated that the stable vortices can be formed at much higher  $Re$ .

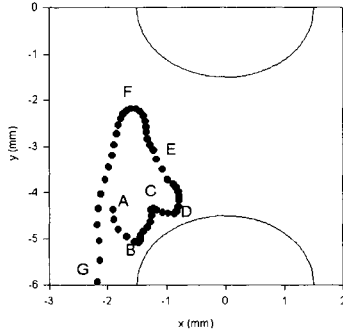


Figure 6a: The trajectory of a particle in the vortex region between two cylinders at  $V_0 = 12.5$  cm/s and  $H_0 = 0$ .

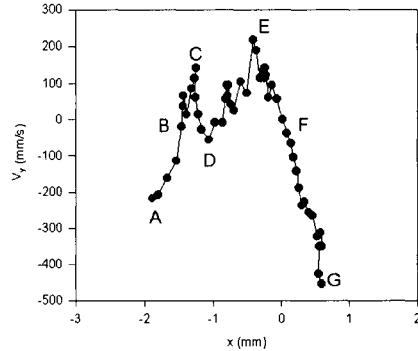


Figure 6b: The variation of  $V_y$  of the particle at different positions in the trajectory in Figure 6a (to make the curve clearer the position of points from D to G on X axis were adjusted).

## Experiments and the experimental results

### *Wollastonite ore*

Wollastonite is mainly used in ceramic industry, paint industry, etc. The sample treated contained 0.35% FeO and its size range was  $\sim 300$   $\mu\text{m}$ . The purpose of the treatment was to reduce the colouring iron-bearing silicates. The experimental results obtained with HGMS and TVMS are listed for comparison in Table I. The expanded metal mesh was used as matrix in HGMS. It can be seen from Table I that when  $H_0 = 1$  T, FeO was reduced to 0.11%. But the recovery of the desired product, non-mags, obtained with TVMS was 9% higher than the one with HGMS. It can also be seen that HGMS's processing rate had to be lowered to 2.9 cm/s to reduce FeO content in the non-mags from 0.35% to 0.09% at  $H_0 = 4$  T.

This resulted in serious mechanical entrapment in the magnetic product and, consequently, the recovery of the non-mags dropped to 47%. On the other hand, TVMS produced very impressive results. With FeO content reduced to 0.09% at 4 T, it can be run at much higher processing rate, 8 cm/s, with the recovery of the non-mags reached 89%. It was 42% higher than using HGMS. The results also indicated that TVMS can provide higher processing rate than HGMS in some cases.

Table I: The purification results of Wollastonite ore with TVMS and HGMS.

$H_0$ (T)	$V_0$ (cm/s)	FeO (%) in non-mags	Rec. of non-mags (% wt)	System
1	8.3	0.11	84	HGMS*
1	8.0	0.11	93	TVMS
4	2.9	0.09	47	HGMS
4	8.0	0.09	89	TVMS

\*The data obtained with HGMS was from the company, the sample provider.

*Feldspar ore*

Feldspar is mainly used in glass and ceramic industry. The aim of magnetic separation was to reduce iron-bearing biotite and muscovite. The sample treated contained 0.66% FeO with particle size being  $<425 \mu\text{m}$ . The experimental results obtained with TVMS and HGMS were listed for comparison in Table II. The expanded metal mesh was used as matrix in HGMS. As can be seen, when the testing conditions were similar in HGMS and TVMS, both the recovery and the iron reduction in the non-mags obtained with TVMS were significantly better than with HGMS.

Table II: The purification results of Feldspar ore obtained with TVMS and HGMS.

$H_0$ (T)	$V_0$ (cm/s)	FeO % in non-mags	Rec. of non-mags (wt%)	System
1	8.7	0.11	86.8	HGMS*
1	8.0	0.10	93.2	TVMS
2	8.7	0.10	85.3	HGMS
2	8.0	0.08	92.6	TVMS

\* The data obtained with HGMS was from the company, the sample provider.

**Conclusions**

Hydrodynamic mechanism involved in the TVMS system was studied by computing simulation with a CFX software package and experiments with a high-speed video camera system. Two main conclusions were reached:

- in classical hydrodynamic theory, stable and symmetrical eddies are formed behind a single cylinder only when  $6 < \text{Re} < 40$ ; in our TVMS system, stable and symmetrical eddies can be formed between two cylinders even when  $\text{Re} > 300$ ;
- in the trapped vortex regions between cylinders, the velocity of the returning flow is much slower than the velocity of the main flow  $V_0$ ; this well explained why TVMS could provide higher recovery of magnetic material at higher processing rate than HGMS.

TVMS system was successfully used to treat the industrial ores, wollastonite and feldspar ores. The comparison between the results obtained with TVMS and HGMS demonstrated that TVMS system can not only produce much better selectivity, but also produce higher throughput. It also indicated that TVMS technology can treat samples with a wide size range.

## GENERAL TRENDS OF GRAVITY SEPARATION

M. Barsky, E. Barsky

The institutes for applied Research, Ben-Gurion University of the Negev, P.O.B. 653,  
Beer-Sheva, Israel

### Abstract

Ascending turbulent two-phase currents are a frequent phenomenon in natural and industrial situations alike. They are exceedingly complex. Attempts to describe the processes involved by analytic means have not met with success. It has been seeking to elucidate the principal mechanisms operating in two-phase flow by examining natural finely dispersed materials moving in channels of varying shape, length and configuration. Visual observation supported by filming reveals that the process is totally chaotic. The motion of each particle is purely random, i. e., it is impossible to predict either the instantaneous velocity of motion of a given particle or the direction of this velocity. Nevertheless, it is possible to formulate a clear-cut physical law that fully characterizes the process under consideration. It has been found that in every concrete case there exists a range of velocities within which the solid phase of the stream is distributed between the upper and lower outlets according to a fixed relationship. The law, it has been formulated and validated experimentally for this range of velocities, is that separation of the various narrow size classes (between the two ends of the channel) proceeds in an identical manner regardless of its configuration and length. This uniformity reflects the invariance of the phenomenon with respect to the size composition of the solid phase, the size and density of the particles, and the velocity and density of the carrier medium. It has been verified for an array of powdered materials of diverse densities in 87 different channels.

*Keywords: gravity separation, particle motion*

### Introduction

Ascending two-phase streams are frequently to be seen in nature, for example in jets of gas or liquid spurting from the ground, in mountain and valley winds, in volcanic eruptions and geysers. They are also frequently encountered in industry, all the way from air-lift devices to fluidized bed furnaces. Flows involving two phases are exceedingly complex. The mass process involved is usually described with the help of the fundamental laws that govern the displacement of single particles. However, these laws give only a first approximation of the mechanism governing the real process, and they have proved inadequate to describing the actual mass movement of the particles.

### Fine particle flow

In the hope of shedding light on this problem, it has been looked at the principal features exhibited by natural finely dispersed materials flowing in a two-phase stream in channels of varying shape, size and configuration (Figure 1). Visual observation supported by filming indicates that, in real life, the process of turbulent two-phase flow displays a wide array of random phenomena, the most important of which are turbulent eddies, unevenness of concentration fields, formation of particle clusters,

non-spherical shape of the particles, inter-particle collisions, and collisions between particles and channel walls (Barsky, 1980).

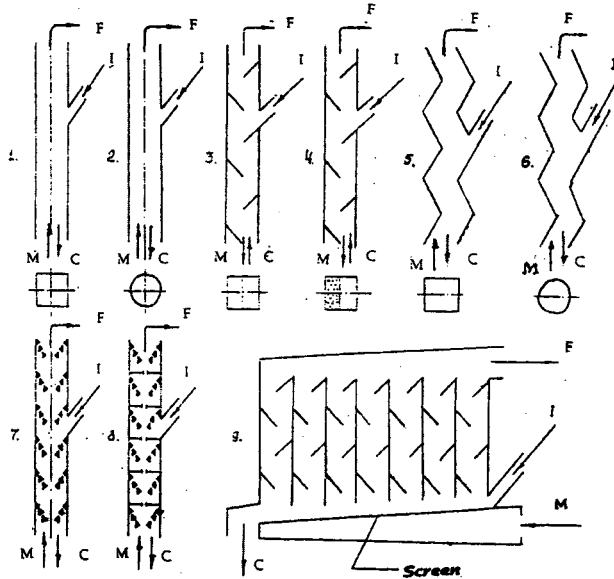


Figure 1: Instruments for powder classification in an ascending air stream. 1: Hollow tube of rectangular cross-section; 2: Hollow tube of circular cross-section; 3: Rectangular tube with baffle plates; 4: Rectangular tube with perforated plates; 5: Zigzag-shaped channel of rectangular cross-section; 6: Zigzag-shaped channel of circular cross-section; 7: Multi-cascade consisting of rectangular tube with concentric rings; 8: Multi-cascade consisting of round tube with concentric rings; 9: Multi-chamber device with sloping screen. i: Input; C: Medium (gas); M: Fine product; K: Coarse product.

These phenomena show up clearly in high-speed motion pictures or on photographs taken with strobe lights (Figure 2): one can see that the movement of individual particles is purely random. That is, it is impossible to predict the instantaneous velocity of a particle or the direction of this velocity, and thus the process as a whole is chaotic in nature. Having realized, then, that chaos is the characteristic feature of the initial distribution, and also that chaos holds the key to the general laws governing the process, it has been proceeded to study the specific physical mechanism that most fully resumed the process under consideration. The laws are related to chaos theory, but they are not subsumed by the settling curve equations. In all the channels, the baffle plates were fixed at angle of  $45^\circ$  to the channel wall.

### Powder separation

Let us look at the results of a concrete experiment with powder separation in a cascade separator (Figure 3).

The solid phase is introduced in the middle of the instrument, while air enters the instrument from below and rises. High velocities of flow assure complete removal of all solid particles from the instrument ( $w > 15$  m/s), while at low velocities ( $w < 2$  m/s) practically all the solid material falls counter to the flow.

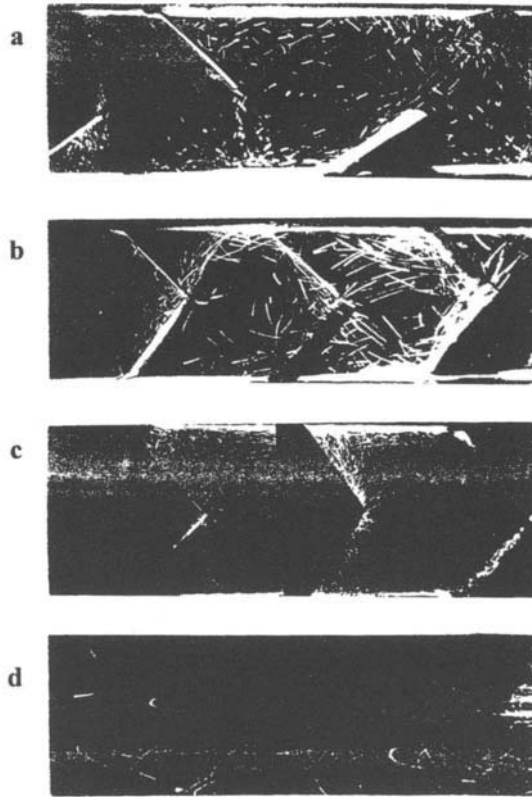


Figure 2: Stroboscopic photographs of particle tracks: a: hollow channel; b: channel with baffle plates in alternating diagonal pattern; c: channel with baffle plates in alternating checker-board pattern; d: channel with baffle plates arrayed to form cascade.

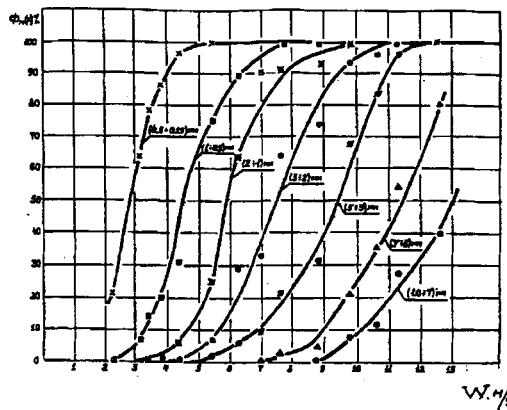


Figure 3: Fractional classification of quartz powder into different size classes as a function of the velocity of the air stream in a cascade-type channel with four elements ( $z=4$ ), feeder in uppermost element ( $i=1$ ).



In a broad spectrum of regimes situated between the regions of high and low air velocities, the material distribute itself between the upper and lower outlets in accordance with a definite relation. This distribution is most fully characterized by a parameter called *fractional distribution*:

$$\Phi_f(x) = \frac{n_i(x)}{N_i(x)} \quad (1)$$

where  $N_i(x)$  is the concentration of a certain narrow size fraction in the initial feed, in %;  $n_i(x)$  is the concentration of the same size fraction in the upper (fine) product, in %; and  $x$  is the mean particle size of this narrow fraction. The grain size distribution of a polymeric material is usually represented in terms of the proportion of particles belonging to a narrow size fraction (this narrow fraction is defined by the ratio  $x_{\max}/x_{\min} \leq 2$ ). As can be seen from Figure 3, at first, as the velocity rises above  $w = 2$  m/s, the fine fractions are drawn into the upper product to a greater degree than the coarse fractions. Later, as the velocity increases further, increasingly coarse particles are entrained as well.

### Fractional separation curves

The process reflected in the graph is obviously more orderly than the situation in the photographs. These curves may be termed *fractional separation curves*. It has been established experimentally that the shape of this curve is independent of the ratio between the various classes in the solid phase. The concentration of a given narrow size fraction in the initial feed (3.3%; 6.7%; 10%; 12.5%; 30%; 50%; 76.7%) has been repeatedly varied, while rigorously maintaining the velocity of flow at a fixed level; within a fixed range of limiting concentrations ranging up to 2 kg/m<sup>3</sup>, all the experimental points were found to lie on the curves. One might discern here a remote degree of physical analogy to Dalton's law for the partial pressure of mixtures of gases approaching an ideal gas in their properties. However, It has been established and verified experimentally that the processes obey a clear-cut general rule: it has been found that in media subject to turbulent regimes of motion, entertainment of the different size classes in a given channel takes place in a uniform manner controlled solely by the geometric characteristics of the flow, namely its length, configuration and boundary conditions. This property of uniformity is independent not only of particle size distribution, but also of the size and density of the particles and of the velocity and density of the medium. The statement in question is validated by experiments also carried out in water. When the abscissa is suitably altered the fractional separation curves in Figure 3 coincide, as shown in Figure 4. The values of expression  $gx/w^2$  have been plotted along the x-axis. This holds for all the channel types shown in Figure 1 without exception. In the most general case, it has been obtained the dimensionless criterion B:

$$B = \frac{gx^2}{w} \cdot \frac{(\rho - \rho_0)}{\rho_0} \quad (2)$$

where  $w$  is the velocity of the stream in m/s,  $x$  is the mean dimension of the narrow size class in m,  $g$  is the acceleration of gravity in m/s<sup>2</sup>, and  $\rho$ ,  $\rho_0$  are the density of the material and of the separation medium, respectively, in kg/m<sup>3</sup>.

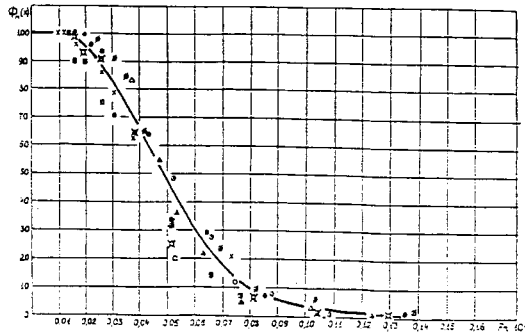


Figure 4: Fractional classification of quartz powder into different size classes as a function of  $Fr = gx/w^2$  for  $z = 4, i = 1$ .

The validity of this rule was tested in an array of powdered materials of various densities (1,070 kg/m<sup>3</sup>, 2,200 kg/m<sup>3</sup>, 2,675 kg/m<sup>3</sup>, 3,170 kg/m<sup>3</sup>, 4,350 kg/m<sup>3</sup>, 6,210 kg/m<sup>3</sup>, 7,810 kg/m<sup>3</sup> and 8,650 kg/m<sup>3</sup>). It was found that the results all lay on one curve (Figure 5).

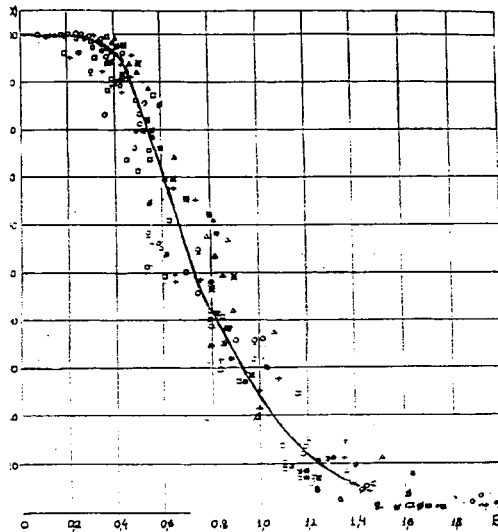


Figure 5: Fractional classification of various materials (of various densities) into different narrow size classes for  $z = 5, i = 2$  as a function of  $B = gx(\rho - \rho_0)/w^2\rho_0$ .

This uniformity is reflected in the following findings:

- The distribution of the solid phase in each specific channel lies uniformly along a single curve irrespective of: original composition of solid phase; limiting size; rate of flow of medium; concentration (up to 2÷8 kg/m<sup>3</sup> for different configurations of the channel); density of material and supporting medium.

- For  $B = \text{constant}$ , the different classes of size and density are distributed in a similar manner. This fact makes it possible to predict the results of the separation and to calculate the process.
- Since the universal curve obtained is identical over the entire set of technical factors reviewed above, its position in the coordinate system  $\phi_m(x) = \phi(B)$  only reflects the nature of the channel in which the process is taking place.
- From this rule, certain conclusions may be drawn regarding the minimal information required about the process and the separating device on which the process is realized. In principle, this minimal information is contained in a single experiment, from the results of which it should be possible to derive the universal curve in its entirety.
- The phenomenon of equivalence applies to any conceivable regime of motion for streams with suspended material, from those in which the solid phase falls counter to the direction of flow, to pneumatic transport.

### **Conclusions**

To sum up, a new, simplified relationship pertaining to the process of separation has been obtained reflecting the uniform character of the process of entertainment of the various size and density fractions of the solid phase in ascending turbulent two-phase flows.

### **References**

Barsky, M., 1980. Powder classification (Fraksionirovanie poroshkov). Moscow, Nedra.

## **FLOTATION – KINETICS AND MODELLING**

This Page Intentionally Left Blank

<b>An Investigation into the Enrichment of Phosphate Slime by Column Flotation</b> H. Ipek, H. Ozdag	<b>C8a-1</b>
<b>An Investigation on the Effects of Ore Grade and Particle-Liberation Size in Gold Recovery by Coal-Oil-Gold Agglomerate Flotation</b> Y. Cilingir, S. Sen	<b>C8a-6</b>
<b>Characterization of Rigid Spargers and Selection for Flotation Columns</b> C.O. Gomez, R. Escudero, J.A.Finch	<b>C8a-14</b>
<b>An Interactive Dynamic Flotation Model Framework</b> O.A. Bascur	<b>C8a-21</b>
<b>A Computational Fluid Dynamics (CFD) Model for a Bubble Separation Tank</b> P.R. Desam, A. Datta, J. D. Miller	<b>C8a-32</b>
<b>Characterization of the Flotation Froth Structure and Color by Machine Vision (Chaco)</b> G. Bonifazi, V. Giancontieri, A. Meloni, S. Serranti, F. Volpe, R. Zuco, H. Koivo, J. Hätönen, H. Hyötyniemi, A. Niemi, P. Sipari, H. Kuopanporrti, R. Ylinen, I. Heikkila, S. Lahteenmaki, J. Miettunen, O. Stephasson, W. Wang, L.E. Carlsson	<b>C8a-39</b>

This Page Intentionally Left Blank

## AN INVESTIGATION INTO THE ENRICHMENT OF PHOSPHATE SLIME BY COLUMN FLOTATION

H. Ipek, H. Ozdag

Department of Mining Engineering, Osmangazi University, Eskisehir, Turkey

### Abstract

Fertilizers seem to be one of the most important inputs in agricultural production for obtaining more crops from the fields. Phosphate is the main source of fertilizers. Phosphate which is used in the fertilizer industry must contain at least 30%  $P_2O_5$ . The sample used in this study was supplied by the Directorate of Mazıdağ Phosphate minework. Petrographic studies showed that dahllite and colophonite were the major phosphate minerals, and the main gangue mineral was calcium carbonate. The sample's average grade was 20.95%  $P_2O_5$ .

The aim of this study was to utilize column flotation to recover phosphate from Mazıdağ phosphate plant tailings, and compare the results of column flotation with the results of conventional flotation techniques. Although a 31.50%  $P_2O_5$  concentration with 78.80% recovery was obtained in column flotation, a 29.58%  $P_2O_5$  concentration was obtained with 76.69% recovery in cell flotation. A 31.50%  $P_2O_5$  result is acceptable for phosphoric acid production.

*Keywords: Phosphate flotation, column flotation*

### Introduction

Phosphate, which is regarded as a savior of mankind facing famine, is used 95% as a fertilizer in agriculture. Today, the use of fertilizer increases 6% each year and 1/3 of it contains phosphate. The only source of it is the phosphate rock. 75÷85% of phosphate rock is used in the fertilizer industry and the rest is used in the fodder industry, food industry, detergent industry and chemical industry (Lowers, 1985; Yener, 1981). Since it is difficult to produce a phosphate concentration of 30%  $P_2O_5$  for super phosphate production, column flotation was tried and its application to carbonate flotation was examined. Furthermore, its results were compared with those of cell flotation.

### Experimental

#### *Sample used in experiments*

The phosphate sample used in enrichment experiments is slime provided from the Etibank Mazıdağ Phosphate Work. The particle size distribution of the sample was measured with the Malver Series 2600C Droplet and Particle Size device, and it was determined that 80% are under 22  $\mu\text{m}$ .

Under microscopic examination, it appeared that the sample consisted of colophonite, dahllite, apatite, feldspars, calcite and quartz.

The particle size distribution and chemical analysis of the sample are given in Table I and Table II.



*Column flotation tests*

The column flotation tests were carried out in a laboratory-type square column with a 6.25 cm<sup>2</sup> cross-sectional area and 185 cm height. The flotation zone consists of two parts; the cleaning and collecting zones. The bubbles are created by a sparger under the column. Air is provided by a compressor. The wash water rate was set at 6 cm·s<sup>-1</sup>.

Table I: Particle size distribution of the sample

Size (μm)	Under (%)	Size (μm)	Under (%)
118.4	100.0	6.4	27.5
54.9	99.3	5.0	20.5
33.7	93.7	3.9	14.2
23.7	83.8	3.0	9.9
17.7	70.3	2.4	6.1
13.6	58.2	1.9	3.7
10.5	46.1	1.5	2.6
8.2	35.5	1.2	2.0

Table II. Chemical analysis of the sample

Element	(%)
P <sub>2</sub> O <sub>5</sub>	20.95
SiO <sub>2</sub>	6.09
CaO	46.20
Al <sub>2</sub> O <sub>3</sub>	1.86
Fe <sub>2</sub> O <sub>3</sub>	1.60
MgO	4.04
Loss on ignition	25.23

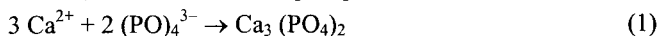
*Column flotation tests*

The column flotation tests were carried out in a laboratory-type square column with a 6.25 cm<sup>2</sup> cross-sectional area and 185 cm height. The flotation zone consists of two parts; the cleaning and collecting zones. The bubbles are created by a sparger under the column. Air is provided by a compressor. The wash water rate was set at 6 cm·s<sup>-1</sup>. The feeding is carried out from 1/3 of the upper part of the column. Since the flotation of phosphate in this study was difficult, the phosphate concentrate was collected at the bottom of the column and the gangue was at the top of the column. Since calcium carbonate and calcium phosphate belong to the polar type salt minerals, their flotation characters are similar. Therefore, it is difficult to separate them by flotation. Also, selectivity in small sizes completely disappears. The sensitivity of these minerals to anionic collectors is quite high. Due to high chemical activity on their surfaces, a chemical adsorption is necessary for collectors to adsorb on the surface. An acid environment is needed to float the carbonate gangue and an alkali one to float phosphate.

*Reverse flotation tests where phosphate is depressed*

With this method, which requires phosphate to be depressed and the carbonate gangue to be floated, acid environment tests are carried out, and phosphoric acid was used as

a pH controlling agent because of its depressing effect towards the phosphate (Fuerstenau, 1962). The depressing effect of phosphoric acid occurs as follows: on the broken surfaces (as a result of crystal lattice being decomposed) of phosphate,  $(\text{PO}_4)^{3-}$  and  $\text{Ca}^{2+}$  ions are present. When phosphoric acid ( $\text{H}_3\text{PO}_4$ ) is added into the pulp,  $\text{Ca}^{2+}$  ions on the surface of the phosphate particles unite with the disassociated  $(\text{PO}_4)^{3-}$  ion of phosphoric acid, and create calcium phosphate.

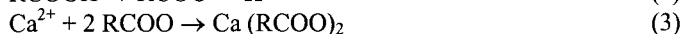


Consequently, the amount of ion on the particles increases due to surplus of  $(\text{PO}_4)^{3-}$  (because  $\text{Ca}^{2+}$  loses its electrical charge due to its unity with  $(\text{PO}_4)^{3-}$  ions) and the surface charge of phosphate particles becomes negative. The effect of the following factors on reverse flotation were examined:

- appropriate choice of collectors;
- collector consumption;
- pH;
- amount of solid in pulp.

#### *Tests for choosing the appropriate anionic collector*

Carboxylate type collectors are used in carbonate flotation. Collectors belonging to this group are organic acids (fatty acids) and their salts. Carboxylic acids affect carbonate with chemical adsorption and make the carbonate surface hydrophobic. This can be explained as follows;  $\text{CO}_3^{2-}$  and  $\text{Ca}^{2+}$  are present on the surface of broken carbonate in the pulp. When carboxyl acid is added into the pulp, the carboxylic group which departs as a result of this creates a reaction with  $\text{Ca}^{2+}$  on the carbonate surface and creates calcium carboxylate. As a result, the element, which is covered with calcium carboxylate, does not get wet in water and floats by sticking to the froth.



If a salt of carboxylic acid is used as a collector, this salt hydrolyses and gives carboxylic acid. This reacts with calcium by disassociation as described above.

In the study are used as collectors  $\text{C}_{17}\text{H}_{33}\text{-COOH} = 2 \text{ kg/t}$  and  $\text{C}_{17}\text{H}_{33}\text{-COONa} = 2 \text{ kg/t}$

Throughout the experiment, the collectors were added in 2 steps with a conditioning time of 5 min., in each step. Results are shown in Table III. The experimental conditions were: quantity of collectors = 2 kg/t; phosphoric acid = 734.4 g/t; pH=4.8; % solid: 12.5; conditioning time = 5 + 5 + 5 min; flotation time = 15 min.

Table III: Recovery and grade of  $\text{P}_2\text{O}_5$  versus anionic collectors.

	Collector	
	Na-oleate	Oleic acid
$\text{P}_2\text{O}_5$ grade (%)	29.40	29.34
$\text{P}_2\text{O}_5$ recovery (%)	79.85	72.28

#### *Deciding on the collector amount*

The following points were kept constant during experiments where different amounts of Na-oleate were used. The effect of amounts of Na-oleate on recovery and grade is

shown in Table IV. The experimental conditions were: phosphoric acid = 734.4 g/t; pH = 4.8; % solid = 12.5; conditioning time = 5 + 5 + 5 min; flotation time = 15 min. It was determined that there was a linear relationship between the amount of Na-oleate and %P<sub>2</sub>O<sub>5</sub> (where the amount of Na-oleate increased, %P<sub>2</sub>O<sub>5</sub> increased). However, the recovery decreased slowly up to 4 kg/t and fast over 4 kg/t.

Table IV: Recovery and grade of P<sub>2</sub>O<sub>5</sub> versus amount of Na-oleate.

	Amount of Na-oleate (kg/t)				
	2	3	4	5	6
P <sub>2</sub> O <sub>5</sub> grade (%)	29.40	30.20	31.50	32.00	32.40
P <sub>2</sub> O <sub>5</sub> recovery (%)	79.85	79.18	78.81	72.20	65.30

When these results were taken into consideration, it was obvious that the best result was obtained with 4 kg/t Na-oleate.

#### *The effect of pH on flotation*

The following conditions were kept constant during the experiment, except for the pH and the phosphoric acid amounts. The experimental conditions were: Na-oleate = 4 kg/t; % solid = 12.5; conditioning time = 5 + 5 + 5 min; flotation time = 15 min.

The best result was obtained at pH = 4.5. However, the amount of phosphoric acid used was too great (1356.0 g/t), a pH = 4.8 was chosen. Since carbonate quickly dissolves, a measurement below pH = 4.5 could not be taken into consideration. It was seen that both the grade and the recovery decreased in alkali environments. The effect of pH on recovery and grade is shown in Table V.

Table V: Recovery and grade of P<sub>2</sub>O<sub>5</sub> versus amount of Na-oleate.

	pH						
	4.5	4.8	5.5	6.0	6.5	7.0	7.5
P <sub>2</sub> O <sub>5</sub> grade (%)	31.62	31.50	30.200	29.46	28.68	28.10	27.88
P <sub>2</sub> O <sub>5</sub> recovery (%)	80.01	78.81	73.26	65.69	45.54	35.68	23.34

#### *The effect of solid amount on flotation*

While various amounts of the solid were examined, the following conditions were kept constant. Five different % of the solid were studied at 10%, 12.5%, 15%, 17.5% and 20%. The experimental conditions were: Na-oleate = 4 kg/t; phosphoric acid = 734 g/t; pH = 4.8; conditioning time = 5 + 5 + 5 min.; flotation time = 15 min.

The effect of amount of the solid on the recovery and grade is shown in Table VI. It was observed that the recovery decreased while % of the solid increased and the best result was obtained at 12.5% solid.

Table VI: Recovery and grade of P<sub>2</sub>O<sub>5</sub> versus amount solid.

	Solid in the pulp (%)				
	10.0	12.5	15.0	17.5	20.0
P <sub>2</sub> O <sub>5</sub> grade (%)	30.50	31.50	27.20	27.10	27.08
P <sub>2</sub> O <sub>5</sub> recovery (%)	79.20	78.81	74.22	68.56	62.43

*The comparison of column flotation and cell flotation*

The experimental conditions were: Na-oleate: 4 kg/t; phosphoric acid: 734 g/t; pH=4.8; solid: 12.5%; conditioning time: 5 + 5 + 5 min; flotation time: 15 min.

As can be seen in the Table VII, column flotation is more advantageous than cell flotation in terms of both  $P_2O_5$ % and recovery. The reason for this can be attributed to flotation time being longer than the cell flotation. The mechanism for this is as follows: hydrophilic pieces that are physically attached to bubbles are detached due to gravity and to the addition of wash water. Chemical analysis of the concentration under best conditions was shown in Table VIII.

Table VII: Recovery and grade of  $P_2O_5$  versus anionic collectors.

	Collector	
	Na-oleate	Oleic acid
$P_2O_5$ grade (%)	31.50	29.58
$P_2O_5$ recovery (%)	78.81	76.69

Table VIII: Chemical analysis of the concentrate.

Element	%
$P_2O_5$	31.50
$SiO_2$	7.90
CaO	33.19
$Al_2O_3$	0.96
$Fe_2O_3$	1.92
MgO	1.83
Loss of ignition	21.64

**Conclusions**

The minerals of carbonate cement Mazıdag phosphate slime that contains 20.95%  $P_2O_5$  are dahllite and collophanite, and calcium carbonate as gangue. As a result of particle size analysis, it was observed that the particle size of slime was below 22  $\mu m$ , whereby the particles were liberated. In flotation tests where carbonate was floated and phosphate was depressed, with a grade 31.50%  $P_2O_5$ , a concentrate and recovery of 78.81% was obtained. The best conditions obtained in column flotation were used in cell flotation, but concentrate grade was 29.58% and recovery was 76.69%. Since surface area increases due to very small particle size, reagent amounts are quite high. The concentration obtained from column flotation is acceptable for phosphoric acid production.

**References**

- Fuerstenau, D.W., 1962. Froth Flotation. 50th Anniversary Volume: A.I.M.E., New York, 666.  
 Lowers, W., 1985. Phosphate Rock. Institution of Mining and Metallurgy A121–A125.  
 Yener, L., 1981. Güneydoğu Anadolu Fosfatları Değerlendirme Çalışmaları Uygulama Politikalar. Türkiye Madencilik Bilimsel ve Teknik 7. Kongresi, TMMOB MMO yayın organı, 187–212. (Turkish Text)

## AN INVESTIGATION ON THE EFFECTS OF ORE GRADE AND PARTICLE-LIBERATION SIZE IN GOLD RECOVERY BY COAL-OIL-GOLD AGGLOMERATE FLOTATION

Y. Cilingir, S. Sen

Department of Mining Engineering Dokuz Eylul University, Izmir, Turkey

### Abstract

Gold recovery methods, which include gravity, flotation, amalgamation and leaching are again under scrutiny today to improve the recovery and decrease the deleterious affects of the processes on environment and human health. On the other hand, new gold recovery methods, which should be less harmful to the environment, in addition to providing higher recoveries than conventional gold processing methods, are also being investigated.

In this study, the effects of the assay and particle size of gold ores on the efficiency of the coal-oil-gold agglomeration processes are investigated experimentally. The effects of these parameters are very important for determining the process efficiency for different ore types. In order to establish the effects of the parameters mentioned above, artificial ores, which have different grades and particle sizes, were utilized as feed materials in the experiments. In last decade, many researchers have studied the optimum oil, coal type and their consumption. Very encouraging results have been obtained (over 90% recovery) by working with high oil and coal consumption. In this study, the experiments were done by using these materials at minimum dosages to provide a method in the range of economic availability. At the end of our studies, it can be clearly said that applying the coal-oil-gold agglomeration method to assist gold flotation gives more desirable results in view of the agglomeration reagents and material consumption.

*Keywords: gold, coal, oil, agglomeration, flotation, grade, particle size*

### Introduction

Agglomeration has become a valid processing method in fine coal and in some ore treatments in the mining industry. Production of agglomerates from fine particles can be provided in a number of ways. The first procedure involves addition of electrolytes to the pulp to cause a reduction of zeta potential and allow colliding particles to cohere. Another method includes using polymeric flocculants to provide the formation of bridges between the particles. A third method that was used in this study is using an unmixable liquid to spread over the particle surfaces. The resulting film on each particle formed by a liquid coating causes formation of "liquid bridges" by the contact of the particles with one another. As a result, the fine particles from the start of the process are converted to the masses that were bound together by liquid bridges called agglomerates (Keller and Burry, 1987).

The use of coal-oil agglomeration method for gold recovery has been object of research for many researchers since it was developed by BP's Mining and Mineral Company in 1983 (Marciano et al., 1994).

The method allows the recovery of relatively fine or coarse gold particles, compared with the conventional gold-recovery methods from certain types of ores. Coal-oil-gold

agglomeration combine a conventional ore processing method with a fine coal treatment process to yield a high grade concentrate and to minimize processing time while providing maximum efficiency.

After the optimum processing conditions are determined, it is possible to recover very fine gold particles that can not be recovered by gravity processing methods, along with the coarse gold particles that can not be effectively recovered by flotation methods of coal-oil-gold agglomeration. However, cyanidation is the most effective technique, when the liberated gold particles are fine or partially locked in the gangue minerals.

This can be highly harmful to environment, if it is not run under proper conditions. In light of the investigations that have been done in recent years, it can be stated that in many aspects, the coal-oil-gold agglomeration method (coal-oil-gold agglomeration and coal-oil-gold agglomerate flotation) can be a valid alternative to conventional gold recovery processes (especially flotation, gravity and amalgamation).

Two main sets of instructions have been reported to prepare the coal-oil agglomerates. The first method involves adding an adequate amount of coal and oil in an agitation tank that includes gold-bearing pulp to form coal-oil-gold agglomerates.

According to the second method, coal agglomerates are produced in a separate step, and then these agglomerates are added into the gold-bearing pulp (Gaidarjiev et al., 1996).

Coal-oil agglomerates may be produced in a two-stage process. In the first stage, a 30÷70% oleophilic material is added under high shear conditions to form the micro agglomerates. In the second step, the rest of the material is added under low shear conditions to increase the size of the agglomerates (Marciano et al., 1994).

Placers, tailings, free-milling ores and certain types of refractory ores (gold must be liberated or liberation can be provided by grinding) can be evaluated by the coal-oil-gold agglomeration method.

However, this method should not be used in some situations where the gold is associated with significant quantities of pyrite, arsenopyrite or other sulfide minerals because of their oleophilicity.

It has been reported that there is no significant difference in gold recoveries for up to 5% sulfides in the feed (Calvez et al., 1998). These types of gold-bearing ores could be used effectively after they were roasted or leached with oxidized sodium cyanide or by some other leaching methods.

After the loaded agglomerates are separated from the slurry by flotation (co-current separation) or screening (current separation), they can be burned to produce a high-grade gold containing coal ash.

Selling the gold containing ash to a refinery might be the most simplest and cheapest option.

To use leaching for the recovery of the gold provides the possibility of very high extraction. Thiourea or thiosulphate may be used to substitute cyanide, if it can not be used as a leachant for the operation.

And it is a very important to note that if cyanidation is used in this stage, the cyanide consumed in the process will be very small, when compared with a conventional gold cyanidation process (House et al., 1988).

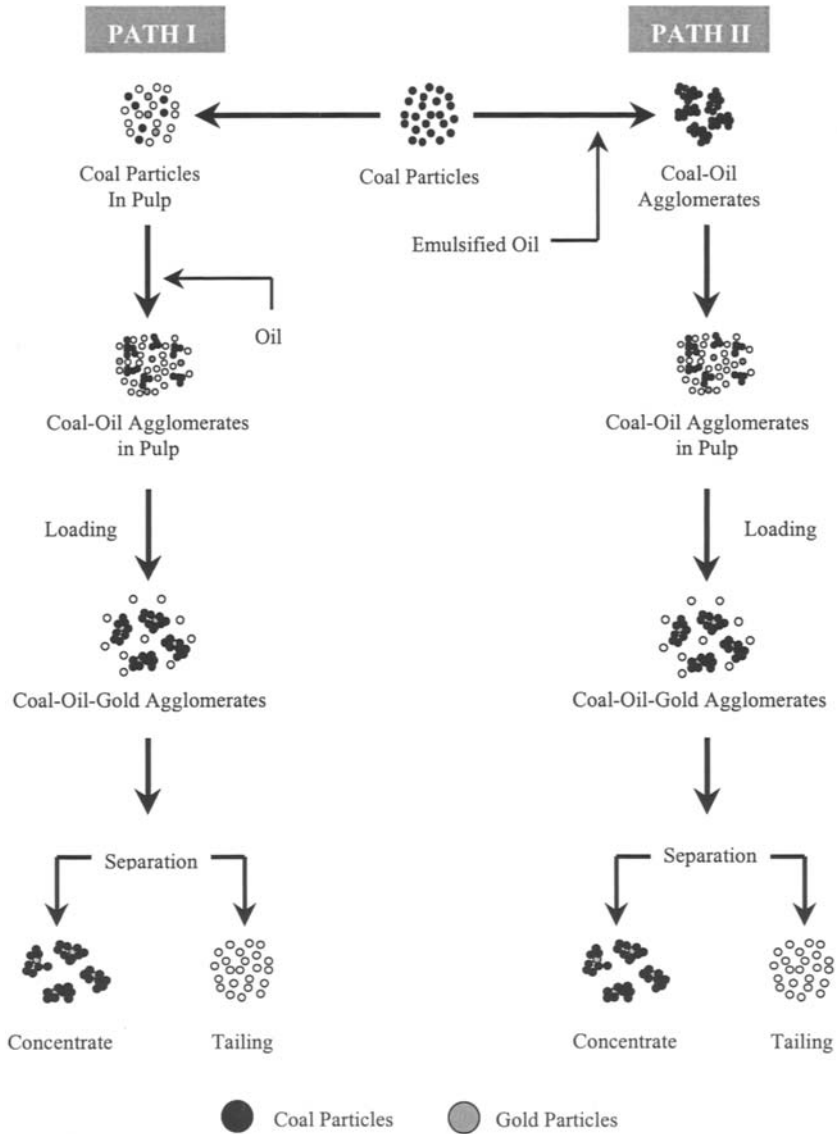


Figure 1: Representation of coal-oil-gold agglomeration process.

**General instructions**

*Materials*

Agglomeration is required for working with oil recovery and for recycling systems in fine coal processing because of the high oil cost of the process. The use of a coal-oil agglomeration in gold processing is also affected, so that the coal-oil-agglomerates’

recycling should be placed in the process flow sheet to prevent this negative effect. This method's applicability on an industrial scale, without any recycling or reused system, is only possible by decreasing this constituent's dosages in the process. For this reason, all experiments were carried out by using the above-mentioned reagents and materials in minimum amounts. Decreasing the coal and oil dosages in the process may probably cause a decrease in the concentrates' recovery and grades. In order to prevent the method from working with lower recovery and grades, some flotation collectors were used. Therefore, this process can be called "coal-oil assisted gold flotation". Coals that are used as agglomerating material should be floatable in order to apply the flotation method to separate the loaded agglomerates from the pulp. Using a good quality coal in experiments may increase the processing cost. For this reason, a lignite coal that was taken from Çanakkale/Çan (7.3% ash content) was subjected to flotation tests, and it responded well to the flotation process. Coal particles were ground to 100% minus 0.150 mm before using the material in the agglomerate preparation step (Table I).

Table I: Çanakkale/Çan lignite coal screening analysis results.

Size fraction (mm)	Weight (%)	Weight (undersize %)
– 0.150 + 0.106	23.59	100.00
– 0.106 + 0.075	38.17	76.41
– 0.075 + 0.053	23.07	38.24
– 0.053 + 0.045	4.26	15.17
– 0.045 + 0.00	10.91	10.91

Olive oil, diesel oil, and fuel oil were used together as agglomerating agents. Some flotation reagents (KAX, Aerofloat promoter 208 and Aerofloat promoter 242) were added to the pulp to provide maximum efficiency and to improve the gold particles' penetration into the coal-oil agglomerates. The consumption of all reagents was kept at a constant rate in all experiments.

Table II: Agglomerating agents' addition.

Agent	Consumption (g/t)
Olive oil	400
Diesel oil	1245
Fuel oil	12.5

Table III: Flotation reagents' addition.

Collector	Consumption (g/t)
KAX	50
Aerofloat 242	50
Aerofloat 208	50
Na <sub>2</sub> SiO <sub>3</sub>	1,000
Dowfroth 1012	250

Providing the same gold grade in all natural gold ore samples is hard work because of the low assays of the gold. This characteristic causes the incapability of studying under different conditions. For this reason, it has been decided to conduct the study



using an artificial ore. Pure quartz has been used to produce artificial gold-bearing ores (100% minus 0.120 mm).

Artificial ore samples with different gold grades were obtained to use in the first step of the study by addition of different amounts of 22-carat gold particles (<0.106 mm) to the gangue material.

For the second step, gold particles were classified in different size ranges, and the samples were prepared by adding these particles to the gangue material.

#### *Determining the assay of samples*

After being separated, agglomerates were burned in a furnace at 900 °C for carbonaceous and volatile material burning.

The roasted material was a mixture of ash and gold particles. The gold content of this material was determined by using a Perkin-Elmer Atomic Absorption Spectrophotometer (model 2280).

#### *Test procedure*

The main goals of this study are to determine the effects of gold ore head grade and the effects of gold-particle size on the coal-oil-agglomeration method's efficiency. Therefore, the studies consist of two distinct parts. Oil consumption and other parameters have been kept at minimum constant rates.

#### First group of experiments

The main objective of this part of the study was to determine the effects of the gold feed assay on process efficiency.

In order to achieve this objective, two different experimental paths were followed (Figure 1).

In the first part of the experiment (Path I in Figure 1), coal particles and oil were added to the gold-bearing pulp directly.

A Denver sub-A flotation machine with speed control was used as an agglomerate formation and recovery machine. Initially, coal-oil-gold agglomerates were produced in the cell.

The loaded agglomerates were separated from the slurry by using conventional flotation. Tests were run under the following conditions:

- 1,000 g of synthetic, gold-bearing ore (25% solids by weight);
- flotation reagents (Table II);
- agglomeration reagents (Table III);
- coal/ore ratio: 2/100;
- 2,000 rpm stirring speed and 20 min agitation for emulsification;
- 850 rpm stirring speed and conditioning for 10 min.

Table IV: The results of the experiments examined to determine the effects of the ore head grade on the coal-oil-gold agglomeration process (Figure1, Path I).

Head grade (g/t)	Weight (%)	Grade (after burning) (g/t)	Recovery (%)
0.46	0.57	63.67	78.77
1.83	0.42	180.43	41.24
4.58	0.41	206.34	18.46
9.17	0.43	357.10	16.75
18.33	0.59	439.53	14.19

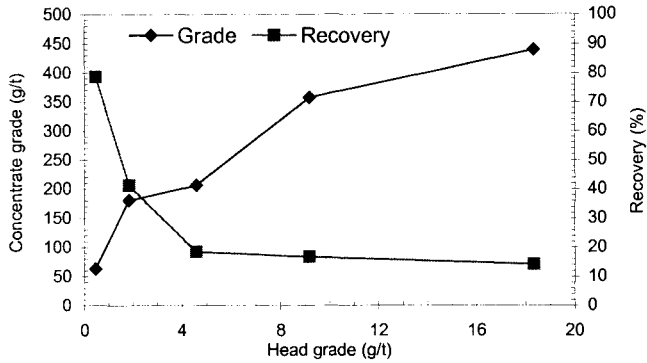


Figure 2: Gold grades and recoveries according to different ore head grades (Figure 1, Path I).

It can be seen from Table IV and Figure 2 that increasing the feed grade of the sample has caused a decrease in concentrate recovery. It was deduced that the main factor affecting the process of recovery was available surface area of the agglomerates. Production of coal-oil-gold agglomerates in ore slurry was not successful, due to low oil concentrations in pulp and slime coating on the coal particles. Hence, only a limited number of agglomerates could be generated. Observations showed that only about 5 g of the 20 g of coal was agglomerated. The agglomerates formed did not provide enough surface area for the penetration of gold particles. These results suggest a relationship between the number of agglomerates generated and number of recoverable gold particles.

In the second part of the study (Figure 1, Path II), the coal particles were agglomerated using oil prior to mixing with the gold-bearing ore pulp. The conditions for agglomeration were as follows:

- stirrer: IKA-Eurostar (Power control-visc);
- agglomeration reagents (Table III);
- emulsification of agglomeration reagents at 2,000 rpm for 5 min;
- coal particles' addition (10% solids by weight) and agitation at 2,000 rpm stirring speed for 5 min.

The solution containing the agglomerates added to the gold-bearing pulp. The mixture was agitated under the experimental conditions below:

- 1,000 g of synthetic gold-bearing ore (25% solids by weight)
- flotation reagents (Table II);
- agglomerates' addition to the gold-bearing pulp and agitation for 10 min at 1,350 rpm stirring speed;
- 850 rpm stirring speed and conditioning for 10 min.

In these experiments, coal particles were completely converted to coal-oil agglomerates. The pre-agglomeration stage provided more available surface area for gold particles' penetration. As a result of these studies, it was observed that the recovery was not affected by the changes in the feed grade, whereas the Au grade of the product increased linearly with increasing feed grade (Table V, Figure 3). A gold concentrate of about 4,375.00 g/t Au could be obtained with a recovery of 76.36% from a gold ore of 18.33 g/t.

Table V: The results of the experiments examined to determine the effects of the ore head grade on the coal-oil-gold agglomeration process (Figure 1, Path II).

Head grade (g/t)	Weight (%)	Grade (after burning) (g/t)	Recovery (%)
0.46	0.28	130.25	79.09
1.83	0.30	485.20	80.45
4.58	0.25	1448.21	77.45
9.17	0.27	2728.26	81.82
18.33	0.32	4375.00	76.36

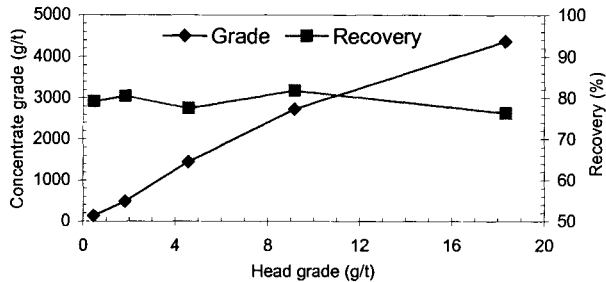


Figure 3: Gold grades and recoveries, according to different ore head grades (Figure 1, Path II).

### Second group of experiments

In this part of the study, the effects of gold particle sizes on process efficiency have been studied using pre-agglomeration. Gold particles of different sizes, assaying 22 carats, were used to produce synthetic gold-quartz samples, after mixing them with 1,000 g of pure quartz amounting to an Au grade of 6.417 g/t. The agglomerate's pre-formation stage was examined by applying the agglomerate pre-formation stage mentioned in the second part of the first group of experiments. 22-carat gold particles in different size ranges were used to produce synthetic gold samples by mixing them with 1,000 g of pure quartz.

Table VI: The results of the experiments conducted to determine the effects of gold particle-sizes on the coal-oil-gold agglomeration process. Ore head grade: 6.417 g/t

Size range ( $\mu\text{m}$ )	Weight (%)	Grade (after burning) (g/t)	Recovery (%)
- 300 + 212	0.45	765.92	53.71
- 212 + 150	0.42	943.40	61.75
- 150 + 106	0.41	932.93	59.61
- 106 + 75	0.41	971.99	62.11
- 75 + 53	0.39	1261.99	76.69
- 53	0.44	1096.60	75.20

It can be seen from Table VI and Figure 4 that the changing particle size of the gold has an effect on the gold grade and recovery, especially for the coarsest fraction (- 300 + 212  $\mu\text{m}$ ). The reason for this behavior is most probably due to the inefficiency of the agglomerates to lift those large (heavy) particles. The decrease in the smallest size (<53  $\mu\text{m}$ ) is considered to be the decrease in the collision efficiency between the agglomerates and the finest gold particles.

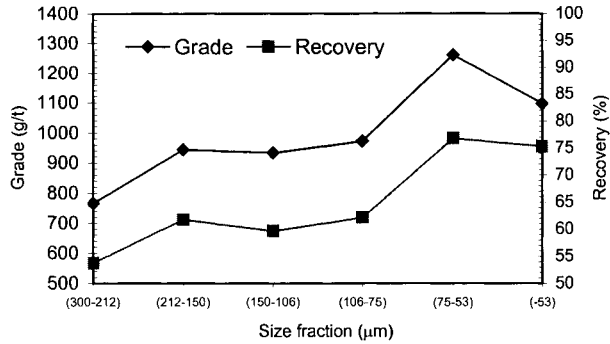


Figure 4: Gold grades and recoveries according to working with synthetic ore samples that have gold particles in different size ranges.

## Conclusions

The studies showed that:

- the applied process can be called “coal-oil assisted gold flotation”, and the method can be considered a successful application;
- the pre-agglomeration stage provides more available surface area for gold particles’ penetration and improves concentrate recovery;
- it can be observed that the recovery was not affected by the changes in the feed grade, whereas the Au grade of the product increased linearly with increasing the feed assay;
- the recovery was affected by the changes in the particle size of the gold in artificial ore samples. Especially in the coarsest and the finest gold particles, it caused a decrease in concentrate recovery.

## References

- Calvez, J.P.S., Kim, M.J., Wong, P.L.M. and Tran, T., 1998. Use of coal-oil-gold agglomerates for particulate gold recovery. *Minerals Engineering*, 11, 803-812.
- Gaidarjiev, St., Stoev, St. and Kireva, R., 1996. Coal-gold agglomeration of alluvial gold. 5<sup>th</sup> International Mineral Processing Symposium, Kusadası, Turkey, 577-581.
- House, C.I., Townsend, I.G. and Veal, C.J., 1988. Coal gold agglomeration. *International Mining*, (September), 17-19.
- Keller, D.V. and Burry, W., 1987. An investigation of a separation process involving liquid-water-coal systems. *Colloids and Surfaces*, 22, 37-50.
- Marciano, A., Costa, L.S.N. and Lins, F.F., 1994. Utilization of coal-oil agglomerates to recover gold particles. *Minerals Engineering*, 7, 1401-1409.

## CHARACTERIZATION OF RIGID SPARGERS AND SELECTION FOR FLOTATION COLUMNS

C.O. Gomez, R. Escudero, J.A.Finch

Department of Mining and Metallurgical Engineering, McGill University  
3610 University, Montreal, Quebec, H3A 2B2, Canada  
e-mail: cesar@minmet.lan.mcgill.ca

### Abstract

Rigid spargers are enjoying renewed interest in some flotation column applications such as de-inking of recycled paper and de-oiling of water. Sparger selection depends on the characteristics of the sparger (material and geometry), the stream to be processed (% solids, presence of surfactants), and on the dimensions of the column. There is no method to predict gas holdup (or bubble surface area flux) for a given duty. Prediction is difficult because there are two processes involved: the formation of a bubble swarm at the sparger and the rise of the swarm against a countercurrent flow of pulp. A method is proposed to predict gas holdup by a combination of two models: one for bubble formation at the sparger which relates bubble size to sparger and stream characteristics; and the second for bubble flow which relates bubble size to gas holdup and phase hydrodynamics. The method requires a set of gas holdup data to characterize the sparger material in the stream of interest (i.e., calibration). Gas holdup can then be predicted for other spargers of the same material processing the same stream in any column. The method is trailed for a set of porous stainless steel spargers in a laboratory column run with water and frother.

*Keywords: flotation, columns, rigid spargers, bubble size, gas holdup, bubble surface area flux*

### Introduction

Gas slurry contactors are extensively used in many branches of engineering. In the case of the minerals industry, their main use is in flotation, in which a suitable air sparging system capable of providing the necessary bubble surface area flux for particle collection must be selected. An efficient sparging system should produce small uniform sized bubbles at the maximum aeration rate with minimum maintenance requirements.

There are several sparging techniques for flotation columns, classified as external and internal depending whether the bubbles are formed inside or outside the column. Internal spargers deliver the air by direct injection into the column through either a porous rigid material, a flexible material (filter cloth or rubber), or a small orifice (Minnovex, Cominco). External spargers inject bubble dispersion formed, for example, by a flow of air and pulp through an in-line static mixer (Microcel). External sparging systems offer the advantage that they can be serviced while the column is in operation.

Rigid spargers have enjoyed renewed interest in some flotation column applications such as de-inking of recycled paper and de-oiling of water. In these applications the formation of small bubbles is crucial to collect the finely dispersed particles. A literature review showed that there is little published information, on sparger selection

and sizing for these duties, other than “rules of thumb” (Xu and Finch, 1989). Rigid sparger performance depends on the physical characteristics of the porous material, feed characteristics, the air flowrate, and the dimensions of the column. Two models, one for bubble formation at the sparger and a second for swarm bubble flow through a column, can be combined to predict gas holdup and bubble surface area flux. This paper illustrates the method for spargers in a laboratory column run with water plus frother.

### **Bubble formation and flow in a flotation column**

The efficiency of flotation is closely related to the effectiveness with which air is dispersed into small bubbles. In the case of flotation columns, one method to obtain small bubbles is by injection of air through a rigid sparger. Bubble size depends on the active pore size and pore density of the sparger material, the physicochemical characteristics of the stream being processed, and the air flowrate. The swarm of bubbles generated rises and distributes across the column. The volumetric fraction of air in the resulting dispersion (gas holdup) is a consequence primarily of the bubble size and, to a lesser extent, of the hydrodynamic conditions created by the flow of air and slurry. It is why gas holdup is generally measured as an indication of the efficiency of the bubble generation process.

Bubble size is difficult to measure and methods to estimate it from column operational data are frequently used. There are two estimation routines based on available models, bubble swarm flow through the column (the most used) and bubble formation from a multi-porous sparger. Drift flux analysis of the flow of bubbles in bubbly regime through the column permits the estimation of bubble size from gas holdup-air flowrate data (Banisi and Finch, 1994). The equations involved in the calculation are implicit and their solution requires an iterative procedure.

Bubble formation from a multi-porous sparger has been modeled from a balance of forces acting during bubble formation (Kumar and Kuloor, 1970). The formation process is assumed to take place in two stages: the growing and the detachment stages. The model assumes that the sparger contains an extremely large number of “potential” pores for bubble formation, but only a fraction of these are “active.” The number of active pores decreases with increasing flowrate. In the first stage, the bubble grows and expands at a definite rate as gas is fed to the orifice. This stage ends as soon as the bubble base starts to move away from the tip of the orifice. This marks the beginning of the second stage, which terminates when the bubble detaches. The estimation of bubble size requires an iterative procedure to solve the equations involved knowing the pore size of the sparger material. Nominal pore sizes provided by the manufacturer have proven inadequate in this calculation. Conversely, if the bubble size is known then the pore size can be back-calculated, referred to as “equivalent” pore size. It is effectively a calibration procedure. The combination of these two models provides a method to predict bubble size (and hence gas holdup and bubble surface area flux). By collecting gas holdup-air flowrate data using a sample of the sparger in a column processing the stream of interest, the bubble size from drift flux analysis can be calculated and subsequently used to determine the pore size of the sparger material. With pore size known, bubble size can be calculated for a given size

and number of spargers of the same material working in any column processing the stream of interest. With bubble size known gas holdup can be calculated for any given air flowrate.

The ideal condition for application of this procedure is when no coalescence occurs after bubble formation. In this way the bubble size produced is directly related to the bubble size causing the observed gas holdup. This condition is approached when there is sufficient surfactant (e.g., frother) that the bubble size is more or less preserved. In many cases of interest in flotation the condition will be approximated. Since it cannot be guaranteed it is best to work with the "stream of interest" (as stressed). In this way the back-calculated pore size reflects any coalescence that has occurred. It assumes that for a given stream the degree of coalescence will remain the same thereafter hence the calibrated pore size is appropriate. The assumption is judged reasonable at this juncture. (An important exception will be water alone. Not only is coalescence extensive in the absence of surfactant but also the bubbles are usually in the range  $0.002 \div 0.010$  m where gas holdup is no longer a function of bubble size).

### Experimental program and setup

A series of experiments was designed to collect pressure loss data for water flowing through a sparger, and gas holdup data in a flotation column as a function of air flowrate. The purpose of the pressure loss data was to establish the homogeneity of the spargers. Experience has demonstrated that porous SS tubes are not homogeneous even if they are from the same batch. A device, which allows the installation of different size spargers in the form of sparging cylinders, was designed (Figure 1). This was achieved by a SS base where the sparging cylinder could be maintained in position by a specially designed nut and bolt (a series of bolts with the same length as the sparging cylinder was made).

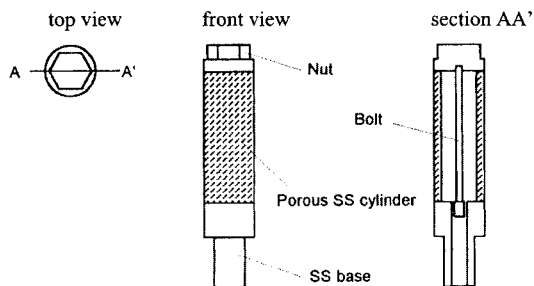


Figure 1: Sparger construction details.

The setup used to collect pressure loss and gas holdup data is depicted in Figures 2 and 3. In the case of pressure loss, the fluid used was water delivered using a centrifuge pump and measured using a magnetic flowmeter (Bailey, model 10D1475). To make sure the sparger was completely immersed in water, it was installed in a short piece of 0.106 m diameter acrylic tube. This tube was provided with an outlet to measure the sparger outside pressure. The pressure drop across the

sparger was measured with a differential pressure transducer (Bailey, model PTSDDD). The water temperature was measured using an ICTD probe (Transduction Ltd., model ICTD). All the instruments were linked to a signal conditioning and interface unit (Transduction Ltd, model Opto 22). Continuous monitoring and registering of the data was performed through a computer running FIX-DMACS, a commercial monitoring and control package (Intellution, type MMI, version 3.1).

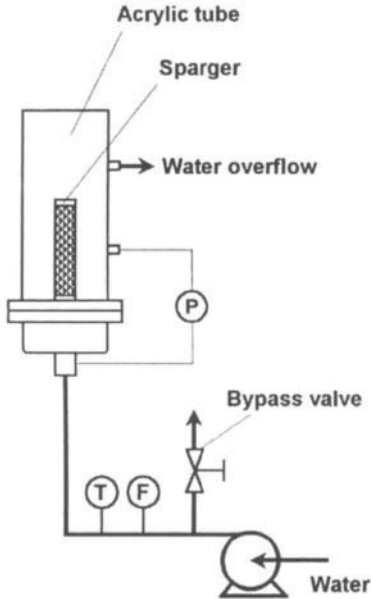


Figure 2: Experimental setup to collect pressure loss data.

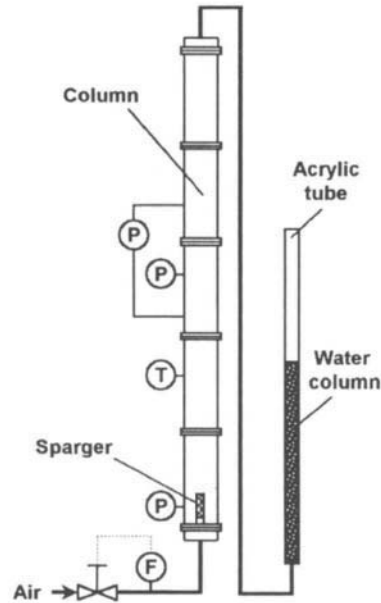


Figure 3: Laboratory flotation column used to collect gas holdup data.

The equipment used to collect gas holdup data was a fully instrumented laboratory flotation column.

The column was 0.1 m in diameter, 4 m high, assembled from flanged sections of acrylic tube, and closed at the top to make possible the control of the pressure head on the sparger, which is mounted at the base of the column.

Pressure head on the sparger is controlled by the height of the water column.

The same instrumentation, electronics and software utilized in the pressure loss setup was used in this column.

Compressed air was delivered to the sparger and controlled using a mass flowmeter/controller (MKS Instruments, model 1562A).

Variables monitored and registered were: air flowrate, water temperature, pressure differential across a 0.9 m test section located at about the center of the column (to measure gas holdup), and two hydrostatic pressure heads (using differential pressure transducers open to the atmosphere), one on the sparger to control the pressure head and the other on the middle of the test section to correct air flowrate.



## Results and discussion

### *Uniformity of spargers; permeability*

Pressure loss data was collected for a set of four spargers nominally of the same porosity (nominal pore size 5  $\mu\text{m}$  according to manufacturer) and lengths 0.026 m, 0.052 m, 0.078 m and 0.105 m, using water as test fluid. The results presented in Figure 4 showed a linear variation of pressure loss vs. water flowrate. This linear relationship is described by the following equation, which was obtained by applying Darcy's law to water radial flow through a cylindrical porous tube:

$$(P_i - P_o) = \frac{Q \mu_w}{2 \pi L k} \ln \frac{r_o}{r_i} \quad (1)$$

where  $k$  = permeability;  $L$  = length of sparging cylinder;  $P$  = pressure;  $Q$  = volumetric water flowrate;  $r$  = radius of sparging cylinder;  $\mu$  = viscosity and  $i$ ,  $o$  and  $w$  mean inside, inside and outside respectively.

Therefore, the permeability  $k$  for each sparger can be determined.

The same data in Figure 4 is presented in Figure 5 on logarithmic axes with water flowrate expressed as sparger water velocity (volumetric water flow/geometric sparger area). The purpose is to facilitate comparison between spargers to establish whether or not they have the same permeability. If the permeability is the same, then all the data points should follow the same straight line of slope 1. The results showed that spargers 0.026 m and 0.052 m are of the same permeability as all the points laid on the same line, but this was not the case for the 0.078 m and 0.105 m spargers.

### *Equivalent pore size*

Although the permeability of the sparger material is known the use of the Kumar and Kuloor model requires the equivalent pore diameter for the material, which can not be calculated from permeability. Therefore, gas holdup data were collected for the four spargers in the flotation column and these data were used for determination of equivalent pore size using the following procedure: bubble size was estimated using the drift flux model, and with bubble size known, the Kumar and Kuloor model was utilized to back-calculate the equivalent pore diameter for the sparger material. The results of this exercise done for the sparger 0.026 m long are presented in Figure 6 as a function of column air velocity (volumetric air flow rate/column cross-sectional area).

This calculation is iterative and is initiated by assuming pore diameter; Figure 6 includes results for three pore diameters: 5  $\mu\text{m}$ , 6  $\mu\text{m}$  and 7  $\mu\text{m}$ . The correlation is better for a pore diameter of 6  $\mu\text{m}$  which is taken as the equivalent pore size of the sparger material for spargers 0.026 m and 0.052 m long.

Gas holdup data for spargers 0.052 m, 0.078 m and 0.105 m was predicted using the pore diameter of 6  $\mu\text{m}$ . The results of the prediction, included as dotted lines in Figure 7, demonstrated that the prediction is accurate for the sparger 0.052 m long (up to the point where flow deviates from the bubbly flow condition), but not for the spargers of length 0.078 m and 0.105 m (which showed a different permeability; hence an equivalent pore size). We have demonstrated elsewhere (Escudero, 1998) that this procedure can be used to reasonably predict gas holdup for different number and size of spargers in any size column processing the same stream.

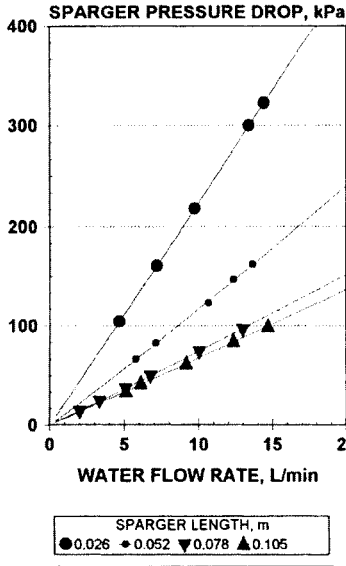


Figure 4: Pressure loss data for set of spargers.

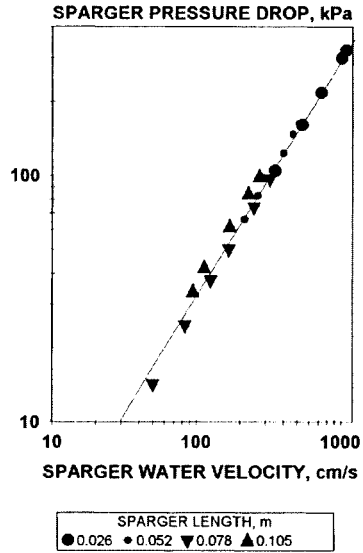


Figure 5: Determination of sparger permeability.

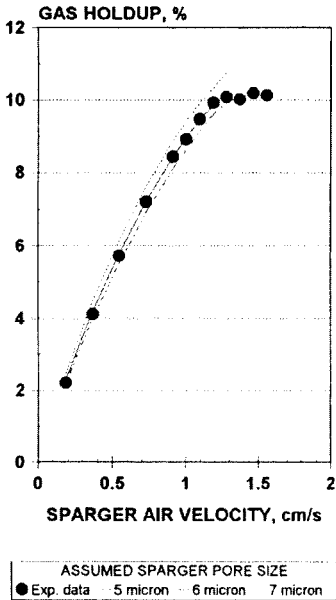


Figure 6: Determination of equivalent pore diameter for sparger 0.026 m long.

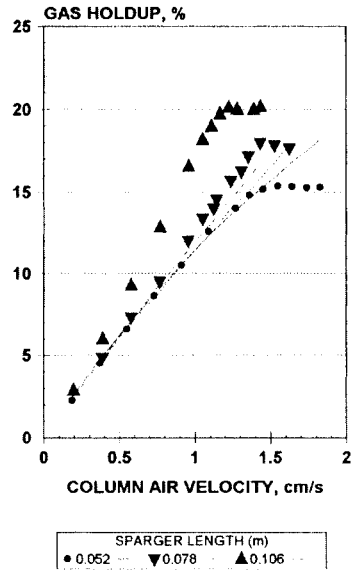


Figure 7: Measured and predicted gas holdup for spargers 0.052 m, 0.078 m and 0.105 m long.

## **Conclusions**

A method was proposed to predict gas holdup in a flotation column operated with rigid spargers. The method is based on a combination of two models: one for bubble formation at the sparger which relates bubble size to sparger and stream characteristics; and the second which relates bubble size to gas holdup and phase hydrodynamics.

The method requires a set of gas holdup-gas rate data with which to calibrate the equivalent pore diameter of the sparger for the stream of interest. The application of the method to a set of spargers in a laboratory column demonstrated that the homogeneity of the sparger material has first to be established. Gas holdup prediction is accurate over the range characterized by bubbly flow.

## **References**

- Banisi, S. and Finch, J.A., 1994. Technical Note: Reconciliation of bubble size estimation methods using drift flux analysis. *Minerals Engineering*, Vol.7, No.12, 1555-1559.
- Escudero, R., 1998. Characterization of rigid spargers and their selection for flotation columns. Ph.D. Thesis, McGill University, Montreal, Canada.
- Kumar, R. and Kuloor, N.R., 1970. The formation of bubbles and drops. In: T.B. Drew, G.R. Cokelet, J.W. Hoopes, Jr., and Vermeulen, T. (Editors), *Advances in Chemical Engineering*, Vol. 8. Academic Press, New York, 256-368.
- Xu, M. and Finch, J.A., 1989. Effect of sparger surface area on bubble diameter in flotation columns. *Can. Met. Quart.*, Vol.28, No.1, 1-6.

## AN INTERACTIVE DYNAMIC FLOTATION MODEL FRAMEWORK

O.A. Bascur

OSI Software, Inc., Houston, TX, USA

### Abstract

A variety of novel flotation technologies have become available in recent years. However, very little research is been done on the hydrodynamics effects on metal recovery. A comprehensive dynamic flotation model was presented at the IMPC 1982. It was the first time that the particle/bubble and water transport description and flotation cell hydrodynamic of flotation were linked. A dynamic flotation framework was developed to analyze and develop process control alternatives. Several new advances to the model have been made.

New developments in mineralogical characterization have simplified the determination of species in a sample stream. With the recent developments of software based on Microsoft technologies dynamic simulation enables process engineers to use ActiveX components under a real time environment to develop process alternatives. The integration of information from the process, laboratory, physical characteristics using latent variables simplifies derivation of operational process models.

Using a framework for flotation knowledge acquisition on industrial process systems is a viable alternative. An implementation of the current process analysis tools and a simplified model are presented to show how this new environment can be used to interactively experiment with flotation. As such, the user could change feed flowrate, % solids, aeration, wash water flowrate, frother flowrate, specific power energy (impeller speed/delta pressure), cell geometry, tails flowrate and see dynamically the effects on grade and recovery.

*Keywords: dynamic flotation framework, hydrodynamic flotation model, froth model, ActiveX development environment, flotation bubbles*

### Introduction

Nearly 2 billion tons of ore are treated worldwide by flotation, (Fuerstenau, 1999), flotation is clearly one of the most important applications of surface chemistry in technology – particularly for control of the solid-liquid interface. Successful flotation separations depend on the selective interaction between solid particles and gas bubbles in aqueous media. Once we define the chemistry, we need to define the best combination of contacting device to mix the air, water and particles to attach them to bubbles. We also need to device ways to hydrodynamically move the froth and not entrain water with the clean classified particles.

In order to improve the operation of a flotation system in a mineral concentration plant, we need to identify the manipulated variables and capture the knowledge of the effect with grade and recovery. Only through good process understanding improved performance can be achieved during the frequent and inevitable mineralogical ore changes and grinding disturbances in most plant. Such an analysis requires the development of accurate, yet easy to implement general dynamic models similar to those available for conventional flotation units (Bascur and Herbst, 1982).

Factors involved in the processing of ores by flotation can be represented by a triangle that shows the interaction between the mineralogical characteristics of the ore, the chemical variables that can be used to regulate the process, and the hydrodynamical characteristics of the contacting and separating equipment. The later one relates to the operational aspects of flotation, the flotation kinetics. The earliest attempt to develop a theoretical basis of flotation microprocesses was T.S. Mika (Mika and Fuerstenau, 1969).

Pate and Herbst (1992) have extended the conventional model to column flotation model. It is interesting that they use a very similar approach.

The paper provides a summary of the work extended by Bascur and Herbst (1982). The major important contribution is the generalization of the turbulence communicated to the pulp/air and particles/bubbles. Also, the critical liquid/froth area is reintroduced by a novel extra manipulated variable in flotation systems as proven experimentally by Sanchez et al. (1997). This critical area is critical in solving the hydraulic part of the dynamic flotation model.

### **The general dynamic flotation framework**

The general flotation framework is based on a population balance model and the hydraulic characteristics of a three-phase contacting device. The model represents the behavior of each mineralogical species and any number of particle sizes. Each of the particle species can exist in one of four states in the cell (free in the pulp, attached to bubbles in the pulp, free in the froth, attached to bubbles in the froth), and water is distributed in the pulp and froth. The air holdup in the pulp and froth is calculated using semi-empirical equations derived from mechanistic models.

Mechanisms of interface transfer are represented by kinetic equations to account for attachment/detachment and entertainment/drainage between the four phases. In each case the influence of important operational variables are included in the model equations. Manipulated variables such as aeration rate, frother addition, agitation degree, pulp level, feed flowrate, percent solids in the feed, grade in the feed, tailings flowrate and froth level are taken into account.

Early workers concerned with the modeling of the flotation process generally concentrated on the behavior of valuable particles tended to neglect the behavior of gangue particles and the effect of cell hydrodynamics and water distribution.

Figure 1 represents a generic-contacting vessel used in flotation. Attention is drawn to the pulp/froth interface, which is highlighted in this paper. A restriction found in two-phase flow is used to determine a critical area. This area is critical in calculating the entertainment and drainage fluxes of water between the pulp and froth volumes. This area is named A3 in the model.

One of the most important factors that control the water distribution in the flotation equipment is the froth. The approach used here to describe the hydraulic transport through the froth involves the assumption that bubbles leaving the pulp phase carry a sheath of water, which moves into the froth phase.

The number, size of the bubbles and the thickness of the water sheath are determined by frother concentration and the agitation conditions in the pulp volume.

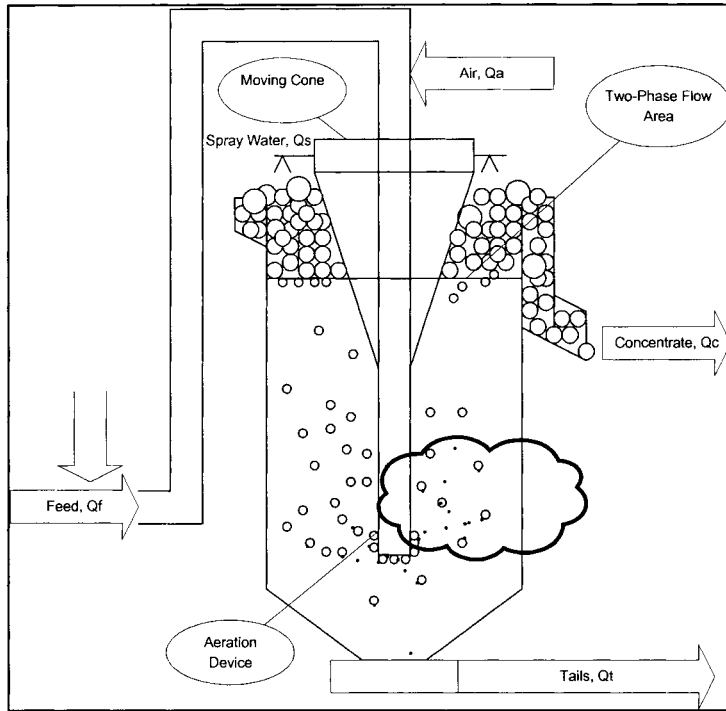


Figure 1. Flotation contacting equipment with a movable froth collector.

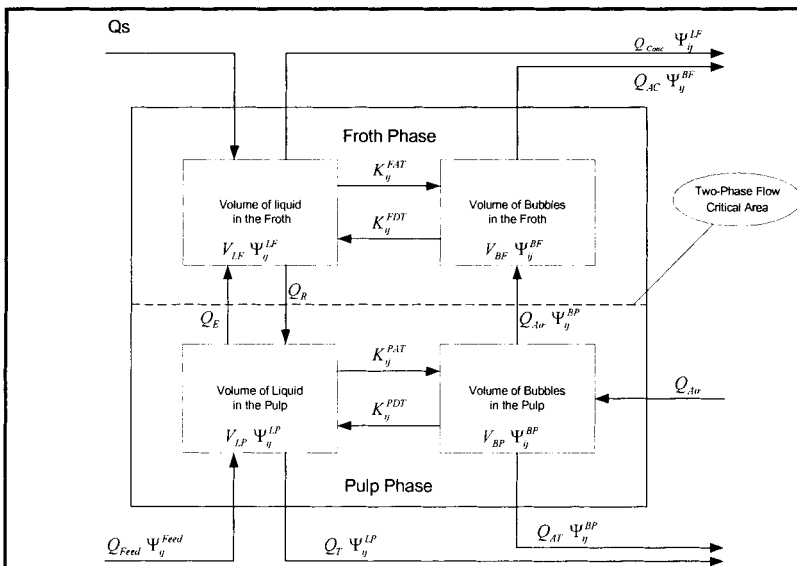


Figure 2: General flotation framework schematic.

Drainage of water back into the pulp is modeled by analogy with the drainage through plateau borders in foams. The height of the froth is determined by the froth removal mechanism in the vessel. For natural overflow, results studies of flow over a weir are used. A detailed description of the flotation model can be found in the references (Bascur, 1982; Bascur and Herbst, 1982).

This dynamic flotation framework has been tested using Illinois n° 6 coal (Bascur and Herbst, 1985), with copper sulfide ores (Bascur and Herbst, 1985; Zaragoza and Herbst, 1988) and phosphate ores (Jamsa-Jounela and Karki, 1990, Jamsa and Niemi, 1989).

### **Flotation hydrodynamic model**

One of the most important factors that control the separation of minerals and water distribution in a flotation cell/column is the froth. Unfortunately, there are very few fundamental models found in the literature. Empirical entertainment models for gangue recovery have been presented by Lynch et al. (1981). Moys (1978) has given a first approximation model for the distribution of water in a flotation cell. Baker (1971), Woodburn et al. (1971) gave good experimental evidence on the effect of aeration and froth behavior.

Based on the flow in multiphase flow, a model of a multiphase suspension was developed to represent in general particles in sedimentation behavior (Concha and Bascur 1975; Bascur, 1991). The general conservation equation is represented by a sinusoidal volumetric balance. This model is also applicable to two and three phase systems, such as flotation. A hyperbolic partial differential equation can be used to represent the dynamic behavior of the froth. This model is used in a lumped form to model the kinematics flow in a flotation cell. Yianatos et al. (1986) extended the approach to model a column flotation. They derived two separated models, a packed bed and an extended bed.

A general framework is suggested to describe the flotation process for mechanically agitated cells and column flotation cells. Figure 2 describes the variables used in performing and species mass balances around a flotation device. The main phenomenological difference between the devices is the degree of turbulence and the geometry of the system. Tables I, II and III show the specific correlations for mechanically agitated vessels and/or flotation columns. Table I shows the flotation microprocesses and the chemical and hydrodynamic factors. Table II shows the characterization of the hydrodynamics of flotation devices. Table III presents the power correlation's for mechanically agitated and column flotation devices.

These empirical models predict the power dissipation per unit of liquid volume, the gas holdup in the pulp, the gas holdup in the froth. The gas/liquid contacting models have been reviewed recently by Lee and Tsui (1999).

### **Relationships involved in a flotation system**

#### *Attachment phenomena in the pulp*

The formation of particle-bubble aggregate proceeds via three important steps (Laskowski, 1974; Jameson et. al., 1977; Yoon, 1999). The formation of a particle-bubble aggregate in the pulp proceeds via three steps, 1) approach of particle to a

bubble, 2) thinning of the water film between the particle and bubble, and 3) reseeding of the residual film to give an air-solid interface. The most relevant approaches to deriving a net attachment rate constant are those of Woodburn et al. (1971) and Bishofgerger and Schubert (1979); both consider the phenomena of turbulence in their development. Bishofberger and Schubert use Abrahamson's equation (1975) for aggregate formation, which depends on the local energy dissipation through the turbulence velocity of the aggregates. It is difficult to explain briefly the theorigyn of turbulence, so the author would like to refer for details to special publications (Batchelor, 1953; Hinze, 1959). In a nutshell, though the velocity and pressure at a certain point in a turbulent field fluctuate irregularly, turbulence may be expressed as a statically continuous function with respect to time and space. The number of collisions,  $Z$ , per unit of volume and time in a flotation system is given by:

$$Z = 5.0 N_{ij} N_B d_{iB}^2 U_i \quad (1)$$

Where  $N_{ij}$  and  $N_B$  are particle and bubble numbers available for collision respectively,  $d_{iB}$  is the mean size of the aggregate of size  $i$ . Liepe has derived the turbulent aggregate velocity,  $U_t$  as (Schubert et al, 1979):

$$U_t = k_t \varepsilon^{4/9} d_{iB}^{7/9} \left( \left( \rho_j - \rho_p \right) / \rho_p \right)^{2/3} (\rho_p / \mu)^{1/3} \quad (2)$$

where  $\varepsilon$  is the average energy dissipation in a flotation cell given by equations in Table 2 depending if it is agitated tank or a column flotation.  $\rho_j$  and  $\rho_p$  are the specific gravity of the species and the specific gravity of the pulp, and  $\mu$  is the viscosity of the continuous phase.

Arranging the terms according to equation  $Z$ , and defining a chemical characteristic for each mineralogical species  $K_j$  in the pulp, the general kinetic rate of attachment in the pulp is given by:

$$K_{ij}^{PAT} = K_j^{PAT} V_{BP} d_i^2 U_t / d_{BP}^3 \quad (3)$$

The respective equation for mechanically agitated flotation cells or column flotation cells presented in Table 1 determine the mean bubble diameter. As such, it is important to have from equipment manufacturers the power curves for flotation cells or the air injection mechanism. The most extensive treatment to evaluate the mixing behavior of mixing tanks is provided by Nagata (1975).

A similar method was used to obtain the flotation power curve to scale, and predict the power intensity in an industrial flotation cell.

#### *Detachment phenomena in the pulp*

Mika and Fuerstenau, 1969, derived an expression for the detachment process based on Thomas' arguments providing a square root proportionality to specific power intensity and the particle diameter squared. Woodburn, King and Colburn (1971) derived an expression based on the maximum deformation stress set up in the bubble skin following a sudden acceleration of the bubble.

Their expression is also dependent on the particle diameter to the power 1.5 and proportional turbulent velocity. It has been shown that the upper size of floatability is determined by the degree of agitation with turbulence as the characteristic parameter (Schultze, 1977).



Table I: Flotation microprocesses, chemical and hydrodynamic factors.

Chemical factors			Hydrodynamic factors
Attachment in the pulp	Contact angle	$K_{ij}^{PAT} = K_j^{PAT} S d_i^2 U_t / d_{BP}^2$ $S = 6\phi_p / d_{BP}$ $U_t = k_t \varepsilon^{4/9} d_{iB}^{7/9} (\Delta\rho_j / \rho_p)^{2/3} (\rho_p / \mu)^{1/3}$	Particle size
	Mineralogy		Solid specific gravity
	Liberation		Pulp bubble size
	Frother conc.		Percent solids, S%
	Water type		Gas holdup
	Gangue type		Turbulent aggregate velocity, $U_t$
	Pulp chemistry		Gas/liquid interfacial area pulp
			Gas superficial velocity
			Surface tension
			Efficiency of particle collision with bubble aggregate
Detachment in the pulp	Same as above	$K_{ij}^{PDT} = K_j^{PDT} d_i^n U_t$	Same as above
			Aggregate size
Entertainment to froth	Same as above	$Q_E = 6 Q_{Air} \delta / d_{BP}$	Bubble loading
			Gas superficial velocity
			Bubble size
			Surface tension
			Gas holdup
			G/L interfacial area pulp
			Water film thickness
			Particle size
			Solid specific gravity
			Critical pulp/Froth area
Drainage from froth	Same as above	$Q_R = KR v^{.53} V_{LF}^{.56} A_3^4 / (\sigma^{.24} d_{BF}^{1.92})$ $d_{BF} = a Q_{Air} + b$	Froth air holdup
	Frother conc.		Wash water
	Critical froth film thickness		Froth bubble size
			Surface tension
			Critical two-phase flow area
			Particle size
			Solid specific gravity
Attachment in the froth	Contact angle	$K_{ij}^{FAT} = K_j^{FAT} \left( \frac{Q_{Air}}{A_3} \right) \left( \frac{d_i}{d_{BF}} \right) \left( \frac{H_F}{d_{BF}} \right)$	Froth height
	Liberation		Efficiency of particle collection in stream line interception
	Mineralogy		Particle size
			G/L interf. area in the froth
Detachment in the froth	Same as above	$K_{ij}^{FDT} = K_j^{FDT} \rho_j d_i^m U_\infty$ $U_\infty = \frac{Q_r}{A_3} (1 - \phi_F)$	Solid specific gravity
	Liberation		Particle size
	Mineralogy		Water drainage flow
			Critical two-phase flow area
			Effective cross section. area
Concentrate removal	Francis law	$Q_C = KC L (H_F - H_c)^{1.5} (1 - \phi_F)$	Laundry size
			High of the froth above
			Gas holdup in froth
			Froth mobility

Schultze points out the dominance of tensile forces both turbulent and shear strengths acting on the aggregates as a function of the specific energy. By analogy, the

detachment rate can be expressed as a function of the particle size and the turbulent velocity. The turbulent velocity is given by Liepe’s equation and n becomes an adjustable parameter.

$$K_{ij}^{PDT} = K_j^{PDT} d_i^n U_t \tag{4}$$

*Attachment phenomena in the froth*

To derive an expression for the attachment in the froth, a froth-line interception mechanism of particle collection is assumed. In this regime, the collection efficiency is given by the ratio of the particle diameter to the bubble diameter in the froth.

$$K_{ij}^{FAT} = K_j^{FAT} Q_{air} \left( \frac{d_i}{d_{BF}} \right) \left( \frac{H_F}{d_{BF}} \right) \tag{5}$$

The second term in brackets represents the number of bubble layers in the trajectory in the froth volume.

*Detachment phenomena in the froth*

The detachment of a particle from a bubble occurs if the shear force exerted by the fluid flowing around the bubble exceeds the binding force. The driven force is due to the mass of the particle represented by the specific gravity of the specie.

$$K_{ij}^{FDT} = K_j^{FDT} \rho_j d_i^m U_\infty \tag{6}$$

$$U_\infty = \frac{Q_r}{A_3} (1 - \phi_F) \tag{7}$$

U is the bulk fluid velocity occurring as a result of the water drainage. The exponent of the particle diameter depends on the flow regime. For the Stokes law the exponent is equal one and for a Newton regime the exponent is equal to two.

Table II. Characterization of the hydrodynamics of flotation devices.

	Pulp, Mechanically Agitated and Columns (Bascur, 1982. Adaptation of Calderbank et al., 1958, and Lee and Tsui, 1999)	Froth (Bascur, 1982)
Gas holdup	$\phi_p = K3 \varepsilon_{VP}^4 \left( \frac{Q_{Air}}{A_1} \right)^6 C_F^{.25}$ $\phi_p = K3 \left( \frac{Q_{Air}}{A_1} \right)^{.578} \sigma_F^{.163} \left( \frac{\rho_G}{\rho_L} \right)^{.062} \left( \frac{\mu_G}{\mu_L} \right)^{.0107}$ <p>(Hikita et.al., 1981)</p>	$\phi_F = K6 \left( \frac{Q_{Air}}{A_3} \right)^{1.2} / \left( \sigma^4 d_{BF}^{1.2} V_{LF}^4 \right)$
Gas/liquid interfacial area	$S_p = 6 \phi_p / d_{BP}$	$S_F = 6 \phi_F / d_{BF}$
Bubble diameter	$d_{BP} = K2 \frac{\phi_p^4}{\rho_p^2 \left( \frac{P_g}{V_{LP}} \right)^4 C_F^{.344}}$ $d_{BP} = K2 \left( \frac{Q_{Air}}{A_3} \right)^{-0.12} \left( \frac{1}{\sigma} \right)^{-0.5} \frac{\mu_L^{0.24}}{\rho_L^{0.74}}$ <p>(Akita and Yoshida, 1974)</p>	$d_{BF} = a Q_{Air} + b$

Table III. Power correlations for mechanically agitated and column aerated flotation devices.

Power in mechanically agitated systems (Nagata, 1975)	$P_o = C \rho_p N^3 D_T^5$		
Power in gas/liquid mechanically agitated systems (Van Landeghem, 1980)	$\frac{P_g}{P_o} = C2 \left[ \frac{Q_{Air}}{ND_T^3} \right]^m$	$\left[ \frac{N^2 D_T^3 \rho_p}{\sigma} \right]^n$	$\varepsilon_{VP} = \frac{P_g}{V_{LP}}$
Pulp viscosity	$\overline{\mu_p} = \mu_L (1 + k_s \phi_s)$		$k_s = 3.5$
Pulp density	$\rho_p = \phi_s \rho_s + (1 - \phi_s) \rho_f$		
Power in gas/liquid in flotation columns	$\varepsilon_{VP} = C_d (\text{Re}) \left[ \frac{\Delta P_{compressor}}{\rho_g} \right]^{1/2}$	$\text{Re} = \frac{U_{Air} \rho_g D_T}{\mu}$	

### Flotation modeling

The approach in modeling the water transport through the froth assumes that bubbles leaving the pulp carry a sheath of water, which moves into the froth. The size of the bubbles and the thickness of the water sheath are determined by the turbulence scale and surface tension condition in the tank (Hartland and Barber, 1974; Barber and Hartland, 1975; Steiner, et.al. 1977). Drainage of water back to the pulp is model by analogy of drainage through plateau borders in foams. The height of the froth is determined by the froth removal mechanism. It is interesting to note that it is a flux equation which it discretized with a jump condition at the pulp/froth interface. As such, the cross-sectional area of the vessel play and important part to satisfy the flux law restriction in multiphase flows. Bascur (1982) described the method to solve this problem by defining a critical area A3 and including all the geometry factors of the flotation device. Unstable stability points exist in the system. It is known that operators do not like to control the level of a bank of floatation cells. It was very important to consider that for a set of operating conditions there only one area (A3) which solve the problem. This is one of the fundamental reasons the froth changes with the height in many flotation vessels. It is well known that flotation cell and column use froth crowders to adjust the two-phase flow to reasonable conditions. Considering Figure 2, a volume balance of the liquid in the pulp phase can be written as an accumulation term of the water in the pulp phase: equal to the volumetric flowrate in the feed less the tails flowrate and the entertainment flow going to the froth volume plus the drainage flowrate.

$$\frac{d}{dt} V_{LP} = Q_{Feed} - Q_{Tails} - Q_{Entertainment} + Q_{Drainage} \quad (8)$$

$$\frac{d}{dt} V_{LF} = Q_{Entertainment} - Q_{Drainage} - Q_{Concentrate} \quad (9)$$

Equations 8 and 9 represent the froth and pulp volumes of the liquid in a flotation vessel. The details for each term are presented in Table I. Many experiments were carried out to characterize the hydraulic behavior of an agitated flotation device. Figure 3 and 4 shows a typical air holdup profile and the conductivity distribution in the flotation cell.

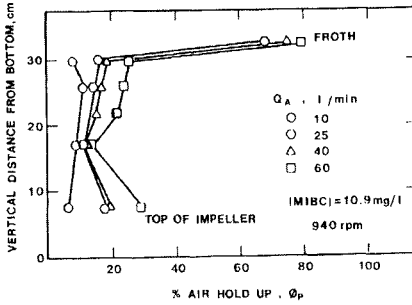


Figure 3: Air holdup distribution.

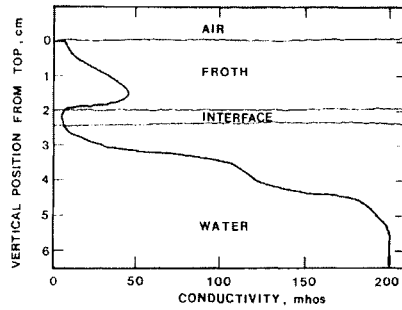


Figure 4: Conductivity measurements.

Guerra and Schubert (1997) showed the effect of fine particle entertainment, froth height, aeration and flotation recovery, supporting the results reported by Bascur (1982). Sanchez et. al. (1997) presented flotation results using the EKOFLOT flotation cell. This cell has a movable area to fine tune the concentrate grade by adapting the flotation froth process to get the critical area for the best water entertainment/drainage. As such, avoiding the need to add additional water on to the froth. It is very important to not the for the dynamic model to work this critical area is calculated such that there is a constant balance. The movable cone provides extended operational flexibility and can adsorb sudden variations of grade in the mineral feed. They report that this type of flotation cell can be used as rougher, scavenger and or cleaner and does not require the use of wash water. The conical effect was included originally in the dynamic equations to represent the Denver type flotation geometry in the original testing of this dynamic flotation framework. Figure 5 shows a display of the dynamic flotation model based on the general flotation framework. Under a real-time container such PI ProcessBook the implementation and testing of the model in and industrial environment can be achieved. Additional software components based on ActiveX technology can be incorporated. The software tools are expanding each quarter with announcements from Microsoft, and for the desktop, there is no competing technology of significant volume. The Microsoft definition is called component object model (COM) and distributed COM (DCOM) which have now been combined to be defined as COM+. A scripting engine is needed to manipulate the objects in the Industrial desktop. The scripting technology in Windows Application is VBA (Visual Basic for Applications). It is a common scripting language for all Microsoft and Microsoft compatible applications (e.g. Word, PowerPoint, Excel, Access, Visio, AutoCAD, and PI-ProcessBook). An original attempt to develop an interactive dynamic model of flotation for training purposes by Bascur and Herbst (1985). Many recent developments in on-line analyzers and on-line process data reconciliation packages make this new framework possible. An example of grinding/flotation integrated computer architecture for such a model to work is described by Bascur (1991). The flotation parameters for this example were obtained manually by characterizing each stream by global composite, by size, each size by mineralogical specie and by chemical composition. Recent advances in mineral characterization will make this framework a reality. QEM\*SEM systems,

which was developed by the CSIRO during the 1980s can produce most the vital data for parameterization and extended validation of the proposed flotation framework. By revealing the content and distribution of minerals in flotation samples, it is possible to characterize and develop general equations which can not only account for the operating parameters (physical) but in addition the chemical parameters. The chemical parameters are required for extended particle size and species characterization. One of the major limitations of the presented framework is the limited number of sizes and species used in the experiments. The major disturbances in flotation processes are the gangue constituents, which are varying, tremendously in real processes. These gangue types use major quantities of reagents and change the surface properties of the particles.

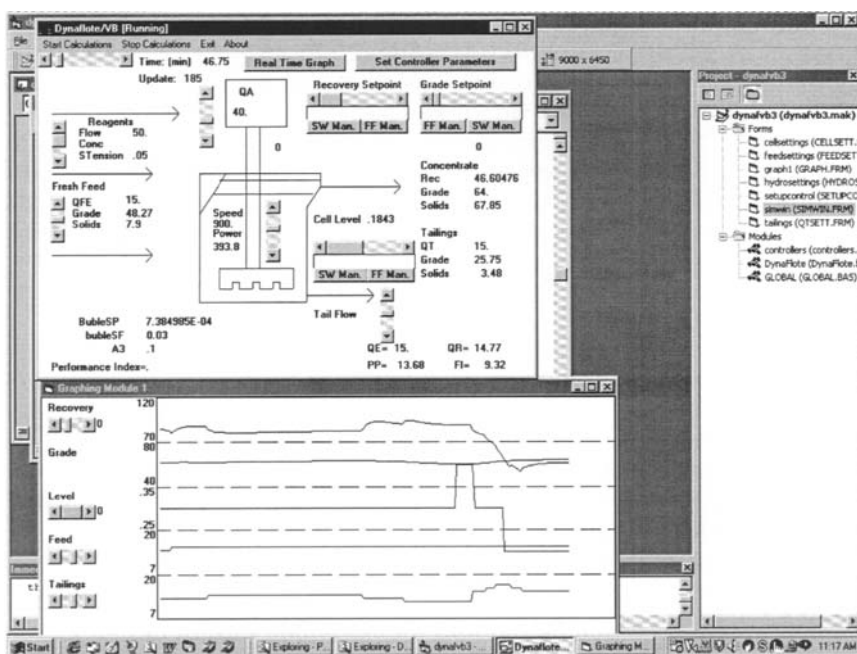


Figure 5: Dynamic simulator for testing the general framework using ActiveX controls.

## References

- Abrahamson, J., 1975. Collision Rates of Small Particles in a Vigorously Turbulent Fluid. *Chemical Engineering Science*, Vol. 30, 1371-1379.
- Baker, I.J., 1971. Investigation into the Effects of Froth Height in a Flotation Cell. M.Sc. Thesis, University of Natal, Durban, South Africa.
- Barber, A.D. and Hartland, S., 1975. The Collapse of Cellular Foams. *Transactions, Institution of Chemical Engineers*, Vol.53, 106-111.
- Bascur, O.A. and Herbst, J.A., 1982. Dynamic Modeling of a Flotation Cell with a View toward Automatic Control. XIV IMPC, CIM, Toronto, Canada.
- Bascur, O.A. and Herbst, J.A., 1985. Dynamic Simulators for Training Personnel. In: *the Control of Grinding/Flotation Systems, Automation for Mineral Resource Development*, Brisbane, July, 1985.

- Bascur, O.A. and Herbst, J.A., 1985. On the Development of a Model-Based Control Strategy for Copper Ore Flotation. In: E. Forssberg (Ed.), *Flotation of Sulphide Minerals*. Elsevier, Netherlands, 409-431.
- Bascur, O.A., 1982. Modeling and Computer Control of a Flotation Cell. Ph.D. Thesis, University of Utah, Salt Lake City, Utah.
- Bascur, O.A., 1991. Integrated Grinding/Flotation Controls and Management. Proceedings of the Copper 91-Cobre 91 International Symposium, CIM, Ottawa, Canada, 411-427.
- Bascur, O.A., 1991. Unified Solid/Liquid Separation Framework. *Fluid/Particle Separation Journal*, Vol.4, No.2, June.
- Batchelor, G.K., 1953. *The theory of Homogeneous Turbulence*. Cambridge University Press.
- Bishofberger, C. and Schubert, H.C., 1979. On the Optimization of Hydrodynamics in Flotation Processes. *Minerals Processing, XIII IMPC*, Warsaw, June 4-9, Laskowski, J. (Ed.), Vol.2., Elsevier Scientific Publishing, NY, 1261-1287.
- Calderbank, P.H., 1958. *Physical Rate Processes in Industrial Fermentation*. Part 1. Transactions, Institution Chemical Engineers, Vol.36, 443-463.
- Fuerstenau, D.W., 1999. The Froth Flotation Century. Adv. In *Flotation Technology*, Edts. B.K. Parek and J.D. Miller, SME, Colorado, 3-21.
- Hartland, S. and Barber, A.D., 1974. A model for a cellular foam. *Trans. Instn. Chem. Engrs*, 52, 43-52.
- Jameson, G.J., Nam, S. and Moo Young, M., 1977. Physical Factors Affecting Recovery Rates in Flotation. *Minerals Science and Engineering*, Vol.9, No. 3, July, 103-118.
- Jamsa, S-L. and Niemi, A., 1989. A Simulation Study of Expert Control System for Phosphate Flotation Process. 6<sup>th</sup> IFAC Symposium on Automation in Mining, Mineral, and Metal Processing, Buenos Aires, Argentina.
- Jamsa-Jounela, S.L. and Karki, E.K., 1990. Expert Control System for Rougher Flotation of Phosphate. IFAC, Tallin.
- Laskowski, J., 1974. Particle-Bubble Attachment in Flotation. *Minerals Science and Engineering*, Vol.6, No.4., October, 223-235.
- Lee, S-Y. and Tsui, Y.P., 1999. Succeed at Gas/Liquid Contacting. *Chemical Engineering Progress*, July, 23-49.
- Lynch, A.J., Johnson, N.W., Manlapig, E.V. and Thorne, C.G., 1981. *Mineral and Coal Flotation Circuits*. Developments in Mineral Processing, Fuerstenau, D.W., advisory editor, Vol.3, Elsevier Scientific Publishing Company, New York.
- Mika, T.S. and Fuerstenau, D.W., 1969. A Microscopic Model of the Flotation Process. Eight International Mineral Processing Congress, Vol.2, Leningrad, Mechanobr, USSR, 246-269.
- Moys, M.H., 1978. Study of a Plug-Flow Model for Flotation Froth Behavior. *International Journal of Mineral Processing*, Vol.5, 21-38.
- Nagata, S., 1975. *Mixing, Principles and Applications*. John Wiley and Sons, New York.
- Schubert, H., Heidenreich, E., Liepe, F. and Neese, T., 1979. *Mechanische Verfahrenstechnik I*. VEB Deutscher Verlag, Leipzig, 75.
- Schultze, H.J., 1977. New Theoretical and Experimental Investigations on Stability on Bubble/Particle Aggregates in Flotation: A Theory on the Upper Particle Size of Floatability. *International Journal of Mineral Processing*, Vol.4, 241-259.
- Steiner, L., Hunkeler, R. and Hartland, S., 1977. Behavior of Dynamic Cellular Foams. *Trans. Instn Chem. Engrs*. 55, 153-163.
- Woodburn, E.T., King, R.P. and Colburn, R.P., 1971. The Effect of Particle Size Distribution and the Performance of a Phosphate Flotation Process. *Metallurgical Transactions*, Vol.2, 3163-3174.
- Yianatos, J.B., Finch, J.A. and Laplante, A.R., 1986. Holdup Profile and Bubble Size Distribution of Flotation Column Froths. *Canadian Metallurgical Quarterly*, .
- Yoon, R.-H., 1999. Bubble-Particle Interactions in Flotation. Adv. In: *Flotation Technology*, eds. B.K. Parek and J.D. Miller, SME, Colorado, 95-112.
- Zaragoza, R. and Herbst, J.A., 1988. Model-Based Feed Forward Control Scheme for Flotation Plants. *Minerals and Metallurgical Processing*, November, 177-185.

## A COMPUTATIONAL FLUID DYNAMICS (CFD) MODEL FOR A BUBBLE SEPARATION TANK

P. R. Desam, A. Datta, J. D. Miller

Department of Metallurgical Engineering, University of Utah  
Salt Lake City, UT 84112, USA

### Abstract

Flow behavior of bubbles in a continuous liquid phase is of interest in many flotation systems such as those used in mineral processing, wastewater treatment, wastepaper de-inking etc., where particles in suspension are separated as bubble-particles aggregates. The fluid dynamics modeling of these multi-phase systems is a difficult task due to the complexities of momentum transfer between different phases. In this work, a general methodology for the computational fluid dynamics (CFD) simulation of a bubble separation tank is described. The continuous phase is modeled with the Eulerian approach while the trajectory of bubbles is computed with Lagrangian frame of reference. The motion of the carrier phase (water) and the dispersed phase (bubble) are coupled via a source term that describes the effect of bubbles on the momentum of the continuous phase. The Particle-Source-In Cell (PSI-Cell) method gives the quantitative description of this source term. With CFD simulations, the effectiveness of different tank design parameters are evaluated in terms of the extent of bubble separation.

*Keywords: bubble separation tank, dispersed phase flow, Lagrangian model, CFD*

### Introduction

The Air-Sparged Hydrocyclone (ASH) flotation technology was developed at the University of Utah (Miller and Kinneberg, 1984, and Miller et al., 1988) in order to achieve higher flotation rate as compared to conventional aerated stirred tank type flotation reactor. The enhanced flotation kinetics is attributed to the presence of high centrifugal field and relatively smaller bubbles in the system. This technology has been applied for removal of contaminants from wastewater (Lelinski and Miller, 1996).

Recently, the researchers in ZPM, Inc., an organization expert in industrial water treatment, have modified the design of ASH to facilitate the separation of contaminants further by improving the water flow pattern and generating more uniform bubble size distribution (Owen et al., 1999). The new design is called as Bubble Accelerated Flotation (BAF) system. The BAF system is an integration of the modified ASH chamber, where the bubble-contaminant attachment is achieved, and a bubble separation tank, where actual separation of the bubble-contaminant aggregates occurs and taken out of the system by an external skimmer (Figure 1). The process and design parameters of this separation tank, such as tank geometry, inlet velocity, inlet and outlet design and the arrangement of baffles determine the nature of the flow field and the extent of separation. The objective of this research study is to explore the existing numerical models for multiphase flows and to investigate the bubble trajectory for analyzing the effectiveness of various design parameters using Computational Fluid Dynamics (CFD) modeling technique.

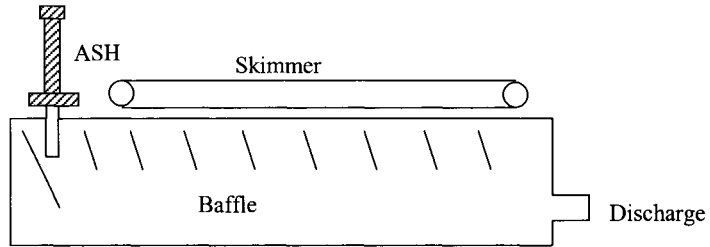


Figure 1: A Schematic of the BAF System with separation tank.

### Numerical models

The fluid flow in the separation tank is a two-phase, gas-liquid flow in which bubbles move in a continuous liquid phase. The gas-liquid phase can be classified into different types depending upon the geometry of their interfaces (Essomé et al., 1994). In our case, the fluid flow in the separation tank can be described as a two-phase, dispersed, gas-liquid flow.

Numerical models for two-phase dispersed phases are thoroughly discussed elsewhere (Crowe, 1982; Durst et al., 1984 and Essomé et al., 1994). Depending on whether the dispersed phase is dense or dilute, there are two numerical models available to simulate the flow. In a dilute dispersed phase flow, the particle motion is controlled by local flow field. The particle-particle collisions influence the particle motion in a dense dispersed flow. The amount of the dispersed phase can be quantified by volume fraction of bubbles. The dilute flows can be better simulated with Lagrangian model, while the Eulerian model is a suitable method for modeling dense flows. However, in both cases the continuous phase is modeled with Eulerian method only (Bird et al., 1960).

In the Lagrangian approach (Essomé et al., 1994), the dispersed phase is represented by bubbles and/or particles that are continually introduced at a given mass flow rate and they coexist with the carrier phase in the flow domain. The conservation equations for the carrier phase are described by Eulerian equations while the motion of the bubbles/particles is described in a Lagrangian frame of reference. In this approach, the trajectory of a single bubble and/or particle can be predicted by considering all the forces acting on it (Durst et al., 1984). The information transfer between the two phases is accounted for by the mass, momentum and energy gains or losses along the bubble and/or particle paths.

This is quantified by means of the Particle Source in Cell (PSIC) method (Crowe et al., 1997), where the computed mass, momentum, temperature transfer of the particles are combined into source terms then inserted into the respective continuum equations. While in the Eulerian approach (Essomé et al., 1994), the large number of dispersed phase present in the liquid is also considered as continuum.

The Navier-Stokes equations are written for each phase along with the appropriate boundary and interfacial conditions.

The Eulerian equations are averaged with respect to time and space. The exchange of quantities between the two-phases can be found by mass, momentum and energy transfer terms. This approach is also called as *two-fluid* modeling.



### Governing equations for Lagrangian model

In this numerical model, the carrier phase equations are written with modifications to allow the interaction between the two phases. This is done by adding the source terms, which describes the effect of the presence of the dispersed phase on carrier phase. As there is no mass transfer or energy transfer between the two-phases that results in their source terms being zero, only momentum conservation equation is discussed here. The momentum conservation equation for an incompressible steady state, turbulent, Newtonian fluid can be written as follows (Essomé et al., 1994).

$$\rho u_j \frac{\partial u_i}{\partial x_j} = -\frac{\partial p}{\partial x_i} + \frac{\partial}{\partial x_j} \left[ (\mu + \mu_t) \left( \frac{\partial u_i}{\partial x_j} + \frac{\partial u_j}{\partial x_i} \right) \right] + \rho f_i + \phi_i^M \quad (1)$$

In the above equation,  $\phi_i^M$  is the momentum source term. This term describes the momentum transfer between the two phases due to drag, gravity force on the bubble and can be quantified using Particle Source in Cell method, which is described later.

The bubble/particle governing equations are written in Lagrangian frame of reference to predict the trajectory by considering the forces acting on the particle. The assumption here is that only drag and gravity are responsible for the particle motion. The relevant equation is (Essomé et al., 1994):

$$\frac{du_i^p}{dt} = \frac{3\mu C_D Re}{4\rho^p D_p^2} (u_i - u_i^p) + \left( 1 - \frac{\rho}{\rho^p} \right) g_i \quad (2)$$

In the above equations,  $u_i$  is the fluid velocity in  $i$  direction,  $u_i^p$  is the particle velocity in  $i$  direction,  $\mu$  and  $\mu_t$  are the molecular and turbulent viscosity of the fluid respectively,  $p$  is the pressure,  $f_i$  is the body forces in  $i$  direction,  $D_p$  is the diameter of the bubble/particle,  $C_D$  is the drag coefficient of the particle,  $\rho$  is the density of the fluid,  $\rho^p$  is the density of the particle and  $Re$  is the Reynolds number.

In PSIC method (Crowe et al., 1997), the dispersed phase particles are regarded as sources of mass, momentum, and energy to the carrier phase. The source term for momentum transfer is calculated by equation 3 (Essomé et al., 1994). In this equation,  $V_p$  is the volume of a particle,  $\eta_j$  is the number flow rate of particles,  $Re^p$  is the particle Reynolds number and  $V_E$  denotes the volume of each element of the Finite Element Method (FEM).

For each time step  $\delta t$ , the source terms of a particle traveling on the  $j$ th trajectory that crosses element  $E$  are evaluated. Then this source term is integrated over the residence time of a particle in an element.

$$\phi_i^M = -\frac{\eta_j}{V_E \delta t} \int \frac{3\mu C_D Re^p V_p}{4D_p^2} (u_i - u_i^p) dt \quad (3)$$

The solution procedure (Essomé et al., 1994) for the Lagrangian model is iterative. The carrier phase flow equations are solved without the influence of dispersed phase. Then the particle governing equations are solved to find out the trajectories of the particles. From this information, the source terms are evaluated and incorporated into the carrier phase equations and a new solution for the flow is computed. The above procedure is repeated till a specific convergence criterion is satisfied.

### *CFD modeling strategy*

In our efforts to initiate the design of separation tank, the complex flow nature in the separation tank is simplified by the following assumptions. The separation tank used in this modeling work is a rectangular tank with one inlet and outlet. The input to the separation tank is imposed with a linear velocity profile despite the swirl flow in the Air-sparged hydrocyclone. A single bubble is tracked rather than a group of bubbles. Only two-dimensional modeling is done to predict the performance of the tank. The carrier phase is water in this set of simulations. The boundary conditions for this model are as follows. The tank inlet is given a velocity inlet type of boundary condition because the fluid is incompressible and the velocity at the inlet is known. The outlet is imposed with pressure outlet boundary condition. The top surface of the flow in the tank is described as a moving wall with zero shear stress and moving relatively with same speed as the adjacent cell. The boundary condition for the remaining part of the tank is fixed wall.

In these simulations a single air bubble is released at the center of the inlet and the trajectory of the bubble is observed. The initial velocity of the bubble is same as the velocity of the fluid at the inlet. The boundary conditions for the bubble are set in a way that it escapes from either the top surface or pressure outlet. Stochastic model is used to simulate the effect of carrier phase turbulence on bubble dispersion. These simulations are carried out by a CFD software called FLUENT 5.0 and this software can model a system up to 10÷12% of the dispersed phase by volume. The turbulence effect of the fluid is modeled with  $k-\varepsilon$  (2 equation) model.

### **Results and discussions**

In this part of study, the influence of inlet velocity, inlet design, bubble diameter, baffle spacing are considered and the effect of each parameter on separation process is described. For all the simulations, the dimensions of the separation tank used are 3 m in length and 0.6 m in height. The inlet and outlet have the identical dimensions of 0.15 m diameter and 0.3 m length. The tank is divided into a suitable number of chambers by baffles and they are denoted by numbers to identify the termination point of bubble. If not mentioned otherwise, inlet velocity is 1 m/sec, bubble diameter is 500  $\mu\text{m}$ , baffle height is 0.15 m, baffle angle is 20 degree counter-clockwise and number of chambers are 10 for all these simulations. A single bubble is released at the inlet and tracked for the number of the termination chamber. The same procedure is repeated for number of times for a particular set of conditions. From this information a probability curve is drawn against chamber number or length of the tank and discussed below. The goal of the tank design should be such that majority of the bubbles (i.e. contaminants) are captured in the initial part of the tank in order to minimize the length of the tank. Thus, the extent of contaminant removal is enhanced for a given length. Therefore, ideally the probability curve should be narrow and the peak of the curve should lie in the initial part of the tank in order to facilitate effective process control.

#### *Effect of inlet design*

The position of inlet plays a very important role in the separation process. Two different kinds of inlets are studied, one is horizontal and the other one is vertical. An

air bubble of 1,000  $\mu\text{m}$  diameter is released and tracked repeatedly in both the systems and the trajectories of the bubble and probability curves of termination are shown in Figures 2 and 3 respectively.

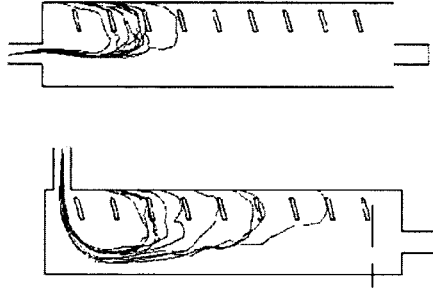


Figure 2: The bubble trajectories for horizontal (top) and vertical (bottom) inlet design.

The probability curve for the horizontal inlet is narrow and lies in the initial part of the tank. It indicates that all the bubbles are coming to the surface in the first few chambers only. But in the case of vertical inlet, the curve is displaced to the right and spread over the whole tank which means bubbles are coming to the surface in all the chambers. The reason for this can be explained as follows. Fluid flow in the separation tank should be as close to laminar as possible for effective separation. From the single-phase velocity profiles, it is observed that the vertical component of velocity for vertical inlet is changing direction to horizontal, which increases disorder in the system and decreases the effectiveness of separation. So, it is concluded that horizontal inlet performs the separation process better than its vertical counterpart.

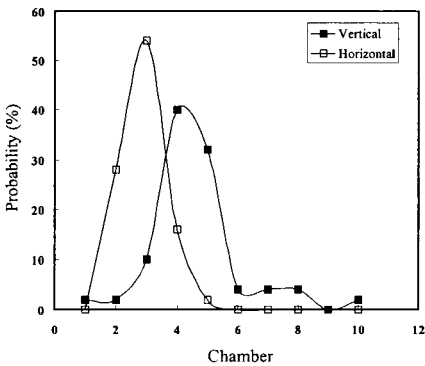


Figure 3: Effect of inlet.

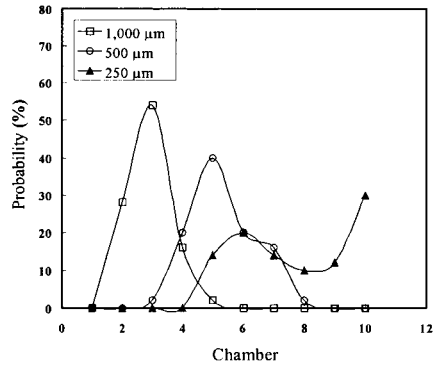


Figure 4: Effect of bubble.

*Effect of bubble diameter*

Bubble diameter is an important parameter in modeling the separation tank because the dispersed phase in real case will have a range of bubbles. Three sets of different diameters are studied and they are 1,000  $\mu\text{m}$ , 500  $\mu\text{m}$ , and 250  $\mu\text{m}$ .

The bigger bubbles rise to the surface in the initial chambers because of the high buoyancy forces associated with them that resists the fluid momentum. This buoyancy force even can overcome the small turbulent eddies in the fluid. The probability curve for 1,000  $\mu\text{m}$  diameter bubble (Figure 4) is narrow and falls in the initial region of the separation tank. But in case of smaller bubbles, the buoyancy force is not quite enough to overcome the fluid momentum and turbulent eddies. So, the effect of turbulence on small bubbles is high, which causes the bubble to disperse in the farther chambers. So, it is concluded that the smaller buoyancy force caused the curve to shift towards right, and the turbulence dispersion caused the curve to spread over the separation tank.

*Effect of inlet velocity*

The separation process is studied with three different velocities and they are 0.5 m/sec, 1 m/s and 1.5 m/s. Probability curves of termination of a 500  $\mu\text{m}$  bubble for different velocities are shown in the Figure 5. The probability curves are showing that as the velocity increases, the curve shifts towards right and spreads over the tank. For high velocity the fluid has more momentum, which forces the bubble to move further. For low velocity like 0.5 m/s, the curve is narrow and only falls into the first few chambers, which is a good characteristic for separation process. In case of high inlet velocity, the curve shifts towards right because of the high momentum of the fluid and spreads due to turbulence dispersion.

*Effect of baffle spacing*

Different baffle spacing is created by changing the number of baffles for fixed length of the separation tank. Three different cases are modeled with 10 chambers, 18 chambers and 34 chambers. Probability curves of termination for the above mentioned three cases are drawn against the length of the tank (Figure 6).

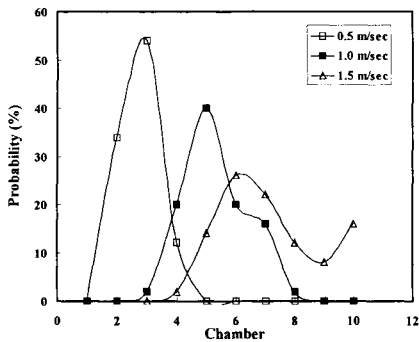


Figure 5: Effect of inlet velocity.

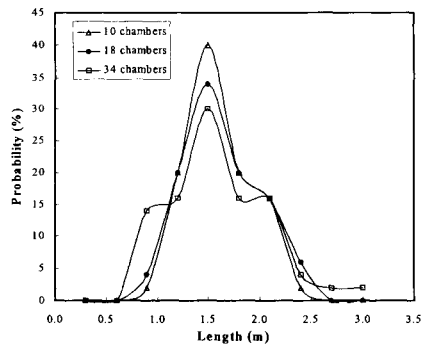


Figure 6: Effect of baffle spacing.

As the number of chambers increases, the curve spreads over more length of the tank. The curve is not shifting to sides because there is no change in the buoyancy force of the bubble and the fluid momentum. The circulation of fluid is more prominent in the entry region when the baffles are spaced widely. This effect causes the separation process little later than the situation where gap between baffles is less. However, it

should be noted that the width of the probability curve is narrower for widely spaced baffles. This is because the turbulence effect on bubble dispersion is present to a limited extent as compared to the case where baffle spacing is less.

### **Conclusions**

The flow domain and the bubble trajectories in the separation tank, which is a part of the recently developed bubble acceleration flotation (BAF) system used for waste water treatment, has been studied using CFD technique. Even for a relatively simple geometry, it has been observed that inlet design, baffle configuration, bubble diameter and inlet velocity had tremendous effect on the separation process. This information is useful for both the design of separation tank and control of the process. However, the future research objectives include further investigation on other design parameters such as baffle height, orientation, outlet geometry and overall tank geometry. Furthermore, the flow pattern with multiple bubbles will also be studied.

### **Acknowledgements**

The discussions with the researchers of ZPM Inc, California, U.S.A. are gratefully acknowledged.

### **References**

- Bird, R.B., Stewart, W.E. and Lightfoot, E.N., 1960. *Transport Phenomena*. John Willey & Sons, New York.
- Crowe, C.T., 1982. Review, Numerical Models for Dilute Gas-Particle Flows. *Journal of Fluids Engineering*, Vol. 104, 297.
- Crowe, C.T., Sharma, M.P. and Stock, D.E., 1977. The Particle-Source-In Cell(PSI-CELL) Model for Gas-Droplet Flows. *Journal of Fluids Engineering*, ASME, 325-332.
- Durst, F., Milojevic, D. and Schönung, B., 1984. Eulerian and Lagrangian Predictions of Particulate Two-phase Flows: A Numerical Study, *Appl. Math. Modelling*, vol. 8, 101-115.
- Essomé, G.R., Haroutunian, V. and Engleman, M.S., 1994. A Lagrangian Based Finite Element Model for Dispersed Two-Phase Flows. *Numerical Methods in Multiphase Flows*, ASME, FED-Vol. 185, 65-72.
- Lelinski, D. and Miller, J.D., 1993. Removal of Volatile Organic Compounds from Contaminated Water Using Air-Sprged Hydrocyclone Stripping Technology. *Proceedings of the International Conference on Analysis and Utilization of Oily Waste*, Supplement, Gdansk, Poland, Chapter 47, 251-274.
- Miller, J.D. and Kinnerberg, D.J., 1984. Fast Flotation in an Air-Sparged Hydrocyclone. *Proceeding of MINTEK 50: International Conference on Recent Advances in Mineral Science and Technology*, Johannesburg, South Africa, Vol. 1, 373.
- Miller, J.D., Ye, Y., Packuet, E. and Gopalakrishnan, S., 1988. Development of Air-Sparged Hydrocyclone – A Swirl-Flow Flotation Column. *Proceedings: International Symposium on Column Flotation*, SME/AIME, Chapter 34, and 305-313.
- Owen, J., Morse, D.E., Morse, W. and Jovine, R., 1999. *New Development in Flotation Equipment for Water Treatment System*. *Advances in Flotation Technology*, B.K. Parekh and J.D. Miller (Editors), SME Publication, 381-389.

## CHARACTERIZATION OF THE FLOTATION FROTH STRUCTURE AND COLOR BY MACHINE VISION (CHACO)

G. Bonifazi\*, V. Giancontieri\*, A. Meloni\*, S. Serranti\*, F. Volpe\*, R. Zuco\*  
 H. Koivo<sup>o</sup>, J. Hätönen<sup>o</sup>, H. Hyötyniemi<sup>o</sup>, A. Niemi<sup>o</sup>, P. Sipari<sup>o</sup>,  
 H. Kuopanporrtti<sup>o</sup>, R. Ylinen<sup>o</sup>, I. Heikkilä<sup>o</sup>, S. Lahteenmaki<sup>■</sup>, J. Miettunen<sup>■</sup>,  
 O. Stephasson<sup>▲</sup>, W. Wang<sup>▲</sup>, L.E. Carlsson<sup>Δ</sup>

\*Department of Chemical, Material, Raw Material and Metallurgical Engineering  
 University of Rome “La Sapienza”, via Eudossiana 18, 00184 Rome, Italy

<sup>o</sup>Helsinki University of Technology, B.O. Box 1000, FIN-02015 Helsinki, Finland

<sup>o</sup>University of Oulu, Kirkkokatu 11A, B.O. Box 191, FIN-90101 Oulu, Finland

<sup>o</sup>VTT, Espoo, Finland

<sup>■</sup>Outokumpu Mining Oy, Pyhäsalmi Mine, P.O. Box 51, FIN-86801 Pyhäjärvi,  
 Finland

<sup>▲</sup>Kungl Tekniska Högskolan, Stockholm, Sweden

<sup>Δ</sup>BOLIDEN, Box 71, S-936 81 Boliden, Sweden

### Abstract

The European Union Long Term Research (LTR) project, concerning the characterization of flotation froth structure and color by machine vision (ChaCo), has been developed with the aim to point out new process parameters, based on froth image inspection, to integrate with the commonly utilized process variables detected for the control of the flotation processes. The main purposes of the project were:

- to analyze the mineral concentration of the flotation froth from the color of froths of different structures;
- to design an on-line froth analyzer by developing software for the color and structure analysis of the froth and for classification using statistical and neural network methods;
- to develop process models and control methods utilizing the on-line froth analyzer.

The resulting products have to be installed and tested at the industrial flotation plants of Boliden (Sweden) and Outokumpu's Pyhasalmi mine (Finland).

*Keywords: flotation process, froth color, froth structure, image processing*

### Introduction

The main results achieved in the framework of the European Union LTR, Project n° 24931, The characterization of flotation froth structure and color by machine vision (ChaCo), carried out by the organizations listed in Table I, are presented.

The aim of the LTR project ChaCo is to utilize machine vision equipment and software for obtaining quantitative information on the pictorial aspects of flotation froth and to use this information in the on-line control of the flotation process (Figure 1). In fact, the fast development of information technologies allows nowadays to automatically acquire images of the froth in real-time (Moolman et al., 1994) and to extract features from the froth images that resemble the more or less heuristic features (Cipriano et al., 1995, 1997) used in the past by the operators in the flotation plants.

Table I: List of the partners involved in the ChaCo project. C = coordinator; P = partner; A = associated partner; S = subcontractor; U = university; I = industry; R = technical research centre.

Organization name	Country	Role	Type
Helsinki University of Technology (HUT)	Finland	C	U
Royal Institute of Technology (KTH)	Sweden	P	U
University of Rome "La Sapienza" (DIC)	Italy	P	U
University of Oulu (UO)	Finland	A	U
Boliden Mineral AB (Boliden)	Sweden	A	I
Outokumpu Mining, Pyhäsalmi Mine (OKP)	Finland	A	I
Information Technology Institute (VTT)	Finland	S	T

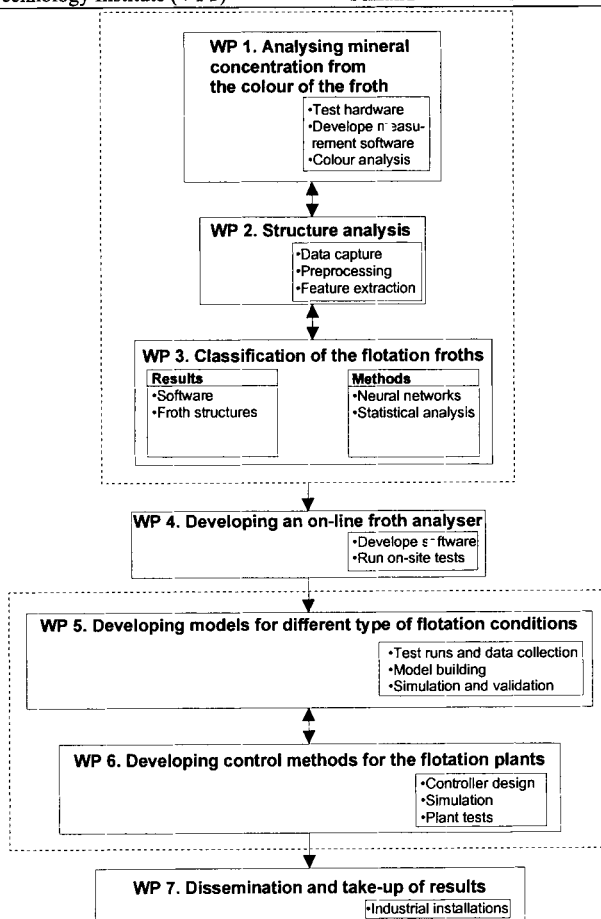


Figure 1: Overview of ChaCo project work-packages.

In such a way, the images coming from a video camera installed over the flotation cells, connected to a computer that processes the data in real-time, could integrate the information concerning flotation process behavior.

The objective of the project has been achieved in different steps (Figure 1), adopting different strategies, that is:

- analysis of mineral concentration in the froth;
- classification of the flotation froths starting from their pictorial aspects;
- development of an on-line froth analyzer imaging based;
- development of behavioral models for different type of flotation conditions;
- development of control methods for the flotation plants.

The research works concerning the color and structure analysis and the classification of the froths were carried out simultaneously as they strongly interact and give feedback to each other.

The on-line froth analyzer was developed by combining together the analysis and software results from the previous topics. Finally the process modeling and controller design was carried out simultaneously.

The research and development were based on standard, fore-front hardware and software for carrying out the project work in a cost-efficient and productive way. For example, standard Pentium PCs with image grabbing and signal processing cards were the basic hardware.

Usual software tools such as MATLAB/SIMULINK with suitable toolboxes (Image Processing Toolbox, etc.) were used in the analysis and software development based on specifically and original developed Fortran and C++ code.

### **Mineral concentration analysis from froth color and structure**

In order to establish criteria for the evaluation of froth structure and color, various digital color image processing methods, together with spectrophotometer based procedures, have been evaluated. Regarding the color analysis, different color reference system were considered (RGB, HSV, etc.) (Pratt, 1991). For the structure analysis different froth bubble segmentation methods have been developed and applied. The computed and analyzed parameters (Bonifazi et al., 1998) can be grouped in the following classes:

- morphological parameters, mainly based on the evaluation of the size and shape characteristics of the bubbles resulting from the segmentation according to the identification of similarity domain criteria of the froth images (Sadr-Kazemi and Cilliers, 1997; Bonifazi et al., 1999a);
- color parameters, mainly based on the analyses of froth images considered as a whole and on the color characteristics inside each domain defined by the bubbles (Oestreich et al., 1995; Bonifazi et al., 1999b);
- textural parameters, mainly based on the evaluation of the neighboring color tone characteristics of the pixels constituting the entire sampled image window (Haralick et al., 1973; Van Deventer et al., 1997);
- closed contiguous domain grouping according to specific morphological and/or morphometrical attributes (Beucher and Meyer, 1993);
- fractal parameters, deriving from the study of the single bubble structure, 2D approach (Bonifazi et al., 2000b) and packing modalities, 3D approach (Bonifazi et al., 2000c);
- other parameters, mainly deriving from the adoption of predefined closed region analysis and multispectral signal analysis.



After parameters detection and collection, the next step was to identify the criteria to correlate froth structure and color with mineral concentration. Different correlation techniques have been evaluated.

A regression analysis was performed showing that in most cases only adopting a multi-parameter approach a good correlation with mineral concentration can be achieved.

As a consequence, a multi-feature statistical classifier (Bonifazi et al., 1999c), was adopted.

### Classification of flotation froths and correlation with process parameters

Tests, with different ore minerals and different flotation conditions, have been carried out in order to establish froth classes and critical froth classes (Figure 2).

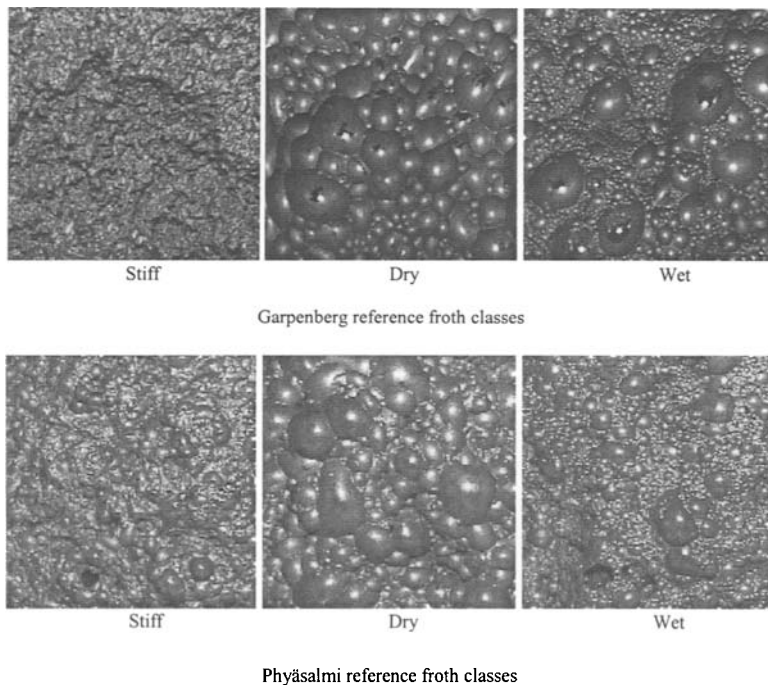


Figure 2: Froth main classes belonging to Garpenberg (Sweden) and Pyhäsalmi (Finland) ores. Froth images presented a wide variability in their visual features, especially in bubble size and shape.

One of the critical factor for the segmentation procedures was lighting conditions. According to color and textural features Garpenberg images resulted *easier* to segment and analyze, in terms of morphological and morphometrical features, than those of Pyhäsalmi ore (Bonifazi et al., 2000a).

Three main lines to perform froth image classification have been adopted. One is the so called simple froth classifier, which measures the similarity of a given froth image against predefined froth classes (Figure 3).

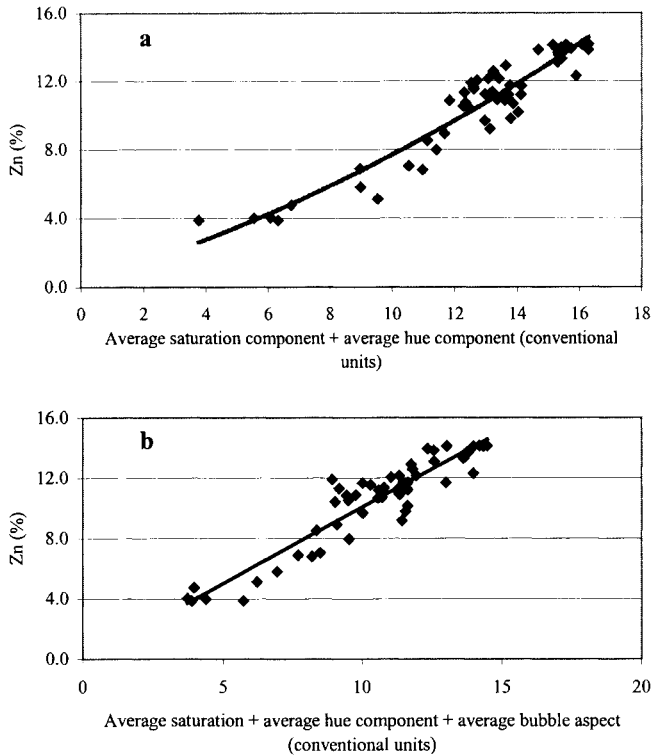


Figure 3: Plots showing the relationship between of the Zn content (%) detected in the froth after Garpenberg (Sweden) ore rougher flotation and the combination of the average saturation component (ASC) in the HSI color reference system and the average hue component (AHC) in the HSV color reference system (a) and furthermore the average bubble aspect (b) after froth image analysis.

The second method applies a tree-classifier to build a local prediction models for a given process variable, where the *local models* should (naturally) improve the prediction accuracy (Figure 4). The third classification method was based on neural nets (NN) (Moolman et al., 1995a, 1995b) and principal component analysis (PCA) to analyze the statistical structure of the data, and to use the *latent variables* produced by the algorithm as variables for monitoring and controlling the process (Figure 5) (Hatonen et al., 1999).

As it was recognized during the statistical analysis of the measurements, partial least squares (PLS) regression method seems to be a good method for modeling the data. In this perspective the procedure was modified in that direction, to incorporate the desired output signals in the construction of the internal model. A general-purpose Matlab Toolbox<sup>TM</sup> was implemented.

The reliability and the robustness of the different image processing algorithms were tested by both collecting data during the current operation of the plant and during special step change experiments.

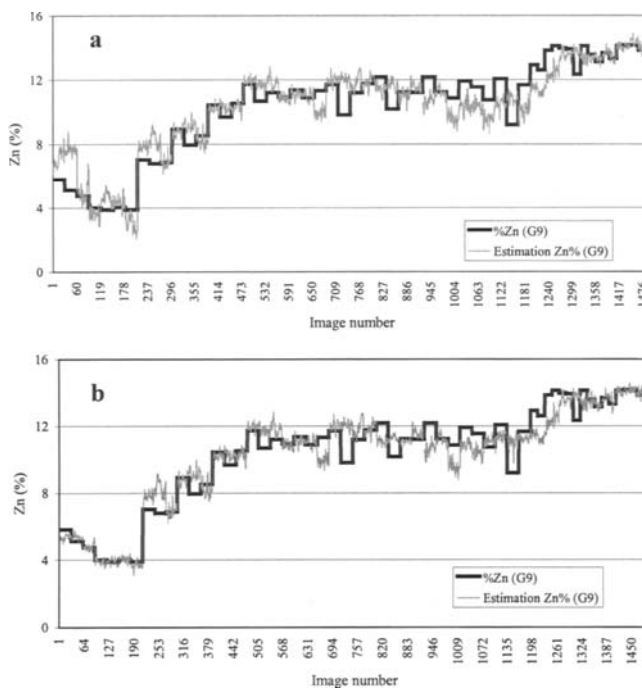


Figure 4: Relationship between the estimated Zn content in the froth and the Zn content after a continuous monitoring in Garpenberg (Sweden) processing plant. a: estimation carried out on the whole set of froth images ( $R_o^2 = 0.863$ ); b: estimation carried out after a preliminary froth classification on the basis of pictorial aspect ( $R_o^2 = 0.907$ ) (Bonifazi et al., 1999b).

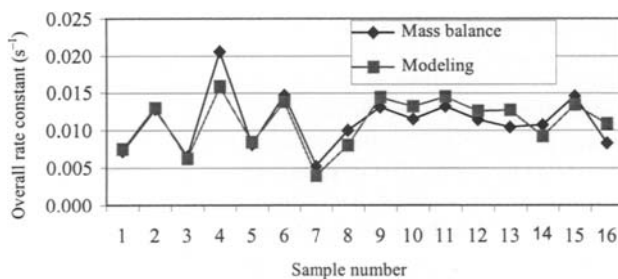


Figure 5: The behaviour of actual and modelled overall rate constant for fine zinc particles in Pyhasalmi (Finland) flotation plant.

### Developing an on-line froth analyzer

An integrated software (SW) and hardware (HW) architecture (prototype), able to incorporate and manage at industrial level (*on-line* analysis) all the previous analyses, has been developed (Figure 6). It manages the images, and the related digital information, in order to create specific data base containing all the requested information in order to

identify, qualify and certify froth characteristics. The first prototype has been installed in Outokumpu's Pyhäsalmi Mine (Finland), the second one in Garpenberg Mine (Sweden).

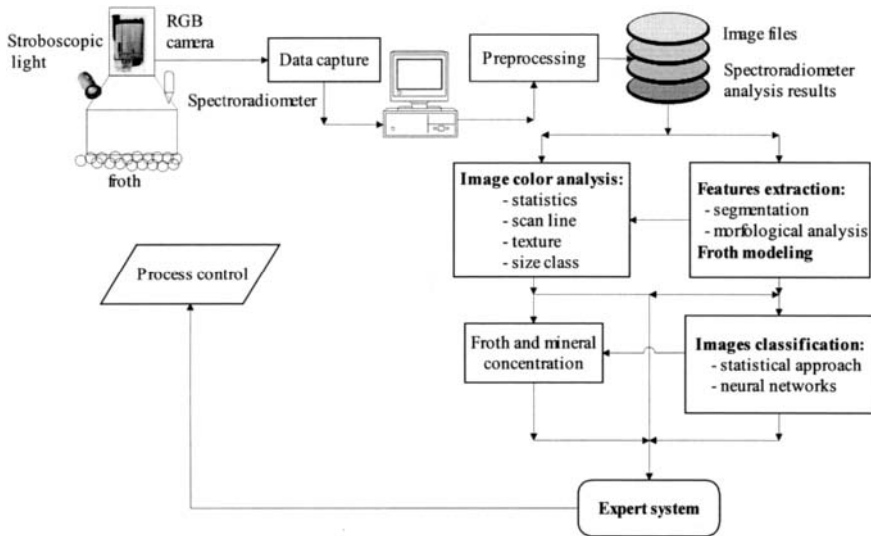


Figure 6: Flow chart of the final software design.

The developed software includes the following routine analysis:

- froth bubbles segmentation;
- froth color analysis as a whole (RGB, HSV and HSI color reference systems);
- single bubble color analysis;
- froth color analysis along a pre-defined alignment (scan-line analysis);
- froth textural analysis;
- 2D and 3D fractal analysis of the froth;
- froth speed;
- froth stiffness
- froth classification.

In Figure 7 it is reported the user-interface of the developed on-line froth analyzer, running inside LabView™ environment.

The user interface enables 4 different sets of functions.

All the control/display front end interfaces are organized as sub-windows.

#### *Image analysis procedure selection*

The user can currently choose to apply on a froth image color analysis, segmentation and morphological analysis based on DIC approach, segmentation and morphological analysis based on KTH approach, dynamical analysis (HUT) and textural analysis (DIC).

#### *Data visualization selection*

The user can select to visualize the results of segmentation (both approaches) and the cross-correlation matrix from an image pair.

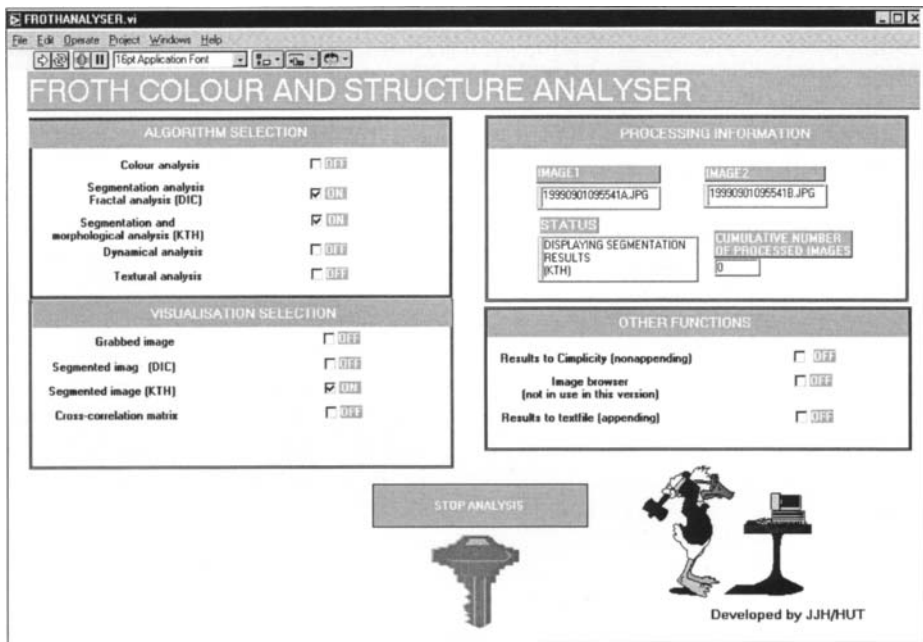


Figure 7: The user-interface of the on-line froth analyzer.

### *Processing chain status*

This area shows the names of the images (where the name corresponds to the time of the grabbing) that are currently being processed, the cumulative number of processed image pairs and the current status of the application, i.e. in what sequence the program is currently.

### *Other functions*

From this area the user can choose to feed the results into the automation system of the Pyhäsalmi mine (Pyhäsalmi specific option). He can also choose to update the image database of the so called *froth image browse* (Pyhäsalmi specific option). Finally all the results can be fed to a text file in an appending format.

### **Developing models for different type of flotation conditions**

Data has been collected by the on-line measurement system; at the same time froth samples were taken from the froth layer. The data and the information from the froth samples have been used for modeling and simulating the flotation process. The non-linear dynamic flotation model was based on the interaction between the froth layer and the pulp and on the assumption that the process taking place within the pulp leaves certain visible signs on the froth surface.

Process dynamics has been described with mass balance equations and overall rate constants, which are divided into several factors. In these factors, the effects of

operational process variables as well as the selected image variables are involved. Different flotation models have been developed for the finest and the intermediate/coarser particles and they have been used to predict flotation rate constants (Figure 5). A simulation system for a flotation cell was created utilizing Matlab's Simulink<sup>TM</sup>. All the necessary input models were either calculated or taken directly from real process data. The simulation was used to predict the recovery of the finest and the intermediate/coarser particles.

The validity of the simulation model was also tested with real process data. Models and simulations were used to find and tune process control parameters in a specific flotation process, and, further, to test, compare and tune the control algorithms for that specific application.

### **Developing control methods for the flotation plants**

As a case study, the control of the xanthate dosage in the zinc rougher bank was studied, also utilizing the image variables produced by the on-line analyzer. From the about 60 image variables only 2 (color red intensity channel, RCC, average bubble size, ABS) were chosen as an input for the xanthate controller.

This was done in order to keep the complexity of the controller down, so that the operators running the plant could understand the reasoning behind the controller.

The selection was made according to operators experience, after the cross-correlation analysis between image data and process variables, and the theoretical work performed during the modeling.

From the available *current* process variables, froth thickness and zinc grade in the rougher tailings were utilized.

The controller user interface is shown in Figure 8.

The logic of the controller is the following.

#### *First step of controlling*

A possible xanthate overdosage is checked by monitoring the froth thickness. If the froth thickness is lower than setpoint then the xanthate dosage is decreased at 2 min intervals until the froth thickness returns above the setpoint.

#### *Second step of controlling*

If the froth thickness is over the setpoint, then the control logic tests the RCC and the ABS. A low value of RCC or high value of ABS indicates lack of xanthate and thus xanthate is increased if the RCC is lower than its low alarm limit or if the ABS is above its high alarm limit.

#### *Third step of controlling*

If the first two tests are untrue, the zinc grade of rougher tailing is compared to its setpoint, which is calculated on the basis of the zinc grade in the feed. If the tailing value is higher than its setpoint then xanthate is increased. The xanthate setpoint is not changed if all the tests are untrue, i.e. when the results are good. The setpoints of the input variables can be modified by the operator. In this way the controller functionality can be adjusted when the ore type radically changes. However, based on the experiences so far, it seems that the controller can improve the recovery of the zinc flotation to some extent.

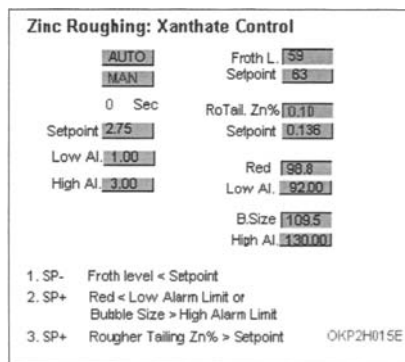


Figure 8: The user-interface of the controller.

## Conclusions

The general objectives of the ChaCo project were to optimize process control and production at flotation plants and thus to give competitive advantage for the European mining industry. New software tools and algorithms for the flotation process control by using existing forefront hardware were developed realizing the following products:

- on-line flotation froth analyzer (color and structure);
- on-line flotation froth classifier;
- mathematical models of the flotation process (especially correlating the dependencies of the visual characteristics of the froth on the process variables);
- control methods and algorithms for the flotation process control by machine vision.

Out of the overall set of the developed procedures, also each specific item can be profitably applied in the flotation industry. As example, the froth analyzer and/or classifier installed in the plant highly increases the operators' ability to control the flotation process on-line. By utilizing the froth analyzer the most serious disturbances due to incorrect reagent dosages can be eliminated, bringing better flotation results, i.e. higher recoveries, and cost savings in reagent consumption. The froth analyzer for its high degree of flexibility is also a useful tool in process studies leading to a better understanding of the process behavior.

## Acknowledgments

The authors wish to thank the European Union for financial support within the framework of the EU LTR Project No. 24931, ChaCo. The characterization of flotation froth structure and color by machine vision.

## References

- Beucher, S. and Meyer, F., 1993. The morphological approach to segmentation: the watershed transformation. In: *Math. Morphology and Image Processing* (Dougherty E.R., Ed.), 433-481, Marcel Dekker, New York.

- Bonifazi, G., Serranti, S., Volpe, F. and Zuco, R., 1998. Flotation froth characterization by optical-digital sectioning techniques. 4<sup>th</sup> Int. Conf. Quality Control by Artificial Vision, Takamatsu, Japan, 131-137.
- Bonifazi, G., Serranti, S., Volpe, F., Zuco, R., 1999a. Flotation Froth Characterisation by Closed Domain (Bubbles) Colour Analysis. Int. Conf. Quality Control by Artificial Vision. Trois-Rivieres, Quebec, Canada, 151-156.
- Bonifazi, G., Serranti, S., Volpe, F., Zuco, R., 1999b. A Combined Morphological and Color Based Approach to Characterize Flotation Froth Bubbles. The Second International Conference on Intelligent Processing and Manufacturing of Materials. Big Island, Hawaii, 465-470.
- Bonifazi, G., Serranti, S., Volpe, F., Zuco, R., 1999c. Software Sensors, Digital Imaging Based, for Flotation Froth Supervision: Algorithms and Procedures. Optimization and Control in Minerals, Metals and Materials Processing (CIM'99), August 22-26, Québec, Canada.
- Bonifazi, G., Serranti, S., Volpe, F., Zuco, R., 2000a. Characterisation of Flotation Froth Colour and Structure by Machine Vision. Computers & Geosciences, in press.
- Bonifazi, G., Hall, S. and Meloni, A., 2000b. 2D Fractal Analysis of Flotation Froth, submitted to Int. Jour. Min. Proc.
- Bonifazi, G., Massacci, P. and Meloni, A., 2000c. Prediction of Complex Sulfide Flotation Performances by a Combined 3D Fractal and Color Analysis of the Froth. Minerals Engineering in press.
- Cipriano, A., Guarini, M. and Soto, A., 1995. Using image processing techniques to evaluate the quality of mineral flotation process. Proc. Int. Conf. on Signal Process. Application & Technology. Boston, USA.
- Cipriano, A., Guarini, M., Soto, A., Briceno, H. and Mery, D., 1997. Expert supervision of flotation cells using digital image processing. Proc. of XX Int. Min. Proc. Con., Aachen, Germany, 281-292.
- Haralik, R.M., Shanmugan, K. and Dinstein, I., 1973. Textural features for image classification. IEEE Trans. Syst. Manage. Cybernet., SMC-3 (6), 610-621.
- Hargrave, J.M., Miles, N.J and Hall, S.T., 1996. The use of grey level measurement in predicting coal flotation performance. Mineral. Eng., 9, 667-674.
- Hargrave, J.M., Brown, G.J. and Hall, S.T., 1998. A fractal characterisation of the structure of coal froths. Coal Preparation, 19, 69-82.
- Hatonen, J., Hyotyniemi, H., Bonifazi, G., Serranti, S., Volpe, F. and Carlsson, L.E., 1999. Using PCA in controller strategy design for a flotation process. 14th IFAC World Congr., Beijing, China, 385-390.
- Moolman, L.W., Aldrich, C., Van Deventer, J.S.J. and Stange, W.W., 1994. Digital image processing as a tool for on-line monitoring of froth in flotation plants. Mineral. Eng., 7, 1149-1164.
- Moolman, L.W., Aldrich, C., Van Deventer, J.S.J. and Bradshaw, D.J., 1995a. The interpretation of flotation froth surfaces by using digital image analysis and neural networks. Chem. Eng. Sci., 50, 22, 3501-3513.
- Moolman, L.W., Aldrich, C., Van Deventer, J.S.J. and Stange, W.W., 1995b. The classification of froth structures of in a copper flotation plant by means of neural net. Int. Jour. Miner. Process., 43, 193-208.
- Oestreich, J.M., Tolley, W.K. and Rice, D.A., 1995. The development of a colour sensor system to measure mineral composition. Mineral. Eng., 8, 31-39.
- Pratt, W.K., 1991. Digital Image Processing. 2<sup>nd</sup> Ed. A Wiley-Intersc. Publ. John Wiley & Sons, Inc., New York.
- Sadr-Kazemi, N. and Cilliers, J.J., 1997. An image processing algorithm for measurement of flotation froth bubble size and shape distribution. Mineral. Eng., 10, 1075-1083.
- Van Deventer, J.S.J., Bezuidenhout, M. and Moolman, D.W., 1997. On-line visualization of flotation performance using neural computer vision of the froth texture. Proc. XX Int. Min. Proc. Cong., Aachen, Germany, 315-326.



This Page Intentionally Left Blank

**FLOTATION – SURFACE CHEMISTRY AND  
REAGENTS**

This Page Intentionally Left Blank

<b>New Synthetic Polymeric Depressants for Sulfide and Non-Sulfide Minerals</b> D.R. Nagaraj	<b>C8b-1</b>
<b>Valorisation of Molybdenite from Majdanpek Copper Concentrate</b> D. Salatic, V. Salatic	<b>C8b-9</b>
<b>Characterisation of the Surfaces of Galena and Sphalerite in the Presence of Dithionite</b> C. Sui, J.A. Finch, J.E. Nasset, J. Kim, S. Lajoie	<b>C8b-15</b>
<b>Collector Properties of New Flotation Reagent Z-96</b> Z.S. Markovic, R. Stanojlovic, G. Milenkovic, Z. Petkovic	<b>C8b-23</b>
<b>Beneficiation of Fine Bituminous Coal by Column Flotation</b> B. Gürsu, C. Hiçyılmaz, S. Bilgen	<b>C8b-29</b>
<b>Studies of Surface and Sorption Behaviour of Saline and Clay Carbonate Minerals in Electrolytes</b> S. Titkov, N. Panteleeva, A. Chistyakov, L. Pimkina, I. Mikhaylova	<b>C8b-36</b>
<b>Activation of Xanthate Flotation of Pyrite by Ammonium Salts Following it's Depression by Lime</b> X. Xiaojun, Ş. Kelebek	<b>C8b-43</b>
<b>Modified Hydroxamate Collectors for Kaolin Flotation</b> C. Basilio, R.A. Lowe, A. Gorken, L. Magliocco, R. Hagy	<b>C8b-51</b>
<b>Monitoring the Distribution of Flotation Chemicals at an Industrial Mineral Processing Plant</b> M.S. Miettinen, P.M. Stén, J.O. Leppinen, H.J. Lehto	<b>C8b-56</b>
<b>Azine Compounds Application in Separation of Polymetallic Sulfide Concentrates</b> T.I. Yushina, A.A. Abramov	<b>C8b-63</b>
<b>On Certain Aspects Controlling Selectivity of Non-Sulfide Mineral Flotation</b> A.V. Kurkov, V.V. Shatalov, I.V. Pastukhova	<b>C8b-71</b>
<b>Purification of Brazilian Kaolin Clay by Flotation</b> A.B. Luz, I. Yildirim, R-H. Yoon	<b>C8b-79</b>
<b>Ways to Increase the Efficiency of Flotation Process for Complex Ores</b> V. Beloborodov, K. Fedotov	<b>C8b-84</b>

This Page Intentionally Left Blank

## NEW SYNTHETIC POLYMERIC DEPRESSANTS FOR SULFIDE AND NON-SULFIDE MINERALS

D. R. Nagaraj

Cytec Industries Inc.,  
Stamford Research Laboratory, 1937 West Main Rd., Stamford, CT 06904, USA

### Abstract

Flotation operations use a wide variety of depressants for sulfide and non-sulfide minerals to achieve both simple and complex separations. These depressants are conveniently grouped into inorganic, small organic and polymeric compounds. The use of polymeric depressants is limited to a few niche applications involving several types of polysaccharides (such as guar, starch and CMC) and, to a lesser extent, other polymers and organic byproducts. Several *synthetic* polymeric depressants have been developed in the last few years by Cytec Industries to address many of the drawbacks associated with the traditionally used depressants. These synthetic polymeric depressants offer many advantages: better dosage-performance and lower treatment cost, ease of handling, lower toxicity, lower transportation and storage hazards, ease of structural modification to suit different applications and ore variability, and consistency from batch to batch. The chemistry, applications and advantages of synthetic polymeric depressants are discussed in this paper using laboratory and plant performance data.

*Keywords: polymeric depressants, polyacrylamides, depressants, flotation, sulfides, non-sulfides*

### Introduction

Modifiers, which comprise depressants, pH and Eh modifiers, dispersants and activators, play a critical role in flotation, which is often overshadowed by the great importance placed on collectors. In addition to producing optimum conditions for collector adsorption on minerals (hence optimum flotation), modifiers make some of the virtually impossible separations possible. The importance of modifiers is far greater in non-sulfide flotation than it is in sulfide flotation because of the general lack of selectivity of most non-sulfide collectors, and because of the great similarity in surface properties among the various non-sulfide minerals. Among the modifiers, depressants present some of the greatest challenges in flotation research and development. Discussion in this paper is restricted to advances made in the development of new, synthetic depressants. Depressants fall into three major categories: inorganic, small organic, and polymeric molecules. Most of the modifiers used are inorganic, and were developed a long time ago. Small organic molecules (for ex. organic dyes, organic acids, S-containing compounds etc.) have found limited commercial use (Nagaraj et al., 1986); cost-effectiveness is a major factor (Nagaraj, 1994). The use of polymeric depressants is limited to polysaccharides and other natural products and byproducts. As in the case of collectors, numerous new depressants have been proposed, but these have remained a laboratory curiosity. In view of the fact that most of the practical and inexpensive inorganic compounds have been evaluated in the past several decades, there is virtually no hope of inventing any better inorganic modifiers (Nagaraj, 1994).

Advances of any commercial significance have been made in the area of development of synthetic, water-soluble polymeric depressants. The general concept is one of incorporating specific functional groups such as complexing or chelating moieties into water-soluble hydrophilic polymers (Nagaraj et al., 1987). These depressants offer many advantages over the currently used depressants, viz. better dosage-performance and lower treatment cost (the efficiency of a large molecule), ease of handling, lower toxicity, lower transportation and storage hazards, ease of structural modification to suit different applications and ore variability, and consistency from batch to batch. The chemistry and applications of the new, synthetic polyacrylamide-based depressants developed recently by Cytec Industries will be discussed in this paper with laboratory and plant data. The discussion in this paper is restricted to depressants (i.e. dispersants or selective flocculants are not discussed). Certain synthetic water-soluble polymers (ex. polyacrylates) are used in the minerals industry as dispersants or selective flocculants for clays and slimes, but the discussion in this paper is restricted to depressants. The discussion is also restricted to synthetic depressants (polysaccharides are not discussed). For a general review of the use of organic polymers in flotation, the readers are directed to the useful articles in the literature (Bulatovic, 1999, and references therein; Pugh, 1989).

### **Depression of non-sulfide minerals**

The first successful synthetic polymeric depressant appears to be the phosphate depressant introduced in 1982 (under the trade name ACCOPHOS® 950) by American Cyanamid Company (Nagaraj et al., 1987).

This was a polyacrylamide-based polymer containing hydroxyl and carboxyl groups (structure I) developed as an alternative to the polysaccharides (such as starch and dextrin) which have many drawbacks. It is used commercially in the phosphate-silica separation in the amine flotation circuit. A depressant of related chemistry has been found to be a silica depressant in the fatty acid flotation of phosphate (Nagaraj et al., 1988).

Typical results for phosphate-silica separation in the amine flotation circuit are given in Table I. Note that in this circuit, silica is floated with an amine collector, and apatite is depressed using the polymer.

It is evident from these data that the addition of the polymeric depressant at even low dosages, ex. 5-20 g/t, resulted in:

- a large increase in the phosphate recovery, 10% units at 20 g/t;
- a drastic reduction in %BPL (Bone Phosphate of Lime =  $2.18 \cdot P_2O_5$ ) lost to silica tails (which is reflected in the increased phosphate recovery);
- little or no change in the grade of the phosphate concentrate (74.4% BPL and 2% Insols, see Table I).

In the phosphate depressant molecule, there is considerable freedom in selecting the proportions of the segments x, y and z, and the molecular weight (typically low) of the polymer to meet the optimum metallurgical performance requirements. The mechanism of adsorption of these polymers on phosphate minerals such as apatite is not fully understood.

The functional group, for example  $-\text{NH}-\text{CH}(\text{OH})-\text{COOM}$  (see structure I,  $\text{R}_2=\text{COOM}$ ), appears to hold the key because in the absence of this group, the depressant activity is inferior (Nagaraj et al, 1987). This functional group can form stable complexes with  $\text{Ca}^{2+}$ .

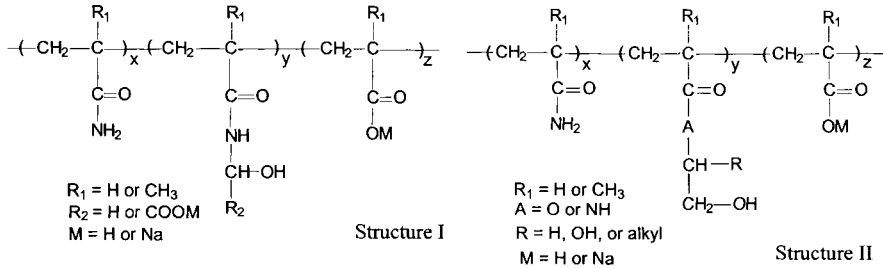
Table I: Metallurgical data for the effect of phosphate depressant (Structure I) on phosphate separation from silica (amine 500 g/t; deslimed feed BPL 58% after Nagaraj et al., 1987).

Depressant (g/t)	Yield (%) concentrate	BPL (%)		BPL (%) recovery	Insols in concentrate (%)
		tailings	concentrate		
0	68.0	23.7	74.4	87.0	1.94
5	74.0	10.9	74.4	95.1	2.13
10	75.5	8.5	74.6	96.3	2.10
20	75.5	7.0	74.0	97.0	2.20
50	75.5	7.5	74.4	96.8	2.30
200	78.4	3.8	72.3	98.6	3.60

The presence of the  $\alpha$ -hydroxy group should provide increased stability to the Ca-complex relative to the complex with  $\text{COO}^-$  alone.

Polyacrylamide-based depressants have also been developed for the depression of Mg silicates, such as talc, serpentines and pyroxene (Nagaraj et al., 1996 a & b).

A schematic representation of the polymer is given in structure II. In addition to these, graft copolymers comprising acrylamide grafted onto polyvinyl alcohol have also been developed.



Results obtained with depressants of structure II for the rejection of Mg silicates (talc, serpentines and pyroxenes) in Ni ores and a PGE (platinum group elements) ore are given in Figures 1a, 1b and 2.

It is evident from these results that in all cases the synthetic depressants provided advantages either in terms of lower dosages or better metallurgical performance or both, relative to the polysaccharides used.

For the Ni ore in Figure 1a, both the synthetic polymers, A and B, gave better rejection of Mg silicates at a lower dosage than guar gum. Ni recoveries with the synthetic depressants were almost the same as those with guar gum.

For the Ni ore in Figure 1b, the synthetic depressant gave the same performance as the CMC, but at a significantly reduced dosage: 75 g/t vs. 275 g/t.

In the case of the PGE ore (Figure 2), the synthetic depressant gave slightly better Pt recovery and concentrate grade at a reduced dosage (400 g/t vs) relative to. the CMC dosage of 500 g/t.



The mechanism of the depressant action of the synthetic polymers of structure II is not known at present. It is expected to involve a combination of influences from hydrogen bonding, hydration and hydrophobic interaction (Gong et al., 1999; Morris, 1996; Pugh, 1989).

### Depression of sulfide minerals

In the mid-1980's, two other classes of synthetic polymeric depressants (structures III and IV) were introduced by American Cyanamid Company, which have been further refined over the years.

These depressants are for a) the depression of iron sulfides (pyrite, pyrrhotite, marcasite) in base metal sulfide flotation (Rothenberg et al, 1990; Nagaraj and Wang, 1996) and b) the depression of copper sulfides (and also any associated iron sulfides) in the Cu-Mo separation from the final bulk copper concentrates (Lipp and Nagaraj, 1989).

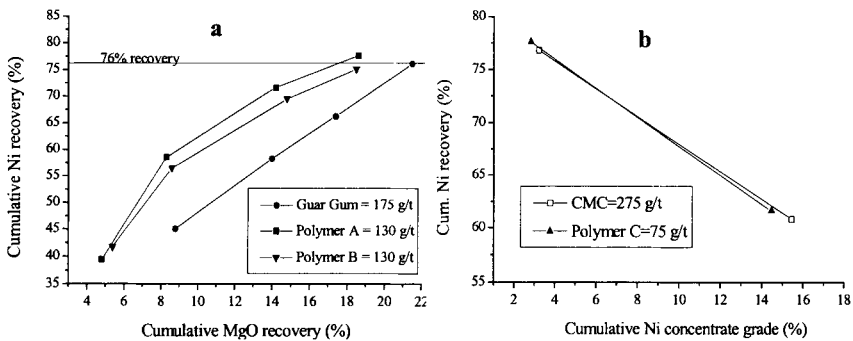
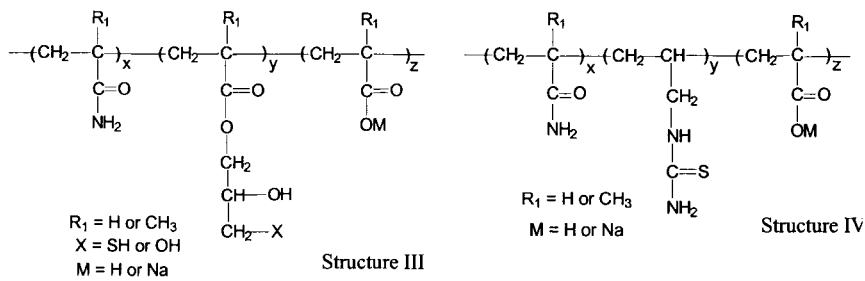


Figure 1: Results for the depression of Mg silicates in a Ni ore using synthetic polymers (structure II)

a: relative to guar gum; feed assay: 2.25% Ni and 27.7% MgO;

b: relative to CMC; feed assay: 0.85% Ni and 39.0% MgO.

Two of the successful applications for the iron sulfides depressant (structure III) have been the depression of pyrrhotite during pentlandite-chalcopyrite flotation from Ni ores and depression of pyrite and pyrrhotite in Zn circuits. Although the mechanism of depression of iron sulfides is not fully understood, the functional group containing either -CH(OH)-CH<sub>2</sub>-OH or -CH(OH)-CH<sub>2</sub>-SH appears to play a key role.

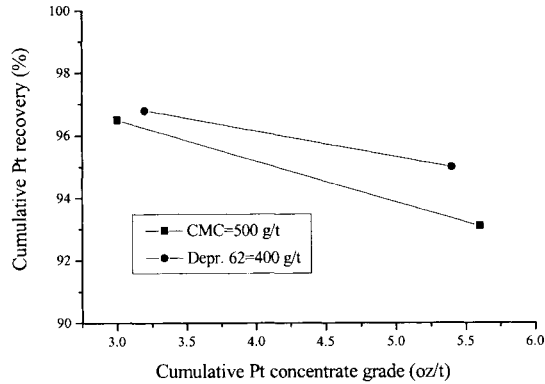
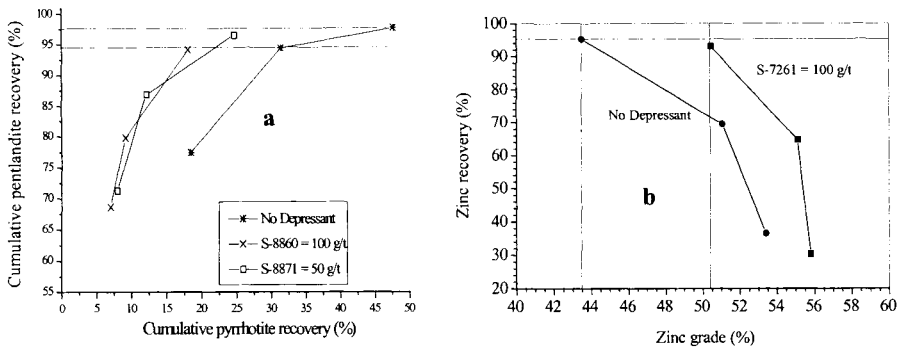


Figure 2: Results for the depression of Mg silicates in a PGE ore using a synthetic polymer (structure II) relative to CMC.

Typical results for a Ni ore containing pyrrhotite are given in Figure 3a. Results for the depression of iron sulfides in a Zinc circuit are given in Figure 3b.



Figures 3: Results for the depression of iron sulfides using polymers of structure III in:  
**a:** pentlandite-chalcopyrite ore; feed assay: 1.3%Ni and 28% pyrrhotite;  
**b:** zinc circuit; feed assay: 4.4% Zn and 17% Fe.

In the case of the Ni ore (Figure 3a), S-7261 depressant decreased pyrrhotite recovery by about 50% while maintaining pentlandite recovery. In the Zinc circuit (Figure 3b), with 100 g/t of reagent S-7261 Depressant, the overall rougher concentrate grade increased from about 43.5% to 50.5% Zn with almost no effect on Zn recovery.

In Cu-Mo separation, the depressant containing the thiourea functional group (structure IV) has shown excellent activity in depressing the copper sulfides and any associated iron sulfides at dosages that are often one-tenth of those required for the traditional depressants such as NaSH and Nokes reagent.

Under certain conditions, a combination of polymer and NaSH has provided improved performance. In such cases, NaSH is used only to adjust pulp potentials initially in the range of -450 to -500 mV (Au electrode, vs. Ag/AgCl) (Lipp and Nagaraj, 1989; Nagaraj et al, 1992). The amount of NaSH required to reach such a potential is

relatively small compared to that required to *maintain* such a potential as is the case when NaSH alone is used as the depressant. The overall economics of the polymer/NaSH system is still more attractive than the NaSH system alone.

One of the important advantages of the polymer is that the depressant effect does not deteriorate by aeration as it does in the case of NaSH alone. In other words, sulfide minerals depressed by polymer remain depressed in the circuit for long periods of time; such is not the case with NaSH.

The depression effect of the polymer could be reversed, however, with the addition of more collector.

The thiourea functional group is necessary for the polymer to function as an efficient depressant (Nagaraj et al, 1992). The adsorption of the polymer is via the thiourea group (complexation with copper on the sulfide surfaces), while the remaining polymer segments provide hydrophilicity to the surface after the polymer has adsorbed.

Results obtained with a formulation of the thiourea-containing polymer, viz. reagent S-8460 depressant, for Cu-Mo separation are given in Figure 4. Relative to the currently used depressant, the Nokes reagent, at 23 kg/t, the polymeric depressant at 10 kg/t gave a significant reduction in Cu recovery (from 22% to 14.5%) and an increase in Mo recovery (from 96% to 98.6%).

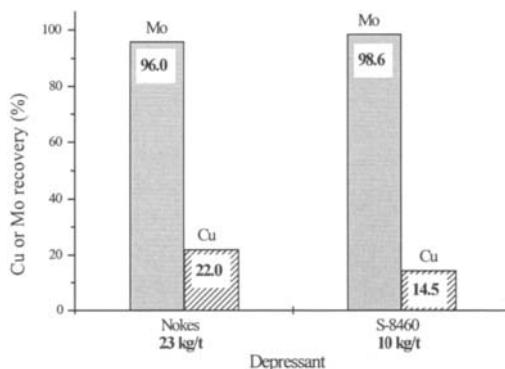


Figure 4. Results for copper depression in Cu-Mo separation using Reagent S-8460 depressant relative to Nokes reagent. Feed assay: Cu % and Mo %.

Plant data for the use of a combination of the thiourea-containing polymer, reagent S-7260 depressant, and Na<sub>2</sub>S in another Cu-Mo plant are given in Table II. These results demonstrate also that the use of the polymeric depressant reduced the overall dosage of the depressant significantly, and provided better concentrate grade of Mo, while maintaining Mo recovery.

Table II. Plant trial data from a Cu-Mo plant: polymer S-7260/Na<sub>2</sub>S (weekly averages).

Depressant	Dosage (kg/t)	Grade of final concentrate		Mo recovery (%)
		Mo (%)	Cu (%)	
Na <sub>2</sub> S	23.2	52.5	1.17	93.3
S-7260/Na <sub>2</sub> S	14.1	54.3	1.00	93.3

### Practical aspects

All of the synthetic depressants discussed in this paper are clear, colorless to pale yellow, low viscosity aqueous solutions, with little or no odor. Their molecular weights are typically <100,000. They dissolve almost instantaneously in water, and aqueous solutions of any strength can be prepared. They can be added to the circuit either at full strength or as dilute solutions, though the latter is recommended for better dosage control. The best addition point is determined by laboratory testing, and it depends entirely on the type of separation in question. The order of addition of collector and the synthetic polymer varies also with the type of separation and the metallurgical objectives, but the laboratory and plant experience with these polymers seem to suggest that addition of the polymer *after* collector addition provides better selectivity and control. It has been observed that these depressants are fully compatible with most of the collectors; in other words, no antagonistic effects have been observed. These depressants do not alter, and do not require any adjustment or control of, pulp redox potentials.

### Conclusions

The chemistry and applications of the recently developed polyacrylamide-based depressants for separation of non-sulfide and sulfide minerals are discussed. These synthetic depressants offer many advantages over the currently used inorganic compounds and polysaccharides. For example, the synthetic depressants provide better dosage-performance and lower treatment cost, batch-to-batch consistency and quality (unlike the polysaccharides), ease of handling, and ease of structural modification to suit different applications and ore variability. They are also relatively non-hazardous. Laboratory and plant data are presented for several separations such as a) phosphate depression in silica flotation, b) Mg silicate depression in Ni and PGE flotation, iron sulfides depression in Zn circuits, and Cu and Fe sulfides depression in MoS<sub>2</sub> flotation. These results demonstrate the advantages of the synthetic depressants in terms of either reduced dosages and treatment cost or improvement in metallurgy or both.

### References

- Bulatovic, S.M., 1999. Use of Organic Polymers in the Flotation of Polymetallic Ores: A Review. *Miner. Eng.*, 12-4, 341-354.
- Gong, W., Jenkins, P. and Ralston, J., 1999. Polyacrylamides at the Talc-Aqueous Solution Interface. In: J.S. Laskowski (Editor), *Polymers in Minerals Processing*. The CIM, Ottawa, Canada.
- Lipp, D.W and Nagaraj, D.R., 1989. US Patent 4866150 (to American Cyanamid Co); Wang, S.S. and Nagaraj, D.R. 1990. US Patent 4902765.
- Morris, G.E., 1996. Ph.D. Thesis, University of South Australia, Adelaide, Australia.
- Nagaraj, D.R., 1994. A Critical Assessment of Flotation Agents. In: P.S. Mulkutla and W.A. Hancock (Editors), *Reagents for Better Metallurgy*. SME, Littleton, Colorado, 81-90.
- Nagaraj, D.R., Basilio, C.I., Yoon, R.H. and Torres, C., 1992. In: R.Woods and P.E. Richardson (Editors), *Proc. Symp. Electrochemistry in Mineral and Metals Processing*. The Electrochem. Soc., Princeton, 108-123.
- Nagaraj, D.R., Rothenberg, A.S. and Lambert, A.S., 1988. US Patent 4720339.

- Nagaraj, D.R., Rothenberg, A.S., Lipp, D.W. and Panzer, H.P., 1987. Low Molecular Weight Polyacrylamide-based Polymers as Modifiers in Phosphate Beneficiation. *Int.J. Min. Proc.*, 20, 291-308.
- Nagaraj, D.R. and Wang, S.S., 1996. US Patent 5,531,330.
- Nagaraj, D.R., Wang, S.S., Avotins, P.V., Dowling, E., 1986. Structure-Activity Relationships for Copper Depressants. *Trans. Inst. Min. Metall.*, 95, C17-26.
- Nagaraj, D.R., Wang, S.S., Lee, J.S. and Magliocco, L.G., 1996. US Patent 5,533,626.
- Nagaraj, D.R., Wang, S.S., Lee, J.S. and Magliocco, L.G., 1996. US Patent 5,525,212.
- Pugh, R.J., 1989. Macromolecular Organic Depressants in Sulfide Flotation: a Review. *Int. J. Miner. Process.*, 25, 101-130.
- Rothenberg, A.S., Lipp, D.W., Wang, S.S. and Spitzer, D.P., 1990. US Patent 4902764.

## VALORISATION OF MOLYBDENITE FROM MAJDANPEK COPPER CONCENTRATE

D. Salatic, V. Salatic

Faculty of Mining and Geology, University of Belgrade, Belgrade, Yugoslavia

### Abstract

Molybdenite often appears in porphyry copper ores. The separation of copper and molybdenum values implies depression of either one of them. Depression of molybdenite involves dextrin and starches, which at the present time have little practical application. On the other hand, depression of copper and iron sulphides is a far more commonly used technique and is almost universally accepted.

In Yugoslavia molybdenite is found in two types of porphyry deposits: in Machkatica deposit in which molybdenite is a predominant useful mineral and in Majdanpek and Veliki Krivelj deposits in which copper minerals are predominant values and molybdenite may be recovered as a by-product.

Both copper deposits are unevenly mineralized with molybdenite. Content of molybdenum in the copper ore is between 0.001% and 0.005%. It is assumed that the average content is 0.003% what is much lower than in the main world copper mines which also produce molybdenite concentrates as by-products. To increase the molybdenite flotation recovery in copper concentrates, the collector diesel oil was added. This brought to slight increase of molybdenite recovery. Later on, by studying the Syntex-L influence on the diesel oil dispersion and on reduction of the negative electrokinetic potential on molybdenite surfaces, it was established the role of Syntex-L on the molybdenite recovery increase in the flotation cycle of copper flotation. The achieved Mo recovery was more than 80% with about 50% of Mo in the concentrate.

The objective of this paper is to present both the basic and applied researches with the aim to extract selective molybdenum concentrate. Attention has been given to the researches carried out in Yugoslavia, particularly to the molybdenite concentrate production from Majdanpek copper ore.

*Keywords: molybdenite, copper minerals, collector desorption, copper depression, selective flotation*

### Introduction

Molybdenum is found in very small amounts in nature. Its concentration in crystalline rocks varies between 1.0 and 1.5 ppm. The number of molybdenum mineral species is very small. Molybdenite is found naturally in different rock types, but for all practical purposes only two of them have significance: quartz veins, in which its concentration may range between 1.0% and 20.0%; and highly disseminated porphyry deposits, where its concentration varies between 0.01% and 0.50%. We have distinguished, essentially, two types of porphyry deposits: those in which molybdenite is a predominant metal value and those in which copper is the predominant value and molybdenite is recovered either as a by-product or co-product. An example of the first type is well-known Climax deposit and second one types are Bingham in USA, Chuquicamata in Chile, Kadzharan in Russia and other copper-molybdenum deposits in the world (Sutulov, 1978).

Particular characteristic of molybdenum world reserves is a very selective distribution in the earth's crust. Some of 87% molybdenum reserves are found in the Western Hemisphere, mainly in the USA, Canada and Chile. The opinion prevails that about

95% of the world's reserves of molybdenum are located in porphyry copper ore deposits.

Molybdenite is known as one of the most floatable mineral owing to physico-chemical properties of its surfaces. However, although it is strongly floatable and has been separated by flotation for a rather long period, the mechanism of its flotation has been explained only recently.

Although flotation is one and only process for obtaining molybdenum concentrate, yet it is still, as Sutulov says (Sutulov, 1975), "more the art than the science because of its complex physico-chemical system that encompasses numerous variables and components, most of which are either unknown or insufficiently defined".

### **Investigations of floatability of sulphide minerals**

Investigations of floatability of numerous sulphide minerals, and molybdenite as well, dated more than 70 years ago, when Taggart published (Taggart et al., 1930) in 1928 the results he obtained during his study on mechanism of xanthate sticking to sulphide mineral surfaces. The knowledge of Taggart was greatly improved and advanced by Plaksin (Plaksin, 1960) who used microautoradiography to prove the irregular distribution of xanthate on mineral surfaces thus discovering the important role of oxygen in sticking of reagents to mineral surfaces. The presence of oxygen increases a positive electrochemical potential to the value when xanthate ions oxidize into dixanthate. Addition of oxygen into a system has to be strictly controlled and homogenous as the absence of oxygen frustrates flotation while the excess in oxygen or the longer contact of the same a mineral surface, reduces flotation properties.

#### *Fundamental investigations of molybdenite floatability*

The floatability of molybdenite was studied by Chandler and Fuerstenau (Chander and Fuerstenau, 1972) within the context of the Deriaguin electric double-layer model (Deriaguin, 1960). They established that molybdenite, due to its specific structure, is characterized by completely surface properties comparing to other sulphide minerals. Its structure is stratified, i.e. sandwich-like, with horizontal S-Mo-S layers built one upon the other, and each metal atom is surrounded by 6 sulphur atoms at the tops of triangular prisms. These layers are mutually connected by weak Van der Waal's forces although strong covalent bonds exist within each layer. Such a structure facilitates the outstanding cleavage of molybdenite crystals along horizontal plane. This plane is strongly hydrophobic as it in fact represents a layer of exposed sulphur atoms, while the edges of a sandwich or layer along which strong covalent bounds are discontinuous, can be polarized and show hydrophilic properties and thus can become attractive for oxidation and other chemical reactions.

The principal conclusion from these studies is that surface potential of molybdenite is controlled by  $\text{HMoO}_4$  and  $\text{MoO}_4$  and that adsorption of these ions contributes to the hydration of surfaces, thus preventing closer approach and bubble attachment to the particle. They could also prove the high surface activity of calcium ions, which apparently actively react with oxidation products of molybdenite and potential-determining ions -  $\text{MoO}_4$  and  $\text{HMoO}_4$  - and neutralize them, thus provoking changes in zeta potential. The best floatability is achieved when the zeta potential is minimum and equal to zero.

Fundamental investigation carried out by Salatic et al. (1979) at molybdenite from Majdanpek copper deposit proved that zeta potential of molybdenite surface can be reduced by adding small quantities of sulphated oil of coconut, known at the market as Syntex L. According to the author's opinion, Syntex adsorbs specifically along edges of molybdenite matricles when it is hydrophobically connected with molybdenite plans through hydrocarbon chain. Such form of adsorption enables zeta potential to become independent from pH medium and molybdenite floatability to improve considerably.

#### *Applied investigations of molybdenite flotation from bulk Cu-Mo concentrate*

As we said before the separation of copper and molybdenite values implies depression of either one of them in a selective flotation circuit for the other. Depression of molybdenite involves dextrin and starches, which at the present time have little practical application. On the other hand, depression of copper and iron sulphides is a far more commonly used technique and is almost universally accepted. The initial works on separation of molybdenite from copper ore containing molybdenum dated some 60 years ago. Nowadays, production of molybdenum concentrate from bulk Cu-Mo concentrate has been performed in many mines. Generally speaking, there are two ways in separation of molybdenite: flotation of molybdenum minerals and depression of copper minerals.

Depression is carried by thermal or chemical processes. The main depressing agents of copper minerals can be sodium sulphide ( $\text{Na}_2\text{S}$ ), sodium hydrosulphide ( $\text{NaHS}$ ), Nokes reagent, various cyanides, ammonium sulphides, mixtures of sodium hydroxide and phosphorpentasulphide (known as reagent LR-744), mixture of sodium and arsenotrioxide (reagent Anamol D) and other similar mixtures. Desorption of a collector layer from surfaces of bulk Cu-Mo concentrate can be done even by thermal process, i.e. by heating concentrate from 90 °C to 110 °C or by roasting at temperatures ranging from 250 °C to 350 °C. The latter process can be performed only in cases when aerofloats are used as collectors in bulk flotation of Cu-Mo minerals.

#### **Investigation of selective flotation of molybdenite in Majdanpek Copper Mine**

The Yugoslav copper mine Majdanpek contains far less concentration of molybdenum compared to the world's copper mines. Its concentration ranges from 0.03% to 0.15% Mo in bulk Cu-Mo concentrate that is obtained by bulk flotation from the ore containing 0.003% Mo approximately.

Already in 1962 the first investigations concerning the possibility of separation of selective molybdenum concentrate from Cu-Mo concentrate were performed at Majdanpek flotation plant (Salatic, 1967). Within a long period a particular attention has been paid to studying a great number of flotation reagents, especially depressing agents of copper minerals and collectors of molybdenite. Investigations have been carried out in laboratories and pilot plant. For desorption of collector layer from the surface of bulk Cu-Mo concentrate either sodium sulphide and sodium hydro sulphide were used or by heating of pulp of bulk Cu-Mo concentrate under normal pressure in a conditioning tank and under higher pressure in autoclave. To increase recovery of molybdenum in Cu-Mo concentrate petroleum, kerosene or diesel oil as a secondary



collector were added. During selective flotation of molybdenite, kerosene and Sintex-L are proved to be the best collectors. In course of copper depression good results were obtained by potassium ferro and ferri cyanide. Sodium silicate was successfully used in depressing of barren minerals. The best results were obtained when the pH values of pulp ranged between 7.5 and 8.5.

Fundamental research on pure molybdenite were performed in order to establish its floatability and explain occurrences on the surface of this mineral in the presence of different flotation reagents (Salatic et al., 1991).

New knowledge enabled considerable increment in recovery of molybdenite in bulk Cu-Mo concentrate by adding diesel oil and Syntex-L. Results obtained in laboratories were confirmed in industrial process at Majdanpek flotation plant. By adding mentioned reagents into bulk flotation the recovery of molybdenum in Cu-Mo concentrate was increased up to 86%.

Concentration of molybdenum in bulk Cu-Mo concentrate changes in dependence of the content of molybdenum in ore and with the regime of reagents, particularly with utilization of diesel oil and Syntex-L. Definite bulk Cu-Mo concentrates contain 0.03-0.15% Mo. Performed investigations showed that a commercial molybdenum concentrate can be obtained by selective flotation of molybdenite from bulk Cu-Mo concentrate.

During investigations of influence of different technologies for desorption of collector layer from surfaces of mineral grains of bulk Cu-Mo concentrate, the best results were obtained by sodium sulphide. Besides, sodium sulphide ( $\text{Na}_2\text{S}$ ) secures the most simple process for copper depression in selective flotation of molybdenite (Salatic et al., 1995). Also, the conclusion was made that a successful depression of copper minerals and high recoveries of molybdenite from its concentrate requires reduction of pH value of pulp down from 12 to value of 9. Further, it was noticed that a very high pH value in flotation of bulk Cu-Mo concentrate has a negative influence on recoveries of molybdenite as well as of gold and silver. Moreover, it requires much more of sulphuric acid in order to reduce pH value of pulp in selective flotation of molybdenite.

Experiments of molybdenite flotation showed that active carbon plays a very important role in separation of selective molybdenum concentrate from bulk Cu-Mo concentrate. Its role is particularly seen in maintaining the stability of process, and also has influence on results of flotation of molybdenite (Salatic, 1996). A certain quantity of active carbon floats together with molybdenite thus reducing content of Mo in concentrate. This however, is not a problem as immediately after entrance of concentrate into metallurgical plant, the coal burns and thus increases the quality of Mo concentrate comparing to the one produced in flotation.

Investigations proved that very good collectors of molybdenite are diesel oil D-2, kerosene and Syntex-L. All the mentioned collectors give satisfying technological results, but their combination give the best one. Then, for depressing of copper and other sulphide minerals, sodium sulphide gives excellent results, and for depressing of barren minerals, particularly silicates, utilization of sodium silicate (water glass) is very useful. As to frothers in bulk Cu-Mo flotation, it is desirable, apart to Dowfroth

or pine oil to add a small quantity of methylisobuthilecarbinol. In selective flotation of molybdenite, methylisobuthilecarbinol or methylamyl alcohol should be only used. At the end of this conclusions we can say that this study undoubtedly shows the successful separation of commercial molybdenum concentrate by selective flotation of molybdenite from definite bulk Cu-Mo concentrate from Majdanpek copper flotation plant. Production of selective molybdenum concentrate under industrial conditions of work in Majdanpek Copper Mine will be realized according to the flowsheet of technological process given in Figure 1.

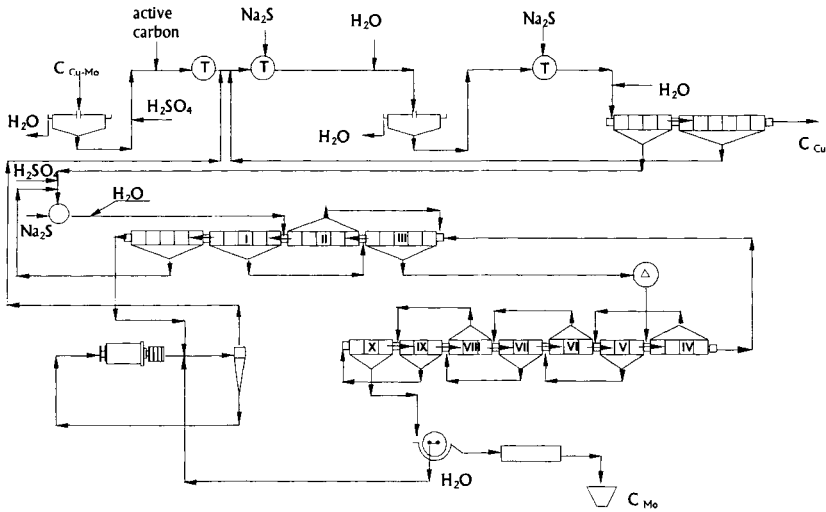


Figure 1: Flowsheet of selective flotation of molybdenite in Majdanpek copper mine.

The technological process is consisted of the following. The bulk Cu-Mo concentrate is fed to the thickener for dewatering purposes. Such a thickened concentrate after addition of sulphuric acid, to decrease pH of the pulp, is transferred to the conditioner where is conditioned with active carbon. Second conditioner is used for desorption of collector layer with sodium sulphide.

The desorbed concentrate, with water addition, is fed to the second thickener to wash off desorbed reagents. The last, third conditioner, is used for additional depression of chalcopyrite with sodium sulphide. After thorough conditioning where sufficient copper depression is achieved, the flotation of molybdenum can start. It is consisted of rougher and scavenger flotation. The scavenger tails are final copper concentrate and scavenger concentrate is returned to the second conditioner. The rougher concentrate goes to the conditioner where sulphuric acid and sodium sulphide is added and slurry prepared for first phase of molybdenum cleaning stages (I-III). First cleaning tails goes to cyclone, which works in a closed circuit with a regrind mill. Cyclone overflow is returned to the second conditioner. The molybdenum third cleaning concentrate, via conditioner, goes to the rest of the cleaning stages (IV-X). A final molybdenum concentrate after tenth stage of cleaning goes to filtration and after to the dryer.

## Conclusions

Based upon research laboratory work and pilot plant test results as per above described flowsheet (Figure 1) it was proved that selective molybdenum concentrate can be produced from bulk Cu-Mo concentrate of Majdanpek Copper Mine. If this flowsheet and reagent scheme is followed, the results presented in Table I, can be expected in industrial conditions.

Table I: Expected metal balance in Majdanpek molybdenum flotation plant.

Products	Weight (%)	Assay (%)		Distribution (%)	
		Mo	Cu	Mo	Cu
Cu-Mo concentrate	100.00	0.09	22.00	100.00	100.00
Mo concentrate	0.15	51	4.00	85.00	0.03
Cu concentrate	99.85	0.0135	22.03	15.00	99.97

## References

- Chander, S. and Fuerstenau, D.W., 1972. On the Natural Flotability of Molybdenite. *Trans. AIME*, 252, pp. 62.
- Deriaguin, B.V., 1960. Theory of flotation of small and medium size particles. *Trans. Inst. of Mining and Metallurgy*, 70, 221.
- Plaksin, I.N., 1960. Using microautoradiography for the study of the interaction reagents with minerals in flotation. *Final Proc. Int. Min. Process. Cong., London, England*, 253.
- Salatic, D., 1967. Tehnosloske mogućnosti izdvajanja molibdena iz koncentrata bakra flotacije u Majdanpeku (Technological possibility of separation of selective molybdenum concentrate from copper concentrate in Majdanpek flotation plant). *Rudarski glasnik (Mining Journal)* 2, 33.
- Salatic, D., 1996. Possibilités actuelles de la flottation sélective de la molybdénite et perspectives de son application en Yougoslavie. (Possibilities actual of selective flotation of molybdenite and the perspectives of its application in Yugoslavia). *Bull. Séanc. Acad. r. Sci. Outre-Mer, Bruxelles*, 42 (4), 863-874.
- Salatic, D., Grujic, M., Deusic, S. and Salatic, V., 1995. Development and progress in the Flotation of Copper Mine Majdanpek on the XXI Century. *Final. Proc. 16th World. Mining Congr., B8, Sofia, Bulgaria*.
- Salatic, D., Pustric, S. and Deusic S., 1979. Uticaj sinteksa na flotabilnost molibdenita iz rude bakra lezista Majdanpek. (Influence of Syntex-L on floatability of molybdenite from Majdanpek copper ore deposit). *Final Proc. 7th Yugoslav Min. Process. Symp., Zabljak, Yugoslavia*, 301.
- Salatic, D., Pustric, S., Deusic, S. and Salatic, D., 1991. Izbor tehnoloskog procesa flotiranja molibdenita u Rudniku bakra Majdanpek. (Selection of technological process of flotation of molybdenite in Copper Mine Majdanpek). *8th Yugoslav Min. Process. Symp., Vrnjacka Banja, Yugoslavia*, 369-384.
- Sutulov, A., 1975. *Copper porphyries*. San Francisco.
- Sutulov, A., 1978. *International molybdenum encyclopedia 1778-1978*. Santiago de Chile.
- Taggart, A. F. et al., 1930. Chemical reaction in flotation. *Trans. AIME*, 87, 217.

## CHARACTERISATION OF THE SURFACES OF GALENA AND SPHALERITE IN THE PRESENCE OF DITHIONITE

C. Sui\*, J.A. Finch\*, J.E. Nasset<sup>o</sup>, J. Kim<sup>o</sup>, S. Lajoie<sup>o</sup>

\*Department of Mining and Metallurgical Engineering, McGill University, University Street, Montreal, Quebec, H3A 2B2, Canada, e-mail: caroline@minmet.lan.mcgill.ca

<sup>o</sup>Mineral Processing Laboratory, Noranda Technology Centre, 240 Hymus, Pointe Claire, Quebec, H9R 1G5, Canada

### Abstract

Dithionite has been used as a reducing reagent to control electrochemical reactions in flotation, notably to reduce oxidation of sulphide minerals. However, chemical side-reactions between the reagent and, for example, metal ions such as  $Pb^{2+}$  may also affect surface properties and thus floatability of sulphide minerals. In this study, the effect of dithionite on Pb ion production and xanthate adsorption on galena and sphalerite (from a mixture with pyrite and galena) was investigated. Lead concentration on the surface of minerals was determined using EDTA extraction, the surface species were characterised by X-ray photoelectron spectroscopy (XPS) and the effect on xanthate adsorption was determined by ultra-violet spectroscopy (UV). Addition of dithionite significantly decreased pulp potential, leading to suppression of galena oxidation and a lower Pb concentration in solution and on sphalerite. However, Pb concentration on the surface of galena increased compared to in the absence of dithionite attributed to precipitation as lead sulphite. The EDTA results and XPS analysis were consistent with the interpretation. Adsorption of xanthate on both galena and sphalerite was reduced. This is attributed to the presence of lead sulphite in the case of galena and the reduced surface concentration of Pb in the case of sphalerite.

This study shows that dithionite suppresses galena oxidation and Pb contamination of sphalerite and suggests that improved selective flotation of galena against sphalerite may be achieved using dithionite. However, formation of lead sulphite on galena, which hinders xanthate adsorption on galena, needs to be controlled.

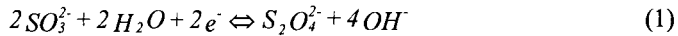
*Keywords: galena, sphalerite, reducing agent, dithionite, XPS analysis, EDTA extraction, xanthate adsorption*

### Introduction

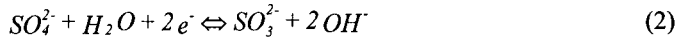
Oxidation of sulphide minerals leading to generation of metal ions is a potentially significant factor in flotation of complex sulphide ores. It is well known that metal ions, especially heavy metal ions like Cu and Pb, may cause accidental activation of pyrite and sphalerite in Cu/Pb flotation, resulting in reduced selectivity. In a previous study we showed that surface Pb could represent as much as 10% of the bulk Pb concentration when ores contained fine galena (e.g.  $<10\ \mu\text{m}$ ) and a high ratio of pyrite to galena (e.g.  $>10$ ) (Sui et al., 1999).

Brunswick Mining and Smelting (BMS), division of Noranda Inc. treats a fine-grained, highly complex ore bodies. The main economic minerals of interest are sphalerite (with  $\sim 7\%$  Fe), galena and chalcopyrite with the main diluent being pyrite (60%). Fine grinding is required to liberate the minerals, which results in a significant amount of Pb ion release

from galena particles. A comprehensive survey attributed about 60% of the Zn loss to the Cu/Pb rougher concentrate to accidental activation mainly by Pb ions (Kim et al., 1997). To prevent oxidation of sulphide minerals, reducing reagents such as dithionite, sulphite, bisulphite, sulphur dioxide can be used. Among these dithionite is the strongest reducing reagent with standard reduction potential of  $-1.12$  V when oxidised to sulphite:



Sulphite can be further oxidised to sulphate with standard reduction potential of  $-0.93$  V:



Batch flotation tests on ores from BMS (and Heath Steele, another complex) (Kim et al., 1997) showed that less sphalerite was lost to the Cu/Pb concentrate when reducing reagents were added to the grinding mill. The interpretation was that under low pulp potential conditions, oxidation of galena was suppressed, and thus the amount of Pb ions produced was reduced. If a high dosage of a reducing reagent was added, sphalerite loss could be further decreased but at the expense of low recovery of Cu and Pb. This may be attributed to too low a pulp potential that retards flotation of chalcopyrite and galena (Kim et al., 1997; Sui et al., 1997). Another possibility is that Pb ions released from galena may react with the  $SO_3^{2-}$ , an oxidation product of dithionite, to form insoluble  $PbSO_3$  on a mineral surface. Such insoluble species may hinder adsorption of xanthate and flotation. The fundamental study presented here aims to address effects of dithionite on Pb ion production, on the type of Pb species formed on the minerals, and on xanthate adsorption. The concentration of Pb on the surface of minerals was determined using EDTA (ethylene diamine tetraacetate) extraction followed by atomic absorption spectroscopy (AA). Species on the surface were characterised by X-ray photoelectron spectroscopy (XPS). XPS, which has been widely used to characterise the surface of minerals, provides quantitative surface composition for elements (except H and He), information about the chemical bonding environment of the atoms (such as chemical state and valence), and quantitative surface depth profiles (Smart, 1991). Two minerals were studied, single galena, and sphalerite isolated from a mixture with galena and pyrite. Minerals were conditioned in water or a dithionite solution. Xanthate adsorption on the conditioned minerals was determined by difference using ultra-violet spectroscopy (UV) analysis of solutions.

## Experimental

### Reagents

The reagents used were sodium dithionite ( $Na_2S_2O_4$ ) and sodium ethylene diamine tetraacetate (EDTA) (analytical grade, J. T. Baker Chemical Co.),  $KNO_3$ ,  $HNO_3$ ,  $NaOH$ , and  $CuSO_4 \cdot 5H_2O$  (analytical grade, Anachemical). Potassium ethyl xanthate (KEX, Cyanamid) was purified by dissolving in acetone and re-precipitated by petroleum ether. Xanthate solutions ( $2.5 \cdot 10^{-5}$  M,  $pH = 9.5$  by soda ash) were prepared daily.

### Minerals

Pyrite (Py), galena (Ga), and sphalerite (Sp) samples, from Ward's Natural Science Establishment, were crushed, and hand picked specimens were ground and screened to obtain two size fractions ( $-74 + 38 \mu m$  and  $-212 + 150 \mu m$ ). The samples were washed

in pH = 2 water (HCl) and rinsed with distilled water until pH = 6 to remove oxidation products. The sample was then rinsed twice with acetone and stored under acetone. Prior to use, the samples were dried, weighed and rinsed with distilled water. Chemical analysis showed the minerals were >97% pure compared to their stoichiometric formula.

### *Experimental methods*

#### Single galena

For each test 1 g galena (– 74 + 38  $\mu\text{m}$ ) was immersed in 200 ml distilled water or dithionite solution and shaken on an orbital shaker at 200 rpm for 60 min. The pulp was filtered, the solution analysed to determine the amount of ion species released into the aqueous phase, and the solids were treated with EDTA, xanthate, or dried in air for XPS analysis.

#### Mixture of pyrite, sphalerite, and galena

In the three mineral mixtures, different particle sizes were used. Sphalerite was fine (–74 + 38  $\mu\text{m}$ ), and other two were coarse (– 212 + 150  $\mu\text{m}$ ). Three minerals were mixed at a ratio of 1:5:5 of Sp:Ga:Py and conditioned in the solutions in the same way as for single galena. The pulp was then filtered, the solution analysed, and the sphalerite was screened out and treated with EDTA, xanthate, or dried in air for XPS analysis.

#### Solution preparation

The dithionite solution was prepared by adding 0.05 g of  $\text{Na}_2\text{S}_2\text{O}_4$  in 500 ml distilled water of pH = 9.5 (by soda ash) to obtain  $5.7 \cdot 10^{-4}$  M of dithionite solution. The decreased pH (4÷5) was adjusted to 7.3 by adding soda ash.

#### Potential measurement

The potential was measured with a Ag/AgCl (Pt) electrode and reported against the standard hydrogen electrode (SHE). The electrode was checked by a standard Fe(II)/Fe(III) solution before being used.

#### Determination of Pb ion production using EDTA

EDTA treatment involved contacting 50 ml of 0.05 M EDTA solution (pH = 6÷7) with the mineral sample for 30 min. The extract was analysed (by AA) to measure the amount of Pb ion extracted. This is taken as a measure of Pb ions present on the surface. Repeat tests showed an error of 4.5% at 95% confidence interval.

#### Determination of xanthate adsorption by UV

A Milton Roy Spectronic 1201 UV-Visible spectrometer was used to analyse xanthate concentration in solution. The area under the characteristic xanthate peak at 301 nm was used to obtain the xanthate concentration using an external standard calibration curve obtained from KEX solutions prepared daily. The amount of xanthate adsorbed was calculated from the initial and residual xanthate concentration and expressed as mole xanthate adsorbed per gram mineral (mole/g). Repeat tests showed an error of 2.4% at 95% confidence interval.

#### Surface analysis by XPS

Spectra were recorded using an ESCALAB 220i-XL spectrometer with an  $\text{AlK}\alpha$  anode ( $h\nu = 1486.6$  eV) at a normal take off angle and a band-pass energy of 50 eV

corresponding to an energy resolution of 0.1 eV. The x-ray was monochromated and the instrument was calibrated against the  $Ag_{3d5/2}$  Fermi edge. The sample was prepared by pressing the powders onto a foil of adhesive-backed copper tape and surrounding with a stainless steel washer (for charge removal). The samples were maintained under the instrumental background pressure ( $10^{-9}$  mmHg) for about half-hour in the sample chamber before spectra acquisition. The charge compensation was adjusted on each sample in order to obtain the maximum signal possible. An initial survey of the surface was made to determine the elements present, then the regions of interest were scanned to measure atomic concentrations. The atomic concentrations were determined from the relative peak areas knowing the sensitivity factor and are expressed as a percentage of all elements scanned. The peak areas were obtained using XPSPEAK95 v 3.1, XPS peak fitting program (Kwok, 1997). The XPS spectra were charge shifted according to the C1s peak at 284.8 eV (Briggs and Seah, 1990) before peak fitting was performed.

## Results and discussion

### *Solution potential*

The potential was measured before mineral particles were added (initial) and after 1 h conditioning (end) (Table I). Addition of sodium dithionite significantly decreased the potential to  $-230$  mV/SHE, i.e., the mineral was conditioned in a strongly reducing environment. At the end of 1 h conditioning, the potential recovered, especially for the mixture of three minerals because the presence of pyrite accelerated oxidation processes.

Table I: Potential of the solutions (mV/SHE).

	In water		In dithionite solution	
	Initial	End	Initial	End
Ga	380	368	-230	304
Sp/Ga/Py	380	383	-230	340

### *Pb ion production*

Total Pb concentration was lower in dithionite compared to conditioning in water (Figure 1).

This is attributed to the strong reducing environment ( $-230$  mV) suppressing oxidation of galena, and thus, fewer Pb ions were generated.

Lead ion concentration on the surface of galena, however, was higher in dithionite than in water with virtually no Pb being detected in solution.

It is speculated that the Pb ions released from galena reacted immediately with  $SO_3^{2-}$  ions to form insoluble lead sulphite ( $PbSO_3$ ) and sulphate ( $PbSO_4$ ):



As a result of the decrease in Pb ion production, Pb concentration on the surface of sphalerite decreased by 35%, and total Pb (= on sphalerite surface + in solution) decreased by 60% (Figure 1).

Clearly the suppressed galena oxidation and probably formation of insoluble  $PbSO_3$  and  $PbSO_4$  decreased Pb ion production and prevented Pb ions from migrating to sphalerite.

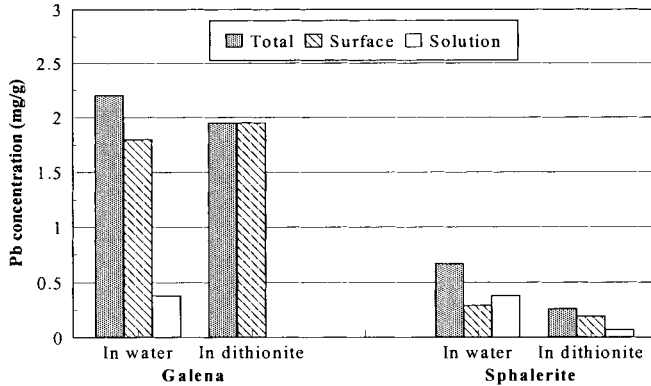


Figure 1: The Pb concentrations in solution and on the surface of minerals (by EDTA extraction). (For sphalerite, Total = on the sphalerite surface + in the solution, Pb on pyrite and galena was not measured).

### XPS analysis

#### Galena

The EDTA results were confirmed by XPS analysis as shown in Table II. The atomic concentration of Pb ([AT]%) on the galena surface was 19% and 20% corresponding to the 1.80 mg/g and 1.95 mg/g from EDTA extraction when conditioned in water and dithionite solution, respectively.

Table II: The atomic concentration [AT] of elements on the surface of galena.

Element	Binding energy (eV)	[AT] (%)	
		in water	in dithionite solution
Lead (Pb4f)	137.2+142.2	17.0	16.9
	139.1+143.9	1.9	3.0
	Total	18.9	20.0
Sulphur (S2p)	160.6+161.8 ( $S^{2-}$ )	18.5	16.9
	164.6+164.8 ( $S^0$ )	8.0	4.1
	167.4+167.5 ( $SO_3^{2-}$ )	0	1.9
	Total	26.5	22.9
Oxygen (O1s)	531.2+531.6	20.1	19.9
Carbon (C1s)	284.6	34.4	32.0

The doublet at 142.2 eV and 137.4 eV on the lead (Pb4f) spectra (Figure 2a) is assigned to Pb in sulphide. The shoulders on the high binding energy side of these two peaks at 143.9 eV and 139.1 eV were observed when galena was conditioned in dithionite solution. The two shoulders may result from PbO, Pb(OH)<sub>2</sub>, PbCO<sub>3</sub>, PbSO<sub>3</sub>, PbS<sub>2</sub>O<sub>3</sub>, and PbSO<sub>4</sub> (Fornasiero, et. al., 1994), among which PbSO<sub>3</sub> was the important contributor according to the sulphur spectrum (Figure 2b). The doublet at 161.8 eV and 160.6 eV on the sulphur (S2p) spectra (Figure 2b) is assigned to sulphide ( $S^{2-}$ ) from PbS. The peak at 164.8 eV is assigned to elemental sulphur ( $S^0$ ), and the peak at 167.5 eV to sulphite ( $SO_3^{2-}$ ). The sulphite peak was detected only when galena was conditioned in dithionite solution. On the carbon spectra (C1s) the additional peak at 286.4 eV was observed when



galena was conditioned in water only (Figure 2c). This peak may be assigned to carbon from carbonate ( $\text{CO}_3^{2-}$ ), corresponding to the peak at 533.0 eV on the oxygen (O1s) spectra (Figure 2d). Other lead species containing oxygen, such as  $\text{PbO}$  and  $\text{Pb}(\text{OH})_2$  were also probable contributors to oxygen peak at 531.2 eV.

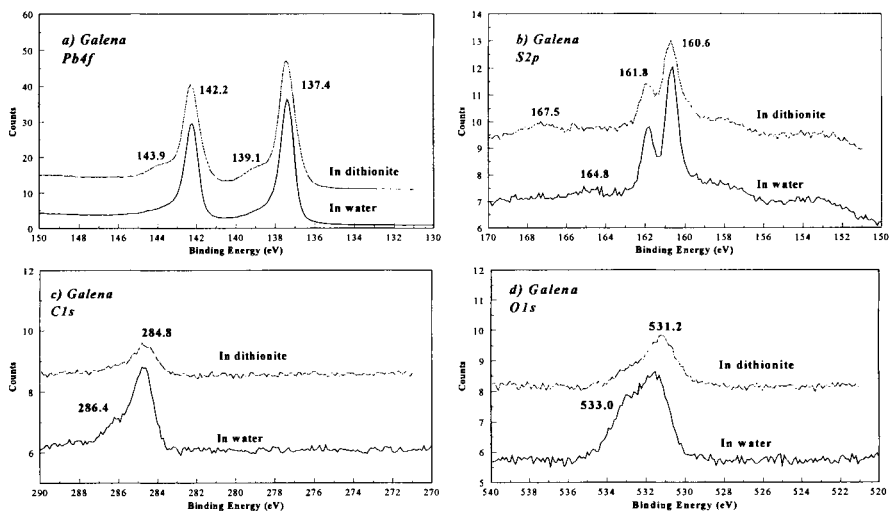


Figure 2: XPS spectra of galena treated with water or dithionite solution.

XPS analysis suggests that  $\text{Pb}(\text{OH})_2$ ,  $\text{PbO}$ , and  $\text{PbCO}_3$  are the main species on the surface of galena conditioned in water while  $\text{Pb}(\text{OH})_2$ ,  $\text{PbO}$ , and  $\text{PbSO}_3$  are the dominant species in the presence of dithionite. The contribution of these species to the total surface species depends on the conditioning solution. It should be recalled that XPS is an ex-situ analytical technique, therefore, the soluble species adsorbed on the surface of galena (i.e.,  $\text{Pb}^{2+}$ ,  $\text{PbOH}^+$ , and soluble lead sulphony species) are not retained and detected with this method.

### Sphalerite

Two peaks at 139.1 eV and 143.4 eV were observed on the lead ( $\text{Pb}4f$ ) spectra, similar to the peaks found on the surface of galena (Figure 3a).

The peak at 139.1 eV is composed of  $\text{Zn}3s_{1/2}$  (139 eV) and  $\text{Pb}4f_{7/2}$  (137 eV) due to their overlap. Such overlap was considered when atomic concentrations were calculated for sphalerite. XPS analysis supports the results of EDTA measurements (Table III).

The atomic concentration of Pb was 1.5% and 0.6% corresponding to 0.29 mg/g and 0.19 mg/g of EDTA extracted Pb on the surface of sphalerite in water and dithionite solution, respectively. The doublet at 161.3 eV and 162.5 eV on the sulphur spectra (Figure 3b) was similar to that from galena (Figure 2b) and is attributed to the sulphide ( $\text{S}^{2-}$ ) of sphalerite. No peaks assignable to sulphite were detected on sphalerite. This suggests that there was no  $\text{PbSO}_3$  formed on sphalerite, and  $\text{Pb}(\text{OH})_2$  and  $\text{PbO}$  are probably the main contributors to these lead peaks since there were no noticeable changes in the sulphur,

carbon, oxygen, and zinc (Zn2p) spectra of sphalerite when minerals were conditioned in water or in dithionite solution (Figure 3c-e).

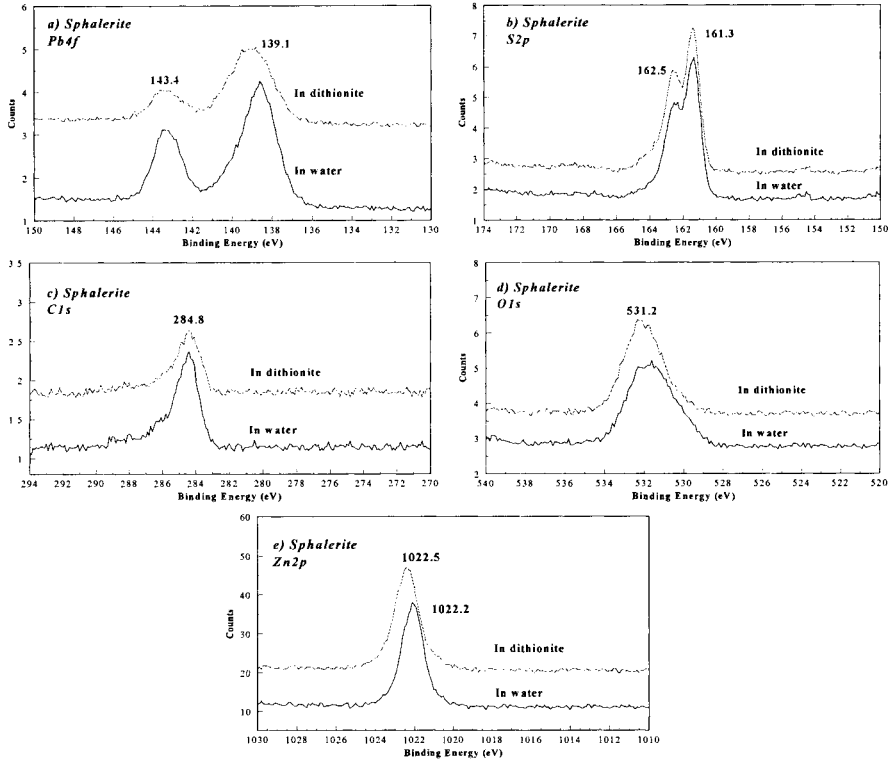


Figure 3: XPS spectra of sphalerite (from mixture with pyrite and galena) treated with water or dithionite solution.

Table III: Atomic concentration [AT] of elements on the surface of sphalerite (from Sp+Ga+Py mixture).

Element	Binding energy (eV)	[AT] (%)	
		In water	In dithionite solution
Zinc (Zn3s, Zn2p)	139.1, 1022.2	18.6	23.3
Lead (Pb4f)	139.1, 143.4	1.5	0.6
Sulphur (S2p)	161.3+162.5 (S <sup>2-</sup> )	24.4	27.2
Oxygen (O1s)	532.3	28.2	30.6
Carbon (C1s)	284.6	27.3	18.3

*Xanthate adsorption*

For single galena, xanthate adsorption was not proportional to Pb concentration on the surface (Table IV). This is attributed to formation of insoluble PbSO<sub>3</sub> (Pattison, 1983).

However, xanthate adsorption did increase with the amount of Pb on the sphalerite surface because the main Pb species were oxy/hydroxyl species that can react with xanthate.

Table IV: Xanthate adsorption on the surface of minerals.

Mineral	Galena		Sphalerite/(Sp+Ga+Py)	
	in water	in dithionite	in water	in dithionite
EDTA extracted Pb (mg/g)	1.80	1.95	0.29	0.19
Xanthate adsorption ( $\times 10^{-7}$ mole/g)	5.8	3.8	2.3	1.6

The results suggest that the suppressed galena oxidation and formation of  $\text{PbSO}_3$  precipitates significantly reduce Pb ion production and migration to sphalerite, and thus, reduce accidental activation of sphalerite. However, insoluble  $\text{PbSO}_3$  forming on the surface of galena may decrease floatability of galena. Therefore, the dosage of reducing reagent used should be controlled at a level at which the pulp potential is sufficiently low to suppress oxidation of galena, but minimises depression of galena through formation of  $\text{PbSO}_3$ . Batch flotation tests on the ores from BMS and Heath Steele proved that a "window of opportunity" existed where accidental activation of sphalerite was controlled while galena recovery was maintained (Kim et al., 1997).

## Conclusions

Addition of dithionite significantly decreased pulp potential, leading to suppression of galena oxidation and reduced Pb concentration in the solution and on the surface of sphalerite.

In dithionite, lead sulphite formed on galena and was considered the cause of the decrease in xanthate adsorption observed.

No lead sulphite was detected on the surface of sphalerite. Xanthate adsorption was proportional to the EDTA extractable Pb. This suggests that the dominant Pb species on sphalerite were oxy/hydroxides, which react with xanthate.

EDTA and XPS measurements proved to be complementary.

## References

- Briggs, D. and Seah, M.P., 1990. Practical Surface Analysis. 2<sup>nd</sup> Ed., Vol.1, Auger and X-ray Photoelectron Spectroscopy, Wiley, New York.
- Fornasiero, D., Li, F., Ralston, J. and Smart, R., 1994. Oxidation of galena surfaces, I. X-ray photoelectron spectroscopic and dissolution kinetics studies. *J. Colloid and Interface Science*, Vol.164, 333-344.
- Kim, J., Lajoie, S. and Nessel, J.A., 1997. Internal report. Noranda Technology Centre, Quebec, Canada.
- Kwok, R.W.M., 1997. XPSPEAK95 v 3.1, Dept Chemistry, The Chinese University of Hong Kong.
- Pattison, I.G., 1983. The Aus. IMM Conference, Broken Hill, 399.
- Smart, R.St.C., 1991. Surface layer in base metal sulphide flotation. *Minerals Engineering*, Vol.4, 891-909.
- Sui, C., Finch, J.A., Kim, J. and Nessel, J.A., 1997. Galena oxidation products and floatability. *Processing of Complex Ores*, Editors, J.A. Finch, S.R. Rao and I. Holubec, 133-142.
- Sui, C., Grimmelt, J.C., Rao, S.R. and Finch, J.A., 1999. Lead ion production: Test of pyrite/galena ratio and locked particle effect. Accepted by Canadian Metallurgical Quarterly.

## COLLECTOR PROPERTIES OF NEW FLOTATION REAGENT Z-96

Z.S.Markovic\*, R.Stanojlovic\*, G.Milenkovic°, Z.Petkovic°

\*University of Belgrade, Technical Faculty Bor, VJ 12, 19210 Bor, Yugoslavia

°Chemical Industry "ZUPA" -Krusevac, 37000 Krusevac, Yugoslavia

### Abstract

Some electrochemical and flotation properties of brand new flotation reagent Z-96 were presented in this paper. A mixture of Z-96/PEX (potassium ethylxanthate) in the ratio of 30/70 gives the best results in flotation experiments. All investigations were carried out on copper ore "V. Krivelj" from Yugoslavia. Presented results show good corrosion inhibition properties of reagent Z-96 in the grinding stage, as well as good collector properties of the mixture Z-96/PEX in the flotation of copper minerals. With the addition of Z-96, ball wearing was decreased for 32.2% in laboratory tests to 10.33% in full industrial test. With the mixture Z-96/PEX as a collector for copper minerals, copper recovery was increased by about 2% in both the laboratory and full industrial tests. Also, laboratory flotation tests presented better hydrodynamics effects with the Z-96/PEX mixture as a collector, compared to that with PEX itself as a collector.

*Keywords: reagent Z-96, inhibitor of corrosion, copper ore, collector, flotation, hydrodynamic*

### Introduction

In a joint venture, the Mineral Processing Department of the Technical Faculty of Bor and the "ZUPA" Chemical Industry of Krusevac, Yugoslavia have made a brand new flotation reagent under the working title "Z-96". The name of reagent Z-96, its characteristics as well as technologies for its applications are still subjected to patent's procedures. Reagent Z-96 presents a chemical combination between a kind of xanthate collector and a corrosion inhibition chemical compound. It is available in liquid form. For the industrial scale experiments about 30 t of this reagent has been produced. Reagent Z-96 was proposed as an inhibitor of corrosion in the grinding process and partly substitutes PEX in the flotation process. The reagent Z-96 has strong corrosion inhibition properties with unsatisfying collector properties in the flotation of copper minerals. In order to improve collector properties with addition of Z-96, some investigations were carried out in a mixture of Z-96/PEX collectors in various ratios. The ratio of 30/70 of Z-96/PEX was chosen as most suitable when the flotation recovery of copper increased by about 2%. Investigations were conducted under laboratory conditions on various copper ores from Yugoslavia, and under full industrial conditions on the Yugoslavian copper ore "V. Krivelj". This paper deals only with results for copper ore "V. Krivelj" because of better understanding with this problem, but similar results were obtained on other copper ores. The effect of reagent Z-96 on the hydrodynamics conditions in flotation cells has been tested in the laboratory and those experiments are still in progress. Preliminary results show that as a collector, the mixture Z-96/PEX spreads regions of air consumption in flotation

cells, and at various rotor speeds, compared to those obtained only with PEX. Introducing Z-96 in the grinding stage caused a decrease in steel consumption by inhibition of corrosion, from 32.2% to 10.33%, as the mixture Z-96/PEX has better collector properties and causes an increase in copper recovery, from 1.5% up to 2%. These effects are also not to be ignored as they present an important role in operating costs and economical processing of copper ore (Stanojlovic, et al. 1999).

## Experimental

This paper presents experimental results obtained on the porphyry copper ore "V. Krivelj". The main copper sulfide mineral in this ore is chalcopyrite. However there is a small amount of chalcocite while the major sulfide mineral is pyrite. Copper content in the ore body is about 0.36% and sulfur content is less than 3%.

All conducted experiments have had a two-fold task:

- identifying corrosion inhibition properties and quantifying corrosion effects in the ore grinding stage, in the presence of reagent Z-96, both under laboratory and full plant conditions;
- identifying and quantifying effects such as collector properties and some hydrodynamics effects caused during the flotation stage in the presence of reagent Z-96, which is in the form of a mixture of Z-96/PEX, under laboratory and full plant conditions.

### *Corrosion inhibition property*

These kinds of experiments were carried out in the laboratory under static and dynamic conditions and under full dynamic plant conditions. The static laboratory experiments were conducted on a single grinding steel ball in water solutions of reagent Z-96 in various concentrations. Figure 1 presents the potentiometric titration curve with relative corrosion speed plotted against the concentration of Z-96 in a water solution

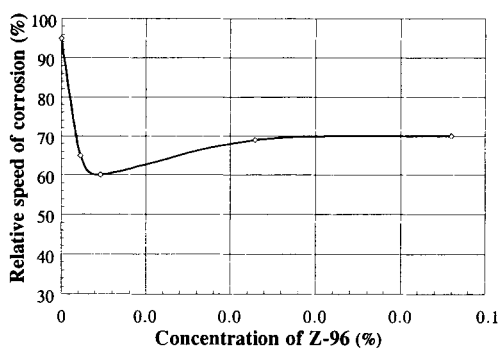


Figure 1: Relative corrosion speed of steel ball vs. concentration of Z-96, at pH = 10.

The relative speed of corrosion rapidly drops with an increase in the concentration of Z-96 to 0.01% and then slightly increases as the reagent concentration increases. The best corrosion inhibition effect can be seen at a low concentration of Z-96, at about 0.01% in water solution, when the relative corrosion speed reaches a value near 40%.

After such initial experiments, the laboratory batch wet grinding experiments were performed on the "V. Krivelj" copper ore. These experiments were done in a wet laboratory steel ball mill in two parallel series, one without Z-96 and another with Z-96. The ball charge was measured after a certain number of batch grinding cycles and results were compared, as given in Table I. The steel balls' savings, less wearing in the environment of reagent Z-96, compared to results obtained without this reagent, reach the level of 32.20%. It is in accordance with the results obtained by potentiometric titration. Each single batch grinding test was performed under constant conditions (1 kg copper ore under a 3.3 mm grain size, pH = 10 adjusted with lime, 75% solid contents, 20 min grinding time). Only the reagent Z-96 was changed. The laboratory results presented in Table I refer to concentration of Z-96 at 15 g/t of feed ore. With these encouraging results, a full industrial test was proposed at the industrial flotation plant "V. Krivelj" for the same copper ore. One of the mill sections was operated with reagent Z-96, which was introduced in a wet steel ball mill. Another two sections were operated without this reagent. Each mill section processed about 500 t/h copper ore. Comparing results obtained among mill sections less ball wearing was found for the section where the grinding had been performed in the Z-96 environment. In Table I, results of ball wearing (savings) for period of 15 days and for period of 70 days' continuous plant operation were presented. The period of 70 days was chosen to present the whole ball charge replacement in the ball mill. The obtained results were expected, in spite of sever winter conditions, which caused a standstill in operation at times.

Table I: Steel grinding balls' savings (%) with Z-96.

Test	Ball savings (%)
Laboratory test	32.20
Industrial test (after 15 days)	14.30
Industrial test (after 70 days)	10.33

#### *Laboratory flotation tests*

Laboratory batch flotation tests were carried out at the same time as the laboratory grinding tests, in order to determine copper flotation behavior with reagent Z-96. The primary goal, of introducing this reagent as an inhibitor of corrosion in the grinding stage was finding such conditions when it could not disturb the flotation process of certain minerals. For that reason, many flotation tests were carried out under various pulp and reagent conditions to find certain collector properties of Z-96 for sulfide copper minerals. All flotation tests were performed on a Denver DR12 laboratory batch flotation machine in a cell volume of 1.4l, in an alkali pulp pH (from 8.5 up to 11.8) adjusted by lime, in various reagent concentrations in pulp at various ratios. Laboratory batch flotation tests were done on several types of domestic copper ores, and the results were similar. Here results related to the copper ore "V. Krivelj" were presented. In Figure 2 a group of flotation results was presented for a mixture of PEX a Z-96 collectors used in all ratios at two chosen pH values. With a 60% <0.074 mm particle size for solids in the pulp, a constant concentration of collectors (PEX+Z-96) of 40 g/t of solids, frother Dowfroth 250 10 g/t of solids and flotation time of 15 min the following can be concluded:

- as single collectors, neither PEX nor Z-96, gave satisfactory results for both pH regions;
- the mixture of Z-96/PEX in the ratio of 30/70 as collector, gives the best results as a collector, with higher flotation recovery of copper minerals.

This mixture ratio was tested in flotation under many different conditions and was thus adopted as the best suitable ratio, with the best collector properties regarding single collectors. Such improved collector properties of PEX with the addition of Z-96, as well as the corrosion inhibitor property of Z-96 alone, warranted further investigations with full industrial tests under plant conditions.

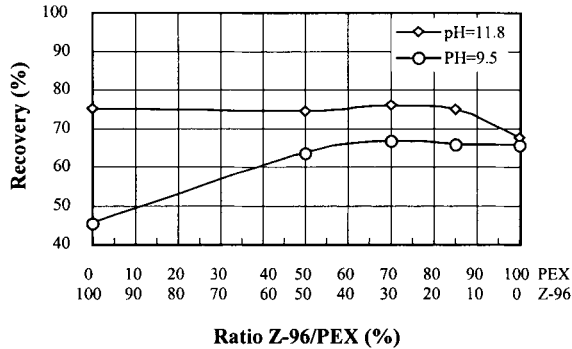


Figure 2: Effect of collector ratio (PEX/Z-96) on flotation recovery.

#### *Industrial flotation tests*

The industrial grinding tests were previously described. Simultaneous with the industrial grinding tests on the "V. Krivelj" flotation plant, flotation constantly observed. Such observations of the flotation process during the grinding tests had the primary goal of not allowing experiments with Z-96 to cause any kind of disturbance of certain processes. If the flotation process had gone wrong, the experiments would have been stopped. However, the flotation results were little better than ordinary results during the grinding experiments.

After the grinding experiments, an extra period of time was devoted to the flotation process. During this period, the collector properties of reagent Z-96 were fully examined and the ratio Z-96/PEX at 30/70 was once again proven as the best suitable ratio of the collectors. Obtained results with such a mixture of collectors were compared to those obtained by applying PEX alone. The increase in copper flotation recovery was up from 1.5% to 1.8%, with a mixture Z-96/PEX (30/70), was found under all conditions investigated. Aside from copper flotation recovery, the other parameters (Table II) were controlled during this investigation, such as: ore grindability (Bond work index), particle size, pulp density, pH of pulp, reagents' regimes, and copper content. Table II gives summary values of controlled parameters in flotation, which were maintained within quoted limits.

#### *Hydrodynamics tests*

These kinds of experiments are still in progress. Besides collector efficiency, hydrodynamics conditions in flotation cells greatly affect flotation results. These investigations were proposed for determination of other characteristics of reagent Z-

96, which were indicated in previous experiments. The hydrodynamics tests are performed only under laboratory conditions, and some results were presented here. Presented results were obtained on the "V. Krivelj" copper ore, comparing hydrodynamics effects of the collector mixture Z-96/PEX (30/70) and of PEX alone in a Denver laboratory flotation cell, as described above in the section "Laboratory flotation tests". The new variable parameters were rotor speed and introduction of air.

Table II: Controlled parameters in flotation

Bond Work index		13.42÷14.87 kW/t
Particle-size	Feed	58÷63% <0.074 mm
	Concentrate	68÷74% <0.074 mm
	Tailings	54÷58% <0.074 mm
Pulp density	Feed	1.200÷1.240 g/cm <sup>3</sup>
	Tailings	1.200÷1.230 g/cm <sup>3</sup>
pH		9.5÷10.0
Collector Z-96/PEX (30/70)		35÷40 g/t
Collector PEX (alone)		35÷40 g/t
Frother Dowfroth 250		5÷10 g/t
Copper contents in feed		0.38÷0.42% Cu
Cu-Recovery increase Z-96/PEX		1.5÷1.8%

The particle size of solids was 60% <0.074 mm in all experiments, collectors = 40 g/t, frother Dowfroth-250 = 20 g/t, pH = 10.5 and flotation time = 21 min. Obtained results were presented in Figures 3 and 4. Figure 3 presents the dependence of copper flotation recovery on variations of rotor speed, with a constant air-flow rate of 300 l/min, for both PEX collectors and for the mixture Z-96/PEX. One can see that the optimal rotor speed for both collectors is 1,200 rpm, but collector mixture Z-96/PEX gives slightly higher recovery and a wider region of rotor speed, and thus offers better conditions when such optimization is needed.

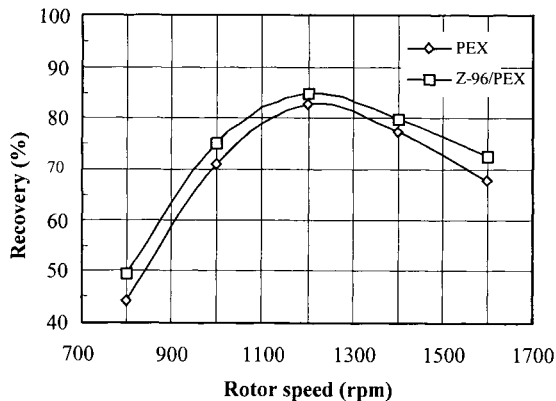


Figure 3: Effect of rotor speed on copper flotation recovery

Figure 4 presents the dependence of copper flotation recovery for variations in airflow rate, with a constant rotor speed of 1,200 rpm, for both collectors PEX and the mixture of Z-96/PEX. Also, it can be seen that the optimal air flow rate is 300 l/min, for both collectors, but the collector mixture Z-96/PEX gives a slightly higher



recovery and a wider region of air flow rate variations. Thus, this offers better conditions when such optimization is needed. In the extreme conditions of airflow rate, on flotation recovery, the collector mixture Z-96/PEX is less sensitive, comparing to the collector PEX alone. Both cases presented may have great importance in industrial practice where flotation cells operate non-uniformly due to the wearing of their working parts. Here the collector mixture Z-96/PEX can act as a buffer of the air supply.

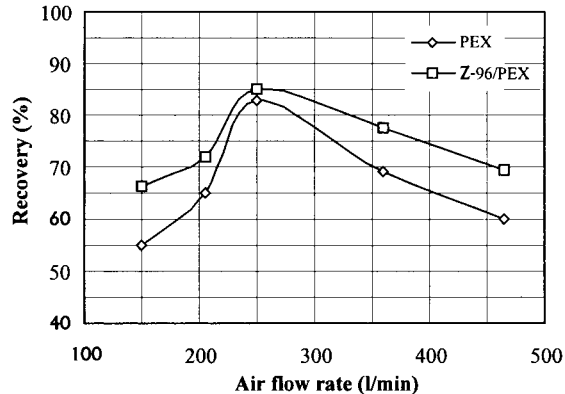


Figure 4: Effect of air flow rate on copper flotation recovery.

## Conclusions

According to the presented results, some conclusions can be made, as follow:

- the new reagent Z-96 has strong corrosion inhibition properties, which cause less wearing of the steel grinding media in the wet grinding processes: thus the savings of steel can be from 32.2% under laboratory conditions to 10.33% under full plant conditions;
- reagent Z-96 used alone has unsatisfied collector properties for copper minerals, but its mixture with PEX in the ratio of 30/70 gives better results for flotation as a referent collector compared to PEX alone: increases from 1.5 to 1.8% of copper recovery were observed in both laboratory and plant experiments;
- overall, reagent Z-96 does not increase the collectors' consumption; the consumption remains the same, but it only substitutes one part of PEX (30%), so the overall collector dosage remains unchanged (35÷40 g/t) from PEX introduced alone: this was proven both in laboratory tests and in industrial tests;
- the presence of Z-96 in the flotation pulp clearly changes the hydrodynamic effects in flotation cells; these results refer to laboratory experiments, but similar ones should be expected in industrial flotation cells; its presence in pulp causes less sensitivity to air flow rate and rotor speed, compared to results when it is absent: So the flotation process becomes more elastic and easier to optimize.

## References

- Stanojlovic, R., Markovic, Z.S., Milenkovic, G. and Petkovic, Z., 1999. New domestic flotation reagent Z-96 as inhibitor of corrosion and collector. Final Proc. VIII Balkan Mineral Processing Conf. Belgrade, Yugoslavia, 265-268.

## BENEFICIATION OF FINE BITUMINOUS COAL BY COLUMN FLOTATION

B. Gürsu\*, C. Hiçyılmaz\*, S. Bilgen<sup>o</sup>

\*Middle East Technical University, Mining Eng. Dept., 06531, Ankara, Turkey

<sup>o</sup>Mersin University, Civil Engineering Department, Mersin, Turkey

### Abstract

The bituminous coal fines (<0.5 mm) of the Zonguldak Central Coal Washery Plant belonging to Turkish Hard Coal Enterprise is burned in power plants. In this research, cleaning of the fines having 47.52% ash was attempted with column flotation. The flotation tests were carried out systematically in a 5×5×200 cm<sup>3</sup> plexiglass column having an internal sparger. Column flotation parameters, such as froth depth, superficial air-flow velocity and frother dosage, were investigated to obtain clean coal suitable for coking. A rougher concentrate having an ash content of 10% and a combustible recovery of 73.52% was obtained. Cleaning of rougher concentrate with and without vibration were also investigated. By this cleaning process, a concentrate containing 5.88% ash was obtained, with a combustible recovery of 59.27%.

*Keywords: column flotation, fine bituminous coal, vibration in flotation*

### Introduction

For many years, froth flotation has been accepted as the most practical and cost-effective method for cleaning fine coal. However, the optimum size of coal particles that can be recovered by conventional flotation (i.e. 100÷300 µm) is more than the grind size required to liberate the finely disseminated mineral matter present in coal (Luttrell et al., 1988). In addition, there are also ultra-fine minerals (i.e. clay) in fine coal, and this causes hydraulic entrainment. Therefore, high ash values are commonly obtained for the products when conventional flotation is used for micronised coal. Nowadays, column flotation is used in order to overcome these disadvantages for the flotation of micronised coal. Hydrodynamic analysis showed that using small air bubbles and a counter-current feeding arrangement increases the particles' bubble-contact efficiency, which improves the recovery of micronised particles. High collection zones also increase opportunities for particle-bubble contact. In addition, wash water is very efficient to prevent hydraulic entrainment, which decrease the ash content of concentrates. In this study, column flotation of bituminous coal fines from the Zonguldak Washery Plant of Turkey was performed by investigating the effect of column flotation parameters (collector dosage, froth depth, superficial air velocity, feeding point, feeding rate, superficial wash-water velocity, frother dosage). A mechanical vibration was also externally applied to the froth zone during the cleaning of the rougher concentrate to improve the purity of coal.

The bituminous coal fines (<0.5 mm) left over in the Zonguldak washery plant are currently sent to the thermal power plant after being mixed with slate. The object of

this research was to achieve a coal product having less than 10% ash content to be utilizable in the coking industry, which can be evaluated much more efficiently.

### Materials, equipments and test procedure

A sample of <0.5 mm coal from the Zonguldak washery was obtained for flotation experiments. As soon as the sample was received, the coal sample was divided into approximately 1,000 g representative lots and placed in plastic bags in order to prevent oxidation. The ash and sulfur content of the coal sample were determined to be 47.52% and 0.37%, respectively. Approximate analyses are given in Table I.

Table I: Approximate analyses of sample.

Approximate Component	Content
H <sub>2</sub> O	2.08%
Volatile matter	16.43%
Fixed carbon	34.24%
Ash	47.52%
Sulfur	0.37 %
Calorific value	4,495.90 (MJ/kg)

Prior to flotation, the coal sample was ground about 80% passing 53  $\mu\text{m}$ . Before feeding the sample to the column, the pH of the pulp was adjusted to 5.5, which was the optimum (Gürsu, 1998). As a collector (1 kg/t unless otherwise noted), Kerosene was conditioned for 10 min, and as a frother, MIBC (514 g/t, unless otherwise noted) was conditioned for 1 min before feeding the slurry to the column.

Flotation experiments were conducted by using a 5×5 cm<sup>2</sup> Plexiglas column made in Mining Engineering Department of METU, with a length of 200 cm. Unless otherwise noted, the following conditions were used throughout the experiments. Wash water (0.05 cm/s) was introduced at a predetermined rate through a distributor located 10 cm above the top of the column. The feed slurry was introduced to the column at a point below almost 60 cm from the top. Bubbles were generated internally by using an air generator and introduced from the bottom of the column. Air-flow velocity (1 cm/s) was controlled by using a flowmeter. Tailing was continuously taken at the bottom of the column. Flowrates of wash water, feed and tailing slurries were controlled by peristaltic pumps. For each experiment, froth depth was kept constant by changing the tailing rate. After a predetermined retention time of 16 min (retention times given were calculated 3 times in order to obtain a balanced system), the concentrate, tailing and feed samples were taken for one minute. The pulp density during flotation was 10% solid by weight.

### Results and discussion

#### *Collector dosage*

In general, collectors are used in small amounts, substantially those necessary to form a monolayer on particle surfaces. When the concentration increases, this tends to float other minerals, and thus the ash content of coal increases. However in column flotation, a higher amount of collector is used since the lower pulp density in

conventional cells. In order to determine the optimum amount of kerosene for Zonguldak bituminous coal fines, it was changed from 0 to 3 kg/t of sample.

As can be seen from Figure 1, without any addition of kerosene, coal particles were also floated, probably due to the natural hydrophobicity of coal and the entrainment of air bubbles within the floc structure. As can be seen, combustible recovery and ash content increase as the collector dosage increases up to 1 kg/t, which was chosen as the optimum dosage. Above this value there is no significant change in combustible recovery while increasing the ash content, because excess kerosene covers the ash minerals with a thin layer of film.

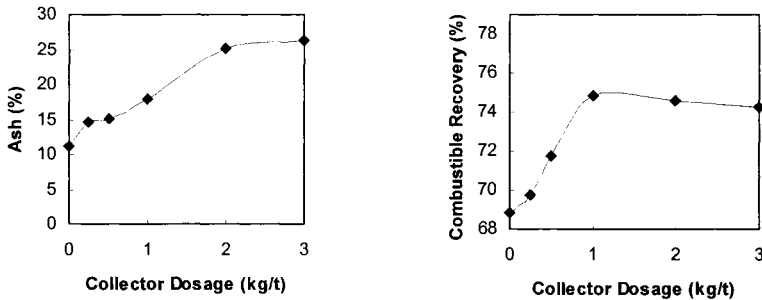


Figure 1: Effect of collector dosage on column flotation of Zonguldak bituminous coal.

#### *Froth depth*

Column froth can show selectivity between particles differing in the hydrophobicity, and this may be related to froth depth. Froth depth was changed from 20 cm to 60 cm in this research. As seen from Figure 2, change in froth depth did not significantly affect the combustible recovery or ash content.

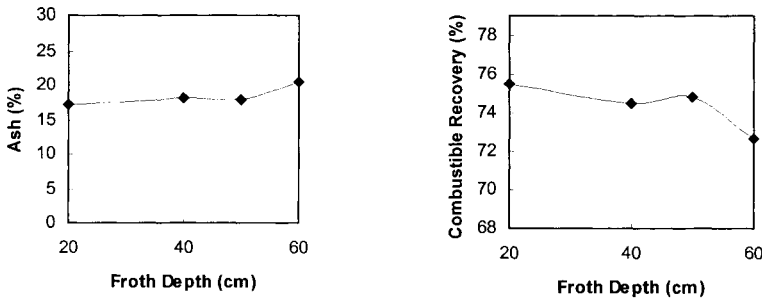


Figure 2: Effect of froth depth on column flotation of Zonguldak coal.

In the literature, in order to obtain low-grade ash, it is recommended that froth depth must be as high as possible. On the other hand, froth depth in industry is from 60÷180 cm (Rubinstein and Badenicov, 1995). However, the froth depth could not be increased more than 60 cm in this column, which was designed so that feeding point and pulp/froth interface close to each other, short-circuiting possible increases. A 50 cm froth depth was chosen as the optimum value for this column. The experiments that follow were performed at this froth depth.

### Superficial air velocity

Air rate is an important parameter, which affects both recovery and grade (Parekh et al., 1988). A series of flotation experiments were done in order to determine optimum airflow rate. It was varied from 0.33 cm/s to 3 cm/s. As seen from Figure 3, combustible recovery and ash content increased with increasing superficial air velocity. There was a sharp increase in ash content above the air velocity of 2 cm/s. There may be two reasons for this situation. One of them is that increasing the number and total surface area of bubbles improves the ash particles' collection. The second reason may be the deterioration of bubble-flow regime to a churn-turbulent flow (Mangiu Xu et al., 1991). A 2 cm/s. superficial air velocity was chosen as the optimum value.

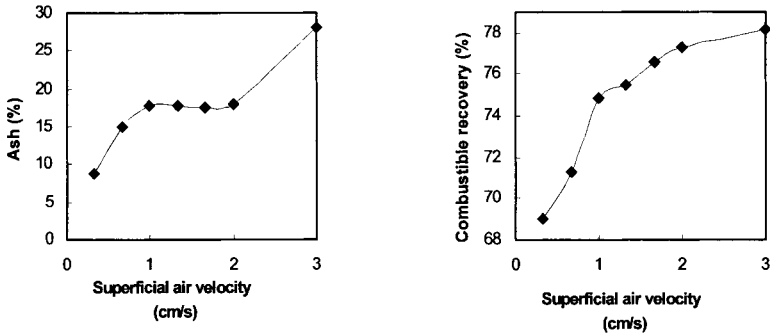


Figure 3: Effect of superficial air velocity on column flotation of Zonguldak coal.

### Feeding Point

Feeding point affect flotation results.

Experiments were conducted with 60 cm, 70 cm and 80 cm feed injection locations from the top of the column. The results are shown in Figure 4. An increase in the ash content and decrease in the combustible recovery have been put in evidence.

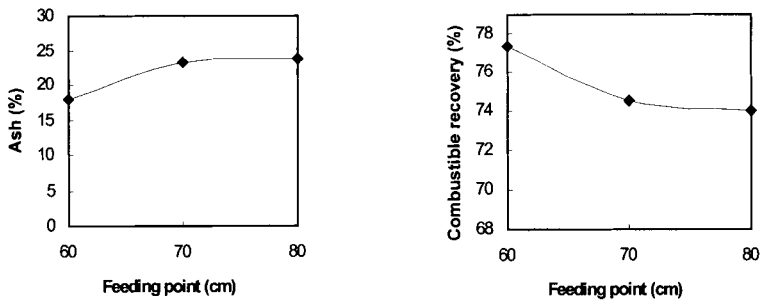


Figure 4: Effect of feeding point on column flotation of Zonguldak coal.

### Feeding rate

Retention time of particles in the column is the main factor that controls both recovery and grade (Parekh et al., 1988). Adequate time must be provided to facilitate

bubble-particle attachment (Narasimhan et al., 1988; Yanchausti et al., 1988). Related retention times were 16 min, 15 min and 14 min, respectively, which were calculated by the formula of:

$$\text{retention time (min)} = \text{volume of the column from bottom to feed injection point (cm}^3\text{)} / \text{feeding rate (cm}^3\text{min}^{-1}\text{)}$$

In the experiments, three different feeding rates were used, and these were 437 cm<sup>3</sup>/min, 655 cm<sup>3</sup>/min and 1,166 cm<sup>3</sup>/min.

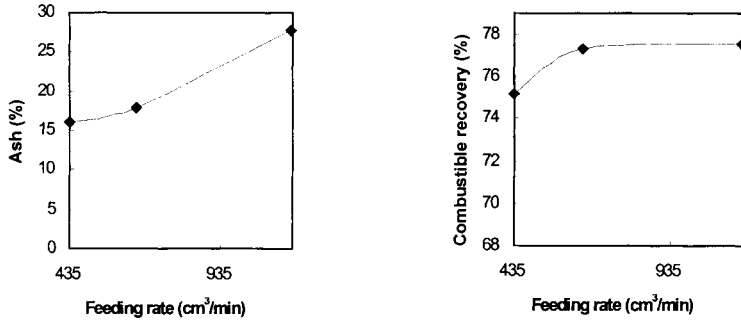


Figure 5: Effect of feeding rate on column flotation of Zonguldak coal.

As seen from Figure 5, low feeding rate (i.e. high retention time) caused the decrease in ash content. The low ash content obtained at high retention time is due to the time spent by coal particles in the froth-washing zone, which helps to remove entrapped impurities from it.

#### *Superficial wash water velocity*

Wash water is used to reduce entrainment and to obtain high-grade concentrates in the column. The froth zone in the column, which is formed by rising the froth bed, is washed counter-currently. Some wash water is taken with the concentrate, whereas the rest, called the bias water, is drained away from the froth stability. The amount of slime entrained in the froth is sensitive to changes in the bias flow caused by varying feed or wash-water flows. In this research, wash-water velocity was varied from 0 to 0.2 cm/s. The results given in Figure 6 show that as the superficial wash-water velocity was increased, combustible recovery and ash content of concentrate decreased. In the case of high superficial wash-water velocity, the positive bias will be high, and wash water will force some coal particles into the collection zone, together with ash minerals.

#### *Frother dosage*

The dosage of the frother, namely MIBC, was varied from 42.85 g/t to 771.3 g/t. As seen in Figure 7, as the frother dosage increased, ash content increased. There were two reasons for this, which were related to bubble size. One was that bubble size, and thus the rising velocity, decreased with an increase in frother dosage, so gas held in the collection zone increased. This resulted in an increase in ash content. The second reason was that the bubble surface area increased with reducing bubble size, and water penetration into the froth layer increased, which again increased ash content.

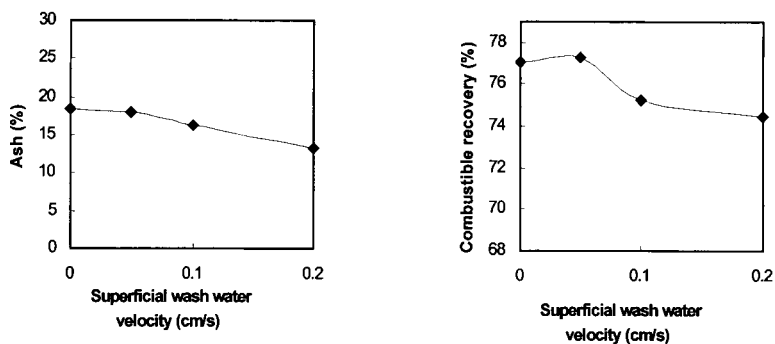


Figure 6: Effect of superficial wash water velocity on column flotation of Zonguldak coal.

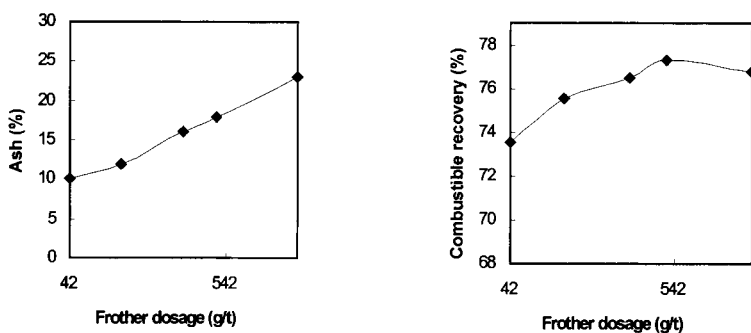


Figure 7: Effect of frother dosage on column flotation of Zonguldak coal.

#### *Cleaning of rougher concentrate*

The effect of vibration was also tested by cleaning of a rougher concentrate. A vibration mechanism was installed externally at the level of the froth zone of the column. The cleaned concentrate was taken with and without vibration.

Table II: Cleaning of a rougher concentrate of Zonguldak coal.

Type	Ash (%)	Combustible recovery (%)
Without vibration	6.03	59.27
With vibration	5.88	52.77

Table II shows the effect of vibration. It decreased the ash content, as well as combustible recovery, due to causing a drop in ash minerals as well as coal fines from the froth.

#### **Conclusions**

It can be concluded that under optimum conditions (kerosene = 1 kg/t, froth depth = 50 cm, superficial air velocity = 2 cm/s, Feeding point = 60 cm,

feeding rate =  $655 \text{ cm}^3/\text{s}$ , superficial wash water velocity =  $0.05 \text{ cm/s}$ , frother dosage =  $205 \text{ g/t}$ , a concentrate produced with a combustible recovery of 73.52% contained 10% ash. After single-stage cleaning, the ash content of the concentrate was reduced to around 6%, with 59% combustible recovery.

However, it can also be seen that a concentrate having 8.68% ash, with 69% combustible recovery, was also possible by lowering the superficial air velocity to  $0.33 \text{ cm/s}$ .

### References

- Gürsu, B., 1998. Column flotation of Zonguldak washery of fine coal. M.Sc. Thesis of METU.
- Luttrell, A.T., Weber, G.T. and Yoon, R.H., 1988. Microbubble Flotation of Fine Coal. In: Column Flotation 88, K.V.S. Sastry (Editor), 205-210.
- Mangiu Xu, Finch, J.A. and Uribe-Salas, A., 1991. Maximum gas and bubble-surface rates in flotation columns. *International Journal of Mineral Processing*, 32, 233-250.
- Narasimhan, K.S., Singh, R.N., Bhatia, R.T. and Madhsudhanan, K.P., 1988. Column Flotation for Fine Coal Recovery in India (A Techno-Economic Assessment). In: Column Flotation 88, K.V.S. Sastry (Editor), 243-247.
- Parekh, B.K., Groppo, J.G., Stotts, W.F. and Bland, A.E., 1988. Recovery of Fine Coal from Preparation of Plant Refuse Using Column Flotation. In: Column Flotation 88, K.V.S. Sastry (Editor), 227-233.
- Rubinstein, J. and Badenicov, V., 1995. New aspects in the theory and practice of column flotation. *Proc. of XIX Mineral Processing Congress, San Francisco*, 23-25 October, 113-116.
- Yanchausti, A., McKay, J.D. and Food, Jr., D.G., 1988. Column Flotation Parameters - Their effects. In: Column Flotation 88, K.V.S. Sastry (Editor), 157-172.



## STUDIES OF SURFACE AND SORPTION BEHAVIOUR OF SALINE AND CLAY CARBONATE MINERALS IN ELECTROLYTES

S. Titkov, N. Panteleeva, A. Chistyakov, L. Pimkina, I. Mikhaylova

Research and Development Institute of Halurgy, St. Petersburg, Russia  
"Uralkaliy" Joint-Stock Company, Berezniki, Russia

### Abstract

Separation of water-soluble minerals by flotation is the most important present-day method of potash ore processing. It has currently come into use in the production of carnallite, that is, the raw material for the production of metallic magnesium and various fertilizers. The paper describes studies on the influence of both hydration of surfaces of alkaline halogenide crystals and that of changes in morphology of sylvite surface in saline solutions having different compositions on cationic collector sorption at saline minerals. The paper also considers the effect of cationic collector composition on the efficiency of clay-carbonate slimes protection by reagents-depressors and on floatability of sylvite and halite at different temperatures and compositions of electrolyte solutions. As a result of work, it has been suggested the optimal compositions of reagents-collectors for the separation of water-soluble minerals by flotation.

*Keywords: flotation, sorption, saline minerals, cationic surfactants*

### Introduction

Since flotation of water-soluble minerals is performed in saturated saline solutions ( $\text{KCl-NaCl-H}_2\text{O}$ ,  $\text{KCl-NaCl-MgCl}_2\text{-H}_2\text{O}$ ), colloid-chemical properties of reagents, as well as in sorption and crystal-chemical properties of particle surfaces of minerals subject to separation, undergo certain changes in accordance with compositions and temperatures of the saline solutions.

Sylvite ( $\text{KCl}$ ) flotation by monoaliphatic amines is a well-studied process. It is known that this process may be successfully performed at normal temperature by using hexadecylamine as a collector (Schubert, 1967; Alexandrovich, 1973; Titkov et al., 1982). If the saline solution temperature increases from  $18\div 20$  °C to  $30\div 37$  °C (in summer or under deep ore mining), as well as if  $\text{MgCl}_2$  content in the solution increases (in case if the sylvinitic ore under processing contains carnallite), hydration of sylvite crystal surfaces increases, the contact angle decreases (Figure 1), and sylvite floatability decreases (Titkov et al., 1985). In addition, an increase in amine sorption at clay-carbonate slimes and weakening of hindering the amine sorption at slimes by reagents-depressors take place, which also leads to degradation of sylvite floatability (Titkov et al., 1982).

Recently, flotation of water-soluble minerals with the use of aliphatic alkylmorpholines as cationic collectors came into use for halite recovery from a mixture containing carnallite (mixture of pure salts crystallized in evaporative ponds during the processing of the Dead Sea brine) (Amira and Darius, 1991). Research is

now underway towards the development of a method of processing carnallite ores by flotation in order to obtain carnallite ( $KCl \cdot MgCl_2 \cdot 6H_2O$ ) as a cell product of halite flotation. Carnallite is a raw material for production of metallic magnesium and various fertilizers (Titkov et al., 1997; Sabirov and Titkov, 1997). The unavailability of data for effect of alkylmorpholine composition on halite floatability hinders the development of this flotation method.

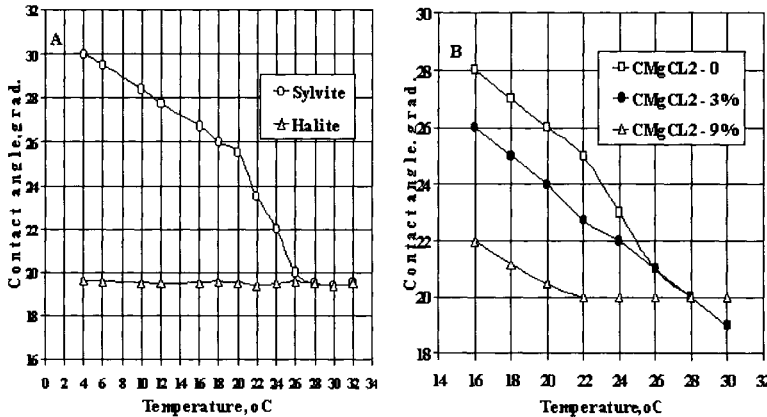


Figure 1: Effect of temperature and  $MgCl_2$  concentration in the saline solution ( $KCl-NaCl-H_2O$ ) on hydrophilicity of sylvite and halite surfaces (Titkov et al., 1985).

The paper presents the results of studying the effect of temperature and composition of saturated saline solutions on sorption and flotation behavior of alkylamines and alkylmorpholines. The properties of saline mineral surfaces as a function of electrolyte solution composition are also considered.

**Experiment**

The morphology of  $KCl$  and  $NaCl$  crystals was studied using a micro-crystallization cell. The temperature was increased and decreased by  $1\text{ }^\circ\text{C}$  or  $2\text{ }^\circ\text{C}$ . The accuracy of saturation temperature for each substance was  $\pm 0.1\text{ }^\circ\text{C}$ . The amounts of amine and alkylmorpholine at saline minerals and clay-carbonate slimes of potash and carnallite ores were determined by photocolometry. The flotation of sylvite ( $KCl$ ) and halite ( $NaCl$ ) was studied using samples of potash and carnallite ores from Upper Kama (Russia) deposits (Table I) in solutions of  $KCl-NaCl-H_2O$  (sylvinitic solution) and  $MgCl_2-KCl-NaCl-H_2O$  (carnallite solution), as shown in Table II.

Table I: Chemical and mineralogical composition of potash ore samples (% wt).

Minerals	Potash ore	Carnallite ore	Salts	Potash ore	Carnallite ore
Sylvite	27.5	0.17	$KCl$	31.5	20.61
Halite	70.5	22.20	$NaCl$	65.0	22.20
Anhydride	-	0.98	$CaSO_4$	-	0.98
Carnallite	-	75.40	$MgCl_2$	-	25.72
Water-insoluble residue	2.0	1.25	Water-insoluble residue	3.5	1.25

Table II: Composition of saturated saline solutions used in research works.

Components	Solution temperature (°C)					
	18	20	35	11.5	18.5	29.0
	Sylvinite solution			Carnallite solution		
KCl (%)	8.9	10.4	11.9	2.33	3.13	3.59
NaCl (%)	21.5	20.7	20.1	1.99	1.98	1.90
MgCl <sub>2</sub> (%)	-	-	-	25.62	25.78	25.86
H <sub>2</sub> O (%)	69.6	68.9	68.0	70.06	69.11	68.65

## Results

### *Alkylamines*

Sorption of alkylamines at KCl (sylvite) crystals is affected by saline solution temperature and composition as well as by the presence of clay-carbonate impurities actively adsorbing amine. The increase in temperature of the saline solution KCl-NaCl-H<sub>2</sub>O leads to an enhancement of hydration of the KCl crystal surfaces (Figure 1a), which may be explained by variations in hydration of Cl anions. As it is known, the temperature increase leads to an increase in ion hydration. Using nuclear-magnetic resonance, Krestov and Abrosimov (1967) have shown that at certain temperatures hydration of Na and Cl ions changes from negative to positive (at  $11\pm 3$  °C for Na<sup>+</sup> and at  $27\pm 3$  °C for Cl<sup>-</sup>). An increase in the density of hydrate envelope has to weaken amine sorption at KCl.

Increase in MgCl<sub>2</sub> concentration in the saline solution also enhances hydration of the KCl crystal surfaces (Figure 1b). By studying KCl crystallization in the KCl-NaCl-H<sub>2</sub>O solution and surface morphology of KCl crystals arising at different MgCl<sub>2</sub> concentrations of the solution (from 0% to 20.01%), it has been discovered that even at low MgCl<sub>2</sub> concentrations (1.06÷3.36%) the surfaces of the KCl crystals become imperfect. A large number of imperfections, such as microcracks and cavities, has to hinder amine sorption at sylvite and hydrofobizing of its surface. The most remarkable variations in KCl crystal morphology were observed at the MgCl<sub>2</sub> concentration of 5.3%. The studies also showed that micro-grains of carnallite can arise at the KCl crystals at the MgCl<sub>2</sub> concentration considerably lower than 25%, i.e., out of the range of its stability (Kuzina et al., 1992; Franke et al., 1992). Substantial enhancement of hydration of KCl crystals with increasing MgCl<sub>2</sub> concentration may be explained through absorption of magnesium ions having energy several times higher as compared with K<sup>+</sup> and Cl<sup>-</sup> ions at KCl crystals (Figure 2b). Concurrent increase in the solution temperature and MgCl<sub>2</sub> concentration is expected to lead to substantial weakening of amine sorption at KCl.

Studies of sorption provided data in favor of existence of harmful effect of increase in hydration of KCl crystal surfaces on alkylamine sorption at KCl. The studies have shown that amine sorption decrease with increasing temperature of the saline solution. Increase in MgCl<sub>2</sub> content in the saline solution also leads to substantial weakening of amine sorption at KCl. The most remarkable decrease in amine sorption at sylvite is observed in the case of concurrent increases in the saline solution temperature and MgCl<sub>2</sub> concentration (Figure 2). Studies of amine sorption at KCl of different particle sizes demonstrated that the most considerable weakening of amine

sorption takes place at sylvite fractions with particle sizes exceeding 0.25 mm. Amine sorption at fine-grained sylvite fractions, whose specific surface is quite large (more than  $75 \cdot 10^{-3} \text{ m}^2/\text{g}$ ), changes relatively slightly. Therefore, the strongest adverse effect of the increase in temperature and  $\text{MgCl}_2$  concentration of the saline solution is experienced by flotation of large sylvite particles.

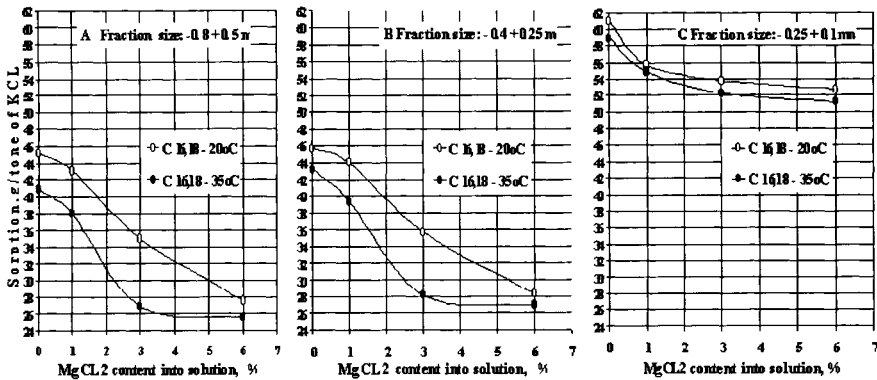


Figure 2: Effect of temperature, KCl-NaCl-H<sub>2</sub>O solution composition, and  $\text{MgCl}_2$  concentration on sorption of primary aliphatic amine C<sub>16</sub> - C<sub>18</sub> at KCl of different particle sizes.

The energy of amine sorption at KCl depends strongly on the energy of dispersion interaction between hydrocarbon radicals (Schubert, 1967) that reaches its highest value in case of C<sub>15</sub>, C<sub>16</sub> (and so on), hydrocarbon radicals having linear structure without isogroups and unsaturated bonds characterized by the index iodine number (J). Studying the velocity of amine sorption at sylvite, it has been found that the longer the hydrocarbon chain the faster amine sorption at KCl. The fastest sorption was observed for C<sub>20</sub> and C<sub>22</sub> amines (Figure 3). This allowed us to conclude that in order to improve cationic collector sorption at sylvite surface (especially in case of increase in hydration of KCl crystals in saline solutions having temperatures above 29÷30 °C), it is expedient to add to the collector amines with C<sub>20</sub> hydrocarbon chain (and longer). It also has been found that increasing number of amine unsaturated bonds leads to deterioration of KCl flotation (Figure 4) and of amine thermal stability (Titkov et al., 1982).

The most important condition for successful flotation of sylvite is efficient protection of the surface of clay-carbonate slimes from amine sorption by treating the flotation feed by reagents-depressors (organic oligomers or polymers). According to the known requirements to the reagents-depressors, they are to decrease amine sorption at slimes no less than by 25÷40% (Titkov et al., 1982; Titkov et al., 1999).

The studies showed that the protective effect of reagents-depressors on clay-carbonate slimes depends considerably on the cationic collector composition. As Figure 5 demonstrates, the decrease in amine sorption is weaker when the amine has small molecular mass and a large number of unsaturated bonds (iodine number higher than 10÷15). The studies resulted in the decision to use amines with combined fractional composition and hydrocarbon chain length corresponding to C<sub>12</sub> - C<sub>24</sub>.

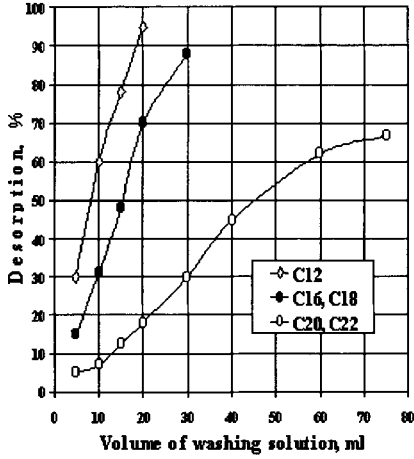


Figure 3: Fastness of sorption of amines with various length of hydrocarbon radical.

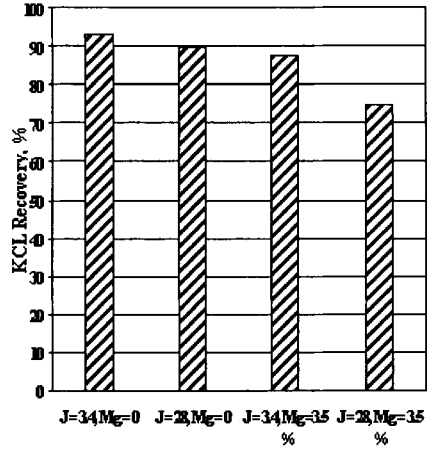


Figure 4: KCl flotation by amines with various numbers of unsaturated bonds in saline solutions of various compositions. Amine consumption = 70 g/t of ore.

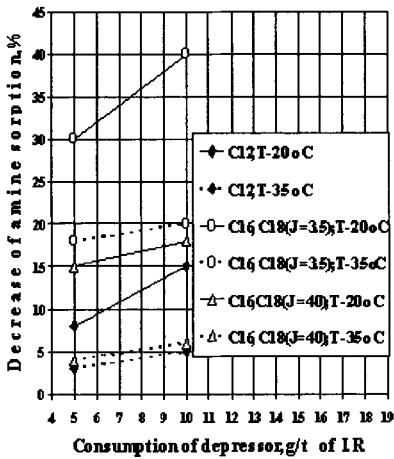


Figure 5. Effect of amine composition and temperature on efficiency of depression of amine sorption at slimes.

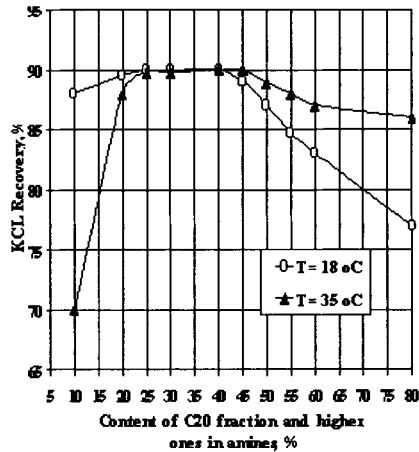


Figure 6. KCl flotation with collection by amines with different contents of C<sub>20</sub> fraction (and higher ones). Amine consumption is 70 g/t of ore.

Varying the ratio of the fractions, flotation properties of a collector used for KCl flotation in saline solutions with different temperatures and compositions (Titkov et al., 1996) can be optimized. Flotation tests showed that, varying the content of C<sub>20</sub> - C<sub>24</sub> fractions in C<sub>12</sub> - C<sub>14</sub> amines, it could achieve temperature-independent KCl recovery in the 18÷35 °C range of saline solution temperature (Figure 6). Commercial

tests of amines having such a composition at "Uralkaliy" and "Sylvinit" Joint-Stock Companies are the results of laboratory research.

*Alkylmorpholines*

Separation of halite from carnallite by flotation relies on selective sorption of alkylamines at halite (Figure 7). Contrary to sylvite in KCl-NaCl-H<sub>2</sub>O solutions, halite is floated in solutions with predominant concentrations of MgCl<sub>2</sub> (carnallite saturated solution, see Table II). Studies of morphology of NaCl crystal surfaces in carnallite saturated solutions demonstrated the absence of KCl crystals at these surfaces and presence of a small amount of carnallite grains. It promotes selective recovery of halite.

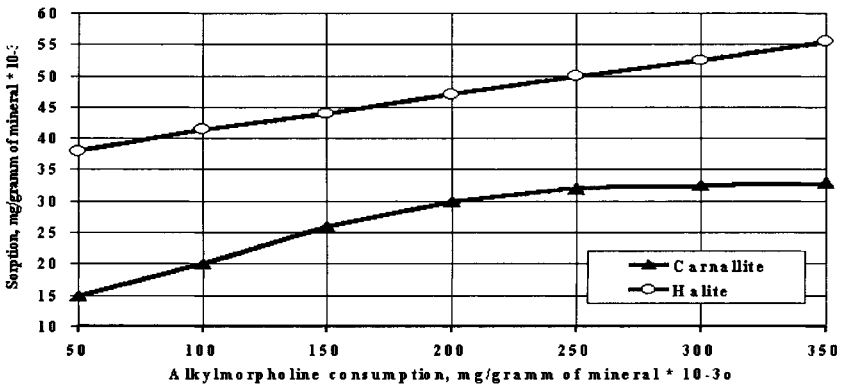


Figure 7. Isotherms of alkylmorpholine C<sub>16</sub>- C<sub>18</sub> sorption on carnallite and halite in carnallite solution.

Studies of effect of carnallite solution temperature on alkylmorpholine floatability demonstrated that at flotation temperature from 18 °C to 20 °C, the best floatability takes place if hexadecylamine is used (Figure 8).

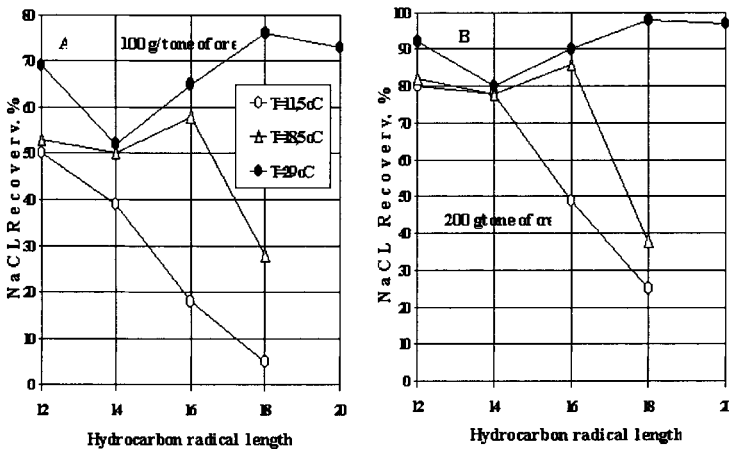


Figure 8. Halite flotation from carnallite ore by alkylmorpholines of various compositions (collector consumption is 100 g/t and 200 g/t of ore).

## Conclusions

Our studies have shown that variations in saline solution temperature and composition affect hydration of surface of alkaline halogenides, morphology of their crystal surfaces, and sorption fastness of cationic reagents-collectors (alkylamines and alkylmorpholines) at the crystals.

It has been found that the efficiency of reagents-depressors in flotation of potash ores depends on fractional composition and structure of the hydrocarbon radical of the cationic collector.

The optimal fractional compositions of cationic collectors used for sylvite and halite flotation have been determined.

## Acknowledgements

We are very grateful to the staff of "Uralkaliy" and "Sylvinit" Joint-Stock Companies, Russian Scientific Centre "Applied Chemistry" and Akzo Nobel Company (Sweden) who were an important help and provided us with reagents for our research.

## References

- Schubert, H., 1967. *Aufbereitung fester mineralischer Rohstoffe*. Leipzig.
- Alexandrovich, H.M., 1973. *Fundamentals of Using Reagents for Flotation of Potash Ores (Osnovy primeneniya reagentov pri flotatsii kaliinyh rud)*. Science and Technica, Minsk.
- Titkov, S.N., Solov'ev, E.I. and Mamedov, A.I., 1982. *Concentration of Potash Ores» (Obogaschenie kaliinyh rud)*. Nedra, Moscow.
- Titkov, S.N., Sokolov, I.D., Ryzhova, M.M., Struzkov, V.N. and Panteleeva, N.N., 1985. Development of new effective Process for flotation Concentration of potash ores with high clay content. XV International Mineral Processing Congress, Cannes, part II, 122-133.
- Amira, G. and Darius, R., 1991. Concentration of carnallite ore by gravitational separation and flotation, XVII International Mineral Processing Congress, vol.6.
- Exploiting Dead Sea potash, 1996. *Phosphorus & Potassium*, March - April, 26-33.
- Titkov, S.N., Sabirov, R.H., Panteleeva, N.N. and Kololeev, N.V., 1997. Production of Carnallite by Flotation. XX International Mineral Processing Congress, Aachen (Germany), September.
- Sabirov, R.H. and Titkov, S.N., 1997. New Process for Production of Beneficiated Carnallite - the Basis for Manufacturing Complex Mg-bearing, Fertilizers. *Fertilizer Focus*, October, 60-65.
- Krestov, G.A. and Abrosimov, V.K., 1967. *Journal of structural Chemistry (Journal struktornoj khimii)*, 8, 822-826.
- Kuzina, Yu.V., Franke, V.D., Kir'yanova, E.V., Titkov, S.N., Gurkova, T.M. and Vaysberg, E.A., 1992. Morphology and imperfections of crystals of halogenides of alkaline metals in the process of parallel growth from solutions. 8 All-Union Conference on Crystal Growth, Harkov, V.2, 68-69.
- Franke, V.D., Kir'yanova, E.V., Glikin, A.E., Titkov, S.N. and Vaysberg, E.A., 1992. Formation of KCl crystal surface geometry in multicomponent solutions with amines. 8 All-Union Conference on Crystal Growth, Harkov, V.2, 87-88.
- Titkov, S.N., Panteleeva, N.N. and Gurkova, T.M., 1999. Use of polymer reagents for processing of potash ores containing clay slimes. 38<sup>th</sup> Annual Conference of Metallurgists of CIM, International Symposium on Fundamentals of Mineral Processing "Polymers in Mineral Processing", Quebec, 375-392.
- Titkov, S.N., Pimkina, L.M., Chistyakov, A.A., Mikhaylova, I.A., Sabirov, R.Kh., Chumakova, T.G., Aliferova, S.N. and Boldyrev, A.V., 1996. A method for ore enrichment by flotation. Russian patent No 2116839.

## ACTIVATION OF XANTHATE FLOTATION OF PYRITE BY AMMONIUM SALTS FOLLOWING IT'S DEPRESSION BY LIME

X. Xiaojun\* , Ş. Kelebek°

\*Department of Resources Exploitation Engineering, Kunming University of Science and Technology, Kunming, Yunnan Province 650093, P. R. China

°Department of Mining Engineering, Queen's University, Kingston, Ontario, K7L 3N6, Canada

### Abstract

Some concentrators in China have adopted the use of ammonium sulfate and ammonium hydrocarbonate for activation of iron sulfides that were previously depressed by lime. This action of ammonium salts has recently been undertaken as a research topic, and the results of flotation and XPS investigations are reported in this paper, with some details. Ammonium sulfate, ammonium hydrocarbonate and ammonium chloride can all restore the floatability of pyrite, without the need to use copper sulfate or sulfuric acid. These salts lower pulp pH to a value below 9.0, and wash off calcium and ferric hydroxide layers on the surface of the pyrite. It is also proposed that activation involves the catalytic promotion of xanthate oxidation to dixanthogen by the ammonium ions. The activation mechanism has three main aspects: desorption of the calcium species, precipitation in solution, and activation. As a result, the recovery of pyrite increases substantially, e.g., from less than 10% to more than 85%.

*Keywords: lime depression, pyrite activation, flotation, ammonium salts, XPS spectra*

### Introduction

Pyrite and pyrrhotite are the most common type of iron sulfides in nature. On demand, they can be a primary resource to produce elemental sulfur and sulfuric acid for various further use in the chemical industry. As they co-exist with other sulfide minerals, such as those containing copper, lead and nickel, their excessive presence in the concentrates of such non-ferrous metals is not acceptable. Therefore, depression of iron sulfides is essential to produce high-grade concentrates. However, in certain cases, activation of iron sulfides is required for further treatment. This is especially so when they constitute the main middling fraction of the ore being processed.

Activation of iron sulfides previously depressed by lime can be accomplished by use of  $H_2SO_4$ ,  $CO_2$ ,  $Na_2CO_3$ , and  $Cu_2SO_4$  (Zhu and Zhu, 1996). In some cases, however, the nature of the process precludes use of acid, especially when cyanide is also involved as a reagent in a previous stage. In general, acid addition increases damage to the process equipment due to corrosion, while it is unsuitable for ores with a significant amount of carbonate gangue. The effect of copper sulfate as an activator in highly alkaline circuits is questionable, especially when there is a lack of retention time in the circuits. In addition to these aspects, the level of reagent consumption involved in such applications is quite high, contributing significantly to the overall



cost of processing. Because of such factors, many flotation plants in China do not favor re-activation of iron sulfides by these methods. Ammonium salts have various advantages, such as relatively low cost, ease of use, effectiveness, and environmental compatibility. Therefore, they are considered to have a potential activating effect for pyrite depressed by lime. Use of ammonium salts as modifiers in xanthate flotation is not new. Many decades ago, their activation effect for copper oxide ores in xanthate flotation was noted. They were also shown to be effective for depression, when used in combination with other reagents in the flotation separation of poly-metallic sulfide ores. However, it is only within the last decade that the technology of using ammonium salts for activation of iron sulfides has been developed and applied commercially in some non-ferrous-based metal and gold operations of China (Ruan and Huang, 1994; Yin, 1996; Deng, 1998). Despite industrial applications, the activation mechanism is still unclear, due a lack of systematic investigations on the subject. The purpose of this paper is to report some recently obtained results on this topic and discuss the mechanism of pyrite activation by ammonium salts.

### **Experimental materials and methods**

A massive specimen of pyrite was received from Yunnan Sin Industry Company. This sample was crushed, and visible impurities were rejected manually. The 100-200-mesh fraction of the pyrite sample was separated through screening and saved for flotation tests. Chemical analysis of the sample indicated 50.4% S and 43.7% Fe. This suggests that the pyrite sample, used in this work, has a purity of about 94%.

The purity of sodium butyl xanthate (BuX) was 96%. Other reagents used in the experimental work were of analytical grade. The flotation tests were carried out using distilled water and a 5.0 g pyrite sample in a small-scale flotation cell. The order of reagent addition in a typical test was lime, ammonium salt, xanthate, and frother with conditioning periods of 4 min, 3 min, 2 min, and 1 min. Flotation time in each case was 5 min. The surface species on pyrite was analyzed by means of XPS.

### **Results and discussion**

#### *Flotation Tests*

Figure 1 shows the influence of the concentrations of three ammonium salts on pyrite floatability at pyrite's natural pH, namely, ammonium hydrocarbonate, ammonium sulfate and ammonium chloride. The flotation recovery of pyrite is improved by an increase in the concentration of these three salts. In each case, the flotation recovery shows an increase up to about 1 g/l, then establishes a plateau. The order of activation is ammonium hydrocarbonate > ammonium chloride > ammonium sulfate. Although the activation of pyrite is quite apparent, the effect in this case is not a particularly strong one. We observed a much more dramatic effect on a cobalt bearing pyrite and pyrrhotite (unpublished results). In this particular case, however, these cobalt-bearing iron sulfides were highly oxidized, compared to a relatively fresh sample of pyrite, considered in Figure 1. It seems, therefore, that one aspect of this activation is related to a reduced stability of ferric hydroxides in the presence of ammonium salts.

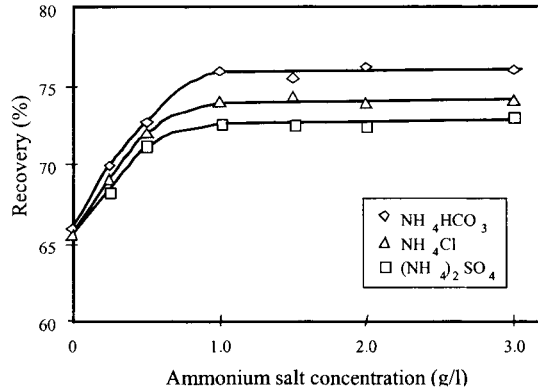


Figure 1: Influence of ammonium salt concentration on flotation recovery of pyrite (natural pH; BuX = 10 mg/l).

The flotation response of pyrite (previously depressed by lime) to activation by ammonium salts is shown in Figures 2 and 3. In these cases, pyrite depression was effected by addition of lime at 800 mg/l and 15 mg/l, respectively. In both cases, activation is highly effective. In the previous case, flotation recovery is about 90%, 89% and 80%, respectively, when the concentration of ammonium hydro-carbonate, ammonium sulfate and ammonium chloride are at 2.5 g/l, 3.0 g/l and 3.0 g/l. However, activation follows a different order, i.e.: ammonium hydrocarbonate > ammonium sulfate > ammonium chloride. It can be seen from Figure 3 that when a low concentration of lime is involved in the depression of pyrite, the concentration of ammonium salt required to activate it for high recoveries is also low. Figure 4 shows the influence of ammonium salt concentration on the recovery of copper-activated pyrite. In this case, copper activation was introduced after lime depression of pyrite.

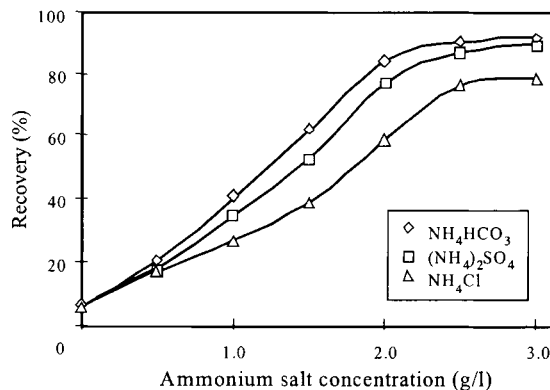


Figure 2: Activation effect of ammonium salts on pyrite previously depressed by lime (CaO = 800 mg/l; BuX = 50 mg/l)

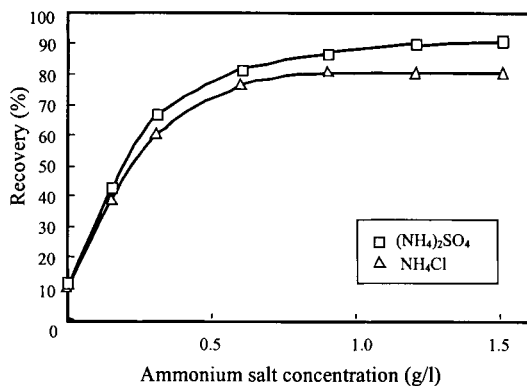


Figure 3: Activation of ammonium salts on pyrite after depression by lime  
(CaO = 15 mg/l; BuX = 20 mg/l)

These observations demonstrate that ammonium salts hinder the flotation of copper-activated pyrite. This is obviously attributable to deactivation of pyrite, resulting from complexation of copper ions in the presence of ammonium salts.

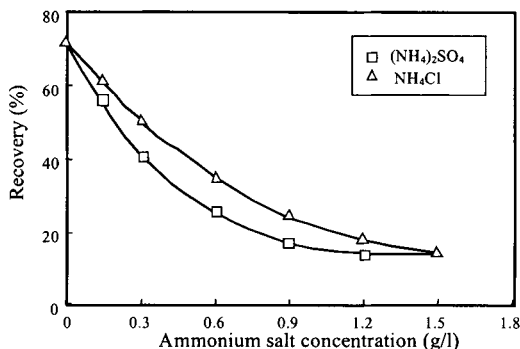


Figure 4: The relationship between pyrite flotation recovery and ammonium salt concentration  
(after copper activation of pyrite that had been depressed by lime in the previous stage,  
CaO = 15 mg/l; CuSO<sub>4</sub> = 10 mg/l; BuX = 15 mg/l).

#### *Nature of calcium coating on pyrite surface*

When lime is used as a depressant for pyrite, the depression is attributed to the adsorption of both the calcium and hydroxide ion originating from lime, especially in the presence of oxygen (Gaudin and Charles, 1953, Gaudin et al, 1956). Generally, the surface of pyrite is negatively charged in a pH above 7.0, and it readily adsorbs calcium ions by electrostatic attraction to form a calcium coating. This reduces the number of active sites for adsorption of xanthate and for oxidation of xanthate to dixanthogen. The hydrophilic species that can form on the pyrite surface include calcium sulfate, carbonate, oxide or/and hydroxide and ferric hydroxide (Zhu and Zhu, 1996). Figures 5 and 6 show the results of XPS analysis of the pyrite surface in the absence and presence of lime. The presence of calcium complexes (Ca<sub>2p</sub>: 347.3 eV, Ca<sub>2s</sub>: 466.1 eV) on the pyrite surface, after it has been contacted with lime, is

quite clear in Figure 5. The expanded XPS spectrum of  $Ca_{2p}$  (Figure 6) indicates that the calcium coating on the surface consists predominantly of  $Ca(OH)_2$ ,  $CaSO_4$  and  $CaO$ . The formation of calcium sulfate is obviously attributed to the surface reaction between calcium ions and sulfate ions from the oxidation of the pyrite surface.

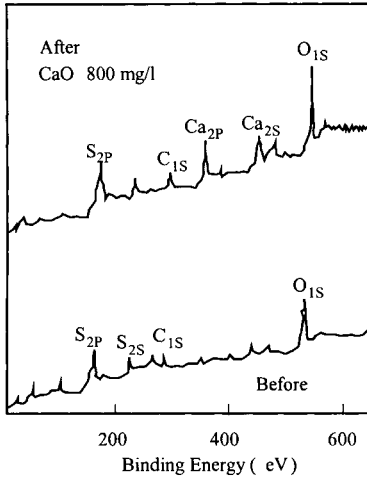


Figure 5: XPS spectra of the pyrite surface before and after treated by  $CaO = 800 \text{ mg/l}$ .

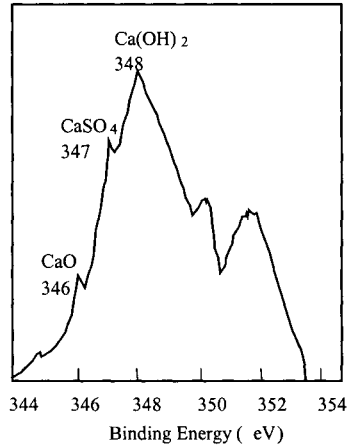


Figure 6: XPS expanded spectrum of  $Ca_{2p}$  in Figure. 5.

On the other hand, it is also known that ferric hydroxides are readily formed on pyrite due to the oxidation of its surface, which is pH dependent. Thus, xanthate flotation of pyrite will be effectively hindered by the formation of a complex coating of hydrophilic products, involving several species of calcium and ferric hydroxide.

*Influence of ammonium salt on calcium coating*

As shown in Figure 7, peaks of  $Ca_{2s}$  and  $Ca_{2p}$  clearly disappear, but a new  $N_{1s}$  peak

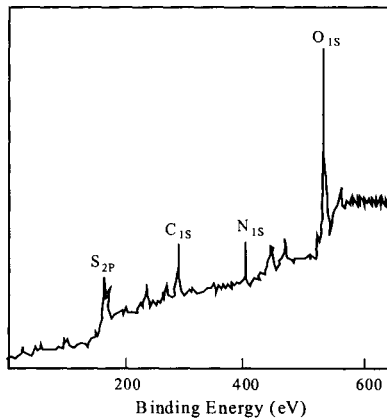


Figure 7: XPS spectrum of the pyrite surface, after lime-depressed pyrite was activated using  $3 \text{ g/l}$  ammonium sulfate.

(401.6eV) appears on the XPS spectra following treatment of the pyrite with ammonium sulfate.  $\text{Ca}_{2p}$  peaks are not identifiable in the XPS expanded analysis. These results indicate that hydrophilic calcium coating has been effectively removed from the surface of the pyrite, and that Ammonium ion/ammonia molecule is adsorbed on the pyrite surface to function as a further activation site on the pyrite.

#### *Solution-chemistry aspects*

The equilibrium involving  $\text{NH}_4^+$  and  $\text{NH}_3(\text{L})$  species in an aqueous solution is:



It can be seen from equilibrium equations (1) and (2) that the aqueous solution of ammonium salt has the characteristics of a pH buffer. The equilibrium constant of equation (2) is defined by

$$K = \log\left\{\frac{[\text{NH}_4^+][\text{OH}^-]}{[\text{NH}_3]}\right\} \quad (3)$$

Equation (3) can be written as

$$\log\left\{\frac{[\text{NH}_4^+]}{[\text{NH}_3]}\right\} = \text{p}K_b - \text{pH} \quad (4)$$

Here:

$$\text{p}K_b = -\log(K_w/K) = 9.25 \quad K_w = [\text{H}][\text{OH}] = 10^{-14}$$

Then, it follows from equation (4) that

$$\log\left\{\frac{[\text{NH}_4^+]}{[\text{NH}_3]}\right\} = 9.25 - \text{pH} \quad (5)$$

According to equation (5), the ammonium ion is the predominant species in a solution below  $\text{pH} = 9.25$ ; the free ammonia molecule is the predominant species above  $\text{pH} = 9.25$ ; the ammonium ion and free ammonia molecule coexist around  $\text{pH} = 9.25$ .

It has been known that ammonium salts can react with hydroxide ions or hydroxides. As shown in Table 1, ammonium salt can effectively lower the initially high pH value of a lime suspension. When the concentration of ammonium salt exceeds 1.0 g/l, the pH value of the lime solution (800 mg/l) decreases from 12.4 to less than 9. The ammonium ion is also able to dissolve away calcium hydroxide and ferric hydroxide coatings on a pyrite surface when ammonium salts are used as an activator.

Table 1: Influence of ammonium salts on the pH value of pulp with 800 mg/l lime.

Concentration (g/l)	pH value observed as a function of ammonium salt concentration						
	0.0	0.5	1.0	2.0	3.0	4.0	5.0
$\text{NH}_4\text{HCO}_3$	12.4	9.05	8.67	8.39	8.36	8.36	8.36
$(\text{NH}_4)_2\text{SO}_4$	12.4	9.65	9.21	8.95	8.78	8.70	8.50
$\text{NH}_4\text{Cl}$	12.4	9.27	9.04	8.80	8.65	8.59	8.56

Free ammonia molecules have one free electron pair, which can react with many heavy-metal ions to form different stability-coordination compounds. On the other hand, because the dipole moment of free ammonia ( $D = 4.9 \cdot 10^{-30} \text{ C}\cdot\text{m}$ ) is less than that of water ( $D = 6.17 \cdot 10^{-30} \text{ C}\cdot\text{m}$ ), adsorption of free ammonia is expected to reduce the stability of the hydrated layer. This is believed to facilitate the adsorption of xanthate on the surface. It is also believed that adsorption of ammonium ions on a negatively charged pyrite surface can improve the adsorption of xanthate on its surface by electrostatic action. Therefore, both the free ammonia and ammonium ions can facilitate the interaction of xanthate with the pyrite surface.

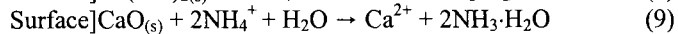
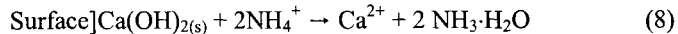
### Mechanism of activation

#### Desorption of calcium coating

This involves two aspects. Firstly, as ammonium salt effectively lowers the pH value of the pulp (Table 1), calcium hydroxides with low solubility ( $K_{sp} \approx 5.5 \cdot 10^{-6}$ ) will dissolve from the pyrite surface into an aqueous solution. The relevant reactions are as follows:

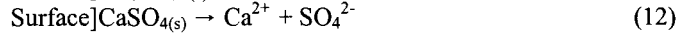
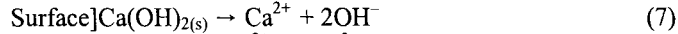


This decreases the amount of calcium coating on the pyrite surface. Secondly, the ammonium ion reacts with the remaining calcium hydroxide on the surface, which results in further dissolution and dropping of the calcium film off the surface. That is



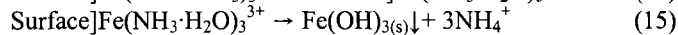
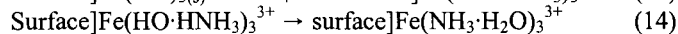
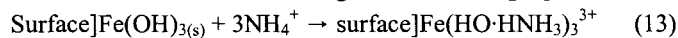
#### Precipitation of calcium ion in pulp

It has been well known that  $\text{SO}_4^{2-}$  and  $\text{CO}_3^{2-}$  ions react with  $\text{Ca}^{2+}$  ions to form sparingly soluble precipitates of calcium sulfate ( $K_{sp} = 9.1 \cdot 10^{-6}$ ) and calcium carbonate ( $K_{sp} = 2.5 \cdot 10^{-9}$ ), respectively (Yan and Wang, 1987). When ammonium sulfate or ammonium hydro-carbonate is used as an activator and is at high concentration,  $\text{SO}_4^{2-}$  or  $\text{CO}_3^{2-}$  ions can react with  $\text{Ca}^{2+}$  ions to form precipitates in the aqueous phase. This precipitation will also result in the dissolution and the dropping-off of the calcium coating.

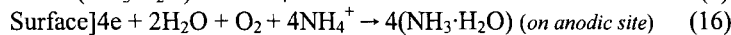
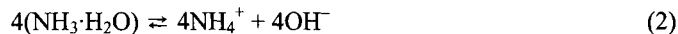


#### Chemical activation on the surface

While ammonium salt decreases the pH value and washes away the calcium coat, it can also react with ferric hydroxides to wash out the hydrophilic ferric hydroxide film on the pyrite surface. The reactions in equations (1), (6), (13), (14) and (15) may describe the process. The ammonium ions and ammonia molecules wash off ferric hydroxides and are adsorbed on the surface according to the following equations:



On the other hand, the ammonium ion and ammonia molecule adsorbed on the activated pyrite surface can promote the oxidation of xanthate to dixanthogen.



Thereby, the ammonium ion acts as a catalytic promoter of the oxidation of xanthate to dixanthogen, which is known to be a strongly hydrophobic species for pyrite flotation.

**References**

- Gaudin, A.M. and Charles, W.D., 1953. Adsorption of calcium and sodium on pyrite. *AIME Transact.*, 196, 195-200.
- Gaudin, A.M., de Bruyn, P.L. and Mellgren, O., 1956. Adsorption of ethyl xanthate on pyrite. *AIME Transact.*, 204, 65-70.
- Deng, H., 1998. Recovery of pyrite depressed strongly by lime with activation and flotation from lead-zinc tailing. *Non-Ferrous Metal (Mineral process.)* 1, 19-22. (in Chinese)
- Ruan, J. and Huang, X., 1994. Study and practice of activation of ammonium sulfate on pyrite in alkaline pulp. *Non-ferrous Mining and Metallurgy*, 3, 16-21. (in Chinese)
- Yan, X. and Wang, C., 1987. *General Inorganic Chemistry. ISBN13209.160*, Beijing University Press, *Beijing*, 117-423. (in Chinese)
- Yin, W., 1996. Study and application of using ammonium sulfate as activator to improve gold flotation recovery. *Non-ferrous Mining and Metallurgy*, 3, 17-19. (in Chinese)
- Zhu, Y. and Zhu, J., 1996. *Chemical Principles of Flotation Reagents. ISBN7-81020-936-1/TD.042*, The Central-South University of Industrial Press, Changsha, China, 317-320. (in Chinese)

## MODIFIED HYDROXAMATE COLLECTORS FOR KAOLIN FLOTATION

C. Basilio\*, R.A. Lowe\*, A. Gorken<sup>o</sup>, L. Magliocco<sup>o</sup>, R. Hagy<sup>o</sup>

\*Thiele Kaolin Company, Sandersville, Georgia, USA

<sup>o</sup>Cytec Industries Inc., Stamford, Connecticut, USA

<sup>o</sup>Cytec Industries Inc., South Charleston, West Virginia, USA

### Abstract

Reverse flotation has emerged as one of the most efficient beneficiation process for removing discolored impurities, mainly titanium and iron-containing minerals, from kaolin. In kaolin flotation, tall oil has been traditionally used as the collector. This requires activation of the discolored impurities with metal ion (i.e.,  $\text{Ca}^{2+}$ ) to enhance tall oil adsorption. On the other hand, hydroxamates have been demonstrated to be more effective and do not require an activation step. In this study, the flotation performance of a series of newly developed hydroxamate collectors was evaluated on different crude clays from Georgia, USA. These new modified hydroxamates provide improved properties and performance over the standard tall oil collector and the current commercially available hydroxamate collector (Aero Promoter 6493) used in the kaolin industry.

*Keywords: kaolin, flotation, hydroxamate collectors, anatase*

### Introduction

Kaolin clays are naturally occurring in sedimentary deposits composed largely of kaolinite mineral. Typical impurities in these deposits are iron oxides, titaniferous minerals, silica, feldspar, mica, sulfides and organic matter. The majority of kaolin clay produced in the world is used in the paper industry as coating and filler materials. This mineral also makes an excellent filler, carrier, opacifier, and diluent in a variety of industrial products such as paints, plastics, cement, rubber, pharmaceuticals, etc. To make kaolin acceptable for use, crude kaolin deposits require beneficiation to remove the associated impurities. The colored impurities, specifically titaniferous minerals and iron oxides, are generally removed by reverse froth flotation, high gradient magnetic separation, selective flocculation and/or leaching.

Froth flotation has proven to be an efficient method of removing titaniferous impurities (mainly iron-rich anatase) from kaolin clays. Fatty acid reagent, primarily tall oil, is used extensively in the reverse flotation of these impurities. This flotation collector typically requires divalent cations (usually  $\text{Ca}^{2+}$ ) to activate the colored impurities and enhance collector adsorption. This is not very selective since the tall oil can also absorb on the kaolinite particles. Alkyl hydroxamate collectors are relatively new in the kaolin industry but provide significant advantages (Yoon and Yordan, 1992). Hydroxamates do not require activators, substantially increases the removal of colored impurities and are very selective. In this study, the flotation performance of a series of newly developed hydroxamate-based collectors was evaluated on different crude clays from Georgia, USA. These new collectors provide



improved selectivity over the standard tall oil chemistry and the commercial hydroxamate reagent, Aero Promoter 6493 (AP 6493). The modified hydroxamates have the advantages of higher activity, easier to handle, more stable, increased floatability if desired and can be tailored via the use of different carriers and methods of synthesizing the reagent.

## **Experimental**

### *Reagents*

The newly developed modified alkyl hydroxamate reagents (from Cytec Industries) tested in this study include S-8704, S-8704D, S-8705, S-8706, S-8706D and S-8765 while the reference collectors used were Aero Promoter 6493 (also from Cytec) and tall oil. The crude clays were dispersed using sodium silicate while soda ash was used to adjust the pH. The frother used in the flotation tests was Aerofroth 70.

### *Clay sample*

Tests were conducted on “soft” and “hard” kaolin clays from Georgia, USA. Soft kaolins are relatively coarse-grained (coarser than 65% <2  $\mu\text{m}$ ), found in Cretaceous age strata, and typically have low  $\text{TiO}_2$  contents (1÷3%). The hard kaolins are fine-grained (finer than 80% <2  $\mu\text{m}$ ), found in Eocene age strata and have higher  $\text{TiO}_2$  contents (2÷8%).

### *Procedure*

The laboratory test procedure used in the different flotation tests is basically composed of three stages: blunging, conditioning and flotation. Blunging (or dispersion) of the crude clay is carried out in a Cowles Dissolver at 60% solids (by weight) using sodium silicate as the dispersant and soda ash (to pH 9) as the pH modifier. After the clay has been dispersed, conditioning is conducted in the same vessel using the required amount of collector. After the conditioning step, the pulp temperature and pH are recorded and the pulp is diluted to 25% (by weight) with water and transferred to the flotation cell. The required amount of frother is then added to the slurry and mixed for a minute prior to flotation. Flotation tests are carried out either in a batch Denver cell or laboratory-sized flotation column (7.62 cm diameter). The froth reject and the slurry remaining in the cell (or underflow in the flotation column) were collected, dried, weighed and analyzed for  $\text{TiO}_2$  using XRF spectroscopy. Plant trial tests were conducted at Thiele Kaolin Company's flotation plant employing Microcel flotation columns. The flotation responses of the kaolin samples to the various flotation collectors were measured using the separation efficiency (S.E.) index. This index combines both grade and recovery to describe the efficiency of the beneficiation process (Wills, 1992). The mathematical expression used to compute the separation efficiency is  $\text{S.E.} = \text{R}_m - \text{R}_g$ , where  $\text{R}_m$  and  $\text{R}_g$  are, respectively, the % recovery of the valuable material (kaolin) and the gangue ( $\text{TiO}_2$ ) into the product.

## **Results and discussion**

Reagent screening tests were conducted on the different modified hydroxamate reagents. The alkyl hydroxamate activities of the modified reagents are higher than

that of AP 6493 (i.e. >30% active). These reagents also have different carrier solvents that allow the alkyl hydroxamate to remain soluble at ambient temperatures. In addition, some of the reagents use a carrier solvent that has some frothing properties; thus reducing the frother requirement for flotation. Flotation tests were conducted on a soft kaolin sample that is known to have good response to flotation (sample A). A laboratory Denver cell was used in these tests and the results are presented in Table I. Using tall oil as a collector, the flotation performance is relatively poor, as shown by the low flotation recovery. This shows the poor selectivity of tall oil in kaolin flotation. Another test was conducted using the flotation chemistry given in U.S. Patent 5,522,986 (Shi and Yordan, 1996). This invention uses a blend of alkyl hydroxamate and tall oil as the collector. The results for this chemistry (AP 6493/tall oil blend) show good flotation recovery and a significant reduction in TiO<sub>2</sub>. The use of a higher AP 6493 dosage without tall oil added produced a significantly lower TiO<sub>2</sub> grade at comparable flotation recovery, thereby increasing the SE index.

Table I: Denver cell flotation testing of sample A (soft kaolin with good flotation response).

Collector	dosage (kg/t)	Product TiO <sub>2</sub> (%)	Clay recovery (%)	Separation efficiency (%)
AP 6493/Tall oil	0.5/0.5	0.84	84	40.5
AP 6493	1	0.27	80	66
Tall oil	1	0.79	67	32
S-8765	1	0.80	81	41
S-8765	2	0.54	84	56
S-8704	0.5	0.55	96	64
S-8704	1	0.44	86	62
S-8705	0.75	0.50	84	58
S-8706	0.625	0.33	96	75

For the modified reagents, the use of S-8765 resulted in poorer flotation performance. A relatively high S-8765 dosage is required to obtain comparable results. However, S-8704, S-8705 and S-8706 gave significantly improved TiO<sub>2</sub> rejections at equal to higher clay recoveries. Reagents S-8704 and S-8706 showed the most promise of the new collectors. S-8706 has a higher hydroxamate activity than AP 6493 and uses a carrier solvent with some frothing properties. This collector produced a considerably lower TiO<sub>2</sub> grade with very high recovery of 96%. The separation efficiency for S-8706 is almost twice that for the AP 6493/tall oil blend. The next series of tests was carried out on a soft kaolin sample that is known to respond poorly to flotation (sample B). Tests were carried out using S-8704 and S-8706, the two most promising reagents found for sample A. Table II shows that a very low product TiO<sub>2</sub> grade was obtained with AP 6493 but the clay yield was poor. The flotation performance was even poorer for the sample floated with tall oil. The modified hydroxamate, S-8704, gave a flotation performance identical to that for AP 6493. On the other hand, reagents S-8704D and S-8706D gave significantly higher clay recoveries with almost similar amounts of TiO<sub>2</sub> removal; thus, giving higher S.E. values.

Tests were also conducted on a soft kaolin sample with relatively higher TiO<sub>2</sub> and iron content (sample C) than the other soft kaolin samples. Table III shows that flotation with tall oil gives poor flotation performance. Using AP 6493, the grade and

recovery are both improved resulting in higher separation efficiency. The modified hydroxamates, S-8704 and S-8706D, give significantly higher TiO<sub>2</sub> removal but with slightly lower clay yields. Higher collector dosages are probably required to improve the flotation response of sample C.

Table II: Denver cell flotation testing of sample B (soft kaolin with poor flotation response).

Collector	dosage (kg/t)	Product TiO <sub>2</sub> (%)	Clay recovery (%)	Separation efficiency (%)
AP 6493	0.5	0.25	47	41
Tall oil	2	0.48	38	28
S-8704	0.5	0.26	47	40
S-8704D	0.5	0.24	53	47
S-8706D	0.5	0.39	60	47

Table III: Denver cell flotation testing of sample C (soft kaolin with high TiO<sub>2</sub> and Fe content).

Collector	Product TiO <sub>2</sub> (%)	Clay recovery (%)	Separation efficiency (%)
AP 6493	0.81	71	39
Tall oil	1.06	60	25
S-8704	0.53	58	41
S-8706D	0.66	64	41

Hard kaolins from East Georgia, USA are known to give poor response to flotation (Yordan et al., 1994). The efficacy of S-8704 and S-8706 are tested on sample D, a fine hard kaolin with TiO<sub>2</sub> content of 2.45% and particle size distribution of about 88% <2 μm. Using tall oil as the collector, the product grade is still high and the resulting separation efficiency is low (see Table IV). Results for AP 6493 show improved anatase removal and a resulting increase in S.E. value. Reagent S-8706 gives further improvement in anatase removal but not S-8704. However, the S.E. values are all relatively low, showing the poor flotation response of fine-grained kaolin clays.

Table IV: Denver cell flotation testing of sample D (hard kaolin) using S-8704 and S-8706.

Collector	Product TiO <sub>2</sub> (%)	Clay recovery (%)	Separation efficiency (%)
AP 6493	1.37	61	28
Tall oil	1.73	68	20
S-8704	1.17	45	24
S-8706	0.96	61	38

The results for the different crude samples show that S-8706 and S-8706D are the most promising of the different collectors tested. These reagents showed improved TiO<sub>2</sub> removal with relatively good clay recovery for either soft or hard kaolins. To further test the efficacy of these reagents, column flotation tests were conducted on sample A. The results of the different flotation tests are presented in Table V. As shown, significantly higher S.E. values were obtained with the use of the flotation column (see Table I). Using S-8706 alone, improved flotation performance is obtained at a lower collector dosage. In the case of the hydroxamate/tall oil blend, replacing AP 6493 with S-8706 results in an increase in S.E. value. Flotation with S-8706D, a derivative of S-8706 using a different carrier solvent, results in similar

flotation performance as AP 6493 but requires a lower collector dosage. These results show the improved flotation performance of these modified hydroxamates.

Table V: Column flotation testing of sample A using S-8706D and S-8706.

Collector	dosage (kg/t)	Separation efficiency (%)
AP 6493	1	66
AP 6493/Tall oil	0.5/0.5	67
S-8706	0.625	73
S-8706/Tall oil	0.5/0.5	70
S-8706D	0.75	66

To further prove the efficacy of S-8706 and its applicability on a full-scale, a plant trial was conducted at Thiele Kaolin Company's flotation plant (Table VI). The average S.E. value obtained with AP 6493 before the trial run was 70. Replacing AP 6493 with S-8706, the flotation performance during the trial run improved to 73. After the plant trial run with S-8706, the measured S.E. value for AP 6493 averaged about 68. This trial shows the improved flotation performance obtained with the use of S-8706.

Table VI: Plant trial data - soft kaolin using S-8706.

Collector	Average separation efficiency (%)
AP 6493 (before trial)	70
S-8706	73
AP 6493 (after trial)	68

## Conclusions

New modified hydroxamate collectors were developed with the following improved properties: higher activity, easier handling, improved stability, and can have increased frothing property. Flotation tests were conducted on different soft and hard kaolin crude samples from Georgia, USA. Laboratory screening tests were conducted to identify the most promising modified hydroxamate reagent. The results show that S-8704 and S-8706 give better flotation performances than AP-6493 for coarse-grained soft and fine-grained hard Georgia kaolins. In a full-scale plant trial using flotation columns, S-8706 showed better flotation performance in the flotation of soft Georgia kaolins than the current commercially available reagent, AP 6493.

Reagent S-8706 has a higher hydroxamate activity and better stability (i.e., remained liquid at ambient temperature) than AP 6493.

## References

- Shi, J., and Jordan, J., 1996. U.S. Patent 5,522,986. Process for removing impurities from kaolin clays.
- Wills, B., 1992. Mineral Processing Technology. Fifth edition. Pergamon Press, Tarrytown, New York, 33-35.
- Jordan, J., Yoon, R.H., and Hilderbrand, T., 1994. Hydroxamate vs. fatty acid flotation for the beneficiation of Georgia kaolin. Reagents to Better Metallurgy, Chapter 22, SME.
- Yoon, R.H., and Jordan, J., 1992. Beneficiation of kaolin clay by froth flotation using hydroxamate collectors, Minerals Engineering, Vol. 5, no. 3-5, 457-467.

## MONITORING THE DISTRIBUTION OF FLOTATION CHEMICALS AT AN INDUSTRIAL MINERAL PROCESSING PLANT

M.S. Miettinen, P.M. Stén, J.O. Leppinen, H.J. Lehto

Technical Research Centre of Finland (VTT), Chemical Technology,  
Mineral Processing, P.O. Box 1405, FIN-83501 Outokumpu, Finland

### Abstract

A sensitive oxidation technique was applied to quantitative analysis of flotation chemicals adsorbed on mineral surfaces in quartz-feldspar ore processing. Distribution of flotation chemicals on single minerals was further calculated using a mathematical method. This method combines chemical analysis, mineral analysis and process data.

In parallel to the process studies, laboratory experiments were conducted with a specially-designed system to examine the competitive adsorption of amine between quartz and feldspar. The experiments showed that the adsorption rate plays an important role in the distribution of amine.

*Keywords: competitive adsorption, chemical distribution, flotation process, quartz, feldspar*

### Introduction

Selective adsorption of flotation chemicals is needed to efficiently separate minerals in the flotation process. Therefore, a better control of the flotation chemicals could result in cost savings, environmental benefits and higher grade mineral products. However, in practise, the fate of flotation chemicals at concentrating plants is not usually known in detail. This is mainly complicated by the low contents of flotation chemicals.

Several analytical methods have been used to directly analyse mineral samples for an adsorbed collector. Pugh and Husby applied the selective oxidation technique to determine the amounts of collectors adsorbed on fluorite, galena and quartz using a specially-designed analyser (Pugh and Husby, 1986). Recently, a commercial combustion analyser was modified in our laboratory to determine flotation chemicals bound to mineral surfaces in flotation processes (Stén et al., 2000). This sensitive method enabled us to study the distribution of flotation chemicals at an industrial mineral processing plant for analysing the various process stages. These analyses provide the total amount of chemicals in specific samples, which have multi-mineral compositions. A mathematical method was developed and applied to determine the distribution of chemicals on various minerals.

Using the classical approach to conduct adsorption tests on single minerals and translating this information to multi-mineral systems can be misleading. In this work, a specific set-up was used to investigate the distribution of flotation chemicals in conditions where the single minerals share the same solution. Consequently, the competitive adsorption can be studied in the presence of the ions dissolved from all minerals representing more realistic process conditions.

## Materials and methods

### *Minerals, process samples and reagents*

Pure mineral samples of quartz and feldspar were used in the laboratory experiments. The samples were subjected to dry grinding in an agate mill. Finally samples were dry-screened and the selected fractions were used in the adsorption studies.

Process samples were filtered prior to drying at room temperature. The elemental composition of the process samples was determined by XRF analysis using Philips PW 1400 instrument and further calculated to obtain the mineral composition of the samples.

Analytical grade sulphuric acid and hydrofluoric acid were received from Merck. A primary amine acetate of commercial grade was used for the laboratory experiments.

### *Combustion method for chemical analysis*

The analysis is based on the oxidation of organic compounds to generate carbon dioxide, which is subsequently detected and quantified. LECO RC-412 analyser is capable of oxidizing selectively over various carbonaceous species by altering the furnace temperature. Moreover, the presence of organic carbon can be verified by coincident CO<sub>2</sub> and H<sub>2</sub>O peaks.

The sensitivity of the instrument was increased by an order of magnitude by making minor modifications in the gas flow. The analysis of low carbon concentrations also requires careful treatment of samples and sample crucibles as well as the use of high-purity oxygen (99.999%). Commercial standards were employed to calibrate the response of the IR cell. This combustion technique is described in more detail in another paper (Stén et al. 2000).

### *Mathematical method for distribution studies*

In this section a mathematical method is introduced for obtaining the amounts of reagents adsorbed on particular minerals by combining process data with the analysis of collector and the mineralogical composition of the various flotation products. Therefore, we need to present the adsorption parameter  $J_i$ , which represents chemical contents of certain minerals ( $i$  = feldspar F, mica M or quartz Q). Chemical C is added to the feed of the process and this chemical is assumed to adsorb on the mineral surfaces according to the equilibrium. Hence, the following equation for the mass of chemical in the feed ( $m_{C(\text{feed})}$ ) can be written:

$$J_F * m_{F(\text{feed})} + J_M * m_{M(\text{feed})} + J_Q * m_{Q(\text{feed})} = m_{C(\text{feed})} \quad (1)$$

Here  $m_{F(\text{feed})}$ ,  $m_{M(\text{feed})}$  and  $m_{Q(\text{feed})}$  are the mass of feldspar, mica and quartz in feed, respectively. After flotation, a concentrate and a tailing are obtained, where mineral compositions and also the amounts of chemicals are different. Therefore, equations (2) and (3) are presented:

$$J_F * m_{F(\text{conc})} + J_M * m_{M(\text{conc})} + J_Q * m_{Q(\text{conc})} = m_{C(\text{conc})} \quad (2)$$

$$J_F * m_{F(\text{tailing})} + J_M * m_{M(\text{tailing})} + J_Q * m_{Q(\text{tailing})} = m_{C(\text{tailing})} \quad (3)$$

Furthermore, the total amount of chemical in the concentrate and tailing has to be the same as the amount of chemical in the feed:

$$m_{C(\text{feed})} = m_{C(\text{conc})} + m_{C(\text{tailing})} \quad (4)$$

### *Competitive adsorption experiments*

The competitive adsorption of amine between quartz and feldspar were examined with specially-designed apparatus. The apparatus consists of three symmetrically located mineral compartments, timer, pneumatic unit, glass beaker and magnetic stirrer. The mineral compartments are equipped with 25  $\mu\text{m}$  screens located below the minerals. The glass beaker contains the desired solution (250 ml) with flotation chemicals and additional reagents. The minerals (5 g) are dipped into the solution and the required delay on both up and down is adjusted with the timer. The compartments are shifted up when their solution level corresponds to the solution level in the glass beaker and the compartments are allowed to drain almost empty before the next immersion in the solution.

The experiments were carried out in an environment as similar as possible to that prevailing during the actual flotation of feldspar. Therefore, pH was set to a value of 2.5 with sulphuric acid prior to addition of hydrofluoric acid (2.3 mg/l, 40%) and amine (40 mg/l). Mineral samples contained size fractions of  $- 500 + 250 \mu\text{m}$  (30%) –  $250 + 125 \mu\text{m}$  (40%) and  $- 125 + 45 \mu\text{m}$  (30%). The surface areas determined by the BET method were  $0.105 \text{ m}^2/\text{g}$  (quartz) and  $0.118 \text{ m}^2/\text{g}$  (feldspar).

## **Results and discussion**

### *Analysis of process samples*

The mineralogical composition of the process samples is presented in Table I.

Table I: Composition of process samples.

Process stage	Quartz (% wt)	Feldspar (% wt)	Mica (% wt)
mica circuit, water separation overflow	31.80	61.55	4.10
mica circuit, flotation feed	32.51	59.87	5.17
mica circuit, flotation overflow	21.05	47.28	28.47
mica circuit, flotation underflow	33.76	62.66	1.99
feldspar circuit, flotation feed	37.27	56.30	6.03
feldspar circuit, flotation overflow	9.89	81.35	8.49
feldspar circuit, flotation underflow	89.54	7.86	2.14

Results from the analysis of flotation chemicals for various process samples are presented in Table II. Unfortunately, samples from the mica and feldspar circuits were not taken simultaneously. The analysed content of organic carbon can be converted to the chemical content knowing the percentage of organic carbon present in the chemical. In addition, we must take into account the impurity organic carbon on the surfaces, such as oils and native organic carbon. This is referred to as "0-carbon" and is subtracted from the original organic carbon contents. Since the sample of water separation overflow of the mica circuit represents the feed sample without chemicals, its organic carbon content can be used as 0-carbon and, consequently, subtracted from the chemical contents of the flotation samples.

While the content of chemicals in the flotation overflow of the mica circuit is by far the highest of all samples, the amount of chemical adsorbed on flotation underflow is very low. This finding revealed that a good selectivity of flotation chemicals is obtained in the flotation of mica. The result also confirmed that mica has the ability to

adsorb large amounts of chemicals, which is not surprising considering the large surface area of mica.

Table II: Analysed contents of flotation chemicals in process samples.

Sample	Content of organic carbon (g/t)	Content of flotation chemicals (g/t)
mica circuit, water separation overflow	14.2	0
mica circuit, flotation feed	84.6	96.4
mica circuit, flotation overflow	766	1030
mica circuit, flotation underflow	22.7	11.6
feldspar circuit, flotation feed	161	201
feldspar circuit, flotation overflow	284	370
feldspar circuit, flotation underflow	56.4	57.8

A similar analysis of feldspar flotation showed a lower selectivity of chemical, which suggests a competition for the amine collector when the minerals share the same solution. It is of interest, therefore, to determine the adsorbed amounts of chemicals on particular minerals and study competitive adsorption under various conditions. Before this, we further calculated the mass balance of flotation chemicals in the process. Tables III and IV present back-calculated and analysed chemical dosages for the mica and feldspar circuits. Such calculations validate the direct analysis of the flotation chemicals. Accordingly, the total amount of chemical in the flotation feed, overflow, and underflow is calculated using mass flow data.

Table III: Mass balance of mica circuit.

Sample	Mass flow (t/h)	Chemical content (g/t)	Amount of chemical (kg/h)
Flotation feed	15.1	96.4	1.46
Flotation overflow	1.4	1030	1.44
Flotation underflow	13.7	11.6	0.16
Calculated chemical dosage		106	1.60

Table IV: Mass balance of feldspar circuit.

Sample	Mass flow (t/h)	Chemical content (g/t)	Amount of chemical (kg/h)
Flotation feed	13.4	201	2.69
Flotation overflow	7.1	370	2.62
Flotation underflow	6.3	57.8	0.36
Calculated chemical dosage		223	2.99

In the mica circuit, the calculated chemical dosage was 1.60 kg/h and this agrees well with the analysed dosage of 1.46 kg/h. Furthermore, the analysed amount of chemical (kg/h) is approximately the same as the actual chemical dosage in the process. Similarly, in the feldspar circuit, the calculated and analysed dosages agreed well with each other, 2.99 kg/h and 2.69 kg/h, respectively.

#### *Distribution of chemicals on different minerals by using mathematical method*

Using the equations presented earlier, the values for adsorption parameters  $J$  in feldspar flotation were 28 g/t (quartz), 234 g/t (feldspar) and 1,533 g/t (mica). The



proportion of chemicals adsorbed on different minerals in various process samples is further calculated and shown in Table V.

Table V: Distribution of chemicals on quartz, feldspar, and mica in the feldspar circuit.

	Percentage of chemical in quartz (% wt)	Percentage of chemical in feldspar (% wt)	Percentage of chemical in mica (% wt)
Flotation feed	4.4	56	39
Flotation overflow	0.8	59	40
Flotation underflow	33	24	43

In the flotation feed, the percentage of chemical on feldspar was higher than on mica, 56% compared to 39%, although the adsorption parameter for mica is almost an order of magnitude greater. This is due to fact that the flotation feed contains significantly more feldspar than mica. The remaining proportion of chemical in quartz was fairly low, 4%. Practically identical results were obtained for the flotation feed and the flotation overflow regarding the percentage of chemical in mica and feldspar, which indicates similar flotation behaviour of these two minerals in the prevailing process environment. On the contrary, the distribution of flotation chemical suggests a reasonable good selectivity between quartz and feldspar.

A careful mineral analysis is an essential prerequisite for obtaining reliable results with this mathematical method. The method is far more tolerant of minor errors in chemical contents or mass flow values. In the presence of minerals with a great surface area, like mica, the calculation could be carried out more accurately by using surface areas instead of masses.

#### *Competitive adsorption experiments*

First, basic adsorption tests were conducted with quartz-feldspar ore and amine to confirm that the distribution of amine between the different compartments was uniform. Samples were taken from all three compartments and analysed with the combustion technique, standard deviation of amine contents being max  $\pm 4\%$ . After these promising results, experiments were carried out with pure minerals.

Apparently, when similar amounts of minerals are present, mica adsorbs a major part of the chemical, thus making it difficult to study the competitive adsorption of amine between quartz and feldspar. Therefore, only quartz and feldspar were chosen for the experiments. The analysed contents of flotation chemicals on quartz and feldspar under various conditions are given in Table VI.

Table VI: Competitive adsorption experiments with quartz-feldspar system.

Water	HF 40% (mg/l)	Conditioning time with HF (min)	Adsorption time	Amine content on quartz (g/t)	Amine content on feldspar (g/t)
Contains NaCl	2.3	0	5 min	115	99.2
Contains NaCl	2.3	0	10 min	124	138
Contains NaCl	2.3	0	1 h	77.1	248
Contains NaCl	2.3	0	5 h	2.9	328
Contains NaCl	2.3	0	24 h	23.6	461
Contains NaCl	0	0	5 h	276	206
Contains NaCl	2.3	10	10 min	128	140
Ultra-pure	2.3	0	1 h	34.4	122

The adsorption tests were carried out with both ultra-pure water (Barnstead Nanopure) and NaCl containing water (4.3 g/l). The presence of NaCl seems to increase the coverage of amine on quartz, while the coverage on feldspar decreases. This indicates that electrolytes, like NaCl, influence the nature of the amine adsorption.

The effect of adsorption time on the coverage of amine in quartz and feldspar is shown in Figure 1, where values of amine contents are plotted as a function of various adsorption times.

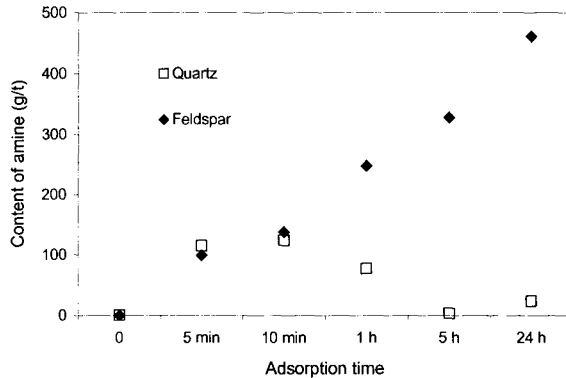


Figure 1: Contents of amine on quartz and feldspar at different adsorption times in the presence of HF.

The contents of amine on quartz and feldspar after 5 min adsorption was high and almost identical, which indicates that the adsorption rate is initially fast and identical on both minerals. The influence of hydrofluoric acid became significant after an adsorption time of 10 min. However, the time for attaining equilibrium in the system, that is the time at which the adsorbed amounts on minerals reaches equilibrium, was several hours. Even the adsorption time of 5 h did not provide maximum amine coverage on feldspar. Unfortunately, the adsorption rate in the experimental system is slower than that prevailing in the actual conditioning stage and, hence, only relative conclusions can be drawn. On the other hand, this experimental arrangement enables detailed study of fast adsorption processes.

It is well known in practise that hydrofluoric acid (HF) activates feldspar and suppresses quartz flotation. However, the basis for this action is not fully understood. Bolin reported that the addition of HF lowers the zeta potential of the feldspar surfaces and has almost no effect on the zeta potential of quartz surfaces (Bolin, 1983). The present results suggest that at least part of this activator-depressant action of HF is due to changes in the amine coverages on the surfaces of quartz and feldspar. As a consequence, the feldspar surface is assumed to become more hydrophobic, while the quartz surface is rendered more hydrophilic. However, the mechanism of selective amine adsorption in the presence of HF remains unknown. The influence of HF addition was confirmed with 5 h test carried out in the absence of HF. In that case, the content of amine was even higher on quartz than on feldspar.

Normally experiments were conducted by adding HF and amine simultaneously. One experiment was carried out where quartz and feldspar were conditioned intensively for 10 min in the HF solution prior to amine adsorption. Nevertheless, the contents of amine on quartz and feldspar were similar to those obtained without conditioning. This indicates that fluoride anions present on the mineral surfaces prior to amine addition do not have an influence on amine adsorption.

### **Conclusions**

The major conclusions of the present work are described below.

The combustion method developed was demonstrated to be a suitable tool for analysing low contents of flotation chemicals in process samples. The analysis is fast and the detection limit was found to be approximately 10 g/t. However, organic impurities on mineral surfaces decrease the sensitivity of the method.

Using a mathematical method, it is possible to determine the flotation chemicals adsorbed on single minerals by combining process data with the analysis of the chemical and mineralogical composition of the various flotation products. This method requires a careful mineral analysis.

Competitive adsorption was examined in laboratory tests with a multi-mineral system. A specially-designed apparatus enabled adsorption kinetics studies at various pulp densities and solution compositions.

The competitive adsorption of amine favoured feldspar over quartz. This was observed for process samples by using a mathematical method and was confirmed by adsorption studies with the quartz-feldspar system. The selectivity between quartz and feldspar of amine adsorption was attributed to the influence of hydrofluoric acid.

### **References**

- Bolin, N.J., 1983. A study of feldspar flotation. *Erzmetall*. 36, 427-432.
- Pugh, R.J. and Husby, K., 1986. Quantitative Determination of Collector Adsorbed on Fluorite, Galena and Quartz Particles by Selective Oxidation Surface Analysis. *Int. J. Miner. Process.* 18, 263-275.
- Stén, P.M., Miettinen, M.S., Bäckman, S. and Leppinen, J.O., 2000. Determination of chemicals bound to mineral surfaces in flotation processes. *Minerals Engineering*. Submitted for publication.

## AZINE COMPOUNDS APPLICATION IN SEPARATION OF POLYMETALLIC SULFIDE CONCENTRATES

T.I. Yushina, A.A. Abramov

Mineral Processing Department, Moscow State Mining University, Moscow, Russia

### Abstract

The rational choice of flotation reagents is one of the main facilities for selective mineral separation. As a result of investigation concerning flotation, electrochemical, FT-IR and electronic spectroscopy and the other methods it has been established that dyes of azine group can be used as an additional efficient depressor for copper sulfides in lead-copper concentrates separation with cyanide.

Efficiency of azine compounds is conditioned by their selective interaction with copper sulfide surfaces. Nigrosine doesn't adsorb on galena and doesn't change its surface properties.

The mechanism of depressing action of azine compounds is caused by their chemisorption on the copper sulfides surfaces through the coordination mechanism with formation of hard-to solve hydrophilic compounds. At nigrosine presence the leaching of copper cations by cyanide is slowed down and "copper-cyanide" optimal ratio in the pulp is supported at the smallest cyanide concentration.

The results of verification of laboratory finding at pilot-scale conditions have proved the efficiency of nigrosine use in separation of lead-copper concentrates. It allows to increase in copper and lead recoveries to their concentrates by 1.5% and copper concentrates quality by 0.5±0.7%, to decrease the consumption of toxic cyanide by 50÷70% and reduce the dissolved metals losses with thickener overflow, to improve ecological conditions in the plant region.

*Keywords: azine, nigrosine, nucleophilic reagents, copper, lead, selective separation, leaching*

### Introduction

The analysis of modern reagent regimes condition of lead-copper concentrates selective flotation testifies to reserves their more efficient use both at the expense of recovery of metals and of use of low-toxic selective reagents-modifiers allowing to replace sodium cyanide partially or completely having raised thus ecological cleanliness of the process.

The rational choice of flotation reagents is one of the main control facilities of selective mineral separation, therefore steadfast attention is given recently to questions of selective reagents collection and finding out of their action mechanism. The available representation in this area has received a new explanation due to attraction of coordination compounds chemistry laws.

At the present time of flotation theory development, nucleophilic reagents chemisorption on mineral surfaces in general form is considered as a process of mixed coordinated-type surface compounds formation, proceeding on donor-acceptor (acid-basic) mechanism (Bogdanov et al., 1990). The role of acid Lewis's adsorption centers are performed by partially charged metals cations located on mineral surfaces, which are not saturated coordinately relative to dispersed environment. The role of solidophilic functional centers of nucleophilic reagents is performed by steric

accessible atoms or groups characterized with excessive density of electronic charge. Chemisorbed flotation reagents form internal coordinational sphere of metal-complexing agent on mineral surface equally to crystal lattice anions.

Modern representations concerning coordination mechanism of flotation reagents adsorption are in accordance with principle of hard and soft Pirson's acids and bases and concept of characteristic nuclear groups (CNG). Taking into consideration this mechanism the intensification action on depression of copper sulfides during flotation may be connected to the presence in the reagent structure of electron-donating nitrogen-containing CNG as active solidophilic agents. For providing necessary hydrophobic degree, a reagent should contain appropriate groups (Ryaboi, 1982).

From among these compounds water-soluble nitrogen, concerning to a group of azine dye was chosen as rather cheap, little toxic and produced in industrial scales reagent. Nigrosine isn't individual compound (Stepanov, 1984).

The intermolecular polarisation analysis of nigrosine molecules electronic density has shown that structure of nigrosine-entering compounds and steric accessibility N- and O- donor atoms correspond with solidophilic activity condition of characteristic atomic dye groups: -N= groups of heteroaromatic cycle, imido -NH- groups of phenylamine fragments and sulpho -SO<sub>3</sub>- groups. The preliminary laboratory tests have confirmed rather high efficiency of nigrosine application in selective lead and copper sulfide flotation process (Abramov et al., 1990).

### **Experimental results and discussion**

Nigrosine action study on flotation of sulfide minerals (galena, chalcopyrite and chalcocite) has been carried out by frothless flotation method on powders by a size of - 125 + 44 μm.

With realization of experiences the dependencies of minerals floatabilities on the consumption of the collector butyl potassium xanthate (BPX), nigrosine, sodium cyanide and pH values of a mineral suspension liquid phase were investigated.

The results of conducted researches have shown that copper sulfides depression grows with the increase of the nigrosine consumption and depends on the collector concentration and the medium pH value (Figure 1). Chalcopyrite flotation is depressed most efficiently while galena is depressed insignificantly, down to the value of 15÷20 mg/l nigrosine concentration in solution. The further increase of nigrosine concentration is lowering efficient because the increase of galena recovery into cell product is observed and the process selectivity is broken.

The study of nigrosine attachment firmness on sulfide mineral surfaces and its influence on the subsequent adsorption activity of the collector tests were carried out with a changed sequence of reagents feeding. Results of these researches, which have been conducted within pH = 7÷9 region, where the copper sulfides greatest depression by nigrosine is obtained, have shown, that with increase of the dye concentration in solution sulfides recovery in cell product, especially appreciable for chalcopyrite and chalcocite, raises. With 20 mg/l nigrosine concentration minerals depression percent makes: chalcopyrite = 80÷85%, chalcocite = 70÷75%, galena = 7÷9%. Flotation research of "mineral-xanthate-nigrosine-cyanide" system has shown that copper mineral treatment with nigrosine provides the same results of

depression by cyanide as well as in case of copper sulfide flotation depression by single sodium cyanide but twice of greater concentration.

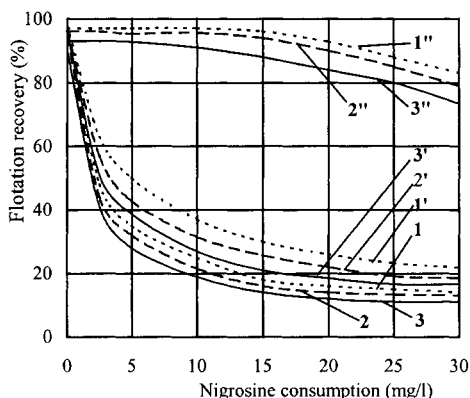


Figure 1: Flotation (with 5 mg/l BPX) of: 1-3: chalcopyrite; 1'-3' chalcocite 1''-3'': galena. Influence of nigrosine consumption and of pH: 1, 1'': pH=7.5; 2, 2'': pH = 9; 3, 3', 3'': pH = 10.

The study of quantitative nigrosine sorption laws and exchange sorption between collector and dye ions on lead and copper sulfides surfaces was carried out using spectrophotometric method. It has been established that nigrosine adsorption increases in a row:  $PbS \ll Cu_2S < CuFeS_2$ . At mineral treatment with nigrosine solution till 100 mg/l concentration, complete rectification of isotherms is not observed (see Figure 2a). Maximum nigrosine adsorption on chalcopyrite and chalcocite surfaces is observed in neutral and slightly alkaline solutions; this fact is quite in accordance with results of monomineral suspension flotation researches. It has been established that even insignificant sorbed nigrosine amount evokes essential change of copper minerals surfaces condition, promoting to sharp collector adsorption reduction in a range of nigrosine concentrations up to 20 mg/l. With increase of nigrosine amount adsorbed by surface, the further decrease of xanthate adsorption on minerals is observed (Figure 2b). Reduction of BPX sorption on minerals depending on nigrosine concentration has made (in % from BPX sorption by clean surface): galena =  $9.0 \div 9.5\%$ , chalcopyrite =  $60 \div 63\%$ , chalcocite =  $40 \div 42\%$ .

The researches, carried out on lead and copper sulfides previously processed with BPX of various concentrations, have shown that nigrosine displays desorbed properties in relation to collector sorbed on mineral surface, especially appreciable in relation to chalcopyrite and chalcocite. The xanthate replacement by nigrosine from chalcopyrite surface almost in 7 times (and from chalcocite surface in 4.5 times) is higher than from galena surface.

As a result of electrochemical researches, it has been established that, with nigrosine introduction into "mineral-water" system, the cathode shift of chalcopyrite electrode potential reaching the greatest value ( $\Delta\phi_{NG}^{CuFeS_2} = -25$  mV) in slightly alkaline media (pH =  $7.5 \div 9$ ) is observed; the value of galena electrode potential thus remains

practically constant ( $\Delta\varphi_{\text{NG}}^{\text{PbS}} = -0.5 \text{ mV} \div -1.5 \text{ mV}$ ). The observable change of chalcopyrite electrode potential in cathode area reaching maximum significance's first five minutes after nigrosine feeding, is irreversible and allows to consider the reagent as a donor of electrons with its adsorption on copper sulfides, that is as a nucleophilic agent. The skip value of the chalcopyrite electrode potential ( $\Delta\varphi_{\text{NG}}^{\text{CuFeS}_2} = 20 \div 25 \text{ mV}$ ) corresponds to significance's noticed with chemisorbed interaction without covalent bonds formation.

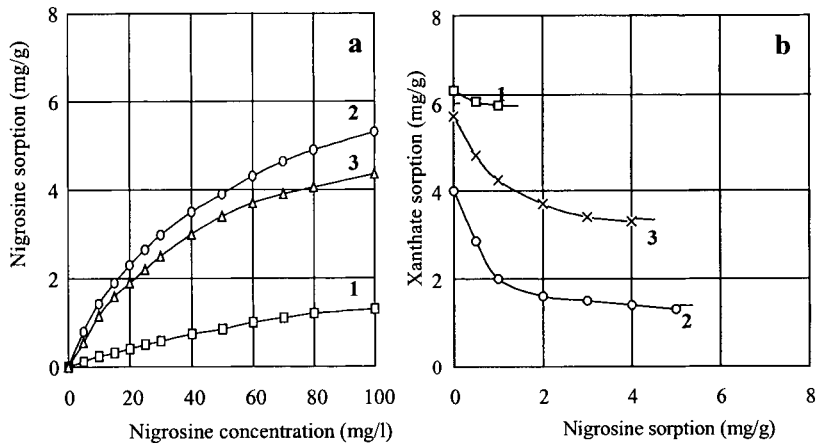


Figure 2: Isotherms of reagent adsorption at pH=8 on: 1: galena; 2: chalcopyrite; 3: chalcocite.  
 a: nigrosine concentration influence on its sorption on minerals;  
 b: influence of sulphide minerals previous treatment with nigrosine of 30 mg/l BPX sorption.

For estimation of mineral surface wettability change after treatment with nigrosine the researches on determination of air bubble detaching force from mineral electrode were carried out by attachment indemnification with elevating force of a float with bubble. All the researches on mineral wettability studies were carried out in a borate buffer solution (pH = 9.18). Wettability change of researched mineral surfaces, depending on collector concentration, was determine first. The least surface wettability was observed at 150 mg/l collector concentration for chalcopyrite and since 50 mg/l for galena (Figure 3, curves 1). The values of stationary electrode potentials of researched minerals thus are shifted in negative area, what confirms xanthate sorption (Figure 3, curves 2).

At various nigrosine concentrations dosing in "sulfide mineral - collector" system, significant reduction of air bubble detaching force value from surfaces of chalcopyrite electrode was observed (Figure 3, curves 3). For the galena electrode in the researched dye concentrations range (0÷20 mg/l) essential changes of detaching force values in comparison with these ones without nigrosine wasn't observed at xanthate 50 mg/l concentration. The restrictions in nigrosine solutions concentrations (<20 mg/l) were carried out by visual observation difficulties of processes of air bubble placing and detaching on mineral electrode surface in consequence of deep black-blue color of dye solutions having concentrations more than 20 mg/l.

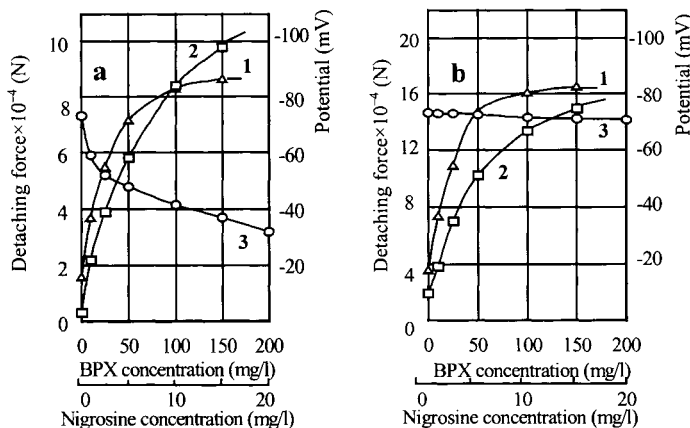


Figure 3: Influence of xanthate (1) and nigrosine (3) concentrations on change of air bubble detaching force from chalcopyrite (a), galena (b) surfaces and their electrode potentials (2) at 50 mg/l xanthate concentration.

The received results have confirmed our assumption about nigrosine adsorption on surfaces of copper sulfides, accompanying with formation of difficulty soluble hydrophilic compounds.

Products composition researches of sorption interaction between nigrosine and chalcopyrite and galena surfaces were carried out using FT-IR spectroscopy method. The received FT-IR spectra of nigrosine surface compounds on chalcopyrite are reproduced well in all the range of pH values conforming to conditions of reagent intensive adsorption on copper minerals without and after treatment them with xanthate (Yushina and Abramov, 1996).

The appearance on the spectrum of chalcopyrite treated with nigrosine of an intensive  $470 \text{ cm}^{-1}$  absorption bend (conforming to metal-nitrogen valence oscillations frequency), absorption bend shifting (conforming to valence oscillations of C-N- and C=N- groups and  $\text{SO}_2^-$  groups in more low-frequency spectrum area on  $40 \div 85 \text{ cm}^{-1}$ ), and pendulum and deformation oscillation of -NH- groups (in more high-frequency area on  $50 \div 130 \text{ cm}^{-1}$ ) testify to a metal-nitrogen coordination bond. The presence of several characteristic absorption bends concerning -N-H- group oscillations indicates existence of a number of these groups' conditions differing by interaction (hydrogen bonds) and orientation. The absence of the characteristic for dixanthogen ( $1,265 \text{ cm}^{-1}$ ) bend on the spectrum of chalcopyrite treated sequentially with BPX and nigrosine testifies about dixanthogen desorption. The appearance of the -OH groups valence oscillations bend ( $3,472 \text{ cm}^{-1}$ ) indicates the presence of coordinated-bound water on mineral surface (Nakamoto, 1986).

The electronic spectra analysis of combined nigrosine solutions with conforming lead, copper and iron soluble salts and BPX has shown absence of chemical interaction in systems "nigrosine-lead nitrate" and "nigrosine-BPX". At Fe(III) salts dosing into nigrosine solutions instant change of color from blue-black to gray-yellow occurs, the solution becomes colloidal and black amorphous precipitate formation is observed. The filtrate spectrum points to nigrosine absence in the solution, i.e.



nigosine interactions with Fe (III) cations with formation of highly hydrated multinuclear nigosine-aquacomplexes of iron. The X-ray research of precipitate has confirmed this assumption.

After mixing nigosine solutions and copper sulfate the deepening of solution color is observed: depending on the spectrum of component-concentrations ratio significant bathochromatic shift of nigosine characteristic maximum ( $\lambda_{\max} = 580$  nm on  $15 \div 40$  nm) is observed. Hyperchromatic shift on  $10 \div 20\%$  to the side of optical density increasing and absorption band geometric area increasing are also observed at comparison with nigosine spectra of similar concentrations.

Proceeding from the complexing theory of organic heterocyclic compounds with metals, it is possible to make a conclusion about the chelate copper-nigosine complex formation at the expense of covalent-coordination binding of a copper cation with nitrogen and oxygen atoms of two nigosine molecules with stable six-membered cycles formation.

Analyzing the researches results of FT-IR, electronic and X-rays spectroscopy, it is possible to make a conclusion that nigosine in water solutions interacts as with a clean chalcopyrite surface as with the mineral previously treated with collector. In this case chemisorbed nigosine layer formation coordinated by cations of mineral surface and physical co-adsorbed nigosine molecules ensuring sufficient surface hydrophilicity as a whole by coordinate-bound water with conforming CNG not participating in coordination is observed. In the case of consecutive chalcopyrite surface treatment with the collector and nigosine it has to be observed the followings:

- the last one desorbs dixanthogen from the sorption layer changing the collector sorption forms ratio; and also interacting with acid Lewis's sorption centers of mineral surface free from the collector (a nigosine ion may be coordinated simultaneously at least by two metal cations) "blocks" the collector action increasing total surface hydrophilicity;
- the flat structure and structural complementation of dye molecules also provides physical co-adsorption at the expense of hydrogen bonds and weak intermolecular interactions of nigosine molecules as free as in the form of volumetric complexes with metals from the solution (back-directed layer);
- this also promotes surface hydration increase and mineral depression (Yushina and Abramov, 1996).

Thus, on the basis of chemical, physico-chemical and flotation researches and in view of the fact that nigosine adsorbs in insignificant quantities (outside sensitivity of FT-IR, roentgenophase and differential-thermal analysis methods), it is possible to present the mechanism of nigosine intensifying action on copper sulfide depression as follows:

- nigosine chemisorption has an electron donating, or nucleophilic, character in relation to copper surface;
- nigosine attachment has a specific adsorption character, which is realized as at the expense of coordination dative  $\pi$ -linkage of nitrogen atoms including in chromophore  $\pi$ -system of connected bonds, as at the expense of covalent-coordination chelate linkage between nitrogen atoms of the imido group -NH- of

oxygen of salt-forming sulpho-group  $-SO_3^-$ , taking place in the ortho-condition on the other phenylamine fragments of the dye and acid Lewis's sorption centers of minerals.

As a result of this interaction difficultly soluble stable hydrophilic compounds are formed "armoring" surface and slowing down leaching process of copper cations by cyanide in pulp. It results in sharp reduction of the sodium cyanide consumption, intensifies depression of copper minerals and provides the optimal "copper-cyanide" ratio in liquid phase of flotation pulp (Yushina and Abramov, 1996).

On the basis of the received results of regularities and azine group reagents action researches with lead and copper sulfides selective flotation, the reagent regime of their selection using nigrosine was developed and confirmed under laboratory conditions at industrial lead-copper concentrates.

The results of laboratory researches at industrial concentrates have shown, that the increase of collective lead-copper concentrates selection process indexes with complex polymetal ores processing can be achieved by selective flotation reagent regime perfection based on nigrosine using as a copper sulfides additional depressor. It has been established that the lead-copper concentrate pre-treatment by an organic reagent-complexing agent of the azine group allows raising the efficiency of chalcopyrite depression at the expense of mineral surface hydrophilization. It occurs as a result of difficultly soluble compounds formation of crystalline lattice copper and iron cations with the reagent.

Thus "armoring" of chalcopyrite surface by insoluble compounds reduces copper cations leaching velocity in pulp, what results in sodium cyanide consumption reduction, and surface hydrophilization is provided at the expense of presence in organic depressor structure the appropriate atomic groups.

Advantages of the developed regime are preservation of basic, accepted at plant selection technology of collective lead-copper concentrates; an opportunity of nigrosine feeding to the concentrate preparation cycle; the small nigrosine consumption, what allows to use the developed regime at the plant with insignificant capital expenses.

On the basis of laboratory researches positive results at plant were obtained: the pilot-scale tests of the developed method of lead-copper concentrates selection have shown that the bulk concentrate treatment by nigrosine, before the rough lead flotation, allows a gain of lead and copper concentration recovery of 1.5% with copper quality increase of 0.5÷0.7%. Corresponding reduction the sodium cyanide consumption of 50÷70% has been observed (Abramov et al., 1990).

Thus it is necessary to take into account that the developed regime allows reducing dissolved copper, gold and silver losses with copper thickener overflows sharply (Table I).

Table I: Ion composition of the liquid phase in the scavenging flotation operation.

Regime	Ion composition (mg/l)				
	$CN^-_{fr}$	$CNS^-$	Au	Ag	Cu
with NaCN use	90	80÷120	0.2÷0.6	6÷10	210÷250
with nigrosine and NaCN use	10÷20	30÷40	0.03	0.8÷1	50÷70

## Conclusions

It has been established that as an additional depressor of primary and secondary copper sulfides with lead-copper concentrates cyanide selection it is necessary to use reagents of the azine dyes group. Azine compounds interact with copper sulfide surfaces on the coordination mechanism. Nigrosine doesn't adsorb on galena and doesn't change its surface properties.

The depression action of azine compounds is caused by the following processes:

- nigrosine chemisorption on copper sulfide surfaces on coordination mechanism with difficulty soluble hydrophilic compounds formation;
- partial dixanthogen desorption, causing collector sorption forms ratio change and mineral surface hydrophoby reduction.

At nigrosine presence the copper cations leaching processes by cyanide are slowed down and "copper-cyanide" optimal ratio in flotation pulp liquid phase is supported.

The developed regime of lead-copper concentration separation using nigrosine has been tested under pilot-scale conditions at plant. The test results have shown an opportunity of metals recoveries increase in the same concentrates of 1.5% with copper concentrate quality improvement of 0.5÷0.7% and high toxic sodium cyanide of 50÷70%. They also will allow reducing dissolved metals losses in the copper thickener overflow, to raise ecological cleanliness of processes and improve ecological conditions in the plant action area.

## References

- Abramov, A.A., Yushina T.I., et.al., 1990. Increasing of copper-lead concentrate selection efficiency using an additional copper sulfides depressor (in Russian). In: Obogashchenie mineralnogo syria. Moscow Mining Inst., Moscow, 42-46.
- Bogdanov, O.S., Maksimov, I.I., Podnek, A.K., et.al., 1990. Theory and technology of ores flotation (in Russian). Nedra, Moscow.
- Nakamoto, K., 1986. Infrared and Raman spectra of inorganic and coordination compounds. New-York.
- Ryaboi, V.I., 1982. Coordination mechanism concepts development of flotation reagents action (in Russian). In: Physical and chemical bases of mineral raw treatment. Nedra, Moscow, 62-69.
- Stepanov, V.I., 1984. Introduction in organic dyes theory and technology (in Russian). Khimia, Moscow.
- Yushina, T.I., Abramov, A.A., 1996. The investigation of mechanism of azine compounds interaction with surface of sulfide minerals (in Russian). In: Sovershenstvovanie tehnologii obogashchenia kompleksnih poleznih iskopaemih. Moscow State Mining Univ., Moscow, 22-28.

## ON CERTAIN ASPECTS CONTROLLING SELECTIVITY OF NON-SULFIDE MINERAL FLOTATION

A.V. Kurkov, V.V. Shatalov, I.V. Pastukhova

All-Russian Research Institute of Chemical Technology 33,  
Kashirskoe Shosse, Moscow 115230, Russia

### Abstract

The mineral/flotation reagent interaction can be considered as an arbitrary equilibrated acid-basic and donor-acceptor process. By changing the energy of these constituents by various collectors, one can effectuate the maximum difference in the adhesive ability on the surface of a valuable mineral and barren rock. Still, the potential of altering the structure of only one collector is rather limited and expensive. Therefore, the method of raising selectivity by reagents' composition seems to be simpler and more feasible economically. The acid-basic and donor-acceptor properties of the collector and consequently, its chemical adsorption, can be controlled with organic diphilic reagents - the reagents of secondary action (RSA), which together with the main collector form an associate with a hydrogen bond. A RSA used under conditions ensuring hydrophobic layer formation for its efficient flotation reduces the absolute value of the zeta potential, making its surface close to isoelectric state and enhancing the hydrophobic flocculation of fine particles (<15  $\mu\text{m}$ ) of the material undergoing the flotation. The RSA classification is given.

Examples of practical application are presented for all above compound groups in the flotation of non-sulfide ores with various mineral compositions.

*Keywords: mineral, collector, reagents, interaction, selectivity, energy*

### Introduction

The results of numerous studies of the last decades (Abramov et al., 1982; Fuerstenau, 1995; Glembotskii, 1977; Rjaboy et al., 1977 and others) investigating the interactions of the mineral with a collector can be generalized as follows.

- The type of the mineral chemical bond and the energy of the latter determine the mechanism, strength and the character of the flotation reagent fixed on its surface. All kind of chemical bonds are involved in the interaction: ion-covalent, donor-acceptor, hydrogen and inter-molecular. Each of the above bonds makes its own contribution to the total interaction energy of all components in the flotation system. The strength of the bond between the mineral and collector is characterized by the difference of energies: one of the lower vacant molecular orbital belongs to the mineral (LVMO) and the other, higher one, occupies the collector's orbital (HOMO). The smaller this difference, the higher the strength of the surface connection.
- There are two general theories formulated regarding the interaction of collectors and minerals. The first considers the interaction as a donor-acceptor one, where the mineral, as the electron acceptor, forms with the collector, an electron donor that is a superficial compound with a coordination bond. The second theory

considers the interaction as an acid-basic one, where the acid role belongs to the mineral, and the base is a flotation reagent.

- As a result of the difference in the electron orbitals (EO) of the ligands, the formation of hydrogen bonds (HB) there causes re-distribution of electron densities within the bond systems of all interacting components. That leads to a compensation dependence of the lengths, charges and energies of the bonds. As follows from Pearson's principle, the theory of the ligands' mutual influence, the strongest and most selective adhesion of the reagent to the mineral, happens in the case when the reagent-mineral bond approximates the bonding in the crystalline lattice of a mineral in its main characteristics (length, energy, coordination number, etc.). It can be reached in the case when the HOMO of the reagent is the closest to the LVMO of the mineral in its energy and symmetry.

The conception of hard/soft acids and bases allows for clear differentiation of the border between sulfide and non-sulfide ores.

The non-sulfide ores are presented by class A-minerals (hard acids), whose cations have a low ionic potential, a high ionization potential and a high electronegativity. The mineral-forming metals, forming mainly ionic bonds with oxygen (Li, Be, Ca) have a basic character. When interacting with water, they have an inclination toward hydrolysis, forming a chemical bond, Me-OH. During the increase in the degree of covalence of the Me-OH bond, the strength of this bond grows, the acidic properties of oxides increase, the inclination to hydrolysis decreases, and the hydration ability, determined by donor-acceptor interaction of the oxide and water, noticeably increases. The strength of their bonding with the reagent (hard base) is conditioned by a large portion of ionic bonding and a high value for the LVMO and HOMO energy difference.

The significant contribution of the s- and p-states is conditioned by the specific structure of metal cations in the molecular orbitals of a mineral, creating prerequisites for their interaction with O-donor reagents (oxyhydril collectors).

The oxyhydril collectors, unlike the sulfohydril ones, have no vacant d- and p-orbits and cannot form a dative bond with the mineral surface. These reagents are of low selectivity.

Therefore, the search for a general approach to the solution of the task of improving selectivity in the flotation process assumes great importance.

### **Forming hypothesis on selecting the structure of the basic collector and an auxiliary reagent**

When dealing with a large number of problems, there is no need to have precise data; it would be enough to know only the course of their change. In this case, one uses a number of simplified approaches with models that make it easy to generalize the experimental and theoretical materials, as well as the prognostication of general relationships.

The energy of the collector and material surface interaction is a function of many factors. Still, relying on the previously formulated general principles regards the mineral and collector interaction. The latter can be generally presented by the following scheme (Figure 1).

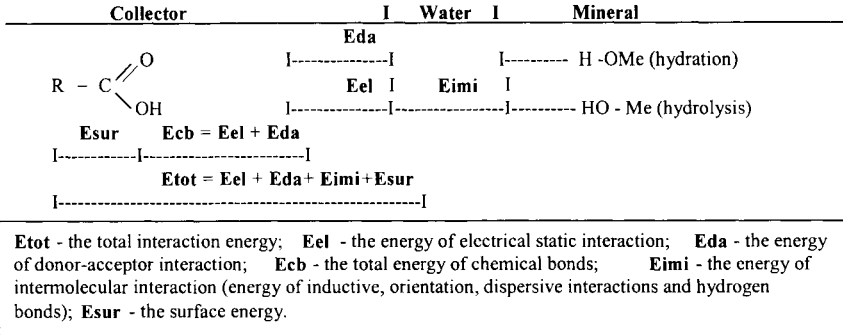


Figure 1: Energy constituents of the mineral and collector interaction.

The collector anion is responsible for Eel. Its protonized form (–OH–group), for the HC formation and the collector participation in the dimerization process, the double-bond oxygen atom, for Eda, and the hydrocarbon radical, for Ecb. It means, that the polar portion of the molecule determines the intensity of the chemical and intermolecular interaction, and the non-polar is responsible for its surface properties, thus being the instrument of the influence on Eel.

Changing the energy of these constituents by altering the collector structure, one can ensure the maximum difference in its fixing strength on the mineral surface of a valuable species and barren rock (Figure 2). The introduction of substitutes producing I- and M-effects (X = Cl, F, COOH, OH, NO2) leads to the reduction both of Eel and Eda. Such collectors are less active flotation-wise but more selective. Increasing the hydrocarbon radical length does not alter Eel but increases Eda. The use of alkyl phosphates and alkyl phosphonates reduces Eel but increases Eda, in comparison with the carboxylic ones.

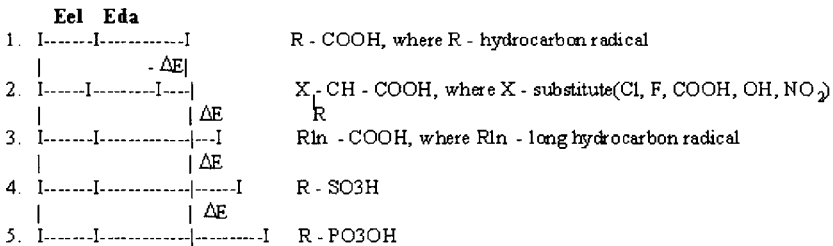


Figure 2: Principle scheme of the interaction energy change in the non-sulfide mineral with a collector.

The interaction here of the mineral and collector has to be considered from the point of view of the singularity of the acid-basic and donor-acceptor interactions. The role of each is determined most of all by electron properties of cation-forming atoms of the minerals, corresponding to their place in Mendeleev’s Table.

Eel corresponds to the part of the chemisorbtional fixing of the collector by the acid-basic interaction, and Eda corresponds to the part of the fixing by the donor-acceptor interaction with a hydrated surface of the mineral. Thus, the character of the mineral

bond determines the direction in which the collector structure changes in order to improve flotation selectivity. Thus, the recovery of the minerals with cation-forming elements of groups I and II (spodumene, beryl), where the acid-basic interaction predominates, should be done with the collectors of type 1 and 2 (Figure 2). The minerals with covalent bonds Me-O predominating (cassiterite) must be recovered with type 4 and 5 collectors (Figure 2), which have reactionary centers of high electron density for the interaction, according to the donor-acceptor mechanism.

Still, considering just one single collector, it should be noted that the potential of changing its structure is rather limited and expensive. A non-sulfide flotation system has all conditions present to facilitate formation of hydrogen bonds (HB), which permits the redistribution of electron density between the interacting components (Table I).

Table I: Peculiarities of the hydrogen bond.

$XAH + BY \rightarrow XA-H \dots BY \rightarrow XA^- \dots H-BY^+ \rightarrow XA^- + H-BY^+$
HB takes place between an acceptor of XAH type, with a highly electro-negative atom A, which has a high degree of the ionic bond A-H and a high positive-effective charge on the hydrogen atom, and between a donor molecule of BY type, which has atom B, with one or more undivided electron pairs.
HB is revealed by groups XA-H, where atom X exhibits strong affinity to the electron (F, O, N).
In the linear fragment A-H...B, there occurs a total shift of the valent electron density from B to A; redistribution of electron charge effects practically all atoms in molecules BY and XAH.
In nature, HB is a variant of donor-acceptor bonding. The dipole moment in a complex with HB increases as compared with the geometrical sum of the dipole moments in isolated molecules BY and XAH.
The specifics of a hydrogen bond is related to the electron structure of the hydrogen atom (i.e. has no electron sheath, is $10^5$ times smaller than other ions, is extremely mobile, and is highly penetrable into electron sheaths of other nuclear-molecular particles).
The greater the HB energy the lower the energy necessary for originating an intermediate complex XA-HBY
HB has an additive property: the involvement of a great number of molecules into the system makes the total HB energy proximate to the energy of a chemical bond.

This presents an opportunity to alter the acid-basic and donor-acceptor properties of the basic collector, its rigidity (Pearson's principle), and the energy of collector mineral surface interaction, respectively, by using it in combination with diphilic organic compounds capable of forming associates with it through a hydrogen bond.

In accordance with their function regarding the basic flotation regiment, it would be proper to call such additive reagents *reagents of secondary action* (RSA). As a rule, under the conditions of a basic flotation regiment, the RSA is taken as a single species, possessing relatively weak collecting properties regarding the minerals to be recovered or for exhibiting their absence. Therefore, the greater the basic collector selectivity, the higher the effectiveness of the flotation ability of its associate with RSA.

The RSA can be subdivided in three groups:

- amphiphilic reagents forming hydrogen bonds both with the oxygen atom and the hydrogen atom (alcohols, hydroxyl-containing compounds);
- organic acids containing anions:  $R-COO^-$ ,  $R-SO_3^-$ ,  $R-OSO_3^-$ ,  $R-PO_3^{2-}$ ;
- organic neutral substances containing groups: C=O, S=O, P=O (ethers of carbonic and phosphonic acids; amides of carbonic, phosphoric and sulfoacids).

A simplified scheme using collector compositions given in Figure 3 shows the contribution of energy given by every reagent group under consideration, i.e. the alteration of fixing forms on the mineral surface:



Figure 3: Simplified scheme of changes in interaction energy regarding a mineral with the collector compositions and RSA.

The use of an acidic RSA will stabilize the basic collector anion, reducing the collector nucleophilicity and hardness. With the increasing force of the RSA, changing accordingly to the growth of the RSA acidity, the tendency toward a donor-acceptor mechanism increases, and the tendency of the interaction of the mineral with the basic collector in the ionic bonding mechanism decreases. In other words, the introduction of RSA into a flotation system with an acidic character reduces its electrostatic energy component and increases the donor-acceptor one; i.e. the part of the physically adsorbed collector increases, and its chemoadsorbed fixing decreases (Figure 3).

Used as an additional reagent, a neutral organic compound of high basicity RP(O)R<sub>2</sub>, containing a long hydrocarbon radical, e.g., amides of alkyl phosphoric acid (R=NR<sub>2</sub>) or alkyl phosphonates, would increase the hardness and nucleophilicity of the basic collector. Therefore, it could be expected that Eda increases and Eel remains unchanged. In this case, the strength of the superficial compound should be higher than that of the case of a dimer (Figure 3).

The long-chain aliphatic alcohols and their analogs (oxyethylated derivatives of acids, amines, alcohols, phenols, amides, etc.) have protodonor capability (not very high) and electrodonor capability. Their use should be accompanied by a slight decrease in Eel and a substantial growth of Eda.

The study of a large number of flotation systems with non-sulfide minerals has shown that the use of RSA under conditions facilitating the formation of a hydrophobic layer for its efficient flotation greatly reduces the absolute value of the zeta potential, making the surface state proximate to isoelectric. This also boosts the hydrophobic flocculation of fine particles (<15 μm) in the material undergoing flotation (Kurkov, 1999).

The suggested performance mechanism of the reagents' combination allows for purposefully choosing the structure of both the collector and RSA, and for efficiently controlling the flotation process, considering the improved selectivity. The development of a selective regiment in the flotation of non-sulfide minerals is therefore increased to ensure maximum correspondence of the electron structure with the collector and mineral. This is due to a preliminary treatment of the mineral surface



with modifiers – the proper choice for the most effective basic collector for control of its fixation energy on the mineral by RSA.

### **Application of RSA in the selective flotation of non-sulfide ores**

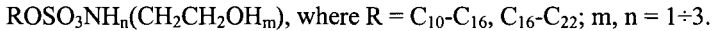
#### *RSA used to improve selectivity and effectiveness of flotation*

In order to improve the efficiency of flotation processes for tin-containing rare metals, copper-molybdenum and fluorite ores, we were the first to suggest using high aliphatic isoalcohols of various fractions (C<sub>8</sub>-C<sub>22</sub>), combined with a basic collector belonging to the class of hydroxamic, fatty acids, xanthates, dithiophosphates, sulphosuccinamates, etc. (Pol'kin et al., 1976, 1977, 1979; Kurkov et al., 1977, 1982). The high flotation efficiency of the suggested combinations has been verified by the work of other investigators (Filippov et al., 1995; Filippov and Houot, 1997). The proposed class of RSA improves the flotation process selectivity, raises the recovery of the mineral in the flotation, cuts down the consumption of the basic collector and flotation time, and improves the froth quality.

The assortment of flotation reagents can be widened on the basis of inexpensive commercial production.

New classes of compounds have been suggested for that purpose: amine salts of alkyl sulphates (ASAS) and alkyl benzene sulphonic acids (ASABSA) (Kurkov et al., 1990, 1995).

The general formula of ASAS follows:



The general formula of ASABSA is:



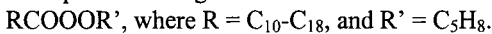
The above compounds present highly-efficient RSA, used in the flotation of cassiterite and minerals of tantalum and niobium with hydroxamic acids. They considerably improve the technological indices of these mineral flotations sharply decreasing the consumption of the basic collector and creating optimal conditions for froth formation.

The effectiveness of these RSA classes have been proved in the beneficiation schemes treating complex rare-earth metals from the Zavitinski, Etykinski and other deposits.

#### *RSA as flotation accelerators*

A rather interesting property is revealed by a number of compounds having no evident collecting properties in their combination with the basic collector. Such compounds are presented by pentaerythritol ether of tall oil from leaf wood (PETO) (Kurkov et al., 1990, 1995).

PETO corresponds to the general formula:



Introduction of some PETO into the basic flotation circuit sharply reduces the flotation time for a certain decrease of the basic collector.

Thus, the flotation of beryllium minerals from the complex of rare metals-fluorite ore from the Ermakovski deposit decreases by more than two times with better technological flotation indices. The flotation time in treating tantalum and tin minerals from the Etykinski deposit ores reduces by three times without altering the technological indices.

### *RSA for flotation under conditions of water recycling*

To increase selectivity of the flotation process with water recycling (including the selectivity of carboxyl collectors, especially under the conditions of strong mineralization of the water) we suggest application of RSA-diphilic compounds with a long hydrocarbon radical and groups with higher electron density in the molecule, i.e. N-methyl amides of alkyl phosphoric acids and ethers of methyl phosphonic acid (Kurkov et al., 1990, 1997, 1998).

The application of small additions of these compounds, together with a basic fatty acid collector, improves the performance of the fatty acid flotation of fluorite and beryl. This completely compensates for the depressing effect of the recycling water, allowing for attainment of even higher technological results than with only a basic collector in fresh water.

### **Conclusions**

To conclude, on the basis of the results obtained in the studies carried out, we introduce the concept of reagents of secondary action (RSA). These are diphilic organic compounds capable of changing the acid-basic and donor-acceptor properties of the basic collector on the surface of a mineral. Accordingly, they are capable of changing the interaction energy of the collector, its hardness and the relationship of the forms it fixes on the mineral surface, which are due to the formation of associates with the basic collector by means of hydrogen bonds. It has been shown that the research and application of RSA are one of the most effective resources for the improvement of the flotation process at present. Using RSA in combination with the basic collector can supersede the expensive procedure of creating a selective collector for the solution of multiple tasks in non-sulfide ore beneficiation by flotation. Small quantities of RSA, used at certain stages in the technological process, will allow for improvement of the selectivity of the flotation operations, create effective water recycling schemes, and sharply decrease the total consumption of flotation reagents and process duration.

### **References**

- Abramov, A.A., Leonov, S.B. and Sorokin, M.M., 1982. Chemistry of flotation systems. Nedra, Moscow (in Russian).
- Filippov, L.O. and Houot, R., 1997. Synergetic effects of a non ionic reagent with heteropolar collectors on the non sulphide ores flotation. Proc. XX Int. Miner. Process. Congr., Vol. 3: Flotation and other Physical-Chemical Processes. GDMB, Clausthal-Zellerfeld, Germany, 427-436.
- Filippov, L.O., Ignatkina, V.A., Shokhin, V.N. and Shaposhnikova, E.L., 1995. Application of an additional non-ionogenic collector for better selectivity in scheelite flotation regarding calcite. Tsvetnye Metally, 11, 67-70 (in Russian).
- Fuerstenau, D.W., 1995. Where we are in flotation chemistry after 70 years of research. Proc. XIX Int. Miner. Process. Congr. V. 3 - Flotation Operating Practices and Fundamentals. Littleton, Colorado, USA, 3-18.
- Glembotskii, A.V., 1977. Theoretical basis of prognostication and modification of collectors properties. Tsvetnye Metally, 9, 61-65 (in Russian).
- Kurkov, A.V., 1999. Reagents of secondary action as an instrument to raise the efficiency of non-sulphide ore flotation. II Congress of CIS Ore-Processing Countries. Abstracts. MISIS, Moscow, p. 63 (in Russian).

- Kurkov, A.V., Pol'kin, S.I. and Adamov, E.V., 1977. Flotation of cassiterite from old tail dumps of the Novosibirsk Tin Plant. *Sci.Tech.Bulletin. Tsvetnaja Metallurgija.*, 15, 9-10 (in Russian).
- Kurkov, A.V., Molodkina, I.A. and Glasunova, R.I., 1990. New reagents-collectors for flotation of non-sulphide Ores. *Issues of Nuclear Science and Engineering Series: Geology and Mining*, 2, 24-29 (in Russian).
- Kurkov, A.V., Shatalov, V.V., Molodkina, I.A., 1995. New classes of reagents for non-sulphide ores. *Proc. XIX Int. Miner. Process. Congr., Vol. 3: Flotation Operating Practices and Fundamentals.* Littelton, Colorado, USA, 259-261.
- Kurkov, A.V., Shatalov, V.V. and Glasunova, R.I., 1997. Flotation technology for high enrichment of rare metalproduction tails. - *XX Int. Miner. Process. Congr., Vol. 3: Flotation and other Physical-ChemicalProcesses.* GMDB, Clausthal-Zellerfeld, Germany, 705 - 713.
- Kurkov, A.V., Stcherbakova, S.N., Gorokhov, I.N. and Pastukhova, I.V., 1998. Phosphororgabic compounds used as additives in flotation of non-sulphide ores. *Mining Information and Analysis Bulletin*, issue, 6, 113-118 (in Russian).
- Kurkov, A.V., Vorobjev, A.D., Rudenko, B.J., Zaitsev, V.G. and Glazunova, R.I., 1982. Using asparal-F in fluorite ore flotation. *Tsvetnye Metally*, 11, 96-97 (in Russian).
- Pol'kin, S.I., Adamov, E.V. and Kurkov, A.V., 1979. Flotation technologies to recover cassiterite from slimes of complex composition. In: *Present and Future in the Development of Flotation Theory.* Nauka, Moscow, 107-115 (in Russian).
- Pol'kin, S.I., Adamov, E.V., Zarakhani, A.I. and Kurkov, A.V., 1976. Control of froth-forming in reagent IM-50 in cassiterite flotation from slime. *Science Engineering Bul. Tsvetnaja Metallurgija*, 1, 20-22 (in Russian).
- Pol'kin, S.I., Adamov, E.V., Kurkov, A.V., Vetrov, I.S and Berger, G.S., 1977. The theoretical principles of the use of organophosphoric compounds for complex processing of rare metals and tin ores. *XII Int. Miner. Process. Congr. Special Publication, Sao Paulo, Brazil*, 2, 53-72.
- Rjaboi, V.I., Bogdanov, O.S. and Zuev, V.V., 1977. Chemical adsorption of reagents on minerals as a process-forming surface compounds with coordination bond. In: *A Study on Developing New and Improving the Present Processes and Technological Schemes for Ore Beneficiation.* Mekhanobr, Leningrad, 59-89 (in Russian).

## PURIFICATION OF BRAZILIAN KAOLIN CLAY BY FLOTATION

A.B. Luz\*, I. Yildirim<sup>o</sup>, R.H. Yoon<sup>o</sup>

\*Centro da Tecnologia Mineral-CETEM, Rua 4-Quadra D-Cidade Univarsitária  
Ilha do Fundão, Rio de Janeiro, RJ, Brazil

<sup>o</sup>Center for Coal and Minerals Processing, Virginia Polytechnic Institute  
and State University, 146 Holden Hall, Blacksburg VA 24061, USA

### Abstract

A kaolin clay from northern Brazil was beneficiated by flotation using an alkylhydroxamate (R6973) as collector. Unlike tall oil fatty acids, this collector does not require activators (divalent cations) for adsorption. Approximately 90% of the particles in the clay sample were finer than 2  $\mu\text{m}$ ; therefore, it was a challenge to remove colored impurities ( $\text{TiO}_2$  and iron oxide) from the clay by flotation. It was possible, nevertheless, to reduce the  $\text{TiO}_2$  content from 1.9% by weight to approximately 1% at 70% to 76% weight recovery. In comparison, the  $\text{TiO}_2$  content was reduced to 0.8% at a 56% weight recovery by using a selective flotation process.

*Keywords: flotation, kaolin clay, hydroxamate collector, anatase, selective flocculation*

### Introduction

Kaolin clay is used extensively for paper coating and filler application, but it has to be processed to meet the industry specifications. It is also used as filler and pigment for various other materials, such as paint, rubber, plastic and resins. Some crude kaolins in northern Brazil as mined, contain colored impurities such as iron oxides and rutile/anatase ( $\text{TiO}_2$ ). The latter are stained by iron and as a result their color varies from yellow to dark brown. The kaolin beneficiation process used in that region consists usually of degritting, fractionation by centrifuge, high-gradient magnetic separation, bleaching with sodium dithionate, filtering and drying (Luz, 1998). In some kaolin clays from that region, titanium oxide minerals occur in fine fractions, lower than 2  $\mu\text{m}$ , thereby making the process difficult. According to Maynard et al. (1969), the conventional methods of classification and bleaching with sodium dithionate, markedly improve kaolin brightness by dissolving ferruginous impurities; however, it has little effect in removing anatase. In fact, the fine fractions from the centrifugation step frequently contain more  $\text{TiO}_2$  minerals than the crude clay or the coarse fraction. The kaolin clays mined in east Georgia, USA, also contain the same kinds of impurities as the Brazilian clays. To remove the colored impurities and bring the brightness to an acceptable level for coatings applications, many different processes have been employed in recent years. As an example, ferruginous impurities are dissolved in sulfuric acid solutions in the presence of hydrosulfites and removed during solid/liquid separation step. One of the most efficient and widely used methods for removing  $\text{TiO}_2$ , including iron-stained anatase, is the froth flotation. The flotation procedure consists mainly of blunging a crude clay in the presence of a dispersant at

the following conditions: solid in weight = 50%; pH to 8.5÷9.5 after addition of alkali; divalent cations such as  $\text{Ca}^{2+}$  and  $\text{Pb}^{2+}$  as activating agents; collector such as oleic acid to float the colored impurities from kaolin clay (Mallary, 1974; Nott, 1978; Smith, 1973; Young et al., 1985). Flotation is useful for processing coarse clays such as those produced in middle Georgia. For processing clays containing finer particles, such as those produced in east Georgia and northern Brazil, it is difficult to remove the anatase impurities by flotation. It has been suggested, however, that the use of alkylhydroxamate can be used for processing east Georgia clays (Yoon and Hilderbrand, 1986; Yordan et al., 1994). Unlike fatty acids, hydroxamate collectors do not require activators, which is a distinct advantage. Shi and Yordan (1996) showed that using a blend of fatty acid and hydroxamate collectors has some advantages.

Because of the difficulty in floating ultrafine particles, selective flocculation is more widely used for the beneficiation of finer clays. In selective flocculation, two different approaches are taken. In one, a kaolin clay is flocculated using a polymeric flocculant, leaving the impurities in the suspension (Smith, 1973; Maynard, 1974; Sheridan, 1974; Chapman, 1980). In another, colored impurities are flocculated, leaving kaolin clay in suspension (Shi, 1986; Behl et al., 1996).

In general, selective flocculation suffers from low recovery due to entrapment. For the case of flocculating colored impurities, a large amount of kaolin is entrapped within the settled material, causing a loss of recovery. Flotation, on the other hand, can give a high recovery except that it has difficulty in removing ultrafine colored impurities. In the present work, Brazilian clay containing a large amount of submicron particles is processed by flotation. The tests were conducted using alkylhydroxamate as collector. The results are compared with those obtained using a selective flocculation process. The flotation results obtained with the Brazilian clay are also compared with those obtained on an east Georgia clay sample.

## Experiments

### *Ore sample*

A crude kaolin clay from northern Brazil was used for a series of laboratory flotation and selective flocculation tests. A 30 kg sample received from a mine was homogenized and split into 1 kg lots at Centro de Tecnologia Mineral (CETEM), Rio de Janeiro. They were sent to Center for Coal and Minerals Processing, Virginia Tech, where laboratory tests were carried out. The crude kaolin clay used in the test work assayed 1.9%  $\text{TiO}_2$  by X-ray fluorescence (XRF) analysis.

### *Reagents*

All flotation tests were conducted using an alkylhydroxamate collector (S6973) from Cytec Industries. Sodium silicate, sodium hexametaphosphate and sodium polyacrylate were used as dispersants. Ammonium hydroxide was used for pH control. A polyacrylamide polymer at 7% anionicity (Nalco 8872) was used for selective flocculation tests. Its molecular weight was approximately 10 million.

### *Procedure*

Each flotation test was conducted using a 500 g bone-dry clay sample, which was obtained by splitting a 1,000 g sample received from CETEM. The sample was

dispersed (or blunged) in the Blacksburg tap water at 42% solids. Sodium silicate (1.5÷6.0 kg/t) and sodium hexametaphosphate (1.2÷3.0 kg/t), or sodium polyacrylate was used as dispersants. Approximately 2 kg/t of ammonium hydroxide was used to obtain pH = 8.5÷9.0. A Hamilton Beach kitchen blender was used as blunger. Following 10 min of blunging at 6,200 rpm, a known amount of collector was added. Agitation continued for another 10 min for conditioning. After conditioning, the pulp was transferred to a 2.5 liter Denver D-12 laboratory flotation cell and diluted to 20% solid. While the clay slip was being agitated at 1,500 rpm, 50 g/t of polypropylene glycol (PPG) with molecular weight of approximately 600 was added as frother. After 2 min of agitation, air was introduced to commence flotation. The froth products were dried, weighed, and analyzed for TiO<sub>2</sub> using an XRF spectroscopy.

#### *Selective flocculation test*

All selective flocculation tests were conducted using a 1 l graduated cylinder. A 500 g bone-dry clay was blunged for 10 min at 50% solids in the presence of 3.75 kg/t sodium silicate, 3.75 kg/t sodium hexametaphosphate, and 0.5 kg/t ammonium hydroxide. The pH of the pulp was 9.5. The dispersed clay slip was conditioned with appropriate reagents specified by Shi (1986), diluted to 12.5% solids, and transferred to a graduated cylinder. Flocculants were then added to the cylinder, agitated for a few min and was let to stand for the separation of flocs from dispersed material.

### **Results and discussion**

Table I shows the results of the laboratory flotation tests conducted on the Brazilian clay sample. At 0.5 kg/t S6973, the TiO<sub>2</sub> content was reduced to 1.36% with a 87.7% weight recovery (or yield). The flotation time was 25 min. At 0.75 kg/t collector, the TiO<sub>2</sub> content was further reduced to 1.34% with a yield of 71.0%. In both tests, 3 kg/t of sodium silicate and 3 kg/t of sodium hexametaphosphate were used as dispersing agents.

Table I: Results of the flotation tests conducted on a brazilian clay assaying 1.9% TiO<sub>2</sub> using S6973.

Collector dosage (kg/t)	Yield (%)	TiO <sub>2</sub> grade (%)	TiO <sub>2</sub> distribution (%)
0.50	87.7	1.36	78.2
0.75	71.0	1.34	77.0

In the next set of flotation tests, substantially larger amounts of R6973 were used. Also, polyacrylate was used in one test together with sodium silicate as dispersant. The flotation tests were conducted using 1 kg/t R6973 initially. After 25 min of flotation time, 1 kg/t of the collector was added again and flotation continued until exhaustion. The total flotation time employed was about 60 min. The results given in Table II show that at the higher collector dosage the flotation product contained much less TiO<sub>2</sub>. It appears also that combination of sodium silicate and polyacrylate gave better results than the case of using sodium silicate-sodium hexametaphosphate combination. A series of flotation tests were conducted on an east Georgia clay, which assayed 2.5% TiO<sub>2</sub> using the same collector, R6973.

Table II: Effect of using 2 kg/t R6793 and different combinations of dispersant.

Dispersant addition (kg/t)	Yield (%)	TiO <sub>2</sub> grade (%)	TiO <sub>2</sub> distribution (%)
-	70.0	1.05	37.7
3 Na Silicate + 3 Na-Metaphosphate	82.9	1.47	59.9
3 Na-Silicate + 3 Na-Polyacrylate	76.3	1.06	41.8

Figure 1 shows the results obtained at different collector dosages. As shown, it was possible to reduce the TiO<sub>2</sub> content to approximately 1% with high recoveries. Higher recoveries may be achieved using an advanced flotation column using smaller air bubbles than those generated in conventional flotation machines.

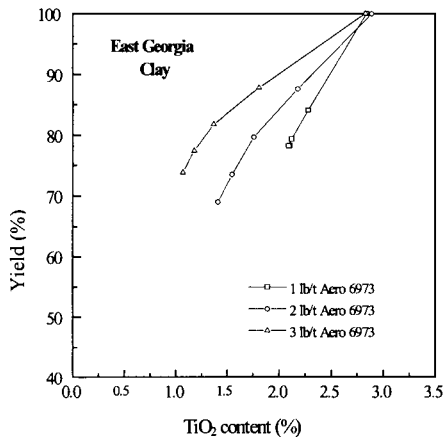


Figure 1: Grade vs. recovery curves obtained with an east Georgia clay using an alykylhydroxamate (R6793). The tests were conducted using a Denver laboratory flotation machine.

A series of selective flocculation tests were also conducted on the Brazilian clay for comparison. The tests were conducted using Nalco 8872. The test procedure was the same as described by Shi (1986). The TiO<sub>2</sub> content was reduced to 0.8% with 56% recovery. The flocculant dosage was 125 g/t. The results showed that selective flocculation can produce clay products with a lower TiO<sub>2</sub> content than can be obtained by flotation. However, the recoveries were higher with flotation.

## Conclusions

Flotation of northern Brazilian clay was able to reduce the TiO<sub>2</sub> content from 1.9% by weight to approximately 1% at 70-76% weight recovery. These results may be compared with that obtained by using a selective flocculation process, which reduced the TiO<sub>2</sub> content to 0.8% at a lower (56%) weight recovery. Thus, flotation may have a limitation in floating extremely fine particles. Further research is on going at CETEM and Virginia Tech to extend the flotation limit to lower particle sizes.

**References**

- Behl, S., Willis, M.J., and Young, R.H., 1996. U.S. Patent. #5,535,890. Method for separating mixture of finely divided minerals.
- Chapman, J.H., and Anderson, D., 1980. U.S. Patent. #4,227,920. Methods of clay beneficiation.
- Luz, A.B., 1998. Estudo de Reoxidação de Ferro Contido em Caulins. Tese de Doutorado pela Escola Politecnica da Universidade de S. Paulo.
- Mallary, M.B., 1974. U.S. Patent. #3, 827,556. Purification of clay by froth flotation.
- Maynard, R.N., 1974. U.S. Patent. #3,808,021. Method of rapid differential flocculation kaolin slurries.
- Maynard, R.N., Milman, N., and Lancinelli, J., 1969. A method for removing titanium dioxide impurities from kaolin. *Clay and Clay Minerals*. Vol. 17, 59-62.
- Nott, A.J., 1978. U.S. Patent. #4,098,688. Brightening of clay by froth.
- Sheridan, III, J.J., 1974. U.S. Patent. # 3,837,482. Process for purifying clay by selective flocculation.
- Shi, J.C.S., 1986. U.S. Patent. #4,604,369. Method of beneficiation kaolin clay utilizing ammonium salts.
- Shi, J.C.S., and Yordan, J.L., 1996. U.S. Patent. #5,522,986. Process for removing impurities from kaolin clays.
- Smith, S.J., 1973. U.S. Patent. #3,744,630. Kaolin flotation process.
- Yoon, R.H., and Hilderbrand, T., 1986. U.S. Patent. #4,629,556. Purification of kaolin clay by froth flotation using hydroxamate collectors.
- Yordan, J.L., Yoon, R.-H., and Hilderbrand, T., 1994. Hydroxamate vs. fatty acid flotation for the beneficiation of Georgia Kaolin. Chapter 22 in: *Reagents to Better Metallurgy*. SME, Colorado.
- Young, R.H., Morris, H.H., and Brooks, R.L., 1985. U.S. Patent. #4,492,628. Method of treating clay to improve its whiteness.



## WAYS TO INCREASE THE EFFICIENCY OF FLOTATION PROCESS FOR COMPLEX ORES

V. Beloborodov\*, K. Fedotov<sup>o</sup>

\*Mining Institute of Kola Science Center of Russian Academy of Sciences,  
fax 47 789 14170, email belobor@goi.kolasc.net.ru, 184200,

Apatity, Murmansk, Russia

<sup>o</sup>Irkutsky Technical University, fax 7 3952 255581

83, Lermontova Str., 664074 Irkutsk, Russia

### Abstract

The flotation separation of mineral products of a composite structure is a multiple-factor process. The increase of flotation efficiency requires a parallel optimization of many factors connected with mineral particles surface characteristics, chemical reactions in the liquid phase of the pulp, and also with hydrodynamic conditions in the flotation cell. The increase of efficiency of flotation of complex ores is possible under simultaneous improvement of three major components of flotation process: operation components, chemistry components and equipment components. Ways to increase the efficiency of flotation of the minerals of apatite and baddeleyite were developed and implemented into practice of beneficiation of complex ore of Kovdorsky deposit. The authors have proposed to increase flotation efficiency at the expense of application of acoustic effects on a flotation system. The method is based on the adoption of high intensity oscillations in the sound frequency range.

*Keywords: flotation, efficiency, acoustic, sound frequency*

### Introduction

As a rule, complex ores containing some useful components are processed by combined technologies of beneficiation with broad application of flotation. The necessity to increase the technological parameters of the beneficiation process, in conditions of a toughening of the requirements on resources-economy and ecological safety, causes the necessity of further development of the theory and practice of flotation separation of mineral products characterized by a complex structure. The flotation of such materials can be considered as a multiple-factor process. The increase of efficiency of flotation requires parallel optimization of many factors connected with a surface of mineral particles, chemical reactions in liquid phase of pulp, and also with hydrodynamic conditions in the cell.

Fuerstenau (1995) and Klimpel (1993) have presented in their works a flotation system by the way of three-dimensional system, in which one part mirrors the *operation components* (parameters connected with initial mineral raw materials), the *chemistry components* (parameters connected with flotation reagents and properties of a liquid phase) and the *equipment components* (parameters of flotation machines and hydrodynamic conditions of minerals separation). Each of set of parameters plays a relevant role in the general process of separation of mineral and should be studied in detail in close correlation with the others.

Now, the authors observed a considerable progress in the study of fundamental properties of minerals surface and in creation of selectively operating flotation reagents for flotation of minerals. A lot of new high-performance flotation machines ensuring high technological parameters of beneficiation of different ores have also appeared. As a follow-up the authors offer the use the fourth component, energy, influence on a flotation system, that is the superposition of acoustic oscillations on a flotation pulp at the moment of flotation. The outcomes of researches, made on the same trilateral scheme and directed on upgrading 933 of flotation process of complex ores, are shown in present paper.

### **Object of researches**

The object of researches was the improvement of the flotation process of a complex iron, phosphorus, zirconium – belonging to Kovdorsky ore deposit (Russian Federation). The ore of the given deposit is at the first stage processed with the help of a magnetic separation for recovery of a magnetite, and then subjects to flotation for recovery of an apatite and subsequent gravity-flotation recovery of a baddeleyite. At the present there is the need to solve a series of problems, connected with an increase of flotation efficiency. There is the necessity to increase the recovery of apatite with a simultaneous decrease of magnesium content in the concentrate. Also, it is necessary to improve the quality of a baddeleyite concentrate and recovery of zirconium dioxide at the expense of improvement of flotation separation of carbonaceous, silicate and sulfide minerals.

### **Outcomes of researches**

The researches aimed to improve the flotation of Kovdorsky complex ore were conducted within the framework of a three-dimensional system, adopted for the basis and describing major significant components of the flotation process. The authors have modified the given system with reference to a real ore.

#### *Operation components of a solid phase*

The study of integral properties of a solid phase (in other words of minerals) of flotation system is a successful way to improve a flotation process. The following characteristics have been assumed as integral properties of the solid phase:

- the grain-size characteristic of particles distribution of ground minerals to be floated;
- the set of crystal-morphological properties of each mineral determining a crystals habitus, crystals surface microrelief and its non-uniformity;
- the value of minerals active surface: the parameter reflecting a specific part of a mineral surface on which the active adsorption-desorption processes with flotation reagents during a flotation process are possible.

The proposed system of characteristics for a solid phase covers the properties of mineral particles from their geometrical sizes and microrelief of a surface up to surface physicochemical features interacting with flotation reagents in a flotation pulp. The grain-size characteristics of baddeleyite-containing products in different areas of the operational technology of processing of Kovdorsky deposit complex ore

were in detail studied within the framework of the given system.

The prominent feature of accumulation of a baddeleyite in circulating load of a ball mill of a secondary regrinding is established. In turn, that results in essential regrinding of friable mineral of a baddeleyite and decrease of recovery. The development of flow sheet of a grinding of the given ore using hydrocyclones together with vibrating screens for a fine screening was the rational decision to the given problem. The flow sheet using a fine screening in regrinding cycle of an apatite-baddeleyite product is shown on Figure 1. The feed is uniformly distributed on 24 Derrick vibrating screens with 0.23 mm screen panel. Finished undersize product with a yield of 53.9% goes to apatite flotation and further to baddeleyite production. The oversize product is fed to ball mills and reground on a normal mode in a close circuit with hydrocyclones. The application of this new technology showed as screening efficiency on the class of 0.20 mm is high enough, about 74.2%. The content of the class of >0.2 mm in a drain of mill hydrocyclones makes 18.6%, and class of <0.071 mm makes 46.3%. The change of the grain-size characteristic towards an increase of a share of middle classes of the raw material prepared for flotation has increased the recovery of valuable mineral apatite in apatite concentrate with 3÷5%, and mineral of a baddeleyite in baddeleyite concentrate with 6÷8%.

The detailed results of study of crystal-morphological properties of mineral of a baddeleyite and main accompanying minerals were reported in a previous works (Beloborodov et al., 1993). These researches have shown that in the ore there are two generations of mineral of a baddeleyite having a different microrelief of the surface. The surface of a baddeleyite of the first generation has a stepwise microrelief with many defects, therefore given generation of a baddeleyite has good flotation activity and can be recovered by the way of flotation. The crystals of a baddeleyite of the second generation have an elongated habitus, has a smooth microrelief of a surface and consequently its low flotation activity is observed.

The third integral characteristic, or value, of an active surface is a parameter, which determines the ability of mineral surface to ion-exchanging process at interaction with a liquid phase of a flotation pulp. With reference to calcium-containing minerals the methods of definition of that parameter were developed. The method consisted in a preliminary measurement of the specific surface area of narrow classes of the ground minerals of flotation coarseness and in the subsequent study of dissolution kinetic curves of the same samples of minerals in water. The dissolution of a mineral particle in solution is described by a known equation:

$$\frac{dN}{dt} = 4\pi R^2 K_s (n_{sat} - n) \quad (1)$$

where  $N$  is a quantity of dissolved substance;  $R$  is a relative radius of a particle;  $K_s$  is the factor characterizing adsorption-desorption properties of a surface of a particle of mineral;  $n_{sat}$  is a density of saturated solution, in which a dissolution goes;  $n$  is a current density of solution. This input equation was transformed taking into account an aspheric shape of particles of real minerals. The value of  $K_s$  can characterize the mean adsorption activity of a surface of a mineral particle, and the value obtained as a result of reference of the given factor to total specific surface area of a mineral particle can serve as the parameter of a specific active surface.

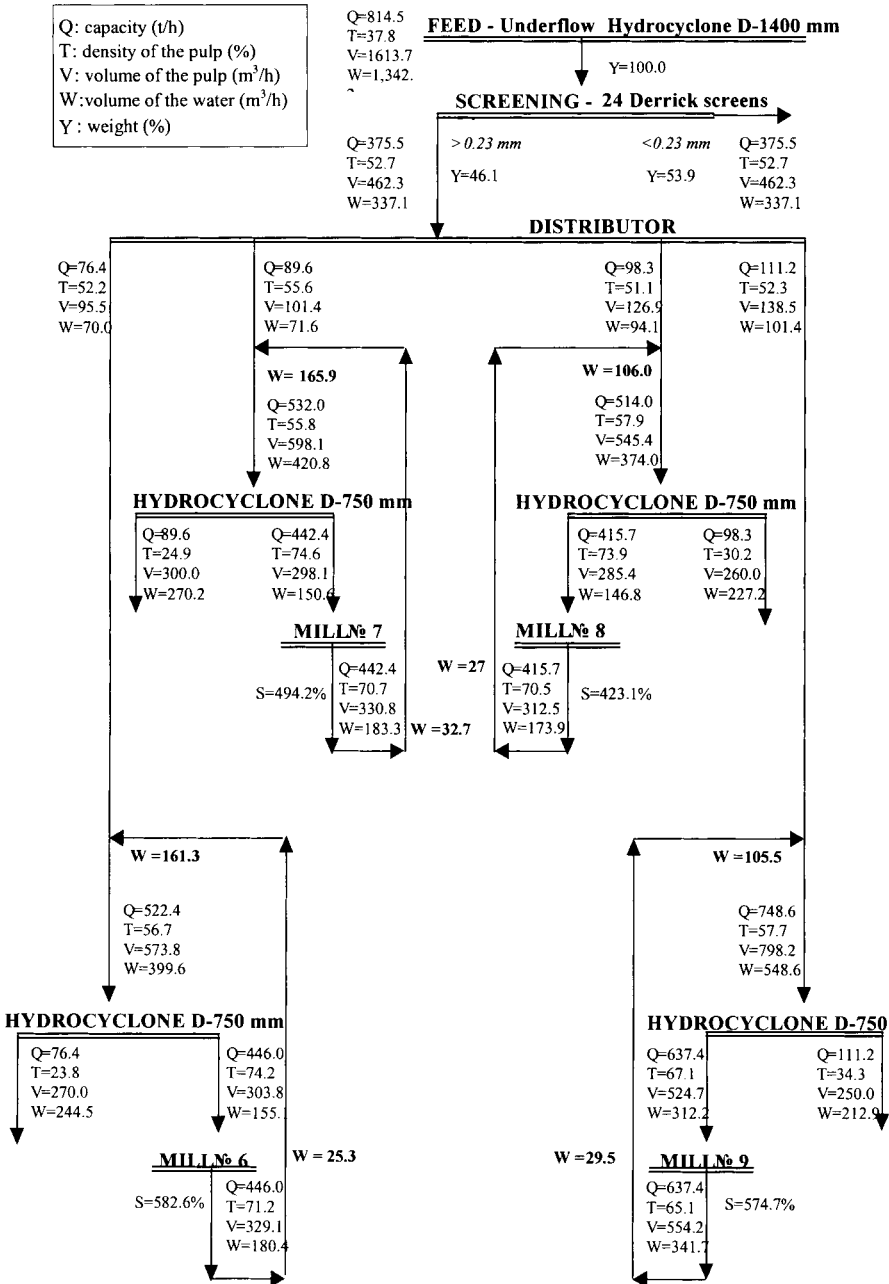


Figure 1: Results of fine screening in grinding circuit of the apatite-baddeleyite complex ore.

The dissolution kinetics of mineral particles in water was studied with the help of potentiometric, ion-selective calcium electrode. The value of activity of the given surface was calculated depending on the speed of transition of an ion of calcium from a surface of mineral into solution. The value was then correlated to total specific surface area of the ground minerals.

Given parameter clearly explains the distinctions in flotation activity of minerals with close physicochemical properties (especially, when the minerals have the same  $\text{Ca}^+$  cation, on which collector is being attached during flotation). More details about this parameter is given in a previous paper (Leonov et al., 1985)

#### *Chemical components of a flotation system*

The following characteristics of that kind of flotation are seems to be significant:

- value of activity of ions determining a potential of minerals surface;
- combination of properties of flotation reagents, or in other words such parameters as surface activity of collectors, efficiency of their linking with the main cations which belong to the structure of a minerals surface, depressant ability of depressants and concentration of reagents;
- pH value of pulp.

A lot of literature and a considerable amount of results exist on this topic. Analyzing the efficiency of linking of a collector with respect to the main potentialdetermining cation of a mineral surface ( $A$ ), it is possible to write by the following formula:

$$A = \frac{M}{C_m} \quad (2)$$

where  $M$  is the equilibrium concentration of ions of metal in solution and  $C_m$  is the total concentration of ions of metal.

The measurement of linking efficiency parameter does not require the information on linking reaction mechanism and on stoichiometric composition of nascent saline, in contrast to the usual values that characterize the process of interaction between molecules of organic compounds with ions of metals such as the constant of instability of complexes or the constant of saline solubility.

The measurement procedure of this parameter is reduced to measure the initial and final concentration of cations of metals after interaction with a portion of the collector. The measurements of concentration of metal ions can be conducted with the help of ion-selective electrode. The same parameter can be used for characteristic of depressants. The usage of linking efficiency parameter can not be replaced during the development of selectively acting mixtures of reagents. In these cases, it is practically impossible to allocate the action of any reagent.

The goal to develop (or to find) a high-performance ways of flotation of composite baddeleyite-containing complex mineral with the purpose to increase the recovery of valuable mineral of a baddeleyite was set as a task with reference to the object of these researches. Practically, the problem was solved adopting two ways of reverse flotation (in relation to a baddeleyite) of the minerals of an apatite, calcite, forsterite, and also sulphide minerals (pyrite and pirrotine). The effective combinations of reagents of a phosphate type were developed and employed.

Q : capacity (t/h)
$\gamma$ : weight (%)
$\beta_1, \epsilon_1$ : rate, recovery $ZrO_2$ (%)
$\beta_2, \epsilon_2$ : rate, recovery $P_2O_5$ (%)
$\beta_3, \epsilon_3$ : rate, recovery $S_{total}$ (%)

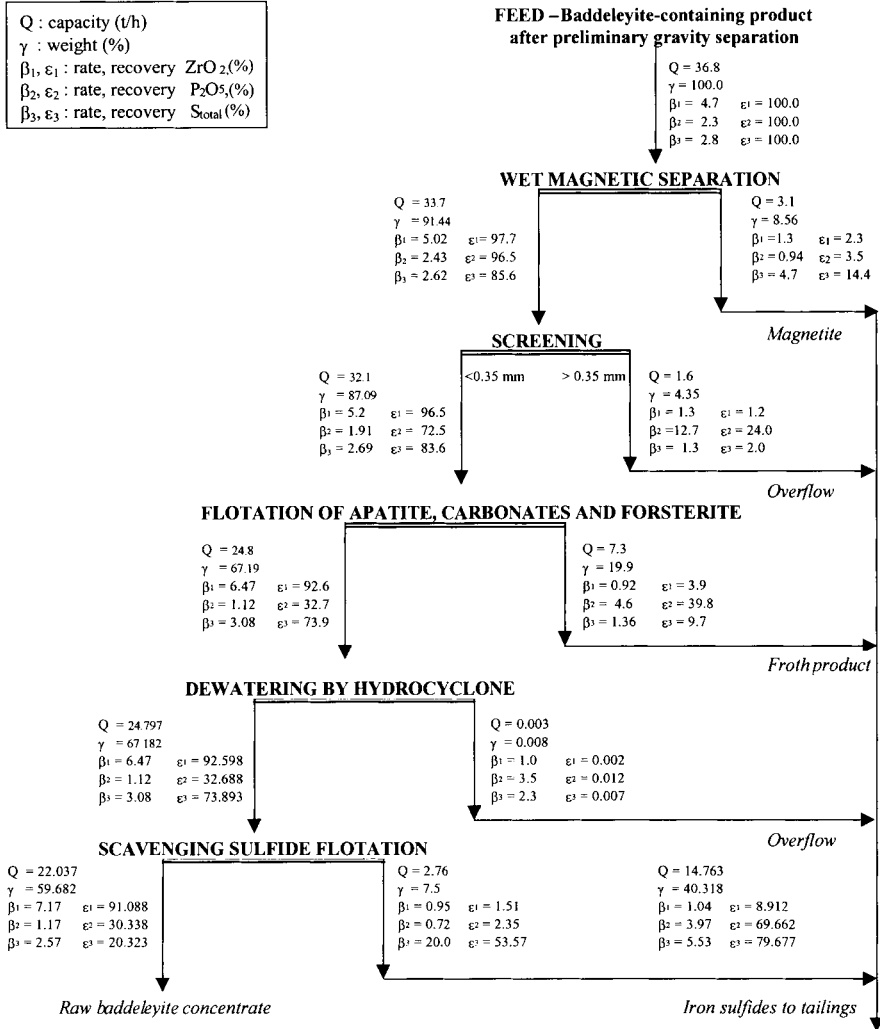


Figure 2: Flow-sheet of beneficiation of baddeleyite-containing product, using reverse flotation.

They are: as the collector: monoethers and diethers of alkyl-phosphorus acid, as the modifier of multifunctional action: monodietheralkylaryletoxyphosphate and depressant tripoliphosphate of sodium. The typical flotation reagents were used in addition. For flotation of an apatite and carbonates: the fatty-acid collectors, and for flotation of sulfide minerals: the potassium xanthogenate. The process flowsheet of implementation of flotation into the combined magnetic-gravitational scheme of beneficiation of baddeleyite-containing ore is shown in Figure 2. The application of the new flotation technology has allowed increasing the recovery of valuable mineral of a baddeleyite in 1.5 times (Beloborodov and Zakahorova, 1999).

### *Equipment components*

With reference to flotation machine as the separating equipment, the authors think that it's rather important to take into account the following main integral parameters:

- the efficiency of pulp mixing (this parameter mirrors the hydrodynamics of process and power characteristics of the machine);
- the aerating ability of an impeller expressed in quantity of air passing through volume unit of machine cell per time unit;
- the dispersion structure of the air bubbles in volume of a cell.

Theoretical calculations and operational practice of flotation machines of different kind shows that only optimal combination of the above-mentioned parameters can ensure an effective flotation process. The authors, guided by the result of researches published in Young, 1982, have chosen the flotation machine AKER for implementation of the designed flotation technology. This pneumomechanical flotation machine has an impeller of *free flow* type that possesses high pumping effect. In addition, the authors have proposed to intensify flotation at the expense of application of acoustic effects on a floatation system. The method is based on usage of high intensity oscillations of sound frequency range. The flotation process using effect of forces of hydrodynamic interaction between bubbles of air and mineral particles in a pulp, subjected to processing by sound is described in work (Fedotov and Leonov, 1997). The results of researches conducted on physical models, on interaction of bubbles and solid particles, suspended in a liquid have shown the actual effects obtained by changing the character of behavior of process of mineral particles joining to bubbles of air. As researches have shown, one of the optimal oscillation frequencies is equal to 330 Hz, and permissible value of vibration acceleration is in a range between 25÷30 Hz. In connection with the fact that mineralization of the air bubbles at hydroacoustic effect lasts for fractions of a second, the supply of prepared pulp and gas phase of a definite degree of dispersion is necessary to conduct in a zone of a vibration source located in the cell of a direct-flow type.

The flotation machine with a unit of acoustic processing of a pulp (acoustic module) works as follows. Having filled the flotation machine by water, actuate the vibrator. Changing quantity of revolutions of a drive motor, vibrator's operational mode is adjusted to the necessary frequency of oscillation. Using two aerators of a jet type, we set the definite diameter of the air bubbles in the cell of flotation machine. The flotation process starts with supply of a pulp from a contact tank into an acoustic module. At the expense of hydroacoustic effect, the interaction of most of mineral particles and air bubbles, passing through a module, happens practically instantaneously. The high-speed flow of air-pulp mixture that is generated at the expense of injection of gas-liquid jets by aerators carries away the formed complexes into the cell of flotation machine. The hydrophobic particles fixed on bubbles, go up to froth and are discharged through a lower nozzle, while hygrophilous particles together with a pulp drain through a bottom nozzle.

Formed flotation complexes flowing out of an acoustic module get into a zone with low intensity of an acoustic field, in which the hydroacoustic effect does not work. Exactly in this zone, where the weak vibrating field is still present, the agitation of flotation aggregates and demineralization of air bubbles from *superfluous* fixed

mineral particles takes place. In other words, here we have the acoustic cleaning of the particles brought to froth. The acoustic module is easily joined to any other flotation cell or flotation machine. The capacity of module depends on the number of aerators installed, and on the power of a vibrational source.

### Conclusions

The results of the study demonstrated as the increase of efficiency of flotation of complex ores is possible under simultaneous improvement of three major components of flotation process: operation components, chemistry components and equipment components. Different strategies to increase the efficiency of flotation of the minerals of apatite and baddeleyite were developed and implemented into practice of beneficiation of complex ore of Kovdorsky deposit. The prove was given to the challenging future of the use of acoustic influence for intensification of flotation process.

### References

- Beloborodov, V.I. and Zakahorova, I.B., 1999. Baddeleyite: valuable raw material for ceramic industry, ways increasing the recovery from the ore. II International Conference Recent Advances in Materials and Mineral Resources, Penang.
- Beloborodov, V.I., Zakharova, I.B. and Nevolina, V.G., 1993. A Study of Crystal-Morphological Properties of Zirconium-containing Minerals and Development of their Effective Recovery Methods from Ores. XVII International Mineral Processing Congress, Sydney, Vol. 4, 1075–1082.
- Fedotov, K.V. and Leonov, S.B., 1997. Flotation under Acoustic Field. Moscow, 81.
- Fuerstenau, D.W., 1995. Where We are in Flotation Chemistry after 70 years of Research. San Francisco, XIX International Mineral Processing Congress, Vol. 3, 3-17.
- Klimpel, R.R., 1993. Froth Flotation: an old process with a new outlook. Mining Magazine, May 1993, 266-274.
- Leonov, S.B., Beloborodov, V.I., Rubinshteyn, J.B. and Polonsky, S.B., 1985. New Ways of Development of Theory and Practice of Benefication of Non-metallic ores., World Congress on Non-Metallic Minerals, Belgrade, Vol. 3, 21–31.
- Young, P., 1982. Flotation Machines. Mining Magazine, Vol. 146, n.1, 114–131.



This Page Intentionally Left Blank

# **PLANT AND PROCESS DESIGN**

This Page Intentionally Left Blank

**Technology for Separation of Non-Ferrous Metal Minerals with Similar Physical and Chemical Properties**

A.V. Tarasov, V.A. Bocharov

C9-1

**Physical Separation Processing of a Bulk Tin-Tungsten Pre-Concentrate Into its Individual Constituents for Commercial Applications**

A.T. Sutaone, S.K. Ghosh, K.S. Raju

C9-7

**Old Tailings Dumps of Concentrating Plants as a Source of Raw Minerals**

V.M. Izoitko, Y.N. Shumskaya

C9-13

This Page Intentionally Left Blank

## TECHNOLOGY FOR SEPARATION OF NON-FERROUS METAL MINERALS WITH SIMILAR PHYSICAL AND CHEMICAL PROPERTIES

A.V.Tarasov, V.A.Bocharov

State Research Center of Russia – State Research Institute of Non-Ferrous Metals, “GINTSVETMET”, Moscow, Russia

### Abstract

The uneven dissemination of minerals, including emulsion-type inclusions, the high degree of sphalerite activation, and the presence of a wide range of copper minerals, as well as generations of sphalerite, pyrite, chalcopyrite, and bornite, are the cause of low recoveries and performance values of ore beneficiation processes. An ore processing technology is proposed ensuring production of high-grade monoselective flotation concentrates containing copper, zinc, and pyrite concentrates, as well as copper-zinc sulfide product. Individual unit operations of the proposed process technology have been tested and proven. This technology makes it possible to improve copper, zinc and precious metals recoveries by 3÷5%, 15÷25% and 10%, respectively.

*Keywords: minerals, sphalerite, chalcopyrite, flotation, metals recovery*

### Introduction

Many types of combined sulfide and oxide ores of non-ferrous metals from Russian deposits contain minerals with similar physical and chemical properties and their separation during ore beneficiation and extractive metallurgical stages is therefore extremely difficult (Tarasov, 1999). Such ores have the following characteristic features: non-uniform fine, emulsion-type inclusions of disseminated minerals; presence of different minerals of copper in the form of sulfides (both primary and secondary), carbonates, oxides, silicates and sulfates; intense oxidation of copper and iron minerals and activation of sphalerite; presence of associations of chalcopyrite, bornite, pyrite, and sphalerite with isomorphic impurities therein, etc. The selection of a suitable processing technology is dependent on many factors, but the most decisive of them are: activation of sphalerite, variety of minerals and their associations, as well as structural properties of minerals. It has been found that different minerals of non-ferrous metals are liberated to different degrees in the process of grinding. Structural characteristics of ores vary within an extremely wide range: massive structures with varying grain size; colloform, banded, and emulsion-type structures. Different generations of minerals have different densities and microhardness and contain various impurities. Of special importance for selective flotation of copper-zinc ores is the degree of oxidation of the surface of sulfide minerals. That is why it is necessary to develop innovative processing techniques at the stage of ore beneficiation ensuring an improved efficiency of minerals separation.

On the other hand, with the use of state-of-the-art highly intensive autogenous smelting processes, high-temperature autoclave leaching, solvent extraction and ion-

exchange methods permitting recovery of main and associated metals from products of varying grades and quality, it has become essential to modify traditional ore processing flowsheets and incorporate both pyro- and hydro-metallurgical techniques in order to ensure integrated utilization of raw materials (Mantsevich et al., 1999; Tarasov, et al., 1996).

### Investigation of intensive flotation methods

An analysis of the causes resulting in loss of metals during selective flotation of combined sulfide and oxide non-ferrous ores has indicated that the bulk of metals lost report into tailings or pyrite concentrate due to both sludge formation and insufficient liberation of mineral intergrowths. Zinc lost with copper concentrate is primarily in the form of free fine grains of sphalerite activated with copper cations. Precious metals are mainly closely associated with pyrite and partially with copper sulfides and are distributed between flotation products in accordance with recoveries of these sulfides into one or another product. The distribution of precious metals throughout the ore beneficiation products is greatly dependent on the presence of lime, cyanide, and sodium sulfide, which suppress flotation of free gold and carrier minerals.

A significant problem related to selective flotation of copper-zinc ores is associated with the presence of secondary copper minerals, as well as carbonates, oxides, sulfates and silicates (Figure 1).

To improve the recovery of secondary copper minerals and reduce their activating effect on sphalerite, it is necessary to subject secondary sulfides to flotation after each grinding stage using softer depressors (i.e., sulfo compounds, organic modifiers) for inhibiting sphalerite and pyrite flotation and carry out the process at moderate pH values. This technology has been introduced commercially at a number of ore processing plants.

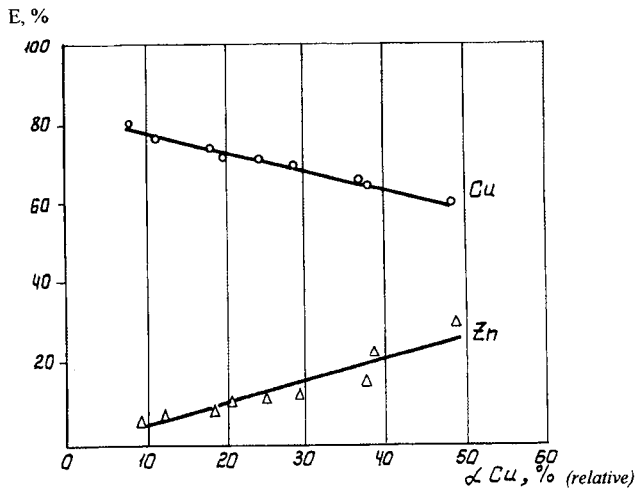


Figure 1: The results of selective flotation depending on secondary copper sulfides content.

In order to improve the efficiency of flotation of oxide minerals, it is advisable to apply sulfidization with sodium sulfide, elemental sulfur, etc. A two-stage sulfidization method has been proposed and implemented: the first stage is performed at pH of about 7 using elemental sulfur, the second stage proceeds at pH of about 8.5-9.5 using sodium sulfide. A mixture of autogenous gases (elemental sulfur, hydrogen sulfide, sulfur dioxide) ensures a higher degree of sulfidization. As a result, covellite is formed over the surface of oxides and carbonates. Complete sulfidization is reached at a temperature of 230-290 °C.

If the ore has a considerable content of secondary copper minerals, "copper head" is recovered by natural flotation between grinding stages or prior to bulk flotation. Up to 50% of copper is recovered into the "copper head" with a minimum requirement of collector (1-5 g/t) and depressors (20 g/t of sodium sulfide, 100 g/t of zinc sulfate). Classical processing technology is used for most ores including separation of bulk concentrate with subsequent copper and zinc flotation steps. For ores with a high content of secondary sulfides, a flowsheet is applied comprising segregation of bulk concentrate with production of final zinc concentrate as underflow from the copper flotation and depression of sphalerite with sodium sulfide and zinc sulfate.

The mechanism for suppression of sphalerite flotation depends on the ionic composition of the pulp and pH values of the medium. In our publications it has been pointed out that ions of  $\text{HSO}_3^-$  and  $\text{SO}_3^{2-}$  are stable at pH values of about 5-7, while ions of  $\text{SO}_3^{2-}$  are stable at pH = 7-9 and  $\text{S}^{2-}$  at pH >9. Depressors used for this process can form a wide range of these sulfocompounds, but at certain pH values, the concentration of one of the ions will be higher than that of any other. This particular anion will determine to a significant extent the mineral depression effect. Theoretically, it is possible to control the sulfide oxidation by adjusting accordingly the pH value creating thereby such an anionic composition of the liquid phase which will ensure suppression of sulfide flotation, but in the practice this effect must be enhanced by adding the missing amount of sulfur-containing modifier. In the case of some ore types, it is sufficient to use only zinc sulfate and lime to inhibit sphalerite flotation due to the natural floatability of minerals.

An investigation of the oxidation-reduction condition of sulfide pulps has permitted the authors to adopt a new approach to selection of optimum process conditions for segregation of minerals, ensuring elimination of the use of a substantial portion of the main modifier, i.e., sodium sulfide, and substitute zinc salt of carboxymethyl cellulose (CMC) type. In this case, suppression of sphalerite proceeds in the following manner: leaching of copper cations and collector from the surface with sodium sulfide, formation (sorption) on the surface of various hydrophilic zinc-containing compounds and multilayered coatings of carboxyl groups of CMC. It is also possible that the latter interacts with free metal cations on the surface of minerals. The use of CMC salt reduces twice the requirement of sodium sulfide and improves the segregation (Figure 2). Instead of sodium sulfide, the following reagents can be successfully used: sodium sulfohydrate, sodium thiosulfate, polysulfides, sulfur dioxide, sodium sulfite, etc.

A mixture of butyl and isopropyl xanthates is used as a collector for flotation of sulfide copper-zinc ores. In order to improve the activity of the collector, electrolyte



was added which facilitated penetration of ions to the surface of the mineral by displacement of hydrate films. The use of mercaptobenzothiozole in combination with butyl xanthate results in a reduction in losses of metals and sulfur with tailings, lower requirement of zinc sulfate and total requirement of collector and frothing agent. There was a trend recorded toward improvement of the copper concentrate grade and better recoveries of precious metals thereto.

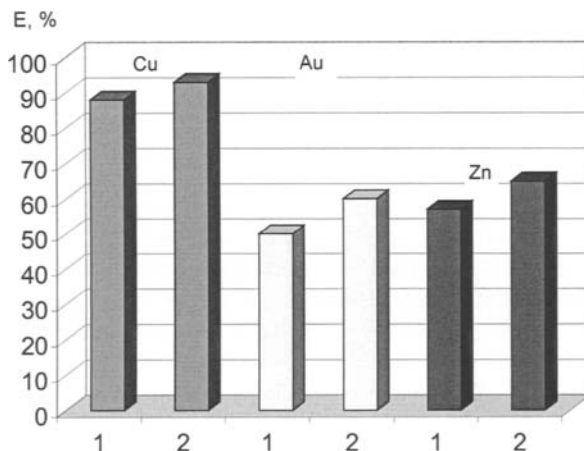


Figure 2: Recovery of metals into the copper concentrate during the flotation with Na<sub>2</sub>S + ZnSO<sub>4</sub> (1) and CMC + ZnSO<sub>4</sub> (2).

### Technology for production of selective concentrates and sulfide polymetallic products

The complexity and the wide variety of mineral compositions of non-ferrous ores is the cause for build-up of sulfide minerals in intermediate products which are difficult to separate and segregate by conventional techniques. Refractory grains of sulfides are distributed between concentrates and tailings and increase the loss of valuable metals and affect the quality of concentrates. We have developed a processing technology ensuring production of copper, zinc and pyrite concentrates along with sulfide products. The latter contain hard-to-flotate free fine sulfide grains and fine intergrowths of sulfides. Two types of copper-zinc products can be separated without any appreciable decrease in the recoveries of copper and zinc into flotation concentrates. A low-grade product is separated in the following circuits: cleaner flotation of pyrite concentrate; thorough scavenging of tailings from a concentrator; cleaner flotation of rough zinc concentrate. This product may contain 1÷3% copper and up to 10% zinc. A technique has been developed for processing this low-grade product using chloride-sublimation roasting with subsequent hydrometallurgical treatment of volatile chlorides of metals. This technology permits a recovery of 98÷99% of valuable constituents. The low-grade product can be also subjected to bacterial leaching to recover zinc. The high-grade product is produced by dezincing of copper concentrate; it can be further treated by hydrothermal autoclave leaching of zinc sulfides with spent electrolyte. The product contains 3÷5% copper and 13÷25%

zinc. As a result of leaching, zinc solution and residue are produced. Zinc is precipitated from the solution after its purification using alkalis or by electrolysis. The copper-containing pyrite leach residue is subjected to repeated flotation and serves as raw material for autogenous processes (Tarasov et al., 1996).

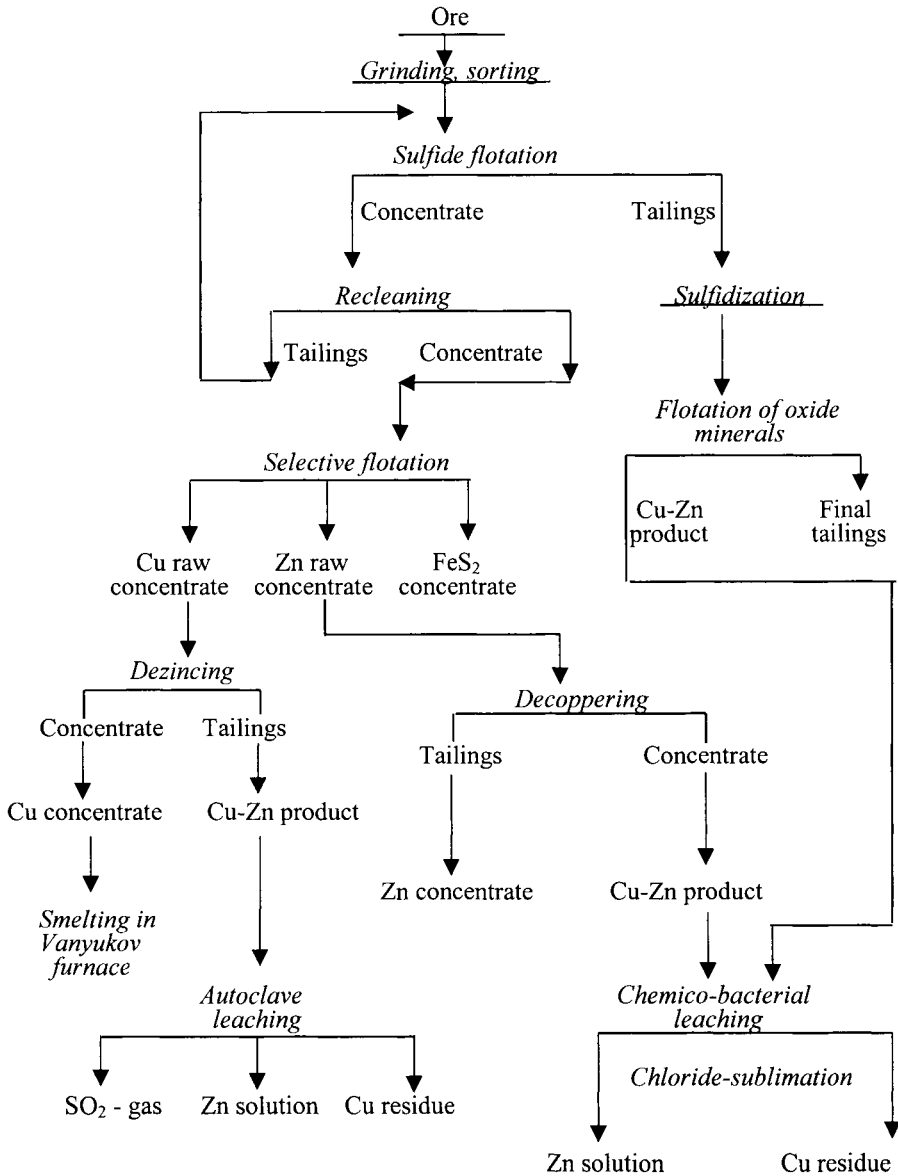


Figure 3: Flowsheet of the combined processing technology for hard-to-beneficiate copper-zinc ores.

High-grade copper-zinc products can be treated using autogenous resource-saving smelting technology in a double-zone Vanyukov furnace, a shaft furnace, a flame-smelting furnace with sparged bath, a combined smelting furnace with sparged bath and thorough utilization of heat (BAGUT process, which is a Russian abbreviation widely used in Russian metallurgical literature), with sublimation of zinc in its reducing zone or with subsequent recovery of zinc from slag by slag-fuming, which makes much easier the problem of precious metals recovery (Tarasov et al., 1995; Paretsky et al., 1993) (Figure 3).

### Conclusions

Separation of sulfide products along with high-grade flotation concentrates at the stage of ore beneficiation and their processing using combined flotation/hydrometallurgical flowsheet makes it possible to more completely utilize the raw materials, improves the overall recoveries of copper of 3÷5%, zinc of 10÷15% and precious metals by 10% (Figure 4).

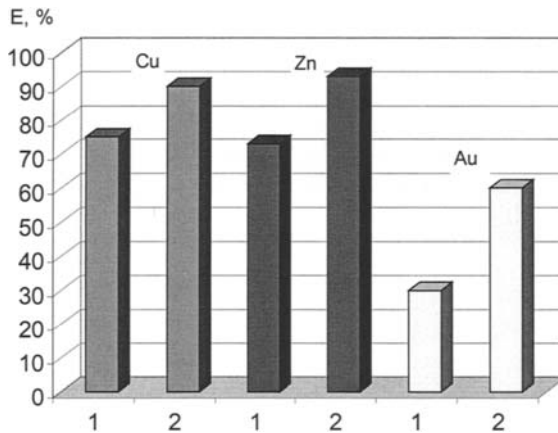


Figure 4: Recovery of copper (Cu), gold (Au) into the copper concentrate and into the zinc (Zn) concentrate by using flotation and combined processing technology.

### References

- Mantsevich, M.I. and Khersonskaya, I.I., 1999. Prospects for development of combined technologies for processing of ores of heavy non-ferrous metals. *Clean Technology: Third Millennium Challenge. Int. Mining and Environmental Congress. Lima, Peru*, pp. 281-285.
- Paretsky, V.M., Generalov, V.A., Tarasov, A.V. and Klushin, S.D., 1993. Oxygen-flame converting of nickel mattes. *Extractive Metallurgy of Copper, Nickel and Cobalt. Proceedings of the Paul E. Queneau International Symposium. Denver. Vol. 1. Fundamental Aspects*, pp. 531-536.
- Tarasov, A.V. and Kovgan, P.A., 1995. Smelting of sulfide copper concentrates in a combined bubbling furnace. *Copper-95. Int. Conference. Santiago, Chile. Vol. 4*, pp. 383-388.
- Tarasov, A.V. and Bocharov, V.A., 1996. The combined technology of pyritic copper-zinc ores processing. *SWEMP'96 Fourth Int. Conf. on: Environmental Issues and Waste Management in Energy and Mineral Production. Cagliari*, pp. 415-419.
- Tarasov, A.V., 1999. Environmental aspects of innovative non-ferrous ore beneficiation and extractive metallurgical process. *Clean Technology: Third Millennium Challenge. Int. Mining and Environmental Congress. Lima, Peru*, pp. 785-791.

## PHYSICAL SEPARATION PROCESSING OF A BULK TIN-TUNGSTEN PRE-CONCENTRATE INTO ITS INDIVIDUAL CONSTITUENTS FOR COMMERCIAL APPLICATIONS

A.T. Sutaone, S.K. Ghosh, K.S. Raju

Indian Bureau of Mines, Nagpur, India  
Fax +91 0712 533631, e-mail [ibmnag@mah.nic.in](mailto:ibmnag@mah.nic.in)

### Abstract

The steel and most base-metal industries are currently experiencing low prices in the international market, due to a global economic recession that has resulted in low production. On the other hand, tin and tungsten metal prices are showing an upward trend, giving a scope to the processing of tin & tungsten ores for production of these metals, which will result in their higher prices, aside from maintaining their strategic importance. The mineral sectors in India have been opened to multi-national companies and to the international market, due to the liberalization of the mineral policies of the Indian Government. Likewise, outside opportunities have been opened for Indian mining companies, as well as international mining companies based in India (Indian Minerals Yearbook, 1997). Keeping these aspects in mind, an international mining company, based in India, with the intention to make a mining lease outside India, sponsored a beneficiation study for tin-tungsten bulk pre-concentrate in the modern mineral-processing laboratory of the Indian Bureau of Mines in Nagpur. The objective of the study was to separate the bulk pre-concentrate into two sellable components, one containing more than 40% Sn for tin smelting and the other one containing 44%  $WO_3$  for producing ammonium para tungstate (APT). A combination of gravity, magnetic and electrostatic separation yielded a tin concentrate assaying 61.0% Sn with Sn recovery of 78% and a tungsten concentrate assaying 44.21%  $WO_3$ , with  $WO_3$  recovery of 71.4%, meeting the stipulated chemical specifications, including the tolerance limit of impurities. This paper deals with the details of test work in developing a suitable beneficiation processing flowsheet, to produce individual concentrates of tin and tungsten for possible commercial application.

*Keywords: pre-concentrate, APT,  $WO_3$  recovery, tolerance limit*

### Introduction

A tin-tungsten pre-concentrate obtained after crushing, grinding and two-stage tabling was subjected to bench-scale beneficiation studies in the mineral-processing laboratory of the Indian Bureau of Mines in Nagpur (India). The pre-concentrate was sent from a tin-tungsten mine outside India by an international consulting firm. The objective of the study was to develop a processing flowsheet for the production of a tin concentrate assaying >40% Sn for tin smelting and a tungsten concentrate assaying >44%  $WO_3$ , with maximum possible recovery. The tungsten concentrate should be used as a raw material for production of Ammonium para tungstate (APT), according to specifications stipulated by a prospective buyer (a Chinese firm).

### Characteristics of the sample

The as-received sample was gray to grayish-black in color. The chemical analysis, size composition and mineralogical composition are given in Table I, II and III.

Table I: Chemical analysis of as-received pre-concentrate.

Sn (%)	WO <sub>3</sub> (%)	Mn (%)	Fe <sub>2</sub> O <sub>3</sub> (%)	SiO <sub>2</sub> (%)	Al <sub>2</sub> O <sub>3</sub> (%)	CaO (%)	MgO (%)	S(T) (%)	Cu (%)	Pb (%)	As (%)	B <sub>2</sub> O <sub>3</sub> (%)	TiO <sub>2</sub> (%)
25.2	17.0	1.33	6.6	19.09	7.25	6.24	3.4	1.33	0.25	0.61	0.05	4.2	0.31

Table II: Size composition.

Size (Tyler mesh)	-10+28	-28+35	-35+50	-50+65	-65+100	-100
Weight (%)	25.3	10.8	20.3	20.0	13.8	9.8

Table III: Mineralogical composition.

Mineral composition (%)	Tourmaline	Cassiterite	Scheelite/Wolframite	Mica (Biotite-Muscovite)
	35	30	15÷20	3+4
Mineral composition (%)	Calcite	Quartz	Sulfides	Fe oxides/others
	4÷5	3÷4	2÷3	2÷3

### Processing technology

The sample was subjected to thorough microscopic examination for liberation studies. It was observed that most of the lighter silicate gangue minerals are liberated from the tin and tungsten minerals at a size of around 65 mesh. A final flowsheet was developed after preliminary tests. The flowsheet includes: i) grinding of all of the sample to <65 mesh; ii) tabling of the ground product; iii) drying of the table concentrate, iv) high intensity magnetic separation of dry concentrate to obtain a non-magnetic fraction as tin concentrate and a magnetic fraction as tungsten concentrate; v) high-tension electrostatic separation of the non-magnetic to obtain high grade tin concentrate (conductor), medium grade tin concentrate (middlings) and additional tungsten concentrate (non-conductor).

### Tabling

A representative portion of sample is stage-ground in a rod mill to over 65 mesh size and is treated on a laboratory model of a Deister table to reject most of the lighter silicates and quartz. The metallurgical results are given in Table IV.

Table IV: Results of tabling test at &lt;65 mesh.

Table products	Weight (%)	Assay (%)		Distribution (%)	
		Sn	WO <sub>3</sub>	Sn	WO <sub>3</sub>
Concentrate	60	39.84	26.17	95.1	91.1
Tailings	40	3.10	3.86	4.9	8.9
Calculated feed	100	25.15	17.24	100.0	100.0

Minerals in the table products: table tails = mostly silicates and quartz, with very slimy tin and tungsten minerals; table concentrate = tin, tungsten minerals, tourmaline.

### Dry, high-intensity magnetic separation

After drying, the table concentrate was subjected to high intensity dry magnetic separation at field strength of 2.1 T and two fractions - magnetic and non-magnetic - were collected. The metallurgical results are given in Table V.

Table V: Results of dry, high-intensity magnetic separation.

Products	Yield (%)	Assay (%)		Distribution (%)	
		Sn	WO <sub>3</sub>	Sn	WO <sub>3</sub>
Magnetic	17.7	10.18	48.27	7.1	49.6
Non-magnetic	42.3	52.26	16.90	88.0	41.5
Feed (table concentrate)	60.0	39.84	26.17	95.1	91.1

It can be seen from the results that cassiterite is distributed mostly in the non-magnetic fraction, but the distribution of tungsten mineral is approx. 55/45. These fractions were subjected to detailed mineralogical examination.

### Mineralogical observations

The non-magnetic fraction mostly contains free cassiterite, along with scheelite, whereas the magnetic fraction contains a lot of wolframite and tourmaline. Besides, in the magnetic fraction was observed also scheelite: this is due to alteration of wolframite in scheelite along the grain boundaries and cracks.

This scheelite, which appears under ultraviolet light, still retains the magnetic properties of wolframite. The degree of replacement of wolframite by scheelite varied from place to place and in case of complete replacement, the tungsten minerals totally behave like scheelite and join the non-magnetic fraction along with cassiterite. The above observations were based on detailed microscopic studies and the microphotographs are given in Figure 1.

### High-tension electrostatic separation

A simple high-tension separator employing a pinning effect, or an electrostatic separator using a lifting effect, were not found suitable for separating tin and tungsten minerals effectively. However a combination of both was found necessary to treat the non-magnetic fraction.

After thorough drying, the non-magnetic fraction was first treated on a high-tension separator (Carpco-make) employing multiple stages to yield conductors as high-grade tin concentrate, and a mixture of non-conductors containing tin and tungsten minerals.

This fraction was further treated on a plate-type electrostatic separator (Carpco-make) to yield a second-grade tin concentrate as a conductor (which is defined as middlings in Table VI) and a tungsten-rich fraction as a non-conductor. The metallurgical results are given in Table VI.

Table VI: Results of high tension electrostatic separation.

Products	Weight (%)	Assay (%)		Distribution (%)	
		Sn	WO <sub>3</sub>	Sn	WO <sub>3</sub>
Conductors	24.9	65.0	7.58	64.3	10.9
Middlings	7.3	47.07	20.80	13.7	8.8
Non-conductors	10.1	24.65	37.10	10.0	21.8
Feed (non-magnetic)	42.3	52.27	16.92	88.0	41.5



Figure 1: Photomicrographs: top: wolframite (W) as fine inclusions within cassiterite (C) and scheelite (Sh); bottom: scheelite (Sh) replacing wolframite (W) around grain boundaries and cracks.

The overall metallurgical results are presented in Table VII. The processing flowsheet with materials balance is given in Figure 2.

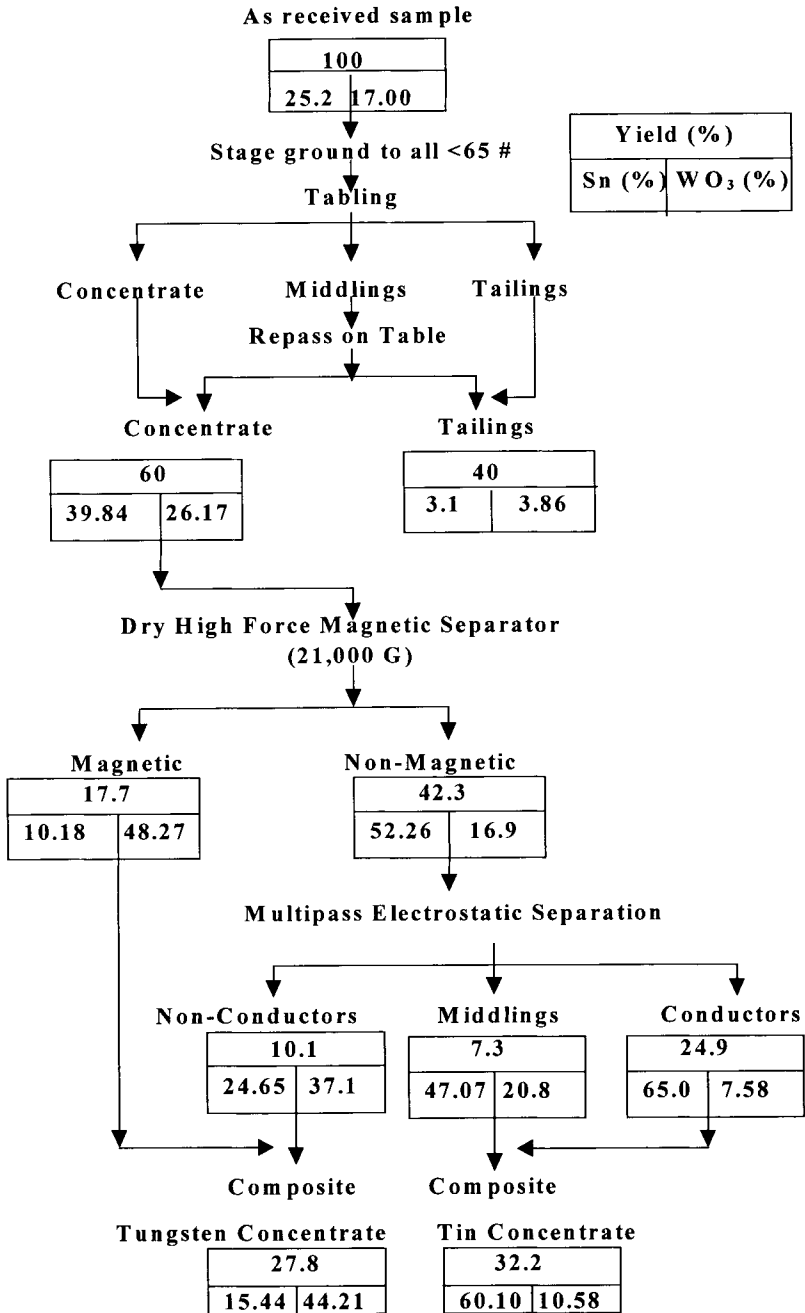


Figure 2: Processing route.



Table VII: Overall results of tabling/magnetic-electrostatic separation.

Products	Yield (%)	Assay		Distribution	
		Sn (%)	WO <sub>3</sub> (%)	Sn (%)	WO <sub>3</sub> (%)
1. Conductors	24.9	65.0	7.58	64.3	10.9
2. Middlings	7.3	47.07	20.80	13.7	8.8
3. Non-Conductors	10.1	24.65	37.10	10.0	21.8
4. Magnetic	17.7	10.18	48.27	7.1	49.6
5. Table tails	40.0	3.10	3.86	4.9	8.9
Calculated feed	100.0	25.15	17.24	100.0	100.0
6. Composite* tungsten conc. (3+4)	27.8	15.44	44.21	17.1	71.4
7. Composite** tin conc. (1+2)	32.2	61.0	10.58	78.0	19.7

Concentrate analysis	Pb (%)	As (%)	Bi (%)	S (%)	Sb (%)	Mo (%)
* (1+2)	-	0.095	0.85	-	-	below det.
** (3+4)	0.57	0.023	0.07	0.70	below det.	-

### Observations

The misplacement of tin in tungsten concentrate and tungsten in tin concentrate is mainly due to the fine dissemination and inclusions of wolframite within cassiterite, besides the fine interlocking of scheelite and cassiterite. Further tests conducted on finer grinds could not help in improving the misplacement, but rather enhanced the losses of both tin and tungsten minerals in the form of slimes, due to their friable nature. However, the other impurities indicated in the concentrate analysis are within the desired limits.

### Summary and conclusions

A tin and tungsten pre-concentrate assaying 25.2% Sn, 17% WO<sub>3</sub>, 6.5% Fe<sub>2</sub>O<sub>3</sub>, 19.09% SiO<sub>2</sub>, and 7.25% Al<sub>2</sub>O<sub>3</sub> was received from an international consultant firm for beneficiation studies, and develop a flowsheet to obtain separate tin and tungsten concentrates as saleable, marketable products. By employing a combination of unit operations of tabling, drying, dry-high intensity magnetic separation and electrostatic separation, it was possible to obtain: i) a high- grade composite tin concentrate assaying 61% Sn, 10.58% WO<sub>3</sub>, 0.57% Pb, 0.023% As, 0.07% Bi, 0.70% S, and Sb (below the detection limit), with a tin recovery of 78% (yield of 32.2% wt); and ii) a composite tungsten concentrate assaying 44.21% WO<sub>3</sub>, 15.44% Sn, 0.85% S, 0.095% As, and Sb (below the detection limit), with a tungsten recovery of 71.4% (yield of 27.8% wt). The tin concentrate is suitable for smelting, and the tungsten concentrate is suitable for manufacturing ammonium para tungstate. Thus, this gives a scope to the sponsoring of the processing of tin and tungsten ores and to the marketing of the concentrates. The mine locations, the lease-granting authority and the marketing/processing companies are known and have been identified by the sponsor.

### References

Indian Minerals Yearbook, 1997. The Controller of Publications, Delhi, India.

## OLD TAILINGS DUMPS OF CONCENTRATING PLANTS AS A SOURCE OF RAW MINERALS

V.M. Izoitko\*, Ye.N Shumskaya<sup>o</sup>

\*JSC, <sup>o</sup>Mekhanobr Engineering, Russia

### Abstract

Based on many years of research, conducted by Mekhanobr's staff, a possibility has been found for enhancing the complex utilization of raw minerals by means of an additional recovery of non-ferrous and precious metals from concentrating plants' tailings. The high economic efficiency of the currently employed technological processes lies in the fact that the latter were tailored to match the mineral composition of tailings, usually rich in metals, and in the reasonably low cost of commercial products produced. Besides, such an approach favorably affects the ecological situation around the mining area.

*Keywords: complex utilization, tailings, technological processes, ecology*

### Introduction

Mining industry is the largest source of solid and liquid wastes, gas and dust emissions. Many years of intensive operation on mining and concentrating enterprises have caused the accumulation of an enormous amount of solid wastes accounting for about 80% of the total rock mined. This amount constantly increases at of rate nearly 70 billion t/y. Simultaneously, the costs are increasing of disposal, storage, and protection of the environment against the hazardous impact of wastes of which every thousand tons occupies an area of 0.1 ha.

In many cases discarded wastes become modified with time by either gaining or loosing mineralization due to the removal of a number of constituents. As a result, water reservoirs and subsoil water often get contaminated with copper with copper, iron and zinc vitriols as well as with soluble metal oxides. An intensive dusting is observed on the surface of old dumps.

Tailings of concentrating plants are known to have the highest concentration of metals, in many cases exceeding the original ore mineralization. These tailings have been accumulating at a rate of 600÷700 t/y. The basic valuable metals contained in the wastes of a number of ore-processing sectors vary in their concentration within the following ranges:

- copper sector: Cu = 0.1÷0.9%; Zn = 0.1÷0.9%; Au = 0.1÷1.5 g/t; Ag = 3÷21 g/t; Re up to 0.6 g/t;
- polymetallic sector: Pb = 0.2÷0.7%; Zn = 0.03÷1.4%; Cu = 0.05÷0.4%; Cd up to 0.003%; Ga up to 0.003%; Se up to 0.0002%; Tl up to 0.0002%; Au = 0.2÷3.0 g/t; Ag = 3÷40 g/t;
- tungsten-molybdenum sector: Mo = 0.01÷0.03%; W = 0.03÷0.3%; Cu = 0.03÷0.3%; Bi = 0.03÷0.06%; Re = 0.1÷0.2%; Se = 0.5÷2 g/t; Tl = 0.5÷2 g/t;
- gold mining sector: Au = 0.1÷5.0 g/t; Ag up to 20 g/t.

Until recent times little attention was accorded to ore concentration wastes as a topic for informational, ecological, technological, and economic discussion. The numerous research efforts undertaken so far have shown that it is possible to distinguish between objective and subjective causes for metals being lost in tailings.

The objective group of causes includes a variety of forms of occurrence of the same metal in the ore (e.g., copper in the form of sulphides, sulfates, carbonates and silicates in stratiform deposits); simultaneous of the metal both in mineral and isomorphous forms (nickel in pentlandite, pyrrhotite, chalcopyrite, pyrite, olivine and pyroxene in copper-nickel deposits); forms not amenable to conventional methods of processing (organic compounds of platinum in coal shales); submicroscopic pattern of minerals, etc.

The subjective causes include an inadequate knowledge of the mineral composition of the ore; use of technologies which are either totally or partially incongruous with the mineral composition of the ore, and the adherence to a non-market economy. In order to reduce metal losses in tailings, the respective causes of such losses shall be analyzed for a particular plant along with the improvement of flow sheets.

The study of polymorphic and technological peculiarities of minerals, including their generations, allows concluding that the major metal losses (up to 20%) are provoked as early as at the ore comminution stage because of the inadequate liberation of aggregates and overgrinding. Since the liberation mechanism is governed by the energy of contacting minerals, a stereological method of analysis was developed in St. Petersburg enabling to determine the optimal grinding size, after which sliming is inevitable. A series of combined flowsheets has been worked out with particular stress made on pre-concentration processes with the aim of separating a maximum amount of gangue to be subsequently processed (e.g. by X-ray/radiometric separation, gravity separation, etc.).

Thus, for example, an additional treatment of polymetallic ores from Altai by heavy-media separation, on concentration tables or by lump-ore jiggling, resulted in higher (3% on average) lead and zinc recoveries, but also in a reduced consumption of toxic reagents, water, electric power and compressed air; lesser volumes of waste water and final-ground tailings: it helped reduce the environmental impact in the region. The problem of processing old tailings appears to be most pressing in the densely populated regions of the Urals, Caucasus and Altai. Meanwhile, it is essential that the value of the concentrates thus produced should exceed the costs, involved in mining and processing of the material, which run at 1.8÷2.5 US\$/t.

The principles, underlay new process flow sheets being developed for tailings concentration, from the regularities observed in the spatial distribution and modification of minerals across the tailing dumps. In most cases such sites have two zones enriched with commercially valuable components: a near-dam zone (mostly coarser particles of  $-1.0 + 0.3$  mm) and a pond zone (mostly fine fractions  $<0.01$  mm). In permafrost regions, the distribution of ore minerals is naturally associated with interlayers of ice-mineralization is recorded at the footings of annual mining cycles, i.e. supraglacial zones.

The study of tailings, discarded by copper-zinc pyrite ore processing operations in the Urals (over 220 million t of dry matter assaying up to 0.47% Cu, 1.22% Zn, 0.25%

Pb, 2.7 g/t Au, 23.2 g/t Ag and other metals), has shown that the biggest economic effect is achieved when precious metals are additionally recovered. A number of tailing dumps have been inspected to show that the highest gold concentrations are to be found in a slimy portion (50÷50% minus 74  $\mu\text{m}$ ) of their central parts (Sample I) as compared with the beach material (50÷60% minus 74  $\mu\text{m}$ ).

Free gold accounts for 8÷13%. Any further grinding improves this figure by a mere 2÷3%. The bulk of gold mineralization is represented by aggregates with sulphides, submicroscopic inclusions in pyrite and chalcopyrite and is concentrated in finer fractions (see Table I).

Table 1: Size distribution of old tailings-material at a copper-zinc concentrator.

Samples	Size class (mm)	Yield (%)	Mass fraction of Au (g/t)	Recovery of Au (%)
1	- 2 + 0.044	54.4	1.10	33.6
	- 0.044 + 0.010	19.4	1.30	14.2
	-0.010	26.2	3.55	52.2
Total for tailings		100.0	1.78	100.0
2	+ 1	2.46	0.47	0.51
	- 1 + 0.3	20.38	0.50	4.54
	- 0.3 + 0.1	31.44	0.63	8.82
	- 0.1	45.72	4.23	86.13
	Total for tailings	100.00	2.25	100.00

Table II: Results of gravity-flotation concentration of old tailings.

Products	Yield (%)		Mass fraction Au (g/t)	Recovery Au (%)	
	by operations	of initial feed		by operations	of initial feed
Sample 1					
Gravity concentrate	1.47	0.8	25	33.42	11.23
Gravity tailings	98.53	53.6	0.74	66.58	22.37
Size - 2 + 0.044 mm	100.00	54.4	1.10	100.00	33.60
Sample 2					
Gravity concentrate	1.16	0.6	30	60.80	8.12
Gravity tailings	98.84	51.22	0.23	39.20	13.24
Size - 1 + 0.1 mm	100.00	51.82	0.58	100.00	13.36
Flotation of gravity tailings after regrinding Sample 2					
Concentrate 1	1.37	0.7	10	59.32	3.11
Tailings 1	98.63	50.52	0.095	40.68	2.13
Feed	100.00	51.22	0.23	100.00	5.24
Flotation of size fraction minus 0.1 mm					
Concentrate 2	28	12.8	11	72.80	62.70
Tailings 2	72	32.92	1.60	27.20	23.43
Size - 0.1 mm	100	45.72	4.23	100.00	86.13
Total for old tailings		100.00	2.25		100.00

The coarser fractions of the tailings (>0.1 mm) were treated on a Knelson concentrator, while fine fractions (minus 0.1 mm) were subjected to regrinding and flotation. Notably, the gravitational recovery of free gold gave positive results on both samples, while the flotation technique was successful on Sample 2 only: beach section of the tailing pond (see Table II).

Production of high-grade gold concentrates from old tailings involves heavy gold losses. These are drastically reduced in hydrometallurgical processing of low-grade concentrates (direct vat cyanidation). However, this technique cannot be profitable (gold recovery of 60%) without a preliminary concentration of the old tailings. Since 40% of the gold in the concentrate is in pyrite, the process of autoclave oxidizing leaching is suggested, to break up the pyrite, with the following parameters:

- leaching temperature: 170 °C;
- oxygen pressure: 4÷5 atm;
- solids in pulp: 25%;
- retention time: 1 h.

After the autoclave leaching the pulp was cyanated, with the gold recovery for the operation being 95% (Table III).

Table III: Results of hydrometallurgical processing of technological products.

Samples	Technological products	Metallurgical results				
		Yield (%)	Mass fraction of Au (g/t)	Gold recovery from feed (%)		
				in product	in cyanidation	
				I	II	
1	Gravity concentrate	0.8	25	11.23		
	Slimes <0.044 mm	45.6	2.59	66.40		
	Total	46.4	2.98	77.63	50.60	73.80
	Rejects	53.6	0.74	22.37		
	Total for old tailings	100.0	1.78	100.00		
2	Flotation concentrate I from gravity tailings	0.7	10	3.12		
	Flotation concentrate II	12.8	11	62.7		
	Gravity concentrate	0.6	30	8.02		
	Total	14.1	11.76	73.84	48.00	70.20
	Rejects	85.9	0.68	26.16		
	Total for old tailings	100.0	2.25	100.00		

Note: Concentrate cyanidation: I = direct, II = after hydrometallurgical oxidation in autoclave.

Judging from the results cited, both types of cyanidation provide similar gold recovery figures: 50.6% and 48%; 73.8% and 70.2%.

At the same time, the volume of technological products from the beach zone tailings (Sample 2) is three times less, and this, naturally, the total cost of gold recovery. It follows then, that the cost of the commercial product, produced from a ton concentrator's old tailings, will come to 13.5÷15.8 US\$/t, which is many times the production cost. Particularly attractive for the extractive metallurgy are the tailings from the concentrating plants copper-nickel ores.

The existing tailings dumps have accumulated materials with over 300 million t of dry matter, containing up to 0.5% of copper and nickel, as well as platinoids with a combined concentration of 1÷5 g/t and a Pd/Pt ratio of 0.5÷4.5.

The bulk of the platinum mineralization is associated with the minus 0.140 mm material, and the set of the platinum-containing minerals is the same as in copper-nickel ores.

The technological research, conducted on centrifugal separators of various models, has proved their high efficiency (Table IV).

Table IV: Metallurgical results of processing old tailings from copper-nickel concentrators.

Products	Yield (%)	Content				Recovery (%)			
		Pt (g/t)	Pd (g/t)	Rh (g/t)	Ni (%)	Pt	Pd	Rh	Ni
Gravity concentrate	1,76	22,1	35,5	2,0	2,07	64,66	56,81	44,0	28,0
Final tailings	98,24	0,216	0,48	0,045	0,095	35,34	43,19	56,0	72,0
Old tailings	100.00	0,6	1,1	0,08	0,13	100.00	100.00	100.0	100.0

The basic process flow sheet provides for a preliminary screening of material at 0.074 mm size and concentration of >0.074 mm material in spiral sluice boxes, producing a middlings concentrate and final nickel-containing tailings No. 1. The middlings from the spiral sluice boxes are mixed with the minus 0.074 mm fraction and upgraded in a sluice-hydrocyclone unit from which a finished platinum concentrate (see Table V) and final tailings N° 2 are obtained.

Table V: Description of rougher concentrate.

Metal	Content	Depth of concentration	Recovery (%)
Pt	4.4÷13.6 g/t	10.3÷18.9	78.6÷94.1
Pd	18.7÷71.4 g/t	9.4÷19.8	53.2÷75.7
Rh	0.52÷13.1 g/t	9.2÷12.6	52.7÷75.0
Au	2.5÷2.8 g/t	9.6÷21.6	77.9÷88.0
Ni	1.62÷2.03%	8.5÷14.1	57.9÷70.9
Cu	4.15÷6.53%	11.7÷21.1	87.6÷94.0

The combined concentrates are shipped to a sintering plant for further processing, while tailings N° 1 and N° 2 are pumped to a new tailing pond where they are used for dam filling. The investment into old tailings processing may bring an annual profit of up to 600% while favorably affecting the ecological situation in the industrial region and in the Arctic as a whole.

The analysis of the data available has shown that the efficiency of the tailings processing business depends not only on the high concentration of metals in tailings, but also on some other factors:

- average size of particles within the – 0.074 + 0.044 mm size group, which substantially reduces the cost of power-intensive crushing and grinding;
- a possibility of a complex utilization of wastes and the use of conventional ore dressing methods (flotation, gravity separation, etc.); geo-technological methods and low-cost heap leaching. This also allows using and expanding the existing production facilities of operating plants.

The above-listed factors make the tailings processing business highly profitable and contributing to the improvement of the environment in industrial regions.

This Page Intentionally Left Blank

## **PROCESS OF COMPLEX ORES**



This Page Intentionally Left Blank

**Pre-Concentration of a Low-Grade Sulfidic Copper Ore from Murgul-Çakmakaya Region of Turkey**

A. Gül, G. Önal

C10-1

**Processing of Valuable Vein-Minerals, as Molybdenite, Monazite, Magnetite, Pyrite and Ilmenite**

M. Zlagnean, N. Tomus, C. Vasile, I. Vasile

C10-5

This Page Intentionally Left Blank

## PRE-CONCENTRATION OF A LOW-GRADE SULFIDIC COPPER ORE FROM MURGUL-ÇAKMAKKAYA REGION OF TURKEY

A. Gül, G. Önal

Istanbul Technical University, Mining Faculty, Mineral and Coal Processing Section,  
Maslak, Istanbul, Turkey

### Abstract

In this study, a sulfide ore with 0.28% Cu was subjected to pre-concentration by the application of gravity separation. Sink and float tests were carried out on low-grade copper ore crushed to <9 mm and classified before beneficiation. In this way, it was established that 45% of the ore was discarded with 0.04% Cu and a loss of metal recovery of only 6.1%. The pre-concentrate obtained in this manner had a grade of 0.48% Cu and a recovery of 93.8%.

*Keywords: pre-concentration, low-grade, copper ore, gravity separation*

### Introduction

Costs of mining and beneficiation by flotation become prohibitive for low-grade ores, due to excessive grinding costs. Therefore, it becomes important to first treat these ores by pre-concentration. The concentration of ores already pre-concentrated in coarse sizes provides a decrease in investment costs as well as grinding and flotation costs. The concentrate obtained has higher grade and recovery figures (Aytekin et al., 1976; Bergmann, 1969; Burt, 1984; Gül, et al., 1997; Heide and Hegner, 1974; Kieffer, 1987; Özkol, 1986).

Tailings discarded should have metal content less than or equal to flotation tailings, in order to have an economically viable pre-concentration process. Discarded coarse tailings must be studied for utilization in other areas. These can be used as filling material in underground mining. The amount of discarded tailings in pre-concentration, storage of tailings and flotation costs are important parameters. The cost of storing discarded tailings is of particular importance, and the geomorphological situation of the district must be taken into consideration as well (Bergmann, 1969; Helms and Mersch, 1998; Kieffer, 1987; Lange, 1973; Leininger and Erdmann, 1984).

Pre-concentration is applied to many ores, including sulfide ores. In pre-concentration, a heavy-medium cyclone, cones, jig and shaking tables, magnetic and electrostatic separations, and optical sorting are the usual methods employed (Bergmann, 1969; Burt, 1984; Heide and Hegner, 1974; Kennedy, 1985; Lange, 1973; Wright, 1971).

### Materials and methods

#### *The ore sample*

In this study, a low grade, 0.28% Cu, sulfide copper ore from the Murgul-Çakmakkaya District was used in pre-concentration tests; the ore sample used was

taken from the Murgul-Çakmakkaya deposit and was discarded due to the overburden of the ore. The chemical composition of the ore sample is given in Table I.

Table I: Chemical analysis of the ore sample.

Element	(% wt)
Cu	0.28
Zn	0.02
Fe	2.94
S	3.36
SiO <sub>2</sub>	84.52
CaO	0.07
MgO	0.23
Al <sub>2</sub> O <sub>3</sub>	0.24
LOI	3.39

Mineralogical studies show that the ore contains pyrite, chalcopyrite, sphalerite, covellite, pyrrhotite and molybdenite as economic minerals. Gangue minerals are mainly quartz and a small amount of calcite-dolomite and barite. Partially impregnated single crystals of pyrites appear alone and interlocked with chalcopyrite and quartz.

Pyrite grains vary in sizes from a few  $\mu\text{m}$  up to 300  $\mu\text{m}$  to 350  $\mu\text{m}$ . Chalcopyrite grains show variation from 10÷15  $\mu\text{m}$  to 0÷0.7 mm. Very minute pyrite and quartz grains are observed in coarse chalcopyrite grains.

Quartz, the main gangue mineral, has crystal sizes that vary from 0.4÷0.5 mm to 20÷30  $\mu\text{m}$ .

The majority of quartz particles are more than 0.1 mm in size. Furthermore, in small quantities, calcite-dolomite and barite, can be countered as gangue minerals. Economic minerals, as well as gangue minerals in the ore, have a hydrothermal genesis.

The ore is completely crushed to <9 mm. Table II indicates the distribution of the Cu % according to size-class.

Table II: Cu distribution of <9 mm ore sample according to class-size.

Size (mm)	Yield (%)	Grade Cu (%)	Distribution Cu (%)
- 9 + 6	36.6	0.20	25.7
- 6 + 4	20.8	0.22	16.1
- 4 + 2	19.0	0.24	16.0
- 2 + 1	8.3	0.34	9.9
- 1 + 0.6	3.5	0.46	5.7
- 0.6 + 0.42	1.9	0.55	3.7
- 0.42 + 0.2	3.2	0.69	7.8
- 0.2	6.7	0.64	15.1
Total	100.0	0.28	100.0

It is clearly seen that as size becomes finer, the grade of copper is increased. This property can be ascribed to chalcopyrite being more friable than pyrite, and therefore requiring less energy in grinding.

### Sink and float tests

A <9 mm ore sample is classified into - 9 + 4.76 mm, - 4.76 + 2 mm, and - 2 + 1 mm fractions, and sink and float tests are executed by use of bromoformium, applying densities of 2.65÷2.70 g/cm<sup>3</sup>. The results of these tests are given in Table III and combined results are presented in Table IV.

Table III: Sink and float test results.

Size (mm)	Density (g/cm <sup>3</sup> )	Yield (%)	Grade Cu (%)	Distribution Cu (%)
- 9 +4.76	+ 2.70	6.1	0.96	20.6
	- 2.70 +2.65	13.8	0.22	10.7
	- 2.65	21.6	0.04	3.0
	Feed	41.5	0.24	34.3
- 4.76 +2	+ 2.70	5.7	0.91	18.3
	- 2.70 +2.65	9.3	0.21	6.9
	- 2.65	17.5	0.04	2.5
	Feed	32.5	0.24	27.7
- 2 +1	+ 2.70	1.3	1.28	5.9
	- 2.70 +2.65	1.7	0.23	1.4
	- 2.65	5.9	0.03	0.6
	Feed	8.9	0.25	7.9
- 1	Feed	17.1	0.5	30.1
Total	Feed	100.0	0.28	100.0

Table IV: Combined results of sink and float tests.

Product	Yield (%)	Grade Cu (%)	Distribution Cu (%)
Coarse concentrate (+2.70 g/cm <sup>3</sup> )	13.1	0.97	44.8
Middling (- 2.70 +2.65 g/cm <sup>3</sup> )	24.8	0.22	19.0
Coarse tailing (- 2.65 g/cm <sup>3</sup> )	45.0	0.04	6.1
<1 mm	17.1	0.50	30.1
Total	100.0	0.28	100.0

According to Table IV, 45% of tailings by weight are discarded, with a grade of 0.04% Cu and a metal recovery loss of 6.1%. The remaining 55% by weight, comprising concentrate, middling and <1 mm fractions with a copper content of 0.48% Cu, can be upgraded by flotation.

### Results and discussion

Tailing obtained after sink and float tests shows similarities in grade and recovery to flotation tailing (grade 0.03% Cu and recovery of 6÷8%). In this regard, pre-concentration is possible, as it is compatible with the data obtained in the literature, whereas tailing in sink and float tests has a grade of 0.04% Cu, and metal loss is 6.1%. Concentrate obtained after pre-concentration is subjected to flotation has a grade of 0.48% Cu. In order to apply sink and float tests on an industrial scale, a heavy-medium cyclone can be recommended. The proposed flowsheet appears in Figure 1.

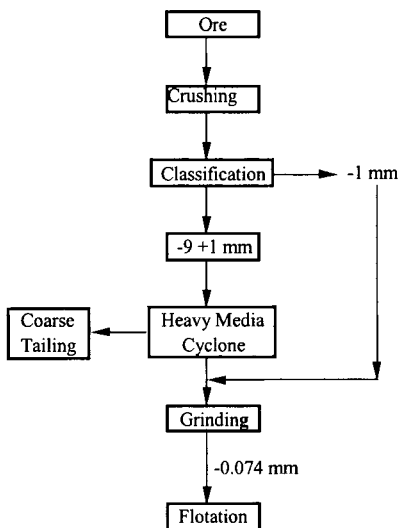


Figure 1: Flowsheet of pre-concentration circuit.

## References

- Aytekin, Y., İzdar, E., Dora, Ö., Köktürk, U. and Acar, E., 1976. Dogu Karadeniz Bölgesindeki Bakır-Kursun-Çinko-Kompleks Yataklarının Cevher. Hazırlama Yönünden İncelenmesi. Tübitak Yayını, No. 303 (in Turkish).
- Bergmann, A., 1969. Die wirtschaftliche berechtigung einer gravimetrischen voranreicherung vor der flotation. *Erzmetall*, 22, 286-289.
- Burt, R.O., 1984. Gravity Concentration Technology. *Developments in Mineral Processing*, 5, Amsterdam-Oxford-New York-Tokyo, 550-555.
- Gül, A., Önal, G., Sirkeci, A.A. and Gürkan, V.B.I., 1997. Preconcentration of low copper grade sulphide ores. In 7<sup>th</sup> Balkan Conference on Mineral Processing, Vol. II, 26-30 May, Vatra Dornei, Romania, 36-38.
- Heide, B. and Hegner, W., 1974. Erfahrungen mit schwertrübezyklonen bei der aufbereitung von metallerzen. *Erzmetall*, 27, 14-22.
- Helms, W., and Mersch, T., 1998. Vergleich feinkörniger aufbereitungsabgänge im hinblick auf die verwendung für versatzzwecke. *Erzmetall*, 51, 533-540.
- Kennedy, A., 1985. Mineral processing developments at Hammaslahti, Finland. *Mining Magazine*, 122-129.
- Kieffer, P.E., 1987. Die erweiterung der bergevorabscheidung in der aufbereitung des erzbergwerks grund und ihr einfluß auf das metallurgische und wirtschaftliche ergebnis. *Erzmetall*, 40, 165-170.
- Lange, J., 1973. Die aufbereitung des blei-zink-erzbergwerks grund. *Aufbereitungs-Technik*, 6, 355-364.
- Leininger, D. and Erdmann, W., 1984. Neuere entwicklungen bei der verwertung von aufbereitungsabgängen im steinkohlenbergbau. *Erzmetall*, Bd. 37, 72-78.
- Özkol, S., 1986. Untersuchungen zur Aufbereitung des Haldenerzes der Kupfergrube Ergani in der Türkei; Diss. RWTH-Aachen.
- Wright, F., 1971. Preconcentration of copper ore by heavy media separation at icon sullivan joint venture. *Proceedings of the Third Annual Meeting of the Canadian Mineral Processors Held at Mines Branch Department of Energy, Mines and Resources*, Ottawa, 78-83.

## PROCESSING OF VALUABLE VEIN-MINERALS, AS MOLYBDENITE, MONAZITE, MAGNETITE, PYRITE AND ILMENITE

M. Zlagnean, N. Tomus, C. Vasile, I. Vasile

Research and Design Institute for Rare and Radioactive Metals, Bucharest  
Manufacturing Factory, Feldioara, Brasov, Romania

### Abstract

The mineral dressing methods used for processing vein-type mineralizations depend on the valuable mineral grades, their nature, grain-size, superficial properties and physico-chemical characteristics. In developing the proper treatment process the production of rare metals (ilmenite, monazite, molybdenite) and sulphides (pyrite) concentrates was followed. The process developed for the vein-ore is a serie of mineral dressing methods (raw material preparation, molybdenite and ilmenite concentration) which comprises the following operations: molybdenite flotation, pyrite flotation, hydrogravitational separation on spirals and shaking tables, electric and magnetic separation.

*Keywords: flotation, magnetic separation, electric separation, monazite, molybdenite*

### Ore petrography and geology

The alkaline massif Ditrau, extended over an area of 110 km<sup>2</sup>, is localized in the pre-Permian crystalline veined structures, which later have undergone the alpine tectonic phase of the Eastern Carpathians. So that, near the massif is localized the meso-cretaceous Bukovinian layer, represented by Rebra, Negrisoara, Tulghes and Bratila litho-stratigraphic series. At the contact with the crystalline schists Ditrau massif presents a large (over hundreds meters) thermal aureole made of hornfels. The rocks of the Ditrau massif can be included in various, well-delimited petrographic associations:

- the complex of rocks from the endo-contact (granites, syenites and quartziferous monazites);
- Jolotca complex (diorites, meta-diorites and hornblendes);
- Putna complex (syenites and monazites);
- the central complex of the massif (fayalites, miaskites and alkaline diorites).

The mineralization of molybdenum and lantanides is basically made of veins (simple, composed and systems of veins) aligned on EW direction with 40÷70° dips towards N, associated with impregnations, nests and fine systems of little veins. The vein distribution is over an area of hundreds of meters long and 0.05÷1.5 m thick, sometimes even 20 m. The following mineralogical associations have been identified:

- sulphides: pyrite, molybdenite, galena, calcopyrite, sphalerite, marcasite, pyrrhotine;
- oxides: rutile, ilmenite, magnetite, hematite;
- phosphates: monazite, xenotime;
- silicates: allanite;
- carbonates: parisite, bastoesite;
- free elements: gold, silver, copper.



The mineralization gangue is represented by carbonates (calcite, manganiferous calcite, dolomite and ankerite), chlorites, quartz, albite, etc. The main useful elements which can be rendered profitable from Jolotca mineralization ore are: molybdenum and lanthanides (La, Ce, Nd, Th). Of economic interest can be considered also the following elements: S, Th, Zn, Pb and eventually Fe. From the chemical point of view the Ditrau mineralization shows the following values:  $\text{SiO}_2 = 40.8\%$ ,  $\text{Al}_2\text{O}_3 = 11.19\%$ ,  $\text{Fe}_2\text{O}_3 = 0.93\%$ ,  $\text{P}_2\text{O}_5 = 0.99\%$ ,  $\text{MnO} = 0.75\%$ ,  $\text{CuO} = 0.015\%$ ,  $\text{PbO} = 0.02\%$ ,  $\text{ZnO} = 0.19\%$ ,  $\text{NiO} = 0.01\%$ ,  $\text{Mo} = 0.057\%$ , etc. From the mineralogical point of view the studied ore contains monazite = 1.2%, xenotime = 0.05%, orthite = 0.1%, molybdenite = 0.1%, pyrite = 6%, ilmenite = 2%, magnetite = 1%, quartz = 17%, etc. The monazite is present as isolated grains, up to 0.25 mm or in micrograined radially nests associated especially with carbonates, but also with orthite, pyrite, etc. Xenotime appears subordinately associated with monazite. The orthite shows up isolated or in radially micrograined aggregates associated with carbonates and monazite (Zlagnean et al., 1994a). The molybdenite is present as very fine impregnation and curve-lamellar crystals. It is associated with oxides and sulfides.

### **Monazite, molybdenite, ilmenite, magnetite and pyrite processing**

When we elaborated the processing technology we had in mind some facts which are specific to Ditrau ore: the characteristic technology, the mineralogical associations, the size-distribution of the individual minerals (grains of monazite up to 0.25 mm) (Craiescu, 1985), etc. In order to recover the molybdenum, the pyrite and the monazite it has been designed a technological flowsheet, which combines flotation with gravity, electric and magnetic processing (Zlagnean et al., 1994b). So it has been optioned for molybdenite and pyrite flotation and for the recovery of monazite through electric and magnetic separation after gravity concentration. The flowsheet for Ditrau ore is presented in Figure 1. The basic flowsheet comprises the following operations.

#### *Grinding and classification of the raw-ore*

The grinding circuit is composed of a mill ( $\text{Ø} = 2,400 \times 2,500 \text{ mm}^2$ ) in a closed circuit with a double spiral classifier ( $\text{Ø} = 100 \times 6,500 \text{ mm}^2$ ). The fineness, at the 70.5% of ground and classified product, is  $< 0.080 \text{ mm}$ .

#### *Flotation of molybdenite and pyrite*

Flotation of molybdenite and pyrite from the classifier overflow is based on direct-selective flotation. The main phases of the flotation process were:

- pulp conditioning in order to adjust the dilution and the reagent addition;
- rougher flotation of molybdenite followed by 9 cleaning stages of the rougher concentrate;
- scavenger flotation in 3 stages in order improve Mo recovery from the rougher tailings,
- cleaning of the scavengers in 5 stages.

The capacities of the molybdenite and pyrite cells were  $2.8 \text{ m}^3$ ,  $0.6 \text{ m}^3$ ,  $0.05 \text{ m}^3$  and  $2.8 \text{ m}^3$ , respectively. The processing conditions for the molybdenite and pyrite flotation are presented in Table I. The technological results obtained from the scavenging of the molybdenum concentrate are shown in Table II.

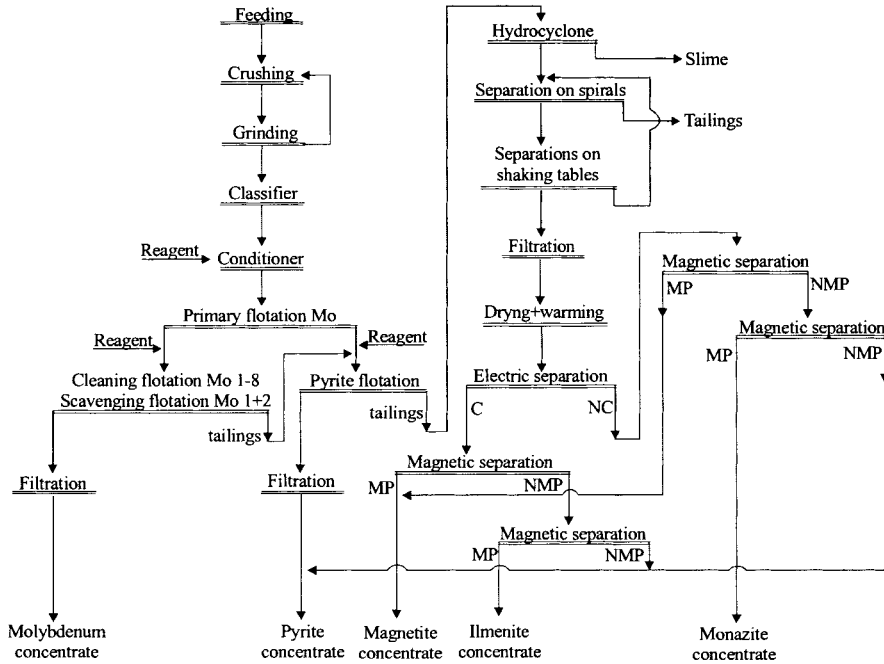


Figure 1: Flow-sheet for obtaining molybdenite, monazite, pyrite, magnetite and ilmenite concentrates.

Table I: Processing parameters adopted for molybdenite and pyrite flotation.

Parameters		Molybdenite flotation			Pyrite flotation
		rougher	cleaning	scavenging	
pH		8.5	8.5	8.5	8.5
Weight solid	(%)	15	20	12	15
Dilution, solid/liquid		1:5.67	1:4.00	1:7.33	1:5.67
Cell capacities	(m <sup>3</sup> )	2.8	2.8; 0.6; 0.05	2.8	2.8
Reagent consumption					
CaCO <sub>3</sub>	(g/t)	85	10	10	-
NaCN	(g/t)	60	20	10	-
Oil	(g/t)	50	50	30	-
Na <sub>2</sub> SO <sub>4</sub>	(g/t)	80	85	80	-
AGF	(g/t)	10	-	-	-
CuSO <sub>4</sub>	(g/t)	-	-	-	250
XE	(g/t)	-	-	2.6	80

Table II: Technological values at the scavenging of the molybdenum concentrate.

Products	Yield (%)	Molybdenum	
		grade (%)	recovery (%)
Molybdenum concentrate	0.23	21.15	71.54
Pyrite concentrate	10.52	0.14	21.9
Tailings from flotation	89.25	0.005	6.56

*Tailings desliming*

Desliming of the tailings coming from the pyrite flotation is carried out by hydrocyclones ( $\varnothing = 250$  mm), the classification size being 0.063 mm.

*Gravity concentration*

At the hydro-gravitational concentration of tailings (sizing more than 0.063 mm) coming from pyrite flotation is carried out using Carpco spirals, after a flowsheet, which comprises a primary concentration and a scavenging on Deister concentration tables (with re-circulation of the intermediate products). Adopting gravity pre-concentration of the flotation tailings it is obtained the pre-concentration of the rare earths (RE) assaying 14.25% RE<sub>2</sub>O<sub>3</sub> (recovery = 70.69%) at yield of 5.06%.

The pre-concentrate contains also 8.25 % TiO<sub>2</sub>, 15.70 % SiO<sub>2</sub>, and 23.50 % Fe.

*Cleaning of the gravity pre-concentrate*

Processing of tailings coming from gravity pre-concentration was carried out by magnetic and electric processes. The cleaning flowsheet contains drying, electrical separation, dry magnetic separation, and shaking tabling.

The electrical separation was carried out on a Carpco separator at a tension voltage of 35 kV, material temperature of 150 °C and distance between the electrodes of 6.5 cm.

The dry magnetic separation was carried out adopting 3 different magnetic field intensities (H = 0.01 T; 0.5 T and 1.2 T) in order to remove magnetite, ilmenite and other tailings and to obtain a final concentrate of rare earths. After the cleaning stage of the pre-concentrate are obtained the products as shown in Table III.

Table III: Results obtained after cleaning of the gravity pre-concentrate.

Products	Yield (%)	RE <sub>2</sub> O <sub>3</sub>	
		grade (%)	recovery (%)
Monazite concentrate	20.13	51.15	88.91
Magnetite concentrate	2.23	1.44	0.28
Non-magnetic product	1.59	5.48	0.75
Conductor product	9.24	3.56	2.84
Mixed product from table	16.2	3.82	5.34
Tailings from table	50.61	0.43	1.88

On the whole, combining the flotation with hydro-gravitational concentration, magnetic and electric separation in order to obtain the molybdenum and rare earths concentrates from Jolotca ore, we got the following results (Table IV). The results shows the possibility of obtaining a molybdenite concentrate with 21.15% Mo (Mo recovery of 74.84%) and a concentrate of monazite assaying 52.15% RE<sub>2</sub>O<sub>3</sub> at a metal recovery of 56.24%.

Table IV: Final results of the molybdenite and monazite concentration from Jolotca ore.

Products	Yield (%)	Mo (%)		RE <sub>2</sub> O <sub>3</sub> (%)		S (%)	TiO <sub>2</sub> (%)
		grade	recovery	grade	recovery	grade	grade
Molybdenum concentrate	0.23	21.15	74.84	-	-	14.8	0.96
Pyrite concentrate	10.52	0.086	13.86	-	-	48.38	0.14
Monazite concentrate	1.06	-	-	52.1	56.24	5.78	4.28
Magnetite	0.94	-	-	0.05	0.05	5.85	6.16
Ilmenite	0.40	-	-	0.05	0.02	2.8	45.15
Tailing from tabling	2.87	-	-	0.56	1.6	2.35	4.04
Preconcentration tailings	68.27	0.008	8.4	0.15	10.45	0.15	1.02
Slimes	15.71	0.012	2.9	1.97	31.64	0.37	0.82

## **Conclusions**

Applying a flowsheet, based on flotation, gravity separation and electric and magnetic separation on the Jolotca ore, could obtain a molybdenum concentrates assaying 14.33% Mo, a monazite concentrate assaying 52.15% RE<sub>2</sub>O<sub>3</sub>, a pyrite concentrate assaying 41.75% Fe and 47.38% S, a magnetite concentrate assaying 59.9% Fe and a ilmenite concentrate assaying 45 % TiO<sub>2</sub>.

From the qualitative point of view the mineral concentrates satisfies the metallurgical necessities. Tests, carried out in an industrial plant during many weeks, have lead to suitable performances.

## **References**

- Craiescu I., 1985. Prepararea substantelor minerale utile. Ed. did. si ped., Bucuresti, Romania.
- Zlagnean M., Vasile I., Vasile C., Tomus N., Georgescu D., 1994a. Technological research for monazite. ICPMRR. Bucuresti. Romania.
- Zlagnean M., Vasile I., Vasile C., Tomus N., Georgescu D., 1994b. Extraction of the concentrates of molybdenite and monazite from Jolotca ore. ICPMRR. Bucuresti. Romania

This Page Intentionally Left Blank

**PROCESSING OF RAW MATERIALS FOR GLASS AND  
CERAMICS**

This Page Intentionally Left Blank

<b>Carrier Flotation of Alunite from Kaolin Clay</b> S. Koca, H. Koca	C11-1
<b>Multicolor Optical Sorting: a Large Scale Application in a Feldspar Treatment Plant in Sardinia - Italy</b> B. Anselmi, H. Harbeck	C11-9
<b>Beneficiation of Low Grade Feldspar Ores for the Ceramics Industry</b> M. Agus, R. Angius, M. Ghiani, R. Peretti, A. Serci, A. Zucca	C11-17
<b>Beneficiation of Sand from the Sava-River Bed</b> B. Salopek, G. Bedeković	C11-26
<b>Controlled Processing of Raw Materials for Ceramic Paste Components</b> F. Durão, L. Cortez, T. Carvalho, C. Pires, A. Felicio, I. Rodrigues, R. Lourenço, C. Tareco, G. Brito	C11-32
<b>Beneficiation Studies on a Spodumene Ore From Portugal</b> A. Botelho de Sousa, M.M. Amarante, M. Machado Leite	C11-40



This Page Intentionally Left Blank

## CARRIER FLOTATION OF ALUNITE FROM KAOLIN CLAY

S. Koca\*, H. Koca<sup>o</sup>

\*Osmangazi University, Mining Engineering Department, Eskisehir, Turkey

<sup>o</sup>Anadolu University, Bozuyuk Technical Collage, Mining Department,  
Eskisehir, Turkey

### Abstract

A kaolin sample with high SO<sub>3</sub> content, obtained from the Balikesir-Sındırgı region, was used to study separation of alunite from kaolin by carrier flotation. Several parameters believed to be effective on separation were tested. Collector amount, pulp pH, size and amount of carrier mineral, agitation time and speed, and pulp temperature were varied and separation conditions were optimized. The best results obtained under the optimum conditions were as follows: 1.03% SO<sub>3</sub> content and 57.95% kaolin recovery.

*Keywords: carrier flotation, alunite separation, kaolin beneficiation*

### Introduction

Kaolin is one of the main raw materials of the ceramic industry, and the growth of the ceramic industry in Turkey in recent years has resulted in the need for high quality industrial minerals. There are not enough high quality kaolin deposits to meet the demand, and an important amount of kaolin has been imported from overseas. It is, therefore, necessary either to search for new kaolin deposits or to upgrade the existing material.

Ustaer and Gurgey (1975) reported the existence of large kaolin deposits, located mainly north-west of Anadolu, that contain alunite as an impurity. It is impossible to utilize such alunitic kaolins without purification, due to SO<sub>3</sub> contents coming from alunite impurities. SO<sub>3</sub> gas emission during the firing process leads to the occurrence of pores in the ceramic materials, which are of low quality.

A number of researches performed on alunitic clays has been reported in the literature (Dixit and Miller, 1980; Jungheng, 1984; Hwang et al, 1986; Koca and Ozdag, 1994; Ustaer and Gurgey, 1975; Sumer, 1991). The main methods for separation of alunite from kaolin include thermo-chemical, physico-chemical and physical methods.

Utilization of thermo-chemical methods requires heating of the material over 1,000 °C, and this may create problems in the utilization of kaolin in the ceramic industry due to the loss of its plastic properties. On the other hand, thermo-chemical methods are not economical in comparison with other methods. Therefore, physical and physico-chemical methods are essential in the separation of these minerals for both better utilization and economics.

Although the separation of alunite from kaolin were successful in the case of artificial mixtures by both flotation and flocculation (Ustaer and Gurgey, 1975; Jungheng, 1984; Koca and Ozdag, 1994), the concentration of natural ores by conventional methods were not satisfactory (Sumer, 1991; Koca, 1992). It was pointed out by

many investigators that the liberation of alunite is obtained at very fine size ranges, around 10  $\mu\text{m}$  (Miller and Ackerman, 1980; Hwang et al, 1986). A liberation study of alunitic kaolins from the same region revealed that the liberation of alunite was obtained at less than 10  $\mu\text{m}$  in size (Koca, 1992). Therefore, it is very clear that the major problem in the separation of alunite from kaolin is liberation size. The separation must be conducted at very fine size ranges, where the conventional methods generally become inefficient (Fuerstenau, 1979; Senneth and Young, 1979). It is well known that carrier flotation has been successfully used either for the beneficiation of ultrafine particles (Liang et al, 1997) or in the removal of minute quantities of impurities. The removal of anatase from kaolin by carrier flotation has been investigated and successfully applied both in laboratory and on commercial scale (Greene and Duke, 1962; Yang, 1979; Senneth and Young, 1979; Fuerstenau, 1980; Wang and Somasundaran, 1980; Chia and Somasundaran, 1983). In this study, carrier flotation of alunite from kaolin was investigated by using coarse calcite particles as a carrier.

## Materials and method

### Sample

Chemical composition of kaolin sample obtained from Balıkesir-Sındırgı region is given, in Table I.

Table I: Chemical analyses of sample.

Component	(% wt)
Al <sub>2</sub> O <sub>3</sub>	31.35
SiO <sub>2</sub>	50.23
Fe <sub>2</sub> O <sub>3</sub>	0.50
SO <sub>3</sub>	8.03
K <sub>2</sub> O	1.65
Na <sub>2</sub> O	0.10
CaO	0.20
MgO	0.10
LOI	7.84

Kaolin sample was comminuted in a ceramic ball mill and its particle size distribution is given in Figure 1. Particle size distribution was determined by using MALVERN Instruments Master Particle Sizer M6.10. As can be seen from Figure 1, 95% of the particles are less than 12  $\mu\text{m}$  and 90% of the particles are less than 10  $\mu\text{m}$ .

Calcite used as a carrier was extra pure and was ground to minus 0.106 mm. The ground calcite sample was wet screened and divided into four size fractions: - 0.106 + 0.075 mm; - 0.075 + 0.05 mm; - 0.053 + 0.038 mm, and - 0.038 mm.

Sodium oleate and sodium silicate (SiO<sub>2</sub>:Na<sub>2</sub>O=3.33) used were laboratory grade purchased from Riedel-de Haen Chemical Company.

### Method

Flotation experiments were carried out in a specially built microflotation cell made of

glass, 250 ml in volume, and air was supplied to the cell by a compressor through a sintered glass filter, which was able to generate air bubbles. Dispersion and conditioning of kaolin were performed in a one liter beaker, using a multi speed mechanical impeller. In the tests conducted to determine the effect of conditioning temperature, beaker was kept in a water bath to maintain the conditioning temperature within  $\pm 1$  °C. 22 g of sample was dispersed in 200 ml of distilled water at 1,500 rpm in the presence of  $\text{Na}_2\text{SiO}_3$  (1 kg/t) for 15 min. Carrier mineral, calcite, and sodium oleate were added to suspension and pH was adjusted. The suspension was then conditioned at a desired conditioning speed, time and temperature. The conditioned pulp was transferred to the microflotation cell and floated at 1250 rpm for 5 min. The flotation products were separated from calcite by washing on a screen, and dried, weighed and analyzed for  $\text{SO}_3$ .

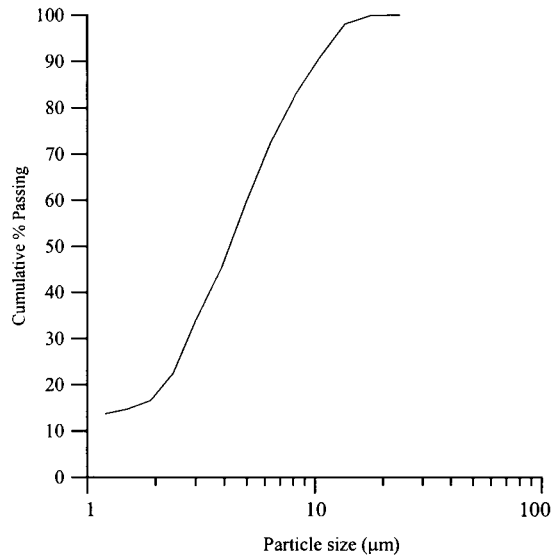


Figure 1: Particle size distribution of sample.

## Results and discussion

Carrier flotation can be achieved via the enhanced aggregation between fine (carried) and coarse (carrier) particles under intense agitation and followed by froth flotation. The common and critical requirements for carrier flotation are: (1) presence of coarse particles; (2) use of higher energy agitation and (3) hydrophobicity of the carrier (coarse) and carried (fine) particles (Subrahmanyam and Forsberg, 1990).

Under the influence of the above description, carrier flotation of alunite from kaolin was investigated and important parameters were tested. The froth fraction, which contains alunite and calcite, was referred to as tailings, and the fraction, which contains kaolin was referred to as concentrate. The results are illustrated in graphs in terms of  $\text{SO}_3$  content and kaolin recovery in the fraction, (concentrate). The effect of

pulp pH on carrier flotation of alunite from kaolin was evaluated under the following conditions:

pulp pH	= 8÷11
sodium oleate dosage	= 1 kg/t
sodium silicate dosage	= 1 kg/t
dispersant conditioning time and speed	= 15 min and 1,500 rpm
collector conditioning time and speed	= 15 min and 1,750 rpm
pulp density (w/w)	= 10%
the ratio of carrier amount/kaolin amount	= 10%
carrier size	= $-0.053 + 0.038 \text{ mm}$
frother amount	= 1 ml/l
flotation time	= 5 min

The pulp pH was adjusted after the addition of carrier particles and sodium oleate. It was varied from 8 to 11, and results are illustrated in Figure 2. As it can be seen from this Figure,  $\text{SO}_3$  content and kaolin recovery in concentrate decreased with increasing pH, indicating that the amount of floated material increased at high pH values. It was reported in the literature that from pH = 7 to pH = 10 complete depression of calcite was achieved in the presence of sodium oleate and sodium silicate, and at pH = 10 complete flotation was obtained (Fuerstenau, 1982; Fuerstenau et al, 1984). Infrared studies of sodium oleate adsorption on calcite surface was carried out in another work and showed that sodium oleate was adsorbed chemically on calcite surface at pH = 10.5 and calcium oleate precipitates on surface (Peck, 1963). Chemisorption and surface precipitation of oleate on alunite surface was also shown in infrared studies at pH = 9.7 (Dixit and Miller, 1980). The anionic flotation of alunite was achieved at strong alkali solutions (above pH = 9), and the presence of  $\text{Na}_2\text{SiO}_3$  did not affect the electrokinetic potential of alunite significantly. (Miller and Ackerman, 1980; Koca and Ozdag, 1994). From the foregoing discussion it can be concluded that oleate is strongly adsorbed on both alunite and calcite particles, so that the hydrocarbon chains orient towards the bulk solution (Chia and Somasundaran, 1983). Strong aggregation between alunite and calcite is therefore expected in carrier flotation systems. Oleate adsorption on kaolin is not expected in the presence of  $\text{Na}_2\text{SiO}_3$  and under the intense mixing conditions since the electrokinetic potential of kaolin is around  $-90 \text{ mV}$  under studied conditions (Chia and Somasundaran, 1983; Koca and Ozdag, 1994). It was shown that high surface charge reduces the aggregation due to repulsive energy between particles (Somasundaran, 1980). Therefore, the aggregation of kaolin-calcite or kaolin-alunite is not expected.

The effects of collector amount on carrier flotation were studied at the same conditions given above and pH was set as 11. The collector dosage was varied between 0.25 g/t to 1.5 g/t, and results are given in Figure 3. Both  $\text{SO}_3$  content and kaolin recovery were decreased with increasing collector dosage up to 1 kg/t. At high collector dosage (1.5 kg/t),  $\text{SO}_3$  content was increased significantly and kaolin recovery was decreased further, indicating the excess amount of sodium oleate caused both the flotation of kaolin and the reduction of alunite-calcite aggregation. It was explained by Chia and Somasundaran (1983) that when dosages of oleate are too high, the adsorption of oleate on particle surfaces takes place in multi layer forms

resulting in a reverse orientation (polar head of the collector oriented towards the bulk solution). This reduces the hydrophobicity and aggregation. It explains the increase in SO<sub>3</sub> content of concentrate.

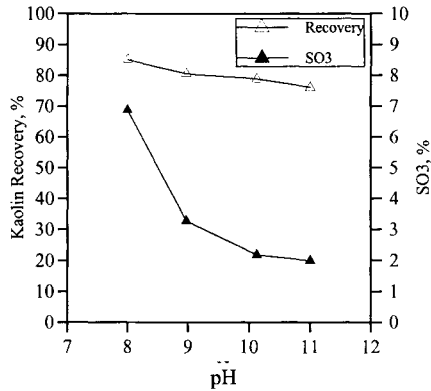


Figure 2: Effect of pulp pH on separation.

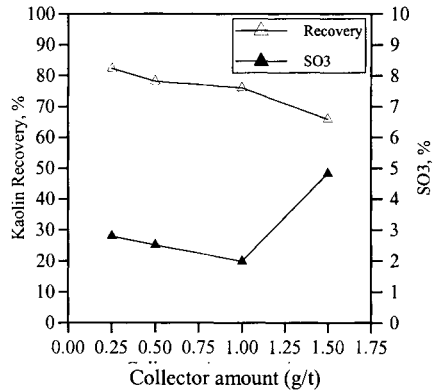


Figure 3: Effect of collector amount on separation.

Role of carrier size and carrier amount was determined under the same conditions and the results are illustrated in Figures 4 and 5, respectively. As the carrier size was decreased SO<sub>3</sub> content of the concentrate was decreased significantly. When carrier amount was kept constant, the decrease in particle size causes an increase in the number of particles present in the system. Since collision rate is a function of particle concentration, the decrease in particle size is expected to increase in alunite removal in the form of calcite-alunite aggregates.

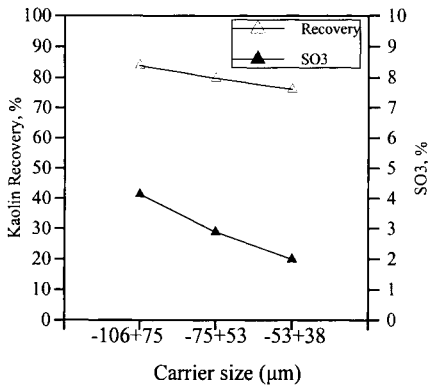


Figure 4: Effect of carrier size on separation.

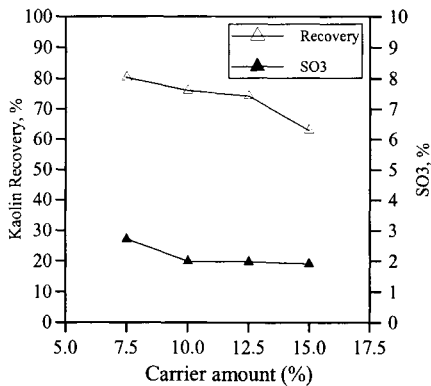


Figure 5: Effect of carrier amount on separation.

The effect of carrier amount can also be explained by increased collision and aggregation rate caused by the increase in particle concentration. It should be noticed that at a high carrier amount (15%), kaolin recovery decreased while SO<sub>3</sub> content was not changed significantly. It could be due to mechanical entrapment of kaolin particles.

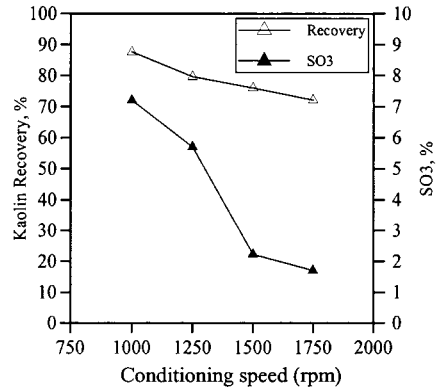
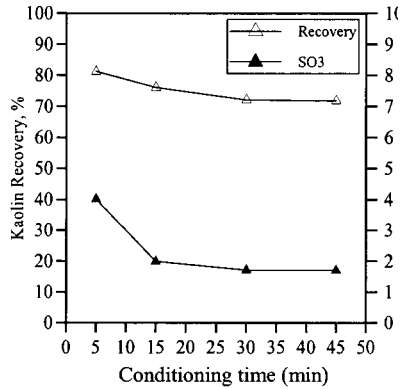


Figure 6: Effect of conditioning time on separation. Figure 7: Effect of conditioning speed on separation.

Conditioning time and conditioning speed were found to be primarily responsible for the extend of separation. The effects of conditioning time and speed were studied under the same conditions and the results are illustrated in Figures 6 and 7, respectively.

As it can be seen from the Figure 6, 30 min conditioning produced better results and, therefore, 30 min conditioning was set as optimum in determining the effects of conditioning speed. SO<sub>3</sub> content of the concentrate markedly decreased with increasing both conditioning time and conditioning speed. The weight yield of the concentrate also decreased. The prolonged conditioning time and speed lead to improved aggregation and consequently to better separation. Better separation in alunite-calcite carrier flotation with increasing conditioning time can also be attributed to increase in collector adsorption on minerals as well as improved aggregation conditions.

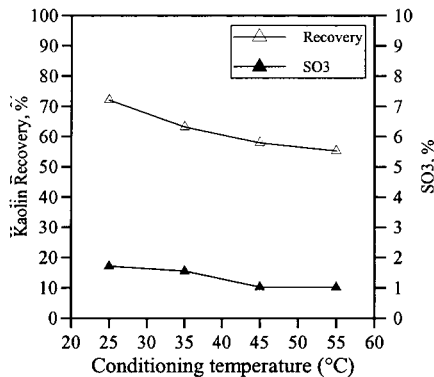


Figure 8: The effect of conditioning temperature on separation.

The effect of flotation temperature on floatability of alunite and calcite aggregates was investigated between 25 °C and 55 °C. SO<sub>3</sub> content and kaolin recovery in the

concentrate decreased with increasing pulp temperature (Figure 8). It was reported in the literature that the increase in temperature can affect system parameters such as better collector adsorption on minerals, better solubility of collector and minerals, reduced viscosity of the liquid medium, enhanced frothing property of collector, etc (Wang and Somasundaran, 1980; Dixit and Miller, 1980; Miller and Ackerman, 1980). The adsorption of sodium oleate on alunite and calcite was shown to be chemisorption in nature (Peck, 1963; Koca, 1992). Since chemisorption increased substantially with increasing temperature, the collector adsorption on minerals is also expected to increase leading to improvement in flotation.

### Conclusions

The separation of alunite from kaolin by means of carrier flotation was investigated and the results revealed that carrier flotation produced better results than conventional flotation, reported in another study with kaolins from the same region (Koca, 1992). Studied variables, collector amount, pulp pH, size and amount of carrier mineral, agitation time and speed, and pulp temperature were determined to have strong effect on separation; the optimum conditions are given below:

collector amount	= 1 kg/t
pulp pH	= 11
carrier size	= $-0.053 + 0.038 \text{ mm}$
the ratio of carrier amount/kaolin amount	= 10%
agitation time and speed	= 30 min and 1,750 rpm
pulp temperature	= 45 °C

The best results obtained under the optimum conditions were as follows:

SO <sub>3</sub> content	= 1.03%
kaolin recovery	= 57.95%.

### References

- Chia, Y.A. and Somasundaran, P., 1983. A theoretical approach to flocculation in carrier flotation for beneficiation of clay. *Colloids and Surfaces*, 8, 187-202.
- Dixit, S.G. and Miller, J.D., 1980. Flotation chemistry of alunite oleate system. AIME Anuel Meeting, SME, Nevada, USA.
- Fuerstenau, D.W., 1979. The recovery of fine particles by physical separation methods. In: P. Somasundaran and N. Arbitor (Editors), *Beneficiation of Mineral Fines*. AIME, Michigan. 3-59.
- Fuerstenau, D.W., 1980. Fine particle flotation. In: P. Somasundaran (Editor), *Fine Particles Processing*, Vol 1, AIME, Maryland, 669-705.
- Fuerstenau, M.C., 1982. Semi-soluble salt flotation. In: R.P. King (Editor), *Principles of Flotation*, South African IMM, Johannesburg, 199-213.
- Fuerstenau, M.C., Miller, J.D. and Kuhn M.C., 1984., *Chemistry of Flotation*, AIME, Tennessee, USA.
- Greene, E.W., and Duke, J.B., 1962, Selective froth flotation of ultrafine minerals or slimes. *Trans. AIME*, 223, 389-395.
- Hwang, J.Y., Kullerud, G., Friedlaender, F.J. and Takayasu, M., 1986. Ultrafine particle processing: a method for alunite beneficiation. *Trans. AIME*, 280, 1961-1964.
- Juncheng, Z., 1984. Separation of alunite from kaolin by selective flocculation. *Industrial Inorganic Chemicals*, 28-32.
- Koca, S., 1992. Kaolin ve alunitin reaktif adsorpsiyon mekanizmalarının flotasyon reaktiflerinin seçimine etkisi. Ph.D. Thesis Anadolu University, Eskisehir, Turkey. (In Turkish, with English Abstr.)



- Koca, S. and Ozdag, H., 1994. Flotation of alunite from kaolin. 5 th Int. Minerals Processing Symposium, Coppedocia, Turkey, A.A. Balkema, Rotterdam, 135-140.
- Liang, R., Numata, Y., Fujita, T. and Wakamatsu, T., 1997. Studies on carrier flotation of ultrafine wolframite. XX Int. Mineral Processing Congress, Aachen, Germany, 669-678.
- Miller, J.D. and Ackerman, J.B., 1980. Bench scale flotation of alunite ore with oleic acid. In: P. Somasundaran (Editor), *Fine Particles Processing*. Vol 1, AIME, Maryland, 832-852.
- Peck, A. S., 1963. Infrared studies of oleic acid and sodium oleate adsorption on fluorite, barite, and calcite. U.S. Bureau of Mines, R.I., No 6202.
- Senneth, P. and Young, R.H., 1979. Current problems in beneficiation of kaolin clay. In: P. Somasundaran and N. Arbiter (Editors), *Beneficiation of Mineral Fines*. AIME, Michigan, 115-133.
- Somasundaran, P., 1980. Principles of flocculation, dispersion, and selective flocculation. In: P. Somasundaran (Editor), *Fine Particles Processing*, Vol 2, AIME, Maryland, 947-976.
- Subrahmanyam, T.V. and Forsberg, K.S.E., 1990. Fine particles processing: shear-flocculation and carrier flotation-a review. *International Journal of Mineral Processing*, 30,265-286.
- Sumer, G., 1991. Alunitli kaolinlerin zenginlestirilmesi. M.Sc Thesis, Anadolu University, Eskisehir, Turkey. (In Turkish, with English Abstr.)
- Ustaer, C. And Gurgey, I., 1975. The separation of alunite in alunitic kaolin by selective flocculation. *Clays and Clay Minerals*, 23,468-472.
- Wang, Y.H.C. and Somasundaran P., 1980. A study of carrier flotation of clay. In: P. Somasundaran (Editor), *Fine Particles Processing*. Vol. 2, AIME, Maryland, 1112-1128.
- Yang, D.C., 1979. Flotation in systems with controlled dispersion-carrier flotation, etc. In: P. Somasundaran and N. Arbiter (Editors), *Beneficiation of Mineral Fines*. AIME, Michigan, 295-308.

## MULTICOLOR OPTICAL SORTING: A LARGE SCALE APPLICATION IN A FELDSPAR TREATMENT PLANT IN SARDINIA - ITALY

B. Anselmi\*, H.Harbeck°

\*Maffei spa, Milano, Italy; °Allgaier-Mogensen Gruppe, Germany

### Abstract

Economic and ecological reasons are increasingly asking the mining industry to optimize the utilization of raw material; in close connection with this comes the growing need for smart alternatives to expensive traditional ore beneficiation processes. Maffei sarda srl operates in central Sardinia a large feldspar production unit, including two main open pit mines and a treatment plant. The total Maffei Sarda feldspar production has dramatically increased in recent years and is expected to reach half a million tonnes in year 2000. As a first step in a rationalization program for all production facilities in Sardinia, Maffei Sarda decided to install a 100 t/h optical sorting circuit in the treatment plant at Orani (NU). Optical sorting was chosen mainly because of its low operating costs and versatility, and was expected to improve both the final product overall quality and mine recovery. All bulk material that can clearly recognize by their surface optical characteristics can be classified using the MikroSort. Even insignificant optical nuances can be taken into account. After a simple preparation by size classification, the product stream is fed into the sorters; during the free fall at the end of a vibratory feeder the material fragments are scanned by high-resolution optical system and evaluated by parallel processor technology. The selection is made by accurate compressed air impulse jets that remove unwanted particles. The multicolor optical sorting technology is described with particular attention to the optical system, the image processing methods and the selection criteria. Then the industrial installation and the flow sheet are illustrated and the processing results reported.

*Keywords: optical-sorting, feldspar, Sardinia*

### Introduction

More than 95% of the entire Maffei Sarda srl feldspar production is sold to the ceramic market to floor tiles manufacturers. In recent years this market sector experienced some major changes in terms of raw material consumption and production areas. First of all, in Italy the growing importance of 'gres porcellanato' (fully vitrified) compared to the declining 'monocottura' (single firing) tiles, determined an overall increase of feldspar consumption and in particular of high quality 'white firing' materials. The main historical Maffei Sarda ore-body, the 'Orani-Ispaduledas' deposit, found itself unbalanced, containing too much 'monocottura' type feldspar and too less white feldspar. Production had nevertheless to follow the market, forcing the exploitation toward selective mining. As a side effect, the waste-to-ore ratio increased from 1:1 in 1989 to the 3:1 in 1998. Moreover, in the past decade, Spain progressively strengthens its importance amongst European tile producers, more than doubling its total throughput from 1990 to 1997. That did not involve Maffei Sarda until 1998, when in Spain the 'gres porcellanato' production started a sharp raise and increasingly amounts of high quality sodium feldspar, not

locally available, had to be purchased abroad. Although, Maffei Sarda, strategically located in West Mediterranean sea, was in the position to become a major supplier to both the Italian and Spanish 'gres porcellanato' industries, the growing and changing market demand required the modernization and expansion of its production facilities.

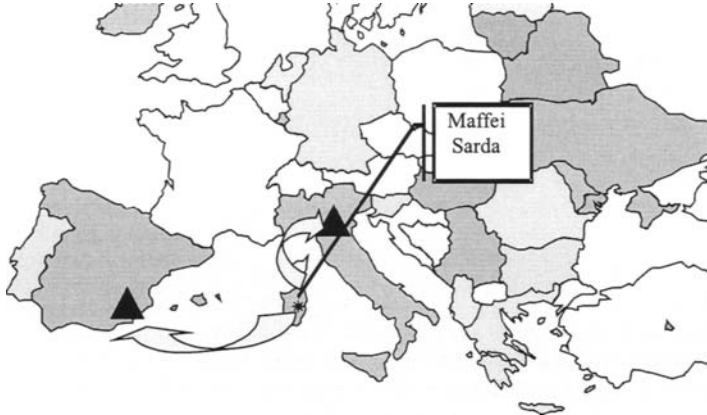


Figure 1: Maffei Sarda srl location.

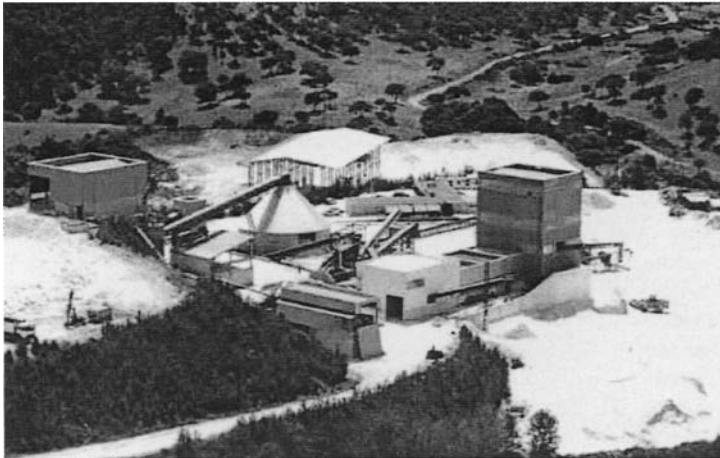


Figure 2: Orani treatment plant

### **Development program**

Four were the main objective of the development program.

Exploration and new mine development: exploration carried out from 1996 to 1999 outlined 6.5 million tons of new feldspar ore reserve to sustain expanding sodium feldspar production (Table I). Product diversification: development of new products,

characterized by different levels of oxide contents (Na, K, Fe, Ti, Mg), together with the necessary flexibility to produce them, is essential to meet client's requirements.

Table I: Maffei Sarda srl sales trend

	Sales 1996	Sales 1997	Sales 1998	Forecast 1999	Budget 2000
Production	259,000 t	308,000 t	380,000 t	370,000	550,000 t
Monocottura	19%	13%	12%	5%	3%
N° of products	9	11	13	14	15

Product diversification: development of new products, characterized by different levels of oxide contents (Na, K, Fe, Ti, Mg), together with the necessary flexibility to produce them, is essential to meet client's requirements. Logistic/production rationalization: the increase of the traffic toward Spain, necessitated the re-organization of the logistic to maintain price competitiveness. That included the construction of a new 90 t/h crushing plant. Beneficiation processes and expansion: the high quality standards needed for the 'gres porcellanato' production, require some beneficiation process beside traditional washing and screening to upgrade the natural ore-body quality. Several processes were investigated, magnetic separation, flotation and optical sorting. Also the installation of additional capacity was needed and realized. Ore sorting was chosen to start with, because of its low operating costs and its great impact on mine recovery and waste-to-ore ratio.

## The technology

### *Technological concept*

The main components and phases of the optical sorting system are as follows:

- material fed into hopper;
- individualization of particles in the integrated vibration feeder;
- transition to free-fall area;
- scanning of "Product curtain" by high-resolution optical sensor system;
- image evaluation by rapid parallel processor technology;
- product selection by means of high-accuracy compressed air impulses;
- removal of separated product streams;
- field bus network interface to central control.

### *Image capture*

Image capture is performed by one or two CCD color line scan cameras each with three color channels for the primary colors red, green and blue. Each color channel has a resolution of 8 Bit with the result that up to 16 million colors can be reproduced. Even when this resolution capacity cannot in practice be fully utilized because of external influences, extremely accurate color sensing is, nevertheless, realizable. The color sensing system scans the surface of the product stream over its entire width. As the product stream is 1.2 m wide and is moving at a speed of 1.5 m/s, the scanning rate and the working width must be such that the resolution of the product stream is adequate.

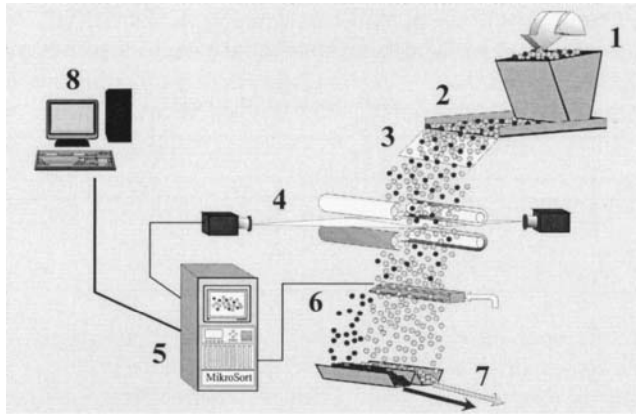


Figure 3: Operational sequence

Example: particles with 3mm diameter

Resolution: 5 scanning lines, 45 pixel in total

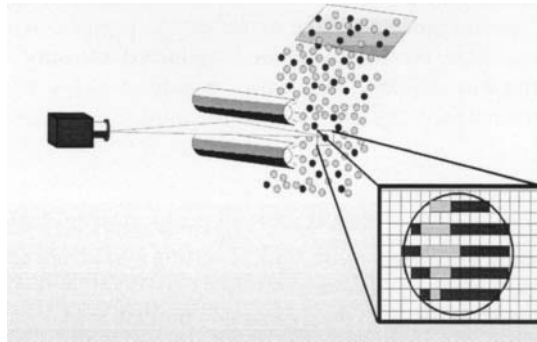


Figure 4: Data capture using line scan cameras.

The product stream is evaluated by means of transmitted light in the case of transparent particles and by means of light reflected from the particle surface in the case of non-transparent particles.

Capacity data are as follows:

- 16 million colors;
- horizontal resolution of 0.5 mm for a working width of 1,000 mm;
- up to 5,000 lines per second;
- processing of a maximum of 30 million scan points per second;
- high light sensitivity, so that it is possible to operate using simple fluorescent tube lighting;
- optional single- or multi-sided image capture.

With reference to figure 4 it can be seen that the number of pixels analyzed per each fragment is very high: it can vary from 45 for a 3 mm diameter particle on one side to around 400,000 for a 200 mm diameter fragment on two sides.

### Colour camera interface

The color camera interface principally fulfills the functions of camera control and the digitalization of the camera data. The color preprocessing has the following functions:

- capture of the three 8-Bit incoming information streams and image formation on an output stream having regard to the sort criteria;
- estimation and normalization of the input data;
- color class formation.

In order to fulfill the processing speed requirements the colour pre-processing is provided with extensive hardware capacity.

The image processing carries out object recognition and evaluation.

These procedures are carried out stepwise from the data received from each colour sensor via data reduction algorithms up to the point of the sorting decision.

The numbers of pixels in the colour classes are assessed specifically in relation to the material and then related to each other and to the total object surface area.

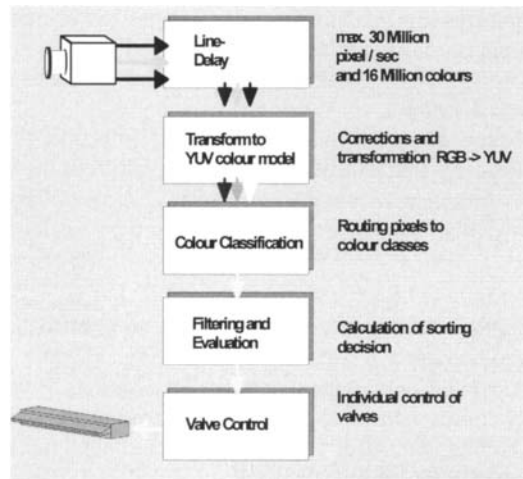


Figure 5: From Image Capture to Sorting Decision

### Product sorting

The sorting of the product stream is achieved using high-accuracy compressed air impulses. Compressed air valves and jets are chosen for this function to match the material being processed. The valves and jets are controlled via semi-conductor switches.

The following technologies have been installed in the product sorting zone:

- mini-dimensioned ejector elements (special valves and air jets);
- up to 256 compressed air valves and jets;
- rapid-action separation equipment; switch cycles are less than 10 ms;
- minimum falling distance between scanning and air jets;
- air impulse duration and number of air jets determined in relation to object size;

As a result of these measures the following advantages have been achieved:

- minimum system pressure and air consumption;
- minimum product losses.

### Sorting criteria

The opto-electronic sorting system offers a wide selection of sorting criteria. The efficiency of the system rests on the combination of these criteria. In this way all loose bulk materials, which are unequivocally classifiable on the basis of their optical characteristics, may be sorted. Even relatively insignificant optical nuances can be taken into account MikroSort make use of the following product characteristics in the application of sorting technology:

- **Real Color:** MikroSort offers a special facility for use with materials, which are not homogeneously colored. The allowable size limit for false-colour inclusions can be predetermined, i.e. if the false-colour portion of a predominately „good“ particle lies under this value, the particle will not be rejected. The benefit of this is a distinctly reduced product loss.
- **Particle Size:** the surface area as well as the horizontal and vertical dimensions are determined for each particle scanned. These are the classic selection characteristics and in using the them MikroSort assumes function of an electronic sieve.
- **Brightness:** brightness information is evaluated from transmitted light data in the case of transparent particles and from light reflected from the particle surface in the case of opaque objects. Brightness is measured in 256 steps and classified according to various criteria.
- **Shape:** simple shape recognition is possible in the case of loose bulk materials in so far as the difference-characteristics may be derived from the sensor data within a reasonable consumption of computing capacity. A decisive factor here is the number of objects, which must be evaluated during the free-fall phase.

### The run-of-mine

The versatility of optical sorting is such that it can be used to help in controlling composition and consistency of several ore-types. We are now focussing on the Orani-Ispaduleddas deposit only, where sorting was expected to have the maximum impact on mining operation, improving both mine recovery and overall ore quality. In the r.o.m. it is possible to identify 3 main ore-types making up more than 90% of the total mass: *white*, strictly the sodium feldspar; *green*, still sodium feldspar in which the color is due to variable contents of chlorite minerals and; *gray-reddish*, typically an altered granite rock constituting the main pollutant of rom. The objective was to reject the *gray-reddish* material, controlling the content of the GREEN fraction.

Table II: Orani-Ispaduleddas ore-types analysis.

Ore type	Al <sub>2</sub> O <sub>3</sub> (%)	Fe <sub>2</sub> O <sub>3</sub> (%)	TiO <sub>2</sub> (%)	Na <sub>2</sub> O (%)	K <sub>2</sub> O (%)	CaO (%)	MgO (%)
<i>white</i>	18.1	0.12	0.23	8.6	0.14	2.00	0.24
<i>green</i>	15.7	0.50	0.28	7.0	0.83	1.75	1.25
<i>gray-reddish</i>	16.6	1.28	0.22	4.0	3.51	1.95	0.45

### The installation

In figure 6 a schematic flow sheet of the Orani treatment plant is reported. The plant has a throughput of 140 t/h of r.o.m., yielding some 110÷120 t/h of finished products,

- 6 + 0 mm grits and - 15 + 5 fraction. The ore sorting circuit is inserted between the intermediate stockpile and the secondary crushing, so that it can be bypassed when treating ore-types that do not need sorting. A detailed scheme of the sorting circuit alone is in figure 7: the - 200 + 5 mm feldspar is fed at around 110 t/h to a 1,500x4,000 triple deck vibrating screen. The minus 15 mm, some 15÷20 t/h, due to its size, may not be economically sorted, so it can be stockpiled for later reclamation or, directly sent to secondary crushing.

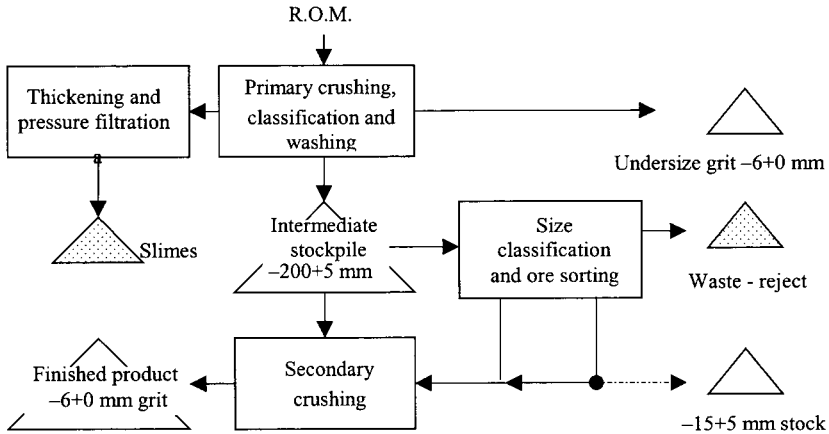


Figure 6: Orani treatment plant flow sheet

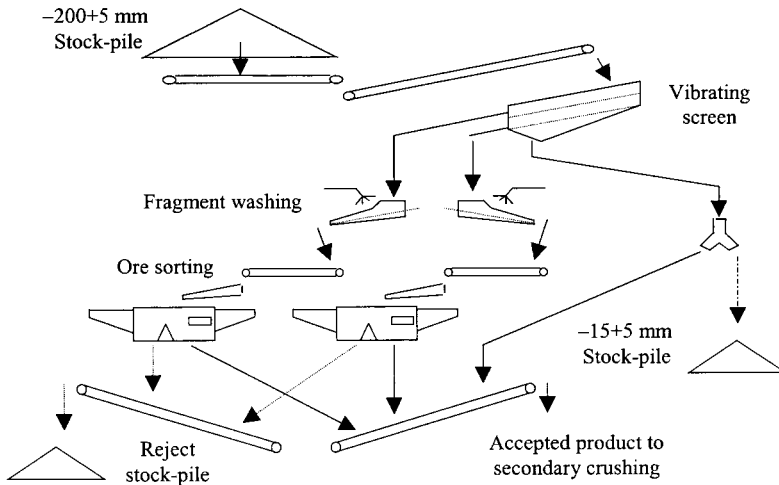


Figure 7: Sorting circuit flow sheet.

The rest of the material is classified into - 40 + 15 mm, 20÷25 t/h and - 200 + 40 mm, 70÷75 t/h. The rock fragments are then spray washed onto vibrating feeders to remove all fine particles and to enhance colors by wetting their surface.



After this simple feed preparation two MikroSort operate the selection; rejected waste is stockpiled to be taken to dump, the accepted feldspar is conveyed to secondary crushing. Air for sorters operation is ensured by two 12,500 l/m, 9 bar compressors; a sleeves filter maintain the sorting areas under constant negative pressure.

### The results

Given the complexity in the determination of the granite content in the sorter feed and products, the efficiency of the extraction of the GRAY-REDDISH fraction is evaluated on the basis of the iron content (Table II for composition). Table III shows the sorting results obtained during plant commissioning and the first period of operation.

Table III: Ore sorting analysis

Date dd/mm/aa	Feed			Accept			Reject		
	Fe <sub>2</sub> O <sub>3</sub> (%)	Na <sub>2</sub> O (%)	K <sub>2</sub> O (%)	Fe <sub>2</sub> O <sub>3</sub> (%)	Na <sub>2</sub> O (%)	K <sub>2</sub> O (%)	Fe <sub>2</sub> O <sub>3</sub> (%)	Na <sub>2</sub> O (%)	K <sub>2</sub> O (%)
12/10/99	0.50	7.97	0.50	0.34	8.60	0.30	0.88	6.50	1.40
01/10/99	0.41	7.75	0.50	0.33	7.50	0.35	1.60	7.00	1.50
29/09/99	0.35	8.40	0.60	0.29	8.50	0.35	1.90	6.00	1.70
22/07/99	0.35	8.20	0.40	0.29	8.60	0.25	0.70	6.50	1.40
21/07/99	0.43	8.40	0.60	0.33	8.80	0.35	0.95	6.40	1.80
20/07/99	0.36	8.60	0.50	0.30	8.70	0.30	0.55	7.00	0.80

In Figure 8, the iron extraction is plotted vs. the feed grade and compared with the theoretical extraction obtained by accurate hand sorting and the plant design data coming from reduced scale test-work.

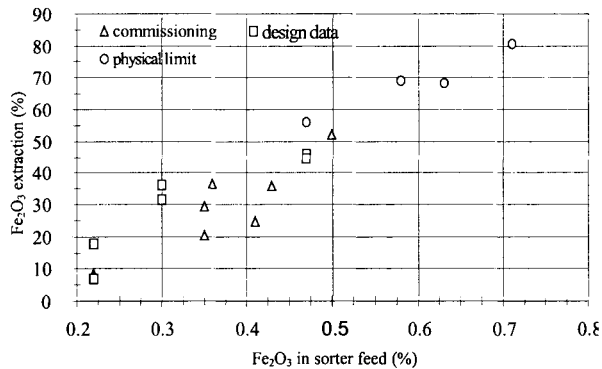


Figure 8: Sorting results – commissioning.

Notwithstanding the extremely variable ore composition the MikroSort reached very rapidly a good level of efficiency, close or equal to design expectancy.

## BENEFICIATION OF LOW GRADE FELDSPAR ORES FOR THE CERAMICS INDUSTRY

M. Agus\*, R. Angius\*, M.Ghiani<sup>o</sup>, R.Peretti\*, A.Serci<sup>o</sup>, A.Zucca\*

<sup>o</sup>DIGITA - Department of Geoengineering and Environmental Technologies, Italy

\*CSGM - Mineral Science Study Centre of CNR , University of Cagliari, Italy

### Abstract

The decline in the production of single fired ceramic tiles has made it difficult to find a market for the poorer quality feldspars. Producers are thus faced with the problem of improving the quality of their products also with a view to increasing profit margins. In this context, the paper addresses the problems involved in enhancing the value of some raw materials currently sold to the less profitable markets or considered as waste material. Three different cases have been examined and the results of experimental studies have demonstrated the feasibility of applying basic mineral processing techniques such as magnetic separation, surface attrition and selective flotation for obtaining concentrates with high added value and as such more readily marketable. The processing flow sheets, usually a combination of the above techniques, become more complex and more expensive, the higher the quality desired of the final product.

*Keywords: feldspar ores, beneficiation, mineral processing techniques, ceramics industry*

### Introduction

Because of their low melting temperature alkaline feldspars are an essential constituent of ceramic mixes. In recent years the ceramics industry has been undergoing major expansion worldwide, especially in Italy, one of the largest users of feldspathic materials for the ceramics industry. Thus the demand for feldspar minerals has grown accordingly (Canetti, 1998; Benedusi, 1998). The main sources of feldspar minerals are pegmatitic rocks and feldspar sands and, to a lesser extent, other acid granite differentiates such as aplites and eurites.

Unfortunately the current trend in the ceramics market, namely increased production of porcelain stoneware tiles and a decline in the single fired tile sector, strongly disadvantages the poorer quality minerals (Benedusi, 1998; Bornioli, 1998). As a result, only a minor proportion of the huge ascertained reserves can be mined and marketed without some kind of treatment to enhance their value. Owing to the low economic value of feldspar minerals, it would also appear unreasonable to start prospecting in hitherto unexplored areas to increase high quality mineral reserves, also bearing in mind the additional cost of transportation. Predictably, the growing demand for high quality feldspar materials will thus have to be met mostly by treating the increasingly larger volumes of extracted or potentially exploitable rock that cannot be marketed directly.

This is true: i) of the ore contained in portions of deposits left in place because of the change in market conditions; ii) of low value products that are suitable for the less

remunerative sectors; iii) and lastly of quarrying and processing waste that is available cheaply also because of the necessity to dispose of it.

The problems associated with enhancing the value of such materials are discussed here and three different exemplificative cases are examined:

- A. a massive albitite deposit: the product could be diversified and part of the material currently sold for use in the single fired tile industry diverted to the more remunerative porcelain stoneware tile and tile glazes sectors;
- B. a pegmatite dike deposit: the raw material, here again destined for the less profitable semi-vitreous tile market, could not only be upgraded to attain typical quality requirements for the production of porcelain stoneware tile but the low grade mineral contained in the outer portions of the deposit could also be mined, thereby increasing reserves;
- C. granite quarrying waste: estimated to account for at least 50% of the material extracted its disposal creates urgent environmental problems (Montani, 1995).

The processing flowsheets proposed and the experimental results achieved are described here. The possibility has been demonstrated of obtaining good quality commercial products, suitable for use in various sectors of the ceramics industry, from low value or waste rock using different mineral processing techniques or a combination thereof. The higher the quality of the commercial product it is desired to achieve, the more complex the treatment becomes.

### **The albitite ore (A)**

The mineral concerned is mined from a deposit consisting of a lens hosted in granodiorites, whose formation is related to soda metasomatic alteration of primary granites and pegmatitic facies (Bornioli and Marini, 1994). The outcropping mineral body has rather homogeneous mineral composition, does not contain foreign inclusions and is characterized by a high albite content accompanied by chlorite (clinocllore of secondary origin), quartz and minor amounts of orthoclase, plagioclases and secondary accessory minerals such as titanite, epidotes and iron oxides. Table I shows the chemical composition of a representative sample of the ore on which the experiments were carried out. As can be seen it is of average quality and as mentioned is used in the production of semi-vitreous tiles.

For the purpose of enhancing the value of the ore to obtain products with greater added value by reducing the mafic material contained therein, essentially Mg, Fe and Ti, dry magnetic separation, surface attrition performed wet and selective flotation techniques were applied. Magnetic separation was carried out using a permanent magnet Permroll separator (Clark, 1985), capable of developing a magnetic field strength of 1.6 Tesla, operating over the entire particle size range of the mineral ground to below 2 mm and dedusted dry using a 50  $\mu\text{m}$  screen.

Attrition was performed on the same size fraction of the ground mineral using a Denver attrition cell varying time and at a solids concentration of 72%. Efficiency of surface attrition was assessed by comparing the chemical composition of the  $-2 +0.25$  mm size-fraction before and after attrition. Flotation experiments were conducted via the inverse procedure on mineral feeds simply wet ground to dimensions of less than 0.25 mm or deslimed in the hydrocyclone, operating both in neutral pulps and in

pulps acidified with hydrochloric acid. In the first case a carboxylic collector was used to float the impurities (Pamak 4, Hercules Powder Co.), in the second a phosphoric ester collector (Flotisor SM15, Hoechst AG).

The efficiency of the three treatments is summed up in Table I, where for simplicity the yields and chemical composition of the concentrates obtained from the different treatments are reported. Note that the results obtained for attrition refer to a residence time of 10 min in the attrition cell. In the flotation treatment, on the contrary, 500 g/t of phosphoric ester collector were used in an acid pulp of the deslimed feed, on account of the fact that this procedure proved technically superior to the alternatives experimented.

Table I: Albitite mineral. Yield and chemical composition of the concentrates obtained from the different treatments.

N°	Procedure applied	Yield (%)	Assays (%)							
			Na <sub>2</sub> O	K <sub>2</sub> O	CaO	MgO	SiO <sub>2</sub>	Al <sub>2</sub> O <sub>3</sub>	Fe <sub>2</sub> O <sub>3</sub>	TiO <sub>2</sub>
1	Feed	100.0	8.6	0.25	1.10	2.9	66.3	18.3	0.52	0.42
2	Magnetic separation	86.5	9.4	0.25	1.05	1.9	67.5	18.5	0.32	0.31
3	Attrition	69.8	9.1	0.22	1.00	1.4	68.0	18.4	0.25	0.26
4	Flotation	69.9	9.8	0.17	0.80	0.3	69.0	18.6	0.06	0.02

The experimental results demonstrate that it is possible to successfully attain the objective of enhancing the value of the albitite mineral so as to find more profitable outlets for this product.

Of the three treatments, only magnetic separation gave disappointing results, as the products obtained do not meet even the least exacting quality specifications of the porcelain stoneware tile industry. By contrast, on account of its ability to concentrate the various impurities in the froth, the flotation treatment using an acid medium proved technically by far the most efficient process yielding products of superior quality suitable for use in the porcelain stoneware tiles and tile glazes sectors.

However, it should be noted that the demand for feldspathic materials in this particular sector, though in expansion, appears to be rather limited (Bariosarda SpA, 1990) thus it may be difficult to market the considerable quantities that can be produced via integral flotation treatment of the ore. Consequently the process flowsheet should be designed to be flexible so as to diversify the product, variable amounts being destined for use in ceramic mixes for porcelain stoneware tile as well as for superior quality products.

The treatment proposed here, whose process flowsheet is schematized in Figure 1, is based on a combination of the surface attrition and flotation treatments described above. The crude ore is ground to dimensions of less than 2 mm and then subjected to attrition. It is then split into two size fractions – 2 + 0.25 mm and – 0.25 mm. Variable proportions of the first of these size fractions is then ground wet in closed circuit to less than 0.25 mm, mixed with the original – 0.25 fraction and deslimed in the hydrocyclone. The cyclone underflow is used as feed in the flotation treatment. The outcome of experimental trials in the laboratory, adopting the flowsheet whereby 50% by mass of the – 2 + 0.25 mm product subjected to attrition is reground and further treated via flotation, are summed up in Table II.

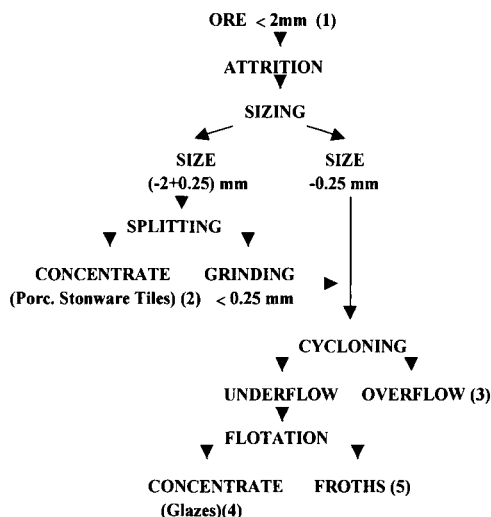


Figure 1. Flowsheet proposed for treating the albitite ore.

Table II: Albitite mineral. Yield and chemical composition of the products obtained from the treatment schematized in Figure 1.

N°	Products	Yield (%)	Assays (%)							
			Na <sub>2</sub> O	K <sub>2</sub> O	CaO	MgO	SiO <sub>2</sub>	Al <sub>2</sub> O <sub>3</sub>	Fe <sub>2</sub> O <sub>3</sub>	TiO <sub>2</sub>
2	(- 2+ 0.25 mm) attrition	39.6	9.2	0.25	1.00	1.3	68.0	18.5	0.25	0.25
3	Cyclone overflow	11.3	5.8	0.44	1.25	10.0	57.0	19.8	2.00	0.85
5	Float	12.8	5.6	0.32	2.00	9.0	57.0	16.0	1.45	1.70
4	Concentrate	36.3	10.2	0.19	0.76	0.24	69.4	18.4	0.07	0.03
1	Feed	100.0	8.7	0.27	1.07	2.9	65.9	18.3	0.54	0.42

The numbers beside the products refer to the same products in Figure 1.

The results confirm the possibility of using the attrition and flotation products in the manufacture of porcelain stoneware tiles and tile glazes respectively.

### The pegmatite ore (B)

The ore comes from a thick acid dike deposit hosted in a granitic pluton made up of formations of the "two-mica leucogranites" type.

The structure of the mineralization is typically pegmatitic, composed chiefly of sodaplagioclase, albite or twin albite-pericline crystals, minor potassium feldspar (microcline), quartz, ferro-magnetic minerals in the form of chlorite and accessory minerals (titanite, epidote, zircon).

Though the genesis of the mineral deposit is related to a single process of prevalently albitic metasomatism, caused by the rising of a pegmatitic fluid rich in soda but containing few volatile constituents, its mineralogical composition is far from homogeneous.

In fact three different rock types can be distinguished, hereafter denoted with  $\alpha$ ,  $\beta$  and  $\gamma$  respectively:

- rock type  $\alpha$ , characterized by incipient albitization and in which the original granitic structure can be recognised, is found in the outer portions of the deposit containing low-grade ore;
- rock type  $\beta$  has undergone a more pronounced metasomatism with enrichment in soda and larger proportions of quartz than rock type  $\alpha$ , intimately intermingled with the feldspar;
- rock type  $\gamma$ , found in small dikes throughout the deposit is composed almost wholly of albite, with rare quartz and titanite as accessory mineral.

The above rock types account for around 20%, 60% and 20% of total ascertained reserves respectively.

Table III shows their average chemical composition.

Actually the material extracted by non-selective mining of rock types  $\beta$  and  $\gamma$  is suitable simply for use in ceramic mixes for the semi-vitreous tile.

Table III: Average chemical composition of the different rock types of the pegmatitic formation.

Rock type	Assays (%)							
	Na <sub>2</sub> O	K <sub>2</sub> O	CaO	MgO	SiO <sub>2</sub>	Al <sub>2</sub> O <sub>3</sub>	Fe <sub>2</sub> O <sub>3</sub>	TiO <sub>2</sub>
$\alpha$	6.0	1.6	1.0	1.0	72.7	14.4	1.6	0.24
$\beta$	7.1	0.9	0.6	0.3	74.7	14.9	0.5	0.04
$\gamma$	9.7	0.4	0.7	0.7	67.9	19.1	0.2	0.33

Experimental studies were conducted to explore the possibilities of enhancing the quality and thus the value of the mineralization concerned, and also of increasing mineable reserves.

A representative sample of pegmatite ore was subjected to the same treatments as the albite mineral based on magnetic separation, surface attrition and flotation.

Though on the one hand the experimental results demonstrated that the ore was refractory to these three techniques when applied singly, on the other it was shown that the mineral could be upgraded using a suitable combination of dry magnetic separation and flotation.

Experimental trials using the flowsheet schematized in Figure 2 produced the results shown in Table IV.

As can be seen, they confirm the technical feasibility of the proposed solution.

Table IV: Pegmatite mineral. Yield and chemical composition of the products obtained from the treatment schematized in Figure 2.

N°	Products	Yield (%)	Assays (%)							
			Na <sub>2</sub> O	K <sub>2</sub> O	CaO	MgO	SiO <sub>2</sub>	Al <sub>2</sub> O <sub>3</sub>	Fe <sub>2</sub> O <sub>3</sub>	TiO <sub>2</sub>
1	Feed	100.0	7.3	0.96	0.70	0.52	72.9	15.6	0.73	0.13
2	Dedusted	92.6	7.4	0.94	0.67	0.47	73.8	15.3	0.56	0.11
3	Non magnetic	84.4	7.6	0.89	0.54	0.26	74.3	15.4	0.27	0.08
4	Cyclone underflow	75.2	7.5	0.87	0.60	0.22	74.7	15.2	0.22	0.08
5	Flotation concentrate	66.0	7.8	0.73	0.42	0.13	75.4	15.2	0.08	0.02

The numbers beside the products refer to the same products in Figure 2.

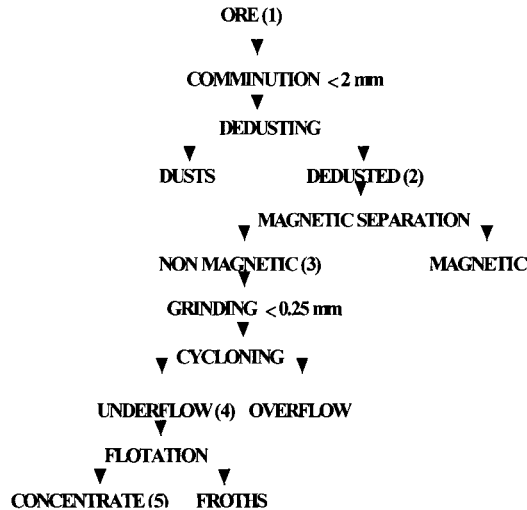


Figure 2. Flowsheet proposed for treating the pegmatite ore.

### Granite quarrying waste (C)

The growing volumes of waste material from granite quarrying and processing are posing serious management and environmental problems (Montani, 1995).

It is not possible to significantly reduce the quantity of waste material produced, by perfecting extraction techniques. The only available option for the disposal of the waste accumulated in existing dumps and for minimising current production of waste from quarrying and processing granite is to find economically convenient outlets for this material. One solution proposed, and in some cases applied, is to use it as aggregates in the manufacture of concrete, as granulates for roadbeds or for other underlayers for civil engineering works (Alfano et al., 1989).

The possibilities of disposal of waste material in this way are limited however by the relatively reduced capacity of absorption in local markets and transportation over long distances of quarrying waste of little value is uneconomical (Alfano et al., 1992).

An alternative form of disposal could be as raw materials in the production of feldspars and quartz for use in the ceramics and glass industries. The relatively high market value of these products, which theoretically can be obtained from such wastes applying mineral processing techniques, means that significant quantities could be economically disposed of. The authors have examined the possibility of treating the more common types of Sardinian granite using traditional gravity separation, magnetic separation and flotation techniques, or a combination of separation and flotation treatments. (Ghiani, et al., 1996; Ghiani et al., 1997). The technical feasibility of enhancing the value of quarrying waste has been experimentally demonstrated at least for some of the granites tested.

As an example the results obtained for a particular type of granite known as "Sardinian Grey" are reported here. The technical and chromatic features of this stone

make it one of the finest quality granites in Sardinia (Del Bono, 1994) and on first sight its textural characteristics appeared favourable.

The sample used in the experiments, waste from squaring granite blocks, shows no alteration at all and is composed of 27% K-feldspar, 35% plagioclases, 34% quartz and 4% micas. The mineral constituents can be satisfactorily liberated at dimensions of around 3 mm, with the exception of the micas, which require finer comminution to less than 1 mm. Experimental results indicated that different processes had to be designed depending on the desired quality of the final products. For example, to obtain materials suitable for use in the production of lower quality semi-vitreous tiles, one-stage dry magnetic separation was sufficient. The feed was first crushed to relatively coarse dimensions of around 3 mm and then dedusted.

On the other hand, to obtain products of greater value (for porcelain stoneware tile) magnetic separation techniques are still applicable but at least two stages are required and a greater degree of liberation is needed in the feed.

Lastly, if the products are to meet even more exacting quality specifications (tile glazes) then this can only be achieved using a combination of magnetic separation and selective flotation.

The flotation treatment is based on techniques traditionally used for separating feldspars from quartz by means of cationic collectors (Amine MFA10, AkzoChemie) in pulps acidified with hydrofluoric acid (Ghiani and Massacci, 1970; Rau, 1985). For the sake of conciseness, only the experimental results obtained for the combined treatment described above are reported here.

The process flowsheet is schematized in Figure 3 and Table V shows the yields and chemical composition of the resulting products.

Table V: Granite waste. Yield and chemical composition of the products obtained from the treatment schematized in Figure 3.

N°	Products	Yield (%)	Assays (%)							
			Na <sub>2</sub> O	K <sub>2</sub> O	CaO	MgO	SiO <sub>2</sub>	Al <sub>2</sub> O <sub>3</sub>	Fe <sub>2</sub> O <sub>3</sub>	TiO <sub>2</sub>
1	Granite waste	100.0	3.9	4.7	1.0	0.10	74.8	13.7	1.26	0.08
2	Dust	6.9	5.2	4.7	1.5	0.13	65.8	20.0	1.45	0.08
3	Non magnetic	78.3	3.8	4.5	0.9	0.01	77.9	12.7	0.06	0.01
4	Magnetic	14.8	3.6	5.7	1.3	0.56	62.8	16.0	7.50	0.45
5	Slime	10.3	3.4	4.7	0.6	0.03	77.5	13.3	0.05	0.01
6	Feldspar float	45.0	5.8	6.7	1.3	0.01	67.2	18.8	0.08	0.01
7	Quartz concentrate	23.0	0.15	0.15	0.1	trace	99.0	0.42	0.01	0.01

The numbers beside the products refer to the same products in Figure 3.

The results confirm the technical feasibility of obtaining feldspar concentrates from granite processing waste to be used in different market sectors in agreement with the observations made previously for the albitite mineral (A).

Technological characterization tests (vitrification, linear shrinkage, water absorption, etc.) conducted on the products obtained via magnetic separation showed that their properties are not unlike those of similar materials employed in the preparation of mixes for porcelain stoneware tile.

On the other hand the high quality flotation products may be suitably used for the production of tile glazes.



The flotation reject containing large proportions of silica may well be suitable for use in the glass industry. Of course, as already mentioned, the mix design will depend on market conditions and logistic conditions in which the producer operates.

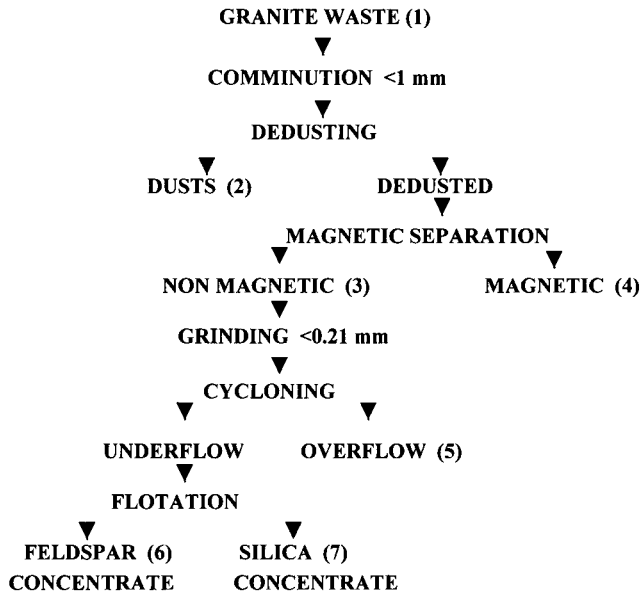


Figure 3: Flowsheet of integrated treatment of granite waste.

## Conclusions

The paper is concerned with the results of experiments conducted for the purpose of enhancing the value of some low-grade feldspar minerals which presently find outlets in the less remunerative sectors of the ceramics industry or are rejected by other processes and as such are waste material.

Some cases have been examined for which the technical feasibility of enhancing the value of the minerals, by means of treatment based on traditional mineral processing techniques used alone or in combination, has been experimentally demonstrated.

In particular, for one of the cases examined (A), it has been shown that inferior quality products presently suitable for use in mixes for semi-vitreous tile can be upgraded using a combination of surface attrition and selective flotation. Variable proportions of the resulting product can find outlets in the more profitable porcelain stoneware tile and tile glazes industry. The second example (B) concerned an ore which, after treatment consisting of magnetic separation followed by inverse flotation of the non-magnetic product, not only exhibited superior quality, but also total mineable reserves could also be increased.

Lastly in the third example (C) it has been demonstrated that the granite processing waste produced in some granite quarries may also be well suitable for producing

feldspathic materials for use in the ceramics industry. With the proposed treatment, based on magnetic separation and selective flotation, it would appear that, similarly to case (A), variable proportions of the finished product can be obtained. It can be destined for the porcelain stoneware tile and tile glazes industry, thereby contributing to solving the environmental problems created by the proliferation of granite waste dumps.

In conclusion, it is shown that the application of flowsheets of various designs, depending on the chemical composition of the ore and the desired quality of the marketable product, can enhance the value of the original product, resulting in higher profits for the producers.

#### Acknowledgements

This work has been carried out with the financial support of MURST and the National Research Council (CNR).

#### References

- Alfano, G., Ciccu, R. and Ghiani, M., 1989. Problemi di utilizzazione economica degli scarti delle cave di granito. Situazione e Prospettive dell'Industria Lapidea. Atti delle Giornate di Studio, ANIM, Cagliari, 339-342.
- Alfano, G., Ciccu, R., Ghiani, M. and Manca, P.P., 1992. Produzione di granulati dalle discariche delle cave di granito: panoramica del settore e soluzioni progettuali. Eurocave '92, Saint Vincent.
- Bariosarda SpA, 1990. Unpublished report.
- Benedusi, S., 1998. Feldspar in Sardinia. In pole position for ceramic markets. *Industrial Minerals*, N. 365, 57-59.
- Bornioli, R., 1998. La miniera di feldspato sodico di Orani. In: *Le materie Prime Minerali Sarde: Problemi e prospettive*. University Press, C.U.E.C., Cagliari, 55-71.
- Bornioli, R. and Marini, C., 1994. Il giacimento di feldspato sodio di Badu 'e Carru (Sardegna centrale), *Ceramica Informazione Speciale*, suppl. al n. 342.
- Canetti, A., 1998. Struttura produttiva e mercato della ceramica. In: *Le materie Prime Minerali Sarde: problemi e prospettive*. University Press, C.U.E.C., Cagliari, 254-257.
- Clark, G., 1985. Magnetic separation, *Industrial Minerals*, May, 24-25.
- Del Bono, C., 1994. Il granito in Sardegna. Osservatorio economico e finanziario del Banco di Sardegna. Quaderno n. 4.
- Ghiani, M. and Massacci, P., 1970. Sul ricupero dei feldspati e del quarzo da rocce granitiche e da sabbie. *L'Industria Mineraria*, anno XXI, 1-19.
- Ghiani, M., Oi, M., Peretti, R. and Zucca, A., 1997. Production of raw materials for the ceramic floor and wall tile industry using waste from granite quarries: case of the material from Sarule. *Ceramica Acta*, n. 2-3/97, 5-17.
- Ghiani, M., Peretti, R. and Zucca, A., 1996. Production of raw materials for the ceramic and glass industries from granite quarry waste. *Proceed. SWEMP*, R. Ciccu (ed), Cagliari, 1003-1010.
- Montani, C., 1995. Stone. *Repertorio Economico Mondiale*, Faenza Editrice, 80.
- Rau, E., 1985. Nonmetallic industrial minerals. *SME Mineral Processing Handbook*, N.L. Weiss Ed., Sect. 29.7, Am. Ins. of Min. Engrs, New York, 29, 9-29/11.

## BENEFICIATION OF SAND FROM THE SAVA-RIVER BED

B. Salopek, G Bedeković

Faculty of Mining, Geology and Petroleum Engineering  
University of Zagreb, Zagreb, Croatia

### Abstract

Gravel from the Sava-river bed contains coal particles, which remain in sand after classification. The coal content in class <4 mm ranges from about 0.5% to 2%, while in relatively close classes, such as  $-1 + 0.5$  and  $-2 + 1$  mm it is even up to 6.23% and 6.37%, respectively. The possibility of separating coal particles from sand was tested on standard equipment used at gravity concentration, which are: the jig, the shaking table and the spiral. The tests were made with classes  $-4 + 1$  mm;  $-4 + 0.5$  mm;  $-2 + 1$  mm;  $-1$  mm;  $-1 + 0.5$  mm and  $-0.5$  mm, where the coal content in sand was 1%, 3% and 6%. The best results were reached with the jig, where sand recovery ranged from 73% to 80%, while the coal content in separated sand was 5 to 6 times lower than in the feed. The tests with spiral showed recovery even to 98% but the coal content was only 3 to 5 times lower than in the feed. The separation tests made on the concentration table showed relatively good results with recovery from 80% to 97%. On the ground of investigations carried out on adequate samples it is proposed that for the elimination of coal particles from Sava sand air jigs must be used, so that by sand quality the prescribed norms can be satisfied.

*Keywords: gravity concentration, sand, coal particles, grade, recovery*

### Introduction

The City of Zagreb is the biggest consumer of construction building material in Croatia. In the surroundings, along the Sava river, there are some ten establishments for sand exploitation and processing, the yearly production reaching about 1,500,000 m<sup>3</sup> (Salopek, 1997). The gravel in the Sava-river bed contain coal particles that after classifying remain in the sand. The coal content in the sand size range of <4 mm fluctuates from 0.5% to 2%, and in relatively tight sizes (like e.g.  $-2 + 1$  mm and  $-1 + 0.5$  mm) even more than 6%. After the Croatian Norms the organic impurities in construction sand may not exceed the mark of 1%, therefore the biggest part of that sand does not satisfy the prescribed norms. Sand with more than 1% coal is mostly used in less demanding works or mixed with sand from other deposits to acquire the needed grade. Usually, these solutions are not justified (neither economically nor technically), therefore among the undertakers there is growing interest for means to secure the winning of appropriate sand. Consequently, an investigation program has been set up with the aim to put forward a technical process acceptable both from the technical and the economical aspect. In that, the standard equipment of gravitation concentration was used: jigs, spirals and tables (Bohle, 1995; Burt, 1984; Neuman et al., 1995; Schubert, 1995).

### Experimental work

Gravel and sand samples from the Sava bed were taken in four deposits along an alignment of about 30 km. Each of the four main samples was composed of a fair

number of smaller individual samples. After homogenization and quartering, the size distribution was determined by dry screening in standard laboratory sieves; the results are presented in Table I.

Table I: Size distribution of the raw gravel and sand.

Size class (mm)	Sample 1 Weight (%)	Sample 2 Weight (%)	Sample 3 Weight (%)	Sample 4 Weight (%)
+ 31	4.8	13.2	4.1	2.7
- 31 + 16	29.3	26.1	11.0	14.8
- 16 + 8	32.8	21.3	27.3	36.4
- 8 + 4	11.7	9.6	18.7	14.3
- 4	21.4	29.8	38.7	31.6

Further on, the size distribution of the size category <4 mm was determined as well as the coal content in each category. This was done after the Croatia Standard Determination of the percentage of light particles in aggregates, where as dense medium a suspension of  $ZnCl_2$  with the density of  $1.6 \text{ g/cm}^3$  is used. The results are shown in Table II.

Table II: Size distribution and coal content of the size class &lt;4 mm.

Size class (mm)	Sample 1		Sample 2		Sample 3		Sample 4	
	Sand (%)	Coal (%)	Sand (%)	Coal (%)	Sand (%)	Coal (%)	Sand (%)	Coal (%)
- 4 + 3.15	19.3	0.24	20.7	0.15	16.5	0.48	16.2	0.28
- 3.15 + 2	12.4	0.73	14.9	0.29	10.8	1.63	8.1	1.07
- 2 + 1	11.4	2.49	11.8	1.23	14.6	6.37	11.4	4.18
- 1 + 0.5	9.4	5.77	7.1	6.23	12.3	3.28	8.9	4.38
- 0.5	47.5	2.43	45.5	1.82	45.6	0.52	55.3	0.45

### Jigging

The testing was carried out in a Harz type jig with a sieving surface of  $490 \text{ cm}^2$ , screen opening of 0,5 mm, amplitude of 26.6 mm and frequency of  $180 \text{ min}^{-1}$ . Sand samples of the size categories - 4 + 1 mm, - 2 + 1 mm and - 4 + 0.5 mm with a coal content in the feed of 1%, 3% and 6% were examined. Depending on the sample mass ( $900 \div 3,000 \text{ g}$ ), the bed thickness was 1 cm, 2 cm and 3 cm, and the stratification time  $10 \div 50 \text{ s}$ . The coal share in the jigging products were determined by float-and-sink analysis (Figure 1). Figure 1 shows that the best concentrate was won from class -2 + 1 mm, not so good was class - 4 + 1 mm, and the worst product comes from class -4 + 0,5 mm. The class - 2 + 1 mm also is least dependent on the bed thickness and coal content in the feed. The minimum coal content in the concentrate ( $0.04 \div 0.11\%$ ) was achieved with a bed of 1 cm and 1% coal in the feed, and the maximum ( $0.58 \div 1.37\%$ ) with the same bed thickness and 6% coal in the feed. With the increase of bed thickness also the coal content in the concentrate increases at a coal content of 1% in the feed, then decreases at a content of 3% in the feed, and when the feed contains 6% coal at first it decreases to bed thickness of approximately 2 cm, and then begins to increase uniformly with the bed thickness. It is evident that a minor coal content in the feed requires a thinner jigging bed, and reversal; in our conditions that thicker bed may be approximately 2.5 cm. The sand recovery in the concentrate varied from 73% to 80%, and was determined on the ground of nine specially executed tests.

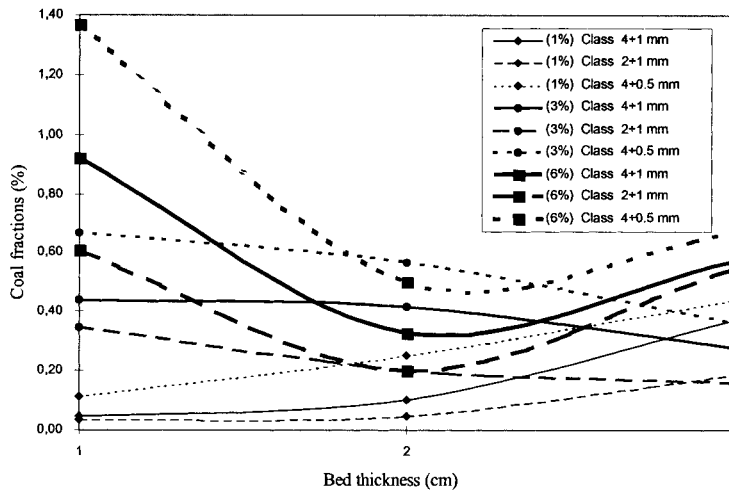


Figure 1: Coal fractions in connection with bed thickness, size classes and coal content in the feed.

*Humphreys spiral tests*

The tests were carried out in a standard Humphreys spiral with a diameter of 55 cm and with six spirals. Investigated were sand samples of size categories – 1 mm, - 1 + 0.5 mm and <0.5 mm with coal content in the feed of 1%, 3% and 6%. The samples of 4,000 g were dosed by a water flow of 4.5÷5 l/min. The results are shown in Figure 2.

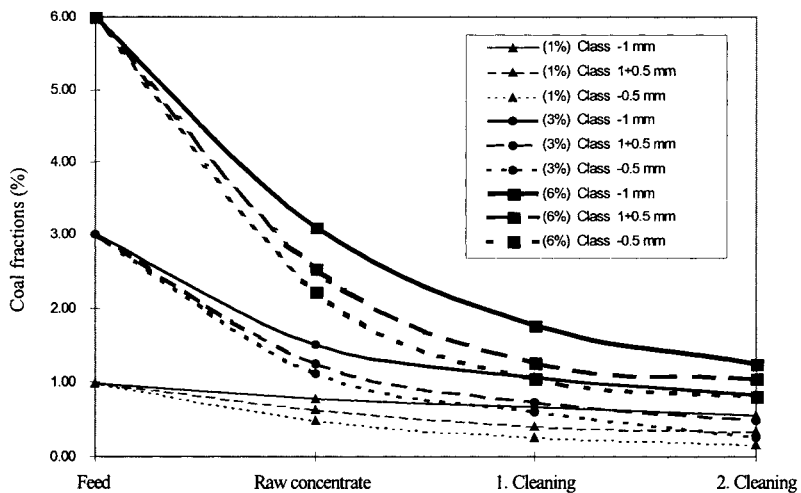


Figure 2: The coal fractions in the concentrate in connection with cleaning steps, size class, and coal content in the feed.

By following the influence of water flow and the switch position on the outlets it was concluded that the needed coal content in the concentrate of approximately 0,5% cannot be achieved, regardless if the recovery increases or decreases. Therefore it was decided to carry out the tests in most favorable conditions for the achievement of high recovery by trying to increase it by cleaning. In Figure 2 it can be seen that only the raw concentrate of class <0.5 mm with 1% coal in the feed can reach the value of approximately 0.5% coal. In all other instances the coal component is bigger and increases with the granular span of the class and the coal amount in the feed. The poorest result, 2.53% coal in the concentrate, was acquired in class <1 mm and with 6% coal in the feed. After the first cleaning, the concentrate quality was increased, but a coal share lesser than 0.5% was obtained only in the sizes of <0.5 and - 1 + 0.5 mm, eith initially 1% coal in the feed. After a second cleaning a coal component of approximately 0.5% was reached in all three examined classes at 1% coal in the feed, as well in the classes <0.5 mm and - 1 + 0.5 mm with 3% coal in the feed. The sand recovery in the concentrate was generally very high, it varied from 95% to 98%.

#### Shaking table tests

The samples were tested on a Wilfley concentration table of  $104 \times 38 \text{ cm}^2$ , with a stroke of 5 mm and frequency of  $270 \text{ min}^{-1}$ . Sand samples of size categories <1 mm, - 1 + 0.5 mm and <0.5 mm, with a mass 500 g and a coal content in the feed of 1%, 3% and 6% were fed at a water inflow of 3.5 l/min and a table slope of  $3^\circ$ ,  $6^\circ$  and  $9^\circ$ .

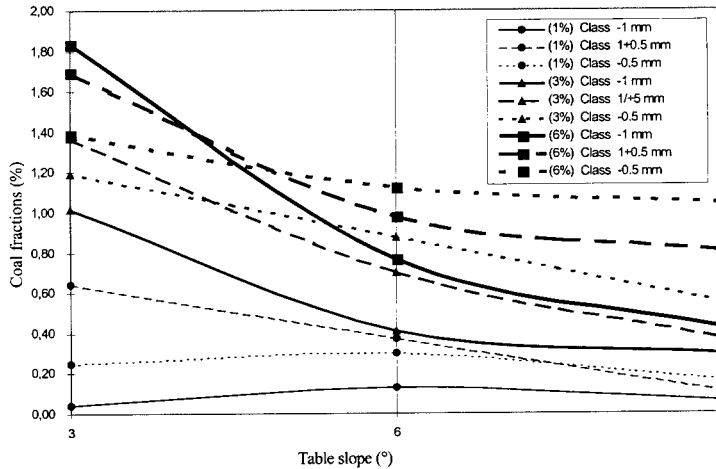


Figure 3: The coal fractions in the concentrate in connection with the table slope, class-sizes and coal quantities in the feed.

From Figure 3 it can be seen that the coal fractions in the concentrate increase with the increase of the coal share in the feed. At a table slope of  $3^\circ$  the highest coal values in the concentrate were acquired, except the classes <1 mm and <0.5 mm with 1% coal in the feed, where at a slope of  $6^\circ$  somewhat weaker results were reached than at  $3^\circ$ . Increasing the slope to  $6^\circ$  the quantity of coal in the concentrate decreases, and

that more in the classes  $<1$  mm and  $-1+0.5$  mm than in the class  $<0.5$  mm. By a further increase of the table slope to  $9^\circ$ , the coal quantity in the concentrate decreases further too: in 2 or 3 cases it is lesser than 0.5%. The sand recovery in the concentrate varied in the span from 80% to 97%.

### Proposal of a flow-sheet for the beneficiation plant

The firm IGM-Trstenik is one of the near ten establishments in the Zagreb environs working on sand exploitation. The sand and gravel is won by suction dredges of  $100 \text{ m}^3/\text{h}$ , and the raw gravel is by trucks transported to the preparation plant (Figure 4), where it is washed and sized in multi-deck vibration screens (1, 2); the gained products ( $+31$  mm;  $-31+16$  mm;  $-16+8$  mm;  $-8+4$  mm and  $-4$  mm) are used in the making of concrete and asphalt mixtures. After sizing, the size category  $<4$  mm goes into a spiral-classifier (7) for desliming; there slime particles  $<0,1$  mm are eliminated. For decreasing the coal content in the size category  $<4$  mm, on the basis of previous investigations it was proposed to construct a line of air jigs (8) for the treatment of the sand separated in the spiral classifier. The clean sand, together with the jigged material, goes after dewatering in (9), to the stock-yard for the size category  $-4$  mm, and the eliminated coal is removed to the dump. To increase the production of the  $-4$  mm size, the coarser sizes are crushed in two centrifugal mills (5, 6) which are working in closed circuit with vibrating screens (3, 4). The won sized products are dumped on the corresponding stock-yards.

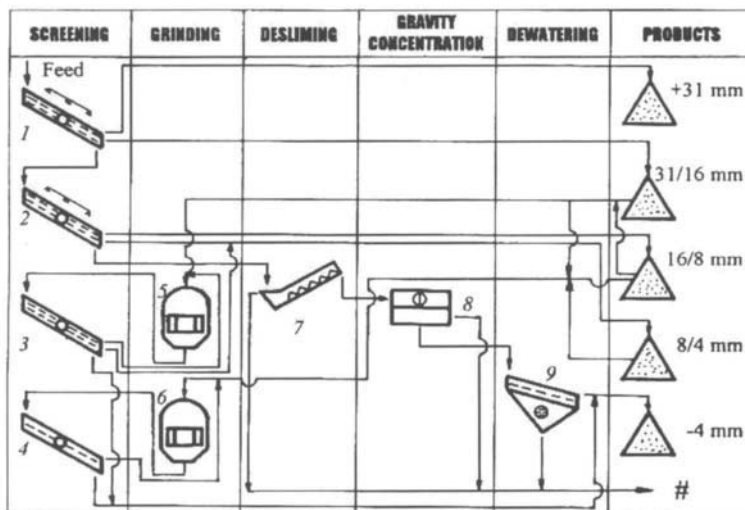


Figure 4: Flow-sheet of the beneficiation plant IGM-Trstenik (proposal).

### Conclusions

The accomplished investigations have shown that jigging gives the best results as to the concentrate quality. Independently of the coal content in the feed, the share of coal

in the concentrate from all treated size categories decreased under the value of 0.5%. But the bed thickness had to be about 2.5 cm.

Somewhat weaker results were acquired by tests on the shaking table. The best result was obtained at a table slope of  $9^\circ$ , when in two third of the tests the coal component in the concentrate could be decreased under 0.5%.

The poorest results as to the concentrate quality were obtained in the Humphreys spiral; there it is not possible to get a concentrate with less than 0.5% coal without on or two cleaning phases and that only in one third of the tests.

The highest recovery value for the sand in the concentrate was acquired in the spiral,  $95\div 98\%$ , somewhat lower on the table,  $80\div 97\%$ , and the worst in the jig,  $73\div 80\%$ .

On the ground of all carried out investigations it is proposed to equip the IGM-Trstenik separation plant with a line of air jigs. In that way the coal content in the size  $<4$  mm would be decreased and so the quality of the separated sand would satisfy the prescribed norms.

#### References

- Bohle, B., 1995. Hydrozyklone und Sortierspiralen - eine einfache Lösung für wirtschaftliche Sortierung und Rückgewinnung von Feinsand. In: Der europäischen Kies-und Sandindustrie, 36, 12, pp. 554-561.
- Burt, O.R., 1984. Gravity Concentration Technology. Elsevier.
- Neuman, Th., Snoby, R.J., Strangalies, W., 1995. Fraktionirte Schadstoffabtrennungen aus Sanden und feinen Kiesen mit alljig-Feinkornsetz-maschinen. Aufbereitungs-Techn. 36,12, pp. 562-567.
- Salopek, B., Bedeković, G., 1997. Environmental protection in the production of gravel and sand in Croatia. Proceedings MPES '97, Ostrava, Czech Republic, 3-6 September, pp. 953-958.
- Schubert, H., 1995. Zu den Grundlagen der Sortierung. In: Hydrorinnen, Aufbereitungs-Techn. 36, 11, pp. 497-505.



## CONTROLLED PROCESSING OF RAW MATERIALS FOR CERAMIC PASTE COMPONENTS

F. Durão, L. Cortez, T. Carvalho, C. Pires, A. Felício, I. Rodrigues, R. Lourenço,  
C. Tareco, G. Brito

C.V.R.M. / I.S.T., Mining and Georesources Department,  
Technical University of Lisbon, Portugal

### Abstract

Within the scope of a European research project, a specific industrial target was to improve the physical and technological properties of ceramic pastes produced from two different types of raw materials, feldspathic ores and raw clays. To accomplish this objective, the chemical/mineralogical composition of the raw materials needs to satisfy some industrial specifications. Several laboratory bench scale tests were carried out in the C.V.R.M. in order to get a suitable flow sheet. The feldspathic ores were treated by differential grinding and screening, or HIMS, followed by froth flotation (without fluoride activation). The raw clays were processed through a combination of hydrocycloning and froth flotation. Bench scale tests show that the technical specifications can be achieved by using a simple flow sheet. A main final target of the project is the design and construction of a pilot plant prototype based on mechanical and column flotation, with a fuzzy-based supervisory control.

*Keywords: flotation of feldspathic ores, raw clay processing, mechanical and column flotation*

### Introduction

Ceramic products are mainly based on raw materials supplied by industrial mineral producers. This is a rapidly developing and evolving sector of the industry. As more and more mineral consumers require stringent raw material specifications, it is becoming increasingly important for suppliers to keep pace with the latest technology in order to meet this constantly changing demand.

The quality of these raw materials is far from considered constant. The variability of their chemical/mineralogical compositions can be as great as  $\pm 100\%$  deviation from the expected average compositions, due to the heterogeneous nature of the geological bodies and also to the exploitation of several different geological formations.

In order to ensure the production of homogeneous lots with the chemical/mineralogical specifications required to satisfy the physical/technological properties of the ceramic materials, processing unit operations, like differential crushing and grinding, combined with screening/hydroclassification, are the most widely used. Systematic controlled blending can be used in case of several different geological formations, and magnetic separation is also applied as a cleaning operation. All the above solutions have limitations and disadvantages. Froth flotation can also be applied by using mechanically stirred cells. However, the application of these processes should tolerate a large range of variation of the input stream's composition and the output stream's specification.

A flotation process carried out in columns, whether associated or not with mechanical

cells, is very suitable for separating quartz from feldspar, for cleaning feldspathic ores (removing biotite and other dark colored minerals) and also kaolinic sands or clays in the fine size range. Simultaneously, this can be adapted to different output stream specifications, when controlled on line, using non-linear adaptive controllers inspired in fuzzy logic inference systems. Such a combination (flotation with adaptive fuzzy control) is used nowadays to model non-linear multivariate relationships, and as such, to build non-linear process controllers. This would lead to several industrial benefits, such as: a reduction of non-conformities with specification of the ceramic paste components, a reduction of the overall operational costs, an increase in the quantitative and qualitative range of the acceptable ore type's response capacity to the plant unit, and the beneficiation of the environmental conditions of the plant.

### **Objectives of the project**

Within the scope of a European research project including Portuguese, Spanish, French and German partners, a specific industrial target was to improve the physical and technological properties of ceramic pastes produced from two different types of raw materials – feldspathic ores from Portuguese granite ore bodies and raw clays from Spanish deposits. To accomplish this objective, the chemical/mineralogical composition of the raw materials needs to satisfy some technical specifications.

With regard to the feldspathic ores, one type, designated C, had no direct industrial application because of the high iron content, due mainly to the occurrence of biotite. The other type, designated A, is an important lithium source and also a very important feldspathic ore. Concerning the raw clays, two important types (large geological reserves), designated Z and V, were chosen because of their high iron/titanium content (about 6±7%), which consists of coloring elements. The industrial objective is to reduce the iron/titanium grade below 2%.

One main final target of the project is the design and construction of a prototype of a mobile and compact pilot plant, with a simple flow sheet based on froth flotation and column flotation, with the respective automatic control equipment, including several sensors/actuators, a programmable logic controller, an on-stream analyser and a personal computer (which is in charge of the supervisor/regulator fuzzy control). This unit can be installed in an industrial plant, in order to disclose the adequate industrial treatment policy for different types of input materials and various output specifications.

### **Characterization of the raw materials**

#### *Feldspathic ores*

Two types of Portuguese ores have been tested:

Type A, corresponding to a litiniferous pegmatite. This rock consists mainly of quartz, alkaline feldspars (microcline/albite) and micas (muscovite/lepidolite), often presenting beryl, bluish-green topaz, spodumene and other minor minerals. The grain size is fine to medium, with some fractured quartz sections. A typical chemical composition is given in Table I. The high content of aluminum and sodium are related to sodic feldspar. The high value of lithium is associated with the presence of lepidolite.

Table I: Typical chemical composition of type A ores.

LOI (%)	SiO <sub>2</sub> (%)	Al <sub>2</sub> O <sub>3</sub> (%)	Fe <sub>2</sub> O <sub>3</sub> (%)	CaO (%)	MgO (%)	Na <sub>2</sub> O (%)	K <sub>2</sub> O (%)	TiO <sub>2</sub> (%)	MnO (%)	P <sub>2</sub> O <sub>5</sub> (%)	Li <sub>2</sub> O (%)
2.95	66.38	20.56	0.066	0.21	-	2.56	3.32	0.006	0.122	0.72	1.40

Type C, corresponding to a porphyroid granite. Its mineralogical composition consists mainly of quartz, sodic and potassic feldspars (normally in separated, large crystals) and biotite, with some minor inclusions. Table II shows a typical chemical analysis.

Table II: Typical chemical composition of type C ores.

LOI (%)	SiO <sub>2</sub> (%)	Al <sub>2</sub> O <sub>3</sub> (%)	Fe <sub>2</sub> O <sub>3</sub> (%)	CaO (%)	MgO (%)	Na <sub>2</sub> O (%)	K <sub>2</sub> O (%)	TiO <sub>2</sub> (%)	MnO (%)	P <sub>2</sub> O <sub>5</sub> (%)	Li <sub>2</sub> O (%)
0.64	69.48	14.93	4.07	1.84	1.11	1.67	5.10	0.632	0.049	0.29	0.03
0.96	64.33	19.68	2.97	1.93	1.78	2.23	4.68	0.371	0.054	0.43	0.04

This rock has a high value of potassium associated with the potassic feldspar. The high content of iron is related to the presence of a large quantity of biotite.

#### Raw clays

Likewise, two types of spanish ores were selected for testing – Type V and Type Z, both consisting mainly of kaoline, illite, quartz, feldspars and some coloring minerals, such as siderite, magnetite and goethite. Table III gives the respective chemical compositions. Particle size analysis shows that 80% of the cumulative mass was finer than 5 µm in Type V and than 10 µm in Type Z clays.

Table III: Typical chemical analysis of clay Types V and Z.

	SiO <sub>2</sub> (%)	Al <sub>2</sub> O <sub>3</sub> (%)	Fe <sub>2</sub> O <sub>3</sub> (%)	TiO <sub>2</sub> (%)	CaO (%)	MgO (%)	K <sub>2</sub> O (%)	MnO (%)	Na <sub>2</sub> O (%)	P <sub>2</sub> O <sub>5</sub> (%)	LOI (%)
Type V	56.14	23.91	6.21	1.14	0.55	0.04	2.85	0.08	0.16	0.21	8.23
Type Z	66.16	17.59	6.26	1.51	0.23	0.002	1.42	0.03	0.1	0.11	5.73

### Laboratory processing of raw material small samples

#### Objectives of the bench scale tests

In order to achieve the objectives pointed out previously, several laboratory bench scale tests were carried out:

#### Feldspathic ores

The main goal was the optimization of the iron-bearing minerals' removal by froth flotation, followed by quartz/feldspar separation and by froth flotation, but without using the classical hydrofluoric acid method, to avoid its environmental and maintenance drawbacks. Furthermore, Type A granites should be studied, keeping in mind production of high-grade lithium concentrates, together with quartz and feldspar products.

#### Raw clays

The objective is the production of final clay samples with an iron grade of 1.5÷2% Fe<sub>2</sub>O<sub>3</sub> and reduced titanium grade. Bench tests should improve the selectivity of iron minerals' flotation, producing clay samples for ceramic tests.

### Sample preparation

So far, more than 100 complete laboratory bench-scale flotation tests were carried out, using a 2 l lab-cell developed by C.C. Dell from Leeds University, with automatic control of the level, rotor-speed regulation and air-flow rate control, besides other regulations and controls (pHmeter, etc.). The clay processing also involved very fine size classification by hydrocyclones, whose underflow (over 10  $\mu\text{m}$ ) was used for flotation. Concerning the feldspathic ores, the material was reduced to minus 1 mm and divided into small samples of about 1.2 kg each. For flotation tests, only fraction sizes less than 400  $\mu\text{m}$  were used.

### Flotation tests of Type C feldspathic ores

The final flow sheet used is shown in Figure 1. This includes two desliming steps to remove the slime fraction and four flotation stages to recover the iron-bearing minerals. The mass balancing corresponding to a typical test is given in Table IV. Only the three more relevant oxides are represented, although eleven were analysed. Overflows #1 and #2 consisted essentially of feldspars. The floated products were mainly iron-bearing minerals. The final underflow of the flotation (about 71% by weight) was a quartz and feldspar product, with nearly 0.6%  $\text{Fe}_2\text{O}_3$ , from a feed material with about 2%  $\text{Fe}_2\text{O}_3$ . The removal of iron exceeded 80%.

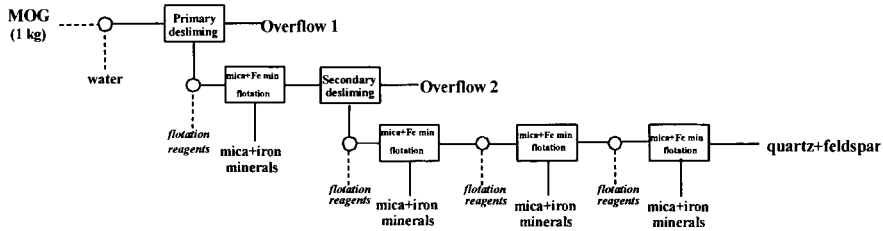


Figure 1: Final flow sheet used for processing the feldspathic ores (Type C).

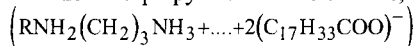
In these tests, Flotigan C with Aero 825 were used as collector reagents in the first three flotations, replaced by Aero 840 with a diamine (Duomeen TDO) in the fourth. Aerofroth 70 was always used as frother. pH was adjusted to 3.5 with  $\text{H}_2\text{SO}_4$ . During conditioning, the pulp was 50% solid by weight, and was diluted to 30% for the flotation stage.

### Flotation tests of Type A feldspathic ores

A similar flow sheet was used, with only one desliming step. In Table V, the mass balancing of a typical test is shown. The floated products consisted mainly of biotite and lepidolite, where more than 50% of the total  $\text{LiO}_2$  was recovered, with a mean grade about 3.5%  $\text{LiO}_2$ . Similar to Type C, the overflow of the desliming stage was essentially formed by feldspars and the final underflow of the flotation by quartz.

Flotigan C alone was used as the collector in the three flotation operations, with fuel oil as the frother and  $\text{pH} = 3.0$ .

It must be emphasized that all flotation tests were carried out using Duomeen TDO as feldspar collector, an N-tallow 1.3-propylene-diamine-dioleate, with the general formula:



with  $\text{H}_2\text{SO}_4$  to keep the pH less than 3.5. Therefore, the hydrofluoric method was avoided.



Particle size classification using hydrocyclones is mandatory, due to the very fine size distribution of the ground clay: over 50% is finer than 8  $\mu\text{m}$ . Table VI shows the results of a typical test (from the previous ones, with two hydroclassifications). In these last tests, the size classification of the first overflow was introduced in order to slightly decrease the iron content of final overflow 2. Note that only the four most relevant elements are presented, although eleven elements were analyzed.

In these tests, the collector was a combination of Aero 825 and Aero 845, with pH = 3.0. As frother fuel oil was used. Iron/titanium flotation was processed in a pulp with 15% solids by weight.

Table VI: Mass Balancing of a typical test (Type Z).

Products	Yield (%)	Grades (%)			
		SiO <sub>2</sub>	Al <sub>2</sub> O <sub>3</sub>	Fe <sub>2</sub> O <sub>3</sub>	TiO <sub>2</sub>
Raw clay (feed)	100.00	67.3	17.16	5.62	1.44
Overflow 1	62.29	54.9	26.23	5.22	1.37
Underflow 1	37.1	87.8	2.18	6.29	1.56
Overflow 2	53.07	51.7	28.44	5.25	1.34
Underflow 2	9.22	73	13.51	5.02	1.53
Froth product Fe-Ti 1	3.89	69.5	7.77	10.82	5.99
Froth product Fe-Ti 2	2.8	73.3	7.47	11.06	3.26
Froth product Fe-Ti 3	2.63	78.5	6.6	9.05	1.77
Flotation product	27.77	86.2	5.64	3.85	0.45
Flotation product*	0.63	37.3	5.23	38.06	0.46

### The pilot plant prototype

As stated in the introduction, a final target of this project is the design and construction of a pilot plant prototype based on mechanical and column flotation, with a fuzzy-based supervisory control.

This prototype will be installed in C.V.R.M., using some equipment already existent and other equipment constructed by the project partner, Eckart Montanconsult und Planung. The laboratory tests carried out will help determine the operational conditions of the future pilot plant. In Figure 3, the schematic flow sheet of the pilot plant is given.

The controller tasks are split into two levels. At the first level, the direct digital control (DDC) is carried out by a programmable logic controller (PLC). At the second (higher) level, a personal computer (PC) is in charge of the supervisory control, which computes the new set points to the DDC. The PC has another important task to interact and present all the relevant information to the human operator.

The supervisory control is based upon fuzzy logic inference systems, using rule data bases provided by an expert and based on experience, particularly that given by the laboratory tests. So, to implement a fuzzy logic based controller (FLC), it is necessary to assemble experimental data quantifying the effects of the main flotation variables on grades and recoveries.

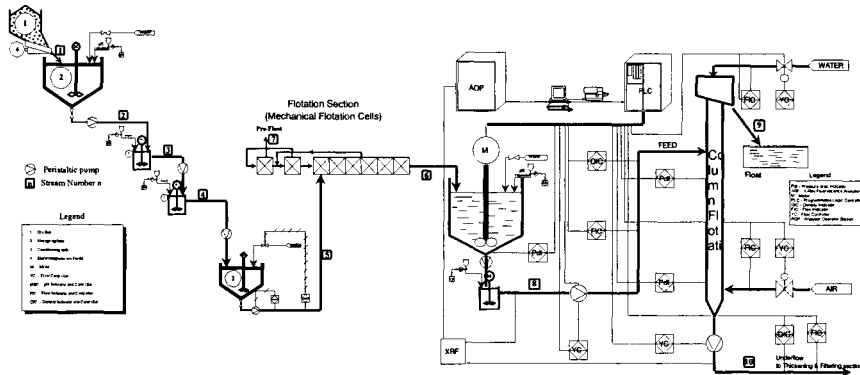


Figure 3: Schematic flow sheet of the pilot plant prototype.

## Conclusions

### *Feldspathic Type C ore*

The main drawback of this ore is its high content in iron, due to the occurrence of biotite. The results of bench scale tests show that the coarse-size of biotite can be removed by dry, high-intensity magnetic separation. Fine-size biotite and other iron-bearing minerals can be separated by froth flotation carried out in mechanical cells. The quartz/feldspar assay ratio can be met by froth flotation using the combination of a H<sub>2</sub>SO<sub>4</sub>/diamine collector, without fluoride activation.

### *Feldspathic Type A ores*

The removal of lepidolite from quartz/feldspar is imperative, because the fluor element is part of its chemical composition. Currently, the lithium mica is separated by differential crushing/grinding, combined with screening. However, the results of bench-scale tests show that the lithium mica can be separated by froth flotation, much like biotite, producing a quite clean lithium concentrate and a quartz/feldspar product. Separation of feldspar from quartz can be achieved using the above combination of flotation reagents. For good flotation results (grade/recovery) with feldspathic ores, the feed preparation phase must include a desliming operation. Kinetic studies carried out at the C.V.R.M. laboratory showed that a 20 min flotation mean residence time is required to recover about 90% of biotite and other iron bearing minerals. Regarding Type A, it is possible to produce a mica concentrate with 4% Li<sub>2</sub>O.

### *Raw clays*

The results obtained show that it is feasible, using froth flotation, to recover more than 85-95% of the clay, with an iron grade of around 3% Fe<sub>2</sub>O<sub>3</sub> or less. The best method was size separation by hydrocyclones, followed by froth flotation of the iron/titanium-bearing minerals of the underflow product, by using sulfonate-based collectors in an acid circuit. The flotation clay product is to be mixed with the hydrocyclone overflow product. Although the results of bench-scale tests show that the proposed objectives are not yet completely accomplished, it seems that with this approach, reduction of the coloring elements' content can be achieved to produce raw clay samples within the range of 2-3% Fe<sub>2</sub>O<sub>3</sub> from ground ores with a high iron/titanium content (about 6-7%).

### **Acknowledgments**

This study was performed within the scope of the European Project (D.G. XII) No. BE-96-3700, "Controlled Processing for Ceramic Pastes Components (CONPAST)", under the financial support of Brite-EuRam III Programme (Contract No. BRPR-CT97-0412). The authors wish to thank the European Commission and the partners of the CONPAST Project, namely, École des Mines d'Ales, École Nationale Supérieure de Ceramique Industriel, Minera Sabater S.L., Pegmatítica Lda, Gresart-Ceramica Industrial S.A. and Eckart Montanconsult und Planung, for their permission to publish this paper.

### **References**

CONPAST Project: 1997-1999. Periodic Reports at 6 Months, 12 Months, Mid-term and 24 Months. C.V.R.M., Instituto Superior Técnico, Lisbon.



## BENEFICIATION STUDIES ON A SPODUMENE ORE FROM PORTUGAL

A. Botelho de Sousa, M.M. Amarante, M. Machado Leite

Laboratório do Instituto Geológico e Mineiro  
Rua da Amieira, 4465, S. Mamede de Infesta, Portugal  
e-mail: ana.botelho@igm.pt; manuela.amarante@igm.pt; machado.leite@igm.pt

### Abstract

A study carried out on processing of a spodumene ore occurring as aplite-pegmatitic lodes in granites located in Northern Portugal, in order to obtain lithium and feldspar concentrates, is described. The Lithia content in this deposit is somewhat variable, with assays between 0.9% and 3.0%  $\text{Li}_2\text{O}$ . The ore also contains feldspar, quartz and mica. Its beneficiation was carried out by heavy media separation (HMS) and flotation. The HMS tests were performed on a sized feed samples ( $4.75 \pm 2.0$  mm) containing ~2.5%  $\text{Li}_2\text{O}$ . A glass-grade spodumene, assaying ~5%  $\text{Li}_2\text{O}$ , was obtained in the sink products.

The flotation testwork was carried out on  $300 \div 75$   $\mu\text{m}$  deslimed feed. However, it was only possible to obtain concentrates with commercial grades, only starting from a feed assaying more than 1.5%  $\text{Li}_2\text{O}$ . Recleaner concentrates, assaying 7.75%  $\text{Li}_2\text{O}$ , were obtained from feed containing ~2%  $\text{Li}_2\text{O}$ . A feldspar concentrate, assaying >17% alumina and >6% alcalis (Na/K ~4/3) with a low iron content, was obtained from the spodumene tailings.

Two beneficiation processes were developed, (i) treatment by flotation, envisaging mainly the production of a high-grade spodumene concentrate, followed by a glass-grade feldspar concentrate, and (ii) pre-concentration of fraction size under 500  $\mu\text{m}$  by HMS, with the advantage of reducing to less than 40% the amount of ore to be processed by flotation. Different ranges for the final products would therefore be obtained, where decreasing in the amount of high-grade spodumene concentrate could be compensated by increasing the quantity of glass-grade spodumene concentrate, with a higher overall recovery and a decrease of the losses into slimes.

*Keywords: spodumene, lithium concentrates, flotation, heavy media separation*

### Introduction

Spodumene is lithium aluminum silicate,  $\text{LiAl}(\text{Si}_2\text{O}_6)$ , containing approximately 8%  $\text{Li}_2\text{O}$ , is one of the richest lithium bearing minerals in nature. Typical consumer product demands include high-grade spodumene assaying at least 7.25%  $\text{Li}_2\text{O}$ , glass-grade spodumene at 5.0%  $\text{Li}_2\text{O}$ , petalite and lepidolite concentrates at 4.4%  $\text{Li}_2\text{O}$  and 4.0%  $\text{Li}_2\text{O}$  (Skillen, 1993).

The main objective of the study was to optimize the treatment of this spodumene ore, in order to obtain commercial concentrates. Lithium concentrate in addition to glass and ceramic bodies, lower process melting points, increase the cooling speed, and reduce coefficient of thermal expansion and viscosity, and therefore eliminate the use of more toxic chemicals (Ober, 1990), contributing to significant energy savings. These characteristics justify the large use of lithium concentrates in the manufacturing of vitroc ceramic, ovenware, floor tiles, thermus flasks, etc. The use of spodumene has advantages over other mineral concentrates, such as lepidolite, because they do not

contain fluorine, a penalty-incurring element. The present study envisages the beneficiation of a spodumene ore occurring as aplite-pegmatitic lodes in granites located in Northern Portugal in order to obtain lithium for the glass and ceramic industries.

## Geology

Lithium-rich aplite-pegmatitic bodies, intruding the metamorphic basement of Northern Portugal, constitute a small percentage of an important two-mica granite complex (Charoy et al, 1992). The spodumene or lepidolite bearing aplite-pegmatite population of Covas do Barroso district, situated between the "Zona-Galiza-Média-Trás-os-Montes" in the north, and the "Zona-Centro-Ibérica" at the South, represents a small fraction of all the lithium mineralization, which appears as spodumene, amblygonite and lepidolite.

Spodumene commonly occurs in the pegmatitic lodes, but also appears in a few of the associated aplites. These lodes are enclosed in metasediments of a siluric age, constituted mainly by mica-schist and quartziferous schist interbedded with black schists.

The detailed cartography of the lodes at 1/5,000 scale and a borehole campaign were carried out in this area, defining an aplite-pegmatitic field, following a NW-SE direction for over more than 20 km (Brandão, 1997).

## Beneficiation studies

### *Crushing and size analysis*

Two representative samples collected from different areas of the deposit were crushed and submitted to a size analysis, with the objective of determining the possibility of a preferential Lithia concentration.

As it can be seen in Table I, there is not a significant preferential concentration in any size fraction.

Table I: Size Analysis and Li<sub>2</sub>O assays in the various fractions.

Size (mm)	Sample 1		Sample 2	
	Weight (%)	Li <sub>2</sub> O (%)	Weight (%)	Li <sub>2</sub> O (%)
+6.68	8.5	0.81	7.4	1.80
- 6.68 + 4.75	17.3	1.10	15.1	1.80
- 4.75 + 3.35	22.1	0.91	22.3	1.80
- 3.35 + 2.36	12.4	0.82	12.3	1.80
- 2.36 + 2.00	4.2	0.70	4.2	1.70
- 2.00 + 1.40	7.1	0.73	7.1	1.80
- 1.40 + 0.85	6.6	0.73	7.3	1.90
- 0.85 + 0.60	2.8	0.78	3.0	2.20
- 0.60 + 0.50	1.6	0.78	2.6	2.60
- 0.50 + 0.30	3.9	0.90	4.9	2.80
- 0.30 + 0.21	2.2	0.97	2.9	2.80
- 0.21 + 0.15	2.7	0.96	3.0	2.50
- 0.15	8.6	0.68	7.9	1.60
Total	100.0	0.86	100.0	1.78

### Flotation testwork

Various batch tests were performed using a Denver flotation machine, in order to optimize the flotation conditions. From the preliminary tests, the following information was obtained:

- grinding to 95% <500  $\mu\text{m}$ ;
- desliming at 74  $\mu\text{m}$  prior to flotation;
- the need of a high reagent consumption, i.e., 500÷800 g/t of collectors and 1.5÷3.0 kg/t of fuel oil;
- the collector combination, which led to the best grade/recovery compromise, was the mixture of oleic + naphthenic acids together with fuel oil able to promote process selectivity at pH = 8.5÷9.5 (Amarante et al., 1998).

The most meaningful results achieved for the rougher and cleaning operations on the samples 1 and 2, are shown in Table II, and in Figures 1 and 2. These results were obtained without the addition of depressants.

Table II: Rougher flotation results achieved on sample 1 and 2.

Flotation products	Sample 1			Sample 2		
	Yield (%)	Li <sub>2</sub> O (%)	Li <sub>2</sub> O recovery(%)	Yield (%)	Li <sub>2</sub> O (%)	Li <sub>2</sub> O recovery (%)
Concentrate	28.8	2.20	77.2	25.7	4.41	60.0
Tailings	47.2	0.10	5.8	46.5	0.85	21.0
Slimes	24.0	0.58	17.0	27.8	1.30	19.0
Total	100.0	0.82	100.0	100.0	1.89	100.0

In the Table II, it can be noted that high-grade spodumene concentrates could only be obtained from sample 2, assaying c.a. 1.9% Li<sub>2</sub>O, after two stages of cleaning.

From sample 1, assaying less than 1% Li<sub>2</sub>O, it was not possible to obtain concentrates with commercial grades. Significant increases in the concentrate grade could not be reached with sequential cleaning, because the concentration ratio was quickly approaching the value 1.

### Heavy media separation (HMS)

Spodumene has a density between 3.15 g/cm<sup>3</sup> and 3.20 g/cm<sup>3</sup>; the other minerals present in the ore are mainly quartz and feldspar with density ~2.7÷2.8 g/cm<sup>3</sup>. Taking into consideration that the liberation size appears to be situated between 3 mm and 4 mm; so that their separation seems to be possible by a gravity method (Taggart, 1945).

The HMS testwork using bromoform, was conducted with feed samples classified into four different fractions, with particle sizes from 2.0 mm to 6.7 mm. Sink product assaying ~5.0% Li<sub>2</sub>O, which comply with the specifications for glass grade spodumene, was obtained with this method.

Li<sub>2</sub>O recoveries of 39÷61% and yields between 21% and 28%, corresponded to this sink fraction, which means that ~75% of the feed material was removed to the light minerals fraction.

For feed sizing less than 4.75 mm, the Li<sub>2</sub>O recovery into the sink product was between 50÷61% (Amarante et al., 1999).

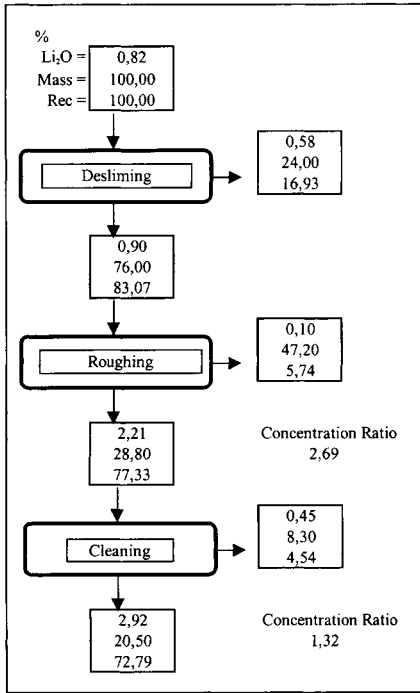


Figure 1: Rougher and 1st cleaner flotation results achieved with Sample 1.

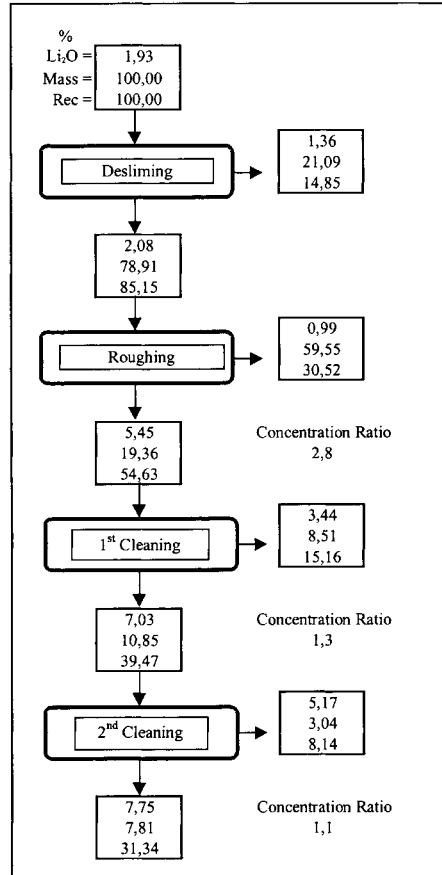


Figure 2: Rougher, 1<sup>st</sup> and 2<sup>nd</sup> cleaner flotation results achieved with Sample 2.

*Production of a feldspar concentrate from the spodumene tailings*

The spodumene flotation tailings are basically a mixture of feldspar and quartz, therefore it was decided to include a feldspar flotation in the experimental set-up.

The procedure followed was based on results previously attained for the flotation of feldspar from an arkosic ore (Botelho de Sousa et al., 1997).

The assays of the feldspar concentrate and the sink product, which contains most of the quartz, are presented in Table III.

It can be seen that a concentrate, having a feldspar/quartz ratio of at least 5:3 and an alkalis content more than 6%, at a Na/K relationship of 4:3, was obtained.

The total Fe content can be decreased by magnetic separation.

Table III: Assays of the feldspar concentrate and the sink product obtained from spodumene tailings.

Assay (by XRF)	Feldspar concentrate	Sink product
SiO <sub>2</sub> (%)	74.00	96.33
Al <sub>2</sub> O <sub>3</sub> (%)	17.22	1.99
total Fe (%)	0.52	0.37
MnO (%)	<0.04	<0.04
CaO (%)	0.09	<0.02
MgO (%)	<0.04	<0.04
Na <sub>2</sub> O (%)	3.88	0.39
K <sub>2</sub> O (%)	2.86	0.22
TiO <sub>2</sub> (%)	<0.02	<0.02
LOI (%)	1.09	0.15

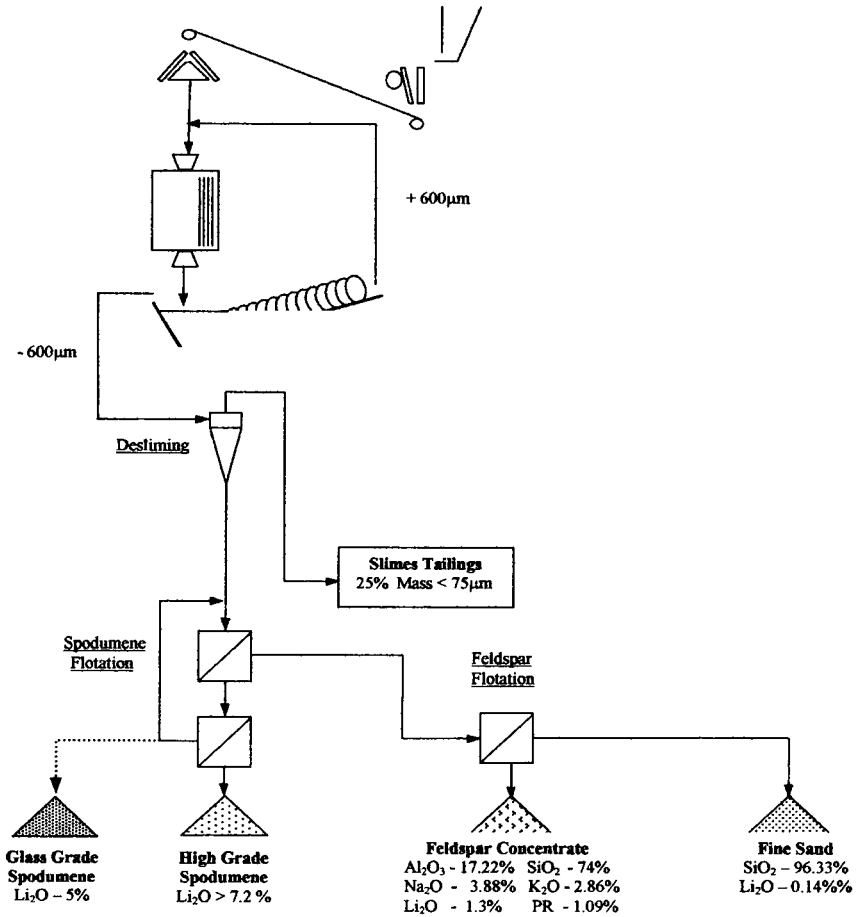


Figure 3: Treatment only by flotation, after crushing and desliming of the ore.

**Proposed flow sheets**

According to the results achieved in the testwork, two flow sheets were proposed, which are presented in Figure 3, where the treatment process only includes flotation after crushing and desliming of the ore, and Figure 4, including HMS prior to flotation.

It can be seen in Figure 3 that 25% of the feed is rejected during desliming, so, a dam would have to be built to store these slimes. In Figure 4, concentration starts at greater particle sizes, after size reduction in a rolls crusher, followed by HMS, to produce a glass-grade concentrate (~5%  $\text{Li}_2\text{O}$ ) at recoveries of ~50%. In this case, only 40÷50% of the feed are treated by flotation. With this option the amount of feed rejected during desliming decreases substantially to values between 8% and 10%.

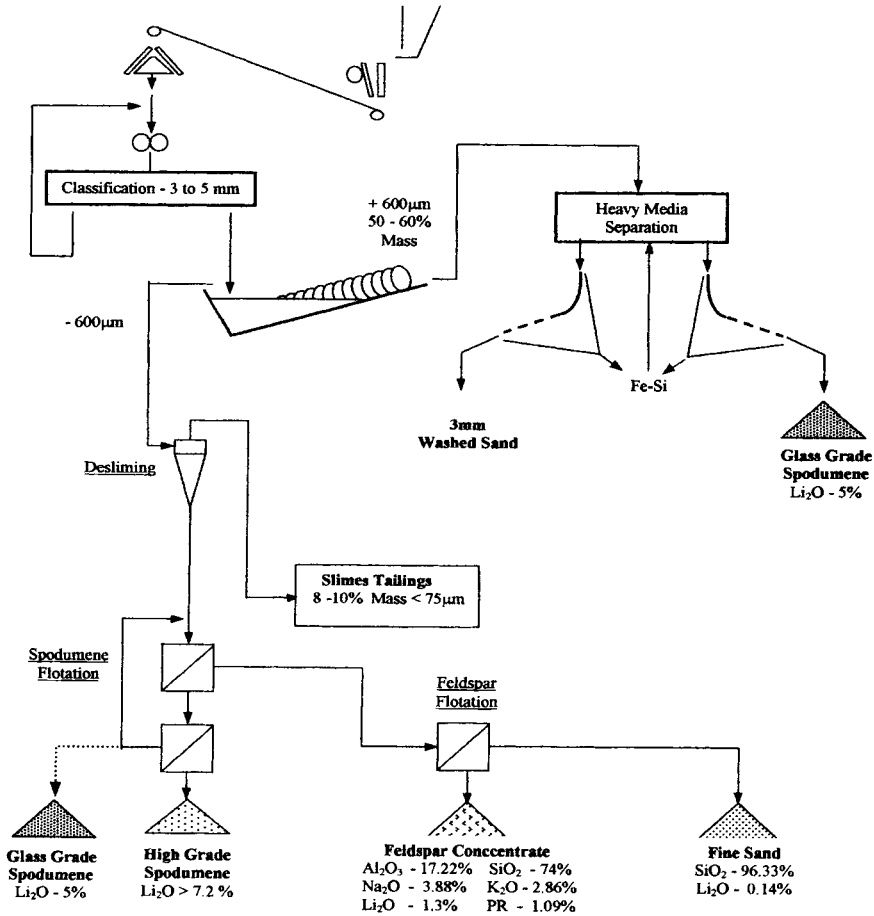


Figure 4: Treatment including HMS prior to by flotation, after crushing and desliming of the ore.

## Conclusions

The beneficiation by froth flotation needs a particle size reduction to <500  $\mu\text{m}$ , although the liberation size starts at  $\sim 4$  mm. This method requires a previous desliming, from which about 25% of the feed are lost. With this method, it was possible to obtain concentrates capable of being used by the industry for feed grades greater than 1.5%  $\text{Li}_2\text{O}$ , corresponding to mean roughing recoveries of  $\sim 55\%$  and cleaning recoveries of  $\sim 40\%$ , for concentrates assaying respectively 5.4%, and 7.0%  $\text{Li}_2\text{O}$ . A second cleaning stage, to obtain a high-grade spodumene concentrate assaying 7.75%  $\text{Li}_2\text{O}$ , resulted in a substantial decrease in the recovery to 31%.

When HMS was included prior to flotation, it was possible to obtain concentrates containing 5%  $\text{Li}_2\text{O}$ , at mean recoveries of  $\sim 50\%$ , and to reduce the losses in the slimes less than 10%.

## References

- Amarante, M.M., Botelho de Sousa, A., Machado Leite, M., 1998. Processing a spodumene ore to obtain lithium concentrates for the glass and ceramics industries. 4<sup>th</sup> Conference on Environment and Mineral Processing, Part I, 205-210.
- Amarante, M.M., Botelho de Sousa, A., Machado Leite, M., 1999. Technical Note. Processing a spodumene ore to obtain lithium concentrates for addition to glass and ceramic bodies. *Minerals Engineering*, Vol. 12, No 4, 433-436.
- Botelho de Sousa, A., Amarante M.M., Machado Leite, M., 1997. Processing a feldspar ore by flotation, using HF or  $\text{H}_2\text{SO}_4$  as pH regulators. *Proceedings of the XX IMPC, Aachen*, 21-26 September, 637- 644.
- Brandão, J.L., 1997. Portuguese Geological and Mining Institute, Internal Report.
- Charoy, B., Lhote, F., and Dusausoy, Y., 1992. The crystal chemistry of spodumene in some granitic aplite-pegmatite of Northern Portugal. *Canadian Mineralogist*, Vol. 30, 639-651.
- Ober, J.A., 1993. Lithium, *Minerals Yearbook*. Volume 1, 1990, pp 699-707, U.S.A. Department of the Interior, Bureau of Mines, U.S. Government Printing Office, Washington.
- Skillen, A., 1993. Lithium minerals, *Industrial Minerals. Raw Materials for the Glass and Ceramic Industries*. 2<sup>nd</sup> Edition, 87-92, A. D. Skillen & J. B. Griffiths.
- Taggart, A.F., 1945. *Handbook of Mineral Dressing - Ores and Industrial Minerals*, 11-02, John Wiley & Sons, New York.

## **WASTE TREATMENT AND RECYCLING**



This Page Intentionally Left Blank

<b>Comminution of Scrap and Metals in Shredders with Horizontally and Vertically Mounted Rotor</b> G. Timmel, S. Sander, G. Schubert	C12a-1
<b>Employment of Foundry Wastes</b> M.C. Zanetti, C. Clerici, D. Sandrin, M. Operto	C12a-9
<b>Production of Magnetite Powder and Recovery of Non-Ferrous Metals from Steel Making Residues</b> A. Delalio, Z. Bajger, P. Baláz, F. Castro	C12a-15
<b>Interactions Between the Toner Composites and Cellulose and Their Implication to Flotation Deinking</b> Y. Hu, D. Wang, J.D. Miller	C12a-20
<b>Beneficiation of Brass Ashes</b> S. Timur, S. Gürmen, G. Orhan, C. Arslan, I. Duman	C12a-27
<b>The Liberation of Impregnated Gold from Wood Chips</b> W. Martin, F.W. Petersen, A.B. Nesbitt	C12a-34
<b>Recycling of Industrial Waste Materials: Recovery of Aluminum from Leftover Bottle Cap-Liner Materials</b> S. Sano, M. Nikaidoh, K. Yanagawa, Y. Kanda	C12a-40
<b>Characterization and Recycling of Amalgam from Dental Clinics</b> J.Y. Pereira Leite, C. Pereira de Souza	C12a-46

This Page Intentionally Left Blank

## COMMINUTION OF SCRAP AND METALS IN SHREDDERS WITH HORIZONTALLY AND VERTICALLY MOUNTED ROTOR

G. Timmel, S. Sander, G. Schubert

Freiberg University of Mining and Technology, Institute of Mechanical Process Engineering and Mineral Processing, Agricolastr. 1, D-09599 Freiberg/Sa., Germany

### Abstract

Shredders are of extraordinary importance for the comminution of scrap. With regard to their design they can be divided into horizontal shaft shredders (HS) and vertical shaft shredders (VS). This work investigates the microprocesses of comminution of metals in small-scale shredders of both types. Moreover, an impact apparatus and a modified Izod pendulum are applied. Four stages can be distinguished during the comminution of platy test bodies.

With five different materials the performance of the two types of shredders were compared. To produce a set product characterized by the mean fragment size, the mean fragment weight and fragment deformation the same specific energy is needed. Differences could be detected regarding the residence time of the fragments.

*Keywords: comminution, metals, scrap, microprocesses, shredder*

### Introduction

The processing of wastes and other secondary raw materials is frequently required in order to make use of their metal content. Since it is used to influence the physical properties of the feed material according to the requirements of the subsequent processes and to secure the liberation of the metals, comminution is usually one of the most important unit operations in waste processing.

For the comminution of scrap, shredders (high-speed hammer crushers) are the most common types of equipment. With regard to the position of their rotor they can be divided into horizontal shaft shredders (HS) and vertical shaft shredders (VS). HS's have been proven for the comminution of end of life vehicles, new and obsolete aluminum scraps, chips, batteries and household appliances. VS's are frequently used for preliminary fragmented steel scrap with less wall thickness, electronic scrap and municipal waste.

For the sake of further development of the known equipment and a successful application of shredders for other purposes, a detailed knowledge of the microprocesses, taking place inside these machines, is essential.

### Experimental

The comminution of the test bodies was conducted on small-scale VS (Figure 1) and small-scale HS (Figure 2), respectively. Both shredders are operated with identical impacting tools (hammers) and at a circumferential speed of 50 m/s. Differences consist in the design of the rotor and the surrounding parts of the housing (especially

the geometry of the anvils and the discharge), which becomes obvious when comparing Figure 1a and Figure 2.

The number of the hammers is also different. The variation of specific energy was achieved by means of batch-tests (HS) and different numbers of rotor units (VS), respectively. Since most of the scraps are characterized by a thin wall thickness, the majority of the experiments were conducted with test bodies made of sheet metals with well-defined properties.

For the evaluation of the experiments the weight and the size of the feed and the fragments, the growth of surface area (considers only new surface area formed by cracks and fractures) and the specific energy per unit mass and per unit growth of surface area, respectively, were measured.

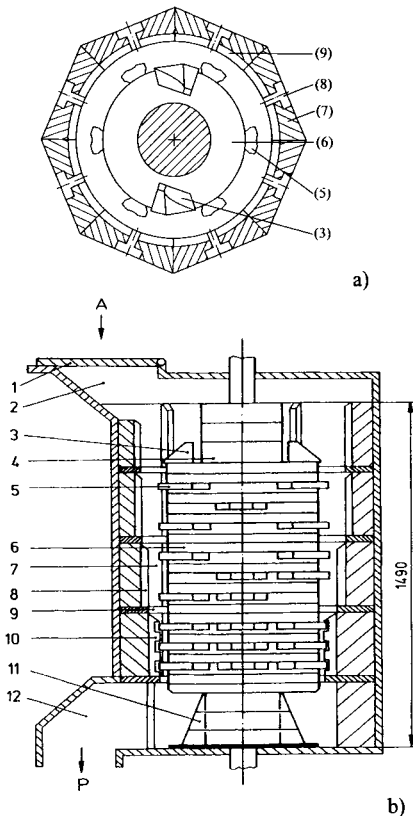


Figure 1: View from above on the comminution chamber a and cross-section b of the small-scale vertical shaft shredder. 1: flap; 2: feed chute; 3: preliminary comminution tool; 4: rotor; 5: impacting tool - hammer; 6: rotor unit; 7: baffle plate; 8: anvil; 9: retaining baffle; 10: comb-shaped anvil; 11: discharge plate; 12: discharge; A: feed; P: product.

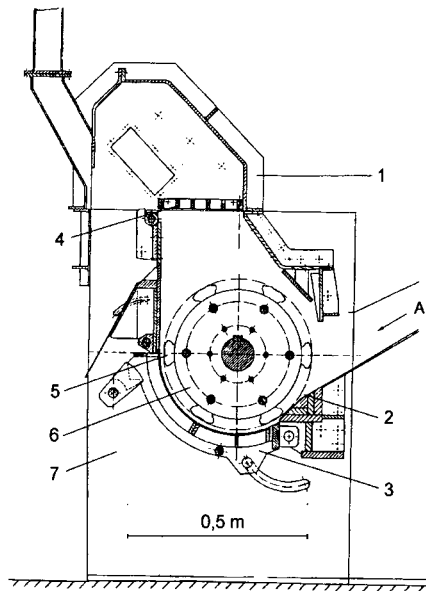


Figure 2: Cross-section of the small-scale horizontal shaft shredder. 1: housing; 2: anvil; 3: lower part of housing - flap; 4: upper part of housing-discharge grate, baffle plates; 5: impacting tool - hammer; 6: rotor; 7: discharge.

In order to investigate the influence of the width of the clearance between impacting tools and anvil and of the main dimensions of the specimen on the first stage of comminution, a modified Izod pendulum was used. Moreover, an impact apparatus was applied, in which the specimens are shot against a vertical baffle plate at a velocity of 50 m/s. There, the dependency of the breakage probability on the number of impacts and therefore on the specific energy was investigated. In addition to that, the determination of the material properties was conducted on testing machines known from material science.

## Results

### *Microprocesses*

From earlier experiments with the small-scale HS (Kirchner and Schubert 1997, Kirchner et al., 1998) it is understood, that four stages can be distinguished during the comminution of platy test bodies:

1. Tearing off of large fragments from the feed by tensile stress in combination with bending and torsion.
2. Intensive deformation (bending to compaction) of the large fragments (and the feed not fragmented in the 1<sup>st</sup> stage) as a result of the formation of abutments. This leads to crack formation and, eventually, to fractures by tensile stress in combination with bending and torsion.
3. Deformation (compaction) of the smaller fragments by load (impact, without formation of abutments), which results in crack formation and fracture propagation, respectively, and fractures.
4. Further compaction of the fragments and formation of fine particles by the combined action of load and shearing at the surface of the fragments.

1<sup>st</sup> stage: Comminution tests on both shredders gave evidence that no fragments are torn off from platy test bodies. Therefore, this kind of feed is only bent at low specific energies, which results in a decreasing mean fragment size whereas the mean fragment weight remains at an unchanged level (Figure 3). A fragmentation could only be observed when using platy test bodies with artificial cracks (in the order of more than 90% of their cross section) or voluminous test bodies with a thin wall thickness. Investigations with the modified Izod pendulum showed that far narrower clearances between the anvil and the impacting tools are required for the formation of fragments from a platy test specimen during the 1<sup>st</sup> stage.

2<sup>nd</sup> stage: The further deformation of the fragments of the 1<sup>st</sup> stage and the platy feed, respectively, leads to the formation of initial cracks and fracture propagation and, thus, to a growth of surface area (Figure 4). In the beginning, the amount of specific energy per unit growth of surface area required for that is very high. Since the deformation enables the formation of abutments and is likely to influence the properties of the material (e.g. hammer hardening, formation of flaws, etc.) the specific energy per unit growth of surface area decreases with the growth of surface area. The importance of preliminary stress of the feed can also be derived from Figure 4. The test bodies stressed by bending before the comminution show a completely different behavior than the ones described above. The flaws formed as a result of the bending

are used for crack formation and propagation and, thus, the formation of surface area at a much lower level of specific energy per unit growth of surface area.

The results of tensile tests carried out using sheet zinc specimens, which were pre-stressed by bending, are given in Table I. They give a hint of how the properties of the material are influenced by the bending. With an increasing number of bendings the tensile strength decreases insignificantly whereas the elongation at fracture drops drastically.

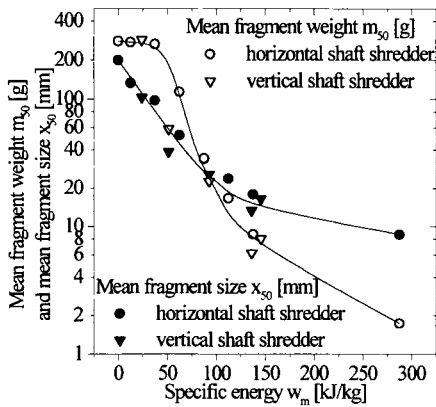


Figure 3: Mean fragment size  $x_{50}$  and mean fragment weight  $m_{50}$  versus specific energy. (feed: Zn ( $200 \times 200 \times 1$ )  $\text{mm}^3$ ; circumferential speed of the hammers: 50 m/s).

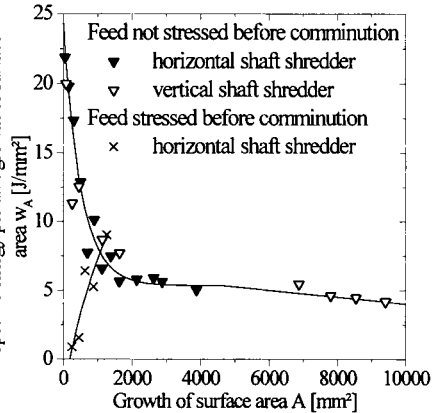


Figure 4: Specific energy per unit growth of surface area versus growth of surface area.

This results in a decrease of the specific energy per unit growth of surface area. The fracture occurs exactly in the spot of the specimen pre-stressed by bending, which leads to the assumption that flaws and micro-cracks are formed as a result of the preliminary stress.

Table I: Results of tensile tests carried out using sheet zinc specimens pre-stressed by bending.

Number of bendings	Tensile strength	Elongation at fracture (%)	Specific energy per unit growth of surface area ( $\text{J}/\text{mm}^2$ )
	( $\text{N}/\text{mm}^2$ )		
0	177.0	35.6	3.1
1	169.5	10.2	0.8
2	153.5	2.2	0.2

3<sup>rd</sup> stage: In order to get an idea whether or not pieces of sheet metal will form fractures as a result of impact, some investigations with an impact apparatus were conducted. In the case of platy specimens, the number of impacts and, thus, the specific energy required for fracture strongly depends on the size (Figure 5), which is due to the different leverages affecting the bending. When using fragments of a product from the small-scale HS this dependency is still visible but weakens. However, the preliminary stress by the comminution turns out to be crucial for the specific energy required for fracture. Since the fragments have flaws and cracks, they

also show a higher breakage probability. The results of comminution tests in both small-scale shredders can be seen in Figure 6. Obviously, the comminution of the platy test bodies, which are too small to form abutments inside the shredders (Zn (25×25×1) mm<sup>3</sup> and Zn (50×50×1) mm<sup>3</sup>, respectively) requires a higher specific energy than the comminution of the larger ones (Zn (200×200×1) mm<sup>3</sup>).

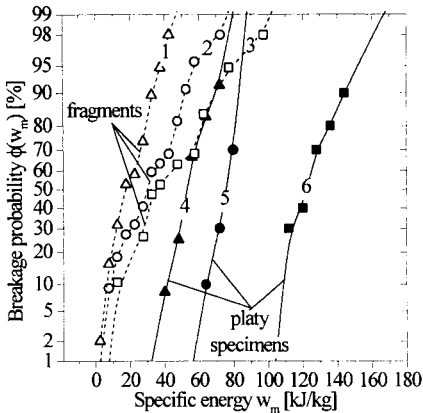


Figure 5: Breakage probability versus specific energy with fragment-weight as a parameter for platy specimens (zinc) and fragments from the small-scale HS (zinc).  
 1:  $m=25\div33$  g; 2:  $m=6\div9$  g; 3:  $m=1.8\div3$  g;  
 4:  $m=31$  g; 5:  $m=7.8$  g; 6:  $m=2.1$  g  
 (wall thickness: 1 mm; velocity: 50 m/s)

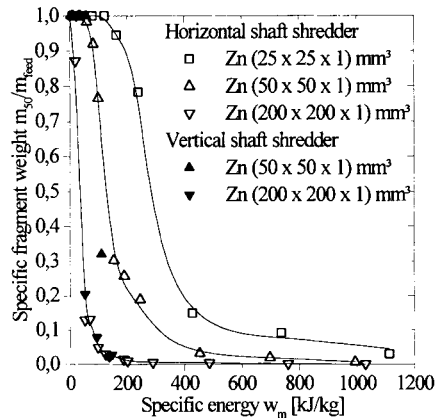


Figure 6: Specific fragment weight versus specific energy with feed-size as a parameter for platy test bodies.  
 (circumferential velocity of the hammers: 50 m/s)

The results of a comparison of the behavior of the two types of smaller test bodies (Zn (25×25×1) mm<sup>3</sup> vs. Zn (50×50×1) mm<sup>3</sup>) are in good conformity with the ones derived from the investigations on the impact apparatus. In order to reach the same specific fragment weight the larger test bodies require less specific energy than the smaller ones. However, no differences between the HS and the VS can be observed.

**4<sup>th</sup> stage:** Basically, the formation of fine particles by wear occurs during each contact. The mechanism of wear, however, is dependent on the properties of the material. Figure 7 shows a typical example of abrasion on the surface of a fragment (sheet zinc). The particles, which can be seen in Figure 8, had been further deformed. Therefore it is difficult to draw conclusions as to their formation.

#### *Comminution tests in the horizontal shaft shredder and vertical shaft shredder*

To study the comminution of platy test bodies experiments were carried out with five materials (Table II).

Test bodies with main dimensions of (200×200×1) mm<sup>3</sup> were investigated. In order to compare both types of shredders it was necessary to produce identical products. For this reason the HS had a discharge grate (Figure 2, number 4) with square apertures (20×20) mm<sup>2</sup>. The VS was used with a configuration as shown in Figure 1. The results are shown in Table II.



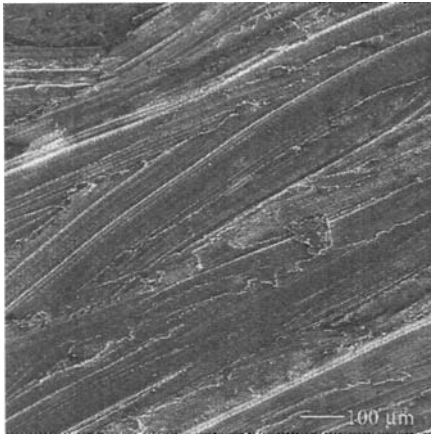


Figure 7: Typical surface of a fragment after stressing in the horizontal shaft shredder.

(feed: Zn (200×200×1) mm<sup>3</sup>; circumferential speed: 50 m/s; batch-test: 60 s)

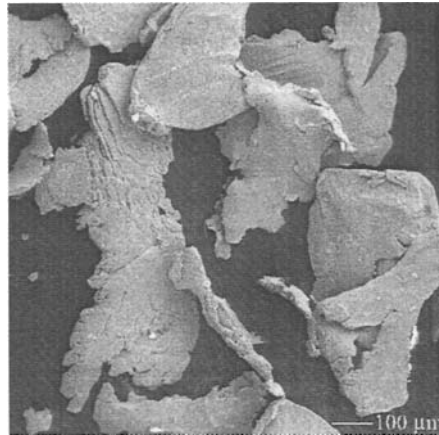


Figure 8: Typical particles of the size interval 0.2÷0.6 mm out of the product of the horizontal shaft shredder.

Table II: Results of the comminution of five materials in the HS and the VS.  
(feed: (200×200×1) mm<sup>3</sup>, circumferential speed of the hammers: 50 m/s)

		Horizontal shaft shredder				
		Zn	Al	St14	MS63	AlMgCu1
$x_{50}$	(mm)	11.0	12.0	12.5	10.0	10.5
$m_{50}$	(mm)	4.1	2.2	5.9	2.4	0.5
$w_m$	(kJ/kg)	170.5	376.4	373.1	168.0	165.4
$\tau_{50}$	(s)	16.3	13.5	19.1	12.7	14.4
		Vertical shaft shredder				
		Zn	Al	St14	MS63	AlMgCu1
$x_{50}$	(mm)	12.5	13.2	13.3	12.0	10.8
$m_{50}$	(mm)	5.5	2.6	6.1		0.71
$w_m$	(kJ/kg)	136.4	253.1	278.6	141.1	135.0
$\tau_{50}$	(s)	26.4	23.7	34.9	27.0	24.0

Obviously, there are only little differences between product sizes of the VS and the HS for each material (mean fragment sizes  $x_{50}$ ).

Each product is composed of fragments with different shape. To detect the different shape of fragments the correlation between fragment weight and fragment size can be used (Figure 9). Hence, differences in deformation of the fragments can be revealed by means of plotting the fragment weight versus fragment size. Figure 10 shows the relation between specific fragment weight and fragment size for three materials. As it can be seen there is the same relation between fragment weight and fragment size for both types of shredders. Thus, the products of both shredders do not differ regarding the deformation of the fragments.

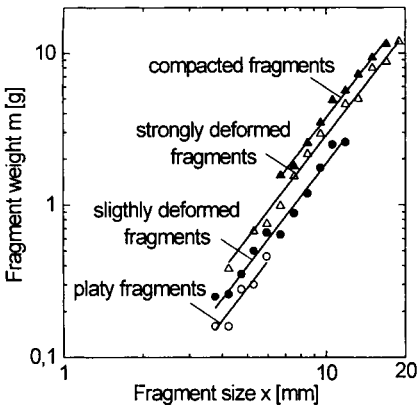


Figure 9: Correlation between fragment-weight and fragment-size with fragment-shape as a parameter.  
 feed: Zn (200×200×1)mm<sup>2</sup>;  
 circumferential speed: 50 m/s, small-scale VS

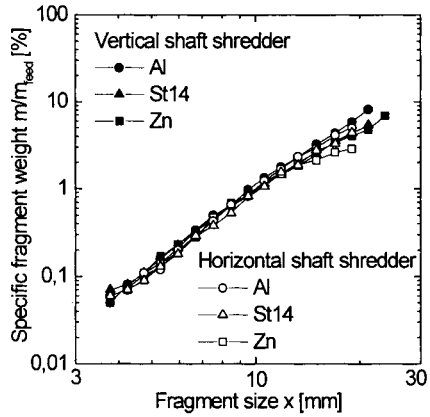


Figure 10: Specific fragment weight vs. fragment-size with material as a parameter.  
 feed: (200×200×1) mm<sup>2</sup>;  
 circumferential speed: 50 m/s

Regarding platy test bodies our experiments confirmed the results of Kirchner et al. (1998). For both types of equipment the same correlation between mean fragment weight and specific energy was observed (Figure 11). In contrast to this the relationship between mean residence time  $\tau_{50}$  and specific energy  $w_m$  is very different (Table II and Figure 12).

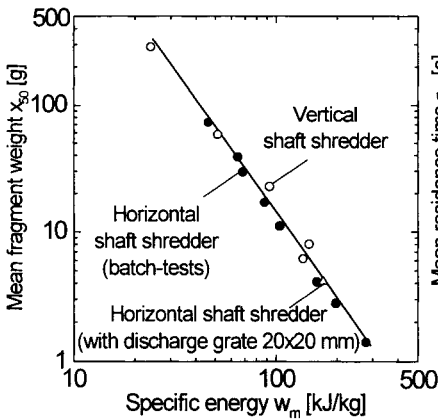


Figure 11: Mean fragment weight versus specific energy.

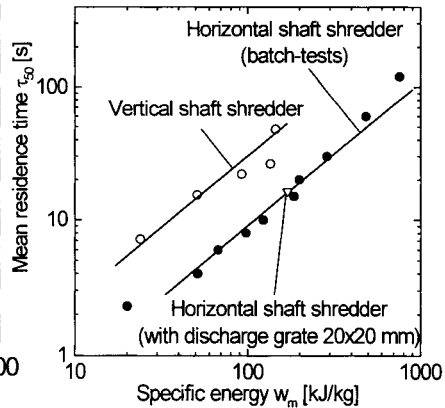


Figure 12: Mean residence time versus specific energy.

(feed: Zn (200×200×1) mm<sup>2</sup>; circumferential speed: 50 m/s)

For similar products the mean residence time of fragments in the VS is much higher than in the HS.

This is a result of details in design of the comminution chamber.

In the VS the comminution starts with low intensity.

This is because of the wide clearance between the preliminary comminution tool and the baffle plate (105 mm). In the HS the feed is stressed very intensively at the beginning of comminution because of the small clearance between anvil and circle of the impacting tools (5 mm).

### **Conclusions**

For the comminution of platy test bodies it has been shown that in both types of shredders the same microprocesses occur. For this reason the same correlation between product size and specific energy is observed. To get the same product there are significant differences in residence time, though. The residence time of fragments in the VS is much higher than in the HS. However, small fragments can leave the VS after short residence times because of the missing discharge grate. This is advantageous for the liberation of waste and scrap. Small, liberated fragments can leave the shredder without further comminution to a fragment size, which would be necessary for discharge through a discharge grate.

### **References**

- Kirchner, J. and Schubert, G., 1997. Comminution of Scrap and Metals by Shredders. Preprints XX Int. Mineral Processing Congress. Gesellschaft für Bergbau, Metallurgie, Rohstoff- und Umwelttechnik, Aachen, Germany, Volume 2, 37-47.
- Kirchner, J., Timmel, G. and Schubert, G., 1998. Comminution of Metals in Shredders with Horizontally and Vertically Mounted Rotors - Microprocesses and Parameters. Preprints 9<sup>th</sup> European Symposium on Comminution. European Federation of Chemical Engineering, Albi, France, Volume 2, 475-484.

## EMPLOYMENT OF FOUNDRY WASTES

M.C. Zanetti, C. Clerici, D. Sandrin, M. Operto

Department of Land and Territory, Politecnico di Torino, Torino, Italy

### Abstract

The processes and fluxes of two foundry plants were analyzed in order to determine the amount and kind of wastes generated from the different activities. The main fractions are molding and core sands, furnace dusts coming from cycloning and bag filtering, exhaust limes, furnace refractors, metallic shotting and sludges. Molding and core sands can be treated and recycled in production operations. A representative sample was collected from different sections of the foundries and it underwent to a treatment cycle in order to evaluate the potential recovery efficiency. The obtained product was chemically and physically characterized. The results show no substantial difference from the values measured employing the fresh silica sands thus validating hypothesis of recycling.

*Keywords: wastes, foundry, molding sands, reutilization*

### Foreword

Cast iron production determines a high amount of wastes (0.7÷1.2 t/t of produced cast iron) (Assofond, 1969) and actually there are no new available technology useful for waste minimization at source. Therefore in this work the cast iron production process was examined and, particularly, the different kind of produced wastes, trying to understand sources, quantities and the potential recovery solutions.

Two cast iron plants were examined, belonging to the same firm, located in the North of Italy. The Crescentino plant produces 900÷1,000 t/d of casts iron (85% gray iron and 15% globular). These casts are employed for car details: flat cars for industrial vehicles and cars, drive shafts and drums. The just in time production is made by means of two hot air cupola furnaces with maximum potentiality equal to 40 t/h. The melt casts is realized by three production lines, in which molding operations, core assembling and shakeout are performed. Then there are finishing sections, where shotting and thermal treatment operations are realized. The Carmagnola plant produces about 600 t/d of cast iron (85% globular and 15% of gray). The produced details are mainly camshafts, piston rods, suspensions, braking parts. The melting is performed by means of two furnaces. One furnace is exclusively employed for globular cast iron production with a potentiality equal to 40 t/h and the other one is utilized both for gray and globular cast iron production for a total of 30 t/h.

In the two plants, the globular cast iron desulfurization is performed by means of shaking ladles employing lime or porous plug ladles by means of calcium carbide.

The melt of casts in the Carmagnola plant is realized in seven production lines.

### Inflows and outflows

The main foundry operations are the followings:

- mould dressing, corresponding to the external shape of the occurring piece;

- core mould dressing, corresponding to hollows of the considered piece;
- shape dressing by means of the mould: this operation is performed employing silica sands, bentonite and black mineral;
- core dressing by means of the mould employing silica sands and resins;
- shape composition;
- melt dressing in the furnace;
- pouring of the melt in the shape;
- shakeout;
- finishing operations;
- fresh sand dressing and recycling sands.

The foundry inflows can be divided in two categories: materials for molding and core operations (Table I) and materials for the cast iron production (Table II).

Table I: Materials for the production of molding sands and cores.

Materials	Crescentino	Carmagnola
Silica sands	500 t/d	107 t/d
Cores	25 t/d	25 t/d
Bentonite	85 t/d	75 t/d
Black mineral	30 t/d	22 t/d
Others	23 t/d	1.2 t/d

Table II: Materials for the cast iron production.

Materials	Crescentino	Carmagnola
Iron Materials	2235 t/d	583 t/d
Calcium Carbonate	90 t/d	38 t/d
Silica Carbide	85 t/d	40 t/d
Calcium Carbide		1.5 t/d
Lime	3 t/d	15 t/d
Coke	225 t/d	170 t/d
Others	18 t/d	25.5 t/d

Silica sands utilized in the Crescentino plant are signed as LA32 and BE31 (French sands) while the ones utilized in the Carmagnola plant are signed as LA32, LA35 (French sands) and Viareggio 4 (Italian sand) (Figure 1). Molding sands are made by silica sand, black mineral (7.8%), bentonite (9÷10%) and water (2÷3%). Coke, fed in the melt production, is useful for heating the metallic charge and to provide the cast iron with the occurring carbon content.

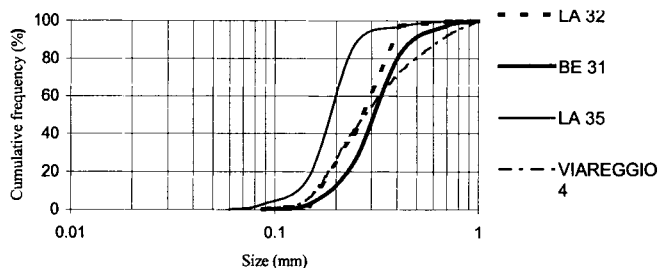


Figure 1: Particle-size distribution for fresh silica sands.

Silica carbide is utilized for the cast iron graphitization and calcium carbonate to eliminate the coke cinders. Wastes coming from the two plants of Crescentino and Carmagnola are reported in Table III. Molding sands are a noticeable fraction of wastes in the two plants. Actually these sands are sold to the concrete industry and/or landfilled. Melting slags are totally sold to concrete plants. Muds are sold to the concrete plants and/or landfilled. All other wastes are landfilled.

Table III: Wastes produced from the two foundry plants.

Materials	Crescentino	Carmagnola
Molding sands	450 t/d	86 t/d
Slags	100 t/d	88 t/d
Muds	125 t/d	120 t/d
Dusts	73 t/d	34 t/d
Exhaust lime	6 t/d	16 t/d
Exhaust carbide		15 t/d
Others	120 t/d	1.2 t/d

### Potential recovery of wastes

Recovery of wastes for the reutilization and reemployment is often the best environmental solution because it allows a reduction of residues and a raw material saving. Reutilization of suction and finishing dusts has been examined (Tonda et al., 1997). In fact the daily production of this kind of waste in the two plants is about 90 t/d with an average iron content about 40% (Zanetti et al., 1999). Metallic product can be recovered by means of magnetic separation and then briquetted in order to reintroduce in the charge of the cupola furnace. Exhaust calcium carbide, coming from the cast iron desulfurization of the Carmagnola plant, can be employed for the acetylene production in a batch reactor plant. This gas can be distributed by a pipeline network to satisfy the factory site demand (Fiore et al., 1999).

In this work the potential reutilization of molding sands in the production activity was considered. A careful characterization of this kind of refuse has been carried out on samples coming from different sections of the considered plants. A treatment process was realized on a representative sample and the resulting material was tested for evaluating potential employment in core dressing.

#### *Molding sands characterization*

Several samples were collected from different sections of the two foundry plants of Crescentino and Carmagnola. These samples were physically and chemically characterized (particle-size distribution and silica, iron and black mineral content). Black mineral content was measured by roasting at the temperature of 900 °C for half an hour. Difference (% wt) between the starting sample and the one obtained after roasting gives the searched value. Metal content was gathered by means of strong acid oxidation performed in microwaves and after flame AA measurements (Perkin Elmer 1100 B). Silica content was measured by the difference (% wt) before and after acid attack (hydrochloric acid, nitric acid and hydrofluoric acid). Results are shown in Table IV. On the grounds of gathered data a representative sample of employed molding sands was prepared and it underwent to some treatment operations.

Table IV: Molding sands characterization.

Products	Quantity (t/d)	d <sub>50</sub> (mm)	Silica (%)	Iron (%)	Black mineral (%)
Molding sands of the Crescentino plant					
Employed foundry sand	350	0.3	76	0.3÷0.5	5.5
Foundry sand coming from shakeout	100	0.4	74	0.6	-
Molding sands of the Carmagnola plant					
Foundry sand coming from soil	8	0.13	45	6	11.8
Foundry sand coming from sieves	12	8	11	18	1.5
Foundry sand coming from the charge "parco"	40	0.3	67	0.2÷0.3	4
Employed foundry sand	20	0.3	62.5	0.7	5

### *Treatment process*

The employed molding sands are mostly made by silica, bentonite, black mineral and a small fraction of iron and water. The bentonite, after the melt, originates an oolitic layer. The oolitic layer is a shell that surrounds silica grains and the corresponding thickness indicates the ageing degree of the sand. This layer must not be too much thick nevertheless casts may present some surface defects. Besides the employed molding sands contain small inert particles made by non-active bentonite, ashes coming from the black mineral combustion and silica particles. A large quantities of these fine particles (2÷4%) may determine some surface defects in casts.

Therefore the treatment process for the silica sands reutilization has to:

- to eliminate fine particles below the 0.1 mm in size (as shown in Figure 1);
- separate the magnetic fraction: in fact the iron particles have both large size (above the 0.6 mm) and particle-size distribution equal to fresh silica sands;
- clean silica grains by means of scrubbing operations (the oolitic content has to be below the 2%); this operation can be performed in wet or dry conditions: however the scrubbing operation efficiency is better in wet conditions.
- eliminate large particles above the 0.6 mm in size (as shown in Figure 1, only the Viareggio 4 sand presents a noticeable fraction above this size, being the 1% of the totally utilized fresh sands).

The laboratory treatment cycle is reported in Figure 2. The starting operation consisted in wet sieving to eliminate large and small particles. Then, magnetic separation has been performed to recover the iron fraction. After this, there was a scrubbing phase employing dilute hydrochloric acid solution (5%) adopting a drive shaft at 800 rpm. The scrubbing cell had a volume equal to 1 liter and a total solid concentration equal to 75%. The operation lasts 10 min.

The ending phase consisted in wet sieving at the size of 0.1 mm to eliminate the oolitic content and the black mineral in the liquid phase coming from the scrubbing operation. The obtained silica product (69.8% of the total treated sample) underwent to some tests in order to understand if it can be reused in core dressing.

### **Results**

The performed laboratory tests were the following: thinness index, oolitic content, the acid request, linseed oil absorption and silica, black mineral and metals content.

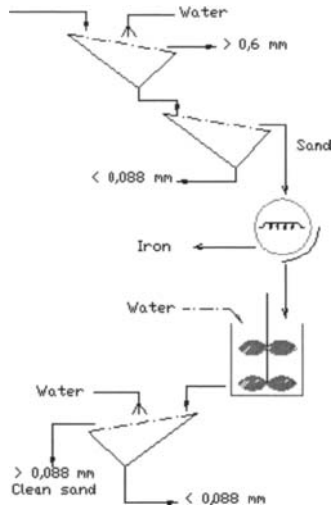


Figure 2: The treatment flowsheet.

#### *Thinness index*

This parameter indicates the number of silica grains kept per  $\text{mm}^2$  of the sieve surface. Therefore a greater index shows the existence of a higher number of fine particles. This index is evaluated after particle-size distribution analysis, each elementary percentage being multiplied for a fixed number. The sum of these values divided for the total weight of the sample determines the thinness index. The resulting thinness index is 50.57 AFA, that is a valid number because the prescribed lower and upper values are 44 and 52 AFA.

#### *Oolitic content*

Oolitic content indicates the ageing degree of the sands as before mentioned. This parameter is measured attacking the sample by hot hydrochloric acid and potassium hydroxide. The difference (% wt) between the fed sample and that one coming from the acid and basic attack furnishes the oolitic content. The measured value is 1.7%.

#### *Acid request*

Acid request is the acid quantity that the basic substances contained in the recovered sand succeed in neutralizing. This parameter is very important in core dressing because the value indicates if the sand and the involved resin can work together. This value is determined adding 0.05 l of water and 0.05 l of dilute hydrochloric acid solution (0.1 N) to a sample of 0.05 kg. Then some ml of a dilute sodium hydroxide solution (0.1 N) are added till reaching a pH value equal to 5. The acid request comes from the difference between 0.05 l and the added quantity of sodium hydroxide solution. The obtained value is 0 ml with upper limit value equal to 6 ml.

#### *Linseed oil adsorption*

Two cylindrical samples (0.05 m diameter and 0.05 m height) are prepared with sand and linseed oil according to foundry prescriptions. These samples were weighed and



underwent to permeability tests (Zanetti et al., 1999) and compression strength tests. Permeability tests indicate how the developed gas during the cast iron melt will flow through cores and they were performed by means of a Fisher permeameter. The compression strength tests were performed by means of a press. The obtained values are shown in Table V.

#### *Black mineral, silica and metals content*

The data concerning chemical analysis were collected according to the mentioned modalities. The results are shown in Table VI. On the grounds of performed chemical analysis the total oxides content is below the prescribed limit value of 1%.

Table V: Results of permeability and compression strenght tests.

	Measured values	Lower limit values
Weight ( $10^{-3}$ kg)	164.8	150
Permeability ( $10^{-6}$ Nm <sup>3</sup> /s)	2.58	2.5
Compression strength ( $10^3$ Pa)	140	110

Table VI: Data concerning chemical analysis.

Black mineral	Silica	Ca	Mg	Zn	Fe	Na	K
(%)	(%)	(%)	(%)	(%)	(%)	(%)	(%)
1.53	94	0.04	0.07	0.01	0.11	0.03	0.04

## Conclusions

Results of the treatment process on the representative sample of molding sands coming from the two plants of Crescentino and Carmagnola are good. In fact all the performed laboratory tests accomplishes with the foundry prescribed parameters for core dressing. Therefore the reutilization of molding sands could allow a raw material saving (in fact, considering a recovery efficiency equal to 70%, the clean silica sands would be about 350 t/d) and waste reduction with noticeable environmental and economic advantages. Large-scale industrial test (500 t) is foreseen in the next future for careful evaluation of the involved economic parameters.

## References

- Assofond, *Associazione Nazionale delle fonderie*, 1999. La formatura nella fonderia di ghisa. Milano.
- Fiore, S., Zanetti, M.C., Onofrio, M., 1999. Treatment process definition for the reuse of manufacturing dusts from metallurgical slugs. Proceedings of the 2<sup>st</sup> National Congress Valorisation and Recycling of Industrial Wastes. Series of Monographs on Material Science, Engineering and Technology. L'Aquila, luglio 1999. In press.
- Tonda, E., Zanetti, M.C., Clerici, C., Operto, M., 1997. Iron Recovery from Foundry Wastes. Proceedings of the 1<sup>st</sup> National Congress Valorisation and Recycling of Industrial Wastes. Series of Monographs on Material Science, Engineering and Technology. L'Aquila, luglio 1997, 89-95.
- Zanetti, M.C., Giordanetto, L., Clerici, C., 1999. Recovery of an old landfill: wastes treatment and recycle. Proceedings Sardinia 99 Seventh International Landfill Symposium. S. Margherita di Pula (CA), 4-8 ottobre 1999, 595-600.

## PRODUCTION OF MAGNETITE POWDER AND RECOVERY OF NON-FERROUS METALS FROM STEEL MAKING RESIDUES

A. Delalio\*, Z. Bajger<sup>o</sup>, P. Baláz<sup>o</sup>, F. Castro<sup>□</sup>

\*Ecometal, s.r.l., Brescia, Italy,

<sup>o</sup>Research Institute Vítkovice, j.s.C., Vítkovice, Czech Republic

<sup>o</sup>Institute of Geotechnics, Slovak Academy of Sciences, Košice, Slovakia

<sup>□</sup>University of Minho, Guimaraes, Portugal

### Abstract

The zinc content of Blast Furnace (BF) and Basic Oxygen Furnace (BOF) dusts and sludges is relatively high, however is generally not economically to treat these residues to recover zinc. Taking into account that they have a high iron content, removal of zinc would allow economical recovery of the iron values. On the other hand, due the increasing rate of incorporation of galvanized steel, the dusts collected in Electric Arc Furnace (EAF) installation present very high content of zinc and lead.

The processing aspects of this research, investigated:

- recovery the iron content of BF, BOF, EAF residues as magnetite by solid state treatment;
- extraction of magnetite product by magnetic method;
- recovery of non ferrous metals as saleable product;
- reuse the remaining residue as fluxing agent in iron and steelmaking furnaces.

*Keywords: metallurgical wastes, steel-making residues, non-ferrous metals recovery, magnetite production*

### Introduction

The steel-making industry produces large amounts of residues presenting, for an important part of them, eco-toxicity characteristics that lead often to the classification as hazardous residue. Hence, there is an immediate need for treatment before disposal. Beneficiation methods have been studied over decades (Barrado et al., 1998; Broomberg et al., 1999; Delalio et al., 1999; Delalio et al., 1998), taking into account that some of these kinds of residues contain valuable non-ferrous metals. This is the case for electric arc furnace dusts, whose content of zinc, lead and cadmium, being the cause of its great eco-toxicity, represents also a potential for valorization. Several processes have been developed for the treatment of these residues, (e.g. flash smelting, fluid bed pyrochloridization), but only the pyrometallurgical Waelz process is still operating, serving some few percent of all the dusts produced in the world. Hydrometallurgical methods have been also developed (Kaminski and Nunez, 1999), but they have proven hard to make economical. Among them, the modified Zincex process, ammoniacal leaching and Amax process could be mentioned. The decrease in non-ferrous metals prices has rendered this situation yet more difficult, treatment being normally un-economical. On the other hand, the final residues of the treatment processes are often also eco-toxic residues, not solving completely the overall

environmental problem. The employment of magnetite to treat wastewater is a new and promising process (Lupi et al.; 1999, Olper, 1994; Soutwick, 1998). Being iron oxides and an important part in the composition of dusts and sludge of the steel-making industry, these residues may be considered as relevant raw materials for high quality magnetite production.

The aim of this work is to verify a new process by which magnetite is produced at the controlled reduction of metallurgical dust with the coal. Metallic zinc and lead behavior will be discussed too.

## Experimental

### Equipment

A special furnace with external heating was constructed for performing reductive tests. The furnace is provided with a condensation chamber. The capacity of the equipment is 10 kg of treated mixtures. The maximum heating temperature was 1,400 °C.

### Procedures

After laboratory testing it was decided to produce magnetite in two consecutive steps:

- the reduction step in N<sub>2</sub> atmosphere and
- the re-oxidation step using CO<sub>2</sub> atmosphere and H<sub>2</sub>O stream, respectively in order to re-oxidize the metallic iron to Fe<sub>3</sub>O<sub>4</sub>.

This treatment enables the reduction of zinc and lead too as well as consecutive evaporation. Volume magnetic susceptibility measurements have been achieved in the apparatus Kappabridge KLY-2 (Geophysics, Czech republic) under the following conditions: intensity of magnetic field 920 Am<sup>-1</sup>, homogeneity of the field 0.2%, frequency 920 Hz.

Specific surface area has been determined by the low temperature adsorption method in Gemini 2360 apparatus (Micromeritics, USA). The qualitative determination of iron phases by XRD method was performed on a DRON 2.0 diffractometer with GUR-5 goniometer (Techsnabexport, Russia) under the following conditions: FeK $\alpha$  radiation, 24 kV, 10 mA and 1°min<sup>-1</sup> goniometer rate. Mössbauer measurements have been made in transmission geometry using a conventional microcomputer-controlled spectrometer in constant acceleration mode. A Co/Rh X-ray source was used. The velocity scale was calibrated relative to <sup>57</sup>Fe in Rh.

### Materials

Two samples of metallurgical wastes were tested for magnetite preparation the chemical composition and origin of which is described in Table I.

Three samples of magnetite: artificial (A), commercial (C) and mineral (M) were used for Mössbauer measurements.

Table I: The origin and chemical composition of samples.

Sample	Origin	Chemical composition (%)					
		Fe	FeO	Fe <sub>2</sub> O <sub>3</sub>	Zn	Pb	C
COP3	Fine sludge (Vítkovice, Czech Rep.)	8.6	50.9	11.0	2.43	0.55	5.1
COP4	EAF dust (Vítkovice, Czech Rep.)	0.43	13.9	39.8	16.17	3.23	0.7

## Results and discussion

The samples COP3 and COP4 were treated by magnetic separation, which led to the production of magnetic (MF) and non-magnetic (NMF) fractions. The efficiency of the treatment is given in Table II.

Table II: The efficiency of magnetic separation.

Sample	Efficiency (%)	
	magnetic fraction (MF)	non-magnetic fraction (NMF)
COP3	65	35
COP4	94	6

The samples were analyzed for metallic iron and iron compounds as well as zinc and lead content. The results are given in Table III.

Table III: The chemical analysis of the samples.

Sample	Assay (% wt)							
	Fe	FeO	Fe <sub>2</sub> O <sub>3</sub>	Fe <sub>3</sub> O <sub>4</sub>	Zn	Pb	C	S
COP3 (MF)	24.2	25.3	1.66	5.67	3.4	3.2	2.78	0.74
COP3(NMF)	5.43	11.9	2.56	3.91	3.5	1.7	19.0	0.63
COP4 (MF)	41.9	<0.01	0.45	44.2	0.06	0.18	4.16	0.2
COP4(NMF)	1.73	1.63	1.46	0.43	0.2	0.16	52.4	0.38

It follows from the chemical analysis that elemental iron, ferrous oxide FeO, ferric oxide Fe<sub>2</sub>O<sub>3</sub> and magnetite Fe<sub>3</sub>O<sub>4</sub> are presented in all samples. Magnetite and elemental iron prevail in the magnetic fraction of sample COP4, while the elemental iron and ferrous oxide are in lesser amounts in magnetic fraction of sample COP3. There is a big difference between MF and NMF fractions of both samples as regards magnetic susceptibility, which illustrate the efficiency of the magnetic separation process. The samples were analyzed for values of magnetic susceptibility and mineralogical forms of iron compounds presented. The magnetite (commercial) values are given in Table IV for comparison. The results are given summarized in Table IV. It follows from the data presented in Table IV that different iron compounds are present in the sample. The magnetite Fe<sub>3</sub>O<sub>4</sub> was identified in both magnetic fractions. It seemed be very probable that desulphurized coal used as a reduction agent in the samples under study is an effective substance for performing the transformation. All samples except for non-magnetic form may be classified as ferromagnetic materials. The method of Mössbauer spectroscopy was tested for the evaluation of phase composition of magnetite samples. The results are given in Table V and VI and on Figure 1.

Table IV: The volume magnetic susceptibility,  $\chi$  and XRD analysis.

Sample	$\chi$ ( $10^{-6}$ SI units)	XRD identified phases
COP3 (MF)	432 143	Fe, FeO (wüstite), Fe <sub>3</sub> O <sub>4</sub> (magnetite)
COP3 (NMF)	11 460	FeO (wüstite), Fe <sub>3</sub> O <sub>4</sub> (magnetite)
COP4 (MF)	504 247	Fe, Fe <sub>3</sub> O <sub>4</sub> (magnetite)
COP4 (NMF)	16 768	Fe <sub>3</sub> O <sub>4</sub> (magnetite) ?

Table V: The origin, surface area,  $S_A$  and volume magnetic susceptibility,  $\chi$  of magnetite samples.

Sample	Origin	$S_A$ ( $m^2 g^{-1}$ )	$\chi$
Magnetit A	Artificial (prepared by precipitation)	14.2	0.644628
Magnetit C	Commercial	0.7	0.593681
Magnetit M	Mineral (Diamantina, Brasil)	0.2	0.888472

Table VI: The iron forms in magnetite samples.

Sample	Site populations (%)			Magnetite
	$Fe^{2+}$ impurity	$Fe^{3+}$ impurity	Hematite	
Magnetite A	-	-	-	100
Magnetite C	3.83	1.51	21.55	73.11
Magnetite M	-	-	11.60	88.40

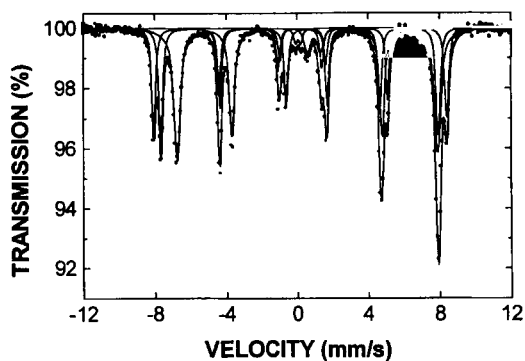


Figure 1: The Mössbauer spectra of sample magnetite C.

The artificial magnetite is a pure compound with 100% of magnetite phase. On the other hand, commercial magnetite has the lowest content of this phase and the highest content of hematite as well as  $Fe^{2+}$  and  $Fe^{3+}$  impurities.

## Conclusions

The new process to recover magnetite by the controlled reduction of metallurgical wastes with the desulphurized coal followed by magnetic separation was tested in this work. The lateral products of the process were metallic zinc as result of the zinc oxide reduction and condensation of gaseous zinc. Zinc rich dust after the appropriate leaching operation allow the recovery of zinc and lead. The final residues of the process are classified as inert. The method of Mössbauer spectroscopy was tested for the iron compounds characterization.

## Acknowledgements

This work was performed in the frame of contract N° ERBC IC 15CT97-0704 thanks to the financial support of the European Commission (DG XII) and efficient guide of Dr. P. Härtwich. The authors wish to express their thanks to Dr. V. Šepelák for performing the Mössbauer measurements.

**References**

- Barrado, E., Prieto, F., Vega, M. and Fernandez-Polanco, F., 1998. Optimization of the operational variables of a medium-scale reactor for metal-containing wastewater purification by ferrite formation. *Water Research* 32, 3055-3061.
- Broomberg, J., Gelinas, S., Finch, J.A. and Xu, Z., 1999. Review of magnetic carrier technology for metal ion removal. *Magnetic and Electrical Separation* 9, 169-188.
- Delalio, A., Bajger, Z., Baláz, P. and Castro, F., 1999. A new treatment process to recover magnetite zinc and lead from iron and steelmaking dusts and sludges. ECSC Workshop, Pre-prints, Bilbao.
- Delalio, A., Bajger, Z., Baláz, P., Castro, F., Magalhaes, J. and Curilla, J., 1998. Characterisation and pre-treatment of steelmaking dusts in order to recover valuable products. *Acta Metallurgica Slovaca*, Special Issue 4, 55-59.
- Kaminski, M.D. and Nunez, L., 1999. Extractant-coated magnetic particles for cobalt and nickel recovery from acidic solutions. *J. Magnetism and Magnetic Materials* 194, 31-36.
- Lupi, C., Cavallini, A., Ferrone, D., Pilone, P., Mililla, P. and Mussapi, R.A., 1999. Hydrometallurgical way to recover zinc and lead from EAF dusts. *Proc. EPD Congress*, Warrendale, Pennsylvania, 621-629.
- Olper, M., 1994. The Ezinez Process. *Proc. EPD Congress*, Warrendale, Pennsylvania, 513-523.
- Soutwick, L.M., 1998. Recycling zinc recovered from electric arc furnace dust: is there a better way? In: *Proc. EPD Congress*, Warrendale, Pennsylvania, 465-482.

## INTERACTIONS BETWEEN THE TONER COMPOSITES AND CELLULOSE AND THEIR IMPLICATION TO FLOTATION DEINKING

Y. Hu\*, D. Wang\*, J.D. Miller<sup>o</sup>

\*Department Mineral Engineering, Central South University of Technology, Changsha, P.R. China

<sup>o</sup>Department Metallurgical Engineering, University of Utah, 412 WBB Salt Lake City, USA

### Abstract

Deinking is very important for paper recycling and usually flotation is used for deinking. In the case of office wastepaper, photocopy and laser-print toner particles are thermally fused and bonded to cellulose fibers, which makes deinking some more difficult than common waste paper. In this paper, the surface physico-chemical properties such as electrokinetics and wettability of the toner composites such as carbon black, some polymers and cellulose have been determined through zeta potential and contact angle measurement. The interaction forces between the toner composites and cellulose have been calculated and their implication to flotation have been discussed based on interfacial polar interaction theory and extended DLVO theory.

*Keywords: interactions, toner composites, cellulose, flotation deinking*

### Introduction

Technology for deinking and cleaning of the cellulose fiber plays an important role in the waste paper recycling which is becoming an increasingly important part of industry papermaking fiber (Claydon, 1990; Raysbro, 1991). Paper is a felted sheet of cellulose fibers formed during the papermaking process. Because of its large content of oxygen-functional groups (mostly —OH and —O— linkage) cellulose exhibits a distinct hydrophilic character. On the other hand, the photocopy laser-print inks exhibit strong hydrophobic character because they contain mainly dry powder polymer as binder and carbon black as pigment. Therefore the separation of ink particles from wastepaper pulp by froth flotation should be a reasonable processing strategy. Air and chemicals are added to the suspension, ink particles attach to the air bubbles, collect in a froth, and hence are separated from the hydrophilic cellulose fiber (Putz et al., 1990; Yu et al., 1992).

In the case of photocopied office waste, where the photocopying ink is photothermally fused and bonded to the cellulose fibers, which make the surface properties of ink much changed, flotation deinking has been much less successful when compared to the flotation deinking of waste newsprint (Shrinath et al., 1991; Nie and Miller, 1995). Further fundamental studies are needed for a better understanding of the surface chemical reaction and changes in photocopying inks during the photocopying process so as to optimize the flotation deinking. The electrokinetic

behavior and wettability of polystyrene, polyacrylic acid, carbon black, which are the dominant components of ink and cellulose have been tested in this study.

#### Interfacial interaction theory

According to the extended DLVO theory, the particle interactions which govern the stability of particle suspensions in a dielectric medium are determined by the repulsive electrostatic interaction force ( $F_e$ ), the attractive London-van-der Waals' force ( $F_w$ ) and non-DLVO forces ( $F_{nd}$ ) (Yotsumoto and Yoon, 1993; Hu and Wang, 1994). The non-DLVO forces have been recognized in many colloidal systems, especially for very hydrophilic or hydrophobic system, during past two decades by surface force measurements and other studies (Veerasamuneni et al., 1997; Van Oss et al., 1988; 1990; Ducker et al., 1991; Tsao et al., 1993; Rutland et al., 1992; Vigil et al., 1994). The total extended DLVO forces can be written as:

$$F_{ed} = F_e + F_w + F_{nd} \quad (1)$$

according to the constant potential model, the electrostatic force ( $F_e$ ) between two dissimilar spheres of radius  $R_1$  and  $R_2$  is given by (Schulze, 1984; Sivamohan, 1990):

$$F_e = \pi \epsilon_a \frac{R_1 R_2}{R_1 + R_2} (\Psi_{01}^2 + \Psi_{02}^2) \left( 2 \frac{\Psi_{01}^2 \Psi_{02}^2}{\Psi_{01}^2 + \Psi_{02}^2} p + q \right) \quad (2)$$

Van der Waals' force is one of the most important interactions between macroscopic bodies. In addition to calculation from the effective Hamaker constant, the Lifshitz-van der Waals' force can also be obtained from surface energy measurements (Van Oss et al., 1987, 1988, 1990; Israelachvili, 1991). The interaction energy between substances 1 and 2 immersed in a liquid 3 according to Van Oss' approach is:

$$\Delta G_{132}^{LW} = (\sqrt{r_1^{LW}} - \sqrt{r_3^{LW}})(\sqrt{r_3^{LW}} - \sqrt{r_2^{LW}}) \quad (3)$$

where  $r_i^{LW}$  is the Lifshitz van der Waals' or apolar component of surface energy of a solid or a liquid.

For two spheres of radius  $R_1$  and  $R_2$ , Lifshitz-van der Waals' interaction forces are expressed by:

$$F_w = 2\pi \frac{R_1 R_2}{R_1 + R_2} \Delta G_{132}^{LW} \left( \frac{D_0}{D} \right)^2 \quad (4)$$

where  $D_0$  is the minimum equilibrium contact distance between two substances,  $D_0 = 0.158 \text{ nm} \sim 0.163 \text{ nm}$  (Israelachvili, 1991).

The non-DLVO force for two spheres with radius  $R_1$  and  $R_2$  can be calculated by the equation:

$$F_{nd} = 2\pi \frac{R_1 R_2}{R_1 + R_2} h_0 \Delta G_{132}^{AB} \exp\left(-\frac{D_0 - D}{h_0}\right) \quad (5)$$

where  $h_0$  is the decay length;  $\Delta G_{132}^{AB}$  is the interfacial polar interactions (Lewis acid-base interactions) energy between substances 1 and 2 immersed in a liquid 3. In the light of Van Oss' interfacial polar interaction theory:

$$\Delta G_{132}^{AB} = 2[(\sqrt{r_3^+} - \sqrt{r_2^+})(\sqrt{r_1^-} - \sqrt{r_3^-}) + (\sqrt{r_3^+} - \sqrt{r_1^+})(\sqrt{r_2^-} - \sqrt{r_3^-})] \quad (6)$$

where  $r_i^+$  and  $r_i^-$  are, respectively the electron acceptor (proton donor) and electron donor (proton acceptor) components of polar component of the surface energy of a solid or a liquid surface. All the surface energy parameters of a solid ( $r_i^{LW}$ ,  $r_i^+$  and



$r_i^-$ ) can be determined with at least three liquids with known  $r_i^{LW}$ ,  $r_i^+$  and  $r_i^-$  values (of which two must be polar) using the Van Oss' approach (Van Oss et al., 1988):

$$r_L(1 + \cos\theta) = 2(\sqrt{r_s^{LW} r_L^{LW}} + \sqrt{r_s^+ r_i^-} + \sqrt{r_s^- r_L^+}) \quad (7)$$

by contact angle( $\theta$ ) measurements.

## Experimental

### Materials

The photocopy toner (fresh ink) is Xerox dry plus 5052/1050 (Xerox Co.). The photocopied wastes (used ink) were made by copy machine and collected from the machines discard bottle. Cellulose (CL) (20  $\mu\text{m}$ ) was purchased from Sigma Chemical Co. Standard polystyrene (PST) and polyacrylic acid (PAA) were purchased from Fluke Chemika. Formamide, diiodomethane and glycerol were respectively purchased from Mallinckrodt, Inc., Aldrich chem. Co., and EM Science. Pure graphite was used as carbon black sample. AR grade HCl and NaOH were used for pH modification. All other chemicals used were AR grade. High purity deionized water with a resistivity of 18 M $\Omega$  was provided by a Millie-Q water system.

### Electrophoretic mobility measurements

The electrophoretic mobilities of ink, polymer and carbon black particles were measured by standard procedures with a Malvern Zeta Sizer using a quartz capillary cell with a 4 mm diameter. The finely powdered particles were added into a 100 ml beaker containing pure water. The solid concentration was about 0.02%. The suspensions were agitated enough time to disperse the particles. And transferred to the capillary cell with a syringe and then the electrophoretic measurements were made.

### Contact angle measurements

The sessile drop technique was used for contact angle measurements with a NRL goniometer (Rame Hart, Inc.). A glass slab with a flat and smooth layers of the polymer obtained by depositing a solution of the polymer in an appropriate solvent on the slab was placed in a rectangular glass chamber and a liquid drop was introduced onto the substrate through a microsyringe. The needle was maintained in contact with the drop. The advancing contact angles were measured for different liquid drops with 3÷4 mm drop base diameter at room temperature (22÷23 °C).

## Results and discussion

### Electrokinetic behavior of ink and ink components

Zeta potentials of fresh, photocopied inks and cellulose as a function of pH are shown in Figure 1. The fresh copy ink has a negative zeta potential, which is increased with pH. The negative zeta potential of photocopied ink (used ink) is higher than that of fresh ink and increased more negative with the increase of pH, indicating that change of surface characteristic of used ink comparing to fresh ink. The negative zeta potential of cellulose is increased with the increase of pH and changed to much more negative when heated to 140 °C.

The zeta potentials of polystyrene, polyacrylate and carbon black (graphite), which are dominant ink components, as a function of pH are presented in Figure 2. It can be

seen from Figure 2 that the negative zeta potential of polystyrene, polyacrylate and graphite are increased with the increase of pH. The PZC occurred at pH = 3.8 for polystyrene and pH = 3.5 for graphite. When polystyrene and graphite are heated to 140 °C, which is usually the case in photocopying machine, the zeta potential of polystyrene and graphite are further moved to negative.

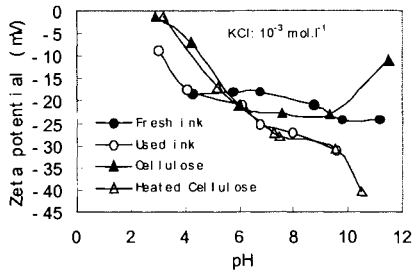


Figure 1: Zeta potentials of fresh, used ink and cellulose as a function of pH.

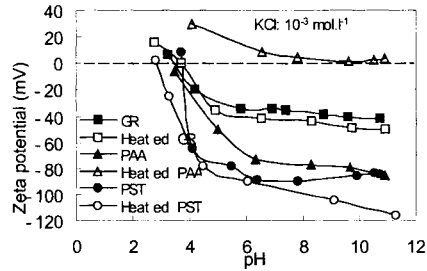


Figure 2: Zeta potentials of polystyrene, polyacrylate and graphite as a function of pH.

The change of zeta potential of polyacrylate when heated to 140 °C is, however, contrary to those of polystyrene and graphite. It changes from negative to small positive. It may be due to the oxidation of acrylic acidic group and decarboxylate reaction because the polyacrylate used here is a copolymer of methacrylic acid and methyl methacrylate.

The change of zeta potential of ink components such as polystyrene, polyacrylate and carbon black when heated comparing to the original ones suggested that the surface physico-chemical properties of used ink would be different from those of fresh ink.

#### *Wettability and surface energy of ink components*

The measured average contact angles of fresh and used inks and various ink components with some polar and non-polar liquids are given in Table I. The calculated values of components of surface energies based on equation (7) are given in Table II. It is obvious that except for polyacrylate, the contact angle and hence the surface hydrophobicity of all substances listed in Table I are decreased when they are heated to 140 °C.

The contact angles, with liquids and hydrophobicity of used ink, are lower than those of fresh ink indicating that the floatability of used ink is some lower than that of fresh ink. It may be also seen that the substance listed in Table II are mostly more electron donor with greater  $\bar{\gamma}^-$  values.

#### *Interactions between ink components and cellulose and their implication to flotation de-inking*

The efficiency of flotation deinking is governed by the hydrophobicity of ink by flotation. In the other hand, it depend on the interaction between cellulose and ink particles which may be repulsive or attractive, mainly affecting the flotation selectively and the whiteness of deinked paper.

In order to find ways to effectively remove the ink from the used paper, the interaction between photocopied ink and fiber paper has been studied.

The Lifshitz-van der Waals' and interfacial polar interaction energy parameters (between ink particles and cellulose and between cellulose and ink components such as polystyrene, polyacrylic acid and carbon black) are calculated in the light of equation (3) and equation (6) and the data in Table II, as shown in Table III. Thus the electrostatic interaction energy curves in various systems can be calculated according to equation (2) and the data from Figure 1 to Figure 2.

The Lifshitz-van der Waals' and interfacial interaction energy curves in various systems can be calculated according to equations (4) and (5) and the data in Table III. The decay length is taken to be 2 nm for attractive system and 1nm for repulsive system.

It has been reported the decay length is usually less or equal to 1 for repulsive system and equal to or greater than 1 for all attractive system (Van Oss et al., 1990; Ducker et al., 1991; Tsao et al., 1993; Rutland et al., 1992; Vigil et al., 1994; Israelachvili, 1991). The total interaction energy curves can be obtained based on extended DLVO theory.

Table I: The average contact angles of some substance with polar and apolar liquid.

Substance	Average contact angle, $\theta$ (°)							
	Room temperature				Heated to 140 °C			
	W	GL	DM	FM	W	GL	DM	FM
Polystyrene	89	75	35	65.5	72.5	67.3	27.7	55.7
Polyacrylate	72.3	66	39	56	75.7	70.3	33.7	59
Cellulose	34.7	32.7	21	17	25.9	26		0
Graphite	60	49.8	30.8	35.8	37	35.5		12
Fresh ink	93	79.5	41	68				
Used ink	68.5	67.5	33.5	56.5				

Table II: The values of components of surface energies of some substances.

Substance	Surface energy parameters, $\gamma$ (mJ/m <sup>2</sup> )						
	Room temperature			Heated to 140 °C			
	$\sqrt{\gamma^{LW}}$	$\sqrt{\gamma^+}$	$\sqrt{\gamma^-}$	$\sqrt{\gamma^{LW}}$	$\sqrt{\gamma^+}$	$\sqrt{\gamma^-}$	
Polystyrene	6.37	0	1.39	6.37	0.06	3.42	
Polyacrylate	5.98	0.44	3.43	6.2	0.04	3.21	
Cellulose	6.24	1.4	5.94	6.14	1.46	6.3	
Graphite	6.1	1.23	3.94	7.08	0.73	5.69	
Fresh ink	6.16	0	1.19				
Used ink	6.2	0	3.28				

Figure 3 demonstrated the total interaction force curves between used ink and heated cellulose. It can be seen that an attractive force may exist between the used ink and heated cellulose.

It suggested that even if the heated cellulose is much less hydrophobic than used ink from the data in Table II, the heated cellulose may still be entrapped onto floated

product or the used ink be entrapped into cellulose fiber paper due to the attraction. It may affect the selectivity of flotation de-inking and whiteness of recycling paper.

Table III: The values of energy parameters of Lifshitz-van der Waals' and interfacial polar interactions.

System	Energy parameter (mJ.m <sup>-2</sup> )			
	Room temperature		Heated to 140 °C	
	$\Delta G_{132}^{LW}$	$\Delta G_{132}^{AB}$	$\Delta G_{132}^{LW}$	$\Delta G_{132}^{AB}$
Used ink/W/CL	- 4.81	- 3.932		
Fresh ink/W/CL	- 4.685	- 19.189		
PST/W/CL	- 5.345	- 17.818	- 5.345	- 17.729
PAL/W/CL	- 4.119	- 3.62		
GR/W/CL	- 4.496	- 1.303	- 7.575	- 12.362

It is also obvious from Figure 3 that the attractive interaction between used ink and heated cellulose may be attributed to the attractive interactions between ink components, such as polystyrene and polyacrylate, and the heated cellulose, which are attractive. In contrast the interaction between the cellulose and carbon black, which is the other component of ink, is repulsive as seen from Figure 4.

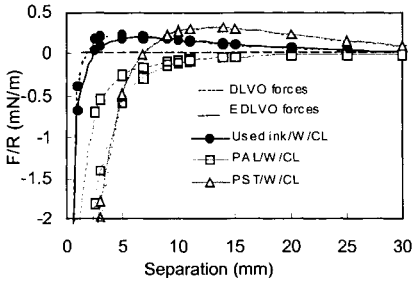


Figure 3: The total interaction force curves between used ink, ink components and cellulose.

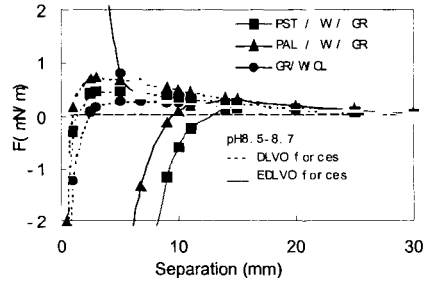


Figure 4: The total interaction force curves between graphite and polystyrene, polyacrylate, and cellulose.

Figure 4 also shows the total interaction force curves between the heated polystyrene, polyacrylate, and carbon black. The interaction between the heated carbon black and cellulose is repulsive which may not make harmful effect on flotation de-inking. However, a strong attraction exists between the heated polystyrene, polyacrylate and carbon black as seen from Figure 4, which will make the carbon black come together with the polymers. Therefore, the difficulty in flotation de-inking from photo-copied paper is that there exist the attractive interactions between cellulose and ink components such as polystyrene, and polyacrylate, as well as between ink component themselves in pulp. To achieve successfully separation used ink from used paper requires modifying the surface properties of used ink and heated cellulose by addition

of some modifiers and surfactants. It is required that the addition of modifiers or surfactants may change the surface physico-chemical properties of ink components such as polystyrene and polyacrylate resulting in the repulsive interactions between the polymers and cellulose so that the ink can be effectively floated out from used paper in pulp. The more details will be reported elsewhere.

#### Acknowledgements

The authors would like to thank the National Natural Scientific Foundation to support this research.

#### References

- Claydon, P., 1990. Recycled fiber: the Major furnish component. In: *Quality Newsprint Production, Pulp & Paper, Canada*, 91(12), 135.
- Ducker, W.A., Senden, T.J. and Pashley, R.M., 1991. Direct measurement of colloidal forces using an atomic force microscope. *Nature*, 353, 239.
- Hu, Y., Wang, D., 1994. Particle interaction: the theory of extended DLVO and its applications in flotation. *J. CSIMM*, 25(3), 310-314. (in Chinese, with English Abstr.)
- Israelachvili, J.N., 1991. *Intermolecular and Surface Forces*. Academic Press., Harcourt Brace & Company, Publishers, 2nd Edition.
- Nie, X. and Miller, J.D., 1995. Thermogravimetric/Mass Spectrometric (TG/MS) characterization of toner particles from photocopied wastepaper and the impact of these features on flotation deinking. The proceedings of the 1995 TAPPI Pulping Conference, Chicago, USA, 179-202.
- Putz, J., Torok, I. and Gottsching, L., 1990. The role of surfactants in flotation deinking of wood-containing wastepapers. *Wochenbl. Papierfabr.* 118(18), 793.
- Raysbro, O., 1991. Utilization of Waste Recycling Technology. *Kagaku Kagaku*, 55(1), 27.
- Rutland, M., Waltermo, A. and Claesson, P., 1992. pH-dependent interactions of mica surfaces in aqueous dodecylammonium/dodecylamine solutions. *Langmuir*, 8, 176-183.
- Schulze, H. J., 1984. *Physico-chemical Elementary Processes in Flotation*. Elsevier, Amsterdam.
- Shrinath, A., Szewczak, J.T. and Bowen, I.J., 1991. A review of ink -removal techniques in current deinking technology. *Tappi J.*, 85.
- Sivamohan, R., 1990. The problem of recovering very fine particles in mineral processing-a review. *Int. J. Miner. Process.*, 28, 247.
- Tsao, Y.H., Evans, D.F. and Wennerstrom, H., 1993. Long-range attractive force between hydrophobic surface observed by atomic force microscopy. *Science*, 262, 547.
- Van Oss, C.J., Chaudhury, M.K. and Good, R.J., 1987. Monopolar surface. *Adv. Coll. Inter. Sci.*, 28, 35.
- Van Oss, C.J., Chaudhury, M.K. and Good, R.J., 1988. Interfacial Lifshitz-van der Waals' and polar interactions in macroscopic systems. *Chem. Rev.* 88, 927-941.
- Van Oss, C.J., Giese, R.F. and Costanzo, P.H., 1990. DLVO and non-DLVO interactions in hectorite. *Clays clay Miner.*, 38, 151-160.
- Veeramasuneni, S., Hu, Y., Yalamanchili, M.R. and Miller, J.D., 1997. Interaction forces at high ionic strengths the role of polar interfacial interactions. *J. Coll. Inter. Sci.*, 188, 473-480.
- Vigil, G., Xu, Z., Steinberg, S. and Israelachvili, J., 1994. Interactions of silica surfaces. *J. Coll. Inter. Sci.*, 165, 367.
- Yotsumoto, H. and Yoon, R.H., 1993. Application of extended DLVO theory: Stability of rutile suspensions. *J. Coll. Inter. Sci.*, 157, 426-433.
- Yu, Q., Ye, Y. and Miller, J.D., 1992. Dispersion and aggregation of newspaper pulps for fiber recovery by deinking flotation. Engineering Foundations Conference, Palm Coat, Florida, USA, 15-20.

## BENEFICIATION OF BRASS ASHES

S. Timur, S. Gürmen, G. Orhan, C. Arslan, I. Duman

Istanbul Technical University, Chemical and Metallurgical Engineering Faculty,  
Metallurgical and Materials Engineering Department 80626 Maslak, Istanbul, Turkey

### Abstract

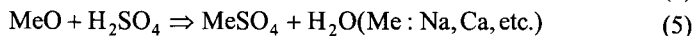
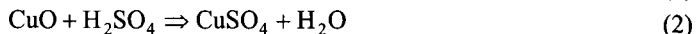
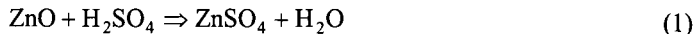
Slags formed during brass smelting contain a significant amount of metallic value. The glassy and oxidized portion of the ground slag, usually referred to as "brass ash", consists of compounds such as ZnO, ZnO·SiO<sub>2</sub>, Cu-Zn, CuO, Cu and Zn/Cu/B oxide, and its colored-metal content may vary between 28÷52% Zn and 8÷16% Cu. These ashes are classified as harmful wastes, due to their high Zn content, and are considered to be secondary raw materials that should be treated accordingly, from an economical viewpoint. The aim of this experimental study is to investigate the possibilities of beneficiating brass ashes by treating it with H<sub>2</sub>SO<sub>4</sub> or (NH<sub>4</sub>)<sub>2</sub>CO<sub>3</sub>+ NH<sub>4</sub>OH mixtures. Effects of temperature, air sparging and addition of oxidizing agents, such as MnO<sub>2</sub> and Fe<sub>2</sub>(SO<sub>4</sub>)<sub>3</sub>, are investigated on copper and zinc leaching recovery. As a result of both acidic and alkaline leaching experiments, it is observed that more than 90% of Zn and more than 65% of Cu was leached out. Two separate process flow sheets are proposed for the possible treatment of brass ashes.

*Keywords: brass ash, zinc recovery, copper recovery, fertilizer, amines, leaching*

### Introduction

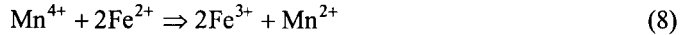
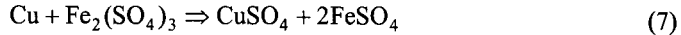
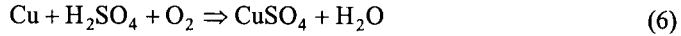
There are numerous small-scale brass casting companies in the vicinity of Istanbul-Turkey, in addition to some medium-scale ones across the country. These small-scale brass-casting companies, however, do not have recycling units for re-evaluating their brass-smelting slags, due possibly to their restricted budgets or to insufficient environmental regulations. Some other small factories purchase these slags for partial evaluation, through which these smelter slags are first wet-ground in roll mills to flatten the metallic bullions, so they will have larger surface areas. These bullions are accumulated on the bottom, while the glassy portion of these ground slag particles are carried with the water overflow. This ground slag is called brass ash and is not treated with any means, while the metallic portion is recycled (Timur and Duman, 1993).

There are two different hydrometallurgical methods for the treatment of brass ashes: acidic and alkaline. The following reactions may occur during the sulfuric acid leaching of brass ashes (Kammel, 1986; Holleman and Wiberg, 1995):

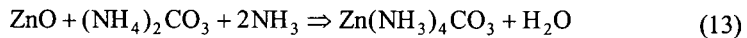
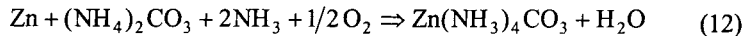
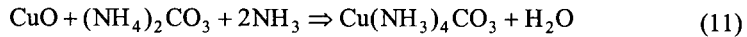
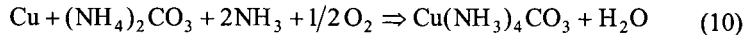


Leaching may be carried out either as a single- or two-step process. Addition of oxidizing agent to the system is necessary to increase the copper-extraction efficiency, either during the second step of two-step leaching process or the single

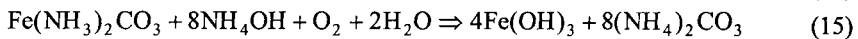
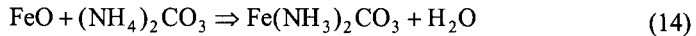
step leaching process, where a Zn-Cu mixed salt solution is produced. Air,  $\text{Fe}^{3+}$ , and  $\text{Mn}^{4+}$  are used as oxidizing agents, and possible reactions are given as follows:



As it is well known, Zn and Cu can also be dissolved under alkaline conditions by forming amine complexes. The main reactions taking place in ammoniacal leaching, where  $(\text{NH}_4)_2\text{CO}_3$  and  $\text{NH}_4\text{OH}$  are used, are listed below (Richardson et al., 1981; Asare, 1981; Akdag, 1986):



Although iron also dissolves under these conditions, it remains in the solid phase as  $\text{Fe}(\text{OH})_3$ , since the reactions are oxidizing in nature:



Moreover,  $\text{SiO}_2$  that exists in brass ashes does not react with ammonia and remains in the solid phase without creating any filtration problems, as was the case in acidic leaching.

## Experimental

### Material

Experiments were carried out with the slag samples collected from different companies. Results of chemical analysis showed that the brass ashes contain some economically important components, such as ZnO, ZnO·SiO<sub>2</sub>, Cu-Zn, CuO and Cu. The chemical composition of these brass ashes shows great deviations (28÷52% Zn, 8÷16% Cu, 0.1÷3% Fe, 4÷8% SiO<sub>2</sub>, and 10÷14% moisture) even in the same company, as there is no classification prior to the treatment of these ashes of various characteristics. The high zinc content of the ashes is due to the high oxygen affinity of zinc as it is selectively oxidized during the smelting. On the other hand, the high iron content of the brass ashes, frequently reaching as high as 3%, may stem from using the low quality and non-classified scraps in brass smelting. However, the iron content of the slag may drop to the level of 0.1% in some factories where standard raw materials are used.

### Method

In this experimental study, brass ashes were treated with  $\text{H}_2\text{SO}_4$  and a mixture of  $(\text{NH}_4)_2\text{CO}_3 + \text{NH}_4\text{OH}$  solutions, in order to examine their beneficiation possibilities. Effects of temperature, air sparging and amount of  $\text{MnO}_2$  and  $\text{Fe}_2(\text{SO}_4)_3$  additions on Zn and Cu recovery were also investigated.

## Results and discussion

### Acidic leaching experiments

The effects of acidic leaching conditions and addition of oxidizing agents (air,  $\text{MnO}_2$  and  $\text{Fe}_2(\text{SO}_4)_3$ ) are investigated in this series of experiments. Figure 1 displays the results of experiments carried out under different acid concentrations in order to investigate the required amount of acid.

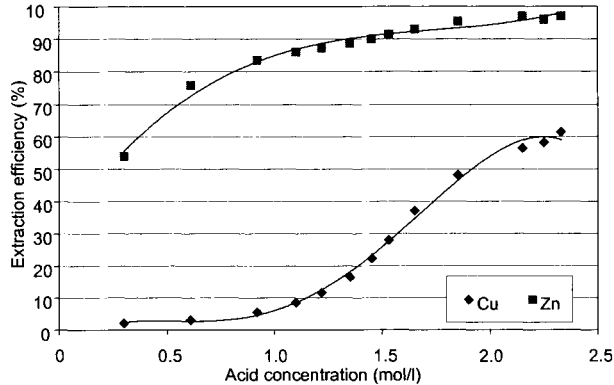


Figure 1: Effect of acid concentration on the extraction efficiencies of zinc and copper.

As seen from this figure, an acid concentration of 1.5 M was satisfactory for significant zinc extraction. There are some filtration problems, however, even at higher  $\text{H}_2\text{SO}_4$  concentrations of 2.04 M due to silica gel formation, and this is overcome by using excess  $\text{H}_2\text{SO}_4$  (i.e. 2.2 M).

Also seen from the figure is that the copper solubility remains low when insufficient acid is used. This difference between the extraction efficiencies of two metals makes it possible to obtain a zinc-rich solution first, and then to leach the remaining zinc and copper in the solid. Dissolved copper can be recovered as cement copper by adding scrap iron into the system after acidic leaching, leaving a zinc-rich solution behind.

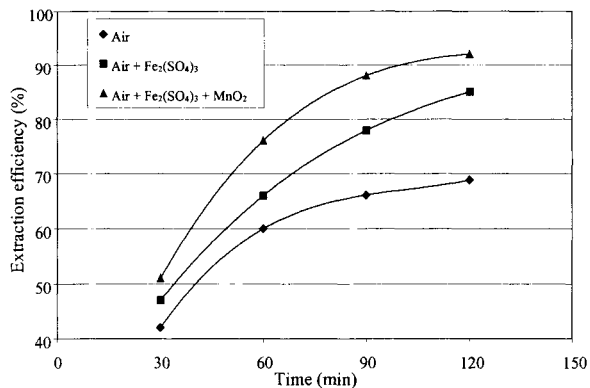


Figure 2: Effect of oxidizing agent addition on copper leaching efficiency (2.2 M  $\text{H}_2\text{SO}_4$ , 0.1 l/s air, 5 g/l  $\text{Fe}^{3+}$ , 2 g/l  $\text{Mn}^{4+}$ ,  $800 \text{ min}^{-1}$ , room temperature).



All experiments in these series are carried out by sparging air (0.1 l/s) into the leaching system. Copper-extraction efficiencies obtained under various oxidizing conditions are shown in Figure 2.

As seen from this figure, extraction efficiency reaches a maximum, as expected, in presence of  $Mn^{4+}$  and  $Fe^{3+}$  ions.

### Alkaline leaching

Figure 3 displays the metal extraction efficiencies obtained by the leaching operations carried out with  $(NH_4)_2CO_3+NH_4OH$ . As seen from the figure, the Zn leaching efficiencies obtained by using amine-based reagents are considerably high, as compared to those of acidic leaching, while copper-leaching efficiencies were almost the same in both types of leaching processes. Therefore, a combined “acidic + amine leaching” process seem to be more economical for the beneficiation of brass ashes, considering the selective metal and salt recoveries from Zn-Cu mixed solutions.

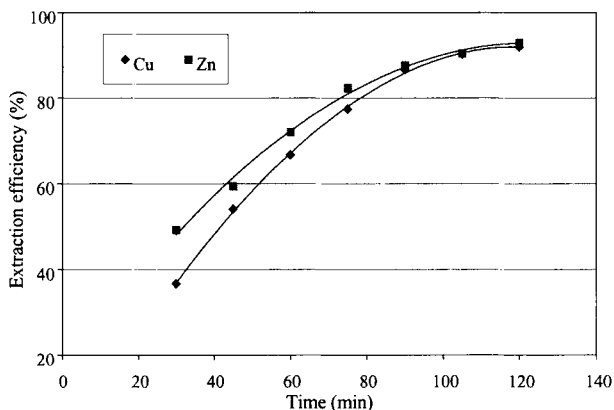


Figure 3: Metal extraction efficiencies in  $(NH_4)_2CO_3+NH_4OH$  leaching.

### Conclusions

The zinc-copper sulfate solution, obtained by sulfuric acid leaching, can be treated via the flow sheet presented in Figure 4. However, this system cannot operate as a closed circuit system, which would include a zinc electrowinning operation as well. It can not be applied industrially either, due to the problems caused by the presence of ions, such as Fe, Al, Na and B, coming from the brass ashes. Therefore, a different approach, “ammoniacal leaching”, has been examined for the beneficiation of brass ashes. The process flowsheet of mixed “acidic + amine” leaching is given in Figure 5. In this process, zinc is dissolved in the form of sulfate by using 1 M  $H_2SO_4$  solution, while allowing only 3÷4% of copper to dissolve. On the other hand, neutralization occurs very fast, since the amount of acid is low, and the pH rises to 5÷6.

Dissolved copper ions, although in very small amounts, go through a cementation process due to the scrap iron added to the system. All iron remains in the solid phase as  $Fe(OH)_3$  by blowing air and adding  $MnO_2$  to the system.  $Fe(OH)_3$  does not create any problem during S/L separation. Recycling the solution can increase the

concentration of  $\text{ZnSO}_4$  solution obtained in the leaching step. However, it is very difficult to recover zinc from this solution electrolytically, due to the existence of salts, such as  $\text{NaAlF}_3$ ,  $\text{H}_3\text{BO}_4$ , etc., used in smelting to obtain a non-viscous and an encapsulating slag. As is well known, elements such as Al, Na, B, etc. cannot be reduced electrolytically from aqueous solutions, and these elements cause problems by constantly increasing in concentration. Therefore, the pregnant  $\text{ZnSO}_4$  solution is used in the production of fertilizers, such as a trace element to ammonium sulfate and ammonium phosphate, instead.

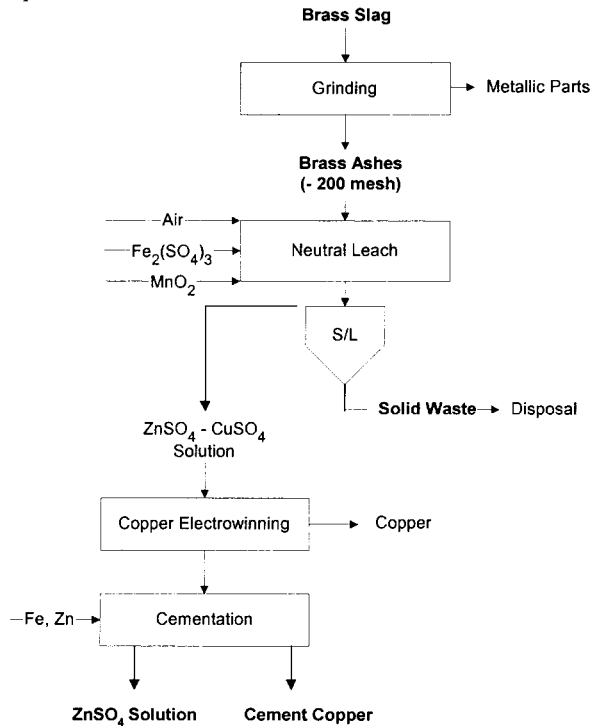


Figure 4: Acidic leaching-process flowsheet for the treatment of brass ashes.

After the acidic leaching of the first step, the solid portion is treated by  $(\text{NH}_4)_2\text{CO}_3 + \text{NH}_4\text{OH}$  leaching, thus dissolving zinc and copper in the form of amine complexes. About 65÷68% of the zinc can be extracted in the form of sulfate, while almost all of the copper that exists in the brass ashes remains in the solid phase. Although it is possible to increase the zinc extraction efficiency at this step, by increasing both the acid concentration and the duration, it would be worthwhile to maintain zinc recovery in this optimum range, in order not to experience any problems in iron precipitation and filtration, and also to restrict copper dissolution. Figure 5 displays some possible routes for the recovery of zinc and copper in the form of salts, after the S/L separation of the “acidic + alkaline” leaching steps.

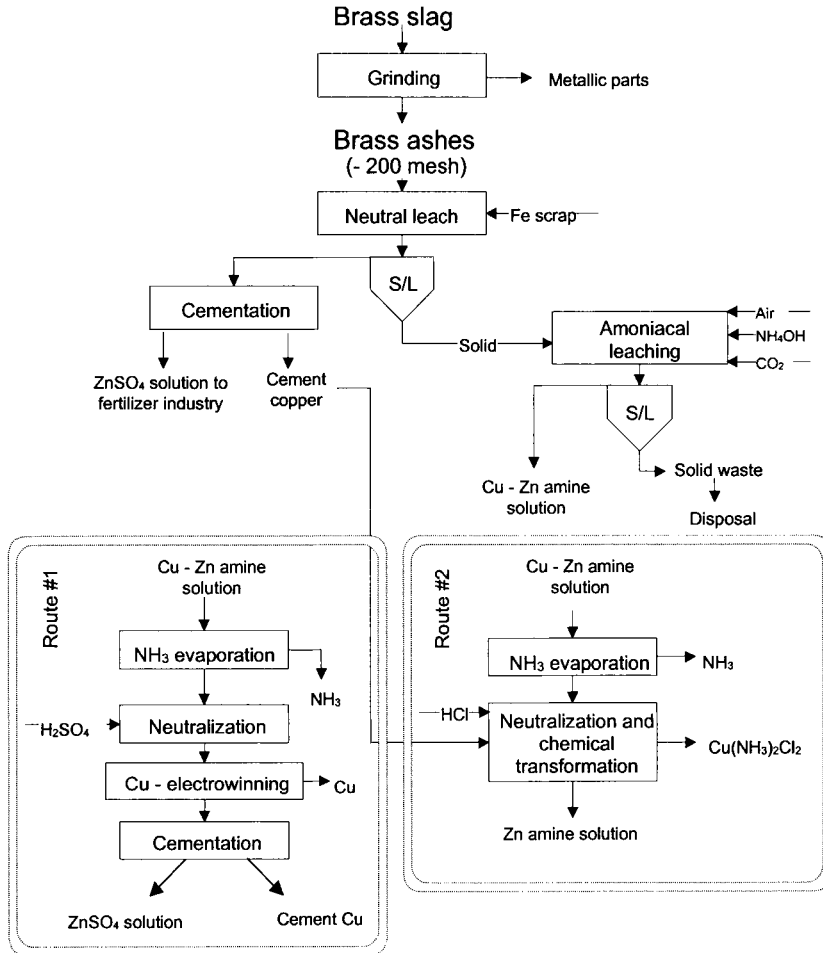


Figure 5: "Acidic + Amine" leaching process flow sheet for the treatment of brass ashes.

Route #1 should be followed if this solution is to be utilized as a raw material in other industrial branches, whereas Route #2 should be chosen if metal production via electrolytic reduction is the aim.

Brass ashes can be economically evaluated by "acidic + amine" leaching. The final extraction efficiencies for copper and zinc are 93÷96% and 90%, respectively. Although longer reaction periods can increase the copper extraction efficiency, it does not prove to be economical. Moreover, especially small-scale companies would have the opportunity to treat their own brass ashes with just very small investment costs.

#### References

Akdag, M., 1986. Extractive Metallurgy. A Publication of 9 Eylül University, Izmir, Türkiye (in Turkish).

- Asare, K.O., 1981. Process and Fundamental Considerations of Selected Hydrometallurgical Systems. AIME, NewYork, 359-369.
- Holleman, A.F. and Wiberg, E., 1995. Lehrbuch der an organischen chemie, 101. Auflage, Walter de Gruyter Verlag, Berlin, 1370-1375.
- Kammel, R., 1986. Nichteisenschwermetalle. In: K. Winnacker and W. Kuchler (Editors), Chemische Technologie, Carl Hanser Verlag, Band 4, 349-388.
- Richardson, J.M., Stevens, L.G. and Kuhn, M.C., 1981. Process and Fundamental Considerations of Selected Hydrometallurgical Systems. AIME, NewYork, 58-59.
- Timur, S. and Duman, I., 1993. Morphology and Sulfuric Acid Leaching of Brass Ashes. 7<sup>th</sup> International Metallurgy and Materials Congress. Ankara, Türkiye, Vol.1, 161-168. (in Turkish)

## THE LIBERATION OF IMPREGNATED GOLD FROM WOOD CHIPS

W. Martin, F.W. Petersen, A.B. Nesbitt

Department of Chemical Engineering, Cape Technikon,  
Cape Town 8000, South Africa

### Abstract

The large quantities of wood chips produced at mines from damaged underground timber contain gold that cannot be completely recovered by cyanidation. A fungus that can degrade a portion of the wood matrix will allow the gold that was previously locked up, to come into contact with the cyanide solution, thereby improving recoveries. The fungus *Phanerochaete Chrysosporium* produces enzymes that use the organic compounds found in lignin as substrate. Consequently, the fungus is able to selectively break down lignin, which is one of the major components of wood.

The average gold grade of chips sampled from Vaal Reefs Mine in South Africa is 2-5 mg/kg. The main sources of gold was identified as discrete gold particles and gold-bearing ore. Only 60% of the gold value were recovered by cyanidation. Comparable weight losses induced by treatment with two different strains designated ME-446 and BKMF-1767 identified the latter as the more aggressive, and this strain was used in all remaining investigations. Transmission electron micrographs show hyphal penetration into cells, removal of the middle lamella between adjacent cells resulting in cell separation and in some instances degradation of entire cells.

*Keywords: wood chips, gold, cyanidation, Phanerochaete Chrysosporium*

### Introduction

Timber is widely used in the mining industry to support underground roofs in connecting tunnels and at the work face. Blasting damages the wood beams, which are consequently replaced, but the splinters or wood chips resulting from the blasts are transported with the ore to the surface where it enters the gold circuit.

Wood chips present problems for reduction plants and especially plants that use the carbon-in-pulp (CIP) process. The most widely adopted method of removing the chips and other trash material is with screens installed at strategic points along the circuit.

The screened chips and logs picked of the belt contain gold and a number of mines stockpile the wood with the aim of recovering the locked-up gold in the future. The gold value originate from ore and discrete gold particles blasted, crushed and milled into the wood fibers and gold adsorbed from the pregnant liquor (Van der Plas, 1998). Unfortunately, direct cyanidation produce an unsatisfactory yield of the gold since the gold-bearing ore and gold particles are locked up inside the wood matrix. Roasting of the chips is carried out on a large scale, but not justified by the large capital outlay and operating costs involved. This study focuses on an environmentally friendly and potentially inexpensive method to biodegrade the chips with a fungal microorganism and cause a collapse of the wood matrix. Degrading the wood matrix will facilitate

greater contact of the encapsulated gold-bearing ore and discrete gold particles with the cyanide solution and yield a higher gold recovery.

### **Background**

The strength properties, natural durability and availability of eucalyptus are the reasons for its use in South African mines. The natural durability of different timber species to the natural process of degradation is dependent on the structure and chemical composition of individual species and eucalyptus is classified as moderately resistant against microbial degradation.

The basidiomycete *Phanerochaete chrysosporium* has attracted interest in the paper and pulping industries because of its ability to selectively remove lignin from wood, which improves paper quality. This task is accomplished by the production of the extracellular enzyme manganese peroxidase and lignin peroxidase under nitrogen limiting conditions. The enzymes reduce the lignin polymer into simpler molecules that are finally mineralized to CO<sub>2</sub> and water. Lignin, together with cellulose and hemicellulose are the major components of wood and typically make up 15% to 35% of the woody mass depending on the species. While cellulose is the material making up microfibrils, the three dimensional lignin polymers are the matrix materials that bind the microfibrils together and make the whole structure rigid. (Preston, 1962; Fengel, 1970; Fengel and Wegener, 1989).

### **Materials and methods**

The approach followed was to divide the research into two parts. The objective of the first part was to gain a better understanding of the value, species and recovery of gold from the refractory chips. The second part focuses on the fungus *P. chrysosporium* and the degradation of wood chips.

#### *Wood chips*

The first part of the research investigating the gold value of the chips was conducted with wood chips taken from the dump at the Vaal Reefs Mine, Klerksdorp. The chips from the mines have a lot of paper, plastics and other trash material with it and was consequently substituted with laboratory prepared chips in the degradation experiments to standardize conditions. All chips were kept in an oven at 80°C to maintain a dry weight and prevent the growth of contaminating microorganisms.

#### *Gold studies*

Adsorption, elution and cyanidation experiments with the wood chips were carried out in batch reactors of height 15 cm, internal diameter 11 cm, and with three evenly spaced baffles of width 1 cm. The chips were kept in suspension by agitating the slurry with a flat blade impeller of width 6 cm and height 5 cm at a stirring speed of 300 rpm. Solution pH was maintained by addition of 1M Ca(OH)<sub>2</sub> as necessary and gold analysis was performed on a Varian GTA coupled to a Varian Techtron AA-1275 atomic adsorption spectrophotometer.

#### *Wood chip preparation and evaluation of degradation*

Eucalyptus logs were debarked and chipped to a nominal size of 5 mm. Virgin eucalyptus chips were kept in an oven at 80 °C to maintain a dry weight and prevent

the growth of contaminating microorganisms. The chips were removed from the oven, allowed to cool in a desiccator and soaked for 24 h in a chemically defined medium proposed by Leatham (1983).

These chips (5 g dry weight per sample) were placed in Erlenmeyer flasks and autoclaved for 15 min at 121 °C. After cooling to room temperature the samples were inoculated with 1 cm<sup>2</sup> plugs from 5 day old plate cultures of *P.chrysosporium* maintained at 39 °C. If not stated otherwise, samples were incubated at 39 °C and 65% moisture and removed after 4 weeks. Humidity was not controlled; instead samples were rehydrated as necessary to the 65% moisture level. The dried out plugs were removed from the samples, the fungal growth rinsed and filtered off and the samples autoclaved. The dry weights of the samples were compared to the initial dry weights to determine weight loss.

## Results and discussion

### Gold value

The mine chips were sieved and analyzed for gold. The average gold value was between 2 mg/kg and 5 mg/kg and the nominal size of the chips ranged from less than 1 mm up to 5 mm. Energy dispersive spectroscopy (EDS) and wavelength dispersive spectroscopy (WDS) show dust consisting of pyrite, silicates and quartz on the chip surface and in wood fibers. An automated gold search of 12 polished samples smaller than 3 mm encountered 4 gold particles with surface areas ranging from 7 μm<sup>2</sup> to 40 μm<sup>2</sup>. The conclusion was that the main sources of gold in the chips are discrete gold particles and gold-bearing ore. Elution yielded only a 17% recovery of the gold. Pregrobbing seems to contribute little to the gold value. Wood chips were stirred in 20 ppm free cyanide in the form of KCN and yielded a 60% recovery prior to treatment with the fungus. The unusual recovery pattern is attributed to particles of activated carbon that are among the wood chips and which adsorb some of the recovered gold from solution (Figure 1).

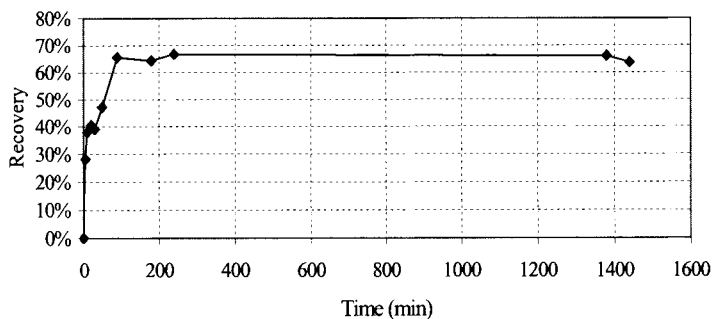


Figure 1: Leaching gold from ore encapsulated in wood chips.

### Fungus screening

Two strains with the designations BKMF-1767 and ME-446 were screened and BKMF-1767 caused 10% greater weight loss of the chips than ME-446 (Figure 2).

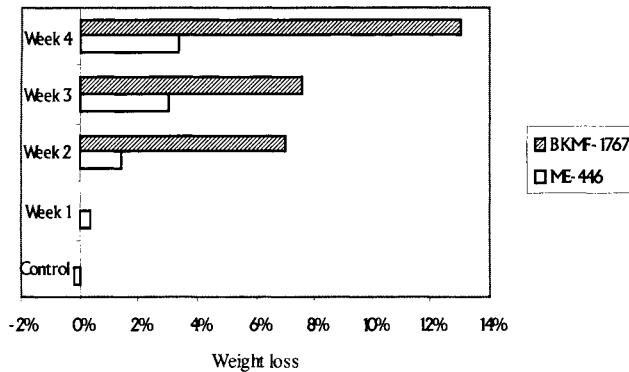


Figure 2: Weight losses caused in virgin eucalyptus chips treated with strains BKMF-1767 and ME-446.

Significant weight losses were only observed from the second week onward, which suggest the fungus remain in primary metabolism throughout the first week and enters secondary metabolism during the second week. The enzymes causing lignin breakdown are produced during secondary metabolism.

#### *Degradation of different size chips*

The effect of different chip sizes on fungal degradation was investigated. The size of the chips had a pronounced effect on the degree of degradation. Highest weight losses of 29% were observed for chips smaller than 1 mm (850  $\mu\text{m}$ ) and lowest (1%) for chips larger than 2 cm. Hyphal penetration is a slow process, which is why the larger exposed surface area of the smaller chips favoured degradation.

#### *Inoculation with different spore numbers*

The number of spores used to inoculate samples had a negligible effect on the degree of degradation. White delignified areas became visible earlier on samples inoculated with higher spore numbers but since the available nutrients are fixed degradation also stop earlier giving the same degree of weight loss over longer periods irrespective of initial spore numbers. However, inoculating with higher spore numbers reduces the risk of other microorganisms growing in samples.

#### *Temperature*

Best results were obtained for samples incubated at 30 °C and 40 °C and no measurable weight losses obtained at 50 °C. The fungus also grew at 20 °C, but its ability to degrade wood was diminished. No weight losses were measured at 10 °C. Contamination was also more commonplace below 20 °C and indicates a reduced ability to compete against foreign fungal microorganisms.

#### *Moisture*

The effect of moisture level on degradation was investigated. The fungus did not grow at 0% moisture, the lowest moisture that could be investigated after addition of the MCDM was 65% (dry basis), and the highest weight losses were obtained at this level. Moisture levels above 65% yielded lower weight losses; growth was observed in samples adjusted to 120% (dry basis) moisture, but weight loss could not be



determined. Fungal growth did not take place in samples adjusted to 150% moisture or higher.

#### *Stationary versus shaken samples*

Samples of chips inoculated with the fungus were vigorously shaken by hand, once every day until all mycelial growth were broken up. Control samples were kept stationary. The difference in extend of degradation between the shaken and stationary samples was small since shaking help distribute the spores, but disrupted mycelial growth that successfully attached to the wood surface.

#### *Microscope studies*

The aim with the microscope studies was to investigate the growth patterns of the fungus and gain a better understanding of the resulting changes caused in the cell material. Micrographs taken of mine chips helped determine the positioning of impregnated ore.

All of the mine chip samples studied under the electron microscopy had foreign material in it. EDMA confirm the foreign material are mostly ore particles and TEM show that in almost all instances the ore are located inside cells (Figure 3), which suggest that any gold dissolved from the ore would need to diffuse through several cell walls before recovery.

Although it was shown that pregrubbing contributed very little to the gold value, some of the gold dissolved from the ore could adsorb onto wood fibers and further contribute to the inefficiency of conventional cyanidation.

Another study show irregular pockets of rot caused on the wood surface by the fungus. Virgin eucalyptus chips has been treated with the fungus for 4 weeks and investigated transverse sections under the microscope. The cells of the control samples remained intact, without any signs of fungal penetration. Sections of samples treated with the fungus showed varying degrees of rot. Hyphal penetration into cells and preferential attack of lignin was observed with separation of adjacent cells after the lignin-rich middle lamella was degraded. Degradation seemed to continue at a distance from the fungal penetration so that it seems physical contact between the hyphal and wood is not essential, but that the enzymes can diffuse over a distance. In the advanced state of degradation whole cells have been removed causing the matrix to break down (Figure 4).



Figure 3: Ore particles inside the wood.

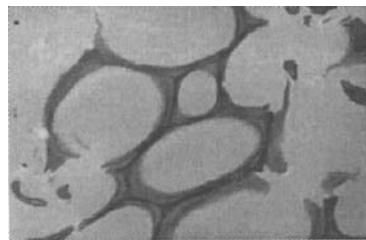


Figure 4: Wood cells in advanced state of degradation showing hyphal penetration in what used to be the cell lumen.

**Conclusions**

Wood chips typically contain between 2 mg/kg and 5 mg/kg gold. The main source of the gold is discrete gold particles and gold-bearing ore. Pregrobbing only contributes 17% of the total gold value, thus the gold grade of the impregnated ore is in the area of 1 to 4 mg/kg. Cyanidation yielded a 60% recovery of the locked-up gold. Of the two strains investigated BKMF-1767 was the more aggressive typically causing a weight loss of 14% in chips with a nominal size of 5 mm. Particle size had a pronounced effect on weight loss, with smaller chips experiencing the greatest losses.

**Acknowledgements**

The financial assistance of the NRF and MINTEK is greatly appreciated.

**References**

- Fengel, D., 1970. Ultrastructural behavior of cell wall polysaccharides. *Tappi*, 53 (3), 497-503.
- Fengel, D. and Wegener, G., 1989. *Wood chemistry, ultrastructure and reactions*. Walter de Gruyter, Berlin.
- Leatham, G.F., 1983. A Chemically defined medium for the fruiting of *Lentinus edodes*. *Mycologia* 75 (5), 905-908.
- Preston, R.D., 1962. *The Physical Biology of Plant Cell Walls*. Chapman and Hall, London.
- Van der Plas, P.J., 1998. The adsorption mechanism of aurocyanide onto wood chips. M.Tech Thesis.

## RECYCLING OF INDUSTRIAL WASTE MATERIALS: RECOVERY OF ALUMINUM FROM LEFTOVER BOTTLE CAP- LINER MATERIALS

S. Sano\*, M. Nikaidoh\*, K. Yanagawa\*, Y. Kanda<sup>o</sup>

\*Department of Chemical Engineering, Ichinoseki National College of Technology  
Takanashi, Hagisho, Ichinoseki. 021-8511, Japan

<sup>o</sup>Department of Material Engineering, Yamagata University 4-3-16, Jyonan,  
Yonezawa, 992-8510, Japan

### Abstract

The inside liners of most bottle caps from drinks are made of aluminum leaf attached by pressure to PE (polyethylene) and PET (polyethylene terephthalate). The punching machine producing the cap liners discharges a large amount of aluminum remains, of which 47.6% is aluminum. So far, these remains have been used in land reclamation as industrial waste. Recently, procurement of reclaimed land has become very difficult, because the movement against environmental destruction is supported by local residents. Moreover, such waste can't be burned, because atmospheric pollution is caused by CO<sub>2</sub>, NO<sub>x</sub> and endocrine disruptors etc. This study has been developed from the point-of-view of effective use of resources and protection of the environment.

Aluminum leaf remains, have been crushed from 10 mm to 20 mm by a primary crusher, and then have been ground to 1 mm by a high-speed hammer mill. Then these aluminum leaf particles have been separated into an aluminum particle group, and a PE and PET particle group by an electrostatic separator. We have learned that recovery of the aluminum particle group is 35.0% of the original material, and the group includes 63.9% aluminum, with a one-time grinding operation. On the other hand, the content ratio of aluminum increases to 71.2% with a three-time grinding operation, and to 75.7% with a five-time grinding operation. The total cost of recycling has not been calculated in detail. This is a considerably effective method, given the low energy cost for refining aluminum. In Japan, it is said that the electric energy cost for refining using recycling materials is about 3% of that when using bauxite as raw material.

*Keywords: industrial waste, aluminum, recycling materials, hammer mill*

### Introduction

In Japan, the recycling of useful components from waste materials becomes a large problem from the viewpoint of air pollution, environmental damage and effective utilization of resources. At present, paper recycling is the most advanced for the solid waste category (Okayama and Nakanami, 1999). This is due to recycling systems that have been established in every self-governing community in Japan (The Japan environment conference, Shuppan, 1994). The recycling of glass bottle waste is being tried next. Concerning glass bottles, bottles of various colors are used. Since there are no regulations concerning colored bottles, an enormous number of bottles of various colors are imported. These colored bottles are not used as glass feedstock, because it is difficult to produce bottles of a certain color with all the recycled bottles of mixed colors (Sano and Nikaidoh, 1999). The only application for these bottles would be as

an aggregate in asphalt or concrete. At present, the utilization as an aggregate is not realized in Japan because of minor regulations concerning strength and composition. The largest amount of discharged waste comes from industry in various forms (Resources and materials, 1997). In this industrial waste, coal ash discharged from thermal power plants, sludge from sewage-treatment plant and construction waste wood, etc. are discharged in large quantities. At present, in Japan, most of this waste is used as landfill. For this reason, the shortage of reclaimed disposal land becomes serious. So the development of reclaimed land has also caused problems of environmental damage. Though small in quantity, many kinds of industrial waste have been otherwise disposed of by reclamation or combustion. Disposal by combustion has caused air pollution with  $\text{NO}_x$  and dioxin, etc. In addition, though it is of small quantity, the industrial waste includes useful metals that can be recycled. If the metal composition and nonmetal components can be separated at low cost, it is thought that such a recycling business could be established.

In Japan, aluminum is imported as a raw material in unrefined states. The energy cost for refining in Japan is highest in the world. It is said that recovered aluminum flake powder uses 3÷10% of the energy costs for refining from bauxite. Also, it is even said that 95% of the water pollution and 97% of the air pollution are reduced. According to this experiment, it is calculated that almost 2 tons of aluminum per day are recovered from several tons of waste materials. There are also underground bauxite resources containing raw aluminum material, which may, in fact, someday be depleted. It is our duty to try to recover as much aluminum as possible, because there are limits to the natural resources. To prolong the life of natural resources, it is absolutely necessary to reduce the amounts of natural resources used in Japan and in all countries. Taking this into consideration, aluminum recycling from leftover bottle cap-liner materials was attempted by using a crusher and an electrostatic separator.

### **Samples and experimental method**

Bottle cap-liner materials consist of 50  $\mu\text{m}$  of aluminum foil held between 20  $\mu\text{m}$  of polyethylene (PE) and 30  $\mu\text{m}$  of polyethylene terephthalate (PET). The aluminum content of this material was almost 47.5%. Finally, under the best conditions, it was possible to recover aluminum flake powder with a grade of 80.5%. Today, cup-noodles, which were invented in Japan, are eaten all over the world, in addition to Southeast Asia. In the manufacturing of cup-noodle containers, the discarding of the leftover materials from the aluminum foil cover sandwiched between PE and PET, is of an enormous quantity in Japan. Recovered aluminum from the leftover materials of the cup-noodle covers was used as a sample. The remaining material has a thickness of 20.7  $\mu\text{m}$ , and it is a three-layered structure with the aluminum sandwiched between PE and PET. The weight ratio of the aluminum layer and the PE. PET layer is 47.5, vs. 52.4. The experiment of aluminum recovery was carried out as in the flow sheet shown in Figure 1. The remaining material of the cover was crushed beforehand to about <math>10\div 15\text{ mm}</math> and then was pulverized by a high-speed hammer mill. The high-speed hammer mill has the structure of six swing hammers, which are rotated at high-speed in a jagged line.

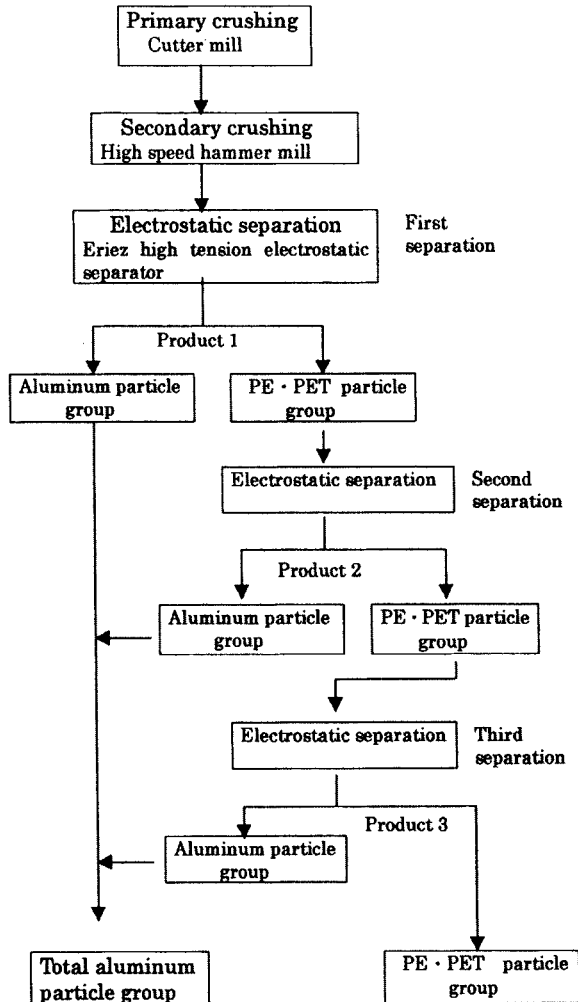


Figure 1: Flow chart of size reduction and electrostatic separation for leftover bottle cap-liner materials.

The motor is 1.5 kW, and the mill shaft is rotated at 9,600 rpm. The rotation diameter of the hammer is 125 mm. Mixed particles of globular aluminum and PE+PET particles, which were made by crushing at 1 mm or less, were almost completely separated from the aluminum particle group and PE+PET group by the electrostatic separator. The PE+PET particle group, which was obtained by electrostatic separation the first time, was separated again 2 more times. We are still running experiments on the cup-noodle covers, and we have not yet obtained enough data. Another separation method was also examined, but since it had a low, 10% aluminum-content rate, the recovery efficiency was not good for this sample. Another method for the cup-noodle covers is shown in Figure 2.

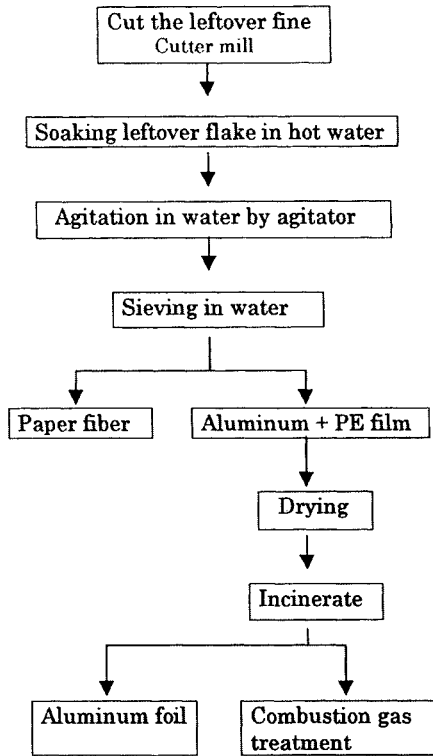


Figure 2: Better method for aluminum recovery from leftover cup-noodle covers.

## Results

The above separation results are shown in Tables I and II. Table I shows the components of each product, which are measured by chemical analysis after separation, and Table II shows the recovery ratio of aluminum from the raw leftover materials. Though two samples were used in this experiment, the results of sample 1 and sample 2 were shown to be almost equal, and the content of aluminum was 80.5% in the first electrostatic separation.

Table I: Components of each product after separation (chemical analysis).

Components	Product 1	Product 2	Product 3	Leftover
Aluminum (%)	80.5	76.5	70.0	42.5
PE + PET (%)	19.5	23.5	30.0	57.5

Table II. Recovery quantities of aluminum from raw leftover materials.

Components	Product 1	Product 2	Product 3	Total
Aluminum recovery (%)	80.5	76.5	70.0	42.5

The results after the second and third electrostatic separations were 76.5% and 70.0% of aluminum content, respectively. By measuring the residual mass, the aluminum content ratio was obtained after the sample was dealt with in nitrohydrochloric acid. In addition, crushing by the high-speed hammer mill, was done 5 times for the preparation of the new sample. These results are shown in Table III:

Table III: Relationships between aluminum content ratio and size-reduction times:one-time separation.

Components	1 time	2 times	5 times
Aluminum (%)	63.1	71.2	75.7
PE + PET (%)	36.9	28.8	24.4

The atmosphere conditions, for electrostatic separation, do not seem to have been good at that time, resulting in a lower aluminum-content ratio (Table I, First separation). However, it was proven that as the crushing frequency increases, so does the aluminum content after separation. With this experiment, it was also learned that the separation operation by the electrostatic separator was greatly affected by the humidity of the atmosphere. It was also learned that we need to be aware of this fact during the actual separation operation. In Table II, the total aluminum recovery quantity for the raw material content is 57.8%. On the other hand, Table III shows an increase for the aluminum content ratio as the crushing frequency increases. Based on this, an increase in the total aluminum quantity can be expected by repeated crushing.

## Discussion

The leftovers of the inside liners contained a large quantity of aluminum metal, so their recycling had an important value. In this experiment, a sample of the leftovers, which was coarsely crushed to <math>10\div 15</math> mm during manufacturing was used. To examine this, it was considered necessary to select the mill construction, in order to obtain better size-reduction efficiency. In short, the adoption of a mill with a powerful peeling mechanism was needed, in addition to the impact of the construction. Since the leftover sample had bonded too strongly with PE and PET, it was difficult to extract only the aluminum.

## Conclusions

At present, aluminum recovery from the leftovers of inside liners disposed has been tried by first by crushing and then by electrostatic separation. The following conclusions have been observed:

- it is possible to recover aluminum from the leftover bottle-cap liners by crushing and electrostatic separation;
- the mill we are using would be better if it generated less heat or if it had a cooling system;
- the high-speed hammer mill used in this experiment hinders the exothermic properties when it is operated continuously; therefore, it is necessary to consider mill construction in order to mill efficiently.
- electrostatic separation is an optimum method for the separation of the particles of this species; over-grinding lowers the electrostatic separation efficiency.

The results of this experiment show that a particle size of about 0.5÷1.0 mm was most efficient. Concerning energy costs, it is the dry-system which separates the aluminum directly, that is more efficient than wet-system.

On aluminum recycling from the cup-noodle covers, 100% recovery was possible by incinerating PE+Al only with regard to Al, after the paper fiber was separated from PE+Al in water.

**References**

- Okayama, T., Nakanami, H., 1999. Preparation of porous materials from wastepaper. Proceedings of Fifth International Symposium on Recycling Technology, Tsukuba, Japan, 143-147.
- Shuppan, J., 1994. The Japan Environment Conference. Consideration of basic law for environmental pollution control. Tokyo.
- Sano, S., Nikaidoh, M., 1999. Effective size reduction of waste glass bottles for manufacturing artificial sand. Proceedings of Fifth International Symposium on Recycling Technology, Tsukuba, Japan, 143-147.
- Resources and material, 1997. Journal of the Mining and Materials Processing Institute of Japan, vol.113, No 12.



## CHARACTERIZATION AND RECYCLING OF AMALGAM FROM DENTAL CLINICS

J.Y. Pereira Leite\*, C. Pereira de Souza<sup>o</sup>

\*Mineral Processing Laboratory, CEFET-RN, Fax  
55 84 2214005, e-mail [jypleite@eol.com.br](mailto:jypleite@eol.com.br)  
Av. Salgado Filho, 1559 CEP 59.056-290 Natal-RN, Brazil

<sup>o</sup>Department of Chemical Engineering, PPGEQ-UFRN, e-mail [carlson@ufrn.br](mailto:carlson@ufrn.br)  
Campus Universitario CEP 59.076-970 Natal-RN, Brazil

### Abstract

Amalgam residue is an environmental problem caused by the odontological practice. Studies of amalgam residues of dental clinics (CEFET-RN) show 27.90% of the total results from manipulation in a consulting room, and there also exists a highly significant amount that is thrown into the spittoon. In Brazil, the law requires these residues to be collected in a selective way, which the great majority of our professionals have been accomplishing. However, sanitary authorities are not familiar with techniques for recycling this material. This work presents an economic and alternative way of obtaining metallic mercury and a silver-alloy with a high grade of silver. The amalgam residues were collected, dried, weighed, put into porcelain recipients and introduced into a retort heated up to 900 °C. The residues of the process were then placed in a furnace where the internal temperature rises to 1,000 °C, melting the elements. This process is economical and easy to develop, and minimizes environmental pollution. The alloys have been characterized with optics and electronic microscopy, Vickers micro-hardness, density, chemical analyses and size distributions.

*Keywords: recovery, dental amalgam, recycle, characterization, raw materials, environment*

### Introduction

Technological development has produced an infinity of products to supply society's avid hunger for consumption. This is associated with a large generation of residues, which are propitiated through phases involving the extraction of related matter and productive manufacturing processes, to the point of the final disposal of the used product. There is a growing increase in the demand for higher levels regarding the destiny of the residues of the production processes and of consumption. This has been contemplated by means of several educational campaigns, with type-ISO 14000 norms for preservation of the environment, and by an increase in scientific recruiting and technological research, with the objective of minimizing degradation of the environment. This work presents the results of the characterization of amalgam residues used in dentistry and of a silver-alloy obtained from the residue. The studies of the residues of human activities and the development of clean technology have been appearing as important themes. Amalgam residue is composed of heavy metals, and in Brazil this has been the object of small studies. The amalgam residues were determined in 27.90% (Leite et al., 1996) of the instruments for condenser amalgam in CEFET-RN dental clinics. Contamination of the air with mercury vapors constitutes an occupational risk to dentistry professionals, resulting from inadequate

manipulation of the amalgam. This increases in an atmosphere that favors the agents' retention (Alves et al., 1999).

## Experimental

### Materials

Samples of amalgam residues were obtained from the dental clinics of CEFET-RN, Natal-RN-Brazil. The particle-size distribution was determined by screen analysis of the amalgam residues, and the results are presented in Figure 1. A high superficial area, as results from size-distribution, will reduce the time of fusion of the residues.

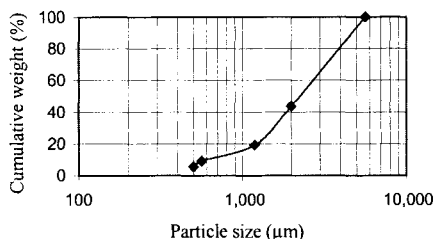


Figure 1: Particle size distribution of the sample of amalgam residues.

### Methods

The investigation has been conducted by using residues amalgam samples taken from Dental Clinic of Federal Center Technological Education - Rio Grande do Norte State (CEFET-RN), Brazil.

The silver-alloy starts to liberate Hg, in the gaseous form on towards the condenser, which transforms the Hg back into its liquid form. The liquid Hg is collected and conditioned in sealing recipients. The system should be set up in a place with a chapel exhaustion. The Hg residues of this separation, which are still in the porcelain recipient, are mixed with fusible elements like borax and sodium carbonate and put into an iron recipient. This mixture is placed in a furnace, and the internal temperature rises 1,000 °C, until the elements melt with attainment of a silver-alloy after solidification.

Figure 2 presents an overall diagram of the entire process for recycling amalgam residues to obtain products with applications in dentistry and other fields. The density of alloys and residues was determined using picnometric, with the results 8.65 g/cm<sup>3</sup> and 11.03 g/cm<sup>3</sup>, respectively.

The results of the silver-alloy indicated the presence of a mixture of others elements in the alloy, such as Cu, Sn and Zn.

Figure 3 presents the preparation process for silver-alloy characterization.

The Min.Proc.Lab.-CEFET/RN, Chem.Eng.-UFRN and Tech.Charact.-USP, were used for the determinations. A microscope, coupled with the hardness test, was used (MPH1000-Carlzeiss). Crowell's solution was prepared according to Voort (Voort, 1984) for the chemical attack of the silver-alloy. The study of SEM-EDS (Stereoscan 440-LEO, Quantimeter 600-LEICA, XLII-LINK-OXFORD) was accomplished in the Laboratory of Tech.Charact.-USP.

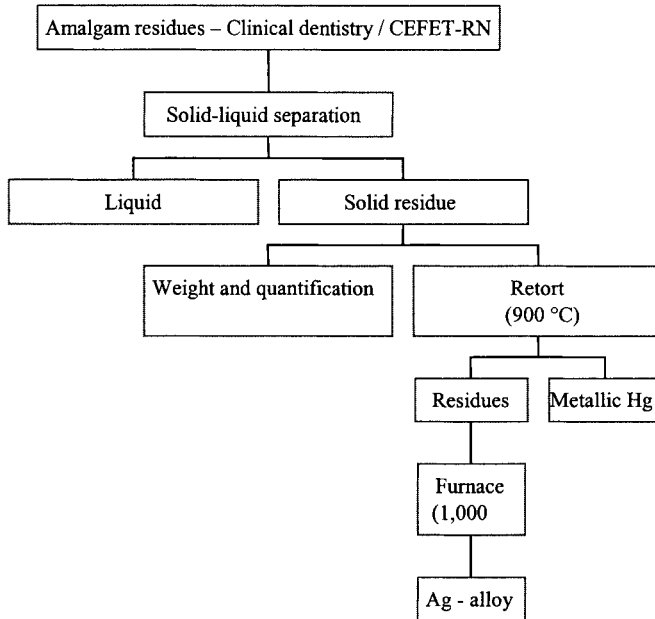


Figure 2: Process for recycling amalgam residues (Leite et al., 1999).

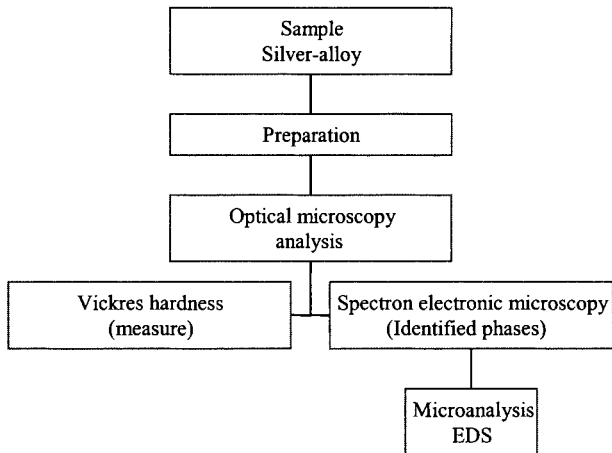


Figure 3: Methods adopted for silver-alloy characterization.

## Results and discussion

In 1998, a questionnaire was applied with a stratified sample ( $n = 140$ ) in the 4 zones of the city of Natal-RN-Brazil. With this data, it was possible to estimate the amounts of mercury and of silver-alloy used by these professionals. They were 6.380 kg Hg and 6.380 kg of silver-alloy per month. These results are quite important, and they

justify studies seeking to minimize the amounts. The studies were realized with scanning electronic microscopy. Figure 4 presents a microphotograph where the four phases present inside a silver-alloy were identified. It can be seen that phase 4 prevails in relation to the other phases regarding the high grad of silver.

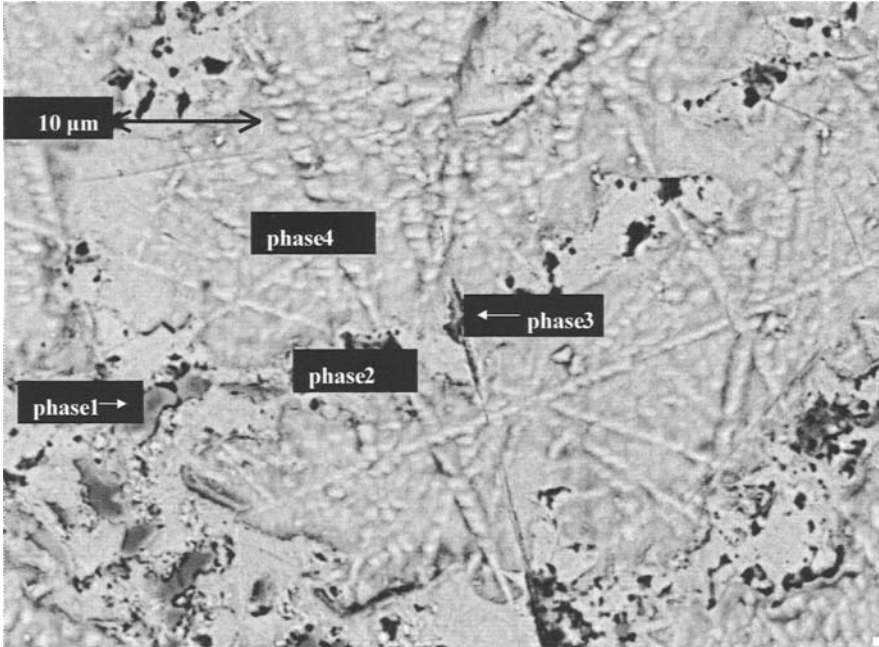


Figure 4: Photomicrograph of silver-alloy obtained from the recycling of amalgam residues.

Table I presents the chemical analysis of four phases realized by EDS. The oxygen present inside silver-alloy can be explained by oxidation of the elements.

Table I: Chemical analysis of the phases present inside silver-alloy.

Phase	O (%)	Cu (%)	Zn (%)	Ag (%)	Sn (%)
Fase 1	1.14	53.31	0.02	5.46	1.14
Fase 2	1.66	3.35	0.15	68.58	1.66
Fase 3	16.98	3.95	0.08	40.29	16.98
Fase 4	1.87	1.14	0.04	82.25	1.87

Figure 5 presents a spectrum of the phase 4, which represents the principal phase of silver-alloy. Studies of optical microscopy realized with the objective of measuring the Vickers hardness (Callister, 1997) of the four main phases, such as phase 4 and the other phases 1, 2 and 3.

The results of Table II showed that phase 4 presents a greater hardness than the other phases, due to the composition and the better dispersion of the components in the phases, 1, 2 and 3. Figure 6 presents the Vickers hardness results for the phases.

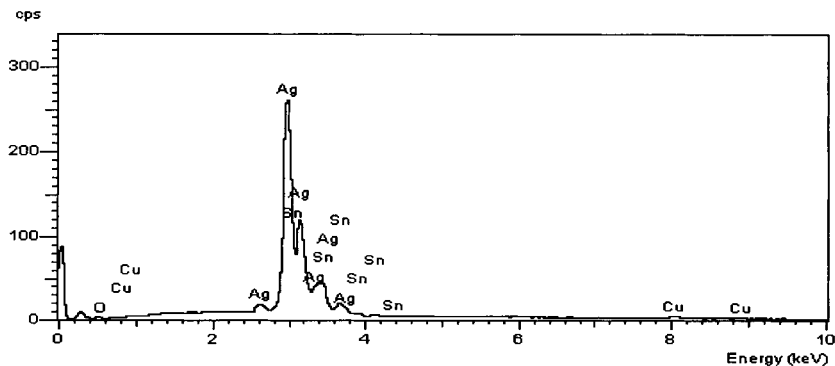


Figure 5: Spectrum of phase 4 - silver-alloy obtained from recycling.

Table II: Measurement results of Vickers hardness for the silver-alloy phases.

Test	Phase 4		Other phases 1, 2 and 3	
	d (mm)	HV <sub>0.05</sub> (kgf/mm <sup>2</sup> )	d (mm)	HV <sub>0.05</sub> (kgf/mm <sup>2</sup> )
1	0.0257	139.8795	0.0332	83.8830
2	0.0264	133.4980	0.0343	78.9929
3	0.0264	133.4980	0.0314	93.9070
4	0.0266	131.4677	0.0349	76.2614
5	0.0257	139.8795	0.0330	84.9154
6	0.0261	135.5758	0.0351	75.3823
7	0.0276	121.9786	0.0359	72.0137
8	0.0272	125.6469	0.0359	72.0137
9	0.0268	129.4833	0.0355	73.6691
10	0.0259	137.7024	0.0361	71.2068
Average	0.0264	132.8610	0.0350	78.2245
Standard Deviation	0.0006	5.9063	0.0015	7.3212
Variation Coefficient (%)		4.44		9.36

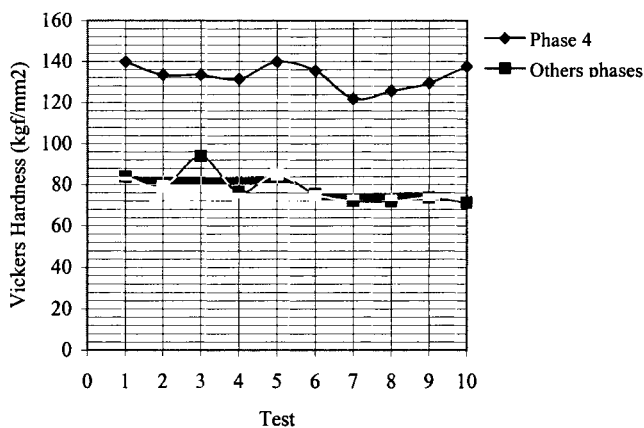


Figure 6: Vickers hardness results of the phases from silver-alloy.

The medium HV results, for silver-alloy in the phase 4 and in the phases 1, 2 and 3, are 132.86 kgf/mm<sup>2</sup> and 78.22 kgf/mm<sup>2</sup>, respectively. In comparison, data of HV<sub>0,1</sub> for the native silver, found in sediments, presented values around 46÷128 kgf/mm<sup>2</sup> (Parfenoff et al., 1970). The silver-alloy obtained has slightly superior average hardness and could be reused in dentistry.

### Conclusions

The present process is applied at Rio Grande do Norte State - Brazil, where the metallic mercury obtained will be reused as dental amalgam, and silver-alloy will be applied in jewels and for researching the best application for this alloy. The HV results for the silver-alloy are compatible with the literature, reinforcing the concept that the recycled material can be reused in dentistry, to develop a non-conventional process that agglutinates a larger value to the material.

### References

- Alves, M.S.C.F., Leite, M.J.V., Leite, J.Y.P. and Medeiros, H.C.S.D., 1999. Analysis of the atmospheres of the private clinics, in relation to the mercurial contamination - Natal/RN. *Journal of Dental Research*, 78(5).
- Callister, W.D. Jr., 1997. *Materials Science and Engineering - An Introduction*. 4<sup>th</sup> Edition, John Wiley & Sons, Inc. New York, 130-137.
- Leite, J.Y.P., Souza, C.P. and Araújo, A.D., 1996. Technological route for the recovery and recycling of amalgam from dental clinics. Porto Alegre: 51<sup>o</sup> Congresso Anual da ABM, IV, 225-233. (in Portuguese)
- Leite, J.Y.P., Souza, C.P., Leite, M.J.V., Alves, M.S.C.F. and Medeiros, H.C.S.D., 1999. Mercury obtaining and silver league from amalgam residues. *Journal of Dental Research* 78(5).
- Parfenoff, A., Pomerol, C. and Tourenq, J., 1970. *Les Mineraux en Grains - Methodes d'Étude et détermination*. Masson et Cia (Editors), Paris, 275-276.
- Voort, G.F.V., 1984. *Metalography Principles and Practice*. McGraw-Hill Book Company, 686.

This Page Intentionally Left Blank

**WASTE TREATMENT AND RECYCLING**  
**(EFFLUENTS TREATMENT)**



This Page Intentionally Left Blank

**New Technique for the Separation of Finely Dispersed Mercury from Philippine Small-Scale Gold Amalgamation Effluent**

L.J.G. Lanticse, E.P. Clemente, H.D. Mendoza

**C12b-1**

**Treatment of Dye Bearing Effluents from Brazilian Agate Industry**

E. Carissimi, T.M. Pizzolato, A. Zoch, C. Mistura, E.L. Machado, I.A.H. Schneider

**C12b-9**

This Page Intentionally Left Blank

## NEW TECHNIQUE FOR THE SEPARATION OF FINELY DISPERSED MERCURY FROM PHILIPPINE SMALL-SCALE GOLD AMALGAMATION EFFLUENT

L.J.G. Lanticse, E.P. Clemente, H.D. Mendoza

Department of Mining, Metallurgy, and Materials Engineering, College of  
Engineering, University of the Philippines, Diliman, Quezon City, Philippines

### Abstract

The removal of finely dispersed mercury from the effluent of small-scale gold mining operations was investigated. The conventional method of amalgamation, or "ball milling", involves the mixing of a substantial amount of mercury with ore to recover free gold during the grinding stage. During grinding, a portion of the mercury is transformed into minute droplets, which readily float and disperse in the effluent. A kilo of gold ore containing 20÷30 g/t, when ground with 3 g of mercury, yields 0.005 to 0.050 mg/l of mercury in the effluent, exceeding the concentration of 0.002 mg/l allowed by law for surface water. A new separation process was introduced utilizing the surface-chemical properties of finely dispersed mercury in aqueous suspension. It was observed that fine droplets of mercury in an aqueous environment readily attached onto a collector having positive surface potentials for pH = 3 to 10. An example of a suitable collector is alumina (Al<sub>2</sub>O<sub>3</sub>) with an iso-electric point of pH = 9.8. This ascertains that mercury possesses negative surface potentials under these conditions. When an effluent, coming from a settling procedure after an amalgamation-grinding stage, is passed through a column-bed packed with alumina fiber, removal and subsequent collection of finely dispersed mercury occurred under acidic conditions, pH = 3÷6. Separation efficiency was around 99.5%, yielding an acceptable quality of water safe for disposal into the aquatic environment.

Presently, there are approximately 100,000 people involved in the small-scale gold operations in the entire Philippine archipelago, using around 26 t/y of mercury. Undoubtedly, the fine mercury droplets that readily float in water are one of the major causes of pollution in rivers and seas. This newly developed technology presents a potential solution to this perennial environmental problem.

*Keywords: mercury dispersion, zeta-potential, collector, attachment, separation, DLVO theory*

### Introduction

The development of a novel technique to achieve solid/liquid separation of finely dispersed particles (<1.0 µm) in aqueous suspension is in line with the growing concern regarding protection of the environment and maximum utilization of valuable resources (Mendoza et al., 1993).

Generally, separation of fine particles from aqueous media becomes difficult when these particles become so small that Brownian movement, rather than gravitational forces, begins to govern their behavior. Moreover, separation becomes difficult when the concentration of fine particles is very low in relation to its bulk media. For these reasons, focus was placed on the distinct surface characteristics of fine particles in an aqueous environment to effect physical separation. Mercury, that is widely used as a collector of free gold in small-scale mining industries, can be transformed into fine droplets during amalgamation and grinding of gold ores. Small-scale gold millers use a conventional method, wherein substantial amounts of metallic mercury are added,

while liberating the free gold from the bulk of waste minerals during the grinding stage. With this practice, which is also commonly referred to as “ball milling”, the mercury in particular is subjected to severe grinding actions, breaking the mercury into minute droplets and forming a dispersion of mercury in the resulting effluent. The presence of these finely dispersed droplets of mercury is one of the root causes of why mercury is easily dispersed and transported through the aquatic environment, leading to the eventual contamination of the surrounding ecology of small-scale gold areas and nearby communities. The concentration of mercury in effluents to surface water allowed by law is 0.002 mg/l (ppm). There are around 6 million small-scale gold miners extensively using mercury in their gold recovery operations in the entire world (Veiga et al., 1997). In the Philippine archipelago alone, there are around 100,000 people directly and indirectly involved in gold small-scale mining operations who are likewise users of mercury. In the southern part of the Philippines, where small-scale mining of gold is widespread, a recent survey showed that around 26 t of mercury was being disposed into one of the major river systems annually (Broad and Cavanagh, 1993).

The objective of this study is thus to develop a solid/liquid separation technology and to introduce a feasible mechanism in order to collect and separate finely dispersed droplets of mercury from aqueous suspension using the concept of heterocoagulation. Recently, Mendoza et al. (1996a) developed a rapid separation process for fine particles of hematite from aqueous suspension using a macroscopic glass bead collector and applying heterocoagulation concept by adapting both the tumbling and column-bed techniques. In this study, alumina fiber is used as a collector for finely dispersed mercury from aqueous suspension using the column-bed method. Alumina,  $\text{Al}_2\text{O}_3$ , possesses a positively charged surface under a wide range of pH conditions in aqueous suspension (Parks, 1964). Sasaki et al. (1994) investigated the increased efficiency of collecting colloidal particles using fibers rather than spherical collectors. To investigate the effective collection of finely dispersed droplets of mercury in aqueous suspension, this study is divided into two parts.

The first part involves the preparation of a well-defined suspension of finely dispersed mercury in aqueous media using ultrasonic irradiation and/or grinding, and the subsequent separation of the mercury from the suspension.

The second part involves the simulation of the actual grinding operation, as practiced on a small-scale in the preparation of a suspension containing minute droplets of mercury and ore, followed by separation of mercury from the suspension. In both cases, the collection of mercury by the heterocoagulation mechanism with an alumina fiber collector is conducted by using the column-bed technique.

## **Experimentation**

### *Materials*

The mercury used was of technical grade. The mercury was washed with soap and rinsed thoroughly with double distilled water before it was used. Alumina fiber is also of technical grade, has a diameter ranging from 40÷80  $\mu\text{m}$ , and is of various lengths, from 2÷4 cm. The alumina fiber was soaked in 1 M  $\text{HNO}_3$  for 6 h to restore the original surface and was later repeatedly washed with double distilled water.

The column-bed used is similar to the one used by Mendoza et al. (1996b). The column is composed of two parts. The upper portion, which is the main column, contains the alumina fiber collector. The lower portion has a stainless steel screen (38  $\mu\text{m}$  aperture) to hold the alumina fibers. These two parts connected by the 'O' ring are clamped together. The effluent or washings are collected in a container, which is open to the atmosphere. A fabricated 10 cm  $\phi \times 30$  cm stainless rod mill containing various sized rods was used to prepare mercury dispersion, with or without ore charge.

## Methods

### Zeta-potential measurements ( $\zeta$ )

Electrophoretic velocities of mercury and alumina particles in aqueous suspension were measured using a Ranks Brother Mark II microelectrophoresis apparatus with a flat, rectangular, quartz cell. Mercury dispersions were prepared by ultrasonic irradiation. A cleaned alumina fiber was crushed and re-suspended in distilled water. The alumina suspension was allowed to settle for 30 min, and the resulting supernatant solution was assumed to contain fine alumina particles suitable for electrophoretic measurements. The supporting electrolyte for all potential measurements was 0.001 M NaCl.

### Dispersion of mercury

Mercury was reduced to very fine droplets by grinding action. The tumbling and shearing action of grinding media breaks the physical bonds of mercury, reducing it to very fine droplets or particles. To investigate the production of fine droplets of mercury, which readily float in water, two procedures were conducted. The first procedure investigates the effect of varying the amount of mercury in the initial feed before grinding, while maintaining other grinding conditions constant. The second procedure investigates the effect of varying the grinding time with a constant amount of mercury in the feed, and likewise maintaining other grinding conditions constant. The grinding effluents derived from both procedures were made to stand for various time intervals in 1000 ml graduated cylinders, in order to settle the mercury droplets influenced readily by gravitational forces. The remaining suspensions for each settling time interval were measured for mercury concentration and mercury droplet size distribution. A material balance of mercury was conducted to account for the probable concentration and size of mercury that readily floats in water. Size distribution of mercury in the resulting dispersions was determined by directly measuring printouts of fine droplets of mercury, which were collected using 0.45  $\mu\text{m}$  membrane filters and taken using the Lieca Surface Morphology Microscope.

### Heterocoagulation (separation stage)

The effluent loaded with finely dispersed mercury from the dispersion procedure was made to pass through a column-bed packed with 3 cm of alumina fiber. The effluent, as a result of 3 h grinding of the ore and 3 g of mercury, was used in heterocoagulation tests. Different pH conditions of mercury suspension were poured into a preconditioned (at the same pH condition) packed bed of alumina fiber. The effluents produced were separately collected and determined for the concentration of mercury in the resulting suspension. Material balance calculations determine the collection efficiency of the alumina fiber as a mercury collector. The concentration of

mercury in the head dispersion, effluents and settling products were determined by chemical analysis using an Atomic Absorption Spectrophotometer (AAS).

## Results and discussion

### Zeta-potential measurements ( $\zeta$ )

The  $\zeta$ -potentials of mercury and alumina fiber, as a function of pH, are shown in Figure 1.

The  $\zeta$ -potentials of mercury are generally negative throughout the pH range considered, without a clear indication of its iso-electric point (i.e.p.). Alumina fibers have their i.e.p. at around pH = 9.8.

The potentials of alumina particles measured by other investigations (Hunter, 1981) agree with the above-measured  $\zeta$ -potential values.

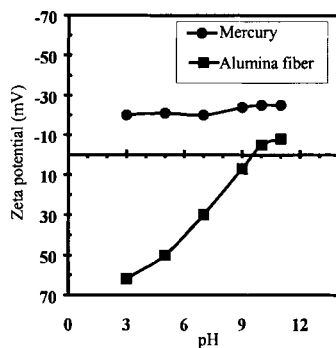


Figure 1: Zeta( $\zeta$ )- Potential measurements for mercury and alumina fiber as a function of pH. Electrolyte concentration of  $1 \cdot 10^{-3} \text{ mol dm}^{-3} \text{ NaCl}$  at  $25^\circ \text{C}$ .

### Dispersion of mercury

Changes in the concentration of mercury in the supernatant solution for various settling-time intervals, considering the grinding of different amounts of starting mercury in the charge, are shown in Figure 2.

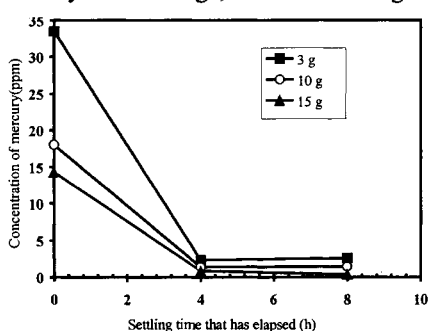


Figure 2: The change on the initial mercury concentration as a function of settling time that has elapsed in the resulting grinding effluent.

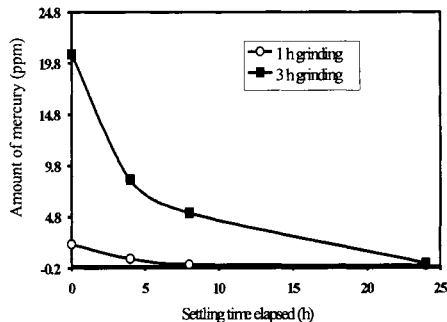


Figure 3: Effect of grinding time in the production of finely dispersed mercury as a function of settling time elapsed. starting amount of mercury is 3 g.

A larger amount of starting mercury produced lesser amounts of finely dispersed mercury droplets. This may be attributed to the presence of more available mercury for coalescence. Figure 3 shows the effect of grinding time in the production of finely dispersed mercury. Extending the time of grinding exposes the mercury to prolonged shearing and tumbling forces, thus reducing more mercury to minute droplets that readily float in water.

The size distribution of finely dispersed mercury that readily floats in water, after allowing some time for dispersed mercury to settle, is shown in Figure 4. Droplets of mercury with a size of less than 14  $\mu\text{m}$  readily float in the effluent.

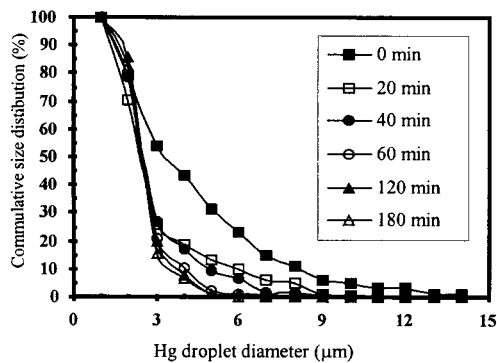


Figure 4: The size distribution of finely dispersed mercury measured at different settling-time intervals.

#### *Heterocoagulation*

The stability of finely dispersed mercury droplets in an aqueous suspension was investigated. The fraction of mercury attached to alumina fiber as a function of pH is shown in Figure 5. There was almost complete deposition of mercury droplets on the alumina fiber under acidic conditions, pH = 3 to pH = 6.

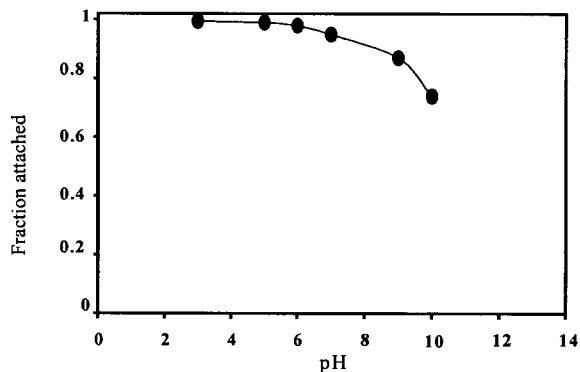


Figure 5: The fraction of mercury attached onto the alumina fiber as a function of pH. Volume of suspension is 100  $\text{cm}^3$ , containing an initial concentration of mercury ranging from 0.005 ppm to 0.050 ppm. Flow-rate is 2  $\text{cm}^3\text{min}^{-1}$ . Electrolyte concentration of  $10^{-3}$  NaCl at 25  $^\circ\text{C}$ .



In the effluent, under acidic conditions, the resulting concentration of mercury is 0.001 mg/l (ppm). This is already an acceptable concentration of effluent under international standards for effluents disposed into surface waters. The recovery of mercury is around 99.5%. This may be attributed to the fact that mercury carries negative potentials, while alumina fiber is strongly positive under these conditions. However, under pH conditions above natural pH, there was still a predominant attachment of mercury onto the alumina fibers, but this time with less recovery, reaching up to 90%. Under a pH = 10 condition, where both mercury and alumina fibers carry negative potentials, recovery decreased to around 70%. Figure 6 shows a picture of the attachment behavior of finely dispersed mercury onto alumina fibers as a collector under acidic conditions pH = 3.

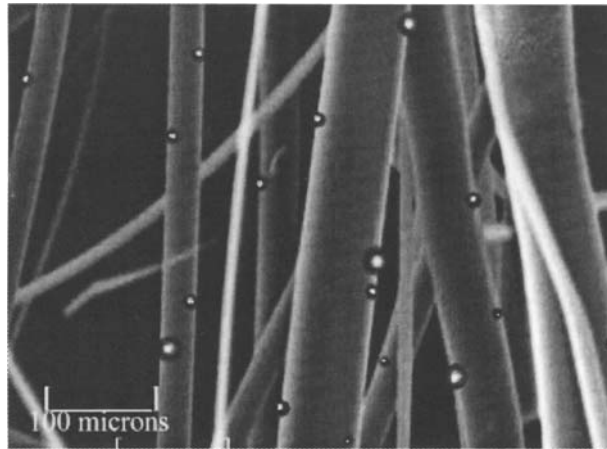


Figure 6: Attachment behavior of mercury droplets onto alumina fiber.

The total potential energy of interaction between a sphere and a plane, which is a simulation of the interaction of mercury (as a sphere) and alumina fibers (as a plane) is given by Hogg et al., (1965) by equating the radius of alumina fiber with infinity:

$$V_t = +\frac{\epsilon a}{4} \left[ (\psi_1 + \psi_2)^2 \ln(1 + \exp(-\kappa H_0)) + (\psi_1 - \psi_2)^2 \ln(1 - \exp\{-\kappa H_0\}) \right] - \frac{A_{132} a^3}{6H_0} \quad (1)$$

where  $a$  is the radius of mercury, and  $\psi_1$  and  $\psi_2$  are the surface potentials of mercury and alumina fiber, respectively;  $\epsilon$  is the dielectric constant of the medium;  $A_{132}$  is the Hamaker constant between mercury (designated as 1) and alumina fiber (designated as 2) in water (designated as 3);  $\kappa$  is the Debye parameter; and  $H_0$  is the surface-to-surface separation. The values of  $\psi_1$  and  $\psi_2$  were assumed to be equal to the  $\zeta$ -potentials.  $A_{132}$  is given as:

$$A_{132} = (A_{131} A_{232})^{1/2} \quad (2)$$

where  $A_{131}$  and  $A_{232}$  refer to the Hamaker constants between identical materials in water, i.e. mercury-water-mercury and alumina-water-alumina, respectively. Usui and Yamasaki (1968) used the Hamaker constant for mercury in water as  $1.3 \cdot 10^{-13}$  erg.

The Hamaker constant for alumina in water is  $4.17 \cdot 10^{-14}$  erg, as proposed by Visser (1972). Using equation 2, the  $A_{132}$  is equal to  $7.36 \cdot 10^{-13}$  erg.

The total potential energy curves for mercury-alumina interaction are calculated as shown in Figure 7. The strong attraction of mercury onto the alumina fibers, as the collector at  $\text{pH} = 3 \div 7$ , is exhibited by the very negative behavior of the energy curves. This explains the high recovery experienced under these pH conditions. It is possible because under these acidic conditions, mercury carries negative surface potentials, while alumina carries positive surface potentials. However, even under conditions where both mercury and alumina exhibit the same negative potentials, a pH above the i.e.p. of alumina, the predominant force, is still that of attraction.

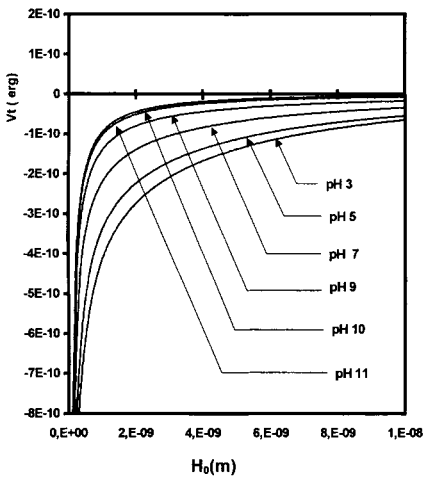


Figure 7: Total potential energy curves for mercury-alumina fiber interaction under different pH conditions, as a function of separation distance,  $H_0$ .  $A_{132} = 7.36 \cdot 10^{-13}$  erg.

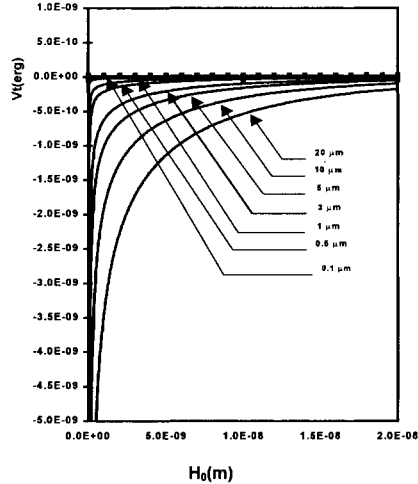


Figure 8: Total potential energy curves for mercury-alumina fiber interaction, at different sizes of mercury droplets at  $\text{pH} = 10$ , as a function of separation distance,  $H_0$ .  $A_{132} = 7.36 \cdot 10^{-13}$  erg.

The mercury that was too small probably initially attached onto the alumina surface, and this might have been detached due to the absence of an energy barrier and to the physical effect of the effluent flow of the suspension through the column. Figure 8 shows the effect of the size of mercury droplets at  $\text{pH} = 10$ , with the total potential energy curves for mercury and alumina interaction.

**Conclusions**

In this study, the following significant conclusions can be deduced:

- mercury carries negative surface potentials under both acidic and alkaline conditions;
- alumina fiber, which carries positive surface potentials under a wide range of pH conditions, can be an effective collector for mercury in aqueous suspensions;
- maximum separation of finely dispersed mercury was observed to occur under conditions when the collector is strongly positive, i.e.  $\text{pH} = 3 \div 6$ ;

- the advantage of using a macroscopic collector like alumina fiber is that a wider range of size distribution for mercury droplets can be effectively collected;
- a decrease in the separation of mercury from the bulk aqueous media was observed to occur under conditions where the potentials for both mercury and alumina collector are the same.

When transformed into minute droplets, mercury easily floats in water and forms a stable dispersion. This warrants some environmental concerns, because at this form, mercury is easily transported into the aquatic environment and will eventually contaminate the surrounding ecology.

The newly developed separation mechanism in this study presents a potential solution that can readily be put into practice to solve the perennial mercury contamination of both marine and soil environments. Though this investigation deals only with the separation of mercury from aqueous media, a substantial area of contamination of mercury can be mitigated.

#### **Acknowledgments**

This report has been made possible through the funding and technical support of the Office of the Research Coordination (ORC), University of the Philippines, Diliman, Grant 09795 NS.

#### **References**

- Broad, R. and Cavanagh, J., 1993. *The Struggle for the Environment in the Philippines, Plundering Paradise*. Anvil Publishing, Inc., Philippines.
- Hogg, R., Healy, T.W. and Fuerstenau, D.W., 1965. Mutual coagulation of colloidal dispersion. *Trans. Faraday Soc.*, 62, 1638-1651.
- Hunter, R.J., 1981. *Zeta-Potential in Colloid Science—Principles and Applications*. Academic Press Inc., London.
- Mendoza, H.D., Sasaki, H. and Sugimoto, T., 1993. New technique for the solid/solid separation of ultrafine particles in aqueous suspension. *First Proc. of the International Conference of Processing Materials for Properties, Hawaii*, 513-516.
- Mendoza, H.D., Sasaki, H., Matsuoka, I. and Sugimoto, T., 1996-a. Rapid separation of fine particles from dilute suspension. *J. Dispersion Science and Technology*, 17(7), 735-765.
- Mendoza, H.D., Sasaki, H., Matsuoka, I. and Sugimoto, T., 1996-b. Selective detachment of silica from co-attached silica and hematite particles on glass beads. *J. Dispersion Science and Technology*, 17(7), 766-791.
- Parks, G.A., 1964. The iso-electric points of solid oxides, solid hydroxides, and aqueous hydroxo complex systems. *Stanford University*, 177-197.
- Sasaki, H., Ibanez, J.P. and Murakami, M., 1994. Utilization of slag fiber as ecomaterial. *Second International Conference on Materials Engineering for Resources, Akita City, Akita Prefecture, Japan*, 35-36.
- Usui, S. and Yamasaki, T., 1968. Adhesion of mercury and glass in aqueous solution. *Journal of Colloid Interface Science*, 29(4), 629-638.
- Veiga, M.M. and Beinhof, C., 1997. UNECA centers: A way to reduce mercury emissions from artisanal gold mining and provide badly needed training. *Industry and Environment (UNEP)*, 20(4), 49-51.
- Visser, J., 1972. On Hamaker constant: a comparison between amaker constant and Lifshitz-Van Der Waals constants. *Adv. In Colloid and Interface Science*, 3, 331-363.

## TREATMENT OF DYE BEARING EFFLUENTS FROM BRAZILIAN AGATE INDUSTRY

E. Carissimi, T.M. Pizzolato, A. Zoch, C. Mistura, E.L. Machado, I.A.H. Schneider

Universidade de Passo Fundo, Faculdade de Engenharia e Arquitetura,  
CEP: 99001-970, Passo Fundo, RS, Brazil

### Abstract

The most common organic dyes used to color agates in the Brazilian industries are Rhodamine B, Crystal Violet, and Brilliant Green. Washing procedures carried out after the staining process release some amounts of these compounds given an undesirable color to the water. The aim of this work is to report the characteristics of the wastewaters and describe the treatment procedures used by the industries. In addition, studies of photodegradation and chemical oxidation for each one of the colorants were conducted at laboratory scale. The results showed that Rhodamine B is more resistant to photodegradation and chlorine oxidation than Crystal Violet and Brilliant Green. The environmental implications of the treatment procedure carried out by the industries are discussed.

*Keywords: agate, chemical oxidation, wastewater treatment, dye*

### Introduction

The agate from Brazil occurs in rich deposits that can be easily and cheaply worked. The most important kind of agate found proved to be the type called "Massik", an evenly grayish colored agate that occurs in huge nodules (Frazier and Frazier, 1988). It is especially suited for staining various colors, including red, blue, green, brown, and black by classical inorganic procedures (Knecht, 1957).

The use of organic dyes increased in the last few years, mainly because of their low cost and the diversity of colors that can be obtained. Commercial dyes have been extensively used, producing wastewaters with an undesirable color. The volumes produced can reach  $10 \text{ m}^3 \text{ day}^{-1}$  in medium and large size staining industries which do not have completely adapted the old treatment plants to this new reality.

The discharge of these high-colored wastewaters to nearby streams are of environmental concern. The colorants and their intermediates can be carcinogenic and to a lesser extent can cause sensitization and allergies (Zollinger, 1987). In addition, high colored waters hinder sun light penetration, decreasing the photosynthetic activities in the aqueous environment.

This work reports the general characteristics of such wastewaters and the treatment procedures commonly used by the local industries. In addition, the individual behavior of the dyes in the presence of the sunlight and sodium hypochlorite is reported. The environmental implications of the treatment procedure carried out by the industries are discussed.

### Effluent characteristics

The most common organic dyes found in the Brazilian agate industries are Rhodamine B, Crystal Violet, and Brilliant Green. The chemical structure, color

index and major absorbency wavelength in the visible spectra for each one of these compounds are depicted in Figure 1.

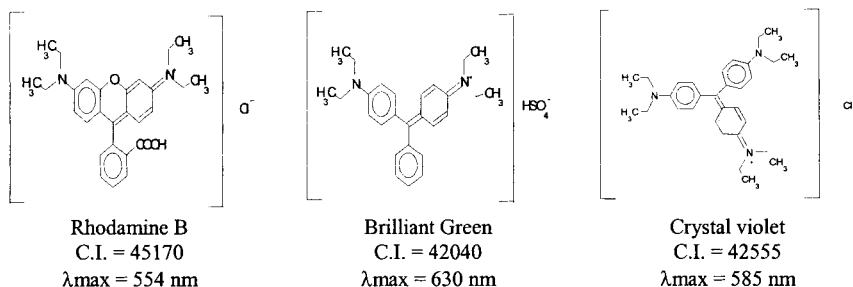


Figure 1: Dyes used in the Brazilian agate industry to give an artificial color to the stones.

The processes of agate staining with organic dyes are carried out in plastic containers, where the stones are placed in a dye alcohol solution (approximately 20 g of dye per 1 liter of ethyl alcohol). After a period of three days the stones are removed from the dye alcohol solution and washed in water. This water, containing residual amounts of dyes and a high color, is the effluent under study. The effluent characteristics are the following: pH = 2.5÷5.6, suspended solids less than 0.1 mg/l, and the concentration of dyes varying from 10 mg/l to 500 mg/l. The visible spectrum of a sample collected in an agate plant containing a mixture of the three dyes is shown in Figure 2.

### Effluent treatment

Decolorization of water streams is possible with one or more of the following methods: adsorption, precipitation, chemical degradation, photodegradation, and biodegradation. A complete mineralization to  $\text{CO}_2$ ,  $\text{H}_2\text{O}$ ,  $\text{NO}_3^-$ ,  $\text{SO}_4^{2-}$ ,  $\text{Cl}^-$ , etc, is the ideal goal (Zollinger, 1987). The effluent treatment procedure preferred by the local industries is chemical oxidation. This method is of simple operation and avoids the solid residues management. Sodium hypochlorite is the most common oxidant used, mainly by economic reasons.

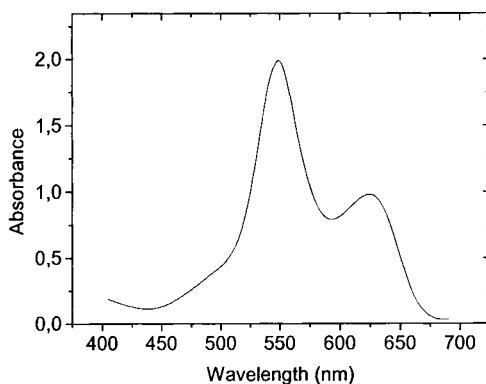


Figure 2: Visible spectrum of an agate effluent.

Other oxidants, like activated hydrogen peroxide ( $\text{Fe}^{+2}/\text{H}_2\text{O}_2$ ,  $\text{UV}/\text{H}_2\text{O}_2$ ) and ozone, can be used (Huang et al., 1993; Masten and Davis, 1994; Bauer and Fallmann, 1997), but are more expensive. The treatment process is carried out in batch systems as outlined in Figure 3. The sodium hypochlorite dose used to decolorize the effluent is in the order of 80 mg/l. The addition of NaOCl promotes an increase in the pH (frequently pH values over 10.0) and a final pH adjustment has to be done to reach neutrality. Most of the time the gravity settling unit is not necessary, but sometimes is very useful when settleable solids are present in the wastewater.

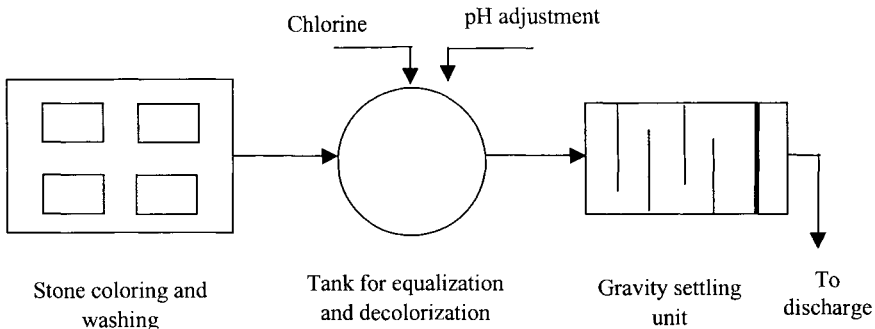


Figure 3: Lay-out of a wastewater treatment plant.

### Individual behavior of the dyes to photodegradation and NaOCl degradation

Photochemical degradation in aqueous solutions, which may occur in lakes and rivers, is likely to progress very slowly since synthetic dyes are in principle designed to possess a high stability to light. However, some dyes have more stability than others.

Figure 4 shows the absorbency as a function of time of the dyes solutions placed in glass bottles and exposed to sun light for a period of two months. It is possible to see that Crystal Violet and Brilliant Green decolorize in a period of two weeks.

The Rhodamine B presents a lower susceptibility to photodegradation than the two other dyes studied.

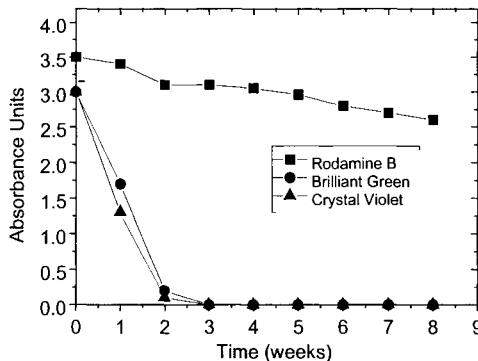


Figure 4: Photodegradation of the dyes as function of time.

This results showed that photodegradation can be a low cost alternative to degrade the dyes Crystal Violet and Brilliant Green. The process kinetics can be enhanced using catalysers (i.e. ZnO, TiO<sub>2</sub>, Fe<sub>2</sub>O<sub>3</sub>). However, the process lay-out shown in Figure 3 should be changed, since the process needs a high exposure of the liquid to the sun light (Legrini et al., 1993; Malato et al., 1996). Figure 5 shows the results obtained using NaOCl to degrade 20 mg/l solutions of the dyes Crystal Violet, Brilliant Green, and Rhodamine B. The experimentation was conducted at pH = 7.0 and pH = 10.0 with different dosages of NaOCl. Crystal Violet and Brilliant Green solutions were decolorized few seconds after the addition of 10 mg/l of NaOCl, in both pH values. However, at the same dosage of NaOCl, or even higher, degradation of Rhodamine B is not possible to occur at pH = 10.0.

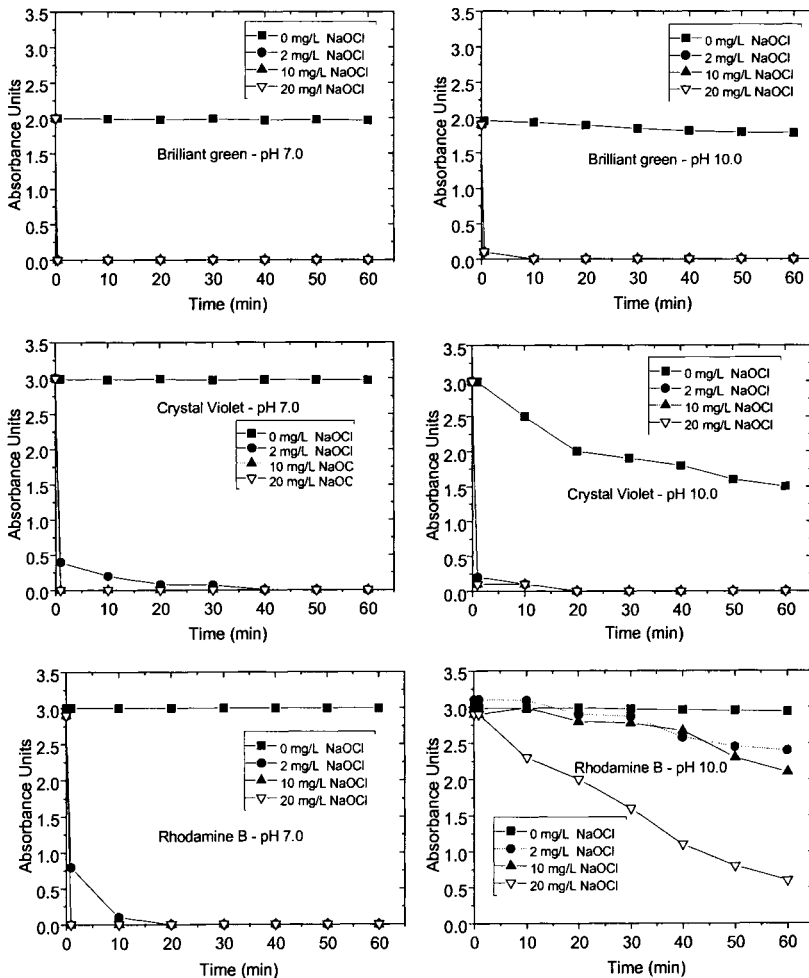


Figure 5: Degradation of the dyes as a function of time at different pH values and NaOCl concentration.

The color removal is more effective at pH values below 7.0, since the HOCl has an oxidation potential of 1.34 V and OCl<sup>-</sup> has an oxidation potential of 1.15 V (Metcalf and Eddy, 1991). The chlorine decolorizing procedure is questioned, mainly because of the misunderstanding of the reactions which can produce toxic compounds (chlorinated hydrocarbons). Chromatographic (GC-ECD and GC-MS) studies being conducted to characterize the byproducts from chlorine degradation demonstrates that, for Rhodamine B, chlorinated compounds are not formed in the process conditions used by the industries. It should be considered that advanced oxidation processes (H<sub>2</sub>O<sub>2</sub>/UV, UV/TiO<sub>2</sub>, O<sub>3</sub>/UV, Fe<sup>+2</sup>/H<sub>2</sub>O<sub>2</sub>), which generate hydroxyl radical (HO<sup>•</sup>) with extremely strong oxidizing power, and chlorine dioxide (ClO<sub>2</sub>) have been considered by many authors as chemical oxidants for organics pollutants degradation without the risks of chlorinated hydrocarbons generation (Liao et al., 1999; Kuo, 1999; Rosemblatt, 1975).

### Conclusions

The effluents originated from staining processes in the Brazilian agate industries contain residual amounts of the dyes Rhodamine B, Crystal Violet and Brilliant Green. The treatment procedure preferred by the industries is chemical degradation using sodium hypochlorite. This method is of easy operation, cheap, and avoids the solid residues management. Rhodamine B is more resistant to photodegradation and sodium hypochlorite oxidation than Crystal Violet and Brilliant Green.

### Acknowledgments

The authors wish to acknowledge the financial support provided by FAPERGS (process 97/1756.2).

### References

- Bauer, R. and Fallmann, H., 1997. The photo-Fenton oxidation – a cheap and efficient wastewater treatment method. *Res. Chem. Intermed.*, 23, 341-354.
- Frazier, S. and Frazier, A., 1988. The Steinkaulengerg in Idar-Oberstein. *Lapidary Journal*, 10, 23-35.
- Huang, C.P., Dong, C. and Tang, Z., 1993. Advanced chemical oxidation: its present and potential future in hazardous waste treatment, 13, 361-377.
- Knecht, T., 1957. Coloração artificial de ágatas. *Ass. Bras. de Gemologia*, 7, 1-9.
- Kuo, W.S., 1999. Effects of photolytic ozonation on biodegradability and toxicity of industrial wastewater. *J. Environ. Sci. Health*, A34(4), 919-933.
- Legrini, O., Oliveros, E. and Braun, A.M., 1993. Photochemical processes for water treatment. *Chem. Rev.*, 93, 671-698.
- Liao, C.H., Kang, S.F. and Hung, H.P., 1999. Simultaneous removal of COD and color from dye manufacturing process wastewater using Photo-Fenton oxidation process. *J. Environ. Sci. Health*, A34(4), 989-1012.
- Malato, S., Richter, C., Galvez, J.B. and Vincent, M., 1996. Photocatalytic degradation of industrial residual waters. *Sol. Energy*, 56, 401-410.
- Masten, S.J. and Davis, S.H.R., 1994. The use of ozonation to degrade organic contaminants in wastewaters. *Environ. Sci. Technol.*, 28, 180-185.
- Metcalf, L. and Eddy, H.E., 1991. *Wastewater engineering*. MacGraw Hill, New York.
- Rosemblatt, D.H., 1975. Chlorine and oxychlorine species reactivity with organic substances. In: *Disinfection Water and Wastewater*, J.D. Johnson (Editor), Chap 13, Ann Arbor Science, Ann Arbor, USA.
- Zollinger, H., 1987. *Color chemistry*. VHC, Weinheim.



This Page Intentionally Left Blank

## **SOIL REMEDIATION**

This Page Intentionally Left Blank

**Microbial in Situ Treatment of Soils Contaminated with Radionuclides**  
S.N. Groudev, P.S. Georgiev, I.I. Spasova

**C13-1**

**Humic Acids from Coal as a Reagent to Soil Remediation**  
E.G. Gorlov., V.V. Rodae, O.G. Ryzhkov, D.M. Koledin

**C13-7**

This Page Intentionally Left Blank

## MICROBIAL IN SITU TREATMENT OF SOILS CONTAMINATED WITH RADIONUCLIDES

S.N. Groudev, P.S. Georgiev, I.I. Spasova

Department of Engineering Geocology, University of Mining and Geology,  
Sofia 1100, Bulgaria

### Abstract

Two experimental plots of agricultural land contaminated with radioactive elements (uranium, radium, thorium) and toxic heavy metals (copper, cadmium, lead) were treated by two different biotechnological in situ methods. The soil in this land was characterized by a positive net neutralization potential, and the soil pH was in the slightly alkaline pH range (from 7.5 to 8.5). The contaminants were located mainly in the upper soil layers (mainly in horizon A).

Both methods were connected with the initial solubilization of the contaminants. Leach solutions containing dissolved organic compounds and carbonate ions were used to irrigate the plots. The solubilization was mainly a result of the activity of indigenous soil microflora. This activity was enhanced by suitable changes at the level of some essential environmental factors, such as water, oxygen and nutrient content of the soil. The first method was then connected with removal of the dissolved contaminants from the soil through the soil effluents. The second method was based on the transfer of the contaminants into the deeply located soil horizon B<sub>2</sub>, where they were immobilized, mainly as a result of the activity of the indigenous sulfate-reducing bacteria. This activity was enhanced by injecting water solutions of organic compounds into horizon B<sub>2</sub> through boreholes located in the relevant experimental plot.

*Keywords: uranium, toxic heavy metals, soil microflora, microbial, sulfate reduction*

### Introduction

Some agricultural lands located in the Vromos Bay area, near the Black Sea coast, Southeastern Bulgaria, have been contaminated with radioactive elements (uranium, radium, thorium) and toxic heavy metals (mainly copper, cadmium and lead), as a result of mining and mineral processing of polymetallic ores carried out in the area for a long period of time. Laboratory experiments carried out with soil samples from these lands revealed that an efficient remediation of the soil was achieved by means of two different biotechnological in situ methods (Groudev et al., 1996). Both methods were connected with the solubilization of the contaminants (located mainly in the upper soil layers), as a result of the activity of the indigenous soil microflora. This activity was enhanced by suitable changes in the levels of some essential environmental factors, such as water, oxygen and nutrient content of the soil. The first method was then connected with the flushing of the soil, by means of leach solutions containing carbonate ions and dissolved organic compounds. The pregnant soil effluents containing the dissolved contaminants were then treated by a passive system of the anoxic-cell type. The barren waters from the anoxic cells were recycled to the soil. The second method was connected with the transfer of the dissolved contaminants to the deeply located soil horizon B<sub>2</sub>, where the contaminants were

immobilized, as a result of the activity of the indigenous sulfate-reducing bacteria inhabiting this anoxic soil horizon. The activity of these bacteria was enhanced by injecting water solutions of organic compounds into horizon B<sub>2</sub>. In 1998, the above-mentioned methods were applied under real field conditions in two experimental plots located in the Vromos Bay area. Some data about this study are shown in this paper.

### **Materials and methods**

A detailed sampling procedure was carried out to characterize the soil and the subsurface geologic and hydrogeologic conditions of the site. Surface and bulk soil samples up to a depth of 2 m were collected by a mechanical excavator. Drill-hole samples were collected up to a depth of 10 m. Elemental assays in the samples were performed by digestion and measurement of the ion concentration in solution by atomic absorption spectrophotometer and induced coupled plasma spectrophotometer. Mineralogical analysis was carried out by X-ray diffraction techniques.

The main geotechnical characteristics of the site, such as permeability and wet bulk density, were measured in situ using the sand-core method. True density measurements were carried out in laboratory, using undisturbed core samples. Such samples were also used for determination of their acid generation and net neutralization potentials, using static acid-base accounting tests. The bio-available fractions of the pollutants were determined by leaching the samples with DTPA and EDTA. The speciation of the pollutants, with respect to their mobility, was determined by the sequential extraction procedure (Tessier et al., 1979). The toxicity of soil samples was determined by the EPA Toxicity Characteristics Leaching Procedure (U.S. Environmental Protection Agency, 1990).

The isolation, identification and enumeration of soil microorganisms were carried out by methods described previously (Karavaiko et al., 1988; Groudeva et al., 1993).

The experimental plots had a rectangular shape and were 400 m<sup>2</sup> in size each (20×20 m<sup>2</sup>). Leach solutions containing carbonate ions and some dissolved organic compounds (mainly lactate and acetate) were used to facilitate the dissolution and transport of the pollutants. The upper soil layers were ploughed up periodically to enhance the natural aeration. Water solutions of dissolved organic compounds and ammonium phosphate were injected through vertical bore-holes into the deeply located soil layers (horizon B<sub>2</sub>) in experimental plot n° 2, to enhance the action of the anaerobic sulfate-reducing bacteria.

The flowsheet also included a system to collect the soil drainage solutions, and to avoid their seepage and the distribution of contaminants into the environment. The system consisted of several ditches and wells, located in suitable sites in the experimental plots. The soil effluents collected by this system were then treated by a constructed wetland located near the experimental plots, to remove the residual amounts of unprecipitated toxic elements in the deeply located soil horizons.

### **Result and discussion**

The soil profile was approximately 100 cm deep (horizon A = 25 cm; horizon B = 55 cm; horizon C = 20 cm). The soil profile was underlined by intrusive rocks, consisting of dense diorite and gabbro. The filtration properties of these intrusive rocks were very

low. The filtration coefficient was approximately  $6 \cdot 10^{-8}$  m/s, and the deeply located rocks were even more impermeable.

The ground-water level was located generally one to two meters below the surface, and ground waters in the site were well separated by the impermeable rocks.

It was assumed that both the geologic and hydrogeologic conditions in the site were suitable for the application of the in situ methods for soil remediation.

Data about chemical composition and some essential geotechnical parameters of the soil are shown in Table I. The concentrations of contaminants were higher in the upper soil layers (mainly in horizon A) (Tables II and III). The contaminants were present mainly in forms susceptible to biological and/or chemical leaching, but considerable portions were present as relevant inert fractions, which were refractory to solubilization. The soil was characterized by a positive net neutralization potential, and the soil pH was in the slightly alkaline range (from 7.5 to 8.5).

Table I: Soil characteristics considered in this study.

Parameters	Horizon A (0÷25 cm)	Horizon B (26÷80 cm)	
Chemical composition (%)	SiO <sub>2</sub>	60.6	61.1
	Al <sub>2</sub> O <sub>3</sub>	14.3	14.0
	Fe <sub>2</sub> O <sub>3</sub>	12.5	5.90
	CaO-	5.72	2.35
	MgO	3.21	1.31
	K <sub>2</sub> O	3.92	3.81
	Na <sub>2</sub> O	0.88	1.94
	S total	0.28	0.21
	S sulfidic	0.14	0.10
	humus	3.7	1.4
Bulk density (g/cm <sup>3</sup> )	1.51	1.63	
Specific density (g/cm <sup>3</sup> )	3.14	3.43	
Porosity (%)	44	41	
Moisture capacity (%)	42	39	
Permeability (cm/s)	$5 \cdot 10^{-2}$	$5 \cdot 10^{-2}$	
pH of H <sub>2</sub> O	7.54	7.65	
Net neutralization potential, CaCO <sub>3</sub> (kg/t)	53	+ 215	

The permeability of the soil was high, and rainwater infiltrated and created conditions favorable for the dissolution of elements. The pore water quality was poor, with high concentrations of contaminants, such as radioactive elements (uranium, radium, and thorium) and some toxic heavy metals (copper, zinc, cadmium, lead). Prior laboratory experiments with soil samples from the experimental plots treated in this study had shown that the dissolution of contaminants was connected with the activity of the indigenous soil microflora. The analysis of this microflora revealed that it included a rich variety of microorganisms (Table IV). In the upper soil layers the aerobic, heterotrophic bacteria were the prevalent microorganisms. Their total number exceeded  $10^8$  cells/g dry soil. Bacteria related to the genera *Pseudomonas* and *Bacillus* were the most numerous in these microbial communities. The fungi were relatively low in number, probably due to the unfavorable soil pH for these microorganisms. Some chemolithotrophic bacteria able to oxidize S<sup>0</sup> and soluble inorganic sulfur compounds at neutral and alkaline pH were also present. *Thiobacillus*



*thioparus* was the main species among these chemolithotrophs, but *Thiobacillus neapolitanus*, the anaerobic *Thiobacillus denitrificans* and some mixotrophic bacteria (mainly such related to the species *Thiobacillus novellus*) were also present.

Table II: Content of pollutants in the soil before and after treatment.

Parameters	U	Ra*	Cu	Cd	Pb
Content of contaminants in the soil before treatment (ppm)					
Horizon A	35	0.540	648	7.0	275
Horizon B	17	0.280	230	3.0	190
Content of contaminants in horizon A after treatment (ppm)					
plot N°1 and plot N°2	9	0.090	240	3.0	95
Content of contaminants in horizon B after treatment (ppm)					
plot N°1	18	0.29	172	2.2	119
plot N°2	27	0.4600	378	4.6	247
Removal of contaminants from the whole soil profile (horizon A + horizon B) (%)					
plot N°1	32.5	37.4	46.4	42.0	48.4
plot N°2	6.2	4.6	7.1	4.1	8.0

\* Ra content is shown in Bq/kg dry soil; all other contaminants content is shown in mg/kg dry soil.

The activity of this microflora was enhanced by suitable changes in the levels of some essential environmental factors, such as water, oxygen and nutrient content in the soil. This was achieved by regular ploughing up and irrigation of the soil, and by addition of some essential nutrients. The optimum soil humidity was about 45 – 50%, from the moisture capacity of the soil, but periodic flushing with water solutions of carbonate and organic compounds was needed to remove the soil contaminants. Zeolite saturated with ammonium phosphate was added to the soil (in amounts in the range of 2-5 kg/t dry soil), to provide the microorganisms with ammonium and phosphate ions and to improve the physico-mechanical properties of the soil.

Table III. Content of pollutants in horizon A of the soil, before and after treatment

Parameters	U	Ra*	Cu	Cd	Pb
Content of toxic elements (ppm)					
before treatment	35	0.540	648	7.0	275
after treatment	9	0.090	240	3.0	95
Bioavailable fraction by DTPA leaching (ppm)					
before treatment	2.6	0.090	68	0.5	0.9
after treatment	0.07	<0.030	14	0.1	0.1
Bioavailable fraction by EDTA leaching, ppm					
before treatment	0.1	0.030	8	0.1	1.4
after treatment	0.2	<0.030	5.3	<0.004	0.14
Easily leachable fractions – exchangeable + carbonate (ppm)					
before treatment	2.7	0.070	28	0.2	0.7
after treatment	0.2	<0.030	1.2	<0.04	0.1
Inert fraction, ppm					
before treatment	12	0.210	125	4.1	161
after treatment	8	0.080	95	2.8	90
Toxic elements solubilized during the toxicity test (ppm)					
before treatment	0.35	<0.030	1.92	0.01	0.08
after treatment	0.03	<0.030	0.21	<0.004	<0.004

\* Ra content is shown in Bq/kg dry soil and Ra solubilized during the toxicity test in Bq/l.

The treatment of the soil was started in March 1998. By the middle of November 1998, it was found that considerable portions of contaminants were removed from the upper soil horizon A and that their residual concentrations, with the exception of radium and lead, were lowered below the relevant permissible levels. It was found that the leaching rates markedly depended on the presence of organic compounds and carbonate ions in the leach solutions. The treatment caused some changes in the composition of the soil microflora, increasing the number of the heterotrophic bacteria. The chemical composition, structure, and main physical and water properties of the soil were altered only to a small extent.

The temperature of the soil also was an essential factor affecting the microbial growth and activity. The highest rates of contaminant solubilization were observed during the summer months (June-August 1998), when the temperature inside the soil profiles was in the range of 17÷35 °C. However, the process was efficient even at temperatures as low as 5÷10 °C (in March 1998), when the well-exposed and the most easily soluble forms of the above-mentioned pollutants were solubilized.

The uranium leaching was connected with the microbial production of peroxide compounds, which turned the tetravalent uranium into the hexavalent state. The  $U^{6+}$  was then solubilized as uranyl carbonate or as complexes with some organic compounds. Radium and the toxic heavy metals were solubilized mainly by means of microbially-secreted organic acids.

In experimental plot n° 1, treated by means of the flushing system, considerable portions of the contaminants were washed out from the soil profile by the soil effluents (Table II). However, considerable portions were accumulated in horizon B<sub>2</sub>. Portions of the toxic heavy metals were present in this horizon as relevant insoluble sulfides. Most of the uranium was present as mineral uraninite (UO<sub>2</sub>). Both the sulfides and uraninite were formed as a result of the microbial, dissimilatory sulfate-reduction taking place in this anoxic zone, regardless of the low content of dissolved organic compounds serving as electron donors. The above-mentioned forms of the contaminants are relatively stable and refractory to leaching, especially under anaerobic conditions. Portions of the non-ferrous metals and uranium, as well as most of the radium in horizon B<sub>2</sub>, were adsorbed on the clay minerals present in this soil horizon. In experimental plot n° 2, treated by means of the detoxification system, only small amounts of the contaminants were washed out from the soil profile by the soil effluents (Table II). The larger portions of the contaminants were retained in horizon B<sub>2</sub>, as a result of the very active process of microbial, dissimilatory sulfate-reduction, which was artificially enhanced by providing the indigenous sulfate-reducing bacteria with high concentrations of suitable electron donors. The population density of these bacteria in experimental plot n° 2 was much higher than in experimental plot n° 1.

The concentrations of dissolved contaminants in the soil effluents from experimental plot n° 2 were much lower than those from experimental plot n° 1. Both types of effluents were treated efficiently by the constructed wetland.

In 1999, the experimental plots were subjected to the same conventional remedial procedures, such as grassing the treated soil, adding suitable fertilizers and animal manure, as well as periodical plough and irrigation. As a result of this, the quality of

the soil was completely restored. So far (as of August 1999), no soluble forms of the above-mentioned contaminants have been detected in the soil pore and drainage waters after rainfall at concentrations higher than the relevant permissible levels.

Table IV: Microorganisms content related to different physiological groups in soil, during treatment.

Microorganisms* n° cells/g dry soil	Horizon A (0÷25 cm)		Horizon B (26÷80 cm)	
			Plot N°1	Plot N°2
Aerobic heterotrophic bacteria	$10^6 \div 10^8$		$10^3 \div 10^5$	$10^4 \div 10^6$
Oligocarbophiles	$10^3 \div 10^7$		$10^2 \div 10^4$	$10^2 \div 10^5$
Cellulose-degrading microorganisms	$10^3 \div 10^6$		$10^2 \div 10^3$	$10^2 \div 10^4$
Nitrogen-fixing bacteria	$10^3 \div 10^5$		$10^2 \div 10^3$	$10^2 \div 10^4$
Nitrifying bacteria	$10^2 \div 10^5$		$10^2 \div 10^3$	$10^1 \div 10^3$
S <sub>2</sub> O <sub>3</sub> <sup>2-</sup> -oxidizing chemolithotrophs (at pH = 7)	$10^3 \div 10^7$		$10^1 \div 10^3$	$10^2 \div 10^5$
S <sup>0</sup> -oxidizing chemolithotrophs (at pH = 2)	$1 \div 10^2$		$10^2 \div 10^4$	$1 \div 10^1$
Fe <sup>2+</sup> -oxidizing chemolithotrophs	$1 \div 10^1$		$1 \div 10^1$	$0 \div 10^1$
Anaerobic heterotrophic bacteria	$10^3 \div 10^6$		$0 \div 10^1$	$10^3 \div 10^7$
Bacteria fermenting carbohydrates with gas production	$10^3 \div 10^5$		$10^3 \div 10^5$	$10^3 \div 10^6$
Denitrifying bacteria	$10^3 \div 10^5$		$10^3 \div 10^5$	$10^3 \div 10^5$
Sulfate-reducing bacteria	$10^3 \div 10^5$		$10^3 \div 10^5$	$10^4 \div 10^7$
Fe <sup>3+</sup> -reducing bacteria	$10^2 \div 10^4$		$10^2 \div 10^4$	$10^2 \div 10^5$
Mn <sup>4+</sup> -reducing bacteria	$10^1 \div 10^3$		$10^1 \div 10^3$	$10^2 \div 10^4$
Methanogenic bacteria	$0 \div 10^2$		$1 \div 10^3$	$1 \div 10^5$
Streptomycetes	$10^3 \div 10^6$		$10^2 \div 10^4$	$10^2 \div 10^4$
Fungi	$10^3 \div 10^6$		$10^2 \div 10^4$	$10^2 \div 10^4$
Total cell numbers	$1 \cdot 10^4 \div 6 \cdot 10^8$		$8 \cdot 10^5 \div 1 \cdot 10^7$	$1 \cdot 10^6 \div 5 \cdot 10^7$

\*The quantitative determination of the different physiological groups of microorganisms was carried out by the spread-plate technique on solid nutrient media or by the most probable number method, using end-point dilutions. The total number of microbial cells was determined by epifluorescent microscopy.

### Acknowledgments

The authors would like to greatly acknowledge the financial support of the European Commission, under the Copernicus project Contract, N<sup>o</sup>: ERB-IC15-CT96-0114, as well as the National Science Fund (Research Contracts N<sup>o</sup> TH-803/98 and VRP-TH-9/99).

### References

- Groudev, S.N., Georgiev, P.S., Spasova, I.I. and Angelov, A.T., 1996. Unpublished results.
- Groudeva, V.I., Ivanova, I.A., Groudev, S.N. and Uzunov, G.C., 1993. Enhanced oil recovery by stimulating the activity of the indigenous microflora of soil reservoirs. In: A.E. Torma, M.L. Apel and C.L. Brierley (Editors), *Biohydrometallurgical Technologies*. TMS Minerals, Metals & Materials Society, Warrendale, PA, 2, 349-356.
- Karavaiko, G.I., Rossi, G., Agate, A.D., Groudev, S.N. and Avakyan, Z.A., 1988. *Biogeotechnology of Metals*. Manual Center for International Projects, GKNT, Moscow.
- Tessier, A., Campbell, P.G.C. and Bisson, M., 1979. Sequential extraction procedure for speciation of particulate trace metals. *Analytical Chemistry*, 51 (7), 844 – 851.
- U.S. Environmental Protection Agency, 1990. Characteristics of EP Toxicity. Federal Register 45(98), Paragraph 261.24.

## HUMIC ASIDS FROM COAL AS A REAGENT TO SOIL REMEDICATION

E.G. Gorlov, V.V. Rodae, O.G. Ryzhkov, D.M. Koledin

Fossil Fuel Institute, Moscow, Russia

### Abstract

Possibilities to produce humic preparations from brown coals by means of alkali extraction have been considered. Conditions for obtaining ballast free sodium humates have been determined which allows to set up their production as a starting material for efficient stimulants of plant growth.

*Keywords: alkali extraction, brown coal, humic salts*

### Introduction

One of the perspective trends of non-fuel usage of coals is the production of humic preparations on its base, which are to be used in different branches of industry and agriculture.

Of interest was to consider the possibilities and conditions for the production of coal-based humic preparations in the form of ballast free sodium humates, especially with the aim of their usage as stimulants for plant growth.

Sodium humate is an environmentally safe stimulant for plant growth and development, which is obtained from humic acids (HA) of brown coals. HA of coals, as a group of natural substances, have much in common with humus of nature, as far as the character of their structure is concerned. They have no principal differences with HA of soils, though they have differences in structural details as their formation depends on bioclimatic factors, stage of coalification, degree of weathering.

It has been established that HA in the form of salts of alkali metals, being absorbed in insufficient amounts by a root system, increase the degree of usage of mineral feed. In addition they play an important role in supporting optimal oxygenation-reduction conditions in soil and plant cells, thus accelerating exchange processes. Humates of sodium and other alkali metals at low concentrations are active preparations, stimulating plant growth and development. They have an effect on chlorophyll formation and photosynthesis and on the income of mineral salts from the environment. However, it should be stressed, that physiologically active humic matters are not a source of mineral feed and do not substitute it, but only increase the coefficient of their usage. Therefore, they should be used as a part of mixture, including mineral fertilizers.

Sodium humate increases the germinating power of seeds and energy of their sprouting, facilitates acclimatization of seedlings and other plants in planting out. It also increases the resistance of plants to decreases an unfavourable effect of soil climatic conditions. It is useful in recultivating of ground, accelerating the ripening of berries, fruits, vegetables, and decreasing the content of nitrates in products.

## Investigations

For the investigation brown coals of Abansky (specimen 1) and Irsha-Borodinsky (specimen 2) deposits of Kansk-Achinsk basin (West Siberia) were taken into consideration. Characteristics of initial coals and HA, derived from them, are given in Table I.

Table I. Characteristics of initial coals and derived free HA.

Indices	Specimen 1	Specimen 2
Brown coals		
Ash content, A <sup>d</sup> (%)	7.7	4.1
Moisture content, W <sup>a</sup> (%)	31.5	32.3
Ultimate composition, daf (%)		
C	71.76	72.90
H	4.98	5.04
N	1.05	0.78
S	0.49	0.74
O (by difference)	21.82	21/24
Atom ratio, H/C	0.84	0.83
Yield of humic acids (%)	25.2	28.2
Humic acids (HA)		
Ultimate composition (%)		
C	66.01	66.63
H	4.92	4.47
N	0.88	0.57
S	0.29	0.32
O (by difference)	27.90	27.01
Atom ratio, H/C	0.90	0.80
Content of active groups (mg eq/g)		
Carboxyl	4.25	2.21
Phenol	3.00	4.13
Chynoid	2.12	1.25

Coals, as a raw material for humic preparation production, are evaluated on the base on HA yield. The method of their determination is herewith important, which should maximally correspond to concrete conditions of a technological process. From single coals, extracted with caustic soda, acidic components proper (so-called free HA) are isolated by means of hydrochloric acid via setting down. At the same time coals may contain a considerably higher amount of HA. Earlier, to destruct organo-mineral HA links, diluted hydrochloric acid was used for coal treatment. At present, in accordance with the acting standard, sodium pyrophosphate is applied. It allows excluding a preliminary treatment by hydrochloric acid and subsequent single alkali treatment gives the possibility to yield common HA from coal.

Special investigations performed with brown coals, of Abansky deposit (specimen 1) have shown that the content of free HA in them (single extraction with sodium hydrate solution) constitutes 25.2%, but pyrophosphatic method, indicating the general content of HA in coals, has resulted in the value of 61.2%. It has been also established, that HA, isolated from alkali solution, are characterized with a greater portion of low molecular fraction. However, the general view of distribution of main fractions as per molecular weights for the studied samples is analogous.

The data of elementary and functional compositions indicate, that common and free HA are proximate in reference to the elementary composition, but different in reference to the content of carboxyl groups: the first is higher than the second. The content of chynoid groups is somehow higher for common HA. It has certain significance for the evaluation of humates used in agriculture as stimulants for plant growth. Indeed, both common and free HA have proximate constitution and structure. They differ in indices which conditions higher solubility of free HA, as compared with common ones. The higher content of low molecular fractions and carboxyl groups is such an index for free HA. Hence, free HA are the main acting factor of humic stimulants for plant growth and include structural groups conditioning stimulating effect of plant growth and development. HA display these properties in a soluble state, penetrating into plants in the form of ions. In this respect free HA have advantage as compared with common ones. Thus, application of ballast free humic stimulants in agriculture is more efficient than coal humic fertilizers of any other type. The base of a skeleton of HA molecules is the aromatic system containing hydroxyl (mainly, phenol ones), carboxyl and methoxyl groups. Ethers and esters, aldehyde groups and others have been found. HA are polydisperse systems, which, depending on pH, may be divided into a number fractions with different molecular weight (as a rule, 500÷50,000). However, all fractions contain, practically, one and the same functional groups, which speaks for their common constitution. Therefore, HA is not a distinguished class of compounds, but are a group of high molecular compounds, having somehow different composition but of a common type of constitution and common properties. As far as chemical functions are concerned, they are aromatic acids and oxy-acids, in which aromatic nuclei are united by section of a non-aromatic character.

### **Experimental results**

Usage of humates in agricultural practice in many respects is connected with biological activity of humic preparations due to the presence within them of a noticeable amount of carboxyl, hydroxyl (phenol) and chynoid groups. Experimental determination of these groups is performed with samples of HA, isolated from initial sodium humates. To characterize sodium humate, as a physiologically active substance derived from brown coal, a simple biological test is suitable. It is based on the increase of size and mass of plants, as compared with the control variant at an early stage of their ontogenesis (as a rule, experiments are carried out with cucumber seeds for the first 7 days of their development).

The resulted experimental data have shown (Table II), that in most cases the content of active functional groups, contained in HA, characterizes biological activity of sodium humates rather well.

The resulted data became a base for creating a general technological flow sheet to produce humic preparations.

The technology of producing sodium humate used at present in industrial practice is based on the interaction of crushed brown coal and concentrated solution of caustic soda followed by the drying of the resulted product without the separation of components. Such a technology leads to the production of a so-called

ballast-containing humates, i.e. humates containing up to 70% of residual coal. Application of ballast-containing humates creates difficulties, connected with the negative effect of unreacted coal on the quality of marketable products, especially when they are used in agriculture, where application of ballast free preparations is needed.

Table II. Content of active functional groups in HA and biological activity of sodium humates, derived from brown coals

Coal deposit	Content of active groups in HA (mg eq/g)			Biological activity (%) (increase of plant mass, as compared with the control)
	carboxylic	phenolic	chynoid	
Tulegansky (Urals)	3.7÷7.2	2.2÷2.9	1.1÷1.7	30÷35
Abansky (Siberia)	4.1÷4.3	2.9÷3.2	1.9÷2.2	30÷35
Beryozovsky (Siberia)	3.0÷3.2	3.5÷3.8	1.0÷1.5	27÷32
Irsha-Borodinsky (Siberia)	2.1÷2.4	3.9÷4.2	1.1÷1.5	26÷31
Bikinsky (Far East)	3.5÷3.8	1.1÷1.4	1.0÷1.2	13÷15
Pavlovsky (Far East)	4.1÷4.4	1.4÷1.6	1.4÷1.6	17÷21

The technology of producing ballast free humic preparations (sodium humates), developed by authors (Rodae and Ryzhkov, 1994), consists of coal preparation (crushing and drying of coal), mixed with a diluted solution of caustic soda followed by mixing the resulted mass at the preset temperature and time. The resulted solution of sodium humate is then separated from residual coal and, after being dried, becomes a marketable product. The residual coal may be combusted or used for other purposes. The process is wasteless and environmentally safe.

### Pilot plant

In accordance with the developed general technological flow sheet an experimental plant of 5 t/y production capacity to produce ballast free humic preparations has been constructed (Rodae and Ryzhkov, 1994; Krichko et al., 1992). The humates produced were successfully used to increase the productivity of a number of agricultural plants in different climatic zones for several seasons.

Operation of the experimental plant has supported the working ability of the process and has allowed the attainment of data for the development of a base project of 500 t/y production capacity to derive sodium humates from brown coals on an industrial scale. The plant of such an output may supply the fertilizer stated to agricultural organizations covering the territory exceeding 100 km<sup>2</sup> of crop area.

Biological activity of humic reagents has allowed creating on their base a number of complex preparations, which were successfully tested in the recultivation of restored and spoilt soils.

### References

- Krichko, A.A., Rodae, V.V. and Ryzhkov, O.G., 1992. The Industrial Technology of Reception the Ballast Free Humic Stimulant of Plant Growth from Brown Coals. *Coal (Rus.)*, No 2, 6-8.
- Rodae, V.V. and Ryzhkov, O.G., 1994. Humic Preparations From Brown Coals of Russia. *Chem. H. Fuel (Rus.)*, No 6, 43-49.

## AUTHOR INDEX

(author's name ▶ volume and number of topic - page)

**A**

Abaidildinov, M. ▶ B10-22  
 Abbruzzese, C. ▶ B11-1  
 Abdel-Aal, E.A. ▶ A6-67  
 Abisheva, Z. ▶ B10-22  
 Abouzeid, A.Z.M. ▶ A4-60  
 Abramov, A.A. ▶ B8a-120, C8b-63  
 Adam, M. ▶ C4-58  
 Adamian, R. ▶ B12b-1  
 Addai-Mensah, J. ▶ C6-1  
 Agatzini, S.L. ▶ A6-22  
 Agus, M. ▶ A5-16, C11-17  
 Ahn, J.H. ▶ C6-29  
 Ahveninen, R. ▶ B8b-40  
 Akbaba, I. ▶ C4-16  
 Akçay, K. ▶ A5-45  
 Akretche, D.E. ▶ B13-1  
 Akser, M. ▶ B8b-109  
 Alcover Neto, A. ▶ C1-17  
 Aldrich, C. ▶ B8a-152, C6-50  
 Alexandrova, L. ▶ B8a-40  
 Alfano, G. ▶ A5-16  
 Aiguacil, F.J. ▶ A6-82, C6-64  
 Alonso, E.A. ▶ B8a-71  
 Amarante, M.M. ▶ C11-40  
 Amelynck, P. ▶ C4-8  
 Anastassakis, G.N. ▶ B8a-64  
 Andrei, L. ▶ B9-24  
 Andres, U. ▶ A2-36  
 Angius, R. ▶ C11-17  
 Anselmi, B. ▶ C11-9  
 Aoe, T. ▶ B13-17  
 Aoki, K. ▶ B13-17  
 Arał, H. ▶ A6-60  
 Arslan, C. ▶ C12a-27  
 Atalay, Ü. ▶ C6-22  
 Ateok, G. ▶ C7-15  
 Augusto, P.A. ▶ C7-9  
 Aurelian, F. ▶ B9-24, C6-84  
 Avan Nierop, M. ▶ C3-39  
 Avdokhin, V. ▶ B8a-104  
 Ay, P. ▶ A5-1

**B**

Babineti, V.S. ▶ B8a-16  
 Bagheri, S.A. ▶ A6-110  
 Bajger, Z. ▶ C12a-15  
 Baláz, P. ▶ A6 – 74, C12a-15  
 Baldauf, H. ▶ B8b-1  
 Barbosa-Filho, O. ▶ A6-41  
 Barres, O. ▶ B8a-111  
 Barsky, E. ▶ C7 – 57  
 Barsky, M. ▶ C7 – 57  
 Bascur, O.A. ▶ A3-83, C8a-21  
 Bashlykova, T.V. ▶ C2-1  
 Basilio, C. ▶ C8b-51  
 Battaglia-Brunet, F. ▶ B12b-9  
 Baudet, G. ▶ A4-21  
 Bazilevsky, A.M. ▶ A7-115  
 Bedekovi, G. ▶ C11-26  
 Beeker, E. ▶ C3-32  
 Beisembaev, B. ▶ B10-22  
 Beloborodov, V. ▶ C8b-84  
 Beolchini, F. ▶ C6-36  
 Bergh, L.G. ▶ C3-24  
 Bertagnolio, A. ▶ A3-100  
 Berton, A. ▶ A3-59  
 Bevilacqua, P. ▶ A7-95  
 Bibawi T.A. ▶ C1-25  
 Bilge, Y. ▶ A5-45, C5-16  
 Bilgen, S. ▶ C8b-29  
 Bissombolo, A. ▶ C4-44  
 Bitimbaev, M. ▶ B10-30  
 Bizi, M. ▶ A4-21  
 Bjelopavlic, M. ▶ A5-69  
 Blazy, P. ▶ B10-1  
 Bocharov, V.A. ▶ C9-1  
 Bochevskaya, E. ▶ B10-22  
 Boehm, A. ▶ A7-35  
 Bogachev, V. ▶ B8b-9  
 Bogdanovich, A.V. ▶ A7-115  
 Boger, D.V. ▶ A5-30  
 Boldižárová, E. ▶ A6-74  
 Bolt, L. ▶ A7-105  
 Bonifazi, G. ▶ A1-52, B8a-178, C8a-39



Bonoli, A. ▶ B12a-56  
Botelho de Sousa, A. ▶ C11-40  
Bouquet, E. ▶ B8a-111  
Boylu, F. ▶ C7-15  
Bozzato, P. ▶ A7-8  
Bradshaw, D.J. ▶ B8a-158, B8b-1, B8b-25  
Bremmell, K.E. ▶ A5-30  
Brito, G. ▶ C11-32  
Broadbent, Q. ▶ B8b-152  
Brochot, S. ▶ A3-108  
Bukurov, T. ▶ B10-22  
Bulut, G. ▶ B8b-103  
Buonomenna, M.G. ▶ A6-95  
Butcher, A. ▶ A1-17

## C

Čalić, N. ▶ B8a-87  
Campbell, J.J. ▶ A4-13  
Carissimi, E. ▶ C12b-9  
Carlsson, L.E. ▶ C8a-39  
Carvalho, M.T. ▶ C3-17  
Carvalho, T. ▶ C11-32  
Casali, A. ▶ A1-9, C4-1  
Cases, J. ▶ B8a-111  
Castro, F. ▶ C12a-15  
Castro, S.H. ▶ B8b-47  
Çelik, M.S. ▶ C5-24  
Cézac, P. ▶ A3-108  
Chahdi, A. ▶ A4-21  
Chander, S. ▶ A5-37, B8b-124  
Chanturiya, E.L. ▶ C2-1  
Chanturiya, V. ▶ B8b-9  
Chen, B. ▶ A3-92, C4-53  
Chen, J. ▶ A5-50, B8b-78  
Chistyakov, A. ▶ C8b-36  
Choi, K.S. ▶ C6-29  
Ciancabilla, F. ▶ B12a-56  
Ciccu, R. ▶ A7-42  
Cieply, J. ▶ C3-72  
Cifuentes, G. ▶ A6-87  
Cilingir, Y. ▶ C8a-6  
Cilliers, J.J. ▶ B8a-158  
Ciminelli, V.S.T. ▶ A6-1  
Cinku, K. ▶ C5-16  
Clemente, E.P. ▶ C12b-1

Clerici, C. ▶ C12a-9  
Clermont, B. ▶ C4-22  
Collantes, J. ▶ A4-77  
Concha, F. ▶ A4-77  
Conger, W. ▶ C4-8  
Cortez, L. ▶ C11-32  
Costa, R.S. ▶ A6-1  
Csóke, B. ▶ A4-132

## D

Da Rosa, J.J. ▶ B9-30  
Dalmijn, W.L. ▶ B12a-49  
Dalvie, M.A. ▶ B8b-25  
Das Kalyan, K. ▶ A5-62, B8a-138  
Datta, A. ▶ C8a-32  
Dawe, J. ▶ C6-1  
De Donato, P. ▶ B8a-111  
De Filippis, P. ▶ B10-9  
De Jager, G. ▶ B8a-158  
De Kretser, R.G. ▶ A5-30  
De Lorenzi, L. ▶ A7-95  
de Oliveira Luz, I.L. ▶ C3-1  
Del Villar, R. ▶ A3-120  
Dela Cuadra, A. ▶ A6-82  
Delalio, A. ▶ C12a-15  
Desam, P.R. ▶ C8a-32  
Desbiens, A. ▶ A3-120  
Dikov, Y. ▶ B8b-9  
Diñçer, H. ▶ A6-9, B8b-103, C7-15  
Diot, F. ▶ A7-27  
Djekic, S. ▶ B12a-43  
Djordem, A. ▶ B13-1  
Dodbiba, G. ▶ B12a-1  
Doğan, M.Z. ▶ C7-15  
Doğan, Z. ▶ B8b-103  
Dolbunin, V. ▶ C7-44  
Donda, J.D. ▶ C4-86  
Donhauser, F. ▶ A4-69  
Dorfner, S. ▶ C7-30  
Dovbysheva, T. ▶ B13-38  
Dowling, E.C. ▶ B8a-163  
Drioli, E. ▶ A6-95  
Drummond, M.A.R. ▶ C4-86  
Drzymala, J. ▶ B8a-79  
Duan, C.H. ▶ A7-121

Duman, I. ▶ C12a-27  
 Dunne, R. ▶ B8b-152  
 Durance, M.V. ▶ A3-108, B12a-26  
 Durão, F. ▶ C3-17, C11-32  
 Dvoichenkova, G. ▶ B8b-9

## E

Eisele, T.C. ▶ B8a-163  
 Eksteen, J.J. ▶ C3-55  
 El Salmawy, M.S. ▶ B8b-160  
 El-Affifi, S. ▶ B10-16  
 El-Hussiny, N.A. ▶ B10-16  
 Els, E.R. ▶ C6-50  
 El-Shall, H. ▶ A5-69  
 Elshin, V.V. ▶ A6-56  
 Eorgescu, D.P. ▶ C6-84  
 Eremin, I.V. ▶ A1-64  
 Escudero, R. ▶ C8a-14  
 Eskibalci, M.F. ▶ B11-9  
 Espinola, A. ▶ B12b-1  
 Esteban, R. ▶ A6-87  
 Ettmayr, A. ▶ C5-8

## F

Faitli, J. ▶ A4-132  
 Fawell, S. ▶ A7-78  
 Fečko, P. ▶ C6-43  
 Fedotov, K. ▶ C8b-84  
 Felicio, A. ▶ C11-32  
 Feng, D. ▶ B8a-152  
 Feng, Q. ▶ B8b-78  
 Ferrara, G. ▶ A7-8, A7-95  
 Ficeriová, J. ▶ A6-74  
 Filip, G.M. ▶ B8a-16  
 Filippov, L.O. ▶ A3-8  
 Finch, J.A. ▶ B8b-87, C8a-14, C8b-15  
 Foerter-Barth, U. ▶ C1-1, C5-1  
 Fordham, M. ▶ B8a-111  
 Fornasiero, D. ▶ B8b-25  
 Forsling, W. ▶ A5-8  
 Forssberg, K.S.E. ▶ A4-1, A7-17, B8a-94  
 Foucher, S. ▶ B12b-9  
 Fourniguet, G. ▶ A3-108  
 Fragomeni, A.L. ▶ B8b-138  
 Francis, J.J. ▶ B8a-158

Franzidis, J.P. ▶ A3-74  
 Fraunholz, N. ▶ B12a-49  
 Frolov, O. ▶ B8a-146  
 Fu, W. ▶ C7-22  
 Fuerstenau, D.W. ▶ A4-60, B8b-62, B9-10  
 Fujita, T. ▶ B12a-1  
 Fukunaka, Y. ▶ B8b-70  
 Furuyama, T. ▶ A5-23

## G

Gaboriau, H. ▶ A4-21  
 Gao, J. ▶ A3-92  
 Gaur, R.K. ▶ B8a-138  
 Georgescu, D.P. ▶ B9-24  
 Georgiev, P.S. ▶ C13-1  
 Geraghty, D. ▶ C4-80  
 Ghiani, M. ▶ A7-42, C11-17  
 Ghosh, S.K. ▶ C9-7  
 Giancontieri, V. ▶ C8a-39  
 Gillet, G. ▶ A7-27  
 Girgin, Ş ▶ C7-15  
 Gliese, R. ▶ A1-24  
 Glover, G. ▶ C3-39  
 Gluba, T. ▶ C4-36  
 Gochin, R.J. ▶ A3-46  
 Gock, E. ▶ B12a-63  
 Golodkov, YuE ▶ A6-56  
 Gomes, L.M.B. ▶ B12b-1  
 Gomez, C.O. ▶ C8a-14  
 González, G.D. ▶ A1-9, C4-1  
 Gorken, A. ▶ C8b-51  
 Gorlov, E.G. ▶ C13-7  
 Gottlieb, P. ▶ A1-17  
 Grigorov, L. ▶ B8a-40  
 Gröger, T. ▶ C7-34  
 Groudev, S.N. ▶ C13-1  
 Guerra, E.A. ▶ B8a-8  
 Guillaneau, J.C. ▶ A3-108  
 Guimaraes, R.C. ▶ B9-17  
 Gül, A. ▶ C10-1  
 Gürmen, S. ▶ C12a-27  
 Gürsu, B. ▶ C8b-29  
 Guyot, O. ▶ C3-45  
 Gyulmaliev, A.M. ▶ A1-64

**H**

- Haarmann, H.C. ▶ C3-32  
 Haas, S.R. ▶ A5-56  
 Háber, M. ▶ A6-74  
 Hagy, R. ▶ C8b-51  
 Hall, S.T. ▶ B8b-33  
 Han, K.N. ▶ A6-33  
 Hanumantha Rao, K. ▶ A7-17, B8a-94  
 Harbeck, H. ▶ C11-9  
 Harris, M.C. ▶ B8a-33  
 Harris, P.J. ▶ B8b-1  
 Haruki, N. ▶ B12a-1  
 Hasu, V. ▶ A3-39  
 Hätönen, J. ▶ A3 – 39, C8a-39  
 Haynes Jr., H. ▶ B10-9  
 Healy, T.W. ▶ A5-30  
 Hebbard, J. ▶ B8a-163  
 Heegn, H. ▶ A1-44, A4-52  
 Heikkila, I. ▶ C8a-39  
 Heiskanen, K. ▶ A4-104, B8b-40  
 Helbig, C. ▶ B8b-1  
 Herbst, J.A. ▶ A3-66  
 Hernández, A. ▶ A6-82  
 Hiçyılmaz, C. ▶ C8b-29  
 Hirajima, T. ▶ C3-8  
 Ho Tun, E. ▶ A1-17  
 Hoberg, H. ▶ B12a-35  
 Hodouin, D. ▶ A3-59, A3-120  
 Hoffman, S. ▶ B12a-18  
 Honores, S. ▶ B8b-47  
 Hoşten, Ç. ▶ B8b-109  
 Hu, W. ▶ B9-10  
 Hu, Y. ▶ A6-111, C12a-20  
 Hupka, J. ▶ B13-31  
 Hussain, S.A. ▶ C6-8  
 Hyötyniemi, H. ▶ A3 – 39, C8a-39

**I**

- Ibrahim, I.A. ▶ A6-67, C1-25  
 Ignatiadis, I. ▶ B12b-9  
 Ignjatovic, M. ▶ A7-52  
 Ignjatovic, R. ▶ A7-52  
 Ilie, P. ▶ B8a-16  
 Inoue, T. ▶ A3-16  
 Ipek, H. ▶ C8a-1

- Ipekoglu, B. ▶ C5-16, B11-9, C5-24  
 Ishii, R. ▶ B8b-70  
 Ismail, A.A. ▶ A6-67  
 Ismail, A.K. ▶ A6-67  
 Izoitko, V.M. ▶ C9-13

**J**

- Jakobs, U. ▶ C7-30  
 Jamal, R. ▶ C6-8  
 Janitschek, R. ▶ C3-32  
 Jankovic, A. ▶ A3-1  
 Jdid, E.A. ▶ B10-1  
 Jeleň, S. ▶ A6-74  
 Jharris, P. ▶ B8b-25  
 Jing, P. ▶ B12a-1  
 Jirestig, J. ▶ A2-36

**K**

- Kähler, J. ▶ B12a-63  
 Kalapudas, R. ▶ A4-104  
 Kalinowski, K. ▶ A3-54  
 Kammel, R. ▶ A6-74  
 Kanda, Y. ▶ C12a-40  
 Kaula, R. ▶ A3-54  
 Kawatra, S.K. ▶ A4-120, B8a-163  
 Kaytaz, Y. ▶ C5-24  
 Kelebek, Ş. ▶ C8b-43  
 Kelebek, S. ▶ B8b-116  
 Keller, K. ▶ C5-8  
 Kelly, B. ▶ C4-80  
 Kennedy, J.P. ▶ A3-83  
 Kerdjoudj, H. ▶ B13-1  
 Kim, H. ▶ C6-29  
 Kim, J. ▶ C8b-15  
 Kim, J.S. ▶ C6-29  
 King, R.P. ▶ A2-16, B9-1  
 Kirjavainen, V. ▶ B8b-40  
 Kishi, W. ▶ B13-17  
 Klimov, A. ▶ C7-44  
 Kmet, S. ▶ B8b-62  
 Koca, H. ▶ C11-1  
 Koca, S. ▶ C11-1  
 Kocakuşak, S. ▶ A5-45  
 Kohad, V.P. ▶ B8a-138  
 Kohmuench, J. ▶ A7-69

Koivistoinen, P. ▶ A4-104  
 Koivo, H. ▶ C8a-39  
 Kolacz, J. ▶ A4-31  
 Koledin, D.M. ▶ C13-7  
 Koltunova, T.Y. ▶ B8a-190  
 Kongolo, K. ▶ A6-14  
 Kongolo, M. ▶ B8a-111  
 Konno, H. ▶ B12b-18  
 Kooijman, S.J.M. ▶ B12a-49  
 K ro lu, H.J. ▶ A5-45  
 Kovachev, K. ▶ B8b-103  
 Kramer, J. ▶ B13-9  
 Krapivny, D. ▶ B8a-146  
 Krasnov, G. ▶ B8a-146  
 Krausz, S. ▶ B8a-16  
 Kudy, A. ▶ C7-44  
 Kuopanporrti, H. ▶ C8a-39  
 Kurkov, A.V. ▶ C8b-71  
 Kurosawa, K. ▶ B12b-18  
 Kur un, I. ▶ C5-24  
 Kusaka, E. ▶ B8b-70, B8b-160  
 Kuyumcu, H.Z. ▶ A4-38  
 Kuzev, L. ▶ A4-44  
 Kuzuno, E. ▶ B12a-1  
 Kyony, P.M. ▶ A6-14

## L

La Marca, F. ▶ A1-52  
 Lahteenmaki, J. ▶ C8a-39  
 Lajoie, S. ▶ C8b-15  
 Lanticse, L.J.G. ▶ C12b-1  
 Laplante, A.R. ▶ A4-128  
 Larin, V. ▶ B8b-54  
 Lascelles, D. ▶ B8b-87  
 Laskowski, J.S. ▶ B8a-71  
 Lavrinenko, A. ▶ B8a-146  
 Lazi , P. ▶ B8a-87  
 Le Guern, C. ▶ B12a-9  
 Le o, V.A. ▶ A6-1  
 Lee, K.H. ▶ C6-29  
 Lehto, H.J. ▶ C8b-56  
 Leite, J.Y.P. ▶ C6-70  
 Lenoir, M. ▶ A7-27  
 Leonov, S.B. ▶ A6-56  
 Leppinen, J. ▶ A4-104

Leppinen, J.O. ▶ C8b-56  
 Levi, R. ▶ A3-100  
 Li, Z. ▶ C7-50  
 Lima, J.R.B. ▶ C4-29  
 Lins, F.F. ▶ B8b-131  
 Liu, J. ▶ C4-53  
 Liu, S. ▶ C7-22  
 Liu, Y. ▶ A3-92, A4-13  
 Lo, Y.C. ▶ A4-112  
 Lopez-Valdivieso, A. ▶ B8b-62  
 Lorenzen, L. ▶ A6-48, C6-50, C7-1  
 Louren o, R. ▶ C11-32  
 Lowe, R.A. ▶ C8b-51  
 Lsandvik, K. ▶ B12a-26  
 Lu, S. ▶ C5-31  
 Lu, Y. ▶ B8b-78  
 Luganov, V. ▶ B10-30  
 Luttrell, G. ▶ A7-69  
 Luz, A.B. ▶ C8b-79

## M

Machado Leite, M. ▶ C11-40  
 Machado, E.L. ▶ C12b-9  
 Madsen, I. ▶ A1-30  
 Maegawa, K. ▶ B8b-70  
 Maffei, A.C. ▶ C3-1  
 Magdalinovic, N. ▶ A7-52  
 Magliocco, L. ▶ C8b-51  
 Mahnke, J. ▶ B8a-56  
 Makavetskas, A.R. ▶ C2-1  
 Maksimov, I.I. ▶ B8a-190  
 Mankosa, M. ▶ A7-69  
 Manlapig, E.V. ▶ A3-74  
 Manouchehri, H.R. ▶ A7-17  
 Mao, Y. ▶ A3-92  
 Maric, R. ▶ A7-52  
 Marion, P. ▶ B8a-111  
 Markovic, Z.S. ▶ C8b-23  
 Martin, W. ▶ C12a-34  
 Mart nez Cavazos, E. ▶ B8b-96  
 Martins, J.P. ▶ C7-9  
 Massacci, P. ▶ A1-52, B8a-178  
 Mathe, Z.T. ▶ B8a-33  
 Matsumoto, S. ▶ C6-15  
 Matsuo, S. ▶ A3-32

Meier-Kortwig, J. ▶ B12a-35  
 Meloni, A. ▶ B8a – 178, C8a-39  
 Meloy, T.P. ▶ A1-37  
 Mendoza, H.D. ▶ C12b-1  
 Merwin, R. ▶ A7-69  
 Mescheriakov, N.F. ▶ B8a-131  
 Mesenyashin, A.I. ▶ A7-89  
 Mfumum, K. ▶ A6-14  
 Micevic, Z. ▶ B12a-43  
 Mielczarski, E. ▶ B8a-111  
 Mielczarski, J.A. ▶ B8a-111  
 Miettinen, M.S. ▶ C8b-56  
 Miettunen, J. ▶ C8a-39  
 Mikhaylova, I. ▶ C8b-36  
 Milenkovic, G. ▶ C8b-23  
 Miller, J.D. ▶ B13-31, C8a-32, C12a-20  
 Milot, M. ▶ A3-120  
 Mistura, C. ▶ C12b-9  
 Miyazaki, T. ▶ B12a-1  
 Moharam, M.R. ▶ B8b-177  
 Molinari, R. ▶ A6-95  
 Monte, M.B.M. ▶ B8b-131  
 Mori, S. ▶ A5-23, C4-44  
 Morin, D. ▶ A3-108, B12b-9  
 Morozov, V. ▶ B8a-104  
 Morrell, S. ▶ A3-1  
 Moshninov, V.V. ▶ A7-115  
 Mostafa S.I. ▶ C1-25  
 Moudgil, B.M. ▶ A5-69  
 Moys, M.H. ▶ C3-39  
 Mulpeter, T. ▶ C3-45  
 Muratoğlu, R.A. ▶ B8b-109  
 Mwema, D.M. ▶ A6-14

## N

Nagaraj, D.R. ▶ C8b-1  
 Nagel, M. ▶ A5-1  
 Nalaskowski, J. ▶ B13-31  
 Naraki, T. ▶ A2-9  
 Nascimento, F.R. ▶ A5-56  
 Natarajan, K.A. ▶ B8a-94  
 Nava-Alonso, F. ▶ B8b-96  
 Navarro, P. ▶ C6-64  
 Nebera, V. ▶ B8b-54  
 Neesse, T. ▶ A4-69, B13-24

Nesbitt, A.B. ▶ C12a-34  
 Nessel, J.E. ▶ C8b-15  
 Neumann, R. ▶ C1-17  
 Nguyen, G. ▶ C6-77  
 Niemi, A. ▶ C8a-39  
 Niewiadomski, M. ▶ B13-31  
 Niinae, M. ▶ B13-17  
 Nikaidoh, M. ▶ C12a-40  
 Nikolov, J. ▶ A1-30  
 Ninova, V. ▶ B8b-103  
 Noaparast, M. ▶ A4-128

## O

O'Connor, C.T. ▶ B8a-33, B8b-1  
 Obraniak, A. ▶ C4-36  
 Oja, M. ▶ C4-64  
 Okano, Y. ▶ A3-32  
 Okaya, K. ▶ A3-16  
 Oliazadeh, M. ▶ A6-110  
 Oliveira, A.P.A. ▶ C6-57  
 Oliveira, J.F. ▶ B8b-131  
 Önal, G. ▶ A6-9, B8b-103, C10-1  
 Operto, M. ▶ C12a-9  
 Örgül, S. ▶ C6-22  
 Orhan, G. ▶ C12a-27  
 Owada, S. ▶ A2-9  
 Ozdag, H. ▶ C8a-1

## P

Pace, D. ▶ A1-52  
 Panayotov, V. ▶ B8b-103  
 Panayotova, M. ▶ B8b-103  
 Panteleeva, N. ▶ C8b-36  
 Panturu, E. ▶ C6-84  
 Parekh, B.K. ▶ B8a-171  
 Passariello, B. ▶ B11-1  
 Pastukhova, I.V. ▶ C8b-71  
 Pate, W.T. ▶ A3-66  
 Paulo, J.B.A. ▶ C6-70  
 Pawlak, W. ▶ B13-9  
 Pereirade Souza, C. ▶ C12a-46  
 Pereiram Leite, J.Y. ▶ C12a-46  
 Peres, A.E.C. ▶ B9-17, C4-86  
 Peretti, R. ▶ A7-42, C11-17  
 Pérez Garibay, R. ▶ B8b-96

Pérez, C. ▶ A1-9, C4-1  
Petersen, F.W. ▶ B12b-33, C12a-34  
Petkovic, Z. ▶ C8b-23  
Petter, C.O. ▶ A1-24  
Pietsch, W. ▶ A4-87  
Pimkina, L. ▶ C8b-36  
Pires, C. ▶ C11-32  
Pitchumani, B. ▶ C4-94  
Pizzolato, T.M. ▶ C12b-9  
Polat, H. ▶ A5-37  
Polat, M. ▶ A5-37  
Possa, M.V. ▶ C4-29  
Potkonen, N.I. ▶ C2-1  
Pradip ▶ A5-62, B8a-138  
Pugachev, V.S. ▶ A7-115  
Pugh, R.J. ▶ B8a-40

## **Q**

Qian, J.C. ▶ A7-121  
Qiu, G. ▶ A6-111

## **R**

Raghuraman, P. ▶ C4-94  
Raichur, A.M. ▶ B8a-171  
Rajiv Raman, R. ▶ C4-94  
Raju, K.S. ▶ C9-7  
Ralston, J. ▶ B8b-17, C6-1  
Ramadan, A.M. ▶ B8b-177  
Rangarajan, V. ▶ B8a-138  
Rao, T.K. ▶ B8a-138  
Rath, R.K. ▶ B8b-144  
Ravaglia, R. ▶ A6-41  
Rets, N.I. ▶ B8a-131  
Reuter, M.A. ▶ C3-55  
Ripke, S.J. ▶ A4-120  
Rodae, V.V. ▶ C13-7  
Rodrigues, I. ▶ C11-32  
Rolf, L. ▶ A4-38  
Romano, D. ▶ A3-100  
Romanov, A. ▶ C7-44  
Rubio, J. ▶ B9-30  
Ryzhkov, O.G. ▶ C13-7

## **S**

Saba, P. ▶ A5-16

Sabedot, S. ▶ A1-24  
Sabirov, R.H. ▶ B8a-131  
Sachweh, J. ▶ C4-72  
Sakaguchi, T. ▶ B12b-25  
Salatic, D. ▶ C8b-9  
Salatic, V. ▶ C8b-9  
Saleh, A.M. ▶ B8b-177  
Salopek, B. ▶ C11-26  
Santander, M. ▶ B9-30  
Samosy, A.P. ▶ A7-115  
Sampaio, C.H. ▶ C1-8  
Sander, S. ▶ C12a-1  
Sander, U. ▶ A4-97  
Sandrin, D. ▶ C12a-9  
Sano, S. ▶ C12a-40  
Sasaki, K. ▶ B12b-18  
Satayev, I.S. ▶ B8a-190  
Sauer, G. ▶ C5-8  
Savaşçı, Ö.T. ▶ A5-45  
Scales, P.J. ▶ A5-30  
Sceresini, B.J. ▶ C6-77  
Schena, G.D. ▶ A3-46  
Schimroszczyk, B. ▶ B12a-63  
Schneider, C.L. ▶ A2-16, C1-17  
Schneider, I.A.H. ▶ A5-56, C12b-9  
Schönert, K. ▶ A4-97  
Schreier, M. ▶ A2-24  
Schreithofer, N. ▶ B8b-40  
Schricker, B. ▶ B13-24  
Schubert, G. ▶ C12a-1  
Schubert, H. ▶ B8a-8  
Schubert, J. ▶ A3-24  
Schulze, H.J. ▶ B8a-56  
Scorzelli, I.B. ▶ B8b-138  
Sedláčková, V. ▶ C6-43  
Seksenov, S. ▶ A4-44  
Sen, S. ▶ C8a-6  
Serci, A. ▶ A7-42, C11-17  
Seron, A. ▶ A4-21  
Serranti, S. ▶ C8a-39  
Shahverdi, A.R. ▶ A6-110  
Shalabi, M.E.H. ▶ B10-16  
Sharma, N.K. ▶ B8a-138  
Sharma, P.K. ▶ B8a-94  
Shatalov, V.V. ▶ C8b-71

- Shen, W.Z. ▶ B8b-25  
 Shibata, J. ▶ C6-15  
 Shibayama, A. ▶ C4-44  
 Shumskaya, L.G. ▶ A1-44  
 Shumskaya, Y.N. ▶ C9-13  
 Simovic, I. ▶ B12a-43  
 Simpson, J. ▶ A6-87, C6-64  
 Singh, A. ▶ A3-24  
 Sipari, P. ▶ C8a-39  
 Sis, H. ▶ B8b-124  
 Solding, M. ▶ A7-59  
 Solozhenkin, P. ▶ B8b-54  
 Somasundaran, P. ▶ A5-62  
 Song, S. ▶ C5-31  
 Spasova, I.I. ▶ C13-1  
 Spencer, S.J. ▶ A2-1, A4-13  
 Stadtmuller, A. ▶ A7-78  
 Stahl, W. ▶ C5-8  
 Stallknecht, H. ▶ A2-36  
 Stanojlovic, R. ▶ C8b-23  
 Steiner, H.J. ▶ A7-35  
 Stén, P.M. ▶ C8b-56  
 Stephansson, O. ▶ C8a-39  
 Stöckelhuber, K.W. ▶ B8a-56  
 Subramanian, S. ▶ B8b-144  
 Sugano, T. ▶ B13-17  
 Sui, C. ▶ B8b-87, C8b-15  
 Sun, Z.X. ▶ A5-8  
 Sung, G.W. ▶ C6-29  
 Surracco, M. ▶ A5-16  
 Sutaone, A.T. ▶ C9-7  
 Sutherland, D. ▶ A1-17, A2-1  
 Swaminathan, C. ▶ B8a-24  
 Sweet, C.G. ▶ B8a-158  
 Sztaba, K.S. ▶ A7-1  
 Szymocha, K. ▶ B13-9
- T**
- Tabatabae, M. ▶ A6-110  
 Tajadod, J. ▶ B8a-49  
 Takeda, K. ▶ A2-9  
 Tarasov, A.V. ▶ C9-1  
 Tareco, C. ▶ C11-32  
 Tarján, I. ▶ A4-132  
 Tavares, L.M. ▶ C4-99
- Teague, A.J. ▶ B8a-24  
 Teipel, U. ▶ C1-1, C5-1  
 Tiberg, F. ▶ B8a-40  
 Tiefel, H. ▶ B13-24  
 Timmel, G. ▶ C12a-1  
 Timoshkin, I. ▶ A2-36  
 Timur, S. ▶ C12a-27  
 Titkov, S. ▶ C8b-36  
 Tolun, R. ▶ A5-45  
 Tomas, J. ▶ A2-24, C7-34  
 Tomus, N. ▶ C10-5  
 Topkaya, Y. ▶ B8b-109  
 Tores, M.L. ▶ B8b-138, C6-57  
 Toro, L. ▶ B11-1  
 Trofimova, E. ▶ B8b-9  
 Tröndle, H. ▶ C7-30  
 Trumic, M. ▶ A7-52  
 Trybalski, K. ▶ C3-72  
 Tsakiridis, P.E. ▶ A6-22  
 Tsukerman, V. ▶ C2-8  
 Tsunekawa, M. ▶ C3-8  
 Tubino, L.C.B. ▶ C1-8  
 Tukul, C. ▶ B8b-116  
 Tumidajski, T. ▶ C3-65  
 Tuunila, R. ▶ C4-64
- U**
- Udrea, N. ▶ B9-24  
 Udrea, N. ▶ C6-84  
 Ukolov, A. ▶ C7-44  
 Ullu, F. ▶ B11-1  
 Ulusoy, U. ▶ C4-16  
 Unland, G. ▶ A1-1  
 Uribe-Salas, A. ▶ B8b-96  
 Usov, A. ▶ C2-8
- V**
- Valderrama, L. ▶ B9-30  
 Valente, C. ▶ B8a-111  
 Valim, A.B. ▶ A1-24  
 Vallebuona, G. ▶ A1-9, C4-1  
 van Deventer, J.S.J. ▶ B8a-24, C7-1  
 van Dyk, W.A. ▶ C7-1  
 Van Houwelingen, J.A. ▶ B12a-9  
 van Tonder, J.C. ▶ C3-39

Vargas, C. ▶ A6-87  
Vargas, R. ▶ A1-9, C4-1  
Vasile, C. ▶ C10-5  
Vasile, I. ▶ C10-5  
Védrine, H. ▶ B12a-26  
Vegliò, F. ▶ B11-1, C6-36  
Vera, M.A. ▶ A3-74  
Vigdergauz, V. ▶ B8a-79  
Villeneuve, J. ▶ A3-108, B12a-26  
Volpe, F. ▶ C8a-39  
von Krüger, F.L. ▶ C4-86

## W

Wakamatsu, T. ▶ B8b-160  
Waldek, U. ▶ B12a-63  
Wang, D. ▶ A6 – 111, C12a-20  
Wang, J. ▶ A6-111  
Wang, W. ▶ C8a-39  
Wang, X.H. ▶ B8a-171  
Wang, Y.M. ▶ A4-1  
Watson, J.H.P. ▶ A7 – 105, C7-50  
Wei, L.B. ▶ A5-50  
Weller, K.R. ▶ A4-13  
Williams, M.C. ▶ A1-37, B9-10  
Witika, L.K. ▶ B8b-168  
Wolf, S. ▶ B12a-35  
Wright, B.A. ▶ B8a-158  
Wu, L.M. ▶ A5-8

## X

Xiaojun, X. ▶ C8b-43  
Xu, D. ▶ C4-53

## Y

Yamamoto, H. ▶ C6-15  
Yan, D. ▶ B8b-152  
Yanagawa, K. ▶ C12a-40  
Yang, D.C. ▶ A7-8  
Yehia A. A. ▶ C1-25  
Yekeler, M. ▶ C4-16  
Yemelyanov, M.F. ▶ B8a-190  
Yen, W.T. ▶ B8a-49  
Yermakov, V.V. ▶ A7-115  
Yianatos, J.B. ▶ C3-24  
Yildirim, I. ▶ C8b-79

Ylinen, R. ▶ A3 – 39, C8a-39  
Yoon, R.H. ▶ B8a-1  
Yoon, R.-H. ▶ C8b-79  
Yoon, S.H. ▶ C6-29  
Yuan, X.M. ▶ B8a-71  
Yüksel, Ö. ▶ C7-15  
Yushina, T.I. ▶ C8b-63  
Yusupov, T.S. ▶ A1-44  
Yüzer, H. ▶ A5-45

## Z

Zagorodnyaya, A. ▶ B10-22  
Zampini, S. ▶ C4-58  
Zanetti, M.C. ▶ C12a-9  
Zanin, M. ▶ A7-95  
Zhang, X.X. ▶ A7-121  
Zhang, Y. ▶ C7-22  
Zhong, K. ▶ A6-111  
Zlagnean, M. ▶ C10-5  
Zoch, A. ▶ C12b-9  
Zshebel, F. ▶ B10-16  
Zucca, A. ▶ A7-42, C11-17  
Zuco, R. ▶ C8a-39  
Zuev, V. ▶ B8b-9



This Page Intentionally Left Blank

**KEYWORD INDEX**

(keyword ▶ volume and number of topic - page)

**A**

*Abrasion* ▶ A4-38  
*Acid-base interaction energy* ▶ B8a-171  
*Acoustic* ▶ C8b-84  
*Acoustic emission* ▶ C3-8  
*Actinoid* ▶ B12b-25  
*ActiveX development environment* ▶ C8a-21  
*Adhesion* ▶ A5-56  
*Adsorbents* ▶ A5-8  
*Adsorption* ▶ A5-69, B8b-144, C5-24, C6-50  
*Adsorption mechanisms* ▶ B8b-131  
*Aeration* ▶ B8a-131, C3-32  
*Agate* ▶ C1-9, C12b-9  
*Agglomeration* ▶ A4-87, A4-132, C3-8,  
     C4-36, C8a-6  
*Aggregation* ▶ C6-57  
*Agitation cell* ▶ A4-38  
*Agitator* ▶ C4-71  
*Air classification* ▶ A4-31  
*Alkali extraction* ▶ C13-7  
*Alumina* ▶ A5-62  
*Aluminate* ▶ B12a-63  
*Aluminum* ▶ A4-44, C12a-40  
*Aluminum recycling* ▶ B12a-35  
*Alunite separation* ▶ C11-1  
*Amines* ▶ C12a-27  
*Ammonium salts* ▶ C8b-43  
*Anatase* ▶ C8b-51, C8b-79  
*Apatite* ▶ B8a-120  
*Apatite flotation* ▶ B9-17  
*Apparent viscosity* ▶ A5-50  
*APT* ▶ C9-7  
*Aragonite* ▶ C6-29  
*ARMAX* ▶ C3-72  
*Arsenic* ▶ B8a-49  
*Ash* ▶ C7-15  
*Attachment* ▶ C12b-1  
*Attrition* ▶ B13-24  
*Attritor* ▶ C4-94  
*Autoclave leaching* ▶ A6-33  
*Autogenous* ▶ C4-79  
*Automated measurement* ▶ A1-17

*Automation* ▶ A3-100  
*Automobile catalytic converters* ▶ A6-33  
*Axial impellers* ▶ B8a-131  
*Axial symmetry* ▶ A4-77  
*Azine* ▶ C8b-63

**B**

*Baffled column* ▶ B8a-16  
*Ball grinding mill* ▶ A3-92  
*Ball milling* ▶ C4-16  
*Barite* ▶ A6-9, B8a-120  
*Base metals* ▶ C6-50  
*Bauxite* ▶ C6-8  
*Bench-scale system* ▶ A7-121  
*Beneficiation* ▶ A5-16, C11-17  
*Bentonite* ▶ A4-120, C5-16  
*Binder* ▶ A4-120  
*Binding mechanisms* ▶ A4-120  
*Bioflotation* ▶ B8a-94  
*Bioleaching* ▶ A6-103, A6-110  
*Bioprocessing* ▶ B12b-25  
*Bioremediation* ▶ B12b-18  
*Biotreatments* ▶ A3-108  
*Blade granulator* ▶ B12a-56  
*Blast furnace* ▶ B11-9  
*Boltzman's model* ▶ B8a-87  
*Brass ash* ▶ C12a-27  
*Breakage* ▶ A4-128  
*Brown coal* ▶ C6-43, C13-7  
*Bubble separation tank* ▶ C8a-32  
*Bubble size* ▶ C8a-14  
*Bubble surface area flux* ▶ C8a-14  
*Building rubble recycling* ▶ A2-24, C7-34  
*By-products* ▶ A4-44

**C**

*CaCO<sub>3</sub>* ▶ C6-29  
*Cadmium* ▶ B8b-138, B12b-1, B13-17  
*Calcite* ▶ A5-56, B8a-120, C4-94  
*Calcium* ▶ B8b-40  
*Carbonation process* ▶ C6-29  
*Carboxymethyl cellulose* ▶ B8b-25

- Carrier flotation* ▶ C11-1  
*Cassiterite* ▶ A3-8  
*Catalysis* ▶ A6-103  
*Cationic collectors* ▶ B8a-40  
*Cationic surfactants* ▶ C8b-36  
*Cellulose* ▶ C12a-20  
*Cement* ▶ A4-1  
*Cement grinding circuit* ▶ A3-32  
*Cementation* ▶ A6-41  
*Centrifugal separator* ▶ A7-115  
*Ceramics industry* ▶ C11-17  
*CFD* ▶ C8a-32  
*Chalcopyrite* ▶ B8a-49, B8b-152, C9-1  
*Chalcopyrite-containing ores* ▶ A6-103  
*Characterization* ▶ C12a-46  
*Chelating reagents* ▶ B8b-70  
*Chemical analysis* ▶ C6-8  
*Chemical distribution* ▶ C8b-56  
*Chemical oxidation* ▶ C12b-9  
*Chromite* ▶ C4-16  
*Citric acid* ▶ B8b-116  
*Classification* ▶ A5-16  
*Classifier* ▶ C4-58  
*Classifying column* ▶ C4-44  
*Classifying index* ▶ C4-53  
*Clean coal* ▶ C7-15  
*Clean soil process* ▶ B13-9  
*Cleanup criteria* ▶ B13-9  
*Cluster analysis* ▶ A5-1  
*Coal* ▶ A1-64, B8a-171, C8a-6  
*Coal flotation* ▶ B9-10, B8b-177  
*Coal organic matter* ▶ A1-64  
*Coal particles* ▶ C11-26  
*Coal-flotation* ▶ C3-32  
*Coarse particle flotation* ▶ A7-69  
*Cobalt* ▶ A6-22  
*Cobalt sulfate solutions* ▶ A6-14  
*Coconut fiber* ▶ B12b-1  
*Colemanite* ▶ A7-52  
*Collector* ▶ B8a-71, C8b-23, C8b-71, C12b-1  
*Collector desorption* ▶ C8b-9  
*Collector mixing* ▶ B8b-177  
*Collector mixtures* ▶ B8b-1  
*Collectors* ▶ B8b-17  
*Colloid stability* ▶ C6-1  
*Color classification* ▶ A1-24  
*Column flotation* ▶ A3-8, C3-17, C8a-1, C8b-29  
*Column method* ▶ C6-15  
*Columns* ▶ C8a-14  
*Combined treatment* ▶ B12a-49  
*Comminution* ▶ A2-16, A2-24, A4-1, A4-13, A4-38, C3-39, C4-44, C4-64, C4-94, C4-99, C12a-1  
*Comminution efficiency* ▶ A4-60  
*Communication* ▶ C3-1  
*Compacting* ▶ A4-132  
*Competitive adsorption* ▶ C8b-56  
*Complex sulfide minerals* ▶ A6-74  
*Complex utilization* ▶ C9-13  
*Complex vibrating-pulsating HGMS* ▶ C7-22  
*Compound distributions* ▶ C3-65  
*Compressed gases* ▶ C5-1  
*Compression* ▶ A4-112, A5-30  
*Computational engineering* ▶ A4-69  
*Concave surfaces* ▶ C4-86  
*Concentrate* ▶ A6-87  
*Confocal laser scanning microscopy* ▶ A5-1  
*Conical cyclone* ▶ A7-95  
*Conroll strategy* ▶ C3-55  
*Contact angle* ▶ B8a-1, B8a-40, B8a-79, B8a-171, B8b-124  
*Contaminated particles* ▶ B13-24  
*Contaminated soil* ▶ B13-9, A3-108  
*Continuous* ▶ C4-71  
*Control* ▶ C4-8  
*Control and regulation* ▶ B8a-120  
*Control strategy* ▶ C3-17  
*Control structures* ▶ A3-54  
*Conventional flotation* ▶ B8b-103  
*Copper* ▶ A4-44, B12a-9, C3-72, C6-64, C8b-63  
*Copper concentrate* ▶ B8a-111  
*Copper depression* ▶ C8b-9  
*Copper minerals* ▶ C8b-9  
*Copper ore* ▶ B8a-87, C8b-23, C10-1  
*Copper recovery* ▶ C12a-27  
*Copper sulphate* ▶ B8a-24  
*Copper-activated sphalerite* ▶ B8b-17  
*Copper-zinc* ▶ B8b-103

*Co-precipitation* ▶ B8b-144  
*Corona discharge* ▶ A7-89  
*Corynebacterium xerosis* ▶ A5-56  
*Counter-rotating vortex* ▶ C4-53  
*Cross-flow gravity separation model* ▶ C7-34  
*Crushing bodies* ▶ C4-86  
*Crystalline structure* ▶ C6-57, C1-25  
*Cu adsorption* ▶ B8b-87  
*Cullets* ▶ A1-52  
*Cu-Ni separation* ▶ B8b-116  
*Cu-Pb sulfide mineral* ▶ C7-22  
*Cu-Zn sulfide mineral* ▶ C7-22  
*Cyanex 302* ▶ A6-22  
*Cyanidation* ▶ A6-9, A6-87, C12a-34  
*Cyanide recycling* ▶ A6-1  
*Cylindrical cyclone* ▶ A7-95

## D

*Data mining* ▶ A3-39  
*Data reconciliation* ▶ A3-59  
*DEM* ▶ C3-39  
*Dense medium* ▶ A7-95  
*Dense medium separation* ▶ A7-52  
*Density concentration* ▶ A7-69  
*Dental amalgam* ▶ C12a-46  
*Depressant* ▶ B12a-49, C8b-1  
*Depressing* ▶ B8b-103  
*Depression* ▶ B8b-25  
*Desliming process* ▶ C4-29  
*Desorption* ▶ C5-24  
*Desulfurization* ▶ C6-43  
*Dewatering* ▶ A5-30, C5-8  
*Diagnosis* ▶ C3-24  
*Diamonds* ▶ B8b-9  
*Diamonds particles* ▶ B8a-131  
*Diethylenetriamine* ▶ B8b-116  
*Discharge* ▶ C2-8  
*Discharge lamp* ▶ B12a-63  
*Discrete element method* ▶ C3-39  
*Disintegration* ▶ A2-36, C2-8  
*Dispersed phase flow* ▶ C8a-32  
*Dispersion* ▶ A5-37, A5-62, B8b-25  
*Dispersion energy* ▶ B8a-171  
*Dissolution* ▶ C6-1  
*Distributed separation efficiency* ▶ A3-46

*Disturbance* ▶ A3-24  
*Dithionite* ▶ C8b-15  
*DLVO theory* ▶ C12b-1  
*DOE* ▶ A3-100  
*Dolomite* ▶ B10-1  
*Donicity* ▶ A7-17  
*Drag* ▶ A5-50  
*Dry* ▶ C4-71  
*Dry fine classification* ▶ A4-21  
*Dry tower mill* ▶ C4-44  
*Dusts* ▶ C6-29  
*Dye* ▶ C12b-9  
*Dynamic* ▶ A3-66  
*Dynamic flotation framework* ▶ C8a-21  
*Dynamic light scattering* ▶ C1-1  
*Dynamic models* ▶ A3-54  
*Dynamic simulation* ▶ A3-83

## E

*Ecology* ▶ C9-13  
*EDTA* ▶ B13-1  
*EDTA extraction* ▶ C8b-15  
*EDTA soluble elements* ▶ A4-104  
*Effect of Ca ions* ▶ B8b-87  
*Efficiency* ▶ A4-112, C4-79, C8b-84  
*Effluent decontamination* ▶ B12b-1  
*Effluents* ▶ A7-27, B8b-138, B12b-9  
*Ejector* ▶ B8a-16  
*Electric charges* ▶ A7-89  
*Electric separation* ▶ A7-42, C10-5  
*Electrical* ▶ C2-8  
*Electrical properties* ▶ A7-17  
*Electrical pulses* ▶ A2-36  
*Electrochemical* ▶ B8b-168  
*Electrochemical treatment* ▶ B8b-103  
*Electrochemistry* ▶ B8b-1  
*Electrode furnace* ▶ B12a-43  
*Electrode potentials* ▶ A4-104  
*Electrodes* ▶ A7-89  
*Electrokinetics* ▶ B8b-168, B13-1, B8b-144, B13-17  
*Electrolyte solutions* ▶ B10-9  
*Electrolytes* ▶ A5-37  
*Electronic waste* ▶ B12a-9  
*Electrostatic* ▶ C7-30

*Electrostatic field* ▶ A7-89  
*Electrostatic force* ▶ B8a-1  
*Electrostatic separation* ▶ A7-89, B12a-1  
*Electrowinning* ▶ A6-87  
*Emissions* ▶ B12a-26  
*Emulsification* ▶ A5-37  
*Enargite* ▶ B8a-49, B8b-47  
*Energy* ▶ C8b-71  
*Energy band* ▶ B8b-78  
*Energy costs* ▶ C4-58  
*Energy saving* ▶ A4-112  
*Energy spectrum* ▶ A3-16  
*Energy split factors* ▶ A4-60  
*Enhanced kinetics* ▶ C6-77  
*Enrichment ratio* ▶ A3-74  
*Enrichment scheme* ▶ C2-1  
*Entrainment* ▶ B8a-8  
*Environment* ▶ B8b-138, B12b-33, C7-30, C12a-46  
*Environmental protection* ▶ B12a-18  
*ESR-spectra* ▶ B8b-54  
*Ettringite* ▶ B12b-33  
*Europium oxides* ▶ B12a-63  
*Expert system* ▶ C3-45  
*Expertise research* ▶ A3-39  
*Extraction* ▶ A6-22  
*Extraction of alumina* ▶ C6-8  
*Extractive metallurgy* ▶ C6-70

## F

*Factorial experiments* ▶ C6-36  
*Falling sphere method* ▶ A5-50  
*Fast gravity flow* ▶ C7-44  
*Fault detection* ▶ A3-59  
*Fault isolation* ▶ A3-59  
*Fault diagnosis* ▶ A3-83  
*Feldspar* ▶ C7-30, C8b-56, C11-9  
*Feldspar ores* ▶ C11-17  
*Ferric sulfate* ▶ C6-22  
*Fertilizer* ▶ C12a-27, C1-25  
*FIELDBUS* ▶ C3-1  
*Filblast* ▶ C6-77  
*Film breakage* ▶ C7-1  
*Film rupture* ▶ B8a-56  
*Filtration* ▶ A5-30

*Fine bituminous coal* ▶ C8b-29  
*Fine classification* ▶ A4-31  
*Fine grinding* ▶ A4-52, C4-94  
*Fine particle* ▶ A5-16  
*Fine particle processing* ▶ C5-31  
*Fine particle sizes* ▶ A7-42  
*Fine particles* ▶ A5-8, A7-8, B8b-70, C5-1  
*Flattening* ▶ A4-128  
*Floatability* ▶ B8a-79  
*Floatstar* ▶ A3-24  
*Flocculation* ▶ A5-1, A5-56, A5-62, B8a-8, C5-24  
*Flocculation kinetics* ▶ C5-31  
*Flotation* ▶ A3-24, A4-104, A6-9, A6-87, B8a-8, B8a-16, B8a-64, B8a-79, B8a-120, B8a-138, B8a-146, B8a-190, B8b-1, B8b-17, B8b-25, B8b-33, B8b-40, B8b-47, B8b-54, B8b-96, B8b-109, B8b-124, B8b-131, B8b-144, B8b-152, B8b-168, B10-1, B10-30, B12a-1, C3-1, C3-72, C7-1, C8a-6, C8a-14, C8b-1, C8b-23, C8b-36, C8b-43, C8b-51, C8b-79, C8b-84, C9-1, C10-5, C11-40  
*Flotation bubbles* ▶ C8a-21  
*Flotation cell geometry* ▶ B8a-8  
*Flotation circuits* ▶ B9-17  
*Flotation column* ▶ A3-120, B8a-163, B8a-190, B8a-131, B9-30, C3-24  
*Flotation deinking* ▶ C12a-20  
*Flotation froths* ▶ B8a-33  
*Flotation kinetics* ▶ B8a-33, B8a-87, B8a-152  
*Flotation machines* ▶ B8a-64  
*Flotation machines hydrodynamics* ▶ B8a-64  
*Flotation of feldspathic ores* ▶ C11-32  
*Flotation process* ▶ A3-39, A3-54, C8a-39, C8b-56  
*Flotation rate* ▶ B8a-1, B8a-87  
*Flotation separation* ▶ B8b-78  
*Flowsheet* ▶ A3-66, B9-24  
*Fluid dynamics* ▶ A4-77  
*Fluidized beds* ▶ A5-50  
*Fluorite* ▶ A5-23, B8a-120  
*Flux pumps* ▶ A7-105  
*Flux tubes* ▶ A7-105  
*Fly ash* ▶ A4-120, B12a-43

*Fly ash utilization* ▶ B12a-43  
*Fly ash beneficiation* ▶ A7-42  
*Folding* ▶ A4-128  
*Foundry* ▶ C12a-9  
*Fractals* ▶ B8a-178  
*Fraction* ▶ A7-59  
*Fractional factorial experiments* ▶ C3-32  
*Froth* ▶ C7-1  
*Froth color* ▶ C8a-39  
*Froth flotation* ▶ A3-74, B8a-24, B8a-152,  
     B8a-158, B8a-178, B13-31  
*Froth model* ▶ C8a-21  
*Froth recovery* ▶ B8a-33  
*Froth structure* ▶ C8a-39  
*FT-IR* ▶ B8a-94  
*Fuzzy approximation* ▶ A3-83  
*Fuzzy control* ▶ C3-17  
*Fuzzy model* ▶ A3-32

## G

*Gain scheduling control* ▶ A3-32  
*Galena* ▶ C8b-15  
*Gas holdup* ▶ C8a-14  
*Gaseous diffusion and chemical reaction* ▶  
     B10-16  
*GAS-process* ▶ C5-1  
*Gas-shear reactor* ▶ C6-77  
*Germanium* ▶ A6-82  
*Gibbsite* ▶ C6-1  
*Glass industry* ▶ B11-9  
*Gold* ▶ A6-41, A6-74, A6-87, B8b-131,  
     C6-22, C8a-6, C12a-34  
*Gold bearing tailings* ▶ B9-30  
*Gold copper ores* ▶ A6-1  
*Gold leaching* ▶ A6-48  
*Gold ores* ▶ B8a-24  
*Grade* ▶ C8a-6, C11-26  
*Grade-recovery curve* ▶ A3-74  
*Grain size distribution* ▶ A2-9  
*Granulation* ▶ C4-36  
*Graphite* ▶ B8a-138  
*Gravitational-magnetic separation* ▶ A1-44  
*Gravity concentration* ▶ C11-26  
*Gravity separation* ▶ A7-8, B9-1, C7-57,  
     C10-1

*Grindability* ▶ A1-9  
*Grinding* ▶ A3-100, A4-44, A4-128,  
     B12a-56, C4-8, C4-71, C4-79, C4-86,  
*Grinding circuit* ▶ A4-31  
*Grinding efficiency* ▶ C4-22, C4-86  
*Grinding kinetics* ▶ C4-16  
*Grinding media* ▶ A4-104, C4-44  
*Grinding plant* ▶ C4-1  
*Grinding selectivity* ▶ C4-86  
*Guar gum* ▶ B8b-144  
*Guars* ▶ B8b-25

## H

*Habitat* ▶ A1-37  
*Hallimond tube* ▶ B8a-79  
*Halogen salts* ▶ A6-33  
*Hammer mill* ▶ C12a-40  
*HCl process* ▶ C6-8  
*Heavy media separation* ▶ C11-40  
*Heavy metals* ▶ B12a-26, B13-1  
*Hematite* ▶ B8a-163  
*Heterocoagulation* ▶ B8a-40  
*Hetero-flocculation* ▶ A5-23  
*Heuristic knowledge* ▶ C3-17  
*Hexametaphosphate* ▶ B8b-25  
*High gradient magnetic separation* ▶ A7-78  
*High intensity conditioning* ▶ B8a-152  
*High pressure jets* ▶ A6-48  
*High pressure roller mill* ▶ A4-97  
*High-performance-attrition* ▶ B13-24  
*High-pressure roll mill* ▶ A4-60  
*High-temperature superconductors* ▶ A7-105  
*Hindered-bed separator* ▶ A7-69  
*Horizontal baffles* ▶ B8a-163  
*Howlite* ▶ A7-52  
*Humic salts* ▶ C13-7  
*Hydrocyclone* ▶ A4-69, A4-77, C1-17  
*Hydrodynamic* ▶ C8b-23  
*Hydrodynamic flotation model* ▶ C8a-21  
*Hydrofloat* ▶ A7-69  
*Hydrogen bonding* ▶ A5-69  
*Hydrogen peroxide* ▶ A6-67  
*Hydrometallurgy* ▶ A6-41, A6-56, C6-70  
*Hydrophobic flocculation* ▶ C5-31  
*Hydrophobic force* ▶ B8a-1

*Hydrophobic surfaces* ▶ B8a-56  
*Hydrophobicity* ▶ B8a-79, C7-1  
*Hydroxamate collector* ▶ C8b-79, C8b-51

## I

*Identification* ▶ A3-54  
*Ilmenite* ▶ C3-55  
*Image analysis* ▶ A1-9, A1-52, A3-46,  
 B8a-178, C1-17  
*Image precessing* ▶ C8a-39, B8a-158  
*Impact* ▶ C3-8  
*Impact crushing* ▶ A2-24  
*Independent components* ▶ A3-39  
*Industrial application* ▶ C7-9  
*Industrial minerals* ▶ A7-27, B9-17  
*Industrial waste* ▶ B12b-1, C12a-40  
*Influence of heterogeneity* ▶ B8a-56  
*Inhibitor of corrosion* ▶ C8b-23  
*Instrumentation* ▶ C3-24  
*Integrated metallurgical complex* ▶ A3-83  
*Interaction* ▶ C8b-71, C12a-20  
*Interface* ▶ C3-1  
*Internet* ▶ A3-83  
*Inverse problems* ▶ A2-1  
*Ion exchange* ▶ C5-16  
*Ion flotation* ▶ B8b-138  
*Iron* ▶ C6-64  
*Iron ore* ▶ A7-8, B8a-163  
*Iron ore pellets* ▶ A4-120  
*Iron oxide* ▶ A5-62  
*Iron removal* ▶ B11-1, C6-36

## J

*Jameson cell* ▶ B8a-163  
*Jet aeration* ▶ B8a-131  
*Jones magnetic separator* ▶ C7-15

## K

*Kaolin* ▶ A1-24, C6-36, C8b-51  
*Kaolin beneficiation* ▶ C11-1  
*Kaolin clay* ▶ C8b-79  
*Kaolinite* ▶ B13-17  
*Kinetic analysis* ▶ C6-36  
*Kinetics interaction forces* ▶ C6-1

## L

*Laboratory testing* ▶ A7-35  
*Lagrangian model* ▶ C8a-32  
*Landfill leachate* ▶ B8b-33  
*Laser light diffraction* ▶ C1-1  
*Leaching* ▶ A6-33, A6-67, A6-82, B13-1,  
 C6-22, C6-43, C8b-63, C12a-27  
*Lead* ▶ C8b-63  
*Lead slimes* ▶ B10-22  
*Lead-zinc minerals* ▶ B8a-138  
*Liberation* ▶ A2-36, C1-17, A2-24  
*Liberation model* ▶ A2-9  
*Lime depression* ▶ C8b-43  
*Liquid-liquid extraction* ▶ B8b-70, C6-84  
*Lithium concentrates* ▶ C11-40  
*Lithology* ▶ A1-9  
*LIX 1104SM* ▶ C6-64  
*Locked cycle tests* ▶ B8a-138  
*Low ash clean coal* ▶ A7-121  
*Low-grade* ▶ C10-1  
*Low-temperature superconductors* ▶ A7-105  
*Luminophore* ▶ B12a-63

## M

*MAA-depressant* ▶ B8a-49  
*Magnesite flotation* ▶ B8b-62  
*Magnesite stability* ▶ B8b-62  
*Magnesite surface chemistry* ▶ B8b-62  
*Magnesium* ▶ A6-22  
*Magnetic classification* ▶ C7-9  
*Magnetic filters* ▶ A7-78  
*Magnetic properties* ▶ A7-35  
*Magnetic separation* ▶ A7-35, A7-105,  
 B10-1, B10-30, C7-9, C7-50, C7-15,  
 C7-22, C10-5  
*Magnetite* ▶ A7-35  
*Magnetite production* ▶ C12a-15  
*Malleable metals* ▶ A4-128  
*Mamdani rules* ▶ C3-17  
*Manganese* ▶ B12b-18, C2-1  
*Manganese ore* ▶ A6-67  
*Manganese sulfate* ▶ A6-67  
*Manganese-oxidizing bacteria* ▶ B12b-18  
*Manganese-zinc removal* ▶ A6-14  
*Mars* ▶ A1-37

*Martite* ▶ A7-35  
*Mass transfer* ▶ C6-77  
*Material balance* ▶ A3-59  
*Material flow analyses* ▶ B12a-35  
*Material flow management* ▶ B12a-35  
*Mathematical characterization* ▶ A1-1  
*Mathematical modelling* ▶ A4-77  
*Mechanical activation* ▶ A4-52  
*Mechanical alloying* ▶ A4-52  
*Mechanical and column flotation* ▶ C11-32  
*Mechanical flotation machines* ▶ B8a-131  
*Mechanical processing* ▶ B12a-9  
*Mechanochemical pretreatment* ▶ A6-74  
*Mechanochemistry* ▶ A1-44, A4-52  
*Media* ▶ C4-8  
*Media mill* ▶ C4-71  
*Membrane process* ▶ B9-24  
*Mercury dispersion* ▶ C12b-1  
*Mesophile bacteria* ▶ A6-110  
*Metal* ▶ A4-44  
*Metal ions* ▶ A5-8  
*Metal wastes* ▶ B12a-18  
*Metallurgical wastes* ▶ A4-1, C12a-15  
*Metals* ▶ B12b-9, C12a-1  
*Metals recovery* ▶ C9-1  
*Metals recovery and concentration* ▶ A6-95  
*Microbial* ▶ C13-1  
*Microcalorimetry* ▶ B8b-1  
*Micronization* ▶ A5-16  
*Microorganism* ▶ B12b-25  
*Microprocesses* ▶ C12a-1  
*Migration* ▶ C7-44  
*Mill* ▶ C4-71, C4-79  
*Milling* ▶ A6-60  
*Milling process* ▶ C4-22  
*Mine drainage* ▶ B12b-18  
*Mineral* ▶ C8b-71  
*Mineral boundary* ▶ A2-9  
*Mineral dressing* ▶ A1-44  
*Mineral liberation* ▶ A2-1, A2-16  
*Mineral processing* ▶ A1-30, A3-59, C6-43  
*Mineral processing techniques* ▶ C11-17  
*Mineral wool* ▶ B12a-43  
*Mineralization* ▶ B8a-131  
*Mineralogical texture* ▶ A2-16

*Mineralogy* ▶ A6-48  
*Minerals* ▶ A5-16, C4-58, C9-1  
*Mine-to-mill* ▶ A3-66  
*Mixture grinding* ▶ A4-60  
*Model* ▶ C3-72  
*Modelling* ▶ A3-8, B8a-104, B12a-26, C1-17,  
     A3-1, A7-59, B8a-33, B8a-120  
*Models* ▶ A3-92  
*Modified bentonite* ▶ A5-45  
*Modifier* ▶ B8a-71  
*Molding sands* ▶ C12a-9  
*Molybdenite* ▶ C8b-9, C10-5  
*Molybdenite flotation* ▶ B9-10  
*Monazite* ▶ C10-5  
*Monothiophosphinic acid* ▶ A6-22  
*Morphogenesis* ▶ A5-1  
*Multifeed flotation circuits* ▶ B9-10  
*Multimodal frequency distribution* ▶ A2-24

## N

*Naphthenic oils* ▶ B8b-177  
*Neural networks* ▶ A1-24, A3-92  
*Ni-Cu ores* ▶ B8b-116  
*Nigrosine* ▶ C8b-63  
*Noise* ▶ C3-8  
*Non-conventional extractants* ▶ C6-70  
*Non-ferrous metals recovery* ▶ C12a-15  
*Nonionic surfactants* ▶ B8b-124  
*Nonlinear control* ▶ A3-120  
*Non-polar oil* ▶ C5-31  
*Non-stoichiometric minerals* ▶ A1-17  
*Non-sulfides* ▶ C8b-1  
*Nucleophilic reagents* ▶ C8b-63  
*Numerical simulation* ▶ A4-69

## O

*OCS software* ▶ C3-45  
*Oil* ▶ A5-37, C8a-6  
*Oil flotation* ▶ B13-31  
*Oleate* ▶ B8a-120  
*Oleate collectors* ▶ B8b-62  
*On-line analysis* ▶ A1-30  
*On-line monitoring* ▶ C3-8  
*Operating variables* ▶ A4-21  
*Operational work index* ▶ C4-1



*Optical-sorting* ▶ C11-9  
*Optimization* ▶ A3-66, B9-1, C3-32  
*Optimizing control* ▶ C3-45  
*Ore* ▶ C2-8  
*Ore dressing* ▶ B8b-9  
*Ore microstructure* ▶ C4-99  
*Organo-clay* ▶ C5-16  
*Osmium* ▶ B10-22  
*Osmium (VI) sulfite complexes* ▶ B10-22  
*Oxalic acid leaching* ▶ B11-1  
*Oxidation* ▶ B8a-104  
*Oxidized raw material* ▶ B10-30

## P

*Packed column jig* ▶ A7-8  
*Paenibacillus polymyxa* ▶ B8a-94  
*Paint* ▶ C5-16  
*Papers* ▶ B12a-1  
*Paraffinic oil* ▶ B8b-177  
*Particle breakage* ▶ C4-99  
*Particle classification* ▶ A1-52  
*Particle motion* ▶ C7-57  
*Particle shape* ▶ A7-95  
*Particle shape analysis* ▶ C4-64  
*Particle shape factor* ▶ A4-21  
*Particle size* ▶ A7-59, C1-1, C8a-6  
*Particle size distribution* ▶ C1-1  
*Particulate materials* ▶ A4-87  
*Partition curve* ▶ A7-95, C4-29  
*Penalty cost elements* ▶ B8a-111  
*Pentlandite* ▶ B8b-40  
*PEO* ▶ A5-69  
*Performance prediction* ▶ A3-16  
*Performances* ▶ A4-21  
*Permeability* ▶ A5-30  
*pH control* ▶ B8b-17  
*Phanerochaete chrysosporium* ▶ C12a-34  
*Phase analysis* ▶ A1-30  
*Phosphate* ▶ B10-1, C1-25  
*Phosphate flotation* ▶ C8a-1  
*Phosphate ore* ▶ B8b-124  
*Phosphate rock* ▶ B9-17  
*Phosphoric acid* ▶ B10-1  
*Pilot plant* ▶ C3-1, C4-22  
*Pilot scale studies* ▶ C5-8

*Pitzer theory* ▶ B10-9  
*Plastic bottles* ▶ B12a-56  
*Plastics* ▶ B12a-1  
*Plastics flotation* ▶ B12a-49  
*Plate vibration* ▶ B8a-152  
*Plutonium* ▶ B12b-25  
*Pneumatic machine* ▶ B8a-146  
*Pole placement* ▶ A3-32  
*Pollution* ▶ C7-30  
*Polyacrylamides* ▶ C8b-1  
*Polyacrylic acid* ▶ A5-62  
*Polyelectrolytes* ▶ C7-30  
*Polymer* ▶ C5-24  
*Polymeric depressants* ▶ C8b-1  
*Polymeric flocculation* ▶ A5-30  
*Polyoxyethylene surfactants* ▶ B8b-160  
*Polyvinylpyrrolidone* ▶ A5-62  
*Porosity* ▶ C4-36  
*Post-consumer plastics* ▶ B12a-56  
*Potash-ore flotation* ▶ B8a-71  
*Potential* ▶ B8b-152  
*Powders* ▶ A4-44, A1-37  
*Pozzolanic* ▶ A4-120  
*Precious metals* ▶ C6-50  
*Precipitation* ▶ A6-82, B9-24, B12b-33, B13-38  
*Precipitation mechanisms* ▶ C6-57  
*Precipitation variables* ▶ C6-57  
*Pre-concentrate* ▶ C9-7  
*Pre-concentration* ▶ C10-1  
*Predictive control* ▶ A3-120  
*Preferential breakage* ▶ A2-9  
*Pressure drop* ▶ C4-58  
*Principal component analysis* ▶ A3-83  
*Printed circuit board* ▶ B12a-9  
*Process* ▶ C1-9, C4-8  
*Process control* ▶ A4-13, A4-69, B8a-158, B8a-178, C3-24  
*Process development* ▶ B11-1  
*Process improvement* ▶ A3-100  
*Process mineralogy* ▶ A1-17  
*Process modelling* ▶ A3-108  
*Process simulation* ▶ B9-1  
*Process water* ▶ B8b-40  
*Processing noble metals* ▶ A7-115

*Production* ▶ C4-58  
*Pt-group metals* ▶ A6-33  
*Pulp potential* ▶ B8b-96, B8a-49  
*Pulsating HGMS* ▶ C7-22  
*Pulsating medium* ▶ B8a-146  
*Purification* ▶ A6-14, A7-27  
*Pyrite* ▶ B8a-171, B8b-1, B8b-131, B8b-152, B10-30  
*Pyrite activation* ▶ C8b-43  
*Pyrite oxidation* ▶ A6-110  
*Pyrrhotite* ▶ B8a-24  
*Pyrrhotite depression* ▶ B8b-116

## Q

*Quartz* ▶ A1-37, B8a-163, C7-30, C8b-56  
*Quartz-feldspar flotation* ▶ B8b-160

## R

*Radicals* ▶ B8b-54  
*Radioactive decontamination solution* ▶ B13-38  
*Ramification flotation* ▶ B9-10  
*Rare earth* ▶ B12a-63, C6-84  
*Rare earth residue* ▶ C6-15  
*Rate constants* ▶ A3-46  
*Raw clay processing* ▶ C11-32  
*Raw materials* ▶ A1-1, C12a-46  
*Reagent Z-96* ▶ C8b-23  
*Reagents* ▶ C8b-71  
*Real time process management* ▶ A3-83  
*Recovery* ▶ C11-26, C12a-46  
*Recovery-grade curve* ▶ A3-74  
*Recycle* ▶ C12a-46  
*Recycling* ▶ B12a-18, B12a-63, C6-29  
*Recycling materials* ▶ C12a-40  
*Reducing agent* ▶ C8b-15  
*Refractory ores* ▶ A6-48  
*Regulatory* ▶ A3-24  
*Reichert cone* ▶ B9-1  
*Release analysis* ▶ A3-74  
*Remediation* ▶ B13-38  
*Resins* ▶ C6-50, B10-1  
*RESS-process* ▶ C5-1  
*Reutilization* ▶ C12a-9  
*Reverse flotation* ▶ B8a-163

*Rhenium* ▶ B10-22  
*Rheological additive* ▶ C5-16  
*Rheology* ▶ C4-29  
*Rigid spargers* ▶ C8a-14  
*Rock* ▶ C2-8  
*Roll mill* ▶ A3-100  
*Roll press* ▶ A4-132  
*Rotor-stator-baffle system* ▶ B8a-8  
*Run of mine* ▶ C4-22

## S

*Sadiola* ▶ C3-45  
*SAG mills* ▶ A4-13  
*Saline minerals* ▶ C8b-36  
*Sand* ▶ C11-26  
*Sardinia* ▶ C11-9  
*Saturation* ▶ C4-36  
*Scale-up* ▶ A3-1, A3-8  
*Scrap* ▶ C12a-1  
*Scrap processing* ▶ B12a-35  
*Screening* ▶ A7-59  
*Segregation* ▶ A7-1, C7-44  
*Selective destruction* ▶ C2-8  
*Selective flocculation* ▶ C8b-79  
*Selective flotation* ▶ C8b-9  
*Selective separation* ▶ B8a-111, C8b-63  
*Selective-flotation* ▶ B8a-49  
*Selectivity* ▶ B8b-96, C8b-71  
*Self-organizing map* ▶ C4-64  
*SEM* ▶ C1-9  
*Semiconductor* ▶ B8b-78  
*Sensors* ▶ A1-9  
*Separation* ▶ C3-65, C6-15, C7-44, C12b-1  
*Separation effectiveness* ▶ A7-1  
*Separation efficiency* ▶ C7-34  
*Separation operations* ▶ A7-1  
*Separation rate* ▶ A7-1  
*Shear thinning* ▶ C6-77  
*Shredder* ▶ C12a-1  
*Sierpinski carpet* ▶ B8a-178  
*Silica* ▶ A5-69  
*Silica flotation* ▶ B8a-40  
*Silica sand* ▶ B11-1  
*Silicate minerals* ▶ A7-17  
*Silicosis* ▶ A1-37

- Silver* ▶ A6-9  
*Silver plant tailings* ▶ A6-9  
*Silver-bearing concentrates* ▶ A6-103  
*Silver-bearing ores* ▶ A6-56  
*Simulation* ▶ A1-1, A3-1, C3-39, C4-16, C7-9  
*Simulator* ▶ A3-66  
*Sink-float separation* ▶ B12a-1  
*Size distributions* ▶ C4-36  
*Slag* ▶ B11-9  
*Slip* ▶ A4-97  
*Slurry analysis* ▶ A1-30  
*Small-diameter hydrocyclone* ▶ C4-29  
*Smelting slag foaming* ▶ C3-55  
*Sodium chromate* ▶ B10-16  
*Sodium humate* ▶ B8b-78  
*Sodium metabisulfite* ▶ B8b-116  
*Sodium oleate* ▶ B8b-109  
*Soft-sensors* ▶ A1-9, A4-13, C4-1  
*Soil contamination* ▶ B13-1  
*Soil deoiling* ▶ B13-31  
*Soil microflora* ▶ C13-1  
*Soil remediation* ▶ B13-17, B13-24  
*Soil remediation technology* ▶ B13-9  
*Solid state diffusion* ▶ B10-16  
*Solid-liquid separation* ▶ B9-24  
*Solubility* ▶ B10-9, C1-25  
*Solution analyses* ▶ A4-104  
*Solvent extraction* ▶ A6-14, A6-82, C6-64, C6-70  
*Solvent impregnated resin* ▶ C6-15  
*SOM* ▶ C4-64  
*Sorption* ▶ C6-15, C8b-36  
*Sound frequency* ▶ C8b-84  
*Sound intensity* ▶ A3-92  
*Spacesuit* ▶ A1-37  
*Spectrocolorimetry* ▶ C1-9  
*Spectrum distributions* ▶ A3-92  
*Sphalerite* ▶ C8b-15, C9-1  
*Sphalerite activation* ▶ B8b-87  
*Spin-labeling* ▶ B8b-54  
*Spodumene* ▶ C11-40  
*Spouted bed* ▶ A4-38  
*Start-up* ▶ A3-24  
*Steelmaking flue dust* ▶ A5-8  
*Steel-making residues* ▶ C12a-15  
*Stereology* ▶ A1-1, A2-1, A2-16, A3-46  
*Stirred mill* ▶ A4-112  
*Stirring screw* ▶ C4-44  
*Stochastic models* ▶ C3-65  
*Stratification* ▶ A7-59  
*Stresses on rollers* ▶ A4-97  
*Structural-chemical parameter* ▶ A1-64  
*Structure* ▶ A5-1  
*Structure parameter* ▶ C4-53  
*Sub-aerated flotation cells* ▶ B8a-64  
*Suction media* ▶ C5-8  
*Sulfate reduction* ▶ C13-1  
*Sulfate-reducing bacteria* ▶ B12b-9  
*Sulfide* ▶ B8b-40, B8b-96, B8b-144  
*Sulfide mineral* ▶ B8b-78, B8a-94, B8a-104, B8b-17  
*Sulfide ores* ▶ B8a-152, B8a-24  
*Sulfides* ▶ B12b-9, C8b-1  
*Sulfidization* ▶ B10-30  
*Sulfur* ▶ C7-15  
*Sulfuric acid* ▶ A6-67  
*Superconducting magnetic separation* ▶ A7-27, A7-78  
*Supercritical fluids* ▶ C5-1  
*Supported liquid membrane* ▶ A6-95  
*Surface* ▶ A5-8, B8a-104  
*Surface characterization* ▶ A5-69  
*Surface chemistry* ▶ B8b-138  
*Surface complexation model* ▶ B8b-70  
*Surface forces* ▶ B8a-1  
*Surface phenomena* ▶ B8a-111  
*Surface properties* ▶ B8b-9, B8b-47  
*Surfactant mixtures* ▶ B8b-160  
*Surfactants* ▶ B8b-54  
*Sylvite particles* ▶ B8a-131  
*Synergism* ▶ B8b-160  
*System identification* ▶ A3-120
- T**  
*Tailings* ▶ C9-13  
*Technological mineralogy* ▶ C2-1  
*Technological processes* ▶ C9-13  
*Thermophilic bacteria* ▶ A6-110  
*Thickening* ▶ A5-30

*Thiobacillus ferrooxidans* ▶ B8a-94, C6-43  
*Thiocyanate technology* ▶ A6-56  
*Thiol collectors* ▶ B8b-1  
*Thiol surfactants* ▶ B8b-131  
*Thiosulfate* ▶ A6-74, B8b-40  
*Thiourea* ▶ C6-22, C6-36  
*Thixotropic agent* ▶ A5-45  
*Thorium* ▶ B12b-25  
*Three dimensional modelling* ▶ B8a-178  
*Three-banded* ▶ B12a-63  
*Tolerance limit* ▶ C9-7  
*Toner composites* ▶ C12a-20  
*Tower mill* ▶ A3-1  
*Toxic heavy metals* ▶ C13-1  
*Toxic metals* ▶ B12b-1  
*Tree technique* ▶ A3-74  
*Tribo/contact charge* ▶ A7-17  
*Tribo-electric separation* ▶ A7-17  
*Triboelectricity* ▶ B12a-1  
*Triboelectrostatic separation* ▶ A7-121  
*Triethylenetetramine* ▶ B8b-116  
*Tri-Flo separator* ▶ A7-52  
*Trona* ▶ B10-9  
*Tumbling mill modelling and simulation* ▶  
 A3-16  
*Tumbling mills* ▶ A4-128  
*Turbo classifier* ▶ C4-53  
*TYMS* ▶ C7-50

## U

*U and Th removal* ▶ A6-60  
*Ultra fine* ▶ C4-79  
*Ultra-fine coal* ▶ A7-121  
*Ultrasonic* ▶ A4-112  
*Ultrasound* ▶ B8a-152  
*Upper layer concentration* ▶ A5-23  
*Uranium* ▶ B9-24, B12b-25, C13-1

## V

*Vector database* ▶ A1-52  
*Verti-mill* ▶ A3-1  
*Vibrating HGMS* ▶ C7-22  
*Vibrating screen* ▶ C5-8  
*Vibration* ▶ A4-44  
*Vibration in flotation* ▶ C8b-29

*Vibration milling* ▶ A4-1  
*Viscosity* ▶ C4-29  
*Volatile fatty acids* ▶ B8b-33  
*Vortex* ▶ C7-50  
*Vortex motion* ▶ A4-77

## W

*Wash sulfuric acid* ▶ B10-22  
*Waste treatment* ▶ B12a-26  
*Wastes* ▶ C12a-9  
*Wastewater* ▶ B12b-33  
*Wastewater treatment* ▶ A5-23, A6-95, C12b-  
 9  
*Water treatment* ▶ B12b-18  
*Wear* ▶ C4-8  
*Wet* ▶ C4-71  
*Wet oxidization* ▶ B12a-49  
*Wetting* ▶ B12a-49  
*Wetting films* ▶ B8a-56  
*Wiegel model* ▶ A2-9  
*WO<sub>3</sub> recovery* ▶ C9-7  
*Wood chips* ▶ C12a-34  
*Work function* ▶ A7-17  
*Work index* ▶ C4-1  
*World Wide Web* ▶ A3-83

## X

*Xanthate adsorption* ▶ C8b-15  
*XPS analysis* ▶ C8b-15  
*XPS spectra* ▶ C8b-43  
*X-ray diffraction* ▶ A1-30

## Y

*Yttrium* ▶ B12a-63, C6-84

## Z

*Zeolites* ▶ A1-44  
*Zeta potential* ▶ A5-23, B8b-87, B8b-168,  
 B8a-94, C12b-1  
*Zinc concentrates* ▶ A6-82  
*Zinc recovery* ▶ C12a-27  
*Zircon* ▶ B8b-109  
*Zircon sands* ▶ A6-60  
*Zirconium oxide powders* ▶ C6-57

This Page Intentionally Left Blank